Josef Krautkrämer
Herbert Krautkrämer

Ultrasonic Testing of Materials

4th Fully Revised Edition

in Collaboration with

W. Grabendörfer · M. Gregor · L. Niklas
R. Frielinghaus · W. Kaule · H. Schlemm
U. Schlengermann · H. Steiger

Translation of the
5th Revised German Edition

With 564 Figures

Springer-Verlag Berlin Heidelberg GmbH 1990

Dr. rer. nat. Dr.-Ing. E. h. Josef Krautkrämer, Köln
Dr. rer. nat. Herbert Krautkrämer, Merten near Köln

Collaborators:

Dr. phil. Werner Grabendörfer
Dr.-Ing. Rainer Frielinghaus
Dipl.-Ing. Walter Kaule
Dr. phil. Ludwig Niklas
Dr. rer. nat. Ulrich Opara
Phys. Udo Schlengermann
Dr. rer. nat. Helmut Seiger
Dr. rer. nat. Gerhard Splitt
Dipl.-Ing. Klaus Volkmann
all of Krautkrämer Company, Hürth near Köln
and
Prof. Dr. Erik Primbsch, University of Hamburg

To the Pioneers of
Ultrasonic Testing of Materials

S. Ja. Sokolov (UdSSR)
1897–1957

Floyd A. Firestone (USA)
*1898

Donald O. Sproule (England)
*1903

Preface to the Fourth Edition

This fourth English edition is based on the fifth German one, published in 1986. Compared with the third English edition it contains a basically new treatment of many sections, because in the meantime fundamental research, as well as practical applications, have made much progress.

To avoid undue growth in the size of the book, some sections have had to be omitted or shortened, we hope without losing too much of an overall view of this quickly growing field of non-destructive testing (NDT).

In Part A the sections on basic physics give more emphasis to guided waves, mode changing processes and the diffraction of waves. The useful creeping or head-waves have been introduced as well as a fuller treatment of scattered or edge waves. In the chapter on generation and reception of ultrasonic waves by methods other than piezo-electricity, the various laser techniques have been treated more thoroughly.

In Part B which covers techniques and instrumentation, the rapid progress of microelectronics is the main reason for an enlargement, and further improvements in transducer design and their arrangement as phased arrays has also been reported. Much more space was required in Chapter 13 which covers real-time imaging methods. Though not yet used on a large scale in practice, they hold much promise for the future, especially in the case of computer-assisted holographic methods.

In Part C the evaluation of defect size and characteristics needed more space for reporting on new methods using diffracted waves.

In Part D, in addition to nuclear reactor testing, the Chapters on heavy forgings, railway components and materials, and the problems associated with austenitic welds, composite materials and concrete have all been revised substantially. Hardness testing using ultrasound has been added and the chapter on standardization updated. In Section 33.3 evaluation of materials and their characterization by attenuation and scattering has been given more space.

A difficult problem has been the bibliography. Today there are probably more than 50 000 published papers on ultrasonic NDT and it has been a difficult task of selection to restrict the total to about 1900. The papers of the last three years could be evaluated only very briefly, but the bibliography from the 5th German edition has been enlarged by adding a Supplement containing a further 206 entries identified by an S prefix. We ask authors for their understanding if they do not find their particular papers included, and their pardon if we have overlooked an important publication.

As well as the co-authors mentioned above (mostly of the Krautkrämer Company, Cologne), a number of experts have also collaborated, to whom the authors are very much indebted. These include Dr. K. Egelkraut, Bundesbahn-Versuchsamt

Minden; Dr. W. Mohr, BBC Baden/Switzerland; Mr. G. Künne, Dortmund; Dr. H. Schneider, Mannesmann Forschungsinstitut, Duisburg; Dr. B. Werden, TÜV Essen; Dr. C. Kleesattel, New York; Dr. S. Hirsekorn, IzfP Saarbrücken and Dr. H. Dölle, BBC Baden/Switzerland.

The translation has been carried out by Mr. J. D. Hislop, Derby, England in collaboration with one of the principal authors. It must be stated however that we owe to Mr. Hislop not a literal translation, but a considerable improvement in the presentation as well as the correction of a number of faults and errors. He also contributed many technical details of test methods based on his 38 years experience in ultrasonic testing.

On this occasion we also would like to thank many unnamed friends for their kind interest and their communications concerning specific items. We are always grateful for personal criticisms and for the correction of errors.

Finally we thank the editor very heartily for the excellent preparation of the book for printing as he has done previously for the earlier editions.

Cologne, Spring 1990   J. and H. Krautkrämer

Contents

---

* The sections marked with an asterisk are less important for beginners.

Introduction

Acoustics, the science of sound, describes the phenomenon of mechanical vibrations and their propagation in solid, liquid or gaseous materials. Empty space knows no sound because it is the particles of matter themselves which vibrate, in contrast for instance to the oscillations of light or other electromagnetic waves where the electric and magnetic state of free space oscillates. In air a sound wave moves a discrete volume of air back and forth around its neutral position, whereas a light wave has no influence on its state of rest or motion.

If such mechanical movements in matter, repeated periodically and for a given length of time, are classified according to their number of cycles per second, a range can be defined in which the human ear can serve as detector. The sound is audible if it reaches the ear either through the air or through the body. This requires, however, that its frequency be neither too low nor too high. Sound below approx. 10 Hz (hertz = cycles per second) and above approx. 15 000 to 20 000 Hz is inaudible to the human ear. For the lower limit this statement is, however, strictly correct only where this concerns sinusoidal oscillations. Other forms of vibration are resolved by the ear into harmonics, thus making them audible as noise pulse sequences.

Just as in the case of light waves, where the higher frequencies which are invisible to the eye, are called ultraviolet, so the sound waves above 20 000 Hz are referred to as ultrasound or ultrasonic. It has been suggested that sound waves below 10 Hz be called subsonic. This division is purely arbitrary and dependent on the human ear. Completely different demarcations apply in the case of other generating and detecting methods.

Ultrasonic waves are a rather common occurence in nature and in daily life, and are occasionally of such intensity that we may regard ourselves as very fortunate indeed that our ear is not burdened by them, as for instance in the case of steam whistles. A rotating grindstone when used for grinding a specimen generates in addition to audible noise intense ultrasonic waves with frequencies as high as those used for testing materials, viz. above 100,000 Hz (100 kHz, kilocycles per second) and up to 10 000 000 Hz (10 MHz, megacycles per second).

The numerous technical applications of sound waves and ultrasonics may be divided into two groups. As in medicine where X-rays are used for two completely different purposes, viz. therapeutically for their action on tissue (e.g. cancer irradiation) and diagnostically for studying certain medical conditions (e.g. radioscopy of the lungs), so sound can be used to act physically on a given material, or to explore its physical condition. In the first case the energy of the sound wave is used, for example for ejecting particles of dirt from fabrics during washing, for detaching foreign bodies from a surface during cleaning, for removing metal chips during drill-

ing, for overcoming surface tension during emulsification, for mixing, and for many other applications of mechanical force all concerning the exploitation of sound energy.

In other cases the energy of the sound wave is utilized only to the extent required for transmitting a sufficiently clear signal, for example in public address systems, for locating ships at sea, for sounding ocean depths, locating shoals of fish, and for checking the condition of materials, for example for detecting the presence of flaws, for measuring their thickness, and determining their elastic and metallurgical properties. The sound wave is in these cases the carrier of information and usually one has to transmit an ultrasonic wave into the specimen and to receive a returning one to analyse the information it carries. There are also conditions arising whithin the material itself which are responsible for generating ultrasonic waves when the material is stressed. Then we can speak of acoustic emission, which also plays a certain role in materials testing.

In this book principally the diagnostic applications of ultrasound for materials testing will be reported.

Fundamentally to determine the mechanical properties of a given material, a mechanical method is the most direct and ready to hand. To determine for example whether a shaft is cracked, it can be stressed by tension or bending until the crack manifests itself by an open break. This is a mechanical but unfortunately a destructive test. By contrast, sound and ultrasonics provide, for the same purpose, non-destructive testing methods which basically also use mechanical stresses produced by tensile, compressive, shearing or flexural forces but which are of such low intensity that no material damage will occur.

This does not imply, however, that an indirect testing method, for example a magnetic particle test which reveals the distorted magnetic field lines produced by a crack, may not at times be more suitable, provided the correlation between the mechanical properties of the specimen concerned and the physical means applied, such as magnetism, electricity, radiation, etc., are unambiguous.

Leaving out the restrictive qualification "ultra", ordinary sound has long been used for testing individual specimens, such as for example forgings or castings, where gross internal defects can be detected by a changed ringing note when the specimen is struck with a hammer, a method still practised today. Every housewife knows that a china cup can be checked for cracks by tapping it. One can therefore with justice maintain that testing by sound is one of the oldest non-destructive methods for detecting hidden defects since it is very probable that the inventors of ceramics would already have put it to use. By the application of modern electronics it has become one of the most up to date and most versatile testing tools.

The transition from audible sound to ultrasonic sound has been made possible by modern methods of generation and detection which replace hammer and ear. Whereas the natural vibration produced by a hammer blow depends very little on the hammer but very much on the shape of the specimen and on the striking point, as in the case of a bell for example, the frequency can be predetermined if electrical sound generators are used. In the case of higher frequencies the wavelength of a vibration becomes smaller in inverse proportion, and finally extremely small compared with the dimensions of the specimen concerned. One can then direct a beam

of such waves into a specimen without interference resulting from its shape and dimensions, just as in the case of light from a projector. In this way the specimen is "sounded out" a term already common in popular speech, and a specimen which is defect free and fit for its purpose has long been described as "sound".

Part A | Physical Principles of the Ultrasonic Testing of Materials

1 Ultrasonic Waves in Free Space

1.1 Oscillations and Waves

Ultrasonic testing of materials utilises mechanical waves in contrast, for instance, to X-ray techniques which use electromagnetic waves. Any mechanical wave is composed of oscillations of discrete particles of material. The motion carried out by a small mass attached to a spring as shown in Fig. 1.1 if pulled down once and released, is called an oscillation. Left to itself, the mass oscillates about the equilibrium position. The nature of this oscillation is of particular importance inasmuch as it is sinusoidal, the path recorded as a function of time being a sine curve. It is obtained only if the driving force, in this case supplied by the spring, increases proportionately to the displacement. It is then also referred to as an elastic oscillation. Furthermore, one can imagine the body to consist of individual particles kept in position by elastic forces. Very much simplified, the model of an elastic body can be visualised as shown in Fig. 1.2, but three-dimensionally. Provided such a body is not stressed by compression or tension beyond its elastic limit, it behaves like this spring model. In it, the particles can perform elastic oscillations. How then does a wave arise from an oscillation?

Let us assume that all material particles on the left side of the model are excited collectively in step with the sinusoidal oscillations, for instance by cementing them
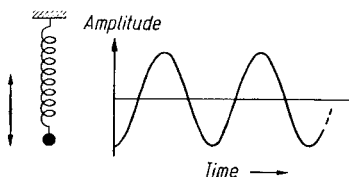
Fig. 1.1. Sinusoidal oscillation of a loaded spring
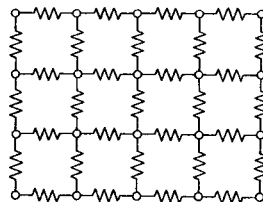
Fig. 1.2. Model of an elastic body
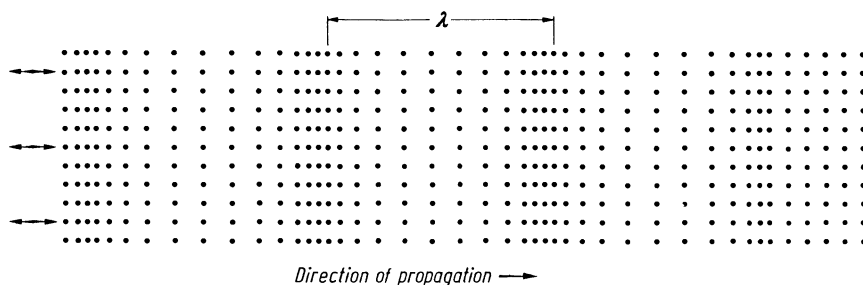
Fig. 1.3. Longitudinal wave

to a diaphragm which is made to oscillate by electrical means, as in a loudspeaker for example. All particles in the first plane are then forced to oscillate with the same amplitude (width of oscillation) and frequency (number of oscillations per second). The elastic forces transmit the oscillations to the particles in the second plane. When these have started to oscillate, the vibratory movement is transmitted to the third plane, and so forth. If all points were interconnected rigidly, they would all start their movement simultaneously and remain constantly in the same state of motion, i.e. in the same *phase*. In an elastic material this is not the case, the motion requiring a certain period of time to be transmitted and the planes reached subsequently lag in phase behind those first excited. While in a certain plane the particles are moving from the right through the point of equilibrium to the left, the particles in a plane further to the right have only just started to move from left to right. Their delay is then exactly one half oscillation. Figure 1.3 shows the instantaneous picture of a section of the model in which a wave travelling from left to right has not yet reached the right-hand edge. It can be seen that the phase shift of the oscillations creates zones where the particles approach each other particularly closely. These compression zones alternate with rarified zones. The chronological pattern of the wave shows that these zones are constantly recreated on the excitation side and that they travel in the body at constant velocity and uniform intervals towards the right. This represents an *elastic wave*.

Of course, Fig. 1.3 cannot vividly demonstrate the movement of the wave, which could only be done on a cine film. The wave phenomenon as such is, however, well known from another kind of wave, viz. waves in water. A wave crest corresponds to a zone of compression. A naive observer might think that the wave crest transports water, because his eye can follow the wave crest. That this is not the case in reality is demonstrated by any small body floating on the water, which merely moves up and down. The only thing that travels in the wave is its state, in the case of elastic waves the state of compression and rarefaction. The particles themselves remain in place and merely oscillate about their positions of rest.

Of course, the model of a solid body can be visualised as consisting of many separate particles of material only if it is uniform (homogeneous) throughout and if it shows the same elastic behaviour in all directions (isotropic). Each point shown in Fig. 1.3 then represents the mass of a small cube.
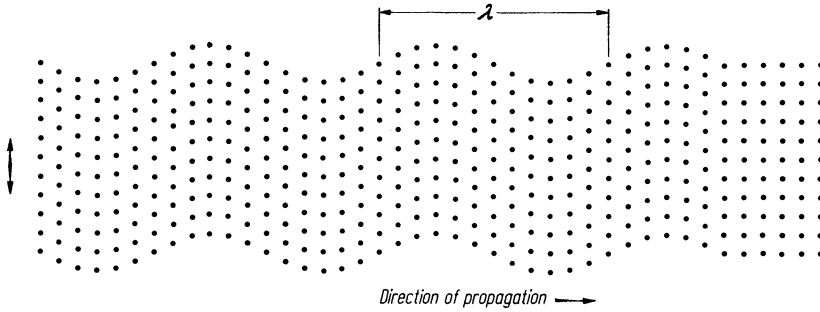
Fig. 1.4. Transverse wave

The spring model shown in Fig. 1.2 cannot be applied to liquid or gaseous substances where the individual particles are not tied to a position of rest but where they are free. Nevertheless, these substances also offer a certain resistance when compressed or expanded, as shown for example by an air pump. They can therefore also transmit elastic waves.

When visualising the models presented in Figs. 1.3 and 1.4, it should be realised that the plane of dots represents only a section of the threedimensional body, in as much as boundary surfaces would modify the wave process considerably. A wave as depicted in Figs. 1.3 and 1.4 can exist in this way only when remote from any boundaries.

A few parameters of a wave will be defined with the aid of Fig. 1.3. The *frequency* of a wave is the number of oscillations of a given particle per second. Within a given wave it is the same for all particles and it is identical with the frequency of the generator which can be chosen arbitrarily. The *wavelength is* the distance between two planes in which the particles are in the same state of motion, for instance two compression zones and it is inversely proportional to the frequency: high frequencies corresponding to short wavelengths, and vice versa. The speed of sound is the *velocity* of propagation of a given condition, for example a compression zone. This velocity is a characteristic of the material concerned and in general is constant for a given material for any frequency and any wavelength. Numerical data and formulae are given in Section 1.3 and Table A 1. For us the most important quantity in a given sound field is the *sound pressure*. At points of higher particle density the pressure is likewise higher than the normal pressure, while in the dilated zones it is lower. A very small and inertia less pressure gauge placed in the path of the sound wave would indicate alternately high pressure and low pressure in sinusoidal sequence. This alternating pressure is the sound pressure. It occurs not only in gases, but also in liquid and solid bodies. The maximum deviation from the normal pressure (without sound wave) is called the amplitude of the sound pressure which is closely connected to the amplitude of movement, i.e. the maximum deflection of the particles from their position of rest.

To indicate shorter wavelengths, in the same way as shown in Fig. 1.3, it would be necessary to choose particles with smaller masses and packed more closely, that is to subdivide the material more finely. This has its limits as soon as atomic di-

mensions are reached. It could then no longer be expected that the masses and forces would be evenly distributed. Elastic waves are therefore possible only in the case of wavelengths which are still very long compared with the distances between atoms or molecules.

The wave described in Fig. 1.3 is called a *longitudinal wave* because the oscillations occur in the longitudinal direction, that is the direction of propagation, is not the only kind of wave although from our point of view it is the most important. Since compressional and dilatational forces are active in it, it is also called a *pressure or compression wave*, and because its particle density fluctuates it has also been given the name *density wave*.

This is the real *sound wave* because it transmits the oscillations of a source of acoustic energy through the air to our ears. Experience shows that the same wave also transmits sound through liquid or solid bodies.

However, in solid bodies another kind of wave can also occur, viz. the *transverse wave*; it is indicated schematically in Fig. 1.4 in the form of an instantaneous picture of the particle motion. It will again be assumed that the wave travels from left to right. It can be seen that in this case the particles no longer oscillate in the direction of propagation but at right angles to it, that is transverse.

The excitations can be visualised as a motion in which the particles on the left-hand surface of the body are moved sinusoidally up and down by a periodical *shear force*. In solid bodies such a shear force can be transmitted to the particles in the adjacent planes but their transverse oscillations will show a lag in time, depending on their distance from the plane of excitation. This wave is also called a *shear wave* and the wavelength is determined by the distance between two planes in which particles are in a similar state. In Fig. 1.4 the wavelength is indicated between two planes in which the particles instantaneously pass through their position of rest in a direction from top to bottom.

The sound pressure of the longitudinal wave is in this case replaced by the alternating shear force, but the name "shear of sound" is not used. The pressure is the force at right angles to the unit surface, while the shear force is defined as the force per unit surface, but parallel to it. Thus, the only difference between pressure and shear is one of direction. In all other respects these two characteristics are identical. In what follows we shall therefore speak only generally of sound pressure even where this refers to the shear force in a transverse wave.

Figure 1.4 indicates that the shear is greatest where the particles pass through their position of rest because at this point the relative displacement of two consecutive particle planes is greatest. At the points of maximum amplitude the shear is zero. The same has been found in respect of the sound pressure in Fig. 1.3: where the particles oscillate through their position of rest they either come closest to each other or are furthest apart. At these points the sound pressure reaches its maximum (or its minimum) value. The generalised sound pressure and the motion of the particles are thus not in phase but transposed a quarter period relative to each other.

Since gases and liquids are in practice incapable of transmitting shear (otherwise they could not flow so readily along walls or through pipes), transverse waves can for the practical testing of materials penetrate appreciable distances only in solid bodies.

1.2 Non-planar Waves; Interference of Waves

The various kinds or modes of wave can occur in different wave forms, by which the form of the *wave front* is meant. Up to now we have described *plane waves*, in which a given phase of the oscillation is always the same in a given plane. This co-phasal plane is the wave front which, during propagation, moves parallel to itself. The wave front need not necessarily be flat and on the contrary is never strictly flat in the case of natural sound generators, but usually of complex curvature. However, for clearer presentation and to simplify the calculations it is preferable to replace natural sound waves by simple wave forms, e.g. plane, spherical or cylindrical waves as approximations.

On a given wave front, for example on a sphere in the case of a spherical wave, only the phase is identical; i.e. the passage through zero at a given moment, but not necessarily the amplitude or the sound pressure. The latter, for instance, may have an appreciable value only within a certain angular sector in a given direction, while in other directions it may disappear completely. This represents a spherical *wave beam* as produced for instance by directional loud speakers in air, and also in most cases by ultrasonic sound generators in the testing of materials.

To avoid any misunderstanding it should be stated specifically that the description of natural acoustic phenomena by means of such simple wave forms for each case is permissible only within certain limits, e.g. in close proximity to a plane sound generator for plane waves, or at great distance for spherical waves.

So far it has been tacitly assumed that the generating oscillation capable of producing one of the described wave types consists of a single frequency and lasts very long. Complex and brief oscillation phenomena can be regarded as consisting of a sum of an infinite, or also finite, number of such sinusoidal oscillations which differ in their amplitude, frequency and phase. In an elastic medium each such partial oscillation produces it own wave. In the case of longitudinal and transverse waves in a large body all frequencies have the same velocity and all partial waves travel equally fast, so that each particle carries out the same oscillation. A complex and brief form of oscillation is thus transmitted by these waves unchanged if energy losses are neglected. Absorption or scattering may of course affect the various frequencies differently, as for instance in air where distant thunder appears to have a lower note since the higher frequencies are attenuated more severely.

In order to demonstrate the influence of one free wave on another within an infinite body, we imagine two waves penetrating each other from different directions. What is the movement of a particle oscillating simultaneously in both waves? Provided both amplitudes do not stress the substance beyond its elastic limit, beyond the so-called linear range, the motions are added vectorally, i.e. according to a parallelogram and are composed of motions which the particle would carry out alone in each separate wave. In this process, however, neither of the waves disturbs the other and the two sound beams change neither their original direction nor their frequency and amplitude.

In one special case, however, one obtains an interesting form of the particle oscillations, viz. *a standing wave*. This paradoxical formation (for the essence of a
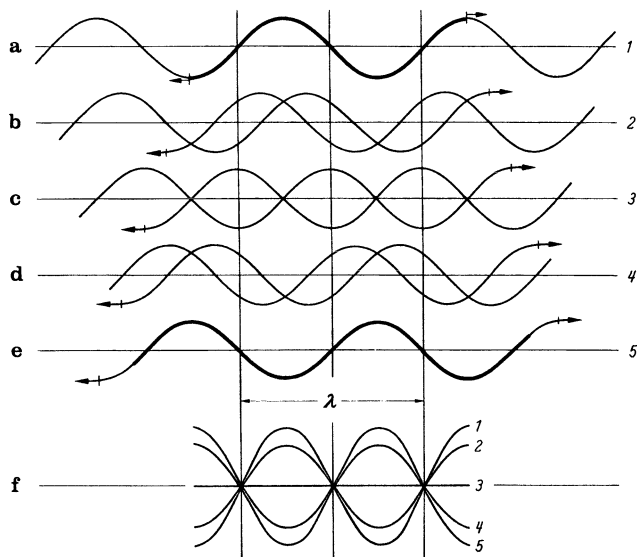
Fig. 1.5. Formation of a standing wave by two waves from opposite directions

wave is that it travels) results from the superposition of two similar plane waves of identical frequency, amplitude and (in the case of transverse waves) direction of oscillation but different direction of propagation. The special case in which they have exactly opposing directions of propagation is shown in Fig. 1.5 for a transverse wave. The sinusoidal curves represent the connecting lines of a series of particles (of matter) at a given moment. Figure 1.5a to e show this state for five consecutive moments. Figure 1.5f is the overall oscillation of the standing wave. The most important fact in this connection is that certain particles constantly remain in a state of rest, which is never the case in an ordinary wave. The points where the two waves constantly cancel each other are called *nodes*, and the points of maximum amplitude between them, *antinodes*.

This form of the wave is generally known from the natural oscillations of taut strings. In the case of the steric standing transverse or longitudinal wave it is, however, necessary to visualise the presentation in Fig. 1.5 supplemented spatially by numerous additional rows of particles. The nodes and antinodes are then located on fixed planes.

It should not be overlooked that the representation of this phenomenon as a standing wave, or as the mutual penetration of two opposing waves, concerns the same physical fact.

The standing longitudinal wave is derived from the representation of a standing transverse wave by regarding the amplitudes of the sinusoidal oscillations in Fig. 1.5 as displacements of the particles in the direction of wave travel or against it (Fig. 1.6). The points of maximum density and dilatation are located in the plane of the nodes spaced one wave length from each other. The nodes of the motion are
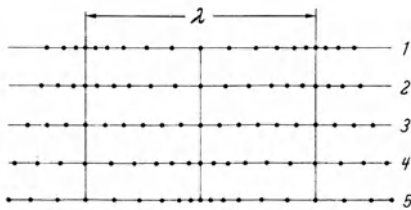
Fig. 1.6. Standing longitudinal wave. Instantaneous pictures at different moments 1–5, corresponding to Fig. 1.5. The nodes of the motion are located in planes spaced $\lambda/2$
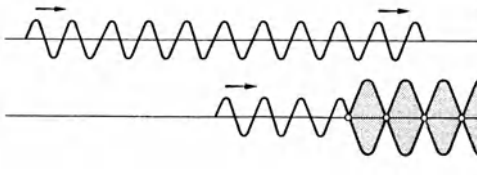
Fig. 1.7. Standing wave produced by reflection at a free wall. Plotted is the amplitude of the particles. At the free wall it has an antinode

therefore simultaneously the antinodes of the sound pressure and vice versa, as is readily seen in Fig. 1.6. The nodes of motion and pressure are thus located a quarter wave length from each other.

In practical ultrasonics, standing waves occur if the material is no longer infinite. At a free surface, i.e. the boundary with empty space, the wave is reflected. In the case of a plane boundary and perpendicular incidence the nature of the incident wave is not changed, but incident and reflected wave have opposite directions, as described in Fig. 1.7 which shows the reflection of a short wave train from a wall, resulting in a brief formation of a standing wave over a distance of a few wavelengths. Figure 1.7 shows the reflection of a wave at a *free wall*, i.e. at the interface between a given substance and vacuum or air, where the wave is totally reflected. According to the boundary conditions the motion of the particles has at that point a maximum, viz. an antinode and the pressure or shear has a node. In Fig. 1.7 is plotted the amplitude of the motion which can be regarded both as longitudinal motion in the case of a pressure wave and as a transverse motion in the case of a shear wave.

Standing ultrasonic pressure waves are produced intentionally when measuring wall thicknesses by the resonance method. In other cases they may cause considerable confusion and should be avoided.

The standing wave is a special case of the superposition of different waves of the same frequency, which is generally called *interference*. This is also the basis of a very vivid method for describing commonly occurring wave forms and wave fields, viz. *Huygens' principle* which will render us good service when explaining the radiation of ultrasonic waves.

Briefly expressed, this principle states that any arbitrary wave form can be constructed from a large number of simple spherical waves of the same frequency, i.e. the so-called *elementary waves*, which must, however, be chosen correctly regarding origin, phase and amplitude. Every wave surface can be visualised as an envelope of such elementary waves whose origin is located on a preceding wave surface. Figure 1.8 makes this clear. It shows in cross-section a piston-shaped sound generator
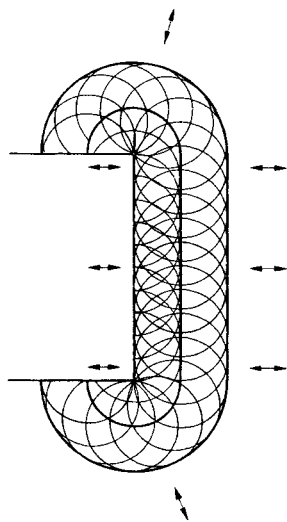
Fig. 1.8. Construction of wave surfaces from elementary waves according to Huygens

with a few wave surfaces constructed according to Huygens' principle. It can be seen that in the centre, in front of the plane sound generator, a plane wave surface is formed which at its edge (seen three-dimensionally) changes into an annular form.

According to the same principle it can also be seen that an impermeable wall produces no sharp shadow in a sound field because its edge can be regarded as the origin of new elementary waves which travel around the wall into the shadow zone.

However, application of this principle cannot provide an answer to the question how strong the excitation becomes at a given point of the sound field, for example in the shadow of the wall. The solution can only be found by a mathematical treatment, according to Fresnel (Chapter 4.2).

1.3 Physical Units for Characterizing Free Waves and the Elastic Constants of Materials

In this chapter we will treat the dependence of the wave properties described above on the characteristics of the transmitting material. If not stated otherwise the international SI units are used. The list below defines the most frequently used quantities and their symbols.

ω	angular frequency	rad/s
f	frequency	$Hz = s^{-1}$
λ	wavelength	m
ξ	particle displacement	m
c	velocity of sound	m/s
v	particle velocity	m/s
ϱ	density	kg/m^3

F	force	$N = kg\,m/s^2$
p	sound pressure	$Pa = N/m^2$
μ	Poisson's ratio	
E	modulus of elasticity (Young's modulus)	N/m^2
G	modulus of shear	N/m^2
Z	acoustic impedance	Ns/m^3
P	acoustic power	W
J	intensity of acoustic power	W/m^2

The following relation between frequency, wavelength and sound velocity is valid for all kinds of wave

$$f\lambda = c. \tag{1.1}$$

Instead of the units Hertz and metre, however, MHz (megahertz or Mc/s) and millimetre are usually used for the frequency and wave length respectively, because this furnishes numerical data of the order 1 which for our purpose are easy to memorise. Thus:

$$\frac{f}{MHz}\frac{\lambda}{mm} = \frac{c}{km/s}. \tag{1.2}$$

For general orientation a few rounded-off values of the wavelengths in steel and water in the frequency range from 0.5 to 10 MHz, which are of main interest in the following pages, are given below (Table 1.1).

Table A 1 in the Appendix gives more accurate values of the velocity of sound, and other constants of additional materials. It should be noted here that the most commonly used frequency, 2 MHz in the case of longitudinal waves in steel, the most common material, corresponds to a wave length of about 3 mm. This at the same time gives an idea of the dimension of a given flaw which can still be detected reliably when using this frequency. Furthermore it should be kept in mind that for longitudinal waves the ratio of the wavelengths in water and steel is fairly accurately 1:4.

In the case of plane and spherical waves sound pressure and particle amplitude are connected to each other by the relation (see [2])

$$p = \varrho c\omega\xi = Z\omega\xi \tag{1.3}$$

Table 1.1

Frequency MHz	Wavelength (mm) in steel		Wavelength in water
	Longitudinal waves ($c_l = 5.9$ km/s)	Transverse waves ($c_t = 3.2$ km/s)	($c = 1.5$ km/s)
0.5	12	6.5	3
1	6	3	1.5
2	3	1.6	0.8
4	1.5	0.8	0.4
6	1	0.6	0.25
10	0.6	0.3	0.15

if the product of density and velocity of sound is abbreviated $\varrho c = Z$ and called *acoustic impedance* (specific acoustic impedance). Materials with high acoustic impedance are called *sonically hard* in contrast with *sonically soft* materials. Steel with $Z = 45 \times 10^6$ Ns/m³ is sonically harder than water with $Z = 1.5 \times 10^6$ Ns/m³ (cf. Table A 1).

Although the sound pressure is, from our point of view, the most important quantity of the sound field, the intensity of a wave is nevertheless sometimes also of interest. In the case of plane and spherical waves it is related to the sound pressure or the amplitude as follows:

$$J = \frac{1}{2} \frac{p^2}{Z} = \frac{1}{2} Z \omega^2 \xi^2 . \tag{1.4}$$

The intensity is thus proportional to the square of the amplitude of the sound pressure. All relations apply equally to longitudinal and transverse waves and it is only necessary to insert the applicable value of the acoustic impedance with the correct velocity of sound. For longitudinal waves one derives from Eq. (1.3) the sound pressure as force per unit surface at right angles to the wave front, and for transverse waves as shear force per unit surface parallel to the wave front.

Sound pressure is here understood to be exclusively the alternating sound pressure. In sound fields there occurs in addition a continuous pressure, the sound-radiation pressure, which in the case of liquids for instance produces a flow and which propels suspended particles away from the source of sound. This is of no interest in the testing of materials.

In Fig. 1.3 the amplitude ξ of the particles has been chosen to be very large for the sake of clarity, viz. 10 % of the wavelength:

$$\frac{\xi}{\lambda} = \frac{J}{\sqrt{2\pi^2 \varrho c^3}} . \tag{1.5}$$

In air with the density $\varrho = 1.3$ kg/m³ and the velocity of sound $c = 330$ m/s, a value of 10 % is reached only at intensities of $J = 10^7$ W/m², which is among the highest values reached to date for very brief periods only. In liquids and in solid bodies the amplitudes would be much smaller for example in water 0.04 % of the wavelength. In reality the generation of such high amplitudes is impossible because at the enormous compressional and tensile forces of about 6×10^6 N/m² ($= 60$ bar) cavitation occurs. When testing materials, an intensity of 10 W/cm² is regarded as already very high, but in steel it produces only an amplitude of $1.8 \times 10^{-6}\lambda$, or about 2 millionths of the wavelength.

The velocities of the various kinds of sound waves can be calculated from the elastic constants of the material concerned, that is the modulus of elasticity E (measured in N/m²), the density ϱ in kg/m³, and Poisson's ratio μ (a dimensionless number),

for longitudinal waves:

$$c_1 = \sqrt{\frac{E}{\varrho} \frac{1 - \mu}{(1 + \mu)(1 - 2\mu)}} , \tag{1.6}$$

for transverse waves:

$$c_t = \sqrt{\frac{E}{\varrho}\,\frac{1}{2\,(1+\mu)}} = \sqrt{\frac{G}{\varrho}} \quad \text{(Modulus of shear } G). \tag{1.7}$$

The two velocities of sound are linked by the following relation:

$$c_t = c_l \sqrt{\frac{1-2\mu}{2\,(1-\mu)}}. \tag{1.8}$$

For all solid materials Poisson's ratio μ lies between 0 and 0.5, so that the numerical value of the expression

$$\sqrt{\frac{1-2\mu}{2\,(1-\mu)}}$$

always lies between 0 and 0.707. In steel and aluminium

$$\mu = 0.28 \text{ and } 0.34, \text{ respectively},$$

$$\frac{c_t}{c_l} = 0.55 \text{ and } 0.49 \text{ respectively}.$$

Calculated roughly for both substances, the velocity of transverse waves is half that of longitudinal waves.

Regarding the velocity of sound as a material constant, it should here also be mentioned, that the values given in the Table A 1 represent true material constants only for materials having an amorphous, vitreous structure. In crystalline materials the elastic properties usually differ in different crystal directions, and therefore so do the velocities of sound. The values in the Table are simply mean values for random agglomerations of crystals and in practice deviations from these can easily occur if a given grain orientation is preferred, i.e. if the material has a texture. It can be recognized by the differences in velocity of sound in different directions of the sample concerned. Formulae valid in the case of anisotropy and texture are listed in [27, Section S 11]. The elastic anisotropy is particularly pronounced in copper, brass and austenitic steel.

In addition the velocity of sound changes in heterogeneous bodies and is usually reduced by a small admixture of a foreign substance. A similar effect is produced by gas pores (for example in porcelain) where porosity can be detected in practice by a reduced velocity of sound.

Finally the velocity of sound depends on both internal and externally applied stress in the material both of which can be measured by this effect (cf. Section 33). In solid substances any temperature dependence is, for practical purposes, insignificant but it plays a definite role in the case of measurements in liquids. The longitudinal velocity of steel decreases with the temperature by about 1 m/s per degree, on average up to 1200 °C, cf. [S. 113]. It increases in water by 3.05 m/s per degree in the range between 10 and 30°C [2].

In Eqs. (1.6) and (1.7) the frequency term does not occur, indicating the velocities are independent of the frequency, and are therefore free of "dispersion". This fact is very important for the use of ultrasonic pulses, which consist of a band of frequencies (cf. Section 2.6). But is valid only for homogeneous materials (cf. Section 6.2 and 33.3).

2 Plane Sound Waves at Boundaries

2.1 Perpendicular Incidence on Single, Plane Interfaces

Analysis of a wave in an infinitely extended substance is possible only theoretically because in practice every substance terminates somewhere, i.e. it has a boundary. There the propagation of the wave is disturbed. If the material concerned borders on an empty space, no wave can go beyond this boundary because the transmission of such a wave always requires the presence of particles of material. At such a free boundary the wave will therefore return in one form or another. At a smooth boundary one then speaks of reflection, and at a rough boundary of scattering. In this connection the roughness of the boundary should be measured in terms of the wavelength. If another material is beyond the boundary, and adheres to the first material so that forces can be transmitted, the wave can be propagated into it, although usually in a more or less changed direction, intensity and mode.

There are three cases where boundaries have a strong influence on the propagation of sound, when testing materials:

— The wave has to penetrate boundaries when passing from a generator into a specimen and vice versa when being received.
— Defects within specimens are detected by the effect of their boundaries on the wave (reflection or transmission).
— Also other boundaries of the specimen may influence the propagation by interfering reflections or by intentional guiding (for example in plates or rods) or by reflecting the wave into areas otherwise not accessible.

Firstly we will consider the simple case of a plane wave incident on a perpendicular, flat, smooth boundary. For reasons of symmetry only plane waves can then be propagated at right angles to the boundary, viz. a reflected wave which opposes the incident wave, and a transmitted wave.

Let us calculate their sound pressures. For this we require the acoustic impedance of the two materials Z_1 and Z_2.

Material 1	Material 2
$Z_1 = \varrho_1 c_1$	$Z_2 = \varrho_2 c_2$
Incident wave	Transmitted wave
Sound pressure p_e	Sound pressure p_d
$\longrightarrow$	$\longrightarrow$
Reflected wave	
Sound pressure p_r	
$\longleftarrow$	

We refer the sound pressures of the reflected and the transmitted waves to the pressure of the incident wave and form the ratios

$$\frac{p_r}{p_e} = R \quad \text{and} \quad \frac{p_d}{p_e} = D.$$

R and D are the coefficients of reflection and transmission, respectively, of the sound pressure and both are dimensionless numerical values.

We can then derive (cf. [34]):

$$R = \frac{Z_2 - Z_1}{Z_2 + Z_1}, \qquad D = \frac{2Z_2}{Z_2 + Z_1}. \tag{2.1}$$

As an example we shall calculate R and D for the interface steel water. According to Table A 1 we have for longitudinal waves

$$Z_1 = 45 \times 10^6 \, \text{Ns/m}^3 \quad \text{(steel)}$$

$$Z_2 = 1.5 \times 10^6 \, \text{Ns/m}^3 \quad \text{(water)}.$$

Thus

$$R = \frac{1.5 - 45}{1.5 + 45} = -0.935, \qquad D = \frac{2 \times 1.5}{1.5 + 45} = 0.065.$$

Expressed as percentages the reflected wave has -93.5% of the sound pressure of the incident wave and the transmitted wave 6.5%, the negative sign indicating the reversal of the phase relative to the incident wave. If at a given instant the incident wave has just reached the positive maximum of the sound pressure (increased pressure), the reflected wave has at the same instant its negative maximum (reduced pressure) at this boundary. This case is shown in Fig. 2.1 a.
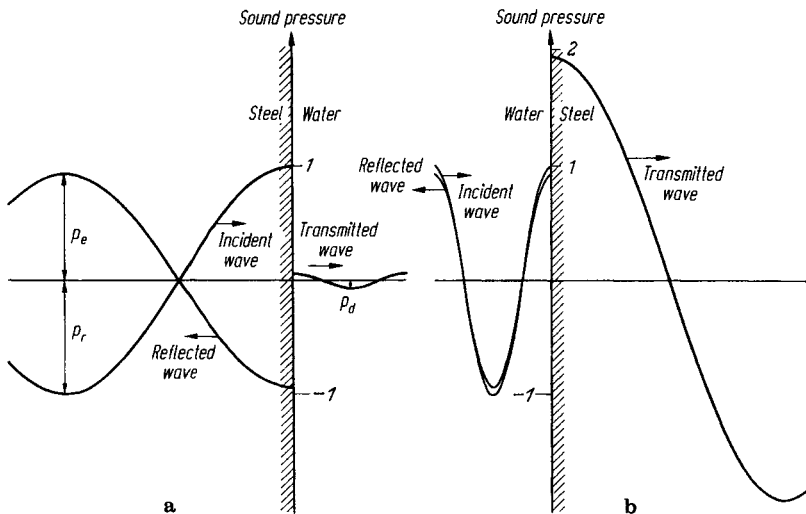
Fig. 2.1. Sound-pressure values in the case of reflection at the interface steel/water: incident wave in steel (a) or in water (b)

If, in the reverse case, the wave coming from water strikes steel, an exchange of Z_1 and Z_2 gives

$$R = +0.935, \qquad D = 1.935.$$

Since R is positive, incident and reflected wave are in phase. The transmitted wave has 193.5 % of the sound pressure (Fig. 2.1 b).

In ultrasonics amplitude (and intensity) ratios are measured in decibels (dB) (cf. Section 6.1). For amplitudes of sound pressure p (or intensities J) the following definition applies:

$$\text{ratio in decibels} = 20 \lg \frac{p_1}{p_2} \, \text{dB} \quad \left(= 10 \lg \frac{J_1}{J_2} \, \text{dB} \right).$$

Applying this to the values of the factors of reflection and transmission in the above example, one obtains for the transition steel/water:
$| R | = -0.58 \, \text{dB}$ (0.58 dB decrease of the reflected amplitude compared with the incident),
$| D | = -23.81 \, \text{dB}$ (23.81 dB decrease of the transmitted amplitude compared with the incident).

For the reverse transition from water to steel one obtains:
$| R | = -0.58 \, \text{dB}$,
$| D | = +5.74 \, \text{dB}$ (5.74 dB increase of the transmitted amplitude compared with the incident).

At first glance a sound pressure exceeding 100 % seems paradoxical and one suspects a contradiction of the energy law. However, according to Eq. (1.4) the intensity, i.e. the energy per unit time and unit area, is not calculated from the sound pressure (squared) only but also from the acoustic impedance of the material in which the wave travels. However, since this impedance in steel is very much greater than in water, the calculation shows that the intensity of the transmitted wave is very much smaller there than in water in spite of the higher sound pressure.

The balance expressed in intensities calculated for a given boundary in the case of perpendicular incidence gives

$$J_e = J_r + J_d$$

i.e. the incident intensity appears again as the sum of the reflected and transmitted intensities, as required by the law of conservation of energy. However, in the case of sound pressure one has

$$p_e + p_r = p_d \quad \text{or} \quad 1 + R = D$$

as is confirmed when recalculating the above two cases.

Phase reversal, characterised by a negative value of R, always occurs in the case of reflection from the sonically softer material. However, since the phase value is usually of no interest when testing materials, we shall generally omit the negative sign in what follows.

Disregarding the sign, the reflecting power is independent of the sequence of two materials but not, however, their transmittance.

In the literature the coefficients of reflection and transmittance are frequently referred to the intensity (Bergmann [2]) or also to the amplitude of the particle motion (Schoch [35]), which can easily lead to misunderstandings. In this discussion these quantities are exclusively referred to sound pressure.

Table A 2 gives values of the coefficient of reflection for certain interfaces between solid and liquid materials, which are of interest in the testing of materials at perpendicular incidence. When measuring these values, which in this case were calculated from the acoustic impedances, higher figures may be obtained if for instance the two materials do not completely "wet" each other. For instance, mercury does not wet bright steel without taking special precautions (oiling or amalgamating), so that an erroneous total reflection results.

Compared to liquid and solid materials, gaseous materials have a very low acoustic impedance. For air it is 0.0004×10^6 Ns/m³, so that for the interface steel/air the coefficient of reflection differs from the value 1 only by about 2×10^{-5}. Where only sound phenomena in liquid or solid materials are considered, interfaces with air can therefore be regarded as interfaces with vacuum, and are called free boundaries.

Equation (2.1) is also valid for transverse waves. Since, however, the velocity of sound in liquids and gases is zero for transverse waves, a transverse wave is always completely reflected (coefficient of reflection = 1) in a solid material at its interface with a liquid or gaseous substance. For transverse waves the formulae are therefore of significance only in the case of solid/solid interfaces.

2.2 Perpendicular Incidence on Multiple Interfaces; Plates and Gaps

In addition to the single interface between two materials of large dimensions, the double interface, as in the case of a plate or a gap, is of interest for the testing of materials. For example when sound is transmitted through a sheet immersed in water, or through a crack in a solid body. The wave coming from material 1 reaches the plate consisting of material 2 and is split into transmitted and reflected waves. After passing through the plate, the transmitted wave is split again at the second interface, and so on, the result being a sequence of reflections in both directions inside the plate. On either side a sequence of waves leaves the plate which are superimposed and whose total sound pressure has to be determined. This cannot be done simply by adding the sound pressures according to Eq. (2.1) for each individual split wave. If the incident wave is of unlimited length, the individual waves are intensified or weakened, depending on the phase position, when they are superimposed, the result being interference.

Using for the ratio of the two acoustic impedances the abbreviation

$$m = \frac{Z_1}{Z_2},$$

d for the plate thickness, and λ for the wavelength in the plate material 2, one obtains (see also Bergmann [2]):

$$D_{\text{plate}} = \frac{1}{\sqrt{1 + \frac{1}{4}\left(m - \frac{1}{m}\right)^2 \sin^2 \frac{2\pi d}{\lambda}}},$$

$$R_{\text{plate}} = \sqrt{\frac{\frac{1}{4}\left(m - \frac{1}{m}\right)^2 \sin^2 \frac{2\pi d}{\lambda}}{1 + \frac{1}{4}\left(m - \frac{1}{m}\right)^2 \sin^2 \frac{2\pi d}{\lambda}}}.$$

(2.2)

Because of the sine functions, both expressions are periodical, i.e. their values fluctuate regularly between fixed limits with increasing thickness.

Minima of R and maxima of D occur at $d/\lambda = 0$, $1/2$, $2/2$, $3/2$ et seq.   and

maxima of R and minima of D occur at $d/\lambda = 1/4$, $3/4$, $5/4$ et seq.

Figure 2.2 shows the transmittance of a steel plate and a Perspex plate in water, plotted against the product of the plate thickness d and the frequency f. At the maxima both plates show complete transmittance and therefore no reflection ($D = 100\%$, $R = 0$).

The presentation of Fig. 2.2 uses the frequency instead of the wavelength because usually the former is given when testing materials. For a given frequency the abscissa can be used as a scale of the plate thickness, or alternatively if the thickness is given, as a scale of the frequency.

Example. A steel sheet with a thickness of 1 mm transmits completely at the exact frequency 2.95 MHz. To permit undisturbed and reflection-free passage of a fre-
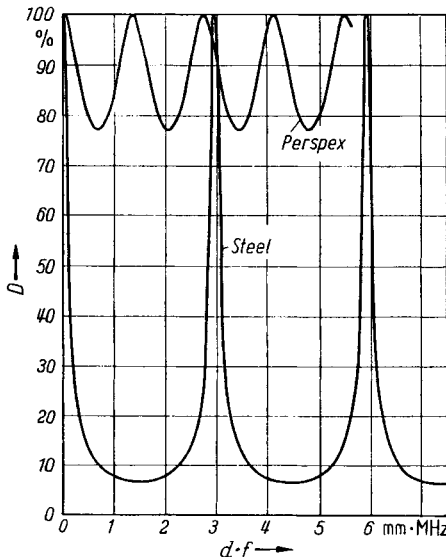
Fig. 2.2. Transmittance D of a steel plate and a Perspex plate, respectively, in water, plotted against the product of plate thickness and frequency

quency of 1 MHz partitions of Perspex can be used having thicknesses of 1.37 mm or 2.74 mm or 4.11 mm.

In the case of steel immersed in water, and similarly for other materials having large acoustic impedance ratios, the transmittance ranges are very small, as in fact Fig. 2.2 shows. Near these points even a small change in plate thickness, or ultrasonic frequency, produces a pronounced drop in transmittance. This is one of the great difficulties in the practical testing of materials with continuous ultrasonic waves.

Since Eq. (2.2) is valid for arbitrary materials 1 and 2, it can also be applied to a sheet of air within a solid body, which in the form of a crack in a given test object plays an important role in the testing of materials. Theoretically the result obtained is a curve of the transmittance similar to that shown in Fig. 2.2 for a steel plate in water, with the difference that the maxima are spaced much more closely at about 1/20 of the distance, and additionally they are so narrow that on the scale used in Fig. 2.2 they could only be indicated by extremely narrow lines. Of practical importance is only the drop from the first transmittance maximum at zero thickness, in the case of very narrow gaps. The remaining maxima could only be obtained with carefully aligned coplanar gap faces at extremely constant frequency.

The result is shown in Fig. 2.3 for the transmittance, and in Fig. 2.4 for the reflection, for a given gap in steel and in aluminium if the gap is filled with air and water, respectively. The scale for the thicknesses is logarithmic so that very narrow gaps can be included in the picture. At a frequency of 1 MHz for example this scale covers the range from 10^{-8} to 1 mm.

Firstly it should be noted from Fig. 2.4 that even at 1 MHz a gap of 10^{-8} mm filled with air produces a *reflection* of 1 % which is readily measurable. This is the principle of the method for detecting cracks in solid bodies by reflected waves. However, with such a fine crack, the *transmittance* could not be distinguished from that of a specimen without crack since according to Fig. 2.3 it remains practically unchanged at 100 %.

However, an air gap of 10^{-8} mm is purely hypothetical since even the most accurate end gauges, if pressed together, still have a separation of 10^{-4} to 10^{-5} mm, and according to Fig. 2.4 such a gap should reflect almost 100 %. However this is by
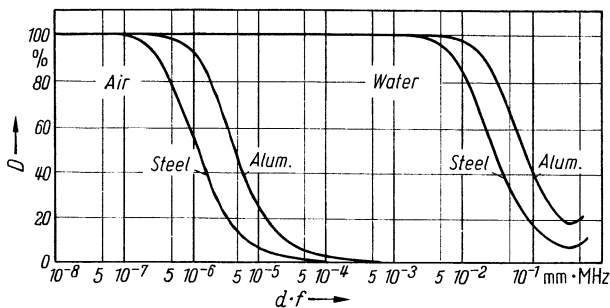
Fig. 2.3. Transmittance of a gap in steel and aluminium when filled with air and water, respectively, plotted against the product of gap thickness and frequency
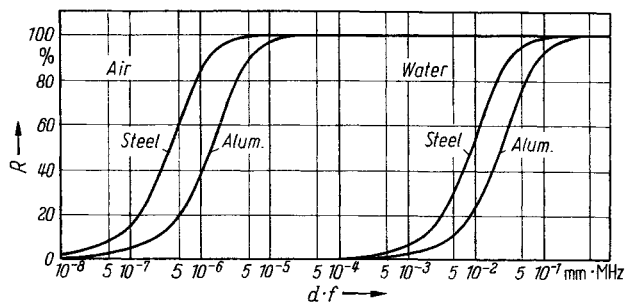
Fig. 2.4. Reflection by a gap as in Fig. 2.3

no means the case because even if it is cleaned most carefully, a foreign layer apparently remains on the surface which reduces the reflection and increases the transmission. The pronounced effect of a liquid in the gap is clearly shown by Figs. 2.3 and 2.4, which theoretically is equivalent to a reduction of the gap width by four orders of magnitude.

Thin air gaps between glass plates can be measured very precisely by optical interference methods and this method has been used to measure the influence of the gap thickness on ultrasonic reflection and transmission.

Clark and Chaskelis [249] have found the values in Fig. 2.5. The reflectivity was much lower than theory indicates but higher than the values of Tarnószy [1506] and Szilard [1496], probably because of the much higher cleanliness of the surfaces. Nevertheless Clark and Chaskelis could still detect air gaps of 20 μm by reflection using frequencies between 5 and 12 MHz. Clark et al. [249, 250] have also measured the reflectivities of liquid-filled gaps for longitudinal and shear waves.

Theoretically, a hairline crack of 1 μm in steel which is filled with oil can still be expected to reflect 6 % at 1 MHz, which would be quite adequate for its detection (24-dB reduction in the reflected amplitude compared with the incident; the acoustic impedance of oil is similar to that of water and thus has a similar influence on the reflection). For materials with an
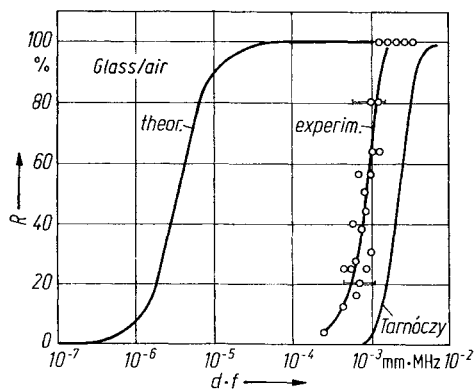
Fig. 2.5. Reflection of an air gap between glass plates according to [249]

acoustic impedance lower than that of steel the reflection for a given gap width is weaker, for example in the case of small gaps in aluminium it would be only approx. one third. To counteract this effect it would be necessary to use an increased frequency, a four-fold frequency increase (to 4 MHz) giving a reflectivity equal to that of steel at 1 MHz. In general, therefore, higher frequencies are better suited to the detection of fine cracks. This is also confirmed by the experiments described in [249] and [250].

The knowledge of the behaviour of thin gaps with respect to ultrasonic waves is important in the testing of materials, because some defects have the form of thin layers or narrow gaps, as for example lack of bonding when using welds or adhesives. It must not be forgotten also, that an air gap between transducer and specimen prevents the transfer of ultrasonic waves and it has to be replaced by a liquid layer (coupling liquid). Therefore what is favourable for the detection of defects is disadvantageous for coupling.

The above discussions all refer to the reflection and transmission of infinitely long waves, i.e. continuous waves. It is, however, important to have a clear conception of the differences which arise in the case of short wave trains, i.e. so-called pulses of only a few oscillations.

The length of the wave train does not occur in formula (2.1) for the reflection and transmission at a given interface. It is, however, necessary to ensure that the reflected and the transmitted waves do not later return to the interface after an arbitrary number of reflections and thus disturb the process by interference. In the case of continuous waves this is in fact often not very easy to prevent.

The conditions are quite different, however, for the reflection and transmission in the case of a plate according to Eq. (2.2). The interesting behaviour of a plate in an acoustic field depends precisely on the disturbances caused by interference in a very long wave train. If the wave train is so short that it cannot "bite its own tail" after a single reflection in the plate, no interferences are produced. In this case a given incident pulse is split into a series of reflected and transmitted pulses completely separate and mutually independent. Each of these can be calculated according to the simple formula (2.1) by applying it repeatedly to the individual reflection and transmission phenomena. As a result of the repeated splitting, the sound pressure of the pulse sequence then decreases continuously, but remains completely independent of the thickness of the plate.

In the transition range between short pulses and continuous waves the wave train partially reaches its own tail, resulting in interference over a certain section of its length. In that case a sequence of connected wave trains with fluctuating amplitude leaves the plate on both sides, the fluctuations depending on the plate thickness and the frequency.

In the case of the above-mentioned thin gaps every pulse, even a short one, is equivalent to a wave train of long duration because the width of the gap is in this case much smaller than one wavelength. The results therefore apply also to pulse transmission [249, 260].

The problem of obliquely incident sound pulses on thin layers is treated in [510] and [695]. Regarding the optimum thickness of the coupling gap see [396, 1369].

Attention is also drawn to the fact that a smooth transition between the properties of two different materials in a given boundary layer changes the results consid-

erably, and reflection may then be completely absent. In the above discussions it has always been presupposed that the transition is sharply defined, or at least very short compared with one wavelength.

2.3 The Law of Refraction for Plane Waves; Mode Changing

If a plane sound wave strikes a plane interface obliquely, at an angle of incidence α_e to the perpendicular (Fig. 2.6), reflected and transmitted waves arise as in optics. The transmitted waves are also called refracted waves because their direction has changed relative to the direction of incidence. The angles of emergence α_r und α_d depend on the angle of incidence and on the velocities of sound of the two materials. The acoustic pressures, which in the case of perpendicular incidence could still be determined by relatively simple formulae, have now become functions of the angles, the velocities of sound and the acoustic impedances. They are tabulated in the Appendix. In contrast to optics, a new phenomenon has now been added in which one kind of wave can be transformed into another, for example longitudinal waves into transverse waves and vice versa.

The transformation of one kind of ultrasonic wave into another is called mode changing. It happens quite often in testing materials, partly intentionally, partly troublesome.

The directions of the reflected and the transmitted waves are determined by the general law of refraction

$$\frac{\sin \alpha_I}{\sin \alpha_{II}} = \frac{c_I}{c_{II}} . \tag{2.3}$$

This law is called *Snell's law* and was first stated by Snell for optics. It is however, valid for all types of wave propagation.

In Eq. (2.3) I and II are two entirely arbitrary waves linked by a reflection or refraction process, and having the velocities of sound c_I and c_{II}.

Example. Let I be the incident wave in Fig. 2.6 with α_e and c_1 (in material I), and let II be the transmitted longitudinal wave with α_d and c_2. Thus

$$\frac{\sin \alpha_e}{\sin \alpha_d} = \frac{c_1}{c_2} .$$

With α_e given, α_d is determined by:

$$\sin \alpha_d = \frac{c_2}{c_1} \sin \alpha_e .$$
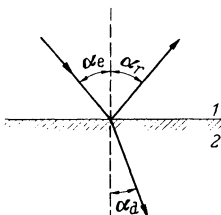
Fig. 2.6. Reflection and refraction of a plane wave at the plane interface between materials 1 and 2 at oblique incidence

Example. Let 1 be water with $c_1 = 1.5$ km/s and let 2 be steel with approx. 6 km/s, thus $c_2/c_1 = 4$. At a $10°$ angle of incidence, $\sin \alpha_e = 0.17$. Therefore

$$\sin \alpha_d = 4 \times 0.17 = 0.68 \,,$$

$$\alpha_d = 43° \,.$$

In contrast to Fig. 2.6 the transmitted wave emerges in this case at an angle greater than the incident angle, the greater velocity of sound being associated with the greater angle. In Fig. 2.6 material 2 has therefore a velocity of sound less than that of material 1.

   If in Eq. (2.3) waves I and II are considered as incident and reflected waves in the same material and if both are either longitudinal or transverse waves, they will of course have the same velocity of sound c_1. Consequently

$$\frac{\sin \alpha_e}{\sin \alpha_r} = 1 \quad \text{and} \quad \alpha_e = \alpha_r \,,$$

i.e. the angles of incidence and reflection are identical. However, the reflected wave can be of a different mode and in that case, although it occurs in the same material as the incident wave, it nevertheless has a different velocity of sound and therefore also a different angle. The general law, Eq. (2.3), however, remains valid.

Example. A longitudinal wave in steel strikes a boundary at $\alpha_e = 60°$ with $c_1 = c_e = 6 \times 10^3$ m/s. A reflected longitudinal wave has the same. Since, however, a transverse wave with $c_t = 3.2$ km/s occurs in steel, a second wave is reflected as a transverse wave according to the law

$$\frac{\sin \alpha_r}{\sin \alpha_e} = \frac{c_t}{c_e} = 0.55 \,.$$

Therefore

$$\sin \alpha_r = 0.55 \times 0.87 = 0.48 \,,$$

$$\alpha_r = 29° \,.$$

The slower transverse wave has a smaller angle than the longitudinal wave reflected at $60°$.

   The same applies to the transmitted waves. Provided transverse waves can occur in the material considered, as is the case for all solid bodies, both types of wave are in general produced but at different angles.

2.4 Sound-Pressure Values after Reflection and Refraction

The law of refraction merely gives information regarding the direction of refracted or transmitted waves but says nothing about their sound pressures. A few examples with combinations of different materials will clarify the situation. The description is much simpler for gaseous or liquid materials as compared with solid materials because gaseous materials behave in practic like empty space as long as we are only interested in the process in the contiguous liquid or solid material, and because only the longitudinal wave can occur in liquid materials.

   With the problem of two contiguous materials, four cases of increasing complexity can be distinguished:

Material 1	Material 2
a) liquid or solid	gaseous (free boundary)
b) liquid	liquid
c) liquid or solid	solid or liquid
d) solid	solid

Case a) Liquid or solid/free boundary can quickly be dealt with for liquid. There is only one longitudinal wave which for all angles of incidence is totally reflected at the boundary.

Figure 2.7 shows the case solid/gas for an incident longitudinal wave and Fig. 2.8 for a transverse wave. Let us visualise in the left-hand quadrant the incident wave concerned, with sound pressure 1 and at angles between 0 and 90°. In the adjacent quadrant the same kind of wave (therefore with the same angle) is reflected, the curve indicating the amplitude of the sound pressure for each angle of incidence. A further quadrant shows the simultaneously reflected wave of the other kind. The vectors for one particular example are drawn in each diagram and the correlated angles are shown separately on the right.

For a more quantitative evaluation the curves for the coefficients of reflection are given in the Appendix together with the formulae.
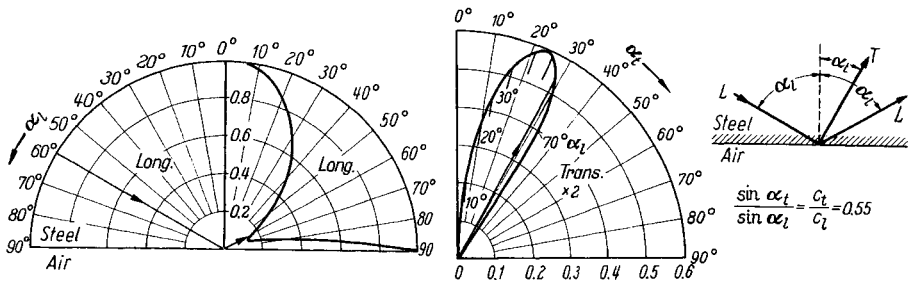
Fig. 2.7. Reflection at the interface solid/gas for an incident longitudinal wave (steel/air)
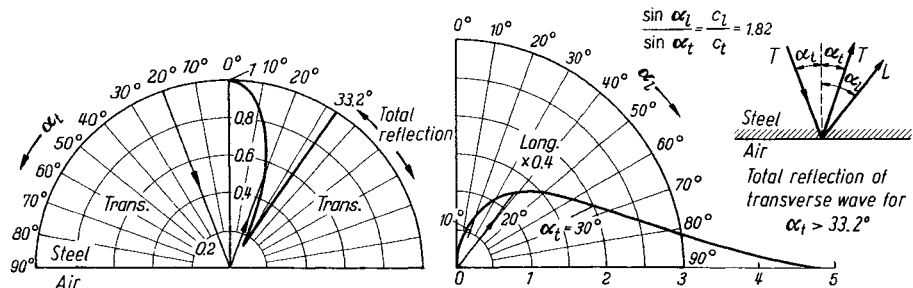
Fig. 2.8. Reflection at the interface solid/gas for an incident transverse wave (steel/air)

It is worth noting that in Fig. 2.7 the incident longitudinal wave is reflected only very weakly between 60° and 70°. Instead, a strong transverse wave occurs below about 30°.

In the case of an incident transverse wave (Fig. 2.8) a similar reflection gap occurs at about 30°. There one finds a strong longitudinal wave in a broad sector up to 90°. A rather interesting phenomenon occurs immediately beyond the 30° angle of incidence since according to the law of refraction, a value greater than 1 would be obtained for the sine, to which of course no real angle belongs. From our point of view this is merely a warning that the wave concerned ceases to be propagated freely. Consequently, the remaining wave must acquire the full sound pressure of the incident wave, i.e. the transverse wave is reflected totally in the sector beyond 33.2°.

The law of refraction (Fig. 2.8, right) reveals that this can always occur if the velocity of sound of the reflected (or transmitted) wave is greater than that of the incident wave.

In view of the fact that the magnitudes of the sound pressure of the reflected and refracted waves differ greatly it was necessary, for the sake of clarity, to use different scales in Figs. 2.7–2.11. As explained already in Section 2.1, a sound pressure of the incident wave greater that 100 % does not contradict the law of energy. However, when evaluating the diagrams and the related tables caution is indicated near a grazing incidence and reflection, i.e. at 90°: in reality the large amplitudes indicated will not be realised due to conversion into a wave with reversed phase which is reflected at the interface.

Case b) Liquid/liquid. The case of two layers of liquid is of no practical importance in the testing of materials and it is therefore not discussed here. For formulae see Appendix.
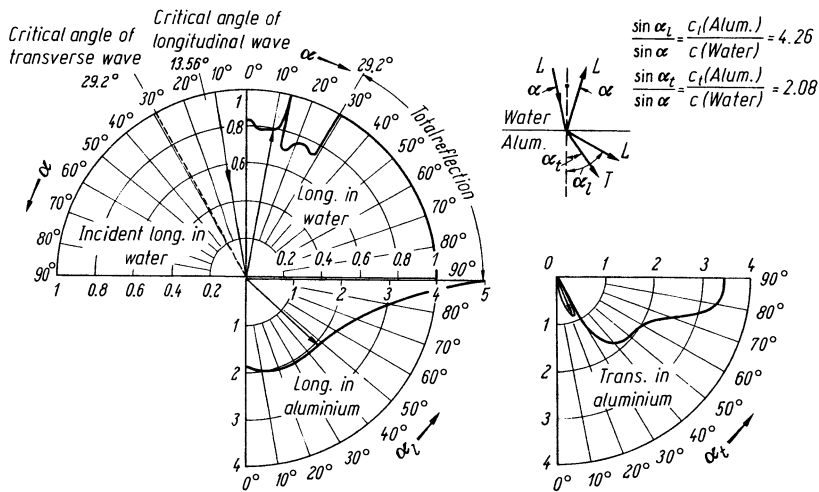
Fig. 2.9. Interface water/aluminium

Case c) Liquid/solid and solid/liquid is of importance in the practical testing of materials because, when locating defects in solid test specimens, an ultrasonic wave must frequently be beamed into the material at an angle oblique to the surface. To achieve this angle, use is frequently made of the refraction between the material of the test specimen and a liquid. Since in this case, because of the occurrence of transverse waves, the conditions are more complex than for instance in the case of the refraction of light rays in optics, they will be explained in Figs. 2.9–2.11, using as examples water/aluminium and aluminium/water. The relevant formulae and diagrams are found in the Appendix.

In Fig. 2.9 we have a longitudinal wave travelling in water and striking the interface. At small angles of incidence (cf. the diagram showing incidence at 10°) a longitudinal wave enters the aluminium with sound pressure and angle increasing rapidly with increasing angle of incidence. Simultaneously, a weak transverse wave (quadrant lower right) is formed with a maximum at 20° in aluminium. The angle of incidence of 13.56° is the so-called first critical angle for the longitudinal wave because it disappears at this point from the aluminium. Immediately, however, a stronger transverse wave appears and this remains with increasing sound pressure in the aluminium from about 30°–90°, while the angle of incidence increases up to 29.2°. This is the second critical angle, that is the critical angle for the transverse wave.

Above this range of incidence no wave whatsoever can be found in the aluminium and it is of no interest therefore for the testing of materials, the incident longitudinal wave being totally reflected. Of more importance is the region between the two critical angles because only the transverse wave is available there when testing solid materials.

Figures 2.10 and 2.11 show the reverse wave path, from aluminium into water. This is of importance for the pulse echo testing of materials, in order to answer the
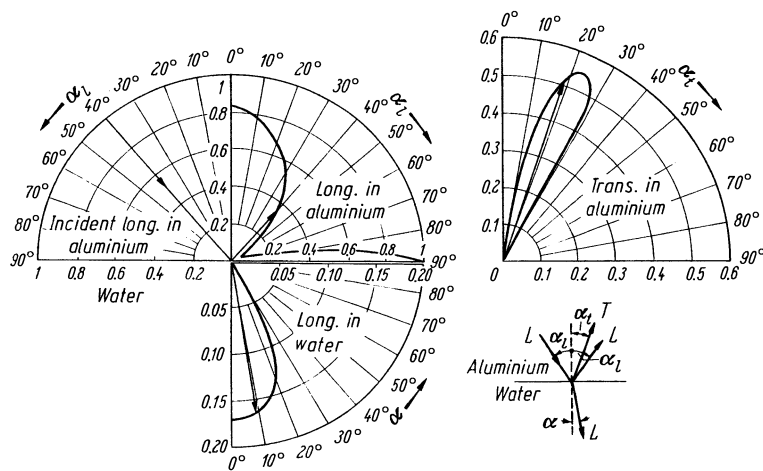
Fig. 2.10. Interface aluminium/water with incident longitudinal wave
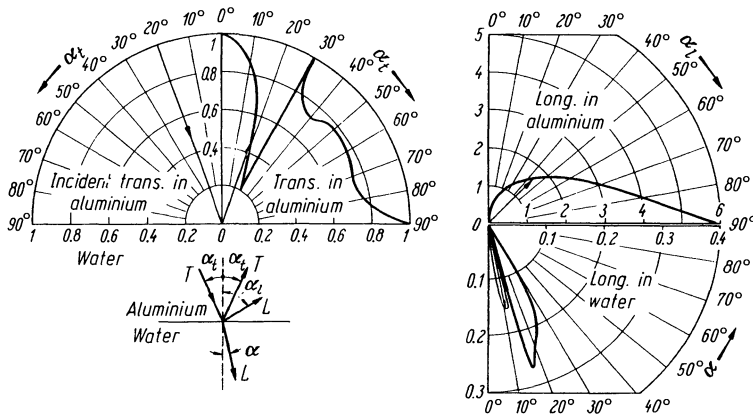
Fig. 2.11. Interface aluminium/water with incident transverse wave

question how much of the wave beamed into the test specimen returns from it as an echo.

Case d) Solid/solid. In this most general case both longitudinal and transverse waves occur in the two contiguous materials. Consequently, the reflection formulae and the presentations become more complex and only a few individual cases have therefore been calculated.

As far as the acoustic contact between the two materials is concerned, two cases can again be distinguished:

d 1) Solid contact, i.e. the two materials are connected to each other by welding, soldering or by a thin solid cementing layer.

d 2) Liquid contact, i.e. the two materials are connected by a thin layer of liquid, which can transmit compressional forces but not, as in the case of d 1, shear forces. In practical testing of materials this case is by far the most important one but attention is drawn to the fact that if high compressional forces are applied (e.g. with a shrink fit) the two surfaces, owing to their roughness, may interlock to such an extent that shear forces also can be transmitted, thus representing physically case d 1 (see Kühn and Lutsch [869]).

In practice refraction at the interface solid/solid with liquid coupling finds wider application when beaming transverse waves obliquely into the material. Figure 2.12 shows the acoustic pressure amplitudes of the refracted transverse wave and the reflected longitudinal and transverse wave for the transition of a longitudinal wave from perspex into steel, as calculated by Kühn and Lutsch [869]. Only the region between the total reflection of the longitudinal and transverse waves, which is of most practical interest, is shown.

If we go from a liquid contact (case d 2) to a solid one (case d 1) we get the dotted lines in Fig. 2.12.

They show that both the sound pressure values for the refracted transverse wave and the reflected longitudinal wave decrease in favour of the reflected transverse
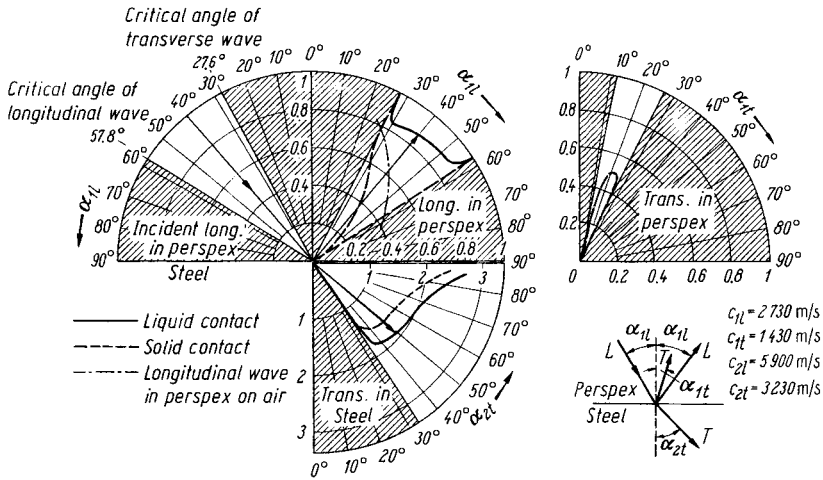
Fig. 2.12. Interface Perspex/steel. Incident longitudinal wave in Perspex

wave. The pronounced dependence of the coefficient of reflection on the coupling conditions in the case of the longitudinal wave in Perspex allows a practical coupling check [953]. For comparison the reflection of the longitudinal wave at the free Perspex interface is therefore also shown (dash-dot-dash line).

When using the echo method for testing purposes it is desirable to transmit as much as possible of the sound wave into the test specimen and to receive the maximum possible echo. According to Fig. 2.9 approx. 80 % of the sound pressure of the incident wave is lost in the reflected wave. Also in the reverse process as shown in Figs. 2.10 and 2.11, large portions of the two types of wave are lost again through reflection when leaving the solid body. Figure 2.13 answers the question how to define a measure for the transmission losses. Assuming a large plane reflector in the second medium the amplitude of the echo is the product of the transmittances in both directions, and it can be called the *echo transmittance* for this specific combination of materials and angle of incidence. Within the solid body we can operate either with the longitudinal or with the transverse wave, having therefore two transmittances E_{11} and E_{1t}. Both are shown in Fig. 2.14 for several combinations of materials.

As in the previous case, it is assumed that the sound pressure of the incident wave is 1. The length of the vector then indicates the sound pressure of the returning wave.
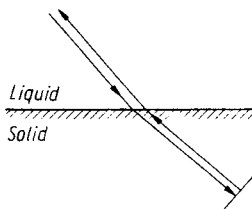
Fig. 2.13. Explanation of echo transmittance at an interface
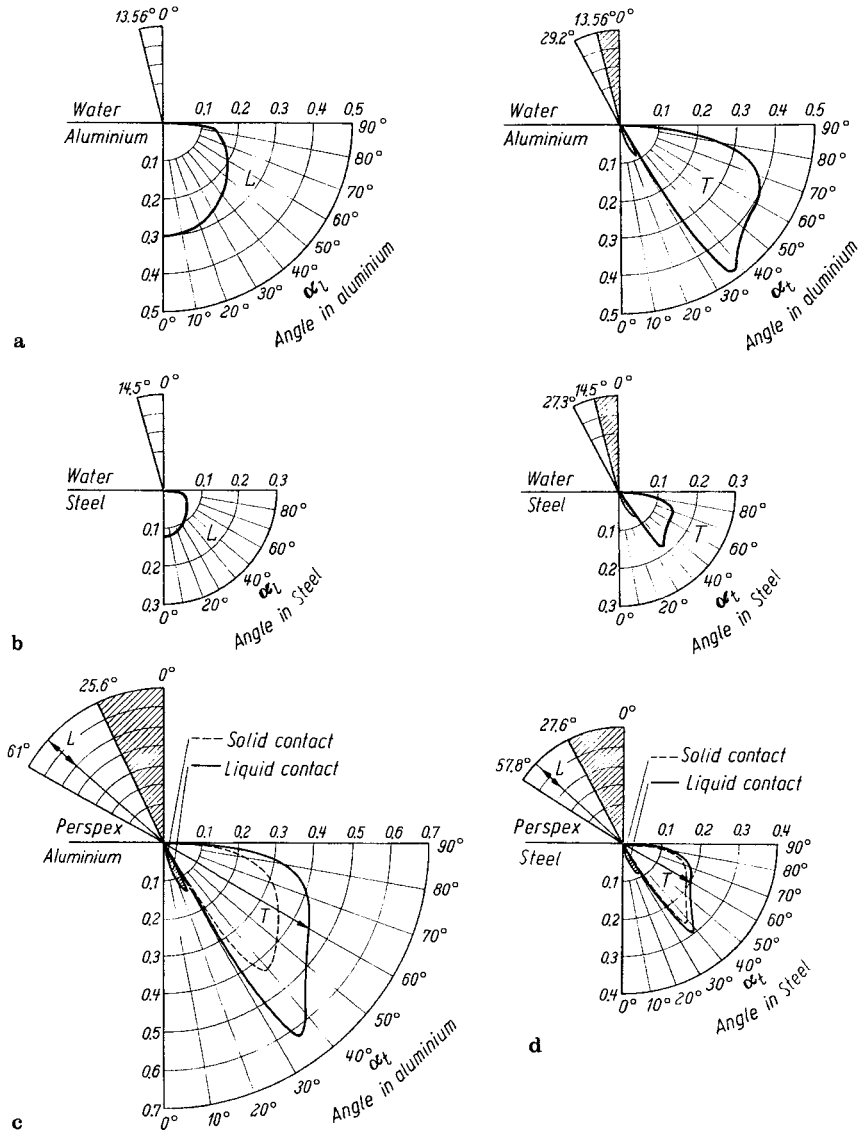
Fig. 2.14. Echo transmittance at various interfaces. **a** water/aluminium; **b** water/steel; **c** Perspex/aluminium; **d** Perspex/steel

For water/aluminium (Fig. 2.14) an echo is obtained via the longitudinal wave from the aluminium at small angles of incidence below 13.56°, containing up to 30 % of the incident sound pressure. At the same time the transverse wave gives only a weak echo of less than 10 % (shaded sector). At greater angles of incidence up to 29.2° an echo is obtained only via the transverse wave, with a good efficiency

of up to nearly 50 %. Figure 2.14 b shows the corresponding values for water/steel. Because of the greater difference in sonic hardness, the efficiency is in this case smaller. As far as the combinations liquid/metal are concerned, it can be stated quite generally that at angles of up to about 30° in metal it is better to operate with longitudinal waves but above about 35° the transverse wave becomes more favourable, a fact widely exploited in the testing of materials. Above 80° the conditions are bad for both kinds of waves.

The corresponding curves for the case Perspex/metal are shown in Figs. 2.14 c and d, but only for the transverse wave in metal, for which so far the two different conditions, viz. solid and liquid contact, have been calculated (Kühn and Lutsch [89]). In the same way as in Fig. 2.12 the efficiency is surprisingly better for liquid contact than for solid contact. Owing to the improved matching of the acoustic impedances, it is of course also better than for the case liquid/solid. The combination Perspex/aluminium returns more than 60 % of the acoustic pressure at the most favourable angle with liquid contact. For quantitative evaluation see Formulae and Diagrams in the Appendix. For further values of echo transmittances for other materials refer to Lutsch und Kühn [946].

The foregoing theory of echo transmittance for unlimited plane waves cannot explain all effects in materials testing because of the use of pulses and spatially limited waves, i.e. beams.

For frequencies between 20 and 80 MHz, and for short pulses, values have been calculated by computer for the case of coupling a generating crystal via a layer of glycerine to steel in [1557].

Regarding the influence of the thickness of a coupling layer at frequencies between 1 and 20 MHz see [1185]. This paper also investigates the influence of a wedge-shaped layer as well as the viscosity and the coupling pressure. Also for the influence of surface roughness see [396, 496, 1544].

Where transverse waves have been discussed in this chapter we have concerned ourselves exclusively with those having a plane of oscillation parallel to the plane of incidence (i.e. plane of drawing in the diagrams).

Since they are generated by refraction of longitudinal waves (Fig. 2.15) one can understand this best by considering that the direction of particle movement in the longitudinal wave is parallel to the plane of incidence. Therefore no particle movement perpendicular to it can arise.

The designation of a transverse wave as parallel or perpendicularly polarised only makes sense if a particular plane is defined as reference plane, as for example
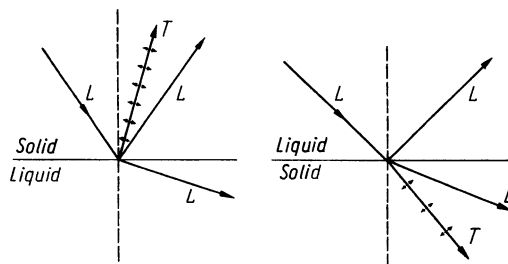
Fig. 2.15. The oscillation plane of a split-off transverse wave is always parallel to the plane of incidence (= plane of the paper)

the plane of incidence in the case of refraction. Within an infinite rigid material all directions of polarisation are identical, but in the case where it has a plane boundary, or if the material is not isotropic, the two directions of polarisation are not identical and we have to distinguish three fundamental types of free wave. This case also happens if the material is stressed in a particular direction, when the two transverse waves may even have different velocities (see Section 33.2).

A wave polarised parallel to a plane surface of a specimen is often called *shear horizontal wave* or *SH wave*, from assuming that the surface is lying horizontally. The other type, as in Fig. 2.15, polarised parallel to the plane of incidence as reference plane is consequently, but not very meaningfully, called *shear vertical wave* or *SV wave*. SV waves, easily generated by the refraction of longitudinal waves, are more frequently used in materials testing than SH waves. These latter are only generated by rigidly coupled transverse wave generating probes or by electromagnetic excitation.

The SV wave at an interface follows the refraction law whereas the SH wave does not. At a free interface, or an interface to a liquid, the SH wave is totally reflected at all angles of incidence and no mode changing can occur. This is of great advantage for guiding a wave along surfaces. By oblique reflection of any transverse wave at a randomly oriented boundary, a transverse wave of any direction of oscillation may be generated. For the calculation of its further behaviour it has to be separated into two components (transverse waves) with polarisations perpendicular to one another. Regarding measurement of the direction of polarisation see Section 16.4 and [1693].

There sometimes arises the need to launch a wave from a solid body via a liquid layer into another body of the same or similar material (Fig. 2.16). The perpendicular transit has been treated in Fig. 2.2. For oblique incidence a longitudinal wave passes through without a mode change so long as the angle of incidence lies between zero (perpendicular incidence) and the first critical angle (15° in steel). However, the liquid layer must be quite thin compared with the wavelength, or interference will take place by multiple reflections and lateral beam shift.

An SV wave also goes through in the range of angles beyond the second critical angle (from 30° to 90° theoretically, but in practice from 35° to 80°). In this case we have a longitudinal wave within the liquid layer but the other transverse wave (SH wave) cannot be transmitted.
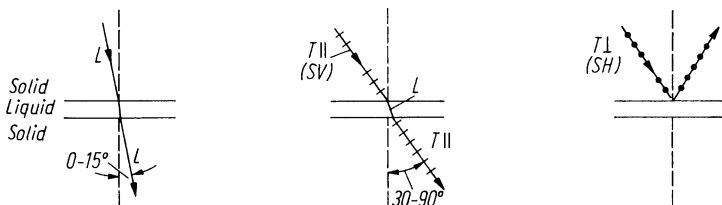
Fig. 2.16. Oblique penetration of a liquid layer between two solids

2.5 Mode Changing of Incident Sound Beams at Interfaces; Guided Waves

Up to now we have considered waves unlimited in space and time but in practice we use beams with a short length of oscillation, i.e. pulses. The direction of a beam is not exactly defined since it comprises a certain angular range in space, in the same way that a pulse comprises a certain range of frequencies in time.

That is the reason that certain new effects arise when a beam enters a solid body (Fig. 2.17) and from this will also come the generation of certain new wave modes.

According to Fig. 2.12 the critical angle of total reflection for a longitudinal wave refracted from Perspex into steel is about 28° in the Perspex and 75° in steel. Shortly before this critical angle is reached a *creeping wave* (also called *head wave*) is split off and is guided along the surface but quickly losing its energy by splitting off a transverse wave. The creeping wave has the same velocity as the longitudinal wave.

In Fig. 2.17a the transverse wave, arriving at a second free and parallel surface of the specimen, generates a secondary creeping wave C' as well as the reflected transverse wave.

The fact that the incident longitudinal wave is still present at the critical angle, and that in practice a somewhat smaller angle has to be chosen, can be explained by the difference between a theoretical unlimited wave and a beam.

The name "creeping wave" is somewhat misleading since the wave is actually as fast as the longitudinal one. We will later deal with another type of creeping wave, which is a degenerated surface wave, and therefore the first one would be better called a longitudinal creeping wave.
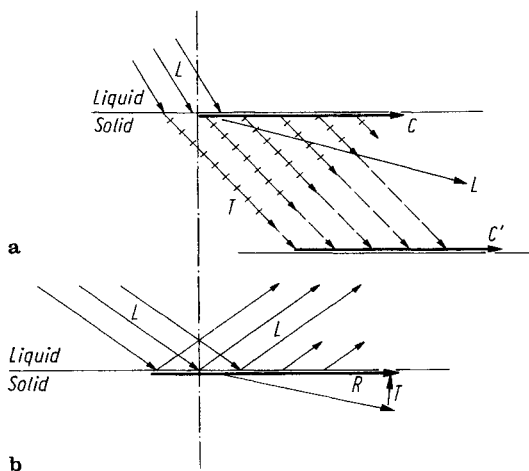
Fig. 2.17. The two critical angles of an incident longitudinal-wave beam: **a** first critical angle with the creeping wave C, further transforming into the transverse wave; **b** second cricital angle of total reflection with the surface or Rayleigh wave R

At the second critical angle with total reflection of the transverse wave (at about 58° in Perspex to steel, when the transverse wave in steel also disappears) a *surface wave* (called also a *Rayleigh wave*) is split off (Fig. 2.17 b). Its velocity along the surface is somewhat smaller than that of the transverse wave and it tends to lose its energy continually into the liquid coupling medium. This can be prevented by keeping dry the surface immediately in front of the generator and then, on the free boundary, the Rayleigh wave can travel for long distances damped only by the surface roughness, the absorption of the material and the beam spread.

Both types of boundary wave are used for material testing and can easily be generated by an incident longitudinal beam.

Another Rayleigh wave is generated if a transverse wave within a solid body strikes a free boundary at the critical angle of 33° in steel, as in Fig. 2.17 b from the lower left.

The damping of the creeping wave cannot be avoided and its useful range is reduced to about the width of the incident beam.

Both wave modes are so-called inhomogeneous or transverse damped waves, the amplitude of the particle movement decreasing perpendicular to the propagation direction, and the penetration depth being comparable to the wavelength. Both types of wave are reflected by surface cracks or by edges in their path, which can both be detected in this way when testing materials. Whereas the creeping wave is only sensitive to inhomogenities within and beneath the surface and does not follow a curvature, the Rayleigh wave is also sensitive to dirt and liquid drops sticking to the surface and it follows the surface contour so long as the radius of curvature is not too small.

At any edge on the surface a Rayleigh wave at perpendicular incidence is partly transmitted and partly reflected without a mode change. The reflectivity coefficient depends on the sharpness of the edge and its angle. Only at an edge like a knife will it be almost 100 % reflected [53].

Both the Rayleigh and the creeping waves can be directly reflected back to the generator and are there retransformed into a longitudinal wave to give a signal from the reflecting feature.
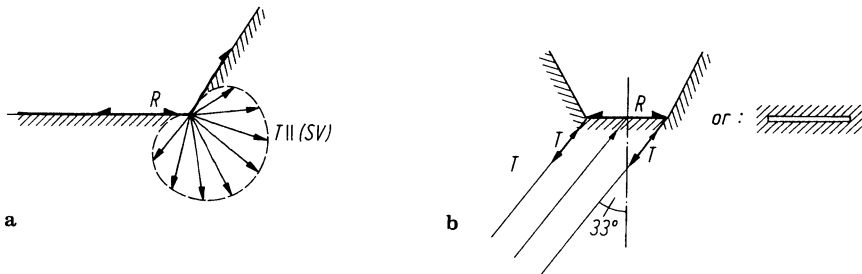
Fig. 2.18. A Rayleigh wave at edges. a splitting into a reflected and a transmitted Rayleigh wave and additionally a diffracted free transverse wave (characteristic of angle only schematic); b on a surface with two parallel edges or a hollow space in shape of a strip or disc. The reflected free transverse wave has been omitted for clarity

The Rayleigh wave undergoes a mode change into a diffracted free transverse wave as illustrated in Fig. 2.18a as well as undergoing the beforementioned transmission and reflection at an edge, provided it has the shape as shown.

This SV wave (polarised parallel to the drawing plane) is an example of a diffracted wave, always generated when any wave is incident on a perpendicular edge and they are therefore called *edge waves*. Applying Huygens' principle we have to imagine the incoming wave generating new elementary spherical waves at points along the edge. From a free line of sources in space, for example a thin wire), the diffracted wave would be of cylindrical shape buts at an edge as in Fig. 2.18a, the directional characteristics are more complicated.

From the diffracted wave we can also get echoes from reflectors within the solid body, but fortunately in most cases they are weak compared with the echo from the edge itself.

Naturally the diffracted transverse wave in Fig. 2.18 a may be detected at any convenient surface of the body by a receiver for transverse waves provided its direction of polarisation is perpendicular to the generating edge.

On the other hand the two transverse edge waves in Fig. 2.18b can be received by the generator of the incident transverse wave. When working with pulses, they show a distinct time lag between them, from which the separation of the two edges, or the diameter of the hollow disc, could be measured (for example for an artificial defect).

For further treatment of edge waves, see Section 2.7.

As distinct from the two free wave types we can describe the waves bound to surfaces as *guided waves*. Let us consider the movement path of the particles in a Rayleigh wave (Fig. 2.19). It has the shape of an ellipse with an anticlockwise rotation if the propagation is assumed to be from left to right. The deformation of the surface is not sinusoidal, as is also the case with waves on the surface of water, but the form of oscillation becomes increasingly more circular and of smaller amplitude with increasing depth beneath the surface.

If the propagation of a surface wave (Fig. 2.20) is limited by an edge parallel to its beam direction, the particle movement is exclusively parallel to the side wall.
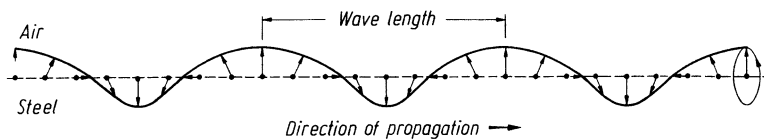
Fig. 2.19. Rayleigh wave on a steel surface. The ellipse of oscillation is shown on the right (cf. [35]; ratio of the axes: 0.44 to 1)
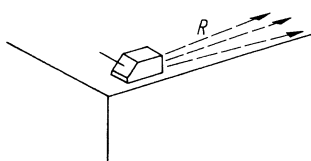
Fig. 2.20. Rayleigh wave along a right-angled edge

This means that no phase shift will occur at grazing incidence and therefore the wave does not cancel itself along the side wall, but is reinforced, and guided, by it.

A wave similar to the Rayleigh wave can exist at the interface between two solid materials (Stoneley [1475]) and other similar types of wave can be guided in layers of a solid material coated onto another one (Love [592]). These and other types of guided wave have not yet found much application in material testing.

For the free propagation of a Rayleigh wave on a surface the solid material must have sufficient thickness perpendicular to this surface. Otherwise, in case of a plate, for example, the wave will be increasingly distorted with decreasing thickness. It degenerates into a *Lamb wave* (Fig. 2.21 b and c) and waves of this type are called *plate waves*, of which a very simple one, the SV transverse wave is already known to us (Fig. 2.21 a). It can be transmitted within plates for long distances because this type of transverse wave does not undergo a phase shift at grazing incidence.

Of more importance for materials testing are the plate waves of Fig. 2.21 b and c, the so-called Lamb waves, especially for the testing of plates. These two are the fundamental types of Lamb wave, the symmetric (or stress) wave and the asymmetric (or bending) wave and to these also belong an unlimited number of harmonics.
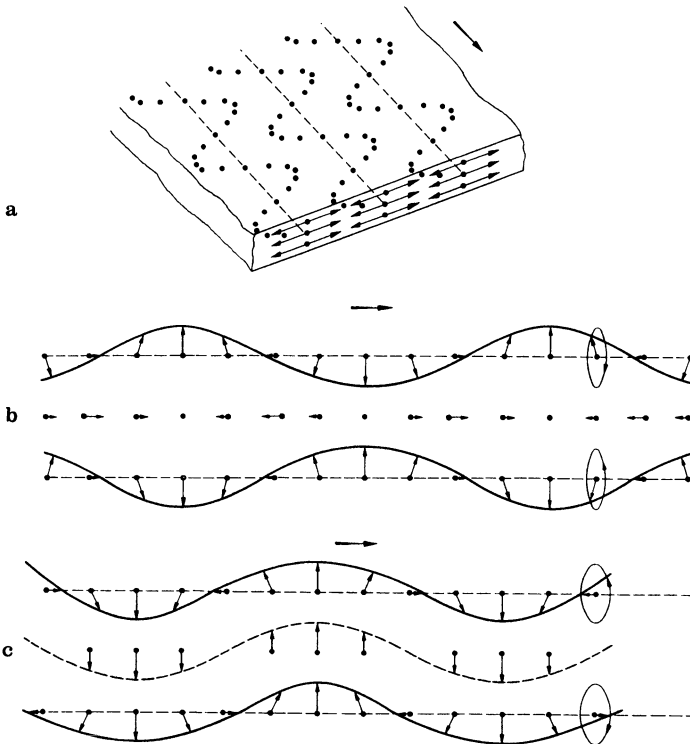
Fig. 2.21. Waves in plates. **a** transverse wave parallel to surface; **b** and **c** Lamb waves, symmetrical and asymmetrical fundamental waves in aluminium calculated according to [35] (ratio of axes of oscillation ellipses depending on thickness of plate)

The particles of the middle zone, or the neutral plane, perform in the case of the stress wave purely longitudinal oscillations, and in the case of the bending wave purely transverse oscillations. The other particles oscillate, in the case of both types, elliptically.

All these boundary waves appear to be new wave types as additions to the two fundamental ones in free space. Mathematically, they can all be made up from the fundamental ones, by taking into account the complicated reflections and phase shifts they undergo at the surfaces (see p. 38).

Also in other elongated bodies, for example in rods, there can be generated other types of guided wave. Within round or square rods the dilatational type wave similar to Fig. 2.21a is sometimes used and is called a *rod-wave*. There are in addition a large number of bending, torsion or radial waves, together with their harmonics, but they are rarely used for materials testing. For generating such waves the piezo-electric method is less useful than the electromagnetic one (see Sections 8.4 and 8.5).

For more information about creeping waves see [411, 412, 264, 413, 1680, 1240, 400, 395]. About surface waves; [32, 35, 180, 259]. About Love waves [667]. About plate waves [888, 35, 457, S 187]. About mode changing see the theoretical papers [1373, 145, 180, 1198, 1005, 879].

2.6 Velocities of Guided Waves; Dispersion

The longitudinal creeping wave has the same velocity as the free longitudinal wave. The SH plate wave (polarised parallel to the surface transverse wave) has the same velocity as the free transverse wave. The other wave types have velocities smaller than the longitudinal wave, and they can be calculated from the material constants E, μ and ϱ (Section 1.3). The velocity of the Rayleigh wave is, according to an approximation by Bergmann [2],

$$c_R = \frac{0.87 + 1.12\mu}{1 + \mu} \sqrt{\frac{E}{\varrho} \frac{1}{2(1 + \mu)}}, \tag{2.4}$$

which gives according to Eq. (1.7)

$$c_R = c_t \frac{0.87 + 1.12\mu}{1 + \mu}. \tag{2.5}$$

Thus the Rayleigh wave is always somewhat slower than the free transverse wave, for steel 92 % and for aluminium about 93 %.

Neither frequency nor wavelength terms appear in Eq. (2.4), just as they are also absent from Eqs. (1.6) and (1.7) for the free fundamental waves. This means that they are free of velocity dispersion. This is true also of the creeping wave but it is by no means self-evident. We have seen already that the Rayleigh wave has velocity dispersion, when it travels on curved surfaces. For example at a radius of curvature $r = 3\lambda$, it is about 10 % higher on a solid cylinder and lower on the surface of a hollow cylinder, see also [1375, 1570].

In addition the Rayleigh wave has some dispersion if the quality of the surface differs from the base material, for example by surface hardening or stress [168].

Love waves also experience dispersion if a surface layer in which they propagate has a thickness comparable to the wavelength and this method can be used for the thickness measurement of layers. Even the fundamental waves experience appreciable dispersion in heavily scattering material (cf. Section 33.3).

Additionally the previously mentioned guided waves (e.g. Lamb waves) also undergo dispersion. Their velocities depend in a very complicated way on the material, on its thickness and the ultrasonic frequency (cf. Table 9 in the Appendix). For materials other than steel Pursey [1216] has calculated the velocities for Poisson's ratios $\mu = 0.25$, 0.33 and 0.375 and values for aluminium are given by Firestone [457].

Fig. 2.22 explains the formation of a Lamb wave from zigzag-reflected fundamental waves. For simplicity we illustrate here only the transverse wave. For a narrow beam, as in Fig. 2.22 a, the single sections of the zigzag wave do not influence one another. With a broader beam (Fig. 2.22 b) the two sections travelling in the same direction partially overlap each other, and hence interference may take place. In Fig. 2.22 b interference is shown to be destructive and with a broad beam this would mean extinction takes place. At another angle for the reflected transverse wave (Fig. 2.22 c) the superposition may be constructive and we have a wave combination giving good propagation.

At first glance it seems strange that such a simple geometrical requirement – that the reflected beams should not cancel each other – demands such a complicated relationship between plate thickness and the most favourable angle as shown in Table 9 in the Appendix. This complication results from the fact that in the case of the oblique reflection of sound beams on surfaces of solid bodies phase shifts occur which in turn depend on the angle.

The relationships become even more complicated when one examines the velocity of these Lamb waves in a direction parallel to the surface. The phase shift during reflection results in the reflected beam being transposed relative to the incident beam so that the path of propagation is not zigzag-like but trapezoidal, see [1125]. The extent of this transposition of
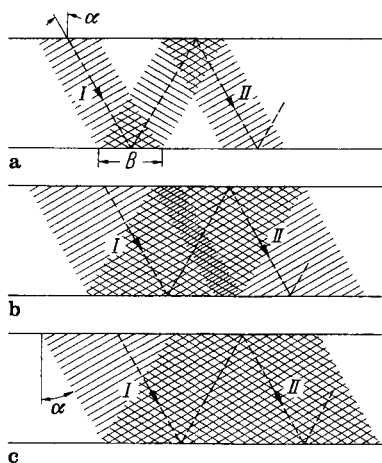
Fig. 2.22. Generation of a Lamb wave from a zig-zag-reflected transverse wave. a Narrow beam obliquely reflected; b broad beam with unfavourable phase; c favourable phase obtained by variation of the angle of incidence

the beam depends on the angle α and the frequency. It may amount to several wavelengths, particularly near the glancing incidence of the longitudinal wave (33.2° in steel), with the result that in the case of plates with a thickness of only a few wavelengths, the velocity differs greatly from the simple geometrical relation $c_l \sin \alpha$ and $c_l \sin \beta$ (β = angle between the longitudinal wave and the normal to plate) which could be expected to follow from the elementary presentation in Fig. 2.22. Only at $\alpha = 45°$ does the phase shift, and thus also the transposition of the beam becomes zero; in this case the simple geometrical sine relation is valid by way of exception.

In addition to these wave types which manifest themselves as longitudinal and transverse waves propagated along a zigzag path, thick plates also have Rayleigh waves. If the thickness of the plate becomes less than the penetration depth of the surface wave, the latter degenerates and is split into two branches with different propagation velocities, viz. the branches marked a_0 and s_0 in Diagram 9 in the Appendix. The corresponding mode of oscillation has already been shown in Fig. 2.21. In a certain sense these waves a_0 and s_0, and the surface wave, are also degenerated zigzag propagations. The wave surfaces are almost perpendicular to the surface of the plate or are even inclined backwards, against the direction of propagation. Consequently, the wave beams no longer detach themselves from the surface, the oblique paths through the plate (I and II in Fig. 2.22) are suppressed, and the wave motion now consists only of the reflection at the plate surface and the continuous conversion of longitudinal waves into transverse waves resulting from this process. Mathematically this degeneration corresponds to the change of α from a real to an imaginary quantity; viz. $\sin \alpha$ becomes greater than 1. As far as the excitation of these wave types is concerned, it should be mentioned that like the true waves reflected along a zigzag path they can be excited by exploiting the law of refraction (Eq. (2.3) and Fig. 2.6) in which the sine of the angle of refraction is made, purely formally, greater than 1 (values of $\sin \alpha$ in Diagram 9). This results in an entrance angle in the water or plastic wedge used for excitation which is greater than the total reflection angle.

For Figs. 2.21 and 2.22, as well as for the calculation of the Lamb-wave velocities in Diagram 9, systems of unlimited plane waves of the fundamental types have been assumed. In practice we have a beam of limited width and in a restricted angular range. This is one of the reasons why we find rather important deviations between the actual and the theoretical velocities.

A second reason for these differences arises from the use of pulses rather than of infinitely long waves. Figure 2.23 shows a pulse shape as it is often used for materials testing.

It consists of not only a single frequency, as assumed for Figs. 2.21, Fig. 2.22 and Diagram 9, but a band of frequencies which is wider the shorter the pulse. Figure 2.24 makes this clear where by the summing of only three infinitely long waves of frequencies 0.85; 1.0; and 1.21 MHz we get a wave form approximating to a 1-MHz pulse.

The various different frequencies contained in a pulse which generates a Lamb wave pulse have different velocities in accordance with Table 9, and they may even be completely suppressed at the given conditions of plate thickness and angle of incidence. Therefore a pulse, rather short initially, will be increasingly distorted and usually broadened, during its transmission. A certain oscillation, as for example that marked by an arrow in Fig. 2.23, becomes unrecognisable. A measurement of transit time, as for example in distance measurement, is no longer possible. Examples of the distortion of Lamb-wave pulses are shown in Figs. 24.13 and 24.14.
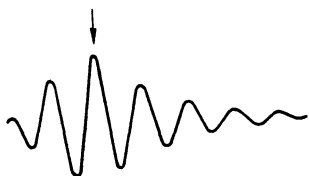
Fig. 2.23. Commonly encountered pulse form when testing materials
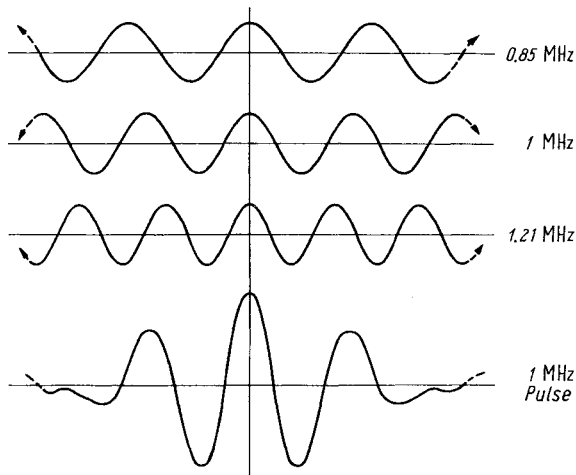
Fig. 2.24. Synthesis of a 1-MHz pulse composed of purely sinusoidal partial waves of 0.85, 1.0 and 1.21 MHz

For a fuller theoretical treatment of sound propagation in solid materials see Mason [21], Achenbach [49] and Pollard [30], for guided waves in layered media see [3] and [S 143], for computer presentations see Nickerson [1119] and Harumi [9].

2.7* Edge Waves

If a free wave within a solid material strikes a discontinuity various additional waves are generated and they can easily be characterised by the requirement to restore the disturbed wave at all points to the original undisturbed wave in both amplitude and phase. In other words they are required to fulfil the physical boundary conditions.

Figure 2.18 b shows a very simplified case, in which the additional or compensating waves tend to be mostly Rayleigh waves propagating from the disturbing edge. Additional diffracted waves are also generated which are not indicated in this diagram and they may be of both the fundamental types. Together with a possible mode change from Rayleigh waves to free waves, the actual details of the full distortion are quite complicated but fortunately all these additional waves are of low amplitude.

We will however consider some specific cases, because the edge waves generated can be of interest for materials testing techniques.

What actually happens when a free wave is distorted by an obstacle has been calculated by Harumi [9]; see also [618, S 65].

Example a (Fig. 2.25 a): Perpendicular incidence of a longitudinal wave on a plane disc-shaped gap or a strip. The illustrations show the wave fronts of the var-
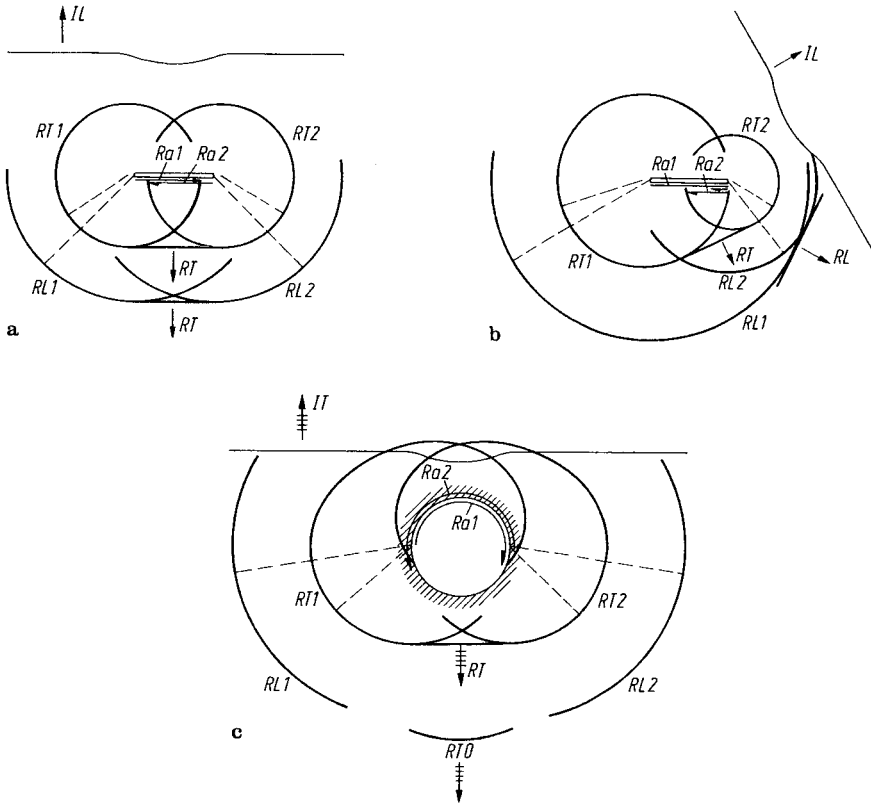
Fig. 2.25. Reflection at a disc, a strip and a hollow cylinder within a solid material to illustrate edge waves. **a** perpendicular incidence of a longitudinal wave on a disc; **b** the same but at angle of 60°; **c** transverse wave incident on a hollow cylinder

ious waves at a moment when the incident wave (IL = incident longitudinal) coming from below has already passed the obstacle. The distortion of its wave front is only indicated qualitatively. Outgoing from both edges are two longitudinal diffracted waves (RL 1 and RL 2). In the centre below the reflector they combine with the specularly reflected longitudinal wave (RL) from which they cannot be distinguished if viewed in the axial direction, but only by angular observation.

Further compensating waves from the edges are two Rayleigh waves (Ra 1 and Ra 2) travelling along the surface of the reflector in opposite directions and generating two transverse edge waves when they arrive at the edges (RT 1 and RT 2).

These latter waves are associated with the Rayleigh waves at their origin, but because their velocity is somewhat higher they seem to originate from a point beyond the edge. They then combine in the direction of the axis as a reflected transverse wave (RT). On either side of the axis they can be received as two separate transverse waves.

Example b (Fig. 2.25 b): A longitudinal wave is incident on the disc at an angle of 60° and the two diffracted longitudinal waves from the edges RL 1 and RL 2 combine with the specularly reflected free wave to form the reflection (RL). The two transverse edge waves RT 1 and RT 2 (connected with the two Rayleigh waves on the surface as in Example 1) combine, at an angle of about 30°, with the reflected transverse wave which has been generated by mode change from the incident wave (RT). In the Figure the Rayleigh wave (Ra 1) is already on the way back from the right hand edge, where it has generated a further edge wave (RT) but which is not shown for clarity. In this way we get a sequence of edge waves, decreasing in amplitude from one to the next.

Example c (Fig. 2.25 c): A transverse wave (IT) is incident on a hollow cylinder and assumed to be polarised perpendicular to the axis of the cylinder, i.e. parallel to the drawing plane (SV wave). It generates the two longitudinal edge waves (RL 1 and RL 2) originating from both sides of the cylinder. In the direction of the axis they cannot be detected because their amplitudes here are zero. Their angular characteristics therefore resemble a plum at the exit points on the surface.

At these points further Rayleigh waves (Ra 1 and Ra 2) are generated surrounding the cylinder and further transverse edge waves (RT 1 and RT 2) arise at these points. They are delayed in time compared with the direct reflected transverse wave (RT 0) and hence they may also be received separately in the axial direction. In this case both the edge waves and the Rayleigh waves are somewhat degenerated since they are continuously connected with the origin of the Rayleigh waves, radiating continuously their energy into the transverse waves. They can however be received at any angle to the axis by a receiver sensitive to transverse waves of the SV type.

The degenerated, continuously fading, Rayleigh wave is sometimes called a "creeping wave". It should be called preferably a "Rayleigh creeping wave" differing as it does from the longitudinal creeping wave described in Section 2.5. Its velocity is somewhat less than that of the normal Rayleigh wave and it depends on the ratio of the cylinder radius to the wavelength.

The amplitudes of all these different types of wave cannot be evaluated from Fig. 2.25. The wave fronts shown give only the positions at the moment considered and they must not be confused with their angular characteristics. Additionally they are not given entirely but only schematically in the main direction of propagation. Numerical calculations for edge waves from artificial defects in selected cases have given pronounced lobes [618].

In the foregoing examples we have exclusively used the longitudinal and the transverse wave of the SV type, i.e. polarised parallel to the drawing plane. We can describe the other transverse wave, the SH wave, very easily since no mode change takes place. The direction of oscillation remains parallel to the surface of the reflector and the compensation waves are diffracted waves of the same type leaving the edge in the form of a circle around the edge.

Artificial defects in the form of surface cracks are important in the practical case and they can be treated qualitatively in the same way. However, the additional plane provided by the surface of the solid body produces numerous additional Rayleigh waves and those arising from their mode changing and splitting off (Harumi et al. [9]).

For the theory of circulating boundary waves on the surface of empty boreholes, as well as those filled with liquids, see [167].

2.8 Reflection at a Right-angled Edge and in a Corner

For the testing of materials, reflections within the angle formed by two surface planes of a test object are frequently encountered (Fig. 2.26). If a ray strikes such a right-angled edge perpendicularly it is reflected parallel to itself at whatever angle it makes with either of the two faces following a double reflection. In the case of a beam (Fig. 2.26 b) there is in addition an interchange of its two sides. If its axis does not strike the edge it is additionally transposed parallel to itself.

If a third plane face perpendicular to the other two forms with them a corner then it reflects a beam, coming from any angle in space, parallel to itself. This effect is exploited optically in the "cat's eye" reflector. A similar effect applies to a plane ultrasonic wave but allowance must be made for the results of the reflection taking place at a solid/gas interface. At each of the two reflections a wave of the other type can be split off so that the total coefficient of reflection largely depends on the angle of incidence. Figure 2.27 shows the angular reflection for a longitudinal wave (a) and a transverse wave (b) in steel. It is calculated as the product of the
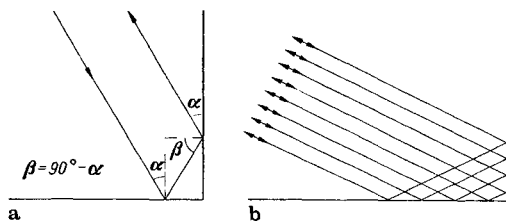
Fig. 2.26. Reflection within a rectangular edge. **a** single ray; **b** beam
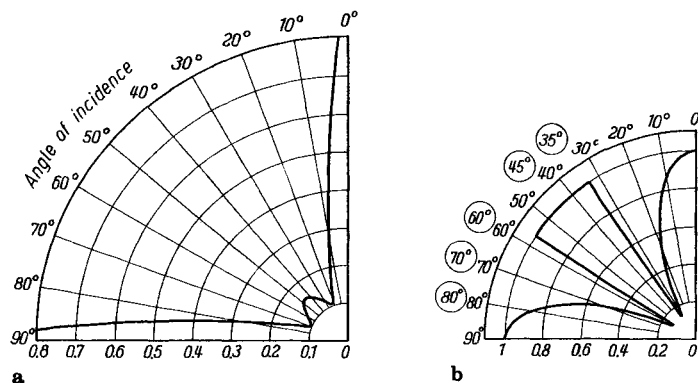
Fig. 2.27. Coefficient of angular reflection in steel for incident longitudinal wave **(a)** and transverse wave **(b)**

coefficients of reflection from Figs. 2.7 and 2.8 for the angles α_l and $90° - \alpha_{l'}$ and α_t and $90° - \alpha_{t'}$ respectively.

Except for a glancing angle incidence to one of the faces, the longitudinal wave shows very bad angular reflection. The reason is that at one of the two reflections a strong transverse wave is always split off which does not return in the direction of the incident wave.

Because it is twice totally reflected the transverse wave is reflected completely in the central range. On either side, however, there are troughs in which practially no reflection occurs. At glancing angles the transverse wave is theoretically again reflected more strongly. Here, however, the supplementary limitation must be made concerning both kinds of waves, that at glancing angles an actual sound beam, in contrast to a theoretial plane wave, loses its sensitivity. Cancellation by interference between the direct and the reflected beam occurs along the wall so that both curves in Fig. 2.27a and b again drop practically to zero at 0° and 90°.

Figure 2.27b also shows the angles frequently used in the testing of materials. It can be seen that for an angle reflection as used for instance for the detection of an incipient crack starting at right angles to the surface, the angles 35° and 45° are favourable. The 60° angle is particularly unfavourable because it lies within a reflection trough.

At a corner it is possible to calculate certain surfaces at which longitudinal waves are only minimally reflected for the greater portion of the steric angle range. For transverse waves a total reflection range is obtained near to the steric angle bisector of the corner but is surrounded by a deep trough. However, this surface is not rotationally symmetrical about the steric angle axis because of the polarisation influence. If it is polarised parallel to one of the planes then there will be no extinction but instead a reinforcement of the grazing wave.

As well as the specular reflection shown at the edge, a mode change into a Rayleigh wave will also take place. It will be of some importance only if there is a further reflecting edge parallel to the first one, where again reflection and mode change can take place, as for example in the case of a rectangular groove. From the bottom of the groove the diffracted edge wave generated by mode changing of the Rayleigh wave may interfere with the main reflection, especially if the groove has only a depth of a few wavelengths. In this case Fig. 2.27 is no longer valid.

A free wave reflected at a boundary with an acoustically soft medium (e.g. air) undergoes a phase reversal. At the edge in Fig. 2.26 therefore two phase shifts will take place regardless of whether a mode change has happened or not. Therefore an echo of a free surface which undergoes only one phase shift will differ from an edge echo in phase.

For reflection from edges and grooves see also [1186, 1187, 1606, 1607, 50, 229, 544, 394], for picture displays see [597], for computer simulations see Sato [1321] and Harumi [617, 9, 618, 619, S 65].
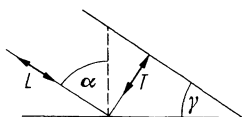
Fig. 2.28. Reflection within a pointed edge

Angles other than 90° are less interesting, but if the angle of incidence of a longitudinal wave (Fig. 2.28) in steel and the angle of a pointed edge are such that

$$\sin \alpha = c_l/c_t \sin \gamma$$

the splitted-off transverse wave meets the second plane perpendicularly and is totally reflected. If α equals about 61°, the mode change back into the longitudinal wave is nearly 100 %; see Section 16.4, 61° reflection.

3 Geometrical Acoustics

3.1 Limits of Validity

Geometrical optics use light rays which can be drawn as straight lines. Applying the simple laws of refraction and reflection at interfaces, it permits a very clear presentation of the effect of mirrors and lenses with curved surfaces for example. We have also used this convenient method when discussing reflection and refraction in Chapter 2. In this connection it should, however, not be overlooked that this method fails to take into account a very important property, both of light waves and ultrasonic waves, viz. the wave structure.

As in optics this produces a number of deviations from purely geometrical constructions, diffraction phenomena occurring at gaps and openings and whenever the dimensions of acoustic sources, reflectors or test pieces are not much greater than the wavelength.

The lengths of light waves are of the order of less than a thousandth of a millimetre but those of ultrasonic waves are of the order of millimetres and therefore, for all dimensions below about 100 mm, i.e. in the range most commonly used in practice, diffraction phenomena can be expected to occur. The simple geometric construction of an ultrasonic field behind a hole in a diaphragm as shown in Fig. 3.1 will therefore in reality be inadmissible for hole dimensions below 100 mm.

In the following sections a few feasible applications of geometric ultrasonic optics will be discussed remembering, however, that where this concerns cases in which the wave length is no longer very small compared with the dimensions concerned, the results obtained are only more or less rough approximations.
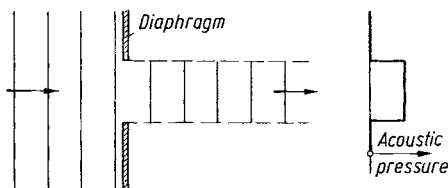
Fig. 3.1. Geometrical construction of the passage of a plane wave through a hole in a diaphragm; on the right the correlated distribution of the sound pressure as a function of the cross-section, valid approximately only as long as the wavelength is very small compared with the diameter of the hole

3.2 The Sound-Pressure Distance Law for Spherical and Cylindrical Waves

Let us investigate how in the case of simple wave forms the sound pressure changes with the distance from the source. In a plane wave the pressure of course remains constant in each plane of the wave, but for waves which are not plane, energy considerations lead to a distance law. Figure 3.2 shows four rays coming from the origin of a spherical wave, which determine a small square on the surface of a sphere with the radius a. On a further sphere with the radius $2a$ the four rays determine a square which is evidently four times greater in area. According to the law of conservation of energy, the ultrasonic energy passing through both squares per unit time must be identical. The energy density per unit surface on the sphere with the double radius is thus only one quarter. Generally the intensities at two different distances are, in the case of spherical waves, inversely proportional to the square of the distances from the source.

Since according to Eq. (1.4) the sound pressure is proportional to the square root of the intensity, the acoustic pressures are inversely proportional to the distances:

$$\frac{p_2}{p_1} = \frac{a_1}{a_2}.$$

If $a_1 = 1$ and the sound pressure at this point is p_1, the law of distance for the sound pressure of the spherical wave gives us:

$$p = p_1 \frac{1}{a}. \tag{3.1}$$

According to this relationship the sound pressure in the source itself (i.e. at zero distance) would become infinite, which is just as unreal as the concept of a point source. Real sources always have finite dimensions and in close proximity to them the acoustic wave is usually not strictly spherical. The law (3.1) therefore applies only to distances very large compared with the dimensions of the source. If this
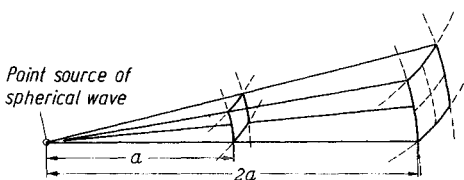
Fig. 3.2. The law of distance for intensity and sound pressure of a spherical wave
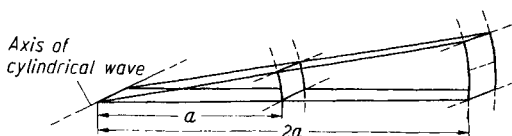
Fig. 3.3. The law of distance for intensity and sound pressure of a cylindrical wave

condition is not fulfilled at unit distance, p_1 refers to a quantity purely specified for determining the strength of the source.

In the case of a cylindrical wave the source is not a point, but the linear axis of the cylindrical wave. According to Fig. 3.3 the area determined by four rays on a cylindrical surface therefore changes only as a linear function of the distance. A square on the inner cylindrical face becomes a rectangle of twice the area on the cylindrical surface with double the radius. The intensity therefore changes only inversely with the distance, that is at a slower rate than in the case of a spherical wave. Consequently, the acoustic pressure decreases only inversely with the square root of the distance:

$$p = p_1 \sqrt{\frac{1}{a}} \, . \tag{3.2}$$

In the testing of materials the spherical wave, particularly where large test objects are concerned, is the most important waveform because the wave generated by a conventional ultrasonic oscillator can be regarded at greater distances as a spherical wave. In practical testing this spherical wave frequently strikes flat, cylindrical, and more rarely spherical surfaces, by which it is subjected to changes by reflection and refraction. These effects will be discussed in the following Sections.

3.3 Reflection and Refraction of Spherical Waves on Plane Surfaces

The reflection of a spherical wave incident on a plane surface is shown geometrically in Fig. 3.4 where each ray is reflected at its own angle of incidence. The shape of the spherical wave is preserved but the reflected spherical wave seems to come from a point 0′ which is the mirror image of the real origin 0. A beam retains its angle of aperature δ, as can be seen from the two rays drawn in the diagram and which form the angle δ.

If one observes the sound pressure along a given ray, it is found that before being reflected it follows the law (3.1). After reflection, the coefficient of reflection for the angle of incidence and the type of interface concerned has to be taken into account, as described in Chapter 2:

$$p = p_1 \frac{1}{a} R \, .$$
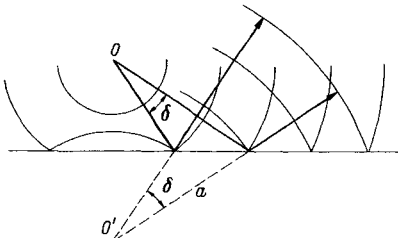
Fig. 3.4. Reflection of a spherical wave at a plane interface (wave fronts only shown partially)
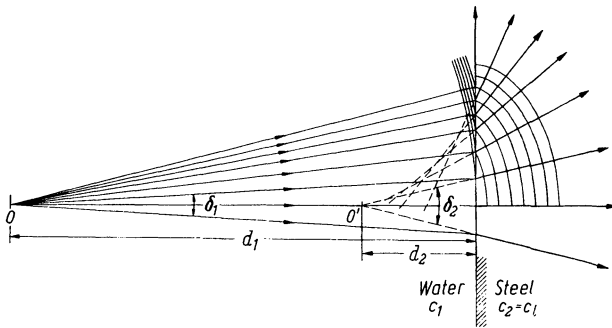
Fig. 3.5. Refraction of a spherical wave at a water/steel interface

Since according to Fig. 2.6 and the following diagrams, this coefficient R depends strongly on the angle, the distribution of the sound pressure on one of the spherical wave fronts may be greatly changed by reflection. The spherical character of the wave is nevertheless preserved.

In the case of reflection of the spherical wave with a mode change, or refraction of the spherical wave, the wave no longer remains spherical, in contrast to the simple reflection. As an example, Fig. 3.5 shows the refraction at a water/steel interface, in which only the longitudinal wave in steel is considered. Only rays which are almost perpendicular still intersect each other after refraction at a virtual origin $0'$. The refracted wave can therefore be regarded as a spherical wave only in this particular zone. Geometry gives us:

$$d_2 : d_1 = \delta_1 : \delta_2 = c_1 : c_2 \quad \text{(here } 1:4\text{)}.$$

The angles of divergence of narrow beams incident at a right angle are in the ratio of the velocities of sound, which for longitudinal waves in steel is four times greater than in water. The pattern of the sound pressure in the second material is determined by the virtual origin $0'$ from which the distance a in Eq. (3.1) must be calculated. In the case of obliquely incident beams with both refraction and reflection with mode conversion, the angle of divergence is dependent on the angle of incidence, as is also the pattern of the sound pressure.

3.4 Curved Interfaces Acting as Concave Mirrors and Lenses

In Fig. 3.6 we consider the behaviour of a spherical wave impinging onto a spherical concave mirror with a radius r. The origin of the wave is at a distance a from the centre of the mirror. After reflection the rays intersect at an image point at a distance b from the mirror. As in optics we call the focal distance f, which is the distance of the image point in the case of plane incident waves. These quantities are related in the formula

$$\frac{1}{b} \pm \frac{1}{a} = \frac{1}{f} = \frac{2}{r}. \tag{3.4}$$
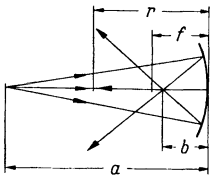
Fig. 3.6. Spherical wave incident onto a concave mirror
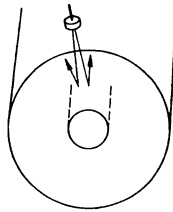
Fig. 3.7. Cylindrical-mirror effect from a forging borehole

The plus sign applies to the concave mirror and the minus sign to the convex mirror. The focal distance should always be taken as positive.

If, in the case of a concave mirror, a negative image distance is obtained, this means a virtual image point behind the mirror. Conversely, if the direction of the rays is taken to be reversed (incident, convergent spherical wave) with apparent origin behind the concave mirror, the distance a should be given the negative sign.

In the case of the convex dispersing mirror all quantities should be taken with the positive sign. Either the image point or the centre of the spherical wave will always appear to be behind the mirror.

In order to calculate the acoustic pressure of the reflected wave, Eqs. (3.1) and (3.2) are used in which the distance from the corresponding image point must now be taken. This image point, or image line in the case of a cylindrical wave, is the source from which the further propagation process can be recalculated, independently of the generation of the image point.

Consider a spherical wave striking a spherical mirror or a cylindrical mirror. The sound pressures of the reflected waves as a function of the distance x from the vertex are:

Spherical wave on spherical mirror   on cylindrical mirror

$$\frac{p_1}{a} \frac{f}{x \mp f(1 + x/a)} \qquad \frac{p_1}{a} \sqrt{\frac{f}{(1 + x/a)[x \mp f(1 + x/a)]}} \; . \quad (3.5)$$

The upper sign applies to concave mirrors, and the lower sign to convex mirrors. p_1 is the sound pressure of the incident spherical wave at unit distance from the centre, so that p_1/a is its sound pressure at the vertex of the mirror. In the case of a spherical wave on a cylindrical mirror, which is the more important one in practice, neither a purely spherical wave nor a cylindrical wave is produced but a combination of two different cylindrical waves which, in accordance with the two terms below the root sign, have also two different image points.

For quantities under the root signs only absolute values will be calculated. In the case of the concentrating mirror the nominator can disappear in all terms, viz. at the real image points, where theoretically the acoustic pressure would become infinite. In reality the geometric construction fails here because of diffraction phenomena. The true concentration and increase of the sound pressure depends on the wavelength.

Figure 3.7 shows a practical test in which a sound beam of spherical waves from the probe meets a cylindrical hole in a forging. The full calculation will be made in Section 3.5.

In this case the surface is air backed and the rays incident at right angles are totally reflected, as is also assumed in Eq. (3.5). According to Fig. 2.7 the rays not strictly normally incident, are not totally reflected but the deviations are only very slight, and for longitudinal waves at 16° are only about 10%. Since Eq. (3.4) is being used, the calculation should in any case be limited to only a narrow beam around the normally incident ray.

If the reflecting surface is not air-backed but for example by water, the reflection will be reduced. Formula (3.5) must then be supplemented by the coefficient of reflection R according to Eq. (2.1). Naturally this does not change the shape of the reflected wave, nor the position of the image point.

At such curved boundaries the transmitted waves can also be traced by considering single rays following the law of refraction (Chapter 2).

A solid/liquid boundary curved spherically or elliptically (Fig. 3.8) acts as a concentrating or dispersing lens, depending on the orientation of the curvature and the ratio of the sound velocities c_2/c_1.

In contrast to optics, in which calculations are made with the "refractive index" $n = c_1/c_2 > 1$, with ultrasonics very different values may occur. For the refraction of longitudinal waves at the water/steel boundary we have $c_1/c_2 = 0.25$ and at the steel/water boundary we have $c_2/c_1 = 4$.

Figure 3.8 shows the four possibilities of a lens between water and steel (cf. the following table).

		Curvature	c_2/c_1
Condensing lens	a	concave	>1
Condensing lens	b	convex	<1
Dispersing lens	c	concave	>1
Dispersing lens	d	convex	<1
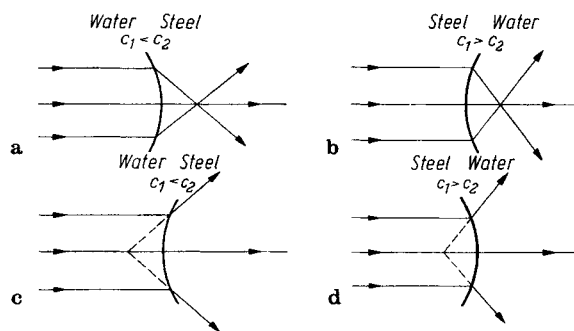
Fig. 3.8 a–d. Lens effect of a curved interface (water/steel)
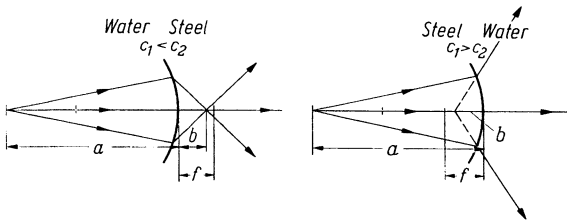
Fig. 3.9. Spherical waves in cases **a** and **b** of Fig. 3.8

The formula for the focal distance:

$$f = \frac{r}{1 - c_2/c_1} \tag{3.6}$$

is only valid for narrow beams small in comparison with the lens diameter. It cannot be used to find the focal distance in the case of focussed transducers supplied commercially (Section 4.5).

If in Fig. 3.8 the incident wave is a spherical one rather than a parallel beam, then in cases a and b we get real image points but in cases c and d only virtual ones (Fig. 3.9).

The focal distance shall always be regarded as being positive, as well as the axial distances a and b of the origin of the spherical waves and their image points from the convex surface. The lens formula

$$\frac{1}{b} - \frac{c_2/c_1}{a} = \frac{1}{f} \tag{3.7}$$

links all three quantities. Anything said above concerning lenses, including Figs. 3.8 and 3.9, also applies to cylindrical lenses. If a plane or a spherical wave is to pass through a spherical or a cylindrical lens, the resultant acoustic pressures are

plane wave
through spherical lens   through cylindrical lens

$$Dp_0 \frac{f}{x \mp f,} \qquad\qquad Dp_0 \sqrt{\frac{f}{x \mp f}} \,, \tag{3.8}$$

spherical wave

$$D\frac{p_1}{a} \frac{f}{x \mp f\left(1 + \dfrac{xc_2}{ac_1}\right)}, \qquad D\frac{p_1}{a} \sqrt{\frac{f}{\left(1 + \dfrac{xc_2}{ac_1}\right)\left(x \mp f\left(1 + \dfrac{xc_2}{ac_1}\right)\right)}}\,. \tag{3.9}$$

The upper, negative sign applies to condensing lenses, (case a and b in Fig. 3.8) and the lower, positive sign to dispersing lenses. Under the root sign only absolute values shall apply and D is the transmission coefficient according to Eq. (2.1).

For the sake of clarity excessively wide beams are used in the ilustrations for which in reality the fringe rays would no longer intersect each other at the focal point.

When testing materials, the mirror and lens effects are often produced naturally by the surfaces of the test objects. Sometimes the effects are used intentionally in order to change the direction, shape or intensity of a wave. The plane mirrors used for this purpose consist of a metal or plastic membrane stretched over a flat surface leaving between them a thin layer of air. The layer of air can of course be very thin without becoming transmissive but as a precaution a dry sheet of paper can be inserted. The membrane itself should be thin compared with the wavelength. Convex mirrors are best made of solid materials, for example steel or lead, with losses of 10 % to 20 %. An absorbing material such as lead can be used to prevent the return of transmitted waves from other interfaces. A parabolic mirror is superior to a spherical mirror since in this case the fringe rays also converge at the focal point.

Occasionally, when testing a complex specimen, reflection by means of mirrors can be exploited to reach points difficult of access (Fig. 3.10). Other examples are shown in Figs. 22.6b and 16.18, and in the latter case the workpiece has intentionally been given a special form to be able to carry out the test by means of the mirror effect.

To obtain high efficiency in the case of ultrasonic lenses, it is important to keep the reflection losses small.

According to Eq. (2.1) this means that the acoustic impedances of lens and contiguous material should be as nearly equal as possible. On the other hand Eq. (3.7) indicates that in order to produce satisfactory refraction, the acoustic velocities should differ as much as possible. The first requirement rules out lenses made of metal immersed in liquid, whereas those made of plastics, for example Perspex or polystyrene, are superior, at least for lower frequencies at which their absorption is not excessive. Liquid lenses consisting of containers made of thin, spun metal sheets, have also been successfully used. For details see [2].

To vary the focal distance lenses filled with liquid between deformable diaphragms have been used, working in a similar way to the lens in the human eye.

In testing materials lenses are also used to focus ultrasonic beams and thus achieve higher sensitivity and better resolution. Finally, another idea has been taken from optics and applied successfully to ultrasonic testing. This is the principle of Fresnel or zone lenses (Fig. 3.11). They have the advantage of being thinner but they can only be used for one special frequency, the zone widths and thicknesses being calculated for a certain wavelength only. Furthermore they can only
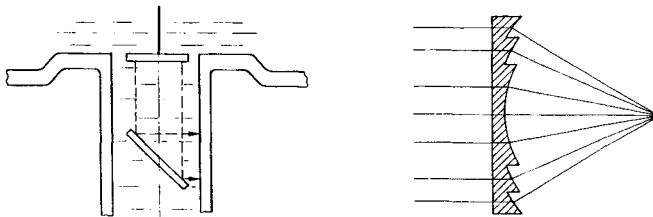
Fig. 3.10. Exploitation of the mirror effect for measuring the cylinder wall thickness of an engine block under water

Fig. 3.11. Fresnel or zone lens made of plastics material in water

operate successfully with ultrasonic pulses of sufficient length to allow constructive and destructive interference between different waves. For lenses see also [1278, 1498, 732] and about materials for lenses see [587].

3.5 Spherical Waves in Hollow and Solid Cylinders

The application of the results of the last section will now be illustrated by the practical cases in which a sound wave passes through a hollow or solid cylinder, either through direct contact with the entrance point of a spherical wave on the surface, or while immersed in a liquid at a distance from the origin of the spherical wave.

For a cylinder with a coaxial borehole as shown in Fig. 3.7, for example a generator rotor with a central hole, the result of the calculation of the sound pressure according to Eq. (3.5) is plotted in Fig. 3.12 for different ratios of internal and external radii. On the axis the theoretical acoustic pressure of the incident spherical wave has been given the value 1. After reflection this value decreases rapidly and remains appreciably smaller than in the case of a reflection from a flat back wall at the same distance.

Of particular interest is the magnitude of the reflection from the centre hole, measured at the entrance point of the beam, as compared with the reflection from a flat back wall. This law is shown in Fig. 3.13.

However, this result applies only if the diameter of the reflecting hole exceeds that of the beam. For instance, a hole of 50-mm radius at a distance of 250 mm gives only 40 % of the reflection from a flat back wall ($r_i/a = 0.2$). The function is derived from Eq. (3.5) for the cylindrical mirror acting as a convex mirror (therefore
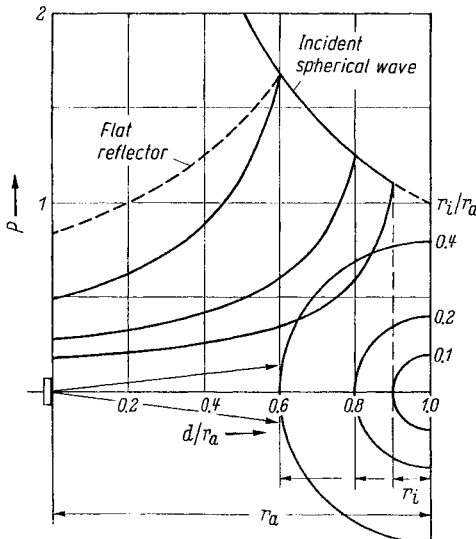
Fig. 3.12. Relative sound pressure p of an incident spherical wave after reflection from a cylindrical hole (sound pressure of spherical wave at distance $d/r_a = 1$ arbitrarily set equal to one)
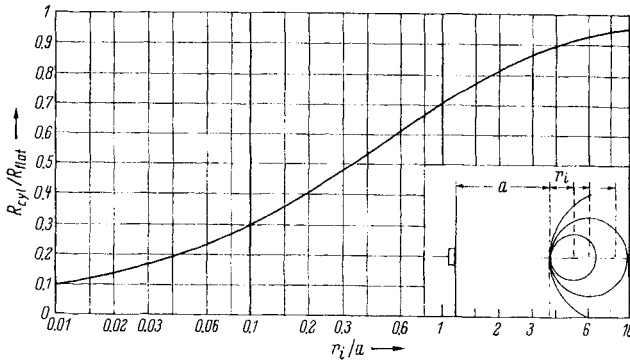
Fig. 3.13. Ratio of reflected sound pressures at cylindrical hole and flat back wall, measured for incident spherical wave at entrance point of beam

lower sign), with $x = a$ and if divided by the sound pressure $p_1/2a$ which the flat back wall would produce:

$$\frac{p_{\text{cyl}}}{p_{\text{flat}}} = \sqrt{\frac{r_i}{a + r_i}} \,. \tag{3.10}$$

In the case of reflection in a solid cylinder, the beam-entrance point is usually located directly on the surface of the cylinder as shown in Fig. 3.14. In this case the back wall concentrates the wave along a focal line F between axis and back wall, at 1/3 radius from the axis. The corresponding law is again derived from Eq. (3.5) for the concave mirror with $a = 2r = 4f$. The presentation in Fig. 3.15 uses the distance d instead of x, measured from the beam entrance point.

In this case too the simple formula fails to give true value of the sound pressure along the focal line. Nevertheless in practice considerably higher acoustic pressures are produced than those of the incident wave at that point. For practical echo sounding this focussing method may result in a small flaw producing a much stronger echo over the longer path via the back wall (W reflection. Fig. 3.16), than along the direct path to and from the beam entrance point.
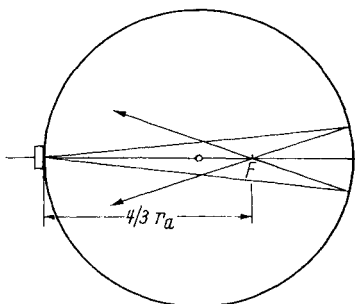
Fig. 3.14. Reflection of a spherical wave in a solid cylinder
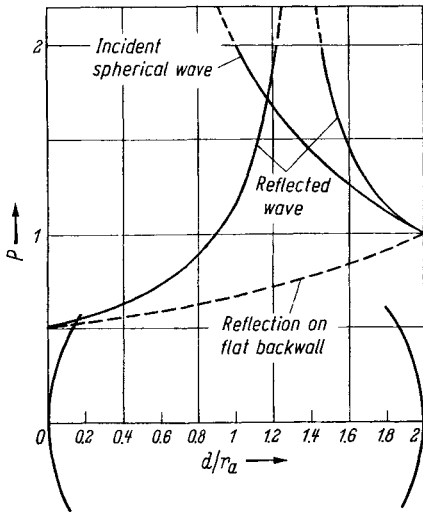
Fig. 3.15. Relative sound pressure p of an incident spherical wave and reflection in solid cylinder (see Fig. 3.14) (sound pressure of spherical wave at distance $d/r_a = 2$ arbitrarily set equal to one)
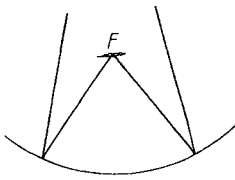
Fig. 3.16. W reflection from flaw F
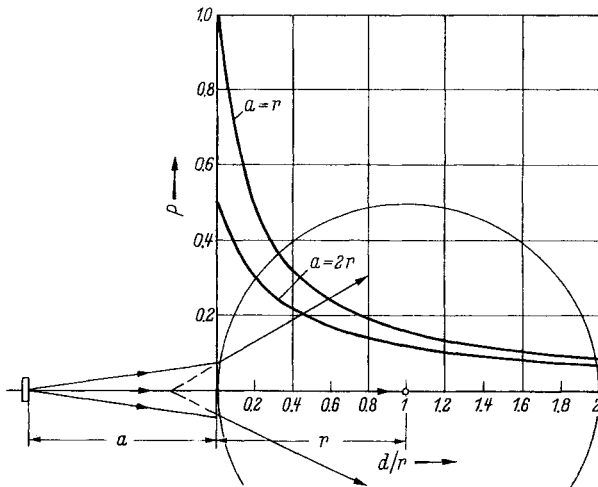
Fig. 3.17. Relative sound pressure in solid steel cylinder for an incident spherical wave from distance a in water

The sound pressure of the reflected wave is also greater along its entire path through the cylinder than in the case of a flat back wall, which is plotted for comparison in Fig. 3.15. They become equal only in the immediate region of the beam entrance point. That is why when comparing a solid cylinder and an equally thick flat plate the back-wall echoes are equally strong for equally strong entering waves, which also applies to the multiple echoes as confirmed by a simple calculation.

The influence of the probe diameter and the radius of a solid cylinder on the back wall echo is the subject of the paper [780].

With reference to the multiple echoes from a cylinder with a central borehole see [781, 979, 782]. The latter proves that the correction factors for the influence of the cylinder radius, as given in Japanese testing standards, are in error.

Often cylindrical test objects are immersed in a liquid, the sound generator being at a distance a from the test object. Figure 3.17 shows that the sound pressure in a steel cylinder immersed in water decreases rapidly with the distance from the surface. With the probe at a distance of 1 radius, viz. $a = r$, the side remote from the probe receives less than 1/10th of the initial sound pressure. At a greater distance ($a = 2r$) the initial value decreases but the pattern becomes generally more uniform.

It must be mentioned again that this relationship, as with the earlier ones, gives approximately correct values only in the case of specimens large compared with the probe diameter.

4 Wave Physics of the Sound Field

4.1 Elementary Description

Ultrasonic waves are generated by a source, the so-called probe, and we require to know how the wave motion propagates into a material as the ultrasonic field.

For this we could make use of the variation of the density of the material to describe the field, or the velocity of the particles, or their displacement. However, for material testing the sound pressure is of greater interest or more precisely the amplitude of the alternating pressure. This defines the amplitude of the signals we receive just as with human hearing the effect is louder for larger variations of the air pressure.

In some simple cases we can calculate the sound pressure at a particular spot or we can measure it with a miniature microphone or in certain materials we can make it visible.

The sound field of a circular, disc-shaped piezo-electric oscillator is quite a simple one (Section 7.2). It oscillates with equal phase and amplitude over its whole surface and communicates its own movement to the contiguous material whether as a thickness oscillator (longitudinal movement) or as a shear oscillator (transverse movement). It acts as an ideal piston oscillator for longitudinal oscillation if we place it into a hole in a solid wall as in Fig. 4.1. We can also assume that a diaphragm of the same diameter in a non-permeable wall irradiated by a wide plane wave must also give rise to the same sound field as the actual oscillator and thus the movement of the particles within the diaphragm, or on the surface of the oscillator, will be the same.
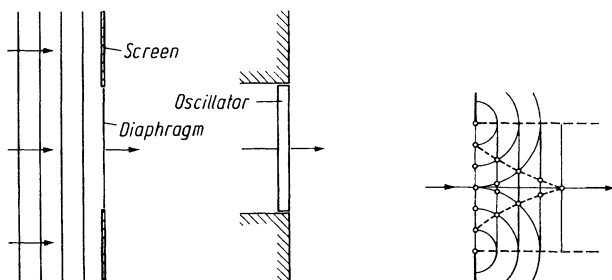
Fig. 4.1. Oscillator in rigid wall produces same effect as a diaphragm in a flat wave with rigid screen

Fig. 4.2. Interference structure of sound field behind diaphragm according to Huygens' principle

According to simple geometric principles the plane wave would beam through the diaphragm a sharply defined cylinder surrounded by a shadow field. In reality the sound field, owing to diffraction phenomena, is changed considerably in both regions. This can be illustrated qualitatively by applying Huygens' principle mentioned in Section 1.2. As in Fig. 1.8, the spherical elementary waves again form plane wave surfaces in the centre zone of the diaphragm. To this is added the edge effect. In the case of a straight edge the elementary waves of the edge form a cylindrical wave whose axis is the edge, while in the case of a circle an annular wave is produced. Superposition upon the plane wave produces a field of maxima and minima of the sound pressure, of which some are indicated in Fig. 4.2. This is clearly demonstrated in Fig. 4.3 where the actual sound beam in front of an oscillator has been made visible (Osterhammel method [1155]).

The ratio of oscillator diameter D to wavelength λ determines the spread of the interference field and the number of maxima and minima.

In Fig. 4.2 the wavefronts have a separation of one wavelength λ and the diameter of the oscillator has been chosen to be 6 wavelengths. In Fig. 4.3 D/λ was about 6.7. The circled points on the dotted lines mark the spots where the path difference between the plane wave and the edge wave reaches an exact multiple of λ and here we have maxima of the sound pressure.

Both illustrations are like instantaneous exposures of the sound field but in a cine film we could see the maxima travelling along the dotted curves towards the axis.

The position of the last pressure maximum on the axis of the disc and the beam depends on D and λ in accordance with the relationship

$$z = \frac{D^2 - \lambda^2}{4\lambda}. \tag{4.1}$$

In most practical cases the diameter is much larger than the wavelength and we can simplify Eq. (4.1) as

$$z \approx D^2/4\lambda = N.$$

The field beyond the last maximum is called the far-field; the one between the probe and the last maximum is the nearfield. N therefore is called the near-field length, and is an important characteristic of the sound field.

Figure 4.4 shows schematically some sections of the sound field perpendicular to its axis. Immediately in front of the oscillator we have an annular system of pres-
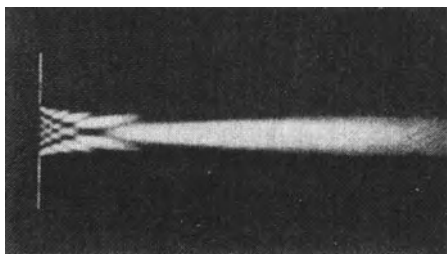
Fig. 4.3. Sound field in front of an oscillator with $D/\lambda = 6.7$ (photograph by Linhardt and Rieckmann [928])
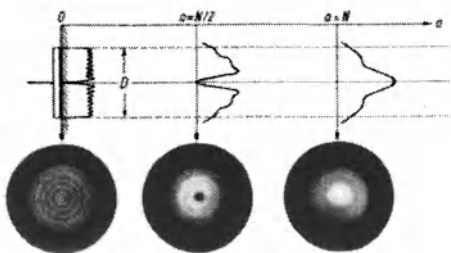
Fig. 4.4. Near-field in front of an ideal piston oscillator, or behind a circular diaphragm in a plane wave, with distributions of the sound pressure along sections spaced $a = 0$, $N/2$ and N, for $D/\lambda = 16$, with correlated photographed simulated images of the beam cross-section
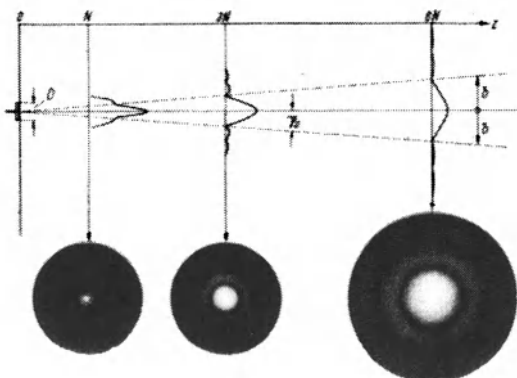
Fig. 4.5. Transition from near-field to far-field with sound-pressure distributions in cross-section as shown in Fig. 4.4 but reduced 1:4

sure minima and maxima the average of which equals the pressure of the plane wave and the number of maxima is D/λ. In the example illustrated there are 16, which corresponds to an oscillator of 24 mm diameter with a wavelength of 1.5 mm, corresponding to a frequency of 4 MHz in steel.

At a distance of about $N/2$ we find the last pressure minimum on the axis surrounded by an annular maximum and there is a single maximum on the axis at the near-field length N (see also Fig. 4.19 below).

The near-field has quite a complicated structure, whereas that of the far-field is much simpler (Fig. 4.5). Here the maximum for all sections lies on the axis and the adjacent minima lie to the side at positions defined by the angle γ_0 (dotted lines in Fig. 4.5). γ_0 is called the angle of divergence.

Since it is difficult to obtain distinct pictures of such acoustic beam cross-sections, the images were produced artificially by photography on the basis of the calculated cross-section curves. Intense brightness corresponds to high sound pressure.

The reason for the variations in the sound fields is of course the interference between different oscillations within the wave trains when shifted in time. The wave therefore must be sufficiently long since otherwise the variations of the sound pressure are reduced and may even disappear completely when short pulses are used.

4.2 Zone Construction of a Sound Field according to Fresnel

In the foregoing chapter we have again made use of the principle of Huygens to explain the sound field and we will now use it to construct an arbitrary sound field graphically without mathematics. The method based on Huygens' principle and developed by Fresnel is called *zone construction*.

Differences of the sound pressure at different points of the sound field result from the fact that Huygens' elementary waves have not travelled along the same paths from all points of the radiating surface. In addition their sound pressure decreases inversely with the distance. The individual sound pressure values of the elementary waves cannot therefore simply be added but their path differences must be taken into account too. Two equally strong waves with a path difference of exactly one half wavelength cancel each other completely and path differences between zero and 1/2 wave length thus result in acoustic pressures between double the value and zero. This can be presented very conveniently by *vector addition* as shown for a few cases in Fig. 4.6. This no longer determines the path difference of two elementary waves by a linear measurement but by an angular measurement in which one full wavelenth corresponds to an angle φ of 360° or 2π. Generally, the path difference l corresponds to the phase angle

$$\varphi = 2\pi \frac{l}{\lambda}. \tag{4.3}$$

In Fig. 4.6 the sinusoidal patterns of the sound pressures of two elementary waves superimposed at a point, are added for given instants and for different path differences (phase angles). In each case the corresponding vectors are added at the right hand side, the result being identical but much simpler and clearer. At arbitrary sound pressures and phase angles therefore the correlated vectors form a parallelogram, the diagonal indicating the sound pressure of the resultant wave in both magnitude and phase.

In the Fresnel method of presentation, all elementary waves radiated from a given surface and producing at a given point of the sound field a resultant sound pressure by adding their individual vectors, are first sorted into groups. Such a
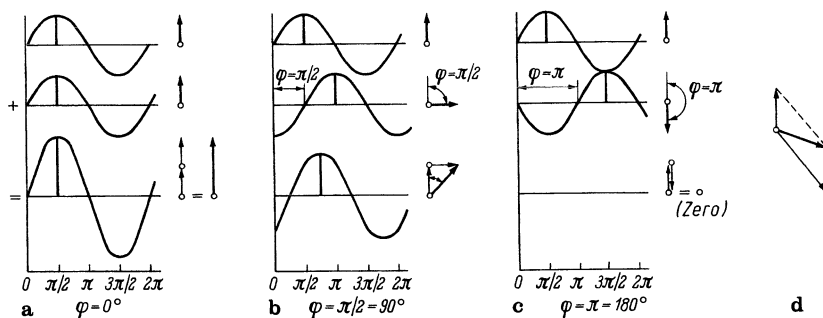
Fig. 4.6. Vector addition. a, b and c with identical amplitude and different phase, d with different amplitudes. a $\varphi = 0$; b $\varphi = \pi/2 = 90°$; c $\varphi = \pi = 180°$; d intermediate value
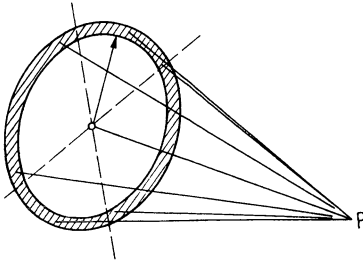
Fig. 4.7. Elementary waves radiated from the face of a circular ring
Fig. 4.8. Fresnel zones of equal area (the radii are in the ratio of the square roots of integers)
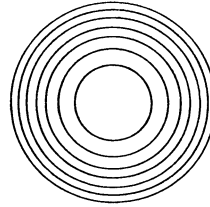
group should have approximately the same phase angle, i.e. the same path length from the area concerned to the point of summation. For a flat radiating surface this is true for instance for all waves radiated from an annular zone whose centre lies at the foot of the vertical (Fig. 4.7). If the radiator oscillates uniformly inside such a zone, all its waves can be added up to a single sound pressure which is proportional to the area of the zone, and inversely proportional to its distance from the point of observation (since they are spherical waves). In the case of a flat area the appropriate zones are concentric, circular rings.

If we divide the surface of the radiator into n annular zones, the jth zone having the area S_j and the path of the waves to the measuring point being a_j, we obtain the sound pressure of this zone as

$$p_j = C_j \frac{S_j}{a_j} \qquad (j = 1, \ldots, n).$$ (4.4)

C_j is a factor of proportionality, which is constant for all zones if the radiator oscillates uniformly over the whole surface. The area of one zone equals

$$S_j = \pi (r_j^2 - r_{j-1}^2) \qquad (j = 2 \ldots n).$$

It is advantageous to equalise the areas of all zones by choosing

$$r_j = r_1 \sqrt{j} \qquad (j = 2 \ldots n)$$

r_j being the inner radius of the jth zone (Fig. 4.8 and 4.9). In this case we have all areas

$$S_j = S_1 = \pi r_1^2 \qquad (j = 2 \ldots n).$$

To add up all vectors we need only the path length

$$a_j = \sqrt{r_{j-1}^2 + a^2} \qquad (j = 2 \ldots n)$$ (4.5)

where $a_1 = a$. The angle of the phase φ_j between the path a_j, and the axis, is obtained from Eq. 4.5

$$\varphi_j = \frac{2\pi}{\lambda} a_j \qquad (j = 2 \ldots n)$$ (4.6)

with $\varphi_1 = 0$.
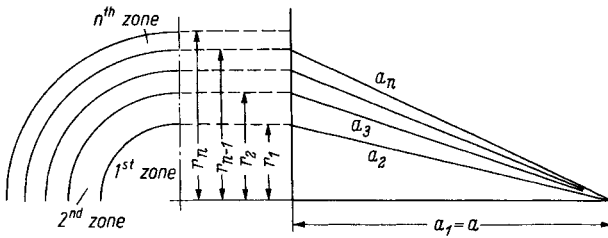
Fig. 4.9. Construction of zones, path $a_j = \sqrt{r_{j-1}^2 + a^2}$
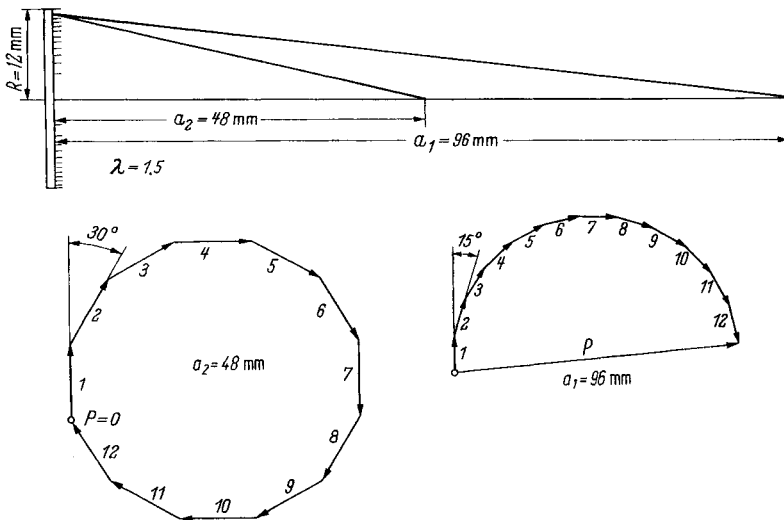
Fig. 4.10. Construction of zones according to Fresnel for two points on the axis at distances $a_1 = R^2/\lambda = 96$ mm and $a_2 = R^2/\lambda = 48$ mm; for $R = 12$ mm, $\lambda = 1.5$ mm $(D/\lambda = 16)$

Figure 4.10 shows the graphical construction of the sound pressure at two points on the axis of a circular disc. It has a value $D/\lambda = 16$, as was also chosen for Figs. 4.4 and 4.19. The two observation points on the axis with distances a_1 and a_2 equal the near-field length N and its half value, i.e.:

$$a_1 = N = \frac{R^2}{\lambda} \qquad a_2 = \frac{a_1}{2} = \frac{N}{2}.$$

The surface of the radiator has been divided into 12 zones with vectors 1 to 12. Their lengths are derived from Eq. 4.4 and Eq. 4.5 and their angles from Eq. 4.6. We realize that the lengths of the wave paths vary only very little if the observation point is at a large distance from the radiator. In addition the differences from one angle to the next get very small.

Here we have at the distance $a = N$, $\Delta\varphi = 15°$ and at $a = N/2$, $\Delta\varphi = 30°$. In the first case the chain of vectors winds up to almost a semi-circle resulting in a total sound pressure at its maximum (and equal to the circle's diameter). In the second case it winds up to complete a full circle and the resultant sound pressure totals zero.

The winding up of the chain of vectors increases as the distance gets shorter and we get more and more maxima and minima of the sound pressure (compare with Fig. 4.19). On the other hand, for large distances, the chain becomes a straight line. That means we can add up the individual vectors without regard to the phase angles and the relationship then becomes:

$$p = C\,(n/a)\,S_1 = C\,(S/a)$$

since all distances a and all the zone areas are equal. Therefore we derive the law, that at large distances from a plane radiator the sound pressure on its axis is proportional to its area and inversely proportional to its distance (as shown already in Section 3.2). Even a large radiator for large distances acts as a point source and its particular shape, whether a circular disc or not, has no influence.

It is interesting to study the influence of different zones on the resulting sound pressure on the axis. At the nearfield end, $a = N$, the outer zones do not contribute much to the pressure. Omission of one or two vectors in Fig. 4.10 diminishes the amplitude very little and the main influence is a phase variation which is usually of no consequence for materials testing. A similar result produces a reduction of the oscillation amplitude in these zones instead of complete suppression but at the distance $N/2$ the effect is quite different. Complete suppression, or even some damping of the oscillation of the outer zones, immediately raises the sound pressure from zero to much higher values. All zero points in Fig. 4.19 behave in this manner and this effect is used to equalize the sound field on the axis in probe construction (Section 4.8).

Such experiments, which can be carried out easily in water, show clearly that because of the wave basis of the sound field one can obtain "more" by "less", which would be impossible to explain by a geometric-acoustic treatment of the sound field.

For points not on the axis, all circular ring zones are no longer located entirely on the surface of the radiator (Fig. 4.11). The areas S_j are no longer identical and the lengths of the p_j vectors become different. But even in this case the construction by the graphical method is simple. The areas are determined by counting the
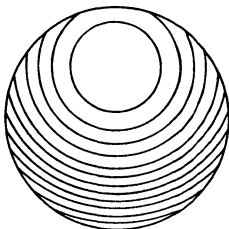
Fig. 4.11. Fresnel zones for a point not on the axis
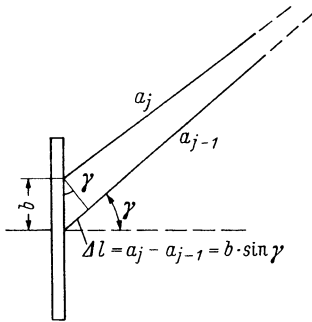
Fig. 4.12. Path difference between two elementary waves for the case of a distant point of observation
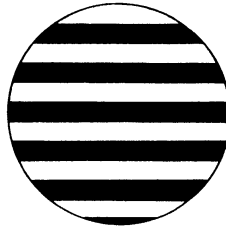
Fig. 4.13. Zonal strip with path differences of $\lambda/2$ at $D/\lambda = 16$ and with $\gamma = 20°$

squares in a drawing of the system on millimetre graph paper and the method is then not limited to circular radiator surfaces.

If the point of observation off the axis moves to infinity, the phase difference for two points of the radiator surface depends only on the angle γ at which this point appears relative to the axis (Fig. 4.12). The ring system from a distant viewpoint then appears as a system of parallel strips which, for a given path difference Δl, have the distance $b = \Delta l/\sin \gamma$. If a path difference of half a wavelength is chosen, two adjacent strips will cancel each other at the point of observation if their areas are equal. Such a system is shown in Fig. 4.13 for the conditions: $D/\lambda = 16$, angle $\gamma = 20°$.

It can be seen that the black strips are in practice almost completely counterbalanced by the white strips, so that nothing, or almost nothing, is left in this direction. This explains the directivity of the radiator in the far-field. At small angles the strips become wider and the total area of the white strips may then greatly exceed that of the black strips, the condition corresponding to the main maximum of the radiation.

As shown above the sound field may be changed by varying the transit-time differences between individual zones. This can be done by using a curved oscillator for which the fringe zones have the same sound path to a certain observation point as have the central ones and we obtain thereby a focussed source. With a Fresnel lens (Fig. 3.11 and [1498, 1499]) the transit-time differences arise from different velocities in the lens material compared with air and by the varying thickness of different sections of the lens. With a zone lens (Fig. 4.36d, see also [1279]) certain annular zones suppress the wave. Finally it is possible to divide the whole oscillator into distinct and separated domains, which are excited electrically by voltages with appropriate phase shifts to produce specially selected beam characteristics (see Section 10.4.1, phased arrays).

With the exception of the first solution, viz. using a curved oscillator, the other methods are only effective if the wave train is sufficiently long to produce the necessary phase shifts with equal amplitudes.

If the wave is produced by some arbitrary shape of the oscillation the resulting sound field must be constructed by adding up the individual sound fields of the individual component frequencies of the oscillation also taking into account their different phases.

Compared with the sound field of a long wave train, a short pulse of the same basic frequency shows substantial distortions away from the axis and its original shape can only be recognized when viewed in the axial direction.
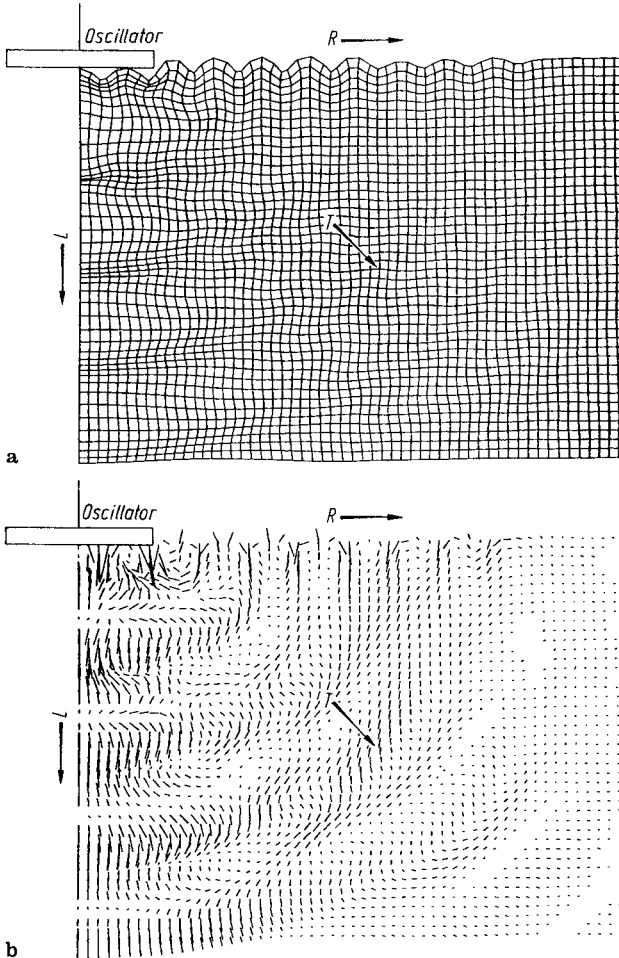
Fig. 4.14. Radiation of a longitudinal wave from an oscillator with a diameter of only a few wavelengths. **a** Net presentation; **b** vector presentation

4.3* Graphical Presentation of Sound Fields

To illustrate sound fields pictorially there are several avilable possibilities. In Figs. 1.2, 1.3 and 1.4 plane waves were represented by a network of individual mass points which are displaced by the force of an ultrasonic wave. In the same way it is possible to represent a complete sound field rather than just an unlimited plane wave. Figure 4.14 illustrates two alternative methods based on a computer simulation which calculates the field in front of a longitudinal wave oscillator.

The *deformation of a network* (Fig. 4.14 a) is a simple illustration representing an instantaneous "snapshot" of the sound field and it can also be displayed by vectors (Fig. 4.14 b) giving both amplitude and direction of individual sound-field elements.

In Fig. 4.14 a we can easily recognize the surface wave, which is radiated simultaneously with the longitudinal wave (cf. Harumi [9, S 65], and for this *finite element method* see also [1195, 163, 733, S 100]).

For the angular characteristics of a sound field a useful method is to measure the amplitude of the wave on the points of a semi-circle around the source and plot them as vectors from a centre point on the radiator (Figs. 4.14 and 4.29). This representation may also be made in perspective (Fig. 4.27). This method gives a good picture of the far-field of a radiator. If we utilise thet decibel values of the measured sound pressure, it is easier to recognize the small values as for example in the side lobes (Fig. 4.15 b). For some applications it is advantageous to represent the angle in a linear diagram (Fig. 4.21), because it makes evaluation easier.

The decibel system of measurement has already been introduced in Section 2.1 and we must remember that the ratio of two sound pressures is expressed in decibels by the formula

$$\Delta p = 20 \lg p_1/p_2 \text{ dB} . \tag{4.7}$$
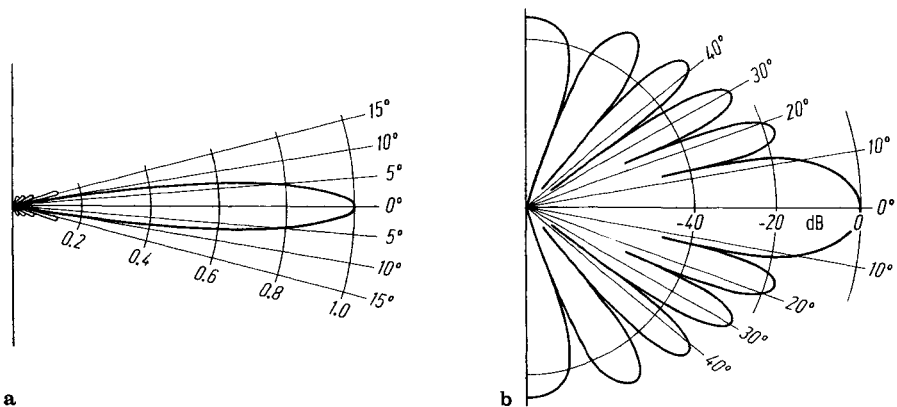
Fig. 4.15. Angular characteristics for large distances from the oscillator. **a** Values of the sound pressure in a linear plot; **b** the same plotted in dB

If the ratio of sound pressures is $1000:1$ then $\Delta p = 60\,\mathrm{dB}$, and $20\,\mathrm{dB}$ represents a pressure ratio of $10:1$.

Isobar presentation. The lines connecting all points of equal pressure in a sound field are called *isobars* and usually their pressure values are calibrated in decibel. The value $-6\,\mathrm{dB}$ in Fig. 4.16 means that the sound pressure on this isobar is about $1/2$ of
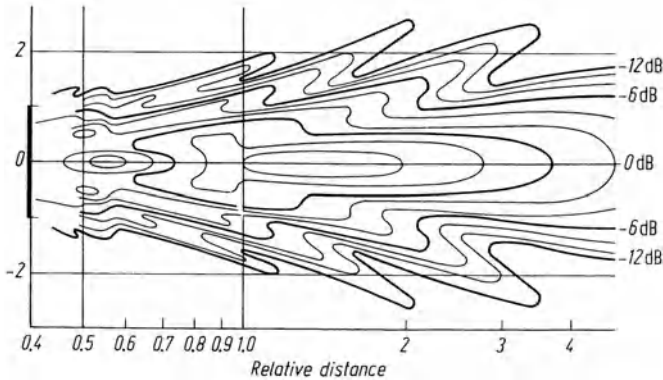
Fig. 4.16. Lines of equal sound pressure, plotted in dB. Also the distance from the radiator is plotted in a logarithmic measure
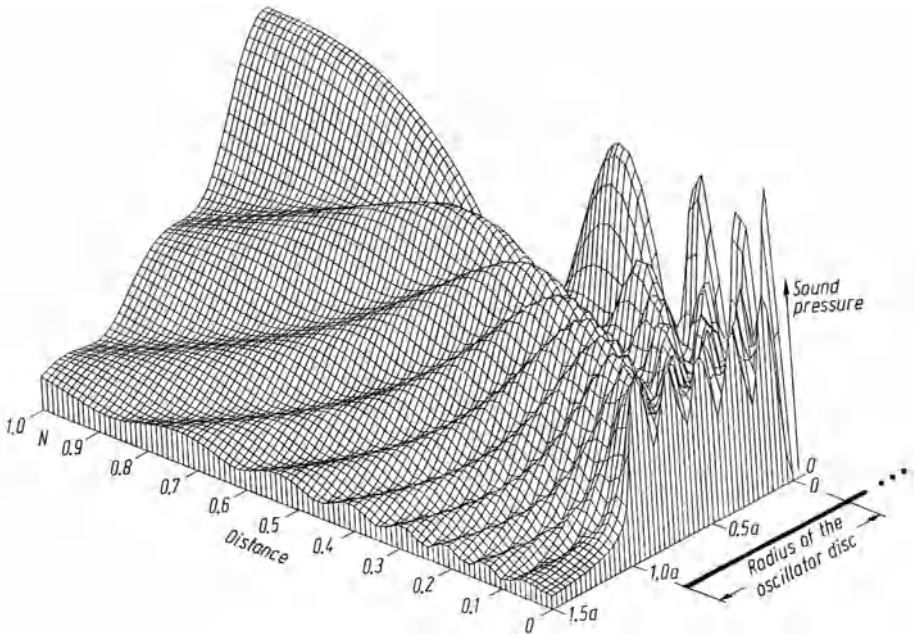
Fig. 4.17. Spatial distribution of the sound pressure plotted in linear values on a half plane through the radiator, [1686]

the reference value, which in this case is on the axis in the same perpendicular section. It might also be used with reference to a fixed value for the whole sound field, for example at the centre of the oscillator, but in what follows we prefer to make use of the former system.

Figure 4.16 represents a longitudinal section through the axis of the oscillator. The spatial field may be circularly symmetrical but need not be since it depends on the shape of the source.

The isobar presentation is well suited for beam plotters or for transparent screens. The zones between the lines may also be coloured for clarity.

Three-Dimensional Display. If the sound-pressure amplitudes are plotted on a plane perpendicular to the axis, we obtain a three-dimensional mountain representing the sound pressure (Fig. 4.17). The shape of the rear-edge section is identical to the presentation in Fig. 4.19.

The axial distances in Fig. 4.17 are plotted linearly, but are normalized in terms of the near-field length N. The distances perpendicular to the axis are expressed in
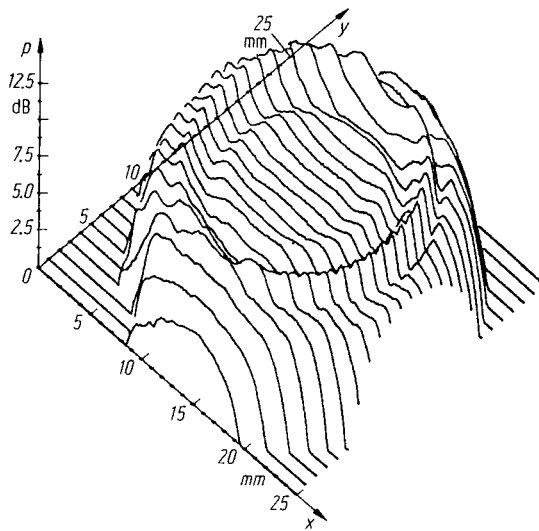
Fig. 4.18. Sound-pressure mountain measured in a plane parallel to the oscillator
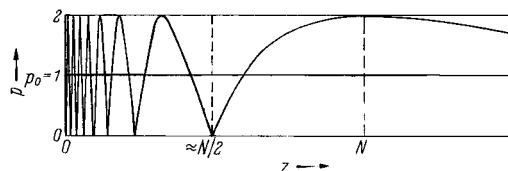
Fig. 4.19. Sound pressure on the axis of a piston oscillator as in Figs. 4.4 and 4.5

multiples of the oscillator radius and we will make more use of this normalized measurement in future treatments of beam shape and configuration.

To obtain a three-dimensional impression of the sound field we may also plot the values perpendicular to a plane across the axis as illustrated in Fig. 4.18. Whereas Fig. 4.17 is derived from calculated values, Fig. 4.18 has been obtained by measurements made line by line with a miniature microphone in an actual sound field, cf. [244 and 790].

Beam Profiles. We obtain much simpler presentations if we plot only a single profile of such a sound mountain either across or along the axis. Figures 4.4, 4.5 and 4.19 are examples.

4.4 Sound Field of a Plane Circular Piston Oscillator

We have already introduced this simplest case of a sound field in Section 4.1. Now we will calculate the beam shape along and across the axis.

According to [38] the sound pressure on the axis is given by the formula

$$p = p_0 \, 2 \sin\left(\frac{\pi}{\lambda}\left[\sqrt{(D/2)^2 + z^2} - z\right]\right) \tag{4.8}$$

where z is the distance on the axis from the centre point of the disc and D its diameter.

As we have seen negative values mean phase reversal.

Figure 4.19 shows the shape in absolute values of Eq. (4.8); see also [38].

Because of the sine function the pressure oscillates between zero and $2p_0$ and the distances z of the maxima are given by

$$\frac{\pi}{\lambda}\left[\sqrt{(D/2)^2 + z^2} - z\right] = (m + n)\pi. \tag{4.9}$$

Therefore we have maxima for $m = 1/2$ and $n = 0, 1, 2, 3 \ldots$
and   minima for $m = 1$ and $n = 0, 1, 2, 3 \ldots$.
See also [975].

If one solves the equation (4.9) to obtain the distance z for the position of the extremes, it follows that

$$z = \frac{(D^2/4\lambda) - (m + n)^2}{2(m + n)}. \tag{4.10}$$

The term $(D^2/4\lambda)$ represents the well-known near-field length N, (Eqs. (4.1) and (4.2)), and if we normalize Eq. (4.10) in terms of this value we obtain

$$z/N = \frac{1 - (m + n)^2 (2\lambda/D)^2}{2(m + n)}. \tag{4.11}$$

Because z must be positive, in Eq. (4.10) only those values of n are allowed for which $z \geqq 0$, and thus

$$n \leqq (D/2\lambda) - m \quad \text{(with } m = 1/2 \text{ or } 1).} \tag{4.12}$$

Therefore a circular radiator such that $D/\lambda = 4$ will have only two pressure maxima and two minima, one of which lies exactly at the center of the disc, where $z = 0$. Table 4.1 gives other values of the positions of maxima and minima.

For large values of z and D/λ, Eq. (4.8) may be simplified as:

$$p \approx p_0 \, 2\sin\left(\frac{\pi D^2}{8\lambda z}\right)$$

$$\approx p_0 \, \frac{\pi D^2}{4\lambda z} = p_0 \, \frac{\pi N}{z} \quad \text{or} \quad = p_0 \, \frac{S}{\lambda z} \tag{4.13}$$

where S is the area of the oscillator, and we see that the sound pressure decreases as $1/z$. This is the same distance law as that of a spherical wave, as seen in Section 3.2. Equation (4.13) therefore means that at large distances the special shape of the radiator is no longer of influence but only its area. In fact all sources at large distances act as point sources. Figure 4.20 shows the sound pressure on the axis according to Eq. (4.9) and also its approximation by a spherical wave. This approximation is too inaccurate at shorter distances and for example at $z = N$ it is $\pi/2$ times too large, i.e. about 57%. However at $2N$ it is 11% inaccurate and at only 3%.

Table 4.1. Position of extreme values of sound pressure on the axis of different circular disc oscillators

	$(D/\lambda) = 4$		$(D/\lambda) = 7$	
	Maxima	Minima	Maxima	Minima
$2(m+n)$	z/N	z/N	z/N	z/N
1	0.93		0.98	
2		0.37		0.46
3	0.14		0.27	
4		0		0.17
5			0.10	
6				0.04
7			0	
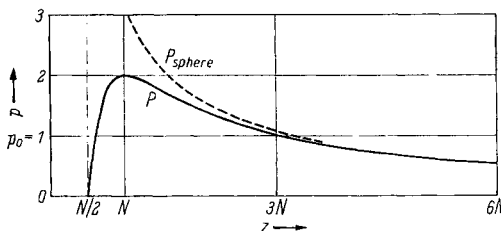
Fig. 4.20. Sound pressure p on the axis of the radiator as shown in Fig. 4.19; dotted line is the sound pressure of a spherical wave

Within the near-field the pressure on the axis oscillates between zero and $2p_0$ but in the far-field it decreases continuously. Not until the 3-fold near-field length, $3N$, is it reduced to the average value of the near-field, p_0. The range between N and $3N$ is sometimes called therefore the *transit field* [1331].

In the transverse section at the points of maximum or minimum pressure we also have peaks and troughs as Fig. 4.5 shows. Here the number of them also depends on D/λ but at the principal axial maximum the side maxima do not reach the principal value, $2p_0$.

In the far-field the maximum sound pressure is always found on the axis and here the description of the field by an angular characteristic makes sense (see Fig. 4.15).

At the distance z the relationship between the pressure and the angle γ is given by the formula

$$p = 2p_z \frac{J_1(X)}{X} \qquad (4.14)$$

where $X = \pi (D/\lambda) \sin \gamma$.

$J_1(X)$ represents a Bessel function, the values of which one finds in mathematical tables cf. [26]. p_z is the value on the axis at z where we have

$$J_1(X)/(X) = 1.$$

Equation (4.14) has been already displayed in polar coordinates in Fig. 4.15 but for better clarity Fig. 4.21 shows it in rectangular coordinates.

With the help of the left-hand angular scale one can determine sound pressure values on either side of the maximum for the special case of $D/\lambda = 16$. For example at $\gamma = 4.3°$ it reaches its first zero point and this angle is called γ_0, the *angle of divergence*. With the right-hand scale other values of D/λ can be evaluated. In this case we have made use of the approximation for small angles

$$\sin \gamma \approx (\pi/180°)\, \gamma° = \gamma°/57°.$$
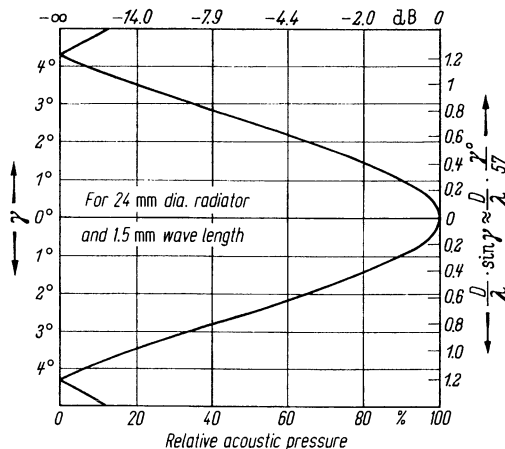
Fig. 4.21. Relative sound pressure in the far-field plotted against angle γ for $D/\lambda = 16$

Example. For an oscillator with $D/\lambda = 4$ ($D = 24\,\text{mm}$, $\lambda = 6\,\text{mm}$, which corresponds to a frequency of 1 MHz in steel) we achieve half of the maximum sound pressure at the value 0.7 on the right-hand scale, from which we calculate the appropriate angle from:

$$4\,(\gamma°/57°) = 0.7: \text{ hence } \gamma° = 10°.$$

The angle of divergence, γ_0 also results from the theory of diffraction (cf. [32]) in which

$$\sin \gamma_0 = 1.22\,(\lambda/D) \tag{4.15}$$

for a circular disc. For small angles, viz. less than 10°, we have approximately

$$\gamma_0 = 70°\,(\lambda/D). \tag{4.15}$$

Specific angles, where the sound pressure has decreased to 50 % or 70 % of the maximum are called $\gamma_{0.5}$ and $\gamma_{0.7}$ or generally γ_α with the value $\alpha \le 1$.

The upper scale of Fig. 4.21 shows the pressure reduction in decibel in which the values 50 % and 70 % correspond to $-6\,\text{dB}$ and $-3\,\text{dB}$ respectively and a sound pressure of zero corresponds to infinite decibel

$$\gamma_{0.5} \triangleq \gamma_{-3\,\text{dB}},$$

$$\gamma_{0.7} \triangleq \gamma_{-6\,\text{dB}}.$$

In the echo method of ultrasonic material testing we are not so much interested in the angular divergence of the outgoing beam (the so-called *free-field*) but more in that of the reflected beam, the *echo field*. Here we need to know what percentage of the maximum axial echo we will still receive from a small reflector lying off the beam axis.

Because the angular characteristics of a given oscillator acting as transmitter is the same as when it acts as a receiver the overall behaviour is provided by the square of the characteristic, and this fact has to be taken into account when angles of divergence are considered. γ_0 is the same in both cases, but not for any other value of γ_α.

If $\gamma_{0.7}$ is considered for example, because $0.7^2 = 0.49 \approx 0.5$, we have

$$\gamma_{0.7\,\text{(free-field)}} = \gamma_{0.5\,\text{(echo field)}}$$

or using decibel-values

$$\gamma_{\Delta\text{dB (free-field)}} = \gamma_{2\Delta\text{dB (echo field)}}$$

and the corresponding angles of divergence are given by the relation

$$\sin \gamma_\alpha = \sin \gamma_{\Delta\text{dB}} = k_\alpha \left(\frac{\lambda}{D}\right). \tag{4.16}$$

Table 4.2 gives the values of the factors k_α for both free-field and echo field in the case of a circular disc.

Equation (4.16) does not depend on the distance z of the source. Equal reductions of an echo from a small reflector, compared to one in the axial position, occur at the same angle to the axis for all distances.

The half width b of a beam at the distance z can be calculated in accordance with Fig. 4.22 as

$$b = z \tan \gamma \approx z \sin \gamma = zk(\lambda/D). \tag{4.17}$$

Table 4.2

Free-field		k_α	Echo field	
α	Δ dB		α	Δ dB
0.84	-1.5	0.37	0.71	-3.0
0.71	-3.0	0.51	0.50	-6.0
0.50	-6.0	0.70	0.25	-12.0
0.32	-10.0	0.87	0.10	-20.0
0.25	-12.0	0.93	0.6	-24.0
0.10	-20.0	1.09	0.1	-40.0
0	$-\infty$	1.22	0	$-\infty$
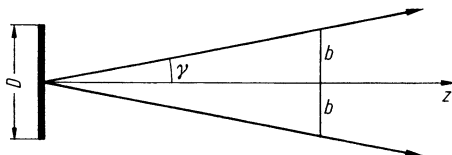
Fig. 4.22. Divergence of the beam from a circular oscillator

Example. What is the width of an ultrasonic beam at the distance N using the edge criterion of a decrease in the echo of 6 dB?

From Eq. (4.17) with $z = N = D^2/4\lambda$ and taking k from Table 4.2 for an echo ($\Delta = -6$ dB gives $k = 0.51$) we obtain $2b = 0.25 D$. This result means that the beam is effectively focussed at the end of the near-field, its sensitivity being concentrated there in a circle with a quarter of the transducer diameter.

Example. How wide is the beam from an oscillator, having $D/\lambda = 16$, at the distance of 500 mm?

From Fig. 4.21 we have $\gamma_0 = 4.3°$ and using Fig. 4.22

$$2b = 2z \tan \gamma_0 = 2 \times 500 \text{ mm} \times 0.075 = 75 \text{ mm}.$$

When using the pulse-echo method of testing we have to expect deviations from the above results if the pulse is shorter than about six wavelengths, or if the oscillator is excited non-uniformly, see Section 4.8.

Equations (4.16, 4.17 and 4.19) are only valid for values of D much greater than λ. With decreasing D/λ the angle of divergence increases to 90° remaining constant thereafter. The free-field characteristics of a small transducer with $D/\lambda = 1$ for longitudinal waves is nearly spherical. The hemispherical shape, often erroneously expected, cannot be achieved, because a free longitudinal wave propagating along a free surface cancels itself since there is a phase reversal at the grazing incidence.

Figure 4.23 represents the angular characteristics of a point-source transmitter according to calculations by Roderick [1275] (see also [442]). It has a nearly spherical characteristic for longitudinal waves, and additionally off-axis transverse waves with two lobes on each side of the axis. It is clear therefore that a small source of longitudinal waves will also transmit transverse waves at an angle and the same is true of a receiver.

The point source directivity diagram has an important consequence in the generation of oblique transverse waves by so-called angle probes (Section 10.4.2). If transverse waves are generated by refraction of a longitudinal beam, the directivity characteristics according to Eq. (4.16) are axially symmetrical, when calculated from the refraction law, Eq. (2.3), only if D is much larger than λ. This would be the "geometrical" directivity, but with decreasing D/λ it
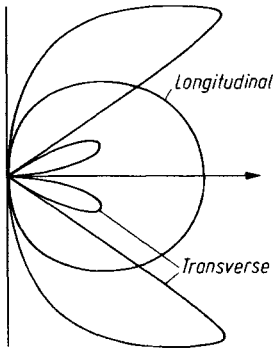
Fig. 4.23. Directivity diagram for a point source on the surface of a solid material, calculated by Roderick for a Poisson's ratio of 0.25

is increasingly affected by the point-source directivity of Fig. 4.23. The calculated angle of refraction is changed and the angles of divergence on each side of the axis are no longer equal (see Wüstenberg [1644]).

In practice is is sufficient to have a simplified model of the beam. Figure (4.24) shows the more interesting cases when the edges of the beam give an echo reduction to 50 % or 10 % of the maximum.

These beam shapes are given in the far-field by the appropriate angle of divergence (in Fig. 4.24 the −6-dB, and −20-dB lines respectively). The beam can be regarded as a search light with an angle of divergence 2γ. From Eq. (4.17) we obtain the beam width as determined by the radius of the oscillator

$$B = \frac{2b}{D} = k_\alpha \frac{z}{2N}.$$

(4.18)
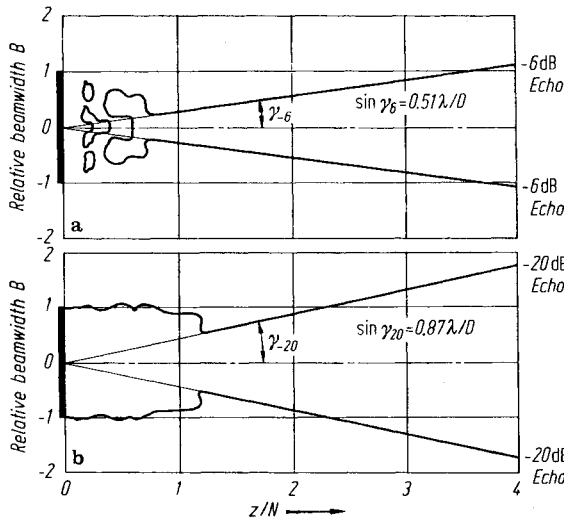
Fig. 4.24. Beam width of echo sensitivity, measured by the oscillator radius. **a** for a small reflector and −6 dB decrease of the echo relative to an axial position; **b** for −20 dB. The shape in the near-field is based on experimental results

According to Fig. 4.24 the -6-dB cone shape can be assumed valid only beyond the distance $0.8N$ and the -20-dB cone only after a distance of $1.3N$. At the near-field end the -6-dB cone has a width $B = D/4$, its quasi-focus. The -20-dB cone at the near-field end is also smaller than the oscillator diameter, being approximately $B = D/2$. It only reaches the full diameter D at $2.3N$.

Regarding mathematical treatments of the sound fields see Cavanagh [221], Zemanek [1686], Tojoetta [1528] (also concerning annular oscillators), Archer-Hall [79, 80].

4.5 Sound Fields of Non-circular Piston Oscillators

For many applications rectangular or square oscillators are in use. We consider rectangular shapes with the larger side $D_1 = 2a$ and the smaller one $D_2 = 2b$ (Fig. 4.25).

In the near-field the isobars are of course no longer circular this shape developing only at large distances. The sound-field structure depends on the ratios D_1/λ and D_2/λ and for a general treatment of rectangular radiators it is useful to normalize the distance z in terms of the quasi near-field length $D_1^2/4\lambda$ and the transverse dimensions in terms of D_1. This normalization is also used in Fig. 4.25 (see also [475, 38]).

The pressure-distance curves depend on the ratio of the two sides. Figure 4.16 shows the isobars in the longitudinal section of a square oscillator whereas Fig. 4.26 represents a more generalized display of the pressure-distance curves for several rectangular radiators with ratios D_1/D_2 varying between one and five times. In the far-field the pressure is reduced in inverse proportion to the distance. There is still a maximum of the sound pressure in the region of the quasi-near-field length $D_1^2/4\lambda$, but it is an absolute maximum only for approximately square oscillators.

Table 4.3. Values of factor h for the calculation of the near-field length of rectangular piston oscillators

ratio of the sides b/a	h
1.0	1.37
0.9	1.25
0.8	1.15
0.7	1.09
0.6	1.04
0.5	1.01
0.4	1.00
0.3	0.99
0.2	0.99
0.1	0.99
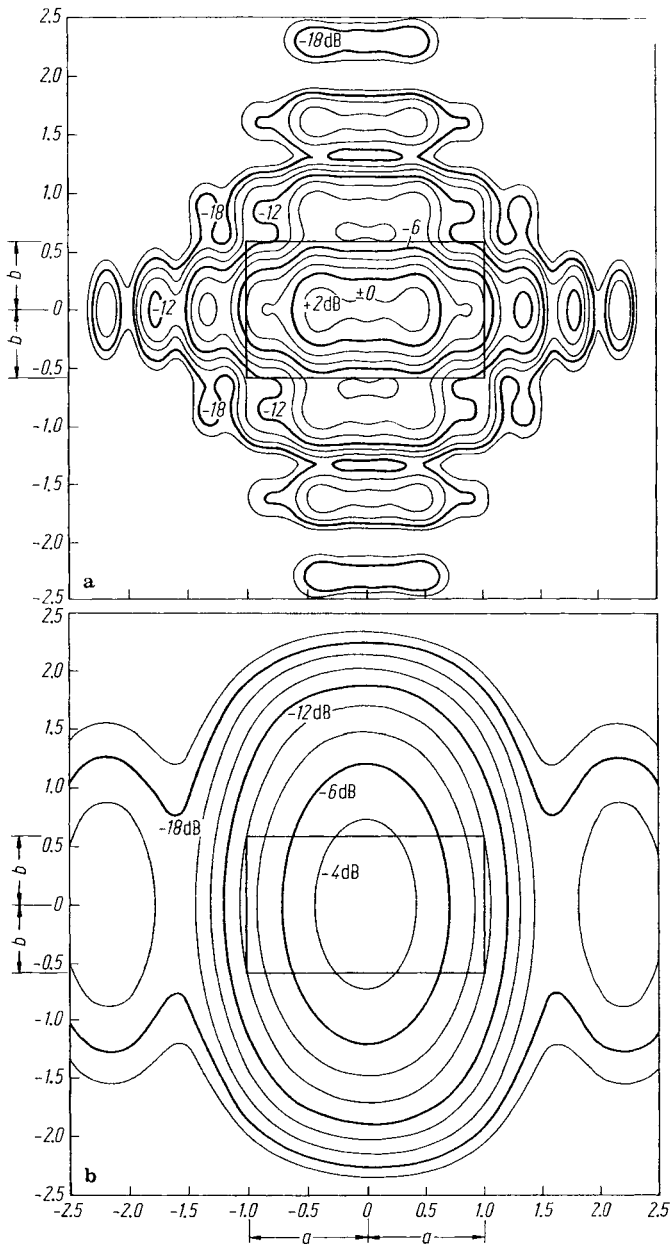
Fig. 4.25. Isobar presentation of the sound field (free-field) calculated for a rectangular oscillator with $b/a = 0.6$. **a** Section at the distance $z = 0.8a^2/\lambda$; **b** at $z = 3.2a^2/\lambda$

A simple formula for the calculation of the axial sound pressure, as in Eqs. (4.9) and (4.14), does not exist and Fig. 4.26 has been calculated by numerical integration [1341]. For rectangular oscillators driven by pulses see [441].

If one defines as near-field length the distance of the last maximum on the axis, Eq. (4.2) is still valid for rectangular oscillators using the values of Table 4.3

$$N = h\,(D^2/4\lambda) = h\,(a^2/\lambda)\,. \tag{4.19}$$

The directivity of a rectangular oscillator is no longer circularly symmetrical. In a similar way to Eq. (4.14) we have

$$p = p_0 \left(\frac{\sin X_1}{X_1}\right)\left(\frac{\sin X_2}{X_2}\right) \tag{4.21}$$

with $X_1 = \pi(D_1/\lambda)\sin\gamma_1,$

$X_2 = \pi(D_2/\lambda)\sin\gamma_2$
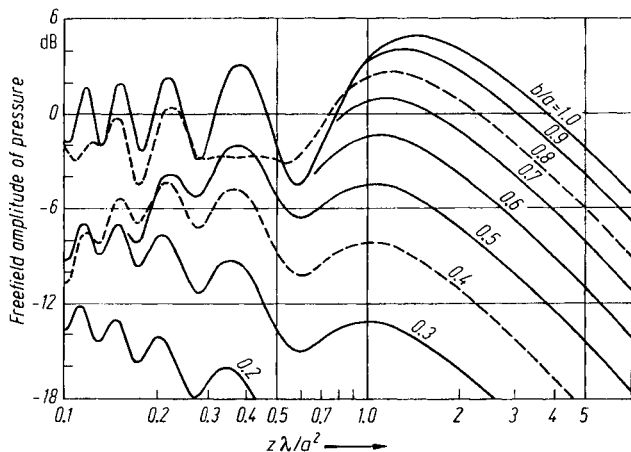
Fig. 4.26. Sound pressure on the axis of several rectangular oscillators with sides ratio b/a (calculated from [1341])
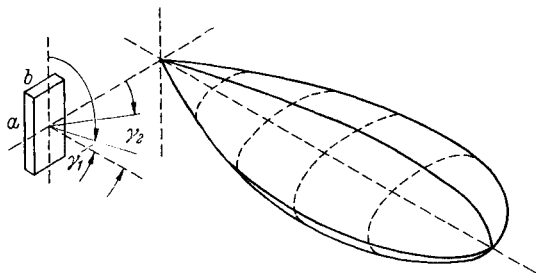
Fig. 4.27. Three-dimensional view of the directional characteristic of a rectangular radiator (without secondary lobes), ratio of sides $2:1$, $D_1/\lambda \approx 4$, $D_2/\lambda \approx 2$

Table 4.4.

Free-field		k_α	Echo field	
α	ΔdB		α	ΔdB
0.84	−1.5	0.32	0.71	−3,0
0.71	−3.0	0.44	0.50	−6.0
0.50	−6.0	0.60	0.25	−12.0
0.32	−10.0	0.74	0.10	−20.0
0.25	−12.0	0.79	0.06	−24.0
0.10	−20.0	0.91	0.09	−40.0
0.00	−∞	1.00	0.00	−∞

using the two independent angles of divergence γ_1 and γ_2. Figure 4.27 illustrates the basic beam shape without side lobes. The larger side has the better directivity, that is the smaller divergence angle. The section through the beam in the far-field is therefore an ellipse with the larger axis parallel to the shorter side of the oscillator. To calculate the angles of divergence and the beam widths of rectangular oscillators one uses Eqs. (4.16) and (4.17) as for circular oscillators, but using the factors k_α from Table 4.4

$$b_1 = z \tan \gamma_1 \approx z \sin \gamma_1 = z k_\alpha (\lambda/D_1),$$
$$b_2 = z \tan \gamma_2 \approx z \sin \gamma_2 = z k_\alpha (\lambda/D_2).$$

(4.22)

For a complete mathematical treatment of rectangular oscillators see [475, 1156] and for experimental measurement of the near-field length see [1336, 1342]. A piston oscillator of arbitrary shape is calculated in [1503]. For sound fields of electromagnetic oscillators see (Section 8.4 and [764, 1172].

4.6 Sound Fields at Boundaries and with Mode Changing

If a sound field penetrates the boundary between two different materials it is of practical interest to know how the near-and far-fields behave. For example in the so-called immersion testing, the sound is first transmitted through a liquid before it enters the specimen. Figure 4.28 shows what happens at an interface without any mode changing. The sections of the beam in each material are modified in inverse proportion to the respective velocities of sound. The sound field in steel is shortened by a factor 4, because $c_{steel}/c_{water} = 4$.

An important point should be noted regarding equivalent distances in the two media. *Distances having equal transit time* are directly proportional to the sound velocities

$$s_1/s_2 = c_1/c_2$$

(4.23)
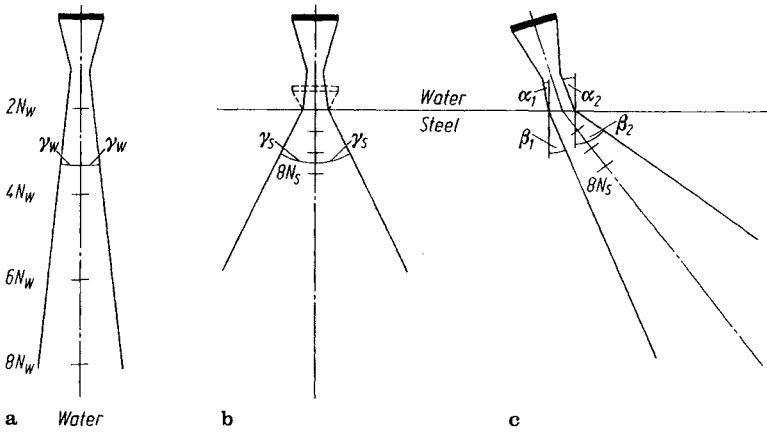
Fig. 4.28. Sound field at an interface without mode changing. **a** Field in water only, simplified; **b** interface water/steel in the far-field, perpendicular incidence; **c** oblique incidence
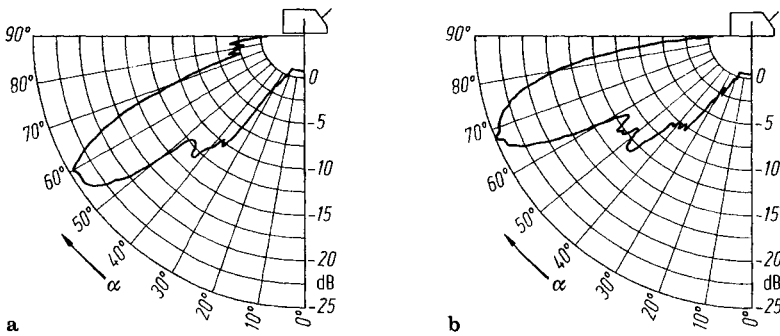
Fig. 4.29. Directivities of angle probes used on steel, measured by [1648]. **a** Nominal angle of refraction 60°; **b** nominal angle of refraction 70°

but measured in terms of near-field length they are in inverse proportion to the velocities:

$$\frac{s_1/N_1}{s_2/N_2} = c_2/c_1 \qquad (4.24)$$

because

$$N = \frac{D^2}{4\lambda} = \frac{D^2 f}{4c}.$$

Therefore distances with equivalent transit times are related to distances equivalent in the sound field in proportion to the squares of the velocities:

$$\frac{s_1}{s_1/N_1} \bigg/ \frac{s_2}{s_2/N_2} = (c_1/c_2)^2. \qquad (4.25)$$

If there is a mode change on refraction, for example longitudinal to transverse at a liquid/solid interface (cf. Sections 2.3 and 2.4), the sound-field characteristics in
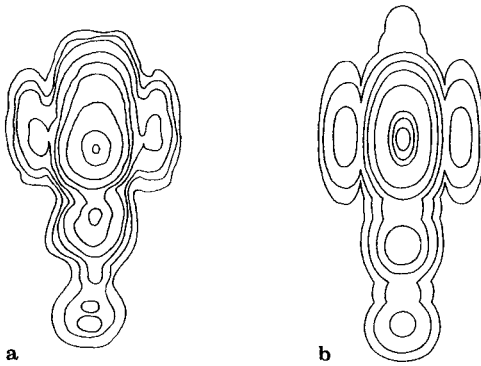
Fig. 4.30. Isobars in a section through the beam of Fig. 4.29a. **a** Measured; **b** calculated by [1648]

the solid material are governed by the transverse velocity. However, since a beam may be considered as being composed of a series of plane waves of different incident angles depending of the width of the beam, the complicated laws of refraction of Section 2.4 have to be applied with the consequence that the refracted beam is no longer symmetrical to the axis of maximum amplitude (Figs. 4.29 and 4.30).

For calculations of the sound field of angle probes used on plane interfaces see [1666, 1621, 564]; on curved interfaces [1550]; and with electromagnetic excitation see [120].

For guided waves the sound fields are similar to those of free waves, keeping in mind that they consist fundamentally of combinations of the two basic wave types.

4.7 Focussed Sound Fields

By focussing a sound beam we can achieve a higher sensitivity and resolution. Usually we understand by the term "focus" a concentration of the beam to a size less than the diameter of the oscillator. In Section 4.4 we have seen already that a circular flat-disc oscillator has a quasi-focus at the end of the near-field, this being a natural one produced by diffraction phenomena. Section 3.4 showed additional means such as curved mirrors and lenses which are able to focus a beam and it is when such devices are used that the term "focussing" is normally used. However, even with "non-focussed" fields the diffraction effects produce an effective concentration of sensitivity and because of the relatively large wavelengths used for testing materials both effects play their focussing role.

We consider the field of a spherically curved circular disc oscillator. According to [1144] the axial pressure is given by the formula:

$$p = p_0 \left| \frac{2}{1 - \dfrac{z}{r}} \right| \left| \sin \left[\frac{\pi}{\lambda} \left(\sqrt{(z-h)^2 + \frac{D^2}{4}} - z \right) \right] \right|$$

(4.26)

where

$$h = r - \sqrt{r^2 - \frac{D^2}{4}}$$
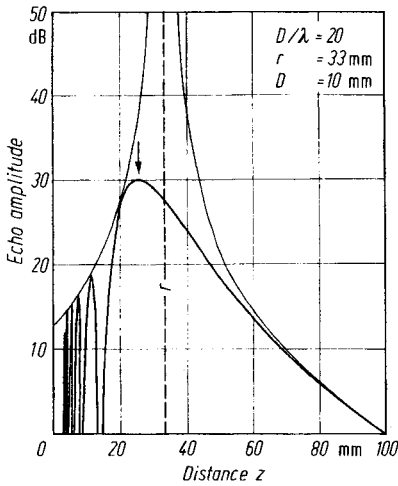
Fig. 4.31. Echo height of a point reflector on the axis of a curved radiator

and r is the radius of curvature of the oscillator. The first hyperbolic factor in brackets represents the influence of the geometry, and the second one represents the diffraction, depending on D and λ.

Figure 4.31 shows the echo of a point reflector in the focussed field of Eq. (4.26), with $D = 10$ mm, $r = 33$ mm, $\lambda = 0.5$ mm.

The position of the maximum sound pressure, or the focus (arrowed), is not at the distance r, as expected from the geometric conditions where it would have an infinite value (as indicated in Fig. 4.31). The finite value of p can be calculated from Eq. (4.26) by iterative methods only.

The ratio of the focal distance to the near-field length of the unfocussed radiator z_f/N is called K, the *focus factor*, and it is always less than 1,

$$\text{i.e.} \quad K = z_f/N \qquad 0 < K \leqq 1. \tag{4.27}$$

Its value as a function of the normalized radius of curvature is shown in Fig. 4.32. For small values of r (i.e. strong curvature) the curve follows approximately the law $z_f = r$, which means that the geometrical focussing effect is the main one, but for
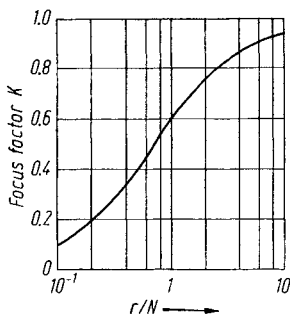
Fig. 4.32. Focus factor K as function of the radius of curvature of the oscillator (normalized by the near-field length) calculated from Eq. (4.26) for $D/\lambda = 20$, but still valid for $D/\lambda = 10$, as long as $r/N > 0.2$

larger radii it approaches unity asymptotically. The focal distance can never be made larger than the near-field length.

The focus factor K also determines the concentration of the beam by the relationship

$$B = KB_\infty \tag{4.28}$$

where B_∞ is equal to the beam diameter characteristic of the plane radiator at the end of the near-field, see [1343, 1345].

If K is greater than 0.6 the degree of focussing may be considered small, and less than 0.3 as strong.

The smallest possible radius of curvature is $r_{min} = D/2$, because then the radiator is a complete hemisphere. For $D/\lambda = 20$ as assumed in Fig. 4.32, we obtain therefore $r_{min} = 0.1N$ (see also [1343]).

The sound-field dimensions of a section perpendicular to the axis can only be formulated at the focus. As with the plane radiator it is given by a Bessel function:

$$p = p_{max} \left| \frac{2J(X)}{X} \right| \tag{4.29}$$

where

$$X = \pi D q / \lambda z_f$$

and q is the distance from the axis. z_f and p_{max} have to be calculated from formula (4.26).

A plane radiator focussed by an added lens is a design usually used within a liquid and since the sound velocity of the lens material is higher than of the liquid the lens must be plano-concave, with the concave surface having a radius r.

The sound field in this case is similar to that of a concave radiator. The axial pressure according to [1332 and 1349] is given by the relationships

$$p = p_0 \frac{2}{1 - \dfrac{z}{z_0}} \sin\left[\frac{\pi}{\lambda} \left(\sqrt{(z-h)^2 + \frac{D^2}{4}} - \left(z - \frac{c_2}{c_1} h\right) \right) \right]$$

where $\tag{4.30}$

$$h = r - \sqrt{r^2 - \frac{D^2}{4}} \,, \qquad z_0 = \frac{h^2[1 - (c_2/c_1)^2] + a^2}{2h[1 - (c_2/c_1)]}$$

and the velocities c_1 and c_2 are those corresponding to the lens and the liquid respectively.

Figure 4.33 gives the curve for the case $D = 10\,\text{mm}$, $r = 33\,\text{mm}$, $\lambda = 0.5\,\text{mm}$, the same values as in Fig. 4.31.

The focal distance is somewhat greater than that in Fig. 4.31. A lens has not the same focussing effect as a curved radiator with the same radius, but the focal distance is much shorter than the geometrically calculated one $z = r/(1 - c_2/c_1)$ in accordance with Eq. (3.6).

The sound-pressure distribution across the axis at the focus is also given by Eq. (4.29), but now the focal distance and the sound-pressure maximum have to be calculated by Eq. (4.30).
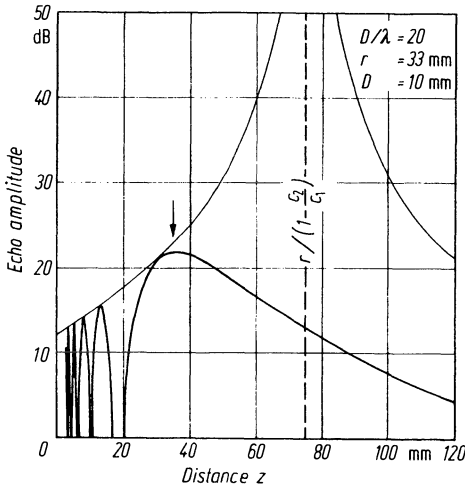
Fig. 4.33. Echo height of a point reflector on the axis of a plane radiator focussed by a lens of Perspex in water
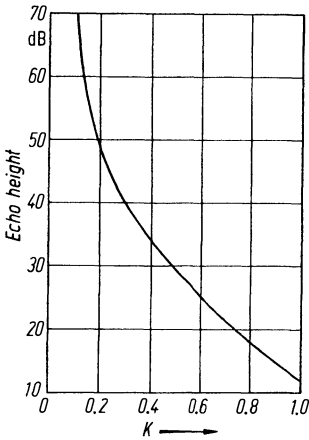
Fig. 4.34. Echo height of a point reflector at the focus of a circular-disc radiator, relative to the average value in front of a plane radiator as function of the focussing factor K, calculated for $D/\lambda = 20$, but also still valid for $D/\lambda = 10$ as long as $K > 0.2$

Example. A plane radiator of diameter $D = 10$ mm, $\lambda = 0.5$ mm, ($N = 50$ mm) is to have its natural sensitivity improved by spherical shaping. The spherical radius must be evaluated for a reduction of focal distance to 25 mm. At this distance $K = 0.5$ and according to Fig. 4.34 the sensitivity improvement is 30 dB. The corresponding radius of curvature must be calculated from Eq. (4.26) by iterative approximation, (by using a computer) the result being $r \approx 33$ mm, which value is also used in Fig. 4.31.

The sensitivity improvement of 30 dB is compared with the echo height immediately in front of the plane radiator so that compared to the natural focus distance (N) where the pressure is $2p_0$ (i.e. an echo 12 dB greater than p_0), we have a nett gain therefore of $30 - 12 = 18$ dB which means an echo-height increase of $8\times$.

The sensitivity of the plane radiator can be improved more simply by using a plano-concave lens of radius 33 mm as a focussing device. Equation (4.30) has been plotted in Fig. 4.33 for this lens curvature and from it the new focal distance f is 35 mm, with a corresponding K value of $35/50 = 0.7$. For these conditions Fig. 4.34 indicates a gain figure of 22 dB, the nett increase being only $22 - 12 = 10$ dB, an echo improvement, by this method, of only $3\times$. Regarding the full theory of focussed circular radiators see [1332, 1337, 1339].
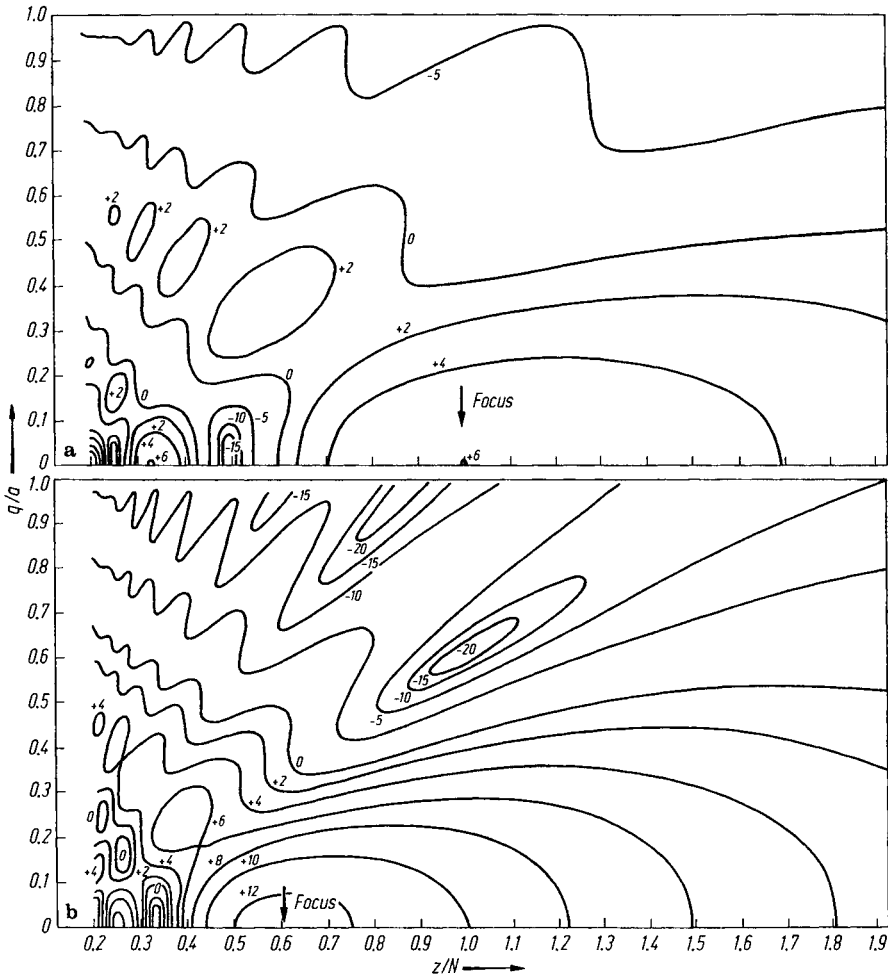
Fig. 4.35. Isobars relating to an axial section. **a** for a plane circular non-focussed radiator; **b** for the same but with spherical curvature giving $K = 0.6$, cf. [222]

The whole sound field of a focussed oscillator compared with a non-focussed one of equal diameter is shown in Fig. 4.35.

To summarize, the following general rules should be kept in mind:

— By geometrical means a plane radiator can be focussed only to distances shorter than its near-field length;

— The complete near-field of the plane radiator is effectively compressed by the focussing into the space between the radiator and the new focus;

— The far-field is also compressed into a range lying nearer to the new focus;

— In the far-field range, beyond the focus, there may also appear some new zones of interference as in the near-field;
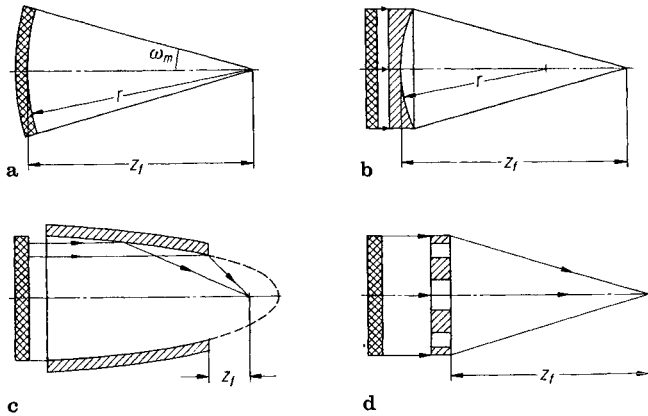
Fig. 4.36. Focussing techniques. **a** Spherically curved radiator; **b** plane radiator with plane-concave lens; **c** plane radiator with hollow mirror; **d** plane radiator with phase plate
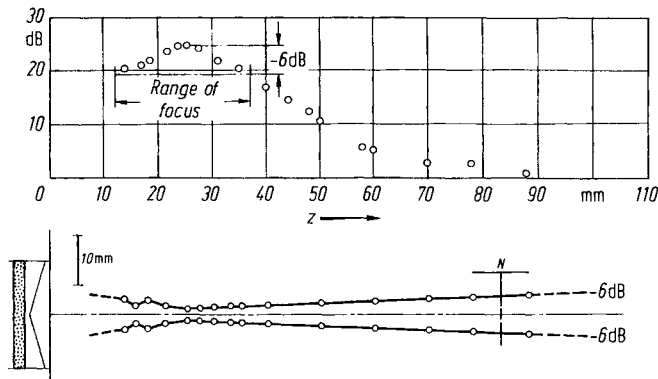
Fig. 4.37. Focussing radiator with cone-shaped lens [1149], $K \approx 0.3$, smallest beam width 2.3 mm, angle of divergence 1.8° measured in steel

— The smallest beam width which can be achieved by focussing depends on the ratio D/λ. For equal size radiators therefore the focussed beam width is proportional to the wavelength.

Figure 4.36 and 4.37 show some possibilities of focussing the field of piezo-electric circular radiators. The examples in Fig. 4.36 are mainly designed for immersion testing, but may be used also for contact in combination with special adaptors. That in Fig. 4.37 may be used for both methods the lens having a conical shape. By this method the focus is less sharp but has a longer axial range (see also Section 10.4). This lens is made from a combination of aluminium and Perspex, but it may also be of a combination of two plastics, for example polystyrene and Perspex.

The principle of the "axicon" has also been used, that is a combination of annular oscillators of a conical shape combined with a concentric conical mirror, cf. [1099].

Focussing of a beam may also be needed in only one plane through the axis so that the radiator may then have a concave cylindrical shape or may be focussed by a cylindrical lens. In both these cases it is preferable to use rectangular radiators cf. [696].

For information regarding focussed ultrasonic fields se also [1332, 574, 130, 1182, 936, 1580]. For Schlieren optical photographic pictures see [470]. For the transformation of the circular-disc field see [1332, 222, 362, 673]. For more examples of the design of focussed ultrasonic probes for the testing of materials see [1343, 1345, 1349]. See further [1343, 417, 1663, 1279], for focussing in one plane only [696].

4.8* Sound Fields with Pulse Excitation and Non-uniform Excitation of the Oscillator

We have already seen that there are considerable differences in the sound fields generated by long oscillations or by pulses. Figure 4.38 shows short pulses originating from different points of a radiator and these may be unable to interfere at the observation point.

Even if two pulses overlap each other with a path difference of one half-wavelength (Fig. 4.39) they are not cancelled completely and hence the sound fields of
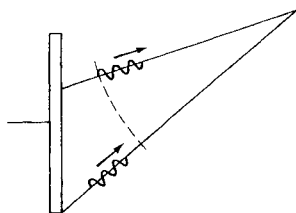
Fig. 4.38. Short pulses may be unable to interfere
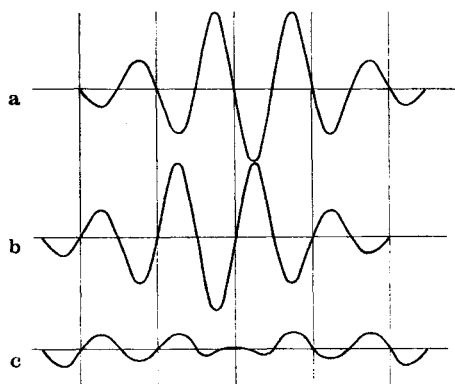
Fig. 4.39. Short pulses cannot completely cancel each other even with a half-wavelength transit path difference

Continous
oscillation
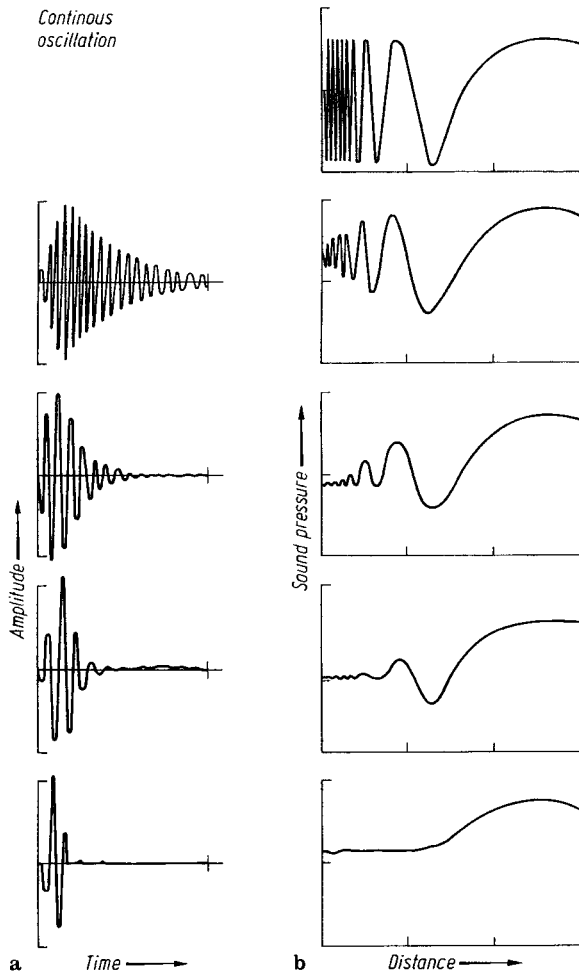
Fig. 4.40. Sound pressure on the axis of a plane circular-disc radiator excited by different pulse shapes [1424]

pulsed radiators have many less fluctuations than have been described above. There are no real zero points and the maxima are smaller.

Figure 4.40 shows, for example, the sound pressure on the axis corresponding to different pulse lengths. In the near-field the differences are substantial but not in the far-field. As well as the changes on the axis for very short pulses the maxima and minima off the axis, as well the side lobes in the directivity diagram, also disappear. Some focussing methods are also influenced if they depend on wave interference. Even when focussing is carried out with curved radiators, when the single wavelets at the focus point are added up without transit time differences, the field away from the focus is changed appreciably (cf. Fig. 4.41).
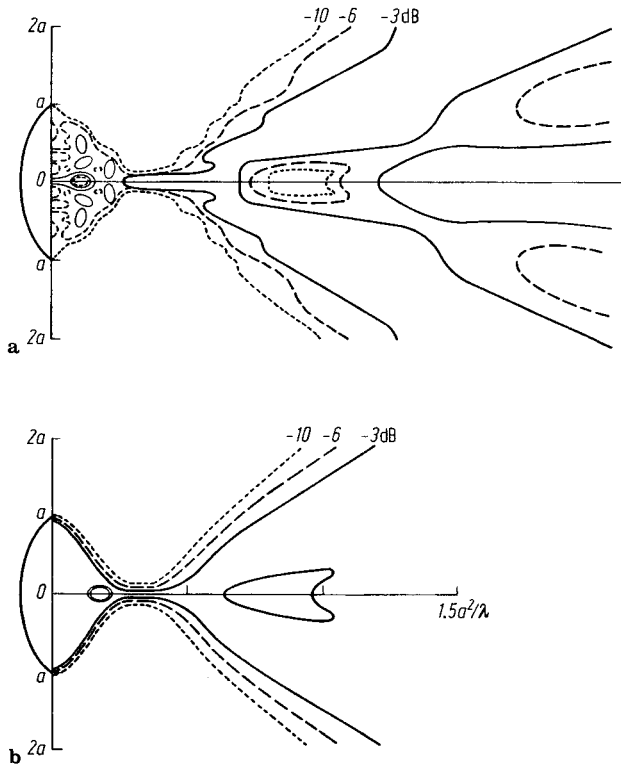
Fig. 4.41. Sound field of a focussed radiator of $D/\lambda = 20$ according to [1611]. a continuous excitation; b excitation by a pulse of two oscillations only

The following general rules should be kept in mind:

— The pulse length does not affect the far-field and the main lobe very much;
— Only pulses of less than six oscillations have a substantial influence on the sound field;
— When there is appreciable material absorption, which is usually greater for higher frequencies, we get pulse prolongation especially at longer transit paths;
— When using focussing lenses unwanted pulse distortion may also take place.

See further the literature [114, 468, 611, 697, 733, 1020, 1462, 1610, 1643, 226, 1274, 1469, 1126, 892, 410, 629, 1598, 1623].

Up to now we have assumed that the whole surface of the radiator is oscillating at the same amplitude, but an oscillator mechanically fixed at its edges will have vibrations of reduced amplitude at that point. Furthermore even a freely oscillating piezo-electric plate excited by an electric field between electrodes on its surfaces, also has less excitation at the edges because here the strength of the electric field is reduced. If a probe has only partial contact with the specimen, for example on a
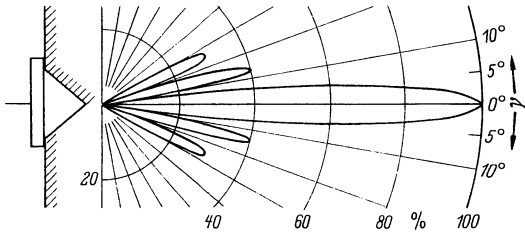
Fig. 4.42. Directivity of an oscillator with $D/\lambda = 16$, but with contact, or oscillation, reduced to an annular zone

curved surface, or when placed in a concentric position over a hole as in Fig. 4.42, the effect on the sound field is the same as that achieved with only partial excitation. The side lobes become more pronounced and the pressure on the axis in the far-field is reduced in proportion to the reduced excitation area.

The near-field length of a radiator which is only excited on a portion of its surface is not affected so long as the edge is allowed to oscillate at full amplitude as for example in Fig. 4.42. If the excitation is reduced progressively from the centre to the edge, then the near-field length is reduced and it is necessary to calculate with a smaller diameter, viz. the effective diameter of the disc, D_{eff}.

Non-uniform excitation is often intentionally used for probe design so as to smooth out variations in the near-field and maintain the directivity in the far-field. To keep the directivity axial all such methods have to be circularly symmetrical. Figure 4.43 shows how the directivity and the axial sound pressure varies if the excitation of the disc from the centre to the edge is varied according to different mathematical functions.

The first example is the *δ-function*, which has the unit value at only one point, here in the centre of the plate, at $\varrho = 0$. This represents the well-known point-source, but in practical terms it is not useful at all. The second example is the uniform excitation over the whole plate, which gives the well-known directivity and pressure functions as shown in Figs. 4.19 and 4.21.

The optimal results are given by the *Gauss-function*, as shown in Fig. 4.44, (curve *b*), as a comparison with the quasi-uniform excitation with edge effect (curve *a*). The advantage may be seen from the axial pressure curve, which has no longer any maxima and minima [850].

The Gauss function is given by

$$e^{-\varrho^2/R_0^2}$$

where ϱ is the radius coordinate as in Fig. 4.43 and R_0 is a particular radius smaller than the physical radius of the disc. The greater the actual radius the better is the uniformity of the near-field and the directivity. In practice an increase of 50 % is ample.
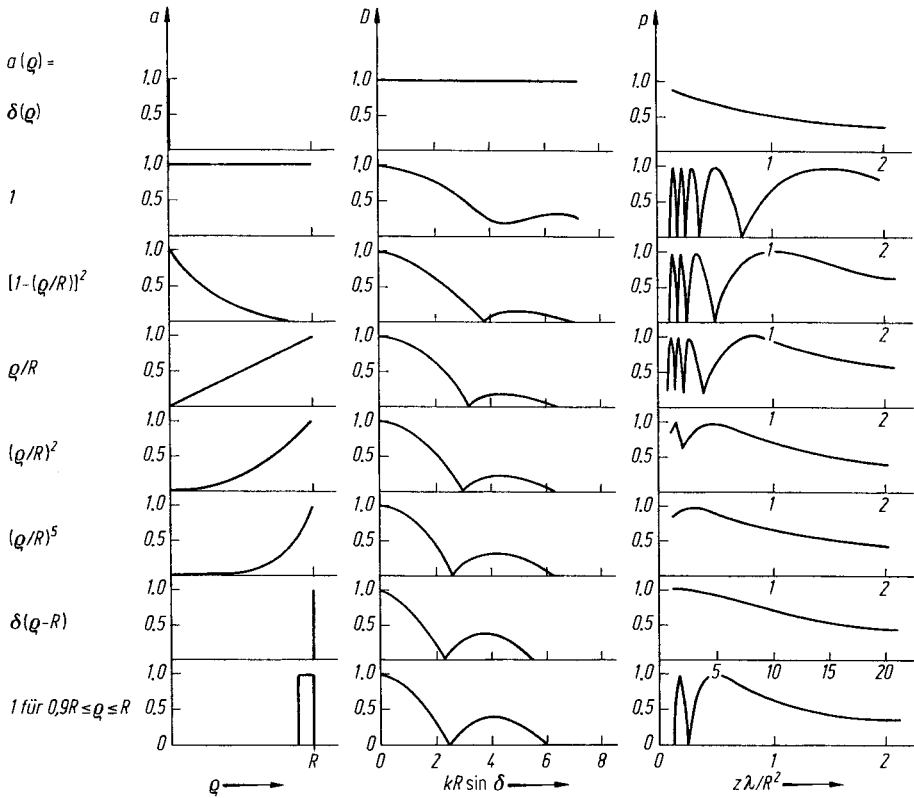
Fig. 4.43. Directivity and axial sound pressure of a circular piston oscillator with different excitation functions over the distance from the centrepoint, ϱ. Radius of the oscillator $= R$ and $k = 2\pi/\lambda$. The so-called "delta Function" $\delta(\varrho)$ (first example) has the value one at $\varrho = 0$, and everywhere else the value zero
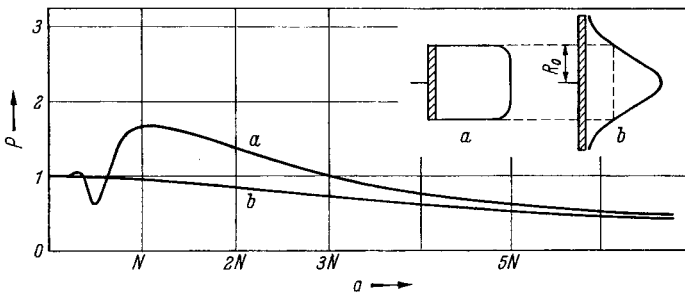
Fig. 4.44. Axial sound pressure of a circular-piston oscillator with two different distributions of the excitation voltage. Type a) Overall excitation by a uniform electric field but reduced at the edge by leaking field lines. This gives a sound pressure curve a with reduced fluctuations. Type b) Excitation in the form of a Gauss function applied over a larger diameter $R > R_0$, which completely suppresses variations in the sound pressure b, [852], [620]

According to [620] the near-field length has now to be calculated as

$$N_{\text{Gauss}} = \frac{R_0^2}{\lambda}.$$

Hence R_0 is the equivalent radius of the Gauss-oscillator.

For practical materials testing the Gauss-probe has one disadvantage. Since the radius is larger than that of an ordinary probe with the same near-field length and far-field sensitivity, the larger contact area required may not be found in all cases.

After these more theoretical principles some methods for the practical manufacture of probes having non-uniform excitation patterns can be mentioned:

— Some regions of the piezo-electric plate can be depolarized by local heating beyond the Curie temperature;
— By subdividing the electrode into several portions for each of which the exciting voltages are different;
— By using electrodes covering only a part of the surface, for example in form of a star.

In the last case the star-shape can be calculated to give a total circumferential dimension at each radial distance corresponding to the reduced voltage compared to the center as required by the Gauss-function. The Gauss-oscillator may also improve the sound field of focussed probes. Its theory is discussed in full in [444].

In addition natural focussing of the field can be improved by appropriate distribution of the exciting voltage. According to [821] the best focussing, without using geometrical methods, is obtained by exciting the edge only in the so-called *annular oscillator.*

As already mentioned the field is always further equalized by using short excitation pulses. The shape of the piston oscillator if it deviates from the circular form also helps in this respect, for example by using square, rectangular, elliptical or even fully irregular shapes. The circular form excited by long pulses is the most unfavourable combination for suppressing the variations in the field. See also [574, 611, 308, 612, 1424, 252, 444, 1291, 1602, 705, 708, 1565, 324, 696, 1529].

5 Echo from and Shadow of an Obstacle in the Sound Field

5.1 Reflection of a Plane Wave by a Plane Reflector

The problems of material testing by ultrasonics can be illustrated qualitatively by an optical experiment.

We can imagine a darkened room having mirror-like walls and to represent defects there are suspended objects made from crumpled aluminium foil. An observer must find these objects by using a sharply defined search-light beam and must evaluate their size from any optical reflections received. Reflections from a wall will only be seen if the incident angle of the search-light beam produces a reflection directed towards the eye of the observer. However, some faint impressions of the walls will also be noticed if the mirrors are dusty or of a rough texture. The "defects" show themselves by the many individual and faint reflections from those small areas of the foil which are just orientated correctly for a good reflection. These will, however, change very quickly according to the geometrical positions of both the search-light and the eye. A suspended small plane mirror will be visible only very rarely if by accident it has the right position, and in this case it will give a rather strong reflection. In other positions, however, the observer may receive only faint scattered indications from its edges.

This illustrative comparison is of course never fully satisfactory because of the large difference between the wavelengths. Nevertheless it does show the difficulties and illustrates that we have to make use of two different types of reflection, the rather rare mirror-like reflection and the indications caused by scattering or diffraction.

We can understand the mathematical method of calculating a reflection with the aid of the Huygens' wavelets (Fig. 5.1). The excitation of a small surface ele-
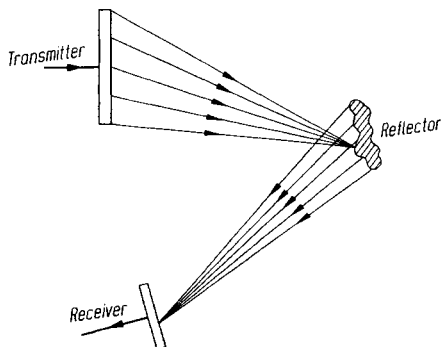
Fig. 5.1. Adding up Huygens' wavelets on the surface of the reflector and the receiver

ment of the reflector is the sum of the effects of all incident wavelets originating from all points of the transmitter and in the ultrasonics case they have to be added up taking account of both amplitude and phase.

If we have thus calculated the excitation of all surface elements of the reflector, we must then do the same for all the surface elements of the receiver which is being excited by the wavelets received from the reflector.

If we consider a piezo-electric receiver (see Section 7), we know that the received sound pressure generates a proportional electric charge and therefore to obtain the total echo charge, we must add up all the individual charges of the surface elements again taking into account both amplitude and phase. The resulting charge is proportional to the average of the sound pressure received.

In mathematical language this means that the echo voltage is proportional to the triple integral of the wavelet $ae^{i\varphi}$ (amplitude and phase) over all area elements ds of the transmitter T, the reflector R, and the receiver E

$$\int_T \int_R \int_E ae^{i\varphi}\, ds.$$

This integral can of course only be solved if all three surfaces can be described by mathematical formulae and cannot be evaluated for the random shape of the reflector. Furthermore it would only be correct if no mode changing has taken place and therefore is only true for longitudinal waves in liquids and gases.

In simple cases one may use graphical methods as in Section 4.2. In a very simple case, however, (Fig. 5.2) we can see the result immediately. The obstacle is a totally reflecting plane disc situated in the path of a much larger plane wave produced by a large plane transmitter. The surface areas can be identified as S_R and S_T respectively. When the transmitted beam strikes the reflector perpendicularly it also emits a plane wave which returns perpendicularly to the transmitter. Because all surface points of the obstacle lie on the same wave front they have the same phase and therefore we can add the amplitudes only, without regard to the phase. The reflected wave is therefore identical to the wave emitted from a piston oscillator of the same size and shape so that we may consider the reflector as a secondary oscillator.

For a circular disc-shaped reflector we know the properties of its sound field from Section 4.1, with the near-field according to Eq. (4.2) and the directivity as shown in Fig. 4.15 a.

In practice the transmitter usually also acts as a receiver when we use pulse excitation. After having sent out the transmitted pulse it receives the echo, after a de-
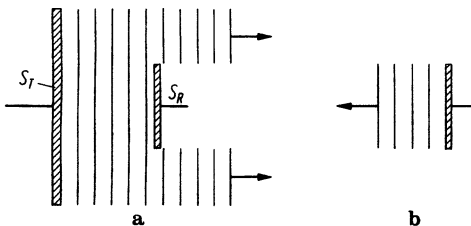
Fig. 5.2. Plane reflector in a plane wave (a) and the reflected plane wave shown separately (b)

lay corresponding to the transit time for the pulse to travel to the reflector and back, and we wish to know the amplitude of the echo received. In Section 7.2 we will see that the voltage generated by a perpendicularly incident plane wave is proportional to its sound-pressure amplitude and to that part of the surface of the receiver struck by the wave. If as in Fig. 5.2 a the wave is reflected by a very large wall, the whole emitted wave is returned without loss, and we can call the corresponding echo height H_0. The limited reflector in Fig. 5.2 b receives only a part of the wave and generates smaller echo voltage H_r and we can see that both echoes are in the proportions of their areas

$$H_r/H_0 = S_R/S_T. \tag{5.1}$$

The echo H_0 is an important reference echo, of which we will frequently make use, and in practice it is generated as the back-wall echo of a plane parallel-sided and smooth plate made of the same material as the specimen in which defect echoes are to be evaluated.

The area of the transmitter S_T in Eq. (5.1) is known and if we can measure the ratio of a reflected echo to the reference echo (usually by way of the signal amplitudes on a cathode-ray tube), we can find the reflector area S_R from this equation. This is the solution of our task.

We may even neglect the condition that transmitter and reflector are of circular shape as long as the transmitted waves can still be considered as plane, otherwise the size of the reflector is under-estimated. Amendments to the method for non-planar waves, for larger distances and for small reflectors follow below (Section 5.3).

At this point we will consider a non-parallel position of the reflector, but without considering any mode change, or the edge waves as described in Section 2.6. In Fig. 5.3 the leading wave front (1) has just reached the distant edge of a plane reflector lying in an oblique position. The corresponding Huygens' wavelet is just being generated and together with the wavelets generated earlier a new wave front is built up and forms the reflected plane wave. Of course no echo signal is produced if the reflected wave fails to strike the transmitter/receiver but in Fig. 5.4 it does reach the receiver and it is often erroneously assumed that an echo can therefore be expected. However, because the surface elements of the receiver are excited at differ-
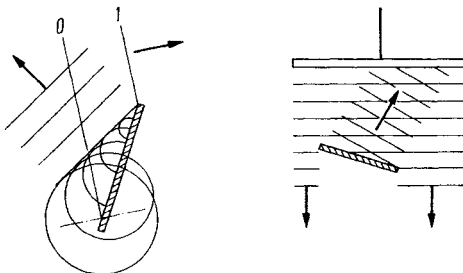
Fig. 5.3. Obliquely reflected wave constructed from the Huygens' wavelets

Fig. 5.4. An obliquely incident reflected wave, because of destructive interference in the piezo-electric partial voltages, generates no echo from which the reflector size can be evaluated

ent phase angles in consequence of the varying transit paths of the wavelets the generated voltages cancel each other and no echo is received except for any diffracted echoes from the edges of the reflector.

In the case of Fig. 5.4 when using short pulses the partial voltages do not cancel each other completely and therefore some sort of echo is obtained in spite of the oblique orientation. However, it is not possible to use this and the edgewave echoes, to evaluate the size of the reflector in the simple way described above.

A way of solving this problem could be to divide the receiver into separated elements, the voltages of which would be added up after applying artificial phase shifts. The directivity of such a "phased array" (see Section 10.4) can be altered by appropriate regular phase shifting so that obliquely incident echoes could also be received efficiently. For other means to make the receiver insensitive to unwanted phase differences see [654].

5.2 Echo of a Reflector, DGS Diagram

The solution of our problem of assessing the area of a reflector from measurement of its echo was straight-foward in the case of the geometry in Fig. 5.2, because both amplitude and phase were constant on the surfaces of transmitter, reflector and receiver. We have approximately the same conditions when there is a large distance between transmitter and reflector as long as they are both planar. Figure 5.5 shows the sound-pressure distribution on the common axis of transmitter/receiver and reflector.

The upper curve is already known to us from Fig. 4.19, but smoothed out as in Fig. 4.44a. At the arbitrarily chosen distance of three near-field lengths ($3N_t$) the reflector acts as a secondary radiator with its own near-field length N_r. Strictly speaking the sound-pressure curve for the transmitter is only valid on the axis, but at large distances it can also be assumed to be almost uniform over the area of a small reflector. So in this case the reflector also acts as a piston oscillator and we
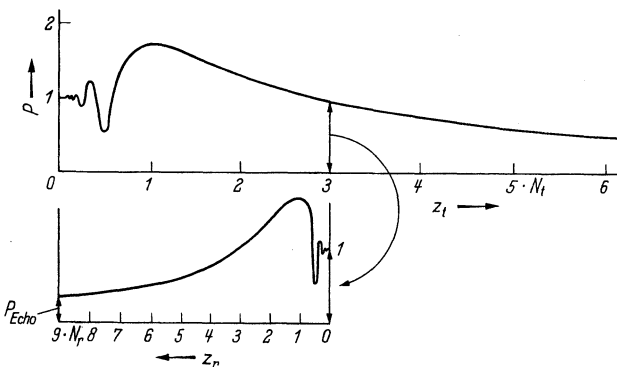
Fig. 5.5. Sound pressure on axis (schematic) for the incident wave (top) and the wave reflected from a reflector in form a circular disc (bottom)

can assume that its axial sound pressure is represented by the lower curve, but travelling from right to left.

For the receiver we may also assume the amplitude and phase of the reflected wave is approximately constant over its surface because of the small path differences which apply between its centre and edge for the large distances between it and the transmitter/receiver.

We can now calculate the reflector area, or its diameter D_r. According to Eq. (4.13) we know that the sound pressure of the transmitter on the axis is

$$p_t = p_0 \frac{\pi D_t^2}{4\lambda z_t} \tag{5.2}$$

and it is also approximately the initial sound pressure on the reflector radiator, p_{0r}. Thus the resulting sound pressure over the whole area of the transmitter/receiver will be

$$p_r = p_{0r} \frac{\pi D_r^2}{4\lambda z_r} = p_0 \frac{\pi^2 D_t^2 D_r^2}{16 \lambda^2 z^2} \tag{5.3}$$

where the distances z_t and z_r are equal and are called z.

The initial sound pressure p_0 of the transmitter can be measured as in Fig. 5.2 with a very large reflector, for example from the back wall of a flat plate, and if we measure the height of this reference echo, as well as the echo of our defect-reflector, (in mm) from the cathode-ray tube screen, we obtain

$$H_r/H_0 = p_r/p_0$$

From this relationship and Eq. (5.3) we can find the reflector diameter as:

$$D_r = \frac{4\lambda z}{\pi D_t} \sqrt{H_r/H_0}$$

or by introducing the transmitter near-field length $N = D_t^2/4\lambda$

$$D_r = \frac{D_t z}{\pi N} \sqrt{H_r/H_0} \ . \tag{5.4}$$

This final relationship is the solution we seek since the diameter and near field length of the transmitter, as well as the distance z of the reflector, are all known.

As already mentioned the reference echo height H_0 is measured as the back-wall echo from a flat plate, having a thickness which is small compared with the near-field length. The back-wall echo must of course not be affected by any defects and the surface quality of the reference plate must closely correspond to that of the surface of the test specimen, so avoiding coupling differences. If the material under test attenuates the ultrasound its attenuation factor (cf. Chapter 6) must be measured and can be taken into account by calculation.

Having found the solution for a small reflector at a short distance (Eq. 5.1) as well as for a small reflector at a large distance (Eq. 5.4) by referring the reflected echoes to the reference echo of a thin plate, it is easy to determine the solution for a large reflector at a large distance such as the back-wall echo for a plane parallel specimen.

According to Eq. (4.13) at a large distance from any source the sound field is equivalent to that from a point source and closely approximate to the spherical wave form, so that its amplitude diminishes inversely with distance. If the beam falls perpendicularly onto a large plane reflector at a distance z_R it is specularly reflected so that the transmitter/receiver acts as a receiver in its own original sound field at a distance $2z_R$. It receives therefore the sound pressure

$$p_R = p_0 \frac{\pi N}{2 z_R}$$

on the axis and assuming as before that the central sound pressure is valid for the whole area of the receiver, we obtain

$$\frac{H_R}{H_0} = \frac{\pi N}{2 z_R}. \tag{5.5}$$

It must be stressed that the reflection from a small reflector is fundamentally different from that of a large reflector, the latter being a mirror-like process whereas the small reflector behaves in accordance with the rules of wave physics. This is to be seen most clearly from the different distance laws for the sound pressures in which the back-wall echo diminishes inversely with distance and the defect echo with the square of the distance.

When using Eq. (5.5) we may incidentally use the specimen back-wall echo rather than that from a reference plate, but in practice this method is attractive only if the test specimen includes a region without any disturbing flaws and has a large plane back-wall.
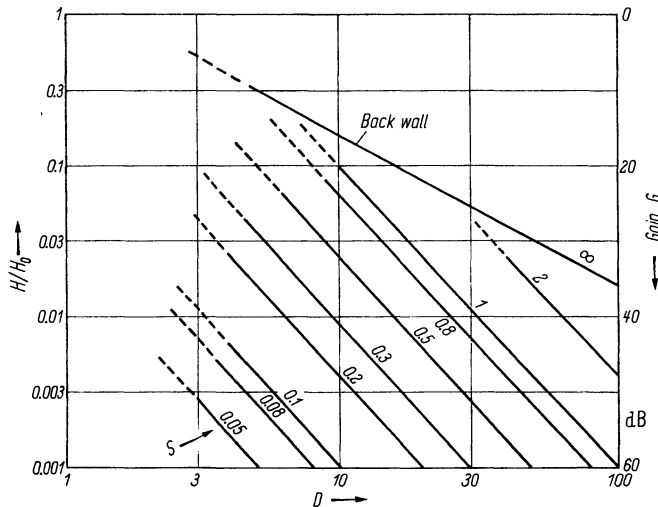
Fig. 5.6. Relation between the distance of a reflector D (measured in terms of the near-field length); relative height of the echo H/H_0 (left-hand scale) or gain G in dB (right-hand scale); and the size of a reflector S (expressed as a fraction of the diameter of the transmitter D_t). (DGS diagram for the far-field)

Up to now we have dealt with situations where extreme conditions for the reflector size and distance apply. The intermediate regions for both size and distance can only be calculated by using higher mathematics. However, for all practical purposes it turns out that this region can be covered with relatively small errors by approaching it from each side. This has been done in Figs. 5.6 and 5.7.

To achieve the most general presentation we can normalize in terms of the basic transmitter characteristics as follows; N = near zone length; H_0 = back-wall echo: D_t = transmitter diameter and thence:

$$\frac{z}{N} = \text{distance of reflector } D,$$

$$\frac{H}{H_0} = \text{amplifier gain } G,$$

$$\frac{D_r}{D_t} = \text{reflector size } S.$$

All the normalized values D, G and S are dimensionless quantities and the gain G represents the ratio by which the reflector echo has to be amplified to make it equal to the reference echo. Introducing D, G and S into the Eqs. (5.4) and (5.5) we obtain for the distant field

$$G_r = \pi \frac{s^2}{D^2} \quad \text{(small reflector)},$$

$$G_R = \pi \frac{1}{2D} \quad \text{(back wall)}. \tag{5.6}$$
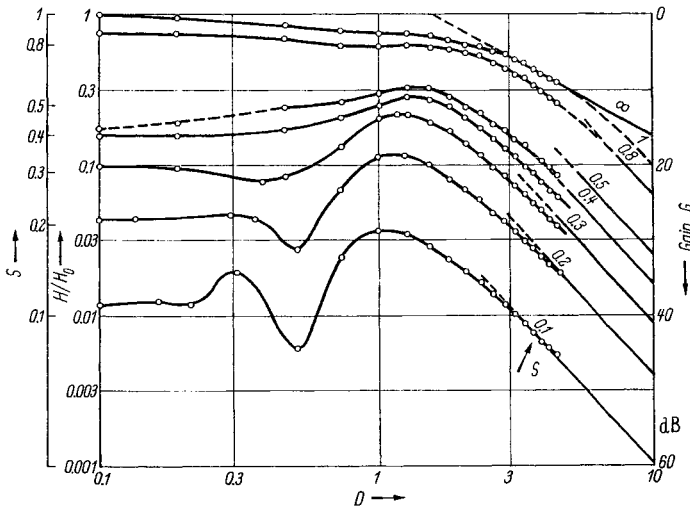
Fig. 5.7. Complete DGS diagram, as a combination of the theoretical solution for reflectors close to the transmitter, Eq. (5.7), scale for S on the left hand; the theoretical solution for the far-field as in Fig. 5.6; and experimental measurements made in the sound field between. Measurements were made with circular-disc reflectors in water [850, 852]

For the reflector very near to the transmitter we obtain according to Eq. (5.1);

$$G_r = S^2 \quad \text{(for } D_r < D_t)$$

$$\text{and} \qquad G_r = 1 \quad \text{(for } D_r \geqq D_t) \,.$$

(5.7)

For a graphical representation of these relationships (Fig. 5.6) logarithmic coordinates are most suited, the gain G being expressed in decibels.

Figure 5.7 is the so-called *general DGS diagram*, where the theoretical solutions for the reflector echoes coming from small distances, and large distances respectively have been linked by echo measurements as in [850, 852]. We see that, for small reflector sizes in the range $S = 0.1$ to 0.3, the experimental echo values fit quite well to both theoretical solutions, derived for the extremes of distance. In the medium size range, for $S \approx 0.5$, differences have been larger but again fit very well for larger reflector sizes and for the back-wall echo. The differences found in the practical tests are towards smaller reflector sizes; that is a reflector or defect in this range is usually measured as too small. In practice this means that it is advantageous to measure a reflector using lower frequencies and with larger transmitters, because then the S value will be smaller and the distance D will be further into the far-field. This is also preferable since the local fluctuations in the near-field depend quite sensitively on the pulse length and the transmitter design. In the intermediate range therefore the general DGS diagram can only give approximate results but for a particular transmitter design a *special DGS diagram* can of course be established by experiment.

We have already seen that the oscillations of the near-field sound pressure more or less disappear when using very short pulses and also when the transmitter is excited in a non-uniform manner over its surface. According to Fig. 4.44b excitation using a Gauss function distribution eliminates all fluctuations in the near-field. In this case the DGS diagram can be fully calculated and differs from Fig. 5.7 especially in the intermediate range cf. [852]. In this case, however, the reflector diameter has to be expressed in terms of the effective diameter of the transmitter which is $2R_0$ and is thus smaller than the actual physical diameter.

In practice special DGS diagrams have found more application since they are determined for an individual transducer, and give directly size and distance values in milimetres. These are usually available from the transducer manufacturers.

DGS diagrams have also been established for transverse waves when used with so-called angle probes, cf. Chapters 19 and 20.

The elementary theory of the reflection of a longitudinal wave by an obstacle does not take into account that this process in solid materials is always accompanied by a partial mode change into transverse waves. In practice when the reflectors are large compared with the wavelength the amount of transverse-wave energy is very small, but with small reflectors the scattered waves of each type have comparable amplitudes but quite different directivities, see Fig. 5.8 according to Harumi [519].

With decreasing diameters the small side lobes disappear for both types, the longitudinal echo approaching a spherical shape whereas the transverse wave exhibits two distinct side lobes. From the angle of these lobes to the axis the diameter of the reflector can be evaluated.
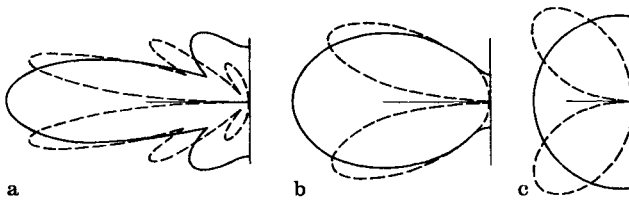
Fig. 5.8. Scattered longitudinal (full lines) and transverse (dotted lines) waves from a small circular-disc reflector in a longitudinal wave field. **a** Diameter 2λ; **b** λ; **c** $\lambda/2$

The sound pressure of the scattered wave according to [441] is directly proportional to the third power of the reflector diameter and inversely to the square of the wavelength. Therefore very small reflectors cannot in practice be detected with certainty even by using more sensitivity and higher frequencies.

For the evaluation of natural defects it is of interest to know how far their shape differs from a circular-disc reflector. Some information can be obtained from measurements at two different frequencies: Eq. (5.3) gives for the frequencies f_1 and f_2 the ratio of the echo amplitudes

$$H_1/H_2 = f_1^2/f_2^2$$

for equal reference echoes from the calibration plate. If this relationship turns out to be fairly exactly satisfied, we can conclude that the shape of the natural defect does not differ too much from a flat disc lying perpendicular to the beam. Also when using the DGS diagram a flat disc-like defect should appear to be nearly of the same size S for two separate probes differing in frequency and/or size.

We mentioned above that the intermediate range of the DGS diagram cannot be fully calculated by simple mathematics but the full calculation has been done by Mundry and Wüstenberg [1086], and in [224]. The exact back-wall echo in this range has been calculated by Seki, Granato and Truell [1398] and special DGS diagrams for normal and angle probes (for both longitudinal and transverse waves) have been calculated by Kimura et al [785], see also [S 78].

Standard reflector shapes other than circular discs. It is of great interest to know the reflection characteristics of those reflector shapes which can be readily made for experimental work in an easy and reproducible manner. examples being spheres, cylinders and strips. The following table gives details of the dependence of the echo height on the diameter or width, d, the distance z and the wavelength λ according to [276].

Reflector surface	Dimensions at right angles to the beam		
	small/small	large/small	large/large
flat	circular disc $d^2/(\lambda^2 z^2)$	strip $d/(\lambda^{3/2} z^{3/2})$	back-wall $1/(\lambda z)$
curved	sphere $d/(\lambda z^2)$	cylinder $\sqrt{d}/(\lambda z^{3/2})$	

The cylindrical borehole is much favored as a reference reflector because it is easily and reproducibly made. Its bore diameter d_{cyl} can easily be related to the equivalent circular disc diameter d_{disc} by:

$$d_{disc} = 0.67 \sqrt{\lambda \sqrt{d_{cyl}z}}$$

which is valid as long as $z > 0.7N$ and $d_{cyl} > 1.5\lambda$. For other reflectors see also [S 47].

As well as making measurements using such artifical defects with longitudinal and transverse wave, Rayleigh and plate wave measurements have been made on saw cuts.

Strictly speaking DGS diagrams may be established for any wave mode and for any type of reference defect, but it should be kept in mind that they will never have a general validity for all probes regardless of their diameter and frequency, and of the distance of the reflector. Only for cylindrical reflectors perpendicular to the beam axis can such a normalized generalisation, within certain limits, be made, cf. [1346]. For further information on DGS diagrams see [405, 408, 1657, 1525, 856, 409, 1427, 1692].

5.3 Shadow of a Reflector

The propagation of a wave is not only disturbed by an obstacle in producing a reflected wave, but also in its shadow. Because we are usually dealing with defects not much larger than the wavelength, we have to expect diffraction phenomena in the shadow too.

To calculate the disturbed sound field behind the reflector we can consider the following propositions. The shadow field will be built up from the undisturbed original field and from interference by a disturbing wave propagating from the rear of the reflector. In the case of a flat, circular, thin disc the characteristics of the interfering wave are easily recognised because the overall excitation on the rear wall must be zero. In this area of full shadow therefore the undisturbed wave and the interfering wave must cancel each other completely. Thus the interfering wave must have the amplitude of the primary wave over the whole reflector area, but with the opposite phase, so that it is in fact the well-known piston oscillator wave of Fig. 4.19 travelling in the same direction as and coaxial with the primary wave. As examples
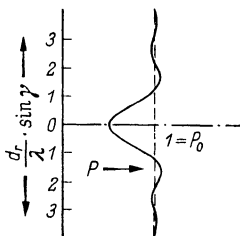
Fig. 5.9. Sound-pressure directivity behind a reflector placed at a distance of six near-field lengths (compare with Fig. 4.21)
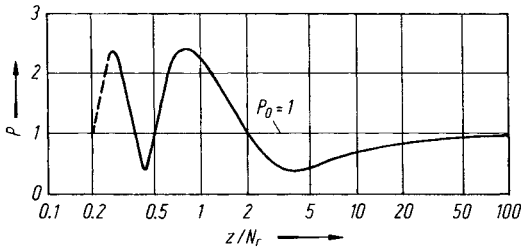
Fig. 5.10. Sound-pressure amplitude in the shadow field along the axis of a circular disc

Figs. 5.9 and 5.10 show respectively the resultant sound pressure directivity, and the pressure amplitude, along the axis, calculated on the assumption that the primary field is a plane wave or in the very distant far-field of a transmitter.

Both figures show the pressure values as they would be measured by a very small microphone but in practice we have to use receivers of larger dimensions which average out the pressure values. The final receiver voltage depends therefore on many parameters and the shadow method can only be used for defect sizing with great reservation.

If it is not possible to work with a plane wave, or in the very distant field of a transmitter, the distances and diameters of transmitter and receiver have also to be taken into account thus preventing the establishment of a diagram of general validity, as the DGS diagram is for echo sounding. It is already clear from Figs. 5.9 and 5.10 that the pressure amplitude in the shadow region may be higher than the undisturbed value, as a result of wave physics. The practical application of the sound-transmission method, which was the first one used for defect detection and evaluation, can therefore only be recommended for defects large compared with the distances and diameters of the transmitter and receiver.

Figure 5.11 shows measured values in water for the special case in which the disturbed wave is reflected back to the transmitter by a back-wall, so being disturbed a second time on the return journey.

The main handicap in using this method for evaluating defect size is the fact that the position of the defect must be known to apply it so that echo sounding is much more advantageous.
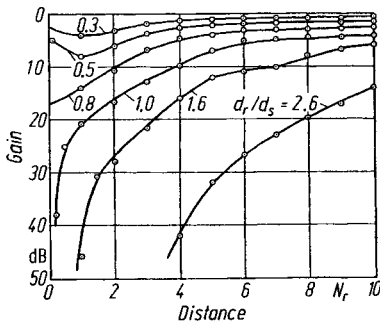
Fig. 5.11. Decrease of the back-wall echo by obstacles of circular-disc shape in water as function of the position between transmitter and back wall at the distance of ten near-field lengths

5.4 Circular-Disc Reflectors in Oblique Positions and Natural Defects

According to Fig. 5.12 the directions of both the echo and the shadow wave of an obliquely oriented reflector are determined by applying Huygens' principle. This shows a wave front of the incident plane wave which has just reached the more distant edge of the circular disc. Elementary spherical waves have radiated from both the front and the back of the disc forming the echo wave and the shadow wave, respectively. It is clear that the shadow wave must have the same direction as the incident wave, while in the case of the echo wave, as in geometric optics, the angle of reflection equals the angle of incidence.

At moderately oblique orientations of the flaw, the form of both waves does not differ greatly from that produced by a flaw orientated at right angles. In Fig. 5.13 both waves have been calculated for their directivities in an elementary manner, that is without consideration of mode changes or edge waves. We know that an exclusive longitudinal reflected wave appears only at very small incident angles, but the shadow wave is always of the same type as the incident one. For larger angles of incidence, besides the longitudinal reflected wave we also obtain a transverse wave at its own angle (cf. Fig. 2.7) with a sharper directivity in accordance with its shorter wavelength.
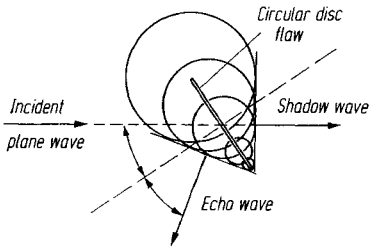
Fig. 5.12. Directions of echo wave and shadow wave of an obliquely oriented flaw plotted according to Huygens' principle
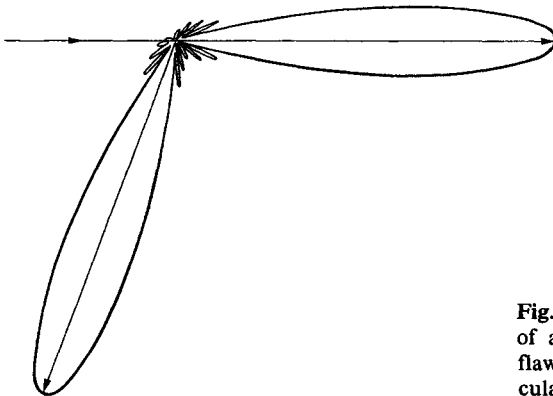
Fig. 5.13. Echo wave and shadow wave of an obliquely oriented circular-disc flaw; directivities of sound pressure calculated for $D/\lambda = 4$

Figure 5.13 has been calculated for a reflector diameter of four wavelengths so that in this case we only receive at the transmitter radiation from the faint side lobes which is in practice blurred and partially hidden by the edge waves. It is therefore just possible to receive an indication of a reflector in this way but no indication of its size.

If the geometry of the specimen allows one can, in this difficult case, consider the influence of the reflector on the back-wall echo but with all the reservations dealt with in Section 5.3.

To be able to evaluate the size of a reflector lying in an unknown position and orientation one would have to use a separate receiver and to vary little by little the positions and directivity angles of both probes until the maximum reflected signal was received. To do this manually would be extremely tedious and difficult, even by an immersion technique. It would perhaps be feasible by using a computer-aided mechanical scanning device.

By using the usual scanning technique, with one transmitter/receiver probe applied at normal incidence one can obtain the best echo possible, but from this it will not be possible to evaluate either the size or the position with accuracy. For the position it is necessary that the directivity axes of both the probe and the reflector coincide. By using a probe with a higher frequency, and hence with a sharper directivity, one can at least try to bring the axes into somewhat better coincidence and from this fact arises the usual recommendation to use lower frequencies in the rapid scanning for defects and subsequently higher ones for localizing them. However, for applying the DGS technique one should keep in mind that the result obtained with a lower frequency probe is likely to be nearer the true size.

In some cases the position of a defect and the geometry of the specimen allow the use of special techniques such as those illustrated in Fig. 5.14. For these so-called *pitch and catch techniques*, when using obliquely incident transverse waves, DGS diagrams have also been established [1350].

In practice, the oblique position of such a flaw does not affect the echo wave as adversely as it might be expected for the following reasons.

Firstly, in the case of short pulses, the secondary lobe region is blurred, giving a more or less even decrease of the sound pressure with the angle.

Secondly, in the case of flaws which are no longer large compared with the wavelength, the angular distributions of the echo wave and the shadow wave can no
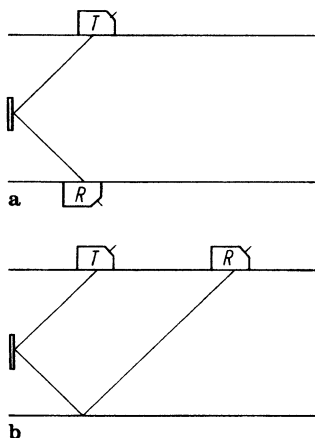
Fig. 5.14. Detection of flaws by oblique transverse waves with separate transmitting and receiving probes. Method b is called a *tandem or pitch and catch* technique

longer be given separately as in Fig. 5.13 but they merge to form a connected, scattered wave. With decreasing ratio of diameter to wavelength this scattered wave becomes more nearly spherical in form (cf. Fig. 5.8) so that finally for small flaws, the influence of the oblique orientation disappears altogether but it should be remembered that the sound pressure also becomes very small and high sensitivities are required to detect them.

For oblique reflectors the edge waves produced are very important since they give, at least, an indication of a defect (Section 2.7). Their amplitude depends on the sharpness of the edges and the angular directivity of the scattered waves. A rounded reflector is much less favorable than one with a sharp edge profile. Of course a transmitter/receiver can only receive waves of the same type as it transmits but there are techniques which use a different type of receiver probe to pick up the scattered wave of the other type (Δ technique: see Section 19.3).

With a regular shaped oblique reflector, such as a disc or a strip, the edge waves scattered from the nearer and the further edges, as seen from the probe, have different transit times and this allows an evaluation of the width or diameter especially when using very short pulses. The amplitude of the edge waves received depend on the length of the edge from which the Huygens' wavelets can combine at the receiver without large phase differences. A reflector with very irregular edges will rarely give useful edge-wave echoes (see Section 19.3).

Natural-defect reflectors differ in several ways from the artificial reflectors used in the theoretical considerations above. Their shapes are not regular nor are their surfaces smooth and plane. Therefore when considering natural defects it is usually not possible to differentiate between the specularly reflected and the scattered waves and they always mutually interfere. This fact explains the fluctuations of echo amplitude arising from small variations of the probe position.

Natural defects are sometimes semi-transparent to ultrasound but it appears to happen in steel less frequently than in aluminium because of the differing properties of the oxides usually associated with cracks. If cracks are air filled they may also be so tight, for example by external pressure, to become partially transparent to ultrasound.

Wavy surfaces militate against the generation of a strong specular reflection, but surface roughness adversely affects the reflectivity only if it is greater than about one tenth of a wavelength.

Reflection of a wave may also be adversely affected if the mechanical properties of the material of the defect, along with any inclusions it may contain, varies only gradually and not at a sharp boundary (i.e. compared to the wavelength). Porosity in castings may also act like such a strong absorber and it may be detected only by its shadowing effect on the back-wall echo.

Regularly uneven surfaces, as for example with milling grooves deeper than a quarter wavelength, may generate strong sideways reflections in the same way as an optical grating behaves. Because this interference phenomenon depends on the pulse length, using a shorter pulse may help to avoid this effect. See also [1654 and 276].

The main task of this chapter has been to evaluate the characteristics of an obstacle from its interference with the sound field, but it cannot be considered as

completed in a general sense. However, the reverse task of calculating the disturbed sound field produced by a given obstacle and including its echo received by a probe, can be solved to a certain extent by the *finite-element* method, if the obstacles shape can be expressed analytically. Up to now only two-dimensional fields, i.e. cross sections through three-dimensional sound fields have been treated (cf. [S 100] and Fig. 4.14). However, by using quick computers the whole field will in future be calculated within reasonable time. Of course in this calculation the comprehensive theory of sound has to be applied, including all wave types and mode changes. Solutions of the above mentioned main task can be expected for reflectors of a relatively simple shape.

6 Attenuation of Ultrasonic Waves in Solids

6.1 Absorption and Scattering

So far, ideal materials have been assumed in which the sound pressure is reduced only by virtue of the spreading of the wave. A plane wave would thus show no reduction whatever of the sound pressure along its path, and a spherical wave, or the sound beam of a probe in its far-field, would merely decrease inversely with the distance from the source. Natural materials, however, all produce a more or less pronounced effect which further weakens the sound. This results from two basic causes, viz. scattering, and true absorption, which are both combined in the term *attenuation* (sometimes also called extinction).

The scattering results from the fact that the material is not strictly homogeneous. It contains boundaries at which the acoustic impedance changes abruptly because two materials of different density or sound velocity meet at these interfaces. Such inhomogeneities may either be foreign inclusions, or gas pores. They may be genuine flaws of the material concerned, or also natural or intentional flaws such as porosity in sintered materials. There are also materials which by their nature are inhomogeneous, for example cast iron, in which an agglomeration of elastically completely different ferrite and graphite grains occurs. In other alloyed materials crystallites of different structure and composition are mixed, as in brass and steel. Even when only a single type of crystal is present, the material may still be inhomogeneous for ultrasonic waves if the grains are orientated at random and the crystal concerned has different elastic properties and different sound velocities in different directions. In this case it is called *anisotropic*. In most common metals elastic anisotropy is the rule, but in different metals it manifests itself to a varying degree.

In a material with very coarse grains of a size comparable to the wavelength the scatter can be visualised geometrically. At an oblique boundary the wave is split into various reflected and transmitted wave types. This process repeats itself for each wave at the next grain boundary. Thus the original sound beam is constantly divided into partial waves which along their long and complex paths are gradually converted into heat because of the always present true absorption (see below).

In the frequency range used for testing materials the grain size is usually smaller than the wavelength and under these conditions scatter occurs instead of geometric division, as when the light of a headlamp is scattered by the small water droplets in fog. In the case of grain sizes of 1/1000th to 1/100th of the wavelength, scatter is for all practical purposes negligible. It increases very rapidly however, approximately as the third power of the grain size, to make itself felt at sizes from 1/10th to the full value of the wavelength, to such an extent that testing may become impossible if the material concerned is anisotropic.

The second cause of the attenuation, viz. true *absorption*, is a direct conversion of sound energy into heat, for which several processes can be responsible [19, 21, 940], discussion of which would fall outside the scope of this book. Absorption can roughly be visualized as a sort of braking effect of the oscillations of the particles, which also makes it clear why a rapid oscillation loses more energy than a slow oscillation, the absorption usually increasing with the frequency, but at a rate much slower than the scattering.

Both losses set practical limitations to the testing of materials, but in slightly different ways. Pure absorption weakens the transmitted energy and the echoes from both the flaw and the back wall. To counteract this effect the transmitter voltage and the amplification can be increased, or the lower absorption at lower frequencies can be exploited. Much more awkward, however, is the scattering because in the echo method it not only reduces the height of the echo from both the flaw and the back wall but in addition produces numerous echoes with different transit times, the so-called *grass*, in which the true echoes may get lost. The scattering can be compared with the effect of fog in which the driver of an automobile is blinded by his own headlights and is unable to see clearly. This disturbance cannot be counteracted by stepping up the transmitter voltage or the amplification because the grass increases simultaneously. The only remedy is to use lower frequencies, which due to the reduced beaming effect of the sound and the increasing length of the waves and of the pulses sets a natural and insuperable limit to the detectability of small flaws.

The sound pressure of a plane wave, which decreases only as a result of attenuation, can for the purpose of calculation be written in the form of an exponential function

$$p = p_0 e^{-\alpha d} \tag{6.1}$$

p_0 and p are the sound pressures at the beginning and the end, respectively, of a section of length d and with the *attenuation coefficient* α.

In literature the attenuation coefficient α is sometimes referred not to the sound pressure but to the intensity. If the latter is called α_I the attenuation law of intensity can be written

$$I = I_0 e^{-\alpha_I d}.$$

Since the intensity is proportional to the square of the sound pressure we obtain:

$$e^{-\alpha_I d} = e^{-2\alpha d},$$

therefore

$$\alpha_I = 2\alpha.$$

The natural logarithm of Eq. (6.1) gives

$$\alpha d = \ln \frac{p_0}{p}. \tag{6.2}$$

This is the *attenuation* proper, or the total attenuation over the distance d, a dimensionless number which is expressed in *nepers* (Np). The attenuation coefficient can therefore be given in Np/cm. Following the practice in electrical measurement,

however, another unit is being given preference, viz. the *decibel* per metre, abbreviated dB/m. The decibel measure is obtained if in Eq. (6.2) the logarithm to base 10 is used and multiplied by 20:

$$\alpha d = 20 \lg \frac{p_0}{p} \text{ dB}. \tag{6.2a}$$

In what follows, α will always be given in the unit decibel per metre (dB/m) because in the frequency range of interest, and the materials in question, the numerical values, which usually lie between one and a few hundreds, can be memorised more easily. For instance, various materials with low attenuation have values from 1.0 to 4.0 dB/m.

According to Bergmann [2] water at 20 °C has an absorption for 4 MHz of 3,5 dB/m. The frequency dependence is given by

$$\alpha = 0.22 f^2 \text{ dB/m} \quad \text{with } f \text{ expressed in MHz}.$$

The influence of the temperature is negative, the absorption decreasing by 3.2 % per degree at 20 °C. At high ultrasonic powers, as can occur in the pulses of a flaw detector, the absorption can be much higher as a consequence of non-linear stressing and the onset of cavitation.

If the attenuation coefficient of a given material is 1 dB/mm, the wave is attenuated by a 1-mm-thick layer by approx. 10 %; by a 20-mm layer by approx. 90 %; at 100 mm the attenuation is the 5th power of 10 and the sound pressure is 10^{-5}. This would already be a very severe attenuation.

Table 6.1 facilitates the conversion of dB values to ordinary figures. The second column applies to negative dB values and gives the attenuated amplitude in %: the third column applies to positive values and gives the gain.

Table 6.1.

dB	Attenuated amplitude in %	Gain	dB	Attenuated amplitude in %	Gain
0.0	100	1.00	10.0	32	3.16
0.5	94.5	1.06	12.0	25	3.98
1.0	89	1.12	14.0	20	5.01
1.5	84	1.19	16.0	15.8	6.31
2.0	79	1.26	18.0	12.6	7.94
2.5	75	1.33	20.0	10.0	10.00
3.0	71	1.41	30.0	3.2	31.62
3.5	67	1.50	40.0	1.0	100.00
4.0	63	1.59	50.0	0.32	316.23
4.5	60	1.68	60.0	0.10	1 000.00
5.0	56	1.78	70.0	0.032	3 162.30
6.0	50	2.00	80.0	0.010	10 000.00
7.0	45	2.24	90.0	0.003	31 623.00
8.0	40	2.51	100.0	0.001	100 000.00
9.0	35	2.82			

Intermediate values are obtained by adding the dB values and multiplying the ordinary numerical values.

Example. A decrease of the amplitude by 23 dB = 20 + 3 dB corresponds to 10 % of 71 % = 7.1 % amplitude, requiring a gain factor of 10.0 × 1.41 = 14.1.

A table of attenuation coefficients for various materials would be of doubtful value. Where values have already been reliably measured, which is difficult below 10 dB/m (see Section 33.3), such values, in the case of metals, depend within wide limits on the various manufacturing parameters (see Section 6.2). Table 6.2, therefore, provides only general information.

For a few values of α from 1 to 300 dB/m, Diagram 10 in the Appendix shows the decrease of the sound pressure of a plane wave as a function of the distance in the form of a graph. It shows the attenuation in dB, or that of the amplitude in per cent, if the pulse-echo method is used, i.e. the height of the echo. If the decrease of the amplitude to 0.1 % is defined arbitrarily as the *range*, Diagram 10 indicates for light metals and fine-grained steel (α = 1 to 3 dB/m) transmission ranges above 5 m when using the echo method, but for grey cast iron (order of magnitude of α approx. 300) only 100 mm. This presentation draws attention to the fact—which in practice is frequently overlooked—that the attenuation increases very rapidly with

Table 6.2. Attenuation of longitudinal waves at 2 MHz and room temperature in various materials

Attenuation coefficient α in dB/m	Low up to 10	Medium 10 to 100	High above 100
Material	*Cast:* aluminium, magnesium, pure and slightly alloyed *Worked:* steel, aluminium, magnesium, nickel, silver, titanium, tungsten (all pure and alloyed) Non-metals: glass, porcelain	Predominantly absorption	
		Plastics (polystyrene, perspex, rubber, PVC, synthetic resins)	Plastics and rubber, with fillers, vulcanized rubber, wood
		Predominantly scattering	
		Cast aluminium and magnesium, alloyed Cast steel, slightly alloyed, high-quality cast iron *Worked:* copper, zinc, brass, bronze, lead, stellite, sintered metals	Cast steel, highly alloyed, lowstrength cast iron, cast copper, zinc, brass, bronze Non-metals: porous ceramics, rocks
Max. thickness that can be tested	1 to 10 m	0.1 to 1 m	0 to 0.1 m, may frequently no longer be tested

the thickness of the layer concerned. While, for instance, 20 mm grey cast iron can still be tested with 25 % of the echo height in a good quality steel, and which reduction can easily be compensated by the gain control, an echo in the same material, but 100 mm thick, has dropped to 0.1 %. This is a value which depending on the transmitter voltage, the design of the probe and the gain may prevent testing. If by increased gain it is nevertheless possible to increase this back-wall echo from the 100 mm thickness to the same value obtained from a thickness of 20 mm, the material at the distance of 20 mm is subjected to a sound pressure 250 times greater than previously, resulting in excessively large indications from boundaries and small flaws in the close range. This is erroneously referred to as increased scattering, although compared with the test at 20 mm thickness nothing has changed. Where there is high attenuation in a given test piece, a comparison of flaw echo and back-wall echo may therefore lead to completely false conclusions.

In view of the fact that at greater layer thicknesses one usually has to work in the far-field of the probe, additional allowance has to be made for the decrease of the amplitude due to the divergence of the beam. According to Eq. (4.6) the sound pressure at distance d from the probe can therefore be written

$$p = p_0 \pi \frac{N}{d} e^{-\alpha d}. \tag{6.3}$$

A numerical example will make it clear that both causes of the decrease follow essentially different distance laws, so that the range will in the one case be determined more by the divergence of the beam and in the other by the attenuation.

Let the sound pressure at a distance of 100 mm be set arbitrarily at 100 %. The sound pressure then is in percentage terms:

At a distance of	100 mm	1 m	10 m
Due to the divergence of the beam alone:	100	10	1
Due to the attenuation alone at			
$\alpha = $ 1 dB/m	100	90	32
10 dB/m	100	35	0.001
100 dB/m	100	0.003	—

Since the two contributing factors have to be multiplied by each other, the divergence of the beam determines the range in the case of materials which can readily be penetrated (fine-grained steel and aluminium at 2 MHz), whereas in the case of higher attenuation this is the predominating factor.

Generally transverse waves are attenuated more strongly than longitudinal waves, particularly in plastics. Contrary to the assumption frequently heard in practice, it is not possible to determine the attenuation coefficient of sound for transverse waves by measuring the attenuation coefficient for longitudinal waves at double the frequency. The elastic resistance of the material exerted against a change in position of the particles (as in the case of transverse waves) is quite different from that against a change in volume (as in the case of longitudinal waves).

The attenuation usually increases with the temperature, particularly in plastics. In the case of steel a maximum appears at the transition point from body-centred-cubic to face-centred-cubic iron (approx. 721 °C) [1168, 1533].

Beyond this point (in the austenitic range) it increases again very strongly as reported in [S 113].

In the case of surface waves, plate waves and rod waves the weakening influence of the roughness of the guiding surfaces must be added; this can be nominally taken into account by adding a certain quantity to α, and in this case also the decrease of the amplitude follows an exponential law.

If an attempt is made to avoid the attenuation of the material by using lower frequencies when trying to detect small flaws, a compromise has to be made; there is an optimum frequency, because the effect of the flaw on the sound field decreases simultaneously. For instance, in the case of a spherical flaw whose diameter D is much smaller than the wavelength, the echo amplitude according to Rayleigh [32] varies by the ratio

$$D^3/\lambda^4 .$$

If the dependence of the attenuation coefficient on the frequency is known from measurements and can be expressed, say by the formula

$$\alpha = p + qf^m$$

where p, q and m are constants, one obtains according to Malecki [819] for a given flaw distance d the optimum frequency

$$f_{opt} = \frac{1}{\sqrt[m]{mqd}} .$$

6.2* Attenuation in Metals; Anisotropy and Cast Structure

In view of the fact that the attenuation, particularly the scattering in the material, is one of the main difficulties encountered in ultrasonic testing and is often the only factor limiting its application, it is of great practical importance to be able to estimate the influence of the crystal structure on the attenuation. So far no general solution has yet been found because both theoretical and measuring difficulties are encountered, and because indubitably, in addition to the directly measurable quantities such as grain size and anisotropy, many other parameters which are difficult to determine have an effect. There are for instance the nature of the grain boundaries and the internal stresses. Frequently, however, not even the grain size can be clearly defined, as demonstrated by micro sections of steels with their complex structures.

A clear and logical law of behaviour can therefore be expected only in the case of simple structures with only one type and form of crystal and a minimum of impurities. This needs not necessarily apply to pure metals since alloys with mixed

crystals are no exceptions in this respect. In such cases the influences of anisotropy and grain size which can readily be interpreted are observed. If for instance two samples of cast aluminium and cast brass of identical grain size are compared, the attenuation in brass is much greater than in aluminium. Further, if two samples of the same material but of different grain size are tested it is found that the change of the attenuation due to grain size is much more pronounced in brass than in aluminium. This last-mentioned comparison can also be made with shorter wavelengths instead of larger grain sizes. A greater ratio of grain diameter to wavelength is thus accompanied by an attenuation which is the greater, the greater the anisotropy.

According to Roth [1301] a number of important materials can be classified according to increasing anisotropy:

W   Mg   Al–Cu   Al   Fe   Ag   Cu   Pb α-brass β-brass

          (95 + 5 %)   (72 Cu + 28 Zn)   (58 Cu + 42 Zn)

The coarser grain produces a disturbance which is the greater, the further to the right the material appears in the above series.

According to Roth, and also Mason and McSkimin [992, 993], the anisotropy can also be specified numerically, but this will not be discussed here, especially since the sequences are not identical for different concepts. In the case of transverse waves permutations within the series may result.

Tungsten should be completely isotropic like non-crystalline materials, for example glass. Tests on samples, however, are usually hampered by porosity introduced during manufacture.

The low attenuation of the pure light metals and aluminium copper alloys with only a few per cent copper has been confirmed. As far as the testing of materials is concerned here the grain size is immaterial.

After iron come the strongly anisotropic materials of which the copper alloy metals in particular cause many difficulties. As far as is known β-brass is the most strongly anisotropic material after austenite.

Iron is considered here only alloyed with carbon and with other metals in the form of steel. The influence of the grain size is considerable, and this is the main reason why, essentially, only frequencies below 5 MHz should be used when testing steel.

In the case of steel the structure is usually not a simple one and does not have only *one* approximately uniform grain size and *one* type of crystal. It is, therefore, not surprising that the results are as yet unclear. As a first approximation the largest dimension of grain groupings or domains should replace the actual individual grain sizes. In relation to the behavior of Austenite see Sections 27 and 28.1.6.

Most materials show a particularly pronounced reduction of the attenuation of sound if their cast structure is destroyed by working, cold or hot, for example during forging, rolling, extruding, etc. To a small extent this effect may be the result of true compaction of the structure by a reduction of the pore volume. In the main, however, the deformation process leads to a destruction of the larger grains of the cast structure, resulting in reduced scattering.

The reduction of the pore volume is usually indicated directly by an increase of the specific gravity; for example cast copper has a specific gravity of 8.3 to 8.9 but

this changes to 8.9 to 9.0 if hammered. Since porosity reduces the velocity of sound the compacting should manifest itself by an increase of the sound velocity.

The effect of the working on the attenuation of the sound is particularly pronounced in the case of non-ferrous metals as well as high-alloyed steels. While in the as-cast structure even small thicknesses can frequently not be penetrated, they can readily be penetrated even after the first pass during rolling. Particularly disturbing in such materials therefore is a zone in the finished piece in which the cast structure has not yet been sufficiently compacted because of insufficient deformation. A special condition of crystallization, for example an austenitic structure, has apparently no great significance in itself, but it is important to know whether this condition is present in the cast structure or the worked structure. For instance, the material of rolled austenitic pipes can readily be penetrated, while an austenitic weld joining them usually shows bad transmission because of its cast structure.

It may be mentioned briefly that the improved mechanical properties of centrifugal casting as compared with chill castings, sand castings or continuous castings, immediately manifest themselves in their ultrasonic behaviour. The centrifugal casting shows better ultrasonic transmittance and is therefore easier to test. It is debatable whether this is merely an effect of the finer grain or of a simultaneously changed condition of the grain boundaries. This has been observed not only in cast iron but also in non-ferrous metals [1453].

Generally the attenuation along the sound path is connected with the dispersion of the velocities, depending on the properties of the material and its structure. Based on this effect a new method has been developed to evaluate the structure from the scattering of sound at the boundaries of the grains and the different solid phases of the material [S 165, S 72–75].

Regarding further theoretical relationships between attenuation, dispersion, frequency, grain size, scattering and anisotropy see also [992, 32, 1627, 1676, 581, 582, 434, 532, 535, 631, and 13, p. 112 f.].

Measurements are reported in [130, 992, 993, 19] on aluminium, magnesium, nickel and brass, metals of simple structure and well defined grain size. They confirm qualitatively the theoretical approach. Measurements on steel are given in [1276, 940, 1161, 88, 21, 433].

Regarding measurement techniques see Section 33.3. The main difficulty, in addition to the measurement technique itself, consists in keeping constant all the numerous extraneous variables within a series of samples except for the one under review.

For the practical purpose of non-destructive testing the results can be summarized by rule of thumb as follows:

1. The scattering produced by a given material increases rapidly with increasing grain size, or decreasing wavelength, if the grain size is about 1/10 of the wavelength or greater. However, the effect becomes disturbing only if the material appears far to the right in the anisotropic series.
2. In complex metallurgical structures the grain size should be defined as the maximum structural dimension which occurs.
3. A cast structure produces stronger attenuation than a deformed structure, even in the case of identical grain sizes.

4. By making a recourse to lower frequencies the attenuation can be reduced con-
    siderably, but this step is promising only if the smallest flaws to be detected are
    still large compared with the grain size, or the factor of reflection of the flaws is
    large compared with the scatter factor of the structure.

According to newer concepts true absorption in crystals is explained by energy-consuming
oscillations of dislocations in the lattice as well as by reciprocal actions on the lattice itself.
(cf. Read [1241], see also Mason's book [21, 19] with further bibliographic references). This
theory also explains the increase in attenuation if the material is stressed by tension or com-
pression, as well as the fatigue behaviour of materials (see Section 33.3 and reports by Truell
et al. [658, 559, 1535, 1536]).

7 Piezo-electric Methods of Generation and Reception of Ultrasonic Waves

7.1 Piezo-electric Materials and their Properties

So far we have discussed the propagation and behaviour of ultrasonic waves in various materials without pre-supposing anything regarding their generation except that they are excited in the material concerned by the contact face of a *radiator* which oscillates with the desired wave-form and frequency. For detection a *microphone* has been assumed which likewise has a contact face and which is capable of measuring the sound pressure of an incident wave. Both devices are referred to in materials testing as a *probe*, or *transducer*, and where applicable as a transmitting probe or a receiving probe. We shall now discuss its mode of operation, which is based almost exlusively on the piezoelectric effect. Other methods for generating ultrasonics are discussed in Chapter 8.

A piezo-electric material has the property that if it is deformed by external mechanical pressure electric charges are produced on its surface. This effect was discovered in 1880 by the brothers Curie. The reverse phenomenon, according to which such a material, if placed between two electrodes, changes its form when an electric potential is applied, was discovered soon afterwards (in 1881). The first in called the direct piezo-electric effect, and the second the inverse piezo-electric effect. The first is now used for measuring, the second for producing mechanical pressures, deformations and oscillations.

Later fundamental research has shown that piezo-electricity is based on a property of the elementary cell of the crystalline structure of the material, which is in this connection the smallest individual symmetrical unit which when multiplied builds up the whole macroscopic crystal. An essential condition for the effect is that the crystal cell should have no centre of symmetry and from the total 32 classes of crystals no less than 21 have this property. Of these 20 crystal types show some piezo-electric properties and there are therefore many different piezo-electric materials. However, only very few of them are useful for our purpose and their description will follow later.

In what follows the piezo-electric effect will be explained using barium titanate as an example since it is a material frequently used in ultrasonics and has a rather simple structure for the elementary cell (Fig. 7.1). Fuller treatments of the subject may be found in the books of Bergmann [2], Hueter and Bolt [11], Mason [20], Cady [5] and Jaffe, Cook and Jaffe [12].

Barium titanate, along with many other piezo-electric ceramics, has the structure of Perowskit, a calcium titanium trioxide ($CaTiO_3$), which can be used as a general designation of the crystal structure. The elementary cell (Fig. 7.1), above a

Ba²⁺   O²⁻   Ti⁴⁺
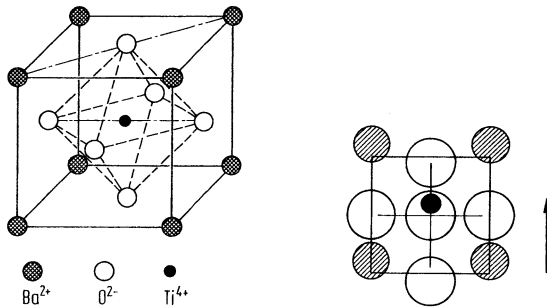
Fig. 7.1. Elementary cell of barium titanate (schematic)
Fig. 7.2. Perowskit structure, tetragonally distorted

certain temperature called the Curie or transformation temperature, has a cubic structure. Below this temperature it is distorted and strained in the direction of the socalled *C*-axis and hence the distances between positively and negatively charged ions are varied (Fig. 7.2). The shift is only a few percent of the length of the cube edge but nevertheless it causes a separation of the effective centerpoints of the electric charges and thus generates a dipole moment . For reasons of energy all these dipole moments belonging to neighbouring cells turn in the same direction within certain crystal domains. Such materials with this property are called ferro-electric which is analogous to the better known ferro-magnetic property.

The direction of polarization of the different domains within a polycrystalline material is randomly distributed, and therefore in a sintered ceramic no piezo-electric effect can be found macroscopically. However, by polarizing the material with an applied strong electric field at a temperature just below the Curie point, a uniform polarization can be achieved for the whole sample. This polarization is "frozen" by cooling down the sample with the electric field still applied. Subsequent reheating will again reduce the ferro-electric properties, and to a greater extent the nearer we approach the Curie temperature, the single polarized domains lose their orientation statistically. Above this temperature no uni-directional polarization is possible because at this point the simple cubic structure of the elementary cell does not have a permanent dipole moment.

When mechanical stresses are applied to a polarized plate of barium titanate, with compression or tension in the direction of polarization, all the elementary cells are deformed thus shifting the centrepoints of the structural electric charge distribution and causing thereby electric charges of the surfaces of the plate. For easier processing of the charges both faces of the plate are coated with a metallic layer, these layers forming an electric capacitor in which the crystal acts as the dielectric. On stressing this plate we can detect and measure the charges as a voltage between the layers, which is proportional to the applied stress. Of course, because of the incomplete insulation of the circuit, the charge falls to zero in the form of a current pulse. When the applied stress is removed we then measure a voltage, or a current pulse, of the opposite sign.

Table 7.1. Constants of Some Piezo-electric Materials[a]

		Lead zirconate titanate		Barium titanate Sonox P1[b]	Lead meta-niobate K-81[c]	Lithium sulfate	Lithium niobate	PVDF	Quartz
		Sonox P2[b]	Sonox P5[b]						
Density ϱ	g/cm³	7.8	7.7	5.3	6.2	2.06	4.64	1.3...1.8	2.65
Sound velocity c	m/s	4200	3800	5200	3300	5460	7320	1500...2600	5740
Acoustic impedance Z	10^6 kg/(m²s)	32.8	29.3	27.6	20.5	11.2	34	2.1...4.7	15.2
Piezo-electric modulus for thickness oscillations d_{33}	10^{-12} m/V	125	340	125	85	15	6	25	2.3
Piezo-electric pressure constant g_{33}	10^{-3} Vm/N	30	24	14	32	156	23	230	57
Piezo-electric deformation constant h_{33}	10^9 V/m			1.5	1.9	8.2	6.7		4.9
Electromechanical coupling factor for thickness oscillations k_t		0.35	0.47	0.33	0.38	0.38	0.47	0.1...0.14	0.1
Coupling factor for radial oscillations k_p		-0.46	-0.57	-0.25	0.07	0		0	0.1
Mechanical quality Q		400	90	350	15	>1000	>1000	<15	>10^4
Dielectric constant ε_r		480	1600	960	300	10.3	30	11.5	4.5
Curie temperature T_c	°C	345	340	120	>400	130	1210	165...180[d]	576

[a] Acc. manufacturers and [720, 23, 550]
[b] Sonox P1, P2 and P5 are trade-marks of the Rosenthal Corporation
[c] K-81 is a materials name of the Keramos Corporation
[d] Melting point

So we can see that the alternating stresses as applied to such a plate by an incident sound wave, generate alternating voltages and their corresponding currents, causing the plate to act as a microphone.

The very thin metal coating does not hinder the operation of the so-called direct piezo-electric effect and the system therefore provides a receiver for ultrasound. The reciprocal effect forms the basis for an acoustic transmitter in which alternating voltages applied across the two metal electrodes cause the plate to oscillate at the frequency of the voltage. If one attempts to prevent the increase or decrease of the plate thickness, it develops compression or tension thereby transmitting a pressure wave into the contiguous medium, its amplitude being proportional to the applied voltage.

However, the deformation of the piezo-electric plate is not only restricted to an alteration of its thickness. As a result of the elastic properties of any solid material any variation of the thickness must always be associated with opposite dimensional variations in the other two coordinates. The extent of this internal coupling depends on the particular crystallographic structure and as an example the size variations in a rectangular plate, cut in the so-called X-direction from a natural quartz crystal, (see also this book, 3rd edition, p. 120), are shown in Fig. 7.3.

Natural quartz was formerly widely used in the probes for ultrasonic materials testing but it is now generally replaced by more sensitive piezo-ceramics (see Table 7.1).

In fact these few illustrated additional variations in the dimensions of a piezo-electric plate subjected to applied electric potentials are not by any means the only ones. A full description and explanation would require a great deal of the theory of elasticity, but for the generation and reception of longitudinal waves the more complex variations do not interfere very much, so we may here restrict ourselves to the variation of the dimensions perpendicular to the thickness as shown in Fig. 7.3 b for the Y-direction.

With a plate cut from a crystal such as quartz variations in both the Y- and Z-directions, have different couplings with the thickness variation whereas ceramics
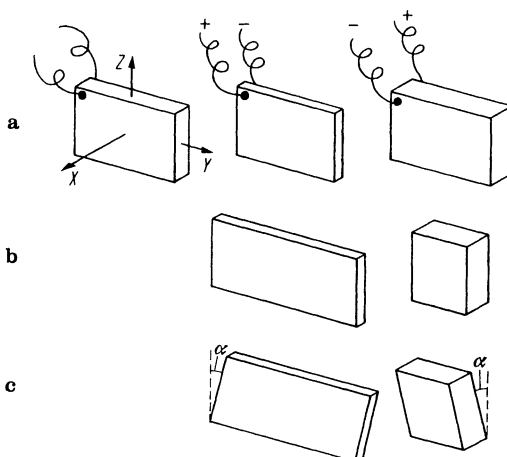
Fig. 7.3. Deformation of an X-cut quartz plate of dimensions $x, y, z = 5,30,20$ mm, for an applied voltage of 1000 volts illustrated on a much exaggerated scale of 1 million to one. a Change of thickness alone; b additional change of Y-axis; c additional shear of the $Y - Z$ plane
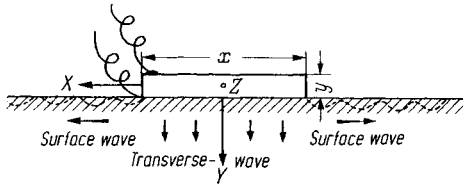
Fig. 7.4. In the solid material the Y-cut quartz plate generates a transverse wave normal to the surface, and a surface wave in the X-direction. The latter is particularly strong if $x : y \sim 7 : 1$
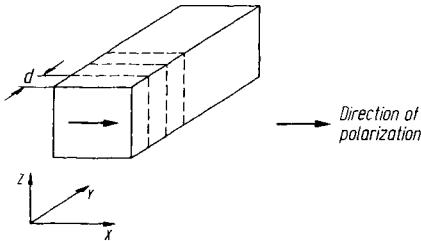
Fig. 7.5. Design of a thickness-shear oscillator

such as barium titanate do not. As a consequence the shape of a circular disc cut from quartz is somewhat distorted when energised whereas a disc made from barium titanate only changes its diameter when oscillating. When rigidly attached to a solid material both transmit a weak shear wave, and a surface wave, besides the normal longitudinal wave (Fig. 7.4). When using a liquid coupling, however, the shear wave cannot be transferred. The surface (Rayleigh) wave is unavoidable however, and can be used intentionally for surface testing, but otherwise it may interfere with longitudinal wave testing by giving unwanted echoes.

The Y-expansion is sometimes made use of for generating low frequency longitudinal waves, which are transmitted from the small X-Z area, since the natural frequency of the plate in this direction is much lower than in the thickness direction (see Section 7.2). It is also an advantage that the radiating contact faces do not have metal electrodes which always suffer from abrasion when in contact with a solid specimen.

Figure 7.5 shows an example of the use of the internal mechanical cross coupling to generate strong transverse waves. A rectangular rod of piezo-ceramic material, with a high cross-coupling factor (see Table 7.1), has been polarized perpendicular to its main axis. It can then be cut into square plates without destroying the piezo-electric properties. Each plate of thickness d, and metallized on the large faces (XZ), can oscillate at the natural frequency corresponding to its thickness, and radiates a transverse wave in the Y-direction when coupled to a solid medium.

As already mentioned in Section 4.8 a piezo-electric plate never oscillates exactly like a piston because of the fringe-field effect. The voltage between the electrodes is in fact uniform over the whole plate, but the electric field strength is actually responsible for the amplitude of the piezo-electric effect. Because at the edges of the plate the field lines tend to curve outwards, the oscillation amplitude is here reduced with unavoidable influences on the ultrasonic field (see Fig. 4.44).

The following basic laws of piezo-electricity are valid for both types of piezo-electric materials. That is the piezo-ceramics which get their piezo-electric properties by being polarized in an electric field at elevated temperatures, and the monocrystalline materials having natural piezo-electricity, such as quartz.

For the following treatment we assume the ideal case of a simple parallel sided oscillator with only thickness deformations. The static case of the twin piezo-electric effects may be written in an elementary manner as follows:

1. Let the applied potential be U_t (the transmitting voltage). The change of thickness Δx_t will then be

$$\Delta x_t = d_{33} U_t \tag{7.1}$$

where d_{33} is the *piezo-electric modulus.*
In the case of piezo-ceramics the direction of polarization is normally identified by the index 3 and a typical value for barium titanate is:

$$d_{33} = 125 \times 10^{-12}\,\text{m/V} \quad \text{(or As/N)}.$$

If an oscillator is to be used only as a transmitter a value of the piezo-electric modulus as high as possible is an advantage.

2. Consider now an externally produced change of thickness Δx_r (receiver). The corresponding open circuit potential, that is the voltage across the oscillator without applied load, is:

$$U_r = h_{33} \Delta x_r \tag{7.2}$$

where h_{33} is the *piezo-electric deformation constant.*
Its value for barium titanate is:

$$h_{33} = 1.5 \times 10^9\,\text{V/m} \quad \text{(or N/As)}$$

but for other crystals the axis and the value of the constant will of course be different.

3. In the latter case one can also start from the pressure p_x, which produces the change in thickness. The voltage produced by the receiver crystal then depends additionally on the thickness d:

$$U_r = g_{33} d p_x \tag{7.2 a}$$

where g_{33} is the *piezo-electric pressure constant.*
It is for barium titanate:

$$g_{33} = 14 \times 10^{-3}\,\text{Vm/N} \quad \text{(or m}^2\text{/As)}$$

A value for g_{33} as high as possible is an advantage when mechanical pressure is to be transformed into a voltage, as for example in a receiver for ultrasound.

Assuming that the total change in thickness of the transmitter is transferred to the receiving crystal so that $\Delta x_r = \Delta x_t$ then the ratio of receiver voltage to transmitter voltage, according to Eqs. (7.1) and (7.2) and using values for barium titanate, will be

$$U_r/U_t = d_{33} h_{33} = k_{33}^2 = 0.19\,. \tag{7.3}$$

The quantity k, defined by this equation (7.3), is the *electro-mechanical coupling factor* which for a piezo-electric material is an indicator of the efficiency of the conversion of an electric voltage into a mechanical displacement or vice versa. For the values above for barium titanate we would get back about 20% of the input voltage. The value of $k = 0.43$ for barium titanate is, however, only valid for rods excited in their axial direction. For thin plates a cross coupling between thickness and transverse oscillations cannot be neglected. The value of k_t (thickness oscillation) for barium titanate taking this into account, is:

$$k_t = 0.33 \quad \text{i.e.} \quad k_t^2 = 0.11$$

which means that only 11% will be obtained. The abolute maximum is about 25% ($k_t = 0.5$, see Table 7.1).

For the thickness oscillation of thin plates also the factor k_p (for radial oscillations) is of importance since from k_p the disturbing oscillations of a probe depend. It should therefore be as small as possible compared with k_t. The higher the value of k_p the more an oscillator differs from the ideal case, assumed above, for a pure thickness oscillator.

In addition to the various piezo-electric constants, its *mechanical quality Q* as well as its *impedance Z* is of importance in considering its performance as an oscillator (cf. Section 7.2).

The mechanical quality Q is a measure of the increase in amplitude if a plate is vibrating at its resonance point as part of an oscillating circuit. It is higher when the oscillation losses of energy in the material are lower. With materials of natural crystalline origin such as quartz it is normally very high and its value cannot be influenced. With ceramic materials it can be varied by making use of small changes in the chemical composition, and available commercial products have mechanical qualities between 15 and 1000 (see Table 7.1).

The acoustic impedance, or sound resistance, Z defined as the product of density ϱ and sound velocity c, determines the passage of sound between two different materials (Section 2.1). For equal impedances the whole sound energy is transferred between two materials and it is therefore better to make an optimum match between the impedance of the transmitter/receiver and the specimen material under test.

For generating and receiving ultrasound in materials testing today piezo-electric ceramics are mostly in use, the commonest being barium titanate, lead zirconate titanate (PZT), lead titanate (PT), lead meta-niobate ($PbNb_2O_6$) and barium sodium niobate ($Ba_2NaNb_5O_{15}$). The properties of these materials can be varied by manufacturing processes within certain limits. Table 7.1 lists values for two typical PZT ceramics (Sonox P 2 and P 5) as well as for barium titanate (Sonox P 1) and lead meta niobate (K-81).

Instead of directly sintering the powder for the manufacture of ceramic transducers it can be mixed with an electrically non-conductive liquid to make a paste and with an applied high-bias voltage it develops piezo-electric properties (Lutsch [955], cf. also [237]). Such paste transducers can be applied directly to the specimen without using a coupling fluid. On rough surfaces they give better coupling but have much lower sensitivity than standard types of transducer. It is of interest that they may be used even at temperatures higher than the Curie

temperature if higher boiling point liquids are used [955]. In addition one may mix the powder material with mouldable hardening resins and produce rigid transducers with low sensitivity but high internal damping.

Pizeo-electric monocrystals such as quartz, lithium sulfate, lithium niobate, lithium tantalate, zinc oxide and iodic acid are rarely used today for materials testing. The reason for not using quartz, the oldest known piezo material, is the low sensitivity, $k_t = 0.1$. For some special cases lithium sulfate and lithium niobate have certain advantages and their constants are mentioned in Table 7.1. Only for the sake of completeness we also mention Seignette or Rochelle salt (potassium sodium tartrate, KNT crystal), potassium phosphate (KDP), ammonium phosphate (ADP), potassium tartrate (DKT), ethylene diamine tartrate (EDT) and tourmaline.

Finally in Table 7.1 we mention polyvinyliden fluoride (PVDF). This is a plastic film used mainly in the packaging industry and its piezo-electric properties have been detected only since 1969 (Kawai [763], Sussner et al. [1489], Ohigashi [1140], Sussner [1488]). Thin films of PVDF in the range 0.1 to 0.005 mm thickness can be polarized by a high voltage after being stretched and in this case molecular chains in the plastic material are aligned rather than being randomly distributed as normally.

When comparing the values given in Table 7.1 one sees from the piezo-electric modulus d, that the first four materials listed give far higher thickness variations than the others and are therefore better suited for use as transmitters at the same transmitter voltage. PZT is the best and the two mentioned PZT types differ mainly in their dielectric constants and their mechanical quality. Type P 2 has a very low dielectric constant ($\varepsilon_r = 480$) compared with P 5 ($\varepsilon_r = 1600$). It is reasonable to select a PZT material which at a given probe diameter allows proper matching of its capacity to the input impedance of the amplifier. The high value of g_{33} recommends PVDF as receiver.

In the case of PZT and barium titanate, the high sensitivity cannot in practice be fully exploited because of their high acoustic impedance. Not only for transmitting into liquids, but also for liquid coupling to solids, the effective impedance is only a few $\times 10^9$ Ns/m². Lead meta-niobate, lithium sulfate and PVDF are in this respect much more favorable.

Another point in favor of lead meta-niobate is the mechanical quality Q which should be as low as possible for the damping of the fundamental oscillations of a plate. In order to obtain short pulses a backing material is usually bonded to the rear face of the crystal both for damping it and for absorbing the penetrating wave. It must be rigid enough to support the crystal but thin enough to maintain the transducer at a handy size. For material with high impedance the compromise may not be easy, and therefore lithium sulfate and lead meta-niobate are preferred. The latter has also a very low Q and may in some cases be used without even a special backing material, which is an advantage for the working sensitivity.

Another important advantage of lithium sulfate and lead meta-niobate is their small coupling factors between co-planar oscillations and thickness oscillations, which is responsible for long-lasting reverberations following a short pulse. Piezo-electric ceramics have radially symmetrical decay oscillations within the plane of the disc and damping by a rear-mounted damping block is only partially effective. A better solution, but one presenting difficulties for the probe construction, is to

use an additional edge damping material around the disc. For this reason barium titanate is not suited for use with very short pulses when compared to lithium sulfate and lead niobate. However, there is another disadvantage of the latter materials which arises from their high sound velocity. This means that discs must be of very small thickness at high frequencies causing them to be rather fragile [550].

Lithium sulfate is water soluble and, for immersion testing, must be protected by water-tight covering layers, usually of cold-hardening resins which can also be used for matching the coupling impedances. When provided with curved surfaces they can even be used to focus the beam when radiating into water, or for matching the profile of a curved surface of the specimen. However, if they are used for contact with solid specimens the plastic surface is easily damaged and the crystal can be destroyed by water so that the surface is usually protected for such applications by a further layer.

The high transformation temperature of lead niobate (1210 °C) allows its use on a hot surface, for example to inspect parts of sodium-cooled nuclear reactors, but the crystal has to be protected against oxidation above 650 °C by an air-tight enclosure (Podgorski [1199]).

Electrical matching of the probe to the amplifier becomes difficult at high frequencies for large crystal diameters because of their high self-capacity. In this case the low dielectric constants ε_r of lithium sulfate and lithium niobate are an advantage compared with piezo-ceramics.

Finally PDVF has very unusual values and in spite of its very low coupling factor ($k_t = 0.12$) it is an interesting material because of its low impedance, low mechanical quality and low dielectric constant. It is suited therefore for high frequency oscillators, having high damping even without backing. Its main advantage, however, is its film character which can be produced at a thickness for which other materials would be extremely fragile. PVDF can be used for transducers working up to 100 MHz, which is only possible with solid transducer materials by exciting them at an harmonic oscillation, as for example the fifth harmonic of a 20-MHz oscillator.

7.2 The Piezo-electric Plate as Transmitter and Receiver of Ultrasound

The above descriptions of the behavior of a piezo-electric plate are strictly valid only for the static case, or as long as the thickness variations only take place so slowly that the inertia of the plate can be neglected. Any plate, regardless of its piezo-electric properties, can oscillate mechanically like the classic system of a mass and spring. The fact that within a plate the mass and the spring's elastic force are uniformly distributed enables it to oscillate at its fundamental frequency, and also at its various harmonics, as in the case of a taut string.

Let us consider the fundamental or first harmonic oscillation in a plate rigidly fixed at its edges as in Fig. 7.6. The material particles of the two surfaces oscillate simultaneously, either outwards or inwards, but within the median plane the parti-

cles are always at rest. If the displacement of the particles at a series of instants 0 to 8 are plotted at right angles to the axis of the plate, as shown in Fig. 7.6, the result is a group of sinusoidal curves having different amplitudes. This phenomenon is well known to us and constitutes a standing wave as explained in Fig. 1.5. It can be thought of as consisting of two waves running in opposite directions through the plate, but at the same frequency. Therefore the thickness oscillation of a plate can be described by a plane wave which is reflected at the first surface with opposite phase (because it is the boundary with an acoustically soft medium), and being re-flected again at the opposite surface, once more with a phase reversal. Thus it un-dergoes a phase shift equal to a full wavelength, and so meets itself in phase.

Using a sound velocity for longitudinal waves c in the plate material, its thick-ness d equals

$$d = \frac{\lambda}{2} = \frac{c}{2f_0} \tag{7.4}$$

and hence the characteristic or natural or fundamental frequency of the plate is

$$f_0 = \frac{c}{2d}. \tag{7.5}$$

A thickness oscillation may also be achieved by transverse waves. For each case, using values for barium titanate (type P 2) ceramic, we obtain:

$$f_{0l} = 2.60/d \text{ MHz},$$
$$f_{0t} = 0.98/d \text{ MHz} \tag{7.6}$$

with the thickness expressed in millimetres.
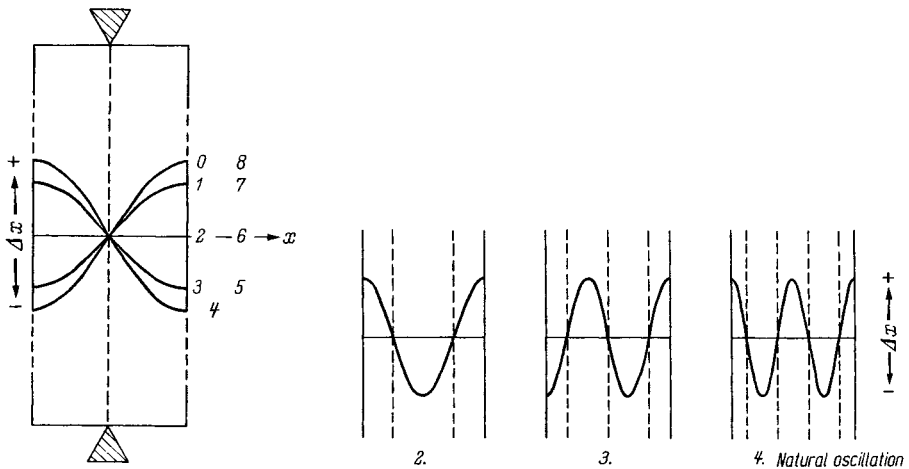
Fig. 7.6. Fundamental thickness oscillation of a plate. Displacement of the particles plotted at equal time intervals, 0 to 8, perpendicular to the axis of the plate

Fig. 7.7. Higher harmonics of a plate. Particle displacement at time zero as in Fig. 7.6.

To produce sound in the audible range with thickness oscillations in a barium-titanate plate, a thickness of 200 mm would be needed, but using thickness of a few millimetres we attain the frequency range of ultrasound needed for testing materials.

Figure 7.7 explains the formation of higher characteristic oscillations, the so-called harmonics. Standing waves will also occur for waves of shorter wavelength, provided they are an exact fraction of the fundamental wave. In these cases two, three or more half-wavelengths fit into the plate thickness so that there are several nodal plains where the particles are always at rest. The corresponding harmonic frequencies are an integral multiple of the characteristic or first harmonic frequency f_0. For the odd harmonics, as well as for the fundamental, viz. at f_0, $3f_0$, $5f_0$ etc., the particles in the two surfaces are subjected to opposing oscillations simultaneously, so that the thickness of the plate varies in the rythm of the oscillation. In the case of even harmonics, viz. $2f_0$, $4f_0$, etc., the particles oscillate simultaneously but in
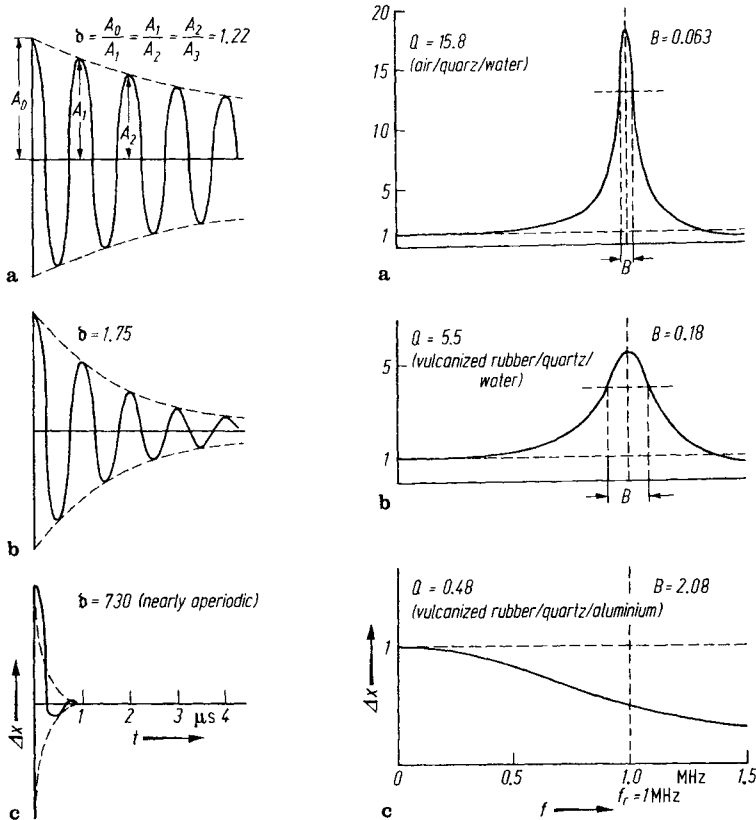
Fig. 7.8. Decay of oscillation of a thickness oscillator for different damping coefficients b (oscillator as in Fig. 7.9)

Fig. 7.9. Resonance curves of forced oscillations of a thickness oscillator as in Fig. 7.8 (Qualities, Q = **a** 15.8; **b** 5.5; **c** 0.48)

the same direction so that the thickness of the plate remains unchanged. From an outside viewpoint it merely oscillates back and forth as a whole.

Mechanical excitation, for example by a physical shock, can produce in a plate higher characteristic vibrations in addition to the fundamental, as well as bending vibrations, resulting overall in a rather complex oscillation. However, thanks to the piezo-electric effect it can be excited electrically in its fundamental characteristic oscillation by applying to its metallized surfaces an alternating voltage corresponding to its characteristic frequency.

If a shock-excited plate is allowed to oscillate freely, its sinusoidal oscillation does not remain constant because the plate constantly loses energy by two mechanisms, viz. internal friction and energy convection in the form of ultrasonic waves transmitted to the mounting and the surrounding material. The first cause is usually insignificant compared with the second which is the real purpose of the oscillator. Due to the loss of energy the oscillation is damped and the amplitude decreases from one oscillation to the next by the factor $\mathfrak{b}$ known as the damping coefficient (Fig. 7.8). As will be explained later, this quantity depends essentially on the material to which the plate is coupled. In the case of the damped oscillation the frequency is in practice that of the characteristic frequency of the oscillation without damping. Only for high values of damping are the frequency deviations appreciable.

If the piezo-electric plate is excited by an alternating voltage of a frequency different from its fundamental, it will oscillate at this applied frequency, after initial build-up, as a forced oscillation with constant amplitude. The amplitude achieved depends on the exciting frequency (Fig. 7.9) and for very small frequencies it is practically identical to the static thickness change of Eq. (7.1), which is arbitrarily taken to be 1 in Fig. 7.9. Up to the resonance frequency f_r it increases to a maximum value which depends on the coefficient of damping, after which it falls again.

At the resonance frequency f_r the plate is excited to the largest amplitudes. This frequency usually differs somewhat from the characteristic frequency f_0 which is the frequency of the free-oscillating plate, whether damped or not.

This increase at resonance is equal to the *quality* Q and is defined as the ratio of the amplitude at the resonance frequency (not the characteristic frequency) to the static thickness change:

$$Q = \frac{\Delta x_{\text{fr}}}{\Delta x_{\text{stat}}}. \tag{7.7}$$

The quality is linked to the damping coefficient $\mathfrak{b}$:

$$Q = \frac{\pi}{\ln \mathfrak{b}} \; (\ln \mathfrak{b} = 2.303 \; \lg \mathfrak{b}). \tag{7.8}$$

The quality is linked also to the band width of the resonance curve. If the band width B of the resonance maximum is defined according to Fig. 7.9, and measured at 70 % (more accurately at $1/\sqrt{2} = 0.707$) of the maximum value, the following equation applies if the damping is not excessive, i.e. for Q-values above say 10:

$$B = \frac{f_r}{Q}. \tag{7.9}$$
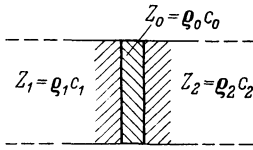
Fig. 7.10. Radiator between two materials 1 and 2

Formulas (7.8) and (7.9) should be regarded only as approximations because their derivation presupposes that the oscillating piezoelectric plate behaves like a mass suspended by a spring However, this is only approximately so, because, particularly in the case of high damping, the deviations are considerable. In the testing of materials by means of sound pulses damping coefficients of this order are necessary, so that when calculating the resonance amplitude and the band width, considerably more complex, exact calculations should be used [1302].

When using a piezo-electric plate as an ultrasonic generator, the relation between the damping coefficient and the constants of the contiguous materials is of interest. Let it be assumed that the plate is located between two materials 1 and 2 with the acoustic impedances Z_1 and Z_2 ($Z = \varrho c$) (Fig. 7.10). As long as Z_1 and Z_2 are both smaller than Z_0, the acoustic impedance of the piezo-electric material, i.e. for sonically soft coupling on both sides, the following applies:

$$\mathfrak{d} = \frac{(Z_0 + Z_1)(Z_0 + Z_2)}{(Z_0 - Z_1)(Z_0 - Z_2)}. \tag{7.10}$$

(For derivation of equations see [1302].)

Equation (7.10) is also valid if both contiguous materials are sonically harder than the piezo-electric material. If, however, one of the two materials is sonically softer while the other is sonically harder, the piezo-electric plate oscillates only at $\lambda/4$ resonance, i.e. the characteristic frequency of the plate damped in this way is only half as high as given by Eq. (7.5), and the damping coefficient in this case is:

$$\mathfrak{d} = \frac{(Z_0 + Z_1)^2 (Z_0 + Z_2)^2}{(Z_0 - Z_1)^2 (Z_0 - Z_2)^2}. \tag{7.11}$$

Example. Let it be assumed that a quartz plate is mounted so that one side borders on air and the other on water. From the values $Z_1 = 0.4 \times 10^3$, $Z_2 = 1.5 \times 10^6$, and $Z_0 = 15.2 \times 10^6\ \mathrm{Ns/m^3}$ it follows that $\mathfrak{d} = 1.22$ (Fig. 7.8 a). This quartz is now cemented at the back to vulcanized rubber. From $Z_1 = 2.8 \times 10^6$ we get $\mathfrak{d} = 1.75$ (Fig. 7.8 b). This applies not only to a plate of 1 MHz, but according to Eq. (7.10) the damping coefficient is independent of the resonance frequency. If, however, we now let the quartz cemented to vulcanized rubber radiate into aluminium instead of water, so that $Z_2 = 16.9 \times 10^6$, the resonance frequency of the plate is now only half as high. To facilitate the comparison Figs. 7.8 and 7.9 however, have been drawn as if a plate of half thickness were used for this test. In this case the damping coefficient should be calculated according to Eq. (7.11); this gives $\mathfrak{d} = 730$, i.e. in this case the plate is already damped almost aperiodically because the amplitude of the second oscillation is now only 1/730 of that of the first and the third only $1/730^2 = 1/533\,000$. For practical applications it must, however, be taken into consideration that a thin layer of cement between crystal and aluminium reduces the effective acoustic impedance of the material so that invariably smaller damping values will be obtained in tests.

In practice, the coupling conditions of a probe may fluctuate considerably with the surface quality, surface shape and material of the test piece, and therefore also the damping. In order to reduce excessively large fluctuations the unchanged acoustic impedance Z_1 of the

damping body cemented to the back can be chosen high. However, this can be done only at the expense of sensitivity because the oscillation-amplitude, and therefore also the amplitude of the radiated sound, decrease with increasing damping factor.

So far the fundamental oscillation of a piezo-electrically excited plate has been discussed. The harmonics will now be analysed and for this purpose we assume that also in this case the plate is on both sides in contact with sonically soft materials. It is found that only the odd harmonics can be excited piezo-electrically, i.e. after the first resonance f_r, further resonances occur at $3f_r$, $5f_r$, etc. Figure 7.9 should be supplemented on the right towards the region of higher frequencies by these additional resonance peaks. The correlated damping factors increase with the order of the harmonic, i.e. they are proportional to 3, 5, etc. Therefore, at constant exciting voltage, the amplitude of the radiated sound wave decreases at the same rate.

Even if the resonance curve shown in Fig. 7.9 is supplemented by the resonance peaks of the harmonics, it still differs from any measured curves because every quartz plate always has additional resonance peaks produced by additional deformations, linked to the thickness oscillation, which have been neglected here.

As far as the testing of materials is concerned, the oscillation amplitude of the piezo-electric plate is less important than the sound pressure of the radiated sound wave. The sound pressure is proportional to the oscillation amplitude and the frequency, so that at frequency 0 the resonance curve starts at zero and not with a finite value as shown in Fig. 7.9. Further, the resonance peak is symmetrical about its resonance frequency. Only in the case where the piezo-electric plate borders on the one side on a sonically hard material and on the other on a sonically soft material, is the resonance peak shifted from the above-mentioned $\lambda/4$ point towards higher frequencies and becomes asymmetrical.

Conversely, if a similar plate is used as receiver, the no-load voltage produced at the plate (i.e. without the load of measuring instruments) is proportional to the amplitude of the oscillation. Therefore, this receiving voltage of the piezo-electric plate again has an asymmetrical form as shown in Fig. 7.9.

If similar plates are used as transmitter and receiver (or, as in the echo method, the same plate is used first as transmitter and then as receiver) and if we consider the ratio of receiving voltage (no-load voltage) to transmitting voltage, the frequency curve with its resonance peak has to be considered twice. Figure 7.11 shows curves of this type calculated according to [1302]. It should be mentioned here that electrical matching of the receiver plate of an amplifer can deform the curves considerably. In calculating the curves shown in Fig. 7.11 it was assumed that no loss of sound pressure occurs between transmitter and receiver as a result of the conditions of propagation.

It should be pointed out that the ratio of receiving no-load voltage to transmitting voltage is independent of the size and thickness of the piezo-electric plate. Figure 7.11 is therefore valid for all sizes of oscillator and the size of the plate influences only the conditions of sound propagation (beam spread, length of near-field).

The sound field of a piezo-electric plate used as transmitter has been discussed in Sections 4.1 and 4.3. It should be added that if the piezo-electric plate is used as receiver it has the same field of sensitivity. According to a general principle, viz. the reciprocity theorem, the transmitter characteristic equals the receiver character-
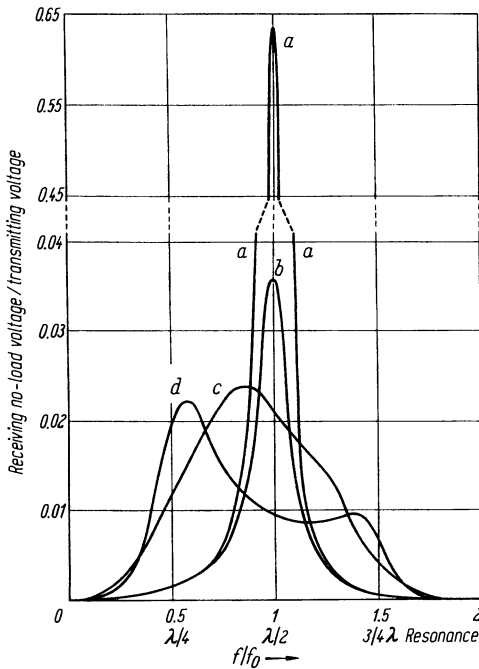
Fig. 7.11. Quartz plate operated simultaneously as transmitter and receiver. The ratio, receiver no-load voltage to transmitting voltage, is plotted for the following damping conditions: Sound radiation in water (curves a and b), in aluminium (c), in steel (d). Damping at back: a air; b, c, d vulcanized rubber (as in Figs. 7.8 and 7.9) (piezo-electric constant $h_{33} = 4.9 \times 10^9$ V/m, see Table 7.1). Loss-free propagation of sound between transmitter and receiver has been assumed

istic. As far as the far-field is concerned this means for instance that an incident wave of constant sound pressure but variable angle of incidence produces in the receiving crystal a voltage which reaches a maximum at perpendicular incidence, and which decreases in the case of oblique incidence according to a characteristic as shown in Figs. 4.15.

In the echo method where the radiator functions both as transmitter and receiver, the directional characteristic in the far-field therefore enters twice as a factor. The same applies to the near-field. The ratio of receiving to transmitting voltage is therefore determined in the case of a small reflector movable in the sound field, by the square of the functions described in Chapter 4 exclusively for the sound field of the transmitter. The characteristic consequently becomes more pointed.

7.3* The Piezo-electric Transducer with Pulse Excitation

Let us first answer the question as to why a low damping of a given piezo-electric plate is not always advantageous. In order to radiate a continuous sound wave at the maximum possible sound pressure and a given frequency, it is logical to excite a suitable plate at its natural frequency and to keep its damping at a minimum. For this purpose it is advantageous to let it be damped only by the coupled material

while it borders on air at the back. In non-destructive testing this is rarely the case, because even if continuous ultrasonic sound is used for the test it will usually be necessary to sweep the frequency to avoid the creation of standing waves in the test piece. In this shifting of frequency the amplitude should remain as constant as possible which, however, a narrow resonance curve does not permit. Ideal would be a frequency curve with a partially flat region, which, however, is difficult to achieve if one does not want to operate with very small amplitudes at frequencies far from the resonance point. A compromise is then made and the resonance curve is broadened as required by introducing suitable damping, resulting in the *band* not being completely smooth but decreasing to only 70 % of the maximum value at its limits.

An adequate band width is particularly important when transmitting short pulses. In the echo method the length of the pulse may prevent the detection of flaws near the surface and pulses of minimum duration are therefore desirable. At high frequencies these pulses may still consist of a large number of oscillations. This advantage is, however, offset by the fact that the damping of most materials increases with the frequency. It is therefore necessary to generate and transmit pulses at frequencies which are not excessively high and with a minimum number of oscillations; it may even be advisable to produce completely aperiodic, i.e. socalled shock pulses or transients.

Every pulse can be presented in sinusoidal form by a Fourier series as the sum of a given number of partial oscillations unlimited in time and contained in a frequency band of given width. Before and behind the pulse these partial oscillations cancel each other exactly. The shorter the pulse, regardless of its shape, the broader is the frequency band of appreciable amplitude. If some of the frequencies are suppressed in the case of pulse transmission by a mechanical or electrical system, the transmission distorts the pulse, and in particular lengthens it. The rule applies that in order to transmit a pulse of duration T without considerable distortion, a frequency band of width $B = 1/T$ is sufficient even if the latter has already decreased to 70 % at both ends, as in the case of the resonance curve shown in Fig. 7.9.

A band width of 0.18 MHz shown in Fig. 7.9 b, therefore, could transmit with practically no distortion a pulse of $1/0.18 = 5,5\,\mu s$ duration, e.g. 5 oscillations of 1 MHz frequency, each lasting 1 µs. If, however, one attempts to place on such a piezo-electric plate a pulse of 1 µs duration, the corresponding frequency band of 1 MHz is not transmitted, and the transmitted pulse would not be shorter than 5 µs as already indicated by the decay process of the plate shown in Fig. 7.8 b.

If a transmission circuit contains several series-connected elements, e.g. transmitting transducer, receiving transducer and amplifier, the above statement applies to the total transmission curve which is the product of the individual transmission curves. The various elements, therefore, must match each other and it is futile to connect a wide-band transducer to a narrow-band amplifier, and vice versa. Also, the material through which the pulse passes in the form of a sound wave may influence the frequency band, because its damping increases rapidly at higher frequencies.

Let us consider various types of electrical pulses and investigate how the piezo-electric plate behaves in these cases. First, let us take an alternating voltage train with 10 oscillations at the natural frequency of the plate (Fig. 7.12 a). At the beginning and end this train suddenly disappears. However, because of its inertia
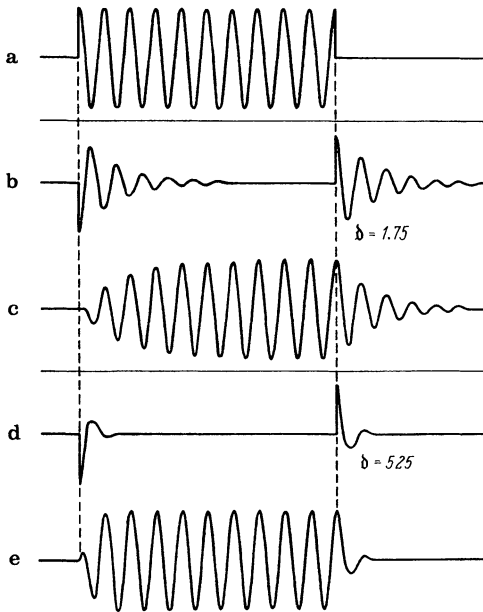
Fig. 7.12. Excitation of a piezo-electric plate by an alternating voltage train with damping coefficients 1.75 and 525, excitation frequency equals natural frequency. **a** Alternating voltage train, identical with oscillation pattern of an inertialess plate; **b** transient oscillation of actual plate for $\mathfrak{b} = 1.75$. **c** oscillations occurring in the actual plate, i.e. the sum of (**a**) and (**b**) · (**d**) transient oscillations for $\mathfrak{b} = 525 \cdot (e)$ oscillation of plate, i.e. sum of (a) and (d)

and the elastic forces, the plate tends to resist any sudden changes and smothes them out at the beginning and at the end of the oscillation by buildup and decay processes. The actual oscillation of the plate is therefore composed of the motion of an inertialess plate subjected to the influence of the voltage, which the plate follows precisely, and the transient oscillations. In Fig. 7.12 the curves a and b should therefore be added, so that the actual oscillation of the plate is obtained in c. Here again a damping coefficient $\mathfrak{b} = 1.75$ was assumed, as in Fig. 7.8 b. The transient oscillation is the free characteristic oscillation of the plate, and Fig. 7.12 b is therefore identical with Fig. 7.8 b; the latter oscillation, however, as a build-up process, should be taken to be negative because it opposes the electrical excitation. However, at the end of the pulse, it acts in the same sense, i.e. it tries to support the electrical excitation.

With higher damping (Figs. 7.12 d and e for $\mathfrak{b} = 525$) the effect of the transient oscillation is less important and the actual oscillation already resembles the exciting voltage much more closely. It should, however, not be overlooked that the amplitude decreases inversely with the damping coefficient; in the illustration this has not been taken into account.

The build-up of the natural oscillation depends entirely on the impressed conditions, for which a particularly simple and clear case has been chosen here, viz. appearance and disappearance of the pulse voltage exactly at a maximum. The correlated build-up process always develops in such a manner that it exactly cancels the motion of an intertialess plate at the beginning.

The shorter the duration of the excitation and the lower the damping of the plate the greater the proportion of transient oscillations in the pulse. In Fig. 7.13 a
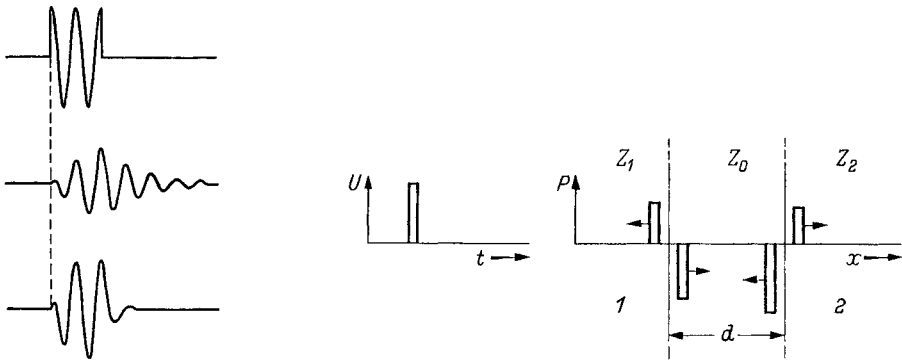
Fig. 7.13. As in Fig. 7.12 but with shorter pulse (corresponding to Figs. 7.12 a, c and e)

Fig. 7.14. Sound-pressure waves, excited by the voltage U as a function of time, along the axis of a transducer plate sandwiched between two materials 1 and 2. For reasons of simplicity, the same sound velocity has been assumed in 1 and 2 and the scale chosen so that the pulse width is the same both in space and in time

pulse of only two oscillations of the characteristic frequency was used for excitation. With $\mathfrak{b} = 1.75$ the oscillation of the plate already fails to reach the maximum value, and build-up and decay already start to overlap. The plate with the greater damping still transmits the pulse almost undistorted, but with smaller amplitude. This disadvantage is partially offset by the fact that this plate reaches its oscillation peak earlier than the less damped plate.

Since short pulses are particularly important in non-destructive testing, the results of a more rigorous treatment of the piezo-electric plate will now be described, which makes it possible to construct correctly the pulse of the sound pressure of interest for arbitrary, exciting voltages by using a rather simple and fruitful method [258, 1246].

Without presenting its derivation, it is recommended that the following, basic rule concerning piezo-electric plates operated as transmitters be memorized (see Fig. 7.14):

If an arbitrary voltage is applied to a piezo-electric plate, sound-pressure waves which show the same chronological pattern as the voltage start simultaneously from both surfaces. They travel into the plate as well as into the materials coupled to it externally, but inside the plate their phase is opposite to that outside. Their amplitudes depend on the acoustic impedances of the materials concerned as follows:

Material 1 (Z_1)	Material 0 (Z_0) (Piezo-electric plate)		Material 2 (Z_2)
$\dfrac{Z_1}{Z_0 + Z_1}$	$\dfrac{Z_0}{Z_0 + Z_1}$	$\dfrac{Z_0}{Z_0 + Z_2}$	$\dfrac{Z_2}{Z_0 + Z_2}$

If the waves inside the piezo-electric plate strike the boundary, the well-known formulae given in Eq. (2.1) apply for their reflection and transmission, together with

the rule: phase reversal at reflection on sonically softer material. Further, they superimpose upon each other without distortion.

It is at this stage already no longer surprising that two waves travel in opposite direction in the plate, if it is realised that we have come to regard the oscillation of a plate in its fundamental and harmonic modes as a standing wave which may be composed of two waves travelling in opposite directions. This concerned the special case of sinusoidal waves, a limitation which is now discarded. Instead of the square waves in Fig. 7.14, any other arbitrary voltage and wave form may be used.

The above rules will now be applied to various boundary conditions and pulse forms. First, a short square wave pulse, as in Fig. 7.15, will be assumed in a thick plate so that the delay in the plate exceeds the duration of the pulse. Further, let us
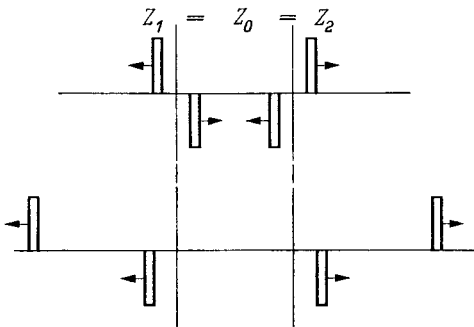
Fig. 7.15. As in Fig. 7.14, but with reflection-free matching on both sides
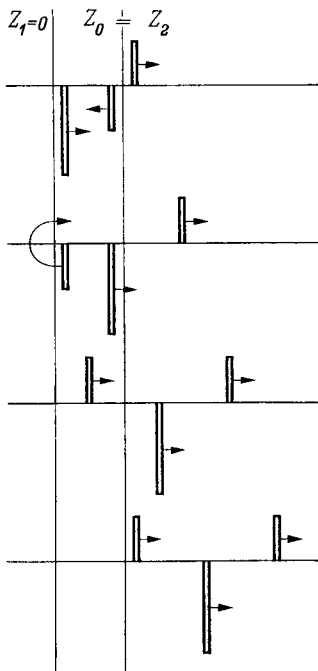
Fig. 7.16. As in Fig. 7.15 but with free boundary on the left and reflection-free matching on the right

first take the simple case of a reflection-free boundary on both sides, viz. $Z_1 = Z_0 = Z_2$, which can approximately be realised experimentally by a quartz plate sandwiched between aluminium, resulting in the four waves being identical. The internal waves pass unimpeded through the opposite faces and completely leave the piezo-electric plate (Fig. 7.15). Thus, outside the plate, two identical, opposing pulses follow each other at an interval determined by the delay in the plate.

Figure 7.16 shows the case where the plate on the left borders on air. The wave from the right is totally reflected with phase reversal. In Fig. 7.17, however, the matching on the right is no longer reflection-free, Z_2/Z_0 being chosen 0.25, which corresponds approximately to quartz/perspex. This results in a sequence of pulses which follow each other at the delay distance of the plate, Fig. 7.18 showing the first eight pulses on an enlarged scale. The second pulse is always twice as large as the first and the later pulses decrease in a constant ratio.

Other terminal conditions, e.g. the sonically hard termination, can be similarly treated. Here, however, only the length of the square wave voltage will be increased, again with reflection-free termination on both sides (Fig. 7.19). If the duration of the square wave voltage equals the transit time, the sound pressure has the form of a square wave oscillation, and if it becomes much longer (or if the piezo-electric plate is thin) only narrow pulses remain at the beginning and at the end. Between these pulses, the next wave (from the opposite plate surface) exactly cancels the first wave because of its reversed sound pressure. In the case of a thin plate, a step voltage, therefore, produces only one narrow pulse if the plate has reflection-free termination. If the square wave voltage is replaced by a sinusoidal voltage, only a
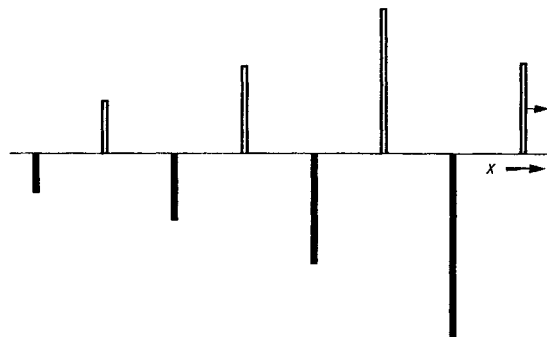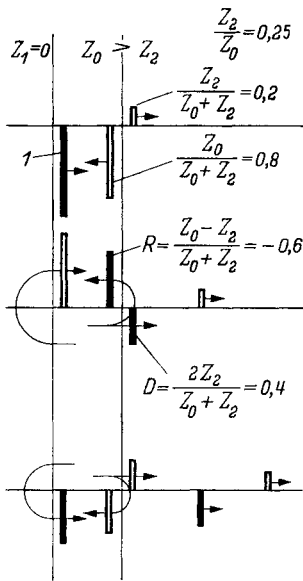
Fig. 7.17. As in Fig. 7.16 but with sonically soft matching on the right. $Z_2/Z_0 = 0.25$

Fig. 7.18. The first 8 pulses of Fig. 7.17 shown on enlarged scale over path x
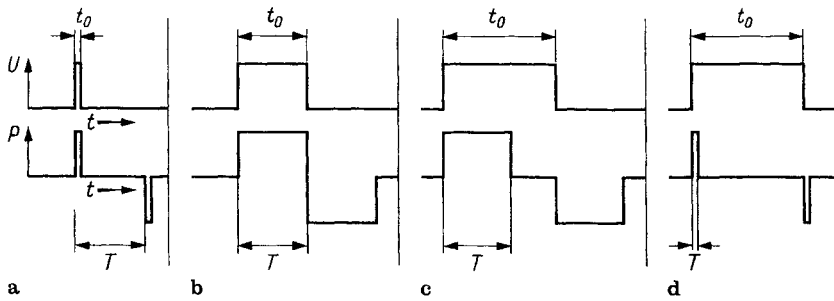
Fig. 7.19. Excitation of a reflection-free terminated oscillator by square wave voltages of different duration relative to the transit time in the oscillator. Pulse duration t_0 transit time T. **a** $t_0 < T$; **b** $t_0 = T$; **c** $t_0 > T$; **d** $t_0 \gg T$ (thin transducer plate)

very low sound pressure remains because two opposing half waves must be added at only a slight relative time lag.

In the case of excitation by several consecutive pulse voltages it is merely necessary to obtain the result for a single pulse and to add similar results, shifted according to the time lag of the pulses, respectively. In this way the sound wave corresponding to a given train of sinusoidal waves can be plotted on the basis of the result of a sinusoidal half wave and one can thus determine the build-up and decay proccesses also in the absence of resonance. In practice this is done by calculation or graphically.

As far as the receiver is concerned, the following rule applies (Fig. 7.20):
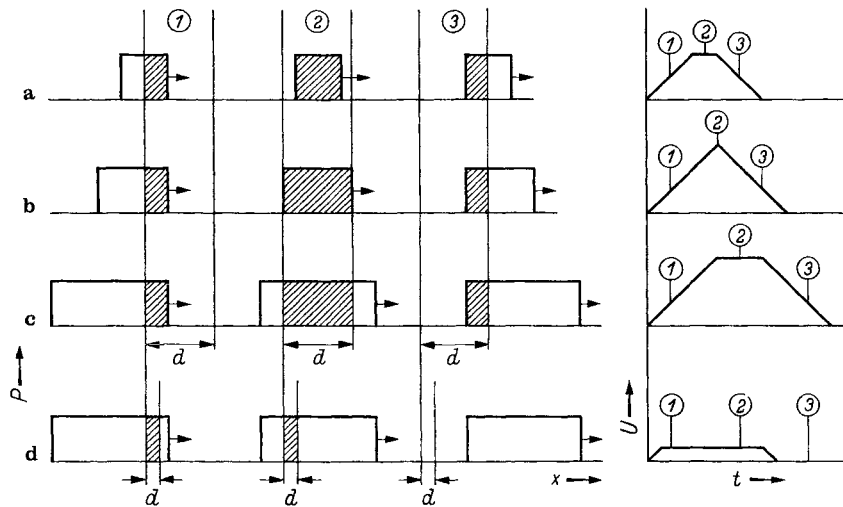
Fig. 7.20. Reception of a square wave by a piezo-electric plate matched on both sides. Receiving voltage U as a function of time for waves of different length. **a** Pulse duration $t_0 <$ delay T; **b** $t_0 = T$; **c** $t_0 > T$; **d** $t_0 \gg T$ (thin receiver)

If an arbitrary sonic pressure wave enters a piezo-electric plate, an electric no-load voltage is produced at its electrodes which is proportional to the area of the sonic pressure curve of the wave which has already entered. If several waves are propagated in the plate simultaneously, e.g. by zigzag reflection, their areas are added with due regard to sign.

The example in Fig. 7.20a shows a square wave which enters a thick plate (duration of wave shorter than transit time). The area inside the plate (shaded) increases linearly, and, therefore, also the voltage. It remains constant as long as the whole wave travels inside the plate. Since it has been assumed that the back of the plate is matched reflection-free, the wave leaves the plate unimpeded and the voltage, therefore, again drops to zero.

If the wave is longer, it can fill the plate completely and the voltage reaches a maximum which persists as long as the plate is filled. Finally, if the wave is very long compared with the transit time (Fig. 7.20d), it increasingly resembles the voltage curve. Thus, if the back of a piezo-electric plate is matched correctly, and the thinner the plate, a sound wave can be transformed into a voltage with increasing faithfulness. In this case, however, the amplitude of the voltage decreases with the thickness of the plate because the area is reduced.

Within a real crystal the area of the diagrams filled by the wave of course means the volume.

In practice it is not an easy matter to terminate a piezo-electric plate reflection-free. If the termination at the back is sonically soft, reflections at this point are produced with phase reversal. A single, short pulse, therefore, produces an alternating voltage of decreasing amplitude (Fig. 7.21).

If one reverses the polarity of a piezo-electric plate, the transmitted pulse also reverses its phase, i.e. it starts with a maximum instead of a minimum of sound pressure or vice versa. If the same plate also serves as receiver the form of the electric pulse will be the same in both cases. The effect of polarity therefore is only of influence if different plates are used.

Finally, Fig. 7.22 shows a case of practical interest calculated by the method described; this concerns the transmission from an X-cut quartz plate backed by vulcanized rubber through water, a similar transducer acting as receiver. The exciting
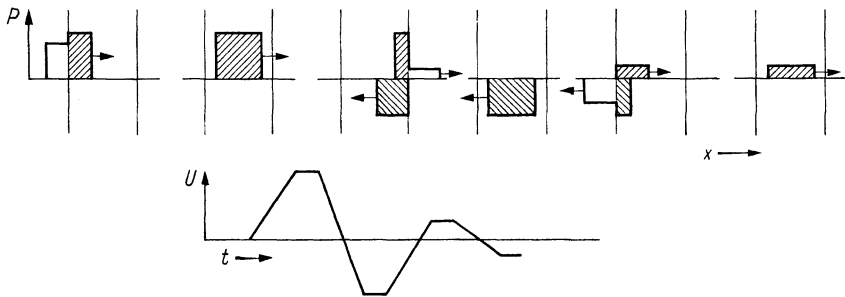
Fig. 7.21. Reception by a piezo-electric plate with sonically soft termination on both sides, left $Z_0/Z_1 = 2$, right $Z_0/Z_2 = 9$. Receiving voltage U as a function of time
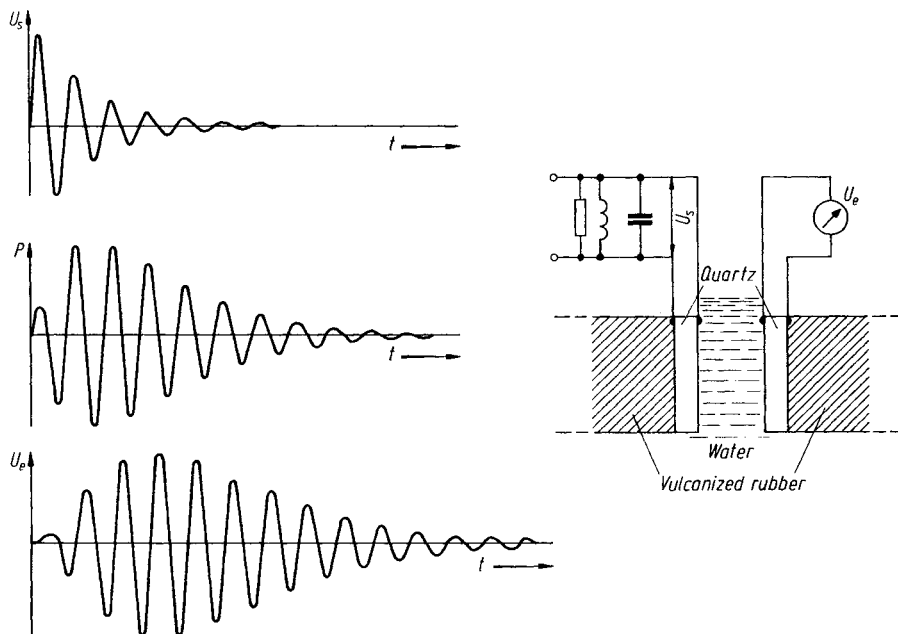
Fig. 7.22. Transmission of an electric pulse in the form of a damped oscillation with $\mathfrak{b} = 1.75$ from transmitter to receiver in resonance at $\mathfrak{b} = 1.75$. Transmitting voltage, sound pressure and receiving voltage as functions of time, maxima arbitrarily shown equally large

voltage, as is frequently done, is the damped oscillation of a resonating circuit with the characteristic frequency of the plate. Both the resonating circuit and the plate have the damping coefficient $\mathfrak{b} = 1.75$, wherein it is assumed that the plate produces no reaction on the resonating circuit and the rest of the generator circuit. This applies approximately to quartz with its small electromechanical coupling.

The example shows how resonance of both the transmitter and the receiver changes the original pulse. The build-up is flattened and the decay increased considerably. Special attention is drawn to the build-up of the receiving voltage, which due to the formation of the area integral is always very flat. The considerable distortion of the pulse can be reduced by better damping as well as by off-resonance excitation.

When coupling a transducer to a solid via a thin layer of liquid the problem becomes more complex due to the multiple reflections in this layer. Basically it can, however, also be solved by adding the individual waves according to amplitude and phase. It turns out that this considerably changes the resonance curve of the transducer, particularly by the appearance of two peaks.

Finally, the matching of the piezo-electric plate to the electric transmitter will briefly be discussed. Greatly simplified, a piezo-electric plate of thickness $d = \lambda/2$ excited at its fundamental frequency can be replaced by its static capacitance C_0 in parallel with an ohmic resistance R_s, as long as the plate is not excessively dis-
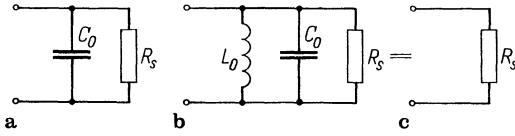
Fig. 7.23. Equivalent circuit diagram of a piezo-electric plate at resonance (**a**). If the static capacitance C_0 of the plate (including the capacitance of the circuit and the cable) is adjusted by means of coil L_0 to electric resonance, only the effective radiation resistance R_s remains (**b**) and (**c**) if other losses are neglected

turbed by contiguous materials (Fig. 7.23). This *radiation resistance* shown in the equivalent circuit, consumes the same energy as radiated by the plate into the contiguous material. If the capacitance, as is customary, is balanced by an inductance L_0 connected in parallel and tuned to resonance, only R_s remains. However, it should also be taken into consideration that by L_0 also the capacitances of the cable and the instrument are compensated. If the instrument is changed or the length of the cable, this may also change the test frequency [126]. If Z_1 and Z_2 are the acoustic impedances of the materials adjacent to the piezo-electric plate, the acoustic impedance (converted according to [633], where a series circuit was assumed as equivalent circuit) is obtainsd from

$$R_s = \frac{1}{S f_r^2} \left(\frac{c^2 (Z_1 + Z_2)}{16 h_{33}^2 \varepsilon_r^2 \varepsilon_0^2} + \frac{h_{33}^2}{\pi^2 (Z_1 + Z_2)} \right) \Omega,$$

where S (m^2) is the area of the radiator, f_r (Hz) the resonance frequency of the undamped oscillation, and $\varepsilon_0 = 8.86 \times 10^{-12}$ As/Vm the universal constant. Typical constants c, h_{33}, ε_r of the piezo-electric material are given in Table 7.1.

Modern transmitter circuits usually have a very low impedance. Therefore electrical matching of a probe is only necessary to the input impedance of the amplifier. If these impedances differ very much, a simple inductance connected in parallel to the input does not suffice and a transformer is necessary. In addition the probe cable has to be terminated with its cable resistance, at least when using long cables and high frequencies, so as to avoid interfering reflections in the cable.

Tuning of the electric circuit to equal the mechanical resonance frequency of the plate will not only improve the sensitivity for the frequency used, but also suppresses interfering frequencies. As we have seen a plate excited by a short shock resonates not only at its fundamental frequency, but also in harmonics and cross oscillations. These latter are related to the much larger transverse dimensions of the plate and therefore have much lower frequencies. So resonance tuning also acts as a filter for unwanted oscillations.

8* Other Methods for Transmitting and Receiving Ultrasound

As well as the piezo-electric effect, other physical properties can be utilized for generating and receiving ultrasound. Although many of these produce weaker signals than are obtainable by the piezo-electric effect, they nevertheless offer a number of advantages which in special cases make their application in the testing of materials useful. In the case of many of these effects the energy is transmitted by electrical or magnetic fields which in principle make mechanical contact with the metallic test piece unnecessary. The conversion into, or from, acoustic energy takes place in the surface of the workpiece concerned. Compared with the piezo-electric oscillator, which is coupled to the workpiece, the surface of the work piece forms in the case of these "direct" methods a part of the acoustic transducer. The direct or dry methods thus require no coupling medium, and so avoid some of the difficulties analysed in the paragraph below.

Wet coupling can introduce various disturbances. Due to the interference of the waves reflected at the two interfaces, the transmissibility of a liquid layer depends to a great extent on its thickness, and can approach zero if the couplant thickness equals a quarter wavelength. Consequently it is necessary to reduce the thickness of the liquid layer to a minimum and to keep it constant. This is not easy if the testing is carried out at high speed as in some automated installations. When testing hot workpieces, the difficulty of finding a suitable couplant increases with the temperature. Finally, a certain amount of wear due to abrasion is unavoidable in all cases where the probes come into mechanical contact with the workpiece.

An ideal method would allow doing without coupling liquid and operate at an appreciable distance from the surface, so that the uncertainties of coupling to the surface could be avoided, as well as wear and tear. In addition such a method could be used on hot surfaces and minimise the problem of protecting the probe from excessive heat.

A further advantage of the direct methods results from the fact that there are no mechanically oscillating components in an electro-acoustic transducer since such components have a natural frequency which influences the overall frequency response. For this reason the direct methods are more suitable for applications where a resonance-free frequency range is important, for example, for shock waves.

The use of effects other than piezo-electricity for the acoustic transformation may also prove advantageous for a quite different reason. If different effects are used for transmitting and receiving the sound, it will be much easier to protect the receiver from direct cross-coupling.

For instance, if in a given test system an electro magnetic transmitter is used in conjunction with an electro static receiving system, the receiver does not react to the magnetic field of the transmitter if the set-up is correct. Consequently, an out-

put signal can be produced only by acoustic pulses coming from the workpiece concerned. Here, a receiver using an induction coil would be unsuitable because in practice it is impossible to decouple magnetically the transmitting and the receiving coil.

In the following all possible physical effects suitable for transmitting and receiving ultrasound for the testing of materials will be discussed and the probes which utilize these effects will be analysed.

8.1 Mechanical Effects

The direct mechanical generation of sound, although not contactless, requires no coupling liquid. Sound can be produced in a body by mechanical shock or friction. This phenomenon, well known in the audible range, produces a wide frequency spectrum with portions in the megahertz range. The spectrum depends on the shape, size and material of the objects exposed to the shock. All types of waves are generated, most effectively in the range from 100 kHz to 1 MHz. Therefore are such methods can be used for testing concrete, cast iron and similar materials. When testing concrete (cf. Section 32.5) electromechanical hammers are used as transmitters. For the excitation in glued honeycomb structures rotating wire brushes have also been used [593].

For reception the effect of the sound radiation pressure in liquids (see Section 1.3) can be exploited. A receiver which uses this principle and which has found some application is the Pohlman cell [2]. However, compared with the conventional probes, it requires considerable sound amplitudes and a long response time (see Section 13.9).

Pressure-sensitive liquid crystals also permit the reception of sound since their optical activity (rotating the plane of polarization of transmitted light) is pressure sensitive.

8.2 Thermal Effects and Laser Techniques for the Generation of Ultrasound

By heating the surface of a body suddenly ("heat shock") the thermal expansion of the material produces mechanical stresses and these initiate sound waves. If the heating is of very short duration (lasting approx. 10 ns), very high frequencies and shock waves can be produced. This requires the thickness of the heated layer to be small compared with the wavelength of the sound [552, 1749, 1616]. All kinds of sound waves are generated.

The required energy is beamed onto the surface of the object concerned and this can be realized in two ways:

1. By electromagnetic waves (microwaves, infrared, visible and ultraviolet light);
2. By corpuscular radiation (electron beams)
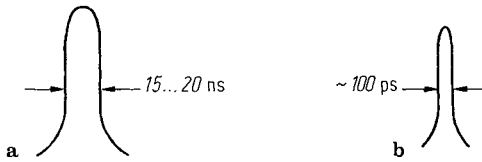
Fig. 8.1. Shapes of light pulses for excitation of sound pulses. **a** Nd-YAG-laser; **b** mode-coupled Nd-YAG-laser
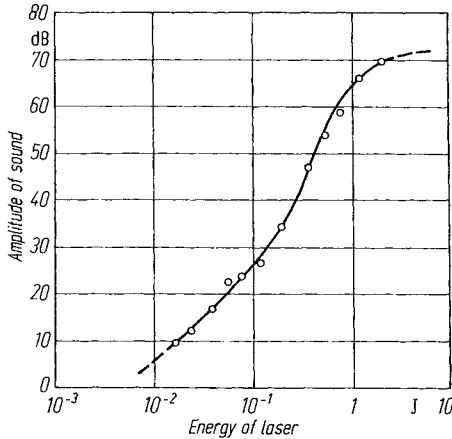
Fig. 8.2. Sound amplitude as function of the laser energy per pulse for a light wavelength of 1.06 μm

The subsequent conversion into heat is effected in several stages which according to [1572] differ for wave and corpuscular radiation.

The sound pulse closely corresponds to the shape of the light pulse and by using an appropriate type of laser one may influence the Fourier spectrum of the sound pulse by the narrowness of the light pulse [1387]. In the range 1 to 30 MHz, which is useful for testing materials, suitable laser pulses are shown in Fig. 8.1. For higher frequencies up to 100 MHz one can use pulses in accordance with Fig. 8.1 b.

The relation between the generated sound amplitude and the energy of the light pulse for longitudinal ultrasonic waves is given in Fig. 8.2. For low light energies the relationship is linear but with higher energies a plasma layer is built up on the surface which increases the sound pressure considerably. This range in Fig. 8.2 goes from 0.3 to 1.0 J, energies commonly used for materials testing. In this range sound pressures can be reached of the same order as those produced by piezo-electric generators, and without damaging the surface of the specimen.

Fundamentally, incident light pulses can excite all types of sound wave, but there are possibilities of exciting certain types preferentially (Fig. 8.3). For example longitudinal waves are generated when the surface is covered by a plasma (Fig. 8.3 b).

The reason for this effect is to be found in the recoil forces of the plasma. If it is required to generate surface waves preferentially a shock must be applied to the surface only over a length small compared to the required wavelength, especially by using a short rise-time of the light pulse. A directional surface wave is obtained by
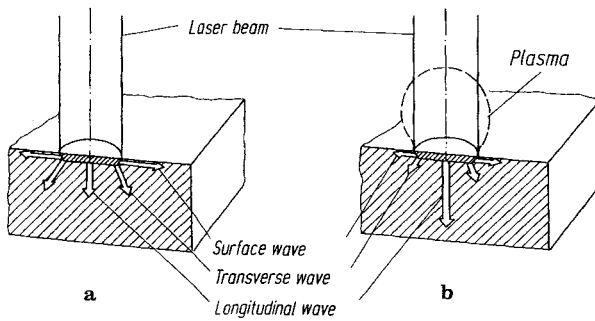
Fig. 8.3. Excitation of ultrasound without (**a**) and with (**b**) plasma on the surface

such excitation on narrow parallel lines by using appropriate slotted diaphragms in the laser beam.

One of the advantages of using laser-pulse excitation is the possibility of using large operational distances of up to 10 m. A further advantage arises from the fact that the velocity of light is high compared to that of sound, which means that all parts of an excited surface area are in practice struck simultaneously. The generated pulse is therefore independent of the angle of the incident light and hence also the angular directivity of the generated ultrasonic pulse does not depend on it. This may however, be influenced by appropriate shaping of the excited surface area. From a very small area we obtain a point source (see Fig. 4.23 in Section 4.4) but from a larger area high-frequency ultrasound is radiated more directionally and low-frequency longitudinal waves propagate in a more spherical shape. Within the large frequency range of a shock wave all this happens simultaneously.

A certain directivity can be obtained by excitation of narrow separated strips which work for selected sound frequencies as the analogue of an optical grating
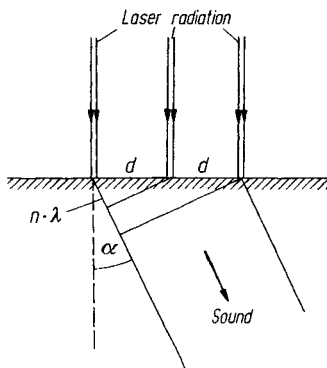
Fig. 8.4. Radiation of sound at an angle to the surface
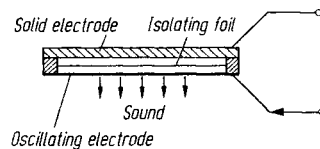
Fig. 8.5. Electrostatic transmitter

(Fig. 8.4). If the strips are separated by the distance d the Huygens' wavelets add up in the correct phase at angles for which:

$$\sin \alpha = \frac{n\lambda}{d}$$

(*n* is an integer, λ wavelength of ultrasound).

By using Huygens' principle we can also calculate the angle of an oblique beam generated by using constant delay times between adjacent strips or for the case in which a complete excitation pattern is moved along the surface at a certain speed.

The temperature of the surface has no noticeable influence.

8.3 Electrostatic Methods

Between the plates of a charged capacitor there are attracting electrostatic forces [28]. This effect may be used for direct excitation of sound in a specimen or for the construction of a transmitter probe. In the first case an electrode can be held at a small distance from the surface of a metallic specimen and subjected to an alternating voltage. The mechanical force on the surface generates an ultrasonic wave at the same frequency as the voltage [906]. Because the forces are perpendicular to the surface, longitudinal waves perpendicular to the surface will be preferentially produced. The resulting amplitudes are usually very small but rather high frequencies and shock waves can be generated by this method.

To build such a transmitter probe a thin metallic diaphragm is mounted at a small distance from a solid metallic electrode as in Fig. 8.5. The radiated ultrasound can be directed into a liquid or even into solids by using a coupling layer.

The effect can also be used for receiving sound by using it in reverse. The voltage across a capacitor energised by a constant electric potential will change if the distance between the electrodes is altered [1518].

8.4 Electrodynamic Methods; EMATs

These methods which are also called magneto-inductive methods, are based on the so-called Lorentz force. This is the force F which acts on a charge e moving in a magnetic field of induction B at a velocity v [28, 580]. The following law applies:

$$F \sim e \cdot v \times B.$$

Transmitting by Means of a Superimposed Magnetic Field

A coil through which an alternating current flows ($i_\sim$) is placed on an electrically conducting body (Fig. 8.6) in which an eddy current is induced of density g (determined by $e \cdot v$) in the small unit volume dV. In this case the force

$$F \sim g \times B$$
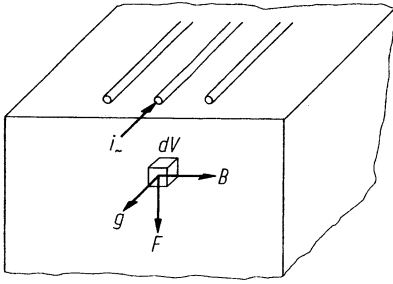
Fig. 8.6. Electrodynamic generation of longitudinal waves
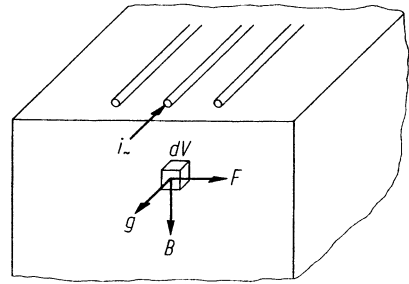
Fig. 8.7. Electrodynamic generation of transverse waves

acts on dV. Here attention should be paid to the directions: the vectors *g*, *B* and *F* are at right angles to each other and *g* opposes the current $i_\sim$ in the coil. By choosing the direction of the magnetic flux *B* one can produce either longitudinal or transverse waves. If *B* is oriented parallel to the surface, Fig. 8.6 shows that the force *F* is perpendicular to the surface and this results in the generation of longitudinal waves.

If *B* is at right angles to the surface (Fig. 8.7), *F* is oriented parallel to the surface, as indicated in Fig. 8.7, and the result is that transverse waves are generated.

The generated sound has the same frequency as the alternating current. The effect produced concerns a volumetric force and due to the finite penetration depth of the alternating magnetic field [28] the necessary condition, that the thickness of the excited layer is small compared with the wavelength of the sound, is fulfilled for ultrasonic frequencies. (Penetration depth here means the depth in the material at which the current has decayed by a factor $1/e$).

This principle can be utilised for the construction of a transmitting probe by placing a flat coil on an electrically and magnetically conducting diaphragm and by orientating the magnetic field as required. Of greater importance, however, are the direct methods using the same principle.

The probes used are designated *EMAT (electromagnetic acoustic transducer)* or sometimes *EMT* or *EMUS*. A survey is given in [492], cf. also [S 77].

Figures 8.8 and 8.9 show the construction principle for testing equipment of this type. The transmitting coil is placed directly on the workpiece which must be electrically conducting. In the drawing the necessary superimposed magnetic field is produced by a permanent magnet. However, since this effect is weak, attempts have been made in practice to increase the efficiency by making the direct field stronger. Electromagnets including those operating by pulsed excitation [465], and even super-conducting magnets up to 11 Tesla (11 T = 110 kG) [1585] have been used.

In the case of the most commonly used flat spiral coils the sound pressure under the centre of the coil has a minimum because the magnetic fields of adjacent sections of the conductors cancel each other at this point.

In practice the maximum working distance is of the order of 1 mm since with increasing probe distance the amplitude of the sound pressure decreases along with
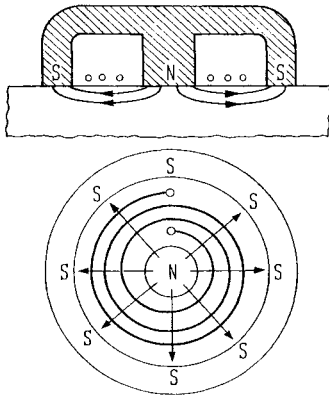
Fig. 8.8. Direct magnetic generation of longitudinal waves in the magnetic field *B* parallel to the surface
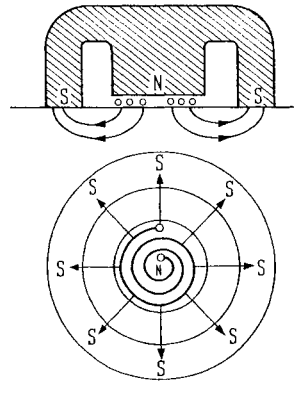
Fig. 8.9. Direct magnetic generation of transverse waves in the magnetic field *B* perpendicular to the surface

both the magnetic field of the AC coil and the DC magnetic field. Due to their different geometries these two fields obey different distance laws and in addition the inductance of the coil changes with distance. Due to the complex interaction of these three effects the decrease in amplitude with distance depends to a large extent on the prevailing test conditions and cannot be expressed by a simple law. For relevant measurements see for instance [33, 1003] where the dependence of the intensity on the DC magnetic field is discussed.

In both the arrangements illustrated in Figs. 8.8 and 8.9, the sound waves are preferentially radiated perpendicular to the surface. The directivity of the longitudinal wave produced in Fig. 8.8 is similar to the beam shown in Fig. 4.15. The transverse wave produced in Fig. 8.9 has, on the other hand, zero amplitude in its axial direction and two symmetrical lobes as shown in Fig. 4.23. The reason is that its direction of polarisation is parallel to the surface but lies radially from the centre point of the probe. Attention must be paid to this fact when a reflector has to be localized (see also [1057]).

The efficiency of the conversion of electrical into acoustic energy is 10^{-3} [580] for a DC field of 1 Tesla (10 kG). If the sound is also received by an identical device (see below) the signals are in consequence at least 50 dB [331] to 100 dB [158] below those obtained with conventional probes.

If the surface is excited by several staggered conductors, particular types of wave and directions of propagation (for example, plate waves, [924]), can be produced due to interference of the waves produced under the individual conductors.

By spacing the current conductors at distances of 1/4 wavelength of the sound and by feeding current pulses which are in phase quadrature relative to each other, preference is given to the radiation of the sound waves in one direction only, see Fig. 8.10.
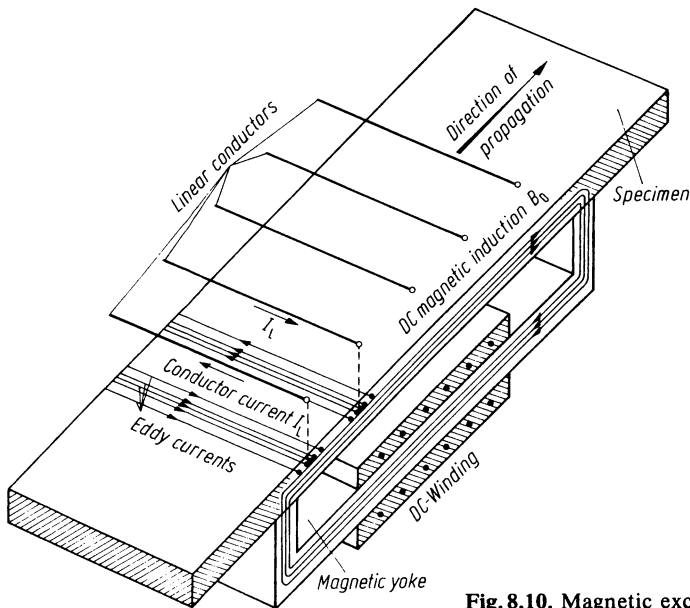
Fig. 8.10. Magnetic excitation of plate waves

By such measures it is also possible to reduce the band width of the sound spectrum in order to suppress harmonics [924]. For details of the sensitivity, directivity and the types of wave which can be generated by an EMAT see [1057].

For a theoretical treatment of the directivity see for example [777, 1172]. Further experimental results are given in [314, 160, 467, 1746, 1747, 493, 1319, 710, 1068, S 6]. [S 109] gives a comprehensive survey on EMATs with many references.

Transmitting without a Superimposed Magnetic Field

If the superimposed magnetic field B in the arrangements described above is omitted a force nevertheless acts on dV because the current $i_{\sim}$ in the coil has its own magnetic field and thus produces at dV an induction $B_{\sim}$. As shown in Fig. 8.11 this results in the generation of longitudinal waves.

Since in this case B oscillates at the same frequency as $i_{\sim}$, F always has the same direction, viz. that of a repelling force between coil and material. The sound has double the frequency of the current in the coil, since both $B_{\sim}$ and g increase with $i_{\sim}$ and F increases in proportion to $i_{\sim}^2$. In addition the force depends on the distance of the coil and the conductance of the material concerned.

As shown above, this effect results from the repelling force between two currents flowing in parallel directions. The eddy currents induced in the material can also be replaced by a second coil through which a corresponding current flows. By this arrangement DC pulses (shock waves) can also be transmitted.
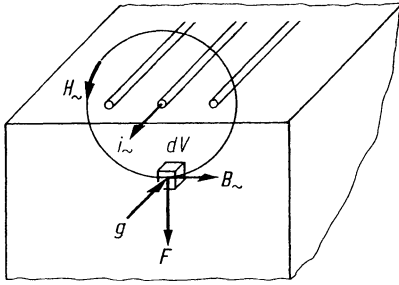
Fig. 8.11. Magnetic generation of longitudinal waves without superimposed magnetic field
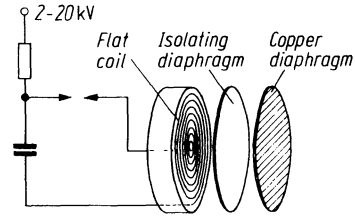
Fig. 8.12. Magnetic transmitter for longitudinal ultrasonic waves without superimposed magnetic field

The magnitude of the force depends only on the numerical value of the product $B \cdot g$. In earlier cases B was chosen as large as possible whereas g was kept relatively small. In the method just discussed the current in the coil should be as strong as possible in order to maximise both B and g, the pulse technique permitting the application of high currents without overloading the coil. This obviates the use of large and heavy magnets and simplifies the construction of the probe shown in Fig. 8.12.

According to [375] the sound transmitter consists of a fixed flat spiral coil facing a copper diaphragm. The strong current pulse is produced by the discharge of a capacitor and a triggered spark gap in air serves as a switch. This is shown schematically in Fig. 8.12, but in practice, alternative circuits for the formation of the pulse can be used.

Due to the skin effect and the increased inductance the amplitude decreases uniformly with increasing frequency. On the other hand, this method can be used at low frequencies, around 100 kHz, in order to produce considerable sound amplitudes.

Consequently this probe is particularly suitable for testing concrete and similar materials.

According to experience the effect lends itself also to the direct generation of sound in conductive specimen. The coil is placed on the work piece concerned and a strong current pulse is passed through it. Also in the case of this method directional radiation of a wave is possible by means of a suitable, spatial arrangement of the conductors and an appropriate phase shift.

Reception

For ultrasound reception a superimposed magnetic field is indispensible and the arrangement is identical to that used for transmission. Various authors have already described pulse-echo methods using the same arrangement for transmitting and receiving in an analogous way to the use of a piezo-electric probe. If the unit volume dV (cf. Fig. 8.6 or 8.7) moves in response to a force F in a magnetic field B, an eddy

current of density g flows which induces a voltage in the applied coil. In a similar way to sound transmission, the direction of the magnetic field determines whether longitudinal or transverse waves will be received. The induced voltage has the same frequency as the mechanical oscillation, and it increases with the magnetic field, but for fields which can be generated economically, it is smaller than that produced by piezo-electric probes.

In the direct method the air gap between workpiece and receiver coil should be kept as small as possible and not greater than about 1 mm. Over a limited range the decrease of the signal with increasing distance can be compensated by the simultaneous inductance increase. This requires that the receiver coil is matched electrically in such a way that its resonance frequency is greater than the sound frequency when the coil is in contact with the material, so that, if the coil is lifted off, its resonance frequency decreases and approaches that of the sound frequency. This increases the electrical signal and partially compensates the reduction resulting from the increased distance.

The sensitivity of this method is too low for the detection of small flaws but is adequate for measuring wall thickness. Another special application, viz. the measurement of the directivity of piezo-electric probes, has been described in [1646], (cf. also [1711 and 162] and Section 10.5.4).

8.5 Magnetostrictive Methods

Nearly all ferromagnetic materials are deformed mechanically when placed into a magnetic field. This phenomenon is called magnetostriction [2].

If this deformation of the material occurs at constant volume, it is called linear magnetostriction but if the volume changes it is volumetric magnetostriction. In practical applications the linear effect is much stronger than the volumetric effect but both reach a maximum value at the magnetic saturation of the material concerned. Linear magnetostriction occurs below the Curie point, whereas above this temperature only volumetric magnetostriction is observed.

Transmitting

In the case of linear magnetostriction the deformation occurs mainly in the direction of the field. It depends on the magnetostrictive constants of the material which are in turn complex functions of the temperature, the magnetic state and the previous treatment of the material concerned.

This effect is independent of the sign of the magnetic field and if an alternating field is applied it results in the generation of sound of twice the frequency. In the case of material with an approximately linear magnetostriction curve (deformation as function of the magnetic field) the working point can be shifted by applying an additional magnetic DC field $H_= > H_\sim$ in such a way that sound of the same frequency is produced.

Due to the finite depth of penetration of the alternating magnetic field the effect is limited to the surface of the material. The generation of sound depends also on the intensity of the alternating magnetic field in the surface layer. Close coupling between the source of the magnetic field and the surface, is therefore essential.

In practice, magnetostrictive transmitter probes have been utilized already for the generation of sound of high output at low frequencies (around 100 kHz). For the excitation it is necessary to magnetize the magnetostrictive body in the direction of the radiation and as in the case of piezo-electric oscillators, magnetostrictive oscillators are operated at their natural mechanical resonance in order to amplify the desired effect. Since at 200 kHz the oscillator is still only approx. 1 cm thick in its direction of oscillation, this makes it necessary to magnetize a disc in the direction of its thickness. In order to keep the losses small at the high frequencies concerned, the oscillators consists of thin sheets, as in the case of transformer cores, into which holes are punched for the winding (Fig. 8.13).

When testing ferromagnetic materials the magnetostrictive effect can also be used for the direct excitation method. The efficiency of the electro-acoustic transformation depends on the magnetostriction parameters. Conversely, the achieved efficiency, i.e. the amplitude of the signal, also permits deductions concerning the magnetostriction parameters. A suitable working point on the magnetostriction curve can be reached by superimposing a direct magnetic field. If the amplitude of the signal is plotted as a function of the direct magnetic field, this furnishes a differentiated magnetostriction curve of the material concerned. Curves of this type depending on the material, may differ greatly. Consequently, a definite form of the curve is characteristic of a material of definite composition and pretreatment. This method, therefore, is suitable not only for the detection of flaws and for thickness measurements, but also for the identification of materials and for tests to prevent mix-ups [754].

The statement in Section 8.4 concerning the dependence of the sound amplitude on the distance between transmitter coil and surface of the test piece applies also in this case. Without a superimposed direct field the counteracting effect eliminates the influence of the distance of the coil on the amplitude of the sound as long as the alternating field exceeds that required for the magnetic saturation of the
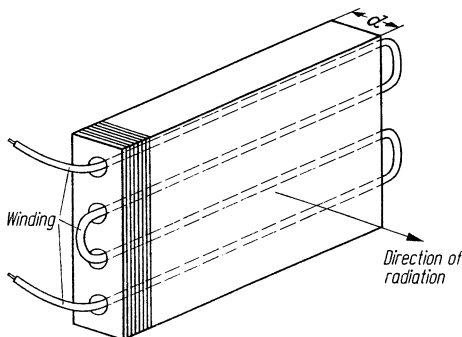
Fig. 8.13. Assembly of a magnetostrictive transducer
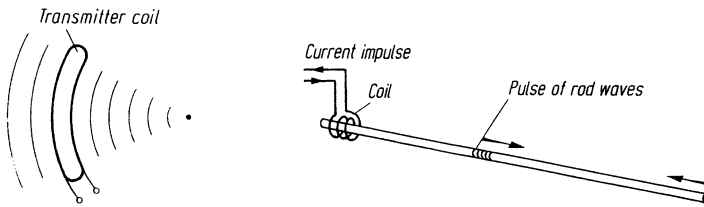
Fig. 8.14. Focussed radiation of plate waves
Fig. 8.15. Magnetostrictive testing of steel rod or wire

material. Exactly as in the case of the magneto-inductive method the preferential radiation in a given direction is controlled by a suitable geometrical arrangement and energising of the linear elements of the coil. The coil may be of special design and thus, for instance, can radiate focussed plate waves. Figure 8.14 shows the principle of this application.

Also the excitation of rod waves as in Fig. 8.15 becomes understandable.

Reception by Magneto-Elastic Effects

Sound waves are received by magnetostrictive material due to the magneto-elastic effect, because elastic stresses arising from the sound waves influence the magnetic properties. In the presence of a magnetic field this changes the density of the magnetic flux and induces a voltage in a coil placed on the surface of the material concerned. For reception it is thus necessary to premagnetise the material by means of an external field. Also in this case it is necessary to shift the working point to the most favorable (i.e. the steepest) part of the magnetostriction curve. The effect obtained is limited to the surface by the skin effect. The direction of the magnetic field should coincide with the direction of the elastic stresses produced by the sound.

It seems feasible to construct magnetostrictive probes by using a suitable material (i.e. ferrite) which has been developed for operation in the MHz range but so far no practical application for routine tests has been reported.

The direct method is however already being applied in the "Ferrotron" instrument, Section 25.1.

Reception due to a Modulated Stray Flux

If the surface of a ferromagnetic material contains a crack, a stray flux appears at this point if the specimen is magnetised at right angles to the crack. This means that the lines of force are densest at the crack on the surface. If sound is transmitted through this specimen which reaches the area around the crack, the stray flux will be modulated via the magnetoelastic effect at the same frequency as the ultrasound. This modulated stray flux can be picked up by an induction coil [755].

In the Ferrotron instrument (see Section 25.1) a combination of several direct magnetostrictive methods is used for detecting flaws in wires. This concerns a com-

bination of surface waves and rod waves which move spirally around the wire and which are recorded by means of the magneto-clastic effect as in the case of the modulated stray flux. Direct magnetostrictive methods, with most materials, give signals which are stronger than those produced by the magneto-inductive methods.

8.6 Optical Methods and Laser Techniques

These concern the effects of sound on light waves and consequently, these methods can be used only for reception. Methods have been developed which evaluate the spatial distribution of the sound field and which make it visible. They are discussed in Chapter 13. The subsequent electronic processing requires that the effects are all converted into an amplitude modulation of the light. This furnishes an electric signal which can be picked up by a photo-electric cell.

Reception

We start with methods in which the effect of sound deflects the light from its original direction or position. If a beam of light impinges on a photoelectric cell of limited receiving area (case a, Fig. 8.16), this cell will receive less light if the beam is deflected (case b). The effective receiving area can be limited by a diaphragm, or by the edge of the cell. The fluctuations cause the photoelectric cell to furnish a corresponding signal. The deflection of the light can be realised in different ways.

If it occurs on the surface of the work piece, this permits the application of direct methods. This possibility will be discussed first.

In the case of a piston-like movement of a reflecting surface an oblique beam of light is shifted sideways. If the surface is deformed when exposed to sound, this causes tilting of the surface elements by a small angle. Beams of light reflected from these surface elements are deflected at twice the tilting angle. In this way Rayleigh waves can be made visible [55]. This method presupposes optically reflecting surfaces.

If rough surfaces are illuminated by laser light the reflected beam consists of irregularly distributed bright spots in its cross-section, the so-called "speckle pattern". By movements of the surface these spots fluctuate and reception is possible using a diaphragm and a photo-cell.

In transparent bodies the light is deflected by a sound wave because the index of refraction varies as function of the pressure (Debye-Sears effect) [2]. A sound
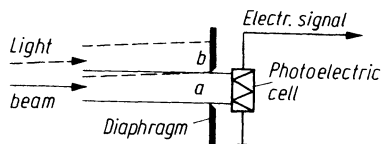
Fig. 8.16. Amplitude modulation with deflection of light

Li = Source of light L_1, L_2 = Lenses   S = Schliere
B = Diaphragm   F = Photoelectric cell
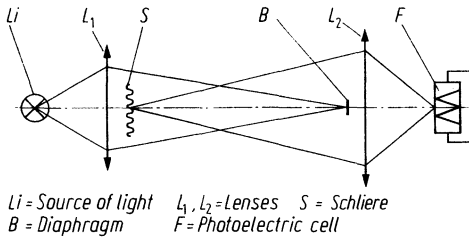
Fig. 8.17. Path of rays in the schlieren-optical system

wave therefore causes zones in which the local index of refraction is different from its value in the surrounding space.

To detect such zones the *schlieren-optical method* is used. The basic path of rays according to [2, 1638] is shown in Fig. 8.17.

A point-like source of light, Li, produces via the lens L_1 an image on the so-called schlieren diaphragm B. If this image appears undisturbed, the entire light from Li through L_1 is intercepted by B and no light falls on F. If a zone of changed refractive index (schliere) occurs between L_1 and B, the light at the edge of the schliere is deflected by refraction from its original direction and the rays by-passing B are focussed by lens L_2 onto the photo-electric cell F where the brightness is proportional to the sound pressure.

If for example an ideal shock wave (a DC wave) passes through the body the wave front generates a moving layer with a changed refractive index. In the case of a wave consisting of multiple oscillations the various layers produced act as a moving optical grating. The spatial structure of the index variations deflects the light into several orders of diffraction (Fig. 8.18). The dimension of the wave fronts in the direction of the light propagation should be not too large. The grating constant is equal to the wavelength.

The grating in this case acts as a phase grating. The Huygens' wavelets scattered at the extremes of pressure, or refractive index, combine into the different orders of diffraction in a way similar to an amplitude grating (Raman-Nath diffraction) [307, 935] see also [3].

For the angle of deflection α at perpendicular incidence of the light on the grating the following applies:

$$\sin \alpha_n = \frac{n\lambda}{2\Lambda}$$

(n order of diffraction, λ wavelength of light, Λ grating constant = wavelength of sound.)
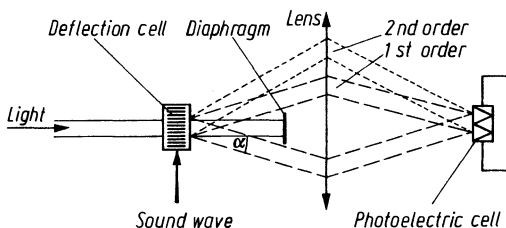
Fig. 8.18. Diffraction of light by the sound field

```
K = Probe
Z = Deflection cell
P = Work piece
B = Diaphragm
F = Photoelectric cell
```
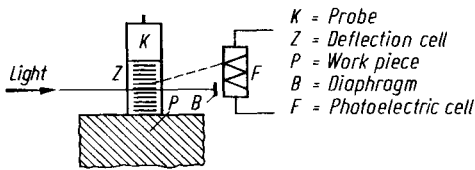
Fig. 8.19. Ultrasonic probe using the method of Fig. 8.18

The sound pressure influences the contrast of the light pattern and hence the intensity of the different orders of diffraction. [935]

The use of this effect for sound receiving probes offers some advantages (Fig. 8.19). The sound is introduced into the diffraction cell which is filled with a suitable liquid, for example xylol. A powerful light source, for example a laser, should be used. Within certain limits the signal from the photocell increases with both light intensity and sound pressure and much stronger signals can be obtained than is possible with piezo-electric receivers.

Another advantage of the system is its insensitivity to electrical interference and in addition the sound field is not disturbed by the act of measurement. By using the arrangement of Fig. 8.19 it is also possible to measure the sound amplitude of a piezo-electric transmitter before entry into a test specimen, as well as of the reflected sound.

By a special optical arrangement it is possible to obtain an electric output in the form of an alternating voltage at the sound frequency, or at an harmonic, or even in DC form.

The diameter of the light beam should be close to the sound wavelength [76].

The schlieren-optical method can also be used for making visible the sound field as a whole [2, 602].

We encounter another diffraction effect of light by a sound wave if the grating (i.e. the wave front) is large compared to the sound wavelength in directions both parallel and perpendicular to the light beam, cf. [797, 637]. This case corresponds to the *Bragg diffraction* of X-rays by a crystal. Similar equations describe the effect in the case of sound, which can also be used for producing an image of the whole sound field (Chapter 13). The principle is a reflection of the light beam at grazing incidence onto the wave fronts (Fig. 8.20).

If the light strikes the wave fronts at the angle α_n then according to [44] it is diffracted at the same angle when:

$$\sin \alpha_n = \frac{n\lambda}{2\Lambda}$$
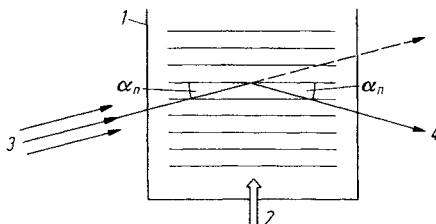
Fig. 8.20. Bragg diffraction of light in a sound field. *1* diffraction cell, *2* sound beam, *3* incident light, *4* diffracted light

Λ sound wavelength, λ light wavelength, n order of diffraction.

The majority of the light is diffracted into the first order spectrum and since the angle of incidence equals the angle of diffraction it is also possible to speak of Bragg "reflection". The light propagates as though it was being reflected by the wave fronts acting as plane mirrors.

A further possibility for the reception of sound is the *photo-elastic effect* which can influence the amplitude modulation of light. Many transparent materials become double-refracting when mechanical stresses are applied. This means that their refractive indices, for light polarized parallel and perpendicular to the direction of stress, are different [2, 13]. The plane of oscillation of polarized light will be rotated as a function of the applied pressure, which in the case of sound is the sound pressure, and this can be measured by using a polarizing filter (analyser) which allows light of only a certain direction of polarization to pass (Fig. 8.21).

A block of material having strong photo-elasticity is illuminated by a polarized light beam. The polarization filter placed behind does not allow any light to pass as long as there is no double refraction in the block. An ultrasonic wave passing through the block causes a rotation of the plane of polarization of the incoming light and hence an electric signal in the photocell. The signal is within certain limits proportional to the ultrasonic amplitude.

In this way a probe similar to that illustrated in Fig. 8.19 could be built, but the effect is of greater importance for imaging the complete sound field within a transparent model made of a photo-elastic material. This serves as a mock-up for a specimen of complicated shape so that it is possible to analyse the propagation of ultrasound in its interior (see Chapter 13 and [598]). In this case it is possible to distinguish between longitudinal and transverse waves by rotating the plane of polarization of the light, since the double-refraction effect depends of the relative directions of polarization and stress.

We will now deal with methods of sound reception where the physical displacement of the surface is used to create optical effects.

The sound signal within a material can be detected at the surface by using a laser beam. The back-scattered light undergoes a *Doppler effect* caused by the velocity of the oscillating surface. This is a frequency change which can be transformed into amplitude at the flank of an optical filter. Very steep flanks are provided, for example, by the absorption lines of iodine vapor in a cell with saturated absorption but nevertheless the overall sensitivity is not sufficient for most practical tasks.

The sensitivity of another optical method is, however, some powers of ten higher. This is the *optical interference method* which can be used in, for example, a *Michelson interferometer*.
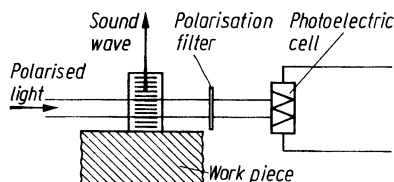
Fig. 8.21. Receiver probe using the photo-elastic effect
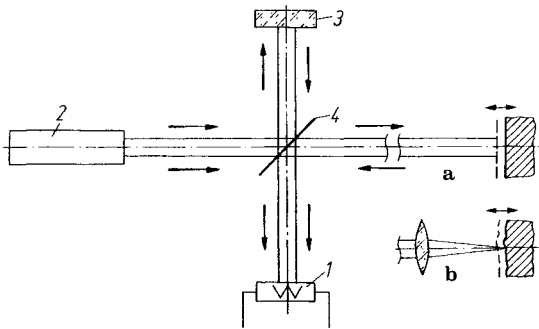
Fig. 8.22. Principle of the Michelson interferometer. **a** With a specularly reflecting specimen; **b** on a rough surface. *1* photo-electric cell, *2* laser, *3* reference mirror, *4* beam splitter

In this the incident light is partially superimposed by the reflected light which is frequency modulated by the vibrations of the surface under test. The frequency differences detected at the output of the interferometer appear as a light signal falling onto a photocell (Fig. 8.22).

A laser beam is used to illuminate the surface of the specimen via an optical beam splitter and the split-off part, or reference beam, travels to the photo-electric cell via the reference mirror. The light reflected from the test surface is also returned to the photocell where it is superimposed onto the reference beam. Because of the Doppler effect caused by the oscillating surface the input to the cell is brightness-modulated [76].

To be properly superimposed the wave fronts of each beam have to be of exactly the same form over their whole sections. This is a very difficult condition to achieve and is not fulfilled if the specimen's surface is somewhat oblique or rough. If (as in Fig. 8.22 b) the illuminated spot on the surface is kept very small by using a focussing lens, certain minor roughnesses may be allowed, but in most practical cases the method is not very useful.

Another type of interferometer has been developed which avoids these handicaps (Fig. 8.23).
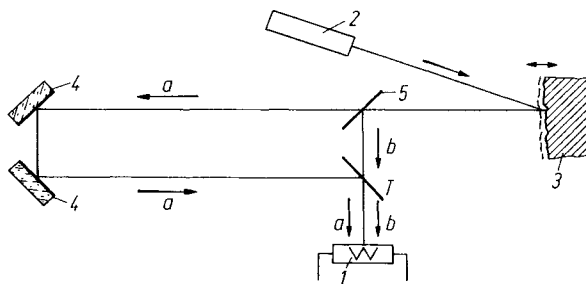
Fig. 8.23. Principle of a transit-time interferometer. *1* photo-electric cell, *2* laser, *3* specimen, *4* mirrors, *5* beam splitter, *T* semi-transparent mirror
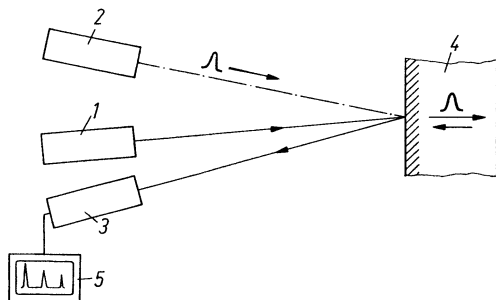
Fig. 8.24. Ultrasonic test system with lasers. *1* illuminating laser, *2* transmitting laser, *3* interferometer, *4* specimen, *5* signal processing

Part of the light reflected, or scattered, from the surface of the specimen takes a longer path *a* and part a shorter one *b* to the photocell. The light wave front taking the longer path via *a* is somewhat delayed compared with the other travelling via *b*. Thus at the photocell two wave fronts of the beam are superimposed, each of which struck the oscillating surface of the specimen, but with differing phases of the ultrasonic oscillation. If the time delay corresponding to the velocity of light by the *a* — path is equal to exactly half the oscillation time of the ultrasonic wave at the surface, then the first wave front undergoes the Doppler effect in opposite phase compared to the second. The wave fronts in both cases are nevertheless unchanged and identical and the interference at the photocell in this case is optimum. If the paths are adjusted to give full darkness at the cell when the ultrasonic oscillation is zero, it will give full brightness when oscillating ultrasonically.

For ultrasonic frequencies between 1 and 30 MHz a time delay for the light of 25 ns is useful but below 100 kHz the sensitivity is zero. Therefore any movements of the specimen are not disturbing, cf. [739]. The complete system (Fig. 8.24) consists of the illuminating laser, the sound-generating laser and the interferometer. The sound-generating laser emits high power pulses of about 20 ns in length and on the surface they generate ultrasonic pulses in the frequency range 1 to 30 MHz. The optical frequency of this laser is arbitrary over a wide range. The illuminating laser operates in a quasi-continuous mode with a long pulse lasting at least for the whole transit time of the ultrasonic pulse. It illuminates the area of the surface where the ultrasonic echoes must be detected. The back-scattered light modulated by the echoes is anlysed by the interferometer as explained above, converted to electric signals and displayed on an oscilloscope screen (see Chapter 10).

Because of the extremely short ultrasonic pulses the echo resolution is very high, and Fig. 8.25 shows an example of the back echo of a thin plate.

The distance separating the whole system from the specimen may be up to 10 m or if one makes use of glass fibers to transmit the light signals it may be even larger. This is of importance since the system has a rather large volume. In this case, a mechanical scanning system has to be installed near to the specimen.

The advantages of the method which are contactless testing with high resolution but without high demands on the quality of the surface, allows new applications of which the testing of red-hot surfaces may be mentioned. As an example Fig. 8.26 shows a method testing red-hot ingot surfaces for cracks in which transmitter and
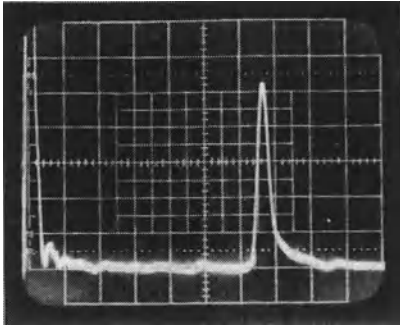
Fig. 8.25. Screen display from a test with the laser system in Fig. 8.24 on a plate 1.2 mm thick
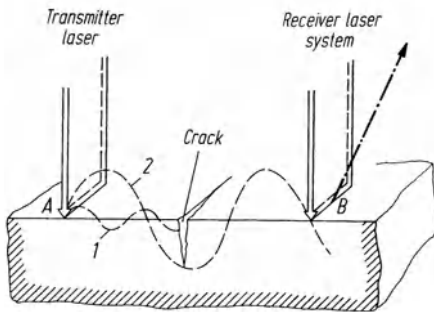
Fig. 8.26. Testing of ingots at red-heat for surface cracks by the laser system, showing schematically the influence of a crack on a short wavelength (1) and a longer one (2)

receiver lasers work on separated parallel strips A and B. The short-wavelength surface wave will be more affected by a crack than will the longer one, and this provides a method of discrimination between cracks of different depths.

Further examples of applications are wall-thickness measurements on thin-walled tubing and on hot tubes during manufacturing, the testing of bonded joints in aircraft structures, and the detection of micro-shrinkage in metals and ceramics. For the latter purpose ultrasonic pulses of 50 to 500 MHz are provided which can be generated in the form of shock pulses with a length of only 100 ps. As the sound generating laser in this case so-called mode-coupled lasers are being used. The test spot is reduced to a diameter of some tenths of a millimetre.

Concerning the application of lasers for ultrasonic testing cf. [S 112, S 116, S 173, S 77, 1387, S 112, S 106, S 105]. In [S 132] laser pulses have been used to measure both ultrasonic velocities in powder metallurgic composites for the evaluation of their elastic constants.

Part B | Methods and Instruments Used for Ultrasonic Testing of Materials

9 Historical Survey of Developments

9.1 Survey and Tabular Summary

Table 9.1 lists all current methods of ultrasonic testing of materials. They are categorized by reference to three basic criteria: namely the type of primary measured quantity, the form of radiated ultrasound used (continuous wave or pulses) and the effect of an anomaly within the material under test or on its surface. Based on the presentation in the Table, each method will be discussed to an extent depending on its practical importance.

The *pulse-echo method* which is the most important one will be described first. A material inhomogeneity, when illuminated by a pulsed ultrasonic beam, reflects an echo which is picked up by a receiver probe. The primary measured quantities are therefore the amplitude of this echo and the transit time of the pulse from the transmitter to the reflector and back (Chapter 10).

If only the transit time, or a corresponding frequency, is made use of so that the amplitude need only reach a minimum detectable value, we have the *transit-time method*. (Chapter 11). If in this case continuous ultrasound is used instead of pulses we have the *resonance method* (Section 11.3.1) or the *phase-measurement method*, (Section 11.4) in which inhomogeneities of the material also act as reflectors.

In the *shadow method* (Chapter 12), as known from X-ray diagnostics, an inhomogeneity between transmitter and receiver produces a shadow which influences the sound amplitude. The method is also called *through transmission* and the primary quantity to be measured is the amplitude. This method can either be used with pulses or with continuous sound. Historically the latter variant was the first method used in an attempt to imitate X-ray fluoroscopy or screening. Because, when using X-or Gamma-rays, the intensity on the screen or the photographic film is important, we can in the case of ultrasound also speak of the *intensity method*, though in physical terms piezo-electric receivers measure the sound pressure amplitude and this is proportional to the square root of the intensity.

Table 9.1

Method	Primary measured quantity			Type of sound radiation		Effect of an inhomogencity (or a boundary)		
	Sound pressure amplitude	Phase	Transit-Time	Continous sound waves	Sound pulses	Reflection	Shadow	Sound generation
Pulse echo method	×		×		×	×		
Transit time method								
1. Transit time method with pulses			×		×	×		
2. Resonance method (transit-time method with continous sound)			×	×		×		
3. Phase measurement method (transit-time method with continous sound)		×	×	×		×		
Shadow method (through transmission method, intensity method	×			×	×		×	
Acoustic holography	×	×		×	×	×	×	
Image methods	×	×	×	×	×	×	×	
Sound emission method	×		×		×			×
Frequency modulation method	×		×	×		×		

If in addition to the amplitude the phase of the received sound is also measured we have the method called *acoustic holography* which is an anlogue of optical holography (Section 13.14). It can be carried out with either continuous or with pulsed ultrasound. A material inhomogeneity will be indicated by both its shadow effect and by its echo.

In principle all the methods mentioned above may be used for *imaging methods* (Chapter 13), by further electronic processing of the primary quantities to form an image. There are in addition a number of other methods, where the piezo-electric effect is used in other ways and also where it is used only for generating ultrasound as, for example, in the schlieren method.

The method of *acoustic-emission analysis* (Chapter 14) plays a special role in which the primary quantities are the amplitudes and pulse transit times of sound energy emitted by the inhomogeneity itself when it changes its shape. This method is also called therefore a passive method, the only one mentioned here.

With the *frequency-modulation* method an inhomogeneity acts as a reflector, as in the pulse-echo method, but continuous sound is used with a periodically modulated frequency (Section 10.7).

9.2 Historical Development

1929 may be considered as the year of birth of ultra-sonic materials testing because it was then that Sokolov first proposed using the shadow method with continuous waves to detect defects in solid materials [1441]: cf. Fig. 12.2. Mühlhäuser obtained in 1931 the first patent for an instrument working with the shadow method [1071]. Further names associated with this development are Kruse [862, 863], Meyer and Bock [1026] Czerlinsky [283, 284], Götz [543] and Shraiber [1411], all using laboratory-built devices with transducers made from piezo-electric quartz plates. The high-frequency generators used for producing potentials up to several hundred volts in some cases, were frequency modulated either mechanically, using rotating condensers, or electronically using noise generators [283]. The latter methods were used to avoid the production of standing waves. The amplifiers and indicating instruments used were standards of the time and to avoid direct crosscoupling between transmitter and receiver they were usually built separately and with effective shielding.

Such laboratory-built instruments were also used for the first practical testing of steel boiler plates for laminations during the second world war by the companies AEG and Borsig in Berlin. The method used was the shadow technique with frequency modulation. The instrument was designed by Berthold and Trost [1534], (see also Fig. 9.6 in the 3rd edition of this book).

Series production of instruments for using the shadow method started after the war at the companies ACEC of Charleroi, Belgium, and Dr. Lehfeldt and Co. of Heppenheim, Germany.

The first experiments for *imaging methods* also started in the 1930s. The first of these, which transformed the sound pressure into a visible image was the *Pohlman*

cell (cf. Section 13.9 and [1202, 1203]). A complete device using this cell, the *Schall-sichtgerät*, was used before 1945 to test steel plates. It had a very large visual field of 500 mm diameter but it found no further practical applications in later years. The principle of the Pohlman cell has recently been used by Ogura et al. [1138] and by Cunningham and Quate in 1972 [280], the latter using a frequency of 1000 MHz for *ultrasonic microscopy* with the shadow method.

The principle of the *relief method* came in 1936 from Sokolov [1442], (Section 13.1). Sound waves at high ultrasound intensities reflected from an immersed specimen onto the water surface generate ripples. This "image" can be observed with special illumination and the method has been developed for frequencies between 50 and 100 MHz for commercial applications as an ultrasonic microscope. (SLAM = scanning laser acoustic microscope or sonomicroscope by Sonoscan, USA).

Another proposal by Sokolov in 1937 [1444, 1445] was to make visible the electric-charge distribution on a piezo-electric disk used as a receiver. Electronic scanning would make the charge pattern visible by presentation on a CR-tube screen *(Sokolov camera)*, Section 13.10.

To avoid the disadvantages of the shadow method when using continuous waves Sokolov proposed in 1941 the *frequency-modulation method* [1445] (Section 10.7). It was however soon overtaken by the pulse-echo method and has not found further applications.

For completeness we also mention the *phase-measuring method* of Hatfield used from 1952 for thickness and velocity measurements [622]. Continuous waves are used and the phase of an outgoing wave is compared with that of a reflected one.

Sound-emission analysis was first recognized as a possible means for non-destructive testing of materials by Kaiser [744]. The first trials to use it in a quantitative manner were made by Mason, McSkimin and Shockley [994]. Though much work has been carried out in the meantime, it is still not possible to accept the method as fully developed. For a recent survey, see Lord [932].

For materials testing continuous waves were replaced by pulses in the 1940s, but they found many applications for wall-thickness measurement using the *resonance method* (Section 11.3.1). This makes use of the fact that the resonance frequency of a plate depends on its thickness. Based on a 1944 patent of Erwin and Rassweiler [418] General Motors Corp. first built the *Sonogage* in 1947 and more applications were later found by the *Vidigage* of Branson Instruments Inc.

Subsequent progress in electronic pulse techniques has lead to the replacement of resonance based instruments by pulse-echo equipment for wall-thickness measurements. The transit time measured by the pulse-echo method gives directly the wall-thickness by using the known velocity of sound.

This, by far the most important method of non-destructive testing of materials by ultrasonics, the *pulse-echo method*, was certainly first used by the bats. In 1798 Spallanza already supposed that bats can orientate by using inaudible sound signals, but this was not proved until 1938 by Pierce and Griffin. The technical realization of the method was facilitated by the discovery by Jacques and Pierre Curie of the twin piezo-electric effects in 1880 and 1881. They used quartz crystals as transmitters and receivers of ultrasonic waves [281, 282]. Lord Rayleigh enunciated the scientific fundamentals of the propagation of sound in solids in his "Theory of

Sound" between 1885 and 1910. Finally in the history of the technique Langevin and Chilowski must be mentioned since they solved between 1915 and 1917 the problem of detecting under-water submarines and icebergs by using ultrasonic pulses [891].

Subsequently the method has found many applications in measuring sea-depths but for materials testing it could not be used effectively before the rapid developments of electronic engineering during the period 1935 to 1938 for use in Radar. (electromagnetic waves used in the atmosphere for aircraft detection; see for example Graff [558]).

The first proposal to use pulse-echo techniques for materials testing came in 1940 from Firestone [451, 454, 456] in the USA.

In an independent development in England, Sproule used the method in about 1942 [558, 313]. In Germany a pulse-echo system was also developed by Kruse [558].

This method has several important advantages over shadow techniques. The sensitivity is much greater for even small defects which may cause only small variations of the sound pressure in the shadow. The transit time also allows the measurement of the reflector distance which is not possible at all with the shadow method. Further only one side of the specimen needs to be accessible for testing and it also overcomes any difficulties with the formation of standing waves.

Ultrasonic pulses have incidentally been used much earlier by Hiedemann and his collaborators to determine sound velocities by measuring transit times [655] (Section 11.3.2).

It has sometimes been claimed that Sokolov was the inventor of the pulse-echo method but strictly speaking this is not true. What he proposed was the shadow method using the rear echo from plates (Fig. 12.1) and to avoid standing waves he even used pulses. However, the echo from the defect itself was not detected and received but only the attenuation of the rear echo [1444].

The first commercial apparatus for using the pulse-echo method were built in 1943 at about the same time by the companies Sperry Products Inc. Danbury, USA and Kelvin and Hughes Ltd., London, based on the work of Firestone and Sproule respectively.

Since then many manufacturers have marketed various units of much smaller size and weight thanks to electronic developments. At the same time their sensitivity and resolution has considerably increased, thanks to piezo-ceramic developments. The size of modern units, which was greatly reduced following the replacement of electronic valves by transistors, is now more or less determined by the size of the CR tube and the AC powerpack or the battery.

In the first few years of pulse-echo applications, considerable success was achieved in testing large forgings using directly coupled quartz probes. In this work longitudinal waves at perpendicular incidence were used and although transverse waves were known they were considered as difficult to control due to mode changing problems. Because of this opinion further applications were confined to axles and plate material. However, in the early 1950s Carlin [210] fitted plastic wedges to longitudinal wave probes to produce transverse waves projected obliquely to the surface. By the use of these a large number of new applications became possible and in particular the testing of tubes and welds. However, the various types of

guided-wave have found only very limited applications up to the present. Quartz is hardly used any more as a piezo-electric material and new materials, such as the piezo-ceramics, are used instead because of their higher sensitivity.

The method of testing used originally was by scanning the surface of the specimen by hand and observing a CR tube screen picture in the form of a horizontal time base with vertical peaks (A scan) and it is still commonly used today. Additionally a number of manual tasks have been mechanized and the screen observation is carried out by electronic devices.

The original aim of getting a visual image of the specimen, with its defects, has also been followed when using the pulse-echo method. There has however not been much success in practice, although a sectional image (B scan) or a plan view (C scan) can easily be obtained with a simple probe-scanning device. More complicated methods (see Chapter 13) have found preferred applications in medicine.

The fundamental papers on *holography* were published in 1948 and 1949 by Gabor [500, 501] (Section 13.14). He proved then that it is possible to obtain an image of a three-dimensional wave field on a two-dimensional film by using a coherent light source. After the invention of the laser optical holography started its development at the beginning of the 1960s [914] and was soon followed by the first experiments with ultrasonic holography (Greguss [570], Mueller and Sheridan [1074] and Thurstone [1522] (in 1965 and 1966). Modern developments have more possibilities for medical purposes whereas practical systems for material testing are still at an experimental stage.

Mezrich and his collaborators [1035] have in 1974 invented a scanning method with lasers using *interferometry*. One of the twin mirrors of a Michelson interferometer is formed by a very thin metallic fòil immersed in a cell filled with liquid. It can follow the particle movement in an ultrasonic wave and a laser beam scans its surface to produce an image (*ultrasonovision* or *RCA camera* see Section 13.2).

The schlieren method (Section 13.5) makes use of the Debye-Sears effect [307, 935] in which the optical refractive index of transparent media is modified by the pressure oscillations of ultrasound. The method is used preferably for imaging the sound fields of probes and the propagation of sound in liquids or transparent models of specimens, rather than for general imaging [1614, 93].

The same physical effect is the base for the method of Korpel [834] here called *Bragg diffraction* (Section 13.4). The oscillations of the refractive index in a transparent material produce an optical grating at which light is diffracted. Imaging by the *photo-elastic effect* (Section 13.6 and 13.7) is possible by using certain transparent materials which become double refracting by the applied stress of an ultrasonic wave. Polarized light rotates its plane of polarisation and can then be analysed by a polarisation filter. The signals from which the image is built up depend on the local ultrasonic sound pressure and applications are the same as with the previously described methods.

Piezo-electric scanning (Section 13.12) with mechanical scanning devices provide at each probe position the echo amplitudes from, and the corresponding transit times for, any reflectors within the specimen, which in most practical cases has been the human body. The results can be displayed on a CR tube screen or re-

corded in many different ways (Dussik 1942 [353], Wild and Neal 1951 [1625], Donald 1955 [336], Suckling and McLean 1955 [1482]).

Mechanical scanning is usually very slow and therefore turning the beam electronically by a so-called *phased array* is much more effective. The individual radiators are phase controlled as was first proposed by Bradfield in 1954 [173] and used by Somer in 1968, cf. also [68]. This method was already known from Radar techniques, from which many other improvements were derived. It is now possible to obtain realtime images for medical diagnostics with moving images akin to cine film.

The latest developments are *digital-image systems*, where after piezo-electric scanning the aperture and the focus of the ultrasonic beam is synthesized. This system of data processing is explained in Section 13.12 for the SAFT-UT method and by using sufficiently quick computers it is possible to obtain sectional images (B scan) in quasi-real time.

The first applications of ultrasonic *tomography* were by Greanleaf and collaborators 1974 [568] (Section 13.12).

Two methods of *ultrasonic microscopy* were developed for practical applications in the early 1970s by Quate et al. (SAM: scanning acoustic microscope) and Korpel et al. (SLAM: scanning laser acoustic microscope) [836, 916] (Section 13.13).

10 The Pulse-Echo Method; Design and Performance of a Pulse-Echo Flaw Detector

10.1 Fundamentals

Figure 10.1 shows the principle of the method in which an ultrasonic pulsed wave, usually in form of a damped oscillation, is generated by a probe and propagates into a specimen with the ultrasonic velocity corresponding to the material concerned. Part of the ultrasound will be reflected if it strikes an obstacle in the form of an inhomogeneity and, if this is not too large, the remainder will travel further to a boundary of the specimen and will be reflected back to a receiver, if the rear surface and the receiver are in favorable positions. The signal obtained from the receiver is displayed as a peak on a base line of a CR tube (Fig. 10.2). The horizontal sweep is proportional to the time, so that the transit times of the pulse to and from the reflector, and to and from the back wall, correspond respectively to the distances on the screen from the initial peak to the echo peaks corresponding to reflector and back wall. To obtain a standing image the pulses and the sweep of the CR tube are synchronised at the so-called pulse-repetition frequency.

By calibration of the base-line in time per unit length the transit times t_R and t_B to the reflector and the back wall respectively can be read from the screen and we obtain for the distance d of any reflector, knowing the velocity of sound c;

$$\frac{2d}{t} = c \quad \text{or} \quad d = \frac{c\,t}{2}.$$
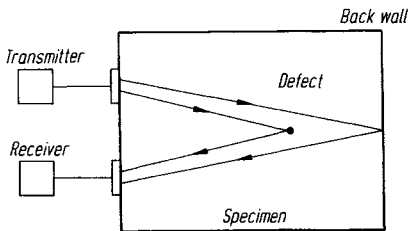
Fig. 10.1. Principle of the pulse-echo method
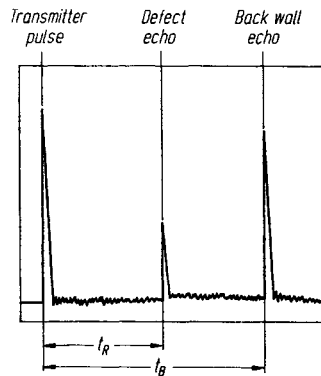
Fig. 10.2. Display on the CR screen (schematic)

Usually the thickness d_B of the specimen will be known and it can serve to calibrate the sweep directly in units of length. Otherwise a testblock of the same material and of known thickness may be used.

Example. A specimen of 100 mm thickness is tested and its back echo is positioned at the right-hand edge of the screen by varying the speed of the sweep. An indication of a defect appears at 30 % of the distance of the back echo which means that the reflection took place at a depth of 30 mm from the surface. In this way a scale can be placed in front of the screen, and the beginning of the transmitter peak and the back-echo peak shifted respectively to the zero and the 100-mm points. The distance of an indication now can be read immediately in units of length.

The amplitude of the received echo depends on several influences, these being:

— Transmitter pulse power entering the specimen,
— Directivity of the transmitter probe,
— Size of the reflector,
— Surface quality of the reflector,
— Position of the reflector,
— Size and directivity of the receiver probe,
— Losses at the receiver by reflection and coupling,
— Attenuation of the wave by absorption and scattering of the material,
— Shadow effect of any defects in front of the reflector
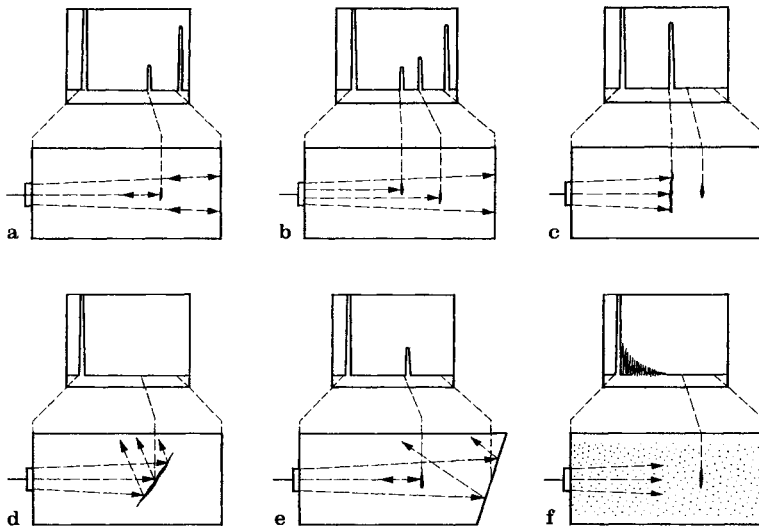
Fig. 10.3. Schematic screen pictures obtained by the pulse-echo method. a Small flaw in sound beam; b two small flaws in sound beam; c large flaw in sound beam, smaller second flaw and back wall masked; d large, obliquely orientated flaw, back wall masked; e small flaw but no back wall echo because the axis of the beam is not incident at right angles on back wall; f strong attenuation of sound beam due to scattering, no echo from flaw or back wall, only "grass"
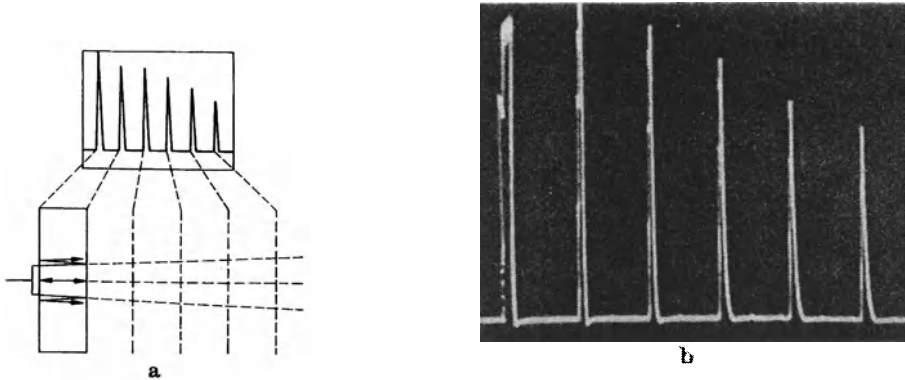
Fig. 10.4. Multiple echoes in a plate. **a** schematic; **b** actual screen picture without time or thickness scale; steel plate 50 mm thick, frequency 4 MHz

Some of these effects are illustrated in Fig. 10.3. Several defects within the beam may be indicated simultaneously, (Fig. 10.3 b), provided that one is not completely hidden in the shadow of the other. In some cases, however, even a smaller defect behind a larger one may be indicated by a wave diffracted at the edges of the first, and of course the back echo may also be screened (Fig. 10.3 c). According to the simple geometrical aspects of the sound wave the back-wall echo would disappear when the defect in front just covers the complete beam. From this fact one can obtain an approximate estimate of the defect size in some cases, especially important for obliquely situated defects. The back-wall echo is also missing from oblique back walls or by too strong an absorption or scattering of the material (Fig. 10.3 e and f).

In the latter case scattering is usually indicated by many close peaks decreasing with distance, the so-called grass.

A specimen of plane-parallel form usually allows several equally spaced back echoes to be visible on the screen if a sufficiently large range of distance is used (Fig. 10.4). This arises from the fact that the echo wave, when it arrives at the test surface, loses only a small part of its energy back into the receiver probe, the larger amount being re-reflected twice, and so on, until the energy is reduced to zero by absorption and beam spread in accordance with Chapters 4 and 5.

The transit times between any two adjacent multiple echoes are equal and very precise, so that they can be used for estimating wall thicknesses by measuring the total separation of n echoes and dividing it by n to obtain a single thickness.

10.2 Basic Functions of a Pulse-Echo Flaw Detector

10.2.1 Block Diagram

Pulse-echo flaw detectors are basically oscilloscopes with special features. Figure 10.5 shows schematically the repetition frequency generator (*1*), sweep syn-
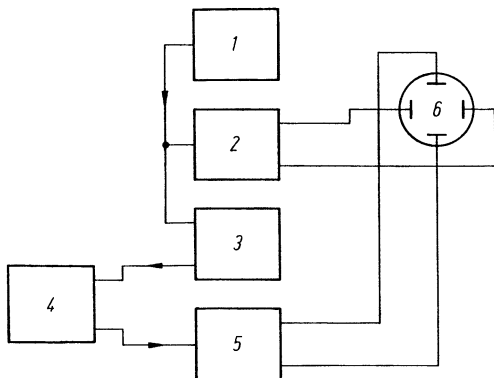
Fig. 10.5. Block circuit of a pulse-echo flaw detector

chronisation (*2*) and the pulse generator (*3*). If only one probe is used as transmitter and receiver (the usual arrangement) the pulse generator excites the transducer (*4*), and the echoes received are amplified by the amplifer (*5*), rectified, and fed to the CR tube (*6*).

10.2.2 The CR Tube

For visual display of the echo pattern electrostatic CR tubes are almost exclusively used (Fig. 10.6). An electron beam is generated in high vacuum marking a luminescent spot of the screen and condensers in both the horizontal and perpendicular configurations vary the beam direction by their applied voltages. The brightness of the spot depends on the beam energy and therefore on the voltage applied to the electron source. The quality of the image depends on the brightness and sharpness of the spot, and on the linearity of the sweep control.

The writing velocity of the electron beam has to be very high, especially for small test ranges. For a calibrated range of 100 mm in steel corresponding for example to 100 mm in length of the base line (imaging one to one) it is about 3×10^3 m/s on the base line, but on the rise of the peaks it must be up to 100 times higher. To make the picture sufficiently bright to be clearly visible, including in the
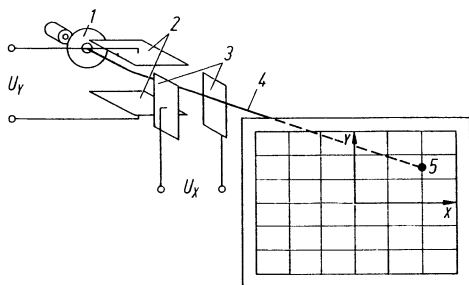
Fig. 10.6. Principle of a CR tube. *1* electron gun, *2* Y-deflection plates, *3* X-deflection plates, *4* electron beam, *5* luminous spot

open air, CR tubes with quite high voltages for the electron gun and for additional acceleration (between 2 and 20 kV), have to be used.

Instead of electrostatic tubes electromagnetic ones have occasionally been tried. However, the deflection coils make it difficult to attain the necessary limit frequency of the deflection system. Otherwise the narrow band width will reduce the precision of the displayed peaks.

10.2.3 The Repetition-Frequency Generator and the Base-Line Voltage

To obtain stationary screen pictures the repetition-frequency generator triggers both the transmitter pulses and the start of the sweep generator. Usually the transmitter pulse is triggered a little later than the sweep so that it is visible on the left-hand side of the screen a little to the right of the start of the sweep, as for example in Fig. 10.4.

Figure 10.7 displays the voltage variations over two periods in a more general case. The delay t_T of the transmitter pulse after the trigger pulse is smaller than the delay of the sweep start t_S, and therefore in this case the main pulse will not be visible during the sweep time and while the trace is bright. Only a few of the echoes will then be visible but in most cases t_T will be a little larger than t_S.

The time base was formerly given a fixed distance scale, which is today usually built into the CR-tube screen, and it was calibrated in various distance ranges for steel corresponding for example to 50, 100, 250 mm etc. by varying the sweep velocity.

For a rough distance measurement it is sufficient to measure the distance of an echo pulse from the rise of the main pulse. For more precise measurements it turns out that there is a certain delay between the rise of the electric pulse on the CR screen and the actual entrance of the ultrasonic pulse into the specimen, due to transit times within the probe. This effect is till more important when using probes fitted with a plastic shoe or for example the perspex wedge of an angle probe (see (Section 10.4.2). This delay is called "error of zero point" and can be eliminated for normal (0°) probes as shown in Fig. 10.8.

The multiple echoes from a plate are adjusted by shifting the whole picture and calibrating the distance scale so that they coincide with the correct graduations of the scale. The main pulse will then start a little to the left of the zero point of the
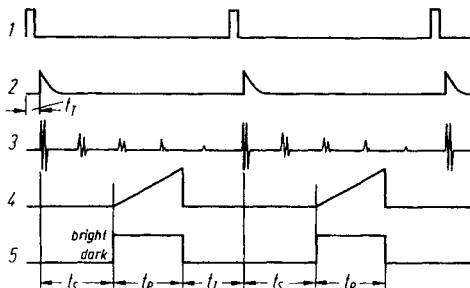
Fig. 10.7. Diagram of time. t_T main pulse delay, t_S delay of the sweep (time base), t_p time of picture, t_I time of interval. *1* voltage of the repetition frequency generator (trigger), *2* transmitter pulse, *3* echo pattern, *4* sweep voltage, *5* bright-dark voltage for the CR tube
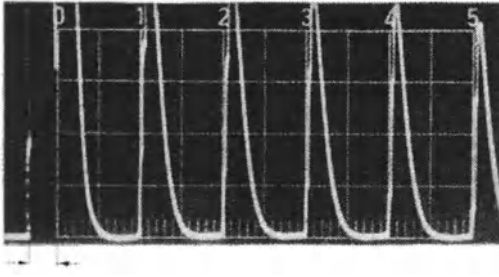
Fig. 10.8. Determination of zero error Δ by means of multiple echoes from a plate (steel, 20 mm thick), using a probe protected by plastic layer approx. 1 mm thick
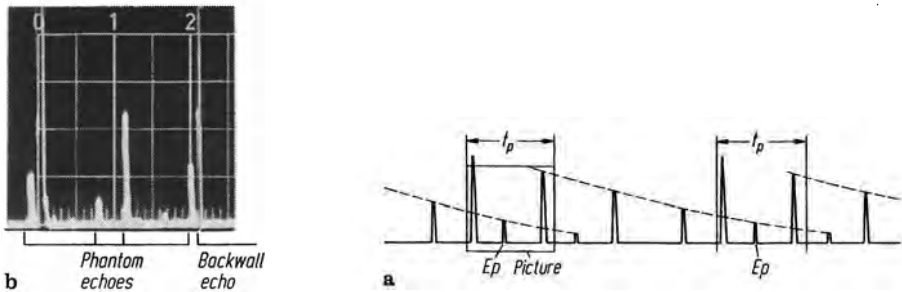
Fig. 10.9. Appearance of spurious flaw echoes (phantom echoes E_p) if pulses are spaced too closely (repetition frequency too high) compared with the thickness of the specimen and its acoustic attenuation. **a** Schematic; **b** traces on screen showing indistinct phantom echoes, also to the left of the transmitting pulse

scale corresponding to the zero error measured for example in millimeters of steel, this being a characteristic of the probe type concerned.

Some designs of flaw detector have the ability to use an external trigger when, for example, several units have to be used simultaneously. In that case the trigger unit is the "master", the others being "slaves".

A high trigger frequency gives a bright picture, but it must be chosen low enough to enable all superfluous multiple echoes to disappear before the next active period is triggered. If it is too high these delayed echoes will be visible (as in Fig. 10.9) and are called phantom echoes.

To avoid such spurious echoes the time interval t_I in Fig. 10.7 must be sufficiently long, which from experience is about 60 times longer than the working time t_P of the picture. Sometimes however this is still not enough, when for example forgings of high quality steel, especially alloys with nickel, which have low attenuation (high transparency) have to be tested.

It is then essential to reduce the trigger rate, or to learn to distinguish the phantom echoes from real ones. This is possible because a trigger frequency of 500 Hz for example is normally somewhat modulated by the mains frequency which causes some jitter in the wrong echoes, and because the time difference between two trigger pulses does not remain exactly constant the delayed echoes also appear less sharply focussed.

Fundamentally the required time interval depends on the testing range and therefore in most designs the trigger frequency and the range are switched together.

The horizontal sweep voltage is usually applied symmetrically to the sweep plates of the CR tube, as in Fig. 10.5. Each plate is fed with the same voltage but with different signs. Line *4* in Fig. 10.7 shows its pattern. One complete period consists of the sweep delay t_S, the picture or working time t_P and the interval time t_I. During the working time the sweep voltage rises uniformly from zero and so shifting the electron beam from left to right. During the interval time the sweep voltage falls back to zero in an arbitrary way, outside the picture time t_p the brightness being reduced to zero by a rectangular voltage (line 5 in Fig. 10.7).

The sweep voltage proportional to time is generated by condensers charging at constant current. The travel time of the luminous spot across the screen is proportional to the ratio of their capacitance to the current. In many instruments this current is controlled by a potentiometer directly calibrated in terms of sound velocity. The values of the capacitors which are switched by the test-range control are proportional to these ranges, so that the full width of the screen is automatically adjusted for each setting in the appropriate units of length, for a given velocity.

For computer-aided instruments the precision of the time base must be much increased, and this is achieved by using a phase-locked loop, the sweep time being controlled by a quartz oscillator.

It is sometimes desirable to magnify a selected small part of the echo picture when the main pulse is of no interest. To achieve this purpose, using a circuit called "scale expansion", a section of the time base is expanded over the whole range of the screen (Fig. 10.10). The section within the test range selected for expansion can
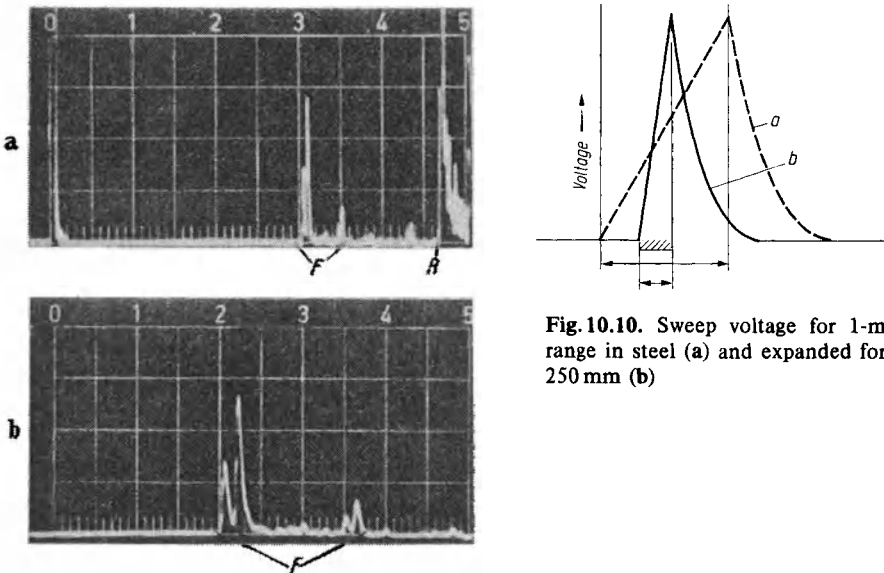
Fig. 10.10. Sweep voltage for 1-m range in steel (a) and expanded for 250 mm (b)

Fig. 10.11. Screen picture of a specimen with back echo *R* and a group of defect indications *F*, with normal sweep at 1-m range (a) and with scale expansion to 250 mm (b)

be moved in the same way as a magnifying glass scans over a subject. Figure 10.10 shows the sweep voltage for the range of 1 m steel together with the scale expansion for a range of 250 mm. The corresponding screen patterns can be seen in Fig. 10.11.

In principle it is not difficult to expand the time base far more and in the case of wall-thickness measurement a 10-mm range may be useful, but in this case the supply voltages must be very constant to avoid jittering of the echoes.

When testing components under water, in so-called immersion testing, the sound pulse has first to travel through water and the interesting testing range starts only with the entrance echo. Because the length of the water path may vary during testing it is of advantage to use the entrance echo to trigger the sweep. The block circuit of Fig. 10.5 would for this case have to be changed. The transmitter generator triggers only the transmitter pulse, whereas the sweep is triggered by the amplifier via a gating circuit (see below).

When using the simplest circuit for starting the sweep by an echo (echo start) the echo itself is not usually completely visible because it has first to start the sweep. If this situation is undesirable and it is required to display the echo fully, then the content of the picture has first to be delayed somewhat before transmission to the CR tube via a delay line.

10.2.4 The Transmitter

To excite the transmitter pulse a voltage pulse of some hundred volts is provided and its amplitude and shape have a great effect on the transmitted ultrasonic pulse.

Although by the use of new solid-state electronic components the circuit details have changed considerably, the principle can still be illustrated as in Fig. 10.12. The condenser C is charged to some hundred volts. The trigger signal closes an electronic switch which discharges the condenser and makes its peak voltage appear at the output to the transducer. The condenser is discharged via the resistor R and the coil L in parallel with the transducer (see also Section 10.4). By means of the electric pulse the transducer is excited to produce a mechanical pulse which is transmitted as an ultrasonic pulse into the specimen via a coupling layer.

The form of the electric pulse is influenced very much by the transducer and even by its coupling conditions. Because at least some of the elements defining the oscillation, for example the coil, are usually incorporated into the transducer, an electric oscillation is not generated before the transducer is connected to the flaw
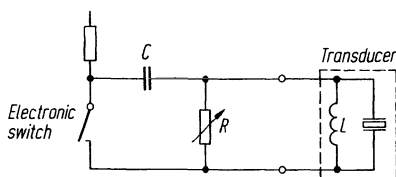
Fig. 10.12. Schematic circuit of a pulse generator

detector. Without this connection the pulse is only a unilateral peak with an ex-
ponential decay (Fig. 10.13).

The upper limit of pulse frequency depends on the risetime of the condenser
discharge and this depends on the switching time of the electronic switch. The
lower frequency limit is given by the size of the condenser.

Formerly gas-filled tubes such as the thyratron (Fig. 10.14 a) have been used as
switches. Today controlled rectifiers (Thyristors, Fig. 10.14 b) or field-effect transis-
tors (VMOS, Fig. 10.14 c) are used. For the excitation of very high frequencies (up
to 100 MHz) avalanche transistors (Fig. 10.14 d) are used as switches since their
switching time is extremely short and is limited only by the inductances and capac-
ities of the circuit.

The field-effect transistors have the advantage (as against thyristors or thyra-
trons) of being opened again at an arbitrary time, for example to greatly increase
the efficiency by switching off the transmitter precisely when the oscillation has
completed its first half wave, (square-wave pulser) since by this means the withdra-
wal of energy from the oscillation by the pulse generating circuit is avoided.
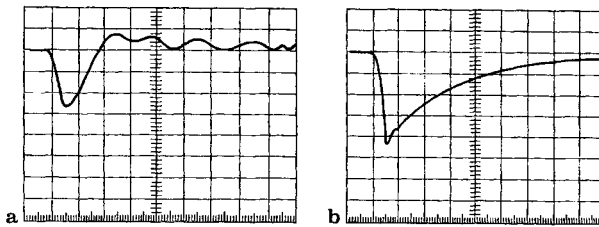
Fig. 10.13. Transmitter pulse of a thyristor-transmitter (a) with transducer connected (b) with-
out transducer (100-Ohm load)
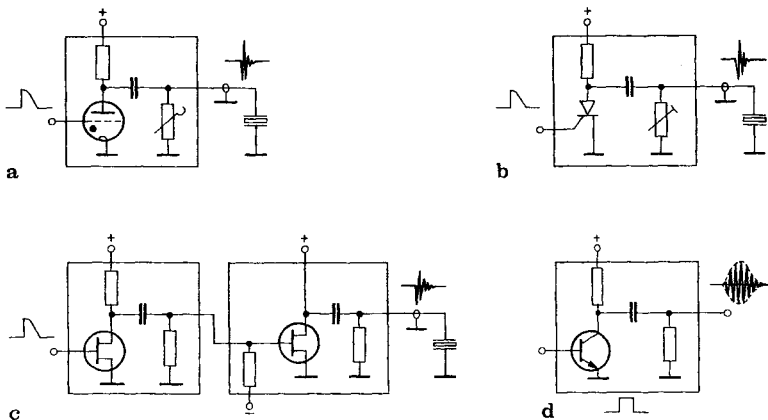
Fig. 10.14. Circuits of pulse generators

A consequence of this idea is the excitation of the transducer by pulses of sine waves, whose frequency equals the ultrasonic pulse frequency (CS controlled signal transmitter [270]). By this means the efficiency is increased, as well providing greater precision for the ultrasonic frequency. By using highly damped wideband crystals it is even possible by varying the exciting sine-frequency, to produce a range of ultrasonic frequencies with only one transducer.

The shape of the transmitted pulse is, incidentally, not too important for the performance of the flaw detector. Of more importance is the shape of the echo signal, which is formed after the pulse has passed through all the various elements of the transmitting chain up to the final display. These include the twofold transformation by the crystal, the properties of the material and the reflector, and the characteristics of the amplifier and rectifier. These all have an influence on the final pulse shape displayed on the screen but the most important influence usually arises from the acoustic properties of the oscillator.

10.2.5 The Receiver

Quite high demands are made on the receiver-amplifier since the voltage which has to be displayed on the screen goes from 30 µV up to 30 V, that is a range of 120 dB.

It is required that the smallest displayed voltage of 30 µV must still be well above the noise and interference levels. On the other hand high voltages of 30 V have to be presented without distortion or saturation. Because of the very short time interval between transmitter pulse and first echo the amplifier must also have a very quick recovery time after overloading because transients following the high amplitude signals may hide small echoes.

The principle of such an amplifier is shown in Fig. 10.15. At the amplifier input we have a voltage limiter (*1*) to prevent the high transmitter voltage damaging the amplifier. Then follows a coarse potential-divider (*2*), by which high echo voltages can be reduced to be within the working range of the amplifier and it usually has several switched steps of 20 dB each. It is followed by the low-noise preamplifier (*3*), the maximum amplification of which is limited by its thermal noise. Then by way of a calibrated fine potential-divider (*4*) (calibrated as a gain control in 2-dB steps) the signal goes into the HF amplifier (*5*) for which a typical frequency band could be 0.5 to 10 MHz in a simple flaw detector. Units with high resolution may have a bandwidth up to 25 MHz and more.
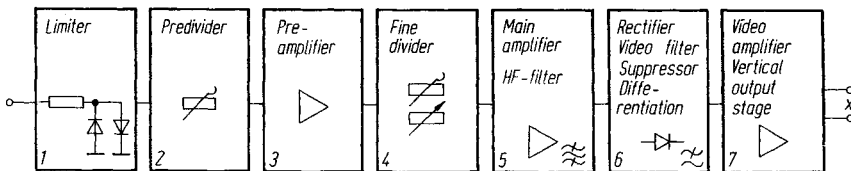
Fig. 10.15. Block diagram for the receiver amplifier

It is essential for high resolution to have highly damped probes and also a wide-band amplifier with flat phase curves in the neighborhood of the probe frequency. These are the conditions to obtain on the screen pulses without transient oscillations. On the other hand a large bandwidth increases the noise level thus reducing the sensitivity for small echoes. For this reason high-quality flaw detectors may have different settings for high and low probe damping to obtain the best compromise.

The signals after having been amplified by the main amplifier proceed to the rectifier (6). Modern units have rectifiers which can be switched from full-wave to half-wave rectification for either the positive or negative half waves. With other units the rectifier may even be switched off, to display non-rectified signals on the screen (Fig. 10.16).

Half-wave rectification is to be preferred if the transit time must be measured, or for a very exact evaluation of the defect distance. The video presentation on the screen then has the steepest rise. The best polarity of the recitifier will depend on the properties of the probe and reflector, and should be determined experimentally. The phase of the echo is, incidentally, changed according to whether the reflector is acoustically softer or harder than the surrounding material.

The full-wave rectifier offers some advantage if the amplitude has to be evaluated because it gives a phase independent presentation. The HF presentation is selected for measurement of the probe frequency and in those cases where distance measurements to reflectors of both hard or soft quality have to be made. This presentation is also preferable if it is necessary to trace small reflectors in the vicinity of strong echoes, as for example with defects close to a surface.

To obtain a clear display of the half waves in Fig. 10.16 b–d the upper limit of the bandwidth of the video amplifier (after the rectifier) including the CR tube, must be several times larger than the probe frequency and this is decisive therefore for the resolution of the flaw detector.
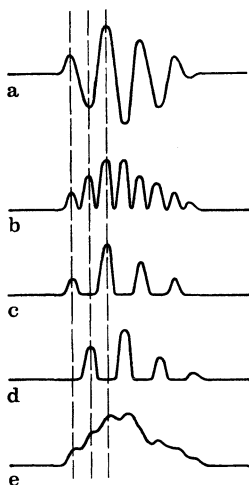
Fig. 10.16. Different types of signal display. **a** High frequency form, unmodified; **b** full-wave rectified; **c** half-wave rectified (positive); **d** half-wave rectified (negative); **b–d** without filter; **e** with filter

Treshold
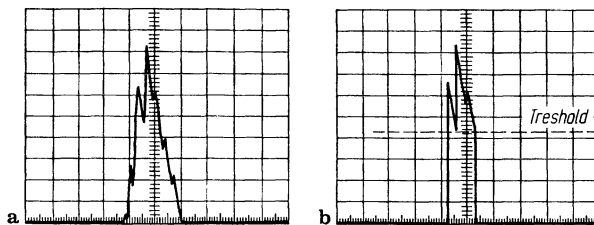
Fig. 10.17. Echo indication. **a** Without suppression; **b** with linear suppression

For most practical applications a smoothed display of the signals is needed, especially if the amplitude of the rectified signal is to be evaluated (Fig. 10.16 e). For this purpose the envelope of the rectified pulse is filtered by condensers and differentiating circuits, which in high quality units can be varied from "without filter" up to "strong filter". By the use of differentiation, or what is sometimes called "screen cosmetics", the decay of the echo pulse can be made to appear steeper, and narrower.

Another important characteristic is *linearity*, which is fundamentally defined by the properties of the rectifier and video amplifier. Perfect linearity is achieved when the echo height on the screen is exactly proportional to the incoming signal amplitude, but full linearity is never reached because of the rectifier characteristics.

To be better able to distinguish an echo within the grass level most units are fitted with means for suppressing small signals. In older designs this was achieved by partial suppression of the base line but this also reduces all the signal amplitudes. Modern units have therefore a "linear suppression" which operates without altering the wanted signals (Fig. 10.17). However, when searching for small defects in a specimen this aid is sometimes strictly forbidden because small but important defects may then be overlooked.

10.3 Special Circuits for Automatic Evaluation of Defect Echoes

10.3.1 Gating Circuits

For those applications of ultrasonic pulse-echo testing, where defect decisions are required, the amplitude of the echo is significant and usually the echo of admissible defects must not be greater than certain limits. If the specimen has plane-parallel surfaces the rear echo is also observed and here the underpassing of reference values may indicate the shadowing effect of large inhomogeneities (Fig. 10.3 d). Electronic gating circuits can relieve the operator from continuously observing the screen and they give an alarm if an echo is greater or less, respectively, than certain predetermined heights within the gated-depth range. Only by using such a supple-
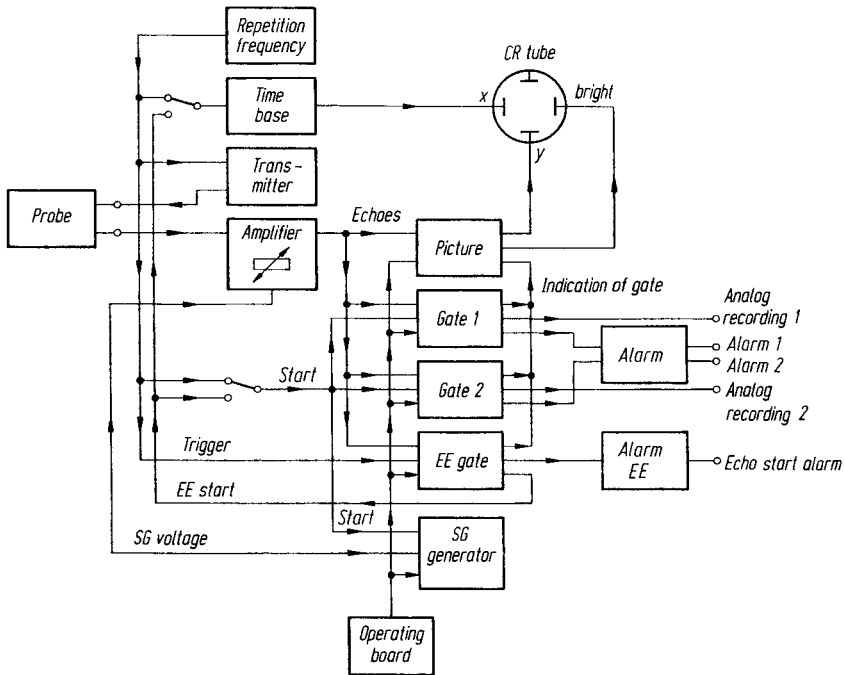
Fig. 10.18. Block circuit of a flaw detector with monitor gates, recording amplifier, entrance-echo start of sweep (EE), and distance-compensated or swept gain (swept gain SG)

mentary device can automatic testing be introduced and so nearly all flaw detectors are provided with gating circuits (Fig. 10.18).

The video output of the amplifier is connected to a comparator circuit, in which the signal is compared to a threshold voltage. By use of a logic circuit any signal greater than the threshold will give an alarm signal provided it occurs within the gated transit time. The threshold voltage, as well as the position and length of the gate, can all be controlled by the same operating panel.

If all defects in the total thickness of the specimen must be indicated, the start of the gate is placed immediately behind the main pulse and is set to end just before the rear echo (Fig. 10.19). By using a second independent gate the rear echo may also be observed.
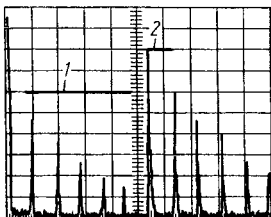
Fig. 10.19. Gate positions for defect indication (*1*) and back-echo monitoring (*2*)

Usually the gating alarm is selected either for coincidence or anticoincidence of a indication with the gate range. The former serves as a defect indicator and the latter, for example, to monitor whether the rear echo maintains a certain minimum height.

Two different ways are used to generate the gate voltage. In simpler designs the gate is fixed on the screen because it is produced by a comparator circuit which compares a controllable reference voltage to the sweep voltage at both the start and the finish (Fig. 10.20 a). In this case the echo pattern is moved relative to the gate if the test range or the main pulse is shifted. With reference to the specimen, therefore, it changes its position and to avoid this disadvantage units of better performance generate the start and finish of the gate independently of the sweep. The gate is therefore fixed in the specimen effectively and a group of defect indications lying within the gate may be observed on an enlarged scale by using the sweep expansion but without losing them from the gate.

Some designs permit the so-called slave function of the gates in which the second is controlled by the first. In this case the second gate stays connected to the first even if the thickness of the specimen changes thereby requiring a change in the gate positions. Only the first must then be adapted and the second, used for example to monitor the rear echo, stays in its correct position automatically.

All these methods usually give an alarm only for echoes within one gate. For a multiple echo pattern the solution may be a so-called gate chain in which one gate is always triggered by the foregoing one. The information may be digitized to give echo transit times (i.e. the depth of the defects). Furthermore there can be introduced a series of stepped thresholds equally spaced for successive gates and then the amplitudes can be digitized. If the gate widths and the threshold differences are sufficiently small, it is possible to do without the
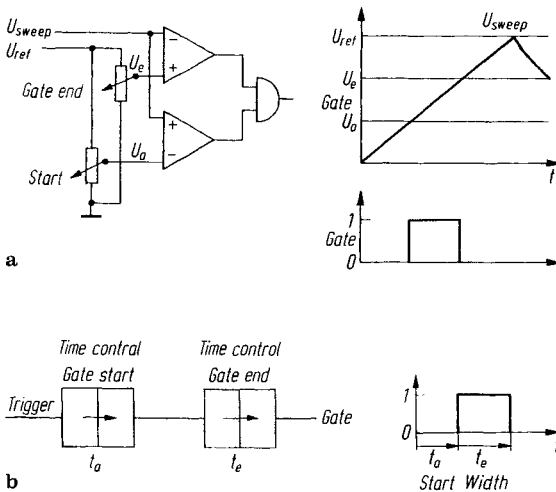
Fig. 10.20. Block circuits for generating the time gate. a From the sweep voltage (fixed relativ to the screen); b independent of the screen (with variable time controls)

screen display thus enabling the use of units without a CR tube, which could be therefore rather small and handy. The disadvantages, which arise if the steps are not extremely small, should not be forgotten since then many features of the fine structure of an echo, and of the echo dynamics when scanning a specimen, are lost (see Fig. 19.8).

One application of the gate-chain, designed for weld testing, is the luminous flaw localizer [944] (see Section 28.1.3 and Fig. 28.12).

For indicating the gate and the threshold level on the screen two alternative ways are possible. Simple units, which often have only a fixed threshold, mark the gate position on the base line with a stepped section (Fig. 10.21 a). In units with variable threshold, both gate position and threshold are indicated by a straight line (Fig. 10.21 b), the height of which gives the value of the threshold, and sometimes both methods are combined (Fig. 10.21 c).

When using a digitized-screen picture, as in Fig. 19.7, the gate can be marked by a contrasting rectangular area at the upper edge of the screen.

The standard controls on the gate operating panel should be protected against unintentional changes. Some modern units have electronic controls, the functions concerned being chosen by a function key. Then the dimensional features are varied by up/down and right/left keys and if the function switch is brought back to its "off" position an accidental adjustment is no longer possible.

The alarm may be given by a warning lamp or by an acoustic device which in some designs may not be cancelled unless a confirmation button is operated.

Many units also have a feature which prevents a single echo pulse within the gate from operating the alarm, because it may arise from electric interference. In this case the total number of successive echo pulses which must appear in the gate are predetermined before the alarm is operated.

10.3.2 Back-Echo Reduction

Usually the signal amplitudes from a defect and from the back echo are widely different, so that operating with both may often not be possible without changing the gain. Some instruments have therefore the means of reducing the gain during a

a   b   c
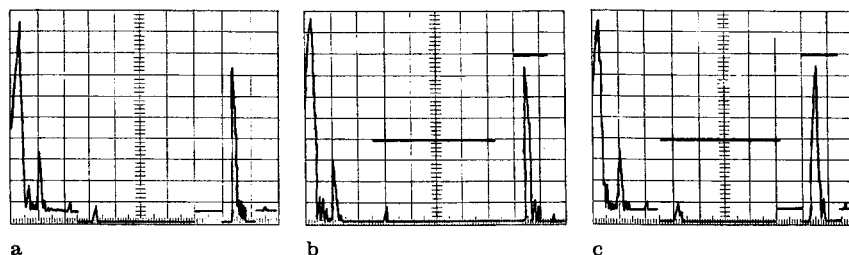
Fig. 10.21. Indications of the gate functions. **a** by steps on the base line; **b** by straight lines; **c** with a combined indication

transit time gate by a preselectable value between 10 and about 40 dB. This brings both echoes into the linear range of presentation and allows the gate thresholds to be placed at comparable heights. To be effectiv, the gain switching must operate very quickly and avoid any interfering electric pulses (see Section 22.3, Fig. 22.14).

10.3.3 Recording Amplifier, Peak Memory

For many testing purposes documentation of the echo amplitudes during scanning of a specimen is desirable. For this purpose a *recording amplifier* is coupled to the gate by which means the maximum received echo height is held for each pulse and then fed to a terminal for a recorder. This voltage is proportional to the echo height in the gate during the immediately preceding period.

If the maximum value is stored until it is cancelled, it is called a *peak-value memory*. It can be very useful for evaluating the maximum indication of a defect, which is detected by slow scanning and during the so-called "growing" of the echo (see Section 19.1). In the same way as with gate functions it may be combined with a counter to ignore random interference. The working speed of the peak memory must be quite high to ensure that the peak value is stored immediately after the echo pulse.

There is a great choice of recorder types which can be used following the recording amplifier output. These fall into two main categories, viz:

— Analog records,
— Analog/digital converters for both digital indications and for computer evaluations.

Digital methods are preferred today and in this case for example an echo of full screen height can be equated to 100 units, the minimum difference of one unit between two different echoes is fully sufficient for recognition and separation.

This system of measuring echo heights is of importance when a logarithmic amplifier is used instead of a linear one (see Section 10.2.5). When using a linear amplifier a maximum amplitude ratio of about 30 dB can be displayed without saturation, whereas with a logarithmic one differences up to a total of 100 dB can be displayed simultaneously, the screen height being divided into 100 parts of one dB each. The analog/digital conversion of a amplitude ratio is directly carried out from the reading on the screen.

10.3.4 Distance-Amplitude-Correction (DAC); Gate Thresholds

The amplitude of a reflector echo depends on its relative distance from the probe and therefore an evaluation threshold cannot be kept constant, but must also be allowed to vary with the distance. For dealing with this problem two methods can be adopted:

— distance dependent threshold by means of a response voltage decreasing with the sweep voltage (Fig. 10.22)
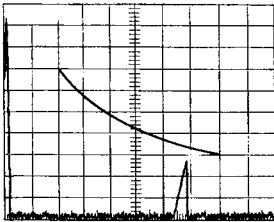
Fig. 10.22. Distance-dependent threshold

— swept gain; i. e. an increase of amplification with distance according to the echo-distance law.

The latter method (DAC) has the advantage of allowing a larger range of variation, up to about 40 dB, and adjusting such a device can be carried out in one of two ways.

1. Empirical adjustment. The apparatus includes a compensating voltage generator which can operate in up to eight linear sections. Adjustment is done by using test blocks which give echoes from the same artificial defect at different depths.

The echoes peak obtained are marked on the screen after which the compensation voltage curve is displayed and by using several controls it is adjusted as a best fit to the echo heights (Fig. 10.23 a). Now the swept gain can be switched on, bringing all the echoes to the same height (Fig. 10. 23 b).

When using a computer-aided instrument it is possible to "teach" the compensation function by using a special program. The echoes from equal artificial test reflectors are automatically brought to the same amplitude, the compensating voltage value for each is stored along with the distance and subsequently the pairs of values stored give the overall compensation function.

2. Adjustment by help of the DGS method (see Section 5.2). The correct compensation function for the swept gain can also be evaluated from the properties of the sound field corresponding to the probe concerned. In some well-developed flaw detectors a number of standard DGS curves are stored so that by choosing the correct parameters for the effective diameter, frequency and attenuation coefficient of the specimen material, distance compensation for any echo is automatically performed.
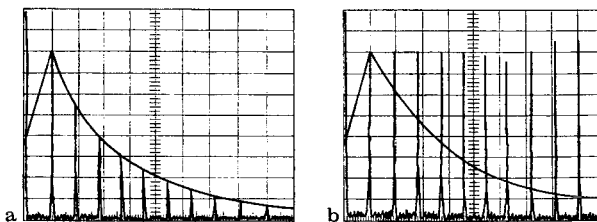
Fig. 10.23. Adjustment of swept gain. a adjusting the compensation voltage curve to fit successive echoes received from increasing distances; b swept gain switched on so that echo amplitudes are made uniform

It is further possible to allow for focussed probes or to choose between the decay law relevant to a circular flat reflector or to a borehole transverse to the beam direction (see Section 5.2).

10.3.5 Wallthickness Meters

The auxiliary devices described above process the echo amplitude into an electric signal suitable for further evaluation. However, the echo transit time is also of interest, either from the probe to a defect or especially to the back wall, giving the wall thickness. The special circuit designs for these measurements are discussed in Section 11.1. If they give the time value in analog form an analog/digital converter is necessary to give the thickness in the digital form usually required. A further circuit will immediately give a digital value, and this can be displayed on the operating panel of the unit as in Fig. 10.24.

With automatic scanning a large number of different values will appear in quick succession and these cannot be evaluated by the eye. In a simplified case it may be only necessary to know whether a given value has been exceeded. Here the wall-thickness measurement can be reduced to a yes/no indication but if one wants to know where the wall thickness has reached a minimum or a maximum value, the reading at each point must be stored for it to be compared with the following ones. Logic circuits will store readings in this way so that each can be compared with the preceding or following values in the scanning range. Finally the extreme values and their positions can be recorded by a commercial printer.

Wall thickness meters incorporated into flaw detectors provide more possibilities to determine:

— Transit time, or distance, between two echoes in two separate gates;
— Transit time between main pulse and an echo within a gate;
— Transit time between main pulse and an echo within a gate corrected by a predetermined delay-line transit (e.g. for angle probes and TR probes; see Section 10.4).
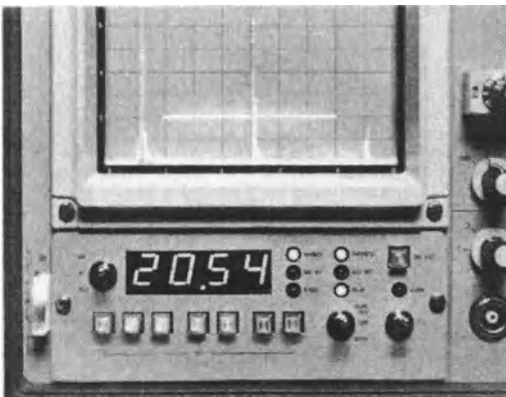
Fig. 10.24. Wall-thickness meter incorporated into a flaw detector

Sometimes this kind of measurement is supplemented by circuits to check whether the two echoes are actually present and so providing a go/no-go signal. A no-go signal can serve to end further scanning or recording, and to keep stored the last measured value. A final purpose for wall thickness circuitry can be to give a very precise control of the gate positions.

10.3.6 Auxiliary Instruments and Documentation Methods

Full documentation of all significant data arising from pulse-echo testing is in principle possible with modern computers. For this purpose the positional data referring to the probe scanning must be transmitted from a mechanical guiding device in addition to the digitized data from the screen. By the many possibilities of data processing a printer can deliver a document in real time and quite complicated data evaluations can follow later. The complete work can of course be very comprehensive but is justified only in special cases, as for example in nuclear reactor testing [636, 1158].

Figure 10.25 shows schematically various schemes of documentation. The so-called A scan can be recorded photographically or with digitized equipment (see Fig. 19.7) using an auxiliary recorder. Such records are mostly of low value, because the probe position data are missing.
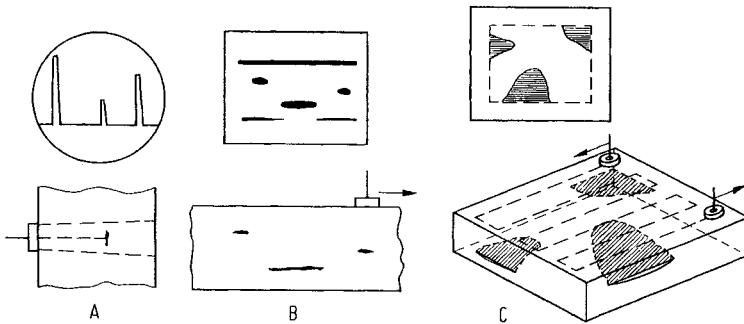
Fig. 10.25. A-, B- and C-scan recording and principle of scanning
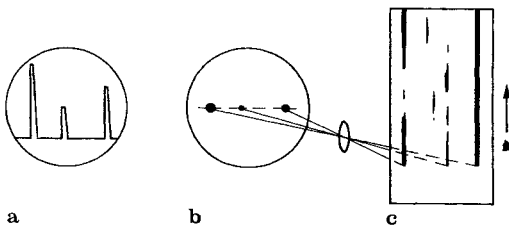
Fig. 10.26. B-scan recording by a brightness-modulated dot display. a Standard A scan; b same with dot presentation, c record on moving film

The B and C scans (Fig. 10.25) are produced by probe scanning and usually involve a mechanical guiding device. The display on the screen is changed from the peak type presentation of A scan to one of light-point writing (Fig. 10.26) which is moved according to the probe displacement. The vertical coordinate in this case corresponds to the transit time, the record corresponding to a section through the specimen. The brightness of the luminous point is controlled by the received echo amplitude. Instead of shifting the luminous point on the screen a photographic film may be moved analog to the probe (Figs. 10.25 and 10.26). To present the full B scan on a screen, large television CR tubes have sometimes been used.

In case of the C scan the mechanical device has to provide a scan in two coordinates. If the luminous point is shifted to follow the two displacements on the screen the CR tube should have a long afterglow to produce the complete C scan, or a storage oscilloscope can be used (Fig. 19.7). More effective is a record on paper produced by one of the many commercial devices available.

With a C scan all echoes within a preselected gate are recorded, or alternatively the echo with a maximum amplitude between front and back echoes. The depth of the defect remains uncertain but by using several gates a depth record is also possible. A three-dimensional presentation could be produced if it was built up from a number of two dimensional recordings.

Figure 10.27 shows a method of producing an isometric presentation from A-scans by moving a film in a direction oblique to the base line, s. [983].

Because photographic recordings are of limited value commercial devices for this purpose are not normally available (see also [1052 and 1056]).

For practical recording, writing or printing devices are to be preferred which obtain their data via gating circuitry as described in Sections 10.3.1 to 10.3.3. Many variations are possible in writing instruments so that if lines are written with perpendicular displacements, for example in the case of a C scan (Fig. 4.18), even with overlapping a clear picture is given of defect positions and size of echo amplitude.
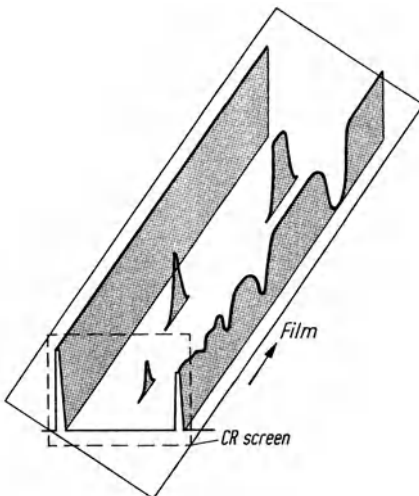
Fig. 10.27. Recording method (Martin and Werner) using obliquely transported film with conventional A scan
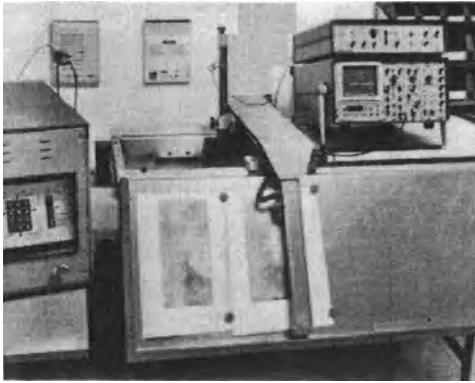
Fig. 10.28. Immersion-testing installation for aircraft parts, using grey-scale C-scan recording (Wells-Krautkrämer)

Figure 4.18 shows an isometric presentation for another purpose and instead of the amplitude of the echo the depth of the defect may also be recorded. If one can omit depth information a simple yes/no recorder will be sufficient for simple plate testing as in Fig. 24.8.

The choice of a recording system depends in the first instance on the limit frequency, which is the frequency of a voltage which it can just follow without much distortion. This criterion also depends on the scanning speed and the required resolution and for simple cases 1000 Hz will normally suffice. There are however much quicker ones available, for example using lasers. Ink is used only for a slower response. Quicker ones can use thermal papers or record directly onto photographic film.

Some recorders using electro-sensitive paper can write with different colour intensities. To obtain an even grey scale with uniform steps the amplitude has first to be processed by a quantizer.

Quantizing is also of advantage if a C record is made via a printer and is useful especially in connection with computer-aided devices (see Fig. 22.17). It may for example write the figures 1, 2, 4 and 8 as measures of echo amplitude.

With the above-mentioned variety of possibilities the cost also increases considerably and may only be justified in cases of great importance when testing critical components for aerospace or nuclear applications. These are usually tested with immersion techniques using a large program and careful recording. Figure 10.28 shows a smaller version of such an installation, the probe movement in the tank being mechanically coupled to the writing electrode on the front-mounted recorder. C scans with a size ratio of 1:1 can be made, with echo heights indicated by eight steps of grey scale.

10.4 Transducers

Transducers, which are also called probes, transform the energy of an electric voltage into an ultrasonic wave, for most applications of materials testing via the

piezo-electric effect (Chapter 7). If the same crystal serves as transmitter, and immediately after transmitting a pulse, also as a receiver we can speak of a single-crystal probe. If on the other hand the echo receiver is a separate crystal we have a twin-crystal or transmitter-receiver (TR) probe.

10.4.1 Single-Crystal Vertical (0°) Probes

With a single-crystal vertical probe also celled normalprobe the generated ultrasonic wave passes into the surface of the specimen in a perpendicular direction and is coupled to it by a liquid coupling layer. As Fig. 10.29 shows it consists mainly of the oscillator disk, a protective layer and the damping block. If necessary there are also electrical matching elements and all are built into a rigid housing with the electrical connector.

Types of probe formerly used which had a direct contact between the (quartz) crystal and the specimen are no longer used (see 3rd edition of this book, p. 210). The protective layer as well as protecting the delicate crystal is also used to match the acoustic impedances for optimum coupling to the specimen.

The damping block absorbs that part of the energy radiated backwards and the oscillator is thereby strongly damped in order to suppress the reverberations of the pulse (see Section 7.3). In addition it also provides mechanical support for the crystal against pressure and against mechanical shocks during practical use.

The thickness of the oscillator plate corresponds to the required frequency and both its surfaces are metallized to act as electrodes. These must be as thin as possible so as not to interfere with the oscillations. The methods of metallizing vary according to the crystal material. With ceramics the surfaces are best painted with a silver emulsion and heated to about 800 °C. Another method is to chemically deposit layers of nickel or/and gold with a thickness of about one micron (10^{-3} mm) and contact wires can then be soldered on. Other piezo-electric materials have electrodes produced by metal evaporation or by spraying conductive paint in which cases the wires can be fixed by a conductive cement.

The choice of a particular piezo-ceramic material depends on the intended purpose of the probe, and it can be decided by reference to Table 7.1. The various physical criteria, as for example coupling factor, mechanical quality Q, cross-coupling properties, the dielectric constant and critical temperature have all been discussed
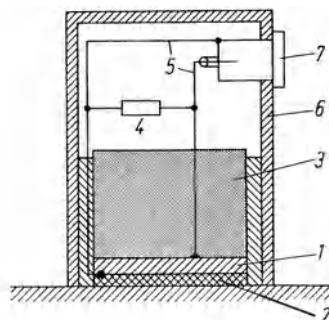

Fig. 10.29. Design of a transducer, schematic. *1* oscillator, *2* protecting layer, *3* damping block, *4* electric matching, *5* wire, *6* housing, *7* connection socket

in Chapter 7 but it should be kept in mind that there is never one optimal material each one having its special advantages and handicaps.

The mechanical bonding of the crystal to both the protective layer and the damping block is of great importance. It can be achieved by cementing, soldering or even by a very thin liquid layer. In all cases the surfaces must be very flat and smooth and it is essential that the cement layer is as thin as possible to avoid oscillations within it, thereby changing the impedance matching. For this purpose it should be less than 5 % of the wavelength and at 4 MHz a typical epoxy cement ($c = 3200$ m/s) should have a maximum thickness of about 0.04 mm. For frequencies above 10 MHz it is quite difficult to keep the bonding layer sufficiently thin so instead of a separate cement layer it is advantageous to cast the damping block and the protective layer as mixtures of liquid resins directly onto the crystal.

The acoustic impedance of the damping block material must be chosen to give the degree of damping required. The maximum effect is reached when both the impedance of the block and of the crystal are equal, since in this case all the acoustic energy of the rearward travelling wave is absorbed without reflection (see Section 7.3). To suppress any reflections from the back face of the damping block it must have sufficiently high attenuation and thickness. The best results are achieved with mixtures of resins and powdered materials and very good impedance values are obtained by using finely powdered metallic tungsten. By using this mixture the impedance can be increased from that of the pure resin (2.7×10^6 kg/m^{2}s) up to the value for lead meta-niobate (20.5×10^6 kg/m^{2}s). The attenuation can also be influenced by the choice of the resin and by admixtures of fine grained materials of high absorption, as for example rubber powder. To absorb the reflected wave porosity and even sawdust have been used as well as being combined with an oblique geometrical shape, or a saw toothed form of the back surface. A combination of effective methods must be found otherwise "grass" or "probe noise" will be produced which is just as annoying as other interfering echoes.

One advantage of using a high proportion of metal powder is that it makes the damping block electrically conductive so that it is not necessary to have a metal electrode on the crystal face.

The damping block is mainly useful in damping the thickness oscillations of the crystal but radial oscillations can also be a nuisance and in case of barium titanate, for example, they are difficult to suppress completely. They can be reduced somewhat by embedding the crystal edges into the block or by using a crystal mosaic design with the intermediate slits also filled with an absorbing material.

As far as the protective layer is concerned it is necessary to distinguish between the hard-faced and the soft-faced designs for suitable acoustic impedances. Reasonable resistance against wear and tear is achieved by using thin, hard layers cemented to the crystal, suitable materials being aluminium oxide, sapphire, boron carbide or quartz. When used on hard metallic surfaces they tend to give large variations of coupling and hence of sensitivity. Moreover such layers suitable for high frequencies are thin and fragile, because they have to be less than 1/10 wavelength thick. The coupling variations arise from small variations in the thickness of the coupling liquid, as a consequence of the great discrepancies in the three impedances: hard layer about 30×10^6, liquid about 1.5×10^6, and specimen about 50×10^6.

Soft-faced coupling probes are constructed with a fixed protective layer of cast resin and these are suitable for immersion testing without making a direct contact with a hard specimen or for use in contact testing with a replaceable plastics film.

The job of matching the impedance of the crystal to that of a liquid can be solved by using a layer with continuously decreasing impedance through its thickness. In practice this can also be achieved by using several superimposed layers with decreasing impedance values. If only one layer is used the best compromise is reached if its thickness is a quarter wavelength and its own impedance is equal to the geometric mean of the other two impedances [837, 170, 859].

The impedance of casting resins can be varied by mixing with filling materials. The thickness has to be quite precisely 1/4 wavelength because otherwise the probe will not produce the frequency required. For use in immersion techniques it is essential to make the probe watertight, because some piezo-electric crystals are readily soluble in water.

For contact testing on rough surfaces one must do without high resolution, and can then use interchangeable films to protect the crystal, these being coupled with a little oil or grease. It is an advantage to use films which combine high resistance against wear and tear with high absorption of ultrasound. The sensitivity is not much affected by the high absorption because of the small thickness, but multiple oscillations within the film which would broaden the pulses are suppressed [987].

The use of soft plastics has the added advantage that variations in the liquid coupling layer do not affect the sensitivity very much and they can be used with low contact pressure and can be shifted more easily.

Sufficiently soft films even allow coupling without the use of liquids at frequencies up to 5 MHz and so such probes can be used for testing materials which are sensitive against liquids or are porous [323].

Further types of soft-faced probes are those using a delay line in front of the crystal (see Fig. 10.30). These are best made of a plastic material with low absorption, for example polystyrene. The usable length depends on the maximum transit time within the specimen and the second echo from the delay line must not arrive

Fig. 10.30. A selection of vertical probes: top and bottom left with hard facing-layer; top centre with exchangable wear-resistant film; lower right with exchangeable delay line, and with cast-resin face for immersion techniques

before the back echo of the specimen otherwise the picture is confused. This type of probe is often used for wall-thickness measurement on thin walls.

For commercial probes crystals between 5 and 40 mm diameter are mostly used. Larger diameters seldom find corresponding flat areas for coupling to the surface of specimens. The disadvantages of using small diameters, especially with low frequencies, are the poor beam directivity and the increased generation of transverse and surface waves. These will produce interfering pulses which can be easily confused with useful longitudinal echoes (see Fig. 4.23). Small transducers also have the handicap of having a low sensitivity.

The height of a back echo in the near-field is proportional to the area of the crystal, but in the far-field it is proportional to the square of the area, i. e. the sensitivity falls with the 4th power of the diameter. The first point arises from the fact that a piezo-electric receiver working with a low termination resistance (as is usually the case) produces a receiver voltage proportional to its area. The second arises from Eq. (5.3), in which initial pressure p_0 is proportional to the area when transmitters of different sizes are compared. It also has to be assumed that the crystal always receives the same transmitter voltage independently of its area.

The diagram of Fig. 10.31 gives details of the near-field lengths, and the directivity angles, for different frequencies (from 0.5 to 20 MHz) and oscillator diameters (up to 40 mm).
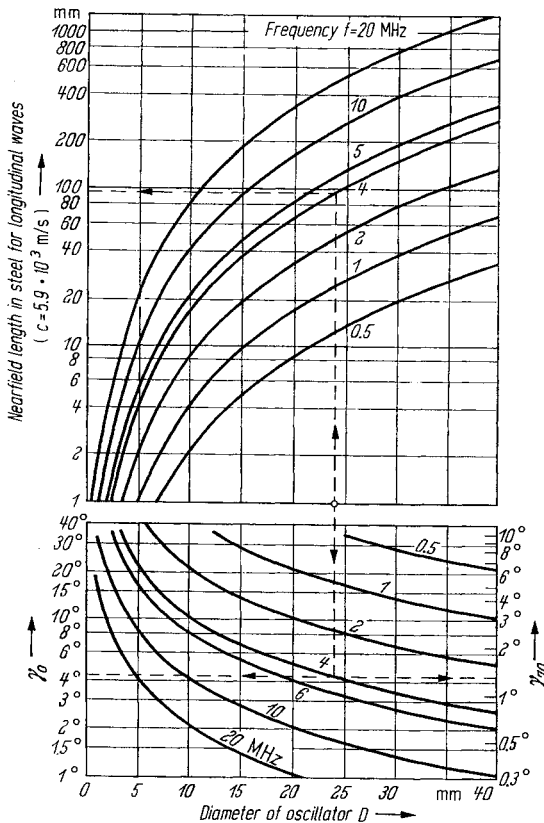
Fig. 10.31. Length of near-field N, angles of divergence γ_0 and γ_{70} for probes with circular-disc oscillators of diameter D, calculated for steel and longitudinal waves (angle of divergence γ_{70} for the echo field)

Example. A transducer of 24 mm in diameter at 4 MHz will have a near-field length of 97 mm and its beam directivity angles $2\gamma_0$ and $2\gamma_{70}$ are $2 \times 4.3°$ and $2 \times 1.3°$ respectively (see Section 4.4).

The effective diameter is actually somewhat smaller than the physical one because of the edge effect (see Section 4.8) and therefore the near-field length shown in the diagram is somewhat smaller than that calculated one. In this example it is only 90 mm and the angle γ_0 is somewhat larger at 4.5°.

The properties required for a "good" probe are on the one hand to have a high sensitivity for defects at larger distances, and on the other to have a good resolution for near-surface reflectors at very short distances. If one has chosen in accordance with the first requirement to have the largest possible diameter and the highest practical frequency then only reduced damping can produce a further increase in the sensitivity. This would, however, clash with the resolution requirement since the longer main pulse would produce a longer "dead-zone" below the contact surface. Such considerations show that for a given piezo-electric material a probe can only be made optimal for either of the two aims but not both.

Figure 10.32 shows a simplified sound-field diagram (Sonogram) for some standard probes. The natural focus at the end of the near field can be seen clearly.
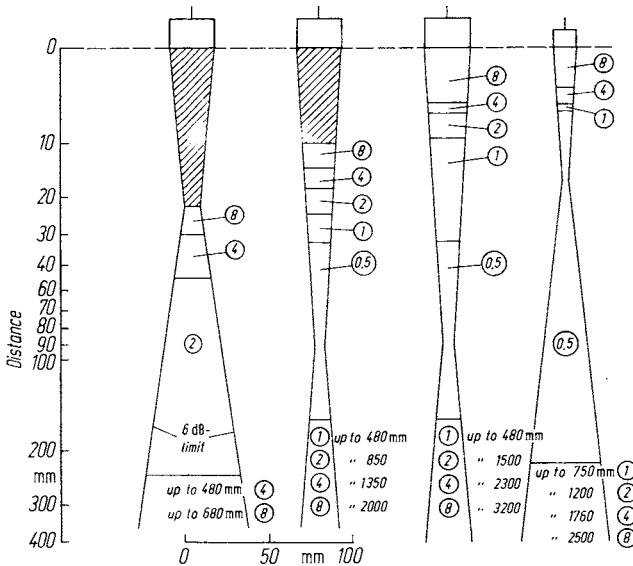
① *smallest discernible size of equivalent defect, e.g. 1 mm diameter*

▨ *dead zone, where no testing is possible*

Fig. 10.32. Sonogram for vertical probes in soft- and hard-faced designs
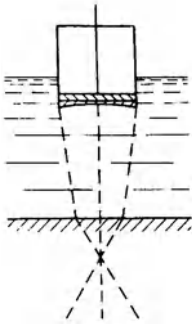
Fig. 10.33. Focussed probe for immersion testing (schematic)

a
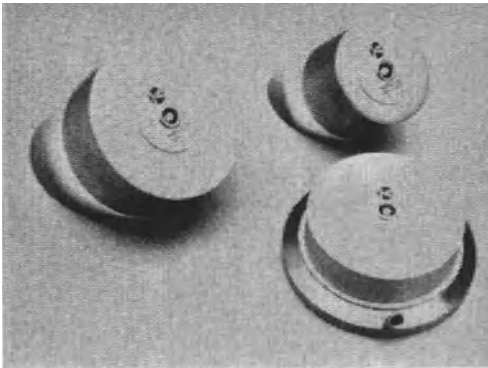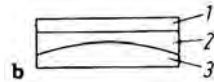
Fig. 10.34 Focussed probes for contact testing: designed by Krautkrämer-BAM (Bundesanstalt für Materialprüfung). **a** vertical and angle probes; **b** cross-section (schematic); *1* crystal, *2* and *3* lenses

If this is not sufficient for any special purpose, as for example in Fig. 10.33, special means for focussing and shortening of the focal distance can be used in accordance with Section 4.7. Such focussed probes are illustrated in Fig. 10.34, but having rather large diameters up to 75 mm, and a lens combination with a flat contact face according to [1655]. A rather large dead-zone has consequently to be taken into account, even if a plastic with absorbent filling material is used to make the focussing lenses.

For scanning of large specimens special broad-beam probes have sometimes been used (Fig. 10.35) up to 100 mm in width and they have also been combined with cylindrical lenses. Using a 75-mm-wide design it was possible to detect a flat-bottomed hole, 1.6 mm in diameter, in aluminium at a frequency of 10 MHz over a depth range between 2 mm and 12 mm below the surface [17, Section 44].

The requirement to test a larger volume with only one scan is difficult to achieve with constant senstivity everywhere. In addition the exact position of a detected reflector is not indicated. A rather better solution is achieved by subdividing
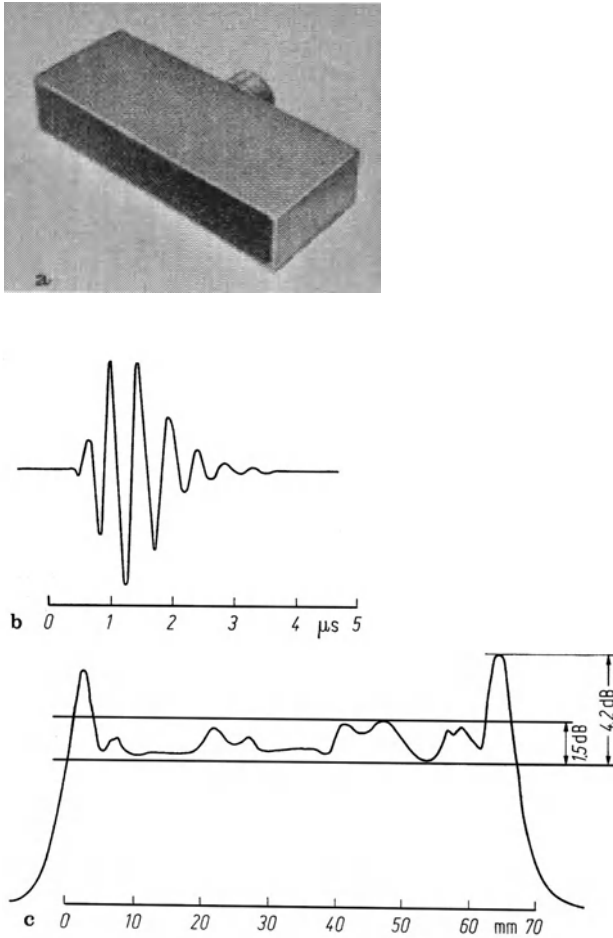
Fig. 10.35. Broad-beam probe (Aerotech), 2.5″ width, frequency 2 MHz.
a view; **b** pulse form of the echo; **c** echo amplitude from a 6-mm diameter steel rod at a distance of 75 mm in water

the long crystal into many single ones each excited separately. This is called a *crystal array* (Fig. 10.36) and it offers many operating possibilities. In the simplest case scanning can be simulated, but with the probe in a fixed point contact, by successively exciting the crystals in which case the sound direction stays vertical to the surface. The sharpness of the beam can be improved by energising several adjacent crystals at the same time and then moving the group. In this way the near-field length can be matched to the requirements. This system is a *linear array*, but for widths larger than about 100 mm there will be many coupling difficulties. Crystal arrays where the phase of the excitation can also be varied, are called *phased arrays*, and offer more possibilities since they can be made shorter. Each single element can have a width of less than a wavelength and they are excited simultaneously, but
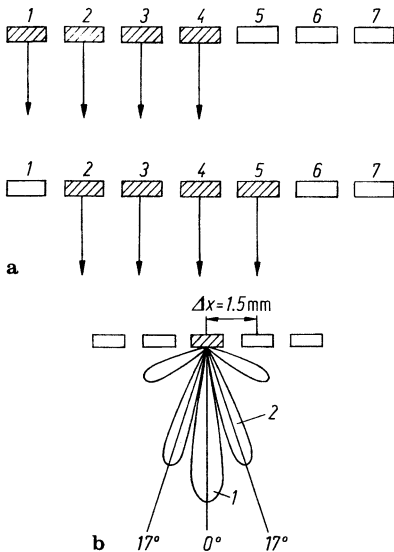
Fig. 10.36. Crystal array for linear scanning. **a** Schematic; **b** sound field calculated with the main lobe (*1*) and side lobes (*2*) for 3.5 MHz in water

with a systematically changed phase shift from one to the next. By this means an oblique beam is generated running at an angle which depends on the amount of the phase shift. The near-field length, viz the distance of best sensitivity, can also be varied and the annoying side lobes of the beam can also be suppressed if the width of the elements is increased towards each end. This can also be achieved by varying the excitation signal amplitudes in the same way as with the Gauss probe (Section 4.8).

Also, when this probe is a receiver it operates as a variable-angle probe. At small angles it radiates longitudinal waves, but at larger angles in solid material mode changes will take place with the production of transverse waves.

Phased arrays can be built for contact testing as well as for immersion techniques. The number of separate crystals can be between about 10 (for coarse swivelling) and several hundred (for medical applications). For materials testing (for example on welds) from 24 to 50 have been used.

For their manufacture individual strips of equal polarity are cemented to a non-conductive damping block, or a long single crystal can be cemented to the block and then cut into individual strips. Electrical contact wires have then to be soldered separately to each element. The overall dimensions can be up to 75 mm in length with a width of 10 to 20 mm. See also [S 110].

Such arrays are already made commercially, apparently because of wide application in other fields, and also electric delay lines (tapped delay lines) for phase shifting are available commercially. If focussing is required, as well as sector scanning, two delay lines are needed in addition to microprocessors [1096] and digital/analog converters, all being available in current standard production.

The electrical circuits for switching and phasing can be built into the crystal housing but in spite of using micro-electronics such a complete scanning device for

materials testing may reach weights of several hundred kilograms. They have found applications in nuclear reactor testing (see Section 13.12 and [1111]).

10.4.2 Single-Crystal Angle Probes

To generate obliquely incident waves in solid materials use is made of the refraction of incident longitudinal waves, with or without mode changing, to transverse waves (Sections 2.3 and 2.4). The effectiveness of this process, as measured by the amplitude of an echo, is shown as echo transmittance in Fig. 2.14. (See also Tables 5 to 8 in the Appendix). For example in the refraction from water into steel every angle in steel can be achieved with incident angles in water between zero and 27°. Between zero incidence and 14.5° we obtain a strong longitudinal wave in the steel, and beyond that, by mode changing, we have a strong transverse wave. The continuous variation of the incidence angle can be carried out easily by moving a longitudinal probe in a water bath but for practical requirements this method is not very useful. Other methods for continuously varying the angle will be described below but for most practical applications probes having fixed crystals for several pre-selected transverse wave angles are in use. They consist of a wedge-shaped intermediate block onto which the crystal is pressed or cemented (Fig. 10.37). Sometimes standard normal probes are used fitted with an exchangeable wedge which defines the angle in the specimen (Fig. 10.38). The replaceable wedge can be changed after wear. When changing the wedge sufficient coupling material (grease or oil) has to be applied, because lack of it will distort the sound field.

If the complete probe is mounted within a housing (Fig. 10.37) the worn contact surface can be reground or replaced after use. The housing can also exhibit a mark indicating the sound exit position (or probe index) on the side wall and from this the axis of the beam has to be calculated for flaw locating.

The angle of sound in the material of the specimen can go up to 90° only if the refraction angle in the material is larger than the angle of incidence, i.e. if the lon-
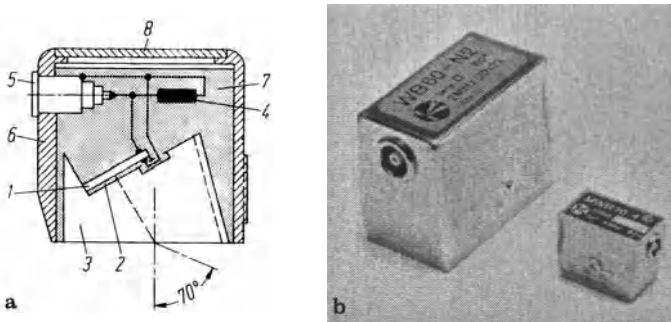
Fig. 10.37. Angle probes (design Krautkrämer). **a** cross-section, schematic, *1* oscillator, *2* coupling layer, *3* wedge of plastic, *4* electrical matching, *5* contact, *6* housing, *7* absorbing material, *8* cover; **b** two different examples
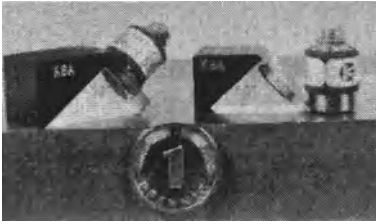
Fig. 10.38. Angle probes with exchangeable wedge (design Krautkrämer-Branson)

Table 10.1. Angle of the transverse wave in come materials corresponding to standard angle probes for steel

Angle in steel	35°	45°	60°	70°	80°
Angle of transverse wave in					
Aluminum	33	42.4	55.5	63.4	69.6
Copper	23.6	29.7	37.3	41	43.4
Grey iron (average value of lamellar iron)	23	28	35	39	41

gitudinal sound velocity in the wedge is smaller than the transverse velocity in the specimen. For steel with $c_t = 3150$ m/s therefore plastics can be used, especially Perspex with $c_l = 2730$ m/s or if a still lower absorption is of importance polystyrene with $c_l = 2350$ m/s.

In certain materials, for example copper ($c_t = 2260$ m/s) or grey cast iron (2200 m/s) the range of angles which can be reached when using Perspex is less than 90°. According to [1228] certain types of Nylon are suitable as alternatives (c_l between 1680 and 2600 m/s) and also Teflon (1350 m/s).

As a first approximation the necessary angle of the plastic wedge can be calculated from Eq. (2.3) using the two velocities. However, as shown in Fig. 4.29 the restricted beam width, rather than a large plane incident wave, is the reason that the calculated value has to be corrected depending on the D/λ value [1654]. The actual angle required is always larger than that calculated. Angle probes having nominal angles for steel are commercially available and when using them on other materials the variation of the angle according to Table 10.1 has to be kept in mind. With 35° probes used on copper and grey iron a longitudinal wave is still present in addition to the transverse wave at angles of 57° and 55° respectively. On these materials it is therefore recommended only to use probes of higher nominal angle.

Figure 10.39 shows the simplified sound field (Sonogram) for several commercial angle probes (cf. Fig. 10.32 for vertical probes). The beam cross sections are not circularly symmetric and in the direction perpendicular to the drawing plane the diameter is usually reduced by about one third, because in this plane no refraction takes place at the surface.

At this point further problems relating to angle probe construction can be mentioned. At the contact face with the specimen a part of the energy is always reflected effectively lowering the echo transmittance as shown in Diagrams 5 to 8 in

Sonogram

Dimension of the oscillator	$20 \times 22\,(mm^2)$	$8 \times 9\,(mm^2)$	$20 \times 22\,(mm^2)$	$8 \times 9\,(mm^2)$
Frequency (MHz)	1	2	2	4
Material	Carbon steel	Carbon steel	Carbon steel	Carbon steel
Attenuation	4 dB/m	8 dB/m	8 dB/m	60 dB/m
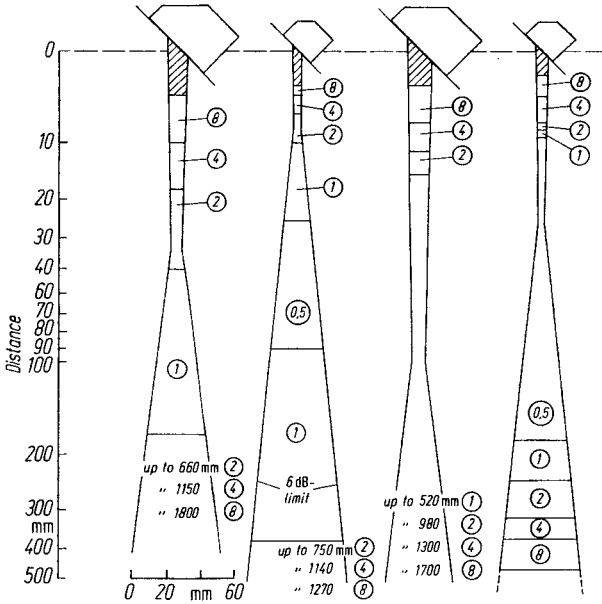
ⓘ smallest discernible size of equivalent defect, e.g. 1 mm diameter

▨ dead zone, where no testing is possible

Fig. 10.39. Sonograms for 45° angle probes

the Appendix. It would be optimal if the acoustic impedances on both sides of the contact face (for longitudinal waves in the wedge and for transverse waves in the material of the specimen) would be equal. For this reason the combination per-spex/aluminum is better than perspex/steel and for steel a wedge material such as lead is theoretically better. However, the unavoidable layer of coupling liquid de-stroys the advantage in practice. In addition the filling of plastic with heavy materi-als makes great difficulties for batch production of uniform quality.

Another problem arises from that part of the wave which is reflected at the con-tact surface back into the Perspex wedge. This is reflected back and forth within the wedge and then arrives back at the crystal. These reflections are responsible for the long dead zone and the principal means of avoiding them is by using a wedge mate-rial of relatively high absorption such as Perspex. In addition all free surfaces of the wedge should be covered by absorbing layers forming an acoustical sump, and these could consist of filled cast resins, or hard rubber blocks. Additionally these surfaces

can be shaped (as visible in Fig. 10.38) in the form of saw teeth or with boreholes filled with absorbing material. A full suppression is not possible, especially at high sensitivities, because there will always be some energy directly scattered from the contact area back to the crystal, especially on a specimen with rough surfaces.

This problem is especially difficult for angle probes generating longitudinal waves in steel, because the wedge angles for angles of 45° to 70° in steel are rather small, being only 19° to 27°. To improve the subsurface resolution the length of the wedge-shaped delay line can be made bigger so that the reflected part of the energy at the contact face cannot be received directly by the crystal. Also, such probes generate a certain additional amount of transverse waves at smaller refraction angles and their effect must be distinguished by the longer echo transit times as Fig. 10.40 shows.

To generate boundary waves such as Rayleigh and creeping waves the same designs of angle probe are used as above but the angle of the wedge is somewhat larger than the second critical angle.

In principle transverse waves can be introduced into solid materials by direct transverse-wave generating crystals, as for example transversely polarized piezo-ceramics or, with lower efficiency, by Y-cut quartz, but direct coupling with rather rigid materials is practical only for steady contact. For oblique radiation it is possible to construct a probe from such a transverse-wave generator cemented to a metal wedge. If the plane of polarization is parallel to the plane of incidence (SV wave), the wave can penetrate a very thin and uniform liquid coupling layer (see Fig. 2.16) in spite of the large acoustic impedance differences between liquid and metal. The practical range of angles is from 30° to 80° as with standard angle probes but steeper incidence angles can only be effected by rigid coupling. Transverse wave generators have also been used in crystal arrays [96].
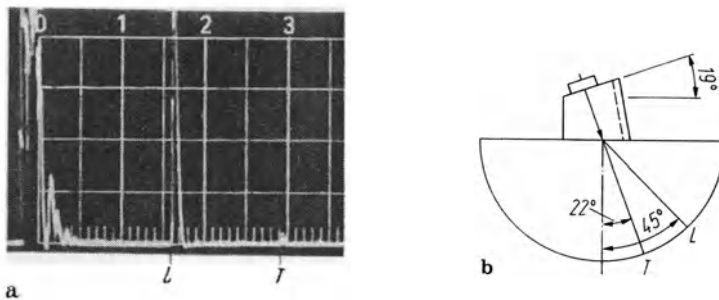
Fig. 10.40. Testing with oblique longitudinal waves at small angles. **a** Screen picture with the echoes from the test block, *L* longitudinal wave, *T* transverse wave; **b** probe with Perspex delay wedge on semi-circular test block of steel
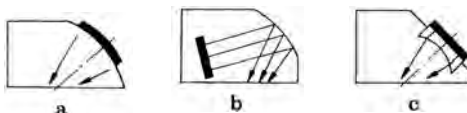
Fig. 10.41. Some designs of focussing angle probes according to [748]. **a** With spherically curved oscillator; **b** with a spherical mirror; **c** with spherical lens

Focussed angle probes have considerable importance for weld testing (Chapter 28) and Fig. 10.41 shows some designs.

For certain testing tasks it becomes desirable to vary continuously the angle of the transverse wave. Some possibilities are shown in Fig. 10.42. In the first illustration [1024] two wedges, one of which carries the crystal, are rotated relative to each other. The angle as well as the plane of incidence is changed. In the second solution, the piezo-crystal is cemented to a semi-cylindrical turntable in a hole in a plastic block, the point of incidence is varied together with the angle. In the third design the exit point remains almost constant as the angle changes. In Fig. 10.43 the complete block is mounted in an oil-filled housing and the exit angle can be read in a window.

The probe design according to Seiger et al [1395] (Fig. 10.44) is an improvement on the principle of Fig. 10.42 b. The angle of the beam, as well as the plane of
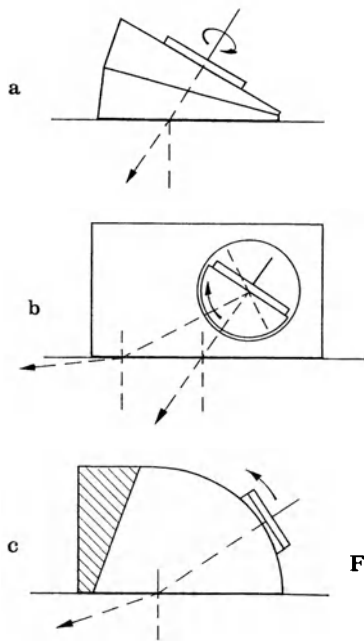
Fig. 10.42. Angle probes with continously variable angle
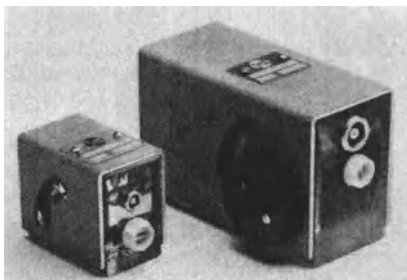
Fig. 10.43. Angle probes with variable angle (design Krautkrämer)
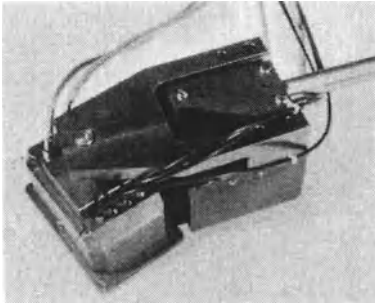
Fig. 10.44. Angle probe with remote control of the angle, the plane of incidence and the size of the oscillator

incidence, can be adjusted by remote control. The crystal is also divided into several individual portions which allows the use of various different crystal sizes, and the corresponding near-field lengths. These can be selected by individual switching of the single sections.

The first operational phased-array, but with only a few crystals and mechanically switched phase delay lines, was built by Bradfield in 1954 [173]. According to [1194] a phased-array has been made in the construction as indicated in Fig. 10.41a. The curved crystal has been replaced by a number of separate ones so that with appropriate phase-shifting the focussing effect of the curved surface can be simulated and even varied geometrically.

Figure 10.45 shows an angle probe which uses a phased-array with ten elements and corresponding delay lines, which are switchable to three different selected angles, according to Kising [1702].

To enable every direction in space to be used, even outside the plane of incidence, one can use a number of the phased arrays described above with even more complicated phase-shifting programs. This usually involves a very large investment but this can be reduced by using a phased-array in the form of a circle, cf. [S 151].

For continuous scanning using a swivelling beam, devices constructed like Fig. 10.42b have been used, with a motor-driven cylinder, while others have used a fixed oscillator and a moveable reflector built into a liquid-filled cell.
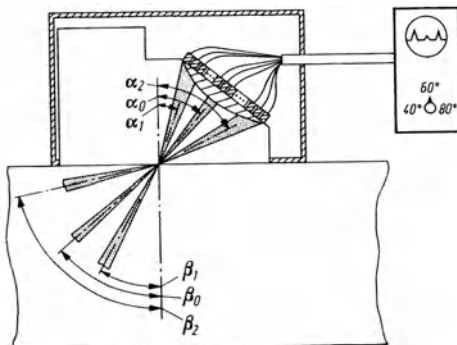
Fig. 10.45. Switchable phased-array angle probe, for three selected angles

Modern computer-aided phased arrays (Section 10.4.1) operate without mechanical movements, but at a far greater cost. The sound beam produced has many possible variations with, for example, perpendicularly incident longitudinal waves, or beams at oblique incidence with longitudinal and transverse waves, individually or combined.

For more information about phased-array angle probes and related literature see Section 13.12.

10.4.3 Transmitter Receiver (TR) Probes

When using single-crystal normal-beam probes the subsurface resolution is often not satisfactory because of the dead-zone which follows the transmitter pulse. Even when using for example a Perspex delay line which replaces the large transmitter pulse by a smaller surface echo, this can also mask a limited subsurface range.

To improve this situation twin-crystal probes are used in the so-called transmitter receiver or TR probes (Fig. 10.46).

The crystals, usually of semi-circular or rectangular shape, are cemented to a delay line and are very carefully shielded from each other, both electrically and acoustically. They are mounted in a common housing with two separate connectors and linked to the flaw detector by twin cables. For the use of these probes the flaw detector must have the means of separating the transmitter from the amplifier with a minimum of cross coupling.

The V-shaped track of the pulse in the specimen in Fig. 10.46 is longer than the double thickness. This "error of detour" has to be compensated when measuring thicknesses (cf. Section 11.2.2).
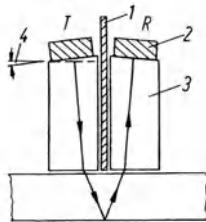
Fig. 10.46. Principle of a TR probe and path of the sound. *1* separating layer, *2* oscillator, *3* delay line, *4* "roof angle"
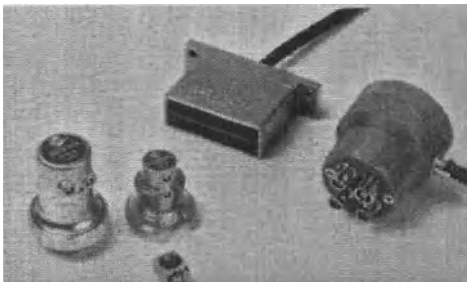
Fig. 10.47. TR probes (design Krautkrämer), left: for manual testing, right: two designs for broad-beam automatic plate testing
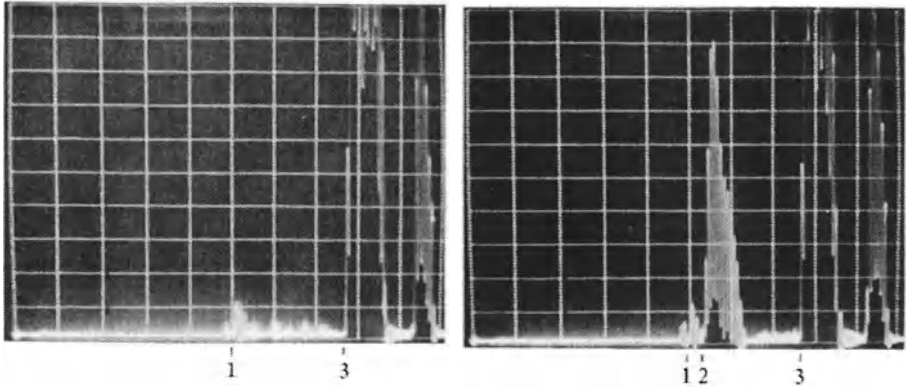
Fig. 10.48. Subsurface-defect indication using a 10-MHz TR probe, left: without defect, right: with defect indication. *1* surface or cross-coupling echo   *2* defect echo (flat bottom hole 0.4 mm in diameter at a depth of 1.2 mm)   *3* back echo of a 6.3-mm titanium plate
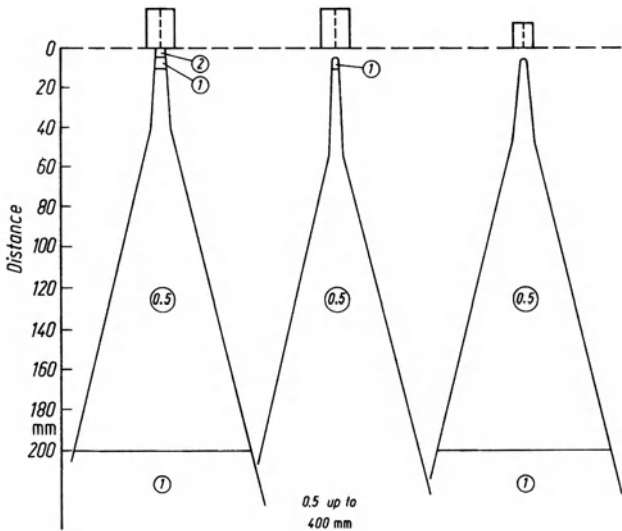
Fig. 10.49. Sonograms of some TR probes

Figure 10.47 illustrates some typical designs. The separating layer between the halves must have very high attenuation for ultrasound and is usually made therefore of a porous material such as cork or foamed plastic. In addition in the neighbourhood of the crystals it must be fitted with electrical screening to prevent electric cross coupling. In an ideal design sound can only reach the receiver by way of the specimen but in practice a residual cross coupling cannot be completely avoided because some energy will find its way directly across the contact surface. The practical quality of a TR probe depends on the extent of this cross-coupling surface echo, a good value being in the range 40 to 60 dB below the back echo from a thin plate (see Fig. 10.48). Figure 10.49 shows more examples of sonograms from typical TR probes, as in Figs. 10.32 and 10.39.

Some applications have also been found for TR angle probes, because the dead-zone of standard types is often far too long. The TR principle has a big advantage for longitudinal wave angle probes (Section 10.4.2) and the use of creeping-wave techniques is only possible with TR probes.

Vertical TR probes are much used for wall-thickness measurement, especially for those cases with a corroded rear surface. They can be used to detect pitting in tubes which would be impossible to find with a standard single-crystal probe. As an example of the resolution obtainable, a flat bottom hole of 0.4 mm diameter can be indicated at a depth of 1.2 mm below a smooth surface, by using a 10-MHz TR probe.

The performance of a TR probe is greatly affected by the "roof angle" which has an important influence on the distance of maximum sensitivity, or the focus distance, as can be seen from the sonogram diagrams. Angles up to 12° can be used but larger angles greatly increase the cross-coupling surface echo.

The electrical matching of TR probes differs in principle from that of single-crystal probes, because it is no longer necessary to compromise between matching a single crystal as both transmitter and receiver. In a TR probe each crystal can be matched separately and even different types of piezo-electric materials can be used to obtain an optimum performance.

10.4.4 Transducers for use at high temperatures and for Special Applications

Standard probes can be used between −20 °C and +60 °C without problems, and even higher temperatures won't damage probes if they are used only intermittently and with intermediate water cooling. For prolonged periods of testing at elevated temperatures special materials can be used for manufacturing probes including the crystal, cements, adhesives and the backing/damping block.
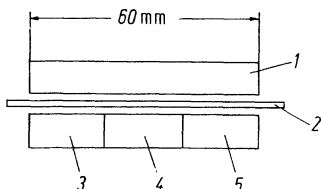
Fig. 10.50. Broad-beam TR probe. *1* transmitter, *2* separating layer, *3, 4* and *5* receiver crystals

Among the piezo-ceramics lead meta-niobate is suited for use up to 300 °C and lithium niobate up to 1000 °C. For backing blocks sintered metals have been proposed in [541] and it is possible to adjust both the acoustic impedance and the velocity of these materials as necessary. In addition to high temperature resistance the thermal expansion must also closely match that of the ceramic oscillator.

Materials for use as delay lines can be either a heat-resistant polyamide (up to 400 °C) or sintered metal (800 °C), or quartz glass (1200 °C) and it is sometimes sufficient to make only the delay line from a heat resistant material and to cool the remainder of the probe by circulating water or air. For wall-thickness measurements TR probes using quartz glass delay lines have been used, which can operate on surfaces up to 600 °C for periods up to 5 s, after which they can be cooled in water.

Crystal cements for use up to 250 °C are commercially available, and there are also types for use at even higher temperatures, but here the quality of the cementing is rather bad since the thickness gets too large and has high attenuation. An alternative way of making contact at high temperature is to press oscillator, delay line and damping block together with screws and springs and by using a high boiling-point liquid for all the couplings. In [939] are described special probes for continuous testing up to 300 °C.

For inspection of nuclear reactors it is necessary to have probes resistant to radiation and usually also to high temperatures. Special suitable materials for cements, oscillators, cables and casting resins are currently available (see Chapter 30).

For testing plates and billets broad beam TR probes as illustrated in Fig. 10.47 are in use. As shown in Fig. 10.50 they contain one large transmitter crystal and three separated receiver crystals. For details of applications see Part D.

In [1652] a special TR longitudinal-wave/angle probe for the generation of creeping waves is described.

Finally a useful multi-purpose probe can be mentioned. If a standard vertical probe is mounted inside a liquid-filled rubber tire (Fig. 15.13), it is possible to roll the tire along surfaces for continuous inspection and/or to swivel the beam through the contact area using longitudinal waves or transverse waves produced by mode changing [684].

10.5 Characteristics of Pulse-Echo Flaw Detectors and Probes

The characteristics and properties of a system consisting of a flaw detector and a probe, as defined below, can only be assessed in accordance with particular applications and therefore we will restrict this treatment to the question of definitions and the different methods used for checking the various physical properties concerned.

10.5.1 General Specifications

1. Ambient Conditions

A testing device must remain fully operational even when subjected to adverse ambient conditions.

According to DIN (German standards) one has to distinguish between "conditions for storage and transport" and "conditions for use". Under the first it is necessary that the device will not suffer any damage when not in use. Under the latter conditions it must be guaranteed that all equipment functions operate in accordance with performance specifications.

The most important ambient conditions which must be taken into account are:

— Range of temperature;
— Humidity of the air and dew point;
— Mechanical stresses produced by shocks and vibrations;
— Stability of the mains voltage;
— Electromagnetic interference fields;
— Rain, sprayed water, dust and dirt;
— Ambient light intensity and its effect on the legibility of the screen picture and/or any digital display

2. Operation, Reliability of Inspection

Another important group of specifications and associated characteristics refer to the practical operation and its relationship to the reliability of the results obtained. These are:

— The time necessary for training an operator;
— Fail-safe properties;
— Reproducibility of the results of any test;
— Brightness of the screen, sharpness of focussing, the size of the screen picture and/or of digital displays;
— Design, lay-out and number of controls;
— Calculating aids for sound beam calibration; for example direct adjustment of the screen display in absolute units of path length by internal calculations of the sweep calibration, based on the velocity of sound and the angle of the beam;
— Simplicity of adjustments;
— Numerical indications of distances, wall thicknesses, position and length of gates, and gain of the amplifier;
— Simple and reproducible data input;
— Documentation of the testing data and of the results;
— Simple means of checking operational functions;
— Potential for connection to auxiliary units, such as computers;
— Use without connection to the mains: time of function using a battery source of power;
— Weight and physical dimensions.

To these general specifications must be added the safety requirements of the VDE (Verein Deutscher Elektrotechniker) and the requirements for possible interference with communications by the German Post Office.

10.5.2 Technical Characteristics of the Flaw Detector for its Applications

There are many different specifications covering the accuracy required of flaw detectors for specific applications and a general survey would not be possible. On the other hand equipment manufacturers usually guarantee data only for individual groups of functions.

In the following discussion we will establish the most important requirements for most applications and their relationship to the functional properties of the units.

Properties specific to each application can be divided into four main groups.

1. The precision of echo-amplitude evaluation and how accurately the size of an equivalent reflector can be equated with that of an unknown reflector. The accuracy of echo-amplitude measurement depends on the precision of the calibrated gain control, the vertical linearity and the stability of the transmitter voltage.

The frequency band of the transmitter pulse and the amplifier also influence the precision of signal amplitude evaluation, and for good measurement reproducibility the basic properties of the probe, viz. oscillator diameter, centre frequency of the pulse and its damping are important.

2. The precision of distance measurement. This property depends on the linearity of the time base, the stability of the pulse relative to the sweep, the width of the screen and the precision possible in reading the screen picture. For devices with numerical indications the accuracy is affected by transit time errors, stability of the gate threshold and the precision of the counting frequency.

Distance measurement also depends on the properties of probes, principally the sound field, the damping and (for angle probes) the position of the beam index and the error of the beam angle. For TR probes the "error of detour" (see Section 11.2.2) has its influence on the precision of wall-thickness measurements.

3. The sensitivity, which can be expressed in terms of the smallest reflector just detectable in a given material at a given distance. This property is determined by the transmitter energy, the limiting sensitivity of the amplifier (viz. noise level and band width) the shape of the sound field of the probe, its damping and the coupling losses.

4. The depth resolution, as expressed in terms of the smallest distance from the surface at which a reflector of a given size can be recognized, or what minimum wall thickness can be measured. This property depends very much on the quality of the probe, and in particular its frequency, its damping and the suppression of reverberation and secondary resonance. In addition the rise time of the transmitter pulse, as well as the amplifier characteristics are important. These include the amplitude and phase as functions of the frequency, the video bandwidth of the rectifier, and the quality of the frequency cutoff. Manufacturers rarely give definitions of these latter properties because of the different requirements a unit must have, according to very different applications. A general difficulty in doing so lies in the fact that precise data can be fixed only for a complete system of flaw detector, probe and test object. Further information on basic probe resolution is given by the

so-called corrogram diagram established for individual probe types by the Kraut-krämer company, see Fig. 10.65.

10.5.3 Checking the Instrument Properties

With the increasing applications of ultrasonic materials testing many official and unofficial specifications have been established concerning specific products (Chapter 34). They always contain certain demands on the performance of flaw detectors but often there are no exact definitions nor generally accepted methods of measuring them. In the meantime this problem has been dealt with by official institutions in different countries. Here we will mention a proposal of the German Society for NDT, see [1711, 1083, 1079], and DIN 54124.

This standard enables the establishment of manufacturing data for general equipment comparability and also for regular checks of units in use. The latter task must be carried out by every operator, without much special training, and so some of the basic properties have to be checked in a simple way for consistency. On the other hand there have to be exact definitions, and methods to measure them on a scientific basis, but this is not possible for all properties. Consequently a class A for elementary checks, and a class B for exact definitions and objective measuring methods, have been proposed. There were already existing check methods using the test blocks 1 and 2 (DIN 54120 and 54122), see Figs. 10.51 and 10.52 and [1079], which have been used for the class A checks.

Difficulties appeared very early when an attempt was made to separately define the properties of a flaw detector and of a probe because the one always influences the other. In addition in different designs the separation of the two elements is not always possible since tuning and matching elements can be housed either within
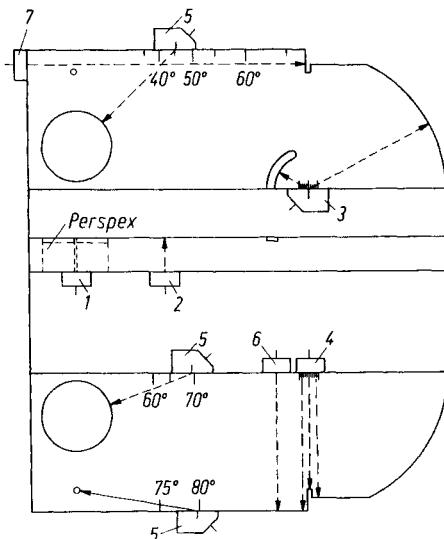
Fig. 10.51. Test block 1 for calibrating the time base (depth scale) of a flaw detector for vertical probes (longitudinal waves) for angle probes (transverse waves), for determining the probe index and beam angle of angle probes, and for checking the short-term consistency of the sensitivity of vertical probes
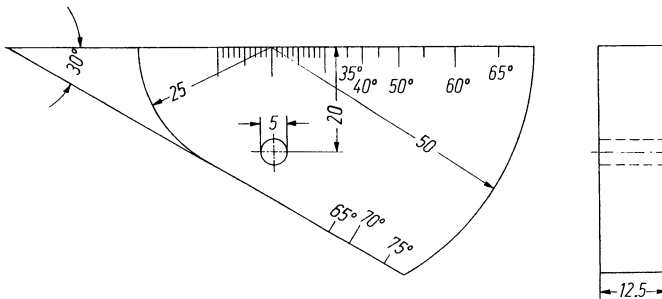
Fig. 10.52. Test block 2 for checking miniature angle probes

the flaw detector or within the probe. At higher frequencies even the probe connecting cable plays a role. For this reason only the properties of the whole system have been systematically defined even when measuring probe data and when the influence of the driving unit is very small.

The whole system can be conveniently divided into the display unit, including the power pack and oscilloscope; the amplifier; and the transducer with its sound field.

10.5.3.1 Properties of the Display Unit

This section can be placed in class A and and is tested mostly by simple methods including the following properties: linearity of the time base; mains-supply variations and behaviour during warming up after switching on; legibility of the screen picture with ambient illumination and at a selected pulse repetition frequency. For all these properties numerical values can be assessed. The legibility of the screen picture is for example measured by the background illumination, in Lux, at which an echo pattern can no longer be recognized by the operator from a certain viewing distance. Some older units score only some hundred Lux in this test but more modern score some thousand Lux and this indicates that the modern designs have been made with a view to be used on site in the open air.

10.5.3.2 Properties of the Amplifier

Here we are concerned with the overall sensitivity, the echo resolution and the amplifier-system's characteristics.

As a very simple method of checking the stability of the sensitivity the number of multiple echoes received from a plastic block was used very early and this plastic block was incorporated into test block 1 (Fig. 10.51, position 1). The method fails at low and high frequencies, and it is also not possible to use it to compare different types of probe. A probe with a soft coupling layer is at an advantage when com-

pared to one with a hard contact surface. Nevertheless the test remains in class A but only for a check of stability of performance.

In class B another test has been established to measure sensitivity by using the *gain reserve*. With this system the maximum obtainable echo is produced, either from the rear echo of a flat plate, or on the test block 1 (Fig. 10.51, position 2) for vertical probes, or for angle probes the echo from the quadrant block (position 3), which approximately equals the maximum echo in this case. For smaller angle probes with a shorter near-field length the test block 2 (Fig. 10.52) has been developed.

The maximum echo is then reduced by using the calibrated gain control until a standard reference height is obtained (about 50 % of full screen height). There is now a degree of amplification in hand up to the maximum possible setting, and this, measured in dB, is the gain reserve. However the noise level of the equipment has also to be considered, since it will also affect the reading of an echo amplitude. It is specified that the noise level (or "grass") must not be more than 50 % of the reference height, when measuring the gain reserve since above this level further amplification would then be useless.

For these measurements a built-in calibrated gain control is necessary but in some simpler and older instruments this is not provided. So a special test unit must then be used, the so-called *test pulse generator*. This will feed into the system an artificial echo pulse of any selected frequency, position and amplitude, thus allowing an indication fo the maximum gain of the unit and therefore also the gain reserve.

Amplifier characteristics are shown in Fig. 10.53 having three different shapes. Type *a* is the ideal linear curve, with saturation only at a high input voltage. Type *b* shows a curved threshold, which suppresses small indications, and type *c* is of the logarithmic type. The saturation point, as well as the threshold, can be identified in class A from a sequence of multiple back echoes, but only qualitatively. For class B the deviations from the ideal curve *a* are measured as the "upper and lower deviation of proportionality" Δ_l and Δ_u (Fig. 10.54). A test echo is adjusted to be at half-scale height for which the amplifier control is set at 0 dB. The measurement is then carried out at -14 dB (10 %) and $+6$ dB (100 %) of the input voltage.

The formerly used characteristic of *dynamic range* was intended to indicate what was the smallest echo just discernible on the base line, when a large echo still showed some variation in its height when the input voltage was increased by 10 %.
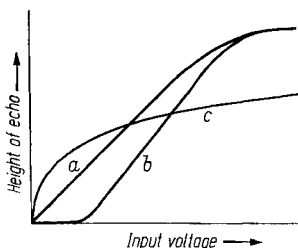
Fig. 10.53. Amplifier characteristic showing echo amplitude above input voltage. a linear amplification; b with threshold; c logarithmic amplification
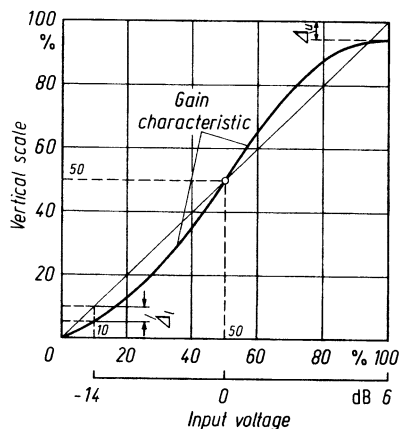
Fig. 10.54. Upper and lower deviations of proportionality, Δ_u und Δ_l

This condition means that the amplifier must not yet be fully saturated but in practice such observations give very subjective values, especially if the base line is not free of noise. A measurement at 10% of the height of the scale is preferable.

A comparison with the maximum echo of a system, as is usual when using the DGS diagram, is allowed only if the amplifier has not yet reached saturation. Therefore as a further important property the *input overloading* is measured.

For use of the DGS diagram, as well as for measuring the attenuation of a material, the *working frequency* of the system has to be known, (viz. the centre frequency contained in the echo), and this can be measured with a calibrated time base displaying the echo in its high-frequency form. At the same time any significant strong pulse distortion can be recognized so that probes with such distortion can be excluded from making quantitative evaluations.

To estimate the "resolution" for class A the base width of an echo is measured and indicated in terms of mm steel. A go/no-go test is possible using test block 1 with a vertical probe placed in position *1*. The three individual echoes must be clearly separated on the screen (Fig. 10.51 [1079]).

In class B the resolution is evaluated quantitatively for all types of probe and one has to distinguish between the resolution following the transmitter pulse and following another echo. The first case refers to the possibility of detecting subsurface reflectors and the second to the possibility of distinguishing two reflectors situated close together.

Figure 10.55 shows the set-up using a generator unit which feeds a test pulse into the system. The test pulse can be shifted from right to left so that it approaches either the transmitter pulse or any other echo. It will be observed that as it approaches up to a certain distance its amplitude will start to change. The reason for this is the interference with small oscillations which follow the larger transmitter or echo pulses, but which are not yet visible on the screen in consequence of the rectifier threshold. Within the high frequency range of the amplifier however they can interfere with the test pulse and hence they create a "dead-zone" in which quantitative evaluation of an echo is impossible. To assess the extent of this so-called *pulse-*
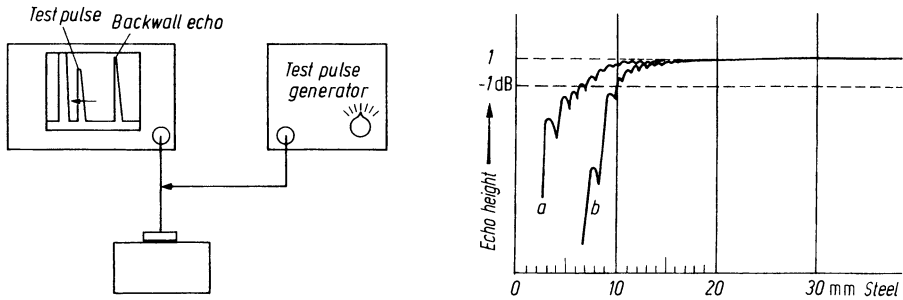
Fig. 10.55. Determination of the resolutions by using a test-pulse generator

Fig. 10.56. Appearance of a 4-MHz test pulse when approaching the transmitter echo at two different amplifier gains. **a** gain adjusted so that the maximum echo of the system reached on a plate equals the reference height (standard gain); **b** at $10\times$ higher gain ($+20$ dB)

influence zone the test pulse is allowed to approach the larger echo up to that point where it decreases by more than 1 dB for the first time (Fig. 10.56). This range applies to both the transmitter pulse or another echo and defines the distance in which a reflector echo cannot be properly evaluated because of the influence of the foregoing pulse. As the test pulse approaches, a position is reached where the two echoes cannot be separated. This is where the saddle between the two echoes is higher than 50 % of the test pulse and the distance measured from the beginning of the first echo is called the *resolution distance* or the *dead zone*. The pulse influence zone ia usually several times the length of the dead zone.

10.5.3.3 Properties of the Sound Field and Probe Data

In this section the probe data and the methods used for their measurement will be defined. As always we assume that the probe concerned is connected to a suitable flaw detector. When changing from one equipment to another the test frequency, according to DIN 54119 [1714], the pulse shape and the sensitivity can change. For this reason the ESI standards [1720 to 1722], require that the manufacturer specifies which flaw detectors and connecting cables are allowed.

For the determination of probe data we can use simple methods applicable by an operator on site (class A) and more fundamental ones which can only be carried out in a well equipped laboratory (class B). The class A tests are specified in the DIN standard 54124 [1717], and the quantities to be measured are widths of transmitter pulse, back echo, entrance echo (for immersion techniques), echo-influence zones, dead zones, cross coupling, noise level and probe index, beam angle and squint angle of angle probes. In addition to the test blocks 1 and 2, a further set of blocks is required for TR probes and the measurement of focal distances.

It should be mentioned, that the values measured by these test blocks do not always correspond accurately to those encountered in practical testing, but they serve approximately to compare the quality of different probes. Wüstenberg [1644] has
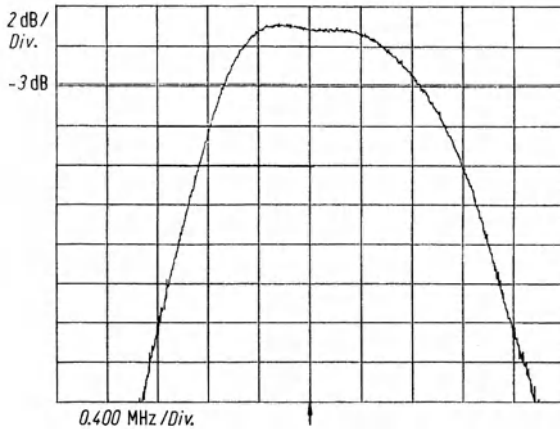
Fig. 10.57. Frequency spectrum of a 4-MHz angle probe (design Krautkrämer)

shown that there can be systematic differences between beam angles measured with the test block and by using the electrodynamic receiver (see Section 8.4 and [1646]). Additionally the width of the standard test blocks sometimes seems to be insufficient when rather broad beams are used.

Additional probe data such as the working frequency, electrical bandwidth and the structure of the sound field in longitudinal or transverse directions, can be measured only with tests under laboratory conditions. The working frequency is the center frequency of the echo pulse at the amplifier input and for its measurement the echo must be gated out and fed to a frequency analyser. A typical result is illustrated in Fig. 10.57, showing the band of frequencies contained in a particular pulse. The lower and upper frequency limits at 3 dB below the peak amplitude are measured and the average value is the working frequency required.

The band width of the probe can be determined from the same test but for these measurements the test block must have no appreciable attentuation in the frequency range concerned.

For immersion testing the probe data are evaluated under water, the sound pressure being measured with a miniature microphone (Fig. 10.58) or as an echo from a small reflector.

Figure 4.18 shows a plot of the sound pressure distribution in front of a 2-MHz probe measured with such a hydrophon. As an alternative a spherical reflector can be used and in this case the result will be the echo field in contrast to the free-field, but a direct observation of the sound pressure immediately in front of the probe is not possible because of the dead zone.
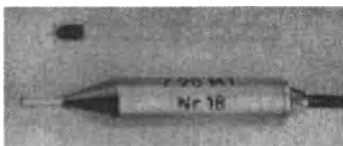
Fig. 10.58. Hydrophon with high spatial resolution and small disturbing effect on the field (sensitive area 1 mm in diameter, frequency range up to 10 MHz)
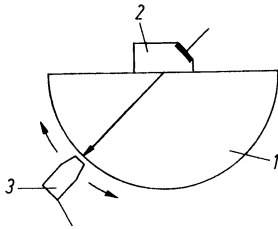
Fig. 10.59. Arrangement to measure the beam angle and the directivity of an angle probe. *1* test block of semi-cylindrical shape made from steel, *2* angle probe, *3* electrodynamic receiver

A qualitative picture of the sound field is produced using the schlieren optical method and the photo-eleastic effect (Chapters 8 and 13).

For contact probes a section through the beam in a solid test block can be measured by scanning the backwall using a small receiver (free-field), or for the echo field by using a block containing a small reflector (for example a flat-bottom hole) by shifting the probe. In the first case an electrodynamic probe is preferably used as receiver because it introduces no coupling difficulties (Section 8.4 and the DGZfP specification [1711].

For the same reason this type of probe is preferably used to measure the beam angle of an angle probe, as shown in Fig. 10.59, a typical result being shown in Fig. 10.60. From this trace one can evaluate the angle with a precision of 0.3°, which is much more precisely than with the test blocks 1 and 2. The directivity angle can also be obtained from this curve as the angle (Fig. 10.60) between the two positions on either side of the peak, where the amplitude has decreased by −3 dB. From this value it is possible to calculate the effective oscillator diameter $D_{T\,eff}$ and together with the measured test frequency of the probe its near-field length can be calculated.

This quantity is an important characteristic of all transducers except TR probes. It is usually measured by immersion techniques from observing the echo of a small spherical reflector (a steel ball or a hollow glass sphere). When the reflector is
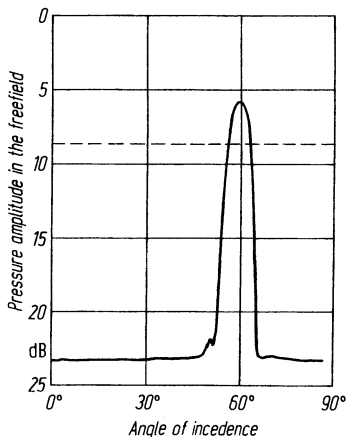
Fig. 10.60. Directivity of an angle probe measured as in Fig. 10.59 at a nominal angle of 60°

moved along the axis of the transducer the echo reaches the maximum value at or close to the end of the near-field. However, for a more exact estimate the absorption of water has also to be taken into account. At 20 °C it is given by:

$$\alpha = 0.22\, f^2\ \text{dB/m}$$

where f is the working frequency in MHz and both forward and return travel paths have to be corrected [491, 1350], see page 110.

At too high sound pressures the absorption of water is increased considerably by non-linear effects, so to avoid errors the method described above should be repeated at reduced pulse power and both results obtained must be equal.

A more precise method makes use of measuring the echo of a small spherical reflector in the transition zone between near- and far-field. Wüstenberg has calculated corrections to the echo height (Fig. 10.62) which change the height-distance echo curve into a straight line if plotted in log-log format (Fig. 10.61).The intersection of this line with the tangent to the peak gives a distance equal to $(\pi/2)\, N$ [1085, 1646].

The advantage of this method is that it can be used with short water paths and still obtain sufficient accuracy. If it is possible to use large distances in water, say up to 10 near-field lengths, the plate-echo method can also be used [49]. The echoes from a large plane reflector in water if plotted logarithmically give the straight line far-field but of course the values have first to be corrected for the absorption of water. The extrapolation of this line to intersect the zero-dB line also gives a distances of $(\pi/2)\, N$. This method can also be used to measure the near-zone of probes which are not round or square but long and narrow, and also for Gauss oscillators and other probes with non-uniform excitation.

If solid material has to be used for these measurements (as for example for vertical transverse wave probes) a set of test plates of different thicknesses or, with precautions, the sequence of multiple backwall echoes from one plate can be used [1083]. Here also the electrodynamic probe can best be used as a receiver on the backwall of solid test blocks to measure the sound fields. Values obtained at several distances, after correction for any absorption, show directly the near-field length in solids with an accuracy of about 5 %.

With angle probes a part of the near-field length lies within the plastic wedge and for measuring and correction methods see the specification [1711].
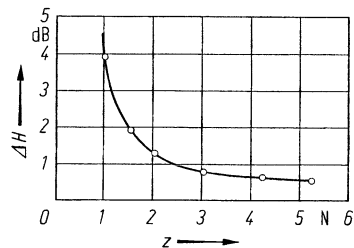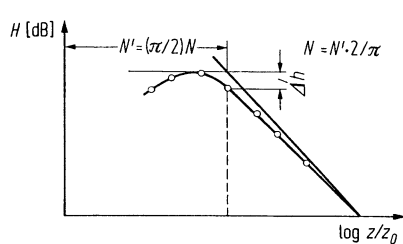
Fig. 10.61. Defining the near-field length from the straight line of the back-wall echo curve
Fig. 10.62. Correction of the echo height using the spherical reflector

TR probes cannot be investigated under water. To establish a DGS diagram as in Fig. 10.63, several test block sets have to be used with increasing thicknesses and with a range of flat-bottom holes as reflectors. The width of such test blocks has to be sufficiently large to avoid side-wall effects.

All this probe data can be listed in a data sheet supplied for each individual transducer when used with the specified connecting cable and flaw detector (Fig. 10.64).
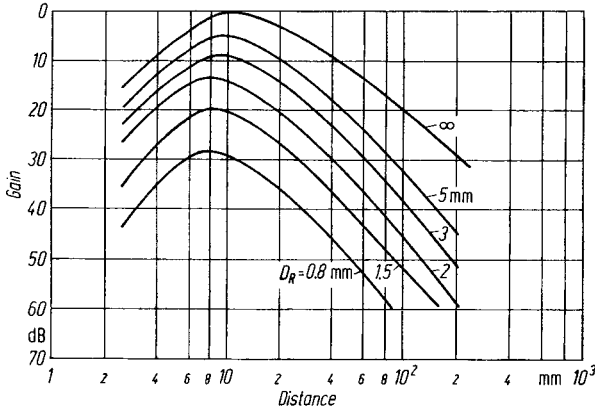
Fig. 10.63. DGS diagram of a TR transducer measured with flat bottom holes of diameter D_R

f_e	4.0 ± 0.4	MHz	P	100	N
N^*	30 ± 4.5	mm	T_a	$-20...+60$	°C
FB_6	1.6 ± 0.2	mm	T_{5s}	150	°C
FL_6	1.2 ± 0.04	mm	V_r	87 ± 6	dB
D_0	$8_{-0.1} \times 9_{-0.1}$	mm × mm	s_0	0	mm
D_{eff}	$7.7 \pm 0.2 \times 8.6 \pm 0.2$	mm × mm	s_{20}	5	mm
β	45 ± 1.5	Grad	s_{40}	17	mm
$\Delta\beta/\Delta T$	0.6 ± 0.1	Grad/10°C	t_0	0	mm
$l_{v(2730m/s)}$	6 ± 1	mm	t_{20}	3	mm
δ	0.8	Grad	t_{40}	12	mm
Z	1	mm	e_0	3	mm
Z_A	± 2	mm	e_{20}	5	mm
φ_6	3 ± 0.4	Grad	r_0	2	mm
ψ_6	2.3 ± 0.3	Grad	r_{20}	4	mm
M	0.5	mm/km	$s; t; e; r$: Tolerance 50%		
M_z	2	mm			

All values refer to steel

*including 5 ± 1 mm delay linie length (near field equivalent)

Fig. 10.64. Data sheet of a miniature angle probe (Krautkrämer)
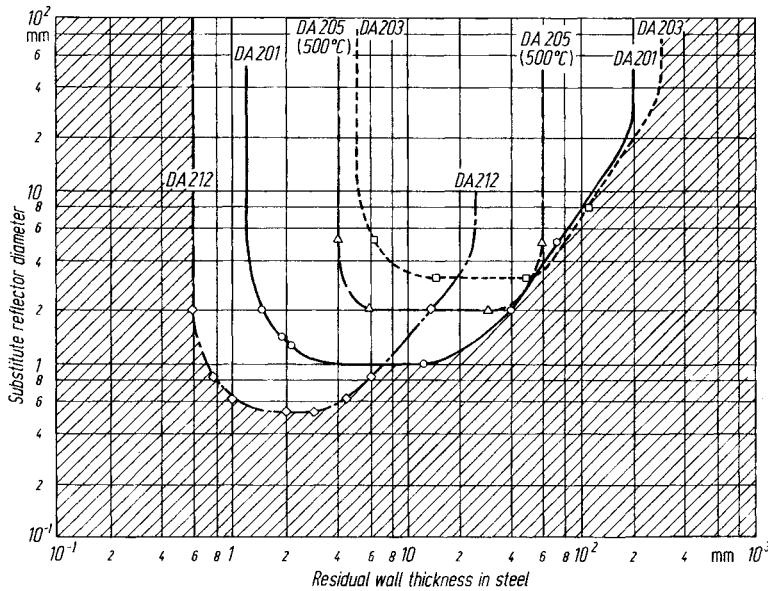
Fig. 10.65. Corrogram for several probes used with the wall-thickness meter DM2 (design Krautkrämer)

The German specifications (DIN [1717] and DGZfP [1711]) include no allowable limits for the data but only specify methods of measurement. In other countries there are often strict requirements laid down. For example the British ESI standards give acceptable limits for the frequency ($\pm 10\%$), the pulse width, the beam angle, the squint angle, the signal/noise ratio and the size of the beam side lobes. Japanese Standards JIS Z 3060 [1731] have also similar fixed limits.

For the problem of wall-thickness measurement, especially on corroded walls, Bosselaar and Goossens [166] have introduced a type of DGS diagram, called a corrogram (Fig. 10.65). It shows the allowable range of distance and equivalent reflector size for different transducers when used with a wall-thickness meter. It is very useful in the case of pitting corrosion and allows the comparison of different wall-thickness meters.

10.6 Instruments Made for the Pulse-Echo Method of Testing

The first commercial instruments have been manufactured in 1943, at about the same time, by Sperry Products Inc. Danbury, Conn. USA and Kelvin and Hughes Ltd, London, England.

Some units from different manufacturers of more recent development are shown in Part D. Thanks to progress in solid-state electronics they have undergone

considerable reductions in size and weight with a simultaneous improvement in their performance, especially in respect of sensitivity and resolving power.

The physical volume of the electronics is already very small by the use of many integrated circuits to that overall size and weight is effectively determined by the CR tube and the power pack (transformer and/or battery).

Miniature flaw detectors weigh about 5 kg with a volume of a shoe box, including batteries for about 12 hours' operation. Further reductions would be possible, but a screen about 70 mm wide is preferred for observation at a distance of 1 m. High trace brightness is also preferred and these requirements necessitate more weight and volume. Units exclusively developed for wall thickness measurement are essentially flaw detectors without a CR tube and can therefore be made much smaller, down to the size of a pocket camera for example.

Modern miniature flaw detectors already possess many special features, which were formerly to be found only in large units. These include for example a wide frequency band (1 to 10 MHz), a dB calibrated gain control, controllable threshold, distance-gain correction and several gating facilities for automatic screen observation. However, sensitivity, resolving power and test ranges may still be inferior. Battery recharging units are usually fitted allowing operation also directly from the mains. CR tubes usually have flat rectangular screens with built-in calibration screen and graticule. When fitted into special housings they can even be made explosion safe and suitable for use under water.

Larger flaw detectors are about 10 to 15 kg in weight and are the size of a small suitcase. They have larger and brighter CR tubes and can interchange various function modules complete with controls, especially those for different monitors and gating devices.

On site these larger units are less often used because the control functions are not quite so easy to manipulate and are preferably used in a laboratory or workshop, for scientific investigations and for simpler automatic testing installations. Battery operation is not often required and a full mains power pack is built in. They also usually have outputs for further data processing.

For automatic testing installations flaw-detector systems usually contain all their functions as plug-in modules. They can cope with complicated inspection functions by testing with several probes simultaneously and with several gating channels including digital data processing. They are then combined with additional rack-mounted units for specific purposes. The CR tube is used only for adjustments and occasional observation of the functions. Special units have been designed for much higher frequencies for high resolution of very small defects [S 178].

In more recent times microprocessors have not only been used in larger installations for automatic testing but also in miniature flaw detectors. Used together with high-capacity memories all functions can be programmed and the screen display digitalized, which allows very bright pictures, but with the disadvantage of a 256×64 pixel raster (see Fig.s 19.7 and 28.5).

Devices using exclusively the electromagnetic pulse-echo method are today no longer built in batches (see for example the Ferrotron, Fig. 25.7). These units need high powers for the generation by electric spark gap of high current pulses thus causing high weights and volumes.

Below are listed alphabetically some of the larger manufacturers of flaw-detector equipment:

Automation Industries, formerly Sperry Products, (USA)

Baugh and Weedon (Great Britain)

Karl Deutsch (Germany)

Gilardoni (Italy)

Krautkrämer-Branson (Germany, France, Great Britain, Italy, Japan and USA)

Mitsubishi (Japan)

Nortec (USA)

Panametrics (USA)

Sonatest (Great Britain)

Sonic Instruments (USA)

Tokyo Keiki (Japan)

Unipan (Poland)

10.7* The Frequency Modulation Method

This method provides echo amplitudes and transit times in a way similar to the pulse-echo system. For some other echo-sounding applications, for example the investigation of the ionosphere, it was used before the pulse-echo method though it is not so easy to understand. It was proposed for material testing by Sokolov in 1941, but is not being used today.

It works with continuous ultrasonic waves, the frequency being periodically increased linearly after which it falls back in the form of a saw tooth. After an interval the cycle starts again and Fig. 10.66 shows the frequency-time pattern. At zero time the frequency starts from f_0 and increases steadily up to f_1. The continuously oscillating probe must necessarily radiate the complete range of frequencies uniformly. An echo-wave from a defect or the back wall, returns after a transit time t and on arrival the head of the wave has still the frequency f_0 which subsequently increases up to f_1.

Example. $f_0 = 10\,\text{MHz}$, frequency increase 5 MHz, up to $f_1 = 15\,\text{MHz}$. Swept frequency rise time $T = 340\,\mu\text{s}$, which is equal to the return trip transit time for longitudinal waves in 1 m steel. Together with the saw tooth interval of 1660 µs we obtain a total time of the cycle of 2000 µs, or a repetition frequency of 500 Hz. Assuming that the leading edge of the echo wave from a reflector at a distance of 400 mm arrives with its frequency of 10 MHz, at the same time as the transmitter frequency has already increased by 40 % of 5 MHz (viz. 2 MHz). This
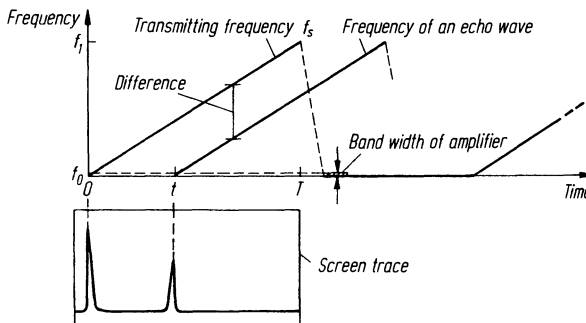
Fig. 10.66. Frequency-modulation method for the measurement of echo amplitude and pulse transit time

difference between the frequencies of the two waves remains constant. A reflector at a distance of 800 mm would for example provide a wave at a frequency 4 MHz below the transmitter wave.

In this method the probe functions as both transmitter and receiver. All signal voltages arrive at the amplifier input, which operates only over a narrow frequency band around the frequency f_0 or a higher one. Therefore at the time t_0 we will have a strong signal from the amplifier, corresponding to the transmitter frequency passing f_0 and a further signal will occur when the same frequency of the echo wave reaches the probe. The appearance of the screen picture is therefore the same as for the pulse echo method, provided the luminous point of the CR tube is swept horizontally at a rate proportional to the frequency sweep and vertically in proportion to the amplitude of the in coming wave.

Some practical disadvantages of the method have been eliminated by Erdman [393, 394] with a more complicated design.

10.8* Electronic Methods of Improving the Indications of a Pulse-Echo Flaw Detector

The "grass" or base noise in the screen picture, where echoes are difficult to recognize due to an inadequate signal to noise ratio, can have different causes and various methods can be used to improve it.

The electronic thermal noise originates in the amplifier and is not correlated with either the repetition or the ultrasonic frequency which means that it has a completely new form for each separate pulse. For this reason, it appears visually as a band by its time averaging. If the pulse power cannot be increased only the use of low-noise amplifiers can help further.

More troublesome in most cases is the noise arising from the grains in the materials under test caused by the multiple scattering at grain boundaries or by small inclusions. These echoes are correlated with the pulse frequency and will therefore stand still when the probe is stationary. When there are small variations in the probe position they will rapidly change their shape, height and position. When a record is made with probe scanning, real echoes can still be distinguished from this noise even when they are of similar amplitude. This dynamic effect is used to measure the depth of the case hardness of chilled grey-iron castings by using a probe which is moved locally [1515, 1689, 1217]. Other scanning methods also make use of this effect for example ALOK, and SAFT (see Chapter 13). Some of these such as the ALOK method use additional electronic pattern recognition systems to separate real echoes from interfering signals [136].

When checking austenitic stainless-steel welds, and for other very difficult crystal structures where strong interfering echoes appear, more complicated methods can help. They are based on the different frequency content of true defect echoes and the interfering ones from grain boundaries [874, 1108, 1361, 540]. The split-spectrum method [498, 1114, 846, S 142, S 158] is based on the fact that the scattered echoes, which arise from multiple reflections, are more changed in their

frequency spectrum than is a true echo. To obtain real-time response the received signals must be digitalized, transformed into a frequency display which is then split into several frequency bands and re-transformed into the time domain. The presentation of the signals from different frequency bands differs somewhat for true and scattered echoes, and these can be recognized by using correlation techniques programmed by an algorithm. An example called the *Minimization algorithm* has proved successful in dealing with problems of austenitic material inspection [151, S 16].

Other signal processing methods, for example by using the so-called Cepstrum operator [S 131, S 11], the separation of two closely adjacent echoes can be improved up to ten times better than when using the conventional method. This is of special importance for thickness measurement and the detection of subsurface defects (see also [S 172, S-33, S 136, S 35]).

Some other methods taken from radar practice have been used to improve distance resolution. A true shortening of the echo pulse would give a wider band width and thus make other difficulties with most materials because of the increased attenuation at high frequencies. However, these electronic techniques mentioned shorten transmitter and echo pulses for an analysis.

The transmitter pulse can also be modified to compensate in advance for those influences which will distort it in transit. If, for example, it will lose much of its higher frequency content by material attenuation, a higher level of these frequencies can be generated in the transmitter pulse *(CS or Controlled Signal technique)*. Other methods such as the *Weiner-filter* and the *Bark-code* [234, 233, 1434, S 34, 1090] require digitizing methods using mini- or microprocessors.

If digital methods are used it is reasonable to digitize the screen picture also, as in Fig. 19.7, which shows an envelope curve of stored echoes after scanning. However, the display of single echoes no longer allows the original frequency to be recognized in the HF display nor in the video display which may be a handicap.

The very rapid development of microprocessors has reduced their price so much that they are readily available in modern flaw detectors (Krautkrämer USD 1 and USD 10, Panametrics EPOCH).

11 Transit-Time Methods

In this Chapter all those methods will be discussed in which the only ultrasonic testing result used is transit time. Information about the amplitude of an echo, which was essential in Chapter 10, is not now considered since it can only be of interest if it should restrict the range of measurement. A variety of instruments have been developed which measure pulse-transit times to evaluate such quantities as wall thickness, residual wall thickness, sound velocity and physical strain with ever improving ease and precision.

At the same time we will include those methods, which are based on frequency measurement rather than on transit time, because the physical information is similar. A particular transit time corresponds to a wall thickness. It also corresponds to a thickness resonance for the specimen and from the resonant frequency the wall thickness can also be derived. The frequency methods were developed before the transit-time methods principally because of the frequency range needed by each. Resonance frequencies below 3 MHz can be used for measuring thicknesses from 1 mm steel upwards but for equivalent transit-time measurements much higher frequencies are necessary to give sufficient accuracy. As a consequence of modern digital circuitry, which is very suitable for these higher frequencies, the older resonance methods have been largely superceded and frequencies up to ten times higher can easily be used.

For more complicated wall-thickness problems see Section 33.1.

11.1 Time-Measuring Methods

The straightforward method to measure a wall thickness is by the direct measurement of a time interval between two markers. The first one, or the start, is usually given by the main transducer pulse or by an entrance echo; the second, or the stop, is given by the back-wall echo. The more precisely that these two markers can be produced the more precise will be the wall thickness measurement. If the two amplitudes are very different one can expect precise markers only from very short rise times at the front edge of the pulses, which means using high ultrasonic frequencies and broad-band amplifiers.

11.1.1 Interferometric Methods

One of the simplest methods of measuring a time interval is by comparing it with one already known. As illustrated in Fig. 11.1 a second probe can be connected in
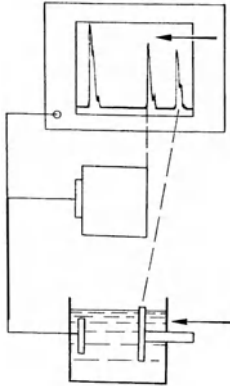
Fig. 11.1. Reference delay line in liquid with adjustable reflector

a   b   c   d
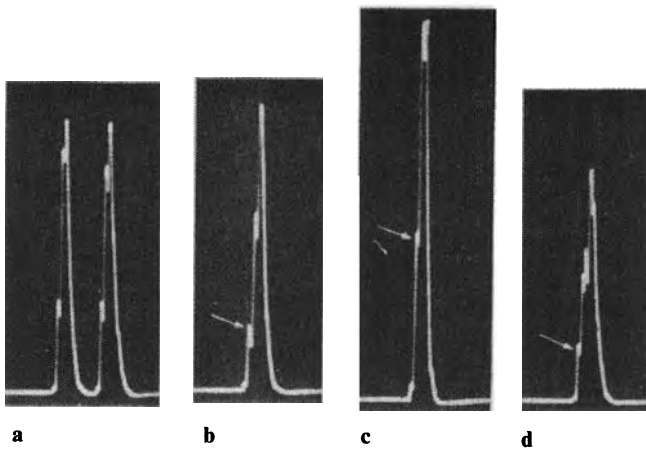
Fig. 11.2. Interferencer of two echoes in different phases. **a** both echoes widely separated, the right (echo of delay line) is being shifted to the left; **b** first minimum of the observed high-frequency node; **c** maximum; **d** second minimum. Reflector shift between **b** and **d** 0.20 mm of water, i.e. change of sound path 0.40-mm water which equals one wavelength, which frequency = 3.8 MHz. Readings reproducible to better than 0,01 mm. Measuring error for 15-mm water section (corresponding to 60-mm steel) is less than $0.01/15 \approx 0.7\,‰$

parallel with the pulse unit, and provided with an adjustable reflector in a water-bath. Two echoes will therefore appear on the screen, one from the specimen to be measured and the other from the adjustable reflector. These can be brought to a coincidence position by varying the water path as in Fig. 11.2. This coincidence can be observed very precisely as long as the high-frequency content of the echoes is not over-suppressed by the rectifier of the unit.

If the length of the delay line is d_0 and the corresponding velocity of sound is c_0 the respective transit times are then:

$$t_0 = d_0/c_0 = d_x/c_x = t_x.$$

The thickness d_x of the specimen is obtained by accurate mechanical measurement and so its sound velocity (c_x) is given by

$$c_x = c_0 \, d_x / d_0 \,.$$

This method is quite time consuming in practice so this and similar intricate methods are currently carried out by using modern electronics [226, 198, 698, 4].

11.1.2 The Integration Method

Figure 11.3 explains why the transmitter pulse is not well suited to serve as a time marker. The time interval between the leading edges of the transmitter pulse and the first echo is always larger than the distances between the subsequent multiple echoes as a consequence of the zero error (Section 10.2.3) and the time delay in the coupling layer or in the liquid or solid delay lines with immersion coupling or with TR probes. The transit time can therefore only be measured between two successive multiple echoes or between an artificially generated zero marker and the first back-wall echo.

When using the integration method these two time markers are first transformed into rectangular pulses (see Fig. 11.4), then into a rectangular voltage between the two leading edges. The first edge switches on a constant current source to charge a condenser, the voltage of which therefore increases until the second edge cuts the connection. The final voltage attained corresponds therefore to the transit time, and is indicated by an analog measuring instrument. The proportionality factor can be varied by the charging current during calibration of the instrument, so
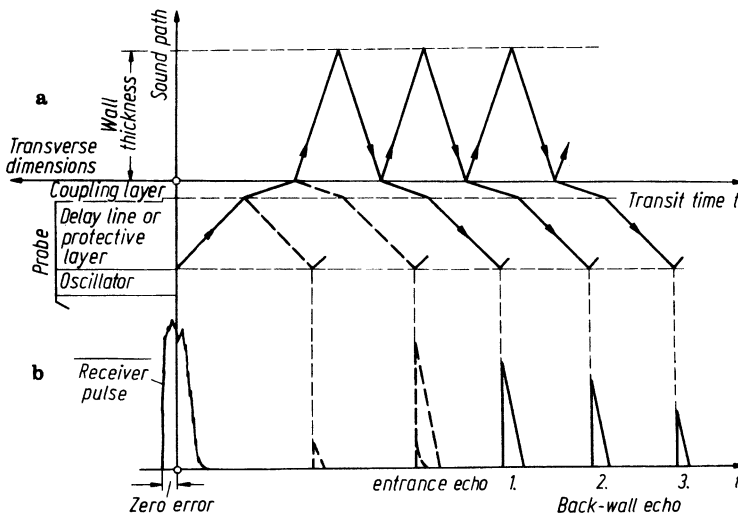
Fig. 11.3. Distance-time diagram. **a** and screen presentation; **b** of the echo pulses in wall-thickness measurements (schematic)
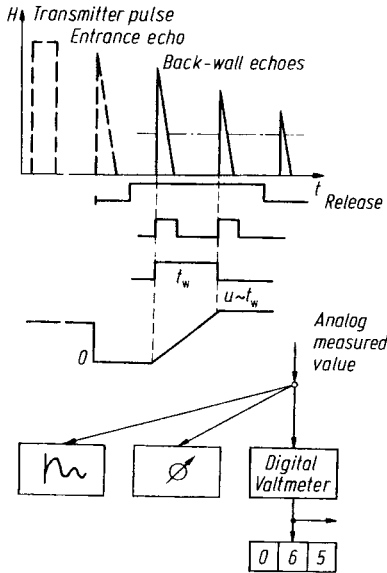
Fig. 11.4. Integration method
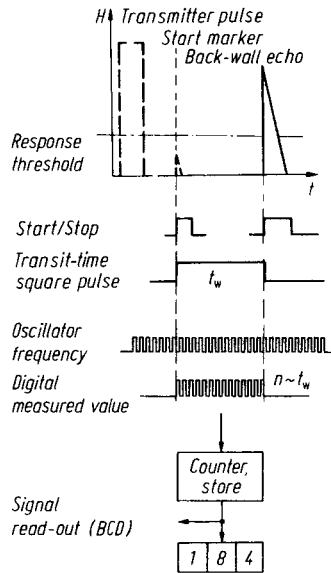
Fig. 11.5. Counting method with artificial start marker

that the indicated value equals the wall thickness of a test block of known thickness and sound velocity.

For further signal processing the maximum voltage reading is stored until a further thickness value appears following the next pulse, after which an analog/digital converter can be used to give a digital display or operate a recorder. The output voltages of the integration method should be stabilized by electronic low-pass filters. In this method the indicated reading corresponds to a time-averaged value.

The critical aspect of the method is the time voltage conversion, which is an analog process and is sensitive therefore to electrical interference and time variations of electronic conditions and components.

11.1.3 The Counting Method

This method is designed to avoid the problems described in the integration method by digital operation. As in Fig. 11.5 the start pulse is artificially generated and coupled to the transmitter pulse. The stop marker is the first back echo but the time measured is of course too short. The difference however is a fixed value which can easily be added to each measurement so avoiding all problems with zero error, and time delays in coupling layers or delay lines. Now the time between the start and stop markers is measured by a quartz controlled electronic oscillator of very stable frequency.

Example. For steel with a sound velocity of 5940 m/s the oscillator frequency has to be 29.70 MHz to attain the accuracy of one wave period, or a thickness accuracy of ± 0.1 mm.

During one wave period the sound travels through 0.1 mm and back again in steel, and for other materials an appropriate frequency can be chosen.

A counting circuit now counts the number of oscillator periods between the start and stop signals, viz. the two edges of a rectangular pulse generated by the start marker and the rise of the first back echo. This counted digital value is fed to a digital display or is stored in BCD-coded form for further data processing.

The possible errors depend on the frequency of the timing oscillator and for manually operated instruments the frequency and precision will usually be sufficient. In automatic-testing installations, however, frequencies up to 3 GHz have been chosen with corresponding increase in measurement accuracy.

When using manual wall-thickness meters a better precision than mentioned above can be achieved by using averaging techniques. If the oscillator is free running, the possible error in the counted number is one, depending on the random position of the pulse relative to the gate. If the counting is carried out 100 times for example the fluctuations of 1 in the final figure of the thickness are averaged. According to the laws of statistical error the computed average is $\sqrt{100}$, (i.e. 10) times smaller than the standard deviation of a single measurement. Simultaneously the measured value is summed from one hundred values thus having two decimal figures more. In practice, however, only one figure more is made use of in most instruments, thus giving a more stable reading without final figure fluctuations [419].

If the fluctuations of the final figure are still troublesome, they can be further stabilised by using even more single shots with the disadvantage of an increased measuring time.

11.2 Instruments using Transit-Time Measuring Methods

Because the main applications of transit-time measurements is the assessment of wall thicknesses, such instruments are simply called ultrasonic wall thickness meters. They are small, light and handy thanks to modern electronic circuitry and the omission of a CR tube. They usually have digital displays as in Figs. 11.6 and 11.10.
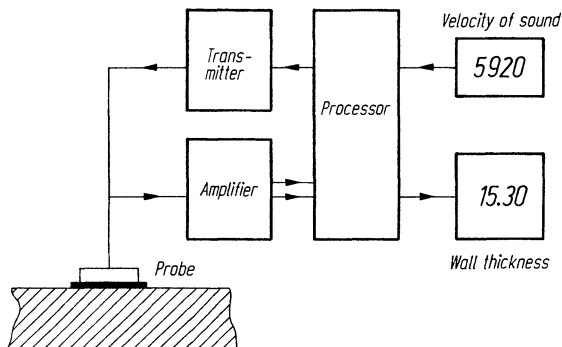
Fig. 11.6. Block circuit of a simple wall-thickness meter

The measured transit time is electronically multiplied by the sound velocity of the material and half this product is the thickness:

$$d = \frac{1}{2}\,ct.$$

The velocity is assumed to be constant for a given material but usually there is a velocity control for correcting the value for other materials the instrument being adjusted by using it to measure a plate of known thickness.

In accordance with differing practical requirements two types of instruments have been developed together with the appropriate probes. The first type which uses a single-crystal probe and measures very precisely, requires that both surfaces of the specimen are of high quality.

The other type is less accurate but is adapted to be able to measure on rough corroded surfaces. In this case it is the residual wall thickness which has to be evaluated, usually using TR probes.

11.2.1 Thickness Measuring on High-Quality Surfaces

For all the methods explained above the precision of the measurement is determined by the stability of the time gate. The start marker is made by the leading edge of the echo and its exact position depends somewhat on the echo amplitude, which in principle should have no influence. To avoid such errors high test frequencies up to 15 MHz are used to obtain short rise times. In addition some wall thickness meters have automatic amplitude control and/or distance corrected gain, to keep the trigger point as independent of the echo amplitude as possible.

Example. In an immersion-testing installation for steel plate the wall thickness meter measures the time interval between the entrance echo and the back-wall echo. The back-wall echo can vary because of coupling differences and the roughness of both surfaces. At a frequency of 5 MHz the trigger threshold has a height -12 dB below the maximum echo peak and if this decreases by 30 % the trigger point is shifted to a somewhat later time, causing an error of 3/100 mm. A reduction by 50 % may cause even 10/100 mm apparent increased steel thickness.

With scanning at high velocity it will not always be possible to compensate these fluctuations automatically but there are other methods of dealing with the problem as follows.

Zero-crossing method [1603] (Fig. 11.7a). If we observe the unrectified echo (i.e. in its high-frequency form), we see that the first crossing of the zero line, after the point of maximum amplitude, does not depend on the pulse amplitude. If this cross-over
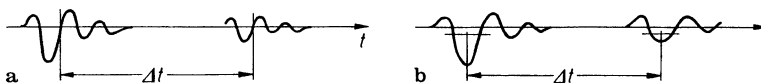
Fig. 11.7. Generation of the time gate. **a** By the zero-crossing method; **b** by the centre-point method

point is used to determine both echo timing points the time interval does not depend any more on the echo amplitudes. In this method no voltage threshold is needed.

Center-point method [1053] (Fig. 11.7b). Here a voltage threshold is used, but the trigger point is not the first crossing with rising amplitude but the mid-point of the section between this and the second crossing, now with falling amplitude. Both these methods are used for larger installations only.

A further condition for a precise measurement is a well damped probe, together with a broad-band amplifier to obtain short pulses. These conditions have two main advantages:

— On thin plate the first echo used as the start signal must be completely decayed before the next echo which gives the stop signal. The narrower the pulse can be made the thinner are the plates which can be measured.
— With low damping (i. e. a narrow-band probe and amplifier) there will be more than a single half oscillation which could trigger the end of the gate if the amplitude varies. This situation must be avoided by obtaining a pulse of only a half wave or by good automatic amplitude control.

Depending on the specific application different probe types are used. These are direct contact, contact via a solid delay line or via a liquid delay as in immersion testing. Thus three different methods for generating the start signal have developed (Fig. 11.8). The first method makes use of the transmitter pulse to start the gate with occasionally an adjustable delay to compensate for the zero error and delay time within the coupling layer. In this quite simple case contact probes are used. Errors can therefore occur by unpredictable variations in the coupling layer and the echo-influence zone following the transmitter pulse makes it impossible to measure small wall thicknesses.
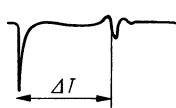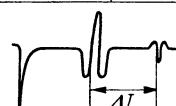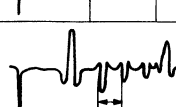
Screen picture	Range (steel)	Error	Probe
1 ΔT	> 0.5 mm	± 0.01 mm	Direct contact
2 ΔT	> 0.5 mm bis 100 mm	± 0.003 mm	With delay line
3 ΔT	> 0.1 mm bis 50 mm	± 0.003 mm	With delay line

Fig. 11.8. Different methods of wall-thickness measurement

The second method generates the start signal from the entrance surface echo when using probes with a solid delay line or used in an immersion technique. Somewhat smaller thicknesses can be measured because the entrance echo usually has a shorter echo-influence zone. The measurement of large thicknesses is limited because the second entrance surface echo must not return before the first back-wall echo.

The third method utilises two or more back-wall echoes, using the first to start the gate. The accuracy is similar to that of the second method, but the range is more extended towards the measurement of smaller thicknesses, because start and stop signals have similar amplitudes. However, direct probe contact is not recommended since the quality of the surfaces must be good and corroded ones cannot be measured reliably.

The attainable accuracy of all wall-thickness measurements depends on several factors:

— The sound velocity for the specimen material is allowed for by adjusting the velocity control of the unit but it might deviate a little from the listed value chosen. Any error therefore affects the measured wall thickness value. Preferably the unit should be calibrated and checked using a sample of exactly the
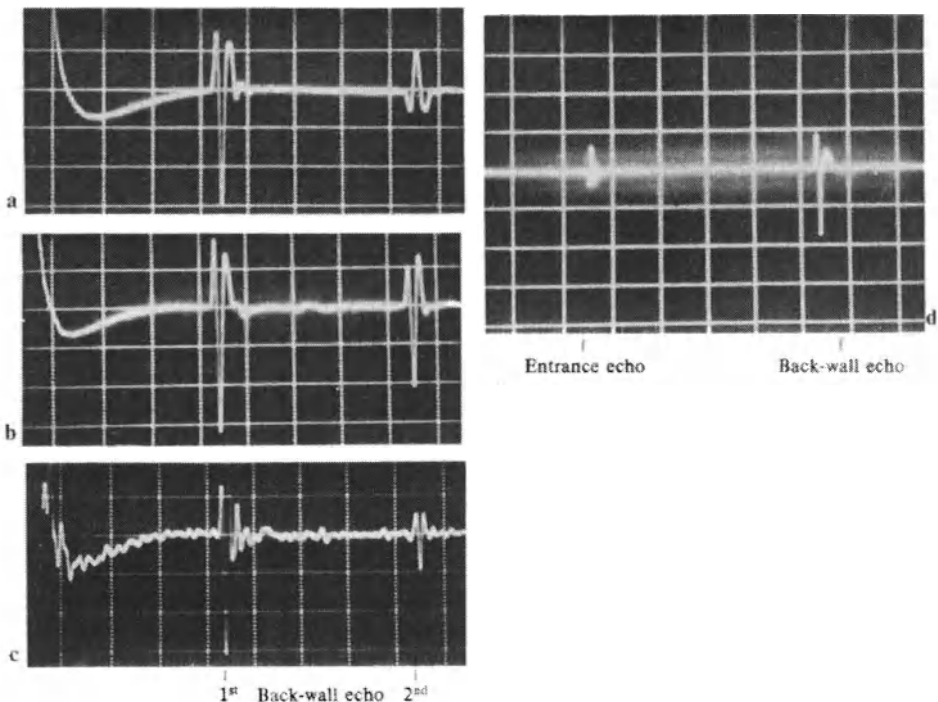
Fig. 11.9 High frequency presentation corresponding to different wall-thickness measurements. **a–c** with hard-faced probe in direct contact. **a** On plastic; **b** on steel; **c** on steel with bad coupling surface; **d** in immersion technique on plastic

same material as the specimen to be tested, using as large a thickness as possible.

— The coupling conditions always influence the precision because they can reduce the amplitude and form of the back echo, especially on curved or corroded surfaces. Improving the surface quality will help in many cases but otherwise the method for measuring residual wall thickness with lower accuracy should be applied.

— High material attenuation can be another handicap, especially when working with high frequencies to obtain high precision. In difficult cases, as for example on layered media such as glassfibre composites (GFC), or on very coarse grained material, using a low frequency system can help but of course with lower precision.

— The sound velocity can actually change within one specimen as for example because of different cooling processes in grey cast iron, or because of differences in temperature in plastic materials.

— Large acoustic impedance differences between the surface of the probe and the material to be tested are unfavorable and for example a hard-faced probe should not be used on soft materials since the range of measurement can then be restricted.

— A further reason for measurement errors can occur because of phase shifts in the echoes. There is a half-wavelength change of phase between the second back-wall echoes from a hard-faced probe when used on plastic and on steel (Fig. 11.9). This can be taken into account by electronic means but otherwise it results in an error equal to a half wavelength.

Various specially developed instruments have been applied to difficult problems (see also Section 33.1):

— cast materials,
— thin plastic items,
— glass-fiber reinforced sheets,
— very thin materials,
— testing installations using multiple channels

Figure 11.10 shows two commercial instruments for high-precision measurements.

11.2.2 Residual Wall Thickness Measurements

In the case of inspecting chemical plants for safety the residual thickness is very often the main interest. This is the thickness of metal left by heavy corrosion, often in the form of pitting. This problem cannot be solved using the methods described above because the mean thickness given by a large echo is not of interest but only the minimum residual wall which is indicated by the small echoes from the individual corrosion pits on the rear face.

The acceptable accuracy can be lower but even very local pitting must be indicated. An automatic amplitude control is of little value because it will reduce the
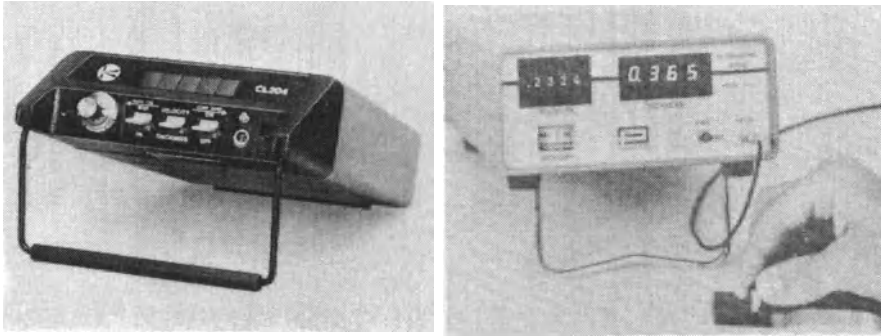
Fig. 11.10. Commercial wall-thickness meters. **a** design Krautkrämer type CL 240; **b** design Panametrics, type 5222
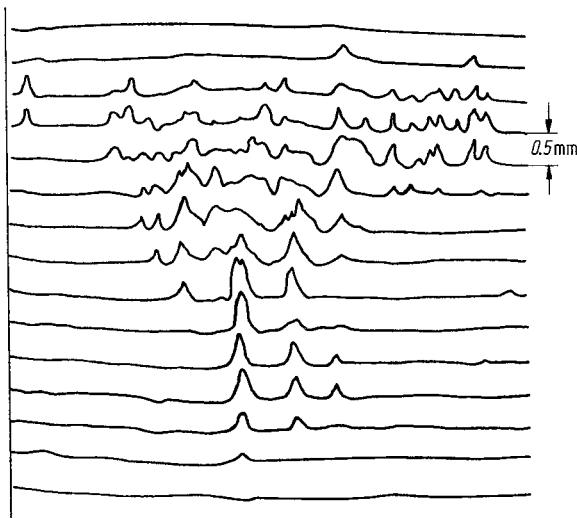
Fig. 11.11. Record of residual wall-thicknesses in tubing plotted by scanning with a residual wall-thickness meter and using a special TR-probe. The amplitude of the peaks indicate the depth of pitting corrosion

main back-wall echo (which is always simultaneously present) so much, that the pitting echoes disappear. Units suited to this problem must omit such circuitry but must have a very high sensitivity and TR probes are exclusively used.

The corrogram in Fig. 10.65 indicates the useful range of various probe types which are different for different designs. To cover an extensive depth range several different types of probe must be used. For example the residual thickness range of about 20 mm is covered by one type and that down to 1 mm by another.

The usual accuracy is about 0.1 mm of steel and Fig. 11.11 shows the recording of a scan on a corroded tube using such probes.
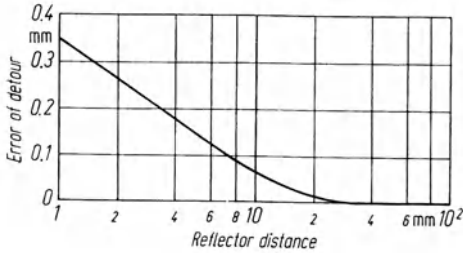
Fig. 11.12. Error of detour, schematic. The actual curve depends on the design of the probe

The error of detour is mainly responsible for the relatively poor accuracy as shown in Fig. 11.12, and Fig. 10.46. The actual distance of the reflector from the contact surface is somewhat less than the track of the pulse because of its V-form and the transit time for small distances below the surface is no longer strictly proportional to the depth. The error can be approximately compensated by a deliberate readjustment of the scale zero and of the velocity but modern units try to avoid the error by using computer circuitry.

Another possible error can occur with measurements taken near to the lower limit of the range. The first oscillation of the echo may be too low to trigger the gate, whereas the second will and thus cause an error of one wavelength. Usually this condition is recognized if contact is improved by shifting the probe position.

A false measurement is also possible by surface-wave cross coupling if the contact surface is rough. The degree of roughness which will still allow the measurement of thin walls is usually indicated by the equipment manufacturer.
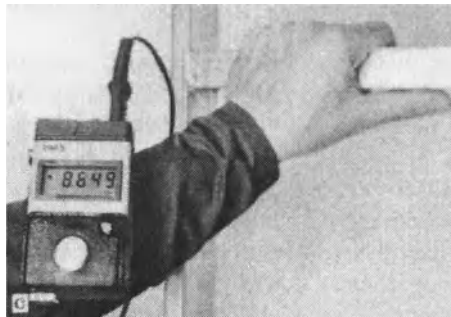
Fig. 11.13. Commercial Corrosion Meters. a Sonatest "Comparagage"; b Teitsu Denshi; c Krautkramer type DM 3 (strapped to an operator's arm)

Figure 11.13 shows some commercial designs of wall thickness meters for corrosion measurement and special units are also available for the following special applications:

— measurements on hot surfaces,
— for materials of high attenuation,
— corrosion measurement under water

In very difficult cases pulse-echo flaw detectors with built in wall thickness meters can be of assistance because in these units any distortion of the echoes or of the echo pattern can be recognized on the CR screen (see also Section 33.1).

11.3 Frequency-Measurement Methods

11.3.1 Methods Using Narrow-Frequency Bands (Resonance Method)

The thickness oscillation of a plate and its resonance with an exciting oscillation has already been described in Section 7.2. In this case the plate represents the wall whose thickness has to be measured. Resonance takes place if a continuous ultrasonic wave is introduced and after being reflected by the back wall coincides with itself with the same phase. This happens firstly if the wall thickness is equal to a half wavelength, provided the wall abuts on both sides onto a soft medium, and thus no phase shift takes place. Then we have:

$$d = \frac{\lambda}{2} = \frac{c}{2f_0}$$

where c ist the velocity of the wave in the material concerned, and f_0 is the resonance frequency. f_0 is also called the fundamental or the first characteristic frequency of the plate, as long as the excitation is carried out without appreciable feedback to the oscillator. Resonance will also take place at the higher harmonics ($d = 3 \times \lambda/2$, $5 \times \lambda/2$, etc.) and hence at the 3rd, 5th etc. characteristic frequencies. To obtain unequivocal results it is necessary to measure the frequencies of two consecutive resonance points. Their difference Δf is equal to twice the fundamental frequency and so the thickness is given by:

$$d = \frac{c}{\Delta f}.$$

The nature of the specimen and its material properties produce the same limitations as those applying to the pulse echo methods in Section 11.2.1. High material attenuation and rough, or even non-parallel, surfaces reduce the sharpness of the resonance and the precision of the measurement.

For acoustic excitation, as well as for indicating the resonance, one probe is used as in Fig. 11.14. This also shows the principle of the circuitry, illustrated with an electronic tube because at the time of these first instruments transistors were not known.
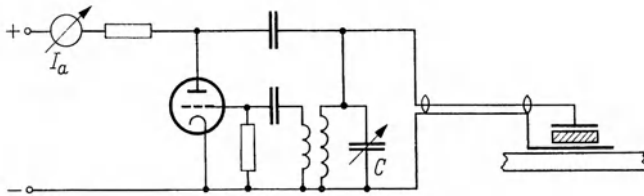
Fig. 11.14. Circuit diagram of a resonance thickness meter

Fig. 11.15. Branson Vidigage, model 14, showing the wall-thickness measurement of 4.2 mm steel
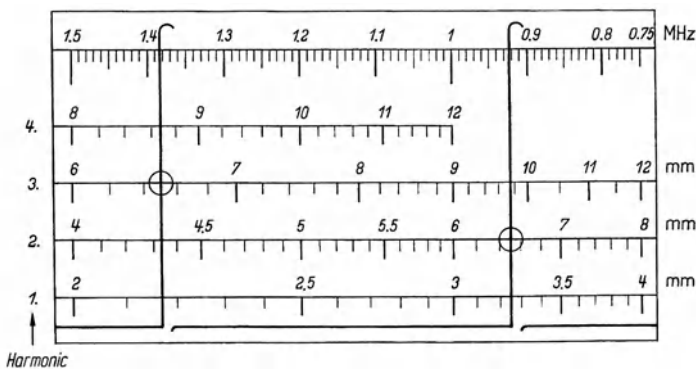
Fig. 11.16. Simplified scale of Vidigage for frequency range 0.75 to 1.5 MHz, with the 1st to 4th harmonic scales. Resonance reading of a thickness of 6.5 mm by the 2nd and 3rd harmonics

With this simple circuit the frequency has to be adjusted manually by using the condenser C. The resonance position is indicated by measuring the anode current I_a, which is maximised at the resonance point. Calibration is carried out as usual using test blocks of known thickness and velocity.

To avoid interference by the characteristic frequency of the probe crystal, only that frequency range below it is used. The sensitivity of the probe in this range should be as high and as uniform as possible in the whole range below its characteristic frequency and is therefore only lightly damped.

Because the probe must be coupled to the oscillating plate it has still a slight influence. In fact we have in effect two oscillating circuits weakly coupled together, and in consequence their resonance frequencies are somewhat shifted. If the same probe is always used, this error can be taken into account when calibrating the scale of the instrument (Fig. 11.15).

Only manual operation of the frequency control was feasible on the first simple units but based on the patents of Erwin and Rasweiler [197], the company General Motors Inc. built in 1947 an instrument which was called the "Sonigage". In this the condenser was driven by a motor and the resonance point could be recognized on a small CR tube. More applications were found using the "Vidigage" manufactured by Branson Instruments Inc. (Fig. 11.15). The frequency was modulated at the repetition rate of the mains voltage and the resonance peaks were seen on a very brilliant and large TV screen. Figure 11.16 shows schematically the screen with indications for a wall thickness of 6.5 mm steel.

In addition to the scale of the frequencies (top) the screen has several thickness scales to evaluate unequivocally the number of the harmonic oscillation. Resonances at the fundamental frequency have to be read from the lower scale and those of higher ones on the upper scales. The value is correct if the thickness indication is the same on two adjacent scales.

The low accuracy of this type of equipment which is a consequence of their performance depending on the surface quality, as well as the progress in electronics design, have made these instruments lose importance as compared to the pulse type instruments. It is of interest to observe that Firestone made use of the first pulse-echo flaw detector for resonance thickness measurement [452]. If the exciting frequency of a standard flaw detector can be continously varied and the probe has low damping, then when it is in contact with a thin plate the transmitter pulse observed on the screen becomes very elongated at the point of resonance. From the corresponding frequency the thickness is evaluated as before.

11.3.2 Methods Using Wide-Frequency Bands (Narrow Pulses)

A resonance can also be established by using the multiple-echo sequence obtained from a plate (Fig. 10.4 and 11.17) [395].

The frequency at which the single echoes follow one another is called the *echo-repetition frequency* and should not be confused with the pulse-repetition frequency or the ultrasonic frequency of the pulse. The latter merely should be as high as possible, in order to obtain echoes which are as short as possible compared with the
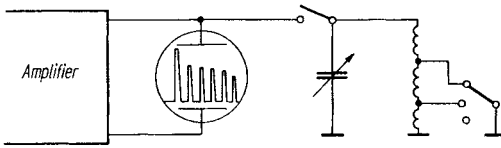
Fig. 11.17. Basic circuit of the wall-thickness gauge attachment

wall thickness therefore defining precisely the echo repetition frequency on the basis of a long sequence of pulses. As customary, the pulse repetition frequency should be low enough to permit the undisturbed formation and decay of an echo sequence betwen successive transmitting pulses.

The basic circuit of a practical application of this method is shown in Figure 11.17. A tunable oscillator circuit is connected to the output of the video amplifier at the leads to the deflection plates of the CR tube. If it is tuned to the echo repetition frequency, each echo of the sequence results again in in-phase triggering of the oscillation circuit and the resonance maximum can be observed directly on the image screen. The scale of the rotary capacitor can be calibrated for a given material directly in transit time or in wall thickness.

Another method for measuring transit times is the *sing-around method* which as the first ultrasonic pulse method had already been proposed and used in 1941 by Hiedemann [655]. In this method the returning echo of a pulse triggers the next pulse and so forth. Consequently, the echo-repetition frequency then equals the pulse-repetition frequency which can be measured with a frequency meter with very high accuracy. The transit time is the reciprocal value of the repetition frequency.

Example. In a section of steel 100 mm thick the transit time is 34 µs. The repetition frequency, therefore, will be 1/34 MHz, i. e. approx. 30 kHz. The repetition frequencies, both the echo-repetition frequencies of the previously described method, and the pulse-repetition frequencies of the sing-around method, are in the case of wall thicknesses of 1 to 100 mm, from 3 MHz to 30 KHz respectively.

This method, however, gives values which are only apparently very accurate. The systematic error which results from the zero error (cf. p.172) is explained in Fig. 11.18. A certain time elapses between the reception of a given echo pulse, its amplification, the triggering of the electric transmitting pulse and the actual start of the transit time of the ultrasonic pulse; this is the zero error by which the measured
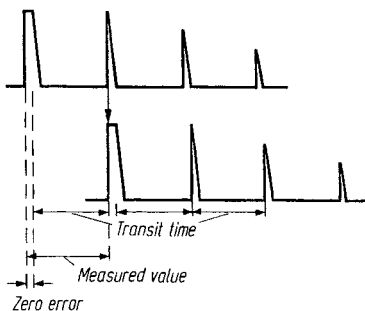
Fig. 11.18. Principle of the sing-around method for measuring the transit time, and its systematic error

time exceeds the transit time. In order to determine and eliminate this error, the method has to be applied to two test pieces of equal sound velocity but of different thicknesses.

For further applications of the sing-around method see [61, 538, 655].

Finally should be mentioned the *PREDEF-method* of Kaule [350, 351]. (pulse resonance with delayed feedback), the principle of which is closely related to digital time measurement (Figs. 11.19 and 11.20)
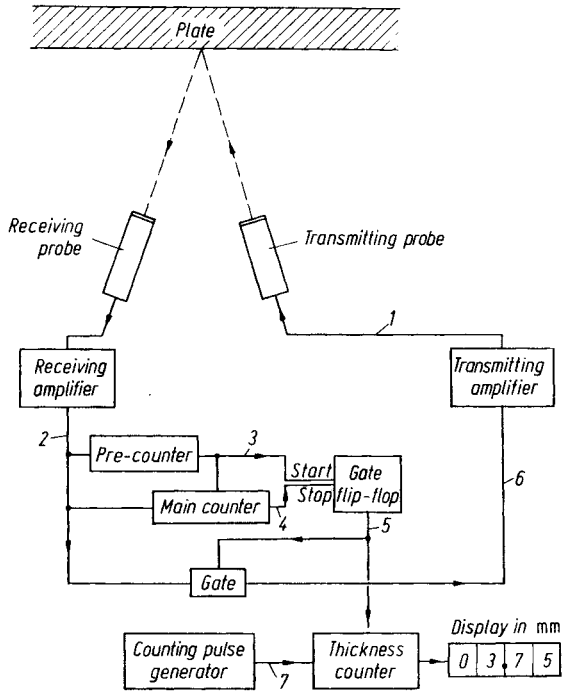
Fig. 11.19. Block diagram of a measuring device according to the PREDEF method (the circled numbers refer to Fig. 11.20)
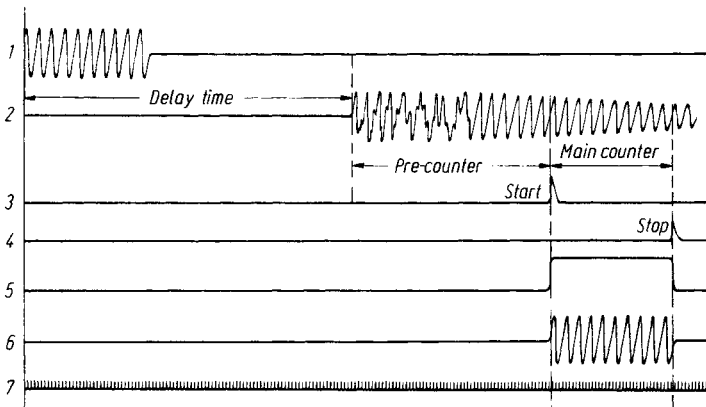
Fig. 11.20. Oscillographs, explaining the mode of operation of the PREDEF method (cf Fig. 11.19)

In a similar way to the sing-around method the wall is excited in a thickness resonance. For the measurement however the free characteristic frequency is used, which shows itself after the excitation has been stopped. Figure 11.20 explains the method and for more details of it see [13], where further variations of the pulse resonance method are also mentioned.

11.4 Other Transit-Time Methods

The *phase method* uses continuous waves of constant frequency. To measure the transit time, the phase of the echo wave is compared with the phase of the emitted wave. If the return transit-time interval in a given plate is less than one wavelength, it can be determined unequivocally on the basis of the phase difference, between zero and 2π, by which the receiving voltage is delayed. For greater thicknesses the measurement becomes ambiguous and to avoid errors consisting of a whole number of wave lengths, the approximate thickness concerned must therefore be known. Since it is also not difficult to use very low frequencies, this method is particularly suitable for measuring thicknesses or acoustic velocities of strongly absorbing materials, such as rubber and plastics and in fact this method is limited in practice to just such materials because multiple echoes impede the measurements. It was mentioned by Hatfield and used for measuring thicknesses in rubber [622].

Finally the *frequency-modulation method* already explained in Section 10.7, can be listed, because it is in principle also a transit-time method.

12 The Shadow Method

This method is also called the intensity-measurement or through-transmission method and is explained in Fig. 12.1. The shadow of an inhomgeneity, which is illuminated by an ultrasonic wave, reduces under certain conditions the intensity of the wave received by a second probe. The name through-transmission method arises obviously from the fact that two probes are often positioned face to face on opposite sides of the specimen but that may not always be the case. Figure 12.2 shows an alternative arrangement of the shadow method where the beam is reflected before being influenced by the defect, and equally is could also be reflected afterwards. In this situation in which a reflection takes place at a free boundary, the two probes can even be combined into one. Nevertheless if only the influence of the defect on the back-wall echo is observed, it is in principle an application of the shadow method, and in addition the shadowing may even have a double influence on both the outward and return sound paths.

A warning is sounded here, particularly for the reader who is less familiar with physics, not to equate the schematic presentations of the ray paths indicated in Figs. 12.1 and 12.2 and many of other diagrams, with the actual propagation of ultrasonic waves. As discussed in Chapters 3 to 5 this presentation of the rays based on geometric-optical concepts of light and shadow is only valid in the extreme case of wavelengths which are very short compared with the dimensions of the probes and the flaws, i.e. conditions which are usually not fulfilled in practice or if so, only as a rough approximation. Unfortunately, wave physics does not lend itself readily to schematic presentation in the form of drawings.

The paradoxical case may also happen, in which an obstacle within the wave increases the intensity at the position of a receiver, as has been shown in Section 5.3 (Figs. 5.9 and 5.10). The method should therefore always be proved using artificial defects, which also allows a defect calibration at the same time.
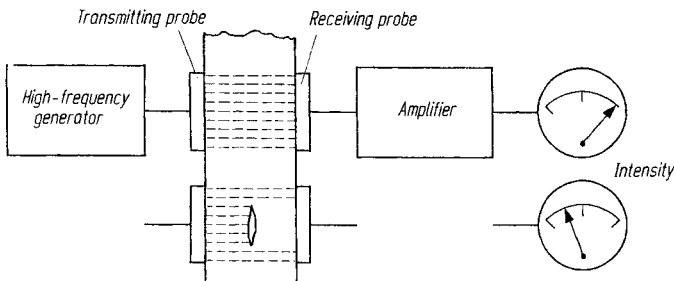
Fig. 12.1. Principle of the shadow method
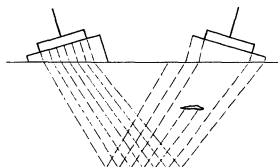
Fig. 12.2. Shadow method with reflection
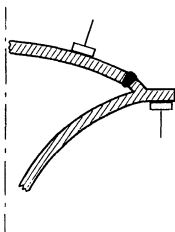
Fig. 12.3. Shadow method with guidance of the sound

In complicated specimens, like Fig. 12.3 which illustrates a weld in a valve body, it could be possible to obtain an indication of a large defect in the weld, though it would not be possible to identify the exact path of the wave or its type. In such cases one could speak of guided ultrasound.

When using continuous waves great difficulties are caused by standing waves. The sound will not only propagate on the intended path from the transmitter to the receiver, but will suffer multiple reflections and build up a field of sound maxima and minima, in which the influence of the defect can be lost completely. This standing-wave field depends very sensitively on the position of the transmitter, the dimensions of the specimen and the sound wavelength so it can never be exactly calculated for most specimens and the sound pressure received will therefore vary strongly with small changes in these values. To avoid this handicap with continuous waves frequency modulation can help somewhat, either using periodic or aperiodic modulation, for example by a noise voltage, and of course the use of pulses also avoids the problem.

The main practical applications of the shadow method are on specimens in the form of plates or shells, accessible from both sides and having planar defects lying parallel to the surfaces. Examples are plate with laminations, layer-structured materials, fiber-reinforced materials and structures such as honeycomb which are commonly used in aircraft production. According to [925] fatigue cracks in tubing can also be detected. For further applications see Part D, and specially for plate testing as described in Chapter 24.

13 Imaging and Methods of Reconstruction

After having located a defect it is of great importance to know something about its size, since this is the basis for a decision concerning its importance for the practical integrity of the specimen which contains it. Its shadow, as revealed by X-ray screening could already be very useful and this is the aim of all imaging methods. By the use of sound sensors, signals are obtained to transform the sound "picture" into a visual image.

The basic handicap of such a transformation is the relatively large ultrasonic wavelength, which is the reason why the optical image can be very different from the "image" first produced by ultrasonic waves. A surface appearing as quite rough in an optical image can be presented in the ultrasonic image as a fully smooth one, since the spatial resolution is far lower being proportional to the ratio of the numerical aperture A to the wavelength, i.e. A/λ.

The method of producing a visual image by ultrasound consists of a two-stage process:

Generation of an ultrasonic field which is influenced by the object under test, and then survey by an acousto-optical transducer which can transform the sound-pressure distribution into an optical image.

To transfer the sound-distribution pattern produced by the object to the position of the acousto-optical transducer, some methods make use of a lens system, imitating the optical process. For lower quality images it may be possible to do without lenses as for example in the simple shadow method. An acoustic lens can also be simulated by electronic means (see below) or acoustic holography can be very well suited to reconstruct the image (Section 13.14).

It must be said that ever since imaging instruments have been developed, none of them has even approached the importance of the manually operated pulse-echo method. The reason is mainly their large size and weight and their lack of flexibility in being only capable of inspecting particular shaped specimens. Nevertheless they will be dealt with here but in Chapter 19 other and simpler methods are described for evaluation of the size and shape of defects.

Compare also the publications of the following authors: Berger [134] (1969); Wade [44] (1976); Ahmed, Wang and Metherell [58] (1979); Haran [609] (1979); Jacobs [717] (1979); Greguss [572] (1980); Hildebrand [601] (1981); Aldridge and Clement [64] (1982); Szilard and Hanstead [1500] (1982); Bar-Cohen [104] (1983).

13.1* The (Liquid Surface) Relief Method

The surface of a liquid is locally deformed by an incident ultrasonic wave and Fig. 13.1 shows how this effect can be used to obtain an image of the wave field.

The wave field in a liquid is modified by an object placed in the beam and the resulting ripple pattern on the surface can be related to the physical conditions of the object. If the surface is scanned, for example by a laser beam, it will be more or less deflected by the surface distortions as compared with its undisturbed parts. By using the edge of a half screen this deflection is transformed into an intensity modulation of the light and presented on a TV screen via a photocell.

The relatively low sensitivity can be improved somewhat by using a metallized plastic foil to cover the surface which gives better reflection of the laser light.

The scanning speed can be very high and the method can therefore be considered as in real time. It has been applied for ultrasound microscopy with frequencies up to 500 MHz (the sono-microscope instrument of the Sonoscan company) see Section 13.13.

Such instruments are also known as SLAM (scanning laser acoustic microscope). The resolution is of the order of one wavelength and hence may be down to a few microns. It has found applications in medicine and for some problems in materials testing for the microelectronics industry (delaminations and porosity). See also Kessler [774]; Kessler and Yuhan [776], with examples for its use and further literature references.
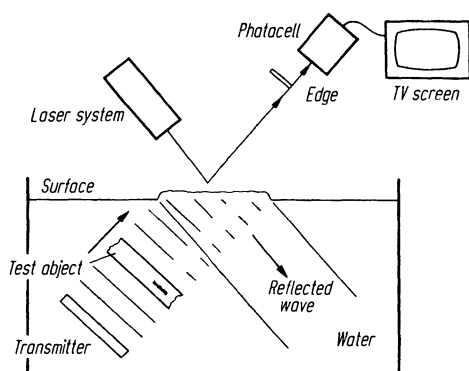
Fig. 13.1. The relief method

13.2* Ultrasonovision (RCA Camera)

In this system the deformation of a thin metallic diaphragm immersed in a liquid is scanned by a laser the diaphragm acting as a mirror in a Michelson interferometer (Fig. 13.2).

The displacement of a surface element of the diaphragm scanned by the laser system changes the phase of the light, which interferes with a reference light beam
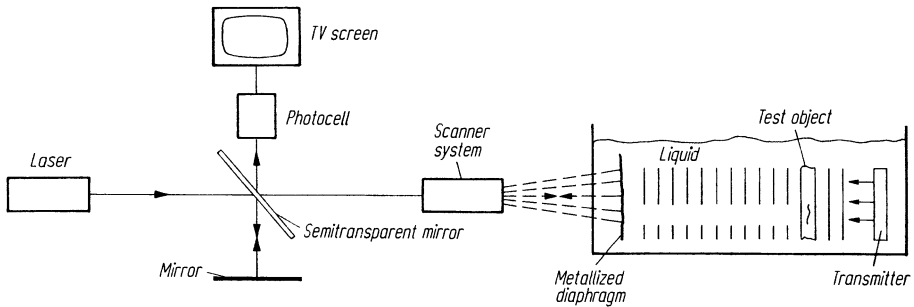
Fig. 13.2. Ultrasonovision method, schematic (RCA Camera)

via the semi-transparent mirror. The variations of light intensity serve, via a photo-cell, to build-up an image of the sound field. The metal foil is thin enough (less than 6 µm) to respond to ultrasonic frequencies up to 10 MHz. The physical displacements can be very small, even less than the wavelength of the light wave and hence the sensitivity achieved is far better than in the previous method. The angular aperture is 50° and covers the whole area of the metallic film 150 mm in diameter. The resolving power is, however, again limited by the ultrasonic wavelength.

For a comprehensive presentation with examples of applications in medicine and materials testing see [1036, 1571]. Reference [875] deals with the application of the RCA camera to an investigation of the propagation of sound in anisotropic materials. For other interferometric methods see [609].

13.3* The Piezo-electric Opto-acoustical Transducer (Parametric Image Converter)

In this method a piezo-electric plate is coated with a photoconductive layer on one face. The film electrode on this layer must be transparent so that if a small area of the photolayer is illuminated by a narrow laser beam any electric charge at this point is allowed to leak away and the corresponding current can be used to modulate the light of a CR tube. By synchronizing the scanning laser beam with the electron beam of the CR tube an image of the electric charge distribution is built up and this represents the ultrasonic image on the receiver crystal.

Conversely local alternating voltage can also be generated by appropriate illumination used to excite the plate and is followed by the transmission of ultrasound. By suitable shielding of the light, for example by a diaphragm in the form of a Fresnel plate, the beam pattern of the transmitted wave (for example its near-field length) can be varied. This can also be carried out for the receiving stage so that by programming the illumination we can obtain a transmitter receiver system with a controllable sensitivity region, near-field length and directivity angle or beam width [91].

13.4* Imaging by Bragg Diffraction

The Bragg-type diffraction which takes place at an ultrasonic wave field, as described in Section 8.6, can be used to produce an acousto-optical image. An object immersed in a liquid cell (see Fig. 8.21) influences the ultrasonic "grating" and this effect can be used to produce an image of the object by using a scanning laser. Ultrasound transmitter, laser scanner and CR tube are all synchronized, and unwanted time periods, for example those including interfering echoes, can be suppressed by using gates in the electronic circuit.

This method operates in real time and is relatively simple but the low sensitivity and the narrow image field (see Fig. 8.29) are disadvantages. It has therefore not found applications either in medicine or in materials testing.

For more details see [57] and [44]. In [624] the method is described for ultrasonic microscopy using very high frequencies in the gigaherz range.

13.5* The Schlieren Method

This has been explained in Section 8.6 (Raman-Nath diffraction). The diffracted light, as in Fig. 8.18, which falls onto a photocell, can be projected onto a screen to produce a visual image of the sound field if the ultrasonic pulses and the illumination flashes are synchronized. By varying the phase lag between them, the pulsed wave is made visible at varying path lengths. The main application of the method is to examine the pulse behaviour after reflection, refraction and mode changes in liquid or solid transparent media. If a sound field is affected by a solid object placed in a liquid an image of the object by reflection, or through transmission, can be obtained.

For examples of the value of this method see Section 13.4. For further details see [1116, 602, 1320, 981 and 609].

13.6* Imaging by the Photo-elastic Effect

See Section 8.6 and Fig. 8.21 for an explanation of the principle. The photocell can be replaced by a camera, or by a screen, to obtain the acoustic image of an object influencing the sound propagation.

The method has a much lower sensitivity than the previous ones but has been used for imaging the ultrasonic field [98, 1614, 1669, 1309, 94, 1421, 598, S 187], and also rarely for materials testing as in [1295, 610, 791]. See also Section 13.7.

13.7* The DUVD Method

The initials DUVD are used for the direct ultrasonic visualization of defects. Figure 13.3 shows a device which uses the Schlieren method or the photo-elastic effect according to [605].

In this method a large transducer projects a pulsed sound wave onto the test object which may contain defects. On their return the echoes pass the transducer and through a lens system which produces a spatial image of the defects within a solid photo-elastic body, or within a liquid-filled cell, for use by the Schlieren method. The defect images are made visible by using a stroboscopic flash.

The quality of ultrasonic imaging by lenses is of course far worse than optical imaging because of multiple reflections and mode changing which takes place in the lenses. For a review of the state of the art in building ultrasonic lens systems see [1500], especially concerning the system of the DUVD method. See further Section 3.4 and [717, 572].

The Schlieren method has been found to be more sensitive than the photo-elastic method, but it is still about 50 dB down compared with a piezo-electric method. Special applications have been proposed in [628]. See also [1500, 104, 103, 627, 981, 609].
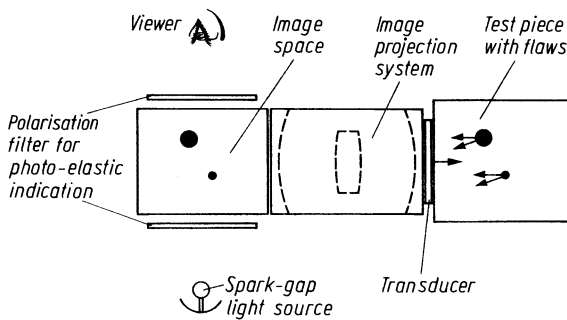
Fig. 13.3. Ultrasonic image projector by Hanstead and Wyatt

13.8* Acousto-optical Liquid Crystal Converter

Liquid crystals are liquids with optical anisotropy, and they behave optically as a typically solid crystal. They are also doublerefracting, which means that they propagate light as two partial-waves, polarized perpendicularly to each other, and to the direction of propagation, as long as the medium is non-absorbent. Because their velocities are different the plane of polarization of incident polarized light is therefore rotated. The usual uniform orientation of the molecules in liquid crystals can be influenced by mechanical as well as by electric forces so that it is possible to produce real time sound pressure patterns.

Liquid crystal displays (LCD) have been the object of much research and the state of the art is reviewed in [320, 601], see also [572, S 147].

13.9* The Acousto-visual Display Unit (Schallsichtgerät) of Pohlman

The Pohlman cell [1202, 1203, 1138] is filled with a liquid in which are suspended very many small aluminium discs of 10–30 µm diameter. The forces within a sound wave try to rotate the discs to lie perpendicular to the direction of propagation of the sound. This effect, known as the Rayleigh-disc effect, has been used to measure the intensity of sound by measuring the turning force experienced by a small disc suspended in a liquid.

In the Pohlman cell the force of the ultrasonic wave is acting against the random Brownian motion. Within the range of ultrasonic intensities of about 1:10; the particles are more uniformly oriented where the ultrasonic intensity is higher. When the cell is illuminated in a direction against that of the ultrasound the regions of high sound intensity appear more brilliant because in these regions more particles will reflect the light towards the observer.

Because of a slow reaction time, a restriction of specimens to the form of flat plates, and because of the bad resolution, the device has not found much practical application.

As a variation from the use of discs, small plastic spheres (diameter 1 µm) have been used [280]. In this system the physical distribution of the spheres is changed by the sound radiation pressure and it is made visible by scattered light. The method has been applied as a shadow ultrasonic microscope, at frequencies up to 1000 MHz, and reaching a resolution of 5 µm. The disadvantages of inertia and low dynamic range are, however, still present [572].

13.10* The Sokolov Camera

In this device the conversion of an acoustic image to a visual one is carried out by scanning a piezo-electric transducer with an electronic beam (Fig. 13.4).

The through-transmission image of the specimen immersed in a liquid is focussed onto a piezo-electric receiver by a lens system. The receiver disc forms part
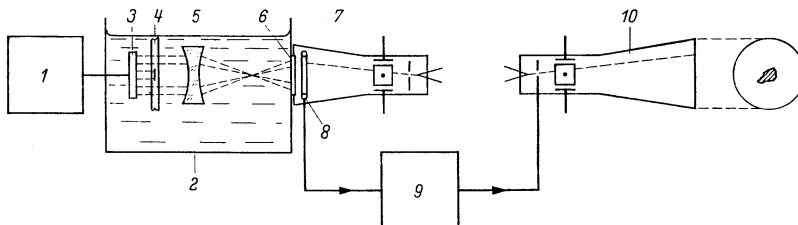
Fig. 13.4. Schematic diagram of an electronic image converter. *1* high-frequency generator, *2* water tank, *3* transmitting quartz plate, *4* test piece, *5* ultrasonic lens, *6* receiving quartz plate, *7* scanning tube, *8* collector, *9* amplifier, *10* picture tube
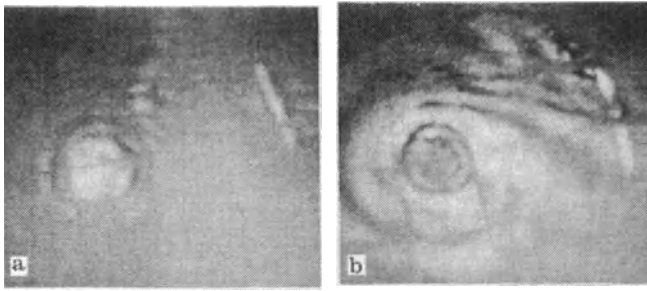
Fig. 13.5. Ultrasonic images of spot welds produced by a Sokolov camera at 10 MHz. **a** No defect (the fine line across the image is generated by the camera); **b** defective with heavy porosity (according to [717])

of a vacuum tube and its surface is scanned by an electron beam. The local discharge currents for each individual spot of its rear surface control the light intensity of a synchronized CR tube.

The main problem met with in manufacturing such a scanning tube is making a strong and vacuum tight joint between a piezo-electric plate and the glass tube. The plate thickness, for reasons of sensitivity, has to be about a half wavelength of the ultrasound. At 1 MHz and for quartz it would be therefore only 3 mm thick, which restricts its diameter, and the test aperture, to only a few centimetres. For better resolution the frequency should preferably be even higher, which would restrict the aperture still more. Of some help would be to use a supporting grid with the plate [719]. This could also be achieved by using a larger plastic plate carrying on its surface, on the vacuum side, a mosaic of small piezo-electric plates or a single large one. Using these methods apertures and testing fields of 9 cm diameter, or 15×21 cm using a crystal mosaic, have been achieved. The plastic disc which borders onto the liquid of the cell must of course be sufficiently transparent to ultrasound.

The sensitivity of the Sokolov camera is not appreciably better than the other methods mentioned above and compared with the direct piezo-electric scanning methods of Section 13.12 has about 40 dB less sensitivity. The Sokolov camera could also be used with piezo-electric polymers instead of solid materials (PVDF, see p. 125).

A Sokolov camera cannot work efficiently with ultrasonic pulses because the scanning of the receiver requires an appreciable time and it has no memory function. Using pulses nevertheless, one for each scanning point, makes the building up of an image a very slow process and in addition the gating out of unwanted interfering waves is also not possible.

An alternative method of operation was also proposed by Sokolov himself [1446]. The receiver plate itself carries on the inside surface a photo-emitting layer. When illuminated with ultrasound the electron emission of a particular point depends on the electric charge at this spot generated by the ultrasonic wave. After a flash illumination the layer is electronically scanned as before [547]. It is also possible to "read out" the charge distribution by a laser scanning system [1439]. According to the proposal by Sokolov the photo-electron emission of the layer when continuously illuminated could be displayed on a CR tube screen at the other end of the tube by electron-optic means and this would not need a scanning process.

Sokolov cameras have been developed for various applications in medicine and materials testing and even used for under water inspections [1589]. Figure 13.5 shows a result of testing spot welds [717]. For further details see [718, 715, 187, 1500].

13.11* The Pyro-electric Camera

Pyro-electric material produces an electric charge when heated and the heat can be generated by the absorption of an ultrasonic wave. If the piezo-electric plate in the Sokolov camera is replaced by a pyro-electric plate or layer it can be scanned by the electron beam thus giving an image of the intensity distribution of the ultrasonic wave over the plate.

The principle became of interest when sufficiently sensitive pyro-electric material was found, for example plastic polymers such as PVF_2 (poly-vinyl-fluoride).

Because of the inertia of the temperature equalization process the scanning can be carried out after the ultrasonic illumination, so that ultrasonic pulses can also be used, the method being quite rapid and in real time, including the possibility of gating-off interfering waves. Another advantage is that sensitivity increases with the ultrasonic frequency, the absorption in the pyro-electric layer increasing with the square of frequency. For the construction of a pyro-electric camera it is advantageous if the pyro-electric layer can be supported by a rigid plate forming the separating wall between scanning tube and cell and hence the field of vision can be rather large; see [716, 717, 1500].

13.12 Scanning Methods with Ultrasonic Pulses

13.12.1 B and C Scan Presentation; ALOK Method

By far the most sensitive acousto-optical imaging method remains that achieved by point to point scanning with a piezo-electric transducer and subsequent building up an image on the screen of a CR tube. Even in the early 1940s such devices were developed, mainly for medical applications (Dussik 1942 [353]) and since the 1970s also for materials testing.

In the early devices which used continuous waves the piezo-electric scanning still had all the handicaps of continuous through transmission. But using the pulse technique the sound image is established point by point, or by a synchronized transmitter in through transmission, or by the pulse-echo method using one transducer only.

Figure 10.25 illustrates the way to extend the A scan presentation to B or C scans, with a much higher information content. However, images produced in this way have several disadvantages.

The transverse resolution of both B and C scans is rather poor because of the broad directivity of the usual probes. Focussed probes have better resolution but only at the focus distance. Some further improvement is possible by using the elongated focus of the probe in Fig. 4.37.

A further problem is the difficulty of getting an image of large planar defects lying not precisely perpendicular to the scanning beam, as explained in Section 5.1. It can be solved by using the so-called *compound scanning* in which each point of a
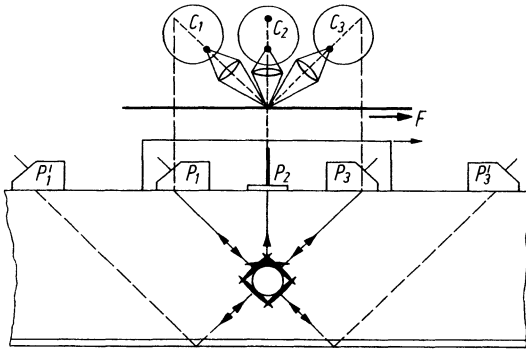
Fig. 13.6. Defect imaging according to Martin and Werner

layer of the specimen is radiated from different directions and the echoes received are attributed by computer to the same spot.

An old application of compound scanning to detect defects in rails is the method of Martin and Werner [983], which is illustrated in Fig. 13.6. The combination of probes P_1 to P_3 are single-crystal transmitter receiver probes separately connected to the CR tubes C_1 to C_3, where the echoes received are indicated by luminous points as in Fig. 10.26. All are projected onto a photographic film F (for simplicity shown as being turned 90° from the drawing plane) which is moved at a speed proportional to the scanning speed of the probe combination along the rail.

Because the time bases of the CR tubes are all inclined to the direction of the film movement at the same angles as between the beams of the probes and the direction of the rail, all echoes received from one location in the rail are combined into one spot on the film. This is demonstrated in Fig. 13.6 using the echoes received from a fish-plate bolt hole. Because of the beam spread the echo points are enlarged somewhat in a direction perpendicular to the beam direction, so that the hole is indicated by three short lines one each from the probes 1 to 3. Additional probes P_1' and P_3' give echoes via the back wall which are also indicated on the film by mirrors (for the sake of simplicity these are not drawn). It is clear that the reproduction of the shape of the defect-reflector is improved with an increase in the number of directions of echo sounding used in producing the image.

This principle has also been used in the ALOK method using modern computer techniques [577, 749, 575, 576, 193, S 186] and Fig. 13.7 illustrates this method.

When a normal probe scans the surface of a specimen which contains a reflector with equal reflectivity in all directions (a small side-drilled hole for example), the amplitude of the echo, because of the directivity angle of the ultrasonic beam, describes a curve with a central maximum directly over the reflector. On the other hand the curve of the echo transit time has a minimum, because the reflector is first detected in an oblique direction. Both the amplitude and the transit-time curves are schematically indicated in Fig. 13.7. The reflector must be positioned on a circle about the probe contact point, and on another circle with a radius proportional to the transit time corresponding to this position. Two different positional circles are indicated and the position of the reflector is at the intersection of
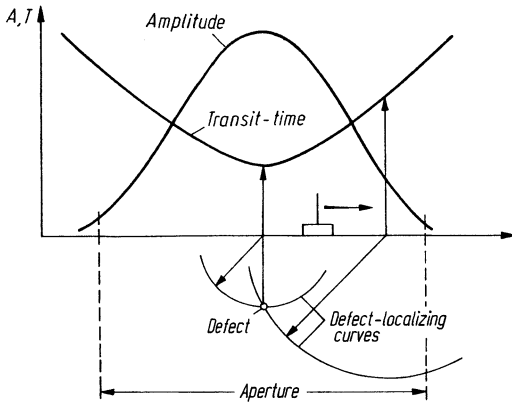
Fig. 13.7. Principle of the ALOK method (Amplituden-Laufzeit-Ortskurven)

the two circles. Of course in space the circles are spherical surfaces and for clarity in Fig. 13.7 transit time and sound path are drawn with equal scales.

This is the well-known *triangulation method* and for probes with separated transmitter and receiver the positional curves are ellipses or in three-dimensional space, ellipsoids. See also [819] and the 3rd edition of this book, page 555, Fig. 30.6.

For locating the defect position the echo amplitude curve is not necessary but it must be wide enough to allow scanning with sufficient echo amplitudes using sufficiently long paths so that a large angle of directivity is preferable.

With natural defects, from which we expect to get an image by the method some difficulties arise. The two curves of Fig. 13.7 are not necessarily symmetrical and they need not reach their maximum values for the same position of the scanning probe but with a sufficient number of sounding directions and positions some averaging takes place. The curves of defect position as written by a plotter and superimposed on one another indicate the actual position and shape of the reflector by a correspondingly high density of shading.

The averaging technique used by this method has also the advantage of suppressing scatter echoes from the grain structure since they change amplitude and position very quickly even with small changes in the probe position and beam angle. In practice the signal to noise ratio is considerably improved and it is particularly useful for example, when testing austenitic material.

Difficulties arising in the ALOK method when oblique specularly reflecting defects are involved can be partially overcome by iterative corrections with the help of computer-modelled defects [749].

The complete installation for using the ALOK method, due to the high-class computer circuitry and associated instrumentation, is quite heavy and voluminous. Nevertheless it has proved its ability in practice and especially in nuclear reactor testing.

A disadvantage of linear or planar scanning of a specimen is the relatively long time needed and by this method imaging in real time, for example in medicine for moving structures within the human body, is not possible. An important improvement was therefore the development of rapid scanners using oscillating probes

and/or mirrors to direct the beam into the specimen and such devices are now used for medical applications using a method called *sector scanning*. Examples for use in materials testing are given in [572, 530, 1639, 739, S 42]. Further progress has been made by avoiding mechanical scanning by using phased arrays, in which the beam angle and focus point are changed electronically (cf. Section 10.4.1).

13.12.2 The SAFT, P-Scan and SUTAR Methods

If the transducer in a linear scanning system, as for example in Fig. 10.25 b, has a very wide directivity angle in the plane of the drawing and a narrow one perpendicular to it, a defect will reflect echoes from different positions of the probe as in the before mentioned sector scanning. An image is obtained by drawing circles around the individual probe positions with radii calculated from the transit times by a computer and as in the triangulation method mentioned above. The intersection of the circles gives more or less the defect position and shape. Such a device by Hanstead [604] works rather slowly and fails if the reflector is a specular reflector inclined to the drawing (or scanning) plane.

This latter handicap is avoided by using a similar, but more complicated system, the so-called SAFT-UT technique (synthetic aperture focussing technique for ultrasonic testing) [503, 531, S 96]. The transducer has a broad beam aperture in all spatial directions and the specimen is scanned two-dimensionally in the form of a meander. The echo pulses are digitized and stored. After the scanning process is completed the defect image is reconstructed by a computer, producing a perspective (third-angle projection) image on the screen. The operational method involves dividing the complete volume of the specimen into small-volume elements and for each position of the transducer each volume element is provisionally considered as being a possible reflector position. All echoes with transit times corresponding to the distance from any particular probe position to each separate volume element are added up, having equal phases only if they are genuine echoes from a reflector in this volume element. All other echoes cancel each other statistically because they have different phases. The summed result for each volume element is a certain amplitude, which has an appreciable value only for elements containing genuine reflectors. The computer effectively synthesizes a transducer with a very large aperture and having a focussed beam directed to each separate point, thus explaining the name of the method. The resolution corresponds to the ultrasonic wavelength and because of the averaging quite high signal to noise ratios are obtained. By using extremely rapid computers it would also be possible to obtain real-time imageing [504, 1403, 1521, 333, 1361, S 149, S 48, S 12, S 44], see also Section 30.5. Real-time imageing by this system is of course only possible if phased arrays could be used in place of mechanical scanning.

Two simple systems still using mechanical scanning will now be described, namely the *P-scan* system (projected image scanning system of the Danish Svej-scentralen, SVC, Danish Welding Institute) and the SUTAR method (search unit tracking and recording system of the Southwest Research Institute of Texas, USA).
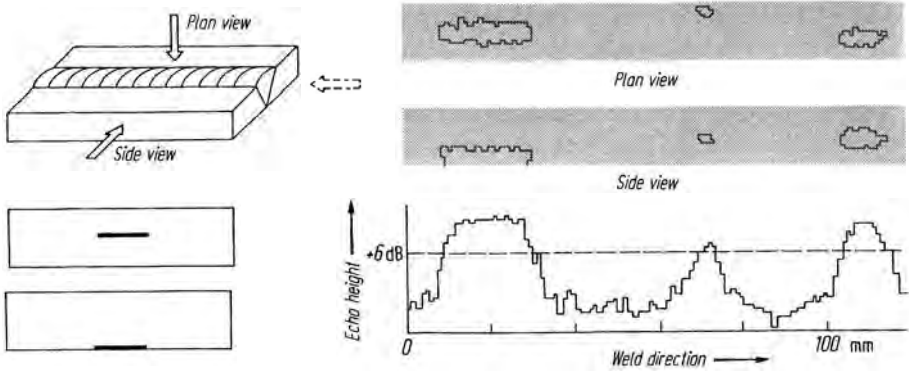
Fig. 13.8. Principle of the P-scan method on a weld

The P-Scan system is specially adapted to weld testing and it records, during mechanical scanning, the probe positional coordinates in addition to the data of signal amplitudes and transit times. As Fig. 13.8 explains the scan produces strip recordings showing C and B scans of the weld, together with the echo-amplitude curve as a function of the probe position coordinates.

In this way the three-dimensional position of a defect is given, along with its echo amplitude, for each section of the weld, and is therefore more informative than an X-ray image, which only gives a C scan. In a recent development a third plane of projection, perpendicular to the weld direction can also be added, as indicated in Fig. 13.8 by the dotted arrow [361]. The system using angle probes for weld testing, can be operated manually or fully automatically and the result can be watched on the screen of the computer even during scanning.

The P-scan method, because of the mechanical scanning, is rather slow, but in the case of much weld testing this is not of great importance. See also Section 30.5 and [945, 1122, 72, S 185].

Working on a similar basis the SUTAR system processes the data of the echo amplitudes, transit times, transducer positions and beam angles to produce a double C-scan image of the weld. Results may also be presented in the tabular form and with a map of the transducer positions during the test. In the case of the P-scan the probe position data is measured by mechanically coupled sensors but with SU-TAR the probe positions are established by using airborne ultrasound signals transmitted from electric spark gaps to microphones mounted on the probes, the microphones working as an array. The transit-time differences allow the transducer to be located and its angular orientation to be determined. See Section 30.5 and [69, S 161].

13.12.3 Methods Using Phased Arrays; Digital B-scan Unit According to Kino; Tomography

Mechanical scanning using a single probe can be replaced by a phased array (Sections 10.4.1 and 10.4.2), enabling much quicker working and avoiding the many problems of coupling a transducer to the specimen at high scanning speeds.

The linear array as in Fig. 10.36 simulates only the mechanical displacement of a single probe, whereas an array using electronically shifted phases when single elements are energized can also simulate swinging the beam direction. Simultaneously focussing of the beam can be simulated, varying with time so that the specimen is scanned in depth.

Real-time imaging of moving features has been achieved in this way in medicine [766]. However, in materials testing the usual poor quality of the surface still influences the sound field of the array. Thus these methods can only be successfully applied if improvement to the surfaces can be made.

The historical development of array methods can best be followed in the conference reports "Acoustical Holography since 1967" (Vol. 1 to 7) and later "Acoustical Imaging", see for example [1017].

The literature has greatly increased in recent years and we will only mention [1017, 59, 968, 660, 512, 517, 96, 971, 144, 81, 87, 106, 1611, 660, 893, 1043, 1502, 107, 680, 346, 1670, 131, 1258, 878, 96, 1194, 1520, 1619, 1661, 306, 614, 915, 1010, 1206, 304, 1546, 1662, 315, 1111, 1521, 517, 99, 1113, 397, 516, S 151].

Some devices can be reported briefly. Firstly there are systems which still use some mechanical movements. In [567] a traditional transmitter illuminates the object and the reflected wave field is received by a linear array after being focussed by a lens system. This system also contains an oscillating prism to shift the ultrasound image in a direction perpendicular to the linear array, which allows two-dimensional scanning.

With another system (EPRI report [121], see also Section 30), the linear array itself oscillates in a direction perpendicular to its length. Simultaneously the direction of receiving is swept through an angle.

In a more advanced system the sweeping of the beam is produced by a phased array and a digital computer, both for transmitting and receiving. At the reception stage the focussing range is simultaneously displaced with constant speed, but synchronized to the transit time of an echo in such a way that the focus is always suitably placed to receive any echo produced.

Many other instruments have been built using all possible combinations of traditional transducers and arrays aided by a computer to swing and focus the beam. For the arrays the phase control is carried out by either analog or digital methods.

The latest state of the art is represented by units which synthesize the aperture and the dynamic focus *after* the scanning is completed. The principle has already been explained for the SAFT-UT method (Section 13.12.2). Figure 13.9 illustrates schematically the system used by Kino and his collaborators [1188, 263, 1189]. The collection of all data takes only 10 ms and in this time each element of the array is used first as a transmitter and immediately afterwards as a receiver. All echoes received are digitized and stored after which the computer generates the synthetic dynamic focussing and builds up the B-scan image point by point. The whole process is equivalent to a single receiver of the size of the whole array, with a lens focussing the beam at each distance. The effective transducer and the fictional lens are synthesized, which leads to the terms "synthetic aperture" and "synthetic dynamic focussing", (because it varies with time). The echoes from each volume element are
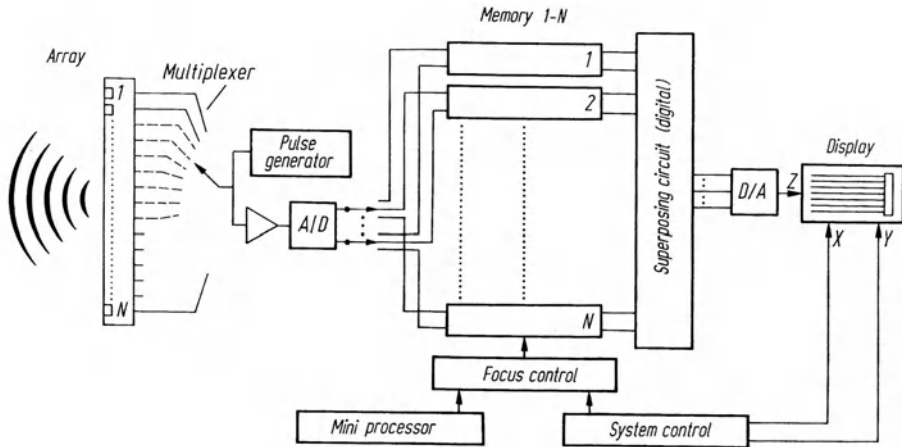
Fig. 13.9. Block diagram of a digital B-scan device [263].
(A/D = analogue/digital converter)

a   b
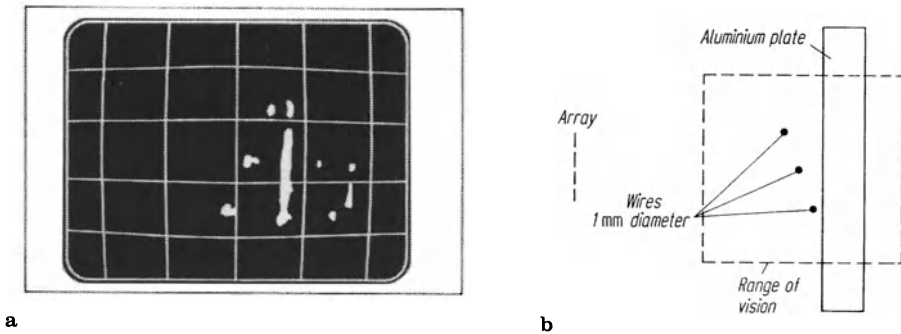
Fig. 13.10. a Acousto-optical image of the device in Fig. 13.9; b test arrangement

added-up by the computer, after artificially adjusting their individual transit times to correspond to the appropriate volume element, give considerable amplitudes by constructive interference only if there have been real echoes from this element. All other random signals cancel each other to produce negligible total values. The scanning plus the construction of an image takes a total of 30 ms, and results in 33 images per second, which can be considered as real-time imaging. Figure 13.10 shows an image of a test piece with artificial defects. Localizing and measuring the depth of natural surface cracks is demonstrated in [1189]. For further digital imaging units see [1748].

A special method of imaging is *tomography*, or sectional scanning, which has been developed for medical X-ray applications. In this system the absorption of X-rays is measured along many intersecting directions within a volume of a body. From the many measurements the distribution of absorption coefficients is recon-

structed, the screen image giving an X-ray B scan in terms of a multiple grey scale. If X-rays are replaced by ultrasound we achieve ultrasound computer tomography. As well as the attenuation of ultrasound, the transit times can also serve as measurement values and the display then also shows the distribution of the ultrasonic velocity. A further variant is reflection tomography or echo tomography, in which, instead of attenuation or transit time, the echoes received in many cross-sectional directions are stored before processing and display. Scanning can be carried out with all available methods, either mechanically or with arrays. Ultrasound tomography has found an application in measuring residual stresses in thick construction elements [662] as well as in medicine. For further information on tomography see [1582, 253, 663, 328, 354, S 182].

13.13 Ultrasonic Microscopy, SLAM and SAM Methods

In principle each of the methods described above can be used for microscopy by using high frequencies and two have been developed for practical application viz. the scanning laser acoustic microscope (SLAM) and the scanning acoustic microscope (SAM). The first one has already been described based on using the relief method (Section 13.1). The latter uses piezo-electric scanning (Fig. 13.11), with a piezo-electric transmitter cemented to the flat end of a glass cylinder, the other end of which is spherically concave and immersed in water. This arrangment generates a sharp focus in which a thin object can be placed for scanning and the receiver has an identical design. The scanning movement is synchronized with the CR-tube sweep. The transmissivity (or if required the reflectivity) of the specimen then controls the image brightness. The frequencies used are in the range from 100 MHz to 3 GHz, corresponding in water to a minimum wavelength of 0,5 μm and giving a
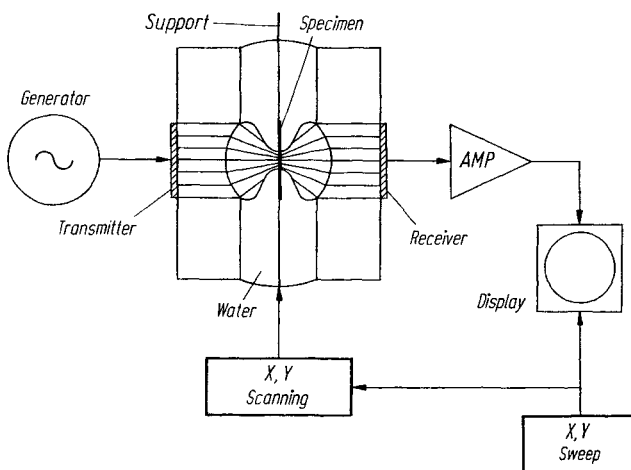
Fig. 13.11. Block diagram of the scanning acoustic microscope
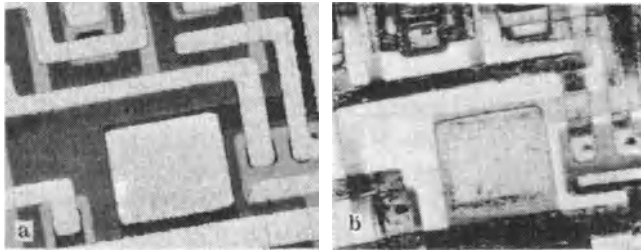
Fig. 13.12. a Optical and **b** ultrasonic image of an integrated circuit, produced by the SAM-instrument (Fig. 13.11) using 3-GHz frequency

corresponding resolution. Possible applications are thus for testing microelectronic products for laminations and porosity (Fig. 13.12).

Scanning microscopes of this type have been developed by Leitz (ELSAM Acousto-microscope) and by Sonoscan (HMS-300). The SAM principle was first described by Lemons and Quate in [916]. For further details see [1218, 776, 86, S 145] and for a general view of ultrasound microscopy see [917].

13.14 Acoustic Holography

13.14.1 Fundamentals

Holography is a two-step method of storing and reconstructing three-dimensional wave fields whether the type of wave is electromagnetic or mechanical.

It makes use of the fact that the total wave field produced by any object is fully defined by the wave field in one selected plane if that is known in both amplitude and phase, on the assumption that no new waves are generated within the space considered. The first step is therefore to record the wave field completely in both amplitude and phase on one plane, the result being called a *hologram*. In the second step, the wave field in the space considered is reconstructed using the same hologram.

Figure 13.13 explains the principle using an optical example after [914]. A laser beam is split into two parts one of which is deflected to form a reference wave in the plane of the hologram and the other part illuminates the object. The wave field reflected from the object is then superimposed on the reference wave in the hologram plane, resulting in a characteristic interference pattern. It is essential that both partial beams are coherent, i.e. that they have the same frequency and a fixed phase relationship, this condition being fulfilled by laser light.

One can understand the process by thinking of the object as a multiplicity of reflecting points or as secondary radiators. Each one emits a spherical wave, which together with the reference wave generates an interference pattern in the form of a circular concentric ring system as in a Fresnel zone plate. The complete hologram is the result of superimposing all these individual ring systems.
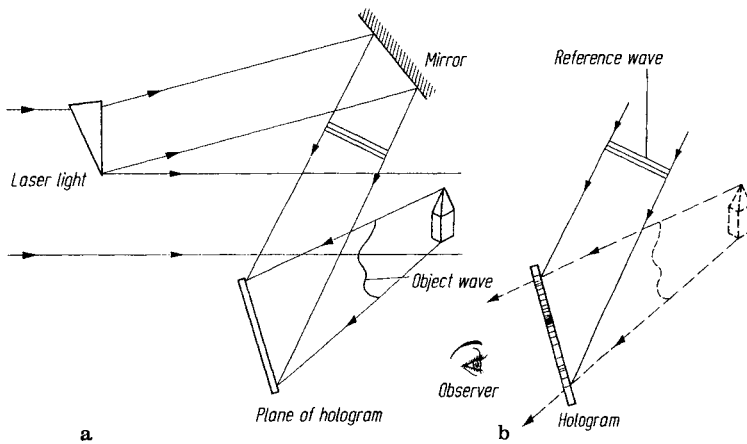
Fig. 13.13. Optical holography. **a** generating the hologram by super-imposing the reference wave and the object wave; **b** reconstruction of the image by illuminating the hologram with the reference wave

The optical hologram can be recorded photographically and the distribution of the photographic density corresponds to the distribution of the light intensity, or to the square of the light amplitude. If only such an amplitude record is used to reconstruct the image, the phase being neglected, the result will be a traditional two-dimensional photograph. However by superimposing the reference wave the intensity of the combined result includes both the amplitude and phase of the object wave and can therefore be used to reconstruct the three-dimensional image of the object.

The hologram must therefore be illuminated by the same laser light (Fig. 13.13) as used for the recording stage and the total object-wave field is reconstructed from the hologram by wave interference. A three-dimensional virtual image of the object is the result, along with a real image beyond the hologram (not shown in Fig. 13.13), but it is usual to suppress one of the two images. In Fig. 13.13 only the virtual image is seen by the eye of an observer.

The observer of the holographic reconstruction obtains a true perspective, three-dimensional, impression of the object when changing his position, especially if the apertures of the laser beam and the hologram are made as large as possible.

The main object of optical holography is the generation of three-dimensional images but the first step of making the hologram also plays a role in holographic interferometry which can also be used for materials testing. Using an object-wave field produced by reflection at the surface of a specimen, even very small surface displacements can be recognized from a change in the interference pattern. These variations can be the result of applied temperature or stress changes and the effect of inhomogeneities below the surface, which are thus made visible [272].

In the case of ultrasonic holography sound waves replace the laser light and generation of a hologram is easy because ultrasonic waves generated by a piezo-electric

transmitter are coherent. In fact two different transmitters energised by the same generator also give coherent ultrasonic waves.

There are several methods of generating the ultrasonic hologram and of reconstructing the image. Some of them use an equivalent of the optical methods, by superposing the reflected wave onto the reference wave in the plane of a detector. In principle all of the methods mentioned in Sections 13.1 to 13.11 are suitable, and all can be extended to become holographic methods, by adding a reference wave.

13.14.2* The Holographic Relief Method

As already explained in Section 13.1 the relief method can also be used for holography as shown in Fig. 13.14. Two transmitters are powered by the same generator and one beam penetrates the object, so generating the object wave, while the other forms the reference wave. The hologram is produced by ripples on the surface as produced by the local sound radiation pressure and optical illumination is made using a laser. In this case the hologram is a phase hologram, which by reflecting the laser light can reconstruct an optical object wave by diffraction, the non-diffracted light being suppressed. Though the quality of the resulting image is not bad the method has not found many applications because of the difficulty of keeping the surface undistorted, and also because of the rapid development of other methods which use piezo-electric scanning. For details see [182, 601].

13.14.3 Piezo-electric Scanning for Amplitude and Phase

In the acoustics field phase-sensitive receivers are readily available, in the form of standard piezo-electric transducers which collect all necessary information con-
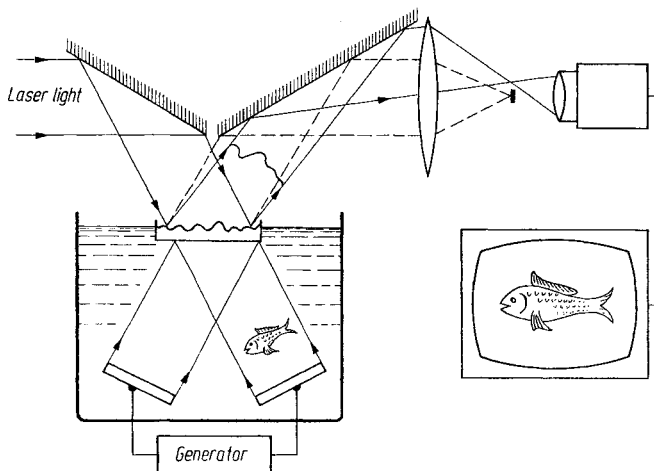
Fig. 13.14. Acoustic holography in real time to allow focussing at a selected depth using the relief method, combined with a TV camera
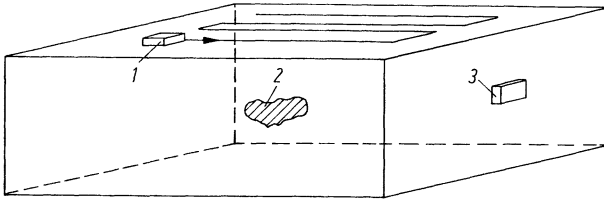
Fig. 13.15. Scanning with movable receiver and fixed transmitter. *1* receiver, *2* object, *3* fixed transmitter

cerning amplitude and phase. As Fig. 13.15 illustrates, a receiver scans the wave field which is generated by a fixed transmitter and subsequently affected by an object. The way in which the object modifies the field, whether it is by reflection or transmission, no longer matters and the wave field at the scanning surface is affected by both, as well as by reflections from the side walls, and it contains all the necessary information concerning the whole tested volume.

For the image-reconstruction a real reference wave is not needed, because it can be simulated electronically. It can even be completely omitted because the piezoelectric receiver measures both amplitude and phase; see [1025].

The reconstruction is better if the surface is fully scanned using a receiver with a very large directivity angle so making the sensitivity as independent of direction as possible. In practice therefore small crystals of about a wavelength diameter are used.

A variation of the arrangement in Fig. 13.15 could also be achieved with a moving transmitter and this can be realized in practice by using only a single crystal transmitter/receiver [1360], or better with a phased array so avoiding the mechanical movement and thus increasing the testing speed.

If the reconstruction must be made optically, the ultrasonic hologram has first to be converted into an optical one, as Fig. 13.16 shows in two alternative ways. The signal from the receiver controls the spot brightness of a CR tube and the sweep in two coordinates is synchronized with the scanning movement. Because of the slow speed of mechanical scanning the CR tube should be of the storage type and in this case the optical hologram can be made photographically. To reconstruct the image laser-light illumination is provided in the usual way.

The large differences between the optical and acoustic wavelengths is the reason for pronounced distortion of the optically reconstructed image. The depth dimensions are magnified in that ratio, i.e. by about 1000x. This distortion can be avoided by reducing the optical hologram in the same ratio but the reconstruction is then so small that it has to be remagnified and the distortion of the depth dimension returns. This is a fundamental handicap of ultrasonic holography by which in practice the three-dimensional properties of the image are lost. Effectively it only contains information about one plane and to obtain more, the scan has to be repeated several times for each important plane in the complete volume.

To generate the reconstruction of an acoustic hologram by a one-step method as in the optical case it is necessary to increase the total aperture in the ratio of the
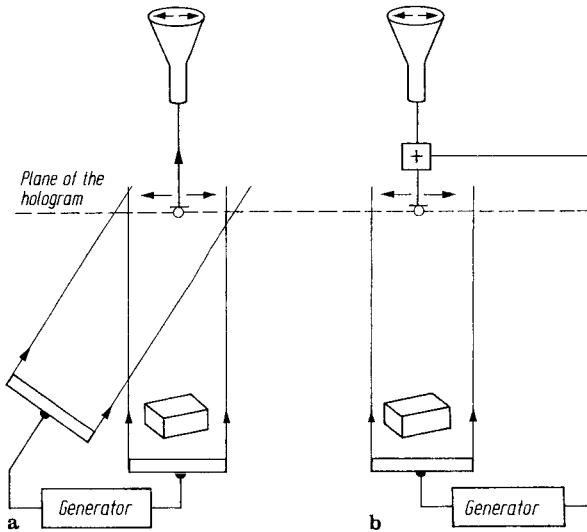
Fig. 13.16. Scanning of an ultrasonic hologram for conversion into the optical form. **a** with acoustic reference wave; **b** with electronically added reference wave

optical and acoustic wavelengths. In practice this means using a scanning surface of several meters in diameter which is impracticable.

The poor resolution in depth of this method is of course the same as that of the relief method, and in practice therefore the reconstruction is only two-dimensional. However, using multiple frequencies the axial resolution can be considerably improved, so that a two-dimensional scan can provide three-dimensional images, [S 18].

13.14.4 Numerical Reconstruction

This method is far more important than by using the optical approach. The signals from the scanning receiver are digitized and stored as in Fig. 13.17, the reconstruction being carried out by computer. The object image can then be drawn by a plotter based on the intensity distribution at the object position. Figure 13.18 shows the reconstruction of an artificial defect of about 2 mm in diameter at a depth of 100 mm in steel. It is only reconstructed in two dimensions because with this method also the depth resolution is poor.

13.14.5 Linear Holography; HOLOSAFT Method

With the system of Fig. 13.17 the evaluation time for two-dimensional reconstructions is still several minutes, in spite of using high speed computers. The amount of instrumentation is also considerable, and for use in materials testing a simplified
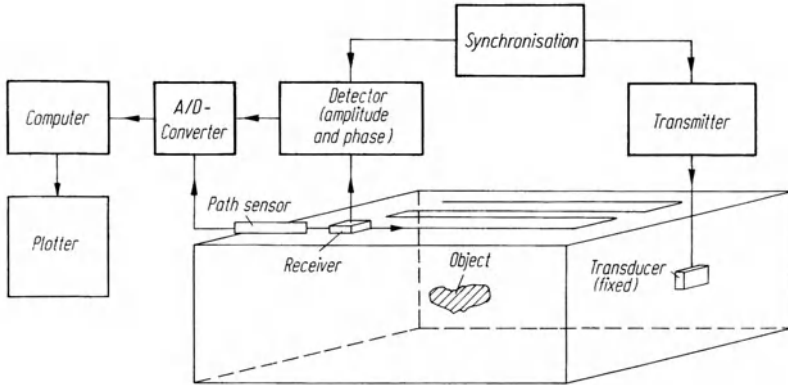
Fig. 13.17. Acoustical holography using mechanical scanning and numerical reconstruction
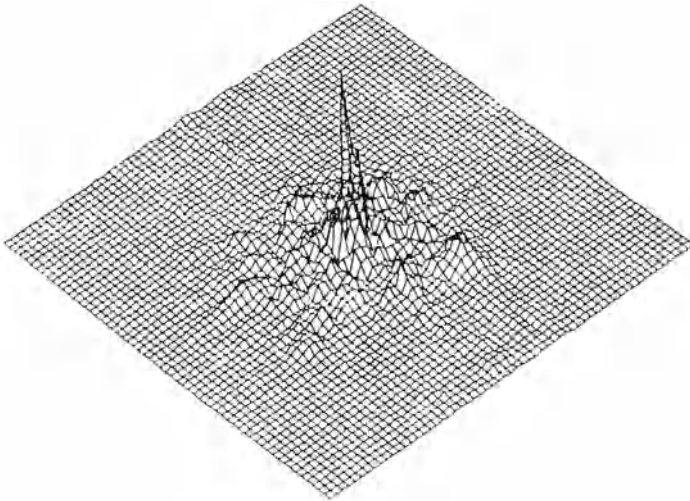
Fig. 13.18. Two-dimensional reconstruction according to [1360]

version has therefore been introduced by Kutzner and Wüstenberg [883, 884]. This is the so-called method of *linear holography*. The sound field reflected by the object is measured for amplitude and phase only along a line rather than over an area.

By using numerical reconstruction it is possible to obtain the dimensions of the reflector within the scanning plane and in particular its in-depth dimension (Fig. 13.19). At 512 individual points along a scanning line, separated by distances of 0.33 mm, both amplitude and phase values have been recorded at an ultrasound frequency of 2.2 MHz. The transmitter/receiver for obliquely incident waves has a 40° wide angle beam directivity, the artificial reflector being two 6-mm strips in water separated by a distance of 2 mm and at a distance below the scanning surface of 70 mm. The sound intensity distribution has been reconstructed along a semi-circle
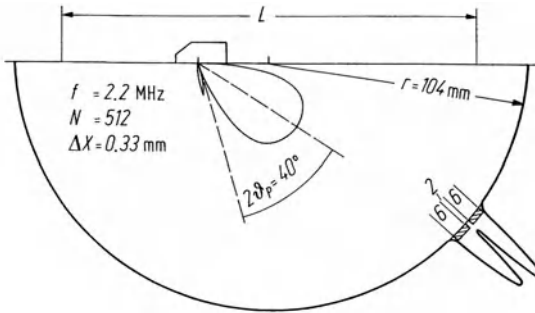
Fig. 13.19. Intensity distribution reconstructed over a circle as evaluated by linear holography. *N* equals the number of measuring points and Δx is the separation distance: *l* is the scanning aperature cf. [880]

drawn around the centre of the aperture. It has a remarkably good transverse resolution, but a rather poor resolution in depth.

For all the above-mentioned ultrasound holographic methods long pulses have normally been used and from this fact results good transverse resolution and a poor one in depth. To improve the latter short pulses can be used, as in the so-called *multiple frequency holography (MFH)* [402, 14]. This method has already been reported under the name SAFT-UT in Section 13.12.2.

The SAFT and MFH methods differ insofar as SAFT uses short pulses, whereas MFH actually transmits long pulses of different frequencies at each point and from these, short pulses are subsequently synthesized.

The volume of data and the time of computing is, however, much longer than with monofrequency (long pulse) holography. Under the name HOLOSAFT a combined system of SAFT and monofrequency holography has been developed [1076].
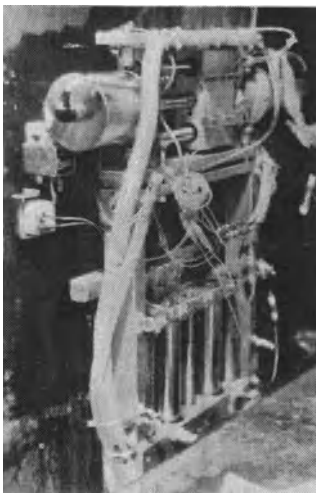
Fig. 13.20. Manipulator for holographic scanning of a weld (courtesy Bundesanstalt für Materialprüfung, Berlin)

It has proved to be a valuable method for testing materials and in particular to obtain information about the size and shape of a defect which has been already detected by simpler pulse-echo methods. It has been successfully used for testing welds in nuclear pressure vessels [1235, 1360, S 42, S 48], see Figs. 13.20 and 13.21.

Extensive description of the acoustic holography has been given by Greguss [572], Hildebrand [60] and Aldridge and Clémant [64]. Many papers are to be found in the proceedings of the international symposiums since 1967 called "Acoustical Holography" (Vols. 1–7) and later "Acoustical Imaging". cf. also the Ultrasonic Testing Documentation of the BAM [4] and the following publications [880, 937, 1649, 1075, 1360, 1363, 58 (containing many earlier references), 60, 1364, 881, S 173].
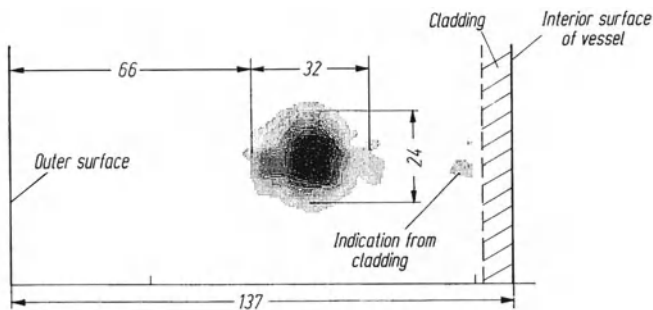
Fig. 13.21. Result of using the device in Fig. 13.20. Reconstruction of a defect with its dimensions in both size and position in the depth dimension (Bundesanstalt für Materialprüfung, Berlin)

14 Sound Emission Analysis (SEA)

This method of non-destructive testing will be treated only briefly because it has little similarity to traditional ultrasonic testing, and also because it has not achieved widespread applications in practice. Testing specifications for pressure vessels have, however, already been produced.

The method depends on energy within a specimen being released in the case of a growing crack or from deformation stresses. It is radiated from its source in the form of sound waves of all frequencies from the audible range up to high ultrasonics. However, for practical reasons observation is confined to frequencies around 1 MHz, because below this frequency there is too much disturbance from ambient noise, and for higher frequencies there is increasing attenuation in most engineering materials which restricts the range of observation. The sensors used are piezoelectric receivers similar to those used in seismology.

The simplest arrangement consists of a receiver, an amplifier and a pulse counter, to use the number of single pulses per second as an indication. Growing cracks for example are indicated by a rising pulse rate, as Fig. 14.1 shows.

This method can be further improved by simultaneously evaluating the amplitude of individual pulses or bursts, and sorting them into groups of different energy levels. The pulse rate depends on the energy thresholds in a characteristic manner,
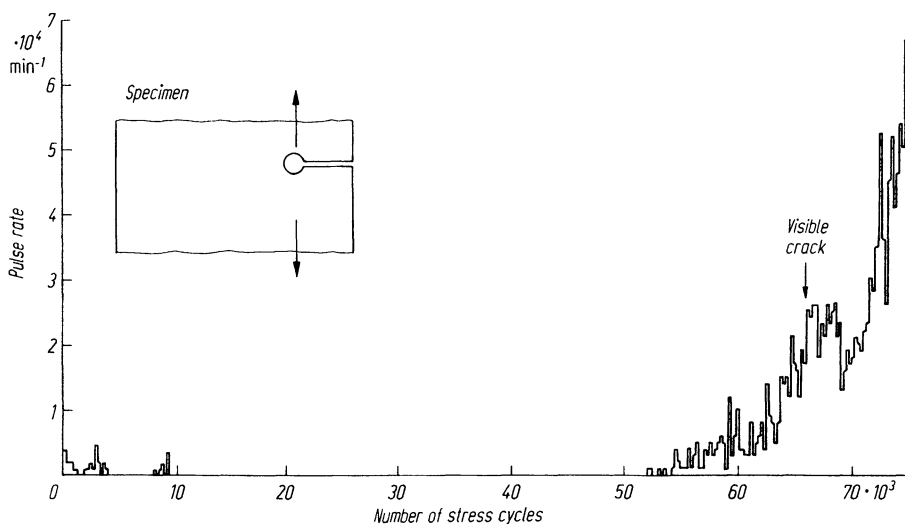
Fig. 14.1. Sound emission from fatigue cracks [1705]

from which certain conclusions about the behavior of the material, and its failure, can be drawn [350].

Another type of measurement uses the product of pulse rate and square of the amplitude to obtain information about the size of the source, and another method consists of analyzing the frequency content of the bursts. Figure 14.2 showing some typical burst shapes.

If more than one receiver probe is used, it is possible to determine the position of the source by triangulation, but the precision in favorable cases only reaches a few centimetres. In non-planar specimens the propagation of sound does not follow simple laws and velocity dispersion makes localizing more difficult [1308, 1592].

Nevertheless there are certain established applications and the best known is the testing of pressure vessels, tubes or other constructional elements by pressure tests or mechanical stressing [133]. The pressure needed is usually only a little higher than for normal use and does not destroy the test specimen. Growing cracks can be indicated by sound emission at their initiation. As well as metallurgical defects leaks can also be found by overpressure tests these showing a very characteristic noise pattern on the screen and is a useful application of SEA.

Fiber-reinforced materials such as GRC and CRC emit ultrasound if fibers are broken and when there are delaminations. Analyzing the pulses allows discrimination between different possible causes [183, 105].

SEA is additionally used to control welding processes in which the distribution of temperature causes large local stresses which can cause sound-emitting cracks. As well as these, phase conversions of the welded material also give acoustic indications if they are accompanied by volume changes. This potentially important application is however often badly affected by many extraneous noise sources [1210].

Further applications for controlling heat treatment processes, monitoring stress-relieving after welding, and the firing of ceramics, have been successful [724]. For further applications, still more remote from ultrasonic testing, see [1705].
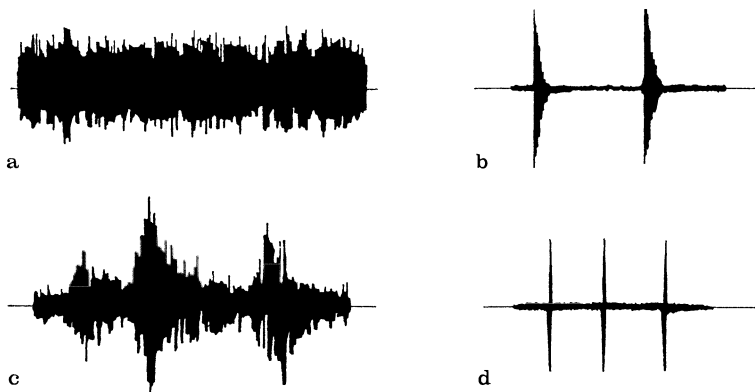
Fig. 14.2. Typical forms of sound emission. **a** Continuous noise from plastic strains or from leakage; **b** bursts of sound from growing cracks or from local areas of friction; **c** signals from wider areas of friction; **d** electrical interference

Part C | *General Testing Technique*

15 Coupling

15.1 Condition and Preparation of Surfaces

In any ultrasonic test the shape and roughness of the test surface is of decisive importance. On the one hand these factors often limit the sensitivity of the method applied, making it necessary to first prepare the surface; on the other they have an important influence on the wear of the probes used for continuous and routine tests if in direct contact with the specimen. The surface conditions, therefore, greatly influence the economics of testing.

All methods require uniform surface conditions for reliable and consistent flaw evaluation. In the case of direct contact where the probe is pressed onto a specimen covered by a thin film of coupling liquid, foreign particles or layers are very disturbing because they can considerably vary the thickness of the liquid film, and thus its transmission characteristics between one test point and another. It is therefore necessary to remove any dirt, loose scale and sand, for which rags, cotton waste and steel brushes are required. Often it is more effective to use a scraper, particularly in the case of loosely adhering layers of rust or paint which form air gaps and which may completely prevent the penetration of sound. In some cases a chisel or grinder may be used, preferably a rotating emery disc with flexible backing which adapts itself to the surface to be treated. Care must be exercised when using grinding wheels to prevent the creation of local concave spots which will result in bad or variable coupling. If large surfaces have to be treated, as in the case of automated testing, blasting with sand or steel shot gives the best results.

Uniform and strongly adhering films such as thin oxide layers or even paint, may not necessarily interfere with testing and are often preferable to an unevenly cleaned surface.

Where the surface can be dressed mechanically, it is more important to obtain a uniformly curved shape than high surface quality with an irregular contour. High surface quality is less important for the commonly used testing frequencies because

a surface roughness of less than 1/10 wavelength (i.e. of the order of 0.1 mm or less) contributes only relatively little to an increase in sensitivity. On the contrary, polished flat surfaces are often awkward to test because the probes stick due to suction and, therefore, cannot be slid along easily. Furthermore, the echo only slowly attains its maximum value on such surfaces after the liquid has escaped from the narrow coupling gap. In the case of contact tests on test blocks a planed surface is therefore preferable in view of the better reproducibility of the echoes. The quality of machined test surfaces in many recent standards is specified to be between 10 µm and 400 µm.

It must be kept in mind that the design of the probe has much influence on the quality of coupling. Hard faced probes (Section 10.4.1) which are often preferred for testing of metallic specimens, change the echo amplitude considerably when variations of the coupling gap thickness occur. For this fact the very variable transmissivity of an acoustically soft layer between two hard media (cf. Section 2.3), is responsible. Probes using soft coupling surfaces react much less than hard faced probes to such gap variations and they are therefore preferable when used on rough cast surfaces. Their basic sensitivity is, however, somewhat lower and the echoes are broader due to echo reverberations.

Such a soft layer of a thin plastic, for example silicone rubber can be permanently cemented to the specimen, thus enabling easy scanning with only little coupling material or even with dry coupling.

A roughness of more than 1/10 wavelength (peak to trough) impairs the coupling markedly. The acoustic pressure in the axial direction is reduced and greater lateral scatter occurs. This also impairs the beaming accuracy and increases the risk of lateral reflections simulating flaws along the axis. Roughness with a uniform pattern, such as turning grooves, can strongly amplify the lateral radiation at certain angles, like an optical grating, resulting in possible locating errors. Finally, very rough surfaces act on the sound beam like frosted glass on light: the beam becomes diffused and is scattered in all directions, making position fixing impossible.

In the case of irregular, uneven surfaces, e.g. with ripples as large as the probe, the coupling layer affects the ultrasonic beam very detrimentally since it is deflected irregularly from the normal and is focussed or defocussed. It is then a matter of chance to accidentally find a spot where the beam is still sufficiently undistorted to reach a given flaw, but even so an evaluation of the flaw by its echo amplitude is not possible. Acceptable conditions are ripples of less than 0.5 mm on an area of 50×50 mm.

A similar effect, however, may be produced by the material itself due to locally varying acoustic velocities, e.g. in grey cast iron or in the heat affected zone (HAZ) of austenitic welds (Section 28.1.6). In such cases a method might be applied in which a given spot in the test piece is irradiated successively along many different beam paths and from different contact points. This would require that the probe changes its beam direction for different contact points so as not to lose the target. The statistically distributed, favorable couplings then should make an individual flaw conspicuous against the interfering background. Some experienced operators already carry out similar practices without the aid of mechanical devices. A probe, particularly one with a soft plastic protective layer and using a liberal supply of cou-

plant, can be simultaneously shifted and slightly tilted and if during this procedure an echo persistently appears, probably indicating a real flaw, the surface may be locally improved for a more satisfactory test.

15.2 Curved Surfaces

Many test surfaces are cylindrical of which convex surfaces are better for making contact than are concave ones. On a convex, cylindrical surface the commonly used flat probe has a reduced contact face in the shape of a narrow rectangle, which enlarges the angle of divergence of the sound beam in the plane normal to the axis of the cylinder (transverse/radial) as shown in Fig. 15.1. In the longitudinal/axial plane the angle of divergence remains unchanged.

The reduced contact area also reduces the sensitivity proportionately as is shown in Fig. 15.2 using the echo from a test object, the sound beam being incident from a cylindrical contact face.
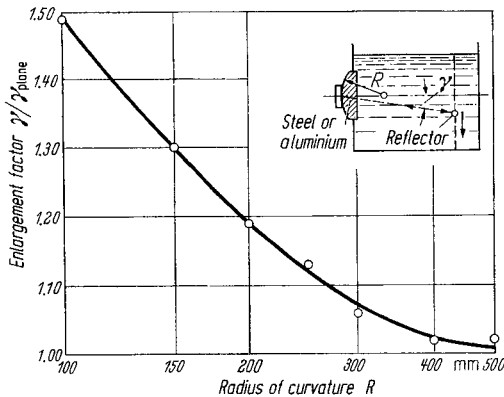
Fig. 15.1. Enlargement of the divergence angle of a probe in contact with a cylindrically curved surface; mean values from measurements on steel and aluminium with a 2-MHz probe, coupled through thin plastic film and light oil. The enlargement of the angle is compared with the free-field angle of divergence for a flat surface. For the echo field the enlargement factor has to be doubled. The measurements were made in the far-field in water
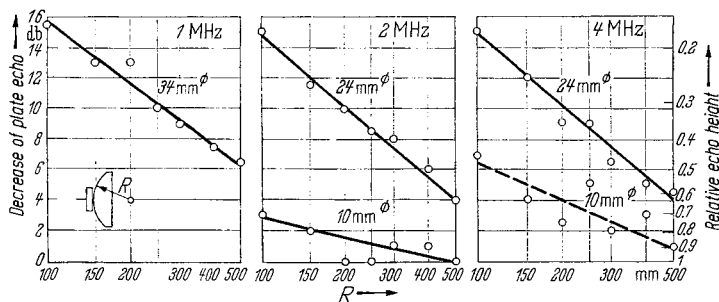
Fig. 15.2. Drop in sensitivity (in dB) in tests from a cylindrically curved surface, indicated by the decrease of the echo from a plane back wall as a function of the radius of curvature; measured in steel with probes coupled through 0.3 mm thick Vulkollan film and light oil

This sensitivity reduction can usually be compensated quite easily by using a higher gain, so that the detection of a defect is no problem. The evaluation of its size is, however, more difficult, because of the change in the sound field which influences the conditions for applying the DGS method. The effect is smaller with a probe of smaller diameter but for more exact measurements a test block with a similar curved surface, and containing artificial defects, can be used.

If angle probes using a plastic wedge are used the contact face can easily be adapted to a single curved surface, either by grinding the plastic wedge accordingly, or by attaching a preformed adaptor, using oil or cement. An exchangeable adaptor makes the angle probe more versatile but it slightly reduces the sensitivity and increases the number of interfering echoes as compared with one cemented-on or using a suitably ground contact face. After rough shaping with a file or grinding wheel the surface of the probe can be trued on the test piece itself by inserting coarse emery cloth and rubbing it in. It is not necessary to polish the surface of the plastic adaptor.

Even if, as indicated in Fig. 15.3 the apex of the curvature is placed at the sound exit point, the angles of the peripheral rays may easily exceed the usual angular sector, the steep angles producing interfering longitudinal waves, and the flatter angles may produce surface waves. If, as in Fig. 15.4, the axis of the curvature of the cylinder is located in the plane of incidence (e. g. tube tested in a longitudinal direction), the lateral divergence of the beam is increased. In the case of shallow beam angles (e. g. 70° and greater) this may likewise result in the appearance of interfering surface waves which leave the probe on both sides at an angle to the forward direction.

In order to avoid such disturbing waves it is advisable in the case of surfaces with strong curvature not to adapt the probe too perfectly but be satisfied with a smaller contact face. Such a face also increases the angle of divergence of the sound beam, acting like a diaphragm, but it avoids the disturbances caused by peripheral rays.

If the contact face is small it is difficult to guide the probe but this situation can be improved by attaching guides or supports which slide or roll on the surface. It is also possible to use a perfectly matched contact face as a guide and to limit the sound beam by sawing lateral slots into the plastic body parallel to the probe surface until the interfering waves have disappeared.
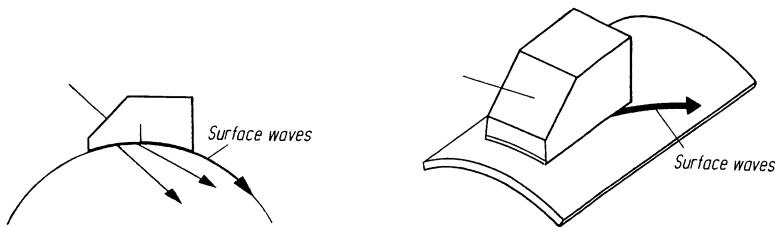
Fig. 15.3. Angle probe on curved surface
Fig. 15.4. Angle probe on cylindrical surface, axis of curvature in plane of incidence
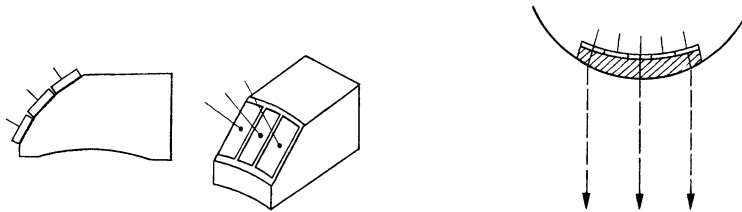
Fig. 15.5. Probes using a strip mosaic for adaptation to curved surfaces as shown in Figs. 15.3 and 15.4

Fig. 15.6. Probe for concave surfaces, using a strip mosaic and adaptor

Specimens with strong curvature of the test surface should preferably be tested by immersion technique, using flat or focussed probes. To avoid interferences by surface waves the end of the near-field (or quasi-focus) should be adjusted to lie on the surface. Figure 15.5 shows another possibility for avoiding problems with curved surfaces in which the sound beam is focussed by using transducers mounted as a strip mosaic.

Although the situation should be avoided wherever possible sometimes flat, normal probes have to be used on concave surfaces. The test sensitivity is then very low because the centre of the probe does not make contact, nor can this difficulty be overcome by using more couplant. It is better to use specially designed rectangular adaptors which, in combination with a focussing arrangement using several crystals, compensate the curvature by a lens effect, as indicated in Fig. 15.6. Mosaic assemblies consisting of several small, spring-mounted transducers have also been used on curved surfaces.

15.3 Coupling Media and Coupling at Elevated Temperatures

Attempts to compensate for the effect of a curved or rough surface by means of a coupling medium have met with little success because all liquid coupling media have a much lower acoustic impedance than the materials of most test pieces. This applies also to liquids containing metal powders in suspension, and to mercury which must be excluded, if for no other reasons than its cost and toxicity. Of all chemically suitable liquids glycerine has the highest acoustic impedance. By far the most generally used couplant is oil, and for contact tests usually an oil of medium viscosity, grade SAE 30. On smooth surfaces, and for making measurements, oil of lower viscosity, or even diesel oil, is preferable and on rough surfaces oil of higher viscosity is useful.

For testing on vertical walls and overhead, a non-dripping couplant is more convenient. Grease and petroleum jelly can be used for this purpose but they are expensive and unpleasant to handle so that a watersoluble paste such as stiff size is preferable.

A suitable paste can readily be prepared on site with cold water and methyl cellulose (wall paper paste). Since the dried-up residue is difficult to remove, glycerine or a substitute can be added to prevent premature drying. Corrosive action of the water on metal surfaces is reduced by adding an inhibitor such as trisodium phosphate.

Cleaning of test pieces, probes and hands, which can be badly affected by oil, when using paste, is best achieved by simple application of water. Therefore, a concentrated sugar solution, which is even cheaper than some oils, is also sometimes used. Compared with oil, ordinary water has the disadvantage that it does not always wet surfaces satisfactorily, which is an important requirement for good coupling. However, by adding a wetting agent water is a very useful couplant either as a stationary layer on horizontal surfaces or in the form of a constant flow of water between probe and surface. In the case of angle probes the liquid can be brought directly to the contact point through a small hole in the plastic wedge.

From a theoretical point of view it is interesting to note that thin metal foils, such as copper 20 µm thick, used in an oil layer, considerably increase the transmission between the transducer and a flat metal surface (Firestone [456]). This effect is explained by the improved matching due to the increased effective acoustic impedance of the whole coupling layer.

Highly viscous materials, such as mixtures of wax, oil, and pitchpine resin can be used for coupling normal (0°) probes generating transverse waves to flat surfaces, because these materials can transfer shear forces when used in thin layers. A bare crystal surface can also be dry coupled by pressing it onto a smooth surface with a clamping device or a heavy weight. In the laboratory the crystal is sometimes stuck onto the surface by a heated sticky wax, by low melting point salts, for example "Salol" (salysilic acid phenyl ester) or even for more extended use with an epoxy resin.

Surprisingly, enough acoustic transmission is still possible on hot surfaces when using water coupling, in spite of the generation of steam. For instance, hot metal plates up to about 250 °C can be tested by the transmission method, using free water jets (see Section 24.1).

Up to 400 °C the coupling can be improved considerably, according to Höller [677, 679, 877], if water is passed at high velocity through a gap between the probe and the plate. In this case it is even possible to use standard TR probes and the echo method, which is indispensible for detecting small flaws in plate. With these methods, the temperature of the surface is presumably reduced locally to about 100 °C [877]. It is always advisable first to wet the test piece with a compressed air-water mixture for example, and even at very high temperatures on red-hot plates, some acoustic transmission can still be observed.

Another solution when testing hot surfaces is achieved by dry coupling a steel roller with a high contact force [741, 77, S 148], the probe being mounted inside the hollow shaft (Fig. 15.7). Using special material for the delay line in the shaft and curved transducers, focussing at the contact point is possible.
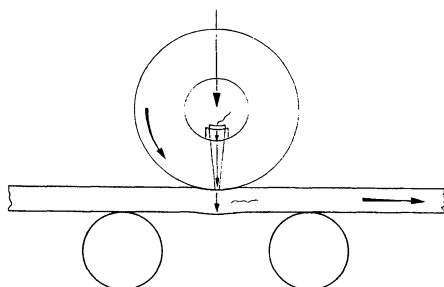

Fig. 15.7. Continuous testing of hot plate by means of a "roller probe" (according to Uozumi and Narushima [1549])

With dry coupling on hot surfaces transverse waves rather than longitudinal waves can also be used. The advantage of the former, in addition to the lower acoustic velocity, is the greater acoustic impedance difference for certain flaws and interfaces giving an improved reflectivity (Lynnworth [962]). In practice a liquid coupling layer inside the roller is not useful so the transducers, (typically six in number) are cemented directly onto the internal surface and are selected electrically in turn. The measuring points on the test piece then are spaced by 1/6 of the circumference of the roller, which for many purposes such as wall thickness measurements in continuous casting (see Chapter 33), is acceptable.

For liquid coupling on hot surfaces up to 300 °C, live-steam cylinder oil with a high boiling point, or special oils such as Shell Nassa oil, can be used. Up to almost 600 °C paste-like materials such as bitumen, Shell Microgel grease, Midland Silicone Ms 550 or a high-temperature coupling paste ZGM of Krautkrämer-Branson have given satisfactory results. The latter consists of a liquid with high boiling point mixed with a powdered insoluble salt. At the lower temperatures the liquid serves as couplant and at the higher temperatures the fused salt [236]. This makes possible brief coupling periods (2 to 3 s) when using probes which are fitted with a heat-resistant delay line. This method can be applied in all instances where the test result is required quickly and where probe cooling during the measurement intervals is possible. This applies, for instance, to wall-thickness measurements on pipelines in accordance with programmed spot checks.

For still higher temperatures metal delay lines are also used, these being water cooled to prevent the heating of the probe by the test piece. For probe contact one of the above-mentioned couplants or also dry coupling with high pressure can be used [1039, S 29, S 113, S 102].

If a photographic record is made of the screen image, the coupling time on hot test pieces can be reduced to fractions of a second, this method being used by Carnevale and Lynnworth [958] for measuring sound velocities and coefficients of elasticity up to 1000 °C. In these tests transverse-wave transducers were dry coupled, or longitudinal – wave transducers coupled with silicone grease.

Using a cooled metal adaptor or nozzle it has also been possible to transmit ultrasound into liquid metal. The liquid metal must, however, wet the adaptor, which is not always easy to achieve. For cast iron Lehtinen [911] has used an adaptor made of stainless steel coated with borax (see also [901, 977]).

According to another suggestion by Farrow [430] hot specimens could be tested by inserting a fusible spacer between transducer and test surface, resulting automatically in liquid coupling but no practical applications of this principle have as yet been reported. Regarding probes for elevated temperatures see Section 10.4.4.

Air should also be mentioned as a couplant, in spite of its very limited application possibilities. Air transmits sound at ultrasonic as well as sonic frequencies, particularly for direct transmission from probe to probe at frequencies below 2 MHz. In this way it is possible to use the sound transmission method to test acoustically soft materials, such as brake linings, gypsum boards, soft rubber or plywood. In this way the internal bonding of such materials, and even of soft rubber layers bonded to steel, have been tested. In this case the acoustic impedance step is not excessive on at least one of the two surfaces of the test piece. As in the case of an air gap in a solid body, which according to Fig. 2.3 starts to transmit if it is thin enough, a thin sheet of steel approximately 0.1 mm thick will transmit the sound coupled to it from air sufficiently well to make testing for laminations appear feasible. Testing of composites by airborne ultrasound is reported in [S 139].

Luukkala and Merilainen have even succeeded in acoustically testing plates of aluminium, brass, copper and steel up to a thickness of 10 mm by using plate waves and air coupling [956, 957]. They used capacitor-type transmitters and receivers at frequencies around 100 kHz. In the most favorable case (0.5 mm aluminium) the transmission loss was only 35 dB, as compared with the direct transmission from the transmitter to the receiver in air.

Sound transmitted in air can be used with the echo method for the measurement of distance from solid objects or for determining certain profile changes, e.g. when testing rails, see Section 23.2. At present, however, conventional pulse-echo testing of solid objects, using air as a couplant, cannot yet be realized [305, 853].

The difficulties which arise when using piezo-electric transducers on hot surfaces do not affect electromagnetic probes (see Section 8.4) or laser methods (Section 8.6). For applications in practice of the former method see [1632, 765, 1047, 1319, 710, 1068, S 91, S 17].

15.4 Checking of Coupling

Uniform coupling at all contact points on a test object is very important for quick and reliable evaluation of the readings. Occasionally coupling uniformity can be checked by means of a back-wall echo and an experienced operator can also do so by means of the varying, small grass indications on the screen display. For this purpose the zero line should always be allowed to show a little "life". When angle probes are used the quality of the coupling can, with a little experience, also be deduced from the sliding resistance when shifting the probe caused by the presence of grit or small foreign bodies, or "seizing" if there is not enough couplant.

In automatic testing, the abovementioned methods of checking which are available in manual operation no longer apply so that other solutions have to be applied. One of these is to use electronic devices which can signal the state of coupling or measure it for use in corrective gain control techniques. It is possible to use a back-wall echo for this purpose although this has the disadvantage that a flaw as well as bad coupling will reduce its amplitude. Similar considerations apply to a through-transmission signal between two angle probes which face each other on opposite sides of a welded joint (see Section 28.1.1) its purpose being to control the gain for the pulse-echo operation of one of the probes. The transmission signal is affected therefore by the coupling variation of the test probe but, additionally by a flaw and by coupling fluctuations of the second probe. The only ideal solution would be a measurement of the acoustic energy immediately under the testing probe which has actually passed through the contact surface. This is possible on a metal surface if the probe is coupled via a non-metallic delay line which combines an electrodynamic-receiver arrangement at the contact point [756], cf. Section 8.4. So far, however, this method has not been exploited.

Another solution has been described by Lutsch [953]. On a crystal transducer with only moderate rear face damping, the intensity of the reverberations depends largely on the degree of coupling. If therefore their amplitude is measured by a monitoring amplifier gated immediately behind the transmitting pulse, the output signal of this amplifier can serve as a measure of the degree of coupling.

According to a suggestion made by van Valkenburg [742] the degree of coupling of an angle probe on metal plate, as shown in Fig. 15.8, can be checked by means of a second crystal which beams through the plastic body normally into the sheet metal, producing a series of multiple echoes. The height of the echoes or the length of the echo sequence can also be converted into a go/no-go indication which actuates a signal.

These multiple echoes are also utilized in some automatic testing installations for gain control.
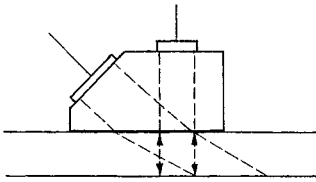
Fig. 15.8. Coupling check with angle probe on plate, using separate transducer

15.5 Coupling Through Intermediate Layers, via Watergaps and by the Immersion Method

Wear and insufficient constancy of the degree of coupling are the reasons for the disfavour into which direct contact of the transducer has fallen. Direct contact makes wear of the transducer unavoidable because the probe, during scanning, cannot always only be placed on and taken off again. Sometimes it must be shifted, because any change in the flaw echo while shifting the probe provides valuable information on the flaw concerned for the examiner. The modern piezo-ceramic materials are far too soft for use in direct contact and so currently probes with protective layers are always used in contact testing. Spacing layers consisting of liquids or plastics cut down the wear but if the pulse-echo method is used a corresponding increase in the amount of interfering echoes must be accepted.

Soft protective layers with properties similar to self-adhesive films allow dry coupling within certain limits on smooth surfaces (cf. [S 25]). Very low frequencies can be transmitted even by dry coupling through conventional soft coupling faces into wood for example [1701], see also [S 28, S 82].

The screen traces shown in Fig. 15.9 demonstrate the effect of spacing layers as a function of their thickness. A layer of 0.1 mm already greatly reduces the sensitivity compared with direct contact and considerably broadens both the transmitting pulse and the echoes because with only moderately damped probes the reduced coupling also reduces the damping. Since the length of a 4-MHz wave in oil or water is about 0.4 mm, the 0.1 mm couplant thickness constitutes a quarter wavelength layer. The out and return path of a zigzag reflection equals half a wavelength, and results in destructive interference (Fig. 15.9 b). In the case of a layer of double the thickness (Fig. 15.9 c) one therefore obtains by constructive interference approximately the same echo height as in case a. The interfering oscillations following the transmitting pulse and flaw echoes have, however, increased.

A 1-mm layer as in case d already produces a very indistinct picture which would make the indication of a flaw in the test plate practically impossible. In addition the echo height is low, so that the gain has to be increased. As shown in Fig. 15.9 e the interfering reflections from the coupling layer can be greatly reduced, according to a suggestion by Martin and Werner [987], by adding to the coupling layer a layer of an absorbing material. In this case Vulkollan was used which, if serving as coupling layer, has the added advantage of high abrasion resistance. The gain, however, has to be increased still further, the same echo height as in the case of direct contact being reached only by a tenfold gain increase.
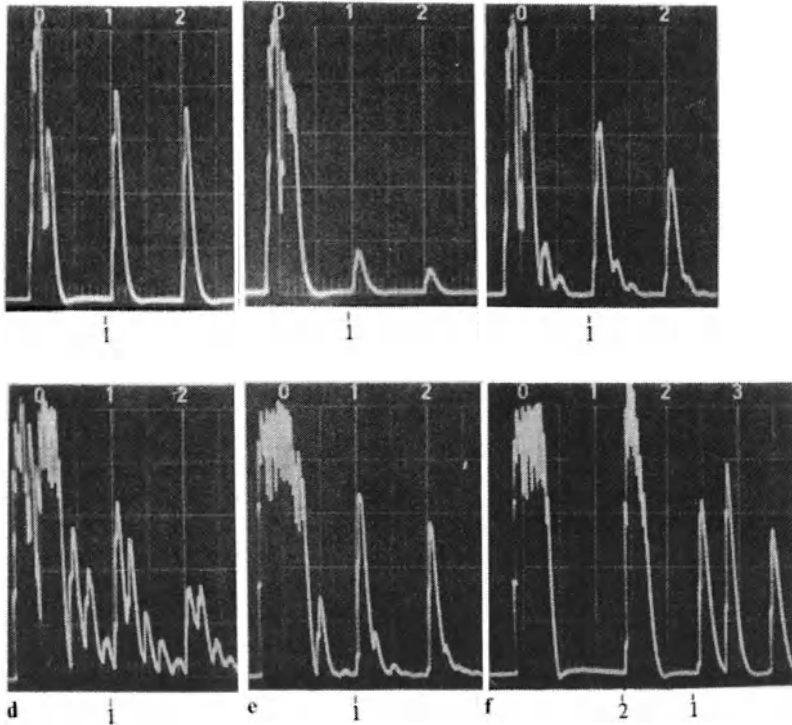
Fig. 15.9. Coupling with increasing layer thickness d (oil or water), probe of 4 MHz on 20 mm steel plate. Calibration: 1 scale division = 20 mm in steel. 1 = back-wall echo, 2 = surface echo. **a** direct contact, $d < 1/100$ mm; **b** $d = 0.1$ mm; **c** $d = 0.2$ mm; **d** $d = 1$ mm, gain compared with **a** to **c**, about 3 times higher (plus 10 dB); **e** $d = 1$ mm, but with inserted Vulkollan film, gain 10 times higher ($+20$ dB); **f** coupling by immersion technique, $d \approx 6$ mm, gain as in **e**

If thicker coupling layers are used the surface echo and its multiple echoes become separated from the transmitting pulse. The screen display then becomes clearer and the first surface echo now takes over the role played by the transmitter pulse in direct contact. If the coupling layer is water it is only necessary to choose a water gap of sufficient length for the second surface echo to occur after the first back-wall echo from the test piece. In the case of steel and water the gap should be greater than 1/4 of the specimen thickness since the ratio of sound velocities is 4:1.

For *continuous automatic testing* good close contact has been achieved in some cases by using an endless plastic belt or a closed tire (Fig. 15.10). In both cases the life time is often quite short, especially on rolled surfaces, due to damage by particles of scale [1700].

As alternatives there are two other possibilities:

1. The *water-filled gap:* There are no wear problems but the thickness of the gap is critical, especially if used without an added absorbing layer.
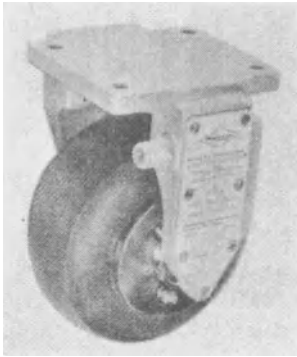
Fig. 15.10. Sperry wheel probe

2. The *water delay line* or the *immersion method:* Because of the presence of multiple echoes between probe and entry surface, the separation distance must be chosen according to the thickness of the specimen. The echoes are not broadened by reverberations, so that the method can be used for thin plate specimens.

For an example of *water-gap coupling* see Fig. 15.11 which illustrates a device for plate testing. The echo pattern (Fig. 15.12) shows a sequence of regular multiple echoes but small defects in the plate would not be revealed by their individual echoes, but only by the reduced length of the main sequence. To detect individual echoes, the standard probe in the device must be replaced by a TR probe, using a water gap of only a few tenths of a millimetre, by which the first surface echo is only broadened a little. If the water for the delay line exits from the probe housing directly onto the plate being tested at sufficient pressure, a water cushion is formed
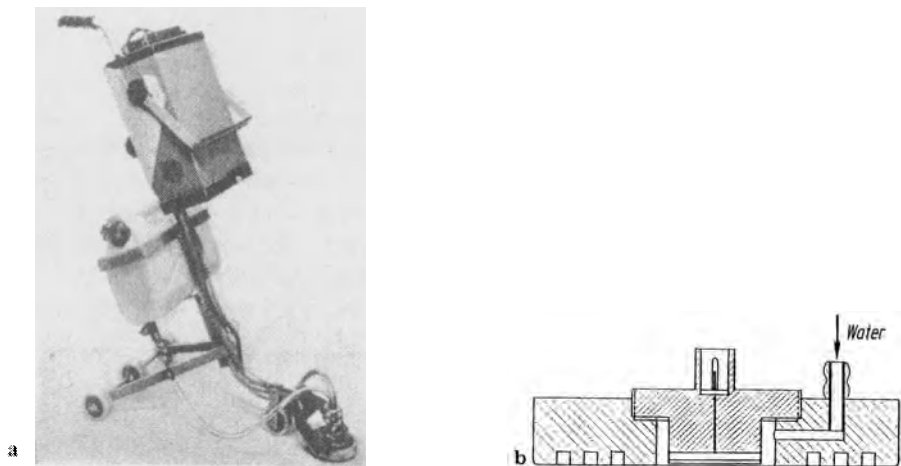
Fig. 15.11. Plate tester, design Krautkrämer, photograph and schematic cross-section
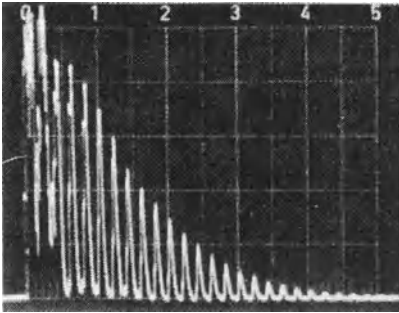
Fig. 15.12. Screen picture of a flawless plate 10 mm thick, tested by water-gap coupling (plate tester of Fig. 15.11)

on which the probe can slide without being in direct mechanical contact with the surface, see Fig. 15.13, Erdman [393].

For a continuous testing method it is preferable to couple such a device to the test specimen from below rather than from above so that the delay line will always be filled with water. Only a small flow or water will then be required to maintain a good coupling to the specimen but with a stronger flow this system can also be applied from above or on a vertical wall. It is of course necessary to avoid air bubbles.

If water is discharged from a pipe at high pressure, a jet is produced by means of which contactless coupling of the probe to the specimen can be effected over a gap of 100 mm and more. This is important in cases where during rapid, automated testing the equipment might be damaged by an uneven surface or by projecting parts of the test piece, for example when testing heavy plate. This water jet technique is also useful for testing curved parts such as aeroplane wings and has been called *squirter technique.*
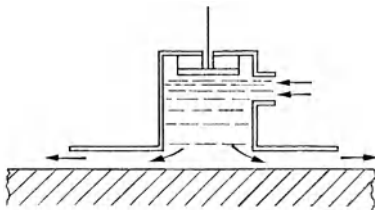
Fig. 15.13. Method of coupling and guiding the probe by means of a water delay line and water cushion, according to Erdman
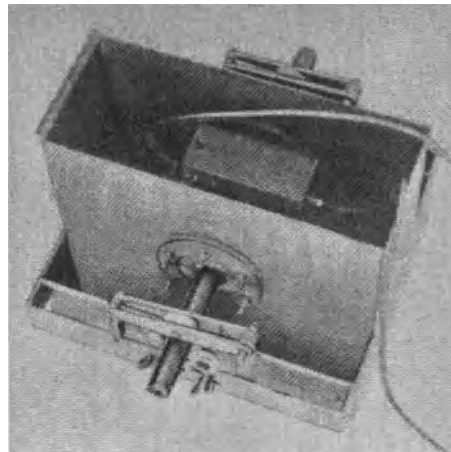
Fig. 15.14. Transit tank with sealed windows for testing round bar or tubing by the immersion technique

When thin water jets are used about 10 mm long, this coupling method is only useful for through-transmission techniques, since splashing at the contact point generates too many interfering reflections. The consequent high noise level prevents the use of the echo method, but if the water jet diameter is about 40 % wider than the crystal diameter, an echo technique can be used, at least for short jets up to about 50 mm long but because of the high consumption of water this method has been rarely applied.

The tire probe of Fig. 15.13 is effectively a combination of an endless plastic belt and a liquid delay line, and is filled completely at elevated pressure. The probe is fixed on the axis of the wheel at a distance of several centimetres from the contact surface and it can also be tilted to introduce transverse waves into the specimen.

Coupling by means of the immersion technique in which the test piece is completely immersed in liquid, was already used during the 1930s for the first tests involving through transmission. Today it has found much favor for automated testing installations since it gives constant coupling without wear and also the possibility of changing the incidence angle to allow the use of either longitudinal or transverse waves without changing the probe. It is largely applied in aircraft and aero-engine manufacture for the testing of plates, discs and extruded profiles, the large costs and space demands being fully justified by the increased reliability and speed of testing.

Modern installations for automated immersion testing make use of digital controls for both the manipulation of the specimen and of the probes. These can be manipulated in three or more different axes by a microprocessor according to a predetermined program, which can also include adjustments of the ultrasonic unit and for carrying out data processing [184].

The immersion technique is also occasionally used for the manual testing of complex parts such as steel and light-metal forgings for aeroplane construction. For this purpose a cylindrical tube (nozzle) is mounted in front of the probe so that it fills with water when held below the surface. Its open end can be plane or shaped to match the form of the specimen and so ensure an easy control of both water gap and beam direction.

For testing long work pieces, such as rods, strips or wires by the immersion technique they can be passed through a water tank either by locally bending down or by passing them through a short test tank with two windows fitted with rubber seals which match the shape of the specimen, as shown in Fig. 15.14. After the specimen is inserted the tank is rapidly filled by a pump.

For the various coupling methods discussed above the costs of the installation increase with increasing complexity but at the same time the economy and testing reliability are also increased. The choise of a system depends therefore largely on the nature and the importance of the testing problem and on the investment costs involved. Practical examples will be discussed in part D.

16 Interference Effects of Boundaries.
   Complex Sound Paths and Screen Patterns

Mode changing by reflection at boundaries of the test piece sometimes results in a basically quite simple testing technique becoming more complicated and interpretation of the screen picture more difficult. The principles of wave propagation discussed in Chapter 2 will therefore be applied to a few frequently occurring cases.

16.1 Effect on the Sound Field of Boundaries Parallel
   to the Beam Axis

Disturbances of normal propagation already occur if the peripheral rays of the lobe strike a lateral boundary as in Fig. 16.1. This affects both the sensitivity and the direction of the original beam and additional echoes are produced by split-off transverse waves.

The reflected longitudinal wave interferes with the direct wave and changes the original sound pressure and the sensitivity, as indicated in Fig. 16.2 by measurements of the echo from a small flaw in comparison with its undisturbed echo height.

Instead of actually measuring the echo height of a small reflector in steel at various distances from the lateral wall, the pattern of the acoustic pressure on the smoothly ground back wall was recorded by means of a small receiver, and the squared values plotted in Fig. 16.2 as echo heights.

The most troublesome disturbance is the strong decrease of the sensitivity close to the wall, making it difficult to detect small flaws such as incipient cracks in this zone. In such cases a common mistake is to move the probe as close as possible to the edge. According to Fig. 16.2 this is wrong because for flaws in the far-field the sensitivity becomes smaller, the closer the probe is to the edge. The result is even worse if the probe projects partially over the edge, because then its maximum sensitivity also decreases in proportion to the remaining contact area. For this situation the probe diameter should be chosen as large, and the frequency as high, as possible. For a given probe and a given flaw distance there is always an optimum dis-
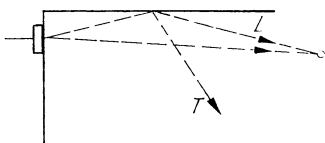
Fig. 16.1. Interference from lateral boundaries
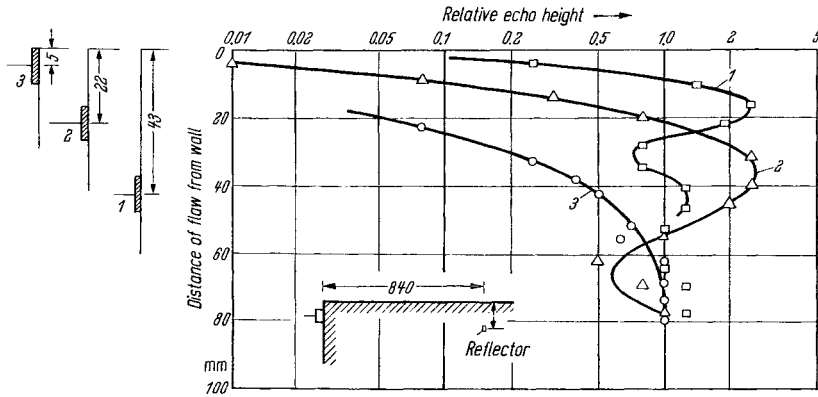
Fig. 16.2. Influence of a plane lateral boundary on the longitudinal sound field: relative echo height of a small flaw plotted as a function of its distance from the wall, measured at a distance of 840 mm in steel, for three positions of a 4-MHz probe of 10 mm in diameter

tance between probe and edge which gives maximum sensitivity and which may have to be determined with the aid of artificial flaws, such as lateral saw cuts. However, close to the side wall the sensitivity is always much lower than in the free-field; such flaws are therefore better located by one of the methods illustrated in Fig. 16.3, which are also much more suitable for size estimation.

The physical cause of the reduced sound pressure close to the lateral wall is the $\lambda/2$ phase change of the reflected longitudinal wave. The nearer the angle of incidence is to 90°, the closer to unity will be the coefficient of reflection and the more completely will the reflected wave cancel the direct wave. This phase reversal occurs also for a transverse wave which oscillates parallel to the plane of incidence and whose sensitivity along the wall is therefore also reduced in the same way. This phase reversal disappears only if the plane of oscillation is parallel to the wall in which case the presence of the wall increases the sound pressure to twice its value.

According to Fig. 16.2, the influence of the wall distorts the directional characteristic of the probe so that it has a shape which is no longer axially symmetrical. It shows maxima and minima but the principal maximum no longer lies on the probe axis but moves away from it, as well as from the wall, by a distance which increases as the probe gets closer to the edge. This disturbance can be vividly described by
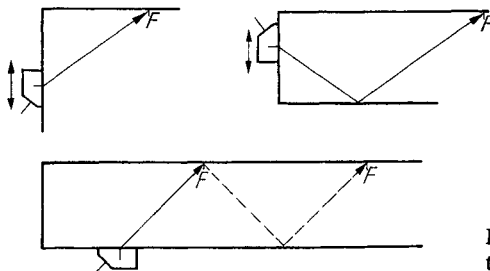
Fig. 16.3. Method for locating flaws close to the surface

imagining that the original sound beam close to the wall is forced away from it so that it appears to bend, the deflection being the greater the more the probe approaches the edge. With such a distorted beam normal flaw locating is no longer possible.

A side wall also influences the back echo which is greatly reduced near such a wall. However, the larger the diameter of the probe, the more it averages the maxima and minima which in general are therefore less pronounced in the back-wall echo than shown in Fig. 16.2. But in any case it should be kept in mind that the amplitude of the back-wall echo can no longer be used as a basis for applying the DGS method of defect sizing, as with an undistorted beam.

Occasionally the side-wall effect can be useful (e. g. for detecting a crack parallel to the axis of the beam as shown in Fig. 16.4) if for some reason the crack cannot be irradiated at right angles. The back-wall echo (or in the case of through transmission, the measured value) reaches a minimum if the crack is exactly in the axis of the beam. It then effectively separates the beam into two laterally deflected lobes. If the crack is not too short in relation to the thickness of the specimen, it may be situated on the front surface, on the back wall or in between with the same effect. For good results in this test, probes with a small diameter and low frequencies should be used.

Another method of detecting such a crack which may lie on the back wall, or in mid-section, is by using the so-called tip reflection. Provided the crack tip is approximately parallel to the surfaces (i.e. perpendicular to the plane of drawing in Fig. 16.4) and has an appreciable extension in this direction, it can be detected from the remote face by using the edge wave generated by the tip (see Sections 2.7 and 19.3). An additional advantage lies in the possibility of assessing the crack depth by measurement of the echo transit time.

So far the disturbance caused by a single side wall has been discussed. In the case of a plate tested from the edge, a second wall is added. For a wave in the plate the disturbance caused by the one wall can be compensated again by the other wall at certain points. Over longer distances and in thin plates however, the longitudinal wave is nevertheless strongly damped and only the parallel polarized transverse wave (SH) can be used, as shown already in Section 2.5, Fig. 2.21 a.

Surface waves can travel with low attenuation along the narrow face of a specimen, as for example in testing the flat faces of hexagon bar. Apparently the side edges do not cause any interference and can even increase the transmission range.
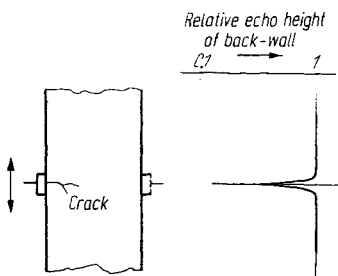
Fig. 16.4. Detection of a crack by disturbance of back-wall echo, reduction of echo height, schematic

If the side faces are not flat but for instance cylindrical, as when round stock is tested longitudinally, the focussing effect of the laterally reflected waves is added. This effect is particularly strong if the sound is radiated into the cylinder coaxially. The wave which is reflected all around the periphery, can, at certain points on the axis, produce much higher sound pressures than the direct wave so that interference is compensated. This has the effect that the sensitivity along the axis of long cylinders may be higher than in the free space. The pattern of the acoustic pressure as a function of distance is, however, not uniform because minima are produced by the interference of waves reflected several times and this makes it very difficult to estimate the size of small flaws.

If the influence of side walls is neglected, this can frequently lead to wrong results when using test blocks with artificial flaws. In the case of the pulse-echo method the minimum distance between the beam axis and a side wall required to avoid disturbing influences can be estimated as follows. The path using a side-wall reflection will be longer than the direct axial path and if the difference exceeds about four wavelengths, the first four oscillations of the pulse will not be disturbed. In the case of short pulses, i. e. when using instruments and probes with a wide frequency band, it is already possible to distinguish the maximum in this undisturbed zone of the pulse from the disturbed zone which follows it. According to Fig. 16.5a this requires that

$$2s - a > 4\lambda$$

or approximately

$$\frac{2d^2}{a} > 4\lambda \,.$$

In steel for example

$$d > 3.5 \sqrt{\frac{a}{f}} \text{ mm} \quad \text{(frequency } f \text{ in MHz).}$$

This applies to the sensitivity along the axis, whereas for an unaffected back wall echo double the length a should be used which gives, according to Fig. 16.5b for steel:

$$d > 5 \sqrt{\frac{a}{f}} \text{ mm} \,.$$

a $d > 3.5 \sqrt{\frac{a}{f}}$ [mm]   b $d > 5 \cdot \sqrt{\frac{a}{f}}$ [mm] f in MHz
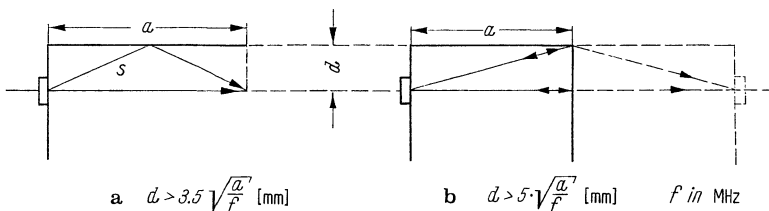
Fig. 16.5. Minimum distance d of a probe from an edge, to avoid interference by the side wall in steel. a For small flaws on the axis; b for the back-wall echo

Thus for an undisturbed back-wall echo the distance from the wall should be greater than that needed for an undisturbed echo of a small flaw on the beam axis.

Example. In order to obtain an undisturbed back-wall echo from a depth of 100 mm with 1 MHz, the probe should be at a distance not less than 50 mm from any side wall. The angle of divergence of the sound beam, i. e. the diameter of the probe, is in this case irrelevant. For an undisturbed echo from an artificial flaw the separation from the side wall must not be less than 35 mm.

16.2 Secondary Echoes Produced by Split-Off Transverse Waves

Transverse waves split-off as shown in Fig. 16.1 leave the side wall of a steel specimen at an angle of about 33° to the normal, and, according to Fig. 2.6 and Diagram 1 (Appendix), almost independently of the angle of incidence of the longitudinal wave, provided this angle already exceeds 70°. In the case of grazing incidence (close to 90°) the amplitude of the converted wave is small, but increases with smaller angle of incidence (acc. Diagram 1 in the Appendix, curve T_{t1}). On the other hand the amplitude of the probe beam lobe decreases for increasing angles to the axis. Because increasing angle to the beam axis means decreasing angles of incidence on the side wall, the mode changed wave reaches a maximum for given values of probe diameter, frequency and distance from the edge, at a particular distance (Fig. 16.6). This maximum moves closer and becomes stronger if the probe is moved closer to the edge.

If this transverse wave is reflected directly back to the probe as shown in Fig. 16.7a, this hardly interferes because the probe is insensitive to it. However, if, for example, the wave is reflected at a corner back along its own path, it is partially retransformed into a longitudinal wave, producing an interfering echo as shown in Fig. 16.7b. On the screen calibrated for longitudinal waves this echo has the apparent flaw distance

$$a_s = a + 1.53\, d \quad \text{in steel.}$$
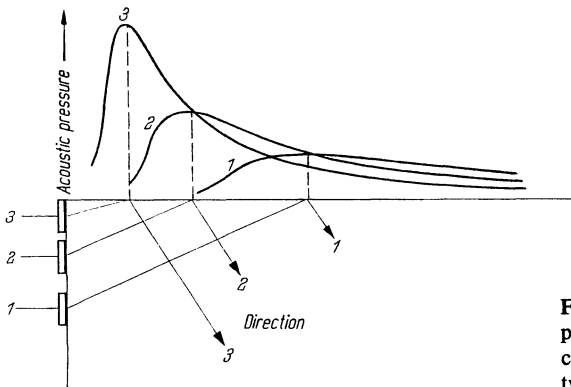
Fig. 16.6. Distribution of sound pressure of split-off transverse wave, calculated for various distances between probe and edge
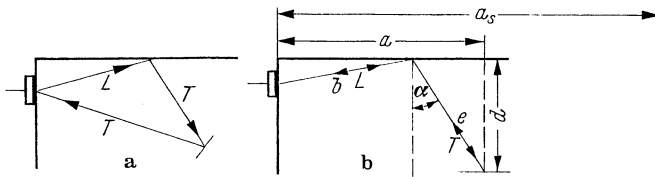
Fig. 16.7. Splitting off of transverse wave. **a** Direct reflection without interfering echoes; **b** mode reconversion into longitudinal wave

Derivation, using the designations of Fig. 16.7 b: The transit time is composed of the time for distance b at wave speed c_l and the time for distance e at speed c_t

$$\frac{a_s}{c_l} = \frac{b}{c_l} + \frac{e}{c_t}.$$

However, in the case of grazing incidence

$$b \approx a - d \tan \alpha.$$

Furthermore, $e = d/\cos \alpha$, and for the critical angle α, $\sin \alpha = c_t/c_l$. Thus generally

$$a_s \approx a + d \sqrt{\left(\frac{c_l}{c_t}\right)^2 - 1} \, . \tag{16.1}$$

The error in this approximation is less than 1 % for waves with angles to the axis up to 10°, i. e. for most cases encountered in practice.

To avoid a false interpretation of those echoes arising as in the examples of Fig. 16.8, the apparent position of the flaw at the distance a_s should be irradiated from another direction, or the test from the same probe position should be repeated by using a more sharply focussed beam. If the echo now becomes smaller, this points to a possible interference phenomenon. Echoes in the form of a *grass mound* are frequently obtained from the rough surface of a hole, or from threads, as shown in Fig. 16.8c. The real reason for this phenomenon is readily demonstrated by the fact that the mound moves closer if the probe is shifted towards the edge or even slightly over it.

If the side walls are parallel, for example in plates, rods, and cylinders, the transverse wave can also travel between the walls along a zigzag path and produce multiple interfering echoes. According to Fig. 16.9 the transverse wave, when it strikes the wall, is partially reflected as a transverse wave at an angle of about 33°, and partially retransformed into a longitudinal wave reflected at a grazing angle. If the test piece concerned is narrow enough, the longitudinal wave, after reflection by the back-wall, can again return directly to the probe. The echo obtained in this way has, however, only half the delay shown in Fig. 16.7 b and will therefore appear only 0.76 d behind the back-wall echo. At the next transverse reflection the reflected transverse wave is again split, resulting in a further secondary echo shifted by 1.53 d. In this way a sequence of secondary echoes is obtained in narrow test pieces behind every back-wall echo or flaw echo, as shown schematically in Fig. 16.10. In
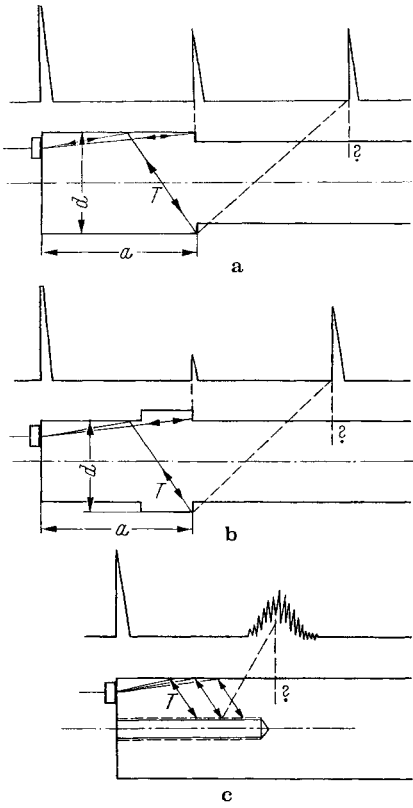
Fig. 16.8. Examples of the creation of interfering echoes by transverse waves. **a** Shaft with shoulder; **b** ditto, but note that d is no longer the diameter; **c** shaft with rough or threaded hole
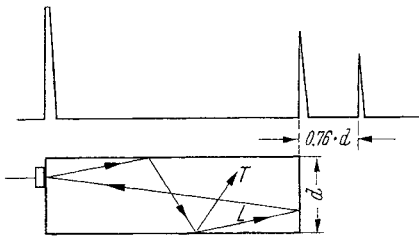
Fig. 16.9. Secondary echoes in a narrow cylinder (steel)
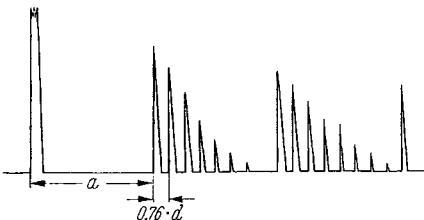
Fig. 16.10. Schematic screen trace of a specimen (plate, round bar or square bar) with $d : a = 1 : 6$, with multiple back-wall echoes and sequences of secondary echoes (steel)

the case of rods of rectangular cross-section this sequence consists of two tele-scoped sequences corresponding to the two different cross-sections.

If such test pieces have no real transverse flaws, the secondary echoes cannot be mistaken for flaws because they appear only after the end echo. However, if true flaw echoes are present, the secondary echoes cause confusion and they may give the impression that there are more flaws in the specimen than are actually present.

For very long and slender test pieces the secondary echoes may be more pro-nounced than the back-wall echoes and they may finally be all that remains, ap-pearing in the form of a "beard" (bell-shaped sequence of closely packed echoes), when the back-wall echoes themselves have already become very weak.

Secondary echoes appear as a long sequence of considerable height only if the conditions for transverse reflection are good at all points because of smooth sur-faces. If, however, in the case of a given specimen these echoes are badly distorted in spite of good surfaces, this indicates longitudinal flaws in the specimens which, while still passing the direct longitudinal wave, suppress the oblique transverse waves.

16.3 Triangular Reflections

In a solid cylinder or a sphere, the peripheral rays from a normal probe making an angle of 30° with the beam axis may produce reflections in the form of a triangle as in Fig. 16.11. The angle of divergence of a flat probe used on small-diameter round stock, or even more so on a sphere, is particularly wide and the triangular echo there-fore very pronounced, as shown in Fig. 16.13. In addition to this reflection path in the form of an equilateral triangle, there occurs also a triangular reflection with wave conversion according to Fig. 16.12. Both types of interfering echoes appear be-hind the first back-wall echo, at the following apparent distances:

triangular wave without conversion: $a_s = 1.30\,d$,
triangular wave with conversion: $a_s = 1.67\,d$ for steel,
    $= 1.78\,d$ for aluminium.
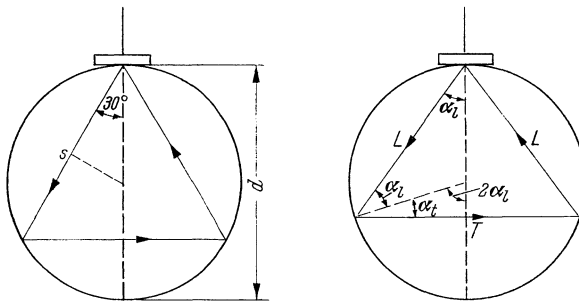
Fig. 16.11. Triangular reflection in round stock without mode conversion
Fig. 16.12. Triangular reflection with mode conversion
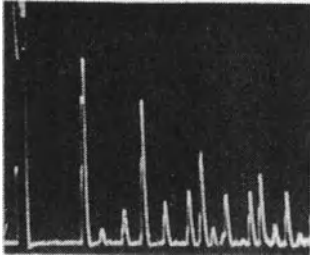
Fig. 16.13. Screen trace when testing round steel bar (40 mm in diameter)

Figure 16.13 shows the screen trace for 40-mm steel round stock at 4 MHz.

Derivation: according to Fig. 16.11, in the equilateral triangle with side s, we have

$$\frac{s}{2} = \frac{d}{2} \cos 30°$$

and the total sound path $3s = 3d \cos 30°$. Of this, however, only half must be taken because the screen is calibrated in distance and not in total echo path. Therefore, irrespective of the material

$$a_s = \frac{3}{2} d \cos 30° = 1.30 \, d. \tag{16.2}$$

From Fig. 16.12 and using trigonometry it follows that

$$\alpha_t = 90° - 2\alpha_l$$

and from Snell's law of refraction (Eq. 2.3)

$$\frac{\sin \alpha_t}{\sin \alpha_l} = \frac{c_t}{c_l};$$

therefore

$$\sin \alpha_l = \frac{l}{4} \left(\sqrt{8 + \left(\frac{c_t}{c_l}\right)^2} - \frac{c_t}{c_l} \right)$$

and the apparent flaw distance

$$a_s = d \left(\cos \alpha_l + \frac{1}{2} \, \frac{c_l}{c_t} \sin 2\alpha_l \right). \tag{16.3}$$

Calculating the angles we obtain for

steel $\alpha_l = 35.6°$, $\alpha_t = 18.8°$,
aluminium $\alpha_l = 36.5°$, $\alpha_t = 17.0°$,

from which the above-mentioned values for a_s can be calculated.

Echoes of multiple triangular paths appear after the second back-wall echo, where they complicate the screen picture. As in the case of all echoes created by peripheral radiation and imperfect contact, the height of the triangular echoes fluctuate considerably with the degree of coupling and the spreading of the couplant. They can interfere with the detection of flaws if the direct flaw echo in front of the first back-wall echo is not used but instead the W echo shown in Fig. 3.16. According to Figs. 3.14 and 3.15 a zone of high sensitivity occurs a little beyond the axis owing to the focussing effect of the cylindrical surface. Therefore, larger flaw echoes usually appear between the first and the second back-wall echo, where the triangular echoes are also located.

In the case of round stock less than 30 mm in diameter, the dead-zone in front of the probe often masks the direct flaw echo. It is then preferable to use a TR probe.

16.4 61° Reflection

Sometimes a reflection of the longitudinal wave takes place in a steel specimen at a boundary inclined at 61° as shown in Fig. 16.14. This is accompanied by conversion to a strong transverse wave and if simultaneously reflection from a side wall occurs, strong echoes from an apparently greater depth are obtained.

Derivation: From the geometrical conditions

$$\alpha_l + \alpha_t = 90°$$

and from Snell's law (Eq. 2.3)

$$\frac{\sin \alpha_l}{\sin \alpha_t} = \frac{c_l}{c_t}$$

the angle α_l, which at the same time is an angle of the prism, is given by

$$\tan \alpha_l = \frac{c_l}{c_t}.$$

The corresponding values are for

$$\text{steel:} \qquad \alpha_l = 61°, \qquad \alpha_t = 29°,$$
$$\text{aluminium:} \quad \alpha_l = 64°, \qquad \alpha_t = 26°.$$

If the entrance point of the beam in Fig. 16.14 is shifted, the apparent echo path, i. e. the transit time, remains unchanged: at first glance this may seem surprising because this changes both the travel distances for the longitudinal and transverse waves. However, the longer path at the higher longitudinal velocity exactly balances the shorter path of the slower transverse wave, as shown in Fig. 16.15. The longitudinal portion of the path along *2-2* is longer by a than along the path *1-1*, while the portion of the transverse wave is shorter by b. The transit times along these paths are a/c_l and b/c_t, respectively. From the triangle it follows that

$$a : b = \sin \alpha_l : \sin \alpha_t$$

and from the law of refraction

$$a : b = c_l : c_t.$$
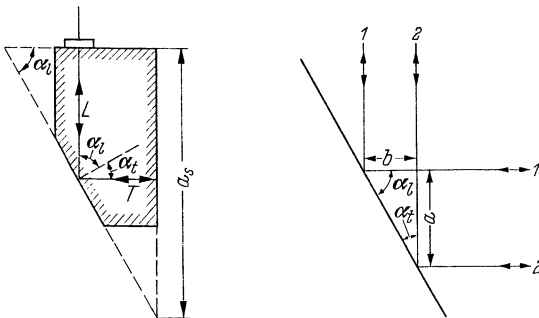
Fig. 16.14. Reflection accompanied by 90° deflection and mode conversion in a 61° steel prism (64° for aluminium)

Fig. 16.15. Conditions for mode conversion in a 61° steel prism

Therefore

$$\frac{a}{c_l} = \frac{b}{c_t}.$$

If the faces of the test piece in Fig. 16.14 are extended so that the dotted triangle is obtained, the transit time of the echo is identical for all beam entrance points along the shorter side and the apparent distance of the echo is equal to the longer side.

Diagram 1 in the Appendix indicates that the product of the two reflection coefficients during the mode conversion, along the outward and return paths, is approximately unity, but the waves of the same mode which also occur are reflected away unfavorably, and are very weak. This device therefore represents an almost loss-free converter from one mode into the other, with 90° deflection. One can also begin with a transverse wave, beamed from the perpendicular wall on the right in Fig. 16.14, assuming that its direction of oscillation is parallel to the plane of the drawing. In the case of aluminium the conversion efficiency is still better.

The effect can also serve to determine the direction of polarization of a transverse-wave generating probe. If the transverse wave (shown as T in Fig. 16.14) falls onto the 61° face there will only be a mode-changed L wave if the polarization is parallel to the drawing plane. The direction of the polarization is found with greater precision by turning the T-wave probe until the L-wave echo reaches its minimum. Then the polarization is perpendicular to the drawing plane. Instead of the L-echo, the through-transmission amplitude with a L-wave receiverprope may also be used.

A practical example of such a mode-change reflection occurs in the testing of a cylindrical hole near a right-angled corner as shown in Fig. 16.16. This could arise for example when checking a high-pressure hydraulic cylinder for the presence of incipient cracks on the cylinder wall. Even when there are no real flaws the following geometrical echoes will occur:

1. Direct echo from hole at distance d_1,
2. Echo from side wall after a 45° longitudinal wave reflection.

This echo appears at the distance

$$d_1 + d_2 + 2r(1 - \sin 45°) = d_1 + d_2 + 0.568\,r$$

irrespective of the material.

It should be noted that at this point the mode-converted transverse wave produces no interfering echo because it is diverted at an unfavorable angle and disappears.
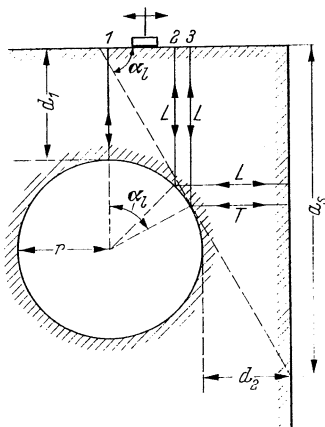
Fig. 16.16. Interfering echoes when checking a cylindrical hole for incipient cracks

3. Echo from side wall after a 61° reflection and L/T conversion.

The apparent distance is calculated by the formula

$$d_1 + d_2 \tan \alpha_1 + r\left(1 - \tan\frac{90 - \alpha_1}{2}\right) = d_1 + 1.82\, d_2 + 0.742\, r$$

for steel.

If, for example, $d_1 = d_2 = r$, the echo distances for cases 1, 2 and 3 respectively are as $1 : 2.57 : 3.56$.

Naturally, in addition to any real flaw echoes, other echoes can also occur depending on the shape of the specimen, such as a back-wall echo for L waves passing through the gap between the hole and the side wall and multiple echoes arising from the above cases.

When testing axles from the end face (Fig. 16.17) phantom echoes can arise from 45° reflections and 61° mode-changing reflections, originating at the journal radii, and these can simulate defect echoes from longer distances.

Sometimes one can make practical use of the 61° reflection as for example when testing a weld as illustrated in Fig. 16.18. The reflecting surface has intentionally been machined at an angle of 61° to allow the test to be made in this way.
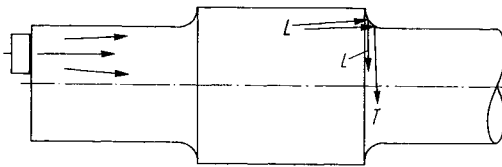
Fig. 16.17. Phantom echoes in axle testing
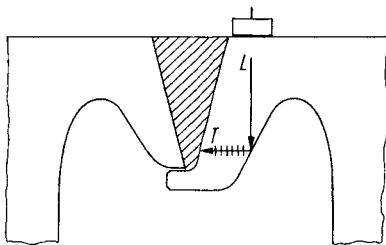
Fig. 16.18. Testing the root of a weld using a 61° reflection
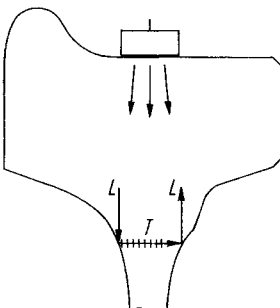
Fig. 16.19. Testing the rim of a monobloc railway wheel with a 61° reflection

When testing the rim of a railway wheel as in Fig. 16.19 an echo can be produced by a double 61° reflection and this can be used to check the probe coupling, or to give an indication of non-reflecting defects in the rim, if it disappears.

16.5 Screen Patterns when Plate Testing

At first glance the screen picture resulting from simple ultrasonic plate testing, as in Fig. 10.4, shows nothing remarkable. In the case of a flawless plate the multiple echoes follow each other at the distance of the plate thickness without intermediate echoes, provided the gain is not too high.

The echo heights generally decrease but not as it is often erroneously assumed, simply exponentially as a result of attenuation, but for various additional reasons. Firstly the path of the rays can be visualized as being repeatedly reversed, as in Fig. 10.4, so that each multiple echo can be regarded as the back-wall echo of a single plate of multiple thickness. In the near-field of the probe the back-wall echo of a given plate decreases only slightly with the thickness, but more rapidly in the far-field, and in fact inversely with the thickness (see Chapter 5). To the true attenuation which varies according to an exponential function, must be added the disturbance introduced by the probe with each reflection of the wave from the front surface because the probe absorbs a portion of the incident energy. Consequently, the reflection over the contact area is smaller than at points around it. Phase shifting, which depends on the design of the probe, may also occur and as shown in Fig. 16.20, a long sequence of echoes may therefore show an irregular change in echo heights, similar to beats, showing minima and maxima, whose position shifts if the coupling is changed slightly. Such a sequence of echoes is not very suitable for quantitative evaluation of the attentuation for example. For this purpose it is preferable to couple via a water column, a condition which is uniform and quantitatively determinable, or at least via a soft coupling layer.

If the plate contains a small flaw which is not big enough to markedly mask the back-wall echo, its echo appears in the same position behind each multiple back-
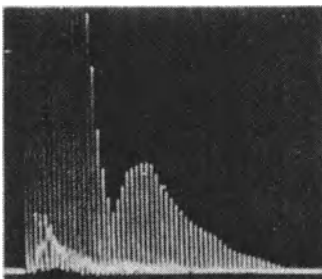
Fig. 16.20. Screen picture of a long series of multiple echoes obtained from a flawless plate in a contact test
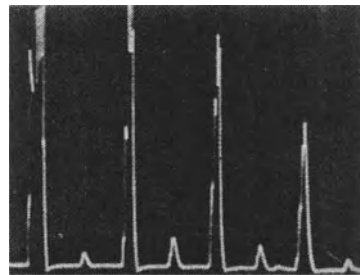
Fig. 16.21. Screen picture of a plate with small flaw
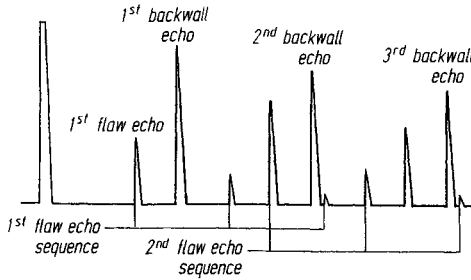
Fig. 16.22. Schematic screen trace of a flaw in a plate showing multiple flaw echoes

wall echo. The flaw-echo height changes, but not however in the same way as the back-wall echo since in the case of the small flaw, according to Chapter 5, the wave structure in the near-field of the sound beam makes itself felt. The point of maximum sensitivity is reached at the end of the near-field while in the far-field the flaw echo decreases inversely with the square of the distance. This explains the screen picture in Fig. 16.21 which shows the different behaviour of flaw echo and back-wall echo. The detailed differences depend of course on the size, frequency and particular design of the probe.

Sometimes the screen picture is further complicated by multiple echoes which follow the flaw echo. As shown schematically in Fig. 16.22 the sequence of flaw echoes may in certain circumstances also extend behind the first back-wall echo where it is superimposed on further sequences of flaw echoes, resulting in a very complex picture. This portion of the picture is however of little significance for flaw evaluation.

The screen picture of a plate may look slightly different from Fig. 16.21, if the flaw does not consist of a small, limited discontinuity which reflects the sound completely, but is a partially transparent layer which, therefore, reflects incompletely. Examples of this type are accumulations of finely distributed inclusions in a given plane of a sheet which are partially transparent like a lace curtain, imperfectly fused laminations as frequently encountered in light metals, and shrink fits and plating, where even a flawless bond may have a certain reflectivity due to different acoustic impedances. This then need not necessarily constitute a defect and the resultant echoes are therefore called *layer echoes*.

The various sequences of layer echoes, as produced by each back-wall echo in a manner similar to that shown in Fig. 16.22 need not decrease uniformly but may show characteristic maxima whose positions depend on the reflection coefficient of the layer concerned. Such an echo picture is shown schematically in Fig. 16.23 which also includes details showing the formation of the individual echoes, each being designated by three indices. Since the pulse when it reaches the layer is split each time into a transmitted and a reflected portion, it breaks up into an increasing number of partial pulses as the number of multiple echo reflections increases. The three indices of such a partial pulse indicate how often it has passed through the entire plate or each of the two sections, which lie above and below the layer respectively. Nearly all echoes then consist of several components with equal transit times. In the case of the echo marked 210 the total number of transits is six, namely three of type 210 and three of type 121. They are shown next to each other above the screen pattern. Each of the six components is shown again in the diagram of the pulse paths under the screen picture. With increasing echo distance the number of separate components participating in a given echo is greatly
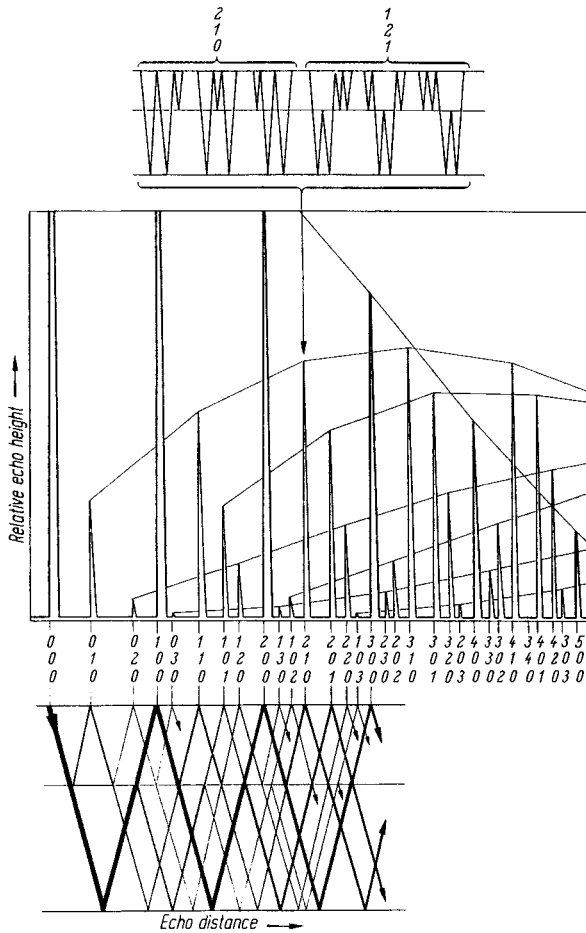
Fig. 16.23. Calculated screen picture of a plate with a partially transparent layer. Multiple back-wall echoes shown in bold lines. Reflection coefficient of layer = 0.2 and of coupling point 0.9. The echoes belonging to a given sequence are connected by curves for clearer indication of their changes in height. Below: pulse splitting at layer. Above: example of an echo composed of six partial pulses

increased so that it can become higher than the previous echo of the same sequence, although the individual partial pulses themselves are smaller [556, 1080], Fig. 16.23 indicates that the echoes of a given sequence—the indices within a given sequence are identical except for the first index—first increase in height and decrease again only after they have passed through a maximum. The envelope of each echo sequence, as well as the envelope of the back-wall echoes, pass in their further progress through alternating zeros and new maxima. These are not shown in Fig. 16.23.

For further theoretical considerations, and for experimental results with layer echoes, see Mundry [1080].

The summation effect of the partial pulses can provide evidence for the presence of weakly reflecting layers by observing the increase of the intermediate echo heights within a
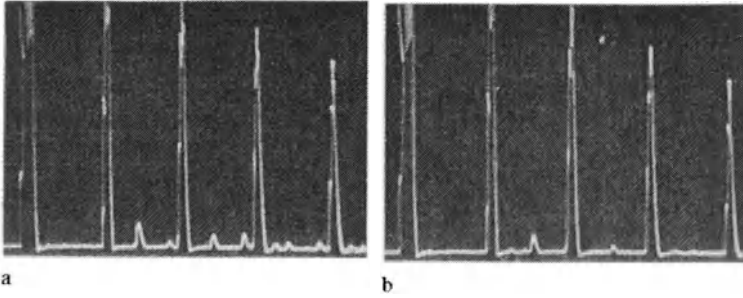
Fig. 16.24. Screen pictures of flawless plates of (**a**) steel and (**b**) aluminium, at high gain

long series of multiple reflections from a plate, the first direct echo being hardly visible before the first back-wall echo. In addition the position of the maxima can give information regarding the coefficient of reflection of the layer and thus, where applicable, the quality of a bond. In evaluating screen pictures of this type it is, however, necessary to take account of interfering echoes the causes of which are described below.

If the gain is high enough, interfering echoes also appear between the multiple back-wall echoes even in the case of a flawless plate. Examples of these echoes are shown in Fig. 16.24 on screen pictures of steel and aluminium plates, respectively. Their position thus depends on the material and according to [556] and [753] these interfering echoes are produced by multiple back-wall echoes which have travelled through the plate along their single or repeated paths as transverse waves. The sound beam from a longitudinal wave probe is not a simple plane longitudinal wave but also contains obliquely travelling longitudinal waves and transverse waves of low amplitude, as shown in Fig. 4.23 for a very small probe. A wave incident obliquely on the back-wall is converted partially into another mode, although at the small angles concerned this conversion is very weak. The probe will also receive echoes of obliquely incident transverse waves because the transmitting and receiving characteristics are always identical. Therefore, a first interfering echo is produced by a wave which on its outward path passes through the plate as an oblique longitudinal wave, and on its return path as a transverse wave, producing a *longitudinal-transverse (LT) echo*. This is, however, also the transit time of a transverse-longitudinal (TL) wave. The next to arrive is a transverse-transverse (TT) wave whose apparent echo path is c_l/c_t times the plate thickness d. Generally the apparent echo path for a combination of m longitudinal paths and n transverse paths is determined by:

$$0.5\, d \left(m + n\, \frac{c_l}{c_t} \right).$$

For the first two paths one thus obtains

for steel	LT and TL:	1.41 d,	TT	1.82 d,
for aluminium	LT and TL:	1.51 d,	TT	2.04 d.

As shown in Fig. 16.24 the first TT-wave echo for aluminium is invisible because it is masked by the second back-wall echo.

These echoes should not be wrongly interpreted as flaw echoes when testing sheets and it should be noted that owing to the above-mentioned summation effect their heights in a longer series of echoes may at first increase.

16.6 Interfering Echoes Produced by Surface Waves

Surface waves are frequently produced unintentionally. Whenever a probe is coupled to a solid they are radiated unavoidably, but usually they are very weak compared with the longitudinal or transverse waves. However, this may no longer be the case if the sound beam is broader and more divergent for small D/λ ratios, as for example with probes of exceptionally small diameter, with incomplete contact, for low frequency probes below say 1 MHz and with angle probes of large beam angle.

Using a 0.5-MHz normal probe on the polished face of a large forging or casting large interfering echoes are arise by surface waves reflected from the edges of the specimen or from the periphery of the polished area. Higher frequencies can be damped by merely touching the surface with an oily finger, and this technique can be used for distinguishing such interfering signals from true flaw echoes. At frequencies below 1 MHz this is, however, more difficult, even if the full palm of the hand is used. If one does not want to use considerably larger probes, which naturally require correspondingly larger coupling areas, specially designed probes can overcome this difficulty. When using square transducer plates, or transducers subdivided into squares, the surface waves in the contact plane are not radiated uniformly in all directions but in a fourlobed directional pattern. By rotating such a probe, interfering echoes can be distinguished from true echoes. Because of interfering surface waves, low frequencies only should be used on rough unpolished surfaces since these quickly damp out the interfering wave and merely produce a little grass.

However, incomplete contact is frequently unavoidable for example when testing round bar stock. On small diameters strong surface waves are radiated even if higher frequencies are used. The original longitudinal waves can then be entirely suppressed by dry coupling using slightly higher contact pressure, and in this way it is possible to exploit the original interference effect for testing by means of surface waves (Section 17.4).

When using the immersion technique boundary waves are produced corresponding to the surface waves and can also produce interfering echoes. These waves are similarly propagated in all directions from the point of incidence of the sound beam, and, compared with the useful sound, they are stronger when the D/λ ratio at the point of incidence is small. On a surface which is not very smooth, the interfering grass produced by the boundary wave may greatly impair the resolution of flaws close to the surface. Boundary waves also occur between two solid layers bonded together but have so far not given any noticeable trouble.

17 Testing with Ultrasonic Waves Radiated Obliquely to the Surface

17.1 Obliquely Radiated Longitudinal Waves

These waves are used only rarely for two principal reasons. As explained in Section 2.3 the longitudinal waves are always accompanied by oblique transverse waves at a smaller angle and these often generate interfering echoes from geometrical features of the specimen. In addition, if they fall on any reflecting surface at an angle other than 90° they lose energy by mode changing. The zigzag technique for example in plates is not useful and even the corner reflection is poor (Section 2.8, Fig. 2.25).

Figure 17.1 shows that a groove cannot serve as a reference reflector for longitudinal waves because it does not give a graduated relationship between echo amplitude and depth of the groove.

Nevertheless there are some useful applications for oblique longitudinal waves in those cases where it is not possible to generate transverse waves by refraction because of the need for using small angles of incidence (Figs. 17.2 and 17.3). Typical examples are for the identification of off-center defects in large cylindrical forgings, for cracks at the root of threads in drill pipe and for the testing of wheel sets (Fig. 23.3). In such cases thin wedges of perspex are fixed to the face of a normal (0°) probe, with a wedge angle between 2° and 10°. For some problems special lon-
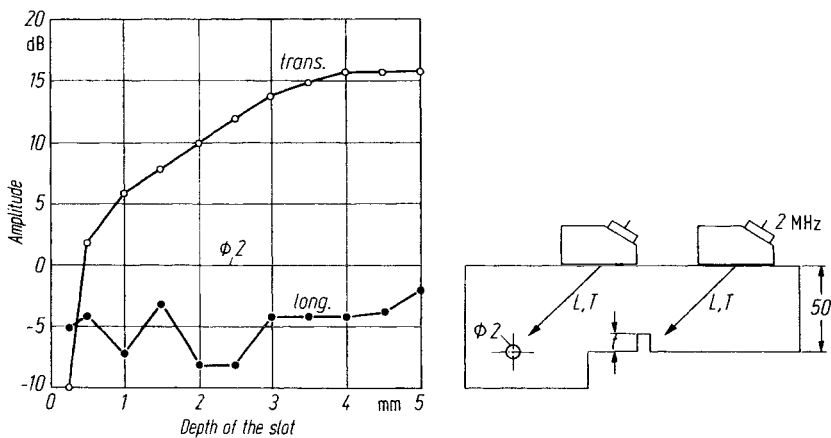
Fig. 17.1. Echo amplitude of a groove, compared with a standard borehole, for longitudinal and transverse waves according to [358]
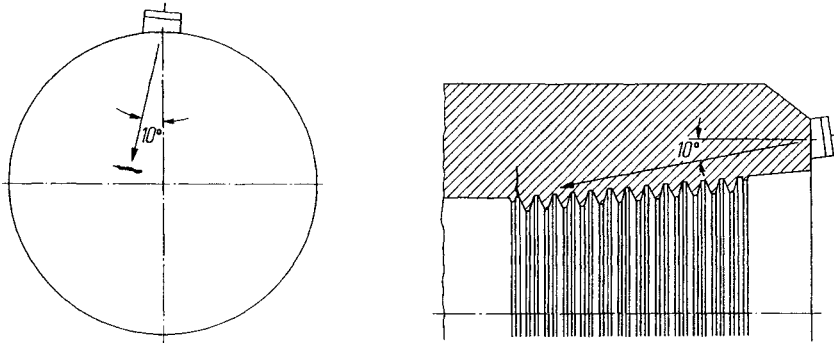
Fig. 17.2. Detection of off-central defects in large forgings by longitudinal waves
Fig. 17.3. Detection of cracks in threads by longitudinal waves

gitudinal-wave angle-probes are used as for example for weld testing in plastics (Fig. 28.17) because transverse waves here have too high an attenuation, and for testing of austenitic butt welds (Section 28.16), because the scattering of longitudinal waves by the dendritic structure of the weld is smaller than of transverse waves [539].

When very good sub-surface resolution is needed, it can be obtained by using longitudinal-wave angle-probes in the TR technique, but when working with such probes it has to be kept in mind that small variations of the perspex wedge angle, for example by wear, changes the beam angle considerably. Therefore the disturbing influence of a rippled or rough surface is much greater for longitudinal waves. This is caused by the fact that the ratios of velocities in the wedge and in a steel specimen for these wave types differ widely: $c_{perspex} = 2730$ m/s, $c_{steel\,(long)} = 5750$ m/s, $c_{steel\,(trans)} = 3150$ m/s so that:

$$\frac{c_{steel\,(long)}}{c_{perspex}} = 2.1, \quad \text{whereas} \quad \frac{c_{steel\,(trans)}}{c_{perspex}} = 1.2.$$

These indices of refraction are responsible for the differences of the behavior of the two wave types.

17.2 Longitudinal Creeping Waves

As described in Section 2.5 (Fig. 2.17) these waves propagate parallel to a plane surface where they have been generated, losing energy continuously by splitting-off transverse waves and have therefore a range of only a few centimeters. They do not follow the contour of a curved surface nor are they affected by its roughness.

Both the split-off transverse waves and the remainder of the longitudinal wave can create interfering echoes which depend on the specimen geometry. On a parallel rear wall a second creeping wave is generated which can also be used for defect detection (Fig. 2.17a).
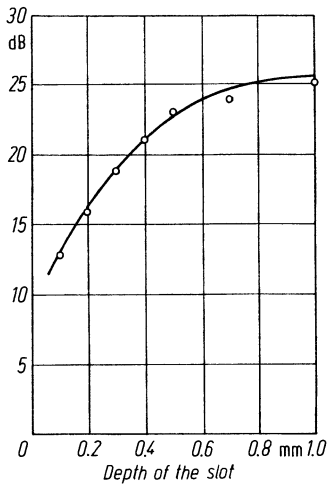
Fig. 17.4. Echo amplitude of a creeping wave at a rectangular groove
Fig. 17.5. Detection of a weld-root crack by creeping waves
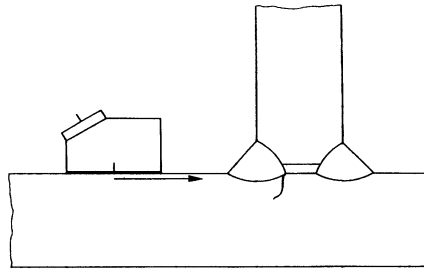
The optimum angle of the perspex wedge for the generation of a creeping wave depends on the longitudinal velocity in the specimen, measured along the surface (if for example it is not isotropic). A change of only 5 %, which can take place between a carbon steel and a high alloy steel, will require a different angle. In critical cases even the ambient temperature may have an important influence because the sound velocity in perspex is strongly affected by temperature.

Tests with rectangular grooves (Fig. 17.4) have shown that the echo of a 2-MHz creeping wave already reaches a maximum value below 1.0 mm groove depth. This means that creeping waves can be used to detect very small defects close to the surface, but not to easily differentiate them according to their depths.

A typical application would be to detect sub-surface defects, which do not form a corner reflector with the surface, for example a small crack in a weld as in Fig. 17.5. See also [400, 395, 401, 413, 230, S 162, S 20, S 118].

17.3 Transverse Waves

When testing curved plates or pipe walls, transverse waves which are propagated along a zigzag path are frequently used (Fig. 17.6). Compared with longitudinal waves their chief advantage here is that if incident at angles greater than 33° in steel (30° in aluminium) they are totally reflected without being split. In such specimens they can therefore travel long distances provided the roughness of the surface is small compared with the wavelength so that losses by scatter reflections do not occur. In addition, the amplitude decreases only according to the law of distance (divergence of beam) and the attenuation of the material for transverse waves.
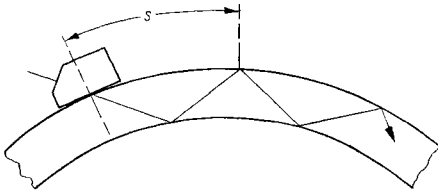
Fig. 17.6. Propagation of a transverse wave along a zigzag path by total reflection
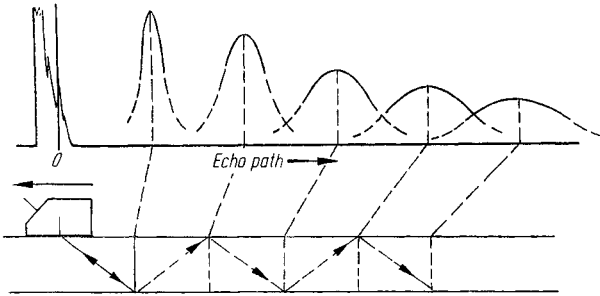
Fig. 17.7. Edge echoes in a plate and their envelope curves, schematic

The plane of polarization for a transverse wave which is generated in the usual way by mode changing on refraction (SV wave) is parallel to the plane of incidence (or the plane of the drawing). The other transverse wave type (SH wave) with perpendicular polarization cannot be generated by refraction but in practice only by electromagnetic methods, (Sections 2.4 and 8.4). This type can also be very useful for defect detection because no other type of wave, not even a surface wave, is split-off. The absence of phase reversal on reflection at a free boundary also allows even simpler propagation in shell-formed specimens, than when using the usual transverse waves (Fig. 2.21a). See also [248, 292, 462, 463, 464, 466, 786, 1366, 1673].

When using the zigzag method the complete cross section of the test piece can be scanned if the probe is shifted through the *skip distance s* (Fig. 17.6). In this way both surfaces can be checked for incipient cracks, and the entire cross section for other defects. A back-wall echo as is obtained when testing normal to the surface occurs only at an end face into the corners of which the zigzag path is incident (Fig. 17.7). If the probe is moved back and forth relative to this end face, corner reflections produce alternately echoes from the bottom or the top edge. In accordance with the divergence of the beam, these echoes reach a maximum and then disappear again, i.e. they pass through envelope curves with a more or less pronounced maximum (Fig. 17.7). For short sound paths in thick plates only one echo at a time is visible, while for longer paths, or thinner plates, the envelope curves are broader and overlap each other. Thus from an edge, just as from a flaw, one has several simultaneously produced echoes, in accordance with the zigzag paths of different inclination (Fig. 17.8). This may make it difficult for the inexperienced examiner to interpret and locate flaws because he is accustomed to viewing the echo traces while the probe is stationary. If, however, a dynamic testing technique is ap-
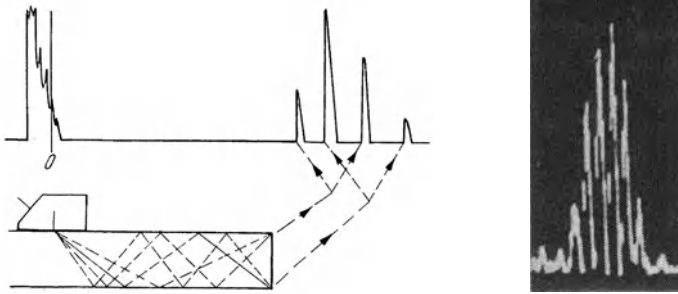
Fig. 17.8. Edge echo along different zigzag paths
Fig. 17.9. Echo of a flaw with zigzag waves in a pipe wall

plied by steadily moving the probe back and forth while observing the screen trace (which requires some skill and practice) it is easy to allocate each echo to the maximum of its envelope curve and this facilitates interpretation.

With longer paths and thin cross-sections, the echoes along the various zigzag paths form a close-packed echo group, as shown in Fig. 17.9 for an incipient crack in a pipe. In this case exact flaw location as well as differentiation between several closely spaced flaws is difficult.

For tracing the zigzag path and the origin of echoes the finger-tip test can be useful: if one touches, with an oily finger, the reflection point of an obliquely incident transverse wave, the echo height in steel may fluctuate by as much as one third. For longitudinal waves, however, there is very little influence and in the case of vertically incident transverse waves none at all.

Flaw location when using the zigzag method, is facilitated if one marks on the viewing screen the reflection points corresponding to the two surfaces by movable pointers. Since this method of flaw location is particularly important for testing welded seams, it is discussed in Chapter 26 in greater detail. In some cases (Fig. 17.10) the reflection points are indicated automatically if the surface is a little
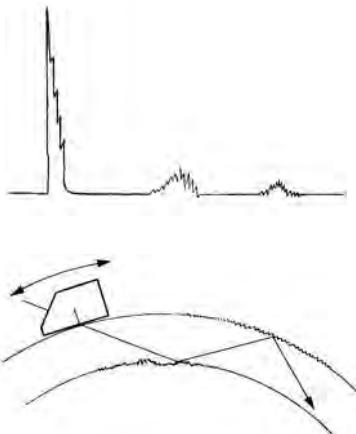
Fig. 17.10. On rough surfaces reflection points can be indicated by stationary "grass mounds"

rough. "Grass mounds" appear at these points on the time base, which, if the probe is shifted, maintain their position whereas individual small echoes move across them. If for example a flaw echo reaches the maximum of its envelope curve exactly at the midpoint between two such points, the flaw is located halfway between the faces of the specimen, and its distance from the probe can be calculated so that its position is therefore completely determined.

In order to check the sensitivity of the angle beam or zigzag test, it is frequently found convenient to use the edge of a rectangular block as in Fig. 17.8, or often simply a piece of plate with one straight edge. According to Fig. 2.27 b, the echo height in the case of corner reflection can, however, be used as a reference echo only with caution: in the case of steel, total reflection occurs only between 33° and 57°, but very little reflection for instance at 60°. This is also important to note when checking the beam angle: in the case of a 60° probe, the peripheral rays of the beam are reflected strongly at 57° and in the usual adjustment technique for maximum edge echo, they shift the apparent beam angle to values smaller than 60°. The beam angle can therefore be measured more accurately using a side-drilled hole and this applies particularly to larger beam angles.

In order to calculate the location of the flaw when the zigzag method is applied, the following simple formulae are used. According to Fig. 17.11a the skip distance in a flat plate of thickness d is

$$s = 2d \tan \alpha \tag{17.1}$$

and the sound path corresponding to a full skip distance

$$w_s = \frac{2d}{\cos \alpha}. \tag{17.2}$$

Finally, the depth of the flaw in the case of an arbitrary, rectilinear sound path w according to Fig. 17.11b is

$$t = w \cos \alpha. \tag{17.3}$$

The corresponding factors for a few commonly used beam angles are

	35°	45°	60°	70°
$2 \tan \alpha$	1.4	2.0	3.5	5.5
$2/\cos \alpha$	2.4	2.8	4.0	5.8
$\cos \alpha$	0.82	0.71	0.50	0.34
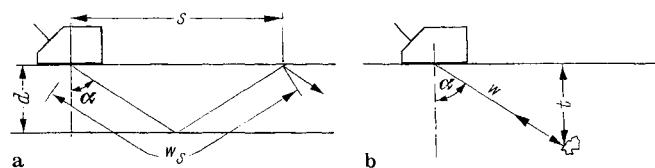
Fig. 17.11. Relation between skip distance s, sound path w, beam angle α and flaw depth t in a plate. **a** With reflection; **b** without reflection
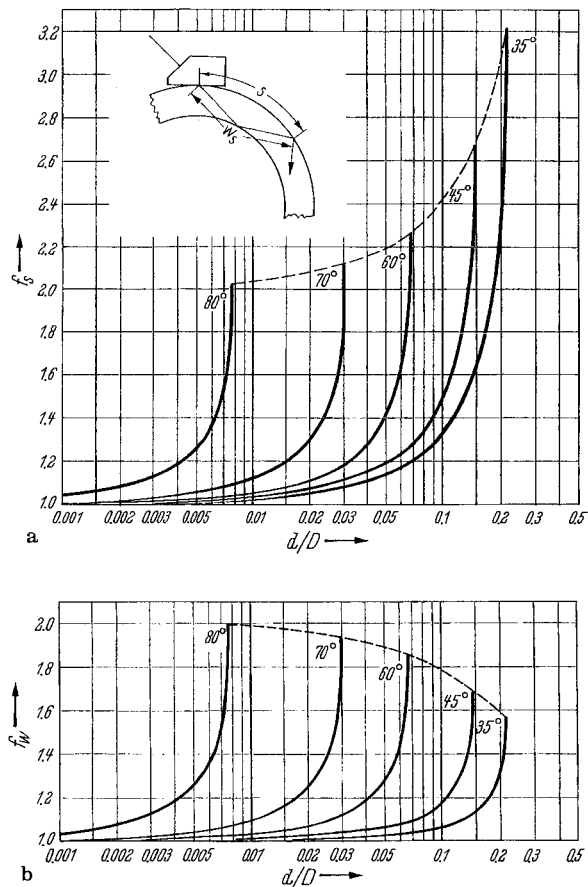
Fig. 17.12. Zigzag waves in the wall of a pipe in a circumferential direction. Ratio of skip distance (a) and sound path (b) in the pipe to the values in a plate of equal thickness, plotted as a function of the ratio of the wall thickness d to outside diameter D

In pipe walls both the skip distance and the corresponding sound path are increased by factors f_s and f_w respectively, the values of which depend on the pipe diameter D and the wall thickness d. Figure 17.12 gives these factors as a function of the ratio d/D and the above-mentioned angles. Where the slopes of these curves are vertical the inside wall is no longer reached by the beam. In the case of round stock and tubing Figure 17.13 shows that only a certain maximum depth d (or wall thickness d of pipe) can therefore be covered by the test and this is determined by the relation:

$$d/D = 0.5\,(1 - \sin\alpha).$$

For the above-mentioned angles one obtains

$$d/D = 0.21 \quad 0.15 \quad 0.067 \quad 0.30$$
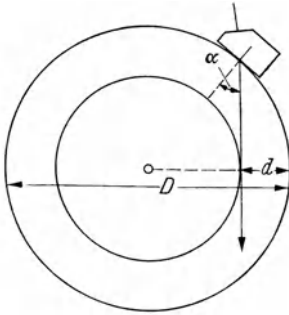
Fig. 17.13. Maximum penetration depth for round stock, or wall thickness of thick-walled pipe, at given beam angle α

and since for oblique transverse waves in steel only angles above 33° can be considered for practical purposes, cylindrical specimens can be tested only to a depth of 0.22 D, i. e. approximately one fifth of the diameter.

Since for the smallest angle of transverse waves we have $\sin \alpha_{\min} = c_t/c_l$ the general relationship for the maximum testing depth is:

$$\frac{d_{\max}}{D} = \frac{1}{2}\left(1 - \frac{c_t}{c_l}\right)$$

which, for aluminium and copper, gives slightly greater values, viz. 0.25 and 0.26 respectively. If, theoretically, the wave still just grazes the internal wall of a thick-walled pipe, the sensitivity is nevertheless already zero as a consequence of the side-wall effect. Therefore, when checking for inside incipient cracks, one can no longer apply the calculated critical thicknesses.

In a flat plate the axial direction of the zigzag path is the same as the axis of the probe casing, making allowance for manufacturing tolerances. If one extends the probe axis by means of a ruler, its edge passes through the projection of a flaw onto the surface, which can then be used for its location. This no longer applies in the case of a test piece whose thickness transverse to the direction of the beam changes, e. g. a wedge or a turbine blade. In this case the zigzag path curves towards the thicker side, which makes flaw location more difficult. Here one can fall back on the finger-tip test to determine the beam direction.

Occasionally transverse waves are used on pipes or solid cylinders, which are beamed into the specimen obliquely to its axis. Their reflection points on the surface are located on a spiral to which the longitudinal direction of the probe is a tangent. This track is therefore more difficult to visualize for flaw location.

In the testing of wedge-shaped specimens, e. g. eccentric pipes in the direction of their circumference (Fig. 17.14) the wave may return along its own path because the angle of inci-

a   b
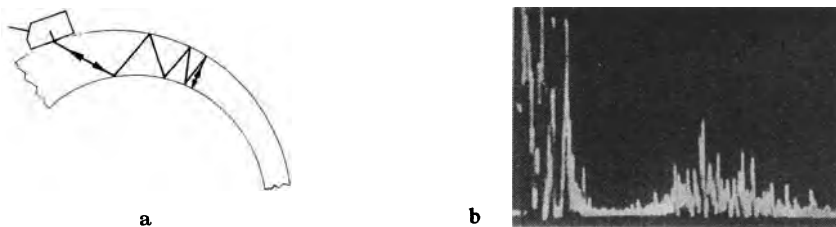
Fig. 17.14. Interfering echoes in the case of an eccentric but otherwise flawless pipe, by reversal of steeply incident zigzag waves

dence decreases with each reflection if the sound is beamed in the direction of the thinner section. Since this involves an angle smaller than that of total reflection, the wave is at the same time strongly weakened by split-off longitudinal waves. This may prevent the detection of flaws beyond the thin section but the difficulty can be overcome by using larger incident angles.

A testing technique with transverse waves known as the *delta technique* (Δ *technique*) utilises the scattered or edge waves of a flaw [268]. According to Section 2.7 the edge wave consists both of a longitudinal wave and a transverse wave and in Fig. 17.15 the test piece is irradiated acoustically by one probe and the longitudinal edge wave is received by a second probe. For scanning purposes both probes should be moved together as well as relative to one another according to a program, which in practice can be realized only by the immersion technique. The received signal records a C scan (see Section 19.3).
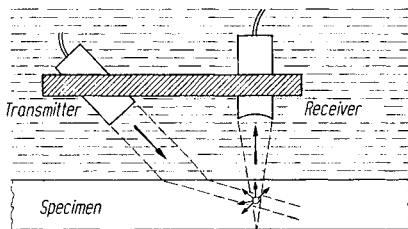
Fig. 17.15. Delta technique, schematic

In practice two separated normal probes working as transmitter and receiver are rarely used, whereas with angle probes this technique is quite common (Fig. 5.14 b). With specimens in the form of flat plate it is called a "pitch and catch technique" and using the double total reflection from a flat flaw perpendicular to the surface it is useful for testing welds in thick plate. To facilitate manual operation of such a technique, devices have been described with mechanical coupling between the two probes to allow the complete scan of a vertical weld section (Section 28.1 and [885]).

17.4 Rayleigh Waves (Surface Waves)

This method is not of great importance for several reasons. On the one hand most defects which it can detect are found more easily by direct visual inspection or with the help of magnetic particle or liquid penetrant methods, which are quicker and cheaper. It also needs clean and smooth surfaces on which the coupling liquid must be restricted to the probe contact point so that echo amplitudes are not affected by surplus liquid.

Rayleigh waves of frequencies above 1 MHz can be damped by touching their path with an oily finger, this technique helping to trace their path and clarify the origin of any echoes received.

As indicated in Fig. 17.16 the wave can also follow a curved surface and travels with little interference over edges if they are rounded with a radius greater than the
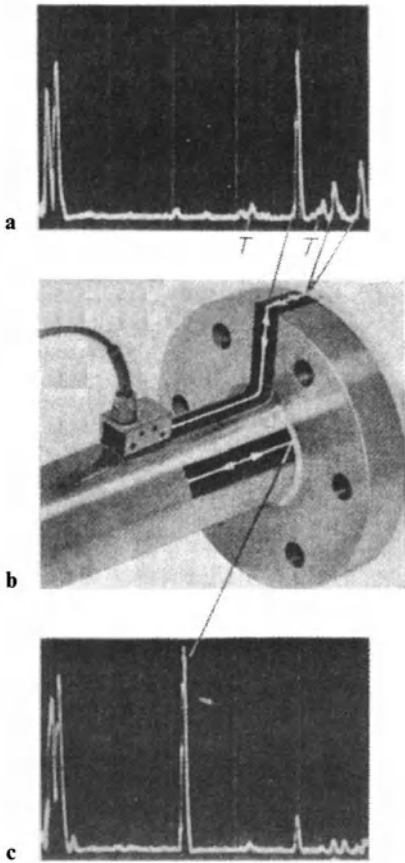
Fig. 17.16. Checking a machined component for incipient cracks by means of surface waves, frequency 4 MHz; depth of crack approx. 0.3 mm. **a** Screen pattern without crack echo, with several surface– and split off transverse wave echoes according Fig. 17.17 (T); **b** specimen with two probe positions and indication of the surface wave paths; **c** screen pattern with crack echo.
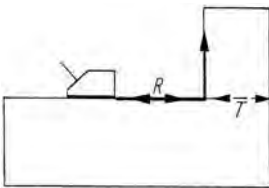
Fig. 17.17. Conversion of a surface wave into a transverse wave and vice versa

wavelength, but even a sharp edge still fails to reflect them completely. The remaining wave travels over it so that in the case of an open crack its depth can be measured by observing the further echo received from the bottom. According to [153] the reflected wave reaches a maximum only in the case of a projecting knife edge.

At a re-entrant edge (Fig. 17.17) a complication can arise: the wave is partially reflected, partially continues, and is partially converted into a transverse wave (Section 2.5) which, if the specimen is shaped as shown in the drawing, can give rise to an interfering reflection. This also happens at a groove sawn into a specimen for

testing purposes and at incipient cracks which a portion of the wave thus bypasses. This can be demonstrated by applying the touch test in which the echo of the transverse wave together with the echo of the corner can be damped by touching the track only *before* the corner concerned, but no longer behind it.

To get the best indication of surface cracks when using Rayleigh waves they should be irradiated perpendicularly. However, if they start at an edge, as in the case of the turbine blade in Fig. 22.20, the beam is preferably directed into the corner formed by the crack and the edge, at any angle between zero and 90° because the Rayleigh wave does not change its phase if reflected at grazing incidence from an edge and there is no mode change either. They can therefore follow a narrow face as in Fig. 22.24, whether or not it is formed between sharp or rounded edges. If the contact area with the specimen is smaller than the full contact surface of the probe, the amplitude of an echo is reduced, but on narrow and curved faces the contact surface can preferably be adapted by grinding to allow better contact and easier guidance.

Echoes by Rayleigh waves cannot readily be used as a measure for the size of the reflector or the depth of a crack. The relation between echo amplitude and crack depth is not definite because the echo increases only up to a depth of 0.4 λ after which it fluctuates, finally reaching a constant value independent of the crack depth [739].

There is also another reason why the amplitude cannot be used to measure the crack depth. Only open cracks reflect the surface wave fully but if they are filled with any foreign material such as that used for grinding or polishing the specimen, they can be quite undetectable by the method so that removal of foreign material is necessary before the method can be used successfuly.

A surface wave test can indicate crack-like defects lying just below the surface at a distance of about one wavelength, but small spherical pores immediately below the surface do not give good echoes apparently because of their poor geometrical reflectivity.

For reception of a surface wave, or of any other boundary wave a laser can be used as explained in Section 8.6, without disturbing the wave by mechanical probe contact. In this way defects can be made visible by the shadow method [739].

Since when a knife edge is pressed dry against a flat surface strong Rayleigh-wave echoes are produced an adjustable delay line for interferometry or for distance calibration can be constructed in this way.

"Grass", caused by the presence of coarse grain or a very rough surface can make locating a flaw impossible. However, it can be used as a quantitative measure of one of these two variables if the other remains constant, for example on turbine blades.

In this connection the possibility should also be mentioned of using surface waves for measuring layer thicknesses on the basis of their velocity, for example of a hardened layer or plating, for determining texture and for checking surface layers for faulty bonding (cf. Sections 29.2 and 33.1).

Using surface waves, Rasmussen [1229] has been able to detect very small incipient cracks on the surface of fatigue-test specimens and he could thus predict the origin of a fatigue fracture.

Of the five possibilities for generating surface waves, viz:

1. Surface-wave probe (conversion from longitudinal waves via a plastic wedge (Section 2.5),
2. Transverse-wave radiating crystal with viscous contact (Section 7.1),
3. Normal hard-faced transducer using linear dry contact under pressure (Section 15.3),
4. Electro-dynamic excitation (Section 8.4),
5. Excitation by laser shock (Section 8.7),

the first is in practice used almost exclusively. However, it has to be kept in mind, that the best efficiency is achieved only if the required angle of the perspex wedge is exactly calculated from the velocity of the material to be tested. A 5 % deviation on either side means that either no waves at all are generated in the specimen or only transverse waves.

The fourth and the fifth methods are still under laboratory development.

The second and third methods are rarely used in practice but for an example of the latter see [13].

Method No. 3 also works with a transverse-wave crystal, pressed onto a dry cylindrical surface. If the direction of polarization is parallel to the axis of the cylinder transverse waves are also generated as well as the Rayleigh waves, and these are polarized parallel to the surface and follow its curvature. They can be distinguished from the Rayleigh wave by their higher velocity (Section 2.6).

Also by this method Love waves can be generated within surface layers, serving for example for bond testing and being more sensitive for this application than the Rayleigh wave. This is because they cannot propagate in a layer of less than half a wavelength and can therefore indicate lack of bonding if the test frequency has been chosen appropriately.

For further testing techniques with Rayleigh waves see also [259, 456, 1568, 1569, 668, 739].

17.5 Plate Waves

Figure 24.2 shows schematically the propagation of a sound beam by zigzag reflections in a plate. At the beginning the zigzag path of the beam is still clearly distinguishable, but after a few repeated reflections, the beam paths overlap so that the entire plate is affected by the vibrations. In a thin plate it cannot be avoided that this overlapping begins directly under the probe. Such waves which in a plate leave no zone free of sound are generally called plate waves.

If the angle of propagation is unfavorable, the overlapping of several reflected beams results in cancellation by interference as shown in Fig. 2.22. Diagram 9 (Appendix) gives the favorable angles of propagation for steel plate at which no cancellation occurs. Apart from the material properties these optimum angles also depend on the plate thickness and on the sound frequency. This explains the phenomenon that some plate-wave echoes have a form different from that of the more usual echoes being broader and consisting of a large number of high-frequency oscillations (Fig. 24.14). This "melting away" of the plate-wave pulse is the more pro-

nounced, the longer the transit path and the steeper the branch of the curve in Diagram 9 for the corresponding plate thickness.

In practice plate waves are used both in reflection and transmission, and the angle probes used for excitation should preferably have an adjustable angle of incidence so that the angle corresponding to the frequency and thickness of the plate can be selected. Usually several favourable angles are found experimentally and very large crystal dimensions give better results. Angle probes with a fixed angle have also been successfully employed by adjusting the frequency and the pulse length.

Electro-dynamic excitation has also been used in practice (Section 8.4 and [676]) and by its non-contact operation it avoids the problem of conventional liquid coupling in which the newly generated plate wave is immediately damped by the front edge of the probe and the surplus couplant liquid.

Instead of conventional liquid coupling, better echo stability is achieved by a full immersion technique. However, because of continuous radiation of longitudinal waves into the water, the sensitivity drops very rapidly.

A reason for the rather uncommon use of plate-wave techniques is that there is no certain relationship between the echo amplitude and the width of a lamination or of a linear inclusion. It is unfortunately of no help that there has been found a correlation between the depth of artificial grooves and the corresponding echo height for certain wave modes [1426]. The method is preferably used for inspection of high-quality plate, where any echo indicates an important defect irrespective of its extent.

Methods using plate waves and rod waves with the appropriate wave forms are treated in detail in Chapters 24 and 25. See further [1282, 1283, 1316].

18 Interference from External High-Frequency and Ultrasonic Sources

In order to correct internal faults of ultrasonic instruments, only the relevant service instructions should be consulted. In the case of external interference, however, certain remedies of general validity apply. If several adjacent pulse-echo instruments with not exactly identical repetition frequencies are used, the pulses are transmitted from one instrument to the other electrically and they travel across the image. This requires synchronisation of the repetition frequencies of the instruments concerned and instruments designed for use in testing installations are usually equipped with this synchronisation facility. If not installed, synchronisation is usually possible by slightly changing the wiring and for this purpose it is recommended to consult the manufacturer.

Since the frequency range of the amplifier largely coincides with that of radio receivers, this may result in radio disturbances which manifest themselves in the loudspeaker by crackling, sizzling, etc. and these may also appear on the screen. These are usually caused by radio-frequency disturbances produced by electrical machines. Occasionally even a powerful, nearby short-wave transmitter may present its program on the screen. Disturbances difficult to eliminate are also caused by the transistor controls of electric drives widely used in modern production plants.

Another, non-electrical type of disturbance can result from the mechanical processing of the test piece. During hammering, turning or grinding generally, ultrasound is generated in addition to audible sound, and this can be received by the probes appearing as crackling on the screen. This concerns non-directional interference sound with a wide frequency range which includes all possible wave modes.

Occasionally this can be exploited usefully: if it is desired, for instance, to determine accurately, according to Fig. 18.1 in a large forging, the point of incidence of an oblique transverse-wave beam, this is found readily by means of a small, high-speed grinding machine by determining the contact point on the surface where the intensity of the disturbance reaches a maximum.

Fast automatic testing is greatly hindered by such external noise conditions and there are several possibilities of avoiding them:

— The position of the test installation must be remote from the place where interference arises.
— Appropriate construction can avoid interfering mechanical noise; for example the skids and rollers for guiding the test objects should be built from plastics.
— The test-frequency band should be kept away from the frequency range of the interfering noise.

For example in a testing installation close to a grinding machine for rods, the noise frequency was below 500 KHz. At the test frequency of 5 MHz the interference could be elimi-
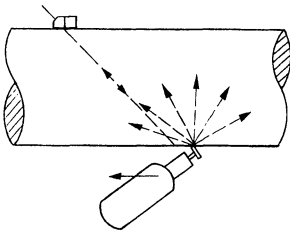
Fig. 18.1. Hand grinder as source of ultrasounds.

nated by using an amplifier having a frequency band with a low frequency cut-off well above the 500-KHz limit.

The first mentioned electrical interference is usually eliminated at its source only at great expense. With visual observation of the screen picture it is easy to distinguish them from real echoes as long as they are not too numerous. For automatic evaluation however, as is usual in big test installations, special arrangements have to be made to allow reliable evaluation. To determine the correct measures it must be kept in mind that there are three different ways in which this interference can enter the amplifier.

The first route is by way of the mains connection. However, most pulse instruments are connected to the mains via interference suppressors, so that in practice it is necessary to connect additional chokes and filtering capacitors only if the echo monitors are connected to mains-operated devices, such as solenoid valves and electrically actuated marking devices. In this connection attention is drawn to the fact that in most countries the maximum capacitance of the filtering condensers is specified, which for safety reasons may not be exceeded. It is recommended, therefore, in the planning and execution of such anti-interference measures to consult an electrical engineer familiar with the local safety regulations.

The second route for entry of interference is via the connection cable between instrument and probe, i.e. the test cable. This acts as a receiving aerial for the electromagnetic fields radiated from the connecting leads of the interference sources. An anti-interference measure can therefore be a compact layout of the testing installation, i.e. the positioning of the instrument close to the probe using the shortest possible test cables. Where for reasons of more convenient operation the instruments are positioned at a greater distance from the point of testing, it is recommended that a coupling unit consisting of transmitter and preamplifier is installed in close proximity to the probe, which amplifies the effective signal above the existing interference level. Most manufacturers can offer such units as accessories to their normal instrument programme. Only in some rare, intractable cases, for example close to short-wave transmitters, will it be necessary to provide additional shielding by housing the probes together with the preamplifier units in a Faraday cage.

The most frequent cause of penetration of interference is the third route, via the earthing leads. In high-frequency engineering a basic rule for interference-free earthing recommends that all earth leads of a given installation should be connected to a single grounding point only. In practice, however, this rule can be followed

only with instruments of compact design and it cannot be realized in installations as such, particularly not in the case of most electric power installations. Consequently, in workshops equipped with electrical machines significant disturbance voltages can usually be measured between any two grounding points even if they are separated by only a few metres. As a remedy star-point grounding can be recommended as far as practically possible, and in addition to apply the remedies recommended in the previous paragraph, i.e. a compact installation and the use of preamplifier units in immediate proximity of the probe. However, since every ground lead also represents an inductive impedance for the high-frequency interference currents and since every instrument module has a capacitance to ground which shunts the star-connected ground leads, it is in practice not always possible to reduce the inductive or capacitive disturbance to an acceptable minimum. Residual interference should be suppressed on the evaluation side of the installation. However, since none of these evaluation measures are 100 % reliable, care is advisable.

A simple method of suppressing interference on the evaluation side makes use of the fact that such signals occur invariably in irregular sequences, and non-synchronized with the repetition frequency of the pulse instrument. If the response time of the monitor is delayed so that it transmits a signal only if during several successive periods a pulse signal appears in the gate, the interference can be suppressed successfully. It is statistically most improbable that such a pulse sequence is produced by interference signals. The same principle is exploited by auxiliary modules which have become known as *flow counter* and which are now marketed by most manufacturers. These flaw counters likewise transmit a signal only if an echo remains in the monitor gate for a preselected number of time periods. Compared with the simpler monitor delay the flaw counter has the advantage that it can be switched and thus can be used also in multiplex operation (probe switching). Both methods, however, can be used only at relatively slow testing speeds because at high testing speeds echo signals from genuine flaws will likewise occur only briefly and thus are evaluated as "interference".

A further method which can be applied without limiting the testing speed picks up the electrical field of the interference by means of an aerial. The signals are amplified and then used for suppressing the monitor indication. However, if the signal reaches the instrument predominantly via earthing currents this method is not fully effective, resulting in the suppressing device still leaving up to 15 % of the interference indications which can still be excessive in the case of strong interference.

Another method which in practice has proved very successful also works without limiting the testing speed and is based on the fact that an echo indication always has a definite, characteristic pulse width. Typical pulse signals from thyristor controls are invariably narrower than echo pulses, whereas the interference signals from contactors and motors are longer. In this case the pulse width is counted by a fast electronic counter which is set between a minimum and a maximum width for the echo evaluation. It is also an advantage that the disturbances due to ambient noise can also be suppressed by means of this device.

19 Detection and Classification of Defects

19.1 Search for Defects, Maximising of Echoes and Selection of Probes

The detection of defects by observing their ultrasonic echoes is usually quite simple and rapid. More difficult and much more time-consuming is the classification of defects according to their type, shape and size. This is fundamentally due to the basic handicap of ultrasonic testing in having a poor lateral resolution because of the relatively long wavelength used. Even when using the most complex imaging methods of Section 13 a precise defect image cannot be expected. Also because these methods have to be restricted in practice to relatively simple-shaped specimens, other means have to be used in the wider applications to establish a little more about a defect than only its geometrical position.

We can in practice always assume that something is already known about the defect since the experience gained from the destructive testing of similar specimens need not be ignored. Often it happens that from the defect position alone one can conclude with certainty that it is of a certain type. The fact that *any* defect exists if often sufficient cause for rejection, without precise indications about its type and size. Thus a clear specification of the testing task can in many cases simplify the problem and save the time used unnecessarily in elaborating the character of defects.

With an extended specimen the test is usually carried out in two parts, the first being a search for defects and the second the measurement of their position and echo amplitude. For the first step, the surface need not be prepared to the best quality, but should be as uniform as possible. The transducer should have a near-field length of at least one third of the largest possible defect distance and the gain used should be sufficient to bring the base line to "life", i.e. showing small indications of the grain structure. The probe should have a soft facing so that with plenty of coupling liquid it can be easily moved along the surface without losing contact too often. If it is compatible with other requirements such as the near-field length, the probe should have a large angle of divergence thus facilitating the scanning of the whole specimen by only a few passes.

For large specimens transducers of 1 or 2 MHz and diameters of 20 to 30 mm are suitable, but for smaller ones higher frequencies and perhaps smaller diameters are useful, especially when there is a rather strongly curved surface. Hard-faced probes should not be used at this stage but should be reserved for the subsequent defect evaluation for both technical and economic reasons.

The observation of the screen when searching for defects can be carried out by a monitor giving acoustic signals, so that the operator can better concentrate on the probe guidance and manipulation.

When using an ample supply of a viscous coupling liquid it can help defect searching to tilt the probe a little to survey a larger angle from one point and a soft coupling surface is advantageous in this case. For similar techniques with angle probes, for example for weld testing, see Section 28.

For the second stage of the inspection in which flaw evaluation takes place the gain should be reduced to bring the echo maxima below the upper edge of the screen. Maximising of each echo is then carried out by careful shifting of the probe, without losing contact, to adjust an echo to its highest value. To use another probe, preferably one with a hard face, can be helpful for this purpose, and in this case the chosen near-field length N should not differ too much from the flaw distance. For the best application of reference blocks with artificial defects or of the DGS diagram the flaw should lie in the distance range between $N/2$ and $3 N$ (see Section 19.2).

For using hard-faced probes satisfactorily the surface can be improved locally, but it should be flat or of a uniform convex curvature and not too smooth. If nevertheless the probe cannot be shifted easily, and the echo amplitude changes too much when moving the probe, a soft-faced probe can be used in practice. For angle probes this is not a problem because contact is made with an acoustically soft plastic wedge.

The inexperienced operator when beginning to use the technique should take the advice of the manufacturer when ordering a set of transducers. Regarding defect localizing see also [1392].

19.2 Evaluation of Equivalent Reflectors, Reference Defects and the DGS Diagram

The defect echo, even when maximised, cannot be related to the defect size without further information about the transducer data and of the gain employed. However, it can be compared with a reference echo produced by the same transducer. The heights of both echoes could be measured in mm but with modern units fitted with calibrated gain controls both echoes separately can be adjusted to the same reference height, by varying the gain. The gain difference in dB is then the basis for indicating the "equivalent defect", which is a term used to refer to an imaginary flat circular reflector at the same position as the real defect, and producing the same echo height.

As a reference echo we have already proposed the rear echo from a thin plate of the same material, and with the same surface quality, as the specimen (Section 5.1). It is the maximum echo which can be generated in this material with the probe concerned. All other echoes obtained with the same probe and material will have negative amplification values, such as $-6\,\text{dB}$ which means half the height of

the reference echo and -40 dB which means 1/100th. This latter ratio would incidentally be impossible to read from a linear screen in millimetres.

As well as the equivalent defect mentioned above, many alternative geometrical shapes have been proposed but the flat circular disc has, however, the big advantage that the reflected echo can easily be calculated, as has been done in Section 5.2, leading to the general law of the DGS diagram, where its size has a definite relationship with the gain and the distance.

Here it must be clearly stated that the area of the equivalent reflector which is given by the diameter resulting from using the DGS diagram is only in rare cases equal to the actual area of the real defect. This could happen in the case of a plane break or separation, struck by the beam perpendicularly to give a coaxial specular reflection. Such a type can occur in steel forgings as so-called flakes for which, even if they deviate to a certain extent from the circular shape, the area would be evaluated quite precisely. Usually, however, the real area of a defect can only be greater than that of the equivalent reflector. In other words a circular flat reflector will generate the maximum echo from the smallest area. A natural defect is always somewhat larger, at best equal, but never smaller than the equivalent flat circular disc.

Instead of using the DGS diagram, the older way is often preferred, of producing a set of test blocks with flat bottom holes of various diameters and with gradu-
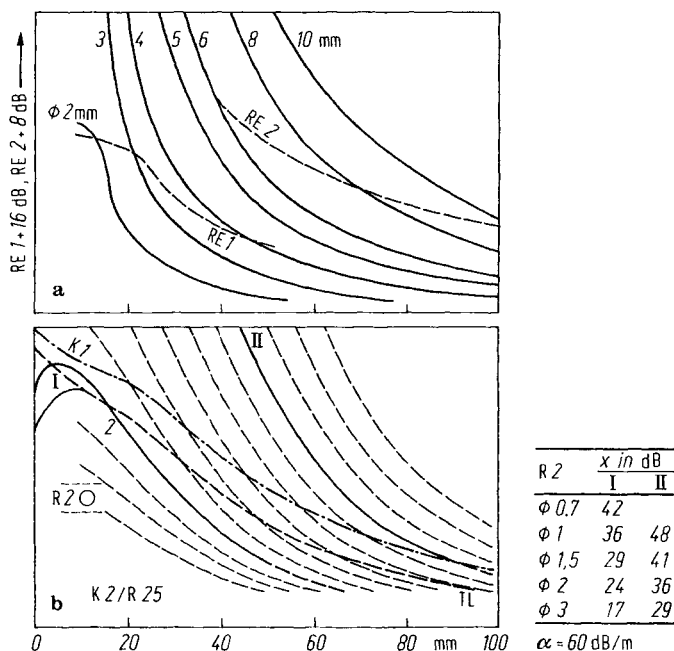

Fig. 19.1. Special DGS scales (design Krautkrämer). **a** For a normal probe of 2 MHz and 10 mm diameter, giving the equivalent reflector diameter over the distance; **b** for an angle probe of 4 MHz and 10 mm crystal and angle of 70°, giving the recording limit over the projected distance (Section 28.1.3)

ated distances from the contact surface. To compare the echo height of a real defect after it has been detected the appropriate distance set has first to be chosen, from which that test block giving nearly the same echo height is selected. If necessary a certain interpolation has to be done between hole sizes. Finally the flat bottom hole in the selected block is found to be the equivalent reflector. The same hole size would of course be found when using the DGS diagram. These test-blocks sets are quite expensive and often are troublesome to use especially on site. In addition they are only useful for limited ranges of distance and diameter, causing considerable errors when the result must be extrapolated by guesswork.

With certain test-block sets, for example those standardized in the USA (Chapter 34), the width of the longer cylinders is not sufficient when probes with a large angle of divergence are used (see Section 16.1). A valid test block for a flaw distance of 500 mm, which is not unusual, cannot be manufactured at all with a width which can be utilized or afforded in practice. The DGS method therefore seems more advantageous. The general DGS diagram which uses the normalized values of distance, gain and size and is valid for all probes and frequencies, may be somewhat cumbersome in use, because the absolute values involved always have to be individually calculated. However, there are now pocket computers available which even consider the attenuation of the material in their programme [1135]. As an alternative individual DGS diagrams, calculated for each probe, are available and can be delivered with them when ordered.

It would be of general advantage for the progress of ultrasonic testing if all manufacturers would deliver their probes along with data sheets which include the appropriate DGS diagram.

Figure 19.1 shows two of such special diagrams to be set in front of the screen instead of the usual scale [319, 1327, 1733]. For the scale of Fig. 19.1a the reference echo is the rear echo of a plate, which has to be brought to the height of the curves RE 1 or RE 2. Then the gain has to be increased by 16 dB or 8 dB respectively.

The scale of Fig. 19.1b serves for weld testing. The reference block is shown in Fig. 10.52, where the echo of the 25-mm radius circular face has to be used. This echo has to be adjusted into the circle R 2. The corresponding table gives the increased gain needed to have the echo of a 2-mm (for example) circular reflector to just reach the recording limits I or II, that is +24 or +36 dB. In weld-testing practice the final equivalent flaw is no longer indicated, but only the number of dB by which the echo exceeds the record limit (see Section 28.1.4 and [172, 725, 1087, 1245, 1262, 1428]).

The result of an equivalent defect size determination by the DGS method can sometimes give an inaccurate answer if very short pulses (e.g. using shock waves from highly damped probes) have been used. The phase of the reflected wave is affected much more by the small reflector than by the reference plate. By observing the HF presentation on the screen (Fig. 10.16a) one sees that the amplitude of the highest positive cycle is reduced in favor of the corresponding negative one, or vice versa, but this doesn't happen in the echo from the reference plate. This effect influences the measurement of echo amplitude when it is made *after* rectification but if one measures the peak-to-peak distance in the HF presentation the DGS results obtained are then precise and reproducible (Wiese [1623]).

It is in practice not possible to manage with only the test blocks already mentioned, i.e. the DGS standardization plate and the two test blocks for angle probes (Figs. 10.51 and 10.52). This is especially true in the case of specimens where the propagation of the sound is affected by side walls since in this case the laws on which the DGS diagram is based are no longer valid. Examples are tubes and plates, where the waves propagate in zigzag paths and defects in the shape of corner reflectors such as surface cracks. In these cases test blocks with artificial defects such as slots, grooves or cylindrical bore holes can be used within certain limits. Often the test block is made to have a shape similar to the test specimen itself.

However, it should be stressed that this type of test block never fulfils the main purpose of the DGS diagram nor of the standard flat bottom-hole test blocks. From these one obtains the so-called equivalent flaw of the first kind; that is one which has the same size for all different frequencies, probe diameters and flaw distances. This "flaw of the first kind", equivalent to a given natural flaw, should be equal for all flaw detectors, operators and test conditions such as probe type and frequency.

However, a slot machined for example in a tube can give only an "equivalent flaw of the second kind", i.e. it is only valid for exactly the same test conditions concerning the type of flaw detector, probe, frequency and distance. It can in fact serve reliably only to check the consistency of the apparatus. Within a testing standard such test blocks should only be specified if at the same time the test conditions are also exactly specified, which in many cases will bring practical problems.

In the past much time has been wasted in carrying out investigations on and with test blocks, although it was well known that the dimensions of an equivalent artificial defect are only rarely closely related to the actual size of a real defect. Artificial reflectors have often been given a shape "similar" to the natural defect; for example a bore hole has been used to simulate a slag line in a weld, or a slot in a tube to simulate a crack. The error in these cases is based on the fact that they are too regular, the sound being reflected specularly, which is not the case with natural defects.

If the single Huygens' wavelets from a specular-reflecting artifical defect which lie in a plane perpendicular to the beam are added up, the phases are almost equal resulting in a large total amplitude. With a natural reflector a distance difference of only a quarter wavelength suffices for the cancellation of one wavelet by the next. Therefore a natural slag line will hardly ever give an echo comparable to that from a borehole, the supposed "similarity" being actually misleading. Unfortunately test reflectors of complete irregularity cannot be reproduced for standardizing.

It makes very little difference in practice if, for example in tubes, slots or boreholes are used as reference defects. They are all equivalent defects of the second kind, and are only valid when used with consistent instrumental conditions. It is in fact easier to specify the echo from a real defect by measuring its difference in dB from the echo of an artificial reflector which can be easily manufactured in a reproducible way. A saw cut, completely through a tube wall, is just as valid a standardization feature as a shallow slot which sets out to simulate a real crack. The relationship of this relative measurement to the actual size of a defect (crack-depth for example) has in all cases to be established by the destructive investigation of a number of similar defects.

The difficulties in using artificial reflectors will be explained in more detail using as an example the popular rectangular groove or slot (see [394, S 135]). According to Section 2.8 the corner reflection of transverse waves is useful only in the range of incident angles between 35°

and 55°. At both ends of this limited range the directivity is distorted and causes big differences if a real crack not exactly perpendicular to the surface is compared with a slot which is exactly perpendicular.

In addition, if we consider the length of both slot and flaw along the surface, an elongated slot obeys a different distance law than does a short crack which is fully covered by the beam cross-section. Also on the smooth walls of a machined slot surface-waves are produced by mode changing and these distort the echo patterns, whereas on the rougher walls of a real crack they have much less influence, especially if the depth of the crack is not uniform over its length. For all these reasons the use of a calibration echo from a slot to measure crack depths gives very unreliable results, especially if the crack depth is less than one wavelength, so that assessing the depth of a real crack by this method is very unsatisfactory. The calibration curve cannot be used for a different beam angle, or for another slot width, or another frequency. If such a procedure is nevertheless necessary the slot cut into a plate or tube should be made by a small circular saw, to give a slot of short length and a depth varying from zero to a maximum thus having approximately the same distance law as a real crack.

It has also been proposed to attach reference reflectors directly to the specimen under test without permanent mechanical changes (Figs. 19.2 and 19.3). They have, however, not found great interest or much practical use being considered too complicated in operation.

For inspection tasks in which a particular probe is specified it is convenient to use the related DGS diagram, either in printed form or on transparent scale mounted in front of the CR screen. It is then usual to have certain equivalent defects specified, a lower one usually called the recording limit and the upper one called the rejection limit. Two lines corresponding to these limits can then be drawn onto the diagram so that indications below the recording limit can be neglected, echoes between the lines can be recorded for further investigation and those defects with echoes surpassing the rejection limit can definitely be rejected without further consideration.

If the DGS method is not used it is of assistance to have the depth dependence of the echo compensated by an amplifier with automatic depth compensation (DAC) which shows the echoes from equal defects with equal amplitudes at all distances (see Section 10.3.4).

In simpler flaw detectors not having such electronic compensation the distance law should be determined by measuring the amplitudes of echoes from a specific type of reference reflector, at different depths, and drawing this curve onto the CR
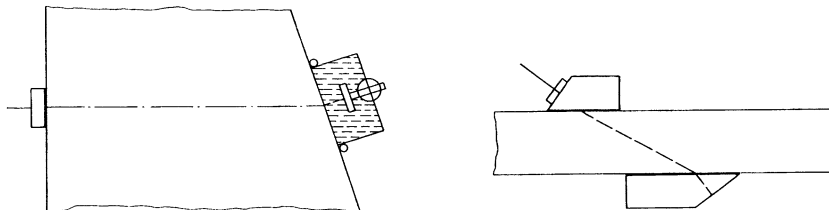

Fig. 19.2. Small reference reflector housed within a liquid-filled container and placed in contact with the back wall of a specimen

Fig. 19.3. Test piece with flat reflecting surface for use with transverse waves in plates, attached to the specimen using liquid contact

scale. In this case the form chosen for the reference reflector is important, because most natural defects follow the law relevant to small circular reflectors (as represented by flat bottom holes) and not to the law relevant to transverse cylinders as represented by boreholes lying perpendicular to the beam. This latter type of test block will give erroneous results, because a natural-defect echo when equalling the echo from a transverse borehole at a certain distance, will be only 50 % of the same borehole echo when both are lying at four times the distance. If for simplicity it is convenient to use transverse borehole test blocks one should correct their echo amplitudes with the help of Eq. 5.8 (Section 5.2).

In practice in spite of all the problems inherent in using artificial defects, evaluation work is carried out using many different types of reference blocks and this leads one to conclude that defect sizing need not be carried out too pedantically, at least within depth ranges not much larger than three times the near-field length of the probe used. A dispute about differences of a few dB in echo amplitudes is pointless having regard to the considerable uncertainties in the relationship between echo amplitudes received from artifical and natural defects respectively.

In some cases the *attenuation* of the material should be taken into account when testing thick specimens or if materials of specially high attenuation are involved. The attenuation coefficient (usually measured in dB per m) for the material is usually known or if not it should be measured (Chapter 33). Its value multiplied by twice the distance gives the dB correction by which the gain figure appropriate to the echo has to be increased. To make this correction still simpler DGS diagrams are available with correction curves for several discrete values of the attenuation.
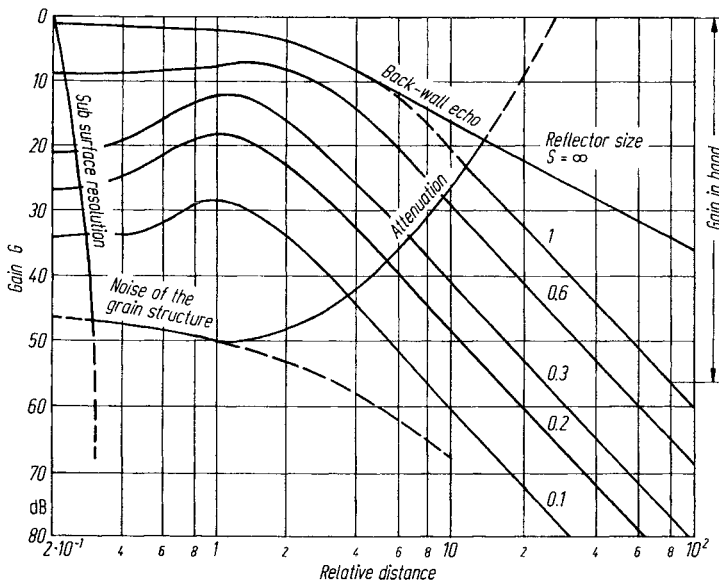

Fig. 19.4. Useful ranges for a DGS diagram, the so-called information field

Curved test surfaces distort the sound field of the probe and are therefore not always suitable for using either the DGS method or flat bottom reference holes without correction. As a convenient rule of thumb it may be mentioned that in practice no special correction is needed provided a probe of less than 24 mm diameter is used to test a cylindrical specimen of 300 mm diameter from its curved surfaces. The corresponding figure for a cylinder of 50 mm diameter is a probe of not more than 10 mm across, the rule being that the probe diameter must be smaller than the square root of the double diameter. In addition soft-faced probes with plenty of coupling liquid should be used.

Figure 19.4 shows the so-called information field based on the standard DGS diagram and taking into account all the factors limiting inspection performance. On the left the useful range is limited by the dead-zone caused by the transients following the main pulse. At medium distances the useful range is first limited for small defects by the grain noise, and later by the attenuation. Each diagram is therefore only valid for a particular probe and test material.

Another very informative diagram is the Sonogram (as shown in Figs. 10.32, 10.39 and 10.40) which illustrates a simplified echo field including the practical limits applying to each probe, if used on steel with practically no attenuation.

The fact that in recent times many ultrasonic testing standards refer to quantitative measurement methods instead of to just a qualitative defect indication as in former times, is an encouraging sign of progress (see Chapter 34). If, however, these documents specify exactly certain probe dimensions, ultrasonic frequency or other data to be used *exclusively*, this seems definitely to be the wrong way. See further [1426, 1732, 1712, 1346, 1695, 1724, 1556, 137].

19.3 Dimensions of Large Flaws, Scanning and Echo Dynamics, Incipient Cracks

Up to now we have mostly assumed the case of small flaws which are fully covered by the beam cross-section, and where the echo amplitude was measured with a stationary probe. To trace the edges of large defects the probe has to be moved, if possible without losing contact, which requires a rather smooth and uniform surface and some operator skill, or even better mechanical guidance for the probe. To im-
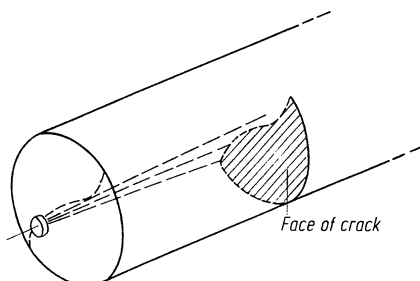

Face of crack

Fig. 19.5. Large flaw normal to the beam axis

prove the constancy of coupling, intermediate layers of plastic have been proposed but at least the coupling surface of the probe should not be hard faced.

The method of assessing the defect from the variations of its echo when scanning the surface with the probe is called *echo dynamics*. It is demonstrated by Fig. 19.5 using a very simple and rare case; a large crack in an axle lying perpendicular to the axis. As long as the side wall does not interfere, the outline dimensions of the flaw can be drawn onto the scanning surface since when the axis of the beam strikes the edge of the crack the echo received drops to half its base height. Following this half-value line traces the contour of the flaw and the system is called the half-value or 6-dB drop method. It is applied also with obliquely incident transverse waves to scan a weld in its longitudinal direction to measure, for example, a slag line, which is longer than the beam cross-section.

If the shape of the specimen allows a back-wall echo to be received this can be used instead of the flaw echo by watching its decrease from maximum to half-value when the probe scans the surface. With through-transmission using two separate probes guided mechanically we have the oldest application of ultrasonic testing [1534].

Figure 19.6 shows schematically the variation of the echoes and the influence of the directivity of the probe. These curves are the basis for the evaluation of the reflector. They are called *envelope curves* and for more precise assessment should be recorded by an appropriate installation with mechanical scanning. Figure 19.7 shows how such recording can be carried out with a digital display flaw detector, where three boreholes perpendicular to the beam have been scanned by hand. Figure 28.15 also shows an example of an envelope curve obtained by scanning a weld perpendicularily to its direction and recorded by a long-time photographic exposure.

The conditions illustrated in Fig. 19.6 for obtaining an envelope curve occur in practice quite rarely. In most cases the reflection obtained consists of waves of dif-
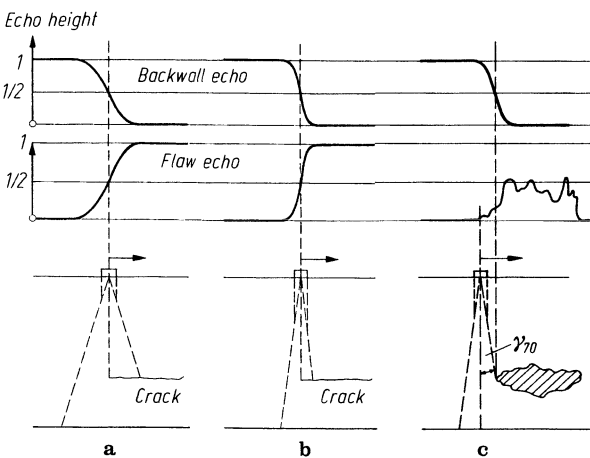
Fig. 19.6. Behaviour of flaw echo and back-wall echo during the scanning of a large flaw; schematic. **a** Large beam angle, **b** small angle, **c** irregular flaw surface
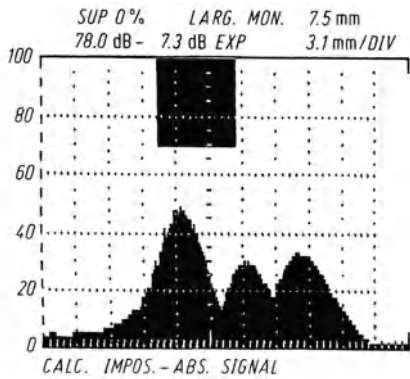
Fig. 19.7. Digitally stored envelope curve from scanning three transverse boreholes of different diameters (device "EPOCH" by Panametrics)
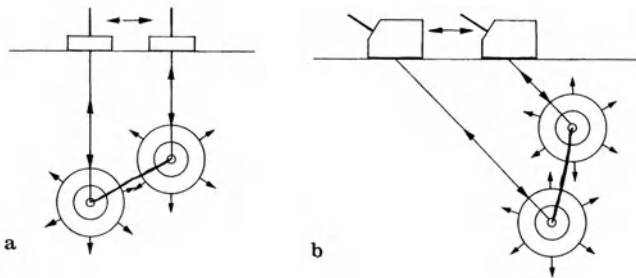
Fig. 19.8. Measuring size and angular position of a flat defect from the edge-wave transit times, when scanned with a sharp beam. a With longitudinal waves; b with transverse waves
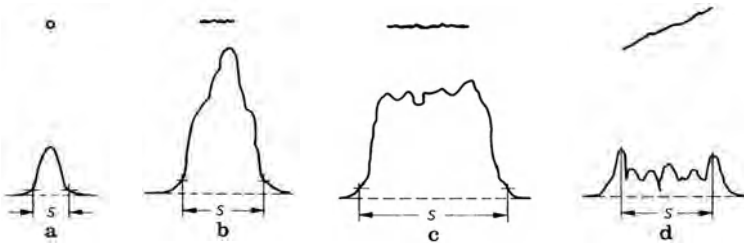
Fig. 19.9. Schematic envelope curves received from different natural reflectors as indicated above. a Rounded reflector such as a pore; b specularly reflecting reflector equal to the beam diameter; c as in b but with larger size of the reflector; d oblique reflector with sharp edges as in Fig. 19.8, but at high amplification compared to a, b, and c

ferent character; the specularly reflected ones (as exclusively assumed in Fig. 19.6), the scattered reflections from a rough surface and the edge waves from sharp edges. The latter type merges with the main reflection when the reflector is perpendicular to the beam, but can be distinguished as in Fig. 19.8a, if the flaw lies obliquely.

Figure 19.9 shows the influence of size and shape characteristics of a reflector on the shape of the envelope curve.

The above-mentioned half-value or 6-dB-drop method often cannot be applied to a natural reflector, because it is not known from which value the 6-dB-drop has to be calculated. The same is of course true of the 20-dB-drop method. For this reason an absolute value of the threshold is often used instead. When scanning, one observes the probe positions where the first indications of the reflector appear just above the noise by choosing high gain, at which setting, the main-echo is, of course, highly over-amplified. With this method as in Fig. 19.9 the overall width s of the envelope curve is measured and is called the "recording length" of the defect, especially for weld testing (Section 28.1.4). The actual length of the defect is of course smaller because of the directivity of the probe. In Fig. 19.9 a this length s has no connection with the actual defect width of for example a small sphere or a narrow cylinder but only represents the beam diameter at the distance of the defect. If the diameter is known, one can use it to correct the results in cases b and c, but this procedure is not of much practical value since the return reflection is also affected by the directivity of the defect, which is not usually known in practice. Therefore the envelope curve or evaluated length of a strongly facetted defect can appear much longer than it actually is, since it also reflects the weaker oblique radiation from the probe. The overall case seems quite complicated to calculate and in practical work, especially with weld testing, one does without these corrections using the recording length as a base for fixing the recording and rejection limits agreed upon in advance (Section 28.1.4).

Figure 19.10 shows the relationship between the half-value width of a reflector and its actual width. It is possible to recognize the difficulty when measuring defects narrower than the diameter of the probe. With regards to the distance of narrow defects it is also possible to see that at short distances (measured in relation to the near-field length), as well as with large ones, there is no possibility of reliably correlating the half-value width to the actual one. Even at the most favorable dis-
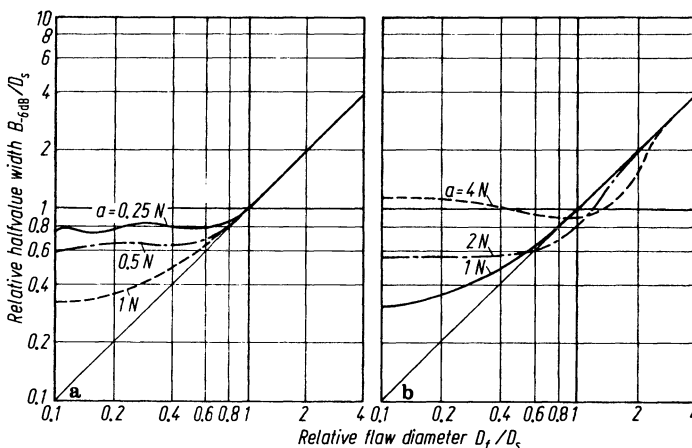

Fig. 19.10. Correlation between the measured half-value width B and the actual circular flaw diameter D_f. **a** In the near-field; **b** in the far-field of a transducer of diameter D_s, measured in water, at various distances a of the reflector measured in near-field lengths

tance, the near-field length, only defects of at least one probe diameter can be measured correctly.

The two maxima in Fig. 19.9d are caused by the edge waves, which can be distinguished from the specular reflection only if the reflector has an oblique position, as in Fig. 19.8, and has sharp edges. They have an appreciable amplitude only if the defect edge lies linear and perpendicular to the beam axis. From the lateral separation of the echoes on the screen and the displacement of the probe during scanning, one can also obtain the angular plane of the defect. For such measurements the beam should be well focussed at the distance of the defect, especially by using high frequencies. In practice therefore this can be carried out only for distances in steel up to about 200 mm, for which range probes of not too large a diameter and frequency are available. At larger distances any scanning of a defect for measuring its size is useless.

At the high gains needed for detection of the edge-wave echoes the noise, or grass, on the screen often make the methods of Fig. 19.8 difficult to apply. The echo of the far edge can be very weak, especially if the face of the defect is illuminated at a very flat angle. The reasons may be the reflector-directivity of the defect and the phase reversal which causes the incident wave to appear to "shy away" from the surface as in Fig. 16.2. This applies to both the longitudinal wave and to the transverse wave with polarization perpendicular to the edge of the defect, but not to the other (SH) transverse wave.

If the envelope curve of Fig. 19.9d displays several regularly spaced maxima, they can arise from the interference of two waves coming from two distinct centers, as for example two pores, or of the two edge waves from one flat reflector [1615]. This can only happen if the probe during scanning is always able to receive both waves by having a large directivity angle. One can calculate the separation of the two wave origins from the separation of two of the maxima and this gives the diameter of a flat defect, a method which in practice had some success in measuring defect sizes.

A shallow *incipient crack* is difficult to evaluate with any of the above-mentioned methods and this defect type will therefore be treated in more detail. In spite of the problems of using saw cuts as reference reflectors for echo amplitude measurements they are nevertheless often used in practice as models for measuring the depth of shallow open surface cracks. If the length of the crack tip lies parallel to the surface and is sufficiently long the method of Fig. 19.11a can be used successfully since a well focussed beam incident from the opposite surface generates an edge-wave echo. Working from the cracked surface the method using two angle probes as in Fig. 19.11b is successful with separate transmitter and receiver probes. Longitudinal waves have proved to be superior for this application because they ar-
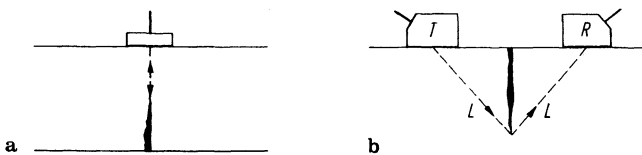

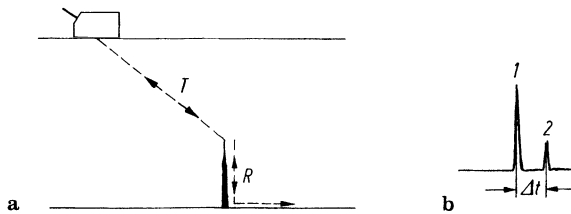**Fig. 19.11.** Measurement of crack tips by edge waves

Fig. 19.12. Measurement of crack depths by satellite echoes generated by mode changing at an edge (Rayleigh wave *R*)

rive at the receiver before any interfering waves. The method of Fig. 19.12, however, uses transverse waves, which by mode changing generate a Rayleigh wave at the crack tip and which can, on a rather smooth crack surface, run down the crack and back, being retransformed into a transverse wave with an echo arriving somewhat later than the direct echo from the tip. From this delay (Δt) the crack depth can be calculated and such echoes have been given the name *satellite echoes*.

The above-mentioned methods however, are not always successful for all types of natural crack. Fatigue cracks are more favorable because they usually have a smooth surface from the prolonged affect of repeated stress cycles and they also usually have a well defined tip edge. Corrosion cracks are on the other hand often more ramified and angulated, and don't have tips lying parallel to the surface. The multi-frequency method of Section 19.4 seems to be more effective in this case [1152]. For closed cracks see [S 36].

If a smooth-edged crack has a tip not lying parallel to the surface, illumination by oblique transverse waves in a direction perpendicular to the tip line can be successful [973]. Cracks with faces pressed together by high internal or external stresses, or those filled with liquid, may not give an indication since they are partially transparent and heating of the specimen can sometimes help.

For literature on crack measuring see [578, 579, 230, 200, 1139, 1422, 192, 1651, S 101, S 52, S 39, S 19, S 30, S 184], especially for the edge-wave method see [750, 218, 1418, 1551, 1587, 650, 1656, 291, 1632, S 66, S 103, S 130, S 150]; for the holographic method see [1653]; and for SH-wave methods see [292].

More elaborate methods based on the scanning system have been reported in Chapter 13 and in particular the *ALOK method* should be mentioned (Section 13.12.1; Figs. 13.6 and 13.7). Using one or more probes at each point of the scanning line the transit-time/position curves of the reflector echo are recorded so that after using electronic interference suppression methods a B-scan image of the reflector in the plane of incidence is obtained. Wide-angled beams are preferred for this method and have proved successful with natural but not too complicated defects.

The Δ *(Delta) method* of Fig. 17.15, see [268], also makes use of the edge waves. Because they have a wide-angle directivity around the crack edge, the axis of the receiver at the position of maximum echo will always be directed towards the edge. The best technique is to use separated transmitter (as illuminator) and re-

ceiver probes, the receiver being sensitive to longitudinal waves because normally scanning is carried out via a liquid layer or by full immersion techniques. The flaw can be illuminated by either longitudinal or transverse waves by way of mode conversion at the liquid interface.

This technique has more recently become known under a new name as the *TOFD-method* (time of flight-diffraction) and is now commonly applied with computer assistance for thick weld testing. It sometimes uses several pairs of transmitter and receiver probes specially designed for their different tasks. Weld testing is a very successful application for such methods because of the relatively short distance from the receiver to the defect, allowing the use of focussed beams from probes of a handy size. See [1414, 1415, 1512, 285, 726, 727, 1070, S 58, S 157, S 7, S 37].

Up to now we have been dealing with methods intended for the evaluation of defect size. However, quite often the size is less interesting than the defect type and its shape, especially for being able to differentiate between planar and globular defects. For castings as well as for welds these shapes can indicate the difference between more dangerous cracks and less important inclusions. Each type of defect differs in regard to its reflecting directivity, as explained in Figs. 19.13 and 19.14. The envelope curve obtained by circular scanning of a flat specularly reflecting defect, or even of a linear reflector, is sharper than that from a rounded reflector. It must be admitted that in practice the difference is often not very clear. Many attempts
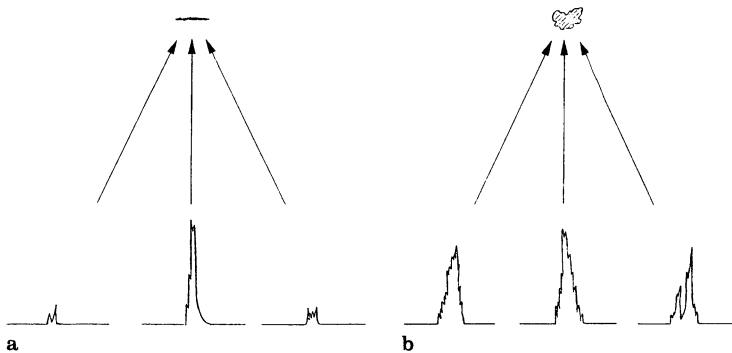

Fig. 19.13. Change of echo height and echo shape when the direction of irradiation is changed. **a** On flat or linear flaw; **b** on rounded flaw
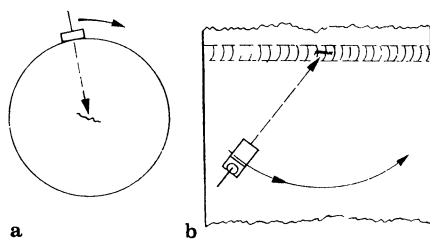

Fig. 19.14. Change in the direction of irradiation. **a** On cylindrical specimens with central defect; **b** on a welded seam

have been made to recognize the differences automatically to allow discrimination between the various flaws.

Certain features of the echo and its envelope curve have been used; for example the rise and fall time of the echo, its width near the base line, the width of the envelope curve, or its plateau length [1297, S 164]. Simple pattern recognition methods have not been successful, apparently because of the complex variations in the echo shape. More successful are mechanized scanning methods using intelligent computers, the so-called learning computers and expert systems. In their memories are stored many basic geometric features of the echo together with an interpretation system using rules derived from practical testing experience [1292, 1298, S 164, S 45]. Frequency analysis of the echo also seems to be very promising, see Section 19.4 and [S 38]. For advanced pattern-recognition methods for weld defects see [S 156, S 26].

A direct imaging method would of course give the size and shape of a reflector and the most promising method in this direction is linear holography which with its good lateral resolution is well suited for measuring the width of a reflector (Section 13.14, [513, 516]).

For using such methods fast computers are indispensable so they may be used simultaneously to control phased arrays thus avoiding mechanical scanning. In some cases, for example nuclear reactor pressure-vessel testing, it is justified to make use of such an installation, although its weight (several 100 kg) and size will be a big disadvantage for more general ultrasonic testing.

For the problem of defect sizing see older papers [1028, 1335, 1525, 1524, 1618, 416, 494, 588, 670, 1659] and more recent ones [1635, 1338, 1695, 1752, 335, 1033, S 181, S 90, S 68, S 47, S 177, S 149, S 45, S 43, S 14, S 155] and the bibliography to the problem compiled by the BAM and DGZfP [S 188].

19.4 The Multiple-Frequency Method, Echo Phase and Spectroscopy

In Section 5.4 it has already been mentioned that by using the DGS method at two or more frequencies one can deduce something more about a defect. A flat reflector which is not inclined very much to the beam axis, is measured as being closer to its actual size (i.e. larger) by the DGS method using a low frequency than when using a higher frequency, whereas with globular reflectors the difference is less pronounced. If one combines this principle with the half-value width method and circular scanning to obtain an evelope as in Figs. 19.13 and 19.14, one arrives at the defect-classification system of Crostack [276] illustrated in Fig. 19.15.

This system produced satisfactory results with defects in castings. The amount of time needed can be reduced if special flaw detectors are used, allowing frequency change without probe change. For this purpose the pulse transmitter must be excited at well defined frequencies and using a probe of sufficiently large band width as in the controlled signal (CS) technique. The reference echo needed for the
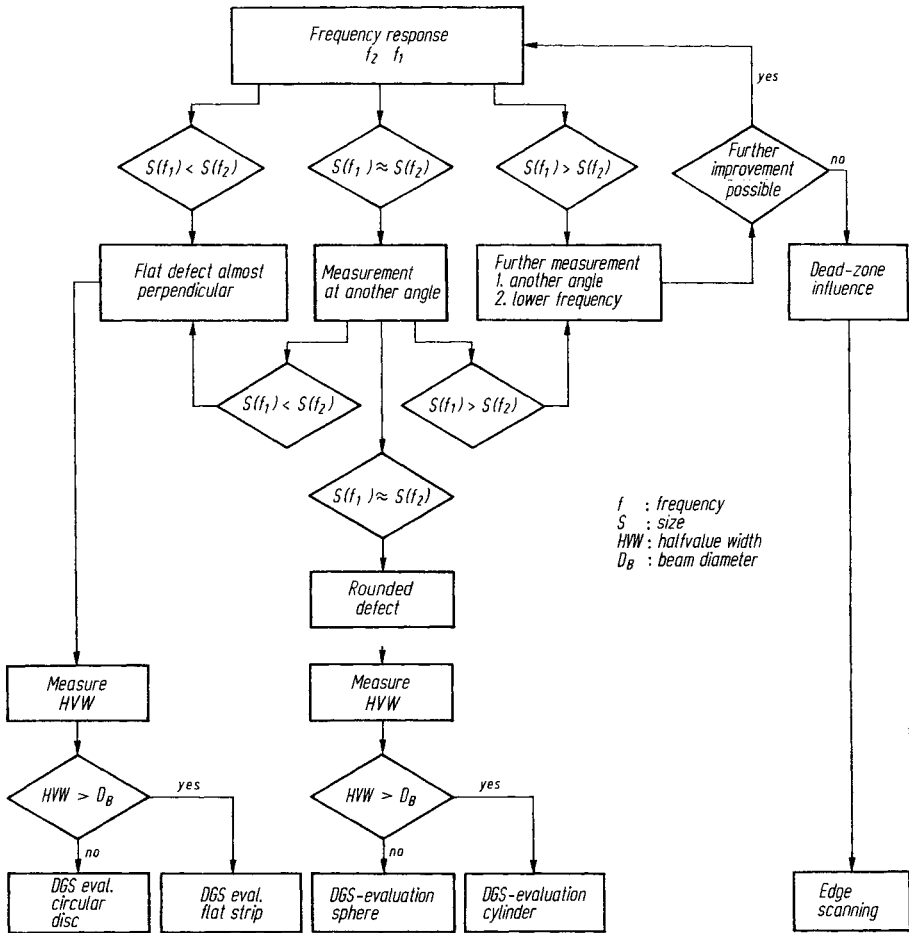
Fig. 19.15. Defect evaluation according to the frequency, circular scanning and half-value method

DGS method (the plate echo) has however to be measured separately for each frequency used.

From the procedure of Fig. 19.15 a new concept can be considered resulting in the definition of a *transition frequency*. A very small defect of any shape, which is illuminated by a sound beam with a wavelength several times larger than the defect, gives a scattered echo more or less independent of its special shape. The corresponding frequency range is called the scatter region. As the defect size increases (or the wavelength decreases) we arrive at a region where its size is comparable with the wavelength and can reflect the beam specularly if it has a flat shape. In the scatter range the echo amplitude normally increases as the wavelength decreases but at a certain point when examining flat defects it can begin to decrease. The transition frequency at which the echo begins to fall again has been measured for small corro-

sion cracks as approximately corresponding to a wavelength of twice the size of the crack. This transition frequency could also have some importance in the choice of the best probe for testing materials such as austenite which have heavy scattering characteristics.

Another possibility for the evaluation of defect types can be found in observing the echo phase when it is displayed in its unrectified HF form on the screen. A pulse which has been specularly reflected at a free boundary has the phase opposite to the transmitter pulse, usually starting with a negative oscillation. On the other hand the echo from a liquid/solid boundary undergoes no phase shift so that it starts with a positive oscillation, cf. also [S 32].

This fact can be made use of when testing bonded joints since the bond line between a plastic layer bonded onto a material of higher impedance will give an echo without a phase shift whereas if it is badly bonded with an air filled interface it will show the usual phase change. This rule will be modified in the practical case of a metal/plastic bond according to whether the test is carried out from the metal or the plastic side of the bond.

It should also be noted that the geometrical echo from a right-angled corner (Fig. 2.26) in a solid body shows no effective phase shift because of the double reflection. According to [1552] the edge-wave echo from the upper edge of an oblique crack, as in Fig. 19.8, has the negative phase compared with a surface echo, whereas the echo of the lower edge has the opposite one, by which it can be distinguished from the echo of a defect. By using the Cepstrum-algorithm for signal-processing the phase of the signal can be recognized more clearly even with high noise levels [S 131].

The use of ultrasonic spectroscopy involves the investigation of an echo to determine its frequency content. This can be done by a frequency analyser used as auxiliary equipment to give an amplitude-frequency curve for the echo. This can be compared with the corresponding curve of the original transmitted pulse, as for example that reflected by a flat back surface. If the material concerned has no attenuation the back-wall echo is identical with the transmitted pulse but the reflection at a defect acts as a frequency filter in the overall system: transmitter-probe-coupling-specimen-defect-coupling-probe-amplifier, [1658]. The wider the frequency band of the transmitter, that is the shorter the transmitter pulse, the better information concerning the defect can be expected from an analysis of the echo frequency spectrum. Broadband probes are therefore indispensible [931, S 10].

Example. If the frequency curve of the echo shows several maxima which are not present in the reference curve, one can conclude that they are the result of interference. Thus the defect either consists of two separate reflectors, as for example two pores, or it could be a smooth-faced separation at which Rayleigh waves are generated, subsequently to excite edge waves which will interfere constructively or destructively depending on the frequency. Such recognizable cases may of course be rare in practice. However, in the field of bond testing spectroscopy has proved successful (Chapter 29). A pulse of moderate length changes its frequency spectrum by the effect of multiple reflections within the bonding layer between two materials, depending on the quality of bond at both interfaces. Within the range from a com-

plete disbond to a well bonded joint the method is often the only reliable one for distinguishing a poor quality bond from good bonding. Some straightforward applications of spectroscopy can incidentally be carried out without a frequency analyzer simply by using an old-fashioned resonance thickness meter (Section 11.3.1).

In the present connection other properties and features of the echo have been considered in the evaluation of a defect, for example to distinguish a flat from a rounded reflector [1292, 1298]. Apparently the method of Seiger and Wagner [1397] is also successful, though purely empirical. A broadband angle probe is used to scan the specimen containing a defect in small steps. At each scanning point the received echo is frequency analyzed. The measured spectra are divided into five equal ranges, for example for a 2-MHz probe into five bands of 0.3-MHz width from 0.7 up to 2.2 MHz. The maximum amplitude occurring in each band is noted and the resulting $5N$ values (where N is the number of scanning steps) are processed by an empirical algorithm resulting in a final value which gives an indication of the flaw type, flat or rounded. The method was astonishingly successful when used to evaluate a series of natural and artificial defects in welds.

To each frequency spectrum there also belongs a phase spectrum, and this has also been used for defect evaluation [1022].

For more literature concerning multiple frequency methods see [270, 276, S 40], and for spectroscopic methods [521, 671, 931, 1212, 1410, 185, 382, 293, 1296, 903, 1347, 338, 1397, 200, 1068, 1613, 148, 1098, 649, 1483, 1298, 1292, S 155, S 159, S 121, S 154, S 61, S 134].

20 Organization of Testing; Staff and Training Problems

Where the same testing problems for identical or very similar specimens occur frequently, it is recommended that the head of the testing department works out a test specification so that the tests can be carried out by a trained examiner. From service experience and information gained from destructive tests, the nature, size and position of flaws will be generally known, so that non-destructive tests can then concentrate on these. The specification should include: designation of the specimen with a sketch, instructions on whether and where the surface should be prepared, type of couplant, setting of instrument and choice of probe for each testing procedure, together with indication of scanning patterns for suspected flaw positions as well as reference to possible echoes which could be confused with flaw echoes. In the case of mass tests, the examiner can, as a rule, be relieved of the necessity of preparing individual reports since on the evidence of the flaw echoes he can quickly make his own decision whether a given specimen should be rejected or not. In the case of more costly test pieces a preliminary sorting out of doubtful specimens is advisable after which these can then be submitted to the more experienced head of the testing department for final decision.

For a number of general testing problems, such as the testing of plates, pipes and welded joints, test specifications are now available whose validity is generally recognized (cf. Chapter 34). The purchaser of products can refer to them if, in the contract with the manufacturer, he has agreed on a test by ultrasonics. They describe in more or less detailed form the test procedure which in particular specifies how the equipment should be adjusted. When testing large quantities of similar test pieces, it is necessary to check at regular intervals the chosen adjustment of the equipment. Previously this was done by means of a test block with properties similar to that of the test piece. In order to obtain definable flaw sizes and flaw shapes for monitoring the adjustment, the test block contained artificial flaws which in respect of size, shape, position and orientation were supposed to show some similarity to the flaws sought.

Today the sensitivity adjustment is usually referred to a standardized test block (cf. Section 10.2.4), the sensitivity adjustment required for the test generally being expressed by decibel values above or below the standard test-block setting.

If evaluation of the specimen is not possible on the basis of the ultrasonic indication alone or if such experience is as yet insufficient, additional non-destructive tests can be applied, for example local tests with X-rays or gamma rays. The ultrasonic test then plays the role of a rapid and inexpensive preliminary test. With greater experience, the ultrasonic test can then frequently become the only test applied, for example on welded seams.

Expensive batch-produced specimens, as well as individual cases, are usually tested according to a written specification. The results are compiled using suitable forms to minimise labor, and using abbreviations and symbols to report the ultrasonic observations as completely as possible. At this stage one does not speak as yet of defects or defect echoes, but only of indications or echoes to avoid any prejudgement of the specimen. The task of the operator is restricted to assemble as many facts about the test as possible, such as the observed variation of echoes during scanning and when using different sound-beam directions. The responsible manager of the test department has to evaluate from these observations the type and size of the corresponding reflectors, although he cannot always decide to accept or reject the specimen without consultation with a design engineer who knows the working stresses for the piece.
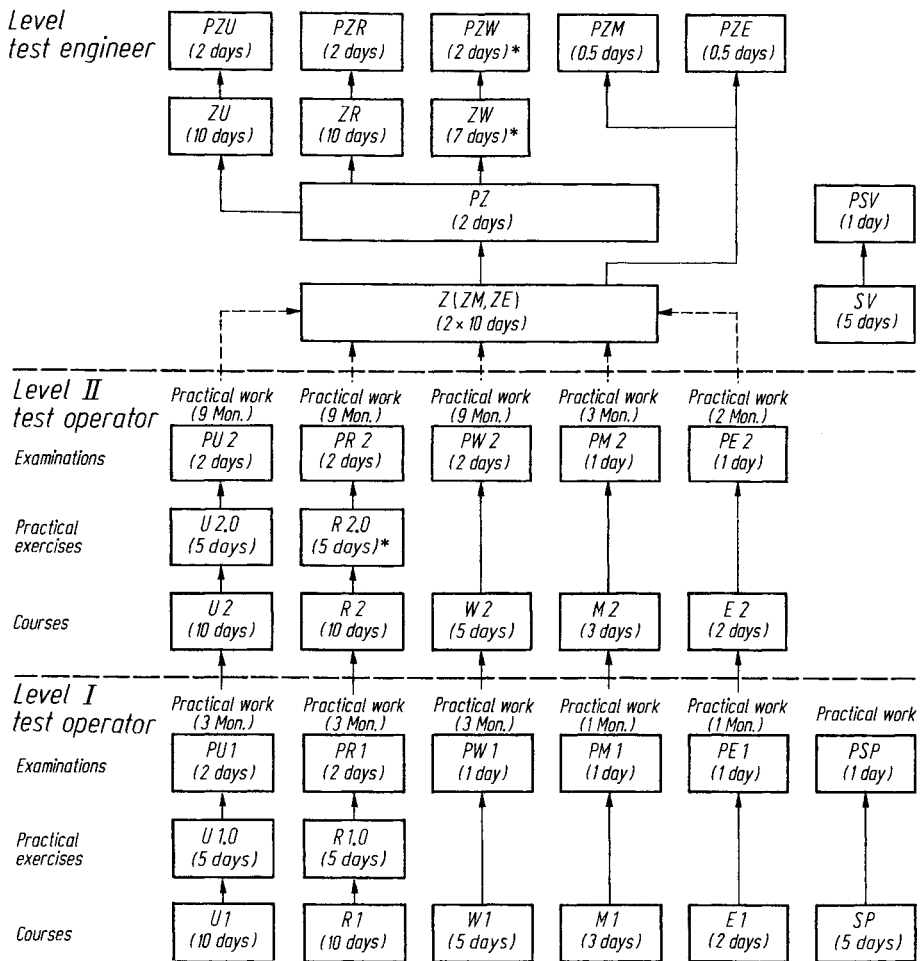

Fig. 20.1. Training program of the DGZfP (according to Egelkraut [1713])

For planning test programmes for complex pieces which may not be accessible from all sides, full drawings will be required so that the correct probes can be chosen, and echoes predicted arising from the form of the specimen, such as those arising from boreholes, edges and remote faces. The drawing, however, may not in all cases correspond exactly to the actual geometrical state of the piece so that any unexpected echoes arising will have to be checked carefully since they may nevertheless be produced by the specimen's shape. Common examples are echoes arising from machining errors which have been disguised or filled. Often also the regular appearance of echoes, or their symmetry when scanned from different positions, make it probable that they are geometrical in origin and not produced by real defects.

Routine tests using only normal (0°) probes, for example on plate or bar material, demand the least experience. Often a training period of a few hours is sufficient if the examiner has good powers of comprehension and a certain dexterity in manipulating the probe without excessive wear and tear so that high-school education is unnecessary. When working with transverse, or surface waves, for the testing of complex specimens, such as shafts, pipes and especially welded seams, more experience is required. The study of a manual of testing methods, a training course, or an apprenticeship with an experienced examiner is desirable. In addition, a certain amount of technical training with a knowledge of elementary mathematics and a good capacity for visualizing objects in space is needed. Before being promoted to the position of unassisted examiner of welded seams and expensive test pieces, the acquisition of a thorough knowledge of the relevant materials and production methods is indispensable. Qualities of character such as diligence and thoroughness are necessary to an even greater extent than for other non-destructive testing methods. Independent application of ultrasonic methods for many different and newly developed tests presupposes at least the study of much physics and mathematics and in addition long practical experience.

The knowledge required for the various testing techniques can be acquired in Germany in a course of the Deutsche Gesellschaft für zerstörungsfreie Prüfverfahren e.V. (DGZfP). Similar courses are also available in other countries for instance in Great Britain at the School of Applied Non-destructive Testing (SANDT) and in Japan at the Nondestructive Inspection Society of Japan. In addition a large number of courses and seminars are organized by manufacturers, users, and other independent organisations, both at home and abroad.

The chairman of the committee for training and professional matters in the German DGZfP has since 1970 systematized the courses for training in the main NDT methods, i.e. ultrasonics (U), radiography (R), magnetic particles (M), eddy-currents (W), liquid penetrants (E). The qualification levels for all sections have been fixed uniformly. Figure 20.1 shows the different training programs according to Egelkraut of the DGZfP.

Figure 20.2 shows the sequence of courses, examinations and practical stages within a given training program, the courses mentioned to the right hand of the dotted line being offered by the society. The stages on the left can also be carried out at certain authorized institutes or by manufacturers of equipment. Extended training college courses also allow the promotion of a level-II test operator to a Test
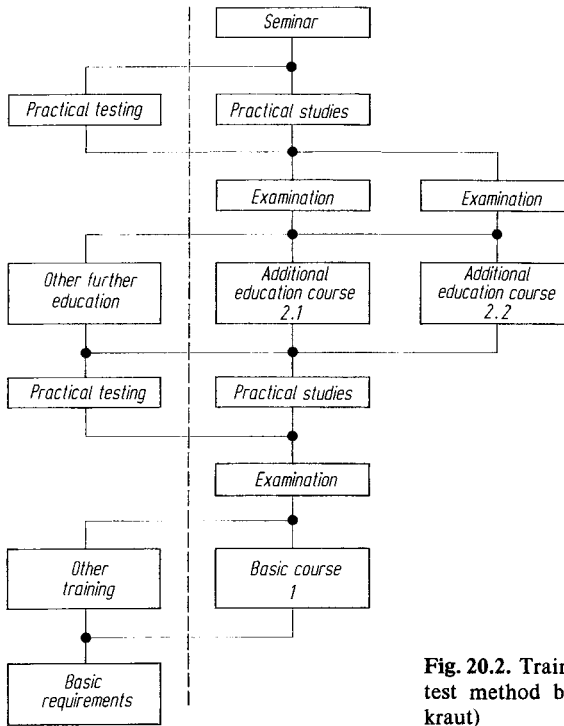
Fig. 20.2. Training performance required for each test method by the DGZfP (according to Egelkraut)

Engineer (Z). However, for this step knowledge of several complementary test methods has to be obtained. (See also the qualifications specification of the DGZfP, [1713] and [369, 370, S 189]).

Equivalent organisations in other countries (see Chapter 34) have also produced specifications and/or recommendations for the training of NDT operators. In the USA (ASNT-Spec SNT-TC-1A); in Austria (ÖGfZP Standard); in Switzerland (SGZP Standard); in France (Cofrend Standard); in Denmark (officially acknowledged rules of Nordtest Corp.); in the Netherlands (Skndo Specification); in Great Britain, (Specs. of CSWIP and PCN); and in the Council for Mutual Economic Assiotance (Government specifications). Full harmonization between the various official requirements has only been fully achieved between the specifications of Germany, Austria and Switzerland up to level III. Work is currently going on for worldwide harmonization of national specifications under the auspices of ICNDT, (International Committee for Non-destructive Testing).

The U.S.A. specification also comprises three levels (I to III), which do not, however, correspond exactly to the German grades. At present therefore full automatic transfer from one to the other is still not possible.

21 Testing Installations and Evaluation of Test Results

In parallel with the gradual mastering by test operators of manual testing methods in the course of time, there came also the development of automated continuous testing installations [1226, 119, 1369] up to the specialised single-piece testing automats [1190]. Examples for the former type of installation are those for testing plate, rods, rails and tubes, which are built into transport roller ways (Fig. 21.1). Example for the second kind are automats for testing steering joints, valves, rollers, balls, and other individual machined construction elements. Their design depends on the shape of the piece for manipulation, and for scanning by the probes (Fig. 21.2). For piece and probe manipulation industrial robots are today used to an increasing degree.

For successful automated testing the signal/noise ratio must be relatively large. Interfering echoes can arise from acoustic scatter at grain boundaries, from mode changing as for example Rayleigh waves in tube testing, from unwanted geometrical reflections and from small bubbles and particles in the coupling water. The incident angle of the beam has to be controlled very accurately because of the strong refraction at the water/solid-interface, thus requiring precise manipulation of the test pieces. This effect can be largely avoided by the use of water-gap coupling in which the final position of the probe is controlled by the surface of the test piece.

For high-speed testing the pulse repetition rate must be quite high since the smallest reflector of interest should be struck by two to five pulses to allow the use of the anti-interference devices mentioned in Chapter 18. The maximum repetition rate which can be used is, however, fixed by the length of the ultrasonic path in the

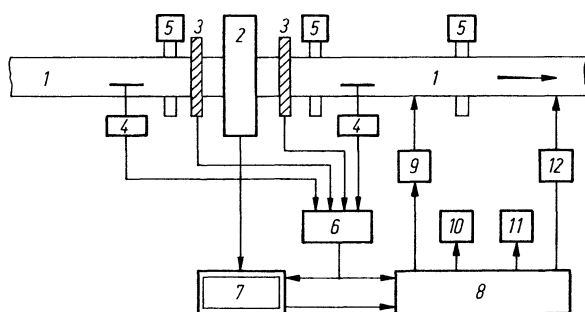Fig. 21.1. Continuously working test installation, schematic. *1* test object, *2* test machine with probes, *3* sensors for beginning and end limits, *4* transport sensors, *5* transport, *6* control of test mechanics, *7* ultrasonics (flaw detector), *8* processing and evaluation of test results, *9* marking of defect, *10* signalling (optically and acoustically), *11* documentation, *12* sorting
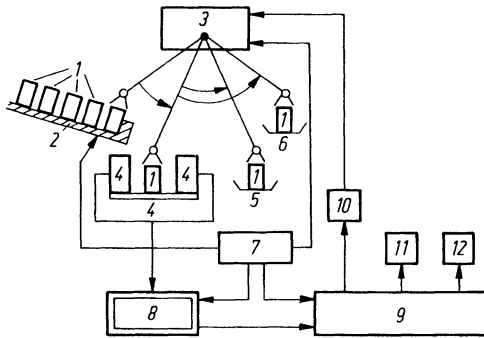
Fig. 21.2. Single-piece automat, schematic. *1* test objects, *2* feed magazine with separating device, *3* object manipulator/robot, *4* object holder with probes and/or probe manipulator, *5* accept container, *6* reject container, *7* control of mechanics, *8* multiplexer electronics, *9* evaluation of test results, *10* sorting, *11* optical and acoustic signalling, *12* documentation

specimen and the water delay line, allowing sufficient extra time for the effective decay of phantom echoes (Section 10.9).

Finally the beam width used influences the choice of scanning speed. In manual testing the operator can readily observe echoes from a reflector struck only by the edge of the beam and can then maximise them. This is not feasible in automated testing, where an indication from a reflector can only be evaluated if it is detected with an echo amplitude only a few decibel down from the maximum. The critical recording and evaluation limits have therefore to be fixed at lower levels than with manual testing.

For certain basic products such as tubes, plates and welds this threshold can usually be fixed according to existing specifications. For other pieces the border between accept and reject must be evaluated experimentally with defective pieces, unless the necessary experience has already been obtained by simple manual testing.

As a reference defect an artificial reflector within a sound piece is sometimes used. This should be as simple and reproducible as possible. As explained in Section 19.2 it is useless to try to simulate the actual shape of natural defects and a simple borehole or a saw cut does the job quite well. The actual reject threshold has to be determined, after confirmatory destructive tests, by reducing the standard echo to a level a certain number of decibel below the reference echo.

Several probes for different beam directions and driven by one flaw detector can be controlled by a multiplexing device, which also controls the gate levels for each probe. For evaluation and documentation several separate sensors have to pass their information concerning the speed and the end limits of the test piece to the evaluation unit (see Fig. 21.1). As well as using optical or acoustical signalling to reveal the presence of a defect, its position on the piece can be marked. An illuminated picture can represent the geometrical position of a defect for a limited time and marking of defective pieces can be carried out by a colour spray, by grinding wheels or by applying a magnetic marking. It can be applied at exactly the defect position or only generally at some other position on the piece. After automatic sorting into different containers the acceptable pieces can be transported for further use and often defect-free pieces are colour-coded to indicate that they have undergone a test.

Documentation of the results can be carried out in many different ways. Firstly a plan of the specimen can be drawn by a recorder complete with indications of defects which are true to position in two planes showing both length and width. Direct recording instruments are provided in this case or sometimes film recording is used in spite of the disadvantages of the photographic process.

A more advanced technique is by the use of digital printers, especially if the amplitudes and transit times of the echoes have been digitized. For repeated periodical tests the complete storage of all results can be done by magnetic tape recording as described in Section 22.2 and Chapter 30. Later results can then be compared with earlier ones very precisely to observe all significant variations.

The simplest method of evaluation is to use a threshold gate for both defects or the back-wall echo. If the go/no-go decision must be carried out later by using documentation the analog output of the monitor must be fed to an analog recorder, but because such instruments operate quite slowly the echo amplitudes are better digitized into several specific levels, as for example 0, 2, 4 and 8, which are more useful for a rapid printer.

Nevertheless high testing speeds demand still more complicated documentation. First the total number of single defects beyond the threshold, or those sections of the specimen with defects can be counted and the specimens are then classified according to this number. Instead of the individual defect echoes one can also count all the single pulses giving an echo. Together with digitizing of the transit time a large variety of computer-aided evaluations are possible.

The flaw-detector electronics for such a variety of test-installations use individual units with modular rack mounting. This allows the use of many probes and different evaluation methods, and special modular plug-in units allows the adaptation of a total installation to different inspection requirements.

Because processing computers are used in many industries today it is reasonable to make use of them also for ultrasonic testing. However, with modern developments the very small microprocessors can easily be used inside the ultrasonic equipment for digitizing pulse amplitudes and transit times close to the probes, and also for digitizing the monitor gates and to operate a distance-compensated amplifier based on a digitized amplitude-distance curve.

An example of such a universal flaw-detector system is the equipment IMPULS 1 of Krautkrämer [1193]. This is controlled by a standard commercial terminal with alpha-numeric keyboard and VDU, providing the dialog between unit and operator who receives the demands for supplying test parameters (type and sequence) from the screen. On the same screen an A-scan for each test channel can be presented in digital form. These can be used for observation and for making adjustments during the test. The adjusted parameters can also be stored for later use which is important when repeated tests have to be made.

The separation between the electronic hardware and the operator's terminal allows remote control to be maintained from one or more separate terminals. An additional feature of such systems should be mentioned, the so-called distributed intelligence for which each plug-in board carries a one-chip computer to control individual functions and to announce on the screen any malfunction immediately it occurs. For the basic functions of the test system standardized software is avail-

able, whereas for specific purposes special software can be provided. The excellent test integrity of such installations is guaranteed by the provision of numerous fail-safe control functions.

Further features are mentioned in the Chapters for specific test problems. See also [636, 1158]. Concerning automation of ultrasonic testing see also [S 167].

Part D | *Special Test Problems*

The classification of the numerous test problems in Chapters 22 to 32 encounters difficulties of a systematic nature. Whereas in Chapters 22 to 30 grouping according to shape and the method of manufacture of the piece is used, the criterion of Chapters 31 and 32 is the material. However, a fully logical classification is not possible and so it may be necessary to consult in this connection the subject index.

Unless stated otherwise, the test methods described are always by pulse-echo equipment.

22 Workpieces for General Mechanical Construction

22.1 Large Steel Forgings

In view of the high machining costs and the long replacement times, testing of large forgings is started as early as possible in the manufacturing process, in order to detect and exclude defects already present in the cast ingots, and which would be dangerous in service for the finished piece.

In earlier times this was specially important when forgings were commonly produced from mould ingots. These can contain typical defects such as

— Primary shrinkage cavities,
— Secondary shrinkage cavities which can disappear during forging if their surfaces are not oxidized,
— Non-metallic inclusions such as Si and Al oxides,
— Foreign bodies such as pieces of furnace linings and unfused workshop tools and equipment
— Flakes (hydrogen embrittlement cracks)
— Segregations

A simple segregation is usually not detected by ultrasonics or perhaps only very weakly. A Baumann or sulphur print, which indicates such segregations, cannot be used therefore for direct comparison with ultrasonic test results. According to [125] metallic sulfide slag, and small alumina inclusions cannot be detected reliably.

Cast ingots are best tested in the direction of the smallest dimension, i.e. transverse to the axis, and scanned along a few longitudinal paths the surfaces of which can if necessary be prepared by grinding. Because of the coarse grain structure and the large dimensions the test is not always satisfactory even when highly damped probes of low frequency (0,5 MHz) are used.

Today ingots made by electro-melting processes are preferably used, where in practice most of the defects mentioned above no longer occur, but only small inclusions widely distributed across the section. This fact makes it unnecessary to test the ingot, a further reason being the trend to save energy by not letting the ingot cool down before starting the forging operation. If, however, during a multi-stage forging process cooling intervals allow testing, this is done along several surface tracks at low frequencies for 0,5 to 1 MHz (see [845]). Testing of hot forgings has not found much application in practice (see [1039, 1328, 1319]) mainly because the strong heat radiation does not permit careful manual testing, and scaled and uneven surfaces affect ultrasonic coupling and prevent mechanical scanning.

For all these reasons the testing of large forgings is usually done after final forging and when heat treatment is complete, but before final machining when

grooves, steps, conical sections and chamfers have not yet been incorporated [1132, 254]. The surface roughness for testing should not exceed 10 to 12,5 µm.

As well as the typical defects arising from the ingot other defects are caused by the forging process especially cracks. They can be caused by forging at too low a temperature or by faulty heat treatment. Inclusions already present in the ingot can assist in the production of such cracks.

After annealing the ultrasonic attenuation is usually very low. For example in rotor forgings it is not measurable with 2-MHz longitudinal waves and even at 4 MHz only reaches 4 to 6 dB/m. Sometimes therefore phantom echoes can occur when using low frequencies and high testing sensitivity as is commonly used today (see Section 10.2.3). In practice they are not always recognized as such but misinterpreted as increased noise level.

This occurs especially with small parts such as test blocks and if it is suspected it is recommended to reduce the pulse repetition rate of the flaw detector or to use a higher test frequency. If the "noise" is then reduced, its origin as arising from phantom echoes is confirmed.

The attenuation for normal incidence can be measured in a simple way from the difference between the first and second back echoes [851] if the loss by geometrical divergence has been allowed for. Solid cylinders behave in this respect as plane parallel plates but forgings with a central bore must be treated differently [979]. In the case of different grain structures between inner and outer zones, or when local zones of coarse grain occur as sometimes in austenitic forgings, this method only gives an average value of the attenuation through the section and in the case of coarse grained zones can be misleading.

For obliquely incident transverse waves the attenuation can be measured, on annular retaining rings for example, using two identical angle-probes in either V- or W-path through transmission. On solid rotor forgings this method is not feasible and one has to use normal (0°) transverse wave probes in the above-mentioned way.

The testing technique depends on the pattern of the forging grain flow as shown in Fig. 22.1 for selected examples. Since flaws such as inclusions and cracks extend by preference in a direction parallel to the grain flow the ultrasound should be directed as nearly as possible in the perpendicular direction. For this reason the test in an axial direction on forgings for turbine or generator rotors is not very informative. Most defects will give very small echoes in this direction, but certainly will reflect strongly if tested in the transverse direction. In addition the long distances in the axial direction are a disadvantage because of reduced sensitivity due to both beam spread and material attenuation.

If when sounding in the longitudinal direction no back echo is received the reason need not always be a real defect. Within the central zone higher attenuation from coarse grain structure may be the main reason, whereas near the outer surface
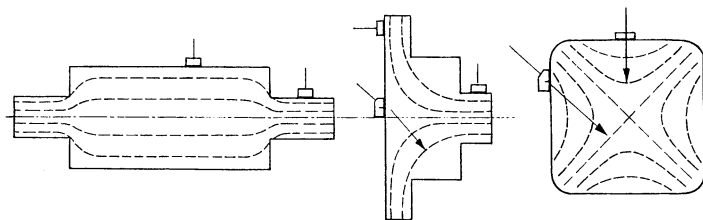

Fig. 22.1. Grain flow of large forgings and optimum testing techniques

the side-wall influence can also prevent an appreciable echo (see Section 16.1). Testing in this direction is an advantage only to detect a large transverse crack, the so-called cold shut, but this can also be detected from the curved surface using 45° angle probes, either directly or by using a pitch and catch technique. During transverse testing with normal (0°) probes these defects often give no direct echoes but can cause loss of the bottom echo, as explained in Fig. 16.4.

The amount of testing a forging will receive depends on its shape and final purpose. Sometimes it will suffice to scan a few longitudinal tracks on the curved surface with longitudinal wave probes. However, it must often be scanned over the complete surface with longitudinal probes and additionally with angle probes in both the circumferential and axial directions, also including pitch and catch techniques. A Sulzer specification for rotor testing demands complete scanning of the whole volume with angle probes as in Fig. 17.2. If the divergence angle of the probe for a 6-dB echo drop is $\gamma°$, several further angle-probe scans have to be made with probes having a beam divergence angle of $2\,\gamma°$. For such as complex test the use of a phased array would be helpful. The frequencies used commonly lie between 1 and 5 MHz, and are mostly chosen as 2 MHz.

The interpretation of the echo patterns can finally give a complete map of all defects concerning their position, angular orientation, size, shape and type. At this stage the concept of "defect" should be avoided so as not to give a judgement on the possibility of using the piece. Modern progress in the methods of fracture mechanics allow quite precise evaluations of critical flaw size for rejection or safe acceptance. Formerly used methods as for example echo amplitude ratios [1038], numerical tables [1238], or purely statistical specifications for acceptance as in the diagram of Rankin and Moriarty [1224, 1225] can no longer be considered as sufficient.

The position of a defect can be determined quite precisely from the echo transit times, if the unit has been carefully calibrated. There are also testing units available which give digitally the distance of a reflector. Evaluation of the angle at which the echo appears is much less precise. This would usually be measured from the normal to the surface at the probe contact point, and there are two reasons for this difficulty. Firstly there may be a lateral deviation between the actual sound beam path and the nominal one, the *squint angle*, and secondly the fact that depending on its inclination and shape a flaw may give its maximum reflection for rays off the beam axis. Additionally the probe can easily be somewhat tilted on curved surfaces giving wrong angular indications of the flaw position. This situation can be improved by using a mechanical guide to keep the probe in a consistent orientation and position. If a flaw must be extracted by trepanning with a hollow bore drill, it is recommended that the exact position is calculated from a triangulation using several beam directions.

To measure the size of a flaw the echo amplitude, as well as the recording length, can be used. Using the DGS method the echo amplitude gives the size of the equivalent flaw (see Section 19.2) but the actual size can be larger, even much larger, than this. For some types of defect correction factors have been determined empirically [813, 1052], but of course these have a rather large scatter range and require a definite knowledge of the defect type.

The opposite case, in which the actual flaw is smaller than the equivalent one can also occur, but very rarely.

In a forging produced from electro-melted ingots small non-metallic inclusions can occur in a very wide distribution. It has been observed at a large distance, and hence a large beam diameter, that the many echoes from small particles can add up with equal phase, so simulating one larger reflector. Focussing of the beam might help in this case, but this is usually impossible at such large distances because of the necessary large probe diameter required. Proposals to evaluate the flaw size in such cases are given in [641].

For the practical measurement of the equivalent defect size Kleinmann [811] has proposed special DGS-graticule scales to be fixed in front of the CR screen (Fig. 22.2). The flaw detector unit has first to be adjusted for depth scale and gain. For the latter purpose the graticule contains a back-wall curve, by which the sensitivity can be adjusted directly on the specimen. As with the standard DGS diagram the maximum allowable echo peaks on one of the equivalent defect curves. Material attenuation, depending on the frequency used, has already been taken into account. According to [1327] the attenuation should be classified in 2-dB/m steps so that the appropriate graticule can be selected, which requires of course a special attenuation measurement in advance.

The introduction of the DGS method into testing practice has not only allowed an exact application of the law of distance, and of material attenuation, but it is also easy to measure the effective signal to noise ratio.

In the course of any test in addition to flaw echoes the constancy of the back-wall echo has also to be observed carefully. If the coupling is apparently good, a substantial drop of the back-wall echo can indicate badly reflecting defects, such as large cold shuts, or local bad annealing. To observe such drops at high testing sensitivities a device by which the height of the back echo can be reduced by a selected amount is useful (see Section 10.3.2).

Certain conclusions about the shape and inclination of a flaw can be drawn from the echo dynamics during probe movement by observation from different angles (Fig. 22.3). In a cylindrical forging a single reflector of approximately cylindrical shape first enters the side of the beam thus giving a small echo at a certain
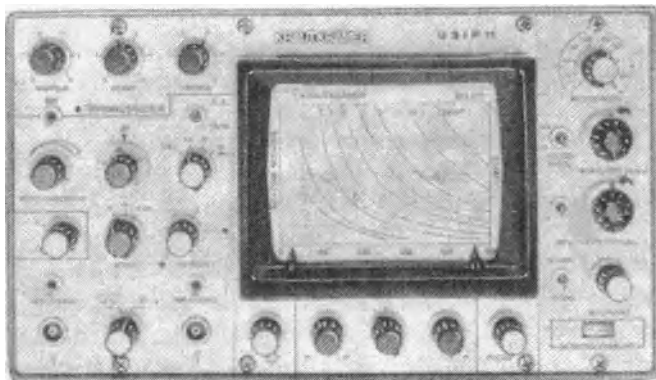

Fig. 22.2. Pulse-echo instrument with DGS graticule for testing forgings
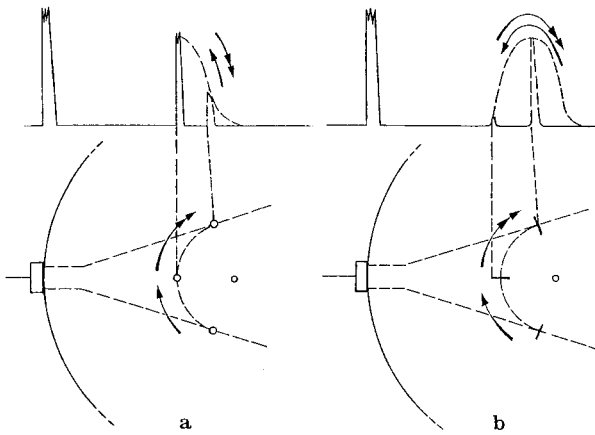
Fig. 22.3. Travelling echoes which appear when a rotor is scanned in the circumferential direction. The envelope of the travelling echo in the case of cylindrical flaws and tangential cracks (**a**) differs from that obtained in the case of radial cracks (**b**)

distance and later a larger echo at a smaller distance. The same behavior of the echo is observed as the reflector leaves the beam. From the movement on the screen it is called a travelling echo. A flatter defect in a tangential position gives a similar symmetrical envelope but with steeper sides. If, however, a flaw has a radial orientation (Fig. 22.3 b) it can give quite a large reflection from a larger distance but falls when it approaches the closest position rising again as it passes to the side of the beam once more. For an inclination between these two extreme cases the envelope becomes non-symmetrical. From such travelling echoes one can deduce the presence of a flat flaw, a likely crack, and therefore a dangerous one [85]. For the

Screen pattern	Shape of echo	Symbol	Screen pattern	Shape of echo	Symbol
	Single echo	EE		Annular zone	RZ
	Group of echos resolved	GA		Many single echos	VE
	Group of echos not resolved	GN		Grass (noise echos from the structure)	WW

Fig. 22.4. Screen pictures with different echo patterns according to ÖNORM 3002

full evaluation of the defect type hints are also provided by its position within the forging as well as by its size and shape. Of course a good knowledge of the manufacturing process of the specimen, and the origin of typical defects which might be caused by the process is indispensable.

For full reporting of all aspects of the screen pattern Fig. 22.4 is of interest, this system being specified by the Austrian Standard ÖNORM 3002 (see Chapter 34).

As an example Fig. 22.5 illustrates the means of distinguishing between inclusions and cracks within a forging. Inclusions often appear in large numbers within a restricted zone, as for example at the center or perhaps within an annular zone. The corresponding screen pattern shows a mountain of echoes between the peaks of which the base line is not visible. Cracks usually appear as single echoes, or at least with larger distances between one and the other, and are more uniform in size. They are usually oriented parallel to the axis of the forging but can be turned round their axes at random angles. Therefore from such a cracked zone one obtains sharp and differentiated echoes with different amplitudes and changing very quickly with change of probe scanning position, the base line often being quite visible between them. The back-wall echo is usually more reduced by a cracked zone than by inclusions. When using a higher test frequency the differences can be more marked, but the pictures are very similar if the cracks are of a small type associated with segregation.

More complex methods for the evaluation of the defect type such as pulse spectrometry and echo tomography with phased arrays (see Chapter 19) are in development [S 182, S 68].
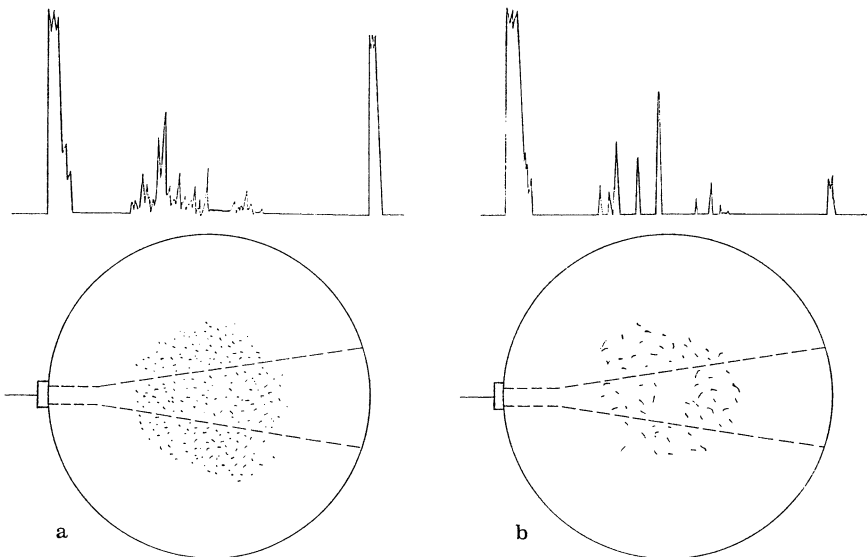

Fig. 22.5. Differences between the indications of inclusions and cracks, drawn schematically and exaggerated for greater clarity. a Inclusions; b flake cracks. The echoes of the more distant flaws, because of divergence and attenuation of the sound beam, are rather weak

As well as the forging manufacturer and the inspection organization further parties may be involved such as the final customer, a classification society and a surveying corporation. Consequently the official *standards and specifications* must be written to refer to unequivocally definable criteria, usually the defect position, the equivalent reflector size, the reduction in the back-wall echo, the echo shape and its behavior during scanning (echo dynamics). In addition the ratio of the useful gain range to the noise level is specified to ensure that the smallest defect which must still be detected can actually be distinguished from the noise. Because of the trend to automated tests the three most useful are the flaw position, equivalent defect size and decrease of back-wall echo since they are readily available for electronic data processing.

International standards and rules of testing (Chapter 34) are restricted to methods of testing, adjustment of the equipment and methods of signal evaluation. They cannot fix reject criteria since this question is usually a matter of agreement between manufacturer and customer [1132]. The limits of acceptance therefore depend more on the service stresses than on the probable defective zones arising from the production process.

With rotor forgings, because of the high centrifugal forces and resultant hoop-stresses, the zone around the central bore is evaluated critically. The parts of steam- and gas-turbine rotors, which are subject to high temperatures and therefore are subject to creep cracking, the zones of blade fixing in turbine and compressor disks, and the region of the slots for housing electrical windings in alternator rotors are all subject to more critical evaluation than the intermediate annular regions.

In addition to the working stresses other reasons for more critical judging criteria play a role as for example on faces to be welded to reduce the risk of the production of weld defects.

Concerning the testing of forgings see also [1450, 740, 1055, 124, 930, 1326, 27 (Sections G 12 and G 13), 461, 968, 1064]; concerning the influence of geometry [1399, 799], and especially about defect sizing [1150, 813, 1055, 822, 1147, S 79, S 14].

The testing of *austenitic forgings* compared to those made from ferritic steels which can be quenched and tempered, does not always give satisfactory results because of the strongly scattering grain structure. During recent years this problem has been the subject of many investigations leading to better forging techniques producing better properties for testing [922, 1132]. The main difficulties resulting from zones of coarse grain can be avoided by choosing a particular temperature for final forging based on recrystallization diagrams. For the testing of these pieces frequencies of 0,5 to 1 MHz with maximum damping are best used, which give good enough axial resolution and an adequate signal to noise ratio [486]. Different design of ultrasonic equipment, as for example by using the CS technique [270] or averaging methods [539] do not provide much improvement in the results.

22.2 In-Service Inspections

The methods described above are applied in the course of and immediately after the production process and are therefore called production tests. To survey highly stressed parts, especially in power plants, repeated tests or in-service inspections are becoming more and more important. In these inspections any defects identified earlier but not being a cause for rejection can be observed for any changes caused by the service conditions. In addition service-produced defects must be detected, these being mainly cracks caused by thermal shock, fatigue or creep, or by corrosion attack.

For both types of test, production and in-service, mechanized scanning of highly stressed parts is often necessary. For some examples see Section 22.3. In most cases, however, it will not be possible to use the results of production testing as a basis for the later in-service test because then other criteria apply and also because scanning equipment has to be specially designed for use on site, for example in power stations.

The first or pre-service inspection has therefore to be performed on the piece in the ready-for-use condition, i. e. at a time when the piece after having been accepted on the basis of production tests, has not yet been affected by its conditions of service. This pre-service test, also called the finger-print inspection, forms the basis for later in-service inspections since they can all be evaluated by comparison with it.

In what follows some examples of in-service tests are given in which an automated scanning installation is not necessary.

In a crankshaft (Fig. 22.6) fatigue cracks develop in the crankpin fillet, starting usually in the 45° direction. Tests with normal probes are therefore less favourable than with 45° angle probes. If a borehole prevents direct observation it can be used as a mirror to reflect the beam. Sometimes the cracks are skewed by the influence of torsional stresses and in this case they can be detected more easily from the side wall as in Fig. 22.7. To avoid unnecessary scanning, experience of the probable position of such cracks is very important. Complementary methods are by using magne-
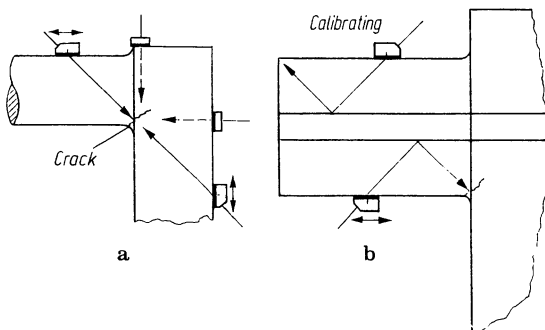

Fig. 22.6. Testing for fatigue cracks on crankshafts and crankpins. **a** Without bore; **b** with bore
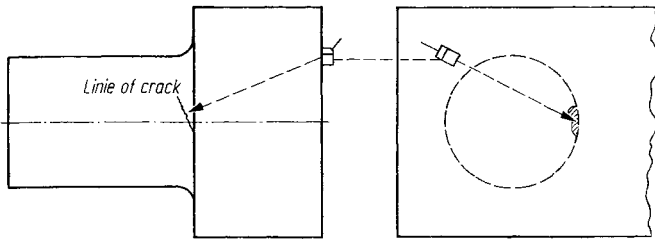
Fig. 22.7. Oblique or skewed fatigue cracks on crankpins

tic particle or penetrant dye techniques, which, however, necessitate dismantling of the machine which is not necessary with ultrasonics. In addition with ultrasonics rough indication of the crack depth can be obtained by comparison with artificial cracks.

When testing heavy machinery, oil-filled holes are frequently encountered. They produce not only the expected echo from the front wall but also a back-wall echo. Because of the lower acoustic velocity of oil, the back-wall echo appears behind the front echo at a distance equal to four times the hole diameter and it is often surprisingly strong.

The supporting columns of heavy presses as well as pump rods are subject to fatigue cracks in the thread (Fig. 22.8) which start at the bottom of the thread and proceed at right angles to the axis. Usually they an be readily detected from the end face if a normal probe is applied near the edge. If this also shows the individual threads they can be identified by their regularity but this makes it more difficult to detect smaller incipient cracks. In this case the optimum angle of divergence of the sound beam can be found by testing a reference specimen with a saw cut at the base of a thread. Angle-probe testing in an oblique direction is in this case less favourable because of the strong indication of the threads and should be considered only if the end face is inaccessible. However, for this problem longitudinal-wave angle probes of small angle can be used to advantage (cf. Fig. 17.3).

Satisfactory tests results are also obtained in the case of reduced ends of pump rods as shown in Fig. 22.9 from which the thread can no longer be irradiated di-
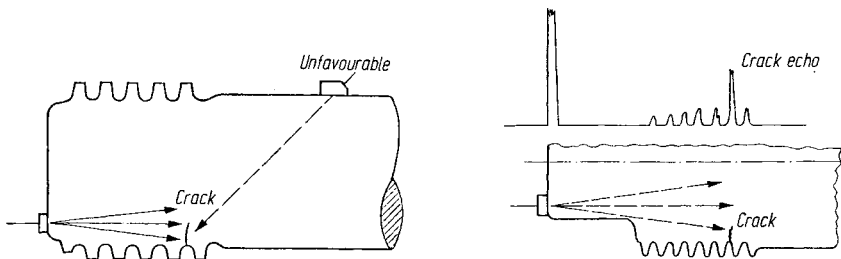

Fig. 22.8. Crack test on press columns, pump rods, etc.
Fig. 22.9. Crack test on thread in the shadow of a sound beam; schematic screen picture above

rectly. The screen picture showed the perfectly regular echoes of these threads, from which the additional crack echo could be clearly distinguished at one point. This was certainly due to diffraction of the wave at the point of narrowing.

For turbine and rotor forgings intended for power plants mechanized scanning and complete recording is necessary, as described in Section 22.3. However, at this point we can say that the designer of these forgings must already consider testability. An old example is shown in Fig. 22.10 in which the four longitudinal machined semi-circular grooves allow inspection of the whole interior volume by using special probes.

If such a forging contains a central borehole it can be used to allow inspection of the stressed zone around it as well as the outer regions (see Section 22.3, boresonic inspection).

Other critical parts in generator rotors are the wedge-shaped retainers which hold the electrical windings against centrifugal forces. These can be affected by fretting corrosion because of the high contact pressures and the bending stresses of the rotor. The usual test for such cracks is carried out using angle probes from the outer faces of the wedges [1376].

End bells or retaining rings (Fig. 22.11) are one of the most stressed parts of an alternator rotor. Their task is also to retain the ends of the windings against centrifugal forces and consist usually of high-strength cold-worked non-magnetic austenitic steel. During service cracks arise as a consequence of stray-current arcing and
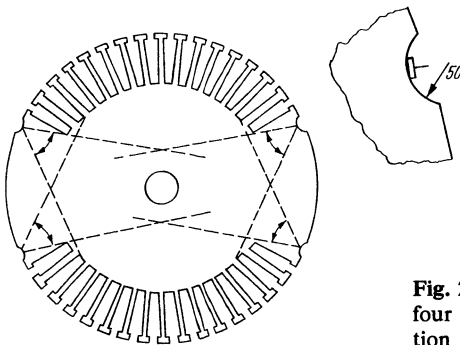

Fig. 22.10. Section through generator rotor with four grooves for inspecting the internal cross-section
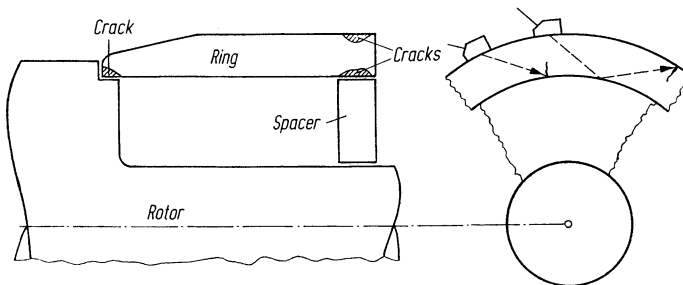

Fig. 22.11. Testing a generator retaining ring or end bell

by stress corrosion caused by humidity. These cracks are detected by manual techniques using angle probes of 35° to 45° and 2 MHz. Occasionally coarse-grained zones require the use of lower frequencies but more reliable testing for in-service inspection is with the help of special manipulators (see Section 22.3).

The rings are initially shrunk on to the rotor and supporting disc and are therefore subjected to considerable static stresses. If they are removed previous definite crack indications may disappear. These must be caused by tight cracks which transmit sound unless opened under the influence of stress, so that the tests should therefore be carried out on the shrunk-on component.

22.3 Mechanized Testing

Figure 22.12 shows a computer-aided test installation in the production line of retaining rings of the Krupp company [1557]. The rings are supported and rotated by two rollers in a tank allowing part of the ring to be immersed in water. With this semi-immersion technique four probes are used, two normal probes (0°) and two angle probes in the range 35° to 60°. One pair consisting of a normal probe and an angle probe contacts the inner surface and the other contacts the outer one. The complete set scans the width of the ring by multiplexing, one of the normal probes also checking the attenuation.

The results are recorded by two twin-channel line-recorders with reversing transport. One channel records the amplitudes of normal echoes received between 0° and 180° and the other between 180° and 360° of the circumference. The second recorder writes the echoes of the angle probes. For the in-service tests this type of inspection and record is, however not suited and other scanning installation had to be developed for this purpose, the main difference being that the inside surface is no longer accessible.

The importance of these production and in-service tests is indicated by more than 30 serious accidents which have occurred in the years before their introduction [1450]. The efficiency of the in-service tests is mainly due to the precisely reproducible probe-guidance mechanism and the data recording. Even the echoes of the grain noise are reproducible and act as a "finger-print" for each retaining ring. During repeated in-service tests it has been possible already to indicate defects when their echoes have not yet surpassed the grain noise [1055]. With a sensitivity adjustment based on this grain noise better results have been obtained than by using a groove 1 mm deep and 25 mm long as reference defect. Öhnfeld [1137] describes an installation for service-testing retaining rings, without the need to lift the rotor, by using very flat probes mounted in the narrow air gap that is available in practice, see also [126].

Automated tests of rotor forgings have been carried out for many years in order to achieve a continuous test. By well-defined probe guidance it was possible to get a record of the complete test rather than the disjointed sequence of A-scan images obtained from visual observation. The goal was to test the complete volume, in which each volume element could be checked in three different, mutually perpendicular directions.
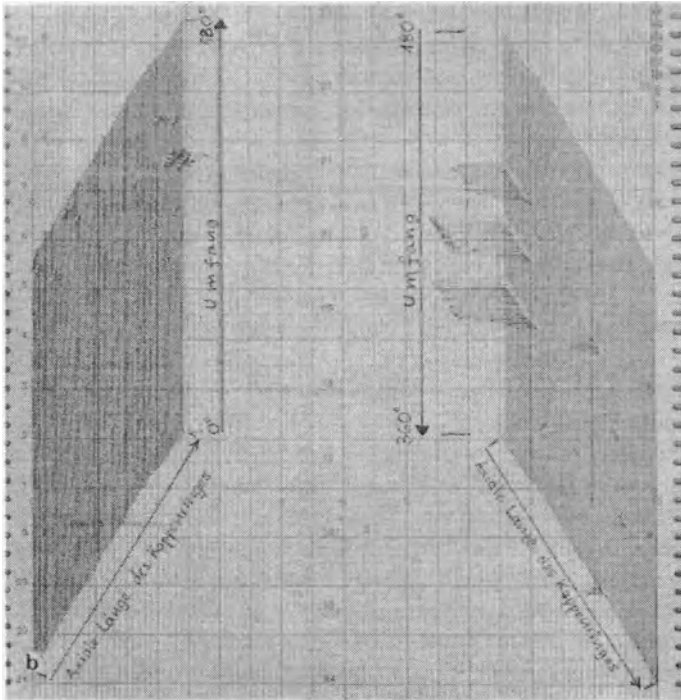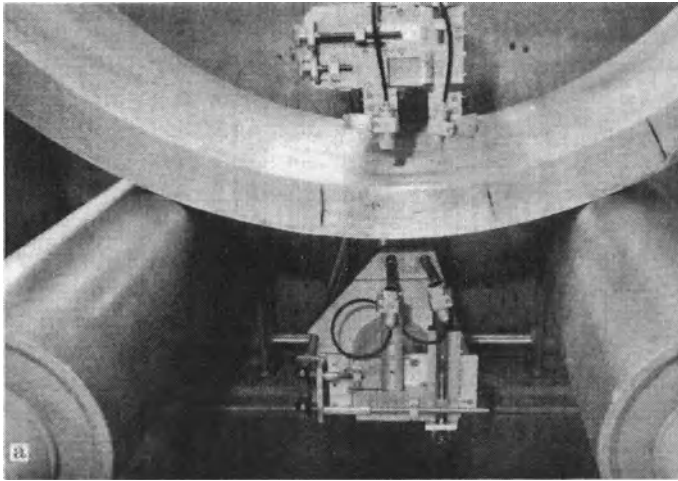
Fig. 22.12. a Test installation for retaining rings; **b** record of a normal probe on a test piece with artificial defects (courtesy Krupp Corp.)

The installation shown in Fig. 22.13 is from the Brown-Boveri Corporation according to Mohr [1052]. It scans the rotor with a multiple-probe system coupled to the surface by flowing oil. The oil container is carried on the test car together with the flaw detector and recording devices running alongside the rotor on rails.

Figures 22.14a and b show the special recording method using photographic film. The base line of the normal A scan (Fig. 22.14a) is projected onto a running film perpendicular to its direction of movement (right). The echoes are themselves shielded, so that the base line blackens the film with the exception of the gaps caused by the echo peaks. The speed of the film transport is controlled by the scanning speed of the probe system. The width of the unexposed gaps is a first indication of the echo amplitudes. Additionally an auxiliary CR-tube shows (4) the amplitude of the back-wall echo and simultaneously the largest amplitude of the complete echo pattern within a range where defects can be expected.

The back-wall echo can be reduced by more than 30 dB so that the sensitivity for defect echoes can be very high. For rotors with central boreholes the back-wall echo is replaced by the hole echo, which can also be reduced to obtain high sensitivity for defects in front of *and behind* the hole.

The travelling echoes are easily recognized from their transit time variations (see Section 22.1). The use of a 4-track imaging recorder to replace the optical camera would allow on-line recording.

For descriptions of older installations offering considerably less possibilities see Goldman and Auger [545, 546] and Cook and Walker [261]. In an installation at the
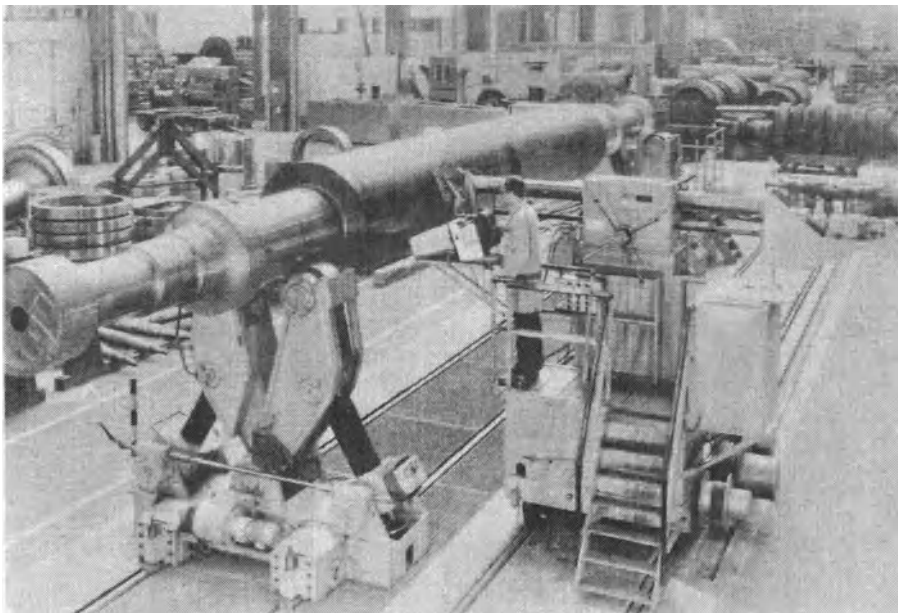

Fig. 22.13. Test installation for rotating forgings up to 150 t weight (courtesy BBC, Baden, Switzerland)

Japanese Steel Works (Okubo et al [1141]) the ultrasonic data is electronically processed. The system gives real time presentation of B and C scans and a classified list of defects with their positional data and equivalent defect size. The computer capacity can deal with rotor diameters up to 2 600 mm, if suitable rotating equipment is available.

Nussmüller describes a smaller full-immersion installation for forgings up to 700 mm diameter and 1 500 mm long. Because of the very uniform coupling testing frequencies up to 10 MHz can be used [1132, 1133, S 121].

Besides these installations for production testing there have also been for some years similar one for in-service inspection.

In the USA several serious accidents have occurred with monoblock rotors because of production defects and creep stress [1354], especially with older machines. When central boreholes are available in-service inspections must now be performed from the inside surface (boresonic inspection) and a number of specially designed installations are in regular use [1526, 542]. Jacobs [714] reports a newly developed system code-named "TREES" (turbine rotor examination and evaluation system). The complete data collection is stored in a computer so that a prediction concerning the residual life time of the machine can be reached.

Another material problem was recognized after a series of serious accidents in Great Britain [746], the USA and South Africa when using low-pressure rotors with shrunk-on discs. Stress corrosion was found to occur at the outer edges of the disc bores, especially originating from the key-way. This lead in the USA to a Standard Revision Plan by the Nuclear Regulatory Commission (NRC [1739]), which de-
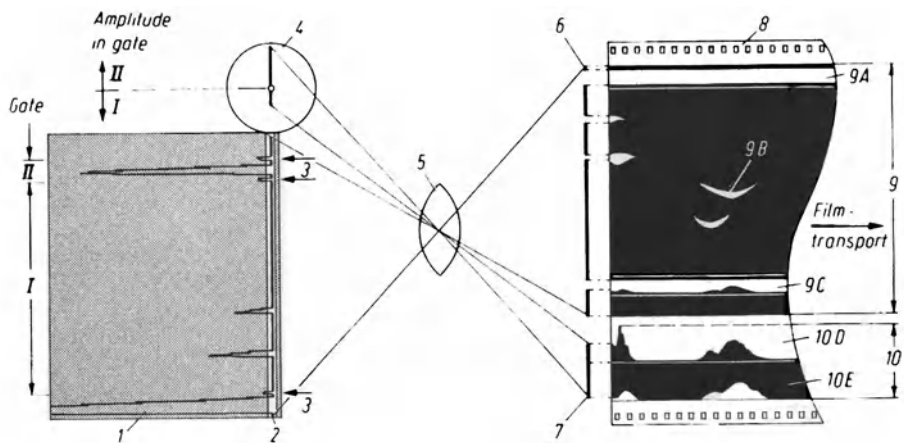

Fig. 22.14 a. Recording system of the installation of Fig. 22.13 (cf. [1052]). Principle of recording. *1* normal A scan; *2* gated base line; *3* indications of the electronic gates; *4* CR tube for echo amplitudes only; *5* camera lens; *6* image of the gated base line; *7* image of the echo amplitudes from CR tube 4; *8* film; *9* transit time/position curve with transmitter pulse A, indications of echoes B, back-wall echo C; *10* amplitude/position curves with maximum echo amplitude D and back-wall echo amplitude E (if necessary reduced within the gate II)
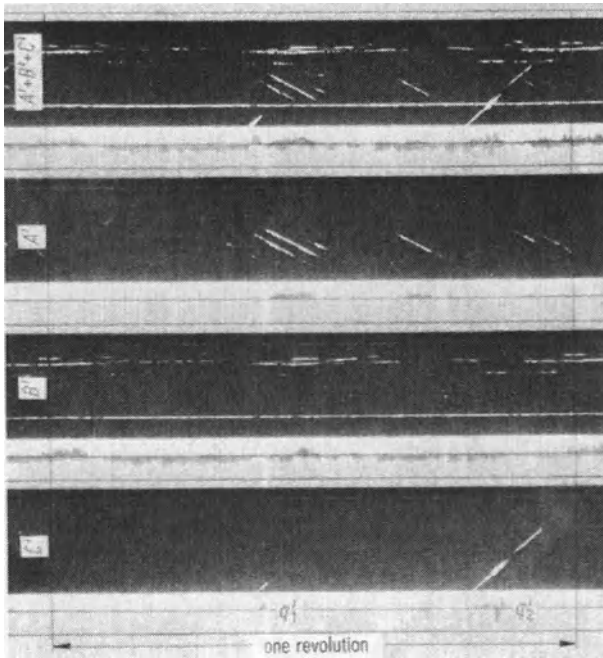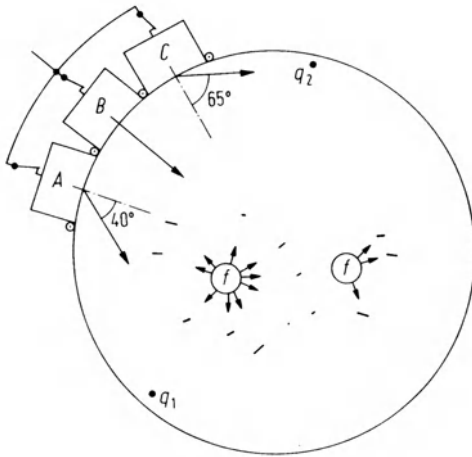
Fig. 22.14 b. Record of a shaft with hydrogen flakes showing probe arrangement.
A angle probe 40°; B normal probe; C angle probe 65°; f flake-type cracks on the front side of the shaft; q_1 and q_2 axial bore holes for reference, 2 mm diameter; $A' + B' + C'$ film record with all 3 probes in parallel; A', B' and C' three films, each for one probe only; q_1' and q_2' amplitude indications of the reference boreholes, drilled transverse to the beams

mands periodically repeated inspections of turbine rotors in nuclear power plants. The various manufacturers involved have designed intallations fitted to their turbines which allows the test to be carried out without dismantling the turbine discs and blades. Figure 22.15 shows such an installation of the KWU company, Mülheim/Ruhr, Germany, [728], for the shrunk-on discs of their low-pressure tur-
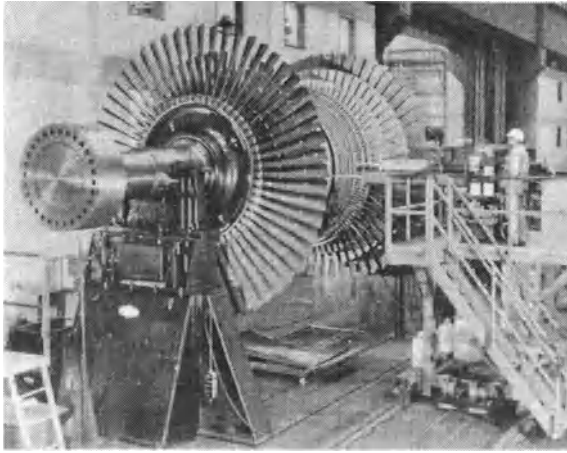

Fig. 22.15. Test installation for low-pressure turbine discs (Courtesy KWU, Mülheim/Ruhr, West Germany) accord. to [728]
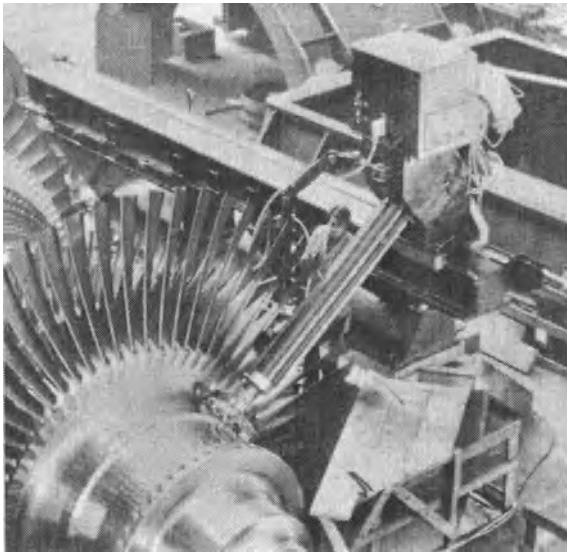

Fig. 22.16. In-service test of the low-pressure shaft of a 1300-MW turbine. The shaft need not be removed from the casing. (Courtesy BBC, Baden, Switzerland; product of Krautkrämer-Geyssel)

bine rotors. The critical region of the disc bores is checked by a combination of several angle probes operating as single probes or with a pitch-and-catch technique. The manipulator carrying the probe assembly is introduced into a gap only 50 mm wide. For further installations of this kind see [70, 1037].

Although this particular problem of the shrunk-on discs does not occur with rotors of other designs (monoblock rotors and those fabricated by welding individual forgings) the test is sometimes demanded for nuclear power plants. An installation for the welded type of rotor has been developed by Mohr for the BBC 1300-MW nuclear turbine group [1056], Fig. 22.16. The shaft can remain within the lower housing during the test and the manipulator is mounted on the jointing flange. Particularly the central zones of the solid discs and the roots of the welds are checked and for this purpose special testing faces are already provided in the design. For recording the results the total depth range is divided into transit-time sections of 1 mm steel equivalent, into which the digitized echoes are sorted. The echo amplitudes are also sorted into 1 dB steps from 1 to 99 dB. The two groups of data are stored on tape for further processing by different programs, for example as B-scans with rated amplitudes as in Fig. 22.17, or for comparison with a later inspection.
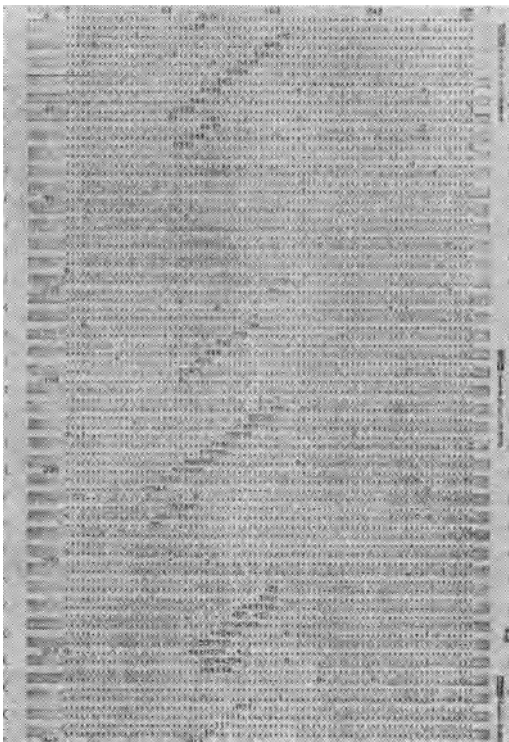

Fig. 22.17. B scan with rated amplitudes of a defective cylinder, recorded by the installation of Fig. 22.16 according to [1056] using 35° angle probes

22.4 Miscellaneous Machined and Semi-finished Parts

No testing information of general validity can be given here in view of the many different shapes and various testing problems. Selected examples will be discussed in as far as they refer to typical or particularly important cases.

Many defects in machined parts can be avoided if the raw material used is defect free, for example rods, bar or shaped sections. These are usually well suited to ultrasonic testing (Chapter 25). After manufacture into forgings only the easily accessible parts can be tested for typical internal forging defects, as far as the proposed use requires it. Surface inspection can be carried out by magnetic particle or liquid penetrant testing.

The ultrasonic method of testing can be used on forgings in aluminium alloys, nickel alloys and titanium, which are widely used in the aircraft industry. Because of the need for constant coupling the immersion technique is very often used, and the excellent surface conditions allow the detection of very small flaws. On complicated shapes the probe is guided manually supported from the surface, and at a fixed distance, by a plastic nozzle, the end of which can be made to fit any surface curvature. For simpler shapes full immersion tanks with probe manipulators and mechanized scanning can be used.

For the highly stressed parts of gas turbines and especially the *discs* and *shafts*, the whole material volume must be tested for production defects. The fully finished component is usually not suited to the test because of it's complicated shape, so the test is carried out at an intermediate stage when the shape is still as simple as possible. Immersion techniques can then be used with normal beams for which the forging defects are well positioned. By tilting the probe defects lying in less favorable orientations, for example near the steps (transition zone between different thicknesses), can be found, where they tend to follow the forging flow lines.

The principle is shown in Fig. 22.18 using simple mechanical scanning and circular recording. With modern computer-aided installations equivalent defect sizes of about 0.5 mm diameter can be set as the rejection limit. Not less than 49 different probe adjustments are required and are provided by the computer programme,
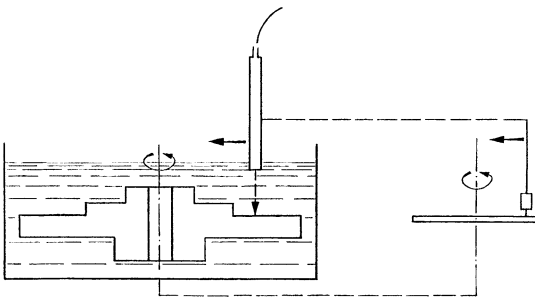

Fig. 22.18. Checking blanks of turbine discs by the immersion technique with circular recorder, schematic
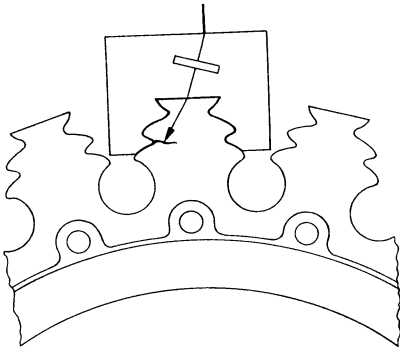
Fig. 22.19. Probe for detecting fatigue cracks in turbine discs (design Krautkrämer-Branson)
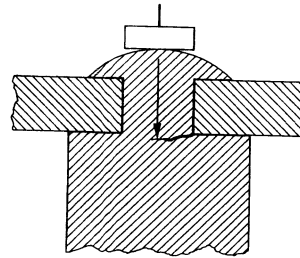**Fig. 22.20.** Detection of cracks in riveted turbine blades

which also contains the various adjustments of the electronic gates, to restrict the test exclusively to that metal volume left after final machining [321, 1133].

The *in-service inspection of turbine discs* is difficult because of the very complicated shape but is also carried out in selected areas by immersion techniques [176]. Probes as shown in Fig. 22.19 have been found successful for detecting fatigue cracks in fir-tree grooves, the transducer crystal being cast into a resin block in situ, which gives very reproducible contact conditions.

Turbine blades are made from many different materials, and in many different shapes, for water, steam and gas turbines. Blades for steam turbines are usually made from magnetic material and can therefore be tested by magnetic methods for fatigue cracks. Ultrasonic testing is often difficult because of severe erosion on the leading edge, and deposits on the surface have to be eliminated by blasting. The surface is then good enough to inspect with Rayleigh waves as in Fig. 22.21, the blades being left in situ.

With some designs the blades are fixed and riveted into a supporting ring, Fig. 22.20. Fatigue cracks in the transition zone between blade and rivet can be detected by high resolution single probes, or by TR probes, provided they extend to a depth down to 0.5 mm.

Raw material for turbine and compressor blades is tested carefully because of the high stresses in service. The cost of testing is not very important because of the consequences of a jet engine failure in an aircraft.

Production defects in blades depend on the method of manufacture, whether die-forged, milled from bulk material or precision cast. The raw material for the first two methods can contain the usual longitudinal defects; see Section 25.1. In the highly heat-resistant nimonic (NiCr) alloys transverse cracks have also been found in the raw material by testing short sections from the flat end faces with small, high-resolution probes.

With precision-cast hollow turbine blades the wall thickness has to be measured with instruments which must have a measuring accuracy of 1/100 mm. Because of the curved outer surface, and the eccentric shape of the internal hole, very narrow beams with high resolution have to be used.
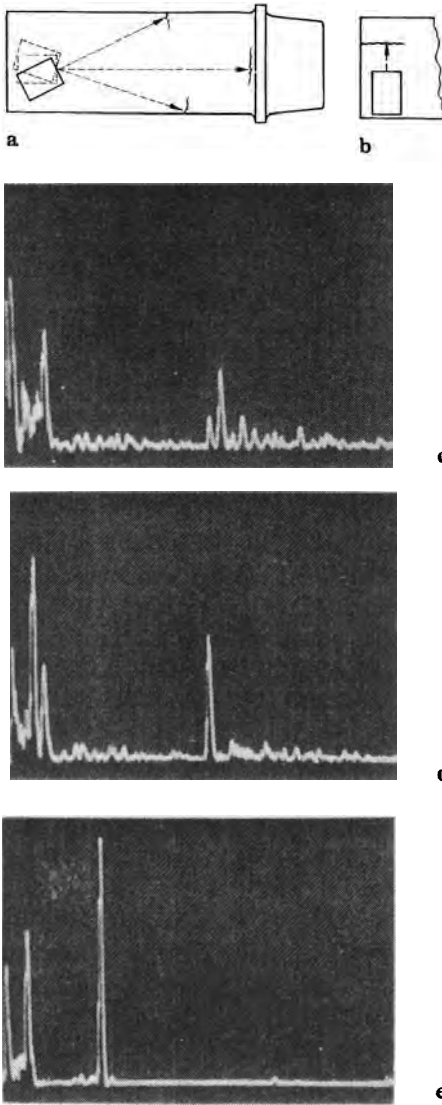
Fig. 22.21. Testing blades with surface waves. **a, b** Positions of probes; **c** screen picture showing small crack in root radius; **d** screen picture from same testing direction on sound blade; **e** screen picture showing small crack at the edge

Small fatigue cracks can occur on both edges, in the blade root radius and in the root itself (Fig. 22.21). The complicated shape of the root usually makes testing very difficult and while a crack as in Fig. 22.22 may still be detectable using special probes, those within the root as in Fig. 22.22 b are no longer detectable by ultrasonics. A favorable case has been reported in [S 95].

Carodiskey [213] has developed a probe, as shown in Fig. 22.23, cast in a resin block for guiding along the curved surface of the blade, and able to detect fatigue cracks as shown. The probe is fastened to a flexible guide rod and can be intro-

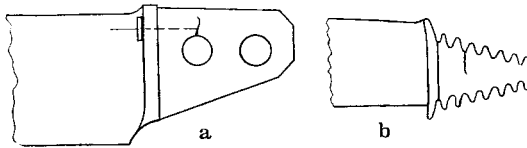**Fig. 22.22.** Cracks in base of blades of different shapes. **a** Possibly detectable while assembled; **b** in fir-tree root, detection very difficult
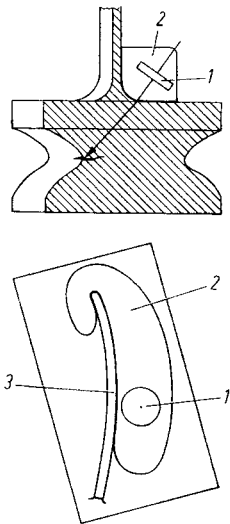

Fig. 22.23. Testing of turbine blade root for fatigue cracks, according to [213]. *1* crystal, *2* cast resin block, *3* blade

duced into the engine through an inspection hole. A drop of coupling liquid is provided through a channel in the resin block by operation of a syringe.

At other positions simpler tests can be performed as in Fig. 22.21, if the surface is not too rough and if the material is not too coarse grained. The test is carried out by Rayleigh waves of 2 to 5 MHz from the convex side of the blade.

Small cracks at the edges are well situated to reflect the surface waves since they usually form a right-angled corner with the edge. Cracks in the blade root radius must be irradiated by a perpendicular beam but the root edges can produce quite high echoes, in front of which an echo from a small crack is not easy to see. For easily reproducible contact the probe is usually fitted to a suitable clamping mechanism if routine testing is needed [943, 1228].

If the flat surfaces of the blade are not accessible it can help to test from the edges as in Fig. 22.24. For this purpose it is advantageous to adapt the plastic contact face of the probe to the edge by forming a groove.

Whereas the sound velocity in Nimonic alloys equals quite precisely that in steel, this is not true for some other materials used for turbine blades, and the perspex wedge angle for angle- and surface-wave probes has therefore to be specially adapted. Copper alloys, as used
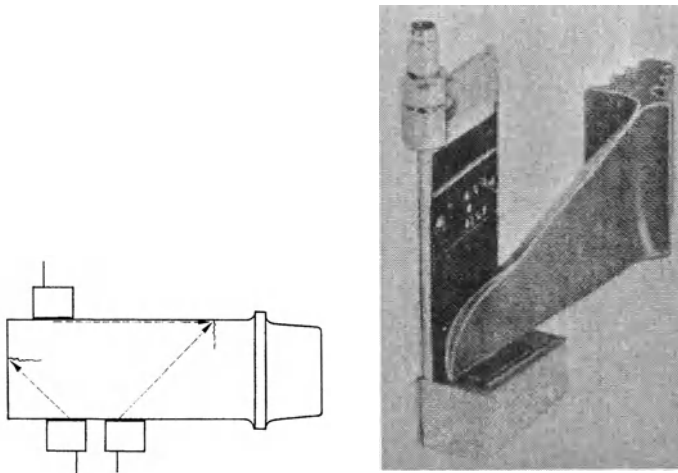
Fig. 22.24. Testing blades from an edge, using surface or transverse waves

sometimes for compressor blades, have very low sound velocities, thus needing the use of other materials for the wedge having a lower longitudinal velocity than perspex.

A serious problem is coarse grain, as already found in forged blades made from nimonic alloys. In this case the edges are sometimes free of coarse grains, thus allowing the use of surface waves in this area. With grains of very large size changing to low frequencies is of no help.

Hitherto the opinion has frequently been expressed that recrystallization is not a disadvantage in operation. Stäger and Meister [1455] have found, however, on nimonic 80 A (with about 19 % Cr and 75 % Ni) that both acoustic velocities decrease with increasing grain size and therefore, also Young's modulus and the shear modulus. Furthermore, fatigue test were strongly influenced by grain coarsening. Elimination of recrystallized blades thus seems advisable, and for this the ultrasonic test could be a possible criterion using either the attenuation of the sound or its velocity. The fir-tree root of the blade is best suited for such measurements.

Screws, bolts and rivets. Manufacturing defects in pressed parts of this type are usually transverse internal separations or the so-called over-drawing cracks, which occur usually near to the head (Fig. 22.25). The test can be made from either end using a normal probe of 2 to 5 MHz, with a diameter not exceeding that of the test piece.

In the shoulder between the head and shaft of a bolt conical defects sometimes occur in the form of a pointed hat, sometimes called chevrons. As Fig. 22.26 shows they can be found by either normal or angle beams. If these defects are still in a formative stage, they may give no recognizable echo but can be indicated by the attenuation of the back echo caused by the disrupted structure. Other manufacturing defects are longitudinal cracks on the axis or at the surface. These, however, are usually caused by defects in the raw material and are therefore better detected by pretesting the bar (Chapter 25).

In service small fatigue cracks often occur in the thread roots or in the shoulder between the head and the shank. The former are best found as shown in Fig. 22.8
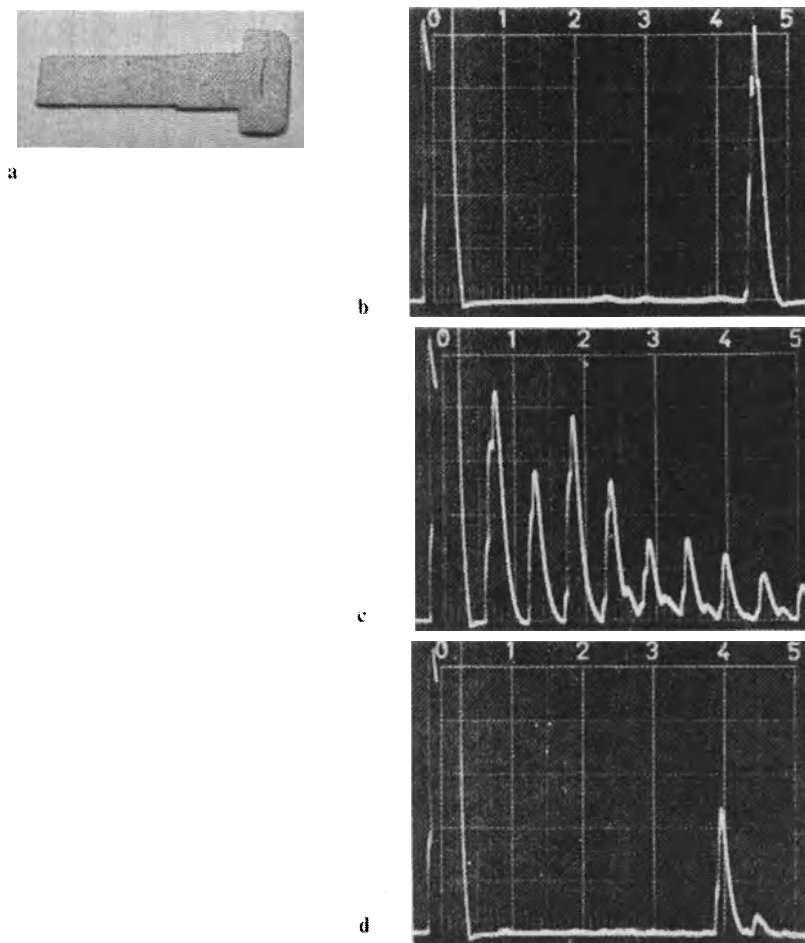
Fig. 22.25. Testing an extruded screw for cracks in the head. **a** Crack in polished cross-section made visible by the magnetic powder method; **b** screen picture of a sound screw tested from the head, 4 MHz, testing range 50 mm; **c** ditto, of screw with flaw; **d** ditto, tested from base. In both cases the faulty screw is easily distinguished from a sound screw

and the latter can be located as in Fig. 22.27 using normal probes, but operating from the shank rather than the head. From the bolt head these cracks, if small, are difficult to distinguish from the ever-present echo of the lower face of the head.

If in service only the bolt head is accessible for testing then the probe should be provided with a guide so that it can be adjusted to give only a small echo from the inner face of the head. A crack causes this to increase noticeably and defects only 0.5 mm deep can be detected by this method.

There is a better chance of detection using angled beams either from the side of the shank or from the inside of a longitudinal borehole using specially designed probes.
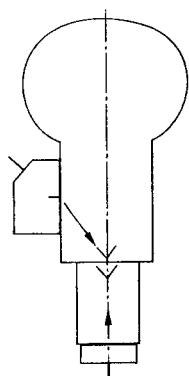
Fig. 22.26. Testing methods for conical defects in a bolt
Fig. 22.27. Testing for fatigue cracks in bolts
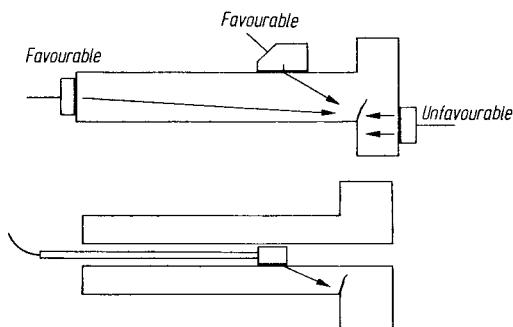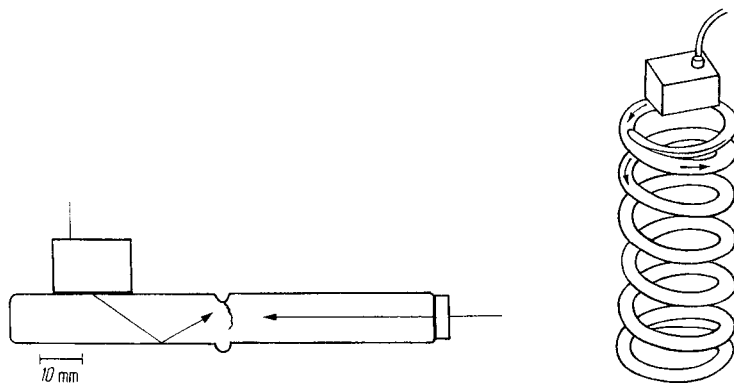
Fig. 22.28. Cross-section through a leaf spring for railway cars with quenching crack showing testing with small angle probe or normal probe. The use of surface waves is unfavorable due to roughness
Fig. 22.29. Testing a helical spring for quenching cracks, using surface waves

For cracks in rivet holes see Section 29.1.

In *quenched work pieces* stress cracks occur which need not necessarily be caused by flaws in the raw material. They appear in finished articles, for example press tools or die blocks, where they do not always reach the surface. Critical zones in such parts should therefore be scanned with normal or angle probes.

On larger and more complex components, such as bolts, leaf springs or helical springs, quenching cracks on the surface can be detected by various methods depending on the position of the cracks and on accessibility. Examples are shown in Figs. 22.28 and 22.29.

Batch testing can be performed according to the principle of Fig. 21.2 in a machine as shown for example in Fig. 22.30.

Fig. 22.30. Single-piece tester for small parts such as rings, bolts, tube sections etc. (type PAR-R, design Krautkrämer)

23 Railway Engineering Items

A separate treatment of this group of testing problems, which individually could be classified under other sections, is justified in view of the extent and the importance of ultrasonic testing in railway engineering. Most interesting in this respect is the detection of defects generated during service by dynamic stresses, especially considering the latest high-speed trains. For these trains acceptance testing is of increasing importance.
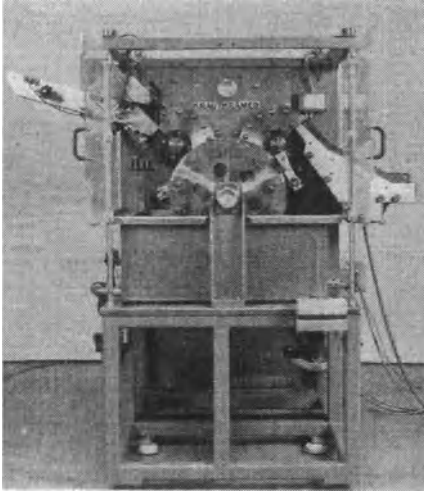
Many of these special types of inspection application can of course be used on test problems in other branches of engineering.

23.1 Axles

The typical types of manufacturing defect are mentioned in Chapter 22 but acceptance tests are, however, not always specified by the customer. The Deutsche Bundesbahn (DB) only requires ultrasonic tests on new axles in selected cases.

In this respect the ISO-Standard 5948 is of interest, in which a check of the attenuation is proposed for rolling railway material to ascertain that in-service inspection for fatigue cracks is possible at all [824, 214].

In-service tests of axles are performed by nearly all railway organisations. In the case of steam locomotives with axles on inside bearings, as in Fig. 23.1, the test according to [67] was especially simple and reliable, because the cracks almost always occurred within the hub seat as shown. The testing of all axles of an express locomotive needed less than 30 min to carry out.

Crank or coupling pin
Hub seat
Bearing stub
Keyway
Probe
Crack
Axle
Wheel body (steel casting)
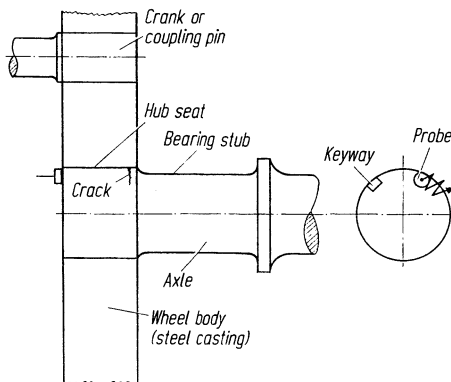
Fig. 23.1. Crack tests on axles of steam locomotives
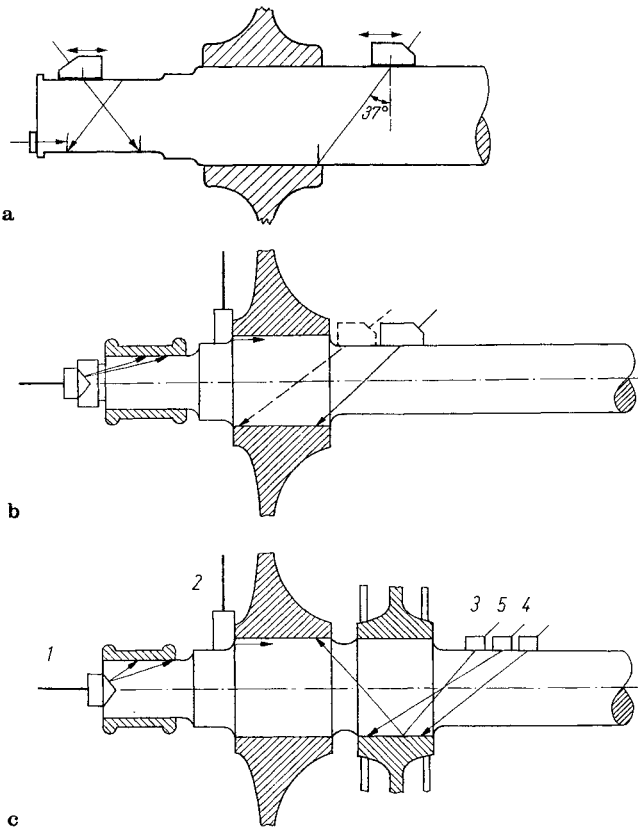
Fig. 23.2. Examples of axles with outside bearings of the Deutsche Bundesbahn. **a** Of goods truck; **b** axle with roller bearing, bearing ring not removed; **c** same with additional brake disc

Small cracks with depths of only a few millimetres could already be detected, although such small cracks were not too important since long experience had confirmed that axle fractures took place only after cracks had reached a greater depth [985, 1710, 1378].

Usually less convenient to test are locomotive and truck axles with external bearings. With the older design of axles using plain bearings (Fig. 23.2a) a 2-MHz 37° angle probe is applied to the bearing stub and, by scanning in length and circumferential directions, the emergency bearing and outer hub seat are inspected. To test the inner end of the hub seat the probe is placed on the inner shaft as shown in Fig. 23.2a. Though here the surface is usually heavily corroded, a reliable test is possible after cleaning with a steel brush.

In the DB the sensitivity of the test is checked with an artificial defect which is a saw cut of 1 mm depth. Axles with crack indications are rejected and those free of any detectable defect have a service life of 5 or 6 years before the next test is needed.

For the detection of rather deep cracks the so-called axle-test pistol (design Sperry) was in use in the USA. It had six crystals coupled to the end face of the axle for longitudinally testing the bearing and the hub seat, using a beam angle of about 10° to the axis. The interval between successive tests had to be shorter, because only large cracks could be detected reliably by this method.

All modern locomotives and trucks use roller bearings with an end face which usually contains grooves, a threaded borehole and a center hole, so that coupling a probe to it becomes impossible. In addition, the diameter of the end face is smaller than the bearing diameter and the inner bearing rings are shrunk-on and should not be taken off, so that the test used for plane bearings cannot be performed. An alternative method is shown in Fig. 23.2 b in which the center boring is conical and can be cleaned and smoothed before the test. Then a special probe (the so-called center-punch probe) can do the test, but it is restricted to the range up to the inner edge of the bearing ring, because some part of the sound can penetrate the shrink-fit and generate interference echoes simulating more distant defects.

For testing the outer part of the hub seat a special TR probe (2 in Fig. 23.2 c) is used with longitudinal waves at an entry angle of 13° and a roof angle chosen to cover just the range from 12 to 20 mm below the surface, where cracks at the outer hub seat usually occur. Because of the very flat design of the probe, it fits into the small gap between the wheel disc and the bearing box. It is coupled to the small radius of the hub seat and requires good cleaning and some skill by the operator. If with other axle designs this access is not available then the outer part of the hub seat has to be checked from the inner shaft.

With axles fitted with brake discs, as in the high-speed passenger trains, the brake disc hubs are also critical at the edges. As shown in Fig. 23.2 c, 3, 4 and 5, the test is performed with angle probes of 37° to 52° from the inner axle shaft.

It has to be kept in mind, that the shrunk-on wheel seat is partially transparent to ultrasound and therefore echoes are sometimes obtained from the wheel hub, with both wave modes, reflected from its faces or even from defects in the cast steel wheel. In doubtful cases one should work with higher frequencies for which the shrunk-on face and the wheel body are less transparent, resulting in interfering echoes becoming less distinct than true defect echoes. At the edges of the shrink-fit sometimes echoes are observed, especially from the outer hub seat, when transverse waves are used. It is probably a case of a diffracted wave, simulating small cracks.

In the DB the intervals between successive tests (400.000 km for locomotives and 600.000 km for passenger coaches) are subject to shortening so that a lower sensitivity can be used, so avoiding the need for highly skilled operators able to distinguish between true crack echoes and interference signals.

The test becomes more difficult if there are many cross-sectional changes between the various wheel discs and especially if there are brake discs and drive wheels too. In this case it is no longer possible to carry out the test by means of angle probes coupled to the surface of the axle. Fortunately hollow axles are often used which permit testing from inside the hole (cf. Fig. 23.3 a, [1378, 364]). Thus, for instance, all modern electric locomotives of the Deutsche Bundesbahn are fitted with hollow axles (inner diameter of 90 mm). An internal 45° angle probe permits convenient testing of all critical zones of the various seats and transitions. This method can also be applied to holes down to 20 mm diameter and all roller-bearing
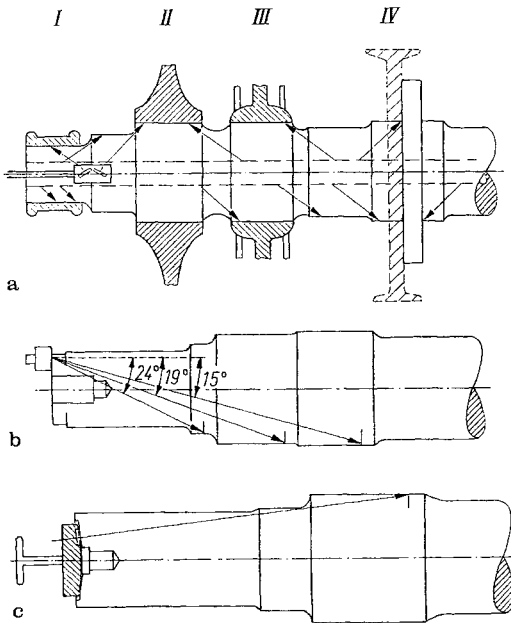
Fig. 23.3. Axle tests with special probes. **a** Hollow axle with several cross-sectional changes (I internal ring of the roller bearing, II wheel disc, III brake disc, IV drive); **b** axle for American Diesel locomotive, probes for longitudinal waves at 15°, 19° and 24° according to Sperry; **c** axle with external bearing (schematic) and conically machined end face using fitted longitudinal-wave probe (Swiss Federal Railways)

supported axles of the new electric railcars of the DB have been fitted with centre boreholes 30 mm in diameter.

Where it is definitely required that the hub seat be tested from the end, larger flaws can be detected relatively reliably with a normal probe (1 to 2 MHz) with a sufficiently wide beam angle. For axles of American Diesel locomotives probes with longitudinal waves and small angles (15 to 24°) have proved successful for this purpose (Fig. 23.3b). The longer dead zone of these probes can be tolerated in view of the greater flaw distances. Another solution is illustrated in Fig. 23.3c. Here the railway administration decided to machine a conical surface on the end face to facilitate testing. All critical points can then be scanned by a probe with suitably fitted transducer in one revolution.

For further reports on differing practices of other railway organizations see [367, 427, 209, 978, 865, 155, S. 167].

In view of the large numbers of truck axles, automated testing installations prove economical. Figure 23.4 shows a test bench designed for this purpose and used by the Deutsche Bundesbahn in several of their repair workshops [522].

The automatic test starts with the hydraulic lifting of the wheel set into position. The wheel set is rotated, the probes are coupled by means of flowing water and switched on one after the other for one revolution each, and the test data from each probe are noted. The angle probes for the bearing stubs contain several parallel-connected transducers so as to cover all possible flaw positions simultaneously without any axial shift. A flaw indication is recorded on the signal display panel at a position corresponding to the position of the flaw. Prior to the scanning by the angle probes used for the hub seat it is tested first by means of normal probes on
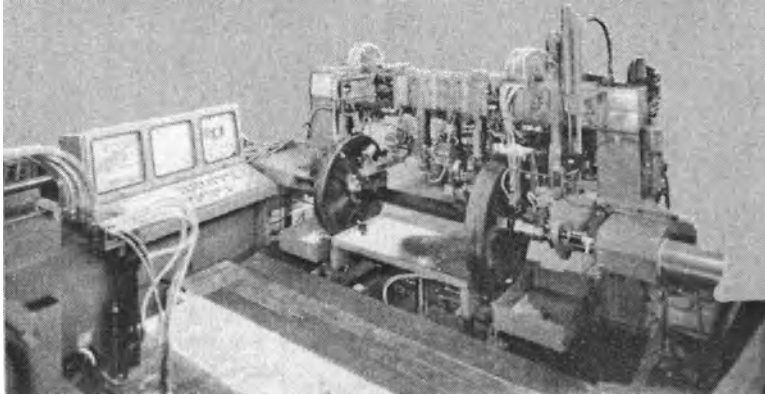
Fig. 23.4. Automated test bench of the Deutsche Bundesbahn for wheel sets (design Hegenscheidt/Krautkrämer)

the basis of the back-wall echo to check whether any serious defects are present which would prevent oblique testing. Only then is the oblique test started. The entire test procedure, including the rolling in and out of the wheel set takes only about 2 min.

23.2 Rails

Manufacturing defects in rails depend on the origin of the steel, those manufactured from cast ingots have rolled-out flaws, and those from continuous casting contain a fine dispersion of non-metallic inclusions. The defects usually occur in the transition zone below the rail head and in the upper part of the web. In addition transverse cracks (the so-called kidney cracks) can occur in the head and true rolling defects are folds in the foot region beneath the web. The usual test positions for probes are shown in Fig. 23.5, and these are 2-MHz TR probes on the top and side of the head, on the web and an angle probe on the foot.

Production testing is usually performed after straightening, as a quality control measure or because it is specified by the acceptance authority. Often rolling mills have incorporated test installations into the production line [471, S 122.]

During service small cracks and inclusions can act as the origin of the Kidney cracks lying transversly in the head of the rail (Fig. 23.6). They are especially dangerous because they can occur in groups over short distances and can therefore cause a short piece of the rail to break out. Similar cracks start at wheel burns, where wheels skid during starting, for example in front of signals, leading to local thermal cracking as a result of overheating.

In England Kidney cracks occur less often, because less hard rails are in use. In the USA, as well as shatter cracks starting from the center of the head, small cracks from the lower edges of the head also occur, contrary to German experience. These
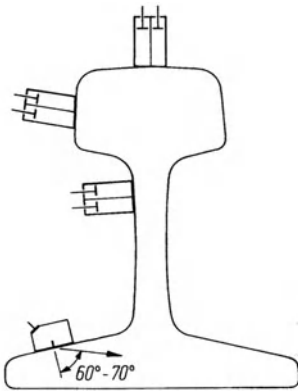
Fig. 23.5. Typical probe positions for rail testing
Fig. 23.6. Kidney crack (transverse crack in rail head)
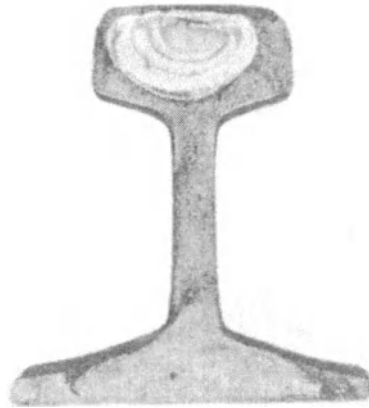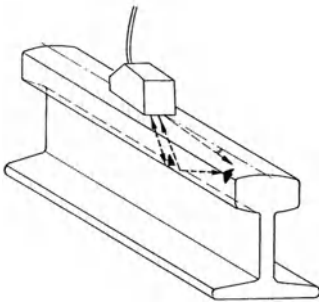
Fig. 23.7. Testing of rails for incipient cracks at the lower edges of the head
Fig. 23.8. Cracks at fish-plate boltholes
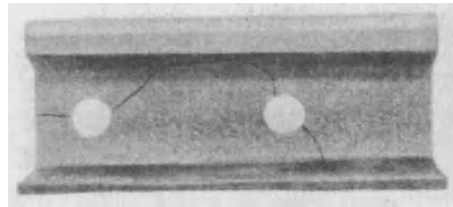
can be detected with 70° angle probes from the rolling surface, if the beam is tilted somewhat (Fig. 23.7). To observe both edges of the head in automatic installations two angle probes are provided, with opposite direction of tilting.

Other in-service cracks are the fatigue cracks at the fish-plate bolt holes (Fig. 23.8) produced by the impact stresses at the rail joint and which may cause a piece of the rail to break out resulting in serious accidents. Depending on the shape and the material of the rail, the flaws encountered in various railway systems can differ greatly regarding their position and frequency, for which the testing method should make allowance. Small cracks in the foot of the rail, if they do not reach the web, are practically undetectable with any of the ultrasonic testing methods used in practice, but they are usually detected by visual inspection.

In the Deutsche Bundesbahn, and also in many other railway organizations, the rails of the most important tracks are routinely tested. Figure 23.9 shows an early model of a manually guided rail tester which contains a battery powered miniature

Fig. 23.9. Rail testing equipment in use by the Deutsche Bundesbahn (Bundesbahn Zentralamt, Minden)
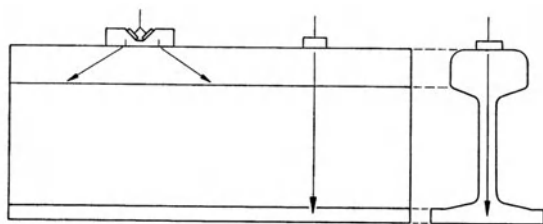
Fig. 23.10. Probe arrangement for testing rails with the rail tester of the Deutsche Bundesbahn

flaw detector. According to Fig. 23.10 a 2-MHz normal TR probe and a pair of TR angle probe can be switched on alternately. Water for use as coupling liquid is contained in a tank of several litres. The normal probe detects cracks at fish-plate bolt holes, quasi-laminations in the head and also cracks in the web. Transverse cracks are detected by the pair of TR angle probes and are indicated as travelling echoes, if the unit is moving. The angle of 70° has been chosen because shatter cracks, the most dangerous, are usually inclined at about 20°. Because both inclinations ($\pm 20°$) occur, a double angle probe indicates both. Based on experience with manual testing the DB has built an ultrasonic testing train (Figs. 23.13 and 23.14) which inspects the whole German rail track once a year.

The rail testing car contains additionally a pair of 35° angle probes in pitch and catch technique, as Fig. 23.11 shows.

Figure 23.12 explains the screen picture obtained with some typical rail defects. The viewing screen shows the simultaneous echoes of the three probes. Characteristic of all defects of appreciable extension in the longitudinal direction is the absence of the bottom echo.

Since the annual routine testing of the track has been carried out by the rail testing car, the additional use of the manually operated device is restricted to critical sections of the track, as for example in tunnels, on bridges and in stations. The operator using this instrument has to give a written report about defects found and
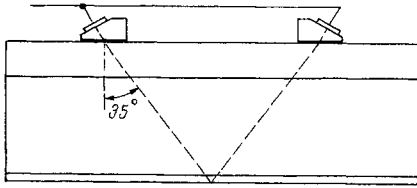
Fig. 23.11. Pair of 35° angle probes mounted on rail-testing train, in addition to the probe assembly according to Fig. 23.10
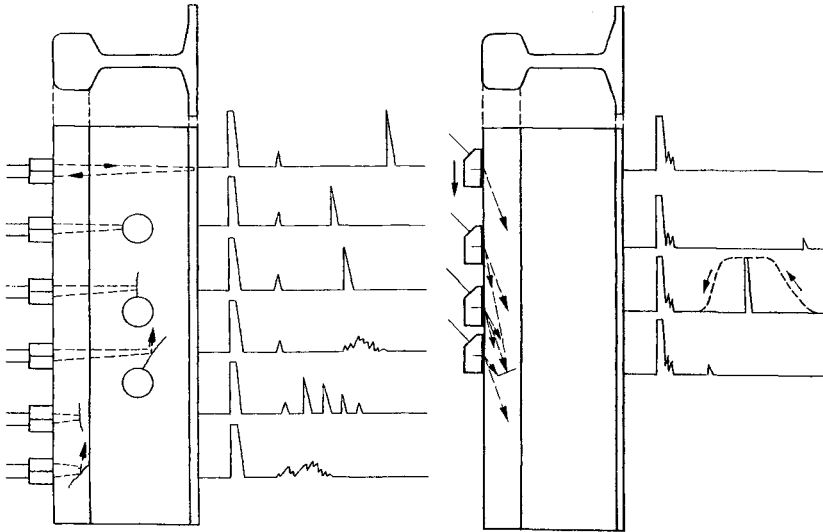
Fig. 23.12. Indications of various rail defects by perpendicular and oblique testing

the speed of testing is on average 5 to 6 km per day (2 rails), depending, however, on the traffic density and the frequency of defects.

Since 1975 the rail-testing train as shown in Fig. 23.13 has been in use [368]. Regarding the earlier design see [984, 366]. It consists of three cars, of which the middle one contains the testing equipment. The two outer ones contain the diesel engines and also house the crew for sleeping and living and contain lavatories and kitchen, the accomodation is thus comfortable even for longer trips.

Beneath the middle car the testing carriage is suspended, containing the pairs of 35° and 70° angle probes and the normal TR probe as mentioned above, one set for each rail. These can be raised or lowered hydraulically either separately or together with the testing carriage. For each rail two ultrasonic probes are arranged additionally directing air-borne ultrasound onto the transition between foot and web to detect welding beads.

The 35° angle probes are switched in parallel, so that each receives the pulse originating from the other after reflection at the bottom face and in addition echoes from fish-plate bolt holes, oblique cracks from the holes and transverse cracks in the foot provided they reach under the web.
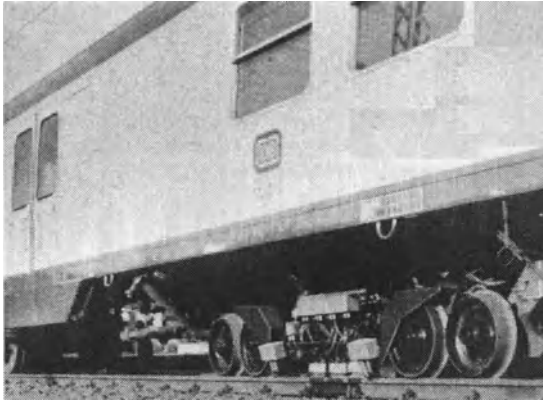
Fig. 23.13. Ultrasonic rail-testing train of the Deutsche Bundesbahn (Bundesbahn Zentralamt Minden)
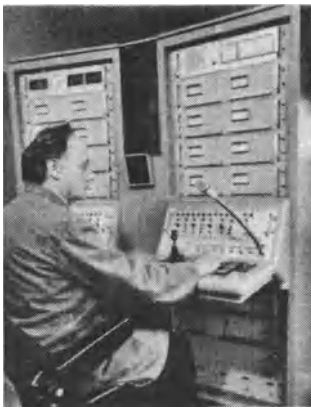
Fig. 23.14. The electronic equipment and the control panel in the ultrasonic rail-testing car
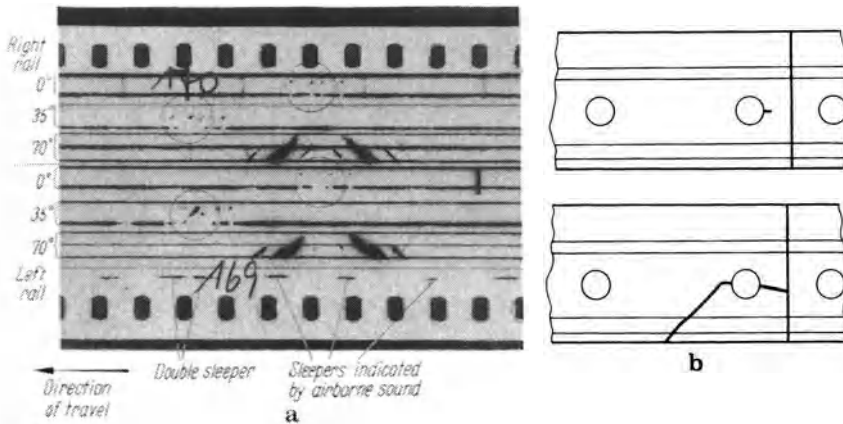
Fig. 23.15. a Record of the rail-testing train at two defective rail joints; **b** reconstruction of two cracks based on the record, marked by circles (Bundesbahn Zentralamt, Minden)

The coupling face is made from plastic and has only to be changed after several thousand kilometers. The several cubic metres of coupling water required for the daily testing distance of 200 km is contained in a tank.

The flaw detector electronics (Fig. 23.14) is arranged in the middle car above the test probes. Each of the probes is connected to a separate CR tube which can be observed by the operator. By glass windows in the car floor, the probes themselves can be seen.

Echoes greater than a predetermined limit are fed to the recording unit and are indicated on CR tubes by luminous points on the non-visible base line (see also Fig. 10.26). All these records are photographed on 35-mm paper (Fig. 23.15). The transport of the photographic paper is coupled to the speed of the car in the ratio of 1:100. An observer operates a recording device at each km post for marking the record. In addition continuously recorded 1-m distance marks facilitate the locating of a defect with an error of ± 2 m. The distance of one defect from another, or from a local indication of a bore hole or a weld in the rails, can be measured with an error of less than 10 cm. The practical testing speed is about 50 km/h (14 m/s) at which defects of an eqivalent size of 3 mm can still be indicated. Sufficiently good coupling is possible up to 80 km/h, but the distance between successive pulses then gets too large for reliable testing. For travel between test sites the train can run at 140 km/h.

The yearly track coverage of the train is about 40 000 km. Within the FRG it is used for routine tests of 10 500 km twice a year, a further 13 800 km once a year and for 2200 km every second year. The surplus time is used for testing trips in the neighbouring countries. The earlier test train was in use for nearly 20 years at a 30 km/h testing speed, covering 120 to 150 km daily, and an overall performance of 348 000 km track and a total distance of 560 000 km.

In Great Britain a rail-testing train has been built in collaboration between British Railways (BRB, Chief Civil Engineers Department) and Wells-Krautkramer Ltd. It was designed to the requirements of British Railways and was based on the same test and recording system [1741]. The testing speed is about 30 km/h, and recording is carried out on commercial 35-mm photographic film, which compared with the paper used in Germany has the advantage of being developed by commercial companies. For this test train the Harwell NDT Center has undertaken development work to enable evaluation to be done in the train by a computer, thus saving film development and visual evaluation at selected centres [507]. Though an on-line defect evaluation system with a printed list of defect position, type and size would be desirable, up to now the method has not yet found full approval in practice.

In other countries as for example Hungary, France, Japan, Argentina and Australia similar, but sometimes also much simpler cars for automatic testing of rails in track have been built, combining ultrasonic testing with eddy-current methods [1543, 769, 1742].

Used rails which are overhauled in the workshops and welded together to full lengths for reuse, are preferably first subjected to automatic testing by ultrasonics. Stationary rail testing benches (see Fig. 23.16) were designed specifically for this purpose of which several ones have been in use since some years. Basically, the
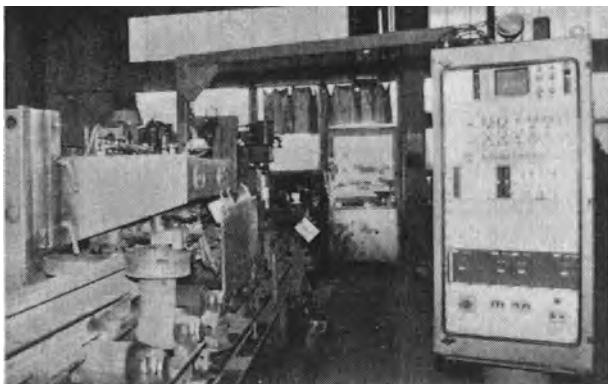
Fig. 23.16. Stationary test installation for used rails in a rail depot of the Deutsche Bundesbahn
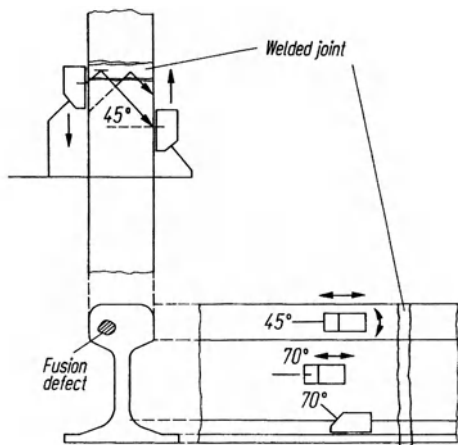
Fig. 23.17. Testing welded rail joints

same method is applied as for testing rails on the track, with the simplification, however, that the rails ends are disregarded because they are invariably cut off.

In the test procedure the rail is transported on a roller bed through the test bench in an upright position. Frequently the test bench follows immediately after the planing machine in which the head of the old rails is machined. The approaching rail actuates a contact roller which controls the position of the probe assembly consisting of two 75° angle probes facing in opposite directions, and one normal probe. Any defects in the rail head or the web actuate a position-true colour-marking device directed against the web by means of auxiliary monitors. When the end of the rail is reached the probe assembly is lifted of automatically. The maximum testing speed is about 1 m/s.

For a general survey of rail-testing methods used in different countries see [367, 179, 135, 768, S 20, S 21].

End-to-end connection of rails is usually carried out today by welding to considerable lengths. In the workshop electric-arc butt welding is usually used, but on the track rails are joined by thermit welding. The most dangerous defect is lack of fusion, because its area extension will always be perpendicular to the rail length. Because such planar defects reflect an ultrasonic wave specularly, a test carried out with a single angle probe can be useless. Figure 23.17 shows the technique of the DB, a double-probe technique using 45° angle probes in the pitch and catch arrangement. Another arrangement, as in Fig. 5.14b, has been used by Farley [428], working exclusively from the smooth and clean runwing surface, testing simultaneously the head, the web and those parts of the foot beneath the web. For the thin-walled web and foot of the rail 70° angle probes can be used as in Fig. 23.17.

Points, or switches which are a critical part of the track usually consist of cast manganese steel, which cannot be tested reliably even with highly damped probes of low frequency (0.5–1 MHz) because of its coarse grained and anisotropic structure.

23.3 Miscellaneous Railway Material

Railway wheels are made in two different designs: monoblock, cast complete in steel, and forged steel tires shrunk on to a cast central portion. In some railway companies an acceptance test for production defects in the tires is obligatory and in this case, as shown in Fig. 23.18, the central volume of the tire, excluding the outer 15 mm layer, is checked in two perpendicular directions. The mechanized installations use 2- or 4-MHz probes including some 30×6 mm rectangular crystals. The working sensitivity is adjusted by using two artificial defects, in the form of 2-mm diameter flat bottom holes.

In cast steel monoblock wheels the transition zone between tire and wheel body is also tested as illustrated in Fig. 23.19. To detect casting defects which do not give good direct reflections, some geometrical echoes are observed for their amplitude. These come from mode-changing reflections at the radiused transitions from the
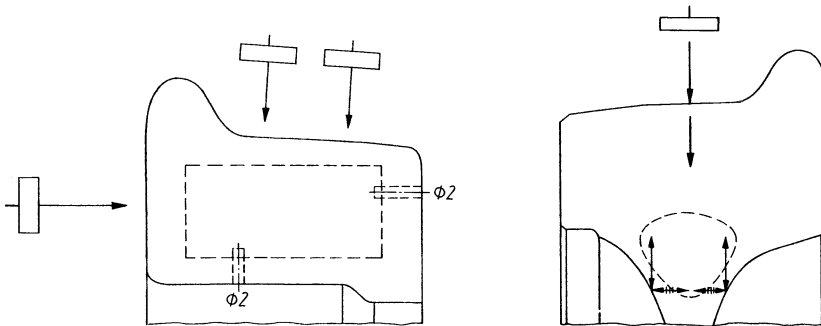
Fig. 23.18. Testing of forged tires for railway wheels
Fig. 23.19. Additional test of the transition zone in cast railway wheels

tire to the wheel body. The equivalent defect size for acceptance is chosen between 2 mm (for high-speed traffic) and 5 mm, but the ultrasonic test of the wheel disc itself is difficult and of questionable value therefore.

For the in-service inspection of railway wheels, tires are occasionally tested manually by a normal probe of 2 or 4 MHz operating from the side face.

The rolling faces of tires are sometimes subject to radially oriented cracking caused by local overheating during braking. They can exist in fairly large numbers but because they are only shallow they are not usually detrimental. However, they can occasionally be deflected into a circumferential direction and can lead to sections of tire breaking out. In the USA, Australia and recently also in Germany techniques to find them by using very low-frequency Rayleigh waves, propagating along the rolling face have been tried [178, 771, S 146, S 190 (paper 63)].

For the tests in Germany [1317] piezo-electric transducers have been replaced by electrodynamic ones, which are built into the rail head. The problem of distinguishing small cracks from deep ones has been solved by choosing different frequencies between 100 and 400 kHz (Fig. 23.20).

Sometimes after the overhaul of tires by the deposit of new metal and welding and re-machining the running face, a check is done for any remaining radial cracks using 45° angle probes as in Fig. 23.21.

The shrink fit of roller-bearing rings is checked successfully by the DB as shown in Fig. 23.22 [1358]. Using 4- or 6-MHz probes the echo amplitude from the pressure joint is observed, the smaller the echo the better the joint, cf. Section 29.5. Sound is also transmitted through the joint so that two multiple-echo sequences appear arising from the nearer joint as well as from the far one. For sensitive testing
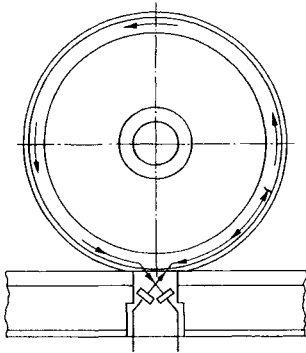
Fig. 23.20. Test of the rolling face of a railway wheel for transverse cracks by Rayleigh waves according to Bray [178]
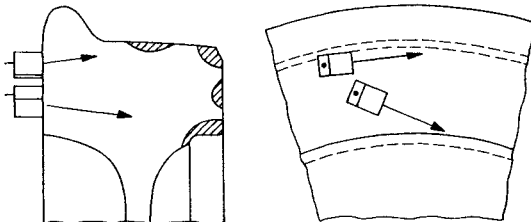
Fig. 23.21. Testing for transverse defects by angle probes from the inner side of the tire

the fifth echo from the first joint is chosen for observation. The final backwall echo is not used because it is affected by both shrink fits. The overall assessment of the shrink fit is based on 400 individual measurements around the circumference.

Testing the shrink fit of tires has not so far been successful, mainly because the rolling face from which the test could be performed is not parallel to the pressure joint face.

The outer rings of roller bearings are also tested for very small areas of damage to the rolling face, for example lost metal chips only a few tenths of a millimeter deep and with an area of some square millimeters [367]. For this purpose a probe is coupled to the outer surface of the ring using an immersion technique in a bath of oil. The usual long sequence of multiple echoes from the ring thickness is much disturbed by small irregularities on the inner surface. Here the amplitude of the tenth echo is used for evaluation tests.

Further railway equipment applications include the successful test of porecelain insulators for cracks and porosity (see Section 32.1). Other miscellaneous applications such as couplings, welded plates, plain bearings and wall-thickness measurement are treated in their respective chapters below.
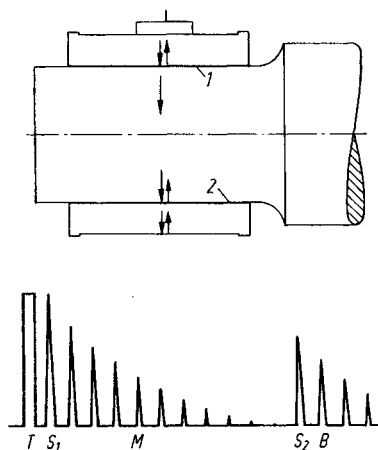
Fig. 23.22. Testing of the shrink fit of roller-bearing rings. T transmitter pulse; S_1 echo of first shrink fit; S_2 echo of second shrink fit, B back-wall echo, M measuring echo of shrink-fit quality

24 Plate and Strip

Test problems for plate are mainly concerned with production testing. However, there are a few applications arising from in-service stresses and working conditions. These will be dealt with first.

In-service cracks almost always occur normal to the plate surface. This applies for instance to corrosion-fatigue cracks caused by caustic embrittlement, cracks at rivet holes, or fatigue cracks in flanges, webs and stiffeners. If the direction of propagation of the cracks is known approximately, they can easily be found by using zigzag transverse waves, and if the surface is good, also by means of surface waves. For cracks at rivet holes, see also Chapter 29, and for corrosion and thickness determination on plate see Section 33.1.

The testing of plate for manufacturing defects is very diversified, which is not surprising in view of the many different uses made of plate in industry, and the resultant varying significance of plate defects, the diversity of the defects according to their nature, shape, position and size, and the wide range in plate thickness from 1 mm to more than 100 mm. Consequently, in this field all the known ultrasonic testing methods are used to a wider extent than in almost any other application. Classification into medium and heavy plate for thicknesses above about 4.5 mm and sheet and strip for thicknesses less than this, seems practical in view of the different problems involved but the demarcation line is fluid.

24.1 Medium and Heavy Plate

If at any time during the production cycle the slab, as the preliminary stage in the manufacture of plate, is available in the cold state, it can be tested in order to eliminate serious defects which would subsequently appear in the rolled plate. This test is, however, controversial because on the one hand small flaws in the slab can be forged together during rolling, and because on the other hand segregations which in the slab are still closed may be opened up during rolling [1477]. Furthermore laminations can be introduced in the plate during rolling so that testing of the finished plate must be carried out in any case. Consequently, slabs are mainly tested only for extended primary pipe, and further perhaps only as a quality-control measure by means of which pieces with a large number of indications can be eliminated.

The surface is cleaned by flame-scarfing or rough milling and then tested at various points by means of 2-MHz normal probes using a liberal application of oil, water or paste. In the case of automatically flame-scarfed surfaces, the quality is suffi-
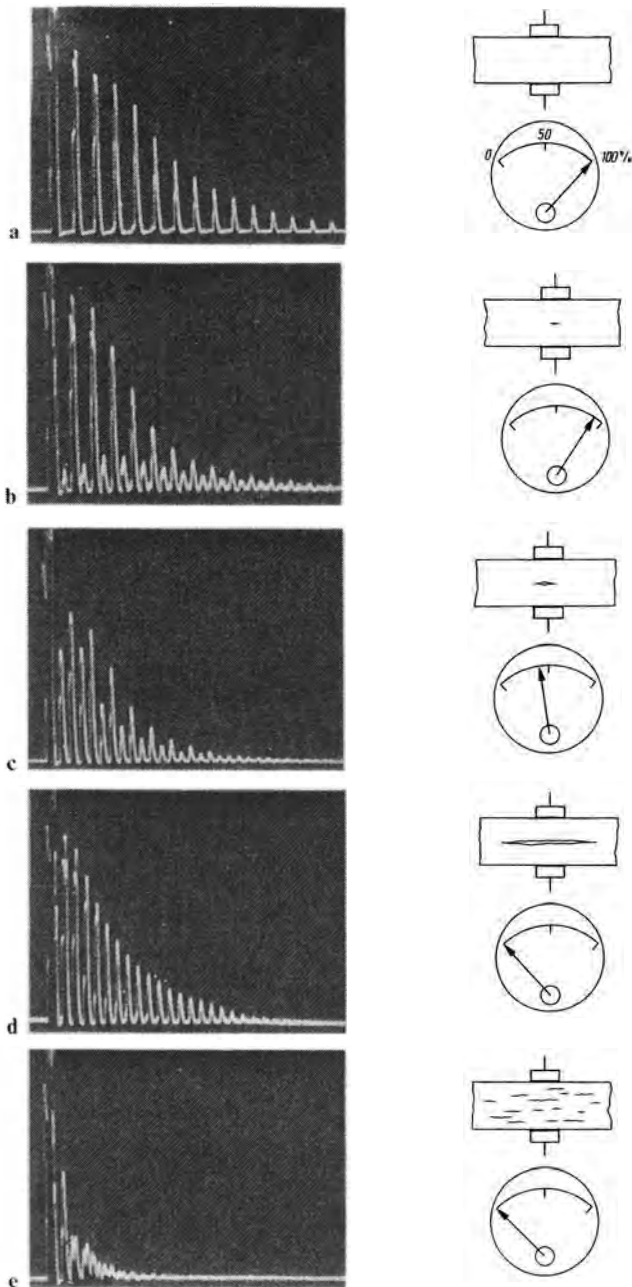
Fig. 24.1. Testing of 15-mm plate with different flaws by the pulse-echo method and by through transmission·

ciently good for continuous scanning with water-gap coupling as in Fig. 15.10. A continuous slab-testing installation has been described by Silber [1412].

Heavy and medium plate may contain defects showing all transitional stages, from the finely distributed layer of inclusions which is partially permeable to ultrasound, to individual inclusions lying singly or together with others in a layer or in several layers, or to open laminations with no mechanical cohesion. Since they originate from central piping, true laminations are usually located at the half-plate thickness. Their extension in the plane of the plate largely depends on the rolling process. A slab rolled not excessively in both directions produces heavy plate in which top and secondary piping extend ribbon-like through the middle zone, whereas other defects show no preferential direction of extension. The extreme case consists of strip which may contain flaws extending for several metres in the rolling direction. These may, however, be only a few millimetres wide and the testing method should make suitable allowances.

Figure 24.1 shows screen pictures obtained with the pulse-echo and through-transmission methods. Contact testing with a probe of about 4 to 5 MHz has been used with a near-field length considerably in excess of the plate thickness.

The flawless plate produces a long echo sequence (a) and an intensity which is adjusted to 100 %. A flaw with an area considerably smaller than the area of the probe produces small intermediate echoes (b), while the intensity drops slightly. Because of the unavoidable coupling fluctuations, this drop in intensity cannot be regarded as a reliable indication of a flaw. For both methods, the indication becomes more distinct if a smaller probe is chosen, but only as long as its near-field length does not become small compared with the plate thickness. A flaw whose area is not much smaller than the area of the radiator produces echoes which are comparable with the still visible back-wall echo (c), while the intensity drops markedly. A pronounced lamination produces an echo corresponding to that of a plate of half the thickness (d), because the lamination is usually at the centre. In the case of a wide open air-filled lamination, the echo sequence may again be very long. Usually, however, the flaw eliminates a portion of the echo sequence, especially if it is filled with slag. In this case only a short echo sequence of half the plate thickness is obtained. In the case of through transmission, zero intensity clearly indicates a separation. In the case of a multilayered defect the various flaw echoes interfere with each other (e). In addition, the sound is then usually attenuated considerably. With through transmission the indication is also zero.

When using the pulse-echo method on thin plates the flaw indication may not be observed but only the disappearance of the long and regular echo sequence ex-

Fig. 24.2. Testing plate with zigzag transverse waves

pected from a flawless plate. The lower thickness limit for this method applied to steel sheeat is reached at about 2 mm for frequencies around 5 MHz but there is no upper thickness limit. On the other hand, the through-transmission method has no lower limit but in practice an upper thickness limit is set by the size of the smallest flaw to be detected.

In addition to the two methods mentioned above it is also possible to test by means of plate waves according to Fig. 24.2. Particularly favorable results can be obtained if the frequency and beam angle are chosen in such a way in relation to the plate thickness that the cross-section of the plate is completely filled by the sound waves reflected back and forth (so that they form a plate wave). This method was tried out first with frequencies above 1 MHz for sheet, and has produced satisfactory results also for plate above 10 mm, using 0.5 to 1 MHz. On defect-free plate it is possible to obtain a distinct edge echo over a width of 4 m. Adjustable angle probes are used for this purpose, the angle being determined empirically to give an optimum edge echo.

Since the three methods respond differently to various types of defect, they have proved to be variously successful in practice for testing plate according to different requirements. The pulse-echo method gives the most complete information, but only if the plate is scanned completely, point by point, which owing to the time required can be considered only in exceptional cases, automation being possible to only a limited extent. The sound-transmission method is reliable in the case of complete laminations (cases d and e), (Fig. 24.1), but less so for areas with clusters of inclusions (cases b and c), particularly where many small inclusions occur predominantly in the center plane. These, however, can be detected readily by plate waves using the echo method and the viewing screen then shows a "beard" of stray echoes whose position and width correspond fairly accurately to the flawed area. Provided the affected zones are not too wide, and the inclusions not too coarse, the wave is still strong enough behind this zone to indicate other flaws and also the plate edge so that a complete display of the tested strip is obtained on the viewing screen. In the case of complete laminations, particularly smooth laminations in an otherwise sound plate, the indication is limited mainly to the point of incidence at the edge of the flaw. Its width is then no longer recognizable and the edge echo the plate also disappears. This attenuation of the wave can, however, be compensated electronically by using a distance-amplitude corected gain.

Occasionally flaws are detected in fillet-welded−joints and angle joints [1028, 199], which manifest themselves as small cracks appearing in the plate material next to the welded joint in the heat-affected zone. The cause is found to be finely distributed slag inclusions in the plate and the flaw is described as "lamellar tearing".

Long ago, Meyer [1028] proposed sound-attenuation measurement at 6 or 12 MHz for plates containing this type of flaw, areas of higher attenuation indicating their presence. Usually inclusions which show themselves by increased sound attenuation can be detected also with TR probes using high gain. However, according to unpublished investigations by Frielinghaus not all inclusions which cause lamellar tearing can be detected by their echoes. Depending on the nature of the manufacturing process, some plates have reduced transverse tensile strength but

show neither increased sound attenuation nor any other properties detectable by ultrasonics when compared with defect-free plates.

When testing large plates in steel mills which, in earlier times, was mostly done by hand, the evaluation by sampling therefore was only statistical. The plates were tested along narrow strips or at points of a grid. For a plate of 4×10 m containing few defects, and test strip separation width of 200 mm, the testing time is, for example, 20 min, i.e. 0.5 min per square meter. If a large lamination is found, its outline is fully traced and recorded, otherwise a code number is entered for the echo height relative to the bottom echo along the scanned strip, e.g. 1 for small readings, 2 and 3 for readings of the order of the bottom echo, or greater, respectively. The theoretically possible case that a large lamination could just fall inside the mesh of the testing grid and fail to be detected while the rest of the plate would be sound, is practically impossible. A flaw never occurs alone, and tests using grids of different density and different orientation have led to practically the same overall evaluation of a given plate.

This geometrical sampling method of testing is suitable only for plate whose utilization does not require closer examination at certain points. If, however, boiler plate is involved, the user will find it desirable to have selected areas tested more closely, where for instance tubes are to be welded in, specifying the maximum permissible flaw. A similar procedure is adopted by the Deutsche Bundesbahn for the acceptance of flange sheets for railway bridges to which web sheets are to be fillet welded. At such points, because of the welding and the transverse stresses produced by the crosspiece, a given flaw is far more serious than on an unencumbered plate. The test specification should therefore make allowance for these special local requirements.

Plates to be used for large-diameter welded pipelines are subjected to special tests of the plate edges. The longitudinal edges of such plates, intended to be welded into pipes with longitudinal or spiral joints, should therefore be defect-free and thus prevent flaws appearing in the joint during welding. Sections of pipe with longitudinal seams are welded together on site using the transverse edges of the plates, so that it is necessary to test the transverse edges also. The total edge test usually requires that a strip 50 mm wide is covered completely. The "Conditions of supply of steel/iron for ultrasonically tested plate" (SEL 072-69) prepared by the VDE in Germany, specify in addition to the general area test also an edge test. (cf. also "Classification of ultrasonically tested heavy plate" and "Classification of heavy plate, tested ultrasonically in the edge zones" [1751].

The wear and tear on probes when used for contact testing by hand is considerable and can represent an appreciable expenditure so that better results have been obtained using coupling by means of a water gap, for instance when using the plate tester illustrated in Fig. 15.10.

In the case of plate thicker than 20 mm, the alarm can be triggered directly by the intermediate choes of a normal probe but in other cases a TR probe can be used in the plate tester, flaw echoes also being indicated automatically in plate as thin as 5 mm.

The plate tester of Fig. 24.3 uses five TR probes of 4 MHz for simultaneously testing five strips having 60 mm distance. By oblique positioning of this array the

Fig. 24.3. Five-channel plate tester (design Krautkrämer)

separation distance can be effectively reduced. The probes are operated by a multiplexer and miniature flaw detector mounted on the trolley and are surveyed by monitor gates.

An installation of similar type has been used by Bethlehem Steel, USA, to check a 450-mm strip using 18 probes, connected by cable to a stationary ultrasonic unit.

Automatic testing devices not only save time but can also evaluate the result according to a given program and provide documentation. A number of them of different detailed designs have been used for many years but they differ regarding the test method, the scanning program and the evaluation of data. Firstly there has been the through-transmission method with coupling by free water jets. Then there comes the pulse-echo method with TR probes and water-gap coupling. Some heavy-plate testing installations are designed to test separate cut plates in which each plate stops, and one or several probes check the face and the edges according to a program (e.g. first testing of all four edges, then scanning of the face of the plate along a meander). Most installations, however, are designed as "transit tests", the plate being tested on a roller bed during normal transport at testing velocities of 1 m/s and higher. The probes are arranged in the form of a comb and in some instances the testing comb oscillates transversely to the rolling direction in order to improve the detectability of long narrow flaws.

The first heavy-plate testing installation using the sound-transmission method and moving plate was described by Höller, Dick and eechky [675].

A testing installation developed by Krautkrämer also uses the transmission method but with free water jets of approximately 75 mm length for coupling. Here no mechanical parts touch the plate which is transported on a roller bed. The gap bridged by the water jets (total 150 mm) also largely prevents any damage to the testing installation by projecting laps or bent ends of the plates. Although completely uncut plates can theoretically be tested in this way, in practice continuous tests are only carried out on precropped plates. Figure 24.4 shows a section of an
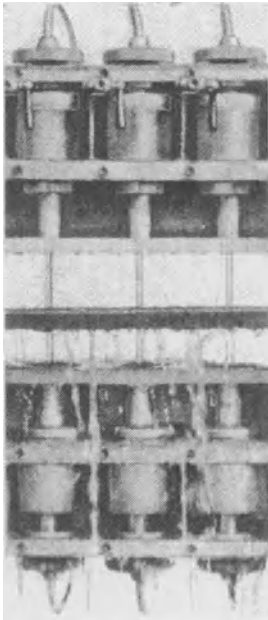
Fig. 24.4. Section of an installation for testing heavy plate, using free water jets (Krautkrämer)

experimental installation which clearly indicates the testing principle. In order to prevent any cross interference from one test point to another they are spaced 100 mm apart. If in practice a greater density of testing tracks is required, (say at 50-mm separation) the test points can be staggered in two rows.

The method of linear testing applied as "whole-plate test" which has been described has of course a statistical character. With a water jet of approximately 8 mm diameter and the test tracks spaced by 100 mm, 8 % of the total plate surface is tested, and in the case of tracks spaced by 50 mm the sample is 16 %.

Figure 24.5 shows such an installation with free water jets which has three extra testing elements arranged in front of the test comb to measure automatically the level of sensitivity at which the plate must be checked, to obtain uniform results for all plates. The required level depends on the individual surface quality, on the temperature of the material, and also somewhat on the thickness. To avoid making a correction measurement on a defective spot, the three probes are distributed over a full width of more than 1 m. The automatic control of the test sensitivity is based on the maximum measured by any one of these three test tracks [870]. The computer for the evaluation is housed in another part of the building.

An interesting feature of coupling via free water jets is that by this method plate can be tested at temperatures up to approximately 250 °C and more recent tests on 35-mm plate found that adequate coupling can still be achieved up to almost 300 °C.

Compared with contact testing, a testing installation using free water-jet coupling has the disadvantage of high water consumption (about 20 l/min, per test point). A portion of the coupling water can, however, be recycled provided the very
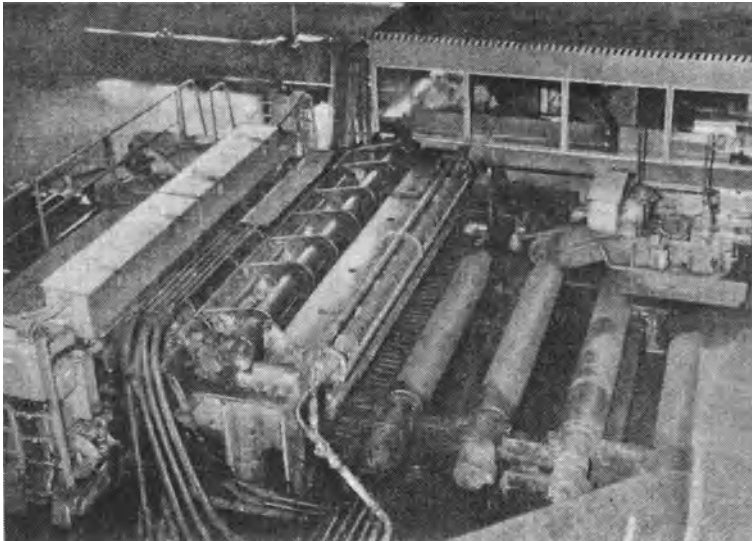
Fig. 24.5. Testing installation for heavy plate, feeding side. On the right the pilot probes; at the top the control cabin (courtesy of Hoesch-Hüttenwerke, Dortmund-Hoerde)
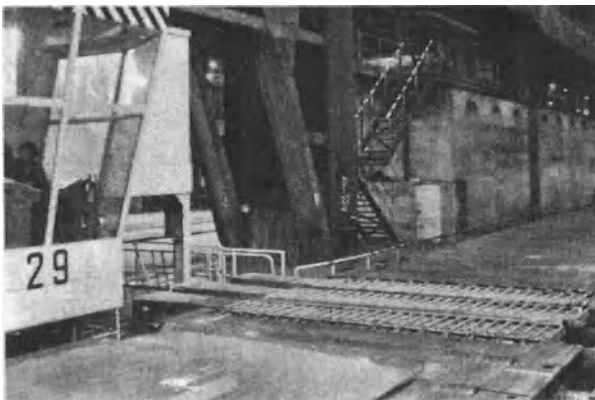
Fig. 24.6. Test installation for heavy plate using broad-beam TR probes from beneath (design Krautkrämer, courtesy of Dillinger Hütte, Dillingen)

dirty water is adequately filtered. Small particles of less than 0.2 mm in diameter, provided not too many accumulate, do not interfere and it is therefore not necessary to use drinking water.

A second testing method, with TR probes and water-gap coupling, is used in some other installations. In the "cut-plate testing installation" of the Hüttenwerke Oberhausen the plate remains stationary. The main surface testing along a meandering line, combined with a test of all four edges, provides the test results in the
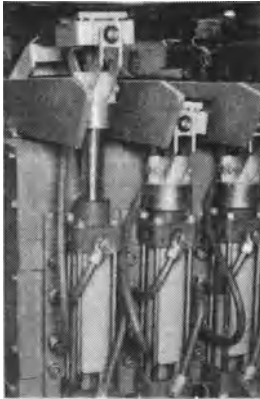
Fig. 24.7. Probe manipulators for the installation in Fig. 24.6

form of an evaluated C scan. In this unit the correct monitor gate position is prese-lected by a computer, which also stores the different delay-line lengths of all TR probes so making it possible to compensate the different wear of each delay line. The computer also controls the entire testing process according to a preselected programme.

A more modern installation shown in Fig. 24.6 uses the same principle but test-ing from beneath, with three rows of 32 probes each, staggered to obtain a testing density of 100%. The 3 times 32 probes are applied in preselected groups by hy-draulic manipulators (Fig. 24.7). The evaluation chart produced by the computer (Fig. 24.8) will be discussed below. The testing speed is 24 m/min.

Figure 24.9 shows a Japanese installation using TR probes with a testing speed of 3.5 m/min.
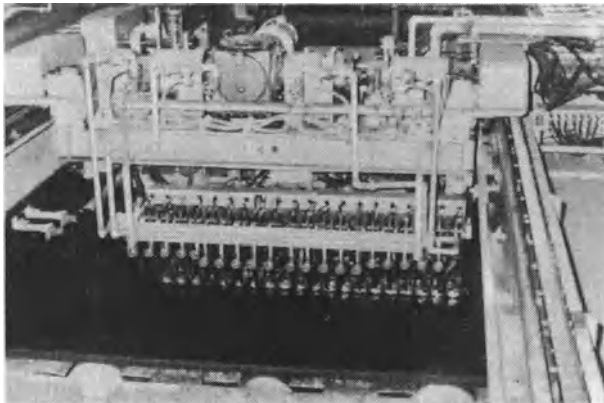
Fig. 24.9. Test installation for heavy plate up to 80 mm thick using TR probes from above (de-sign Mitsubishi Electric Corp., courtesy of Nippon Kokan Corp., Japan)

The Flaw Evaluation

The large number of test points, usually 60 to 80, for the standard plate widths of 3 to 4 m, require special evaluation methods. The simplest way is by a C scan of the plate, in which all test traces are written by a multiple recorder (Fig. 24.8). The scale reduction in the longitudinal direction is usually about 20 : 1 so that for a maximum length of plate of 30 m, a record 1.5 m long is produced. From this record the decision has to be made where to cut the plate and how to classify it according to the specification of the "Technische Lieferbedingungen für ultraschallgeprüfte Bleche" in which 10×10 mm defects have already to be considered, so that the length of the record cannot be further reduced. Therefore further reduction has been made by using digital printers, giving numbers and symbols, classifying the whole plate. Such an evaluated C scan is produced in the following way.

Each longitudinal trace is divided into separate 10-mm lengths (subsections) and ten of these are taken together as one recording section. If at any position in a recording section a defect is indicated, a number is printed which indicates how many defective adjacent subsections have been detected within this recording section. If several groups of adjacent defective subsections have been detected, the largest number is printed. The groups of such numbers give a position-true image of the plate. If a particular plate is found to be unacceptable for one order then the computer can look through other orders to find one for which the plate, after cutting, can be used. The computer automatically then gives the order to produce a substitute plate.

The computer and recorder of the installation in Fig. 24.6 gives a result as in Fig. 24.8, making a point for each defective recording section. On the leading edge ① it shows a defective spot on seven traces, but this will be subsequently cut off. In addition a larger defect is to be seen at 1.50 m from the leading edge. Finally near the rear edge ② (not yet cut off) some scattered areas of lamination are to be seen. All defective spots are totalled up ③, ④ in the length as well as in the width. From this result the general classification of the plate is computed. Simultaneously on the trace numbered ⑤ the thickness is measured and in addition coupling conditions and/or probe failure is indicated.

Plate-Edge Testing

For cut plate or strip to be used for the manufacture of large-diameter pipes, freedom from flaws at the edges is of particular importance because of the subsequent welding process. Therefore in addition to the above-mentioned general plate-testing installations, so-called plate-edge testing is simultaneously in use, using both methods i.e. water-jet through-transmission or TR-probe water-gap testing. Figure 24.10 shows one of the latter design. Usually an edge zone of 50 mm width is checked 100 % by a combination of several broad-beam TR probes (see also Fig. 10.50). As can be seen in front of the probe assembly colour-jet pistols are provided for marking defective areas of the plate.

Another requirement on the raw material for large-diameter pipe production is the absence of subsurface laminations. For this type of defect the methods men-
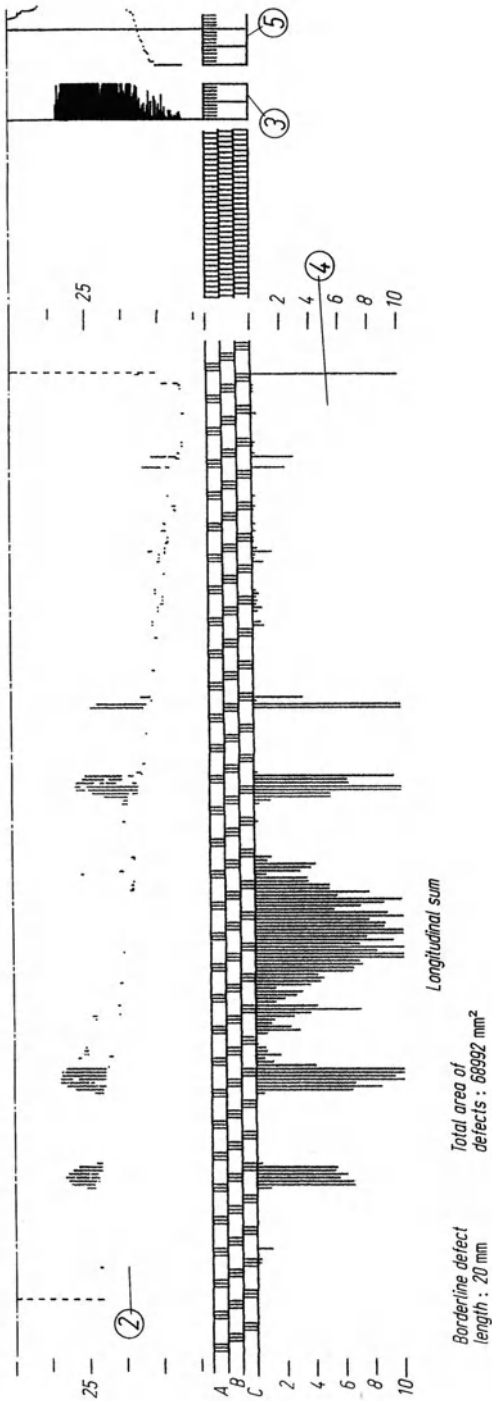
Borderline defect
length : 20 mm

Total area of
defects : 68992 mm²

Longitudinal sum
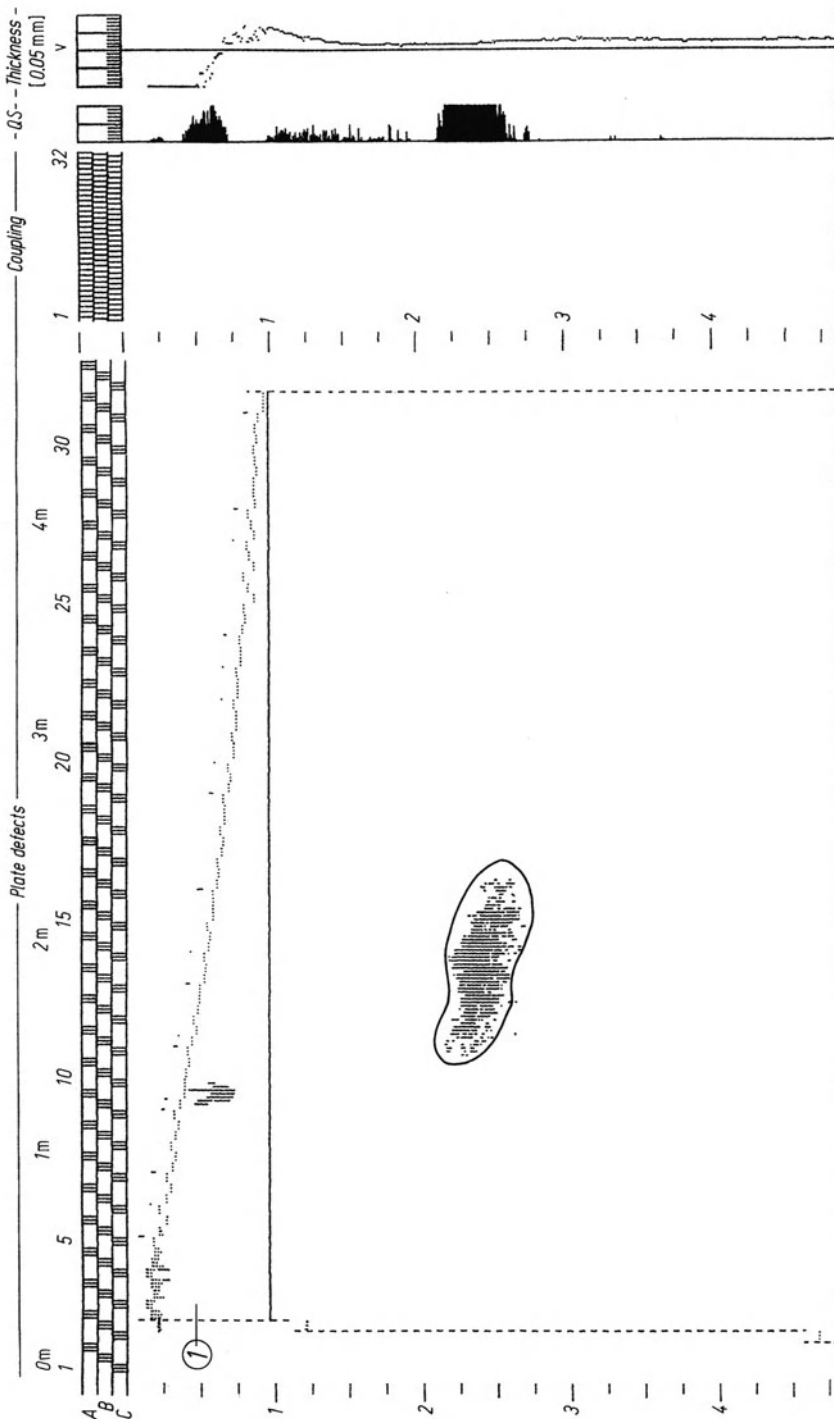
Fig. 24.8. Test record of the installation in Fig. 24.6
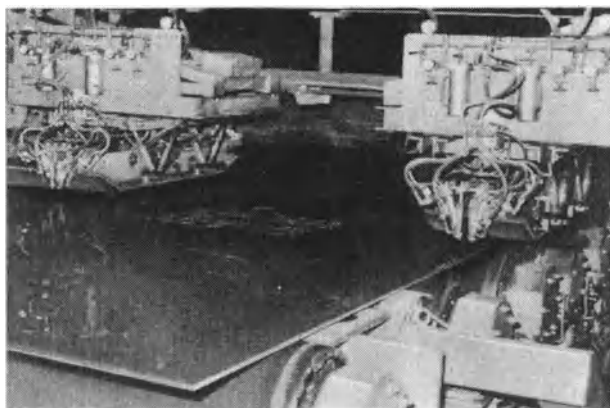
Fig. 24.10. Plate-edge testing installation (design Krautkrämer, courtesy of Italsider, Taranto, Italy)

tioned above fail if the plate is tested by pulse-echo from the opposite side. Schlus-nus [1353] has used a wall-thickness meter using shock waves for high precision and it indicates these laminations by showing a thickness somewhat lower than on defect-free areas. Laminations very close to the back-wall can be found also when scanning, by discriminating between slowly varying wall thicknesses and sudden changes. Even laminations of 0.4 mm distance from the back-wall can be found by this means.

Comparison with Other Test Methods

If one compares the results of ultrasonic tests on metal specimens with chemical or semi-destructive methods, it must be said that exact agreement with the Baumann or sulphur print cannot always be found, mainly because closed segregations are usually not indicated by ultrasonics. Sometimes also a grooved reversebend test is contradictory, when it fractures with smooth separations which give no ultrasonic result. In a plate of a 1 % manganese steel no ultrasonic echoes were found but it had a very pronounced layered structure and the transverse tensile strength was much reduced. After further heat treatment no differences could be found indicating that no real physical separations had been present.

In this connection other ultrasonic tests on a 13 % manganese steel plate should be mentioned in which only a few indications were found at a temperature of 80 °C, but many more after further cooling. The cause was segregations which only opened at low temperature, as distinct from real laminations which are already open at higher temperatures.

In the field of *light-metal alloys* the above observations cannot be applied simply. Light-alloy ingots in the cast state can be tested quite easily and it is useful to use for this purpose the milled surface produced prior to rolling. The demands from the aircraft industry for defect-free final products such as thick plate and continuously extruded profiles are much more critical, and hence ultrasonic tests on the fi-

nal product must be much more sensitive and complete. In the USA large immersion-testing-technique installations have been built incorporating automatic scanning and remote control of the probe manipulator in two horizontal, one perpendicular and two angular coordinates. Horizontal scanning is carried out at about 0.5 m/s and the tank with dimensions of 4×16 m can receive single specimens up to 20 t in weight using a hydraulic lifting mechanism (Curtiss-Wright).

Such large sections of aluminium plate are first automatically scanned at a speed of 2 to 3 m²/min by using a broad-beam probe 120 mm wide. By using a guiding mechanism on the surface the probe is always kept to the correct alignment on the surface of wavy plates. Any defect greater than a certain minimum echo height is indicated under water by a lipstick. Subsequently a small probe is used to evaluate exactly the flaw position and size, comparing the echo received with those from test blocks with flat bottom holes.

Oblique defects can also be evaluated by tilting the probe and because these materials usually contain only very few defects the complete test can be completed within a reasonable time.

For specifications and acceptance standards for steel and aluminium products see Chapter 34. For more information about heavy-plate testing see [998, 999, 867, 868, 1222, 698, 1192, 139, 143, 1049, 101, 1089, 1430].

24.2 Strip and Sheet

The testing problems relevant to the inspection of strip and thin sheet material and their solutions differ greatly according to the fabrication and contract requirements. An example in which a partial test which covers only a few tracks in the longitudinal direction is sufficient, is the *edge test of strip*. In the manufacture of large-diameter pipes from strip by automatic longitudinal or spiral welding, no laminations are allowed at the edges, even if they penetrate only a few millimetres. Testing along the edge, however, is much more difficult than in the body of the sheet. If the
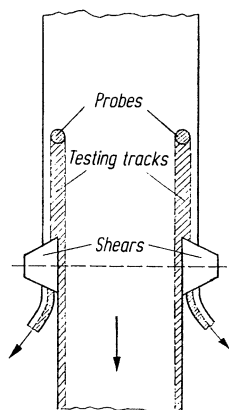

Fig. 24.11. Testing the edges of strip, diagram of probe positions

strip, prior to welding, passes through trimming shears which prepare the edges and in addition cut off a narrow strip of metal it is recommended that the test is made on a slightly wider track within which the subsequent edge will be located (Fig. 24.11). Provided the thickness is greater than 6 mm, TR probes can be used too and the test conditions are more favorable than with plate edge testing. Because of the considerable length of the strip readjustment to other strip dimensions is only needed at long intervals and can be made manually.

The TR probes mounted in sled-like holders are usually lowered onto the strip from above and coupled by flowing water. Monitors indicate the appearance of flaw echoes by means of signals but in this case there is no point in applying position-true color markings to the top surface of the strip because flawed sections cannot be cut out in this continous production process. The strip is usually marked therefore from below preferably as permanently as possible (e.g. by grinding) so that the flaws can be identified after rolling and welding on the outside of the finished pipes. Flaws in the edges of the strip usually cause a defective welded seam which can therefore be checked close to the points marked on the strip. At this stage it can be decided whether the affected section of pipe should be eliminated.

Below a strip thickness of 6 mm, which is the lower application limit for TR probes, the through-transmission method can be used with an immersion technique. Here, instead of simple sound-intensity measurement (as for instance when testing rolled plate with free water jets, see Section 24.1) the pulse transit-time method is used. This is made possible by staggering the probes in such a way that
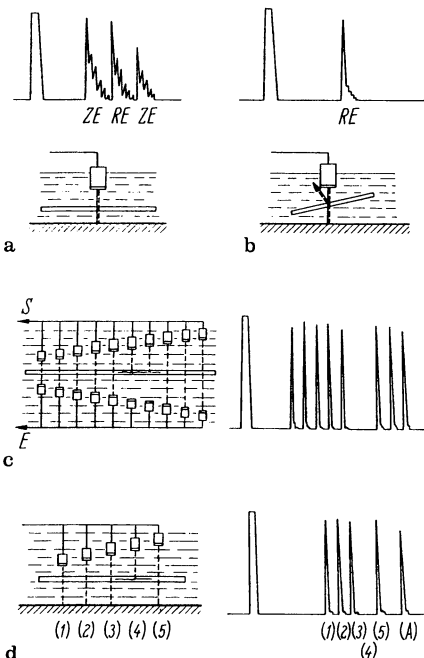
Fig. 24.12. Testing of strip and sheet with the pulse transit-time method by sound transmission, using the immersion technique.
a "Double-sound transmission", sound beam normal to plate, intermediate echoes (ZE) and reflector echo (RE) broadened by multiple reflections; b "double-sound transmission" with inclined plate: the intermediate echoes which interfere in the case of a and the broadening of the echo are avoided; c "single-sound transmission" with 10 parallel tracks, lamination indication by 2 tracks; d "double-sound transmission" with 5 parallel tracks, lamination indication on track (4). (A) = first repetition echo of reflector indication on track (1)

the sound-transmission readings of several scanning tracks are presented next to each other on the screen, which are then evaluated by separate monitoring gates (Fig. 24.12).

One variation, the "double-sound transmission" (Fig. 24.12 d) in which the echo height of a reflector mounted under the sheet is used has proved much more effective for locating small flaws than the simple sound transmission of Fig. 24.12 c. It is advisable to incline the probe-reflector assembly relative to the surface of the sheet in order to avoid broadening of the echoes due to multiple echoes from the sheet. Several testing tracks monitored on a CR screen by adjacent indications can be recorded separately in this way. The maximum number of tracks which can be checked simultaneously by a single flaw detector unit in the case of the "single-sound transmission" is approximately ten, and in the case of the "double-sound transmission" approximately five because of the more critical reflection conditions which in turn depend on the track density.

In practice the immersion technique described is applied by passing the strip through a "transit-testing tank". This tank contains the probes and reflector mounted in a frame which is inclined relative to the strip. The entrance and exit slots of the tank have suitable flexible seals so that the loss of water is reduced to a minimum and submersion of the probes ensured.

For a simple edge test of the strip several water-jet coupled probes have been successfully applied. In general, however, a complete test of the strip using longitudinal multiple test tracks, irrespective of whether the test is carried out by the reflection method with TR probes or by sound transmission, is not justified because the flaws are usually elongated and very narrow, which makes it very probable that they could be situated between adjacent testing tracks. In addition the required testing velocity can be higher than 2 m/s, so that the testing density even with oscillating probes is insufficient. Therefore, for rapid testing of strip, the *zigzag* or *plate wave method* is used in which, according to Fig. 24.2, the entire plate can be covered merely by testing along one edge. Against this advantage must be considered the shortcoming that the flaw echo is no longer correlated quantitatively to the size of the flaw. Moreover it cannot be guaranted that the transmitted mode is being reflected as the same mode by a machined rectangular edge and by a natural defect. Generally the same mode as transmitted can only be received by an equal probe after through transmission. Because of the different velocities of other wave modes generated by conversion at an edge or even from a defect, measuring the distance can give wrong results. Only the same mode as transmitted seems to have been reflected in Fig. 24.14 and in Fig. 24.13 a, c, d and e. On the other hand Fig. 24.13 b shows a mixture of several modes reflected from the edge. For the theory of reflection of plate waves see [S 187].

In practice, any beam entrance angle may be used, but in thinner plate, where the zigzag reflections in the cross-section of the plate overlap increasingly (as in Fig. 24.2 towards the right), it is found that strong energy transmissions are obtainable only with particular beam entrance angles that produce the so-called plate-waves. Figure 24.13 shows the echo from a plate edge for different beam entrance angles. It is always to be expected that at sufficiently high gain different wave modes may appear simultaneously. If their velocity exceeds that of the wave with
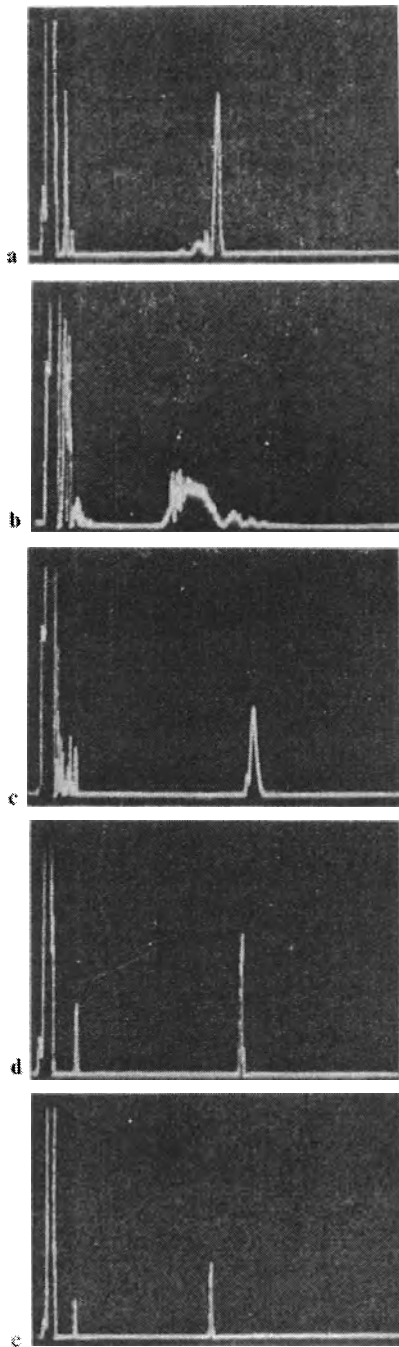
Fig. 24.13. Plate waves of 4 MHz in 1.1 mm thick steel sheet. Echoes of edge at different angles of incident transverse wave (cf. Diagram 9 in Appendix): **a** $\alpha = 20°$ (type s_2); **b** $\alpha = 34°$ (type s_1?); **c** $\alpha = 43°$ (type a_1); **d** $\sin\alpha = 1.05$ (type s_0); **e** $\sin\alpha = 1.1$ (type a_0). Compared with Diagram 9, small deviations of the propagation speed caused by differences in texture may occur. The test parallel and transverse to the direction of rolling may therefore require slightly different angle adjustments

the predominating amplitude, they can easily be mistaken for flaw echoes, which arrive before the edge echo. Two possibilities exist for checking this situation. For frequencies of 2 MHz and higher, plate waves can be damped by the fingertip, so that if a doubtful echo can be damped in this way along the entire wave path up to the edge of the plate, it is merely the edge echo from an unwanted wave. As a further check it can be noted that the distance of the doubtful echo from the main edge echo does not remain constant if the probe is shifted towards the edge, in contrast to that of a true flaw echo.

Since the speed of popagation of the plate waves is also a function of the frequency (cf. Diagram 9 in the Appendix), the echoes of some plate waves are distinctly broadened and bell-shaped, the broadening depending on the path length (Fig. 24.14). The frequency dependence also explains the phenomenon that the individual high-frequency oscillations on these echoes do not move simultanously with the echo if the probe is shifted, but merely travel along its outline and over its peak.

Figure 24.15 illustrates and summarizes the various plate-wave testing methods which are grouped according to the direction of the sound beam relative to the direction of rolling, which is also the usual direction of the length of flaws.

The *transverse test* is particularly suitable for automated strip testing because the probes can then remain stationary while the strip travels past. In the case of methods 1a and 1b (Fig. 24.15), both of which are fundamentally identical through transmission methods, a noticeable reduction of the edge echo can be expected only in the case of flaws several times larger than the thickness of the strip. Inclining the soundbeam direction relative to the rolling direction does not increase the sensitivity markedly in the case of narrow bands of flaws. On the other hand the echo method, 1c, is sensitive to such flaws but without the possibility of relating the echo height quantitatively to the width of the flaw. Thus, even when using the echo method its operation is only a qualitative, go/no-go, indication.

If the detection of larger flaws is all that is required it will be advisable for an automated testing installation, to choose method 1a with continuous-sound transmission using unmodulated frequency because standing waves are hardly to be expected. The pulse method 1b, apart from the saving of one probe offers no advantages but on the contrary, requires more expenditure, especially for recording.
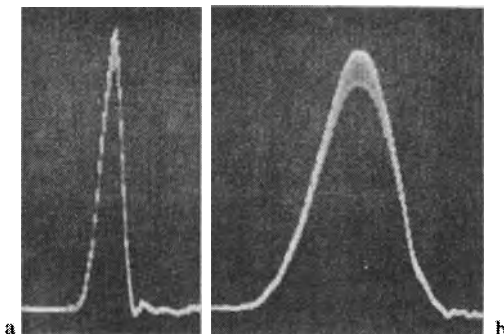
Fig. 24.14. Edge echo of a plate wave. **a** After a path of 100 mm; **b** after a path of 500 mm, on the same scale

	Intensity measurement (with two probes)	Pulse method (single-probe method)
Test *transverse* to rolling direction	Strip	Strip (or thin panel)
Direction of rolling	1a Evaluation of the sound transmission reading (single sound transmission)	1b Evaluation of the edge echo alone (double-sound transmission) 1c Evaluation using flaw echo
Test *in* rolling direction	Thin panels / Strip	Thin panels
Rolling direction	2a Scanning by shifting 2c Oscillatory scanning Evaluation of the sound transmission reading	2b Evaluation of edge echo

Flawtrace   ////, Zones not tested

Direction of strip movement   Direction of movement of probe assembly

Fig. 24.15. Plate-wave test of strip and sheet

For more sensitive testing, echo method 1c with alarm monitor and colour marking or recording with its increased expenditure must be accepted. This method also permits the indications of flaw bands narrower than the thickness of the plate.

The *longitudinal tests* 2a and b can also detect very narrow flaws provided they run in the direction of the sound beam because they then disturb the propagation of the sound over the full beam path.

The disturbance caused by a flaw which is much narrower than the width of the sound beam can be explained in the same way as in Fig. 16.4. The change of the sound beam produced by artificial flaws (grooves) and bands of slag in sheet 0.75 to 2 mm thick has been investigated by Kopineck and Sommerkorn [826]. With beams aligned in the direction of the slag, using methods 2a or 2b, they observed a definite splitting of the central maximum sound lobe into two side lobes.

For continuous strip testing, method 2 a requires that the probe assembly oscillates (Fig. 24.15, 2 c). This testing method is used only on slowly moving strip, for instance at the feeding point of the strip into the welder for large-diameter pipes [867, 868].

Method 2 b, due to the absence of a transverse edge, cannot be used for testing strip. Consequently, this method is used principally for testing individual thin panels.

Based on the fact that different types of flaw affect the various wave modes differently, a probe assembly according to Fig. 24.15, 2 a for the generation of several modes of plate waves has been suggested by Kubiak and Rowand [864], which uses the frequency-modulation method (cf. Section 10.7).

This requires rapid variation of the testing frequency in the range from 2 to 25 MHz, so that all modes can be excited in quick succession. The evaluation is based on the interference frequency of the received waves when compared with the excited wave modes, and on the change in amplitude. This device furnishes a digital read-out of the test values for four selected wave modes but so far no details are available concerning the test results in practical application.

Kügler and Berner [867, 868], with their probe assembly, "Salzgitter" which uses a fixed beam angle and only one frequency in the longitudinal test 2 a or 2 c, have obtained satisfactory results in practical application.

According to Sipek [1425] the wave modes with flat sections in the group-velocity diagram (Diagram 9) in the Appendix give satisfactory results near the minima, for instance at a_1, when the product of plate thickness and frequency is equal to 6. Frequently, however, the most favorable angle and wave mode are found experimentally by carrying out tests on samples with known flaws.

The probe separations usually used in methods 1 a and 2 a are approximately 500 to 600 mm, so that, for a complete test of wider strips several testing tracks should be arranged one behind the other, but relatively transposed. To avoid crosstalk between traces different frequencies are used. For the testing of individual sheets the test result obtained along one track is often regarded as valid for the entire sheet in view of the fact that a particular flaw usually extends over the entire length of the sheet. On the other hand, in the case of strip, most defects usually occur in the central area so that the test tracks along the edges can be omitted.

The probes used in all these methods can consist of conventional angle probes with a plastic wedge. Adjustment of the angle is sometimes unnecessary, because the results obtained with fixed angle probes in the range 35° to 80°, or even a surface wave probe, is completely adequate for rough testing. Alternatively adjustable angle probes should be used and the coupling liquid, which can be water, oil, cutting emulsion or diesel oil, should be fed sparingly so as not to wet the sound path, or alternatively the entire surface should be wetted uniformly. It should be noted that liquid-covered areas on the rear surface also give interfering echoes and a sheet should never be tested on a contaminated support.

For testing from one edge by the echo method, a guiding and holding device as shown in Fig. 24.16 is practical. This moves on three rollers over the sheet and on two rollers along the edge. The narrow gap between contact face and sheet is filled continuously with liquid, thus ensuring uniform contact and minimum wear.
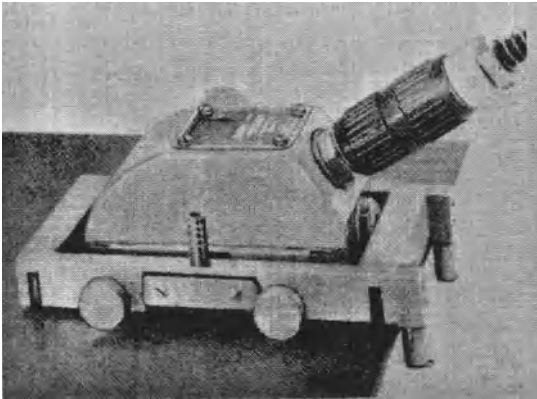
Fig. 24.16. Holder for angle probes suitable for testing plate from the edge by the plate-wave echo method

Up to now only the method of Fig. 24.15, 1 c is being used for continuous strip testing. The probe is arranged in a liquid chamber for oblique beaming by means of an adjustable water wedge.

In practice the test is usually combined with the continuous pickling process and although the condition of the strip surface is adequate prior to pickling, preference is usually given to testing after pickling with strip speeds between 40 and 150 m/min. These relatively high testing speeds require special measures to ensure sufficiently constant coupling and new methods for presenting and evaluating the test data. Direct observation of the CR screen cannot be considered, nor can simple monitor-controlled flaw signalling. No use has yet been made of the possibility of marking flaws on the strip surface or on its edge, to allow the indication of flaws on coiled strip. A method for the documentation and evaluation of defects will be considered later in connection with rod testing (Section 25.2).

The installation shown in Fig. 24.17 uses the method as in Fig. 24.15, 1 c, but with two variable TR angle probes of 0.5 MHz to avoid dead-zone problems (Fig. 24.18) [1433]. They are coupled to the underside of the strip facing in opposite directions and somewhat staggered in the longitudinal direction. The water tanks containing the transducers have a plastic contact face which forms a water gap with the strip, determined by rollers. The probes are actuated by remote control and are controlled by a computer fed with punched cards for each testing programme. The computer obtains from the card the thickness and the width of the strip, and from a stored table the optimum angle, which is based on the plate-wave diagram together with experience obtained with certain types of flaw. In addition, the computer determines the correlated group transit times and adjusts the monitor gates in accordance with the transit time and the width of the strip. The attenuation of the waves as a function of the distance is taken into consideration by several gates of increasing sensitivity, staggered according to the distance, the result being available as a digital read-out.

In the case of both recording methods a pulse generator coupled to the strip carriage is used for a length-true division of the strip into recorded sections and subsections, irrespective of the speed of the strip.
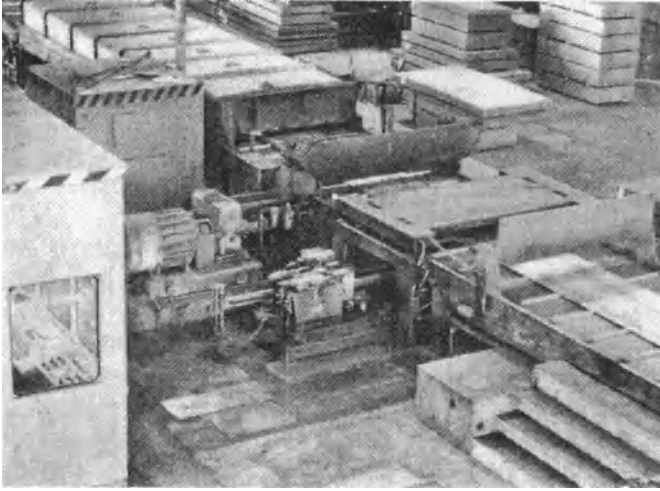
Fig. 24.17. Strip-testing installation (Courtesy of Thyssen Niederrhein, Oberhausen). Both probes at rest position for demonstration
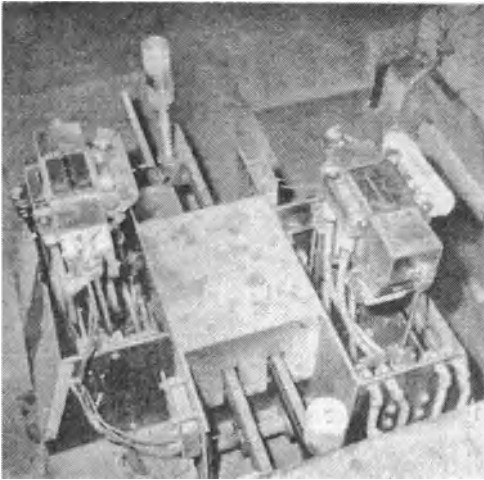
Fig. 24.18. Probe assembly of the installation shown in Fig. 24.17

For strip testing electromagnetic probes (EMATS) have also been used [767].

Thin sheet is today no longer tested on a large scale because of the large quantity which is produced and ordered. For former literature see [456, 457, 1642, 908, 825, 1497] and additionally see [97, 561, 864, 709, 678, 811, 1369].

25 Semi-finished Products: Rod, Bar, Billet and Wire

Manufacturing defects which occur in this group of semi-finished products can either be on the surface or internal (Fig. 25.1). Internal defects originate from ingot defects such as shrinkage cavities and inclusions which have been elongated during rolling and drawing or are rolling or drawing defects, such as piping, particularly in the case of non-ferrous metals, and cracks in the core, which in cross-section appear flat or star-shaped. Surface defects are usually the result of the drawing operation on defects such as radial cracks or laps which reach the surface at a shallow angle. Since all flaws extend in the longitudinal direction, this requires that the axis of the sound beam in a cross-sectional plane lies either normal or obliquely to the surface and for some applications can be surface waves running in a circumferential direction.

25.1 Rod Material

In the case of drawn steel rods, manual testing for internal defects is one of the oldest applications of the pulse-echo method and it made the commonly used pickle test superfluous. To find defects in the core it is sufficient to scan along a few longitudinal tracks using a normal probe, or at least on two mutually perpendicular tracks in order to be sure of obtaining an echo even where cracks are unfavourably orientated.

Thin, bright rods, down to approximately 5 mm in diameter, are preferably tested with a TR probe with its central separations line transverse, or at 45°, to the rod, and it can be easily shaped cylindrically for better guidance. A special probe-holding device greatly facilitates these tests in which two TR probes are placed on the circumference displaced 90° from each other and pressed by spring action
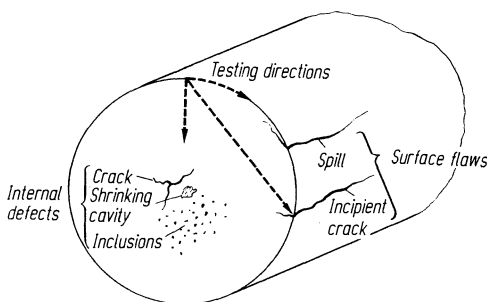

Fig. 25.1. Types of defects in round stock, and main directions of testing

against the continuously moving specimen, a flow of water being used for coupling.

In the case of non-circular rod material as for example square, hexagonal or flat, testing is successful even with diameters below 5 mm because of the higher sensitivity obtained with flat coupling surfaces.

For a go/no-go test it is then sometimes sufficient to observe only the disturbance of the echo sequence occurring between the flat boundary faces. In the case of more complex sections, both the method and the possibility of testing depend entirely on the cross-sectional shape and the probable position of the flaws.

Surface defects can be found with oblique transverse waves or with surface waves as in Fig. 25.1 but the latter can be used only on very smooth surfaces and quantitative differentiation between deeper and shallower crack is impossible. If an angle probe of 45° or 60° is suitably ground as shown in Fig. 25.2, the wide beam after a few reflections fills a zone below the surface fairly completely up to a depth of approximately 20% of the diameter. This technique can therefore detect some internal defects in addition to true surface defects. Any surface defect will produce a considerably stronger echo than an inclusion of comparable size, so that even the minutest surface defect, such as a die line will dominate the test. Surface defects can, however, be distinguished by the fingertip technique.

Since the sensitivity of oblique transverse waves drops after several reflections, the flaw should as far as possible be met in the first half circumference. Thus, in the case of stationary rods, the test should be carried out along two or three longitudinal tracks, or better still, the probe should be moved longitudinally following a zigzag path on the circumference. Flaw echoes then travel back and forth on the CR screen and can be detected and distinguished very much more easily from spurious interfering echoes from the probe. For the same reason it is recommended that the rod be allowed to rotate slowly at a few revolutions par second. Since laps are indicated with greater sensitivity in one incident direction of the wave than in the other (as in Fig. 25.1), the test should be carried out in both directions successively, or better, simultaneously by using a double angle probe.
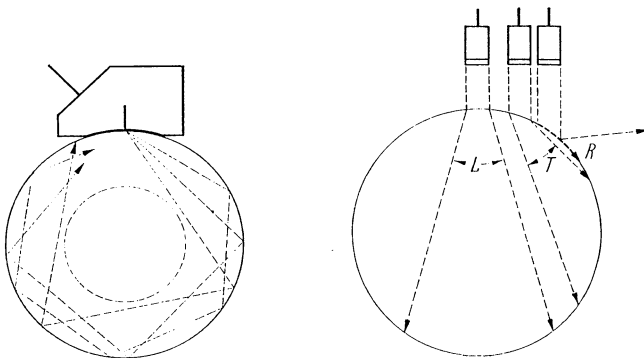

Fig. 25.2. As a result of the beam divergence on entering round material, an oblique beam of transverse waves can cover an outer zone of up to 20% of the diameter

Fig. 25.3. Testing round stock by the immersion technique, beam paths shown for steel in water

The immersion technique can also be used for diameters below about 120 mm, and is the best method for automatic testing. As in Fig. 25.3 all types of waves and testing directions can be obtained by using different probe positions, including a boundary surface wave. When using a broad sound beam, several waves can sometimes be obtained simultaneously and if the surface is not perfectly smooth, this may give rise to troublesome interfering echoes in a zone behind the entrance echo, which in round stock of small diameter may completely mask the echoes of core defects. These interfering echoes are mainly produced by boundary waves which, although they quickly decay on the surface, still produce strong echoes from minute depressions, foreign particles and air bubbles on the surface if they approach the sound entrance point during the rotation of the rod. Therefore, narrow or focussed sound beams should be used, or more simply masks with a circular or slot-shaped opening should be inserted in the sound beam.

To avoid receiving interfering or multiple echoes from a mask, it should be inserted either immediately in front of the probe and/or to lie obliquely to the beam. The mask can be of plastic material with good absorption, such as rubber-containing fillers, or alternatively a thin metal plate covered by a plastic film which makes it impermeable to sound as a result of the trapped layer of air.

The relative positions of probe, mask and bar stock should remain fixed, which in the case of smaller bar diameters is realized most simply by a probe holder such as that illustrated in Fig. 25.4 which is guided by hand. The mask, which is rotatable, is mounted in front of the probe and contains two off-center openings so that depending on their position two transverse waves circulating in opposite directions for detecting shallow defects, or two longitudinal wave beams through the core of the rod are obtained. By using a probe for 4 to 6 MHz it then becomes possible to test rod material with a mill-rough, slightly oxidized surface, down to 12 mm in diameter.

If focussed probes are used in an immersion technique, the reduced sensitivity due to the strong refraction in the rod can be compensated, or the beam can be focussed at a given depth where the presence of any flaws would be particularly dangerous during further manufacturing processes. For correct adjustment, the optimum water gap is found on a specimen with artificial flaws.
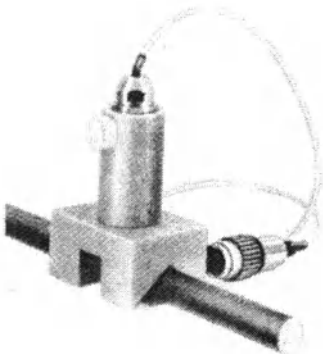

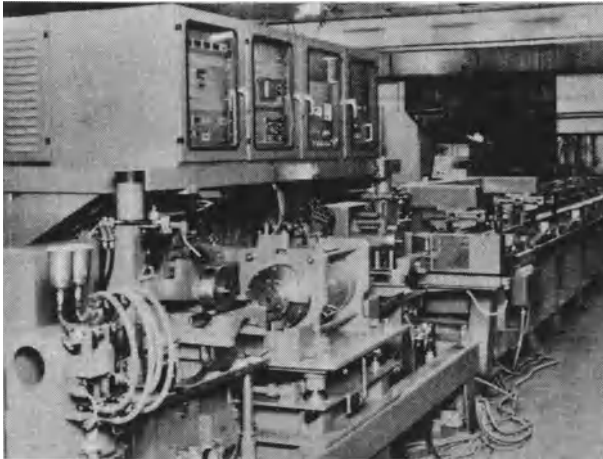Fig. 25.4. Probe holder for testing round stock by the immersion technique

Fig. 25.5. Rod-testing machine with rotating probes for testing of rods up to 80 mm in diameter for longitudinal surface cracks (design Krautkrämer)
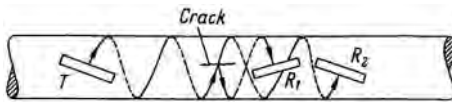

Fig. 25.6. Testing round stock by magnetostrictive excitation according to Kaule [757]. T transmitter; R_1 receiver for crack echoes; R_2 receiver for sound transmission pulse

For defects close to the surface, especially longitudinal cracks, the method to be used is the same as for tubes (Chapter 26, Fig. 26.7). In fact the same testing-installations can in many cases be used for both products, an example being shown in Fig. 25.5 which uses rotating probes.

For small-diameter bright steel rods the magnetostrictive method (Sections 8.4 and 8.5) using the "Ferrotron" instrument has been used for some time. For detecting longitudinal surface defects an array of several coils is mounted in such a way that the electromagnetically excited ultrasonic pulse spirals around the rod with a steeply pitched path (Fig. 25.6).

Receiving coil E_1 is orientated so that it can receive the part of the sound beam reflected by a longitudinal defect, thus producing a flaw echo. The other receiving coil E_2 can receive the spiralling wave directly so that the disappearance of the sound-transmission indication obtained in this way reveals the presence of large defects. Both indications are evaluated by monitors and Fig. 25.7 shows such an installation for testing rods with diameter from 2 to 14 mm, using a Ferrotron instrument. Since the rods need not be rotated while passing the coil array the testing speed can be as high as a few metres per second and for bright stock longitudinal defects down to 0.05 mm deep can be readily detected.

See also [1633] and for further literature concerning rod testing [529, 1548, 115, 1744, 1019].
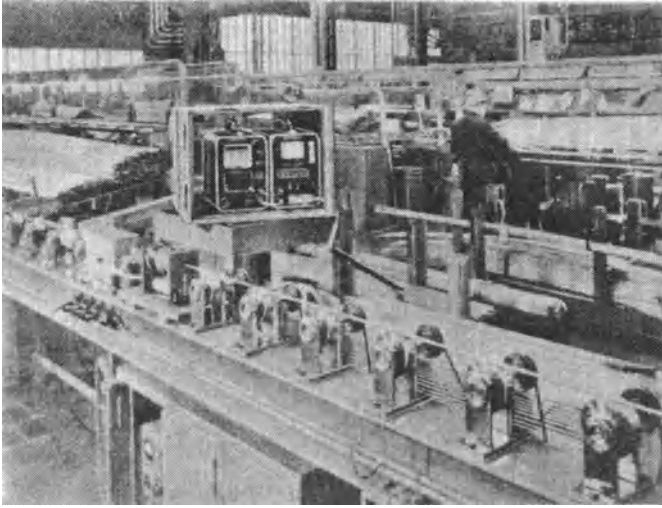
Fig. 25.7. Testing rods with the "Ferrotron" (magnetostrictive principle of excitation of sound waves) (courtesy of Messrs. DEW, Krefeld)

25.2 Billets

Rolled circular billets cannot be tested in the same way as smooth rods and tubes in installations with rotating specimen or probes because of their inferior surface condition.

The larger part of the bulk material is tested with a combination of two normal or TR probes as shown for square billets in Fig. 25.8. For dimensions larger than about 50 mm the number of probes is usually doubled.

In the testing of billets it is not possible to make high demands concerning the detection of either surface or subsurface defects because of the rough surface conditions.

For mechanized testing square billets are best transported on a roller bed as in Fig. 25.8. The probe arrangement consists of twin heads each containing a combination of one normal probe and two broad-beam TR probes. These latter probes are

Fig. 25.8. Testing square billets with two probes connected in parallel

staggered to cover billets up to 250 mm square. In this arrangement the twin heads are pressed onto the billet from beneath after it enters the test machine.

The probe holder has all the necessary freedom of movement to enable it to follow all irregularities of the billet up to a speed of 60 m/min.

In another design (Fig. 25.10) the probe assembly contacts the billet from above after it enters and rides on it.
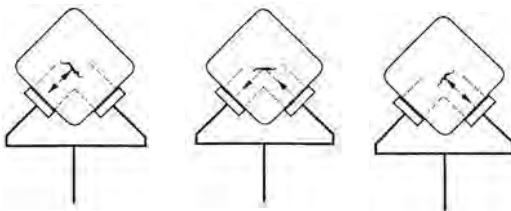
Figure 25.11 shows a test record of the installation of Fig. 25.9. This evaluation system is also valid for similar types of inspection, as for example for strips, tubes and rods. The figures are computed by a microprocessor and printed on a paper strip.

The billet is divided into recording sections of 500 mm, which are themselves subdivided into 50 or 100 testing sections of 10 or 5 mm in length. If an echo exceeds the threshold, the corresponding testing section is recorded as defective but to obtain varying evaluations two different thresholds can be chosen. For each recording section the number of defective testing sections is printed out and in addition the summed length of coupling failures is printed for each recording section. Additionally the total number of defects in a preselected length of billet is summed, so that it is possible to say if the billet contains a defect-free section of a chosen length. At the end of each billet test, the result is summarized and the billet classified according to a specification agreed between customer and manufacturer.

In addition after testing a complete batch the overall statistics are collated to give the number of billets in each classification.

For round and square billets the most important part of the volume is checked in this way. Surface defects, however, cannot be detected so easily because of the
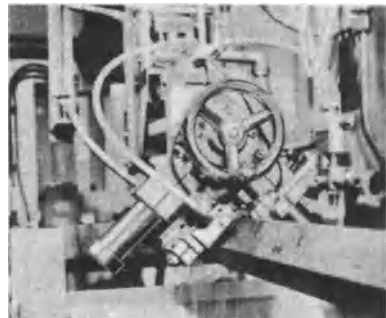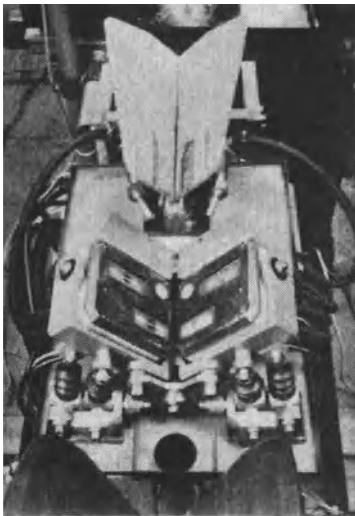

Fig. 25.9. Test installation for square billets (design Krautkrämer)
Fig. 25.10. Test installation for square billets (design Deutsch)

```
PRUEFPARAMETER

DATUM:         19.10.83
SCHICHT:              B
PRUEFER:        MUELLER
SCHMELZE NR.    423716
ARBEITSKARTENNR. 5321
KN-DIMENSION   110 MM
PK-VORLAUF 1    10 MM
PK-VORLAUF 2    12 MM
F-SCHWELLE 1   (3 MM)
F-LAENGE 1      40 MM
F-FENSTER        4 M
K-AUSF.LAENGE 200 MM


KNUEPPEL-NR.  00126

005 50:00     00
010 50:00     00
015 46:01     00
020 38:01     02
025 43:01     01
030 24:01     03
035 00:00     04
040 18:02     01
045 00:00     02
050 12:01     00
055 00:00     02
060 00:00     00
065 00:00     00
070 08:01     01
075 14:02     02
080 00:00     06
085 50:00     05
090 22:02     03
095 06:01     01
100 00:00     04
105 00:00     01
110 00:00     00
115 16:02     03
120 07:01     01
125 08:01     01

FL1:0404 CM   FZ1:017
LK: 043 CM
KN-KL.: 'C'

KN-LAENGE:    1208 CM
```

```
STATISTIK:

ANZ.GEPR.KN:   018

ANZ.KN KL.'A'  011
ANZ.KN KL.'B'  005
ANZ.KN KL.'C'  002
  *  *  *  *  *  *
```

Fig. 25.11. Documentation of billet testing. **a** manufacturing and test-data entered; **b** record of defects in a billet; **c** summary of data; **d** statistics of a batch of billets. Notes ref: **b** 1st column: 500-mm recording sections; 2nd column: length (cm) of defect in the corresponding recording section; 3rd column: corresponding number of defects. For a defect occupying the whole section (i.e. 50 in column 2), the number is not recorded before the section in which the defect ends; 4th column: length (cm) over which coupling fails

roughness and irregularity of the surface. Basically longitudinal defects on the surface of round billets can be found by angle probes or tube-testing probes as explained for rods in Section 25.1. A manual test is feasible only if the requirements for detecting small defects ist not too high. Automatic testing is hardly possible, because the specimen has to be rotated and transported to give a spiral scan and this is impossible for most large round billets because they are not straight enough.

In the testing of square billets for surface defects another problem is encountered. Cracks usually extend from the corners and detection by angle probes is difficult. Occasionally a test with surface waves could be possible, if they are generated on one of the four faces and used for testing the adjacent corner. However, it it necessary that the surface quality is sufficiently good, giving an adequate signal/noise ratio for the smallest defect echoes [142].

The best overall success for these requirements uses a combination of ultrasonic testing for the interior coupled with a magnetic stray-flux test for the surface. Such combined installations have been used for a long time for testing circular rods between 16 mm and 80 mm in one machine or 30 mm and 190 mm in another. For testing of hot slabs and billets at temperatures up to 1000 °C by EMATs see Section 8.4 and [S 91]. For further literature see [116, 701, 529, 119, 858, 815].

25.3 Wires

Rod waves which correspond physically to plate waves in sheet are also used occasionally for testing thin rods and wires. Magnetostrictive excitation of such waves, which is possible only in steel and nickel, according to Fig. 8.15 has the great advantage that no contact is required and a coil is shifted over the end of the rod or wire.

Where the primary objective is to detect longitudinal surface defects in wires, the magnetostrictive method as in Fig. 8.15 with spirally rotating waves can be successfully applied on diameters down to about 2 mm. The flaw detectability starts at depths of about 0.05 mm, at testing speeds of 3 to 4 m/s.

Fine wires, usually less than 1 mm, on which longitudinal and transverse cracks, shrinkage cavities, and inclusions are to be detected, can be checked by a number of different techniques.

In a design according to Böhme [159] a buffer shoe attached to the probe makes dry contact with the wire along a very short section. This excites particularly strong bending waves which are strongly attenuated and reflected by such flaws as longitudinal cracks having a depth greater than 10 % of the cross-sectional area. In the case of frequencies of 1 to 2.5 MHz the coupling fluctuations reach only 10 % of the pulse amplitude. As in the case of plate waves, the pulses are partially broadened as a result of dispersion.

When using the pulse-echo method, one can also operate with standard angle probes and surface-wave probes, the plastic wedge being fitted in the longitudinal direction with a small matching groove. The contact point is continuously wetted with coupling liquid, and the wire moves in a direction opposite to the sound beam to avoid interfering echoes by excess coupling liquid. In the case of coupling under water, as used in the device by Lehfeldt [909], the problem of wear and adjustability of the beam angle is solved in a simple way. A guiding block forces the wire under water for a short distance and in bright wires of less than 1 mm in diameter, even fine scratches are clearly indicated by travelling echoes.

26 Pipes, Tubes and Cylinders

Manufacturing defects are once more the main inspection problem for pipes and tubes, and it also happens that in-service defects such as fatigue cracks and corrosion cracks require the same testing techniques as the manufacturing defects because they are usually in the same position and orientation. Other in-service inspection such as the detection of corrosion and the measurement of wall thickness, are discussed in Section 33.1.

The special cases of pipes produced by casting or by welded fabrication are not included in this chapter because their characteristic defects are of quite different origins.

In seamless rolled tubing the defects which are of interest are similar to those occurring in rod material, that is cracks and laps on the internal and external surfaces as well as inclusions and laminations in the wall which are caused by the manufacturing process as they are in rolled plate (Fig. 26.1).

In some types of manufacturing process transverse or obliquely oriented flaws may occur at angles lying between 30° and 60° to the surface and resemble cracks or laps. When applying a contact test with angle probes to pipes of less than 80 mm in diameter, the beam is transmitted along a zigzag path, partially spiralling around the pipe on either side, as in Fig. 26.2 and this technique will also reveal the oblique flaws mentioned above.
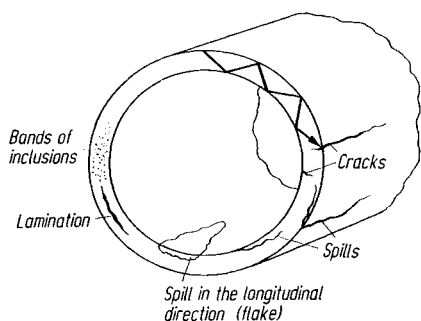

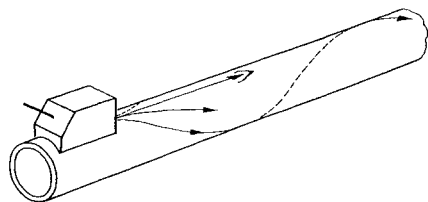Fig. 26.1. Types of defects and main direction of testing in pipes

Fig. 26.2. Longitudinal test on pipes for laps and transverse cracks using zigzag waves (only the path of the wave on the pipe surface is shown)

Transverse cracks also occur as in-service defects on the internal wall of tubular steel moulds used for centrifugally cast pipes, where they are formed regularly in association with longitudinal cracks due to severe thermal stresses and they also occur as fatigue cracks in drill-pipe. Most pipe-testing installations are therefore also fitted with suitably arranged probes for the detection of transverse and oblique flaws.

The testing methods used for detecting the usual longitudinal flaws in pipes differ according to the testing conditions, whether in the pipe mill under production conditions, or for maintenance inspection on pipes already installed. In the factory automated testing installations are installed almost exclusively using the full or partial immersion technique. Manual contact testing is usually used for maintenance inspection and for testing smaller batches in the pipe mill.

The manual testing methods were the first to be developed and were also used at the pipe mills initially. Later on these testing procedures were partially mechanized.

For large diameter pipes above about 400 mm in diameter as used for gas-storage tanks and accumulators for steam boilers, a zigzag shear wave can cover only a small portion of the circumference. Therefore, the pipe should be scanned by hand in the circumferential direction, along separate tracks or along a zigzag path, using angle probes, usually of 45° or 60°. Deep scores on the inner surface produced by the drawing "plug" and which are not readily detectable visually, may make testing rather difficult, and should therefore be avoided during manufacture as far as possible to facilitate the checking for corrosion fatigue cracks.

In the range 25 mm to 400 mm outer diameter (as used mainly for boiler tubes, gas and oil mains, high-pressure pipes and precision steel pipes) a "circular-transit echo" is used which is obtained by means of two probes mounted back to back or in a so-called *pipe probe*, which gives a stationary reference echo as in Figs. 26.3 and 26.4. Here, the reference echo takes over the task which, when normal probes are used, is performed by the back-wall echo since it shows immediately, even in the absence of flaw echoes, whether both the instrument and the coupling are satisfactory. In addition it enables both a direct pulse-echo system to be used as well as a type of through transmission with the sound passing completely round the pipe wall from one probe to the other.

As is shown in Fig. 26.3a, one usually obtains with such a pipe probe two indications from a single flaw, lying equidistant from, one in front and one behind, the reference echo. Since this reference echo is not a true echo but only two pulses travelling from each probe to the other, it has the same total transit time as would an echo from a flaw situated exactly opposite to the probe position. If the reference echo is moved to the center of the CR screen by scale expansion, each half of the pipe is represented by the trace lying respectively to the left and to the right of it. Whether given indications arise from the right or the left half of the pipe cannot be decided if the probe is stationary, but only if it is moved in a circumferential direction. If the flaw echo between transmitting pulse and reference echo, both of which remain stationary as the probe rotates on the pipe, travels towards the transmitting pulse, then the probe is approaching the flaw, and vice versa. Since exact flaw location in pipe testing is usually not required, the pipe probe is usually moved in such
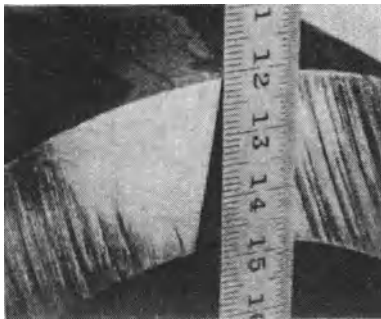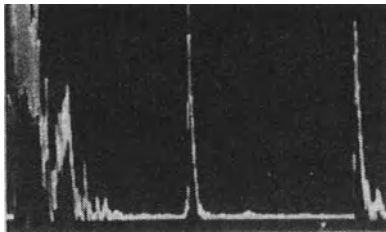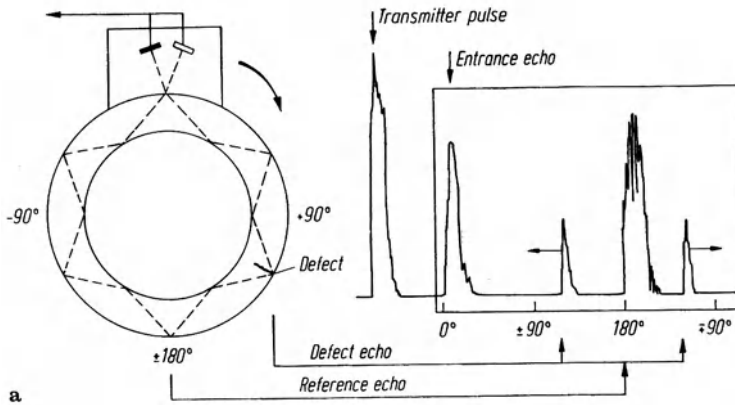
Fig. 26.3. Testing thick-walled pipes by means of the pipe probe. **a** Sound path and screen picture, schematic; **b** screen picture obtained with a pipe of 30×300 mm showing flaw at approximately $120°$ position, frequency 2 MHz; **c** flaw made visible in ground section (lap 3 mm deep)

a way that the flaw echo is located approximately halfway between the transmitting pulse and the reference echo. The flaw is then located at approximately one quarter of the circumference of the pipe (at an angle of $90°$) from the probe.

Unlike the schematic drawing in Fig. 26.3 both flaw echoes and the reference echo are mostly composed of a number of zigzag waves which lie within the range of the angle of divergence. Consequently the indications usually contain several peaks.
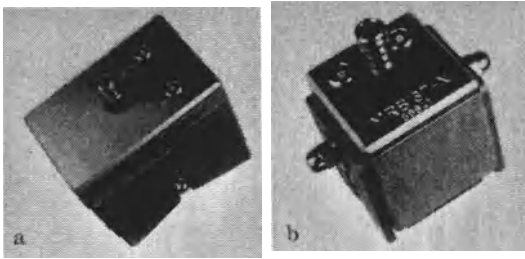
Fig. 26.4. Tube-testing probes, with crystals arranged side by side to get the exit point for both on one line, with irrigation of the contact face. **a** 45°, 2 MHz, for manual testing; **b** 37°, 4 MHz, for automated testing

In the case of thick-walled pipes where the wall is greater than about 10 % of the diameter, the envelope of a flaw echo shows distinct maxima and minima when the probe is moved. The positions of the maximum readings of both internal and external flaws can then be marked on the CR screen using a pipe section with internal and external saw cuts, thus enabling the different flaws to be distinguished from one another.

A fixed pipe should not be scanned along only a single longitudinal track because then the zone below the probe will not be checked, and because the reference echo may mask a flaw lying in the exactly opposite position. For this reason, and also for clearer indication of flaws by using travelling echoes, the probe should be moved along a zigzag path. For the detection of laps it may then be advantageous to observe both flaw indications simultaneously as in Fig. 26.3 a. While in the case of small cracks the right-hand echo with the longer sound path is usually smaller than the left-hand echo, this may be reversed in the case of laps lying in an unfavorable orientation. Otherwise the second echo can be disregarded and the reference echo shifted to the right-hand side of the screen, as in Fig. 26.3. This is particularly effective when testing rotating pipes because a lap always assumes a favorable orientation at one point if the pipe probe is used.

The reference echo, as implied by its name, is used for checking the coupling and the complete circumferential traverse of the sound pulses. Strong reduction of the reference echo intensity usually indicates a defect in the pipe. In the case of new tubes this may be a lamination, which might be directly indicated merely by weak flaw echoes, and in the case of used pipes it might be caused by a corroded area not visible from the outside which causes diffuse scattering of the waves. In the case of thick walls say above about 20 mm, both types of flaw can be distinguished by scanning at right angles to the surface, while in the case of pipes with thinner walls, indirect means must be used if flaw differentiation is essential.

If a wide enough range is selected on the CR screen, multiple reference echoes of decreasing amplitudes are abtained, like the echo sequence from a plate. Any weakening of the pulse due to any of the causes mentioned above is indicated with increased sensitivity by the multiple echo sequence.

Influence of wall thickness. In the case of pipes with a wall thickness which is small compared with the diameter (say less than 5 %), the sound waves will reach the in-

ternal wall at approximately the same angle at which they left the probe. In the case of thicker walls the internal angle of incidence increases and thus the sensitivity for internal defects decreases.

To obtain sufficient sensitivity in practice angles in the range 37° to 45° are preferred but for small wall thickness these angles produce too steep a zigzag path and therefore a reduced testing range with echoes divided into several separate peaks in which case larger incident angles are preferred.

Figure 26.4 shows two tube testing probes, in which the crystals are arranged, as shown in Fig. 26.3. To have the same angle of incidence for all different tube diameters, only the curvature of the contact face has to be adapted. They are usually coupled by running water fed through a hole in the plastic block. The small cross-coupling signal between the crystals, indicates the beam index or entrance point into the tube. When used in an automatic installation it is of advantage to pulse the crystals successively, one following the other, and to generate the reference or circumference echo by both crystals during the third cycle. By this multiplexing method the noise level is reduced considerably. For this purpose the contact points of the two crystals are separately accessible.

According to Section 17.3, wall thicknesses above 20 % of the outside diameter can no longer be checked reliably for defects on the inner surface by means of oblique transverse waves. For these thick walled tubes longitudinal waves at angles up to 30° can be used and these are introduced by using strongly absorbing wedges, of for example vulcanized rubber. This reduces the interfering echoes to a tolerable level (Fig. 26.5) and since a portion of the beam strikes the inner wall perpendicularly, an echo sequence is obtained in which flaw echoes can be distinguished readily by the fact that they travel when the probe is moved.

It is advisable to arrange for the pipe to rotate uniformly and to guide the probe along it. A probe with variable angle coupled to the tube via a water-filled chamber has proved satisfactory (Fig. 26.6). It is then possible to find an optimum beam angle for the pipe diameter concerned and a further advantage of this arrangement is the even coupling obtained.

Manual testing is not recommended for tubes used for canning fuel elements in nuclear reactors because they have very thin walls and thus are easily damaged and because they require very high flaw-detection sensitivity. Accurate guidance sys-
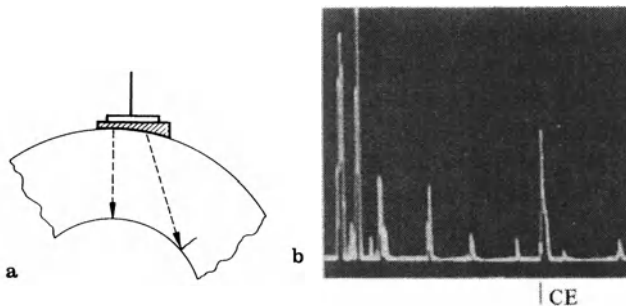

Fig. 26.5. Testing of very thick pipes with longitudinal waves. **a** Schematic; **b** screen trace with crack echo CE
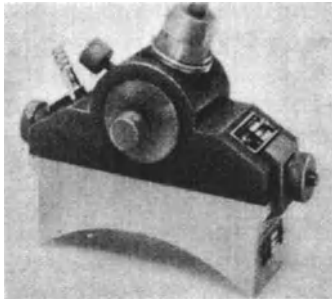
Fig. 26.6. Tube testing with a variable angle probe coupled via a water delay line

tems are necessary and the appropriate testing methods will be discussed along with factory installations for pipe testing.

For high-pressure pipes, seamless large-diameter pipes, oil-field pipes and standard main-supply pipes, and for diameters above about 120 mm, 2 MHz is usually chosen as the test frequency. For boiler tubes and precision tubes (up to about 120 mm diameter), the test frequency is usually 4 to 5 MHz whereas fuel-element canning tubes are tested using sound of 4 to 12-MHz frequency.

Installations for tube testing in manufacturing plants have been operational in Germany since the 1950s and in particular based on DIN testing specifications [1750] (cf. Chapter 34). At first high-pressure gas cylinders for specific purposes were checked for longitudinal cracks by the TÜV (technical supervisory association). The early installations used standard pipe-testing probes in a mechanized holder in combination with a pipe-transporting system. Later full or partial immersion techniques were used.

Fig. 26.7. Tube testing with full or partial immersion techniques. **a** One-probe method; **b** method according to Terry; **c, d** according to Zöllmer and Grabendörfer; **e** according to Pause and Schlengermann; **f** double-probe technique with multiplexing using partial immersion

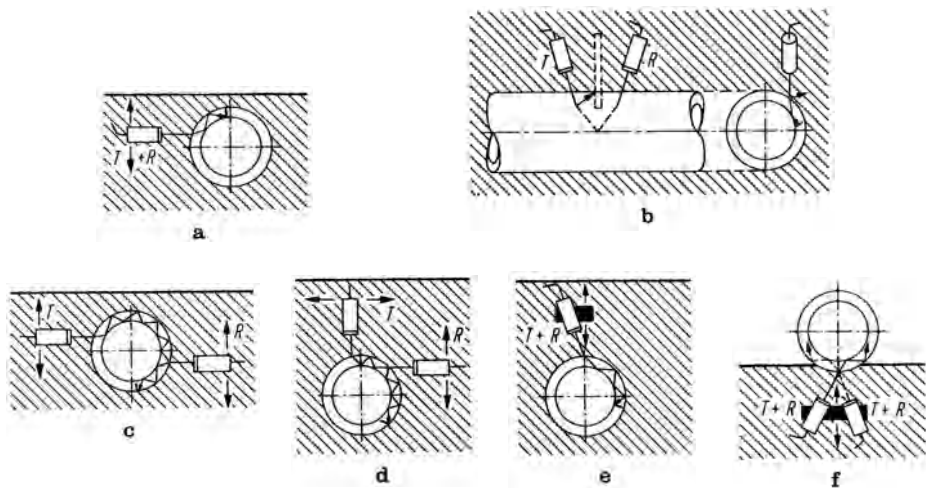Figure 26.7 shows various probe arrangements in automated installations which have been used for testing tubes to detect longitudinal defects. Currently the methods a, e or f are preferred for mass produced tubes such as boiler and main-supply tubes, high-pressure tubes, oil-field tubes, precise tubing and nuclear-fuel canning tubes. Methods b, c and d avoid the annoying direct echo from the tube surface. However, in method d the correct and reproducible adjustment of both probes independently from one another, is difficult. In method c this adjustment is easier but the sound paths and transit times are too long. The surface echo of the single-probe method on the other hand can be useful for a reference and for a fail-safe indication. Usually two complete probe assemblies are used but separated in the longitudinal direction of the pipe, and with sound beam paths in opposite directions. In this way the internal and external laps are covered reliably for both directions of inclination.

To detect transverse defects an additional simple arrangement of a single-probe is used, which generates a 45° zigzag wave along the tube wall in the longitudinal direction. To ensure that unfavorably oriented defects are also detected a second probe pointing in the opposite direction can be added [S 104].

Tube testing installations can be divided in general into two groups of different mechanical design. In the first type the probe arrangement is stationary and the tube is rotated and transported longitudinally to achieve a spiral scan. In the second type the tube is longitudinally transported and the probes rotate around it giving an arrangement which fits better into the production line.

Early installations of the first type were equipped with transit tanks for full immersion of tubes up to 80 mm in diameter, and the probe assemblies were transported by the tube under water. Seals were provided at each end of the tank to avoid much water loss during the test (see Fig. 15.14). Currently most of these units are working in a partial immersion technique, and transit tanks are used only for nuclear-fuel element canning tubes, as shown in Fig. 26.8. The tank contains four
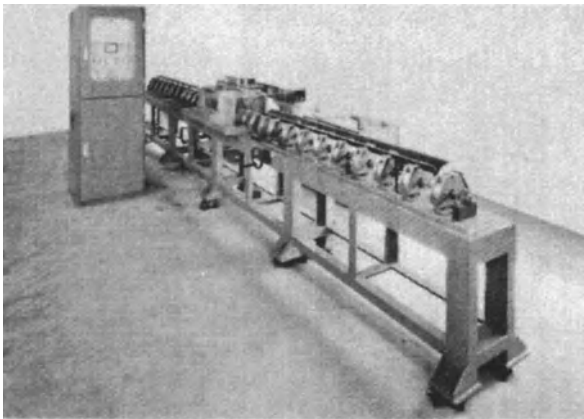

Fig. 26.8. Testing installation for canning and precision tubing up to 25 mm in diameter (type RDR 25 J, design Krautkrämer, Japan)

point-focussed probes of 10 MHz arranged in two planes perpendicular to the tube. One pair tests for longitudinal defects according to Fig. 26.7 a but with opposing beam directions, and the other pair detects transverse defects. Additionally a further probe can measure the wall thickness, or a pair arranged in 180° positions can measure the complete geometry of the tube including wall thickness and outer and inner diameters (see Section 33.2, Fig. 33.4).

Defects as small as 0.03 mm with a length of 0.75 mm can be detected, because of the very precise guidance system of the probe assembly, achieved by riding on the tube. Testing speeds, depending on the minimum defect length to be detected is 2 to 5 m/min.

The installations with a partial immersion technique and spiral transport are used preferably for large tubes, when rotating the probe assembly would be too difficult (Fig. 26.9). When the tube has entered the test machine, the water-filled tank together with the probe assembly is pressed against the tube from below. The installation shown can test tubes up to 600 mm in diameter, and with appropriately smaller tanks down to 25 mm.

Often the probe system is divided into two groups housed in two different tanks, one for longitudinal defects and the other for transverse ones, and for wall-thickness and tube-geometry measurement, if required. They are then mounted in two neighbouring sections in between the transport rollers. The tank in Fig. 26.9 contains arrays of probes for the longitudinal defects to achieve a high testing speed up to 1 m/s, the tube being spiralled at an 80-mm pitch, allowing complete testing of the surface.
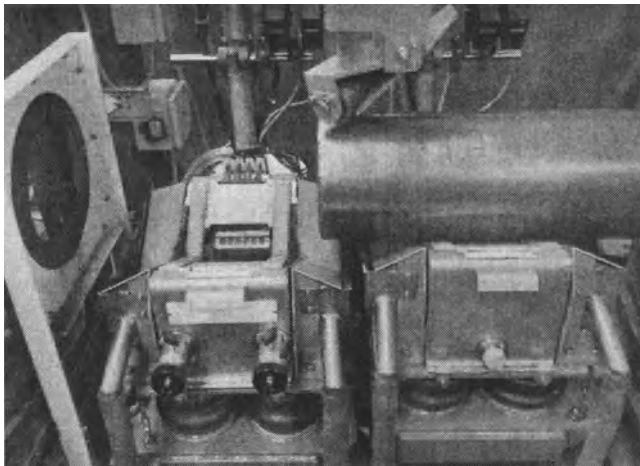
Fig. 26.9. Tube-testing installation (type GRP, design Krautkrämer) for tubes of more than 100 mm in diameter with two testing tanks. The right hand one has already been lifted and pressed against the incoming tube. The exposed left-hand tank shows the linear probe assembly. The coupling water which is introduced after contact with the tube, fills only the small space adjacent the probes
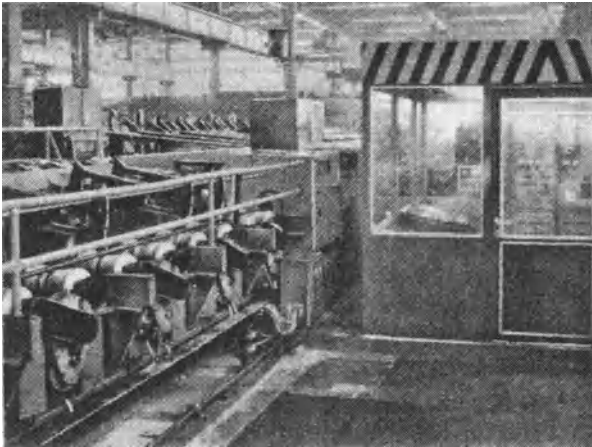
Fig. 26.10. Tube tester for tubes up to 160 mm in diameter with spiral transport (design Deutsch, courtesy Mannesmann-Röhrenwerke, Solingen-Ohligs)

Installations according to Möller [1048] for testing tubes up to 160 mm in diameter have a very elegant solution of the transport mechanism. In both of two transport units three rollers provide the linear transport and simultaneously the complete roller system is rotated around the tube axis. In this way the linear and the rotating feeds can be independently controlled and the system makes it simple to supply both movements to the computer for defect evaluation and recording (Fig. 26.10).

Another type of design (Fig. 26.11) makes use of several individual probe boxes containing water delay lines, which are filled-up after the entry of the tube, so that a section of the tube up to 300 mm long is not tested, which is larger than is usual
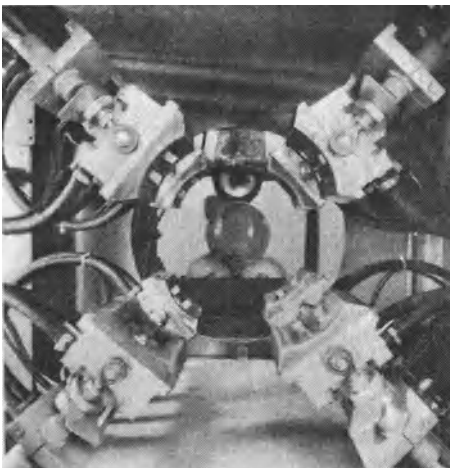
Fig. 26.11. Tube tester with 2×4 probe boxes around the tube circumference with spiral transport (design Krautkrämer)
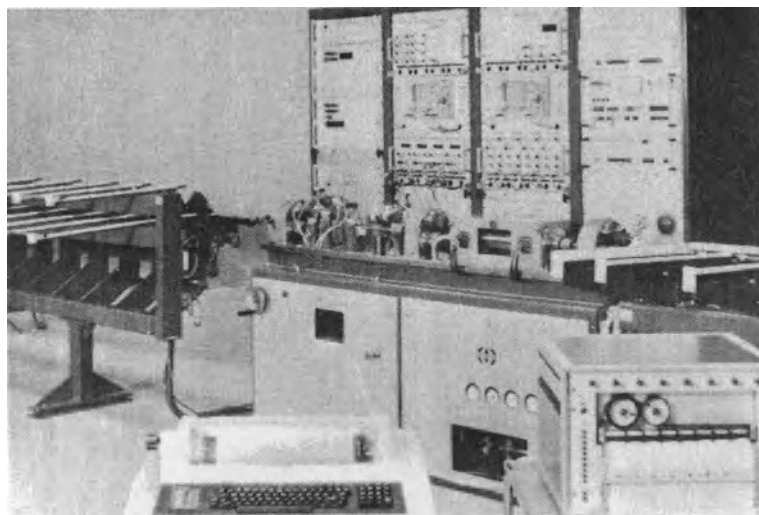
Fig. 26.12. Rotating probe installation for nuclear-fuel canning tubes (Type ROTA 25, design Nukem, Hanau)
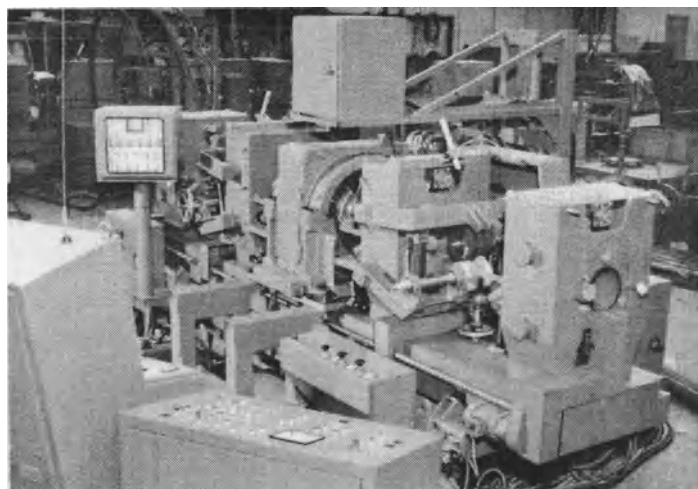
Fig. 26.13. Rotating probe-testing installation for tubes between 20 and 180 mm diameter (type ROT 180, design Krautkrämer)

with the partial immersion technique, but because the surface velocity can reach 2.5 m/s, this type of installation has a greater efficiency than the systems using that technique.

The installations of the second type with rotating probe systems, serve a wide variety of tube diameters, from 5 to 25 mm (canning tubes) up to 600 mm. In most

installations up to 250 mm the probes are housed in a closed water tank and circulate around the tube, also incorprating probes for wall-thickness and geometry measurement (see Fig. 33.4). For larger tube diameters water-gap sliding probes are used.

The installation of Fig. 26.12 for testing canning tubes comprises all of the above-mentioned probe functions at a testing speed of 8000 rpm.

Figure 26.13 shows a rotating probe installation for boiler and high-pressure tubes up to 180 mm in diameter, also equipped with additional probe arrangements for wall-thickness and geometry measurement. In addition laminations very close to the inner surface can be indicated by sudden changes of the thickness during scanning. Probe adjustment for new tube dimensions takes some time, but this can be reduced considerably in a design in which it is possible to vary the position on the circumference of all four probes simultaneously from one control point. This unit is designed for tubes up to 130 mm in diameter and reaches a testing speed of up to 60 m/min (1 m/sec).

To complete this description of operational machines the "jumbo" must be mentioned. Built by Mitsubishi, Japan, it checks tubes from 165 mm up to 600 mm in diameter for longitudinal and transverse cracks and quasi-laminations (Fig. 26.14). The rotating probe container operates at 100 to 300 rpm and the computer-aided system adjusts the probes automatically, using tube sections with reference defects. As well as seamless tubes the machine also tests welded ones.

Stewarts and Lloyds, Dept. of Research and Technical Development, England, formerly developed a machine for tube testing (see [1921]), which now has been improved by BSC under the name RP 500. It can test tubes up to 20″ (508 mm) in diameter with rotating sliding probes. Figure 26.15 shows a general view of this equipment. As well as testing for longitudinal defects the wall thickness is measured con-
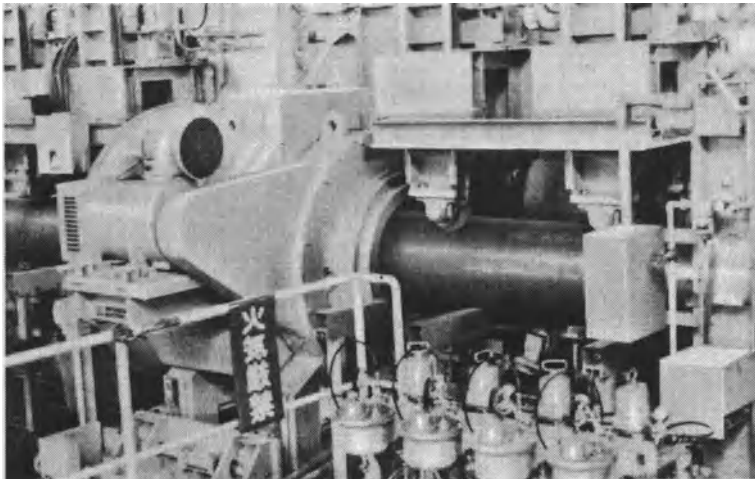
Fig. 26.14. Rotating probe tube-testing installation for seamless and welded large tubes up to 600 mm diameter (design Mitsubishi)
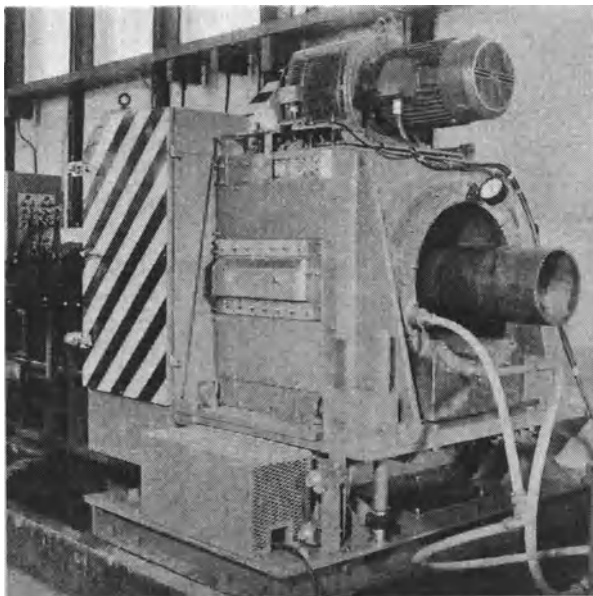
Fig. 26.15. Rotating probe tube-testing installation with sliding probes

Fig. 26.16. Evaluation unit type UCASE, with the two screens for the presentation of the test result of the installation in Fig. 26.15

tinuously, also allowing the detection of laminations. The system can rotate at 300 rpm on tubes of 500 mm in diameter and reaches a testing speed of 25 m/min. The presentation of the results in made on two CR screens (Fig. 26.16) diagrammatically. The Y-axis (perpendicular) corresponds to the length of the tube, the X-axis being divided into five columns, and in the first one is indicated all events, such as failure of probe coupling, exceeding the tolerances of the wall-thickness measurement and defects on the inner or outer surfaces of the tube. The other four columns display details of the different defect indications and their positions in one of the four quadrants. The two screens function alternately, one storing the results from the previously tested tube, and providing a hard copy of the results, whereas the results from the tube under test is being built up on the second screen.

Finally a transportable installation for testing compressed gas bottles should be mentioned (Fig. 26.17). The bottles are removed automatically from a stock and then rotated and checked for longitudinal and transverse defects, and for the wall thickness. The test is, however, restricted to the cylindrical portion and each bottle is provided with a printed record. For another installation see [S 84].

Some particular problems of tube testing demand special methods such as for example if testing is not possible from the outside surface. It can then be carried out from the inside to accommodate tubes with welded-on cooling fins or drilled tubing with conical or non-circular outside shape as for example gun barrels. For the latter an installation has been reported by Sperry in which the probe assembly replaces the cutter on the boring machine. Flaw echoes from the rotating barrel returning from the outer and inner walls are classified and recorded according to their transit times.
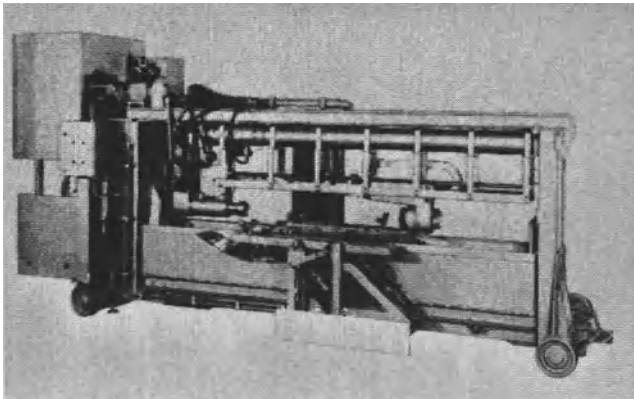
Fig. 26.17. Transportable testing installation for compressed gas bottles (design Deutsch)

Purely transverse zigzag waves can be used for internal testing only as long as the wall thickness is less than 20 % of the diameter. In the case of pipes with thicker walls, the transverse wave transmitted by the probe is split as in Fig. 26.18 into transverse and longitudinal waves when reflected at the outer surface at an angle smaller than 33°. Both wave modes can produce echoes which may complicate the interpretation of the screen picture.
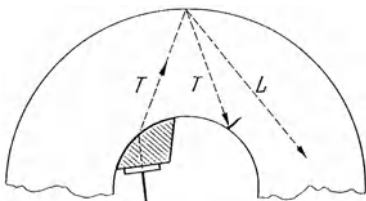
Fig. 26.18. Testing of pipes with very thick walls from the inside
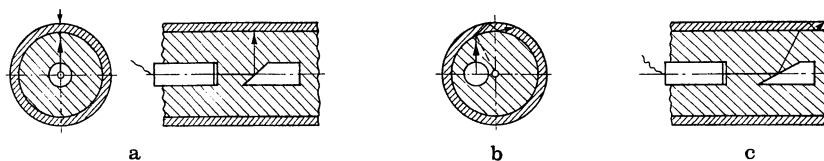
Fig. 26.19. Internal testing of pipes. **a** Wall-thickness measurement; **b** detection of longitudinal defects; **c** detection of transverse defects (according to Robba [1273])

For pipes of small diameter an immersion technique can be used by filling the tube and introducing probes into it (Fig. 26.19). A normal probe placed in the pipe radiates sound axially, a mirror mounted in front of the probe deflecting the sound beam in the desired direction. Depending on the orientation and the shape of the mirror, the reflected beam can be used for detecting longitudinal or transverse cracks, or for measuring the wall thickness. By using a curved mirror, the beam can also be focussed [1273].

The testing of externally finned pipes in order to detect longitudinal defects presents a difficult problem. These pipes are covered on the outside by closely spaced ribs, usually surrounding the pipe in an elongated spiral and permitting testing from the inside only The detection of flaws is difficult because the individual ribs produce echoes. Any deduction concerning the possible presence of longitudinal defects can be obtained only from irregularities in the echo pattern of the ribs. For this purpose the pipe or the probe and mirror assembly is rotated slowly. The detection of transverse defects causes no difficulties [1213].

Much easier is the testing of high-pressure finned pipes (hair-pin pipes) as used in the chemical industry, with fins lying transverse to the axis of the pipe, in order to detect longitudinal cracks.

For further literature concerning tube testing in general see [1048, 1487, 1505, 890, 1344, 638, 1068, 866], concerning computer-aided equipment [45, 751, 1101, 1314], concerning automatic testing of heat-exchanger tubing [1370, 1379, S 111], concerning continuous test of nuclear fuel canning and precise tubing [85, 201, 584, 585, 861, 1215, 1251, 1289, 1307, 1440, 1236, 1184], and concerning the use of electrodynamic excitation of plate waves (tubes waves) see [1368, 1620, 1063].

27 Castings

In castings flaw detection is almost exclusively concerned with manufacturing defects and only rarely as in-service inspection. Suitable testing techniques and the subsequent evaluation of indications in castings is very different from the testing of forged and worked material so that the differences must not be forgotten or difficulties can occur. In-service inspection, as in the case of forgings, depends on the local stresses and the piece geometry so it is not necessary to treat it specially in this section.

Typical casting defects are as follows (see Fig. 27.1):

— Shrinkage cavities, generated by contraction during solidification and insufficient feed of metal. They occur preferentially below feeders, at changes of section and nodal points, and within large wall sections as center-line flaws.
— Blow holes and porosity occur when gas bubbles are released during pouring and cooling or by insufficient degassing of the mould and cores.
— Non-metallic inclusions generated by interaction between the molten metal and the mould material, pieces of the mould material itself, or by oxide films swept along with the metal during pouring.
— Hot tears caused by shrinkage during solidification, in combination with restrictive stresses caused by unfavorable design of the piece or of the mould and by metallurgical influences.

Metallurgical considerations and good casting technique will generally avoid such defects, by providing, for example, a sufficient number of feeders and chills. However, the critical areas will usually be known so helping the operator to restrict any tests to these positions and the appropriate sound beam directions.

The reflectivity properties of typical casting defects is important for ultrasonic testing. Except for true cracks all other casting defects are more or less voluminous and globular. The direction of the sound beam is less important therefore, and Fig. 27.2 shows the results of tests on a 110 mm thick section of spheroidal cast iron
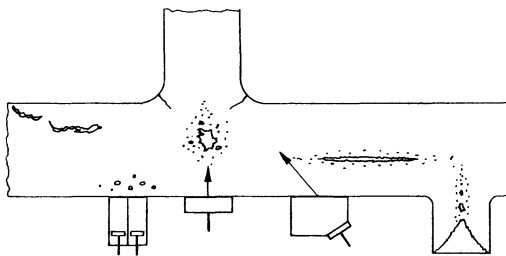
Fig. 27.1. Typical casting defects and their detection methods
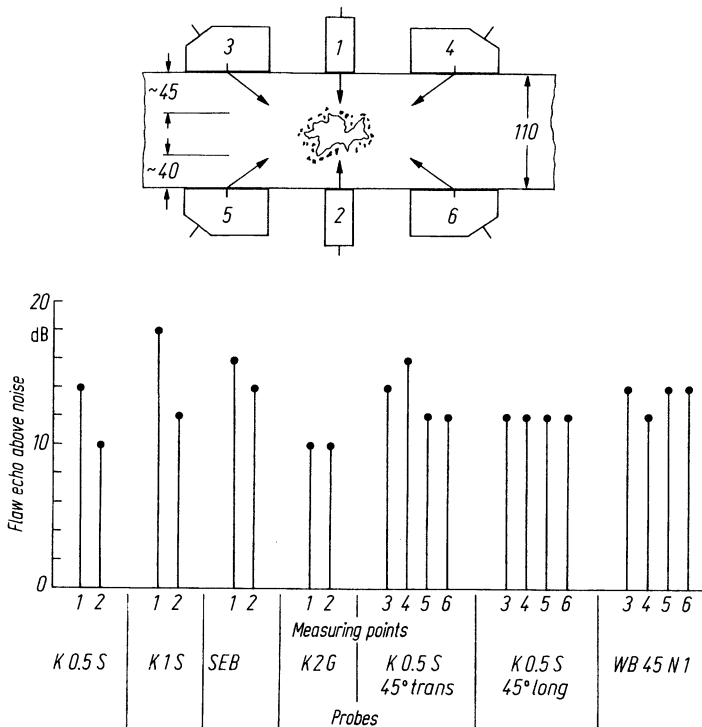
Fig. 27.2. Detectability of a shrinkage cavity

using normal and angle probes in different directions. The diagram shows the maximum echo amplitude received above the noise level and it can be seen that the probe position, ultrasonic frequency and wave type are apparently of minor influence. The echo amplitudes are relatively low because of the irregular shape of such a shrinkage cavity. The rough surface scatters the sound in a wide angle, so that only a small amount returns to the probe, this effect being reinforced by the large number of pores surrounding the flaw in most cases. For these reasons the flaw can often be detected more easily by the shadow effect on the back-wall echo [242].

With other casting defects also, only small areas of their surface are illuminated perpendicularly to give specular reflections so that sizing of the defect from its echo amplitude, as for example with the DGS diagram, is of little value.

An indication of the defect size can be obtained from:

— The amount of back-wall echo reduction,
— Lateral scanning of areas showing a reduced back-wall echo,
— measuring the distance from front and back walls and so deducing the thickness of the flaw

At critical positions which will be stressed in service, smaller flaws can also be evaluated by the DGS method though this will give only a minimum size, often differing widely from the true one.

Cast steel, ferritic		
Cast steel, austenitic		Highly damped probes only
Cast iron, lamellar		Highly damped probes preferably
Cast iron, spherical		
Cast aluminium		
Cast copper and copper alloys		Highly damped probes only

0.5 1   2   3   4   5 MHz 6

Fig. 27.3. Recommended ultrasonic frequencies for testing of various cast materials

The paper [1383] is an example of an unsatisfactory application of the DGS method on cast steel neglecting completely the reduction of the back-wall echo. Compared with X-ray tests only between 7 % and 30 % of the defects were found by ultrasonics. However, much better comparisons were found in other cases where the back-wall echo reduction was taken into account [242, 426]. It should, however, always be kept in mind that excessive requirements for the homogeneity of castings would be unattainable.

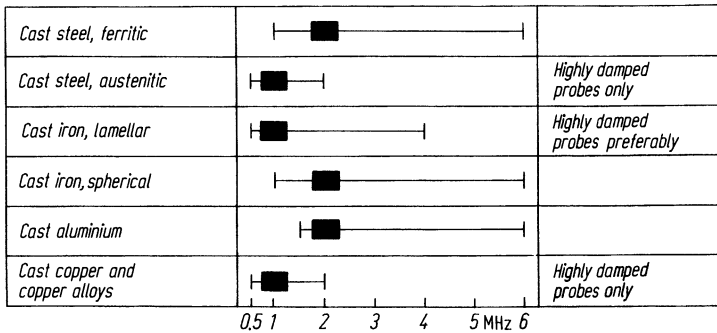Local reduction of the back-wall echo can also be caused by reasons other than flaws. Worse surface roughness, small inclinations between front and back surfaces, inferior coupling caused by local surface irregularities, or variations in the grain structure can all cause back-wall echo reductions. Grain structure is usually very coarse, which in the case of an anisotropic material results in heavy attenuation and scatter. Differences in the grain size can be caused by different cooling speeds between the outer and inner portions. For example in cast iron the size of the graphite particles can differ between such areas, which can change the ultrasonic velocity by several percent. As a result the beam can be bent resulting in local reductions in the back-wall echo without any corresponding defects.

At lower frequencies these influences will usually be less important. Figure 27.3 gives a summary of the recommended frequencies for various cast materials.

Within the recommended band of frequencies the higher ones are used for the thinner specimens. In the case of good surfaces and thicknesses up to about 25 mm, much higher frequencies can be used occasionally, for example 10-MHz TR probes for detecting small inlcusions close to the surface. However, the question which is frequently asked — how much of the surface layer should be machined away to ensure in practice a pore free surface — can only be answered with difficulty.

For the testing of castings the use of highly damped probes shows a great improvement as Fig. 27.4 illustrates. The dead-zone as well as the noise level is much reduced. In addition materials hitherto considered as non-testable can be checked, for example austenitic steel castings [807] and cast copper alloys [1453, 1386], although the smallest detectable defect size is not much less than the probe diameter.
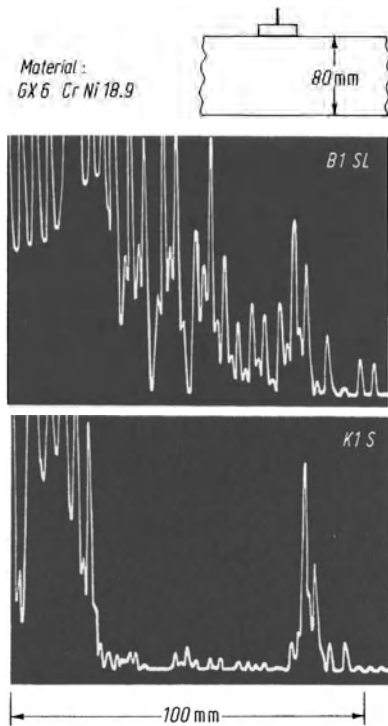
Fig. 27.4. Subsurface resolution with a conventional (B1SL) and a highly damped probe (K1S)

As regards the probe types best used for the testing of castings normal probes suffice in most cases, preferably those with a plastic protection layer. TR probes can also be used to detect defects near the surface. The advantage of a soft coupling layer can be recognized from the following test. The surface of a cast plate was partially left rough, as cast with 0.15 mm roughness, and the rest machined. A 4-MHz normal probe with soft face showed only a 4-dB difference of the back-wall echoes of the two portions, whereas a hard-faced probe displayed a difference of between 20 and 30 dB.

When angle probes are to be used the deviation of the beam angle from nominal has to be considered because of the difference between the shear velocity in steel and in the cast material concerned (see Section 10.4 Table 10.1). They are preferably used for the detection of cracks which form a corner reflector with a surface. Figure 27.5 illustrates some applications of different probes. With an angle probe the defect echo can often more easily be observed as a travelling echo while scanning the surface. Sometimes TR angle probes have been used to measure exactly the extent of shrinkage cavities [385].

The amount of testing applied to a casting varies very much depending on the material and the application. A cast steel turbine housing for example is usually tested by a complete surface scan using a normal probe. At critical points, for example on flanges, at faces for welded joints and areas with defect indications, additional probes and beam directions are often used. In addition in these areas
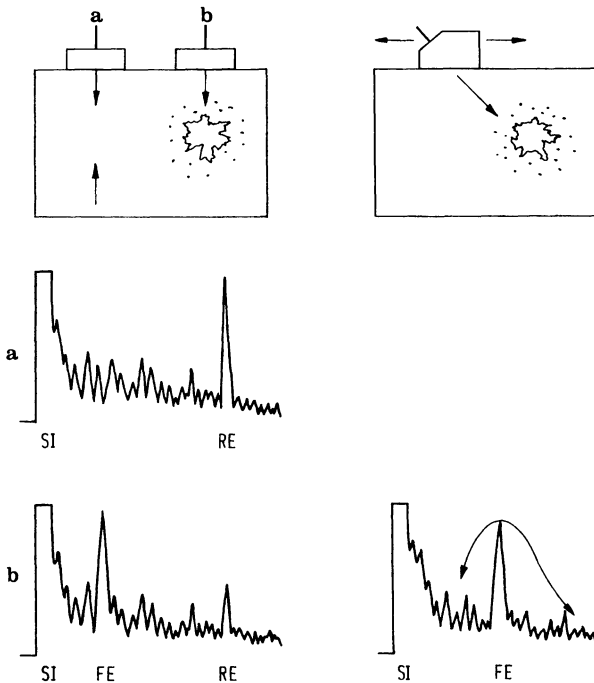
Fig. 27.5. Detection of shrinkage cavities with normal and angle probes

X-radiography or magnetic-particle methods are also used. In more transparent materials such as for example spheroidal cast iron, linear scanning, or on a grid pattern, is sufficient. On mass-produced castings, if a test is at all justified it can be applied only at critical points. In such cases the casting technology has been established in advance by the help of destructive and non-destructive tests [1356]. For an example of the manual testing of mass-produced cast iron parts see [1029].

Since some automobile parts with high safety demands are produced in spheroidal cast iron, mechanized tests have been introduced as Figs. 27.6 and 27.7 show.

Typical parts are swivel bearings, steering knuckles and brake components, usually parts of complicated shape. In the illustrated test-machine each part is tested by an immersion technique at selected critical positions and additionally the sound velocity is measured at a position with local parallel surfaces since this factor is a measure of the quality of the spheroidal graphitic structure. See Sections 31.3 and 33.2 for details.

In the automatic test installation of Figs. 27.6 and 27.7 the parts are taken individually from a magazine, placed in the tank, tested by several probes one after another and sorted into accept or reject containers combined if required with a marking device for faulty parts. Castings with a low sound velocity are also rejected. A magnetic-particle test for surface defects follows on line, the testing speed being six parts per minute [1190].
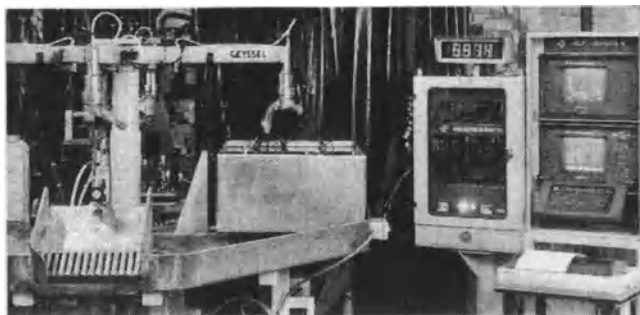
Fig. 27.6. Test installation for cast automobile parts (design Krautkrämer)
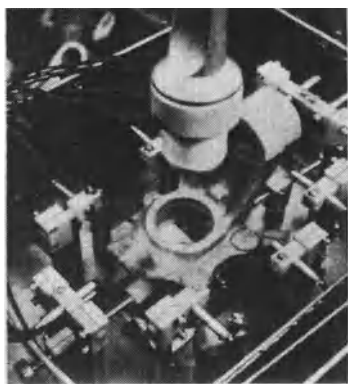
Fig. 27.7. Swivel-bearing in test position in the immersion tank of the installation of Fig. 27.6

A difficulty of testing castings in addition to the complicated shape is also the attenuation of sound by the as-cast structure, which, however, differs greatly for different materials. For example in aluminium castings the porosity can be measured by way of the attenuation by comparing a back-wall echo sequence with that from a specimen with borderline acceptable porosity. In low-alloy or carbon-steel castings the attenuation can be neglected in practice for frequencies of 1 to 2 MHz [386]. For grey cast iron Fig. 27.8 shows the dependence of the attenuation on the type of iron (lamellar or spheroidal) as well as on the thickness. The dependence on the wall thickness arises from the different cooling rates. Generally one can say that in lamellar cast iron with high-tensile-strength testing is possible, but is very restricted for materials with low strength, having many and large graphite flakes. For machine parts made from such material a test is not usually needed, as for example for machine bases and mountings. Additionally materials with very coarse structure such as austenitic castings, hard manganese steels, and for copper and its alloys, tests are only possible for very large defects.

In such cases the through-transmission technique is sometimes the only way. For example on the rim of a 30 cm thick bronze bell a rough test for large shrinkage cavities could be performed with 1-MHz probes guided manually on the inner and
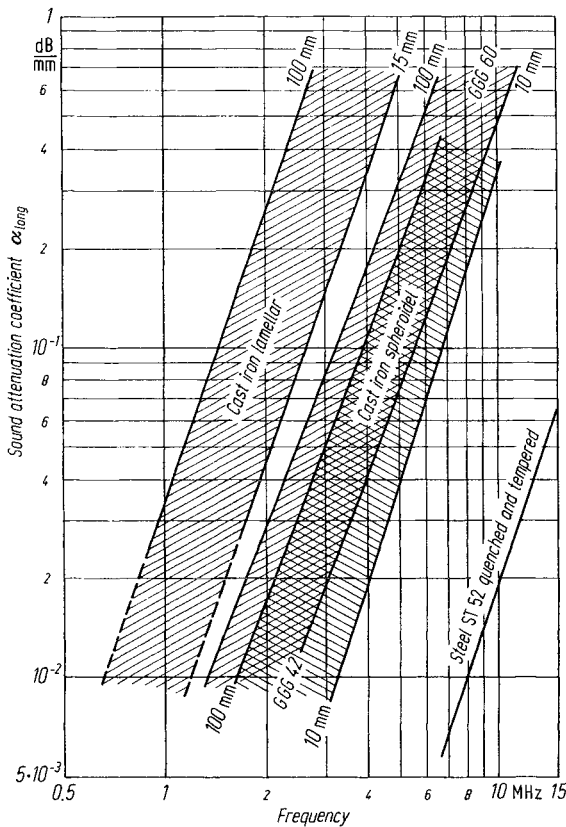
Fig. 27.8. Attenuation of sound in cast iron, depending on the frequency and the wall thickness, according to [386]

outer surfaces. By this means two defect-free positions were found and recommended as contact points for the clapper.

According to [117] cast uranium plates have also been tested by through-transmission methods using pulses, for dimensions of 18 mm × 180 mm in cross-section and several meters in length. However, as explained in Section 5.3, the through-transmission method is very unreliable for the detection of small defects when lying at large distances from the probes.

The inspectability of cast materials depends also on the casting methods. In centrifugal casting for example the metal grain is oriented radially on solidification. In the case of tubes cast in spheroidal cast iron this fact is not important, but with tubes in austenitic steel testing in a radial direction is possible, but only to make a wall-thickness measurement. However, angle-probe testing using an echo technique is impossible. Through-transmission between two angle probes of low frequency can, however, find radially oriented in-service cracks.

Centrifugal castings in spheroidal cast iron can be tested for hot cracks, cold shuts, shrinkage cavities and slag inclusions, using 45° angle probes of 2 to 4 MHz.

However, the method is seldom used in practice because of the difficulty in distinguishing between cold shuts and cracks on the one hand and acceptable inclusions and surface roughness on the inner wall. More recently tests have been made to differentiate them by using several ultrasonic frequencies [276].

Because of their very complicated shape most die castings are only occasionally tested an example being on zinc die castings for automobile door locks, at selected favorable positions.

Of more importance is ultrasonic wall-thickness measurement on castings, in cases where walls are accessible from one side only. These examples are all parts cast with central cores as in cylinder blocks, pump housings, heating-radiators and hollow-cast turbine blades. On other pieces a mechanical measurement could be made but an ultrasonic measurement is easier because of the large size, as for example for process vessels in the chemical industry and mine shaft casings. It is, however, recommended that the wall-thickness meter is calibrated on the piece itself because of the unpredictable sound velocities of cast materials. In the case of anisotropic materials it has also to be kept in mind that adjustment of the meter must be made at a point where the crystallization has the same orientation as at the points to be measured. In grey cast iron the velocity can also be different for different wall thicknesses because of different cooling rates.

Practical experiences of wall-thickness measurements on cast-iron components for diesel engines are reported in [1027]. For testing of steel castings see [1566, 902, 275, 290, 242, 741, 363, 740, 1356, 1104, 337, 219].

28 Welded Joints

28.1 Butt-Welded Joints

The commonly occurring defects in welded joints are porosity, slag inclusions, lack of side-wall fusion, lack of inter-run fusion, lack of root penetration, undercutting and longitudinal or transverse cracks.

With the exception of single gas pores all the defects listed are usually well detectable by ultrasonics. Most applications are on low-alloy constructional steels but welds in aluminium can also be tested, bearing in mind the somewhat smaller beam angle if the conventional probes are used (see Table 10.1 and [487, 995]). For testing austenitic steel welds and welds in plastics see Sections 28.1.6 and 28.1.7.

28.1.1 Testing Methods, General

Testing butt welds with normal (0°) probes is only occasionally possible if the geometry of the specimen is favorable, as for example in Fig. 28.1, where a flange has been welded to a tube, or when forged parts have been welded together. However, for small cross-sections, interference by the side walls must be expected resulting in split-off transverse waves and poor sensitivity for defects lying near the surfaces.

For butt-welded joints in plates and pipes the pulse-echo method using zigzag transverse waves (Fig. 28.2) is mainly used, the reflections between the two surfaces of the plate being utilized. A broad beam would cover a thin joint in one pass but on thicker plates it is necessary to scan the probe in a transverse direction so as to cover the complete cross-section. According to Fig. 28.2 a movement from a half to a full skip-distance is required. In practice a little more is used in view of the width of the joint. As a check and for the sake of greater reliability, the test can be repeated from the opposite side of the weld because some defects are indicated more
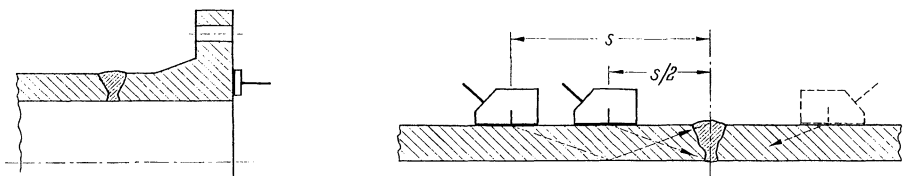
Fig. 28.1. Testing a circumferential pipe weld from the welded-on flange
Fig. 28.2. Sound paths for half and full skip distances
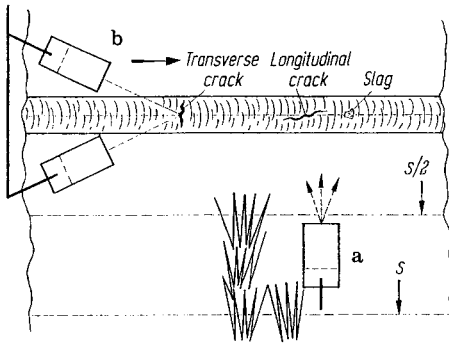
Fig. 28.3. Longitudinal scanning of a weld. **a** For all defect types except transverse cracks; **b** for transverse cracks

favorably if irradiated from one direction rather than from the other. By this method all defects are covered, except for transverse cracks which require a different approach. As shown in Fig. 28.3 a, it is recommended that the backward-forward motion between $s/2$ and s be combined with the longitudinal movement in the form of a zigzag motion, onto which is superimposed a still more rapid swivelling motion, so as to strike slightly inclined flaws at favourable angles. If transverse cracks are suspected, the method according to Fig. 28.3 b should be applied. The two angle probes connected in parallel and mounted in a common holder need only be moved along the seam.

In highly stressed welds the test is usually performed from both sides of the weld, especially if an indication has been obtained from one side and which has to be identified as not arising from a geometric feature such as an excessively high weld crown or from over penetration at the root. In such cases exact locating of the position of the reflector can help (see Section 28.1.3) if the plate thickness is larger than about 10 mm.
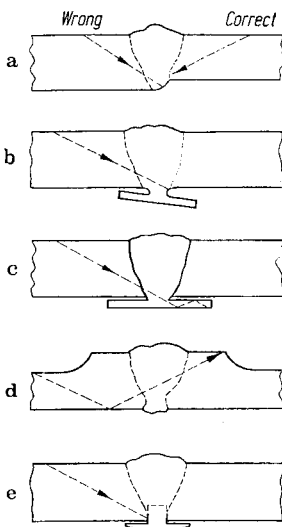
Fig. 28.4. Interfering echoes in the testing of welds. **a** Displaced plates or different thicknesses; **b** and **c** backing strip or fitting ring (circumferential welds on pipes); **d** welded swaged collar; **e** inserted and incompletely fused fitting ring (to be judged as a genuine flaw)

If an echo from a V-preparation weld only appears from one side it can be assumed to come from mismatched plates caused by bad set-up or unequal thicknesses (Fig. 28.4a). The first fault occurs quite often with circumferential tube welds. In the second case one can perform the test from the thinner walled side without problems. Other types of interfering echoes, as illustrated in Fig. 28.4, can come from backing strips, fitting rings in tubes, or from a thicker swaged collar section. A non-fused fitting ring as in Fig. 28.4e has, however, to be considered as a genuine flaw [645].

Welds in steel and aluminium made with a powder flux sometimes have an exaggerated bead thickness which gives an echo from the far side of the weld. This can be used as a coupling and sensitivity check. The test in this case is not adversely affected if it is performed from both sides of the weld and only half of the weld is observed each time.

Further interference with the weld test can take place if laminations and inclusions are situated within the parent plate adjacent to the weld. The quality of the plate should therefore be checked first by using normal probes along two strips equal to a half-skip distance on each side (Fig. 28.2).

For thin plates of less than about 15 mm the weld test can be carried out from a fixed probe distance of about 2 skip distances. This arrangement is preferably used in mechanized test installations see Section 28.1.5.

Manual weld testing on a weld 10 mm thick is illustrated in Fig. 28.5.

If transverse cracks can be expected it is necessary to use additionally the technique of Fig. 28.3b. The two angle probes are connected together in parallel and are scanned along the weld in a joint fixture. If, depending on the welding technique, the cracks are restricted to a definite section of the joint, for example in the sections closest to the surfaces, the probes are arranged so that the inter-section of their beams is located at the appropriate depth. Otherwise for thick plate it will be necessary to scan the weld several times with different probe positions. If the weld crown is machined off, to be level with the adjacent plate, a single probe test can suffice if it is placed directly on the weld crown and oriented longitudinally.

If the welded joint can contain central vertical cracks or fusion defects lying

Fig. 28.5. Manual weld testing in chemical plant construction with digitized miniature, flaw detector USD 10 (design Krautkrämer)
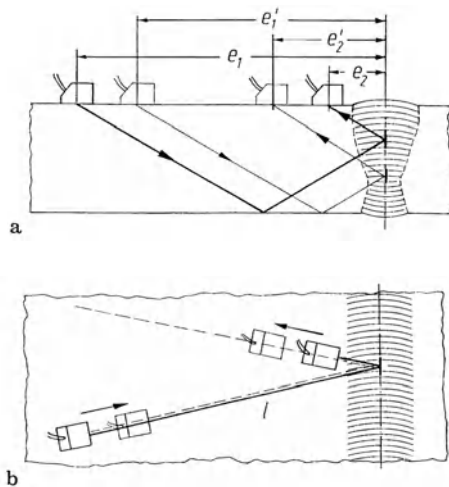
Fig. 28.6. Pitch and catch method. **a** Principle $(e_1 + e_2 = e_1' + e_2' = \text{const})$, **b** guiding device of the probe according to Lack

normal to the surface of the plate, testing with a *single* probe is no longer satisfactory for reliable detection of these defects. The sound pulse is reflected away from the incident beam and thus can be received satisfactorily only by a second probe suitably placed. This probe should be placed at a distance from the first probe depending on the plate thickness and the depth at which the defects can occur (Fig. 28.6a). This twin-probe arrangement, called a "pitch and catch" or "tandem" method, is most commonly used for testing the welded joints in thick-walled vessels [505], specifically in the pressure vessels for nuclear reactors (cf. Chapter 30). This method is also used for narrow welds if one can expect that defects will lie in a plane perpendicular to the surface, as with electron beam or friction welds.

Economic manual testing by this method requires that both probes are mounted in a suitable guide frame which ensures that they maintain the correct angle relative to the weld and at the same time a constant distance from it. A suitable device for this purpose has been suggested by Lack [885], (Fig. 28.6b). Figure 28.7 shows some modern holders.
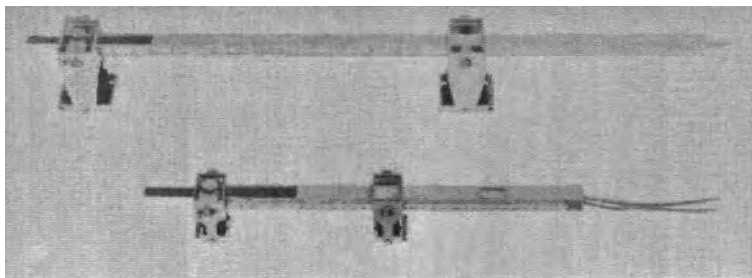
Fig. 28.7. Pitch and catch holders (design Krautkrämer)

The plate surfaces on both sides of the weld must be free of dirt and irregularities which could prevent good coupling, so rust, loose scale, welding spatter, chisel marks and metal burrs should be removed before testing begins. The arithmetical average roughness should not exceed 20 µm and any local surface waviness should not separate the probe face from the surface by more than 0.5 mm at any point. Oil, cellulose paste or water can be used as a coupling liquid care being taken to ensure the couplant "wets" the plate surface. Water sometimes does not wet the surface immediately and it should therefore be applied some time in advance.

By far the best and most constant coupling for probes, particularly for automatic testing, is obtained with flowing water. The higher consumption of water which this entails whether from a main supply or a small pressure pump is almost always worthwhile for extended periods of testing in view of the savings of time for applying couplant and in higher testing rates.

For checking the efficiency of the coupling it has been proposed to work with two probes facing each other from either side of the joint; these would be connected in parallel and, therefore, would produce a double flaw indication in addition to a reference "echo" by through transmission. Although this arrangement has considerable advantages it is unsuitable for testing by hand because the rapid swivelling motions are not easily achieved with it.

In practical manual testing the noise level can be used to keep the sensitivity constant but for mechanized weld testing several arrangements with auxiliary oscillators have been proposed. One of these is a longitudinal wave crystal directing a beam normally through the plastic wedge of the shear-wave probe and using as an indicator the length of the multiple back-well echo sequence.

For further literature concerning this test method see [1413, 700, 934, 1243, 1171, 46, 47, 449, 1708, S 9].

28.1.2 Plate Thickness, Beam Angle and Testing Frequency

The roughness of the weld bead as well as over-penetration at the root can generate geometrical echoes if the beam angle is too steep (45° or less). Therefore larger (i.e. shallower) angles are preferred, using steeper beams only for very thick plates when otherwise the transit paths would be too great. The following practical values can be given as a general recommendation for various plate thicknesses:

Plate thickness mm	Beam angle degrees	Skip distance mm
5–30	70°	30–165
30–60	60°	105–210
above 60	45°	above 120

For the critical inspection of highly stressed welds several tests using a variety of beam angles is necessary, so that planar defects giving a specular reflection can be detected. In these cases reflections from the weld bead are common and they

have to be eliminated by local smoothing of the weld or identified by the touch test with an oily finger and observing the resultant changes in the echo height.

For thin plates below about 10 mm this problem gets worse and below 3 mm plate waves are preferentially generated by all types of angle probe for all beam angles. These waves give echoes from any sudden thickness changes including the weld bead. If the bead cannot be removed completely it sometimes helps to use very high frequencies and focussed probes. For example longitudinally welded tubes in titanium with diameters between 15 and 25 mm and 0.8 mm wall thickness could be tested with 10-MHz probes whereas 4 MHz gave too much interference from geometrical echoes.

Resistance-welded joints may contain fusion defects which cannot be detected reliably with ultrasonics, the so-called stuck-weld. If stressed slightly, the joint cracks along the fusion-zone revealing crack faces with a uniformly dull appearance.

A prepared cross-section does not show any physical separation, only a broken line of minute inclusions by which apparently ultrasonics, including transverse waves up to 4 MHz, are not reflected. As far as is known, no fully reliable non-destructive testing method for this defect is as yet available.

Also in the case of double-V preparation welds having incomplete fusion in the central zone, it has been observed that this defect has not been indicated probably because the plate edges at this point have been forced together by the weld stresses so becoming transparent to transverse waves.

The range of testing frequencies used in weld testing is usually between 2 and 5 MHz, and in practice 4 MHz miniatare angle probes are often chosen because the smaller size of these probes allows easier manipulation and closer access to the edge of the weld bead, whereby defects can be detected in the direct beam. Moreover they have well concentrated beams similar to the larger 2-MHz probes.

In principle it is, however, advisable to make use of lower frequencies to compensate better for any specular reflections from flat reflectors. According to [484] different types of natural defect in a 30-mm weld generally gave smaller indications with 4 MHz than with 2 MHz, compared to a transverse bore hole of 2 mm in diameter. Therefore it seems reasonable to make use of 2-MHz probes on welds above 20 mm in thickness.

Only in the case of defects forming a corner reflector with the surface does the higher frequency give better results [1460].

After having observed an echo the weld must be scanned longitudinally to obtain as precise a measure of the defect length as possible. This is best done using a probe of higher frequency (see Section 28.1.4).

Frequencies lower than 2 MHz are rarely used for weld testing, because from the wide-angled beam increasing interference from the weld bead will occur. Only on austenitic cladded construction components are 1-MHz probes better because the interference is less from the coarse grain structure of the cladding and the transition zone [485].

In ferritic arc welds the as-cast weld structure usually causes no special problems, but for electro-slag welding the corresponding structure is too coarse and only permits a satisfactory test after heat treatment. Also in resistance-welded tubes, in spite of the removal of both inner and outer beads, structural echoes from the weld are sometimes observed, which are only eliminated by suitable heat treatment.

28.1.3 Flaw Locating Methods

Determination of the flaw depth (from the surface) and its lateral position (within the weld cross-section) is desirable, not only to distinguish true weld defects from defects lying outside the weld, such as inclusions in the parent plate or interfering echoes as in Figs. 28.4a and d, but also for assessing the nature and importance of the flaw on the basis of its position within the joint.

The method of location will be readily understood from the geometric configuration of the beam path as indicated in Fig. 28.8. It is assumed that only indications lying between one half and one full skip distance are taken into account and that the flaw is aligned on the axis of the sound beam and its echo maximised.

It is easy to recognize that a particular depth is related to a particular sound path. It is thus possible to attach to the CR screen a flaw-depth graticule valid for a
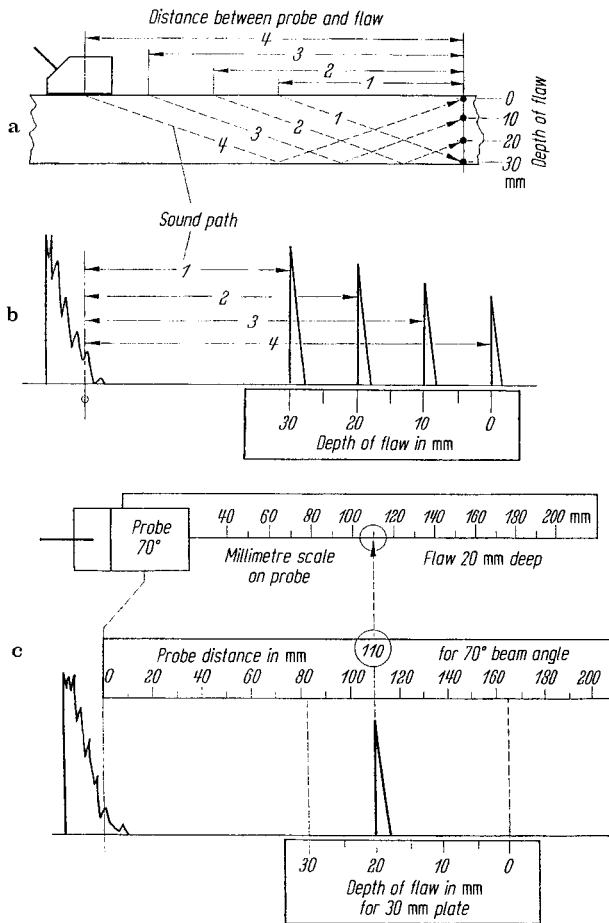

Fig. 28.8. Flaw location in the testing of welds with CR-screen scale for flaw depth and probe distance, selected for a particular plate thickness and beam angle
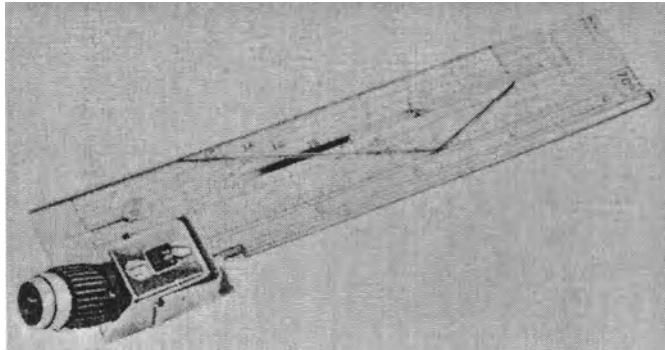
Fig. 28.9. Flaw-locating rule for weld testing, design Krautkrämer

given beam angle (e.g. 70°) and a given plate thickness (e.g. 30 mm), running from right to left. Where only the depth is of interest, this is all that is necessary.

Figure 28.8 a clearly shows that every flaw depth is related to a definite distance between probe and flaw (projected to the surface). At the beginning of the depth scale, i.e. for surface defects, this distance equals the full skip distance. As indicated in Fig. 28.8 c a calculated distance scale can be placed on the CR screen. The distance in millimetres read on this scale for a given flaw echo is then transferred to a scale attached to the probe, so that both the flaw location and its depth can be marked directly on the plate. The distance scale is valid only for a particular beam angle and the depth scale additionally for a particular plate thickness. If no direct depth readings in millimetres are required, the bottom and top surfaces of the plate can be indicated by movable pointers between which the depth of the flaw is estimated, in fractions of the plate thickness d, e.g. 1/4 d from the rear face. In this way the device can be made suitable for any plate thickness.

Formerly, mostly for training purposes, a locating rule was used, fixed to the probe (Fig. 28.9). It has a sliding graticule which can be adjusted for any plate thickness and which gives the flaw depth in millimeters.

As indiated in Fig. 28.10 a scale for the sound path is placed in front of the CR screen. This is identical to the locating rule, but is calibrated in arbitrary units, e.g. 0-5, because the true sound path in millimetres is no longer of interest. Prior to the test this scale is calibrated with the aid of a test block by shifting and expanding it to a total distance of, for instance, 250 mm in steel. The position of the flaw echo is read in scale divisions, e.g. 2.6, and transferred to the locating rule. There, the five-division scale is expanded in such a way that the true probe distance in millimetres can be read from it, or more simply, the location of the flaw is marked directly on the plate next to the edge of the rule. The oblique line starting at the probe, together with the oblique edges of the sliding graticule, indicate the sound path between the two surfaces of the plate, rotated 90° from its true position into the plane of the plate. Thus the depth of the flaw can be read on this line if the probe distance has been transferred to it from the CR screen.
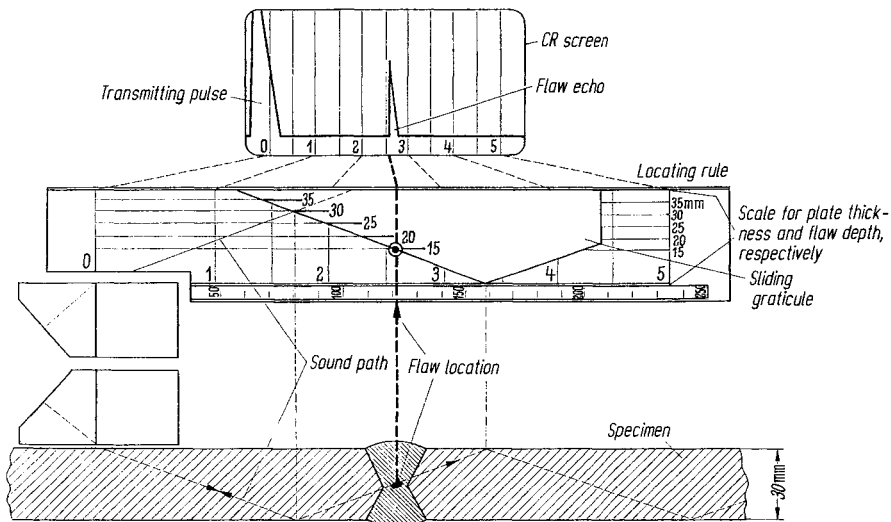
Fig. 28.10. Locating flaws with the Krautkrämer locating rule for testing welded joints

Another very practical solution determines the position of the flaw by the intersection of two straight lines on a traced cross-sectional sketch of the joint [841]. This requires reading on a scale attached to the probe its distance from the center of the weld and transferring it to a locating diagram mounted above the CR screen. On this diagram the true cross-section of the welded seam, i.e. double V, V or U-joint, is drawn to scale. The point of intersection of the normal from the plate surface with the oblique distance line gives the position of the flaw inside, or outside, the welded joint.

Because of its simplicity, the following locating method according to Papke [1170] has found wide application in practice. An engraved graticule is placed in front of the CR screen as "locating scale" (Fig. 28.11). The projected distance p which corresponds to a given sound path w is entered on the abscissa. The beam angle α is entered on the ordinate, indicating the nominal beam angle for the angle probe used and a number of other adjacent angles which may occur during the test, either as a result of manufacturing tolerances of the probes, or uneven wear of the perspex contact shoe. The plate thickness d, which determines the reflection points at the bottom and top of the plate, is selected from the oblique parameter lines. With the aid of the auxiliary lines explained above a cross-sectional sketch of the weld can now be drawn on this transparent diagram (bottom surface = perpendicular through intersection between angle line and plate thickness d, top surface = perpendicular through intersection between angle line and double plate thickness $2d$; in the example in Fig. 28.11 the values $\alpha = 71°$, $d = 20$ mm have been chosen). The shape of the joint can then be drawn symmetrically inside the indicated plate thickness lines.

The instrument is then adjusted by marking the echoes from standard reflectors at given distances as calibration markers for the correct projection distances of the locating scale. The true sound path is then always longer by a factor of $1/\sin \alpha$ than the distance reading of the locating scale. From now on the instrument is no longer calibrated in "sound path w" but in
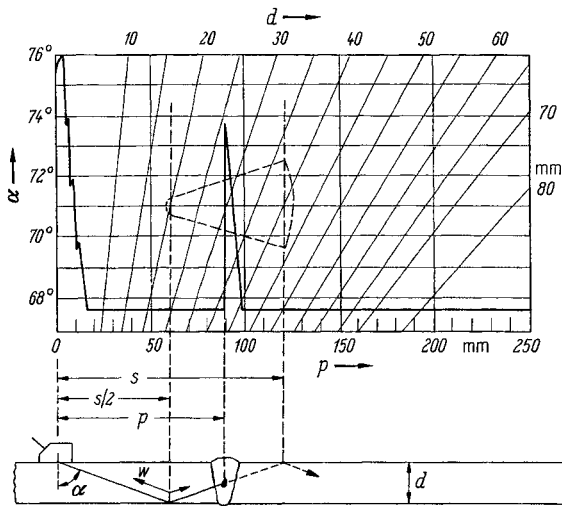
Fig. 28.11. Locating flaws with the locating scale according to Papke [1170]. s skip distance; p projected distance of flaw, i.e. surface distance between flaw and probe index point; w sound path to flaw

"projected distance p". In Fig. 17.7 this would mean that by contracting the time base the maxima of the envelopes would be moved exactly over the reflection points in the lower section of the drawing.

This device greatly facilitates the location of flaws. The flaw echo is, as usual, adjusted to maximum amplitude by shifting the probe and the front edge of this echo immediately indicates the depth of the flaw below the plate surface on the weld cross-section drawing. In addition the projected distance of the echo is read on the locating scale in millimetres; this value is then transferred to the distance scale on the angle probe, and so the lateral position of the flaw is determined as projected onto the surface of the plate indicating immediately the flaw position within the weld or outside it.

In practice the method is often simplified by using exclusively the projected distance and the nominal beam angle, doing without adjacent angles and the plate thickness. Instead of the full projected distance frequently the reduced distance is used as measured not from the probe index but from its front face of the probe against which, during working, it is easier to place a scale.

Miniaturisation of electrical circuits has made it possible to use a modern version of these locating methods, viz. the "luminous locating rule" according to Lund (Fig. 28.12). The scale attached to the probe contains 100 closely spaced light-emitting diodes (LED), each being coordinated to a 100-element chain gate (see Section 10.3.1). If a flaw indication appears in a given gate or gates, the coordinated diode(s) is (are) illuminated. The zero point and the scale calibration of the chain gate, are referred to projection distances for a given beam angle, and a particular flaw echo causes only that diode to light up which is momentarily located exactly above the flaw. Provided the flaw is still covered by the sound beam, due to its divergence, while the rule is moved back and forth, the appropriate diodes above the flaw position will be illuminated.
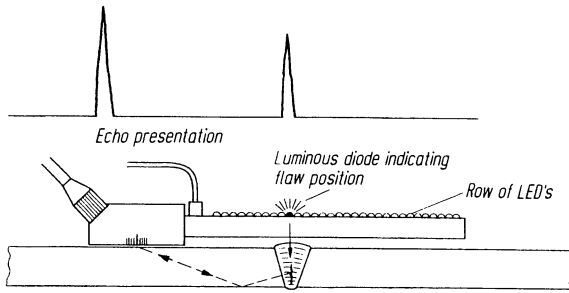
Fig. 28.12. Luminous locating rule, schematical, according to Lund

With this device the inspector recognizes the flaw indication at the point on the plate at which he looks while guiding the probe. At the same time he can determine its lateral position in the weld and also the longitudinal extension of the flaw. Only then will it be necessary to observe the screen to determine on the DGS scale the equivalent reflector diameter and to deduce from the shape and the dynamic behaviour of the echo relevant information concerning its type and shape.

Despite its many advantages the size of the luminous locating rule is a handicap for easy probe manipulation and it has not been widely accepted therefore.

All locating methods discussed so far presuppose flat plates and parallel cross-sections. In the case of pipes these methods can be applied directly only to circumferential welded joints. For longitudinal joints as in Fig. 17.12 both the sound paths and the skip distances are increased so requiring special rules valid only for particular wall thicknesses and particular external diameters. It is therefore usually preferable to use a hand drawn sketch of the pipe cross-section showing the configuration of the beam, even if this is more complicated and less accurate.

The accuracy of measurement for flaw position by any of the locating methods in welds of 20 to 30 mm in thickness is a few millimetres. For thinner welds the error can be larger, but this is not of great importance because repairing the weld in these cases is also easier.

The accuracy of position measurement can be increased by using digital electronics, as an auxiliary device or built into special flaw detectors. The values of distance, sound path and defect depth can then be indicated digitally.

A form as suggested in Fig. 28.13 can be used for the test report and for documentation purposes [1169]. Here the operator enters length, lateral position and depth of any defect, the echo from which is over the recording limit. In addition the equivalent defect size and the suspected type of defect must be recorded. Such a report can take the place of an X-ray film and even gives additional information, viz. the position in depth of the defect, which is very useful for repair purposes.

When comparing these two weld testing methods it must be kept in mind that the detectability of important planar defects such as cracks and lack of fusion is more doubtful by radiography and usually requires additional ultrasonic testing anyway. For thicknesses over 60 mm ultrasonic testing is usually regarded as the only economic and reliable one [688, 752, 1084].

Fig. 28.13. Typical report form for weld testing

28.1.4 Defect Size, Shape and Type

The fundamentals to these problems have been discussed in Chapter 19 so only the special factors relevant to weld testing will be dealt with here.

In ultrasonic weld testing it is a major handicap, that a naturalistic defect image from which could be drawn conclusions on its acceptability for service is missing. Formerly it was attempted to overcome this problem by specifying very low recording limits for indications and by carrying out multiple comparing tests, especially in the nuclear field.

As a measure of defects their echo height and recording length are used (see Section 19.3). For a comparative measure of the echo height either test blocks with side-drilled boreholes, or the DGS method, is used. To convert the echoes of transverse boreholes to those from equivalent flat bottom holes Eq. (5.8) in Section 5.2 can be used. Side-drilled boreholes are easy to manufacture reproducibly, but the test block has to be quite large to avoid side-wall effects (see Section 16.1, Fig. 16.5). For an artifical defect at 200 mm in depth the block should not be narrower than 70 mm.

An added disadvantage is the requirement for a large number of test blocks corresponding to the different thicknesses of plate and for the construction of nuclear power plants for example the full collection of blocks is expensive and bulky [1011, 1538, 1261, 1407].

With the DGS method (see Chapter 19) DGS diagrams or graticules are used (Fig. 19.16). They are available for normal (0°) and for certain angle probes. By using them the recording limit for an echo can be indicated immediately at any distance of the defect. The attenuation of sound for transverse waves cannot be neglected and it is therefore already taken into account in the diagrams, 8 dB/m for 2 MHz and 60 dB/m for 4 MHz. In modern fine-grained steels these values can be at least two times too large, however, and in such cases one can use the DGS diagrams without attenuation-correction and, if necessary, correct the final result by mental arithmetic.

The reference echo for setting the gain to 0 dB is obtained from the quadrant reflector of the reference blocks 1 or 2. The echo peak obtained is adjusted to fall into the small circle

marked R on the graticule in Fig. 19.1 b, after which the gain must be increased by the factor corresponding to the specified recording limit. The small differences between the back echoes from the curved surfaces of the test blocks 1 or 2 (Fig. 10.51 and 10.52) and from a flat back-wall, as required basically for the DGS diagram, have been taken into account in these graticules.

The differing surface qualities which may exist between test block and workpiece can be allowed for by the so-called transfer correction. Using two identical angle probes as separated transmitter and receiver, a through-transmission signal over one skip distance is produced on both the test block and the workpiece. On the graticule a nominal curve for this through-transmission signal is shown for the ideal surface quality. The signal from the workpiece, which because of a generally rougher surface is lower, has to be increased by the transfer function in decibel. The different transit paths of the skip beams because of the different thicknesses of the test block and the plate under test have been taken into account in the curve.

If the DGS method is not applied, a swept-gain circuit (Sections 10.3.4 and 19.2) is very useful. To take account of the material attenuation in this case, Niklas [856] has proposed using the multiple-echo sequence generated by a normal (0°) transverse-wave probe on the plate under test but because of the difficulty of coupling this method is not generally used. The same is true for the DGS graticules provided by Deutsch [319], which use as the distance-law function the average between that for flat circular reflectors ($1/z^2$) and for transverse cylindrical holes $\left(1 \Big/ z^{\frac{3}{2}}\right)$.

For further literature concerning the DGS method for flaw evalution in weld testing see [929, 1242, 1429, 1430, 415, 725, 153a, 640].

Concerning the shape of the defect, if it is large compared with the wavelength, something can be deduced from the echo shape and its scanning dynamics. Figure 28.14 shows echoes from a crack and from slag inclusions respectively when the sound beam is incident either perpendicularly or obliquely to the weld axis. Linear scanning can also reveal additional information about the shape of the de-
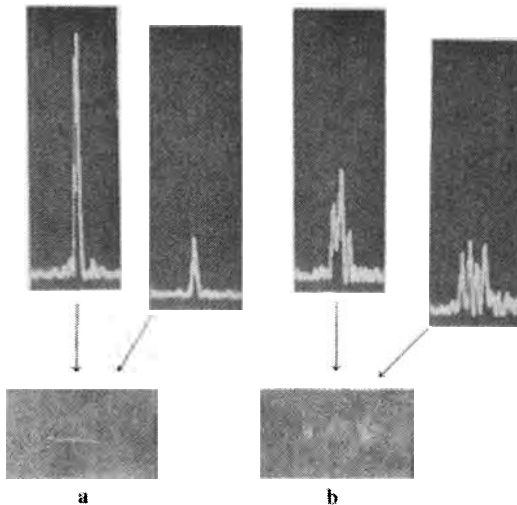

Fig. 28.14. Echo traces of weld defects compared with radiographs, sound in each case beamed normal and obliquely to the longitudinal direction of the joint. **a** Crack in root; **b** slag inclusions and pores in a 50-mm thick V joint. The picture of the crack has been retouched since it was barely discernible in the original radiograph. Probe 4 MHz, 70°
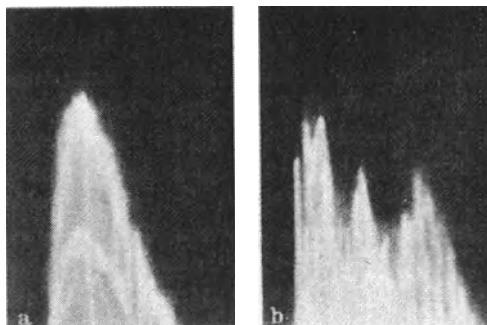
Fig. 28.15. Envelopes of flaw echoes. **a** 3-mm borehole parallel to test surface; **b** crack in a 35 mm thick welded joint, probe 4 MHz, 70°

fect, as explained in Section 19.2 Figure 28.15 shows the variation in two typical echoes when the weld is scanned in a direction perpendicular to the weld axis.

In practice, however, defects which give echoes as in Fig. 28.14 a, or which give a definite plateau in their envelope when scanned as in Fig. 19.9 c, are very rare. The problems with most defects which cannot be definitely identified by the above-mentioned methods have often been overcome by the following rules.

Firstly only the maximum echo amplitude should be taken into account. A certain recording limit (for example a 1-mm circular disc reflector) is decided, leaving all indications which do not reach this level out of account. Larger echoes are recorded and the defect length is measured by scanning, using a fixed or a relative threshold (Section 19.3). If the measured length is greater than the maximum which has been agreed, then further time-consuming methods can be applied, including more precise measurement of its length by taking into account the distance of the defect and the beam divergence of the probe. In addition special focussed probes and precise mechanical scanning devices can be agreed but these additional means are not the standard rule. By these methods the great advantages of ultrasonic testing, viz. high speed and reliability for detecting important large defects, is not affected.

If a recording limit of the echo amplitude is agreed, this is of course based on the experience that the actual flaw size can be larger than the equivalent flaw, so that an important defect should not be overlooked in practice.

In the day to day routine manual inspection of welds all the various methods for distinguishing the shape, whether flat or globular, as well as the direct imaging methods of Chapter 13 cannot find practical application, because they are too time-consuming [1405]. See further [325, 1263, 931, 1211, S 101, S 150, S 26, S 156, S 64, S 26] and Section 19.3.

28.1.5 Mechanizing and Recording of Weld Testing

Manual weld testing comprises the observation of the transitory screen image and making a record of the results either by marks made directly on the workpiece showing defect positions or by completing a form.

Automatic scanning and recording equipment can be installed following an automatic welding machine or as a separate installation for checking thick-walled and highly stressed welded tubes. The systems described in Chapter 13, P scan [945, 1121] and SUTAR [1046], are examples of the automatic recording of amplitudes, transit times and corresponding defect positions displayed as a C-scan picture. In these equipments the probes can still be manipulated manually, or be guided mechanically.

If the probe movement imitates the methods of manual testing, viz. longitudinal and transverse movement combined with swivelling, testing can take too long and the probe wear becomes excessive so that several probes, guided only longitudinally and pulsed by multiplexing are to be preferred.

Automatic testing and recording systems are especially useful if they can operate simultaneously with the welding process. Examples are resistance and inductance-welded tubes and thick tubes welded with powder flux, all with longitudinal welds, because in these cases the speed of welding is not too quick for testing. The same criterion is valid for large-diameter spirally welded tubes.

Tubes between 20 and 80 mm in diameter can be checked during the cooling portion of the production cycle either under water or using water delay lines. The separation of the probe from the weld is sufficiently large to enable the ultrasonic beam to fill the complete wall thickness with the gate covering an extended section of the circumference.

Bad results however are obtained from so-called cold-welds or stuck-welds, which are almost completely transparent to ultrasound. They can, however, be detected if the tube is slightly deformed after welding by a roller system when the cold-weld opens up. A better method of process control would be by an accurate measurement of the welding temperature since a cold-weld usually occurs only when this is too low. These types of pressure-welded tubes often present another testing difficulty as well as their excessive weld beads and cold-welds. These are small areas of lamination and slag in the plate which are not harmful to the use of the tube, but which give indications comparable to weld defects if they occur near the weld. For this reason the method is not favoured for small wall thicknesses, but with larger wall thicknesses above about 5 mm, the ultrasonic probes can be carefully adjusted at a distance where the focussed beam does not strike the inner wall. Then if the outer weld bead has been machined off, a test can be carried out successfully [527]. For further information on pressure welded tubes see also [1583].

Whereas the weld zone of resistance-welded tubes is usually very small, it is quite large on those welded by submerged arc with a double-V preparation
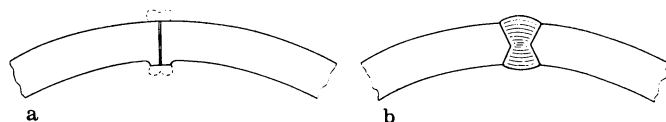

a   b

Fig. 28.16. Cross-sections of joints, schematic. **a** Electric-resistance welded (ERW) longitudinal pipe seam with incompletely removed internal bead; **b** submerged arc-welded (SAW) joint
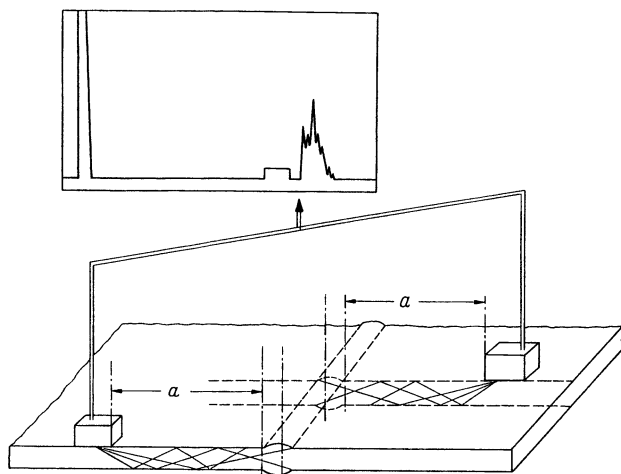
Fig. 28.17. Continuous testing of thin seams produced by automatic welding

(Fig. 28.16). Because of this fact a method has been proposed by de Sterke, to avoid interference by echoes arising from the far edges of both inner and outer weld beads. These echoes have a somewhat longer path than those from a center defect so as in Fig. 28.17 the weld is tested using two probes, somewhat staggered along the weld, each covering by an appropriate gate the nearer two-thirds of the weld width. The central zone will thus be tested twice, and the nearer sections only once so that interference echoes are eliminated.

The probe stagger can cause some confusion however, particularly when recording the flaw indications in their correct position in a longitudinal direction. According to a suggestion by Schlusnus and Koch [1853] this ambiguity in the recordings can be avoided by mounting the two probes exactly opposite to each other and multiplexing them. Such an arrangement has an added advantage since after the two testing cycles both probes can be connected in parallel during a third cycle, resulting in a transmission-pulse reference echo to check the coupling conditions.

If transverse defects can occur, the testing assembly must be enlarged by two additional probes according to Fig. 28.18.

The arrangement of these extra probes depends on the position of the probes used for longitudinal defects. If according to Fig. 28.18 a, all probes are operated in parallel, to distinguish between longitudinal and transverse defects requires that probes 1 and 2 should be arranged at a different distance from the joint compared with probes 3 and 4, the evaluation being made by two different monitor gates.

In the case of the arrangement in Fig. 28.18 b, where the probes for longitudinal defects, as described above, are operated first independently and then in a separate control cycle simultaneously, the probes for detecting transverse defects can be included in the multiplexing programme. The testing point, as drawn in solid lines, can coincide for all probes since the multiplexing excludes mutual interference.
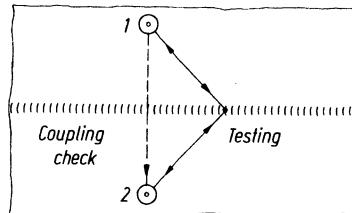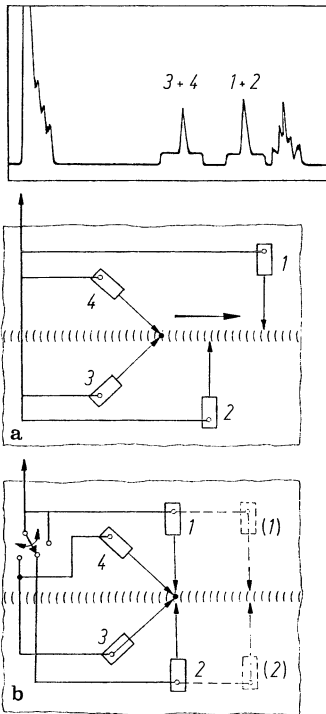
Fig. 28.18. Arrangement for detecting longitudinal and transverse defects. a With parallel-connected probes; b with multiplexed probes, the so-called K arrangement

Fig. 28.19. Arrangement of double-beam probes for detecting transverse defects, combined with a coupling check

However, for reasons of spacing, the testing points for each type of defect are usually separated as shown by dashed lines.

The simple functional and coupling check using the probes for longitudinal defects by means of a through-transmission pulse cannot be applied to the probes for transverse defects. For these another method is used in which an auxiliary crystal is mounted in the angle-probe wedge to send a beam perpendicularly into the material at the angle beam index point (cf. Fig. 15.8). The resulting back-wall echoes serve as a reference for the quality of the coupling and also provide control voltages which indicate the degree of coupling and so can be used to control the gain.

The satisfactory functioning of the probes for detecting transverse defects is checked by using an auxiliary reflector built into the probe to direct a part of the coupling control beam to the test transducer which acts as a receiver. This signal is independent of probe coupling and gives an indication of the correct function of the test transducers and amplifiers.

Another arrangement with special probes has also been used for the functional check of the probes detecting transverse defects. As in Fig. 28.19 the two opposing angle probes transmit and receive beams in two different directions. The "testing beams", at 45° to the joint, are used in the customary way for the detection of transverse defects. The "checking beams" produce a direct through-transmission signal. Since in addition both beams emitted by each probe come from the same crystal, the through-transmission signal monitors the electrical

functioning of the probes. In order to produce two beams from one crystal it is fixed into a slot in such a way that it radiates from both its front and back surfaces. Reflecting surfaces of the wedge then deflect the beam portions in the desired directions. The use of these two "check-beams" for simultaneously detecting longitudinal defects is not feasible due to the critical adjustment requirements of both position and sensitivity. Consequently, the test for longitudinal defects is carried out in the usual way with a separate pair of probes.

In a further system known as the X arrangement, four probes are located at the corners of a rectangle to participate in testing for both longitudinal and transverse defects (Fig. 28.20). The sound beams coincide with the diagonals of the rectangle and their intersection marks the testing point on the joint. The probes T_1 and T_2 at the ends of one diagonal operate as transmitters, the receivers being R_1 and R_2 at the ends of the other diagonal. Longitudinal defects in the welded joint are indicated by probes T_1 and R_1 and simultaneously by T_2 and R_2, whereas a transverse flaw is detected by the combinations T_1/R_2 and T_2/R_1, respectively. This arrangement has the advantage that whenever a flaw is indicated on the CR screen it will be located at the point of intersection of the sound beams, and since the sound paths are identical for longitudinal and transverse defects, the evaluation requires only one monitor gate position. Differences in the dynamic behaviour of an echo reveals whether it comes from a longitudinal or a transverse defect (see Fig. 28.20a and b). In automated installations the probe assemblies are operated successively by multiplexing. Two interposed cycles, during one of which T_2 operates as a receiver while during the other R_2 operates as transmitter, makes it possible to check the functioning and the degree of coupling of all probes.

On the other hand this arrangement has some disadvantages due to the dual function of the probes. The mechanical adjustment of the assembly, as well as of the testing sensitivity, is more critical and more complex than in Fig. 28.18 where the testing for longitudinal and transverse defects is strictly separated. In addition this 4-probe assembly cannot be used for testing near the end of a pipe since as the first two probes reach the end the testing ceases. For the other probe arrangements longitudinal defects can be detected almost to the end of the pipe.

In practice both longitudinal and spiral joints can be tested by the methods described, immediately after the continuous length of pipe leaves the welding machine. In some factories, however, central test installations have been installed in which the pipes produced by several welding machines are all tested separately, the
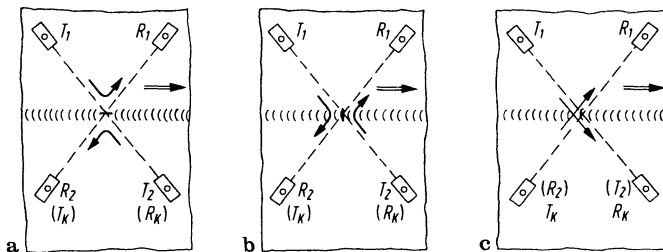

Fig. 28.20. Testing of submerged-arc welded joints by means of separate transmitting and receiving probes. **a** For longitudinal defects; **b** for transverse defects; **c** control cycles
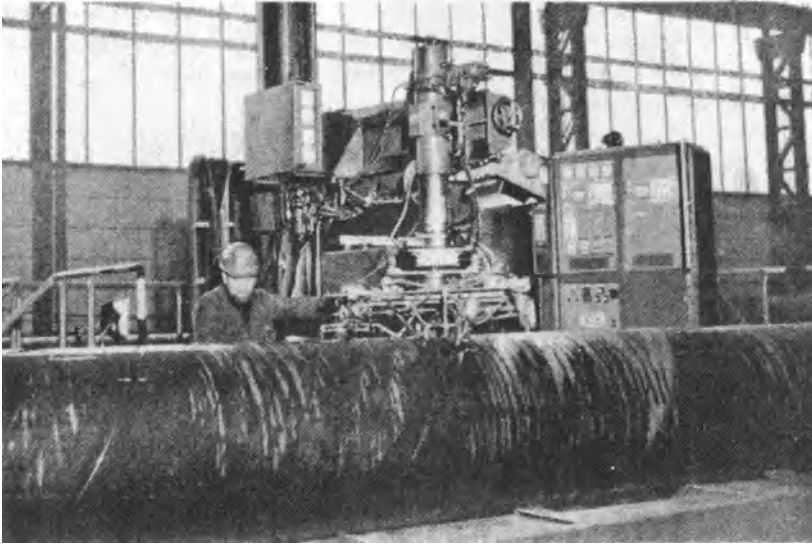
Fig. 28.21. Central test installation for spiral-welded large-diameter pipes for longitudinal and transverse defects (courtesy of Stahlwerke Peine, Salzgitter)

pipes being cut into individual lengths. These are transported by rollers which permit rotation and exact positioning of the joint at the location of the probe assembly. In the case of spiral welds this requires exact control of the drives for rotating the pipe and moving it forward, in accordance with the spiral pitch (Fig. 28.21). In the case of longitudinal joints it is often advisable to test only after the pipe has been expanded by hydraulic pressure, and after straightening, because these processes may cause cracks.

The speed of testing longitudinal welds is up to 30 m/min, and for spiral welds up to 20 m/min.

For tubes with wall thicknesses up to 25 mm testing installations are in use in large numbers. Up to 15 mm in diameter 4-MHz probes are commonly used but for thicknesses above 15 mm 2-MHz angle probes are used because of their larger beam angle. More recently welded tubes with a wall thickness of 40 mm have been produced and here the weld is tested by two angle probes somewhat staggered along the weld, each intended to inspect one half of the thickness.

A very high degree of automation has been reached in the tube-testing installations by Krautkrämer-Japan. Varying the position of the probes and gates is carried out automatically when the tube dimensions have to be changed.

In association with the weld testing for spiral tubes of large diameter, the basic quality of the parent steel plate is often checked at the same time for laminations and large inclusions. This is carried out with one or more normal probes arranged on the top of the tube and locally scanning longitudinally. For a wall thickness of 5 mm and above, TR probes can be used but for thinner walls down to 1.5 mm, shock-wave probes with a water delay line are necessary. The strip edges are some-

times checked before welding at the entrance of the welding machine, because laminations and inclusions can influence the quality of the weld. Similarly the base material is checked at each end of the welded tube to ensure the quality of a connection weld to be made later on site.

On pipeline sites the test of longitudinal welds is occasionally carried out manually using the K arrangement. The probe-holder device is self-guided along the bead of the weld, the probes being connected to a battery-powered miniature flaw detector via a multiplexer.

For the testing of circumferential welds on site Husarek and Ruault [704] have built a semi-mechanized device to assist manual testing. For the same purpose an installation of Krautkrämer-Japan [1409] has been built which records defects according to their size and position within the weld and along the circumferential direction.

A device called ROTOSCAN has been developed by RTD, Holland, especially for testing circumferential welded pipes on board ship, during their installation [1466]. The multi-probe arrangement, working through a 32-channel multiplexer, is moved mechanically along the weld, the results corresponding to different testing zones being documented by a multiple line recorder. This installation has also been used on land, and even under water to test the welds on the legs of drilling-rigs [1128]. In this case the complete device, including an electronic interface needed near the probes, has been made waterproof so that after having been put into position by a diver the test proceeds automatically.

Welds of thick-walled pressure vessels above 40 mm are tested with a combination of several angle probes, working singly or in a pitch and catch technique, [S 104]. Figure 28.22 shows such an installation, where the vessel is manipulated on a roller system, above the probe assembly and its electronics, which travels on rails along the length of the vessel. This installation is equipped with microprocessor-controlled electronics with dialog service. The test data are stored on tape, allowing evaluation to be carried out according to different requirements, for example as an
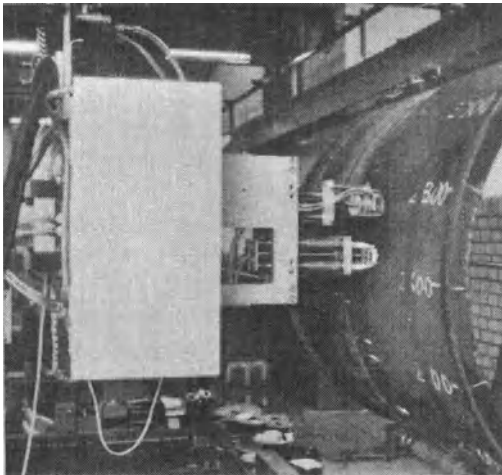
Fig. 28.22. Test installation for welds in thick-walled pressure vessels Type BPA (design Krautkrämer)

evaluated B or C scan. The equipment is reported in more detail in Chapter 30 in connection with the testing of nuclear pressure vessels.

For the evaluation of defect size and type in mechanized weld testing so-called expert systems have been used successfully as for example in the COMSOM system [S 164, S 45]. These methods use intelligent computers, which are programmed with details of the geometrical features of defects and interpretation rules gained from practical operator experiences. For further reports on mechanized and fully auto-matic weld testing see [140, 438, 448, 885, 942, 1058, 1555, 1672, 1270, 1547, 1465, 186, 361, 1208, 579, 615, 816, 1367, 2081, S 80].

28.1.6 Austenitic Welds

When testing single-sided butt welds in austenitic plate material a few millimetres thick it is often sufficient to check only if the weld is fully penetrated or not. This test is effective using 4-MHz 45° angle probes which is sufficient to indicate any non-welded edges. By testing from both sides of the weld it is even possible to de-tect lack of side-wall fusion. However, to find individual defects within the interior
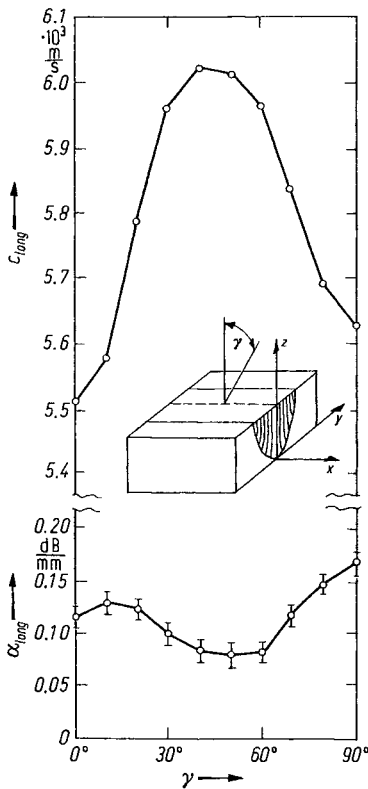
Fig. 28.23. Sound velocity c and attenuation α for 2-MHz longitudinal waves in austenitic welded mate-rial, measured for angles of incidence γ measured from the z-axis in the y/z-plane

of the weld is made difficult by interfering indications from the coarse and aniso-tropic grain structure [48].

If an austenitic weld has been produced horizontally the structure shows elon-gated, rod-shaped crystallites in the weld cross-section as illustrated in Fig. 28.23. They begin perpendicular to the weld flanks and then grow upwards following the temperature gradient [1726, 1416]. Consequently the sound velocity depends on the angle of incidence at the surface. It has been measured for longitudinal waves using a series of specimens cut from a thick austenitic weld, together with the attenuation for 2 MHz (Fig. 28.23) [505]. For vertical incidence (0°) the sound propagation was parallel to the length of the crystallites in the centre of the weld. The strong varia-tion shown has also been predicted theoretically [1183, 1531, 873, 1389, 742, 965, 1677, S 124].

These measurements (Fig. 28.23) have been made with very simplified assumptions con-cerning the propagation of waves in anisotropic materials. A longitudinal wave for example is not propagated in a direction perpendicular to the surface, if introduced by a longitudinal probe. Therefore the angles of incidence shown equal the actual ones only at 0 and 90°, and consequently the values for velocity and attenuation are not certain. For the treatment of wave propagation in anisotropic media see [S 73].

The coarse grain structure combined with the marked anisotropy is the reason for the strong scattering which for a long time has made ultrasonic testing of such
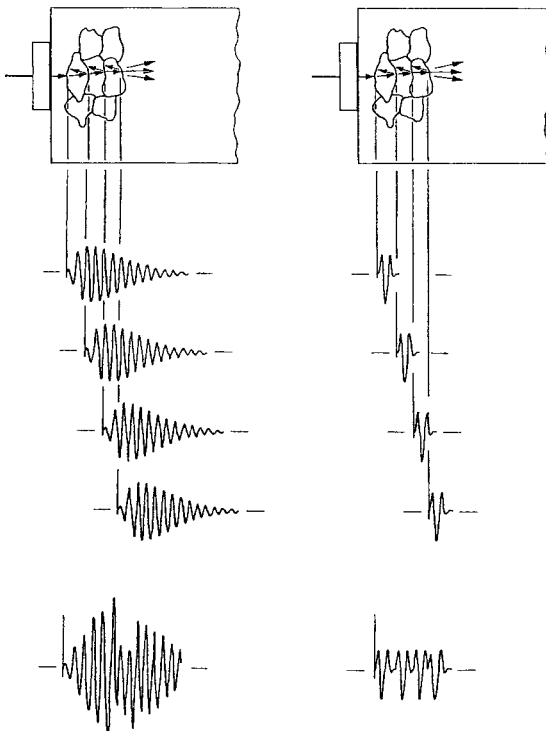
Fig. 28.24. Noise level caused by scatter from the structure of long and short pulses, schematic

structures using transverse waves impossible [1260, 1668]. Important progress has been made in measurements by de Sterke [1183, 1110] using obliquely incident longitudinal waves (see also Section 17.1). According to [1107, 539] the scattering measured for L waves is about 11 dB lower than for transverse waves.

A further improvement has resulted from the use of short pulses and according to [632] there is an optimum pulse length of one to two wavelengths. For longer pulses the different parts of scattered waves add up again (Fig. 28.24). For very short pulses, however, the greater amount of higher frequencies in the spectrum again increases the noise level.

According to [489] the actual attenuation for longitudinal waves in austenitic weld material is not very much higher than in the base material, as Fig. 28.25 shows. The echo from an inclined surface of a specially cut specimen containing weld material (SG) and adjacent base material (GW) shows only a difference of about 2 dB, equalling about 50 dB/m for the weld material. The large reduction in the back-wall echo in the transition zones indicate a splitting of the beam along a
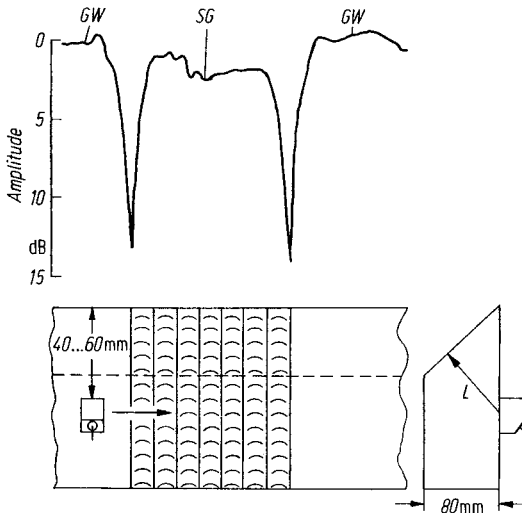
Fig. 28.25. Back-wall echo measured through an austenitic weld
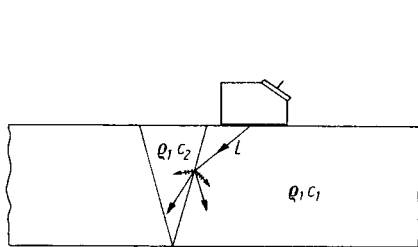
Fig. 28.26. Typical sound propagation when testing an austenitic weld
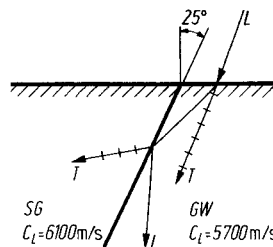
Fig. 28.27. Total reflection of a longitudinal wave at the transition between base material (GW) and austenitic weld (SG)

boundary between different impedances, similar to that explained in Section 16.1.

Figure 28.26 illustrates how this boundary between the austenitic, anisotropic but fine-grained base material and the coarse-grained weld material affects the longitudinal wave by a combination of reflection, refraction and mode change to transverse waves. As these effects vary from point to point because of the different orientations of the grain boundaries one can imagine the destructive effect on the beam. As shown in Fig. 28.27 even total reflection can occur at shallow-angled incidence onto a grain surface. Following a further reflection at the back wall, interference echoes can occur to simulate apparent flaws at completely different positions.

Such echo patterns which occur when testing austenitic welds are shown in Fig. 28.28. On the right-hand screen image one sees the echo indications of the corner between the transition zone and the back surface. The centre image shows the echo of a 2-mm borehole additionally as seen from the right-hand side. The left screen image shows the same hole but seen from the left-hand side through the
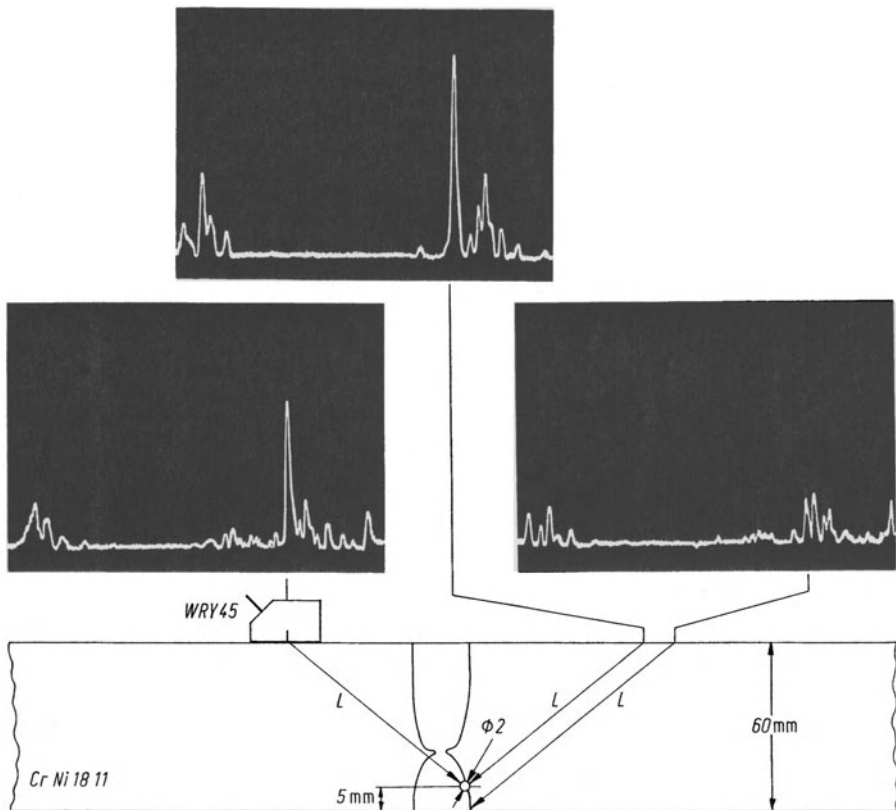
Fig. 28.28. Interference between echoes from the side of an austenitic weld near the plate surface

weld material near the root, but still clearly distinguishable from the following in-terference echoes caused by split-off waves.

At places with unequal penetration of the fused weld metal, and especially in the region of the narrowed root, the beam is distorted [1590, 1665]. Both the evaluation of the defect size from its echo amplitude, and its localisation will be affected by this fact. Some improvement can be achieved by using different beam incidence directions towards the suspected defect position. These difficulties cannot be overcome by using focussed beams or TR probes nor by the frequently proposed means of data processing techniques including signal-averaging or pattern-recognition methods or by the CS technique [1072, 539, 874, 1108, 847, 1361, 540, S 10, S 158, S 123].
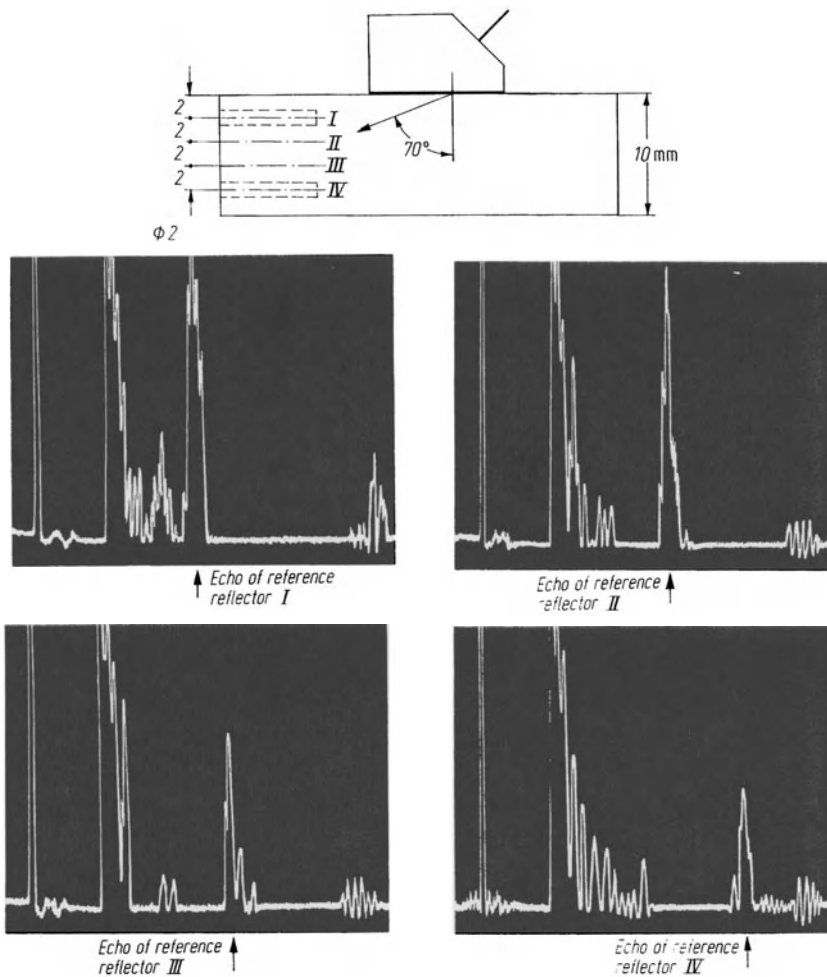
Fig. 28.29. Adjustment of the sensitivity for testing welds in plastics with 2-MHz longitudinal waves at 70° incidence

A considerable improvement in the testability of austenitic welds has been achieved by using appropriate welding techniques. The flanks of the joint should be as parallel as possible, and not tapered, to avoid very narrow root sections and wide top zones [S 125, S 126].

For the technique using obliquely incident longitudinal waves see Section 17.1. The time-base adjustment is carried out with test blocks and the sensitivity is chosen with an echo from a 3-mm transverse borehole [1726]. When using several of these transverse holes at different distance care should be taken that they are not too close together to avoid the possibility of confusion between their echoes and the numerous other echoes arising from mode changed transverse waves.

To estimate the size of larger defects the measurement of their recording length is preferred but for fixing the recording limit the energy losses in the transition zone have to be taken into account [488].

Another way of dealing with the problems of testing austenitic welds has been reported in [462] using SH transverse waves. The testing of mixed connections, for example between ferritic and austenitic components or of austenitic welds between high-alloy steel tubes (such as 20CrMoV 12 11 for example) have proved successful using longitudinal wave methods.

28.1.7 Welds in Plastics

The attenuation in plastics of transverse waves is also extremely high, due however, more to real absorption than to scattering. For testing welds in plastics therefore only longitudinal waves are feasible. This proposal was made by Homes in 1959 [685] but it was not used before the 1970s for welds in hard polyethylene tubes
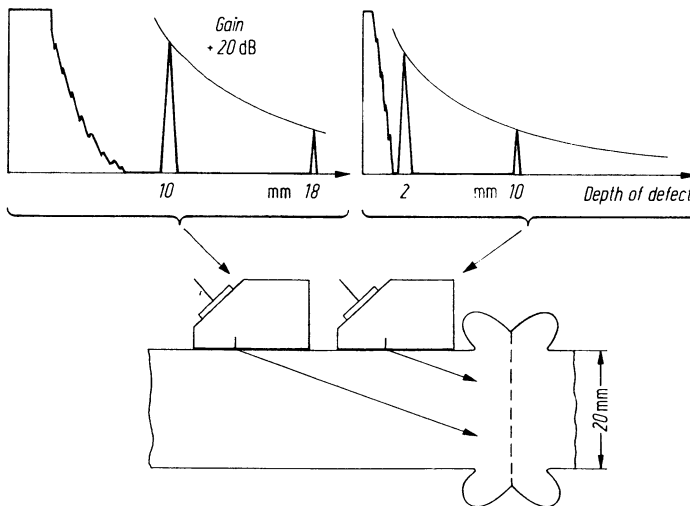
Fig. 28.30. Adjustment of the sensitivity for defects in plastic welds at different depths

[649]. Widely diverging longitudinal wave beams, from 1 to 2 MHz, 10-mm crystals, at angles of about 70° allow checking the complete cross-section from one probe position. Figure 28.29 shows a useful test block with artificial defects in the form of 2-mm flat bottom holes at different depths. According to their depth, the echoes from these reflectors arrive with different transit times and, because of the increasing absorption, with decreasing amplitudes. Larger wall thicknesses need a twin stage testing with increased gain for the lower half, as Fig. 28.30 illustrates. Still thicker walls must be tested from both sides of the sheet with single probes or with the pitch and catch technique using two probes.

The echoes received from the lower bead of the weld, as in Fig. 28.31, arrive with too big a transit time to be confused with real defect echoes. They are a welcome indication of coupling quality if the operator is experienced.
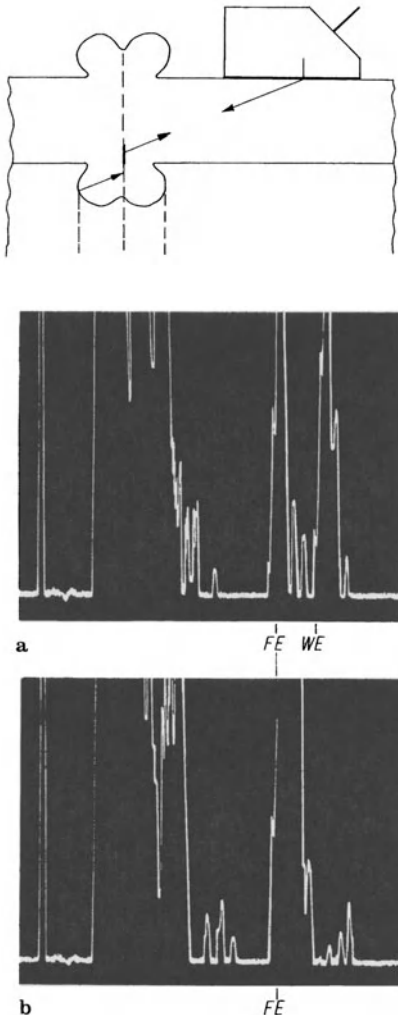
Fig. 28.31. Testing of a weld in a plastic tube of 120 mm in diameter and 11 mm in wall thickness with a 2-MHz, 70° longitudinal-wave angle probe. a Indication of a small lack of bond of about 1.5 mm height (FE) in front of the echo from the weld bead (WE); b indication of a lack of bond of half the wall thickness (FE)
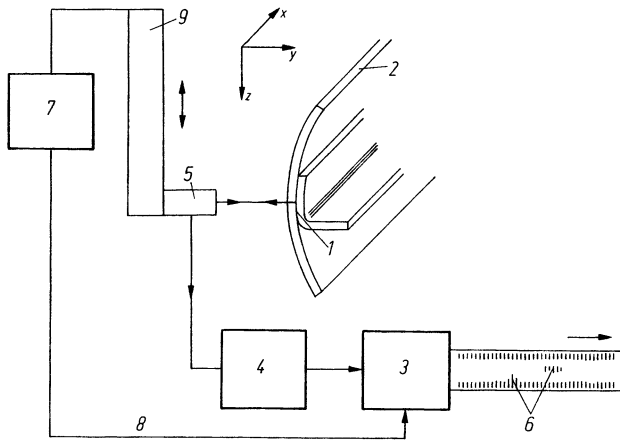
Fig. 28.32. Testing of car bumpers (design Wells-Krautkrämer). *1* welded stiffener, *2* bumper bar, *3* line recorder, *4* flaw detector, *5* probe, *6* non-bonded areas of the weld in the record, *7* analog/digital converter, *8* recording signal, *9* mechanically oscillating probe guide

A critical defect type similar to that found in resistance welds in steel, is the "cold weld" or "stuck weld". The weld zone is usually transparent because the faces are in good pressure contact with one another. On long lengths of weld, however, which have a "stuck-weld" condition throughout there are always intermittent echoes which can indicate the possible presence of the longer defect. In this case a destructive test can easily check if actually, perhaps because of changed welding conditions, a bad weld has been produced. Because immediately after the welding a destructive check is possible without much trouble, the main applications for ultrasonic weld testing in plastics lies in the field of production testing.

Lap welds, as for example are used for sealing 2 mm thick sheets in the dumps for domestic and industrial rubbish, can easily be checked by a 4-MHz normal probe at normal incidence.

The plastic bumpers (fenders) of automobiles are usually welded together from several parts. Figure 28.32 shows the principle of a test installation with oscillating scanning. The test result is recorded on a paper strip, where the defects appear as black on white images. The whole installations comprises the water tank for the immersion testing, a flaw detector and probe of very high resolution characteristics and a computer to control the testing procedure. With a 10-MHz probe lack of bond of about 2×2 mm can be detected, the inspection time being about 5 min per piece.

For butt-weld testing in plastics see a paper of the International Institute of Welding (IIW); see Chapter 34.

28.2 Fillet Welds

In the field of fillet welds there are two main types. Firstly non-penetrating welds for low-stress applications and those with full penetration for more critical requirements (Fig. 28.33).

If the first type of design needs to be tested at all, it can be carried out for thicknesses of the flange exceeding 10 mm, using a TR probe or a high-resolution miniature normal probe. As shown in Fig. 28.33 a a guiding arm following the edge of the flange can help in manipulating the probe manually. As illustrated in Fig. 28.33 a one obtains a multiple-echo sequence on the free flange plate as well as on the non-welded central area. Over the weld itself the sequence disappears completely or it can be replaced by indications from large weld defects. Sometimes echoes with larger transit times also appear resulting from various multiple reflections between the two welds, often indicating that both welds are sufficiently penetrated into both web and flange.

In the fully penetrated, or so-called K weld (Fig. 28.33 b), the flangeplate echo sequence must disappear over the whole width of the weld. Non-penetrated areas and lack of fusion have favorable orientations to be indicated directly. However, for cracks and slag inclusions within the welds angle-probe testing either from the flange or the web can be more favorable, but whereas the normal probe testing as described above can be used with plate thicknesses of about 10 mm and over, the
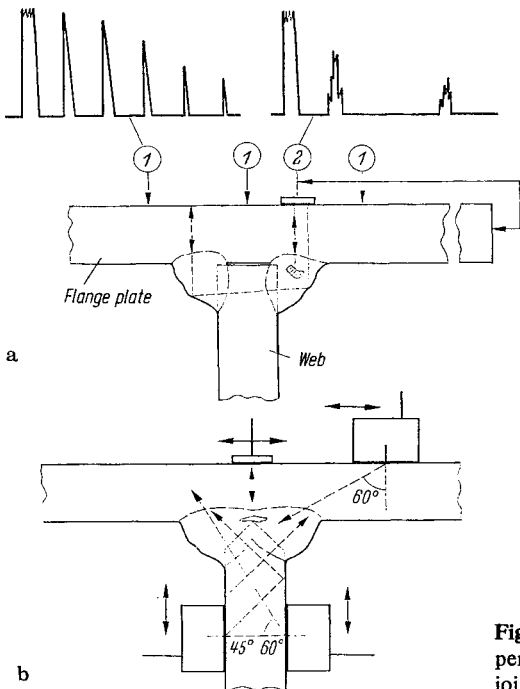
Fig. 28.33. Testing fillet welds. a Joint not penetrated; b joint fully penetrated (K joint)
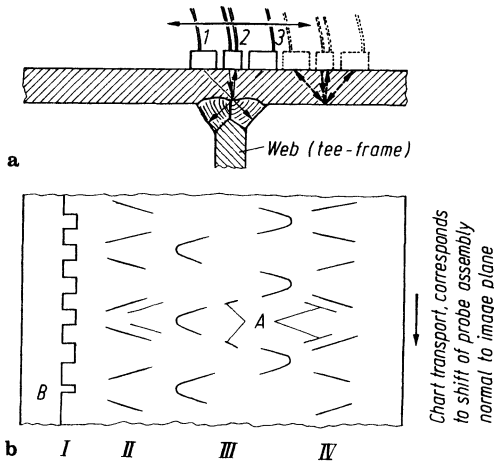
Fig. 28.34. Automatic testing equipment for T-frame welds. **a** Arrangement of probes: *1* and *3* angle probes, *2* TR probe; **b** recording chart, schematic; *I* coupling check, *II* and *IV* recording traces of the angle probes, *III* recording trace of the TR probe, A indication of defect in joint, B indication of coupling failure of the angle probes

use of angle probes require somewhat larger plate thicknesses (Fig. 26.33 b). Then miniature angle probes, 4 or 5 MHz and 45° to 60° can be used. If the flange surface is not accessible the only possible method of testing these fillet welds is from the web surface with angle probes, or from the end of the web plate if it is accessible. This latter technique requires that the web plate thickness exceeds about 10 mm, and that its height does not exceed about 10 times its thickness, and can indicate at least lack of fusion in the center part of the fillet weld.

Recently incipient cracks in non-penetrating fillet welds have also been detected by creeping waves (see Section 17.2). For further information concerning fillet-weld testing see also [1263, 1678, 1154, S 162].

The British Navy has developed equipment for the automatic testing of the welds securing internal T frames in submarine pressure hulls based on the methods illustrated in Fig. 28.34; see [681].

The test installation is carried on flexible guide-rails attached to the hull by suction cups and which run parallel to the direction of the welded joint which is circumferential around the hull. The test assembly advances on these rails step by step while the probe holder oscillates in the perpendicular direction. Both the test assembly and the holder are moved pneumatically, thus avoiding electric interference caused by an electrical motor and its controls. The probe holder contains in the center a TR probe and on each side angle-probes with opposing beam directions (Fig. 28.34 a). A multi-channel spark-discharge recorder records the test results.

The recording of the back-wall echo from the TR probe (absent over the joint) produces the central curved pattern (III) while any defects in the joint show themselves as deviations from the standard pattern. The two traces of the angle probes (II and IV) show the images of the weld surfaces in their characteristic form by re-

Fig. 28.35. Testing a fillet-welded lap joint, or sleeve joint between two tubes (according to von Heesen)

cording the transit times. Since defects will have different transit times, they can be recognized as lines which are parallel to the indications of the weld surfaces.

In a separate cycle the two angle probes are operated in parallel in order to provide a coupling check. As long as the two sound beams meet on the inner surface of the hull plate they prod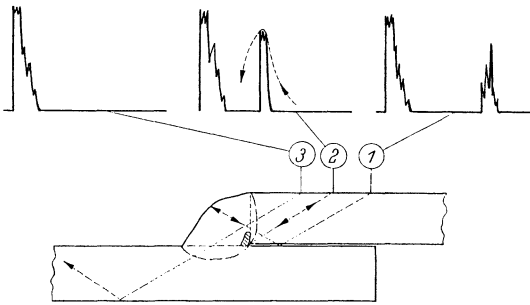uce a transmission pulse which will regularly disappear during the to-and-from movement of the probes above the weld joint. Any irregularity in this sequence of the recording track thus points to unsatisfactory coupling of the angle probes.

Another type of fillet weld which can also be readily tested is a sleeve joint joining two tubes with wall thicknesses above 10 mm as in Fig. 28.35. Here, miniature angle probes of 60° or less have proved successful. Echoes from the weld bead can be obtained in position ① of the probe. When the probe is shifted towards the joint, an area of incomplete penetration produces echoes with a shorter transit time, which can readily be distinguished from the echoes produced by the bead surface. At places without flaws, the beam passes through the weld into the inner tube and gives no echo, see also [918, 972].

Usually less favorable and very much dependent on the specific shape of the joint, are tests on nozzle welds as in Fig. 28.36. For a tube welded into a flat plate the joint, as in Fig. 28.36a, has the same cross-section everywhere and can readily be tested with oblique transverse waves, the echo from the pipe corner serving as a reference echo.

Often, however, the fitting faces show incomplete weld penetration as in Fig. 28.36b. The point of separation can then be distinguished from adjoining flaws only in the case of thick walls and sharply focussed sound beams. Here a better design of joint can more easily be tested, by using for example a pipe joined by a simple circumferential butt weld to extruded apertures in the thicker pipe, cf. [1225, 1516].

Figure 28.36c demonstrates how the complex joint-line curve of two not very dissimilar pipes complicates the test. The sound is propagated in a plane only at four points of the joint (in the longitudinal and in the circumferential direction of the larger pipe). Between these points the zigzag path is distorted and the skip distance continuously changes from place to place so that accurate flaw location is impossible here. If the test is made from the smaller pipe, both the position and the shape of the joint around the circumference also changes, but at least the beam angle remains constant. The latter method is therefore usually more advantageous. Concerning nozzle welds in nuclear power plants see Chapter 30 and [S 166].
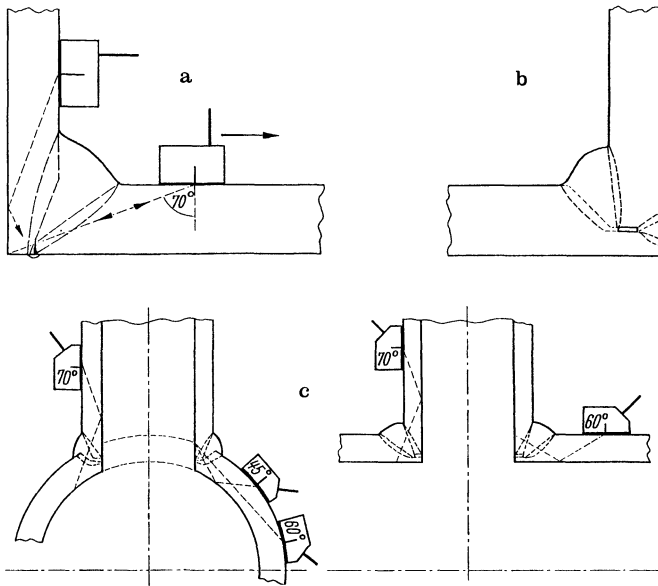
Fig. 28.36. Testing nozzle welds and pipe joints

28.3 Spot Welds

Very early in the history of ultrasonic testing spot welds have already been studied [599, 1095, 1197, 1081, 639]. Testing is made very difficult because of the problem with cold welds or stuck welds, by the need to resolve echoes from thin plates and the bad coupling conditions over the cup-shaped deformation in the surface. The proposal of Wilkens [1002, 318] to build the crystals directly into the welding electrodes was partially successful, but failed because of the problems of maintaining a physical match between the shape of the electrodes and the cooling metal surfaces. Also the method by Crecraft of measuring the thickness profile of the molten metal lens during welding was not applied in practice because of changes in production methods [266].

Another method aimed at detecting a typical defect, the small weld nugget and partial cold weld, uses a very small diameter probe of high resolution coupled to the impressed surface via a short water delay line. Over a good weld it gives a sequence of multiple echoes from the combined thickness of the two plates. Because of the sound attenuation by the as-cast structure of the weld the sequence is relatively short. Over a small weld nugget, however, the attenuation is much lower and in consequence the echo sequence is longer. Around the weld is an unfused area so that there is also an echo sequence corresponding to the thickness of the top plate. With frequencies of about 25 MHz the method was partially successful [S 107].
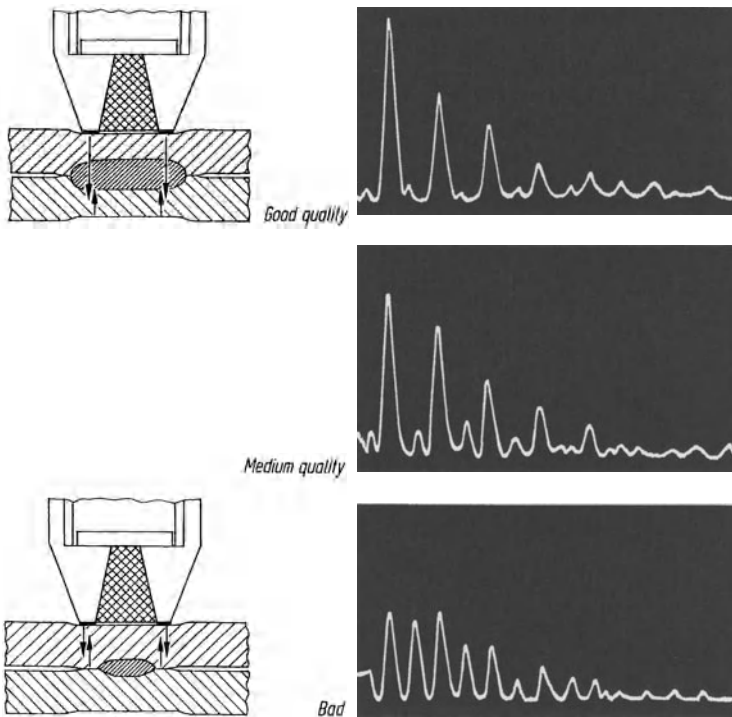
Fig. 28.37. Spot weld testing according to Asai (Toyota)

A further method according to Asai and collaborators, Toyota, Japan, makes use of a small shock-wave probe with a perspex delay line, as shown in Fig. 28.37. The core of the delay line is filled with a highly absorbing material, leaving only an annular beam. Its outer diameter is the nominal diameter of the weld nugget so that for a good weld with a full-sized nugget one gets an echo sequence of the combined thicknesses of the two plates. For a too small weld-nugget diameter a sequence of echoes corresponding to the thickness of the top plate only is indicated. The performance of this device with cold welds has not been reported.

Rolling electrode resistance welds are generally not testable economically. Welded-on bolts of sufficient diameter can be tested by using a small probe in contact with the flat end surface. For a good weld the echo from the end of the bolt will disappear, being replaced by the back echo from the plate with therefore a longer transit time.

28.4 Other Forms of Welded Joints

There is a great variety of welded shapes which are used in all types of mechanical construction. These are mainly small parts which usually are of complicated shape and hardly possible to test by manual methods. Often, however, immersion testing with a certain degree of mechanization is successful, especially using high frequencies up to 15 MHz.

In [S 24] a very sensitive test of a thin electron-beam weld in aluminium is reported using 30-MHz longitudinal waves combined with 7.5-MHz shear waves. Some examples are illustrated by the various diagrams (Figs. 28.38, 28.39, 28.40, 28.41, 28.42).
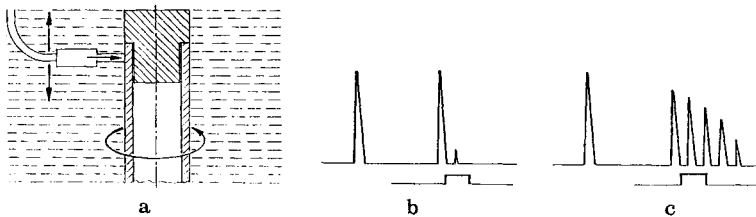
Fig. 28.38. Testing a Magnetweld joint on the end plug of a fuel-element canning tube. **a** general arrangement; **b** echo pattern without defects; **c** with lack of fusion
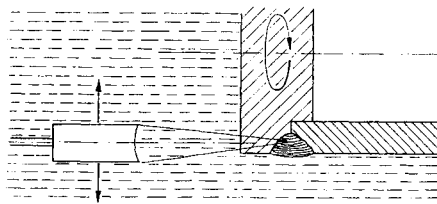
Fig. 28.39. Testing the joint of a sealing cap according to Crowe [277]
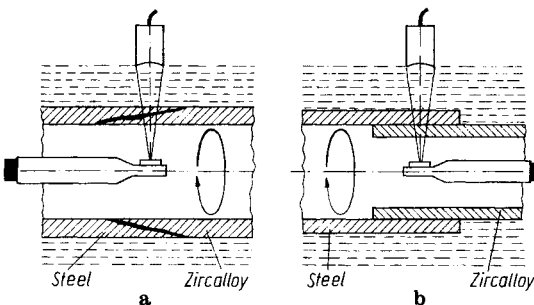
Fig. 28.40. Testing joints between steel and zircalloy pipes. **a** According to the "flow press method"; or **b** the explosive-welding method, using the immersion technique and sound transmission, according to Albertini et al
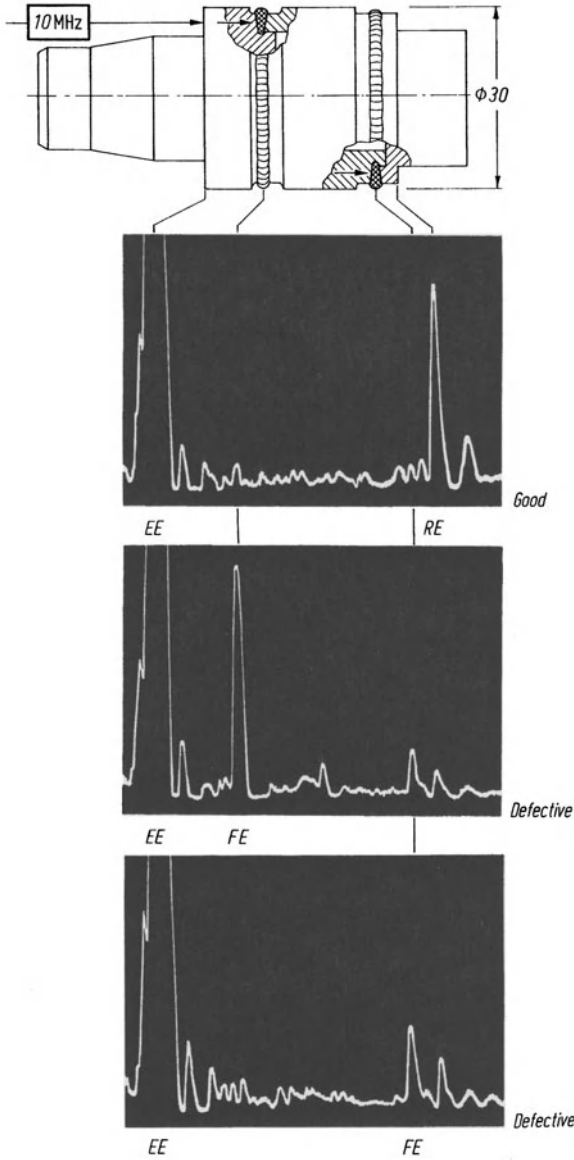
Fig.28.41. Testing of an electron-beam weld (EE entrance echo, RE rear echo, FE flaw echo)
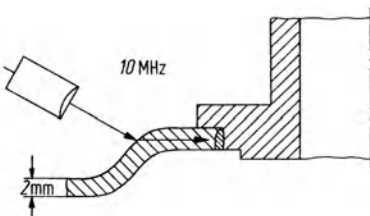
Fig. 28.42. Testing of a laser-beam welded seam

29 Testing of Other Types of Joint and Compound Structures

29.1 Rivets and Rivet Holes

At one time this inspection requirement in steel pressure vessels was very important, but today it is mainly of historical interest. The rivet itself can develop transverse cracks between head and shank and these can be detected by testing from the rivet head, as on bolts (Section 22.4). Figure 29.1 illustrates the formation of inci-
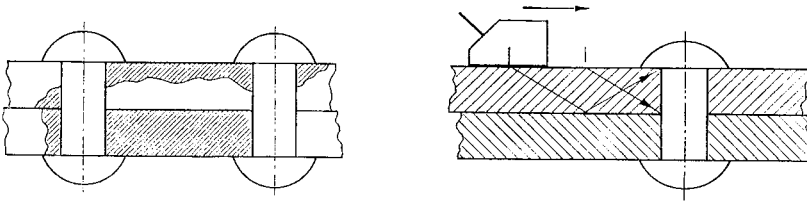
Fig. 29.1. Partially and fully penetrating cracks in rivetted joints
Fig. 29.2. Rivet-hole testing; reference echo from top and bottom edges of the rivet hole
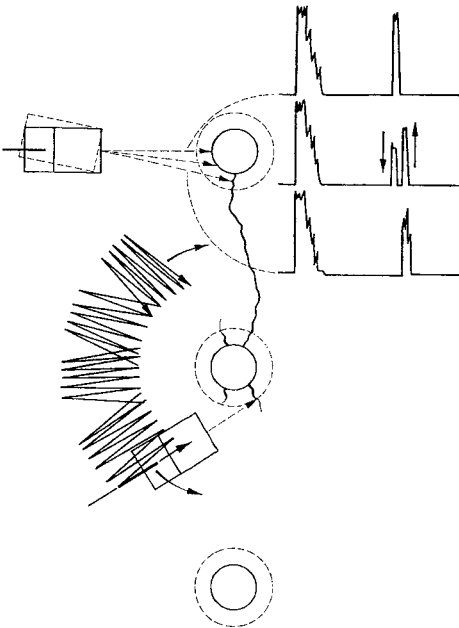
Fig. 29.3. Testing rivet holes, swing-motion of the probe and indication on the CR screen of an incipient crack in a rivet hole

pient cracks at the hole surfaces, which can penetrate through the wall and even extend from one rivet hole to the next. The testing technique is illustrated in Fig. 29.2 and 29.3 and is similar to the probe-scanning movement for welds. The echoes from the top and bottom edges of the hole serve as reference echoes.

The testing of rivet holes has still some importance in airframe construction where the fastener holes can develop corrosion and fatigue cracking beneath the heads of the rivets. Because of the small thicknesses of the aluminium alloy plates involved, the scanning movement is not needed [1706, 595]. The Boeing Company has developed a portable unit for the purpose of finding fatigue cracks in wing skins of their aircraft [1280]. In this application the electromagnetic generation of ultrasound has also found applications [1559].

29.2 Laminar Joints Produced by Soldering, Brazing, Plating and with Adhesives

There is a great variety of types of laminar joint and a corresponding great diversity of applicable ultrasonic test methods. Figure 29.4 gives a summary in which the first two are most widely used. The important question for the choice of test method is whether the lack of bonding occurs because of missing joining material, or bad contact, or if the quality of the bond shall be rated. Finally it must be taken into account that large areas cannot be tested manually in an economic way.

If the bond between two materials with closely similar acoustic impedance is very strong, a resonance test as in Fig. 29.4a amounts to measuring the thickness d_1 (bad) or $d_1 + d_2$ (good). The same applies to the pulse-echo method where the length of the echo sequence serves as a criterion. For both methods it is preferable to measure from the thinner layer because the differences are then more obvious.

As indicated in Fig. 29.4c, large defects can be found with zigzag transverse waves or plate waves which can reach the receiver from the transmitter only if there is no bond, thus allowing positive flaw indication. Instead of the immersion technique where a screen must exclude directly reflected waves, special probes can be used in direct contact [1642].
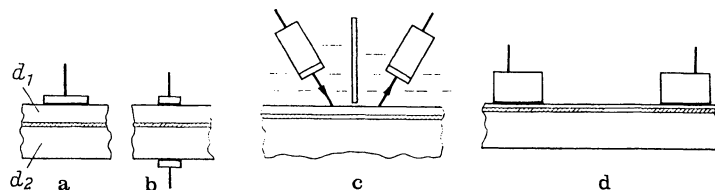
Fig. 29.4. Method for testing laminar bonds. **a** Resonance or pulse-echo method with longitudinal waves; **b** through-transmission method; **c** through-transmission using plate waves or transverse waves within one layer; **d** through-transmission with plate waves or surface waves in the full thickness

Conversely, a bonding defect of thin surface layers may interrupt the propagation of selected wave modes, which can serve as an indication by either reflection or transmission methods (Fig. 29.4 d). Ordinary surface waves or Love waves (transverse waves parallel to the surface) may be used [592]. In both cases the wavelength must be large compared with the layer thickness and these methods have the advantage of testing from one point the whole area of the beam path.

If the bonding material has a markedly different acoustic impedance from the main layers such as in an adhesive bond, a satisfactorily bonded spot will not behave as would a solid specimen. A specimen consisting of two bonded aluminium plates gives a picture different from that of a solid plate of the same total thickness [644]. Conclusions can be drawn from the frequency and the height of resonance peaks regarding the properties of the bonded layer, which provide more information than a simple go/no-go test.

Schematic screen traces applying to the pulse-echo method are shown in Fig. 29.5. If the bonding is satisfactory, the echo pattern depends on the difference of the acoustic impedances as well as the attenuation in the second material. In the figure it is assumed that the influence of the bonding layer is nil but this is not always true.

In the case of some organic cements when using high ultrasonic frequencies, the layer absorbs the sound almost completely and can hide a non-bond.

Further examples of the situation in Fig. 29.5 b are various *metal claddings*, such as special steel on steel, silver on steel, *brazing* of steel or stellite to a steel base, as well as similar bonds between heavy and light metals produced by diffusion bonding or metal spraying techniques.

In addition there are the cases of *enamelling* onto metal and the bonding of porcelain to porcelain. In these cases of the echo sequence of the total layer predominates in the picture. If, however, the second material is not a layer and gives
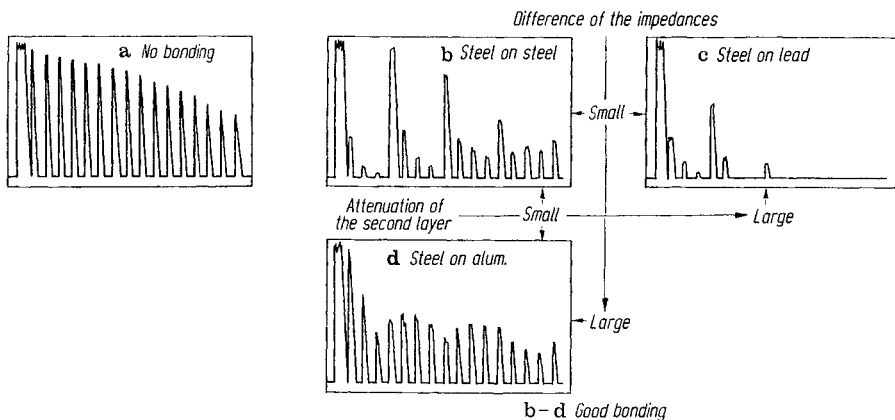
Fig. 29.5. Screen pictures when bonds are tested with the pulse-echo method. **a** No bond; **b** to **d** satisfactory bond; **b** and **c** bond with small difference in acoustic impedances; **d** bond with large difference; **b** and **d** bond with small attenuation in the second layer; **c** bond with high attenuation

no back-wall echo, only weak traces of the sequence a (Fig. 29.5) appear, the difference between good and bad being always very clear.

The case shown in Fig. 29.5c occurs in *homogeneous lead coating.* At low gains a satisfactorily bonded spot produces practically no echoes because the lead layer absorbs all energy. The contrast as compared with an unbonded spot then shows up clearly. The test is best made from the steel side and should be made from the lead side only if absolutely unavoidable. It is then helpful if the lead, by alloying it with antimony and tin, is harder and more transmissive than pure lead. Attention should then be paid to the echoes returned from the steel. According to [1285] a lack of bond is readily detectable, if necessary after the lead layer has been slightly heated and hammered.

Less clearly recognizable is the difference in case d. Since the two transit times are in the ratio 1:4, the various echo sequences partially coincide, producing a picture which may be very similar to that of case a (no bond) if the coupling fluctuates. In general, however, the difference can still be recognized by the mutual interference of the echo sequences. In cases b und d the close echo sequence may show maxima, as in Figs. 16.20 and 16.21, from which deductions can be made on the transmittance of the bonding layer. If the second material in case d is very light, e. g. foamed material, and at the same time the bonding layer very thin, the test is no longer reliable.

The old problem of testing the adhesive bond strength of a rubber/metal bond for example, which could not be solved using the above mentioned methods, seems now to have found a solution by a sort of attenuation measurement of low-frequency waves, called the "stress-wave factor" method (SWF). For details see Section 33.3 and [S 70, S 55].

For bonded laminar joints of parts with thicknesses of the order of a few millimeters and less, high frequencies (10 to 15 MHz) and shock wave probes must be used. Figure 29.6 shows an example of the type in Fig. 29.5b, but with lower amplification. The differences in the impedances between steel and copper as well as between copper and molybdenum are very small, so that from a good bond no echoes from the boundaries are to be seen. The good quality of both bonds is indicated by the rear echo from the complete sandwich, viz. from the rear face of the 0.5 mm thick molybdenum plate. The test has been performed in a mechanized device resulting in a C scan of the assembly as shown in Fig. 29.7.

In the chemical industry the masonry or concrete linings of some process vessels or containers are checked in order to determine whether the lining still adheres to the steel shell. A bonded, dry concrete lining can readily be distinguished from one completely separated when the test is made from the outside, by the higher damping of the echo sequence in the steel, but only very unreliably if the inside is filled with liquid which has penetrated into the gap. If the concrete lining is completely absent, this can sometimes be recognized by a back-wall echo being obtained through the liquid, from the remote side of the vessel, e. g. on steel pipes lined with a centrifugally cast layer of concrete. In another case such as the linings of cellulose digesters, penetrating acid corrodes the wall and these areas can be distinguished from those which are still protected, by the less distinct formation of the echo sequence from the steel wall.
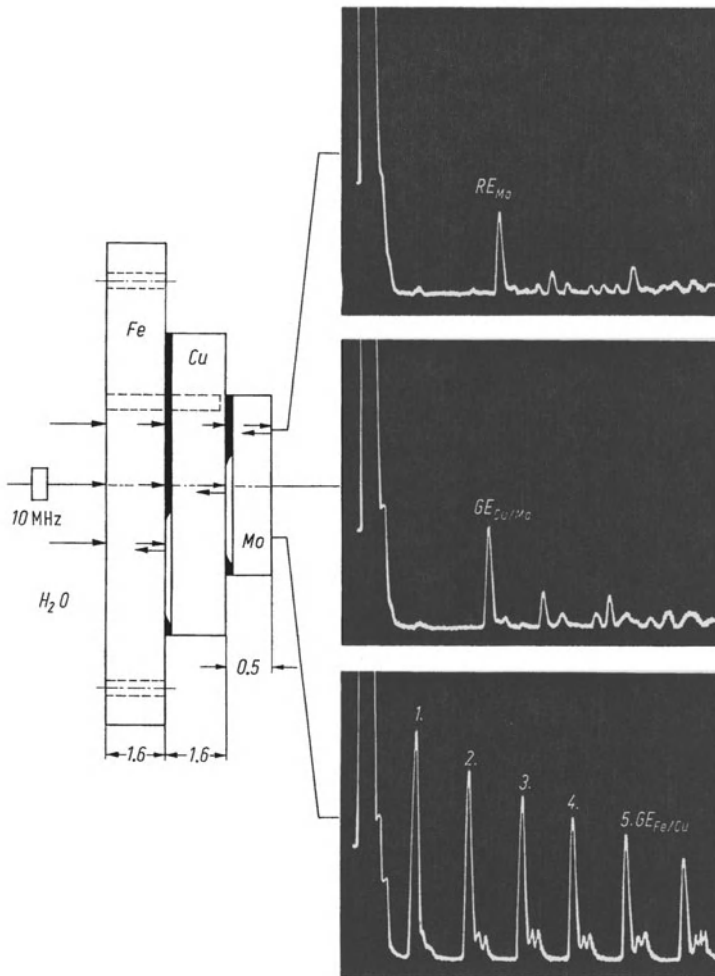
Fig. 29.6. Bond testing of supports for power transistors (drawing not true to scale): RE_{Mo} rear echo from molybdenum layer, GE intermediate boundary echoes
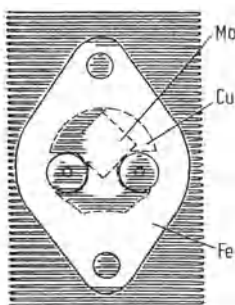
Fig. 29.7. C-scan record of the test in Fig. 29.6

Adhesive bonds of strongly absorbing layers on metal such as linings for brakes or clutches should be treated like rubber-metal bonds. When the echo method is used, they can be tested only from the metal side because of the strong absorption in the lining. Sound-transmission by immersion technique affords low frequencies.

An important application is the testing of adhesive bonds between thin sheets in aircraft construction. Here, it is required to distinguish the cases in Fig. 29.8 a to c (bad), from d (good). For the usual gauges of about 1-mm high-frequency contact probes are required.

It is easy to distinguish cases a and b from c and d. Case c, however, presents difficulties and one can decide on a purely empirical basis from the somewhat different screen traces or use the method of frequency analysis of the echo (see Chapter 19). For this purpose the old type of resonance wall-thickness meter has also been used. Depending on the special circumstances one obtains several resonance frequencies having different amplitudes. From these one can make empirical decisions based on the results obtained from test pieces. This principle is the basis of specially built bond testers [1511]. The use of frequency analyzers as auxiliary instruments to wide-band flaw detectors often allows much finer discrimination. See [1272, 1511, 1550a (with many further references), 1629, 1284, 927, 1164, 66, 227, S. 61, S 134]. According to [1673] SH-transverse waves have been used instead of longitudinal waves (see Section 2.4).

Honeycomb structures (Fig. 29.9), because of their high strength-to-weight ratio, play a considerable role in aircraft and rocket construction. They require the testing of bonds between the sheet skin (usually aluminium but also stainless steel, titanium or plastic) and the honeycomb core (usually aluminium, but also copper, steel or plastic). The bond usually consists of self-curing adhesives, or brazing for particularly strong constructions.

Although the honeycomb walls usually consist of only 0.1 mm or even thinner metal strips, they transmit ultrasound of considerably greater wavelength from one side to the other, and reportedly at 0.5 and 1 MHz even better than at higher fre-
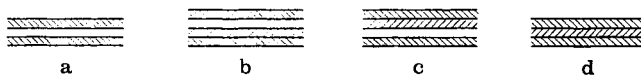
Fig. 29.8. Bonding test of bonded aluminium sheets. **a** to **c** bad; **d** good
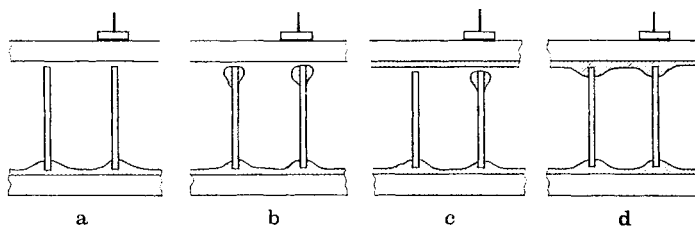
Fig. 29.9. Cross-section through honeycomb structure, schematic, with faulty and good bonding
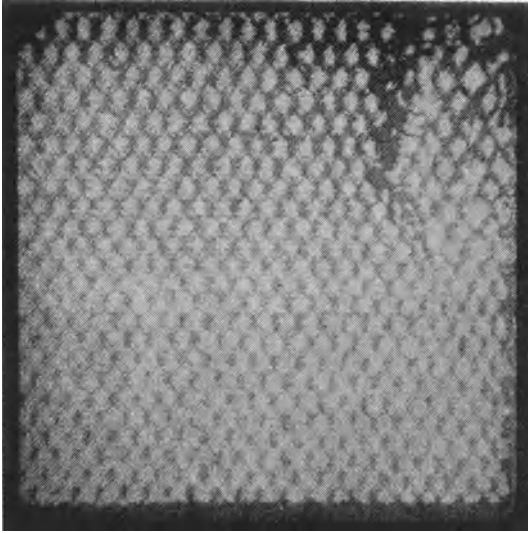
Fig. 29.10. Ultragraph screen picture of a honeycomb structure with defective bonded area (Automation Industries Inc. Pasadena Calif., USA)

quencies. One can thus use the immersion technique with sound transmission and still detect flawed areas of about 1 cm².

Using the echo method, with its usual resolution only cases a and b can be distinguished from c and d (Fig. 29.9). However, since it can be assumed that the condition in c occurs only rarely, this still permits safe differentiation between a good and a bad bond (Fig. 29.10).

Compound castings such as finned aluminium cyclinder-head castings with bonded cast iron lining can be tested from inside the cylinder by the echo method in an immersion technique.

The testing of the bonding of enamel-coatings is best carried out from the enamel side. It is sometimes also necessary to test for cracks in the coating. This can be achieved with an angle probe, for example for 70° in steel, swivelling into all directions because of the random direction of such cracks.

Electroplating is checked from the coating side, if a rear echo from the base object can be obtained. Otherwise surface waves can be used, giving echoes from non-bonded areas.

For further literature see [1586, 273, 692, 435, 1191, 1045, 1102, 149, 150, 1034, 472, 326, 808, 809, 458, 56, 65, 1586, 1191, 1045, 352, 273, 692, 435, 1173, 1464, 593, 1351, 1059, 713, 1388, 1267, 1248, 910, 1264, 1290, S 32]. For using high-frequency ultrasound to test thin soldered joints see [528, 537].

29.3 Laminates, Compound Materials, Composites

This group of materials includes many new examples which have found wide application in the aerospace and missile industries. They consist of metallic and non-metallic layers, including in the latter case composite materials such as fiber-reinforced resins using carbon (CRC), glass (GRC), boron or aramid fibers. For other filled plastics see Chapter 32. The sections to be tested can be from a few millimetres thick up to more than 100 mm and the areas involved go up to several metres square. As well as construction elements for air- and spacecraft with plane and curved shapes, tubes are also produced from these materials.

Possible defects include delaminations, pores, inclusions, cracks and gaps, also transverse to the main directions, which are produced by bonding faults, by insufficient resin, incomplete curing or lack of inter-layer adhesion. The attenuation in these materials is usually very high and can be as high as 1000 dB/m even at 0.5 MHz.

Because of their relatively low impedance plastic composites can also be tested by airborne ultrasound, using high power pulses of low frequencies [S 139].

In this application acoustic emission testing (Chapter 14) has also found application. During stressing fiber fractures and delaminations are easily indicated [1051, 1637, 583].

For measuring thicknesses as well as for angle-beam testing it has to be noted that these materials are usually strongly anisotropic [980].

Manual testing methods are mostly not economic. In practice large installations with mechanized scanning and full immersion techniques, or water-jet coupling with either vertical or horizontal jet directions, is the usual choice. The results are usually presented as C-scan recordings or further evaluation of the data is carried out by a computer.

The echo method is useful only with thin pieces. As a consequence of the low frequency which has to be used the resolution both laterally and in depth is poor. In this case through transmission is of advantage either using two probes, one on each side, or both on one side in a V configuration. One can also observe a rear-face echo or an echo from a reflector placed in the water behind the piece.

With curved complicated surfaces mechanized guidance in contact is less successful than water-jet coupling as illustrated in Fig. 29.11. In this installation large
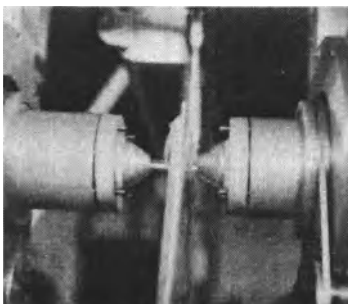
Fig. 29.11. The water-jet (squirter) probes of the test installation of the CANDET company, Toronto (courtesy CANDET)

aircraft parts fabricated from compound materials, or made of a honeycomb structure are tested in the vertical position using three pairs of water jets. The very stable water jets allow even echo techniques to be used. The testing speed is 0.3 m/s, and defects down to a minimum of 30 mm² can be recognized in a C scan recording of 0.9 m total width.

An installation of the Nukem company [905] uses an immersion technique with a horizontal position of the test pieces. The results from two groups of three probes which simultaneously test the structure and measure the thickness, are digitized for further data processing. By logarithmic digitizing very large ranges of signal amplitude are processed without changing the sensitivity controls.

From the computer memory, recordings are provided as required, either a B scan or an evaluated C scan. The computer also controls the probe guidance mechanism when non-planar pieces are to be tested.

For further installations of this kind see [246, 801, 594, 997, 419, 905, 1109]. See further for the general test problem [348, 256, 228, 347, 341, 804, 330, 988, 665, 1255, 1380, 288, S 176, S 62, S 28, S 5], for material attenuation [904, 626, 1567], for acoustic velocity [1322, 1323, S 85, S 60, S 174, S 144], for fatigue cracking in these materials [814, 1628] and especially for the heat shield of the space shuttle see [56, 65].

29.4 Bearing Boxes

On slide or shell bearings the bonding of the tin or lead-bronze liner to the steel backing has to be tested. If the bearing metal is cast-on it is readily penetrated by frequencies up to 5 MHz in the usual thicknesses of up to 10 mm. The bearing alloy has approximately the same acoustic impedance as steel, with the result that a properly bonded boundary gives only weak echoes. Sprayed metal coatings are also transparent but in thin layers only, for example silver of a few tenths of a millimetre thick in miniature bearings. Thicker layers cannot be tested therefore from the coating side.

The test of the bonding is usually performed with the echo method, as recommended in the paper ISO 4386 [1730] s.a. DIN 4386, p. 560.

If the shape, and the material, of the supporting backing member is favorable, the bond can also be tested using the echo from the bond and the back echo of the support. If the quality is to be determined without the use of a back echo, then a reference echo from a simulated test block which gives a back echo can be used after precalibration by destructive methods,

The backing members are usually of simple cylindrical shape, but with oil grooves and fixing flanges. For the test in immersion technique, two halves are fixed together on a turntable and mechanically scanned as in the installation shown in Fig. 29.12 which is a computer-aided system with full evaluation and recording [334]. Bearings of various types can be checked, axial, radial, segmented and combined bearings with either plane or dovetailed bonds. The device also serves to test the bearing material for pores and shrinkage, if sufficient extra thickness has been provided for the finishing operations.
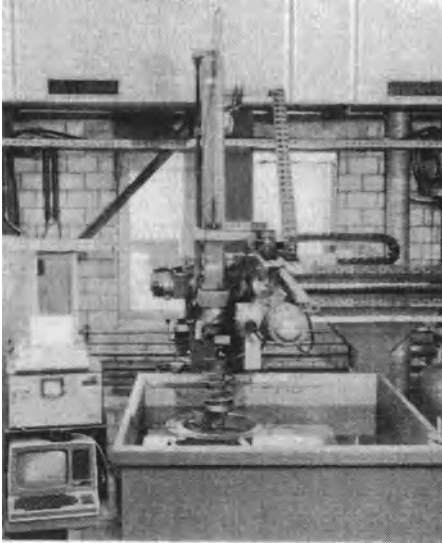
Fig. 29.12. Computer-aided immersion test installation for compound slide bearings (courtesy BBC company, Baden, Switzerland)

If large bearings with linings at least 4 mm thick must be manually tested, a contact probe using a shaped delay line is suitable [986].

Since standard probes cannot be introduced into small cylindrical bearings it is possible in this case to make use of a 45° mirror on the axis of the immersed bearing which deflects the beam onto the bearing surface in a radial direction and focusses it at the same time.

29.5 Shrink Fits

The transmittance of a boundary, separating parts of identical material but with no adhesive between them, depends on the ratio of the residual air gap to the wavelength (Figs. 2.3 and 2.4). Whereas the optically plane faces of precision gauge blocks become almost wholly transmissive if simply placed together without external pressure being applied, to achieve the same result if the surfaces are less perfect requires a substantial external pressure. Thus, the transmission or reflection at such a boundary can be used for determining the external pressure for a given surface roughness, e.g. for the general measurement of high pressures [840] or to determine the quality of a shrink fit between cylindrical surfaces [652, 653].

According to Fig. 29.13 the ratio of shrink-fit echo to back-wall echo where this exists, can be used for qualitative grading according to the following pattern:

1. Shrink-fit echo $\ll$ back-wall echo: shrink fit very good,
2. Shrink-fit echo $<$ back-wall echo: shrink fit good,
3. Shrink-fit echo $>$ back-wall echo: shrink fit moderate to bad,
4. Shrink-fit echo $\gg$ back-wall echo: shrink fit very bad.
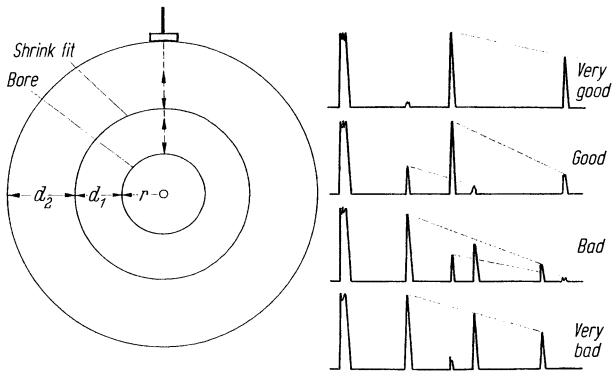
Fig. 29.13. Shrink fit on hollow core and schematic screen pictures (combination echoes have been omitted for greater clarity)

In the last case a long multiple-echo sequence from the shrink fit is obtained.

As far as any quantitative evaluation is concerned, it should be noted that both echoes are a function of the radius of curvature and the sound path. If one operates in the far-field of the probe, it is recommended that the multiplication factors be first determined from Fig. 3.13 so as to calculate the echo amplitudes for flat boundary faces. With these it is then possible to compare the shrink fits of differently shaped specimens if one also makes additional allowances for the distance dependence of the echo amplitude according to the DGS diagram. For instance, using flat plates one can calibrate the echo amplitudes empirically by applying different external pressures and calculating the results for cylindrical shrink fits of various shapes. If the surface conditions are approximately the same, the shrink-fit pressure can then be estimated in absolute figures. To exclude the influence of attenuation, low frequencies should be used.

In a shrink fit onto a solid cylinder, as shown in Fig. 29.14, the sound travels through the interface twice. The back-wall echo then appears as an echo sequence which may start with small echoes as in Fig. 16.22 and which has a maximum. The further back the maximum appears in this sequence, the greater is the reflectivity and the lower the quality of the shrink fit.
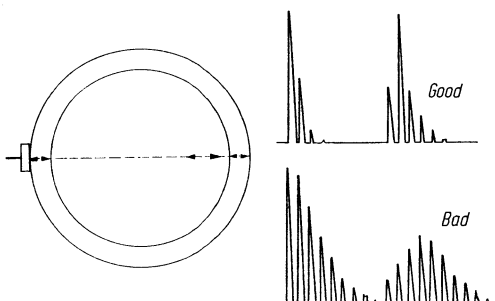
Fig. 29.14. Shrink fit on solid core and with relatively thin shell; schematic screen picture of good and bad bond

If oil has entered the interface, as may happen in the case of old shrink fits which have become loose, the transmittance is greatly increased as shown in Figs. 2.3 and 2.4, so that evaluation according to the above grading table may give misleading results. The evaluation should then be graded down by at least one step. To be on the safe side it is recommended that the oil be expelled by heating; cf. also [1359, 1252, 1358, S 114].

A new method for connecting tubes of several centimetres in diameter is the so-called Cryofit method in which a fitting sleeve of "Tinel" metal is slipped over the adjacent ends of the tubes. Since Tinel has the property of expanding when cooled this allows the sleeve to be fitted easily after cooling in liquid air for example, and thus giving a good shrink fit after regaining ambient temperatures. The subsequent shrink fit has been tested by Tsao et al. at 10 MHz [1541].

30 Nuclear Power Plants

Because of the very high safety demands for nuclear power stations all components of the primary circuit, including the reactor pressure vessel and the circulation system, have to undergo several detailed utrasonic tests. Before the plant is put into service the so-called zero test or "fingerprint" inspection is made. Additionally in-service tests have to be made in Germany of the pressure vessel every 4 years along with 50 % of the remaining components after the first 4 years and the other 50 % at the following in-service inspection, and so on. Other countries have similar specifications, corresponding wholly or in part with the German requirements (see Chapter 34). In several detailed specifications (rules of the Reaktorsicherheits-Kommission RSK [1745], of the Kerntechnischer Ausschuss (KTA) [1732] and DIN-Standards [1719]) the areas of application of the different tests are specified including the relevant sections of the components involved, the timing and extent of testing, and the techniques and equipment to be usded. Ultrasonic testing is specified as the basic method in these requirements.

Additionally the same components are inspected during manufacture by their manufacturer, the constructor of the power plant, and the Technischer Überwachungsverein (TÜV), all independently of one another. This three-fold testing has, however, in practice proved not to be justified [1540]. These production tests are also performed more and more using mechanized devices. For these developments see [1050, 1469, 1277].

The zero or base test provides full data on the initial state of the plant before it enters service. Later tests are compared with these initial results to reveal changes caused by the relevant service conditions.

In-service tests often have to be performed under so-called hot conditions in an environment of intense radiation levels so that they must provide for remote control and rapid mechanized testing procedures.

Short testing times are also desirable from the view of costs and in-service tests are frequently combined therefore with plant shut-downs for other operations such as the change of fuel elements. A complete pressure-vessel test including all preparation can take several weeks even utilising 24-hour working days.

In several countries remotely controlled test installations for nuclear power station components have been developed. We will first describe such developments in Germany and follow briefly with similar developments in other countries. The development has been mainly sponsored by governments and includes remote-controlled manipulators for probes, automated scanning systems, computer-aided data processing and computer software for on-line and off line processing of documentation, as for example B or C scan records. Some parts, for example the probe manipulators, must be designed to allow easy decontamination from radioactive material [S 115].

30.1 Reactor Pressure Vessel

The nuclear reactors used for commercial power generation in Germany are of the the light-water type, which means the pressure vessel is filled with ordinary water. Of this there are two different types, the pressurized-water reactor (DWR) and the boiling-water reactor (SWR) (Fig. 30.1). Within the complete primary circuit which consists of reactor pressure vessel, steam generator, pressure regulator and connecting pipes, the first mentioned is the most important from the point of view of testing. Figure 30.1 shows the two types of vessel which are welded together from many individual component parts. The inside surfaces are cladded with austenitic stainless steel several millimetres thick as a protection against corrosion.

30.1.1 Pressurized-Water Reactor

In this design the nuclear reactor is first removed from the pressure vessel and so it can be tested from inside using a full water-immersion technique but with probes
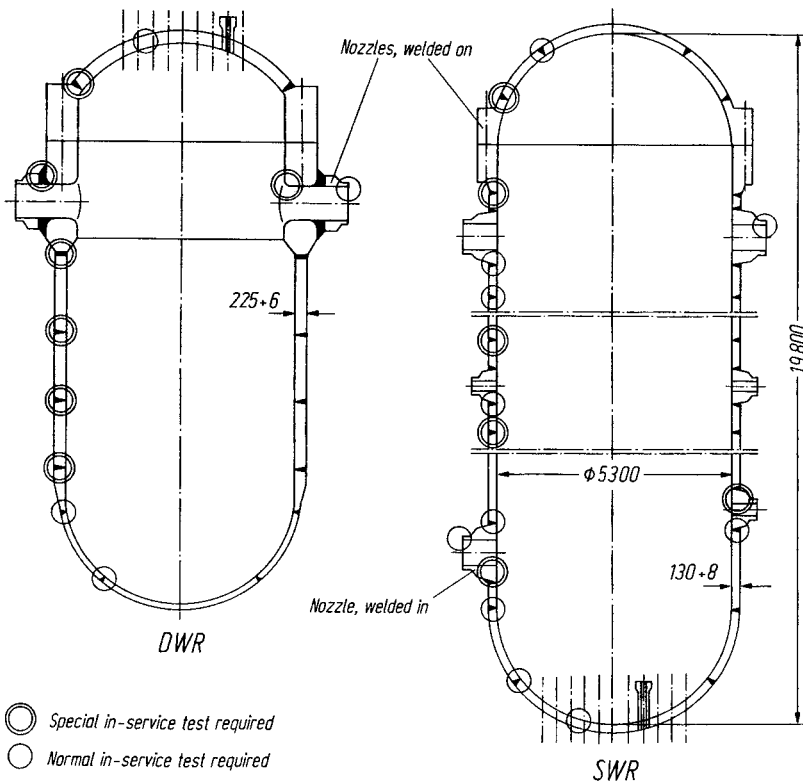
Fig. 30.1. Pressure vessels for pressurized-water reactor (DWR) and boiling-water reactor (SWR) of equal power (600 MW), older design, schematic. Testing zones circled
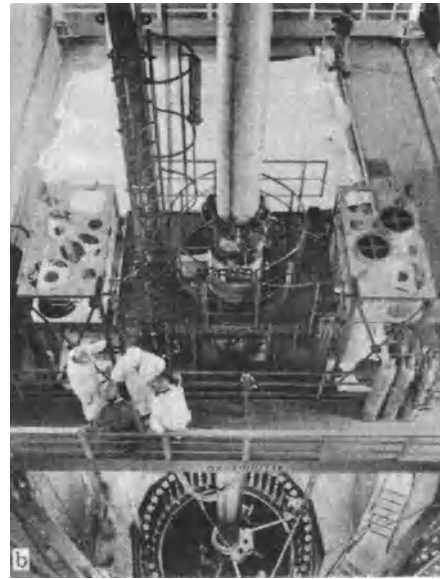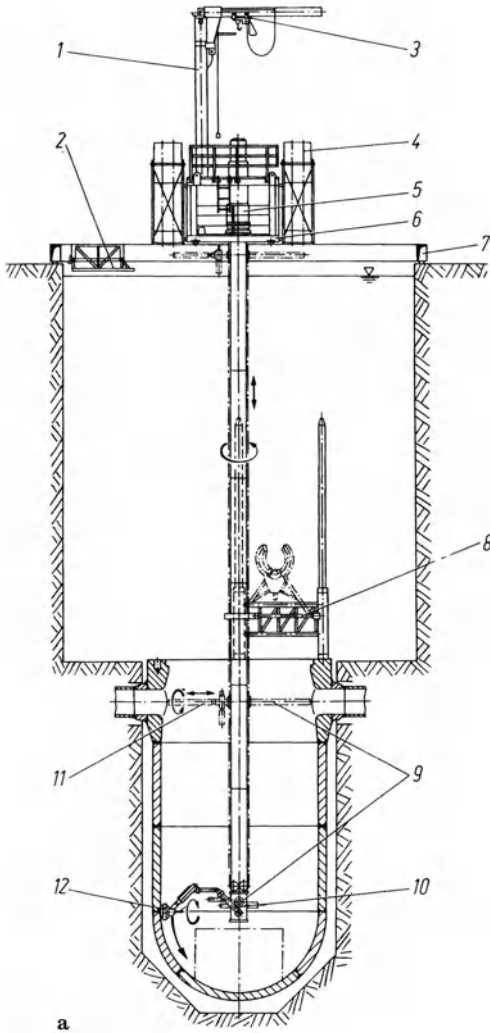
Fig. 30.2. Central manipulator for in-vessel tests of the MAN pressurized-water reactor. **a** Cross-section, schematic, showing *1* slewing column crane, *2* service trolley, *3* monorail-mounted crane trolley, *4* mast sections, *5* mast bearing, *6* cross bridge, *7* manipulator bridge, *8* mast-centering support, *9* telescopic tube, *10* swivel arm, *11* probe-system mount for cylinder and nozzles, *12* probe-system mount for the vessel base; **b** general view (courtesy MAN, Nürnberg)

in close contact with the surface. Figure 30.2 shows the manipulator mast for guiding the different probe systems which are fixed to different mounts for testing the cylindrical welds, the spherical-bottom circular weld and the various welded nozzles. The areas tested are scanned under water and therefore coupling is no problem. The cylinder cap and its fixing bolts are first removed and then tested separately (see below).

External vertical rails are also provided to allow additional testing to be carried out from the outside surface as is necessary for the BWR pressure vessel.

30.1.2 Boiling-Water Reactor

The pressure vessels have to be inspected from the outside surfaces, because it is not possible to remove the reactor from inside. Coupling of probes is carried out with running water, and a continuous coupling check must be provided therefore as distinct from immersion testing from the inside. For the cylindrical portion permanent vertical rails are fixed, on which a trolley can run provided with means for transverse/circular movement (Fig. 30.3). The probe system is mounted on the traverse travelling gear, the probes being universally mounted and arranged to meander-scan the surface. Formerly the trolley had to be transferred manually from one rail to the next, but in recent designs this has also been mechanized to avoid excess
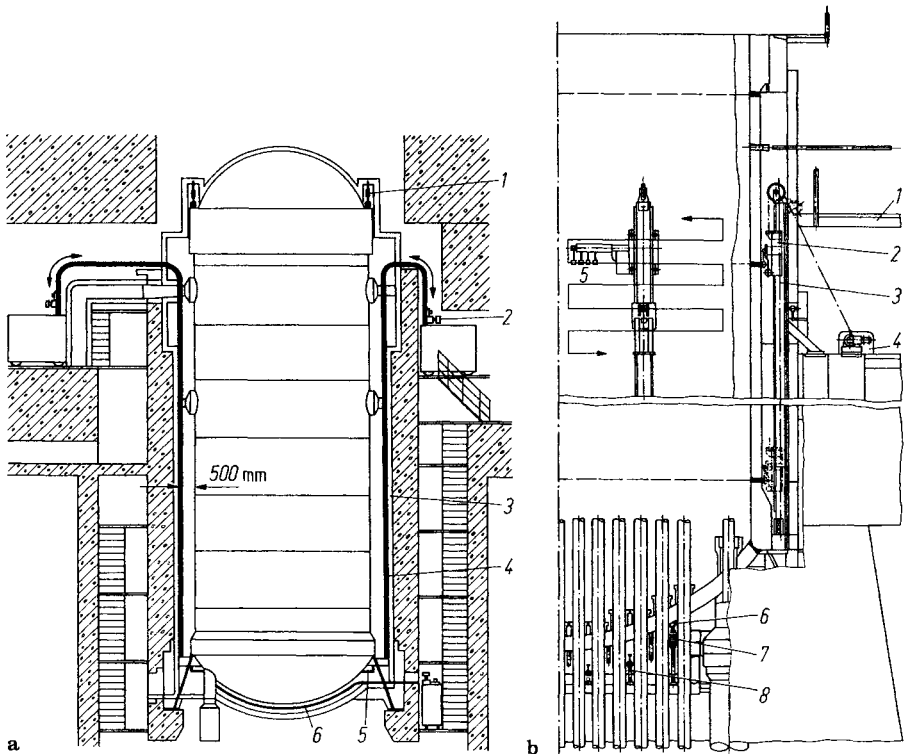
Fig. 30.3. Manipulators for the external testing of a boiling-water reactor vessel. **a** Design KWU, *1* manipulator for the screw bolts, *2* universal manipulator, *3* concrete shield, *4* longitudinal rails for circular- and longitudinal welds (flange seam, nozzle seams), *5* guiding rails for the base circular-seam manipulator, *6* bottom rail; **b** design MAN, *1* service platform, *2* testing trolley, *3* longitudinal rail, *4* lifting motor, *5* probe system, *6* probe for the spherical base, *7* testing trolley, *8* bottom rail

radiation exposure for the operator. This was possible only because now the gap between the pressure vessel and the concrete biological shield is wider. Additionally the nozzle welds are tested by very complicated manipulators also mounted on the same rails. The spherical base of a boiling water reactor (Fig. 30.3 b) carries many nozzles through which the control rods are guided. Probes for testing these run along rails fitted in the gaps between the tubing.

30.1.3 Cylindrical Portion of Pressure Vessels; Multi-probe Systems

The testing speed achieved on the cylindrical portion is about 50 mm/s with a positional accuracy of ± 2 mm. The distance between scanning paths is from 10 to 20 mm.

Figure 30.4 shows schematically the multi-probe system used for testing the cylindrical section of the pressure vessel, and especially the circumferential welds, including the heat-affected zone, for detecting longitudinal and transverse defects. The vessel wall, which can be more than 100 mm thick, is divided into separate testing zones, for application of single-probe and tandem-probe (pitch and catch) techniques. The central zones *2* and *3*, are tested using 45° transverse waves transmitted
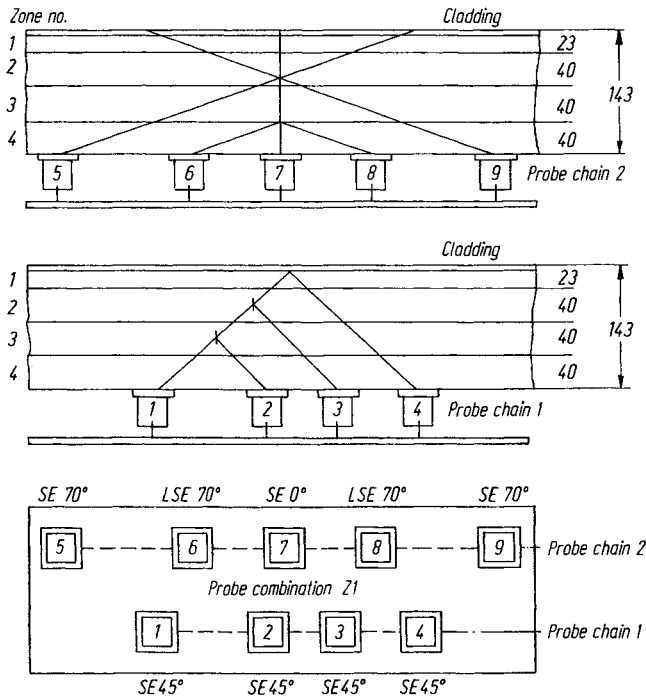
Fig. 30.4. Probe combinations, using two probe chains for testing the cylindrical section of a BWR pressure vessel from the outside (according to the test specification of the Hamburger Elektrizitätswerke for the Brunsbüttel power plant)

by probes *2* and *3.* Dangerous defect types which could be oriented perpendicular to the vessel surfaces, will reflect ultrasound via the back wall to the receiver *4.*

The recording limit is set as 6 dB below the echo from a 10-mm circular flat reflector.

The inner and outer zones are tested simultaneously using 45° transverse-wave probes *1* and *4*, working as transmitter-receiver. Possible reflectors not orientated in the perpendicular through-wall direction are found better by the single-probe echo technique. For the echo technique the recording limit is equal to a reflector 3 mm in diameter when the wall thickness is greater than 40 mm. For the pitch and catch-technique sensitivity see [882].

The outer near-surface zones *1* and *4* are tested with the echo technique at the half and the full skip distances for 45° using probes *1* and *4*. Additionally the layer near the probes is checked by using longitudinal wave TR-angle probes of 2 to 4 MHz (probes *6* and *8*). These probes detect under-cladding cracks when used from the inside surface (see below).

It is advisable to use additional angle probes, with angles other than 45°, especially for the central zones (70° probes *5* and *9*) as well as a normal probes (*7*) for defects lying parallel to the surface. Figure 30.5 shows one of these angle probes for thick welds equipped with a wear frame which provides a small water-filled gap at the surface. Its height depends on the surface quality and is different for the smooth outside surface and the more irregular cladding surface inside [1396].

When testing from outside, the cladded inner surface acts as a reflector for the pitch and catch technique. However, for inside testing it creates difficulties for the uniform propagation of sound. This interference is indicated by the variations in the through-transmission between probes *1* and *4*. The reasons for this are the irregularities of the cladding surface, of the bond line between cladding and basic plate and of its thickness. Additionally variations in the grain structure of the cladding and base material also play a role. The overall effect is that the sound field is disturbed, the attenuation varies and the axes of the beams can be deflected from their nominal position [1703, 1004, 1641]. To take account of these variations they are first recorded over a representative length and the values averaged, from which the additional gain needed is evaluated. This blanket correction means that about half of all amplitude measurements are under-valued and the rest are over-valued. A method which does not use a blanket correction for these disturbing influences, but applies a local adjustment is reported in [339].
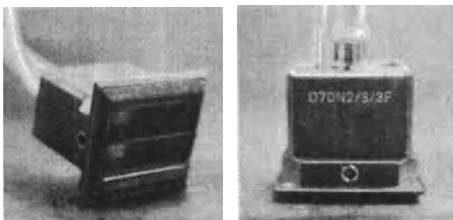
Fig. 30.5. Angle probe for thick welds
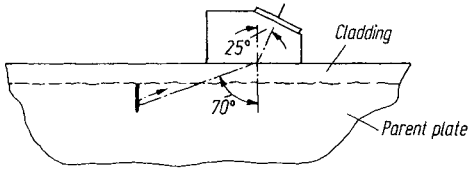
Fig. 30.6. Testing from the cladded surface for undercladding cracks with a longitudinal-wave angle probe

During testing, the V-transmission pulse is recorded continuously to indicate the point-by-point level of local variations and it also helps to detect very large defects by the shadow method.

The test of the zone near the cladding layer is especially hampered by the scattering from the austenitic structure, and by the surface form especially over the grooves between adjacent cladding strips. For the test of this region, where undercladding cracks can occur (Fig. 30.6) the longitudinal angle probe has been used successfully [871]. In recent years under-cladding cracks have been detected in several nuclear power plants [1312, 1281, 1220, S. 47, S 59].

The same probe and inspection technique can also be of value in the test from outside to detect subsurface defects, in addition to the test via a whole skip using 45° probes.

In a SWR the critical sub-cladding zone can only be tested from the outside surface by using the corner reflection with transverse waves of 45° or even higher angles to diminish the noise arising from the cladding structure.

For all these tests frequencies of 1 and 2 MHz are preferred since they have considerably lower fluctuations of through-transmission intensity [1004] and a lower noise level from the cladding. In addition the reliability of detecting obliquely oriented flat defects is higher [438]. Advantages of using higher frequencies are of course better resolution and location of defects, but detectability is better when using lower frequencies.
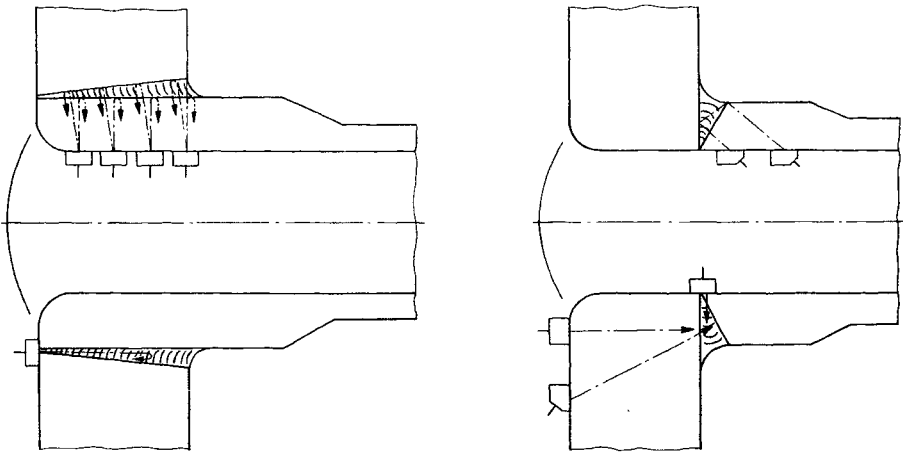
Fig. 30.7. Testing of nozzle welds

When probes are used in sliding contact with the surfaces and follow its contour the deviations of the beam are less serious than with fixed positions when mounted on a manipulator at a distance [1234]. In addition the influence of the water temperature on the beam angle is smaller when using a contact technique.

30.1.4. Nozzle-Weld Testing

For the testing of nozzle welds, probe combinations which are suited to the geometry are used (Fig. 30.7). The nozzle corners are the most critical parts of the pressure vessel because of the high local stress. They are tested with the longitudinal TR angle-probe technique from inside or with the single-probe echo technique from outside (Fig. 30.8) [643, 1647, 1219, 390, 1220, 1382, S 49, S 136, S 140, S 136].
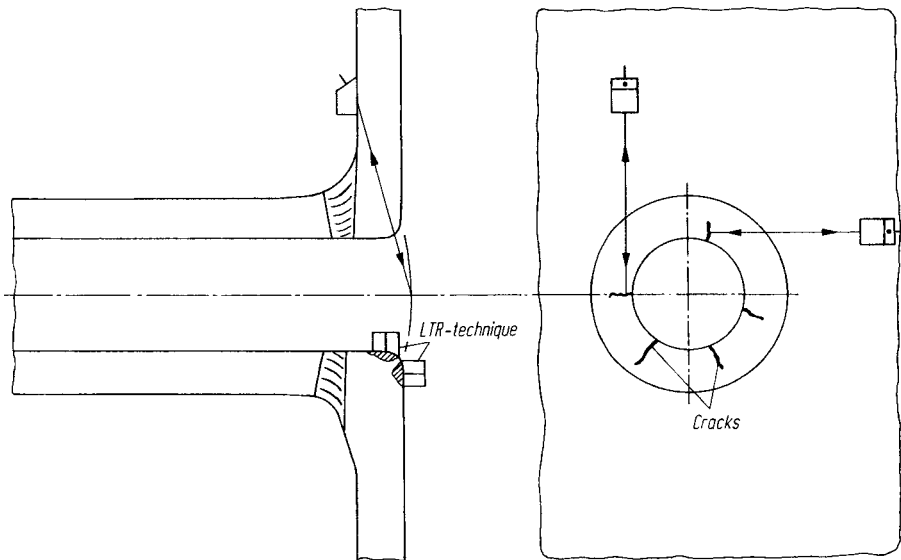
Fig. 30.8. Testing of nozzle edges using standard angle probes and longitudinal-wave TR probes
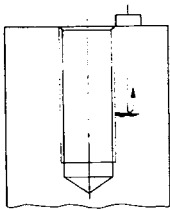
Fig. 30.9. Testing of a bolt socket
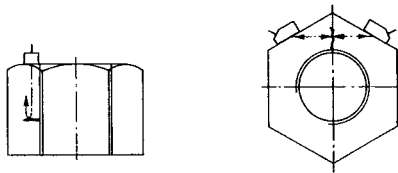
Fig. 30.10. Testing of a nut
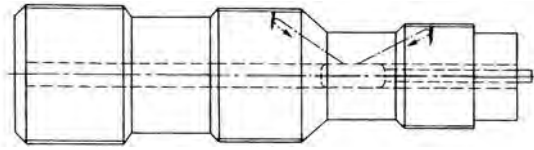
Fig. 30.11. Testing of a bolt
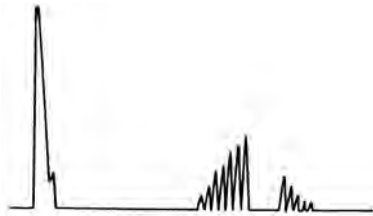
Fig. 30.12. Shadow effect on the thread indications

30.1.5 Bolt Sockets and Nuts

Figures 30.9 and 30.10 illustrate the practical techniques in use. Special probes have been designed for testing of the bolt-hole region of the pressure vessel as well as for the bolts and nuts themselves.

30.1.6 Testing of Bolts

As Fig. 30.11 shows fixing bolts are best tested using special probes from the inside of the axial borehole [1233]. The probes are of cylindrical shape and are fixed to a guide rod. They contain transmitter/receiver transducers for detecting cracks in the threads by the reflection of transverse waves using the corner effect. The optimum beam angle depends on the form of the thread. Larger cracks originating from the
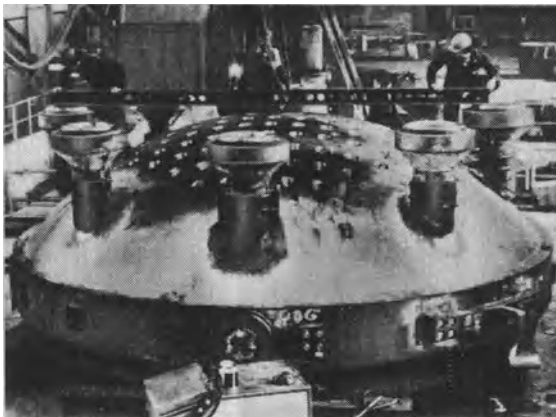
Fig. 30.13. Bottom of a SWR pressure vessel (inverted) during manufacture

root of the thread can also be detected by the shadow effect. As Fig. 30.12 illustrates the threads in front of the crack are clearly indicated whereas the ones immediately behind it are hidden in its shadow. See also [S 99].

30.1.7 Testing of the Perforated Zone

The bottom of the SWR and the cap of the DWR are spherically shaped sections with multiple perforations for the many vertical nozzles (Fig. 30.13). Their inner surfaces are also cladded and the areas between the nozzles are tested in the critical region near the cladding by using obliquely incident transverse waves from the outside surface (Fig. 30.14) [1394]. Here also the test is hampered by strongly scattered
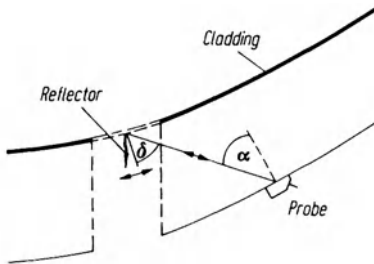
Fig. 30.14. Testing of the nozzle region
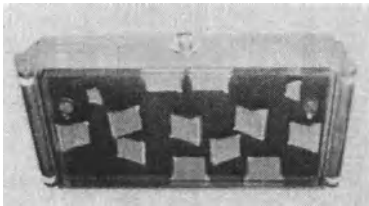
Fig. 30.15. Multi-probe combination for the spherical bottom of a SWR pressure vessel
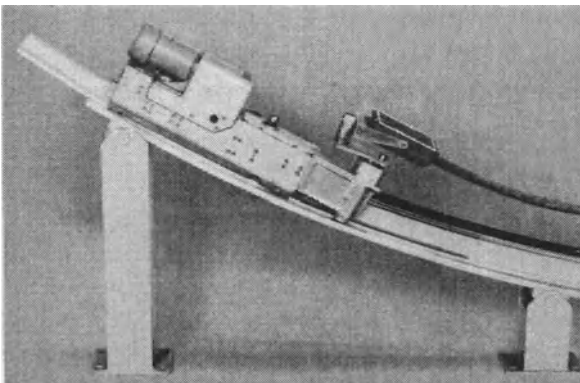
Fig. 30.16. Probe trolley on rail for testing the nozzle region (courtesy MAN)

sound from the cladding so that a frequency of 1 MHz is usually the optimum [1393]. For the choice of the optimum beam angle the bad accessibility had to be taken into account since the test head can only be manoeuvred in the narrow gaps between the nozzle holes. This fact and the complicated geometry which changes from point to point, necessitates a wide choice of probes with different beam angles and orientations, the angles being usually between 40° and 55° [1391, 1393, S 22].

Figure 30.15 shows an appropriate multi-probe combination, housed in a cast resin block which is fitted to the spherical curvature of selected gaps. The block is moved through the gaps by a motor-driven trolley (Fig. 30.16). See also [S 183].

30.2 The Electronic Equipment for Ultrasonic Reactor Pressure-Vessel Testing

A typical electronic test system for the ultrasonic test of the cylindrical portion consists of between 40 and 50 different circuits for test and control functions in each test cycle. They operate with many probe channels using multiplexing methods and in a typical design of Krautkrämer each channel can be programmed individually by digital instructions specifying each individual step (Fig. 30.17).

A cycle starts with the generating of a pulse, which is fed to the appropriate probe. A signal received by the same or by another probe is fed to a logarithmic preamplifier and then to the common main amplifier. It is then digitized by a 8-bit A/D converter. The 100-dB range of the combined amplifiers is divided into 256 parts so that all individual indications can be considered including even the noise from the material structure. Following the A/D converter a digitized A-scan display is available, which is obtained from the maximum amplitudes of the positive or negative half-cycles occurring in the HF form of the echo. Because the different probes corresponding to the various functions and cycles can have different sensitivities, they are equalized by individual gain adjustments. To each function belongs an individual gate position and a corresponding distance-amplitude correction is applied to it.

A similar series of operations follows for each individual probe channel and all the electronic data from each cycle are stored on tape together with the positional data of the mechanical probe system.

When all test and control functions have been completed the probe system is moved forward by 1 mm after which the next cycle begins. At a probe travel speed of 50 mm/s the cycle frequency must be 50 Hz. If one cycle contains 45 functions for example, the pulse-repetition frequency is $50 \times 45 = 2250$ Hz.

During each cycle one control function checks one transmitter or receiver, the result being stored and recorded. Unusual deviations from the nominally expected function generate an alarm signal (Fig. 30.17).

Finally an evaluation unit operates with the equipment which includes a computer and a printer for on-line evaluation. Since printers operate much more slowly than tape recorders some data reduction is necessary. For this purpose the primary amplitude data are subdivided into ten portions so that for each function only the maximum value of a selection of primary data sets is printed in which the number of them can be selected arbitrarily.

Figure 30.18 shows the complete system, but in practice each component is located at a different place during testing. The probe connection box is situated near the manipulator, so that for in-service tests it is within the irradiated area. It contains the pulse transmitters, the preamplifiers, the main amplifier and the A/D converter. The probes are connected to this unit by 35 m long HF cables.
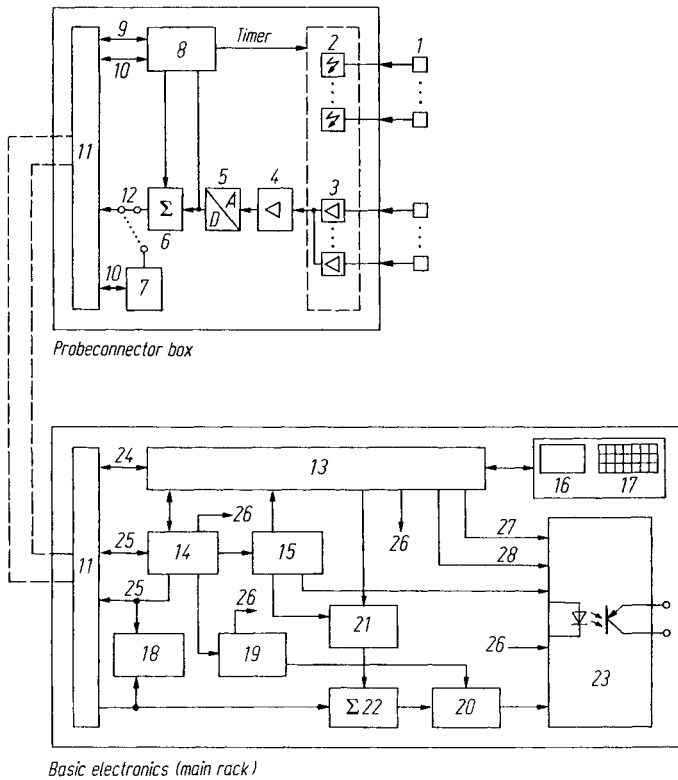
Fig. 30.17. Block diagram of a multi-channel electronic system for ultrasonic testing of nuclear power plants (Krautkrämer design). *1* probes, *2* pulse transmitters, *3* preamplifier, (logarithmic, dynamic range 100 dB), *4* main amplifier, *5* Analog/Digital converter, *6* adder (scaling), *7* line monitoring, *8* control unit (stability check, sensitivity compensation), *9* bi-directional data bus, *10* synchronization, *11* differential line drivers/receivers, *12* echo data, *13* central control unit, multiplexer, *14* trigger control pulse and pulse repetition rate, *15* transit-time unit, *16* display, *17* keyboard, *18* line monitoring, *19* gate unit, *20* maximum-amplitude determination, *21* DAC (distance/amplitude correction), *22* adder stage, *23* optocoupler, *24* bi-directional data bus, *25* synchronization, *26* external synchronization, *27* status, *28* cycle control

During in-service tests the basic electronics (main rack) is housed in an air-conditioned lift-van placed outside the reactor building. It is connected to the probe connection box by 150 m long cables for the controls and for the transfer of the digitized data. This method of transfer suffers much less interference than using analog methods. In the van there it also situated the data-recording unit, the evaluation unit, and the data printer.

More recently so-called active probes have been developed, which also contain the pulse transmitter and the preamplifier, and these units are much less subject to electrical HF interference. They will be working with the latest flaw detector, IM-
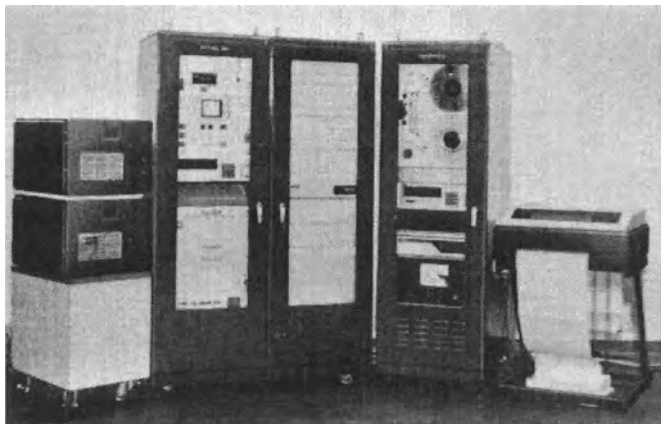
Fig. 30.18. Electronic system for testing nuclear reactor pressure vessels (design Krautkrämer)

PULS-1, of Krautkrämer. For the future highly flexible units (modules with intelligence, using a microprocessor for each module) will also be used for reactor testing exclusively.

30.3 Computer Evaluation

The full evaluation of the data from a complete reactor test must be carried out off-line because of its large volume. The evaluation programs process the data from the magnetic tapes into C scans of a series of selected depth zones. The indicated amplitudes are sorted into ten steps, which are finally printed by using different numerical symbols, resulting in an evaluated C-scan image (Fig. 30.19). The minimum separation of the screen dots is the distance between two adjacent measuring
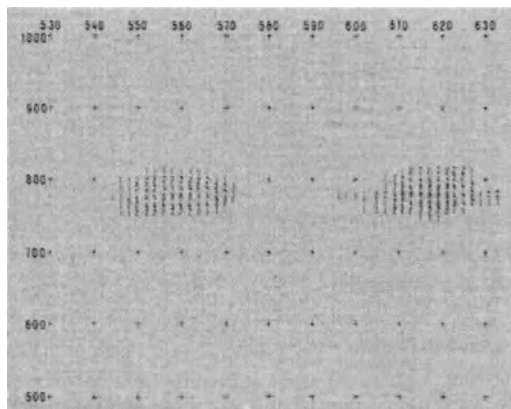
Fig. 30.19. Computer print-out of a digitized C scan from a reactor test (courtesy MAN)

points, for example 1 mm. For larger separations each printed symbol represents the maximum value of several points (Fig. 30.19). B-scans can also be printed, as well as statistical evaluations of for example the fluctuations of the through-transmission signal amplitudes acting as coupling control signals (event-occurrence distribution curve and summaries).

The complete results of the evaluation is called the classification atlas.

More details about the methods of evaluation used by the companies Hamburger Elektrizitätswerke and MAN is given in [590].

In the program of Kraftwerks Union (KWU) the total tested volume is divided into cubic subdivisions of $40 \times 40 \times 50$ mm. From the total of all indications from each test function arising from a particular cubic volume the average is taken, thus reducing the large number to one for each function. Only these average values are used as the basis of the classification atlas. This method is called TIM (Teilvolumen – Integrations Methode; partial-volumes integration method) [1581].

In all systems the base data are stored on tape and are available for later evaluation and for comparison with subsequent in-service tests.

30.4 Analysis of Reflector Types

The pressure-vessel inspections as reported above are often referred to as defect-search tests, because their function is to detect and locate the position of any defect [1392]. For subsequent analysis of the reflectors located other systems are used, for example using focussed probes or acoustic holography, see [397, 225, 459] and Chapter 13. Analysis here means evaluation of the defect shape, whether flat or voluminous [1297, 1362, 1397, 1432]. For measuring the defect depth see [579, 397], concerning the ALOK-method in nuclear power stations see [100, 102, 391].

30.5 Other Components of the Primary Circuit

The testing of welds in piping, pressure-control valves and heat exchangers has also been mechanized. For heat-exchanger tubes see [388, 638]. For the internal surface test of these tubes the eddy-current method is also applied, as for example in the combined probe in Fig. 30.20. For subsurface defects creeping-wave techniques are also used. As already mentioned these tests are often hampered by metallurgical structure as for example in austenitic welds [644, 642, 359, 358, 357, 1470, 540, 860]. Here also the systems P-Scan and Sutar (Section 13.12) find application. To reduce the exposure to radiation for operators permanently built-in rails have also been installed on components of the primary circuit [389, 439, 1221].

A special system has been developed for testing leaking fuel-element cans so that any water-filled fuel element can be removed and replaced. Figure 30.21 shows the principle schematically. A twin probe containing transmitter and receiver crys-
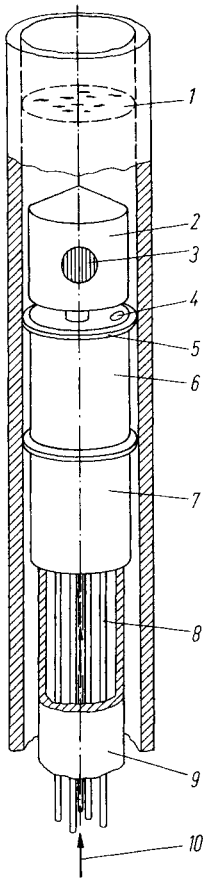
Fig. 30.20. Combined test head for testing heat-exchanger/steam-generator tubes. It contains both ultrasonic and eddy-current probes (design KWU Erlangen). *1* level of coupling liquid, *2* rotating probe head, *3* ultrasonic probe and eddy-current probe, *4* exit hole for coupling liquid, *5* guiding and sealing ring, *6* housing containing electric motor, bearings, gears, electric transfer elements (slip rings), *7* preamplifier, *8* control and test cables, *9* transport cable, *10* feed of coupling medium
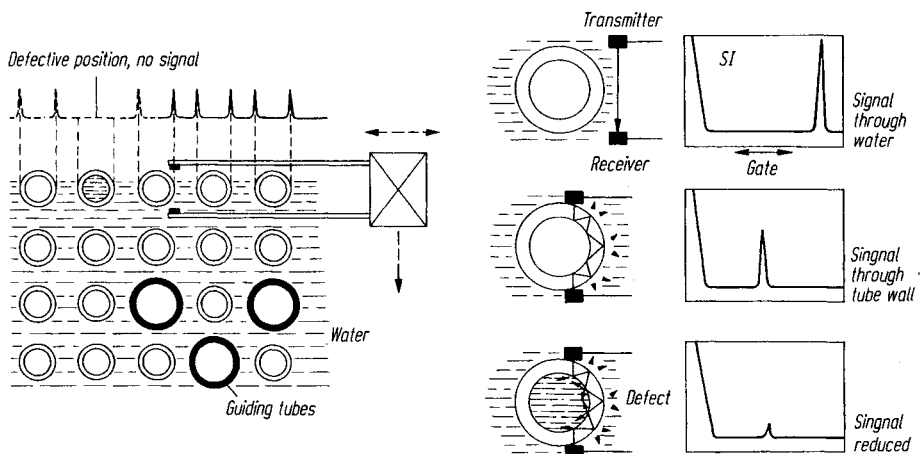
Fig. 30.21. Testing of fuel-element canning tubes (Braun-Boveri and Co. and Babcock Braun-Boveri Reaktor GmbH)

tals is slipped over the canning tube and if the tube is water-filled the through-transmission signal is strongly reduced. Each 10-MHz probe has a thickness of only 1.5 mm, to fit in between the tubes. Length scanning is carried out mechanically as well as the transfer from one tube to the next [1324, 108]. For further literature concerning reactor testing in Germany see [1650, 317, 1073, 1423, 340, S 83, S 48, S 12, S 22].

30.6 Testing of Nucelar Reactors in the USA

In the USA the production inspection of nuclear components is not subject to mandatory ultrasonic inspection. The zero test and subsequent in-service inspections are specified in the ASME Boiler and Pressure Vessel Code, Sections III and XI [1695, 74, 298] and in the Nuclear Regulatory Commission' Guide [1740, 231]. According to these specifications different angles of transverse waves have to be used, 45° and 60°, and 0° longitudinal-wave testing with single-crystal probes. Pitch and catch techniques are not required. These ASME specifications are widely applied in countries using reactors of US design and production. The specifications for in-service tests in the USA and in Germany are compared in [1540, 1539, 387].

In [686 and 251] systems developed in the USA for the defect search test of the pressure vessel are described, and according to [898] these can be considered as finalized. Later developments are concerned with the testing of other parts of the primary circit, for example nozzles and piping [926] and with the techniques of defect analysis, for example acoustic holography [683] and SAFT-UT [712, 504]. See also Chapter 13, and [1060, 296]. Pattern-recognition methods (partially with adaptive learning) are among the more advanced methods used, for example for nozzle-edge testing [1612] and for testing pipe welds [1293]. In [294] the use of EMATs (see Section 8.4) for the test of heat-exchanger tubes is reported. Other systems using phased arrays have also been developed for defect analysis [121] see Chapter 13. Concerning the state of the art for in-service testing of tubes in US nuclear reactors see [1065].

30.7 Reliability of Tests

In the USA a program has been established by the PVRC (Pressure Vessel Research Committee) to check the reliability and reproducibility of ultrasonic weld testing in nuclear pressure vessels. Several thick-walled test specimens have been specially manufactured for this purpose and these have been tested by several inspection teams for locating and sizing of the defects they contain. Eventually they have been investigated destructively [240, 1396]. In Europe similar investigations were commenced in the mid-1970s using three test plates from the second PVRC-program. This was the so-called PISC I program. Ten European countries have taken part

in this work [1145, 220, 1146]. The basis for these tests have been the specifications of the ASME Code, Section XI, for nuclear power reactor testing, but for comparison purposes more advanced techniques, such as pitch and catch and focussed probe techniques, have been used in the PISC I programme. The general results indicated that the existing codes could be amended to ensure that all important defects can be detected by all the inspection teams. For the PISC II programme see [S 119, S 71, S 41, S 63, S 140].

Further international programs including European countries, Japan, Canada and the USA, with the exchange of test specimens are in progress for the evaluation of the reliability of tests on thick-walled welded vessels. [240, 278, 279, S 42]. For national programs of similar scope see [723, 1480, 295, 128, 1069, 75, 1594, 316, 332, 1092, S 31].

30.8 Testing of Nuclear Reactors in Japan

Similar systems to those reported above are also in use in Japan. In [76] the relavant Japanes codes are reported. In addition it covers proposals for reactor designs which facilitate testing, and for the mechanized testing of DWR and SWR reactor vessels and other critical components up to 1981. See further [707] for the current status and development trends in Japan. For austenitic tubes in the primary circuit see [970]. See further [1484, 1408] for Japanese designs for mechanized testing installations, [1676] for pattern-recognition methods for nozzle-edge testing and [1148] for a comparison between destructive and non-destructive tests of natural defects in nuclear components.

30.9 Testing of Nuclear Reactors in Great Britain

Up to now no light-water reactors have been built in Great Britain for commercial power generation because the power industry has concentrated on heavy-water and gas-cooled designs. However, much development work has been carried out for the mechanized testing of nuclear pressure vessels and other components of the primary circuit, because the construction of pressurized-water reactors is planned. For a survey see [1118, 1117, 1417, S 31]. A system developed by the UKAEA (United Kingdom Atomic Energy Authority) called CIRCE [657], is similar in principle to the reported ones.

In [429] a system is described which uses a curved phased array to control the beam angle and for the sizing of defects transit-time methods are also used. In [255] a proposal is made to improve nozzle-edge testing from inside by separated transmitter/receiver arrangements using specular reflection from the faces of a radial crack and this is to be used in the PISC II programme [278].

Installations for remote controlled testing have been developed for some parts of the existing heavy-water reactors (e. g. for pressure tubings, [154]) as well as for

the gas-cooled reactor types Magnox and AGR (Advanced gas-cooled reactor). In a CEGB (Central Electricity Generating Board) report [384] a device for manual testing of welds in Magnox reactors is described including advanced on-line or off line data processing to produce transverse B scans, C scan and D scans (= longitudinal B scan) with colour graphics for the amplitude discrimination. For more details see also [730]. To measure the thickness of oxide layers in these reactors ultrasonic spectroscopy has also been used [1181, 1117, S 37].

30.10 Testing of Nuclear Reactors in France

For the testing of pressurised-water reactor vessels which are widely used in France immersion techniques are used from the inside, using focussed single probes [1313]. Using a central mast the probes are transported and guided without contact with the surface. The complete probe system consists of about 15 probes with different focus depths and beam angles. Defect search and defect sizing is thus performed by a single scan only. The system has been developed by the CEA (Commission a l'Energie Atomique).

Analog B scans are produced in real time and are also stored on video tape for permanent records [1304]. In addition all test data are stored in real time on magnetic tape, from which real-time C scans can be derived or produced for later evaluation.

A second fully digitized system has also been developed, consisting of the interface between ultrasonic equipment and the computer called STADUS, and the software for the computer including the evaluation units, called PRODUS [1311, 473, 1560].

[1564] reports on the important field of testing nozzle welds and edges, and [1537] on the test of austenitic welds with focussed probes by immersion techniques. [741] shows possibilities of improving the test of austenitic welds by pattern-recognition methods with adaptive learning. [894] reports on French standards for the production test of nuclear components.

In-service tests of heat-exhanger tubing is normally carried out with eddy-current methods. There are in addition specially designed rotating probes for ultrasonic testing from inside, equipped with the appropriate mirrors so that testing for both longitudinal and transverse defects can be carried out [1184, 499].

A recent description of French techniques for testing pressurized-water reactors is given in [1310].

30.11 Testing of Nuclear Reactors in the Comecom Region

In the USSR and other countries of Comecom great interest is shown in the fingerprint and in-service testing of reactor pressure vessels. As well as the single-probe techniques using different angles, similar to those mentioned above, pitch and

catch techniques also find application, to detect defects oriented perpendicular to the surface [1214]. In [565] there is a survey dating from 1980 with many references and for the latest state see [414, 648].

30.12 Testing of Nuclear Reactor by Sound-Emission Analysis

SEA (see Chapter 14) has achieved increasing importance, especially during the pressure test of the components of the primary circuit. Small leakages are easily revealed and sound emission can also be used to detect cracks by the emission of acoustic energy during crack growth. This principle can also be used in a permanent survey, for detecting a growing crack during service [1578, 372, 706, 1593, 373, 1671, 132].

30.13 Ultrasonic Testing of Fast-Breeder Reactors

In countries such as Britain, France and Germany, testing methods have been developed, or adapted, to solve fast-breeder reactor problems. The primary-circuit components in sodium-cooled LMFBR (Liquid metal fast-breeder reactors) are made exclusively from austenitic stainless steel, so that the methods mentioned above for testing austenite, such as TR techniques with longitudinal waves and shock-wave pulses, must be considered (see Section 28.1.6). For in-service tests the difficulties are increased by the fact that testing must be carried out at about 200 °C.

Suitable probes are reported in [1000] and for further information see [235, 1704, 1107, 1016, 1105].

31 Metallic Materials and their Specific Problems for Ultrasonic Testing

31.1 Steels

The Table of the sound velocities for different steels, published in the 3rd edition of this book, page 527, shows differences of less than 5 % for different states of working and for the various alloying metals no systematic influence can be recognized. The processing conditions such as heat treatment, hardening, quenching and cold working have a larger influence than the alloying elements. In general both longitudinal and transverse velocities as well as the attenuation decrease as a result of such processes. The deviations from the value 5.93 km/s for most practical applications can be neglected, but not if precise wall-thickness measurements are to be made. Care must also be taken when using angle probes because a change of only 1 % in the transverse wave velocity at a nominal beam angle of 70° causes a change of 1.5°. In critical cases, as for instance at the critical angles for the generation of Rayleigh or creeping waves, velocity changes must be taken into account, and in these cases the decrease of the velocity with temperature also plays a role [437, 1162, 450].

On thin sheets, the influence of texture makes itself felt. For zigzag transverse waves different acoustic velocities and sound attenuations are obtained in directions normal and parallel to the rolling direction. In the case of plate waves, this anisotropy manifests itself by the fact that an optimum excitation angle determined for the one direction is no longer valid for the other.

As a rule, in the forged or rolled condition almost all steels show satisfactory transmittance. However, a few high-alloy steels have a tendency to form coarse grains and this may show great differences between one spot and another, which can be explained easily by the fact that the scatter increases with the third power of the grain size. On the other hand some alloyed steels show exceptionally low attenuation which may also be a disadvantage in testing because delayed multiple echoes could produce phantom echoes (Section 10.2). To suppress this latter phenomenon, the pulse repetition frequency should be reduced. It has not yet been explained whether this effect, which is observed particularly in stainless nickel steels, results from the alloying and the fine-grained structure, or simply from the fact that these steels have fewer inclusions than ordinary carbon steels because of the clean melting in electric furnaces. Regarding austenitic steels, see Holmes [682].

By a suitable choice of probe and at very high gain, small impurities of a few tenths of a millimetre in diameter can be detected in steel. Thus appropriate evaluation makes it possible to check the whole volume of steel test pieces for minute inclusions (cleanliness), in contrast to the currently used, elaborate microscopic methods, which can cover only a particular cross-section. Regarding the develop-
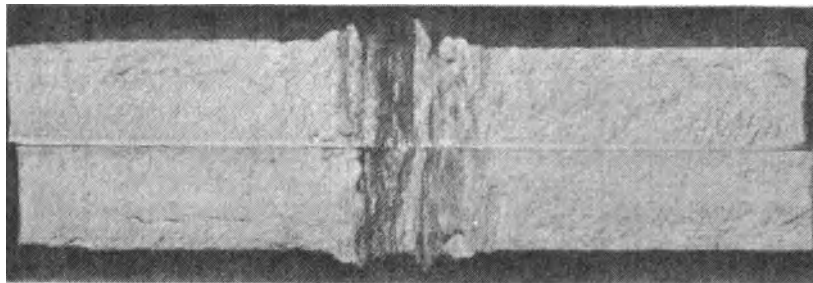
Fig. 31.1. Fracture face of a Cr-Mo steel showing fibrous structure which could not be detected by ultrasonics (according to Marianeschi)

ment of a method recommended by ASTM [1737] and the experiences made with it, see [1061, 1062, 267, 216, 217, 1334, 289].

When testing steel for inclusions and segregation, failures of the ultrasonic method are rare. Dubious cases usually arise when there are closed segregations which produce no echoes. In a few cases it has also been found that the cause was a pronounced banded structure which the destructive test interpreted as a flaw. Another case of a so-called fibrous fracture in forged Cr-Mo-steel blocks of 220 × 220 mm cross-section shown in Fig. 31.1 could not be detected even at 5 MHz. This concerned segregation of chromium oxide.

When finely rolled out, sulphide slag inclusions in steel plate cannot be detected reliably with ultrasound but they can result in reduced transverse tensile strength (lamellar tearing).

See further [1684, 342, 1157, 1435, 67] and on austenite see Chapter 27 and Section 28.1.6.

31.2 Cast Steel

Little is known about differences of acoustic velocities in cast steel. In the case of unalloyed and low-alloy steel castings the attenuation at 1 to 2 MHz is usually so low that specimens of thickness 1 m and more can be penetrated without difficulty. High-alloy cast steel, due to its coarse grain and the anisotropy of its structure, is difficult to test. Manganese-hardened steel, due to its extremely high acoustic attenuation can usually only be tested for coarse defects by the through-transmission method. For cast stainless steel see also [S 93, S 92].

For all types of cast metal is should not be forgotten that the attenuation is also partially influenced by genuine small cavities and impurities, so that the possibility of testing may depend on the metal purity and the method of casting.

For literature on cast steel, see Chapter 27 and [286, 1237, 787, 1485, 1486, 147, 1096].

31.3 Cast Iron

For defect testing, grey cast iron is not very suitable. Figure 31.2 shows how the attenuation caused by absorption as well as by scattering influences the ultrasonic test.

It is perhaps not surprising that the sound velocity, as well as the attenuation, varies within very wide limits if the different constitutions and casting conditions, with their consequences for the structure, are considered.

Frequency

6

4

2

1

0.5 MHz

| 0 dB | 20 dB | 55 dB |
| Gain → | (10 times) | (180 times) |
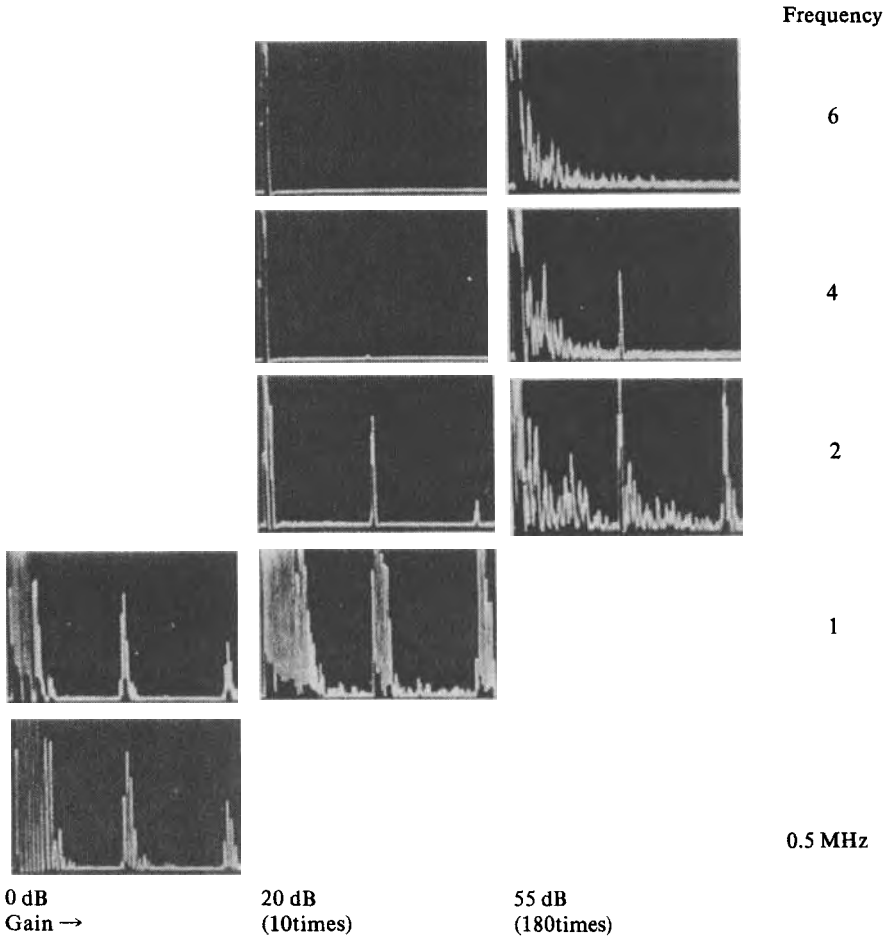
Fig. 31.2. Tests on cast iron 100 mm thick (ASTM 3–4) at different frequencies and sensitivity. All probes have been adjusted to the same echo height on a 30-mm steel plate at 0-dB gain. At 0.5 and 1 MHz the attenuation is of no consequence since a full back-wall echo is obtained at 0 dB, but with 2 MHz only at 20 dB, with 4 MHz only at 55 dB and with 6 MHz none at all. At this high gain (55 dB) the scatter at 2, 4 and 6 MHz is remarkably constant. The difficulty of testing cast iron thus arises from the attenuation and not from the scattering. With 0.5 or 1 MHz the dead zone of about 40 mm prevents flaw detection near the surface. The remedy would be by using a TR probe.

According to the form of the graphite, it is possible to distinguish between lamellar cast-iron (with plate-shaped graphite particles, cf. Figs. 31.8 a and b) and nodular cast iron (with spherical graphite particles, cf. Fig. 31.8 c). The latter can be produced also with an austenitic stucture. Table 31.1 shows the different qualities with their standard codes as used in various countries, together with their relevant tensile strengths.

We should also mention a special form, viz. *white cast iron*, which is obtained either intentionally or unintentionally by rapidly cooling ordinary gray cast iron and which is characterized by great hardness and brittleness. Its acoustic velocity differs only slightly from that of steel, and its attentuation, because of its relatively fine structure (ledeburite), is much lower than that of lamellar cast iron and approximately comparable with that of cast steel. It is produced intentionally in chill castings, for example rolls, providing a local hard surface layer (see below). Workpieces which have solidified with a completely white structure are usually unsuitable and these faulty castings can be sorted out readily on the basis of their ultrasonic properties.

Tabele 31.1

Grey cast iron

UK BS 1452/1977 (1961)	West Germany DIN 1691	France NFA 32-101	ISO R 185	U.T.S.[a] t/sq in	U.T.S. N/mm^2
180 (12)	GG 20	Fr 200	20	12	180
220 (14)	GG 25	Fr 250	25	14	220
260 (17)	GG 30	Fr 300	30	17	260
300 (20)	GG 35	Fr 350	35	20	300

Spheroidal graphite cast iron

UK BS 2789/1973 (1961)	West Germany DIN 1693/1973	France NFA 32-201	ISO ISO 1083/1976	U.T.S. t/sq in	U.T.S. N/mm^2
370/17 (SNG 24/17)	GGG 35-5	FGS 370/17	370/17	24	370
420/12 (SNG 27/12)	GGG·40	FGS 400/12	420/12	27	420
500/7 (SNG 32/7)	GGG 50	FGS 500/7	500/7	32	500
600/3 (SNG 37/2)	GGG 60	FGS 600/3	600/3	37	600
700/2 (SNG 42/2)	GGG 70	FGS 700/2	700/2	42	700
800/2 (SNG 47/2)	GGG 80	FGS 800/2	800/2	47	800

Austenitic spheroidal graphite cast iron

UK BS 3468/1974	West Germany DIN 1694/1977	France NFA 31-301	ISO 2892/1973	USA ASTM A 439	U.T.S. t/sq in	U.T.S. N/mm^2
S-Ni-Cr 20-2	GGG Ni-Cr 20-2	SNC 20-2	S-Ni-Cr 20-2	D2	24	370
S-Ni-Cr 20-3	GGG Ni-Cr 20-3	SNC 20-3	S-Ni-Cr 20-3	D2B	25	390
S-Ni 35	GGG Ni 35	SN 35	S-Ni 35	D5	24	370
S-Ni-Cr 35-3	GGG Ni-Cr-35-3	SNC 35-3	S-Ni-Cr 35-3	D5B	24	370

[a] Ultimate tensile strength
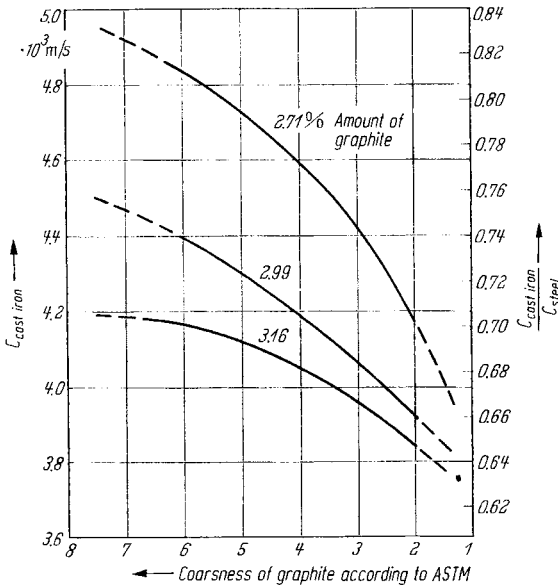
Fig. 31.3. Longitudinal acoustic velocity in lamellar cast iron containing graphite particles of different size and quantity according to Ziegler and Gerstner. The right-hand ordinate shows relative acoustic velocity referred to steel (5.95 km/s).

In *lamellar cast iron* the length of the lamellae, indicating the coarseness of the graphite, is expressed by code numbers from 1 to 8, corresponding to lamella lengths visible in micro-section in the range from 1 mm to 0.015 mm [1697, 889].

The relationship between the properties of cast iron and the acoustic velocities has been investigaged by Ziegler and Gerstner [1688, 525]. The dependence of the longitudinal-wave velocity on the *size and quantity of the graphite* is shown in Fig. 31.3, indicating that with decreasing coarseness and quantity it approaches that of steel. Since in fine-grain lamellar cast iron the amount of graphite is also usually smaller, the rule for practical purposes can be stated as, the finer the graphite the higher the acoustic velocity.

According to measurements by Patterson and Bodmer [1177] the velocity of the transverse waves is linearly related to the longitudinal velocity (Fig. 31.4), even if the spheroidal cast iron discussed below is included.

According to [1688] a second important correlation exists for the saturation of the cast iron with carbon, which can be calculated from the formula:

$$S_C = \frac{C}{4.23 - 0.312 \, Si - 0.275 \, P}$$

given the percentage content of carbon (C), silicon (Si) and phosphorus (P). According to Fig. 31.5 this correlation is given by a straight-line graph with a slight bend at saturation 1, and the method of velocity measurement can replace chemical analysis for rapid determination of S_C provided the shape of the test sample and
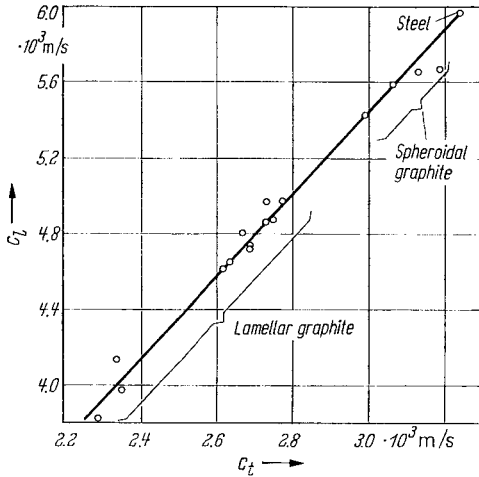
Fig. 31.4. Velocities of longitudinal and transverse waves in grey cast iron containing different amounts and forms of graphite, according to Patterson and Bodmer
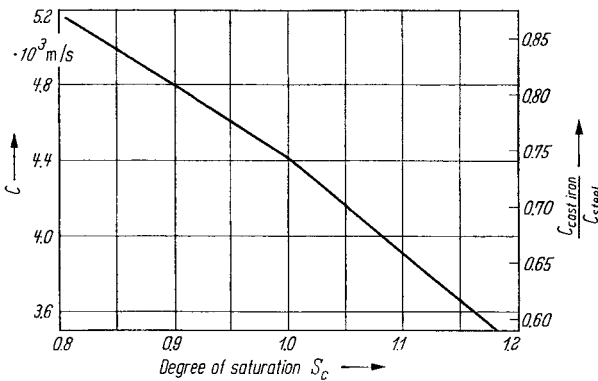
Fig. 31.5. Acoustic velocity of longitudinal waves in lamellar cast iron as a function of the degree of saturation of the carbon, according to Ziegler and Gerstner

the casting conditions remain constant. In this connection Frielinghaus [478] has established in addition a distinct influence of the wall thickness of the casting concerned which can be explained by differences in the cooling speeds which depend on the wall thickness and influence the structure, and therefore the velocity and the attenuation (see Chapter 27, Fig. 27.8).

Finally, the *tensile strength* is also a linear function of the acoustic velocity (Fig. 31.6), as long as the method of melting remains the same (for example medium frequency electric induction furnace or cupola). Surprisingly it is independent of the wall thickness and clearly the influences of both the size and the quantity of the graphite tend to cancel each other. In practice, it is of great importance to be able to measure the tensile strength at various points in a casting having different wall thicknesses, by determining the true thickness d mechanically and the apparent wall thickness d_s by means of an ultrasonic instrument calibrated for steel. The
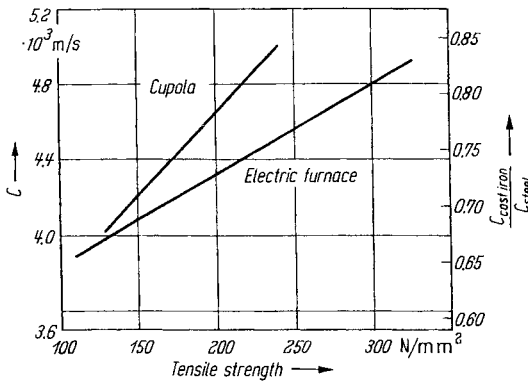
Fig. 31.6. Longitudinal acoustic velocity in lamellar cast iron as a function of the tensile strength, for melts produced in different types of furnace, according to Ziegler and Gerstner

ratio d/d_s (< 1) is also the ratio of the acoustic velocities $c_{cast\ iron}/c_{steel}$, shown in Fig. 31.6 on the right. However, according to [478] a slight influence of the wall thickness is detectable even here. Nevertheless, the relationship between acoustic velocity and strength when determined on similar work pieces has been found to be acceptable as a quality control check and even for acceptance purposes [1688, 98].

The *hardness* can also be related to the acoustic velocity and determined from it empirically if the other conditions remain constant, as confirmed by Thieme [1515] on chilled rolls for the average hardness of the core. Allowance must be made in this case for the very different acoustic velocity in the white iron shell.

In gray cast iron it is often important to be able to measure the wall thickness at mechanically inaccessible points, e. g. in cylinder block castings. However, since the acoustic velocity in turn depends to some extent on the wall thickness, this makes the measurement difficult. A linear relation exists (Fig. 31.7) which, however, depends also on the degree of saturation. Although the latter is constant for a given melt, as well as for the whole casting, it is not always known. To overcome this difficulty in practice one can measure the wall thickness mechanically at two accessible points where it differs as much as possible, interpolating linearly for the
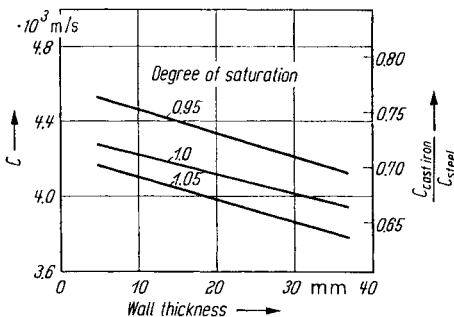
Fig. 31.7. Longitudinal acoustic velocity in lamellar cast iron as a function of the wall thickness at different degrees of saturation, according to Ziegler and Gerstner
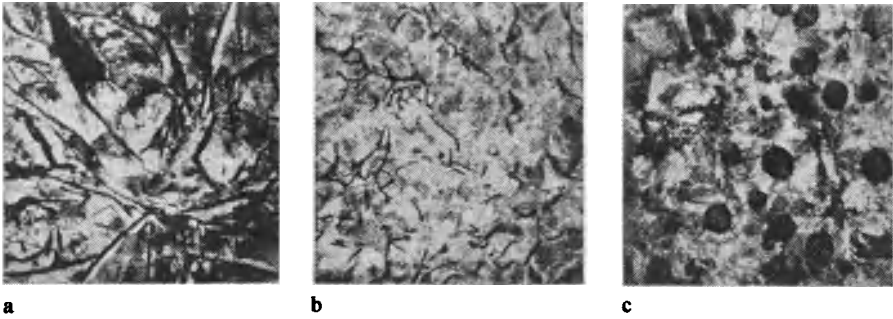
Fig. 31.8. Micrographs of cast iron with different graphite structures (Patterson and Bodmer), **a** and **b** lamellar, **c** spheroidal. **a** Structure A_1, 2.78 % graphite; **b** A_5, 1.7 % graphite; **c** 2.52 % graphite, wholly spheroidal

intermediate points. High accuracy is not possible, but not normally required. Where an error up to 5 % can be accepted, the influence of the wall thickness can be neglected completely if the instrument is calibrated at a mean wall thickness. Sometimes it is only a question of determining whether the walls of the cylinder bore are eccentric. This merely requires comparative measurements at various points with no definite calibration.

Spheroidal cast iron shows markedly different behaviour in respect of both ultrasonic attenuation and velocity, the reasons for which become clear when the microsections (Fig. 31.8) are compared. Even for almost identical total graphite content, as for instance in Figs. 31.8 a and c, the spheroidal form reduces the acoustic velocity to a far smaller extent than the lamellar form and has also a smaller influence on the sound transmission. According to [1688] the acoustic velocity is a unique measure of the ratio between spheroidal graphite and total graphite (Fig. 31.9) as long as the saturation remains constant. Since the latter is approximately known when making the cast, the acoustic velocity can serve as a measure of quality for
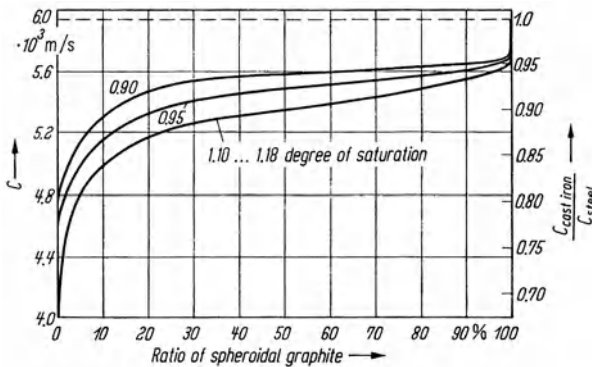
Fig. 31.9. Longitudinal acoustic velocity in spheroidal cast iron as a function of the ratio of spheroidal graphite to total graphite content, according to Ziegler and Gerstner

spheroidal cast iron. In the case of wholly spheroidal graphite the acoustic velocity is at least 96 % of that of steel, irrespective of the saturation, see also [S 81].

More accurate investigations concerning the graphite formation are found in [1374, 169, 1473, 497].

The acoustic attenuation of nodular cast iron in the frequency range normally used for metals testing is independent of the quantity and the size of the spherical graphite particles, and is determined by the structure of the matrix. It is small in the case of a ferritic or perlitic matrix, as commonly used in castings, but can be very high in the case of special castings with an austenitic matrix [481, 1196].

If it is desired to determine the tensile strength of high-quality grades of cast iron of either the lamellar or spheroidal type, on the basis of ultrasonis measurements, it has been shown [1622] that to a first approximation Young's modulus can be determined with sufficient accuracy on the basis of the longitudinal velocity alone. To deduce from this modulus the tensile strength is, however, not generally acceptable. This requires the determination of an additional quantity, for example an indentation hardness, and both measurements can be made on the finished piece [788].

The *attenuation* in grey iron castings also provides a useful possibility for the non-destructive determination of technological properties. Its measurement with satisfactory accuracy is, however, less simple than that of the velocity, particularly on the finished pieces because it requires parallel surfaces.

It has long been known that in general cast iron having tensile-strength values above 200 N/mm^2 is sufficiently transmissive for flaw detection, even at frequencies above 1 MHz. Conversely, the approximate tensile strength can be deduced from the attenuation. However, satisfactory calibration is possible only if in a test series all variables except one are kept constant. As an example, good transmission for flaw detection with 2 MHz can be expected for lamellar cast iron with code numbers above 4 which means having lamellae less than 0,1 mm long.

According to [1622] a correlation exists between the attenuation and Young's modulus in the case of high-quality cast iron with spheroidal graphite, which is independent of the heat treatment and the structure.

The difficulty encountered in measuring absolute values of the attenuation [851] does not prevent the establishment of quality-control checks on the basis of the decrease in echo amplitude of a given echo sequence, which is adequate for practical requirements. One can then use either sample blocks while keeping the conditions regarding dimensions and instrument adjustment constant, or alternatively one can test directly on approximately plane-parallel areas on identical castings with as-cast surfaces. In this way it has been found possible, for instance, to sort out under production conditions brake drums for automobiles according to their strength with an accuracy of ±20 N/mm^2, by empirically correlating the tensile strength to the ratio of the echo amplitudes of two chosen echoes cf. [1253, 1315, 1029].

Here, it should not be overlooked that such a simply defined *attenuation value* in addition to the true attentuation factor, is affected also by the probe because spreading of the sound beam also changes the echo amplitude. It is therefore not permissible to measure simply at different frequencies and deduce therefrom the

frequency dependence of the attenuation nor may different specimen thicknesses be simply compared with each other (cf. Chapter 33).

In addition, Frielinghaus has found linear relationships between the logarithm of the coefficient of attenuation on the one hand, and respectively the degree of saturation, the density and the tensile strength on the other. In all instances, however, the wall thickness appears as an additional parameter. Under certain conditions measurement of the attenuation, provided this can be carried out in practice in an acceptable form, may look more promising than measurements of the acoustic velocity [478, 490]. Zettler has also investigated the correlation between attenuation and the elastic properties of cast iron [1687].

In thick-walled castings the unavoidable different solidification times are responsible for structural differences between the surface and the core, which as a rule do not manifest themselves by distinct echoes during testing because the transitions are gradual. These differences are however, very pronounced if the specimen is tested parallel to the surface. The attenuation is lower, and the acoustic velocity higher, near the surface than in the central zone, because of the finer segregation of graphite which occurs during rapid cooling. Only in the case of chill castings where the choice of a particular composition and deliberately rapid cooling produce a layer of white cast iron near the surface, are the transitions so abrupt and the differences of the acoustic properties so great, that distinct echoes can be obtained from the transition zones, if tested perpendicular to the surface (Thieme [1515, 1689, 1217]). This fact has already been practically exploited for some time for measuring the thickness of the hard surface layer. The high transmittance of the white cast iron makes the use of frequencies up to 10 MHz possible. In the case of thin layers, less than 10 mm thick, the dead zone of a single probe frequently interferes so that the use of a TR probe is recommended.

Finally, of interest from a metallurgical point of view, is the fact that pig iron under certain conditions of production shows relatively good acoustic transmission, resembling in this as well as in other properties, good-quality cast iron (Stäger and Meister [1453]).

Lehtinen has measured the sound velocity also in liquid cast iron [911]; see further [53, 223].

31.4 Light-Metal Alloys

It is well established that for alloys of aluminium and/or magnesium, with small amount of heavy metals (less than 1 %), the anisotropy is so significant that the grain size has little or no effect on the testability in practice. Ultrasonic tests can be made readily in ingots which are continuously cast, in spite of the occasional occurrence of very large grain size. In contrast to steel, testing of highquality light-metal ingots can already begin as soon as they have cooled sufficiently. At this stage a transverse test using longitudinal waves can reveal gross defects, such as radial cracks in the core (spiders). On sawn sections approximately 1 m long it is possible also to detect small flaws, such as entrapped slag (dross) by testing from the cut
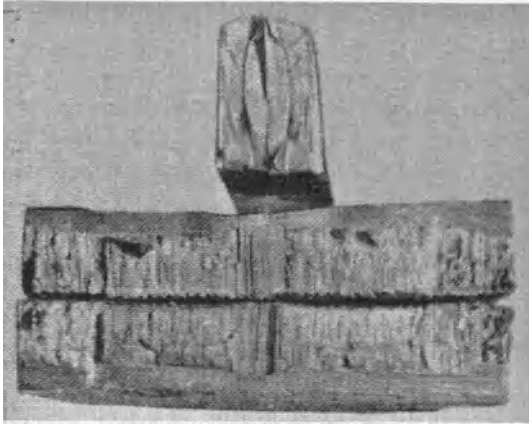
Fig. 31.10. Fracture specimens of extruded light-metal sections with flaws which cannot be reliably detected by ultrasonics. Above: rolled-out shrinkage in flat material (sealed lamination); below: fibrous fracture in 60-mm round stock

faces. Customary frequencies are 1 to 2 MHz. Since the outer skin on continuously cast ingots is very uneven but metallically clean, this is adequate for a rough test but occasionally it may be advisable to grind a few areas or longitudinal tracks. Very good tests can be made on the cast ingot after the rough-milling operation in preparation for rolling. However, the value of excessively sensitive tests is rather questionable because some small flaws are not found again in the finished product.

Failures of ultrasonic tests occur in the case of worked light metal more frequently than with other metals. Firstly, some flaws in spite of favorable orientation normal to the sound beam may be of considerably greater area than estimated by the DGS diagram or by a comparison with flat bottom holes, which is probably due to a certain transmittance of very thin slag inclusions when rolled out. Probably for the same reason it is sometimes possible to observe with ultrasonics rolled-out shrinkage cavities only up to a certain size, although the flaw is actually of greater length and is readily revealed by a destructive test (Fig. 31.10).

Similarly pronounced macro-segregations as in Fig. 31.11 cannot be detected with frequencies up to 5 MHz although the specimen concerned bursts even at moderate load. This particular flaw could only be detected at 10 and 15 MHz but
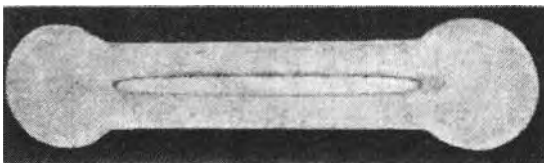
Fig. 31.11. Macro-etching of an aluminium section with a flaw difficult to detect (analysis 0.55 % Mg, 0.80 % Si, 0.33 % Fe, remainder Al) (natural size)

even then only by an echo corresponding to an equivalent defect of 1 mm in diameter. Higher frequencies are therefore preferable for detecting such flaws in light metal but a preceding heat treatment often helps a successful test.

When light metal of any given cross-section is extruded, it is of interest to detect the transition zone between the normal, fine-grained structure and the coarser structure with its inferior mechanical properties, which is sometimes encountered in the extrusion near to the end of the ingot. A very simple ultrasonic method can be used for this purpose in which the pulse-echo instrument as adjusted for a very long measuring range, e. g. 5 m, at high gain. The individual multiple echoes together with various transverse echoes, can then hardly be distinguished from each other (Fig. 31.12) but they form a *brush* the length of which gives an indication of attenuation which, despite being generally very small in light metals, gives marked differences between zones of fine and coarse grain.

Light-metal alloys with greater proportions of heavy metals differ considerably in their behaviour, particularly when cast. The casting method, whether by continuous casting, or casting in sand moulds or ingot moulds, as well as the cooling conditions, have also a great influence, which indicates that the anisotropy in some complex crystals is no longer negligible. No quantitative measurements are available of the attenuation and it is therefore only possible to draw attention to a few general points.

The common alloys produced for extruding and rolling have good to excellent transmission (at 2 MHz) even if they contain several per cent of copper and manganese. According to Stäger, Schütz and Meister [1452] the precipitation-hardening alloy Al-Cu-Ti (4.76 % Cu, 0.27 % Ti) when cast in sand shows low transmission even at 1 MHz. Strong scattering echoes may possibly result from segregations of copper, which still interfere considerably even after heat treatment. The Mg-Al-Zn-Mn alloy with 0.88 % Al, 0.69 % Zn and 0.17 % Mn behaves similarly. By contrast, Mg-Zn-Zr with 3.93 % Zn and 1.1 % Zr shows good transmission, at least when cast in an upright position although some of the zirconium is deposited as insoluble zirconium oxide at the grain boundaries. After heat treatment the attenuation usually decreases slightly, but in some cases it also increases, which would seem more logical, because effective heat treatment results in the segregation of the supersaturated complex crystals. Since the reasons for this behaviour are as yet obscure, it is not possible to draw any conclusions

a   b
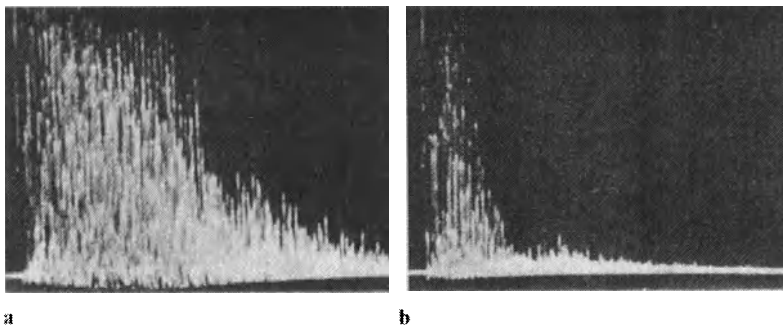
Fig. 31.12. The "brush" method for comparing the attenuation in similarly shaped specimens, applied here at a frequency of 4 MHz for testing the structure in extruded round aluminium bars of 80 mm in diameter. **a** In the normal state; **b** with a coarse structure

concerning the hardening and tempering from the attenuation. However, since it is of practical interest to be able to check this condition by non-destructive means, the measurement of the transverse acoustic velocity may turn out to be a useful method. In the case of the above alloys in the cast state this velocity is increased by hardening and tempering, in contrast to the longitudinal velocity which shows no clear change [1452].

The behaviour of the acoustic velocity of the longitudinal waves in light-metal alloys is still puzzling in some respects. While ordinary extrusion alloys, such as Al-Cu-Mg-Mn-Si (with 4.48 % Cu, 1.26 % Mg, 0.74 %Mn, 0.54 % Si) very closely approach the value measured in pure aluminium (viz. about 6.2 km/s) according to [1452], cast alloys show values some of which are considerably higher, while others are lower. According to [941] the longitudinal-wave velocity in the case of Al-Mg-Si with only 0.57 % Mg, 0.68 % Si, 0.74 % Mn and 0.20 % Fe, $c_1 = 6.72$ km/s in a continuously cast ingot, while the above-mentioned precipitation-hardening alloys if cast in sand have velocity values between 5.4 and 5.7 km/s which in addition distinctly depend on the wall thickness (as in the case of cast iron).

Since, therefore, the structure can have a considerable influence on the acoustic velocity, one must be careful in attributing any change of its value to a change on concentration of the alloying constituents. Lukas and Lutsch [941] have found in the above-mentioned alloy Al-Mg-Si an increase of 1.5 % from the core towards the periphery of a cast ingot and they suspect that this is due to an increase of the silicon from 0.54 % to 0.67 %. However, this seems questionable because this element does not change the acoustic velocity in Al-Cu-Mg-Mn-Si appreciably as compared with pure aluminium, and a quite considerable change of the acoustic velocity has been measured as a function of the grain size in pure aluminium, an effect which can also be assumed to be present in alloys. The change might thus also be explained by differences between the structure in the core and at the periphery.

The pronounced radial texture in continuously cast ingots has already been suspected of being the cause of curvature in the sound beam but this phenomenon can possibly also be explained by the side-wall effect.

For further information see [477, 839, 969, 1299, 1553, 376, 839, 425, 977].

31.5 Copper and its Alloys

Because of the anisotropy of copper, and particularly of its mixed crystals with zinc, the inspector using ultrasonics is particularly wary of copper, brass and bronze in the cast state.

Single crystals and very coarse crystalline material are, however, not particularly difficult to test. Extruded brass plates a few centimetres thick occasionally have clearly visible crystals with dimensions comparable to the plate thickness and the diameter of the probe. During scanning the clearly visible back-wall echo jumps back and forth by a multiple of its width, in accordance with the random orientation of the crystal being irradiated at that moment and the corresponding sound velocity. This demonstrates that the true absorption makes only a minor contribution to the total attenuation, whereas the main contribution in a polycrystalline material is the grain scattering.

As soon as the diameter of the sound beam has become wide enough to cover several adjacent grains, the testability becomes nil where small shrinkage cavities and gas pores up to about the size of a pea have to be detected. This therefore eliminates all untreated sand castings and die castings, and even continuously cast billets. Only for a grain size about 100 times less than that produced by means of

centrifugal casting, the cast structure again becomes readily transmissive and then it can be tested almost as easily as worked material of the same composition. This was confirmed by measurements of Stäger, Schütz and Meister [1453] on a number of copper alloys.

Reference [1453] also showed that suitable heat treatment to relieve residual stresses, below the recrystallization temperature, can slightly improve the transmittance of otherwise non-transmissive material, so that such specimens can possibly be tested for large defects. However, if prior to final working, for example conversion of copper into wire, or brass ingots into plate, a more accurate test is required, there is no alternative to performing this test after the early-rolling passes. The improvement produced is astonishing and the testability of the final product is no longer dependent upon the exact type of material. In the case of wall-thickness measurements it should, however, be noted that the copper alloys have a pronounced tendency to show a rolling texture. If the thickness calibration has been made on a section of one copper plate, gross errors in thickness may result if other plates are measured using this one calibration. The acoustic velocity changes from plate to plate can be very pronounced because of different textures. The instrument should therefore be adjusted directly on each plate to be measured.

The testing problems encountered on centrifugal castings are the detection of pore clusters (best achieved by using frequencies up to 5 MHz, testing from the machined surface and observing the disappearance of the bottom echo), and the detection of large pores and voids. They can be found only if not surrounded by clusters of micro-pores. The overall testability differs little from alloy to alloy, particularly for brass (Cu-Zn 72/28, 58/42, Cu-Zn-Pb 58/40/2) aluminium bronze (Cu-Al 92/8), German silver (Cu-Zn-Ni 63/25/12) and red brass (Cu-Zn-Sn-Pb 88/4/4/4). Concerning the ultrasonic testing of cast brass types Ms 70 and Ms 72, see [312].

For extruded copper as tubes or hollow sections intended for water-cooled electrical conductors, longitudinal cracks and changes in wall thickness are easily detected, as well as transverse cracks with a cup shape in drawn round stock. Rolled or extruded brass rods can readily be tested for core defects and cracks starting from the surface by the same methods discusses for steel. In order to keep interfering echoes on extruded material caused by coarse grain as small as possible, it is recommended to use only 2 MHz for the testing. A special defect encountered in the extrusion of brass is central pipe, caused by core defects in the cast ingot. Depending on the extrusion die, which may be single or multiple, this defect can occur either in the center or on the periphery of round stock (Fig. 31.13). These are separations which in the production of cartridge cases for example can lead to cracks in the wall. In the semi-finished piece this defect is sometimes difficult to detect be-
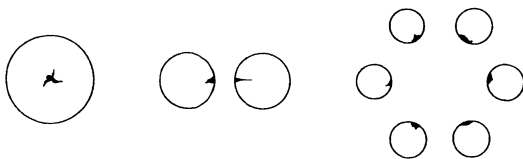

Fig. 31.13. Flaw positions in extruded brass rods, with single, double and sextuple dies

cause it has been rendered partially transmissive by the heavy working. The microsection then shows only microscopic discontinuous bands of inclusions which burst if stressed, clearly showing the nature of the defect in the fracture face. The best solution would be to test after the first working of the cast ingot which, however, is not always possible in practice.

31.6 Other Non-ferrous Metals

Where other metals are to be tested ultrasonically they usually present few problems in view of the relatively small dimensions concerned. Pure *lead* has a very high, true absorption, but lead alloys, particularly those with a few per cent antimony, are harder and more transmissive. When cast into double-walled steel casings used as biological shielding for reactors, it can be checked by an echo method if satisfactorily bonded to the steel casing. Thicknesses of 100 mm and even more can be tested from the outside to detect large cavities using a frequency of about 1 MHz, but smaller pores cannot be easily detected in such lead linings; see also [1636].

Cast *uranium* is markedly anisotropic and it usually has to be tested in the cast state, in the form of plates or rods. Since small defects are of little consequence, thicknesses of a few centimetres can be tested successfully by sound transmission in an immersion technique using 1 to 2 MHz. Sharpe and Aveyard [1404] have succeeded in displaying the structure of coarse-grained uranium by ultrasonics. Patel [1176] mentions a successful test of cast uranium rods using 2.25 MHz, and of rolled rods using 5 MHz.

Little is known of the precious metals *gold, silver* and *platinum* in the cast state, but if worked they are readily testable with frequencies up to 5 MHz. Silver contact rings for electrical machines have been tested for laminations and inclusions.

Zirconium and hafnium are used in nuclear engineering and they are already tested at the ingot stage. Zirconium ingots of 300 mm in diameter, and more than 1 m long, are tested by hand from the machined surface using 1 MHz, preferably with TR probes, so as to be able to detect flaws close to the surface [447, 1640]. Hafnium is made in smaller ingots of approximately 100 mm diameter, which can be tested by an immersion technique with 5 MHz after the surface has been machined [447]. In thin sheets both metals can be tested also at 10 MHz.

Zircalloy tubes, as used in the construction of reactors as canning tubes for fuel elements, must be absolutely free of defects. However, these tubes can be tested without difficulty in the immersion technique using the method described in Chapter 26.

Titanium finds increasing use in aviation engineering and is tested ultrasonically both as an ingot and as a forging for example as landing gear for aircraft, and gas-turbine compressor discs, almost as easily as light metals There are no problems with testing rods for core or welding defects; see [1490, 1558, 92, S 13].

Zinc and its alloys are relatively difficult to test because of their coarse structure and castings made from them are usually too complex and of little value. Door-lock

components made of zinc die castings for automobiles have been tested for porosity.

Tungsten in a dense, sintered state exhibits excellent sound transmission, but nothing is known of testing problems for which ultrasonics could be used.

Nickel and its highly heat-resistant alloys with chromium, aluminium and titanium (nimonic) can readily be tested after being worked (cf. Section 22.4, turbine blades), but in the cast state this is practically impossible. Blades with monocrystal structure, drawn from the melting charge, need no tests because they are always free of defects. Because of the anisotropy of the complex crystals, the formation of coarse grains during forging and also while in use is very troublesome. According to [1455] this phenomenon can be observed indirectly, both by the greatly increased attenuation and by the reduction of acoustic velocity.

Kleint and Johnson have reported on the testing of nickel alloys used in rocket-motor manufacture [800].

31.7 Sintered Materials

All sintered materials have a certain residual porosity, which may either be intended and desirable (sintered iron) or unavoidable during manufacture (tungsten, stellite), or often the result of wrong manufacturing methods (porcelain). Porosity increases the attenuation as a rule but the effect only becomes measurable at frequencies higher than those commonly used in materials testing since the small pore size must be comparable to the wavelength used. In addition, the acoustic velocity decreases, for which presumably the total pore volume rather than the number and size of the individual pores is responsible. This effect is therefore readily measurable at the usual testing frequencies. If all other conditions remain constant, porosity, and thus the degree of sintering, can be measured indirectly via the attenuation or the sound velocity [1200, 548]. In practice this method has so far been applied mainly to porcelain (Section 32.1).

In [S 132] a method is reported of measuring the elastic constants of powder metallurgical components by laser-generated ultrasonic pulses. See further [S 82] for sintered ceramics. For defects in powder metallurgical turbine parts see [S 50].

However, an apparent anomaly exists in respect of the sound velocity for sintered aluminium (SAP), which is practically free of porosity. Its $c_1 = 6.6$ km/s, which is very much higher than normal aluminium at 6.3 km/s.

Sintered aluminium transmits sound as well as ordinary aluminium, and sintered iron and sintered brass are sufficiently transmissive for testing purposes. Numerous small components made of these materials are tested by means of special probes for incipient cracks starting at edges. Nickel carbide, sintered intentionally in very porous form for use as electrodes, can be tested only at the lowest possible frequencies.

All types of *stellite*, consisting of tungsten carbide in a cobalt matrix and containing also admixtures of other carbides such as titanium and tantalum, are very

transmissive and can be tested easily. Occasionally internal cracks are detected which are clearly recognized by the greatly disturbed echo pattern they cause. Plates can be tested by contact using small probes and a high frequency. Since the acoustic velocity can vary markedly for different grades, manufacturing conditions and raw materials, valid deductions regarding porosity can only be made on the basis of the velocity in respect of a given batch. In addition larger and thicker pieces always contain local regions with dinstinctly higher attenuation. This does not necessarily indicate a material fault so that the ultrasonic test has gained little acceptance for this application. When considering echoes received from joints when larger pieces are made up by sintering together several smaller pieces, one must exercise caution because of possible differences in structure which cannot be regarded as defects.

Frequently brazed joints between stellite and steel are tested. If neither the hard metal nor the steel has an available contact face parallel to the brazed face, one can with advantage use the immersion technique by irradiating the brazed face perpendicularly using a refracted beam; see [1130, 1510, 1472, 1166].

32 Testing Problems on Non-metallic Specimens

For testing of composites see Section 29.3.

32.1 Ceramic Materials and Glass

The main application of ultrasonic testing for ceramics and glass material is that used for electrical insulators. The unfired porcelain blanks, the so-called slugs, as long as they are saturated with water, are sufficiently transmissive at frequencies of 0.5 to 2 MHz to be tested in thickness of a few 100 mm for larger voids and insufficiently bonded joints between two or more slugs. In practice, however, tests are not made on the material in this state and dried blanks are no longer transmissive. Densely fired porcelain, as far as transmittance and acoustic velocity are concerned, reaches values close to those for steel. Using longitudinal waves of 5 MHz and higher, 1-m lengths or more can be penetrated ultrasonically. Other dense ceramics used for insulators show similar behaviour, for example steatite, whose acoustic velocity exceeds even that of steel (see below) and glass has also very low attenuation and high velocity.

Typical flaws are shrinkage, cracks, inclusions and a capacity to absorb water. In addition cracks can occur under a metal cap, the so-called transverse core cracks, which result from tensile tests carried out on cap-type insulators. Composite insulators may also have bonding defects where the separate pieces are joined together.

Shrinkage cavities when they occur in porcelain, are usually not of spherical shape but appear as gaps extending in the longitudinal direction, sometimes twisted helically *(snails)*. These defects reduce both the mechanical and the dielectric strength and can be detected by the pulse-echo method using 2 to 5 MHz. On solid-core insulators the end faces prior to attaching metal caps can readily be used for contact testing, especially if they are prepared smooth and planar.

A longitudinal test in fact covers the whole core (the curved external extensions known as petticoats are not normally tested), but because of the long sound path and the unfavorable orientation of the common flaws, a transverse test is customary, at least as a confirmation. This also eliminates the troublesome secondary echoes arising in the longitudinal test from sound which somehow finds its way into the petticoats, particularly on hollow-core insulators with wall thicknesses of a few centimetres. In the transverse test a flat-faced probe is shifted around the circumference from point to point, and simultaneously moved back and forth as far as possible between the petticoats. Nevertheless, a small defect in the core directly under a petticoat, may occasionally be overlooked.

Mass-produced solid-core insulators can be tested for shrinkage, etc. on a conveyor belt provided they can be rotated around their axis. Instead of using oil as couplant, which subsequently has to be cleaned off carefully, one can use flowing

water fed directly to the probe. If the testing is well organized and depending on their size, up to 1000 insulators can be tested per day. One-piece rod-type suspension insulators, and hollow insulators, require more time and are preferably tested by rolling them back and forth on a horizontal surface.

A capacity to absorb water or *absorptive capacity* reduces both the mechanical and the dielectric strength in service. Porosity is undesirable but is dangerous only if the pores communicate and reach the surface. Since separate pores also occur, the designation "hygroscopic" would be more appropriate for a defective insulator than porous. At an early date it had already been suggested that the attenuation indicated by a sequence of back-wall echoes be used as an indication [524], but measurement of the acoustic velocity is more promising [1254, 109].

The *attenuation* can readily be checked qualitatively on a plane-parallel sample, using frequencies above 2 MHz, on the basis of the damping of the back-wall echo sequence, but on a real insulator, because of the unstable coupling conditions, this is possible only with very heavy porosity. There is also some evidence that sometimes a type of absorptive capacity is encountered which only slightly affects the attenuation but has a very noticeable effect on the acoustic velocity.

Figure 32.1 shows how according to measurements by Stäger and Studer [1454], and Ranachowski and Wehr, the acoustic *velocity* increases with the firing temperature, while at the same time the porosity decreases. Absorptive capacity is observed in the range which corresponds to too low a firing temperature. At very high temperatures the acoustic velocity again decreases slightly as a result of a certain increase in porosity, which since it concerns closed pores is harmless. According to Stüber [1479] densely fired porcelain has very different acoustic velocities which vary with the manufacturer (see table below):

	c_l (transverse direction) km/s	c_l (longitudinal direction) km/s	c_t (longitudinal direction) km/s
Porcelain I	5.60	5.80	3.52
Porcelain II	5.67	5.84	3.59
Porcelain III	6.11	6.18	3.68
Steatite	6.45	6.74	3.95

According to a VDE (Verein Deutscher Elektroingenieur) specification the fuchsine pressure test is used as a detecting method on fragments on which the effect of a methyl-alcohol fuchsine solution applied under pressure is observed. For qualitative tests the fragment is then washed and again broken. Sound material should reveal no internal staining. The quantitative determination of the absorptive capacity, as in Fig. 32.1 involves measuring the increase in weight of a small test block.

The permissible velocity values when used for porosity measurement can therefore be determined only for each individual case. Based on investigations by the Deutsche Bundesbahn on almost 100 000 contact-wire insulators [1478], these limits are fixed at about 0.25 km/s below the values quoted above. With this object in mind it is important to measure the acoustic velocities consistently in directions either crosswise or lengthwise with respect to the insulator. The values show that
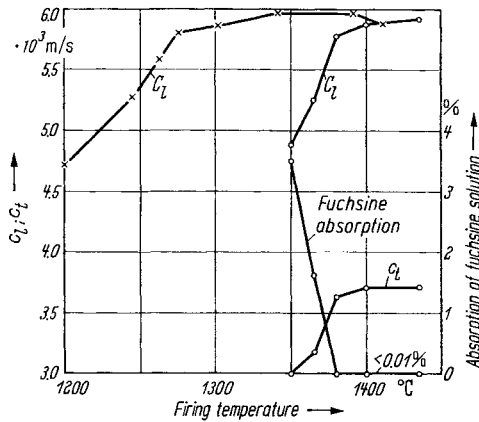
Fig. 32.1. Acoustic velocity and porosity of porcelain versus firing temperature. ——o—— Measurements by Stäger and Studer, ——×—— Measurements by Ranachowski and Wehr

the latter is usually a few per cent higher, possibly because of a certain anisotropy resulting from the working during extrusion of the material [1609]. The measurement is in fact usually made in the transverse direction because any localized absorptive capacity, near the end of the insulator, fails to be indicated when the measurement is made in the longitudinal direction, because of the averaging effect over the full length; see [1406, 53].

Cracks and fissures in the insulator, as well as in the glazing, caused for instance by internal stresses or damage, can be detected by their echoes only when irradiated perpendicularly, because of their very smooth surfaces. In the cylindrical wall of hollow insulators they can be detected as in tubes, by using zigzag transverse waves if, during scanning, the sound beam is swung through a wide angular range. Even fissures affecting only the glazing are indicated but these are also readily detected by surface waves. In one case (Fig. 32.2) oblique cracks in the neck of a hollow cylinder had to be detected, the test being possible only from the end face because of the rough surface of the barrel. They remained completely invisible with parallel beams and only after a probe of small diameter and low frequency was used could they be detected because they were then irradiated perpendicularly by part of the wide-angle beam; see also [778].
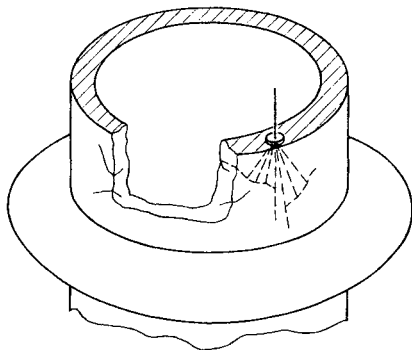

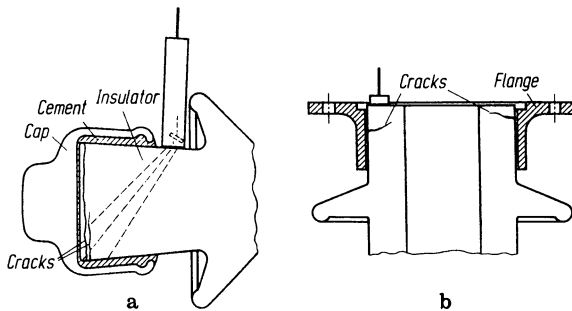**Fig. 32.2.** Cracks in the neck of a hollow insulator

Fig. 32.3. Testing for cracks under the cap. **a** On solid-core insulators; **b** on hollow insulators

Cracks under the cap often occur in solid core insulators (Fig. 32.3 a) or in hollow insulators under the flange (Fig. 32.3 b) if they have been over-loaded during a tensile test. When in service, the stress on the reduced cross-section then leads to further cracks and finally even to a complete break.

Bonding defects on cemented areas of larger pieces can be detected individually by the echo method although the flaw echoes are often difficult to distinguish from the secondary echoes received from the petticoats. Unfortunately cemented areas often produce pronounced echoes at points where a destructive test reveals no significant flaw. According to Weyl [1609] these are caused by a pronounced anisotropy in the structure of the bonding compound but with some practice they can be distinguished from true flaw echoes.

Various specifications have already been drawn up on the testing of insulators with ultrasound cf. [630].

For high-grade special ceramics used for example for turbine blades the defects to be found are so small that they cannot be detected by the conventional frequencies. This is a task for ultrasonic microscopy, see (Section 13.13) [1129, S 120] and high-frequency pulse-echo testing [310, 1257, 1574, S 190, S 51].

In the case of *glass*, the only practical testing of interest is the measurement of the thickness of large plates and this presents no difficulties using either the resonance or the echo method, provided the glass is not too hot.

Junke [738] mentions investigations on safety glass, based on measurements of the acoustic velocities of longitudinal, transverse and plate waves, as well as on measurements of plate-wave amplitudes, in order to obtain information on the fracture behaviour [1690, 1591, S 190]. For older literature see [27, (Section 0.21)].

32.2 Plastics

In view of the wide range of different materials which come under this collective heading the attenuation of ultrasound, which determines the testability, extends from the medium values applying to solid materials without fillers, such as acrylic resins (perspex), ethoxylene resin (cast resin), polystyrene, polyamide and teflon, to

the very high values of the soft varieties of polyethylene (PE), polyvinylchloride (PVC) and polyisobutylene (Oppanol B). The latter group are excellent sound absorbers even at the lowest frequencies used in materials testing. The hardness of a given plastic, unless this has been achieved by fillers or plasticisers, is thus an approximate measure of its testability.

The fact that the semi-solid state shows greater attenuation than either the liquid or the solid state can be observed clearly during the curing of cast resins. After the hardener has been added, the cast resin at first still shows good transmission and this can be observed on the CR screen with a layer a few centimetres thick. When the material starts to set the back-wall echo decreases. Especially in cases where reaction heat is generated the echo can often no longer be observed even at higher gain, until it reappears after curing, at a shorter transit time as a result of increased acoustic velocity.

Among the testing problems encountered on semi-finished plastic material may be mentioned the detection of bubbles in extruded polyamides and teflon. Solid cylindrical stock of diameters up to approximately 100 mm can be tested at approximately 1 to 2 MHz by the echo method with direct contact. The limit of detectability is reached with bubbles of approximately pea size and central piping of about match size. Water or oil is used as couplant and even in the case of a sliding contact the wear of metallized probes is insignificant [555].

Usually, however, TR probes are used due to their superior near-surface resolution in thinner material, particularly in the case of testing frequencies of 1 MHz and lower. As an example of the possible flaw detectability it should be mentioned that in polyethylene rods of up to 150 mm in diameter, 1-MHz TR probes can detect flaws with an equivalent reflector size of 0.3 mm in diameter.

Compared with metals, the immersion technique here offers still better sound transmission, with lower reflection losses and less deflection and splitting of the beam on curved surfaces. Longitudinal waves are better used in the specimen, even at oblique incidence, because transverse waves are usually strongly damped. In this way it has been possible, for instance, to check teflon tubes under water for bubbles in the wall using 1-MHz longitudinal waves, the beam being focussed by a perspex lens mounted in front of the transducer. The tube was moved past the probe and rotated simultaneously.

Thick plates of polyethylene produced by thermoplastic pressing from granules can be checked for homogeneity in thicknesses exceeding 12 mm, using 1 to 2 MHz. Plastic material similarly produced from sheets can be tested for laminations like metal plates. The echo method can no longer be used on thin insulating laminates. If sufficiently hard, they can still be tested by transmission at frequencies above 2 MHz by immersion technique, while wrapped insulating tubes (with resin-bonded paper) already require frequencies below 1 MHz if tested for lamination-like bonding defects.

For the testing of solid-fuel rocket compounds and explosives, in which the detection of voids and cracks is very important, very low frequencies are required, so that only testing by through transmission is possible. If the test specimens are hollow, with a cylindrical internal surface, one of the two probes is placed in contact inside and the sound is passed only through the outer wall under water. It is recom-

mended that pulses of long wavelength are used for which the first half oscillation of the transmitted pulse is not disturbed by multiple reflections in the wall. If the pulse voltage of this first peak is measured, it provides a measure of the transmittance which is independent of small changes in wall thickness and beaming direction. It can be used for flaw recording in automatic testing devices and an instrument using this principle has been designed by the Explosives Research and Development Establishment, Ministry of Supply, U.K. On material with a star-shaped internal cross-section the internal space can then be filled with water, or for case where liquid coupling is not possible a solution has been to use airborne sound with dry coupling [305].

Concerning weld testing in plastics see Section 28.1.7 and for problems connected with fibre reinforced plastics see Section 29.3.

Ultrasonic measurements can also be used for determing the moisture content of plastics. On polyamide, for instance, both the attenuation and the acoustic velocity, change with the moisture content. It is, however, not recommended that the velocity be used as a criterion because differences in structure, between for example the center and periphery of a disc cut from round stock, affect this value. The attenuation decreases noticeably from the dry zone to the zone saturated with moisture, so that 1-MHz back-wall echoes are in the ratio 1:10.

Another problem encountered in the plastics field is wall-thickness measurement on plastic tubing during manufacture, if possible immediately behind the extruder. Although this rather belongs to Section 33.1 (wall-thickness measurement) it is discussed here because the properties of plastics are involved. The formed tube should have a uniform wall thickness, and it should deviate as little as possible from the specified wall thickness in order to save material. These tests can be made along the cooling section by means of a TR probe with sliding contact, or alternatively by means of a strongly damped normal probe in an immersion technique. A difficulty arises from the fact that at this point the tube is still rather hot and the temperature in the wall, due to different cooling, is higher near the inside. In plastics the acoustic velocity is greatly affected by the temperature (e.g., in hard PVC -8 m/s, per degree temperature rise). Consequently, absolute values of the wall thickness can be measured only if the temperature of the pipe wall is uniform and if corresponding correction factors are applied, see also [S 57].

On the other hand, the temperature profile on the circumference of a pipe varies only slightly, even in the case of non-uniform wall thickness, and differences in wall thickness around a given circumference can be determined with an accuracy of 0.1 to 0.2 mm by means of comparative measurements. This accuracy is sufficient to permit correction of the extruder in the case of eccentricity, cf. [480, 1495, 672].

32.3 Rubber

Vulcanized natural rubber containing no fillers can be tested in thicknesses up to a few centimetres with frequencies up to 2 MHz. The usual commercial brands contain fillers such as carbon which greatly increase the attenuation. Here, only frequencies below 1 MHz can be considered. If layers of fabric are added as in automobile tires, frequencies around 100 kHz are used. Besides the bonding of rubber to metal, another important testing problem is the bonding between various layers of rubber and fabric in automobile tires and transmission belts.

Suggestions for inspecting automobile tires in a water bath by swept ultrasonic frequencies and through transmission, date back quite some time [1066, 1067, 907].

In the USA, Halsey [600] mentions evaluation of the quality of automobile tires by the pulse-echo method, using the immersion technique, with strongly damped, focussed 1-MHz probes. A recorder records the amplitudes of the echoes from the transition between rubber and carcase, revealing separations, and simultaneously the transit time of the intermediate echo of the carcase is measured and recorded which monitors the thickness of the tread. The tire is inflated for optimum geometrical conditions.

Klinman et al [1007] in more recent investigations also used the pulse-echo method with highly dampled 1-MHz probes and wide-band amplifiers, which provides additional information for tire evaluation from the distortion of the back-wall echo due to dispersion.

32.4 Rock, Abrasive Wheels and Carbon

As far as *natural rock* is concerned only magmatic material, such as basalt, can be regarded as homogeneous and uniform throughout. In other types of rock both the acoustic velocity and the attenuation vary greatly. According to Malecki [819] granite, for instance, depending on its grain structure, can reach values from 1.7 to 5.0 km/s (see same source for values of many other rocks). Moreover laboratory tests on samples give values which differ appreciably from those obtained "in situ" in underground strata, because of the pressure effect. However, measurements of this pressure on the basis of the acoustic velocity also provide unreliable values because the relationships change from site to site.

In general the attenuation (except in homogeneous materials like rock salt) is so high that only frequencies below 500 kHz can be considered for ultrasonic tests. In the case of layers of sand, clay and even coal, the frequencies have to be reduced to those of audible sound in order to reach transmission distances of 1 m. An added difficulty arises from that fact that rocks usually contain numerous small cracks and inclusions which greatly reduce the transmittance [818, 819, 1574].

Because of the poor focussing obtained with low frequencies, flaw location by the echo method is usually impossible. On the other hand, on blocks with parallel surfaces, large cracks and inclusions can be detected using separate probes for through-transmission techniques.

Lutsch [954] has used the pulse-echo method at 0.5 MHz for detecting fracture zones in dense underground rock and thus indirectly indicating the strength of the solid rock (quartzite and reef formation). A special probe attached to a rod is inserted into a smooth drill hole and oil is used as couplant. It is possible in this way to inspect a volume of a few metres in diameter around the hole. At depths of 1 to 2 m numerous echoes are obtained caused by cracks, but at greater depths the screen picture becomes quite clear. A drill hole of 40 mm in diameter orientated parallel to the test hole and located at a distance of 1 m is still indicated very clearly by its echo. In quartzite acoustic velocities around 6 km/s and attenuation values around 100 dB/m were obtained at 1 MHz.

Wenzel [1604] has used a pure transit-time method for the same purpose and has in this way measured the acoustic velocity between two drill holes using two separate probes. The zone of reduced pressure near the surface gives lower velocity values and smaller transmitted amplitudes. Assuming a value for Poisson's ratio, Young's moduli were determined which

showed good agreement with the results obtained by other methods and which were of great practical interest for the lining of tunnels. In this case the drill holes pointed obliquely downward and were filled with water to ensure satisfactory and uniform coupling. The tests were made with Steinkamp's concrete tester [1458] at a frequency of 30 kHz. In Rofna gneiss and marble the acoustic velocities were about 4700 and 6500 m/s, respectively.

Tests in natural rock have found practical applications only to a very limited extent. On the other hand, measurements of acoustic velocities and attenuations on drilled core samples are used successfully for the purpose of determining elastic constants and other properties of the material for basic research. Core samples of 20 to 40 mm in diameter and from 50 to 100 mm long can be tested at frequencies between 1 and 4 MHz with longitudinal waves, and at 1 MHz with transverse waves, by the through-transmission method. In exceptional cases these measurements can also be carried out successfully at 1 and 2 MHz by the pulse-echo method [1180].

Among artificial rock material the ultrasonic test so far has mainly been applied to refractory bricks used for the lining of furnaces and kilns. The problem is the detection of cracks, extrusion defects and cavities, and the determination of technological properties, such as porosity and cold compressive strength. At moderate porosity levels these materials are sufficiently permeable to sound at frequencies between 50 and 500 kHz. Due to the rough surfaces, grease or paste is used for the coupling and the probes are preferably fitted with protective shoes made of rubber due to their superior adaption to the irregularities of the surface. In moderately porous material the acoustic velocity can also serve to estimate this porosity. For instance, in a given material the velocity changes from 3900 to 3400 m/s if the porosity increases from 20 % to 30 %.

In porous rocks such measurements are possible only by through transmission, whereas densely calcined bricks and ceramic tiles can be tested at 1 and 2 MHz, and even at 4 MHz by the pulse-echo method.

Regarding the testing of refractory rocks, fired bricks, glazed oven tiles and floor tiles, see [518, 1431, 1207, 301, 569, 1681 and 27 (Sections K 21 and K 22)].

Abrasive wheels bonded with silicate transmit sound in the same way as sandstone and can be tested by an immersion technique by means of a sharply collimated beam of 1 MHz. Using the through-transmission method, defects such as cracks or unsatisfactory bonding, which reduce the transmission, can be detected. With the pulse method it is also possible to draw conclusions on the quality of the bonding from the acoustic velocity. Abrasive wheels on a rubber base have low transmission, but by using 0.2 MHz, it has been possible to carry out rough tests on specimens up to 15 cm thick.

Pressed *carbon and graphite blocks* (electrode and reactor material) show very different transmittance. Where it was at all possible to test electrode blocks (with frequencies below 1 MHz), the acoustic velocities, measured normal and parallel to the main orientation of the slabs, differed greatly, viz. 1100 to 2300 m/s and 3200 to 3900 m/s, respectively. Furthermore, the transmittance changed greatly from place to place even in the absence of gross defects, so that flaw detection was not always possible. In another case graphite blocks could readily be tested by sound transmission in an immersion technique, using 0.5 to 1 MHz [1357, 591, 345, 1091, 262].

32.5 Concrete

Checks for defects and strength are of great interest both in large concrete structures fabricated on site as well as for mass-produced prefabricated units. The intrinsic inhomogeneity limits the frequencies which can be used for this purpose to 100 kHz and less where testing distances exceed 1 m. These frequencies, however, no longer permit sharply collimated sound beams as is customary in the testing of metals. To obtain a collimated beam as with 25-mm 2-MHz probes in steel (angle of divergence γ_0 approximately 8°), a transducer used for concrete would have to have a diameter of approximately 350 mm at 100 kHz. In practice probes which are not much larger than the customary ones are usually used and thick oil, grease, coupling paste containing water, glycerine-kaolin slurries, soft soap and similar substances are used for coupling. Occasionally the probes are also semi-permanently attached by means of plaster where observations over a long period are required. There are also probes for dry coupling.

The probe contact face, which is only of the order of magnitude of the wavelength (at 100 kHz, $\lambda \approx 40$ mm), naturally also radiates with appreciable intensity wave modes other than longitudinal waves. A strong Rayleigh wave can always be assumed, which results in so many disturbing echoes of uncontrollable direction that the echo method can rarely be used. As a rule therefore two probes are used with pulse transmission. The lack of any directionality of the probes makes it possible to couple at arbitrary points on different surfaces of the specimen even those inclined to each other (Fig. 32.4a). The first wave received in this way is then always the direct longitudinal wave. This is followed by the transverse and Rayleigh waves which, depending on the shape of the specimen, may already be disturbed by the reflected longitudinal waves. If both probes are placed on the same surface of a given concrete structure, for example on a road paving slab (Fig. 32.4b) the direct longitudinal wave is rather weak (cf. point-source directivity Fig. 4.23).
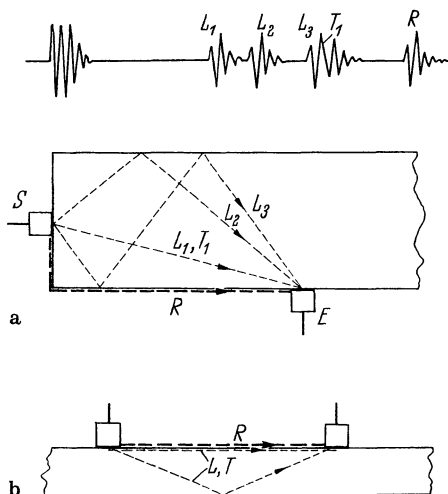

Fig. 32.4. Testing concrete by pulsed sound transmission. **a** With contact on two adjacent sides of a pillar, showing schematic screen pictures and the first pulses received of various wave types; **b** with contact on the surface of a road slab

For the important problem of pavement-thickness measurements a TR-probe arrangement has been reported, consisting of a mosaic of 14 barium-titanate transmitters of 200 kHz, arranged like spokes or slices of pie around a central receiver made of lithium sulphate with a resonant frequency of 5 MHz. By this arrangement the surface cross talk which limits the measurement of small concrete thickness can be greatly reduced [974].

The main application of interest for ultrasonic testing in concrete is for the evaluation of the concrete quality, via its compressive strength. This is linked with the Young's modulus, but not exclusively. However, for a first approximation the quality can be judged from the velocity as shown in the following table:

Longitudinal velocity $\times 10^3$ m/s	Quality of concrete
Above 4.6	Very good
3.6 to 4.6	Good
3.0 to 3.6	Moderate to questionable
2.1 to 3.0	Bad
Below 2.1	Very bad

As long as all other factors of influence are constant, including the type, amount and coarseness of the aggregate, ratio of water to cement, age, humidity content and steel reinforcement, comparisons between different specimen are possible.

Figure 32.5 shows the influence of the water/cement ratio on the velocity for five different mixes of cement, sand and gravel. The specimens had a setting age of 28 days and were saturated with moisture. The compressive strength varies according to the amount of water added when mixing, along one of the calibration lines [736].

Because sometimes wrong decisions have been made which were based exclusively on the measured velocity, the method has been considered as unreliable. However, in combination with other physical measurements made on the material,
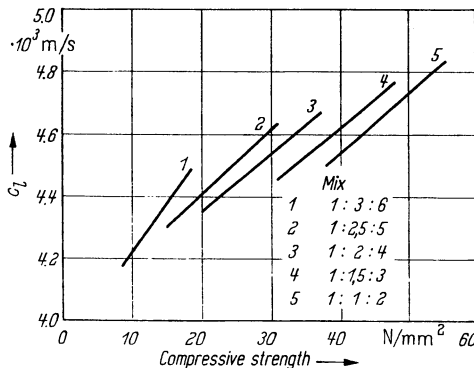

Fig. 32.5. Correlation between longitudinal velocity and compressive strength in concrete specimens with several mixing ratios (cement/sand/gravel) and variable water-cement ratio, as measured by Jones and Gatfield. (1 kp/cm² = 1 kgf·cm² ≈ 10 N/mm²)

such as the hardness measured by the rebound of the Schmidt-hammer on the surface of the specimen, reliable values of the strength can be obtained.

Teodoru [S 168 and S 169] (with many other references)] has combined the ultrasonic velocity and attenuation with the rebound figures of the Schmidt-hammer. By a complex computer program all factors of influence are correlated even for the case of hydrothermal treatment, which is important for the prefabrication of concrete components.

According to Bungey [197] concrete testing with ultrasound can be of interest in the following cases:

— testing of the uniformity of pieces of nominally equal mix to detect demixing, shrinkage cavities, cracks;
— to measure the compressive strength under equal loading conditions, on condition that other measuring methods have been taken into account in a series of measurements, as for example surface hardness, or density;
— checking the maturing process;
— detection of damage occurring by fire or by micro-cracks introduced by stressing.

Bungey has also measured the influence of the reinforcement on the velocity. In the longitudinal direction steel reinforcement bars less than 5 mm thick are of no influence and up to 20 mm in the transverse direction. Correction values for heavier reinforcement have been indicated.

Instruments for concrete testing usually have no CR tube and are restricted to measuring transit times, which in some cases is done digitally and with high precision [302, 445, 736, 919, 1458, 1205].

Older papers on the testing of concrete are [383, 519, 1306, 833, 1491 and 27 (Sections K 112, 121 and 131)]. See further [327, 664, 197, 123, 1201, 743, 1576, 1390, 1021, 1325, 502, 1256, 1532].

32.6 Wood and Leather

One of the earliest applications of ultrasonic testing was the bonding test on plywood by Czerlinsky [284] but instead of swept ultrasonic frequencies pulsed-sound through transmission is used today. A non-existent or faulty glued bond in plywood is easily revealed by its lower transmittance but since couplants containing oil or water are usually undesirable, a slowly evaporating liquid has to be used instead. Automation Industries in the USA use wheel probes [1701] for the continuous testing of plywood by the transmission method, and these require no liquid coupling between the wheels and plywood.

Another problem is the detection of core rot, both in live trees and in wooden poles (dry rot, for example in telephone poles). In wooden poles such central rotting is readily detectable.

The probes are fitted with protective plastic shoes coupled by grease and suitable hinged tongs are used for applying the probes to the poles at the required coupling pressure of about 10 kg so that no coupling liquid is required.
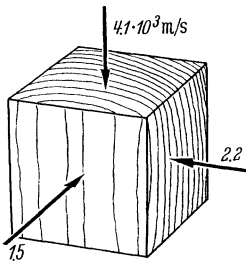
Fig. 32.6. Longitudinal acoustic velocities in a cube of beechwood

As reported by Waid and Woodman [1584], the same method can be applied to living trees and sound transmission in living wood is better than in wooden poles. On the other hand the bark is so impermeable that it has to be removed from two opposing areas which should also be as flat as possible.

For through transmission a frequency of 250 to 500 kHz is required and on sound beechwood satisfactory transmission was obtained even up to 1.2 m diameter.

Due to the pronounced anisotropy caused by fibre orientation it is difficult to use the measurement of the sound-velocity for general quality tests of timber. For instance the acoustic velocity values shown in Fig. 32.6 were measured on a dry beechwood block. At the same time the attenuation at 500 kHz was found to be about 400 dB/m which, compared with metals, is very high.

Quality tests by means of ultrasonics have also been made on other organic materials such as leather [747] but these have so far found no important practical application. Here again the sound velocity is the measured quantity, which depends on the physical structure and fibre orientation. For literature see [203, 204, 205, 976, 745, 820, 190, 1493, 351, 1143, 1174, 1009, 1597].

32.7 Bacon and Meat

As far as these edible "materials" are concerned, the measurement of fat and lean meat thicknesses on live animals, especially pigs and cattle, has found fairly wide practical application. The method is used by animal-breeding institutions since it greatly facilitates the assessment of the market value of the livestock.

The animals readily tolerate the application of the ultrasonic probe, in contrast to the previously practised insertion of needles into pigs in order to determine the thicknesses of the bacon layers. For this purpose the animal is preferably driven into a narrow gate or cage, so as to obtain a steady display on the CR screen while the animal is still. Frequencies around 2 MHz give a good compromise between sound transmittance and definition of the echoes. If probes of approximately 10 mm in diameter are used it is not absolutely necessary to remove the bristles on the pig and oil, grease or water-soluble paste can be used for coupling (Fig. 32.7).

The reflection at the transition layer separating fat and lean meat results from a slight difference in acoustic impedance. In addition some intermediate echoes are obtained from membranes between the layers (Fig. 32.8).
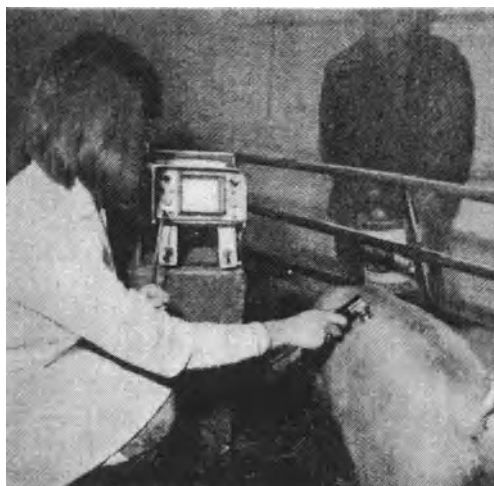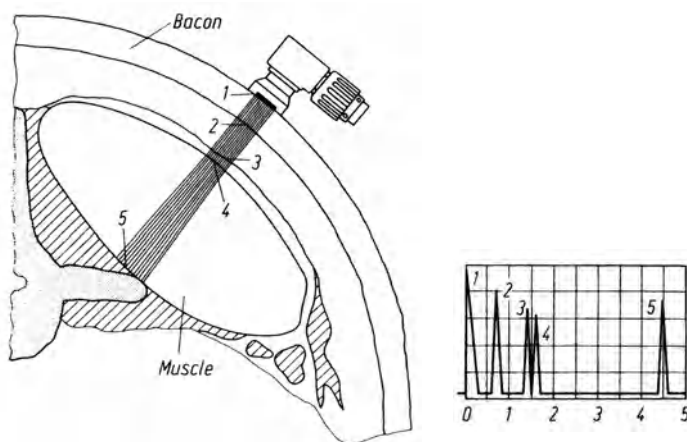
Fig. 32.7. Measuring the thickness of fat on a pig

Fig. 32.8. Measuring the thickness of fat and meat, schematic, with cross-section through the animal. *1* Surface of the animal, *2* and *3* membranes, *4* back muscle, upper side, *5* back muscle, lower side

According to Horst [690] the acoustic velocity in bacon of freshly killed pigs (still warm) is 1430 to 1510 m/s. As the temperature falls the sound attenuation rises steeply which can usually be compensated by using higher gain. In the case of pork, in the long dorsal muscles (cutlets), the velocity is 1650 m/s, and in the case of beef from the hind quarters about 2040 m/s, according to data supplied by Burg-kart [202].

When the instrument is being calibrated, one should observe that in addition to the effect of the temperature, the thickness of the bacon on the hung carcase de-creases because of stretching. According to Lauprecht [895] the accuracy usually
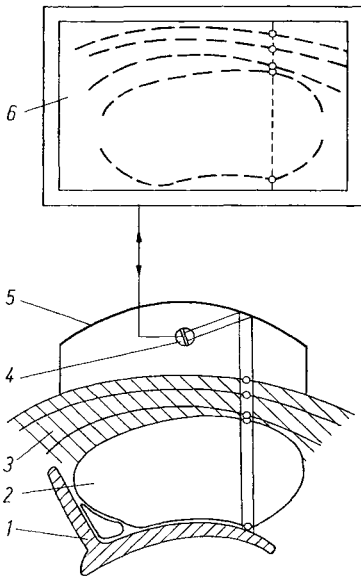
Fig. 32.9. Diagram of the scanning method of the back of a pig by means of the Vidoson according to Horst. *1* bone, *2* lean meat muscle, *3* fat layers with membranes, *4* ultrasonic transducer, *5* parabolic mirror, *6* CR screen

obtained was 1 to 2 mm on thicknesses of about 40 mm, which is quite adequate. Regarding further data on measurements on pigs see [156, 1271, 523].

After measurements of the thickness of the outer layers had given satisfaction until 1959, the possibility of measuring the thickness of the lean meat offered a new way of determining carcase values which were based on the ratio of the cross-sectional area of the dorsal muscle in the back bacon to the overlaying fat (Fig. 32.8). By spot-sampling by hand, and by plotting and integrating the areas concerned, it was possible to determine a quality value, although in practice this was too time consuming. More recently a commercial video instrument developed for human medicine, the Vidoson of Siemens, has been tried out for this purpose [691]. Figure 32.9 shows the scanning principle in which the sound beam from a rotating transducer is directed by a parabolic mirror from a water-filled chamber placed on the back of the pig.

Further applications of ultrasonics in animal husbandry include measurements of the breast muscles in chickens and the measurement of fat and meat in sheep and other pedigree lifestock. In humans the measurement of the subcutaneous layer of fat in young people is used for nutritional research [195].

Concerning suitable instruments for these applications see [212, 1743].

33 Ultrasonic Testing by Determination of Material Properties

This Chapter deals with the measurement of material properties and of elastic constants, as far as they are of interest for materials testing in general and where they can be carried out by using commercial testing instruments. This excludes therefore many purely scientific problems and measuring methods or permits only their brief mention. For further and more detailed studies the textbook of Tietz [41] is strongly recommended.

33.1 Measurement of Wall and Layer Thicknesses

The determination of a given wall thickness, or of an acoustic velocity, is based on the measurement of a transit time t. If the velocity is known, this then provides the thickness, or if the thickness is known the velocity can be calculated.

$$d = ct \quad \text{or} \quad c = d/t.$$

These methods, as well as the instruments, are described in Chapters 10 and 11. The measuring problems encountered in practice can be divided into two groups.

1. In the manufacture of pipes, vessels, plate and strip, continuous measurements, or programmed selective measurements, of the wall thickness are desirable. At the measuring points of these workpieces the walls are usually parallel and the boundary faces smooth.

The demands in respect of accuracy are high, about 1 %, or, in absolute values, 10 μm at wall thickness up to 1 mm, or about 0.1 mm at wall thickness up to 10 mm and over. Local variations in thickness are small so that the exact position of the measuring point is non-critical.

2. In plant maintenance as in power stations, or the chemical industry, the problem is different and consists of checking the thickness of the residual wall on installed pipes, tanks, bends, and vessels, which are exposed to high temperatures and pressures, and to corrosive chemicals. The main problem is the detection of local areas of general or pitted corrosion, and the measurement of the residual wall thickness at the critical points. This is usually at points where no multiple echoes can be obtained from a wall defined by parallel faces.

The first group of problems is the domain of wall-thickness meters of high frequency and high resolution. If perfect back-wall echoes are available, a high precision of measurement can be achieved.

However, this condition is the reason for the fact that such instruments do not work satisfactorily on corroded areas which is the task in the second group. Instrument manufacturers often claim a very wide useful range for their instruments, claiming to be able to measure deeply corroded walls with instruments of the first kind. Because there are no general standards for corrosion such a claim cannot be challenged easily. Anyhow these instruments do not operate well on real pitted corrosion, because in this case the received echoes are very much reduced, compared to a plane back wall.

This is therefore the domain of the second group of instruments, which work with TR probes. One can distinguish one type from the other by reference to the probe, but not by the display. This can be either an analogue or a digital indication (see Section 11.1.3). They use the conventional frequencies of ultrasonic testing, but have more power to obtain echoes from even small corrosion pits. Nevertheless to be able to measure thicknesses of 1 to 2 mm, the TR principle is absolutely necessary. The second group of instruments are also better able to measure at elevated temperature, this being also better performed with TR probes of special design. The contact delay lines are then made from quartz glass which are able to withstand temperatures up to 900 °C for a short time. It is even possible with these probes to work without intermediate cooling, if the probe is applied only for a fraction of a second. The contact surface in this case must be quite smooth to allow quick wetting by a high-temperature coupling medium (Section 15.3). Preferably a device to allow mechanical contact should be used, as in Fig. 33.1.

More difficult wall-thickness measurements occur if the outside of a pipe is not accessible and measurements must be made from the inside. Special probe designs as in Fig. 33.2 can be introduced into the liquid-filled tube, the beam being focussed onto the corroded surface. For small pipe diameters the probe can be mounted axially, the beam being deflected into a radial direction by a 45° mirror which is rotating.

The most difficult problem is the detection of a generally corroded area in a vessel with otherwise smooth surfaces and further measuring the residual wall-thickness within this area. For the first part of this task zigzag or plate wave methods are

Fig. 33.1. Probe holder for short-duration measurement on hot pipes (Krautkrämer)
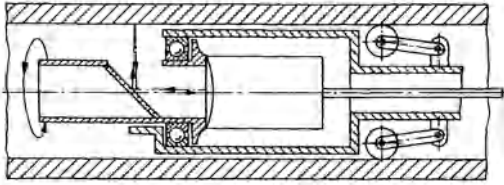
Fig. 33.2. Testing tubes for corrosion from inside

useful to check a whole strip or circumference of considerable length from one position. As described in Chapter 26 a circular transmission method can be used on tubes, for example with a tube-testing probe, or in flat plates a through transmission between two facing angle probes. Such a method is reported in [343] for use on oil pipelines embedded into the desert sand, where corrosion mainly occurs on the lower inside surface (Fig. 33.3). Occasionally the strong attenution of the circular transit echo is alone sufficient to pinpoint a corroded spot and this should also make it possible to roughly estimate the position and depth of the corroded area.

Once the generally corroded area has been located the remaining problem is the location and measurement of the minimum residual wall thickness possibly over an area of a few hundred square centimetres. It is practically impossible to cover such an area completely by manual testing and statistically distributed measuring points are usually selected. It is obvious that only a very conscientious inspector can be entrusted with the selection since one is tempted to omit spots on which a value can be read only by very careful probe manipulation. However, precisely such points may be the critical ones. The best solution would be automatic scanning over a limited surface area. So far no practical solution has been found in view of the elaborate mechanics involved and the difficulty of obtaining uniform coupling.

Fig. 33.3. Inspection of partially exposed pipelines for corrosion (according to Dubresson, Institut de Soudure, Paris)
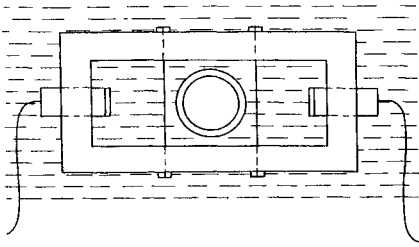
Fig. 33.4. Measurement of the wall thickness and the geometry of tubes with temperature compensation of the velocity of sound in water

On precision tubing (cf. Chapter 26) it is desirable to combine the testing for flaws with a measurement of the wall thickness and the internal and external diameters. As indicated in Fig. 33.4 this problem is solved by measuring the wall thicknesses at two opposite points by the immersion method. Then the distance of both probes from the surface is measured and subtracted from the known spacing of the probes. This provides the external diameter and if now both wall thicknesses are subtracted from the outer diameter, this provides the inner diameter. Each wall-thickness value may be different which in addition provides the eccentricity. These measuring and combination operations are preferably carried out by a computer with digital readout.

In the case of spiral scanning the measuring points on the tube are spaced very closely, which makes it necessary to select the values for practical processing by using only readings which exceed the tolerance value. Such an auxiliary device, which supplements the flaw testing, is provided by an equipment of the Danish Atomic Energy Commission, Risø [584, 585]. There is a problem of the measurement of the acoustic velocity in water whose temperature dependence (see page 534) must be compensated by using auxiliary reflectors in the beam, such as wires. The distances measured in water are calculated using the velocity figures arising from the variable transit times of the auxiliary echoes.

A dry and contactless measurement of wall thickness is possible in principle using electromagnetic probes (EMAT) (Section 8.4). According to [371] variations of several millimetres in the air gap between probe and surface are tolerable, because fluctuations of echo amplitudes up to 20 dB can be compensated. Ito and collaborators [710] make use of EMATs on tubes up to 120 mm in diameter at temperatures up to 900 °C in the production line and Boettger has reported success up to 1200 °C [S 17].

For copper and its alloys there is a risk of wall thickness measurement errors if the specimen, as a result of anisotropy and texture has an acoustic velocity normal to the wall different from that of the specimen used for calibration.

Water or other liquids in contact with the backwall (e.g. on filled pipelines and containers and on ships below the water line) do not usually disturb the thickness measurements. Only in the case of lead-covered cables, where the thickness of the lead sheath has to be determined, does it make much difference whether the inside is dry or filled with oil. Because of the curvature of the surface and the attenuation in the lead, the echoes are in any case rather weak.

Deposits on the inside of pipes and containers have usually a much lower acoustic impedance than the wall itself so that the ultrasonic wave is almost totally reflected at the boundary between wall and deposit and only the genuine wall thickness is measured. However, there are important exceptions, since in oil refineries it has been observed that a layer of iron sulphide forms in furnace tubes if crude oil containing sulphur is used. This layer adheres strongly and apparently has a sufficiently high acoustic impedance to simulate a considerably greater wall thickness. This disturbance has been observed on tubes of 14 % Cr, 1 % Si — steel but is suspected of occurring on other steels too. Where this seems possible, for example if the measured values have increased from one test to the next, an attempt can be made to spall off the layer at a few spots by strong hammer blows in order to be able to check the true wall thickness at such spots. Naturally, this disturbance applies to both the resonance and pulse-echo methods.

A problem of particular importance and wide application is presented by *plate-thickness measurements on ships hulls.* The former trepanning method which requires dry-docking of the ship and subsequent sealing of the holes by welding, is obviated by ultrasonic tests for which the ship can remain in the water. Particularly in oil tankers, the bulkheads and hull plates corrode rapidly because the empty tanks are filled with sea water. Tankers have already been successfully checked by using both resonance [422, 423] and pulse-echo instruments, although the testing conditions of the surfaces are not easy. Grinding or chipping of the measuring points is usually necessary.

Measurements of layer thicknesses with ultrasonics are only possible if the acoustic impedance of the layer differs markedly from that of the base and also if the layer is not too thin. The usual layer thickness of chromium or nickel on steel thus violates both these requirements. With pulse-echo instruments using the shock-wave method which gives maximum subsurface resolution, layers above about 0,1 mm of acoustically softer material on steel, for example, copper, plastic or paint, can be measured by the direct echo method. Thicker layers of rubber on steel, for example, thicker coatings of metals with markedly different acoustic impedances, and the white iron shell on chill castings (see Section 31.3) can be measured with standard pulse echo instruments with a CR tube which are much more suitable for the purpose than digital wall-thickness meters.

A difficult problem arises when measuring the *wall thickness in continuous casting.* The ingot, when cooling and leaving the mould must have a sufficiently thick solid shell surrounding the liquid core to prevent wall collapse. Kurz and Lux [876] have used normal probes with a water gap and a strong flow of water. However, since the reflectivity of the interface solid-liquid is unfavorable due to only a small difference in acoustic impedance, Lynnworth [960, 962] has used transverse waves, cf. [989]. For coupling, dry pressure contact is usually sufficient and this allows a very brief contact by shooting the probe including a delay line at the specimen. Alternatively a water-cooled roller can be used with several transverse-wave transducers firmly cemented to its internal surface.

For measuring the *case thickness* of surface-hardened workpieces the conditions are much more favorable for conventional case hardening than for flame or induction hardening because the former produces a greater change in the composition of

the steel and in its ultrasonic properties. With frequencies of the order of 40 MHz and very short pulses, the measurement has been successful, even for case thicknesses of less than 1 mm (Elion [379]). Thus, the boundary of the case is indicated by scatter which however, with the gradual transition desired in practice does not occur abruptly enough to permit a definite measurement.

While therefore beaming normal to the surface only rarely provides practical results, propagation along the surface still offers promising possibilities. If the transverse velocity in the layer is lower than in the base, the layer thickness will change the propagation velocity of Rayleigh waves and Love waves (Häusler [592]). Investigations are still in progress with a view to determining the extent to which measurements with pulse instruments are feasible in spite of the dispersion of the phase velocity. Unfortuantely, Love waves can be excited only via a solid, or at least a highly viscous, couplant.

Finally, transit-time measurements by the pulse-echo method are used for determining the *length of bolts*, their change when stressed, and thus the *strain in the bolt*. The mechanical method used so far has relied on a torque measurement with a torque spanner which is not very accurate because of unknown frictional restraints. The transit time of the bottom echo is therefore measured from the accessible end of the bolt, both before and during tightening. The transit time does not change exclusively as a result of the true change in length, but also because of a dependence of the acoustic velocity on the stress (cf. Section 33.2). The calculation cannot be based on the normal acoustic velocity therefore and it is preferable to make allowance for both effects by using an empirical calibration curve for the material concerned [526]. Special instruments for this purpose are available from several companies for example Panametrics, VWR Scientific, and Raymond. With the latter equipment the influence of temperature can be compensated by an external sensor. As an indication of the size of the effect it can be stated that in a bolt of 24 mm in diameter and 180 mm long, for a stress of 20 t the transit time is increased by about 1 µs.

A more advanced method of measuring stresses in bolts is reported in [1447]. Instead of measuring the length in both the unstressed and stressed conditions it is instead measured in the stressed conditions using both longitudinal and transverse waves, the ratio of the transit times being correlated with the stress.

For information on hot surface see [1305]; for in-service wall-thickness measurements on vessels filled with liquid zinc for galvanizing see [633]; for measuring tube walls from inside [866]; on heavily corroded tubes [1667] and on plastic tubing [247, S 57].

33.2 Measurement of Sound Velocity and Stress

Since in materials testing our principal interest is in sound velocities in solids, attention is here drawn to the book by Bergmann [2] concerning methods for measuring this quantity in liquids.

From the acoustic longitudinal- and transverse-wave velocities, Eqs. (1.6) and (1.7) give the elastic constants of solid materials [41]:

Poisson's ratio

$$\mu = \frac{\frac{1}{2} - \left(\frac{c_t}{c_l}\right)^2}{1 - \left(\frac{c_t}{c_l}\right)^2}, \tag{33.1}$$

The shear modulus (in N/m²)

$$G = \varrho c_t^2, \tag{33.2}$$

Young's modulus

$$E = 2G(1 + \mu) \tag{33.3}$$

$$\text{or} \quad E = 4\varrho c_t^2 \left(\frac{\frac{3}{4} - \left(\frac{c_t}{c_l}\right)^2}{1 - \left(\frac{c_t}{c_l}\right)^2} \right).$$

These basic relationships, and others mentioned below, indicate that the measurement of velocities of sound has great practical importance and various methods for their determination will be summarized here for convenience.

Using a resonance or pulse-echo instrument calibrated for a definite velocity of sound c (for example in steel) one readily determines an unknown velocity of sound c_x by measuring the steel equivalent thickness d_s of the specimen. The true thickness d having been determined by mechanical measurement, we then have:

$$c_x = c \frac{d}{d_s}.$$

The measurement accuracy is determined by the calibration accuracy of the instrument and in general this will not be better than about 1%.

With the use of interferometers (cf. Section 11.1.1) in conjunction with pulse-echo instruments one aims at accuracies of approximately 0.1%. In the above formula the apparent thickness d_s is then replaced by the length of the reference delay line which can be measured with a micrometer, and c by the accurately known velocity of sound of the delay line. In the case of water we have $c = 1483$ m/s at 20 °C. The velocity value increases in the range between 10 °C and 30 °C by 3.0 m/s per degree.

In order to measure the transverse velocity a transverse-wave normal (0°) probe is used on a solid test piece. These probes use a Y-cut quartz or other piezo-electric transducer polarized for shear waves. Of course with a liquid delay line a longitudinal-wave probe must be used.

A rather convenient method for determining the acoustic velocity in solid samples using a pulse-echo instrument is as follows. First the thickness of the sample with the unknown velocity of sound c_x is measured mechanically and a series of back-wall echoes produced at the same point. The pulse-echo instrument is then adjusted using the controls for velocity of sound and zero shift, so that the back-
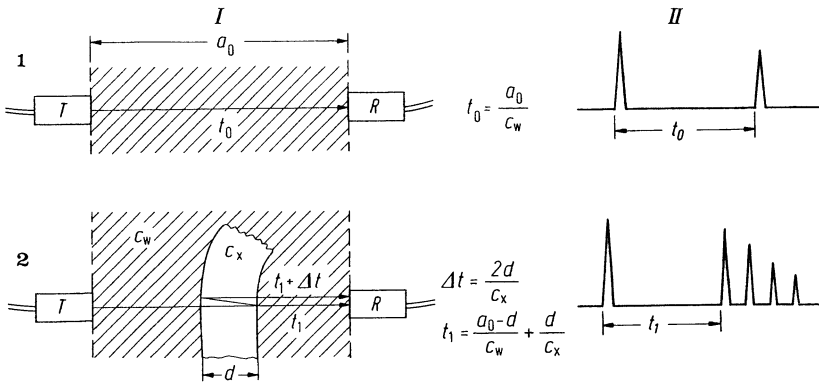
Fig. 33.5. Velocity of sound measurements on spheroidal grey-iron castings for the automobile industry. I immersion technique arrangement, II echo pattern, schematic. *1* measurement without test piece; *2* measurement with test piece inserted

wall echoes for the known thickness of the test piece appear at the "correct" points of the screen calibration scale. Following this adjustment the probe is now placed on a 20-μs transit-time standard. The back-wall echo of this standard will now appear at the point on the adjusted screen which corresponds to the unknown value of the velocity of sound. Since the screen adjustment has been made in respect of the unknown velocity of sound the sound pulse travels in 20 μs (corresponding to a single thickness travel of 10 μs) as many millimetres as correspond to 1/100 of the velocity of sound in m/s. Thus, the indicated thickness value in millimetres multipled by 100 gives the unknown velocity of sound in m/s.

A specially adapted velocity of sound meter can be used for the production monitoring of parts whose thickness remains constant. This thickness is first measured mechanically and the instrument adjusted appropriately, but if the thickness changes too often it makes the measurement of velocity too time consuming. On an instrument of Branson (Fig. 33.5) all these manipulations are automated [371].

Transmitter and receiver probes are arranged facing each other in water at a fixed distance a_0. First the transit time of the water delay line is measured, $t_0 = a_0/c_w$, and then with the test piece inserted, the time t_1 and the time Δt for the two-way travel in the test piece. On the basis of these data and the known velocity of sound in water c_w the computer determines the unknown velocity of sound:

$$c_x = c_w \left(\frac{2}{\Delta t} (t_0 - t_1) + 1 \right)$$

and the thickness and corresponding transit time of the test piece.

Bradfield has used the critical-angle method by a goniometer arrangement as in Fig. 33.6 for determining the velocity of sound in a flat smooth sample. The pronounced amplitude changes at the critical angles (see Diagram 2 in the Appendix) permit the reading of angles to within 0.1° and thus accuracies of the velocity of sound 0.1 %. In particular, Bradfield has measured the surface-wave velocity by this
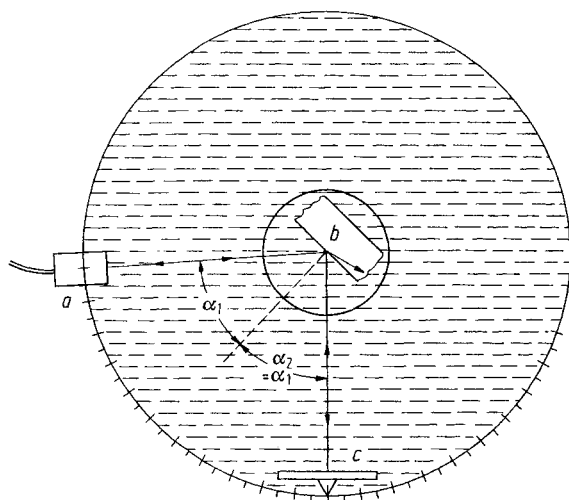
Fig. 33.6. Velocity measurement of Rayleigh waves with the goniometer according to Brad-
field. **a** Probe; **b** test piece; **c** reflector

arrangement, which can provide information on the technological condition of the
surface [171, 1608, 699].

For practical applications of velocity of sound measurements in the testing of
materials the accuracy of the described methods is adequate for determining the
mixing ratio in composites: porosity in porcelain (Section 32.1); moisture content
in plastics (Section 32.2); the structure of metals, preferred grain orientation, struc-
ture of grey cast iron, and its tensile strength (Section 31.3 and [S 91]).

For a method of measuring the elastic constants of powder metallurgical com-
posites see [S 132] and of ceramics and fibre composites see [S 60 and S 76].

There are a number of other problems for which in general a higher measuring
accuracy is required, and these include the measurement of internal and external
stresses, the flow velocities of liquids, and the temperatures of liquids and gases.

When stresses, either internal or external, exist in or are applied to an otherwise
isotropic material it becomes double refracting. This means that the velocity of a
transverse wave normal to the direction of the stress differs, depending on whether
its direction of oscillation is parallel or normal to the stress direction. This is shown
schematically in Fig. 33.7 for a body subjected to an external stress (pressure or ten-
sion).

If the direction of polarization is not known it has first to be found as in Sec-
tion 16.4.

The differences in velocity and hence of transit times are very small so that it is
preferable not to use commercial probes but to cement suitable crystals firmly to
the test piece. The echo sequences of each transverse-wave transducer are fed into
an amplifier and the interference due to the different transit times can be observed
on a CR screen. The first back echo may not show sufficient interference to permit
observation but after several transits, the phase difference can increase to half a
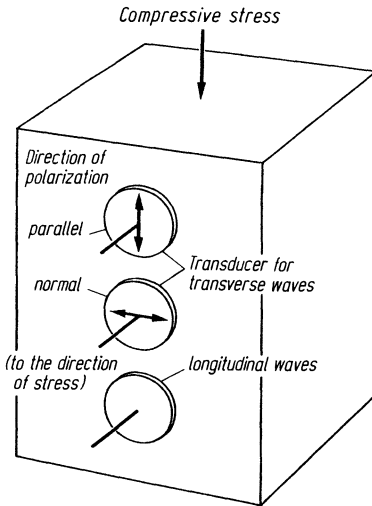
Fig. 33.7. Measurement of changes in velocity of sound caused by mechanical stress

wavelength, thus causing the cancellation of an echo and consequently the echo sequence shows beats. It is also possible to connect in the lead of one of the two transducers an electric phase control [380, 378, 659, 1287, 1288, 1437, 1160, 243]. Crecraft [245] has used the sing-around method instead of wave interference and by using a pressure-coupled transducer assembly was able to make tests at the same point of the specimen by rotating the assembly between measurements.

Instead of using two Y-cut quartz crystals, it is simpler to use only one whose direction of oscillation makes an angle of 45° with the direction of stress. The transmitted wave can then be separated into two components parallel and normal to it, which are propagated at different velocities. As in optics (cf. Pohl [28]), the resultant oscillations are generally in an elliptical or circular path, or in special cases a linear oscillation normal or parallel to the original, depending on the phase shift. If received by the same oscillator the elliptically or circularly polarized waves produce an electrical signal whose amplitude decreases to zero with increasing phase shift, then rises again, and so forth. The result as shown on a CR screen is then exactly the same as in the case of two separate oscillators, that is a sequence of echoes with minima and maxima. In order to obtain distinct and numerous extreme values, the pulse used should contain a reasonably large number of oscillations of equal amplitude. However, in order to keep the pulses short higher frequencies are used. The sensitivity increases with the frequency used and the length of the delay line.

According to Elion [378, 380], two Y-cut quartz plates can also be cemented together as a sandwich, the outer one then transmitting or receiving its wave through the other. Although this requires only one measuring point, the two crystals can be separately pulsed, and the phase shift can be measured after compensation by electrical delay lines before the amplifier. With such probes it is also possible to generate arbitrary, elliptically or circularly polarized waves.

A changing double refraction in a specimen subjected to varying loads, can be followed by the amplitude of a given echo which follows a cosine function of the phase angle and this is simpler than using the minima of the echo sequence for this purpose. Provided the double refraction is sufficiently marked, one can use the first echo for this purpose or, in the case of pulse transmission, a pulse which has travelled trough the measuring distance once only.

During this test it may happen that at the beginning of the application of the load, the height of the echo does not decrease immediately, but at first still increases; this can be the

result of preferentially orientated residual stresses, which thus could also be measured in this way.

Using a Y-cut quartz of 45°, Firestone [456] already was able to determine the texture in thin plate by the pulse resonance method (see Section 11.3.1): When tuning the pulse frequency to resonance (maximum width of transmitting pulse) beats appear in its decay oscillations.

Since this method is the acoustic counterpart to the photo-elastic method used for investigating specimens in the form of transparent models, the term *acousto-elasticity*, in contrast to *photo-elasticity*, has been coined for it.

Figure 380 shows measuring results obtained by Elion [380] during tensile tests on aluminium of 100×100 mm² cross-section. Crecraft [265] however, was unable to confirm this in spite of very careful measurements. No velocity maximum of the polarized wave could be detected and the pattern of the other two is exactly opposite: the parallel-polarized wave decreases and the longitudinal-polarized wave increases in velocity. In the case of nickel, however, the pattern is again reversed. This shows how difficult this problem is.

A further difficulty in the stress analysis arises from the texture of the specimen. However, it has been shown that the separate influences of stress and texture can be distinguished by simultaneous measurement of the changes in both velocity and attenuation. [1366, S 74].

The theoretical fundamentals of the determination of the elastic constants in anisotropic and textured materials have been treated by L. Niklas in Chapter S. 11 of [37].

For experimental determination of the elastic constants from measurements of the velocities see [126, 920, 958, 961, 1168, 1630, 1683, 964, 623, S 85, S 94, S 190], concerning the method and instruments [913, 1136, 181, 355, 775, 211 (also for attenuation measurements)] for measurements of stress [731, 13, 1366, 662, 786, 248, 495, 51, 82, 1365, S 23, S 137, S 197, S 128, S 15, S 74].
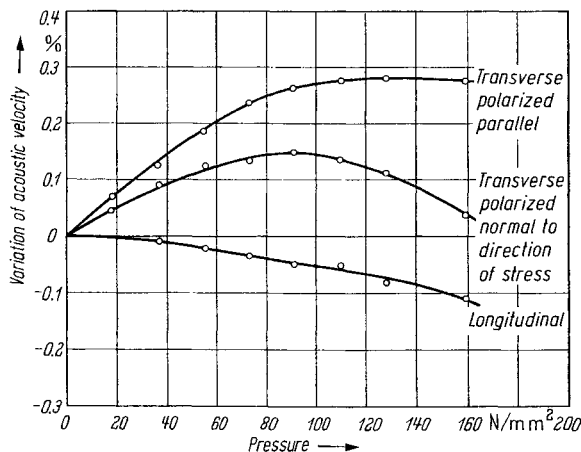

Fig. 33.8. Variations in per cent of the velocity of sound in aluminium subjected to compressive stresses according to Elion

For the investigation of the surface condition after heat- or chemical influence and also for stress and texture measurements the Rayleigh-wave velocity is used in [168] and for similar purposes (hardness and texture) the Love-wave velocity in [667].

33.3 Measurement of the Attenuation, the Scattering of Sound and the Microstructure

To make an absolute measurement of attenuation is very difficult because the echo amplitude depends not only on the attenuation but also on a number of other influencing factors. Relative measurements are easier to make, such as the change of attenuation during a given test, and also simple qualitative tests. For this purpose the shape of the specimen, the probe and the coupling are kept constant while the amplitudes of the back-wall echoes are compared. On an instrument with a calibrated gain control these amplitudes are then adjusted to the same level on the CR screen so that the difference is read directly in decibels. In this way it is, for example, possible to observe the effects of temperature or fatigue by using a crystal cemented to a particular specimen so that its shape has no influence on the measurement. In the case of different specimens of identical shape any deductions concerning attenuation from a back-wall echo or through-transmission signal can be made only if each has the same acoustic impedance and surface quality. Thus, for instance, the fact that an aluminium block gives a larger back-wall echo than a steel block of identical shape, does not necessarily mean that the attenuation in the aluminium is smaller. The more likely cause is better sound transfer in the coupling due to the better acoustic impedance matching.

For absolute measurements it is necessary to use the decrease of the echo amplitude in a given sequence of multiple back-wall echoes. However, in addition to the attenuation of the material, this decrease is caused by the energy losses when sound is reflected at the probe-metal interface and also by the geometrical divergence of the sound beam.

According to Truell [1276] the loss caused by the coupling factor can be made negligibly small by cementing a single piezo-electric plate without backing or sup-
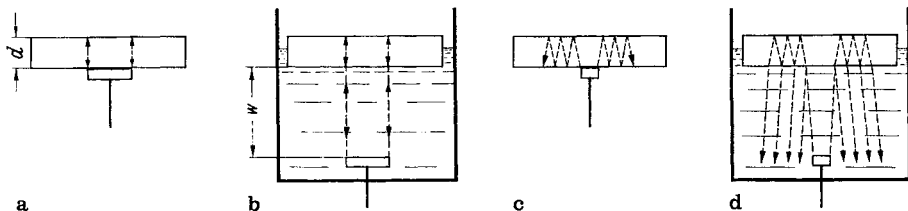

Fig. 33.9. Arrangements for attenuation measurement on the basis of multiple-echo sequences. **a** Direct contact, near-field; **b** delay line, near-field; **c** direct contact, far-field; **d** delay line, far-field

porting structures and exciting it exactly at its natural frequency. When conventional probes are used therefore a certain loss which is not exactly known has to be accepted when testing by direct contact. It is preferable therefore to couple via a liquid delay line when the reflection losses at the boundary can be calculated from the known ratio of the acoustic impedances.

In the case of losses due to beam spread it is possible to operate entirely in the near-field, including all the repeat echoes used in the measurements, in which case the effect of beam spread is negligible. An alternative is to use the far-field, beyond about three near-field lengths where the amplitude decreases fairly accurately in inverse proportion to the distance.

Figure 33.9 shows schematically the arrangement for the four possibilities given and the corresponding formulae for measuring the coefficient of attenuation α in dB/mm are:

$$
\text{a)} \quad \alpha = \frac{1}{2d} S_E, \qquad\qquad \text{b)} \quad \alpha = \frac{1}{2d} (S_E - S_R),
$$

$$
\text{c)} \quad \alpha = \frac{1}{2d} (S_E - S_A), \qquad \text{d)} \quad \alpha = \frac{1}{2d} (S_E - S_R - S'_A). \tag{33.4}
$$

Equation (33.4 a) follows from Eq. (6.1), because if the echo method is used, double the plate thickness d must be used. S_E is the ratio of two successive echo amplitudes H measured in decibels

$$
S_E = 20 \lg \frac{H_n}{H_{n+1}}.
$$

But if an instrument with a calibrated gain control is used, S_E is simply the difference between the two settings required to bring the echoes to a given level on the CR screen.

In the case of Eq. (33.4 b), because of the incomplete reflection at the boundary between specimen and water, the corresponding loss S_R must be taken into account once for each echo:

$$
S_R = 20 \lg \frac{1}{R} = 20 \lg \frac{Z_2 + Z_1}{Z_2 - Z_1}
$$

where Z_1 and Z_2 are the acoustic impedances of the specimen and the water, respectively; see Eq. (2.1).

Equation (33.4 c) follows from Eq. (6.3) with the attenuation S_A due to the spreading of the acoustic beam in the far-field

$$
S_A = 20 \lg \left(\frac{n+1}{n} \right).
$$

In Eq. (33.4 d), the beam-spread correction S'_A has to be subtracted, in addition to the reflection loss and, due to the path w in water, has a slightly different value:

$$
S'_A = 20 \lg \frac{w c_w/c + (n+1)\, d}{w c_w/c + nd}.
$$

The path in water w enters in the formula only after multiplication by the ratio of the acoustic velocities c_w/c, in water and in the specimen respectively.

In Fig. 33.9a it is assumed that the amplitude of the back-wall echo remains constant for the whole of the near-field in a material with no attenuation. According to Truell et al. [1398] this is not strictly true because of diffraction phenomena (cf. Fig. 5.7). Accurate measurements therefore require a correction given in [1398] which depends on the sound path and is approximately 2 dB at the end of the near-field of a true piston oscillator.

In cases b and d of Fig. 33.9 the water can also rise above the metal plate. The correction for the reflection losses is then doubled, and one obtains a second relation for α which can be used in addition for determining the unknown reflection and thus the acoustic impedance of the specimen.

In such measurements the plate should be thick enough to obtain a good separation of the multiple echoes, but not too thick, so that it accommodates as many multiple echoes as possible in the near-field of the oscillator. In case c and d of Fig. 33.9 the lateral dimensions of the metal plate should be large enough for the echoes used not to be disturbed by side-wall effects. It is best to estimate the minimum size on the basis of twice the angle of beam divergence γ_0 (Fig. 10.31). In this respect round specimen plates cause more disturbance than square or irregularly shapes plates.

A variant of the measuring arrangement using a water delay line (Fig. 33.9b, d) is to use a solid delay line made of plastic material or steel, the latter being best for hot test pieces [1168]. The reflection losses at the interface between the delay line and the test piece, and the coefficient of attenuation in the test piece itself can both be determined according to Papadakis [1163] from the amplitudes of the echoes received from the interface and the first and second back-wall echoes from the specimen. According to Lynnworth [963] these quantities can also be determined from the amplitudes of the echoes from the delay line before and after coupling to the test piece, and the first back-wall echo from the test piece; see also [S 53].

According to Truell a rod-shaped specimen with a reduced mid-section, such as a tensile test specimen, produces a collimating effect on the sound beam so that one can work with it as in the near-field although the sound paths are much longer. This would mean that it is not necessary to use the far-field correction factor S_A for the beam spread.

The demands of plane parallelism for a plate specimen are higher the higher the frequency and the required accuracy. According to a calculation by Truell [560] the wedge angle of the plate should not exceed approximately 2.5×10^{-3} degrees (i.e. 9 seconds of arc), if an attenuation of 0.5 dB/µs has to be measured with an accuracy of 10 % at 300 MHz. Note that here the attenuation is referred to transit time instead of to path length (see [211]). This already requires plane parallelism of optical quality.

For measurements on flat plates the arrangements shown in Figs. 33.9a and b are better suited to higher frequencies since with these sufficiently long near-fields can be obtained using convenient oscillator diameters.

Only with the arrangement shown in Fig. 33.9a does the echo sequence approximately follow an exponential function. This is exploited in an attenuation measuring instrument designed by Truell, and sold by Automation Industries, called the "Attenuation Comparator". It uses the discharge of capacitor whose voltage decay curve is also an e-function. Simultaneously with the transmitting pulse a charged capacitor is discharged through a variable resistor. The curve appearing on the CR screen has to be matched to the echo sequence (Fig. 33.10). Since in this case both e-functions have the same exponent, the value αd can be read directly
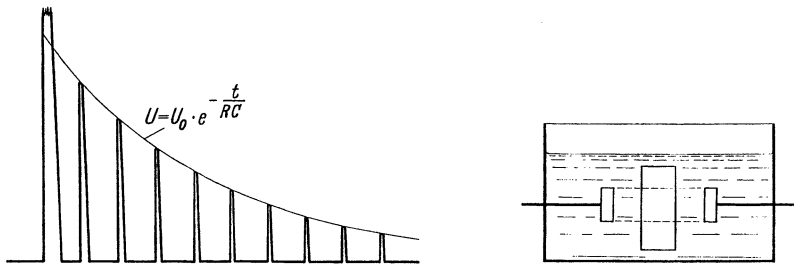
Fig. 33.10. Measurement of the exponential decay of the arrangement shown in Fig. 33.9a, by matching the discharge function of a capacitance C through a resistance R with the echo sequence
Fig. 33.11. Attenuation measurement with through-transmission

on the scale of the control. The instrument operates from 1 to 200 MHz. Correct measurement, however, presupposes that the multiple echoes are all in the near-field and that coupling losses are avoided by using a tuned, undamped crystal.

To be able to observe rapid changes of the attenuation Truell [1536] has developed an instrument for automatic measurements, called the "Automatic Attenuation Readout Adapter". By means of a logarithmic and a differential amplifier the exponent αd is obtained from two gated echoes of the sequence and indicated in real time or recorded continuously.

In a modification of the above arrangements the measurement can also be made by pulse through-transmission (Fig. 33.11). However, if this is used for comparing multiple echoes, and if the entire process takes place in the near-field, it is essentially the same as Fig. 33.9b. Sometimes, however, a single transmission is used and compared with the signal of the free water section without test piece. Thus if the water can be regarded as non-absorptive (only valid for measurements on highly attenuating specimens) the difference between the two signal amplitudes contains a double reflection loss as well as the attenuation in the specimen. If the attenuation of the water is appreciable then it would also have to be taken into consideration and added to the measured value of the material attenuation. The water attenuation depends on both the frequency and the temperature as well as the gas content (cf. Bergmann [2, p. 462]). Because of the short sound paths, this method is suitable for materials with high attenuation and where the sound path of multiple echoes would extend beyond the near-field at the given values of metal thickness, frequency and transducer diameter.

The sound absorption in water and also its frequency and temperature dependence has been described in Section 6.1. Usually it can be neglected but at high pulse powers, even when using conventional pulse-echo flaw detectors, it can increase considerably as a consequence of cavitation onset and non-linear stressing. Then it depends on the the sound pressure and hence on the distance from the probe. To avoid obtaining false results the measurements should be performed at various different distances from the probe, to check whether the results are constant.

Ivens using multiple echoes, has measured with a similar arrangement in the far-field and in the transition zone between near- and far-fields. In this region a

large receiver would have required corrections for the propagation of the sound field which cannot easily be neglected. The measurement was therefore made with a small receiver for which the pattern of the acoustic pressure along the axis according to Eq. (4.8) applies.

Because of the usually strong frequency dependence of the attenuation, the different frequencies contained in the pulse are affected to different degrees, so that the pulse shape becomes more and more distorted as it passes through the material. Therefore a simple comparison of the amplitudes of successive echoes in a sequence can give the wrong results especially when very short (broad band) pulses are used. A better method, which simultaneously gives the frequency dependence of the attenuation, is described by Vary [1558]. Two pulses of the sequence are transformed from the time domain into the frequency domain by a frequency analyzer. Now the ratio of the frequency curves, corrected for the differing geometric losses, gives the true attenuation at each frequency.

All the methods mentioned above require a specimen of the material concerned which has been specially prepared for the purpose. Frequently, however, attenuation measurements on the test piece itself are of interest, when structure has to be evaluated or when corrections must be made to flaw size evaluations.

This requires that a fairly smooth back-wall of the specimen normal to the sound beam can be used for comparison with the back-wall echo of a non-attenuating reference plate. Using the known near-field length of the probe, the ratio of the two echoes is calculated according to Chapter 5, or more simply read from a DGS diagram. As a result of the attenuation, the measured amplitude of the back-wall echo of the specimen is lower than the calculated value. The difference gives the mean attenuation over the thickness of the specimen, which can be estimated directly in dB/m if the equipment has a calibrated gain control. Corrections can also be made for cylindrical test surfaces and back-wall [852].

Example. A specimen of 400 mm in thickness with a plane back-wall and without attenuation should give a back-wall echo 40 % of that from a flat reference plate (i.e. −8 dB) when using a probe with a near-field of 100 mm (Fig. 5.6). If in fact 28 dB difference is measured, 20 dB of it is attributable to the attenuation. The mean attenuation is therefore 20 dB/800 mm = 25 dB/m.

If the specimen shown in Fig. 33.9 c is thicker than three times the nearfield length, the error caused by using a conventional probe in contact can be neglected for practical purposes and the attenuation can be determined according to formula (33.4 c), even on a test piece such as a forging, provided it has plane-parallel faces.

In a solid, cylindrical forging the multiple echoes also behave exactly like those in a plate as a result of the focussing effect [1150]. In the case of a hollow, cylindrical specimen, such as a bored rotor, the beam-spread effect S_A must still be calculated on geometric-acoustic principles (see Section 3.4).

Naturally, the accuracy of such routine measurements is much lower than that of the laboratory methods described above. However, even here it is difficult to keep the error below a few dB/m in the frequency range used in materials testing, which in the case of microcrystalline metals and at 2 MHz is already of the order of magnitude of the attenuation itself. Therefore, for scientific purposes higher frequencies are more commonly used.
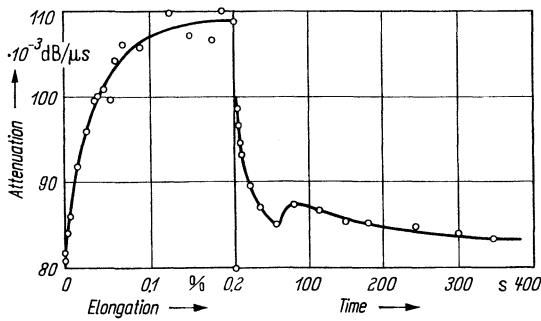
Fig. 33.12. Attenuation in aluminium during a tensile test, according to Truell

The dependence of the attenuation on conditions of mechanical stress may possibly lead to a solution of a very urgent problem of materials testing, viz. the prediction of fatigue-crack development under the influence of alternating stresses. Figure 33.12 shows the relevant results on aluminium according to Truell [1536]. The left half of the diagram shows the increase of the attenuation with elongation in the non-repeated tensile test. The acoustic velocities (see Section 33.2) change at the same time. On the right of the diagram the attenuation is plotted versus time, the elongation reached ultimately in the tensile test being kept constant. The decrease of the attenuation, which after some time reaches an asymptotic value, is called recovery. The changes of attenuation reached during the first part of the test depends on the load as a function of time because the recovery occurs during the same period. This phenomenon is readily explained by the dislocation theory of crystal lattices, as well as the irregular recovery pattern which sometimes shows maxima and minima.

A similar recovery of the material is initially observed after interrupting a pattern of alternating stress loading. However, after a large number of alternating stress cycles this recovery is slowed down progressively and finally disappears completely. When this stage is reached the material is fatigued and cracking is imminent.

In the case of magnetic materials the pattern of the attenuation during the tensile test is different and more complex. If these materials are free of residual stresses, the attenuation decreases during elongation in the elastic range. Here, the points of dislocation play a minor role in contrast to the walls of the magnetic elementary domains (Weiss domains). The elongation reorientates these zones, resulting in improved sound transmission. The same decrease of the acoustic attenuation is also observed during magnetization of the specimen. If, in the case of steel, residual stresses produced for example by cold-working, are superimposed, external stresses and residual stresses oppose each other so that the attenuation value passes through a maximum at a medium elongation (cf. [658]).

Vary [1558] has established methods of inter-relating attenuation with material properties, such as tensile strength, and fracture toughness, in polycrystalline and/or anisotropic and/or inhomogeneous materials. These apply especially to fibre composites thus allowing prediction of their behaviour under stress up to fracture.

The so-called stress-wave-factor method (SWF) (see [S 170]) measures attenuation by a method similar to the brush method described in Section 31.4 for testing aluminium extrusions. Using point-source transmitters and narrow-band receivers usually below 1 MHz, ultrasonic energy is transmitted through the specimen in a random manner. The received signal is displayed in an HF form, showing a number of ring-down oscillations, the number depending on the attenuation. This number, which is digitally indicated, is the stress-wave-factor, and it is normalized by comparison with an identical standard specimen. As well as the correlation with material properties mentioned above it has been shown to measure the strength of a rubber-steel bond (Section 29.2) [S 170, S 70].

In some cases the attenuation of sound also makes possible the determination of the degree of contamination in crystals by foreign atoms, and the observation of their movement during heat treatment. They reduce the attenuation because the dislocation points are pinned by the foreign atoms so that they are prevented from carrying out energy dissipating oscillations in the sound field. This has been observed in germanium, and also in titanium and copper after absorption of hydrogen.

As explained in Chapter 6 the attenuation of sound is caused by true absorption (transformation of energy into heat) and wave scattering. The reason for scattering is the inhomogeneous microscopic structure of polycrystalline material (even if it consists of only one metallurgical phase), caused by the single-crystal anisotropy and the different orientation of the crystallographic axes of the individual grains. Because all metal crystallites are more or less anisotropic the relevant elastic constants for the propagation of sound differ from one grain to the next. At the grain boundaries therefore the sound is scattered as at the boundary between two different metallurgical phases. The scatter is measured by the scattering coefficient, which together with the true absorption coefficient accounts for the total attenuation.
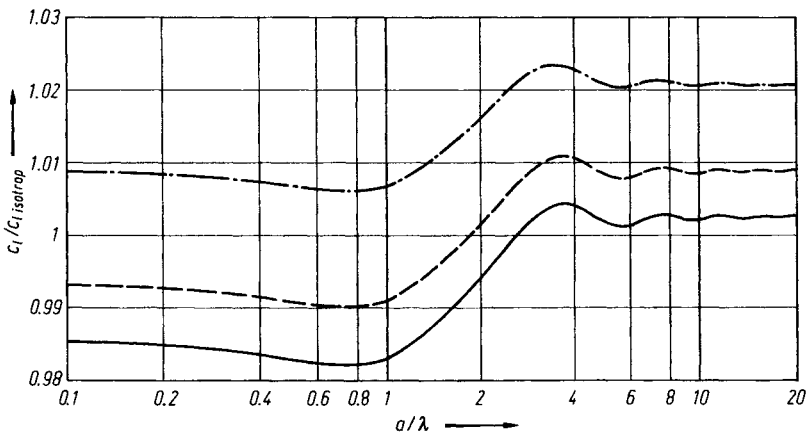

Fig. 33.13. Phase velocity of longitudinal waves in 70 % cold rolled steel, normalized by the velocity in isotropic material. Direction of measurement: ——————— in the rolling direction; — — — — transverse to it; ——— – ——— normal to the specimen
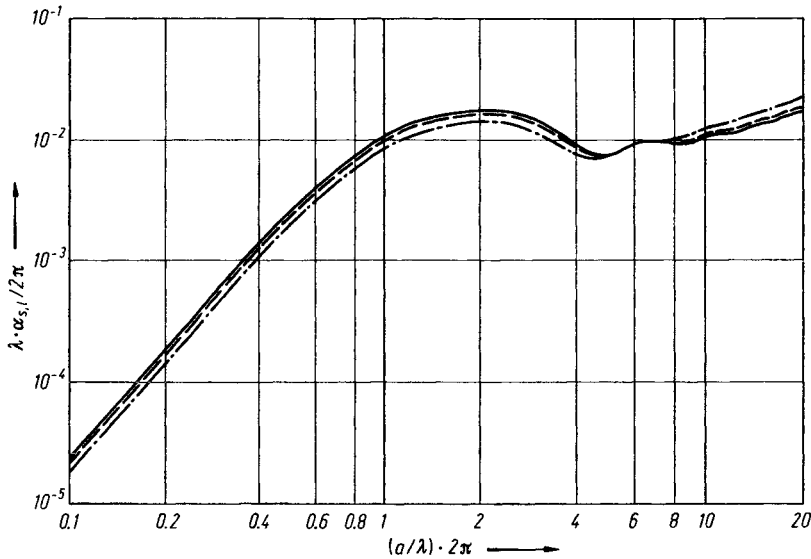
Fig. 33.14. Coefficient of scattering for longitudinal waves in 70 % cold-rolled steel. Direction of measurement: ——————— in the rolling direction; — — — — transverse to it; —— – —— normal to the specimen

The amount of scatter varies with the ultrasonic frequency and the size of the scatterers which is, in this case, the grain size. Scattered waves also propagate in the direction of the ultrasonic beam. Since they are phase-shifted relative to the original beam the super-position of the incident and the scattered waves in polycrystalline materials cause frequency dependent sound velocities and thus exhibit dispersion.

In polycrystalline material showing texture the crystallographic axes of the grains have a weighted orientation distribution. Therefore the ultrasonic velocities and scattering coefficients, as well as their dispersion characteristics, are directional.

The scattering at the grain boundaries, which depends on both the monocrystalline and the structural properties, provides a means of non-destructive structure analysis by making use of measured ultrasonic velocity dispersion and scattering coefficients, if the relationships can be expressed quantitatively. The theory of sound propagation in polycrystalline media [S 165, S 72, S 73, S 74] allows this calculation for both longitudinal and transverse waves. The first three of the papers mentioned deal with the simplest case of single-phase materials with cubic crystal symmetry with or without rolling or fiber texture. The last one presents the first results relating to multi-phase structures.

Figures 33.13 and 33.14 illustrate the velocity and the scattering coefficients for longitudinal waves in cold rolled steel as a function of the ratio of the effective radius a to the wavelength λ of the corresponding homogeneous isotropic medium. The velocity and scattering coefficients are respectively normalized relative to the velocity and wave number, derived from the isotropic averaged elastic constants.

The influence of the direction of measurement, and also the dispersion, are of the order of a few percent, the scattering coefficients also varying considerably with the testing direction.

From these results arises the possibility of evaluating the grain size and other structural parameters from measurements of the velocities and scattering coefficients in different directions and at various frequencies. Structural parameters in-

clude the texture coefficients and the shape, size and volume fractions of secondary phases. In the paper [S 35] from 1975 a method of grain-size discrimination has already been proposed, which uses the approximate results of the scattering coefficients valid in the Rayleigh region, where the wavelengths are large compared with the effective grain diameter. The Rayleigh approximation was already available before the development of the general scattering theory.

This theory allows the directional dependence of sound velocities caused by texture to be calculated, so that ultrasonic techniques for stress determination can be applied to textured materials [S 75].

Ultrasonic attenuation can be determined either by measurement of the reduction in amplitude of an ultrasonic pulse or of the amplitude of the wave scattered into a chosen direction as a function of the sound path. With the pulse-echo method the back scattered amount is measured.

As mentioned above, the scattering amplitude depends on the grain size and within the Rayleigh region it increases with the third power of the effective grain diameter. Therefore coarse grained materials cause high scattering amplitudes and a rapid reduction of signal strength with transit time or path length while fine grained structures produce low scattering amplitudes decreasing slowly with time or path, as illustrated in Fig. 33.15 (see [829]). If the grain size in the material varies with depth the decrease of the scattering amplitude plotted on a logarithmic scale will no longer be linear and will thus indicate macroscopic inhomogeneity of the structure.
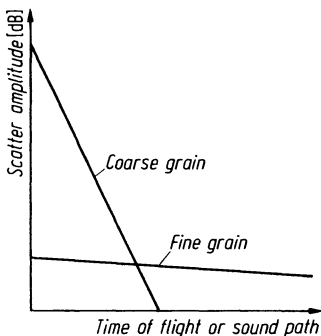
Fig. 33.15. Back-scatter amplitude versus sound path in a logarithmic presentation

According to [830, 431] it is possible to determine separately the amounts of scattering and absorption by measuring the decrease of the pulse amplitude in the propagation direction and also the back scattering amplitude.

The oldest practical application of scattering measurements is the determination of the hardened layer on chilled cast-iron rolls [1515, 1689, 1217]. Here, the transition from the "white iron" surface layer to the "grey iron" core is revealed by the increased sound scattering from the graphite lamellae in the core. Frequencies between 4 and 8 MHz are used with normal (0°) acoustic irradiation.

As with all scattering measurements the analysis of the results is better defined if the probe is moved during the test so as to average the indications from different grains, so that only the effective grain size is responsible for the measured back-scattering amplitude.

According to [829, 831, 832] it is also possible to detect the transition between the martensitic surface layer and the perlitic core in hardened steel rolls by the rise of the scattering amplitude. However, the overall effect is much less than on chilled cast-iron rolls and requires supplementary electronic evaluation circuitry. This measurement is made using transverse waves at an irradiation angle of 45° and with frequencies between 6 and 20 MHz.

In practice, applications of quantitative attenuation measurements for testing materials are still rather rare. Frequently, however, an estimation of the grain size and of the structure, for example in cast iron, can be obtained from the ratio of back echoes from different specimens of similar dimensions. In cast iron, the tensile strength can also be estimated from the attenuation but in this case, exact quantitative measurements are not usually required (see Section 31.3). According to [1040, 843, 1041] the hardness of steel can be derived from its attenuation values. Measurements of grain size are reported in [88, 191, 482, 63, 669, 805, 1249], especially in metals also in [127, 432, 1501, 1134, 635, 535, 563, 586]. A simple distinction between coarse and fine grained structures in forgings is treated in [482]. An installation for grain-size evaluation according to the method of [S 35] is presented in [1112].

Scientific works on sound attenuation are reported in [659, 658, 559, 1535, 1533, 940, 206, 1096, 669, 901 (in liquid steel), 1400, 1436, 381, 1165, 839, 1577, 1249, 1588, 1584 (in natural rock)]. The relation between attenuation and fatique is treated in [1628] for glass fibre-reinforced composites, and in [823] for railway axles. In [737] it is related to the structural changes taking place before cracks appear and during their subsequent propagation. The theory of sound propagation in polycrystalline structures [S 165, S 72, S 73, S 74] provides the basis for additional quantitative methods of using ultrasonics for structure analysis which not only exploit attenuation and scattering amplitudes, but also use the frequency dispersion of sound velocities.

33.4 Low-load Vickers Hardness Testing

It is well known that a vibrating mechanical resonator, a quartz crystal for instance, changes its resonant frequency when it makes contact with another solid body. It is also known that this frequency change increases if the contact pressure is increased, due to the corresponding increase in contact area. This fact suggests the possibility of building hardness-testing equipment based on this effect, in particular a fully automatic, rapid action, Vickers hardness tester.

The theory of elasticity gives a formula for the elastic stiffness of the contact zone, for a constant contact area A_c

$$k_c = C \left(\frac{1 - \nu_1^2}{E_1} + \frac{1 - \nu_2^2}{E_2} \right)^{-1} \sqrt{A_c} \tag{33.5}$$

where C is a numerical factor and E_1, E_2, ν_1 and ν_2 are the Young's moduli and the Poisson's ratios, respectively, of the two solids. The external elastic contact stiffness

k_c is added to the effective stiffness of the contacting resonator, resulting in an increase in the effective resonant frequency of the system.

Now, if it is possible to determine the exact value of k_c by experimental measurement, and if the elastic constants of the bodies in contact are known, the area of contact, A_c, can be calculated from formula (33.5). This makes it possible to measure the contact area resulting from an indentation under external pressure, thus also the indentation hardness. In practice the resonator used for this purpose is a metal rod with a diamond pyramid indenter firmly attached to one end. When a static loading force is applied to the other end in the axial direction, and the diamond is applied to the surface of a test piece, a permanent indentation results. At the same time the resonant frequency of the longitudinally excited rod increases by $\Delta f = f - f_0$, where f_0 is its free resonant frequency. The elastic stiffness of the contact zone can then be calculated from the equation:

$$k_c = k_0 \varphi \left(\frac{\Delta f}{f_0} \right) \tag{33.6}$$

where k_0 is a fixed stiffness term, and φ is a function that depends on the type of mechanical resonator used in the testing equipment.

The elastic term $E_1 (1 - \nu_1^2)$ of the indenter has a fixed value for use in Eq. (33.5). The corresponding term $E_2 (1 - \nu_2^2)$ for the test piece is not usually known, so that it has to be determined by a calibration procedure, for example by using standardized hardness testing blocks as references. When the quantity in brackets from Eq. (33.5) is established, the area A_c can be calculated from the k_c value which results from Eq. (33.6). At this stage the Vickers hardness is calculated from Eq. (33.7)

$$H_v = 0.09457 \frac{P}{A_c} \tag{33.7}$$

where P is the static test load, measured in N, and A_c is the *plane* surface contact area in mm^2 defined by the edges of the indentation when the full loading force P is applied. The plane contact area of a pyramid indentation with straight edges equals $\frac{1}{2} d_1 \cdot d_2$, where d_1 and d_2 are the lengths of the diagonals of the impression.

As the determination of k_c is obtained by the measurement at *u*ltrasonic frequencies, of a *c*ontact *i*mpedance, in which the elastic term happens to be predominant, the test has been named the UCI method. Figure 33.16 shows a portable instrument which operates according to this principle. Fig. 33.17 illustrates the design schematically. Fig. 33.18 shows the equivalent mechanical circuit of the oscillating system.
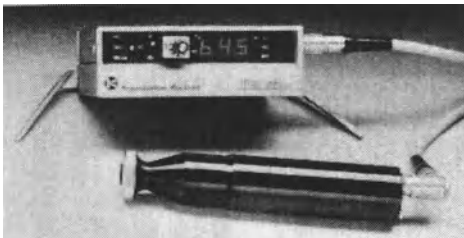

Fig. 33.16. Low-load portable hardness tester (design Krautkrämer-Kleesattel), battery operated, frequency 40 kHz, load $P = 8$ N, hardness numbers from 50 to 950 H$_v$ indicated digitally
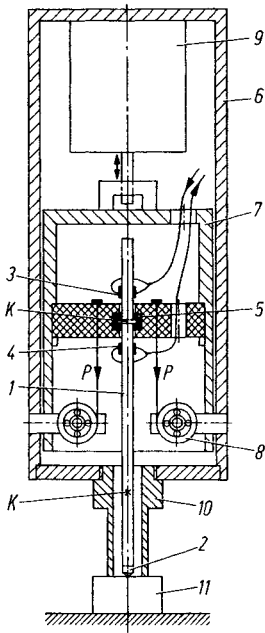
Fig. 33.17. Manual sensor of the UCI hardness tester.
1 resonating rod with two nodes K, *2* indentation body, a Vickers diamond pyramid, *3* PZT-ceramic transducers exciting the oscillation, *4* PZT-ceramic receivers, *5* rod mounting, acoustically soft, *6* outside housing, *7* innerhousing, axially moveable within 6, *8* two closely wound steel springs providing constant load, *9* servo-mechanics for automatic transport of the indenter rod with speed control for shock-free contact with the test piece, *10* protecting nozzle, *11* specimen

The resonant frequency of this system equals

$$f = \frac{1}{2\pi} \sqrt{\frac{k_0 + k_c}{m}}$$

and its free resonant frequency for $k_c = 0$ is

$$f = \frac{1}{2\pi} \sqrt{\frac{k_0}{m}} \ .$$

Hence

$$k_c = 4\pi^2 m \left(f^2 - f_0^2\right) = k_0 \frac{f^2 - f_0^2}{f_0^2} \ .$$

This reduces to

$$k_c \approx \frac{2 k_0}{f_0} \Delta f$$

if

$$0 \leqq \frac{\Delta f}{f_0} \leqq 0.02 \ .$$

For further details of the theory see [794, 795, S 54, S 87, S 86].

34 Standards

The growing importance of ultrasonic testing has persuaded associations for the application of non-destructive testing methods, of manufacturers and users, as well as standardizing organizations, to publish standards ranging from non-compulsory recommendations to specifications with legal status. In every country national standardizing commissions are investigating the specifications proposed by the various associations and societies. In the Federal Republic of Germany this is the DNA (Deutscher Normenausschuß) which publishes the DIN standards. On an international scale the ISO (International Organization for Standardization) is making efforts to reconcile and harmonize the standards of the various countries. For the same purpose on a european scale the CEN in Paris has been established (European Standards Committee). In addition, similar efforts are being made by international professional associations, e.g. in the field of welding, such as the IIW (International Institute of Welding).

In the ISO it is the Committee 135 (ISO TC 135) which is responsible for general nondestructive testing methods of materials. In a number of other committees, subcommittees are likewise engaged in standardizing special applications of nondestructive testing methods: e.g.

TC 11 – Boilers and pressure vessels, TC 44 – Welding,
TC 17 – Steel,   TC 85 – Nuclear energy.
TC 20 – Aircraft,

Any logical system of standards for ultrasonic testing methods should comprise a number of fundamental standards which serve as basis for a number of further standards for special test objects. In the past these latter standards, e.g. for welded joints, frequently were established prior to the fundamental standards as a matter of urgency. This is now clarified by a steering committee of the Deutsche Gesellschaft für zerstörungsfreie Prüfverfahren (DGZfP) [German Association for Nondestructive Testing Methods].

The Table below summarizes the standards of some countries published to date in accordance with this scheme, viz. fundamental standards and special standards, divided into international and national standards and standards of the most important non-official organisations. Where known, standards which are being presently drafted will also be mentioned. It is impossible to present a complete list, especially where this concerns standards of professional associations or even private companies (see [1261]). About the numerous USA standards see also [1736] and about Japanese standards [785]. For abbreviations see p. 579.

Country	Institution or its code (see page 579)	Title, in short	Year
I Fundamentals			
1. Terminology			
	IIW/IIS	List of terms used in ultrasonic testing	1967
BRD	DIN 54119	Zerstörungsfreie Prüfung. Ultraschall-prüfung. Begriffe	1981
DDR	TGL 15 003/01	dto.	1969
F	A 09-300 draft	Vocabulaire utilisé en contrôle par ultrasons	1982
GB	BS 3683	Glossary of terms. Part 4: Ultrasonic flaw detection	1965
USA	ASTM E 500	Standard definitions of terms relating to ultrasonic testing	1986
2. Training			
A	ÖNORM M 3040	Anforderungen an das Prüfpersonal für zerstörungsfreie Prüfungen	
		Teil 1: Allgemeine Richtlinien	1981
		Teil 2: Qualifikationsstufen I und II	1981
		Teil 3: Qualifikationsstufe III	1983
BRD	DIN 65450	Luft- und Raumfahrt. Zerstörungsfreie Prüfung. Anforderungen an Prüfpersonal	1983
USA	ASNT SNT-TC-1A	Personal qualification and certification in nondestructive testing	1980
	ASTM E 543	Practice for determining the qualification of nondestructive testing agencies	
3. Test blocks			
	ISO 2400	Welds in steel — reference block for the calibration of equipment for ultrasonic examination	1972
	ISO 7963	Reference block no. 2 for ultrasonic examination of welds	1985
BRD	DIN 54120	Kontrollkörper 1	1973
	DIN 54122	Kontrollkörper 2	1973
DDR	TGL 15 003/02	wie DIN 54120	1968
	TGL 15 003/03	wie DIN 54122	1968
F	NF A 04-311	Blocs d'étalonnage	1964
	NF A 89-611	Bloc d'étalonnage type No 2 pour le contrôle par ultrasons des soudures et des produits de base (Modèle allégé)	1981
GB	BS 2704	Calibration blocks	1978
J[a]	JIS Z 2345	Calibration blocks type G used in ultra-sonic normal beam testing (STB-G)	1973
	JIS Z 2346	Calibration block type N 1 used in ultra-sonic normal beam testing for steel plates (STB-N 1)	1978
	JIS Z 2347	Calibration block type A 1 used in ultra-sonic angle beam testing (STB-A 1)	1978
	JIS Z 2348	Calibration block type A 2 used in ultra-sonic angle beam testing (STB-A 2)	1978

Country	Institution or its code (see page 579)	Title, in short	Year
	JIS Z 2349	Calibration block type A 3 used in ultrasonic angle beam testing (STB-A 3)	1978
	NDIS 2301	Calibration block P 1 for ultrasonic Lamb wave testing.	1966
USA	ASTM E 127	Fabricating and checking aluminum alloy ultrasonic standard reference blocks	1982
	E 428	Fabrication and Control of Steel Reference Blocks Used in Ultrasonic Inspection	

4. Properties of instruments and probes

Country	Institution or its code	Title, in short	Year
BRD	DIN 54450	Kontrolle der Eigenschaften von Ultraschall Prüfsystemen	
		Teil 1: Einfache Kontrollen	1982
BRD	DIN 25450 draft	Ultraschallprüfsysteme für die manuelle Prüfung von Komponenten und Systemen	1988
F	NF A 09-320	Vérification simple en service des appareillages de contrôle manuel par ultrasons des produits métalliques	1984
	A 09-321 draft	Procédure de réception des appareils à ultrasons	1983
	A 09-330 draft	Définition et vérification des caractéristiques des faisceaux ultrasonores focalisés	1981
	A 09-322 draft	Caractérisation des traducteurs ultrasonores à usage industriel	1985
GB	BS 4331	Performance characteristics of ultrasonic flaw detection equipment	
		Part 1: Overall performance on-site methods	1978
		Part 2: Methods for assessing the perfomance characteristics	1972
	ESI 98-2 (Electricity Supply Industry)	Ultrasonic probes: Medium frequency miniature shear wave angle probes	1979
	ESI 98-7	Normal compression wave probes for contact testing	1982
	ESI 98-8	Low frequency single crystal shear wave angle probes	1982
	ESI 98-9	Ultrasonic flaw detectors	1985
J	NDIS 2105	Evaluation of performance characteristics for portable pulse-echo ultrasonic thickness meter	1976
	NDIS 2107	Measurement and representation of performance of wideband ultrasonic probes	1982
USA	ASTM E 317-79	Practice for evaluating performance characteristics of ultrasonic pulse-echo-testing system without the use of electronic measurement instruments	1979

[a] The Japanese Industrial Standards, as mentioned, base on former recommendations of the Japanese Nondestructive Inspection Society (NDIS) and have been published in English by the Japanese Standards Association.

Country	Institution or its code (see page 579)	Title, in short	Year
	ASTM draft	Evaluating the characteristics of ultrasonic search units	
	ASTM draft	Evaluating the electronic characteristics of sections of pulse-echo ultrasonic inspection instruments	
	ASTM E 317	Evaluating performance characteristics of ultrasonic pulse-echo testing systems without the use of electronic measurement instruments	1985

5. General testing technique

Country	Institution or its code	Title, in short	Year
BRD	DIN 54126	Regeln zur Prüfung mit Ultraschall	
		Teil 1: Anforderungen an Prüfsysteme und Prüfgegenstände	1982
		Teil 2: Durchführung der Prüfung	1982
BRD	DIN 54127 draft	Justierung von Ultraschall-Prüfsystemen und Bewertung von Echohöhen	1987
F	A 09-331 draft	Estimation des dimensions des réflecteurs ultrasonores à l'aide de faisceau ultrasonores focalisés	1981
J	JIS Z 2344	Ultrasonic testing of metals by the pulse echo technique	1979
	NDIS 2408	Measuring method of thickness by portable pulse-echo ultrasonic thickness meter	1979
USA	ASTM Draft	Proposed recommended practice for the detection and evaluation of discontinuities by the immersed pulse-echo ultrasonic method using longitudinal waves	
	ASTM E 214	Immersed ultrasonic testing by the reflection method using pulsed longitudinal waves	
	ASTM E 114	Recommended practice for ultrasonic pulse-echo straight-beam testing by the contact method	
	ASTM E 587	Ultrasonic angle beam examination by the contact method	
	ASTM E 804	Calibration of an ultrasonic test system by extrapolation between flat-bottom hole sizes	

II Special standards

1. Heavy forgings

Country	Institution or its code	Title, in short	Year
A	ÖNORM M 3002	Ultraschallprüfung von Schmiedestücken aus ferritischem und vergütbarem Stahl	1982
BRD	VDEh SEP 1921	Ultraschallprüfung von Schmiedestücken und geschmiedetem Stabstahl ab ca. 100 mm Durchmesser oder Kantenlänge	1985
DDR	TGL 101-267/01	Prüfung von Schmiedestücken durch Ultraschall	1965

Country	Institution or its code (see page 579)	Title, in short	Year
GB	BS M 36	Ultrasonic testing of special forgings by an immersion technique	1970
GB	BS 4124	Ultrasonic detection of imperfections in steel forgings	1987
GB	ESI 98-6	Ultrasonic testing of ferritic steel plate	1981
GB	ESI 98-13	Manual ultrasonic testing of forgings for turbine and generator rotors, shafts and discs	1983
GB	ESI 98-14	Ultrasonic testing procedures for nonmagnetic generator coil retaining rings	1983
J	JFSS 13-77 (Steel Casting Forging Association Japan)	Standard for ultrasonic inspection of marine forgings	1977
	NDIS 2411 JIS dto.	Ultrasonic testing of steel forgings in preparation	1980
USA	ASTM A 388	Recommended practice for ultrasonic examination of heavy steel forgings	
	ASTM A 418	Ultrasonic inspection of turbine and generator steel rotor forgings	
	ASTM A 503	Specification for ultrasonic examination of large forged crankshafts	
	ASTM A 531	Recommended practice for inspection of turbine-generator steel retaining rings	
	ASTM A 745	Ultrasonic examination of austenitic steel forgings	
	ASTM E 588	Detection of large inclusions in bearing quality steel by the ultrasonic method	
	ASTM A 21	Carbon steel axles, non-heat-treated and head-treated, for railway use	

2. *Plate*

Country	Institution or its code (see page 579)	Title, in short	Year
BRD	DIN 54123	Ultraschallverfahren zur Prüfung von Schweiß-, Walz- und Spreng-plattierungen	1980
	VDEh SEL 072-69	Stahl-Eisen-Lieferbedingungen: Ultraschallgeprüftes Grobblech	1977
DDR	TGL 15 003/10	Ultraschallprüfung von Blechen und Bändern	1983
F	NF A 04-305	Contrôles des tôles fortes aux ultra-sons — Définition de qualités — Méthodes d'essais	1983
GB	BS 5996	Methods for ultrasonic testing and speci-fying quality grades of ferritic steel plate	1980
GB	ESI 98-6	Ultrasonic testing of ferritic steel plate	198?
J	JIS G 801	Ultrasonic examination of steel plates for pressure vessels	1974
J	JIS C 901	Classification of structural rolled steel plate for building by ultrasonic test	1983
USA	ASTM A 435	Straight-beam ultrasonic examination of steel plates for pressure vessels	

Country	Institution or its code (see page 579)	Title, in short	Year
	ASTM A 577	Ultrasonic angle beam examination of steel plates	
	ASTM A 578	Straight-beam ultrasonic examination of plain and clad steel plates for special applications	
	ASTM B 548	Specification for standard method for ultrasonic inspection of aluminium alloy plate for pressure vessels	1982
USA	ASTM B 594-82	Method for ultrasonic inspection of aluminium-alloy wrought products for aerospace applications	1982

3. Tubes and other long products

Country	Institution or its code	Title, in short	Year
BRD	DIN 17175	Nahtlose Rohre aus warmfesten Stählen	1979
	VDEh SEP 1915	Stahl-Eisen-Prüfblatt: Ultraschallprüfung an nahtlosen Rohren aus warmfesten Stählen	1977
	VDEh SEP 1918	Ultraschallprüfung auf Querfehler von Rohren aus warmfesten Stählen	1977
	VDEh SEP 1919	Ultraschallprüfung auf Dopplungen von Rohren aus warmfesten Stählen	1977
	VDEh SEP 1921	Ultraschallprüfung von Schmiedestücken und geschmiedetem Stabstahl ab ca. 100 mm Durchmesser oder Kantenlänge	1985
F	NF A 49-870	Tubes en acier — Méthodes de contrôle non-destructif — Contrôle par ultrasons pour la recherche des défauts longitudineaux	1981
	NF A 04-307	Détection par ultrasons des défauts internes des produits longs autres que poutrelles, rails et profilés analogues (contrôle manuel)	1983
GB	BS 3889	Ultrasonic testing of ferrous pipes	1965
GB	ESI 98-5	Automatic ultrasonic testing of tubes, Part 1: Seamless and welded tubes outside diameters of 12 mm up to but not including 160 mm Part 2: Seamless steel tubes outside diameters 160 mm and above	1983
USA	ASTM A 376	Specification for seamless austenitic steel pipe for high temperature central station service	
	ASTM A 450	General requirements for carbon, ferrite alloy, and austenitic alloy steel tubes	
	ASTM A 556	Standard Specification for seamless cold-drawn carbon steel feedwater heater tubes	
	ASTM A 557	Standard Specification for electric-resistance welded carbon steel feedwater heater tubes	
	ASTM E 213	Ultrasonic inspection of metal pipe and tubing for longitudinal discontinuities	1985

Country	Institution or its code (see page 579)	Title, in short	Year
	ASTM E 453	Recommended practice for examination of fuel element cladding including the determination of the mechanical properties	
	ASTM A 376	Specification for seamless austenitic steel pipe for high temperature central station service	1985

4. Castings

Country	Institution or its code	Title, in short	Year
BRD	DIN 17245	Warmfester Stahlguß	1987
	VDEh SEP 1922	Stahl-Eisen-Prüfblatt: Ultraschallprüfung von Gußstücken aus ferritischem Stahl	1989
	VDG P 540 (Verein Deutscher Gießerei-fachleute)	Ultraschallprüfung von Gußstücken aus Gußeisen mit Kugelgraphit	1988
GB	BS 4080	Non-destructive testing of steel castings	1966
GB	ESI 98-4	Ultrasonic testing of ferritic steel castings	1982
USA	ASTM A 609	Specification for ultrasonic examination of carbon and low-alloy steel castings	1983

5. Welded Seams

Country	Institution or its code	Title, in short	Year
	IIW/IIS		
	— 205-66	Draft recommended practice for the ultrasonic inspection of butt welds Handbook	1966
	—	on the ultrasonic examination of welds. Welding Institute Abington	1977
	— VC 422-84	Handbook on the ultrasonic examination of austenitic welds	1984
	— V-732-82	Subcommission VC Working Group: Guidance on the assessment of ultrasonic indications to determine defect type and defect size	1982
	— V-714-821	Recommendations concerning the defect sizing with ultrasound on welds	1982
	— V-664-79	Example for the direct evaluation of ultrasonic indications using the reflectivity diagram method (go/no go-criteria)	1979
	— V-751-83	Danish Central Welding Institute: Quality classes for the arc welded joints in steel materials	1983
	— V-627-78	Herman, H.: Ultrasonic testing of heated tool welded butt joints in hard polyethylene	1978
A	ÖNORM M 3001	Ultraschallprüfung von Schmelzschweiß-nähten ferritischer Stähle	1986
	ÖNORM C 2125	Oberirdische zylindrische Flachboden-behälter aus metallischen Werkstoffen. Grundlagen. Ausführungen, Prüfungen	1982
BRD	DIN 54123	Ultraschallverfahren zur Prüfung von Schweiß-, Walz- und Spreng-plattierungen	1980

Country	Institution or its code (see page 579)	Title, in short	Year
	DIN 54 125	Zerstörungsfreie Prüfung: Prüfung von Schweißverbindungen mit Ultraschall	1983
	DIN 54 125 Beibl. 1	Anwendungshilfen zur Norm	1983
	AD Merkbl. HP 5/3 (Arbeitsgemeinschaft Druckbehälter)	Herstellung und Prüfung der Verbindungen: Zerstörungsfreie Prüfung der Schweißnähte	1981
	Anlage zu HP 5/3	Verfahrenstechnische Mindestanforderungen für die zerstörungsfreien Prüfverfahren	1977
	KTA 3201.3	Komponenten des Primärkreises von Leichtwasserreaktoren: Herstellung	1979
	VDEh SEP 1916	Zerstörungsfreie Prüfung schmelzgeschweißter Fernleitungsrohre für brennbare Flüssigkeiten und Gase	1975
DDR	TGL 15 003/11	Ultraschallprüfung: Prüfung von Schweißverbindungen	1988
GB	BS 3923	Methods for ultrasonic examination of welds	
		Part 1. Manual examination of fusion welded butt joints in ferritic steels	1978
		Part 2. Automatic examination of fusion welded butt joints in ferritic steels	1972
		Part 3. Manual examination of nozzle welds	1972
	BS 3923	Ultrasonic examination of welds	
		Part 1: Methods for manual examination of fusion welds in ferritic steels	1986
		Part 2: Automatic examination of fusion welded butt joints in ferritic steels	1972
		Part 3: Manual examination of nozzle welds	1972
	BS M 42	Non-destructive testing of fusion and resistance welds in thin gauge materials	1972
	ESI 98-5	Automatic ultrasonic testing of tubes, Part 1: Seamless and welded tubes outside diameters of 12 mm up to but not including 160 mm	1983
		Part 3: Longitudinally submerged arc welded steel tubes, outside diameters 160 mm and above	
		Part 4: Longitudinally electric resistance and induction welded steel tubes outside diameters 160 mm and above	
	ESI 98-10	Manual ultrasonic testing of welds in ferritic steel sections	
		Part 1: Butt welds in ferritic steel sections greater than 10 mm thick	1984
		Part 2: Nozzle, brand, stub and attachment welds	1983

Country	Institution or its code (see page 579)	Title, in short	Year
		Part 3: Butt welds in tubes of outside diameters between 25 mm and 120 mm inclusive	1984
	ESI 98-10	Manual ultrasonic testing of welds in ferritic steel sections	
		Parts 1: Butt welds in ferritic steel sections greater than 10 mm thick	1981
		Part 2: Nozzle, branch, stub and attachment welds	1983
J	JIS Z 3060	Ultrasonic testing of ferritic steel welds and the classification of test results	1975
	JIS Z 3061	Method of ultrasonic manual testing for ferritic steel welds on curved material	1983
	JIS Z 3080	Method of ultrasonic angle beam testing and classification of test results for aluminium welds	1982
	NDIS 2407	Methods for automatic ultrasonic testing of steel welds	1976
USA	ASTM E 164	Recommendation for ultrasonic contact examination of weldments	1981
	ASTM E 273	Ultrasonic inspection of longitudinal and spiral welds of welded pipe and tubing	1983
	ASME	Boiler and pressure vessel code Section III: Nuclear power plant components, Appendix IX 3000 Non-destructive methods of examination	1971
	ASTM F 600	Nondestructive ultrasonic evaluation of socket and butt joints of thermoplastic piping	
	ASME	Boiler and pressure vessel code Section III: Nuclear power plant components, Appendix IX 3000 Non-destructive methods of examination	1971
UdSSR	Gost 14 782-69	Schweißverbindungen. Methoden der Ultraschallprüfung	1970

6. Miscellaneous

	ISO 4386	Plain bearings. Part 1: Nondestructive ultrasonic testing of bond for bearing metal layer thickness $\geqq 2$ mm	1987
	ISO 5948	Railway rolling stock material. Ultrasonic acceptance testing	1981
BRD	DIN 25435	Kerntechnische Anlagen. Wieder-kehrende Prüfungen	1979
		Teil 1: Mechanisierte Ultraschall-prüfungen	1979
		Teil 5: Protokollvordrucke zur Dokumentation der Daten mechani-sierter Ultraschallprüfeinrichtungen	1981

Country	Institution or its code (see page 579)	Title, in short	Year
	DKI Werkstoff-Prüfblatt Nr. 831 (Deutsches Kupfer-Institut)	Ultraschallprüfung von Platten aus Kupfer und Kupferlegierungen	1985
GB	BS 4408	Part 5: Recommendations for non-destructive methods of test for concrete. Measurement of the velocity of ultrasonic pulses in concrete	1974
USA	ASTM C 597	Test method for pulse velocity through concrete	1983
	ASTM B 594	Ultrasonic inspection of aluminium-alloy products for aerospace applications	
	ASTM D 2845	Test method for pulse velocities and ultrasonic elastic constants of rock, laboratory determination of	
	ASTM E 494	Measuring ultrasonic velocity in materials	
	ASTM E 664	Measurement of the apparent attenuation of longitudinal ultrasonic waves by immersion method	
	ASTM E 797	Measuring thickness by manual ultra-sonic pulse-echo contact method	
	ASTM G 46	Recommended practice for examination and evaluation of pitting corrosion	
	ASTM D 2966	Test method for cavitation erosion-corrosion characteristics of aluminium in Engine Coolants Using Ultrasonic Energy	

Appendix. Tables, Formulae and Diagrams

Table A 1. Densities, velocity of sound and acoustic impedances of some materials

Material	Density ϱ 10^3 kg/m^3	Velocity of sound		Acoustic impedance $Z = \varrho c_l$ 10^6 kg/m^{2}s
		long. c_l 10^3 m/s	transv. c_t 10^3 m/s	
Metals				
Aluminium	2.7	6.32	3.13	17
Bismuth	9.8	2.18	1.10	21
Brass (58)	8.4	4.40	2.20	37
Cadmium	8.6	2.78	1.50	24
Cast iron (cf. Section 31.3)	6.9 to 7.3	3.5 to 5.8	2.2 to 3.2	25 to 42
Constantan	8.8	5.24	2.64	46
Copper	8.9	4.70	2.26	42
German silver	8.4	4.76	2.16	40
Gold	19.3	3.24	1.20	63
Stellite	11 to 15	6.8 to 7.3	4.0 to 4.7	77 to 102
Iron (steel) (cf. Section 31.1)	7.7	5.90	3.23	45
Lead	11.4	2.16	0.70	25
Magnesium	1.7	5.77	3.05	10
Manganin	8.4	4.66	2.35	39
Mercury	13.6	1.45	—	20
Nickel	8.8	5.63	2.96	50
Platinum	21.4	3.96	1.67	85
Silver	10.5	3.60	1.59	38
Tin	7.3	3.32	1.67	24
Tungsten	19.1	5.46	2.62	104
Zinc	7.1	4.17	2.41	30
Non-metals				
Aluminium oxide	3.6 to 3.95	9 to 11	5.5 to 6.5	32 to 43
Epoxy resin	1.1 to 1.25	2.4 to 2.9	1.1	2.7 to 3.6
Glass, flint	3.6	4.26	2.56	15
Glass, crown	2.5	5.66	3.42	14
Ice	0.9	3.98	1.99	3.6
Paraffin wax	0.83	2.2	—	1.8
Acrylic resin (Perspex)	1.18	2.73	1.43	3.2
Polyamide (nylon, perlon)	1.1 to 1.2	2.2 to 2.6	1.1 to 1.2	2.4 to 3.1
Polystyrene	1.06	2.35	1.15	2.5
Porcelain (see Section 32.1)	2.4	5.6 to 6.2	3.5 to 3.7	13
Quartz glass (silica)	2.6	5.57	3.52	14.5
Rubber, soft	0.9	1.48	—	1.4
Rubber, vulcanized	1.2	2.3	—	2.8
Polytetrafluoroethylene (Teflon)	2.2	1.35	0.55	3.0
Liquids				
Glycerine	1.26	1.92	—	2.5
Methylene iodide	3.23	0.98	—	3.2
Diesel oil	0.80	1.25	—	1.0
Motor car oil (SAE 20 a. 30)	0.87	1.74	—	1.5
Water (at 20 °C)	1.0	1.483	—	1.5

Table A 2. Reflection at boundaries for normal incidence
Upper figures: reflection factor of amplitude in %
Lower figures: gain (dB) needed to compensate the reduced reflection

	Aluminium	Lead	Iron (steel)	Stellite	Copper	Brass	Nickel	Silver	Tungsten	Glass (crown and ordinary)	Rubber, soft	Rubber, vulcanized	Perspex	Porcelain	Glycerine	Methylene iodide	Oil (motor car oil SAE 20 to 30)a. water	Mercury
Aluminium	0	18 15	46 6.8	71 3.0	41 7.8	29 11	49 6.1	38 8.4	72 2.9	10 20	85 1.4	72 2.9	68 3.3	13 18	74 2.6	68 3.3	84 1.5	7 23
Lead		0	30 10	60 4.4	26 12	12 19	34 9.5	21 14	62 4.2	27 11	89 1.0	80 2.0	77 2.3	31 10	82 1.8	77 2.3	89 1.1	11 19
Iron (steel)			0	37 8.6	4 27	19 14	4 28	9 21	39 8.2	53 5.5	94 0.5	88 1.1	87 1.2	56 5.1	88 1.2	87 1.2	94 0.6	40 8.1
Stellite				0	41 7.8	53 5.6	33 9.6	45 6.9	2 34	75 2.4	97 0.2	95 0.5	94 0.6	77 2.3	95 0.4	94 0.6	97 0.3	67 3.5
Copper					0	15 17	8 22	5 26	43 7.4	50 6.0	94 0.6	87 1.2	86 1.3	53 5.6	89 1.0	86 1.3	93 0.6	36 8.9
Brass						0	23 13	10 20	54 5.4	38 8.5	91 0.8	83 1.6	81 1.8	41 7.6	85 1.4	81 1.8	91 0.8	22 13
Nickel							0	13 17	35 9.0	56 5.0	94 0.5	89 1.0	88 1.1	58 4.7	90 0.9	88 1.1	94 0.5	33 9.5
Silver								0	47 6.6	46 6.8	93 0.7	86 1.3	84 1.5	49 6.2	88 1.2	84 1.5	92 0.7	31 11
Tungsten									0	76 2.4	97 0.2	95 0.5	94 0.5	78 2.2	95 0.4	94 0.5	97 0.2	68 3.3
Glass (crown and ordinary)										0	82 1.8	67 3.5	63 4.0	4 29	70 3.1	63 4.0	81 1.9	17 15
Rubber, soft											0	50 6	40 8	80 2	30 11	40 8	3 30	87 1.2
Rubber, vulcanized												0	7 23	65 3.8	6 25	7 23	30 10	75 2.5
Perspex													0	60 4.4	10 20	0 ∞	40 9	72 2.8
Porcelain														0	70 3	60 4	80 2	20 14
Glycerine															0	10 20	25 12	78 2.2
Methylene iodide																0	40 9	72 2.8
Oil (motor car oil SAE 20 to 30) and water																	0	86 1.3
Mercury																		0

Formulae for Reflection and Transmission Coefficients

The following formulae give reflection (R) and transmission (D) coefficients for the acoustic pressure as a function of the incidence angle, calculated for plane waves on plane boundaries and disregarding absorption. The notation of the formulas is based on that of Schoch [35] where, however, they refer not to the acoustic pressure but to the particle displacement.

The following equations do not seem to have solutions in certain angular ranges, especially beyond the critical angle for the total reflection of the longitudinal wave, because an angle is required with a sine function greater than one. This arises from the fact that in the derivation of the formulas complex functions have been used. In this case it helps therefore to replace the real angles by imaginary ones, for example α by $i\mu$ and to use hyperbolic functions (sinh, cosh etc.). The general relationships

$$\cos i\mu = \cosh \mu \quad \text{and} \quad \sin i\mu = i \sinh \mu$$

then apply and the equations can be solved. The solutions will, in general, be complex values, the physical meaning of which is a phase shift (φ) at the boundary, where $\tan \varphi = Im(R)/Re(R)$ and similarly for D. In the figures 2.7 to 2.12 and in the following diagrams only the ratio of amplitudes, given by

$$\sqrt{(Im(x))^2 + (Re(x))^2} \, ,$$

are shown.

If the angular solutions have imaginary values, the corresponding waves are damped transversely, as in the case of the well known surface waves. If the velocity solutions have complex values the corresponding waves are damped longitudinally and propagate as do conventional waves in an absorbing material.

Most of the solutions of Eq. (A 27) for example are of this type. In Diagram 9, however, only the few solutions with real values for the velocity are displayed.

a) Free boundary of a solid. (See Figs. 2.7, 2.8 and Diagram 1). Symbols: the angles of the longitudinal and transverse waves are α_l and α_t, respectively. Thus for example R_{lt} signifies the reflection coefficient of the acoustic pressure for a reflected longitudinal wave reffered to an incident transverse wave. For the reflected *longitudinal wave* we have:

$$R_{ll} = \frac{(c_t/c_l)^2 \sin 2\alpha_l \sin 2\alpha_t - \cos^2 2\alpha_t}{N} \tag{A 1}$$

with the abbreviation for the denominator

$$N = \left(\frac{c_t}{c_l}\right)^2 \sin 2\alpha_l \sin 2\alpha_t + \cos^2 2\alpha_t \, ,$$

for the reflected *transverse wave:*

$$R_{tl} = \frac{2(c_t/c_l)^2 \sin 2\alpha_l \cos 2\alpha_t}{N}, \tag{A 2}$$

with incident transverse wave (oscillation plane parallel to plane of incidence) (cf. Fig. 2.8) for the reflected *longitudinal wave:*

$$R_{lt} = -\frac{\sin 4\alpha_t}{N}, \tag{A 3}$$

for the reflected *transverse wave:*

$$R_{tt} = \frac{(c_t/c_l)^2 \sin 2\alpha_l \sin 2\alpha_t - \cos^2 2\alpha_t}{N} \equiv R_{ll}. \tag{A 4}$$

b) Interface between two liquids. Symbols: the angles of the incident, reflected and transmitted longitudinal waves are α_i, α_r and α_d, respectively. The velocity of sound and acoustic densities of materials 1 and 2 are c_1, ϱ_1 and c_2, ϱ_2, respectively. The reflection coefficient of the acoustic pressure

$$R = \frac{\cos \alpha_i - (\varrho_1 c_1/\varrho_2 c_2) \sqrt{1 - (c_2/c_1)^2 \sin^2 \alpha_i}}{\cos \alpha_i + (\varrho_1 c_1/\varrho_2 c_2) \sqrt{1 - (c_2/c_1)^2 \sin^2 \alpha_i}}, \tag{A 5}$$

the transmission coefficient of the acoustic pressure

$$D = \frac{2 \cos \alpha_i}{\cos \alpha_i + (\varrho_1 c_1/\varrho_2 c_2) \sqrt{1 - (c_2/c_1)^2 \sin^2 \alpha_i}}. \tag{A 6}$$

c) Interface between liquids and solids. Symbols: angle of longitudinal wave in liquid α, angles of longitudinal and transverse waves in solid α_l and α_t, density and velocity of sound in liquid ϱ and c, in solid ϱ_f. c_l and c_t, respectively.

In the case liquid/solid (i.e. incident longitudinal wave in liquid) (see Fig. 2.9 and Diagram 2) we have:

$$R = \frac{1}{N} \left\langle \left(\frac{c_t}{c_l}\right)^2 \sin 2\alpha_l \sin 2\alpha_t + \cos^2 2\alpha_t - \frac{\varrho c}{\varrho_f c_l} \frac{\cos \alpha_l}{\cos \alpha} \right\rangle \tag{A 7}$$

with the abbreviation

$$N = \left(\frac{c_t}{c_l}\right)^2 \sin 2\alpha_l \sin 2\alpha_t + \cos^2 2\alpha_t + \frac{\varrho c}{\varrho_f c_l} \frac{\cos \alpha_l}{\cos \alpha}.$$

$$D_{ll} = \frac{2}{N} \cos 2\alpha_t, \tag{A 8}$$

$$D_{tl} = -\frac{2}{N} \left(\frac{c_t}{c_l}\right)^2 \sin 2\alpha_l. \tag{A 9}$$

In the case solid/liquid (see Figs. 2.10, 2.11) and Diagrams 3 and 4) with incident longitudinal wave, we have for the reflected *longitudinal wave:*

$$R_{ll} = \frac{1}{N} \left\langle \left(\frac{c_t}{c_l}\right)^2 \sin 2\alpha_l \sin 2\alpha_t - \cos^2 2\alpha_t + \frac{\varrho c}{c_f \varrho_l} \frac{\cos \alpha_l}{\cos \alpha} \right\rangle, \qquad (A\,10)$$

for the reflected *transverse wave:*

$$R_{tl} = \frac{2}{N} \left(\frac{c_t}{c_l}\right)^2 \sin 2\alpha_l \cos 2\alpha_t \qquad (A\,11)$$

and for the transmitted *longitudinal wave* in the liquid:

$$D_{ll} = \frac{2}{N} \frac{\varrho c \cos \alpha_l \cos 2\alpha_t}{\varrho_f c_l \cos \alpha}. \qquad (A\,12)$$

In the case solid/liquid with an incident transverse wave:

$$R_{tt} = \frac{1}{N} \left\langle \left(\frac{c_t}{c_l}\right)^2 \sin 2\alpha_l \sin 2\alpha_t - \cos^2 2\alpha_t - \frac{\varrho c}{\varrho_f c_l} \frac{\cos \alpha_l}{\cos \alpha} \right\rangle, \qquad (A\,13)$$

$$R_{lt} = -\frac{1}{N} \sin 4\alpha_t, \qquad (A\,14)$$

$$D_{lt} = \frac{2}{N} \frac{\varrho c}{\varrho_f c_l} \frac{\cos \alpha_l \sin 2\alpha_t}{\cos \alpha}. \qquad (A\,15)$$

The echo transmittances (see Fig. 2.14 and Diagrams 5 to 8) for both cases, solid/liquid and liquid/solid are identical. If in both materials the longitudinal wave is used, we have

$$E_{ll} = \frac{4}{N^2} \frac{\varrho c}{\varrho_f c_l} \frac{\cos \alpha_l \cos^2 2\alpha_t}{\cos \alpha}, \qquad (A\,16)$$

but if the transverse wave is used in the solid,

$$E_{lt} = \frac{4}{N^2} \left(\frac{c_t}{c_l}\right)^2 \frac{\varrho c}{\varrho_f c_l} \frac{\cos \alpha_l \sin 2\alpha_t \sin 2\alpha_l}{\cos \alpha}. \qquad (A\,17)$$

d) Interface between two solids. The values in Diagrams 7 and 8 were calculated from a computer program by Kühn and Lutsch [869]. For the case of coupling through a thin liquid layer, and using the above symbols, the following reflection and transmission formulae apply.

Abbreviations: denominator N (index 1 for material 1, index 2 for material 2)

$$N = 2 \cot \alpha_{1t} + \frac{\cos^2 2\alpha_{1t}}{2 \sin^4 \alpha_{1t}} \tan \alpha_{1l} + \frac{2\varrho_2 c_{2t}^4}{\varrho_1 c_{1t}^4} \cot \alpha_{2t} + \frac{\varrho_2 \cos^2 \alpha_{2t}}{2\varrho_1 \sin^4 \alpha_{1t}} \tan \alpha_{2l}. \ (A\,18)$$

For the incident longitudinal wave in material 1:

$$R_{ll} = 1 - \frac{\cos^2 2\alpha_{1t}}{N \sin^4 \alpha_{1t}} \tan \alpha_{1l}, \qquad (A\,19)$$

$$R_{tl} = \frac{2 \cos 2\alpha_{1t}}{N \sin^2 \alpha_{1t}}, \qquad (A\,20)$$

$$D_{\mathrm{ll}} = \frac{\varrho_2}{\varrho_1} \; \frac{\cos 2\alpha_{1t} \cos 2\alpha_{2t}}{N \sin^4 \alpha_{1t}} \tan \alpha_{21}, \qquad \text{(A 21)}$$

$$D_{\mathrm{tl}} = \frac{2\varrho_2 c_{2t}^2}{\varrho_1 c_{1t}^2} \; \frac{\cos 2\alpha_{1t}}{N \sin^2 \alpha_{1t}}. \qquad \text{(A 22)}$$

For the incident transverse wave in material 1:

$$R_{\mathrm{lt}} = \frac{4c_{1l}^2}{c_{1t}^2} \; \frac{\cos 2\alpha_{1t}}{N \sin 2\alpha_{1l}} \cot \alpha_{1t} \qquad \text{(A 23)}$$

$$R_{\mathrm{tt}} = \frac{4}{N} \cot \alpha_{1t} - 1, \qquad \text{(A 24)}$$

$$D_{\mathrm{lt}} = -\frac{4\varrho_2 c_{2l}^2}{\varrho_1 c_{1t}^2} \; \frac{\cos 2\alpha_{2t}}{N \sin 2\alpha_{2l}} \cot \alpha_{1t}, \qquad \text{(A 25)}$$

$$D_{\mathrm{tt}} = \frac{4\varrho_2 c_{2t}^2}{\varrho_1 c_{1t}^2} \; \frac{1}{N} \cot \alpha_{1t} \qquad \text{(A 26)}$$

Note: For the incident wave in material 2, the indices 1 and 2 should be interchanged.

e) *Velocity of lamb waves.* Referring to Diagram 9: Optimal sound propagation occurs if for the angle α between the transverse wave and the perpendicular to the plate the following equation is fulfilled:

$$F_{1,2} = G \qquad \text{(A 27)}$$

with the abbreviations:

$$a = \pi \frac{d}{\lambda_t}; \qquad q = \frac{c_t}{c_l}; \qquad s = \sin \alpha_t;$$

$$T_1 = \tanh \sqrt{s^2 - 1}\, a; \qquad T_q = \tanh \sqrt{s^2 - q^2}\, a;$$

$$F_1 = \frac{T_1}{T_q} \quad \text{for symmetric Lamb waves,}$$

$$F_2 = \frac{T_q}{T_1} \quad \text{for antisymmetric Lamb waves,}$$

$$G = \frac{4s^2 \sqrt{s^2 - 1} \sqrt{s^2 - q^2}}{(2s^2 - 1)^2} \quad \text{for both.}$$

The correlated velocity of propagation (group velocity) then is [1216]:

$$u_\mathrm{p} = \frac{c_t}{s + a \dfrac{\mathrm{d}s}{\mathrm{d}a}}. \qquad \text{(A 28)}$$

The differential ds/da calculated from (A 27) is:

$$\frac{ds}{da} = \frac{\dfrac{\partial F_{1,2}}{\partial a}}{\dfrac{\partial G}{\partial s} - \dfrac{\partial F_{1,2}}{\partial s}},$$

(A 29)

and explicitly for the symmetric wave modes:

$$\frac{\partial G}{\partial s} = s \frac{8(q^2 - 1) s^4 + 4(3 - q^2) s^2 - 8q^2}{(2s^2 - 1)^3 \sqrt{s^2 - 1} \sqrt{s^2 - q^2}},$$

$$\frac{\partial F_1}{\partial s} = \frac{as}{T_q^2} \left\{ \frac{T_q(T_1^2 - 1)}{\sqrt{s^2 - 1}} + \frac{T_1(1 - T_q^2)}{\sqrt{s^2 - q^2}} \right\},$$

$$\frac{\partial F_1}{\partial a} = \frac{1}{T_q^2} \left\{ \sqrt{s^2 - 1}\, T_q(1 - T_1^2) + \sqrt{s^2 - q^2}\, T_1(T_q^2 - 1) \right\}.$$

For the antisymmetric forms the tanh function should be replaced by the coth function.

Diagram 1. Reflection at free boundary of steel

R_{ll}, reflection coefficient for longitudinal wave versus incidence angle of longitudinal wave, α_l (*bottom scale*), according to Eq. (A 1);

R_{tl}, reflection coefficient for transverse wave versus incidence angle of longitudinal wave, α_t (*top scale*), according to Eq. (A 2);

R_{lt}, reflection coefficient for transverse wave versus incidence angle of transverse wave, α_l, according to Eq. (A 3);

R_{tt}, reflection coefficient for transverse wave versus incidence angle of transverse wave, α_t, identical with R_{ll}, according to Eq. (A 4)
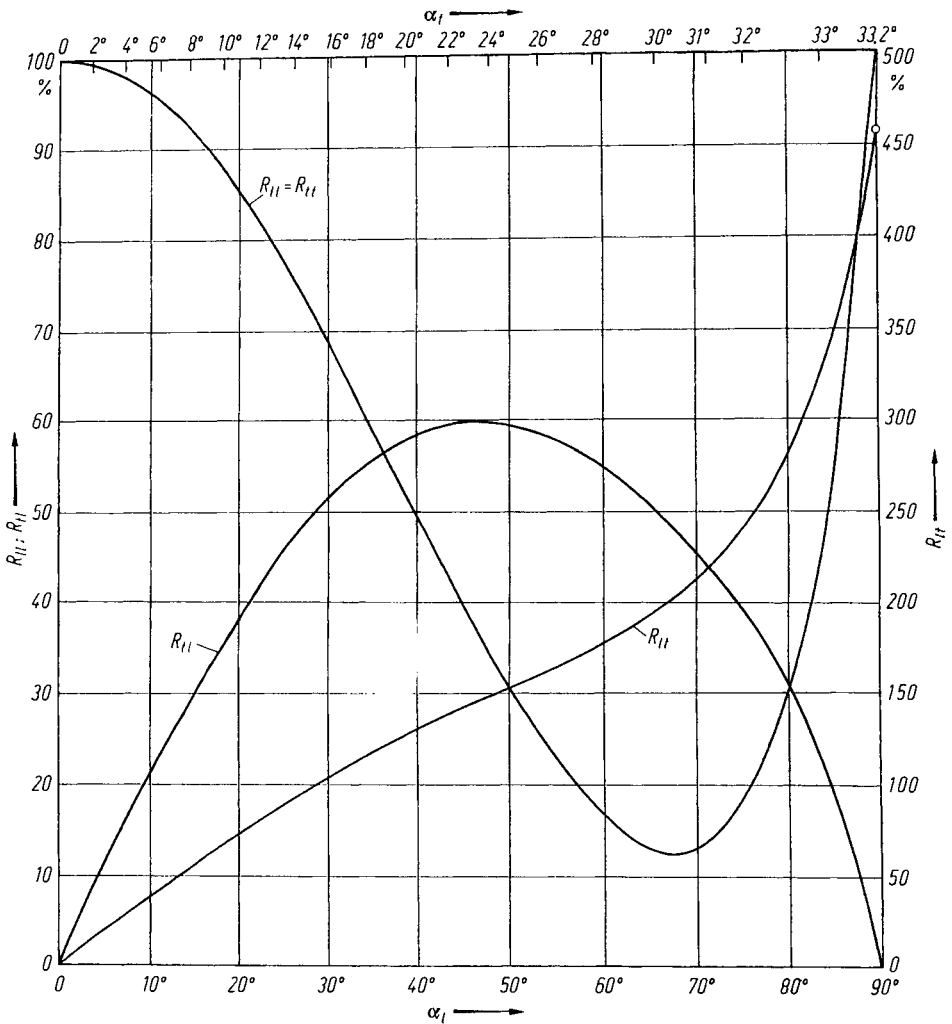
Diagram 2. Reflection and transmission of longitudinal waves at water-aluminium interface

Longitudinal wave incident in water at angle α gives longitudinal wave in aluminium with angle α_1 and transverse wave with α_t. Calculated from Eqs. (A 7) to (A 9) with the constants

$$c_t/c_l = 0.488; \qquad c_l/c = 4.26; \qquad \frac{\varrho c}{\varrho_f c_l} = 0.0888$$
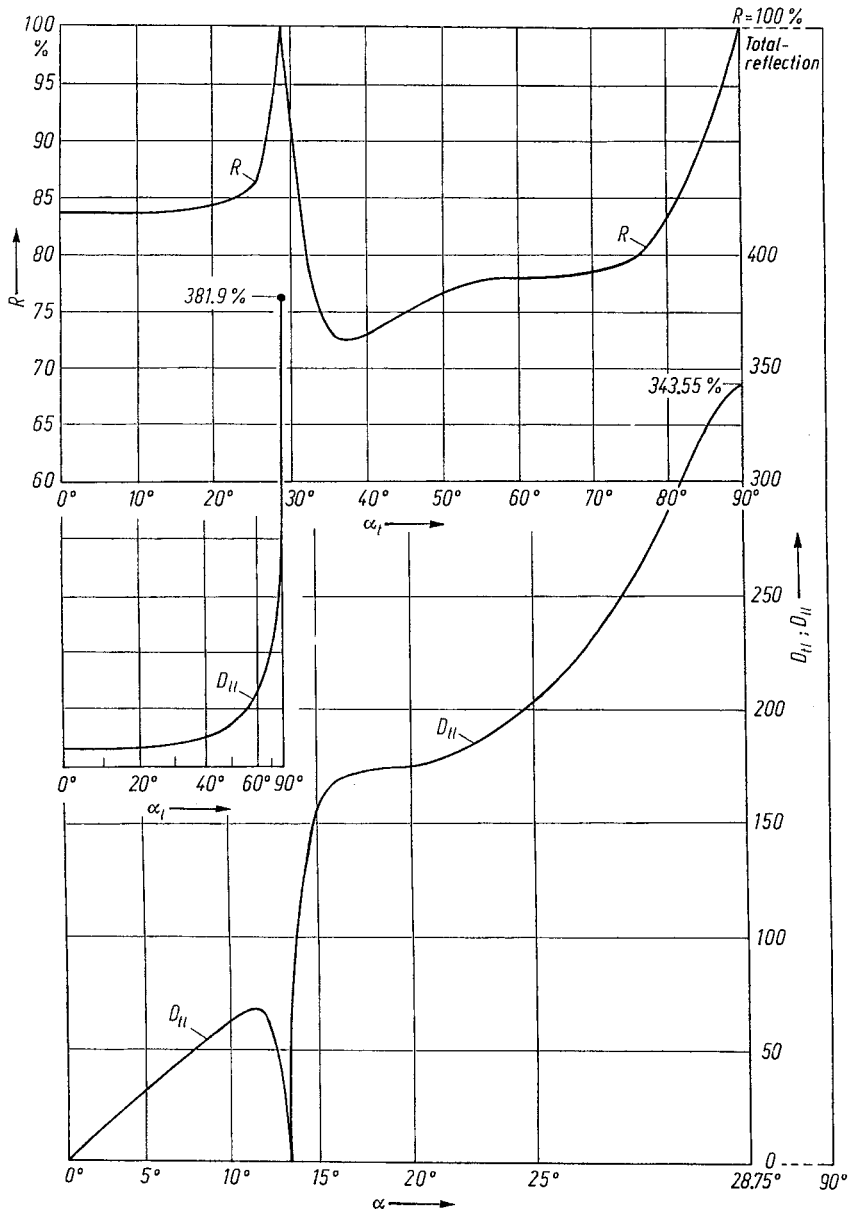
Diagram 3. Reflection and transmission of longitudinal waves at aluminium-water interface

Longitudinal wave incident in aluminium at angle α_1 gives reflected longitudinal wave in aluminium with angle α_1, reflected transverse wave in aluminium with angle α_t and transmitted longitudinal wave in water with angle α (Eqs. (A 10) to A 12), regarding constants, see Diagram 2)
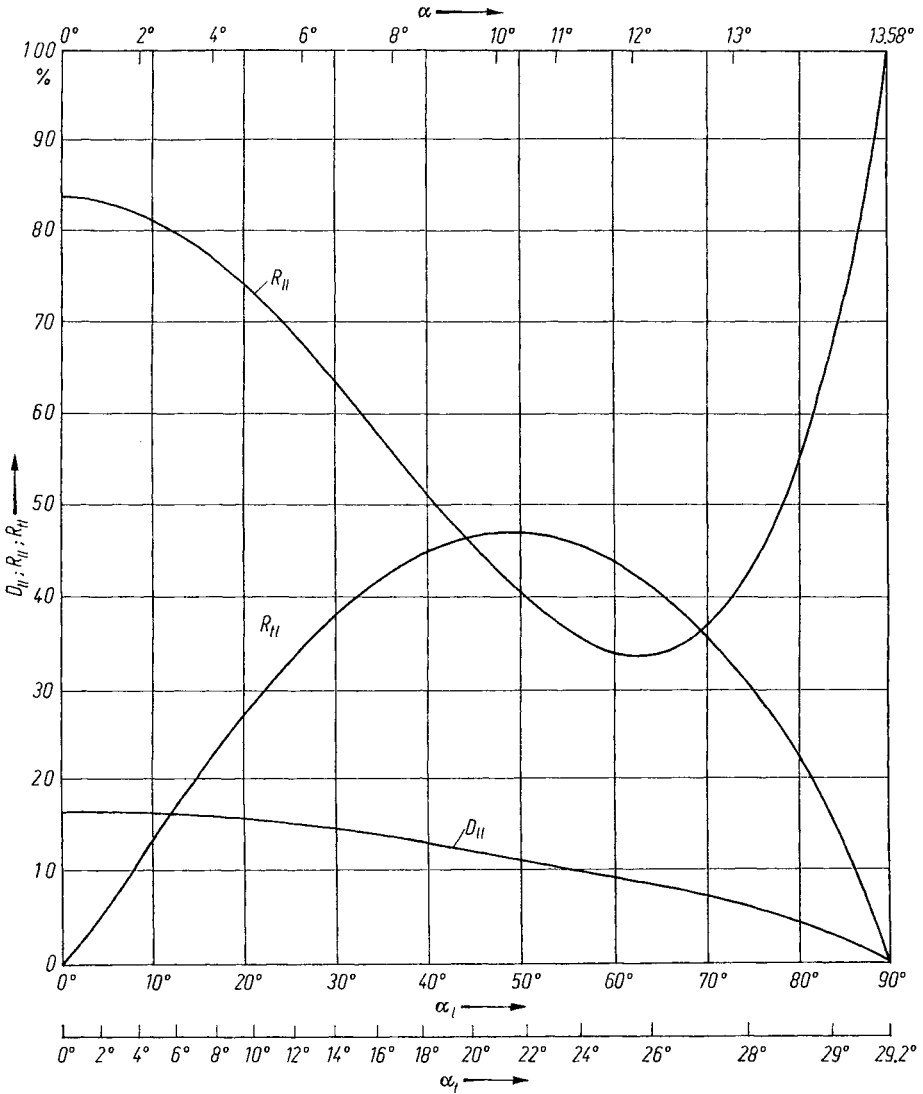
Diagram 4. Reflection and transmission of transverse waves at aluminium-water interface

Transverse wave incident in aluminium at angle α_t gives reflected transverse wave with α_t, reflected longitudinal wave with α_l and transmitted longitudinal wave in water with angle α (Eqs. (A 13) to (A 15), regarding constants see Diagram 2)
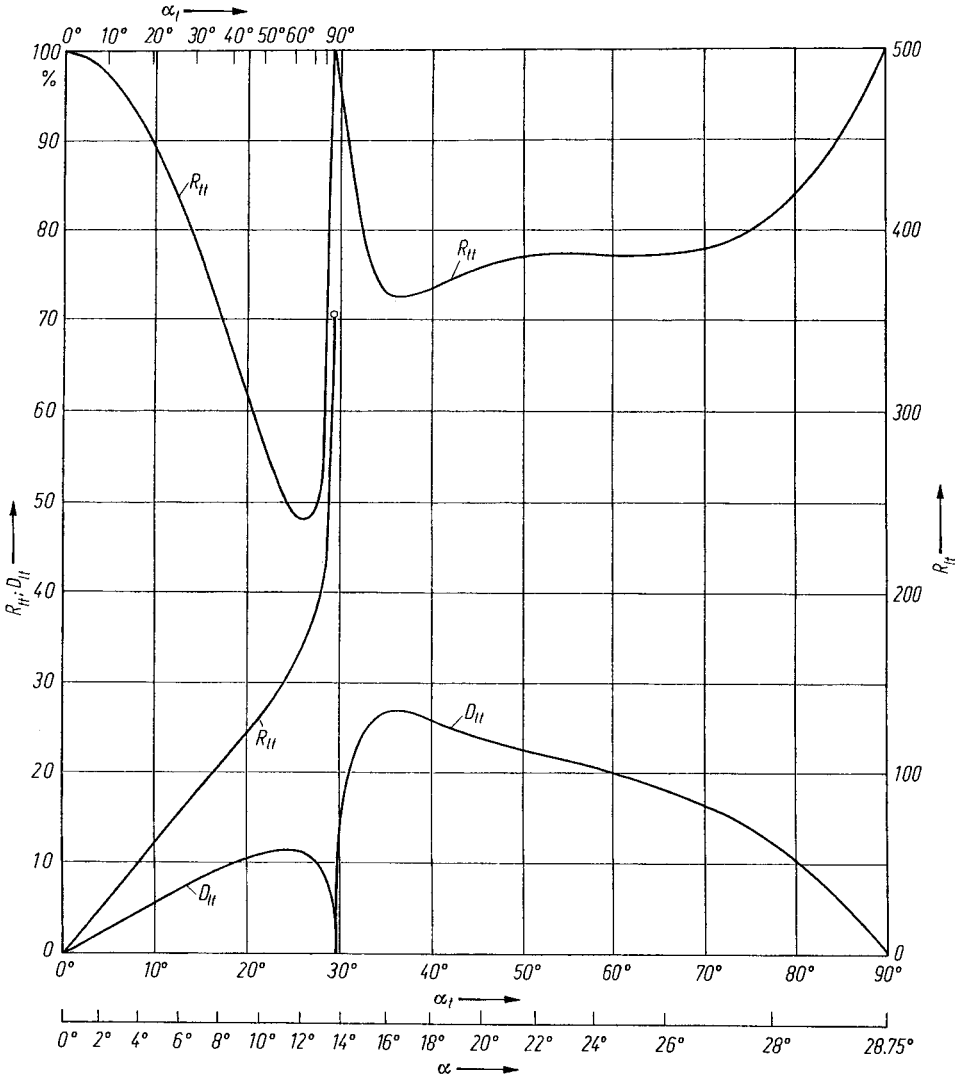
Diagram 5. Echo transmission at water-aluminium interface

E_{ll} and E_{lt}, echo transmittances versus angles of waves in aluminium, α_{l} and α_{t}, respectively (Eqs. (A 16) and (A 17))
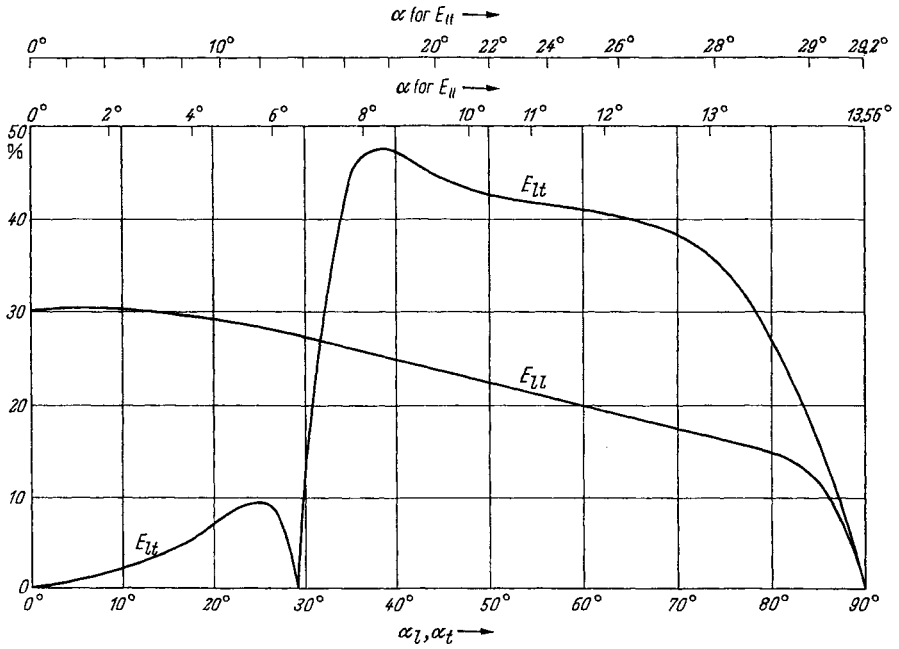
Diagram 6. Echo transmission at water-steel interface

E_{ll} and E_{tt}, echo transmittances versus angles of waves in steel, α_l and α_t, respectively (Eqs. (A 16) and (A 17))
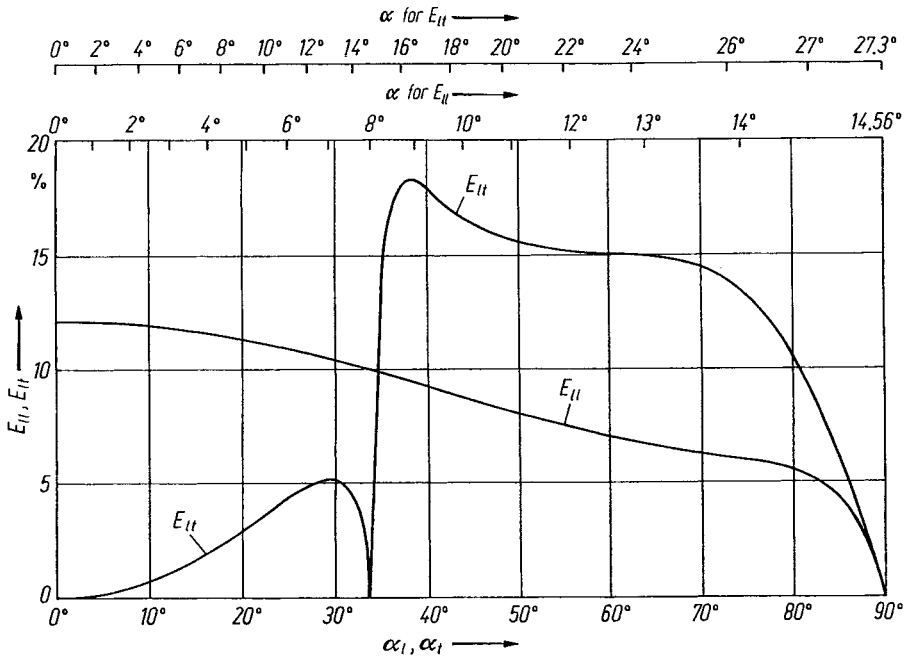
Diagram 7. Echo transmission at perspex-steel interface

E_{lt}, echo transmittance for liquid contact and solid contact (broken line)
Perspex: $c_l = 2.73 \times 10^3$ m/s; $c_t = 1.43 \times 10^3$ m/s; $\varrho = 1,180$ kg/m^3;
Steel: $c_l = 5.90 \times 10^3$ m/s; $c_t = 3.23 \times 10^3$ m/s; $\varrho = 7,700$ kg/m^3
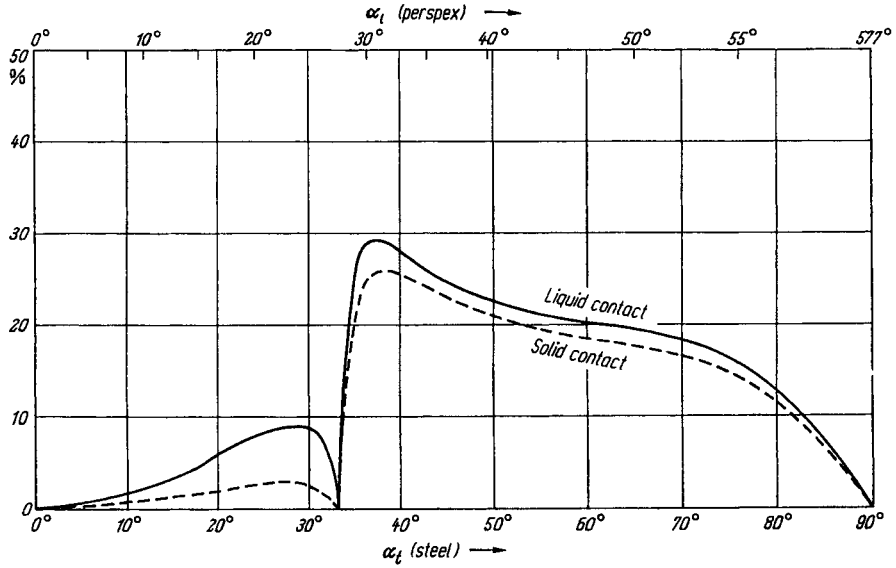
Diagram 8. Echo transmission at perspex-aluminium interface

E_{lt}, echo transmittance for liquid contact and solid contact (broken line)

Perspex: $c_l = 2.73 \times 10^3$ m/s; $c_t = 1.43 \times 10^3$ m/s; $\varrho = 1,180$ kg/m^3;

Aluminium: $c_l = 6.32 \times 10^3$ m/s; $c_t = 3.13 \times 10^3$ m/s; $\varrho = 2,700$ kg/m^3
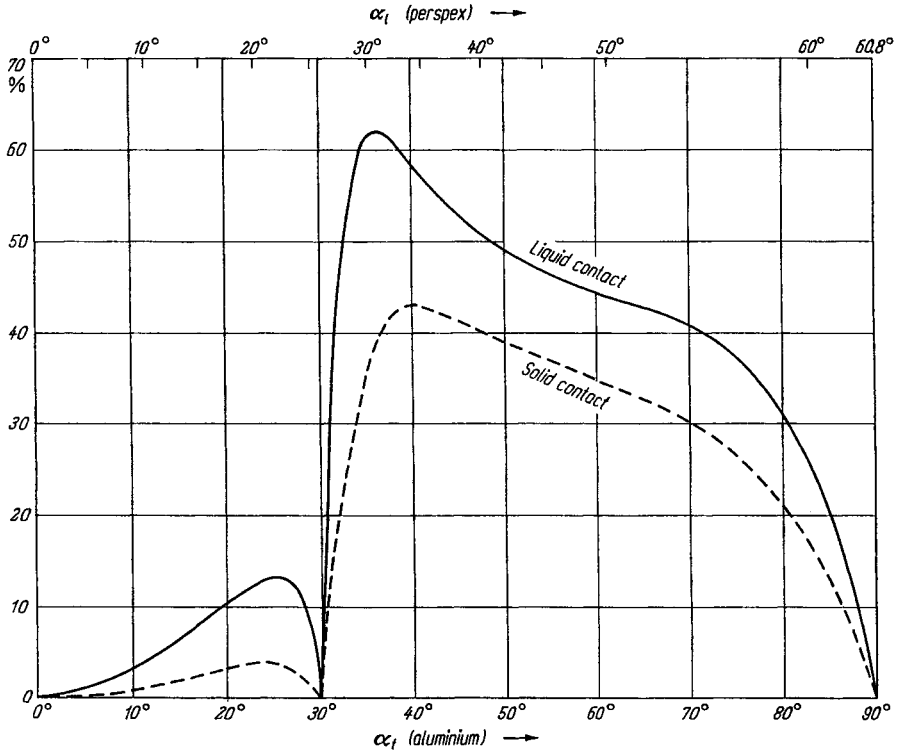
Diagram 9. Velocity of Lamb waves in steel

$c_l = 5.96 \times 10^3 \text{ m/s}; \quad c_t = 3.26 \times 10^3 \text{ m/s}$
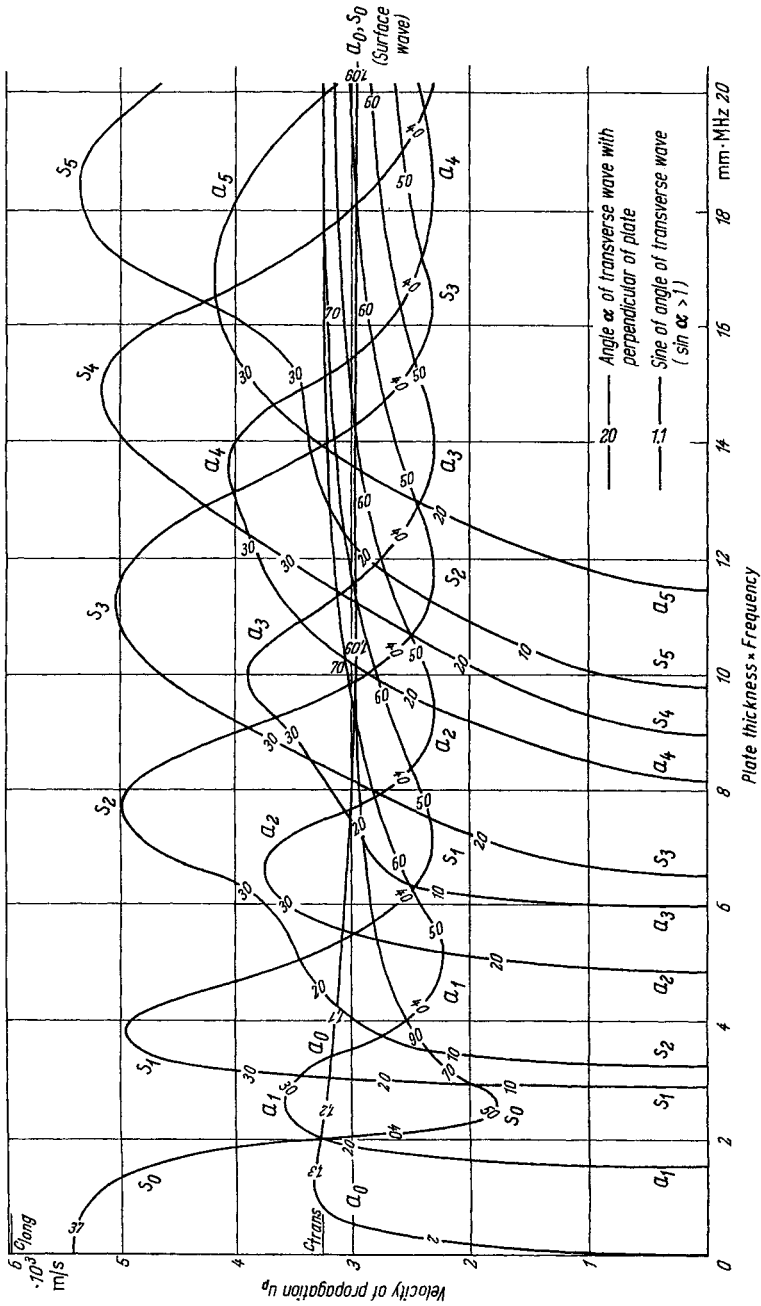
Diagram 10. Attenuation of plate waves

Various attenuation coefficients and layer thicknesses according to the relation $p/p_0 = e^{-\alpha d}$. Scale on *right side*: attenuation in dB, scale on *left side*: sound pressure amplitude and echo amplitude, respectively, in per cent
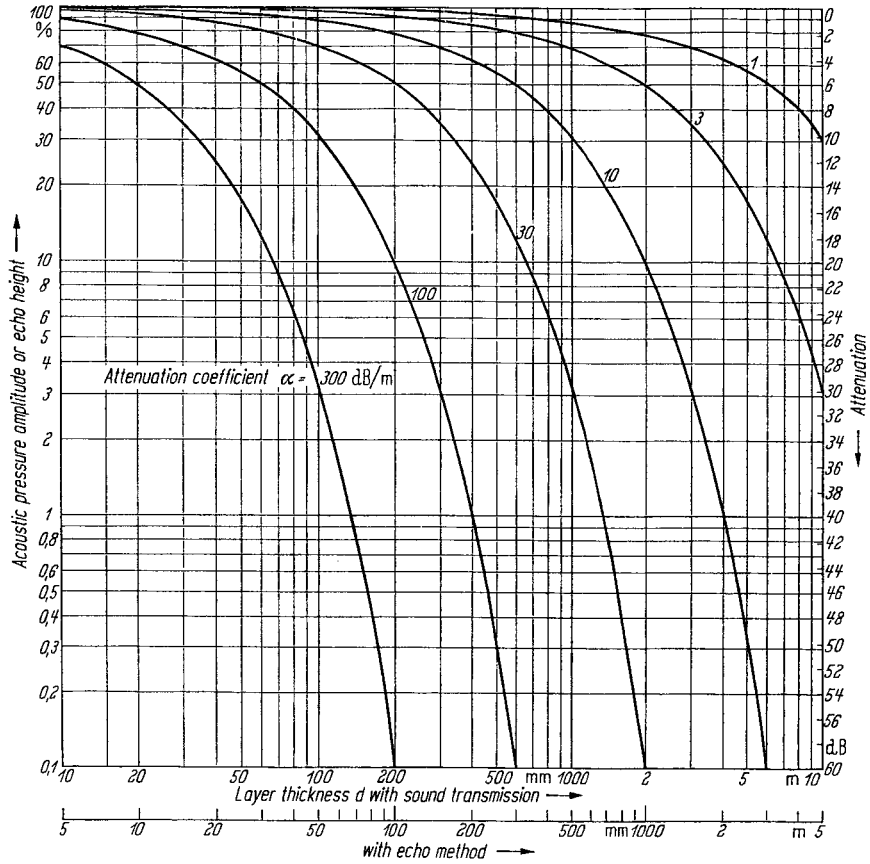
References

The references are arranged alphabetically according to the author's name and consecutively numbered. They are divided into three groups:
1. Textbooks and Handbooks for further studies,
2. Publications in the name of the author or editor, also patent-specifications if the inventor has been named,
3. Publications without named author and of Institutes, Corporations etc.

Abbreviations

API	American Petroleum Institute
ASM	American Society for Metals
ASME	American Society of Mechanical Engineers
ASNT	American Society for Nondestructive Testing
ASTM	American Society for Testing and Materials
AWS	American Welding Society
AVG	Abstand—Verstärkung—Größe (-Diagramm) (cf. DGS)
BAM	Bundesanstalt für Materialforschung und Materialprüfung (Berlin)
CEGB	Central Electricity Generating Board
DGS	Distance—Gain—Size (-diagram) (cf. AVG)
DGZfP	Deutsche Gesellschaft für Zerstörungsfreie Prüfung
DVS	Deutscher Verband für Schweißtechnik
EPRI	Electric Power Research Institute
ESI	Electrical Supply Industry
IEEE	Institute of Electrical and Electronics Engineers
IIW/IIS	International Institute of Welding/Institut Internationale de Soudure
ISO	International Organization for Standardization
IZfP	Fraunhofer-Institut für Zerstörungsfreie Prüfverfahren
JIS	Japanese Industrial Standard
KTA	Kerntechnischer Ausschuß
NASA	National Aeronautics Space and Administration
NDE	Nondestructive Evaluation
NDI	Nondestructive Inspection
NDT	Nondestructive Testing
NRC	Nuclear Regulatory Commission
RSK	Reaktorsicherheits-Kommission
SWRI	Southwest Research Institute
UKAEA	United Kingdom Atomic Energy Authority
VDEh	Verein Deutscher Eisenhüttenleute
VDI	Verein Deutscher Ingenieure
VdTÜV	Vereinigung der Technischen Überwachungsvereine
ZfP	Zerstörungsfreie Prüfung (cf. NDT)

1. Textbooks and Handbooks

1 Auld, B. A.: Acoustic fields and waves in solids. Vol. 1, 2. New York: Wiley 1973
2 Bergmann, L.: Der Ultraschall, 6. Aufl. Stuttgart: Hirzel 1954

3 Brekhovskikh, L. W.: Waves in layered media. London, New York: Academic Press 1960
4 Bundesanstalt für Materialprüfung, Berlin: Bibliography on Non-destructive Testing
5 Cady, W. G.: Piezoelectricity. New York: McGraw-Hill 1946
6 Carlin, B.: Ultrasonics. New York: McGraw-Hill 1949
7 Ermolov, I. N.: Theory and practice of ultrasonic NDT (in Russian). Moscow: Mashinostroenie 1981
8 Filipczynski, L.; Pawlowski, Z.; Wehr, J.: Ultradzwiekowe metody badania materialow. Warszawa: Panstwowe Wydawnictwa Technieczne 1959.
9 Harumi, K.; Okada, H.; Saito, T.; Fujimori, T.: Educational films for ultrasonic engineers. 3rd Europ. Conf. NDT Florence 1984, Vol. 2, pp. 300–312; 399–407
10 Hiedemann, E.: Grundlagen und Ergebnisse der Ultraschallforschung. Berlin: de Gruyter 1939
11 Hueter, T. F.; Bolt, R. H.: Sonics. New York: Wiley 1955.
12 Jaffe, B.; Cook Jr., W. R.; Jaffe, H.: Piezoelectric ceramics. London, New York: Academic Press 1971
13 Krautkrämer, J.; Krautkrämer, H.: Werkstoffprüfung mit Ultraschall, 5th ed. Berlin: Springer 1986
14 Kutzner, J.: Grundlagen der Ultraschallphysik. Stuttgart: Teubner 1983.
15 Lindsay, R. B.: Acoustics — historical and philosophical development. Stroudsburg: Dowden, Hutchinson, Ross 1973.
16 Love, A. E. H.: A treatise on the mathematical theory of elasticity, 4th ed. New York: Dover 1927.
17 McMaster, R. C. (Ed.): Nondestructive testing handbook, 2 Vols. New York: Ronald Press 1959.
18 Malecki, I.: Physical foundations of technical acoustics. Oxford: Pergamon Press 1969.
19 Mason, W. P.; Thurston, R. N. (Ed.): Physical Acoustics, principles and methods. Vol. 16 (1982). Academic Press, New York
20 Mason, W. P.: Piezoelectric crystals and their application to ultrasonics. New York: Van Nostrand 1950
21 Mason, W. P.: Physical acoustics and the properties of solids. New York: Van Nostrand 1958
22 Matauschek, J.: Einführung in die Ultraschalltechnik, 2nd ed. Berlin: VEB Verlag Technik 1962
23 Mattiat, O. E.: Ultrasonic transducer materials. New York: Plenum Press 1971
24 Metherell, A. F. et al.: Acoustical holography. New York: Plenum Press. Vol. 1: 1969, Vol. 2: 1970, Vol. 3: 1971
25 Mollwo, E.; Kaule, W.: Maser und Laser. Mannheim: Bibliogr. Inst. 1968.
26 Morse, P. M.: Vibration and sound. New York: McGraw-Hill 1948
27 Müller, E. A. W.: Handbuch der zerstörungsfreien Materialprüfung. Vol. 1–5. Munich: Oldenbourg 1973
28 Pohl, R. W.: Einführung in die Physik, 3 vols. Berlin: Springer, vol. 1: 1983. vol. 2: 1975. vol. 3: 1976
29 Pohlman, R. (Ed.): Ultraschall-Dokumentation. Laboratorium f. Ultraschall, RWTH Aachen, Stuttgart: Hirzel, vol. III: 1971, vol. IV: 1972.
30 Pollard, H. F.: Sound waves in solids. London: Pion 1977
31 Rayleigh, Lord: Scientific papers. Cambridge University Press 1899–1920. Reprint Dover Publ. 1964
32 Rayleigh, Lord: Theory of sound. London 1926
33 Redwood, M.: Mechanical waveguides. Oxford: Pergamon Press 1960
34 Schlengermann, U.: Das Krautkrämer Taschenbuch, 2nd ed. Cologne: Krautkrämer GmbH
35 Schoch, A.: Schallreflexion, Schallbrechung und Schallbeugung. Erg. d. exakten Naturwiss. Vol. 23. Berlin, Göttingen, Heidelberg: Springer 1950

36 Skudrzyk, E.: Die Grundlagen der Akustik. Wien: Springer 1954

37 Sokolow, W. S.: Testing of Materials (in Russian). Moscow: National Energy Publ. 1957

38 Stenzel, H.; Brosze, O.: Leitfaden zur Berechnung von Schallvorgängen, 2nd ed. Berlin, Göttingen, Heidelberg: Springer 1958

39 Sharpe, R. S. (ed.): Research Techniques in Nondestructive Testing. Academic Press, London. Vol. 1 (1970), vol. 2 (1973), vol. 3 (1977), vol. 4 (1980), vol. 5 (1982), vol. 6 (1982), vol. 7 (1984), vol. 8 (1985)

40 Shutilov, V. A.: Physik des Ultraschalls — Grundlagen. Wien, New York: Springer 1984

41 Tietz, H. D.: Ultraschall-Meßtechnik. 2nd ed. Berlin: VEB-Verlag Technik 1974

42 Vaupel, O. (ed.): Bildatlas für die zerstörungsfreie Materialprüfung. Berlin: Verlag Bild u. Forschung 1954

43 Viktorov, I. A.: Rayleigh and Lamb waves. New York: Plenum Press 1967

44 Wade, G. (Ed.): Acoustic imaging. New York: Plenum Press 1976

2. Publications with named author

45 Abend, K.; Lang, R.; Sternberg, W.: Rechnerüberwachte Anlagenqualifikation mit Kontrollkarte. In: DGZfP (ed.): Int. Symp. Neue Verfahren der ZfP. Saarbrücken 1979, p. 511–524

46 Abrahams, C. J.: Methods used in ultrasonic testing of welds. Weld. Met. Fabr. 35 (1967) 458–463.

47 Abrahams, C. J.: The ultrasonic examination of thin wall tube-to-tube butt welds using assisted hand scanning methods. Br. J. Non Destr. Test. 14 (1971) 141–147.

48 Abrahams, C. J.: The ultrasonic examination of thin wall tube-to-tube butt welds in austenitic steel using assisted hand scanning methods. Br. J. Non Destr. Test 14 (1972) 66–72.

49 Achenbach, J. D.: Wave propagation in elastic solids, Vol. 16: Applied Mathematics and Mechanics. Lauwerier, H. A.; Koiter, W. T. (Eds.). Amsterdam: North Holland 1973.

50 Achenbach, J. D.; Norris, A. N.: Interference of corner reflected and edge diffracted signals for a surface-breaking crack. J. Acoust. Soc. Am. 70 (1981) 165–171.

51 Adachi, K.; Harrison, G.; Lamb, J.; North, A. M.; Pethrick, R. A.: Ultrasonic investigations of morphology and stress relaxation in drawn polypropylene. Polymer 22, No. 8 (1981) 1026–1031.

52 Adams, C. J.; Morris, J. W.: Ultrasonic standards for the evaluation of missile materials and components. ASTM Spec. Publ. Bull. A-273 (1959).

53 Adams, R. D.; Vaughan, N. D.: Resonance testing of cast iron. J. Non Destr. Eval. 2 (1981) 65–74.

54 Adler, L.; Cook, V. K.; Simpson, W. A.: Ultrasonic frequency analysis. In: Sharpe, R. S. (Ed.) Research Techniques in NDT Vol. 3. London: Academic Press 1977, pp. 1–49.

55 Adler, R.; Korpel, A.; Desmares, P.: An instrument for making surface waves visible. IEEE Trans. SU-15 (1968) 157–161.

56 Ahlberg, L.; Tittmann, B. R.; Elsley, R. K.: NDE of simulated space shuttle tile disbonds. In: Thompson, D. O.; Chimenti, D. E. (Eds.): Quantitative NDE, Vol. 1, 1982, pp. 321–325.

57 Ahmed, M.; Wade, G.: Bragg-diffraction imaging. Proc. IEEE 67 (1979) 587–603.

58 Ahmed, M.; Wang, K. Y.; Metherell, A. F.: Holography and its application to acoustic imaging. Proc. IEEE 67 (1979) 466–483.

59 Alais, P.: Real time acoustical imaging with a 256 × 256 matrix of electrostatic transducers. Acoust. Hologr. 5 (1974) 671–684.

60 Albertini, C.; Basile, D.: Statistical evaluation of the results of NDT carried out on SAP reactor pressure tubes. Mater. Eval. 28 (1970) 182–188.

61 Albertini, C.; Jung, J.; Montagnani, M.; Verceletti, G.: A correlation of NDT of zircalloy-steel welded joints for reactor pressure tubes. Mater. Eval. 27 (1969) 185–192.

62 Albertson, C. P.; van Valkenburg, H. E.: Ultrasonic detection, sizing and counting of sub-sieve particles. Proc. 4th Int. Conf. NDT, London 1963. London: Butterworths Sci. 1964, pp. 147–149.

63 Aldrige, E. E.: The estimation of grain size in metals. NDT views, reviews, previews OUP (1969) pp. 31–45.

64 Aldridge, E. E.; Clément, M. J.-M.: Ultrasonic holography. In: Szilard, J. (Ed.): Ultrasonic testing. Non-conventional testing techniques. Chichester: Wiley 1982, pp. 103–166.

65 Alers, G. A.; Zimmerman, R. M.: Ultrasonic characterization of the thermal protection tiles for the space shuttle. Nondestructive Testing Information Analysis Center Newsletter 9, No. 5 (1982) 104.

66 Alers, G. A.; Elsley, R. K.: Measurement of metal to adhesive bond quality using digital signal analysis. IEEE Ultrasonics Symp. Proc., Phoenix 1977, 77 CH 1264-1 SU, pp. 35–40.

67 Allen, D. R.; Sayers, C. M.: The measurement of residual stress in textured steel using an ultrasonic velocity combination technique. Ultrasonics 22, No. 4 (1984) 179–188.

68 Allen, J. L.: Array antennas: new applications for an old technique. IEEE Spectrum 1 (1964) 115–130.

69 Allen, T. L. et al: Automatic data recording during manual ultrasonic inspection. Conf. Periodic Inspection Pressurized Components, London 1979. London: Inst. Mech. Eng. C 36/79.

70 Ammiratow, F.; Wheeler, G. C.: Ultrasonic inspection of in-service shrunk-on turbine wheels. General Electric Information 79 MPL 405, Nov. 1979.

71 Andersen, B. B.; Pedersen, O. K.; Busk, H.; Lund, S. A.; Jensen, P.: Ultra-schallmessungen bei Rindern und Schweinen. Fleischwirtsch. (1970) 843–845.

72 Anderson, E. B.: The evaluation of defects with P-Scan equipment and focused contact search units. Conf. Periodic Inspection Pressurized Components, London 1982. London: Inst. Mech. Eng. pp. 163–168.

73 Anderson, G. P.; Check, B. B.: High sensitivity logarithmic recorder of ultrasonic attenuation. J. Acoust. Soc. Am. 45 (1969) 1343–1351.

74 Anderson, W. F.; Bush, S. H.; Chockie, L. J.: The ASME Sect. XI, Code, past, present, and future. In: Periodic inspection of pressurized components. I. Mech. E. Conf. Publ. 1982-9, London: Mech. Eng. Publ. 1982, pp. 1–6.

75 Ando, Y.: Reliability assessment of non-destructive examination in Japan. In: Nichols, R. W. (Ed.): Advances in non-destructive examination for structural integrity. London: Appl. Sci. Publ. 1982, pp. 357–369.

76 Ando, Y.: Nondestructive examination relating to structural integrity of light water nuclear power plant: Recent trends in Japan. In: Nichols, R. W. (Ed.): Advances in nondestructive examination for structural integrity. London: Appl. Sci. Publ. 1982, pp. 117–137.

77 Andrews, K. W.; Druce, M.: The testing of hot steel by ultrasonics. Br. J. Non Destr. Test. 14 (1972) 6–10.

78 Arave, A. E.: Ultrasonic channel measuring system. AEC Res. and Dev. Rep. IDO 17290/January 1969.

79 Archer-Hall, J. A.; Bashter, A. I.: A means for computing the Kirchhoff surface integral for a disk radiator as a single integral with fixed limits. J. Acoust. Soc. Am. 65 (1979) 1568–1570.

80 Archer-Hall, J. A.; Gee, D.: A single integral computer method for axisymmetric transducers with various boundary conditions. Non Destr. Test. Int. 13 (1980) 95–101.

81 Arditi, M.; Foster, F. S.; Hunt, J. W.: Transient fields of concave annular arrays. Ultrasonic Imaging 3 (1981) 37–61; 4 (1982) 92.

82 Arman, J.: Dispositif de mesure de la vitesse de propagation et du coefficient d'atténuation d'ultrasons dans les polymères. Acustica 43 (1979) 212–216.

83 Arons, R. M.; Kupperman, D. S.: Use of sound-velocity measurments to evaluate the effect of hot isostatic pressing on the porosity of ceramic solids. Mater. Eval. 40 (1982) 1076–1078.

84 Arora, A.: Nondestructive methods for monitoring delayed cracking in reactor pressure tubes. In: Charyulu, V. H. (Ed.): NDE in the nuclear industry — 1980. Metals Park: ASM 1981, pp. 383–399.

85 Astier, P.; Oquidam, B.; Papezyk, F.: Contrôle par ultrasons de la santé interne de tubes moulés en alliage d'uranium. 12ᵉ Colloque de Métallurgie, Saclay (France) 1968 (Institut National des Sciences et Techniques Nucléaires).

86 Attal, J.: The acoustic microscope: A tool for nondestructive testing. NDE of semiconductor materials and devices. Proc. Conf. Frascati 1978, pp. 631–676.

87 Aulenbacher, U.; Langenberg, K. J.: Analytical representation of transient ultrasonic phased array near- and farfields. J. Non Destr. Eval. 1 (1980) 53–66.

88 Aurich, D.; Martin, E.: Voraussetzungen, Möglichkeiten und Grenzen der Korn- größenermittlung durch Ultraschallschwächungsmessungen. Arch. Eisenhüttenwes. 41 (1970) 285–291.

89 Aveyard, S.; Sharpe, R. S.: Applications of ultrasonic pulse interference. Proc. 4th Int. Conf. NDT London 1963. London: Butterworths Sci. 1964, pp. 150–154.

90 Avioli, M. J.; Lapides, M. E.: Development and qualification of a feature based ultrasonic piping inspection system for the nuclear industry. In: Dau, G. J. (Ed.): NDE program. Rep. EPRT-NP-2088 (1982), Paper 10.1–10.4, T103-3.

91 Azim, K.; Wang, K.: Acoustic switching ratios of piezoelectric and electrostrictive OATS. In: Acoustical imaging, Vol. 9. New York: Plenum Press 1980, pp. 121–137.

92 Azarov, N. T.: Examination of the possibilities of the ultrasonic inspection of joints in titanium alloys produced by solid-phase bonding. Weld. Prod. 26, No. 9 (1979) 44–46

93 Baborovski, V. M.; Marsh, D. M.; Slater, E. A.: Schlieren and computer studies of the interaction of ultrasound with defects. Non Destr. Test. 6 (1973) 200–207.

94 Baborovsky, V. M.: Visualization of ultrasound in solids. Phys. Technol. 10 (1979) 171–177.

95 Backhaus, H.; Trendelenburg, F.: Über die Richtwirkung von Kolbenmembranen. Z. Tech. Phys. 7 (1926) 630–635.

96 Baer, R. L.; Selfridge, A. R.; Khuri-Yakub, B. T.; Kino, G. S.: Contacting transducers and transducer arrays for NDE. Proc. IEEE Ultrasonics Symp., Chicago 1981, pp. 969–973, IEEE, New York.

97 Ball, D. F.; Shewring, D.: Some problems in the use of Lamb waves for the inspection of cold rolled steel sheet and coil. Non Destr. Test. 6 (1973) 138–145.

98 Bannink, G. H.: Ultrasone kwaliteitscontrole, Gieterij 2, Nr. 3 (1968) 9–15.

99 Barbian, O. A.; Grohs, B.; Kappes, W.; Hullin, Ch.: Inspection of thick-walled components by ultrasonics and evaluation of the data by the ALOK-techniques. In: Höller, P. (Ed.): New procedures in NDT. Proc. Germany—US Workshop, Saarbrücken 1982. Berlin: Springer 1983.

100 Barbian, O. A.; Grohs, B.; Licht, R.: Signalanhebung durch Entstörung von Laufzeitmeßwerten aus Ultraschallprüfungen von ferritischen und austenitischen Werkstoffen — ALOK 1. Materialprüfung 23 (1981) 379–383.

101 Barbian, O. A.; Hullin, C.: Ultraschall-Grobblechprüfung mit flächengetreuer

Rekonstruktion der Fehlerbilder als Grundlage einer automatischen Qualitäts-
bewertung. Arch. Eisenhüttenwes. 51 (1980) 189–194.

102 Barbian, O. A.; Grohs, B.; Neumann, R.: ISI by ultrasonics in nuclear power plants
using the ALOK technique. In: Periodic inspection of pressurized components.
I. Mech. E. Conf. Publ. 1982-9. London: Mech. Eng. Publ., 1982, pp. 197–208.

103 Bar-Cohen, Y.; Ben-Joseph, B.; Harnik, E.: Compact sensitive instrument for
direct ultrasonic visualization of defects. Rev. Sci. Instrum. 49 (1978) 1709–1711.

104 Bar-Cohen, Y.: Schlieren visualization of acoustically imaged defects. Mater. Eval.
41 (1983) 88–93.

105 Bailey, C. D.; Pless, W. M.: Acoustic emission: An emerging technology for
assessing fatigue damage in aircraft structure. Mater. Eval. 39 (1981) 1045–1050.

106 Bardsley, B. G.; Christensen, D. A.: Beam patterns from pulsed ultrasonic
transducers using linear systems theory. J. Acoust. Soc. Am. 69 (1981) 25–30.

107 Bardsley, B. G.; Christensen, D. A.; Pryor, T. A.: Multifrequency and non-
uniformly-spaced arrays: Effect on grating lobe amplitude. Ultrasonic Imaging 4
(1982) 351–354.

108 Baron, J. A.; Dolbey, M. P.; Erven, J. H.; Booth, D.; Murray, D. W.:
Automated inspection and gauging of fuel channels in CANDU reactors. Conf.
Periodic Inspection Pressurized Components, London 1982. London: Inst. Mech.
Eng., 1982, pp. 67–76.

109 Barthelt, H.: Erfahrungen über die Anwendung des Ultraschallverfahrens in der
keramischen Fertigung. ETZ A 75 (1954) 69–71.

110 Barthelt, H.; Böhme, W.: Die zerstörungsfreie Prüfung der armierten Enden von
Langstabisolatoren nach dem Ultraschallechoverfahren. Siemens-Z. 29 (1955) 206
bis 208.

111 Barteld, K.; Krefting, R.; Becker, H.; Bigge, P.: Erfahrungen mit automatisierten
Ultraschallprüfanlagen in der Halbzeugzurichterei eines Edelstahlwerks. Int. Eisenh.
Tech. Kongr. 1976 Brussels, Düsseldorf, Vol. IIc, Rep. 7.3.4

112 Beaujard, L.; Husarek, V.; Vasset, A.: Signalisation, comptage ou enregistrement
des défauts des produits métallurgiques au moyen du sondage ultrasonore auto-
matique par échos. Rev. Métall. 52 (1955) 240–248.

113 Beaujard, L.; Collette, G.; Drouet, C.: The effect of dispersion and the velocity
of propagation of Lamb waves during the ultrasonic testing of mild steel sheet. Br. J.
Non Destr. Test. 2 (1959) 7–11.

114 Beaver, W. L.: Sonic nearfields of a pulsed piston radiator. J. Acoust. Soc. Am.
56 (1974) 1043–1048.

115 Bechhaus, W.; Weiland, H.: Prüfung und Fehlerbeseitigung in einer neuen Zu-
richtungslinie für Halbzeug und Stabstahl der Thyssen Edelstahlwerke AG. Stahl
u. Eisen 100 (1980) 1404–1409.

116 Beck, H.; Specht, R.: Automatische Ultraschallprüfung von Stahlknüppeln auf
Innenfehler. Conf. of the DGZfP Vienna 1965

117 Beck, W. N.: An ultrasonic scanner and recording system. Non Destr. Test. 15
(1957) 42–43. — Symp. on nondestructive tests in the field of nuclear energy.
ASTM Spec. Tech. Publ. No. 223 (1958) 246–258.

118 Becker, E.: Zerstörungsfreie Prüfung von Erzeugnissen aus Gußeisen. 1. Part: Auf-
gaben und Ziel der zerstörungsfreien Werkstoffprüfung. Gießereitechnik 21 (1975)
271–273. — 2. Part: Beurteilung von Gefüge- und Behandlungszuständen im Spiegel
der Literatur, Section 1. Gießereitechnik 21 (1975) 372–374. — 3. Part: Beurteilung
von Gefüge- und Behandlungszustände im Spiegel der Literatur, Section 2. Gießerei-
technik 22 (1976) 20–23

119 Becker, H.; Pies, W.: Automatisch rechnergesteuerte US-Knüppelprüfung im Pro-
duktionsfluß. Betriebsergebnisse und Erfahrungsbericht. In: Österr. Ges. ZfP (Ed.):
2. Europ. Conf. ZfP Wien 1981, p. 146–150

120 Becker, F. L.; Busse, L. J.: Ultrasonic angle beam profiling in steel using an

EMAT receiver. Battelle Pacific Northwest Lab., Richland, Rep. PNL-SA-10025 (1982).

121 Becker, F. L.; Crow, V. L.; Davis, P. J.; Doctor, S. R.; Hildebrand, B. P.: Development of an ultrasonic imaging system for the inspection of nuclear reactor pressure vessels. Electr. Power Res. Inst., Palo Alto, Final Rep. 1979, EPRI NP-1229.

122 Becker, H.: Ultraschallprüfung austenitischer Schmiedestücke. Fachber. Hütten-praxis Metallweiterverarb. 19 (1981) 446–454.

123 Becker, S.: Der Einsatz der Ultraschallmeßmethode in Betonsperrmauern. Wiss. Ber. d. TH Leipzig Nr. 11 (1979) 35–40.

124 Beckmann, G.: Zur Prüfung schwerer Schmiedestücke mit Ultraschall. Neue Hütte 2 (1957) 169–178.

125 Beckmann, G.; Spiegelberg, K.: Über den Nachweis nichtmetallischer Einschlüsse in Walzmaterial mit Ultraschall. Neue Hütte 6 (1961) 316–321.

126 Beckmann, G.; Spiegelberg, K.: Über die Bestimmung von Elastizitätsmoduln mittels Ultraschallimpulsen. Technik 17 (1962) 81–88.

127 Beecham, D.: Ultrasonic scatter in metals: its properties and its application to grain size determination. Ultrasonics 4 (1966) 67–76.

128 Bell, I. P.; Gray, B. S.; Hudgell, R. J.; Sargent, T.: Reliability assessment of austenitic steel ultrasonic inspections — progress report on a UKAEA programme. In: Nichols, R. W. (Ed.): Advances in nondestructive examination for structural integrity. London: Appl. Sci. Publ. 1982, pp. 269–283.

129 Bell, I. P.; Highmore, P. J.: Developments in data handling, data recording and data analysis — a review of UK work. In: Nichols, R. W. (Ed.): Advances in nondestructive examination for structural integrity. London: Appl. Sci. Publ. 1982, pp. 213–224.

130 Beller, L. S.: Location of focal points of focused continuous wave ultrasonic transducers. EG & G Idaho, Rep. EGG-FM-5656 (1982).

131 Belleval de, J. F.; Fink, M.; Mercier, N.: Focusing of ultrasonic waves at oblique incidence by a linear array of transducers. Ultrason. Int. Conf. Proc. (Novak, Z., Ed.) 1979, 94–102.

132 Bentley, P. G.: Developments in acoustic emission for application to nuclear reactor systems. In: Nichols, R. W. (Ed.): Advances in nondestructive examination for structural integrity. London: Appl. Sci. Publ. 1982, pp. 17–36.

133 Bentley, P. G.: A review of acoustic emission for pressurized water reactor applications. Non Destr. Test. Int. 1 (1981) 329–335.

134 Berger, H.: Ultrasonic imaging systems for NDT. J. Acoust. Soc. Am. 45 (1969) 859–867.

135 Berger, H.: Nondestructive testing of railroad rail. Transportation Res. Rec. 744: Railroad and Facilities (1980) 22–26.

136 Bergman, E. H.; Shahbender, R.: Effect of statically applied stresses on the velocity of propagation of ultrasonic waves. J. Appl. Phys. 29 (1958) 1736–1738

137 Berke, M.: Das Sonogramm — praxisgerechte Darstellung der Schallbündelform und Leistung von Ultraschallprüfköpfen. Qual. Zuverl. 24 (1979) 57–61.

138 Berner, K.: Magnetpulver- und Ultraschall-Rohrendenprüfanlage für Großrohre. Rohre, Rohrleitungsbau. Rohrl. Transport Int. 17 (1978) 529–535.

139 Berner, K.; Gallus, W.: Design of modern ultrasonic plate testing equipment as regards integrating it into the production line of a rolling mill. Proc. 10th World Conf. NDT Moscow 1982, Vol. 3, pp. 413–420. (Acad. Sci. USSR).

140 Berner, K.; Kügler, J.: Zerstörungsfreie Prüfverfahren und -anlagen bei der Her-stellung von spiralnahtgeschweißten Großrohren. Stahl, Eisen 93 (1973) 317–331.

141 Berner, K.; Kügler, J.; Vogt, H.: Evaluation system and preliminary tests for the automatic ultrasonic test of billets for core and surface defects. 7th Int. Conf. NDT, Warszawa 1973, paper C-03

142 Berner, K.; Westkämper, G.: Versuchsergebnisse und Konzept für eine Prüfung

mit Rayleigh-Oberflächenwellen. Oberflächenfehler-Knüppelprüfanlage mit Ultraschall. 2. Seminar Eisen- und Stahlforschung, Berlin 1982. (Neumann, R., ed.), Vol. 1, p. 229–244/KFA Jülich 1982

143 Berner, K.; Westkämper, G.: Betriebserfahrung mit einer computergesteuerten Ultraschall-Grobblech-Prüfeinrichtung in SE-Technik mit EDV Prüfdatenauswertung. Materialprüfung 22 (1980) 291–294.

144 Berson, M.; Ronçin, A.; Pourcelot, L.: Dynamic focusing and compound scanning in linear array of transducers. In: Alais, P. (Ed.): Acoustical imaging, Vol. 10. New York: Plenum Press 1982, pp. 39–46.

145 Bertoni, H. L.; Tamir, T.: Unified theory of Rayleigh angle phenomena for acoustic beams at liquid-solid interface. Appl. Phys. 2 (1973) 157–172.

146 Beyer, R.: Prüfen von Schweißnähten mit Ultraschall-Kleingeräten. Schweißen und Schneiden. Der Praktiker 18 (1966) 136–137.

147 Beyer, R.: Erfahrungen bei der Güteüberwachung von Stahlguß mit Hilfe zerstörungsfreier Prüfverfahren, besonders mit Ultraschall. Gießerei 54 (1967) 123–128.

148 Bieth, M.; Adamonis, D. C.; Jusino, A.: Amélioration de la caractérisation des défauts en ultrasons par l'adaptive learning network. Journées Nationales Cofrend, Paris 1982, pp. 292–307.

149 Biggiero, G.; Canélla, G.; Cicchinelli, S.: Ultrasonic testing for bond efficiency of carbon-to-stainless steel adhesive joints. 3rd Europ. Conf. NDT Florence 1984, Vol. 5, pp. 206–223.

150 Biggiero, G.; Canella, G.; Moschini, A.: Ultrasonic scanning and spectrum analysis for inspection of bond efficiency of metal-to-metal structural adhesive joints. Non Destr. Test. Int. 16 (1983) 67−73.

151 Bilgutay, N. M.; Sanii, J.: The effect of grain size on flaw visibility enhancement using split-spectrum processing. Mater. Eval. 42 (1984) 808–814.

152 Bilgutay, N. M.; Newhouse, V. L.; Furgason, E. S.: Flaw visibility enhancement by split-spectrum processing techniques. 1981 Ultrasonics Symp. Proc. IEEE. New York 1981, Vol. 2, pp. 878–883.

153 Binczewski, G. B.: Standardization and application of ultrasonic surface-wave inspection. Non Destr. Test. 15 (1957) 36–40.

153a Birkholz, P.: Erfahrungen bei der Anwendung von AVG-Vorsatzskalen bei Prüfung von Rohrschweißverbindungen mit Rohrwandstärken <6 mm. ZIS-Mitt. 13 (1971) 654–658.

154 Black, W. S. A.; Murgatroyd, R. A.; Highmore, P. J.: Advances in inservice inspection of the Winfrith Steam Generating Heavy Water Reactor. Br. Nuclear Energy Soc., Proc. Western Branch Symp. on Inspection of UK Reactors 1980

155 Blaser, E.: Achswellenprüfung mit Ultraschall. Technica 27 (1978) 1249–1251.

156 Blendl, H. M.: Die Eigenleistungsprüfung im Feld mittels Echolotverfahren beim Schwein in Bayern. Züchtungskde. 40 (1968) 264–283.

157 Blessing, G. V.; Elban, W. L.: Aluminium matrix composite elasticity measured ultrasonically. J. Appl. Mech. 48 (1981) 965–966.

158 Blessing, G. V., Warren, J. M.: The ultrasonic inspection of depleted uranium rods. Proc. 11th Symp. NDE, San Antonio, 1977, pp. 227–233.

159 Böhme, W.: Ultraschallprüfung von Drähten. Materialprüfung 1 (1959) 111–112.

160 Böttcher, W.; Kopineck, H. J.: Berührungslose Ultraschallerzeugung. Stand der Technik und Entwicklungstendenzen. Fachber. Hüttenpraxis Metallweiterverarb. 17 (1979) 948–955.

161 Böttcher, W.; Kopineck, H. J.; Schlusnus, K. H.; Sommerkorn, G.: Ultraschallprüfkopf zur Prüfung längs vorgegebener Prüfbahnen auf Längs- und Querfehler. Materialprüfung 12 (1970) 170−172.

162 Böttcher, W.; Kopineck, H. J.; Künne, G.: Zur elektrodynamischen Ultraschallerzeugung. Materialprüfung 20 (1978) 62−67.

163 Bond, L. J.: Methods for the computer modelling of ultrasonic waves in solids.

In: Sharpe, R. S. (Ed.): Research techniques in NDT. London: Academic Press 1982, pp. 107—146.

164 Bordoni, P. G.; Nuovo, M.: A tuned capacitive detector for high frequency vibrations. Acustica 8 (1958) 351—362.

165 Borloo, E. E.: An ultrasonic technique for the inspection of magnetic and explosive welds, using a facsimile recording system. Non Destr. Test. 6 (1973) 25—28.

166 Bosselaar, H.; Goossens, J. C. J.: Method to evaluate direct-reading ultrasonic pulse-echo thickness meters. Mater. Eval. 3 (1971) 45—50.

167 Botter, B. J.; Arkel van, J.: Circumferential propagation of acoustic boundary waves in boreholes. J. Acoust. Soc. Am. 71 (1982) 790—795.

168 Bourse; Fremiot; Lambert; Rivenez; Foct: Contribution des mesures de vitesse des ondes de Rayleigh par traitement numerique du signal à l'étude de l'état superficiel des metaux. 3rd Europ. Conf. NDT Florence 1984, Vol. 5, pp. 375–383.

169 Boutault, J.; Tuncer, T.; Margerie, J. C.: Zerstörungsfreie Prüfung der Struktur von Gußeisen mit Kugelgraphit. DGZfP-Conf. Neuere Entw. besond. Verf. ZfP Mainz 1978, Vol. 2, S. 331–338

170 Bradfield, G.: Ultrasonic transducers-1. Introduction to ultrasonic transducers, Part A. Ultrasonics 8 (1970) 112–123.

171 Bradfield, G.: The ultrasonic goniometer and its applications. Non Destr. Test. 1 (1968) 165–172.

172 Bradfield, G.: Correlating echo and flaw magnitudes. Non Destr. Test. 1 (1968) 317–318.

173 Bradfield, G.: Improvements in ultrasonic flaw detection. J. Br. Inst. Radio Eng. 14 (1954) 303–308.

174 Bradfield, G.: Ultrasonic flaw detection in metals. In: Chalmers, B.; Quarrel, A. G. (Eds.): The physical examination of metals, 2nd ed. 1960, Chap. 12.

175 Branson, G. N.: Portable ultrasonic thickness gage. Electronics 21 (1948) 88–91.

176 Bratt, M. J.; Wiegand, V. I. E.: Detection of flaws in jet engine parts by ultrasonics. Non Destr. Test. 13 (1955) 45–47.

177 Bray, D. E.; Dalvi, N. G.; Finch, R. D.: Ultrasonic flaw detection in model railway wheels. Ultrasonics 11 (1973) 66–72.

178 Bray, D. E.; Dalvi, N. G.; Finch, R. D.: Ultrasonic flaw detection in model railway wheels. Ultrasonics 11 (1973) 66–72.

179 Bray, D. E.; Egle, D. M.: Ultrasonic studies of anisotropy in cold-worked layer of used rail. Met. Sci. 15 (1981) 574–582.

180 Breazeale, M. A.; Adler, L.; Scott, G. W.: Interaction of ultrasonic waves incident at the Rayleigh angle onto a liquid-solid interface. J. Appl. Phys. 48 (1977) 530–537.

181 Breazeale, M. A.; Cantrell, J. H.; Heyman, J. S.: Ultrasonic wave velocity and attenuation measurements. In: Edmonds, P. D. (Ed.): Methods of experimental physics, Vol. 19: Ultrasonics. New York: Academic Press 1981, pp. 67–135.

182 Brenden, B. B.: Liquid surface holography. In: Wade, G. (Ed.): Acoustic imaging. New York: Plenum Press 1976, pp. 99–110.

183 Brockmann, W.; Wolitz, K.; Fischer, T.: Prüfung von glasfaserverstärkten Kunststoffbauteilen durch Messung des Schallemissionsverhaltens. In: Techn. Überw. Verein Rheinl. (Ed.): Die Schallemissionsanalyse. Cologne, publisher TÜV Rheinl., 1978, p. 184–199

184 Brook, C.: A new generation of European immersion systems for ultrasonic testing. 3rd Europ. Conf. NDT Florence 1984, Vol. 3, pp. 134–144

185 Brown, A. F.: Materials testing by ultrasonic spectroscopy. Ultrasonics 11 (1973) 202–210.

186 Brown, B.; Rossi, L.: Ultrasonic screening — a mechanised approach. 3rd Europ. Conf. NDT, Florence 1984, Vol. 3, pp. 114–125.

187 Brown, H. P.; Vernon, G. W.: The detection of cracks in underwater steel structures using an ultrasonic camera system. Conf. Proc. Ultrasonics Int. Graz, 1979. Guildford: IPC Sci. and Technol. Press 1979, pp. 384–392.

588   References

188 Brown, P. H.; Randall, R. P.; Sivjer, R. F.; Wardley, J.: A high resolution, sensitive ultrasonic image converter. Conf. Proc. Ultrasonics Int. London 1975. Guildford: IPC Sci. and Technol. Press 1975, pp. 73–79.

189 Brown, T. G.; Rankin, A. B. C.; Haslett, R. G. W.: Improvements in or relating to the ultrasonic testing of materials. GB Pat. 808274 (1955).

190 Bucur, V.: An ultrasonic method for measuring the elastic constants of wood increment cores bored living trees. Ultrasonics 21 (1983) 116–126.

191 Buken, G.: Untersuchungen über die Schallschwächung in unlegierten C-Stählen in Abhängigkeit von der chemischen Zusammensetzung und Gefüge im unbelasteten Zustand und während des Zerreißversuches. Diss. RWTH Aachen 1971.

192 Budenkov, G. A.; Khakimova, L. I.: Measurement of the diameters of spherical and cylindrical defects. Sov. J. Non Destr. Test. 17 (1981) 540–545.

193 Budenkov, G. A.; Gurevich, S. Yu.: Current status of contactless methods and facilities for ultrasonic inspection (survey). Sov. J. Non Destr. Test. 17 (1981) 325–347.

194 Büchl, K.: Der TEA-Laser. Laser u. angew. Strahlentech. 2 (1970) 45–48.

195 Bugyi, B.: Vergleich einiger Methoden zur Bestimmung des Körperfettes und des Magergewichtes bei Jugendlichen. Z. f. Ernährungswiss. 10 (1971) 364–381.

196 Buken, G., Krächter, H.: Zur Frage der Fehlergrößenbestimmung in Schweiß- nähten nach dem Ultraschall-Reflexionsverfahren. Materialprüfung 10 (1968) 329 bis 337.

197 Bungey, J. H.: The use of ultrasonics for NDT of concrete. Br. J. Non Destr. Test. 26 (1984) 366–369.

198 Burckhardt, C. B.; Grandchamp, P. A.; Hoffmann, H.: Focussing ultrasound over a large depth with an annular transducer — an alternative method. IEEE Trans. SU-22 (1975) 11–15.

199 Burdekin, F. M.: Lamellar tearing in bridge girders — a case history. Metal Construction & Brit. Weld. J. 3 (1971) 205–209.

200 Burger, C. P.; Testa, A. J.: Online fast Fourier transform of Rayleigh waves determines the depth of surface cracks. Proc. Ultrasonics Int. 1981, pp. 271–276.

201 Burggraf, J.; Heckhäuser, H.; Richter, H.: Empfindlichkeit zerstörungsfreier Prüf- verfahren für Rohre aus austenitischen Stählen und Nickelbasislegierungen. Bänder, Bleche, Rohre 13 (1972) 17—22.

202 Burgkart, M.; Maucic, D.; Ritter, H. Ch.: Eine Methode zur Ermittlung der Geschwindigkeit von Ultraschallwellen im lebenden Rindermuskel. Bayr. Land- wirtsch. Jb. 40 (1963) S. 567—571.

203 Burmester, A.: Untersuchungen über den Zusammenhang zwischen Schallgeschwindig- keit und Rohdichte, Querzug- sowie Biegefestigkeit von Holzspanplatten. Holz als Roh- und Werkstoff 26 (1968) 113–117.

204 Burmester, A.: Nachweis von Ästen in Kiefernholz. Holz als Roh- und Werkstoff 25 (1967) 157—163.

205 Burmester, A.: Zusammenhang zwischen Schallgeschwindigkeit und morphologischen, physikalischen und mechanischen Eigenschaften von Holz. Holz als Roh- und Werkstoff 23 (1965) 227–236.

206 Busse, H. G.: Apparatur zum Messen der Ultraschallabsorption mittels eines Differenzverfahrens. Acustica 22 (1969/70) 232–237.

207 Butler, J. L.: Maximum sound pressure from a displacement limited circular piston. J. Acoust. Soc. Am. 65 (1979) 1579–1581.

208 Burrows, M. S.; Deane, J. A.; Morton, J.: Experiences with a portable ultrasonic imaging system — MDU. 6th Int. Conf. NDE in the Nuclear Industry, Zürich 1983.

209 Byrne, B. R.; Johnson, P. C.; Farley, P. G.: Ultrasonic inspection of railway axles. Ultrasonics 4 (1966) 143—151.

210 Carlin, B.: Verfahren und Vorrichtung zum Prüfen fester Materialien, insbesondere dünner Platten oder dgl., auf Risse oder Sprünge. DE Pat. 881 266.

211 Calder, I. D.: Calculations of the effects of nonparallelism on measurements of

ultrasonic attenuation and velocity. J. Acoust. Soc. Am. 63 (1978) 967–973.

212 Carlson, D. L.: Automatic digital backfat meter US Pat. 4 359 056 (1982).

213 Carodiskey, T. J.: Ultrasonic transducer probe. US Pat. 4.368.642 (1983).

214 Caroti, F.; Iafelice, A.: Criteria of project of railway axles for a good ultrasonic testability in service. 3rd Europ. Conf. NDT Florence 1984 Vol 2, pp. 68–88.

215 Carson, P. L.; Oughton, T. V.; Hendee, W. R.: Ultrasonic transaxial tomography by reconstruction. Ultrasound in Medicine and Biology 2 (1976) 341–350.

216 Carter, C. J.; Cellitti, R. A.; Abar, J. W.: Effect of inclusions as measured by ultrasonic methods on the mechanical properties of aircraft quality steel. Tech. Rep. AFML-TR-68-303 (1969) (Air Force Materials Laboratory, Wright Patterson Air Force Base, Ohio).

217 Carter, C. J.; Cellitti, R. A.; Abar, J. W.: Ultrasonic test procedure for rating material cleanliness of semi-finished material. Rep. AMMRC CR 69-11 (US Army Materials and Mechanics Research Center, Watertown, Mass., 1969).

218 Carter, P.: Experience with the time-of-flight diffraction technique and an accompanying portable and versatile ultrasonic digital recording system. Br. J. Non Destr. Test. 26 (1984) 354–361.

219 Caspers, K.-H.: Zerstörungsfreie Prüfung von Erzeugnissen aus Gußeisen. 16. Mitt.: Möglichkeiten zur Qualitätssicherung von Motorteilen aus Gußeisen mit Lamellengraphit durch zerstörungsfreie Prüfung. Gießereitechnik 26 (1980) 245–249.

220 Caussin, P.; Crutzen, S.; Deuster, G.; Parry, G.: Analysis of the PISC trials results for alternative procedures. In: Charyulu, V. H. (Ed.): NDE in the nuclear industry — 1980. Metals Park: ASM 1981, pp. 345–360.

221 Cavanagh, E.; Cook, B. D.: Gaussian-Laguerre description of ultrasonic fields — numerical example: circular piston. J. Acoust. Soc. Am. 67 (1980) 1136–1140.

222 Cavanagh, E.; Cook, B. D.: Nearfield description of focused — unfocused transducers and transducer-lens systems. Proc. 12th Symp. NDE Bradshaw, W. W. (Ed.). San Antonio 1982, pp. 202–206.

223 Čech, J.; Zezula, J.; Rusin, K.: Ultraschallmessungen der mechanischen Eigenschaften von Gußeisen. 3rd Europ. Conf. NDT Florence 1984, Vol 4, pp. 243–247.

224 Certo, M.: Mathematical modelling of ultrasonic inspection 3rd Europ. Conf. NDT Florence 1984, Vol. 5, pp. 345–354.

225 Certo, M.; Gammino, G.; Tonolini, F.; Maciga, G.; Regis, V.: Improvements in NDT evaluation of power plant components by an integrated approach with some non conventional ultrasonic techniques. 3rd Europ. Conf. NDT Florence 1984, Vol. 5, pp. 573–586.

226 Challis, R. E.: Diffraction phenomena in the field of a circular piezoelectric transducer viewed in the time domain. Ultrasonics 20 (1982) 168–172.

227 Chang, F. H.; Bell, J. R.: Time domain analysis of ultrasonic propagation in a five-region layered structure. Non Destr. Test. Int. 11 (1978) 275–280.

228 Chang, F. H.; Bell, J. R.; Gardner, A. H.; Fisher, C. P.; Haile, R. W.: A laboratory mock-up ultrasonic inspection system for composites. Mater. Eval. 40 (1982) 756–761.

229 Chapman, R. K.: Ultrasonic reflection from smooth flat cracks: exact solution for the semi-infinite crack. Central Electricity Generating Board, London, Rep. NW/SSD/RR/145/81 (1983).

230 Charlesworth, J. P.; Temple, J. A. G.: Creeping waves in ultrasonic NDT. Ultrasonics Int. 1981. Guildford: IPC Sci. and Technol. Press 1981, pp. 390–395.

231 Charyulu, V. H. (Ed.): NDE in the nuclear industry — 1980. Interdependence of CFR 50 with ASME Sect. XI, NRC Regulatory Guides and ANSI Standards. Metals Park: Am. Soc. Met. 1981, pp. 281–289.

232 Chaskelis, H. H.: Tranducers — Fact and fiction. Non Destr. Test 4 (1971) 375–379.

233 Chen, W. H.; Chung, I. S.: Advanced ultrasonic imaging techniques for NDT.

3rd Europ. Conf. NDT Florence 1984, Vol 3, pp. 75–83.

234 Chen, W. H.; Chung, I. S.; Ding, C. H.: Ultrasonic NDT using Bark-code pulse compression techniques. 3rd Europ. Conf. NDT, Florence 1984, Vol 5, pp. 260–267.

235 Chevereau, G.: Study of the present development status of the in-service inspection of sodium-cooled fast breeder reactors. Draft Final Rep. Novatome. Commission of het European Communities, Contract No. ECI-2652-717-F. Ref. No. VIM 0221/IMD 282 C.

236 Chichos, D.: Verwendung eines Ankoppelmittels für Ultraschallprüfung. DE Pat. 2000641 (1971).

237 Chilowski, C.: Piezoelectric plastic material and method of making same. US Pat. 2,420,864 (1947).

238 Chinnathambi, K.; Prabhakar, O.: Quality control of aluminium alloy castings. Trans. Indian Inst. Met. 33 (1980) 296–300.

239 Chmiel, E.; Przybylowicz, M.: Detection and evaluation method of flaws in rails in polish goverment railways with ultrasonic flaw detector. 7th Int. Conf. NDT, Warszawa 1973, paper C-37

240 Chockie, L. J.: Progress report on a PVRG program on the reliability of ultrasonic examination of heavy section weldments. In: Nichols, R. W. (Ed.): Advances in nondestructive examination for structural integrity. London: Appl. Sci. Publ. 1982 pp. 285–293.

241 Chrétien, J. F., Chrétien, N.: A bibliographical survey of acoustic emission. Non Destr. Test. 5 (1972) 220–224.

242 Christianus, D.; Fischer, K.-H.: Ultraschallprüfung und Abnahme von Gußteilen aus warmfestem Stahlguß nach DIN 17245. Zusammenhang zwischen Durchstrahlungsprüfung nach ASTM und Ultraschallprüfung. Materialprüfung 20 (1978) 295–298.

243 Chung, D. H.; Silbersmith, D. J.; Chick, B. B.: A modified ultrasonic pulseecho-overlap method for determining sound velocities and attenuation of solids. Rev. Sci. Instrum. 40 (1969) 718–720.

244 Chwirut, D. J.: A simple technique for visualizing transmitted or reflected sound fields. Mater. Eval. 37 (1979) 29–32.

245 Ciorau, P.; Mandrila, S.; Grioras, G.: Size evaluation of discontinuities in welded joints by ultrasonic and radiation methods. 3rd Europ. Conf. NDT, Florence 1984, Vol. 1, pp. 470–479.

246 Cipri, F.: Non destructive tests on graphite/epoxy aerospace primary structures. 3rd Europ. Conf. NDT Florence 1984, Vol. 1, pp. 52–65.

247 Cist, J. D.; Smith, J. G.: On-line inspection of plastic pipe by rotational ultra-sonics. Plast. Eng. 34 (1978) 41—44.

248 Clark, A. V.: Determination of stresses in slightly orthotropic plates using off-axis horizontally polarized ultrasonic shear waves. Ultrasonics 21 (1983) 249—255.

249 Clark, A. V.; Chaskelis, H. H.: Measurement of ultrasound reflected from ultra-thin defects. Ultrasonics 19 (1981) 201—207.

250 Clark, A. V.; Hart, S. D.: Measurement of ultrasound reflected from liquid layers of submicron thickness. Mater. Eval. 40 (1982) 866–873.

251 Clark, J. P.; Staley, J. P.: Remote automated ultrasonic inspection: new approaches to reduce radiation exposure and shorten inspection time. In: Clough, R. B. (Ed.): Quantitative NDE in the nuclear industry. Proc. 5th Int. Conf. NDE in the Nuclear Industry. San Diego 1982, Metals Park: ASM 1983, pp. 60–61.

252 Claus, R. O.; Zerwekh, P. S.: Ultrasonic transducer with a two-dimensional Gaussian field profile. IEEE Trans. SU-30 (1983) 36–39.

253 Clément, M. J.-M.; Alais, P.: Ultrasonic computed tomography by electronic scanning of an annular array. Conf. Proc. Ultrasonics Int., Graz 1979. Guildford: IPC Sci. and Technol. Press 1979, pp. 511–517.

254 Clipson, W. R.: Ultrasonic inspection of rotor forgings. Parsons Materials Symp.

Newcastle 1976, Paper M 3.

255 Coffey, J. M.; Wrigley, J. M.: Pressurized water reactor nozzle "crotch corner" inspection: an effective additional ultrasonic technique for radial cracks. Br. J. Non Destr. Test. 25 (1983) 130–131.

256 Collins, R. M.: NDT chronology of advanced composites at Grumman aerospace. Mater. Eval. 39 (1981) 1126—1129.

257 Cook, B. D.; Werchan, R. E.: Mapping ultrasonic fields with cholesteric liquid crystals. Ultrasonics 9 (1971) 101—102.

258 Cook, E. G.: Transient and steady-state response of ultrasonic piezoelectric transducers. IRE Convention Record 1956, Part 9, 61–69.

259 Cook, E. G.; van Valkenburg, H. E.: Surface waves at ultrasonic frequencies. ASTM-Bull. 84, May 1954.

260 Cook, E. G.; Valkenburg van, H. E.: Thickness measurement by ultrasonic resonance. J. Acoust. Soc. Am. 27 (1955) 564–569.

261 Cook, G. G.; Walker, W. D.: Ultrasonic testing of gas turbine discs and heavy rotor forgings. Proc. 4th. Int. Conf., London 1963. London: Butterworths Sci. 1964, pp. 215–217

262 Cook, K. V.; Simpson, W. A.: Improved techniques for the ultrasonic characterization of graphite. Oak Ridge Nat. Lab. Oak Ridge, Rep. CONF-811003-5 (1981).

263 Corl, P. D.; Kino, G. S.: A real-time synthetic-aperture imaging system. In: Wang, K. Y. (Ed.): Acoustical imaging, Vol. 9. New York: Plenum Press 1980, pp. 341–355.

264 Couchman, J. C.; Bell, J. R.: Prediction, detection and characterization of a fast surface wave produced near the first critical angle. Ultrasonics 16 (1978) 272–274.

265 Crecraft, D. I.: The measurement of applied and residual stresses in metals using ultrasonic waves. J. Sound Vib. 5 (1967) 173–192.

266 Crecraft, D. I.; Warner, G.: Ultrasonic evaluation of electrical resistance spot welds. Non Destr. Test. 2 (1969) 40–43.

267 Cressmann, R. N.; Plante, A. J.: Ultrasonic inclusion rating of bearing steel billets. Blast Furn. Steel Plant (1969) 232–238, 251–259.

268 Cross, B. T.; Hannah, K. J.; Tooley, W. M.; Birks, A. S.: Delta technique extends the capability of weld quality assurance. Br. J. Non Destr. Test. 11 (1969) 62–77.

269 Cross, N. O.: An ultrasonic test for measuring the shear strength of clad plate. 6th Int. Conf. NDT, Hanover 1970, paper G 7

270 Crostack, H. A.; Deutsch, V.; Steffens, H. D.; Stelling, H. A.; Vogt, M.: Ultraschallprüfung mit Sendeimpulsen stufenlos veränderlicher Frequenz und steuerbarer Spektralverteilung. Materialprüfung 20 (1978) 372–377.

271 Crostack, H. A.; Deutsch, V.; Vogt, M.: Improvements in ultrasonic testing by means of narrowband transmitter pulses of continuously variable frequency. Br. J. Non Destr. Test. 22 (1980) 166–171.

272 Crostack, H. A.; Fischer, W. R.: Einsatz von Ultraschall in Verbindung mit holographischer Interferometrie zur zerstörungsfreien Prüfung thermisch gespritzter Schichten. Materialprüfung 24 (1982) 49–54.

273 Crostack, H.-A.; Morlo, J.; Wielage, B.: Einsatzmöglichkeiten der zerstörungsfreien Prüfung von Lötverbindungen mittels Ultraschall. Kolloquium Hart- und Hochtemperaturlöten und Diffusionsschweißen. DVS Essen, 1981, Vol. 69, p. 123 to 127.

274 Crostack, H. A.; Oppermann, W.: Einfluß des Spektralgehaltes von Ultraschallimpulsen auf die Fehlerbewertung nach der AVG-Methode. Materialprüfung 23 (1981) 234.

275 Crostack, H. A.; Oppermann, W.: Zur Bestimmung von optimalen Impulsparametern bei der Ultraschallprüfung von Stahlguß mit stochastischer Gefügestreuung. Gießereiforsch. 34 (1982) 33–39.

276 Crostack, H.-A.; Roye, W.; Verbesserung der Ultraschallprüfung von Gußteilen. Fehleranalyse mit der Mehrfrequenztechnik. 3rd Europ. Conf. NDT, Florence 1984, Vol. 4, pp. 11–19.

277 Crowe, J. C.: Techniques for NDE of radioactive waste capsule end cap welds. Mater. Eval. 30 (1972) 93–98.

278 Crutzen, S. J.: The PISC II Programme. In: Nichols, R. W. (Ed.): Advances in nondestructive examination for structural integrity. London: Appl. Sci. Publ. 1982, pp. 315–336.

279 Crutzen, S.; Jehenson, P.; Borloo, E.: PISC II: Status report at the end of an international exercise on NDT effectiveness assessment and decisions of the JRC-ISPRA for its follow-up. 3rd Europ. Conf. NDT, Florence 1984, Vol. 5, pp. 325–334.

280 Cunningham, J. A.; Quate, C. F.: High resolution acoustic imaging by contact printing. Acoust. Hologr. 5 (1974) 83–102.

281 Curie, P. J.; Curie, P.: Développement par pression de l'électricité polaire dans les cristaux hémiedres à faces inclinées. C. R. (Acad. Sci., Paris) 91 (1880) 294–295.

282 Curie, P. J.; Curie, P.: Contraction et dislocation produites par des tensions électriques dans les cristaux hémièdres à face inclinées. C. R. (Acad. Sci., Paris) 93 (1881) 1137–1140.

283 Czerlinsky, E.: Zerstörungsfreie Lagerprüfung mit Ultraschall. Dt. Luftfahrtforschung, Unters. u. Mitt. Nr. 1069 (1943).

284 Czerlinsky, E.: Zerstörungsfreie Sperrholzprüfung mit Ultraschall. Dt. Luftfahrtforschung, Unters. u. Mitt. Nr. 1042 (1943).

285 Dahlberg, P.: A four probe technique for accurate crack sizing using ultrasonic diffraction. Proc. 2nd Europ. Conf. NDT Vienna (1981) 44–45

286 Dalton, R. R.: Ultrasonic inspection of cast HK-40 tubes for creep fissures. Vortrag auf der ASNT Fall Conf., Chicago 1973.

287 Danicki, E.; Dilling, M.: Experimental and numerical analysis of diffraction of ultrasonic surface waves. J. Tech. Phys. 20 (1979) 255–263.

288 Daniel, I. M.; Schramm, S. W.; Liber, T.: Fatigue damage monitoring in composites by ultrasonic mapping. Mater. Eval. 39 (1981) 834–839.

289 Daniel, S. S.; Rege, R. A.: Ultrasonic cleanliness rating of steel. J. Metals (July 1971) 26–37.

290 Dasgupta, S.; Hore, A. R.: Application of ultrasonic echo loss techniques for the determination of heat-treatment quality of steel castings on the shop floor. Br. Foundryman 72 (1979) 228–233.

291 Date, K.; Shimada, H.; Ito, Y.: Monitoring crack extension in fracture toughness tests by ultrasonic surface wave. Non Destr. Test. J. Jap. 2 (1984) 132–137.

292 Datta, S. K.; Fortunko, C. M.; King, R. B.: Sizing of surface cracks in a plate using shear horizontal waves. In: Thompson, D. O. (Ed.): Quantitative NDE Vol. 1, 1982, pp. 227–231.

293 Dau, G. J.: The EPRI NDE program; Proc. 9th World Conf. NDT, Melbourne 1979, Rep. 2B-2.

294 Dau, G. J.: Inservice inspection of steam generators. In: McGonnagle, W. J. (Ed.): International advances in NDT, Vol. 6. New York: Gordon and Breach, 1979, pp. 1–18.

295 Dau, G. J.; Quinn, J. R.: "Reliability" assessments of ultrasonic inspection — pipework and austenitic weldments in the USA. In: Nichols, R. W. (Ed.): Advances in nondestructive examination for structural integrity. London: Appl. Sci. Publ. 1982, pp. 251–268.

296 Dau, G. J.; Quinn, J. R.: Developments in ultrasonic inspection of reactor pressure vessels in the USA. In: Nichols, R. W. (Ed.): Advances in nondestructive examination for structural integrity. London: Appl. Sci. Publ. 1982, pp. 47–57.

297 Dau, G. J.; Lapides, M. E.: Considerations for an optimized system for an

ultrasonic inspection of stainless pipe. In: Charyulu, V. H. (Ed.): NDE in the nuclear industry — 1980. Metals Park: ASM 1981, pp. 61–73.

298 Davis, D. D.: ASME Sect. XI, Design and access requirements for in-service inspection. In: Periodic inspection of pressurized components, I. Mech. E. Conf. Publications 1982-9, London: Mech. Eng. Publ. 1982, pp. 7–26.

299 Davies, I.: An alternative approach to flaw size measurement. Proc. Conf. Ultrasonics for Industry, London 1970, pp. 40–42.

300 Davis, T. J.: A high frequency ultrasonic tester for bond inspection of thinclad nuclear reactor fuels. Mater. Eval. 28 (1970) 257–261.

301 Davis, W. I.; Brough, R.: Ultrasonic techniques in ceramic research and testing. Ultrasonics 10 (1972) 118–126.

302 Dawance, G.; Chefdeville, M. J.: Schallmessungen an Beton. Schweiz. Arch. 21 (1955) 223–234, 313–325.

303 Day, A.: Ultrasound as a possible means of examining swaged joints. Mater. Eval. 31 (1973) 164–167.

304 DeSilets, C. S.; Selfridge, A. R.; Kino, G. S.: Highly efficient transducer arrays useful in nondestructive testing applications. Proc. IEEE Ultrasonic Symp. 1978, pp. 111–116.

305 Dean, D. S.: Air-coupled ultrasonic probes. Br. J. Non Destr. Test. 10 (1968) 56.

306 Dean, D. S.: A review of ultrasonic transducer arrays. Br. J. Non Destr. Test. 21 (1979) 140–146.

307 Debye, P.; Sears, F. W.: On the scattering of light by supersonic waves. Proc. Nat. Acad. Sci. 18 (1932) 409–416

308 Dekker, D. L.; Piziali, R. L.; Dong, E.: Effect of boundary conditions on the ultrasonic-beam characteristics of circular disks. J. Acoust. Soc. Am. 56 (1974) 87–93.

309 De Lano, R. B.: Means for inspecting materials by wave trains. US Pat. 2,507,854 (1945).

310 Derkacs, Th.: High-frequency ultrasonic inspection of a gas turbine ceramics. 4. Ann. Conf. Composites Advanced Ceramic Materials, Cocoa Beach (1980), Ceram. Eng. Sci. 1 (1980) 576–592. Am. Ceram. Soc., Columbus.

311 Deputat, J.; Pawlowski, Z.; Rulka, R.: Ultrasonic testing of metal-metal bond in engine sleeves. 7th Int. Conf. NDT Warszawa 1973, paper C 49

312 Deputat, J.; Mazurek, J.; Pawlowski, Z.: Ultrasonic testing of brass castings. Vortrag, 6th Int. Conf. NDT; Hanover 1970, Vol. E, p. 87–98.

313 Desch, C. H.; Sproule, D. O.; Dawson, W. J.: The detection of cracks in steel by means of supersonic waves. J. Iron Steel Inst. 153 (1946) 319–352

314 Deuble, W.; Hübschen, G.: Elektrodynamische Anregung freier Ultraschallwellen. IZfP Conf. Saarbrücken 1982

315 Deuble, W.; Repplinger, W.: Ein breitbandiges elektromagnetisches Ultraschall Phased Array. Proc. 4th Int. Conf. NDT in Nuclear Techniques, Zürich 1981, p. 683–690

316 Deuster, G.; Issler, L.: Nondestructive testing of a large tensile test specimen under the German component safety programme. In: Charyulu, V. H. (Ed.): NDE in the nuclear industry — 1980. Metals Park: ASM 1981, pp. 197–217.

317 Deuster, G.: Developments in data processing, recording and analysis — review of work in the Federal Republic of Germany. In: Nichols, R. W. (Ed.): Advances in nondestructive examination for structural integrity. London: Appl. Sci. Publ., 1982, pp. 225–236.

318 Deutsch, V.: Zerstörungsfreie Prüfverfahren für die Widerstandspunktschweißungen und ihre praktische Bedeutung. ZIS-Mitt. 10 (1968) 63–75.

319 Deutsch, V.; Schaper, H.; Vogt, M.: Vorschlag einer Vorsatzscheibe zum quantitativen Auswerten der Befunde beim Prüfen von Schweißnähten mit Ultraschall. Schweißen u. Schneiden 23 (1971) 449–451.

320 Diamand, R. D.; Reynolds, P. M.: Ultrasonic inspection for back-end defect in large section copper alloy extrusions. BNF Res. Rep. A. 1939 (1978)

321 Dickhaut, E.: Rechnergestützte Ultraschallprüfung von Turbinenscheiben. Conf. of the DGZfP Essen 1984, paper no. 35

322 Dickinson, W. W.: An acoustic spectrometer system. Non Destr. Test. 1 (1968) 379–382.

323 Dickson, J. K.: Dry coupling ultrasonic method of inspection on composite and metallic honeycomb panels on aircraft structure. Proc. 10th World Conf. NDT Moscow 1982, Session 5-1.

324 Dietz, D. R.: Apodized conical focusing for ultrasonic imaging. IEEE Trans. SU-29 (1982) 128–138.

325 DiGiacomo, G.; Crisci, J. R.; Goldspiel, S.: An ultrasonic method for measuring crack depth in structural weldments. Mater. Eval. 28 (1970) 189–193, 204.

326 Djordjevic, B. B.; Venables, J. D.: NDE of bonded metal and composite structures. Proc. 13th Symp. NDE, (Leonard, B. E., Ed.). Southwest Res. Inst., San Antonio 1982, pp. 68–76

327 Di Majo, A.; Traversa, L.; Giovambattista, A.; Giaccio, G.: Evaluation of concrete structures using ultrasonic pulse velocity methods. 3rd Europ. Conf. NDT Florence 1984, Vol. 1, pp. 214–223.

328 Dines, K. A.; Kak, A. C.: Ultrasonic attenuation tomography of soft tissues. Ultrason. Imaging 1 (1979) 16–33.

329 Dion, J. L.; LeBlanc, A.; Jacob, A. D.: Pseudo-holographic acoustical imaging with a liquid crystal convertor. Acoust. Imaging 10 (1982) 151–166.

330 Djordjevic, B. B.; Venables, J. D.: NDE of bonded metal and composite structures. Proc. 13th Symp. NDE (Leonard, B. E., Ed.). Southwest Res. Inst., San Antonio 1982, pp. 68–76.

331 Dobbs, E. R.; Lewellyn, J. D.: Generation of ultrasonic waves without using a transducer. Non Destr. Test 4 (1971) 49–56.

332 Doctor, S. R.; Selby, G. P.; Heasler, P. G.; Becker, F. L.: Effectiveness and reliability of inservice inspection, a round robin test. In: Clough, R. B. (Ed.): Quantitative NDE in the nuclear industry. Proc. Int. Conf. NDE in the Nuclear Industry, San Diego 1982. Metals Park: ASM 1983, pp. 176–179.

333 Doctor, S. R.; Busse, L. J.; Collins, H. D.: The SAFT-UT technology evaluation. 6th Int. Conf. NDE in the Nuclear Industry, Zürich 1983.

334 Dölle, H.; Schmidt, R.: Automatisierte Ultraschall-Tauchtechnik-Prüfanlage für Schwalbenschwanz-Verbundgleitlager. Conf. of the DGZfP, Erlangen 1985

335 Domarkas, V.; Khuri-Yakub, B. T.; Kino, C. S.: Length and depth resonances of surface cracks and their use for crack size estimation. Appl. Phys. Lett. 33 (1978) 557–559.

336 Donald, I.: Sonar — the story of an experiment. Ultrasound in Medicine and Biology 1 (1974) 109–117.

337 Dorko, J.; Lorincz, L.: Quality assessment of cast iron parts by ultrasonic determination of the elasticity modulus. Proc. 10th World Conf. NDT. Moscow 1982, Vol. 7, pp. 555–562 (Acad. Sci. USSR).

338 Dory, J.: Les possibilités d'application de l'analyse fréquentielle au contrôle non-destructif par ultrason. 7th Int. Conf. NDT, Warszawa 1973, paper C-24

339 Dressler, E.; Oellrich, K.: Ortsabhängige Berücksichtigung des Plattierungseinflusses bei der Anzeigenbewertung mechanisierter Ultraschallprüfungen an Reaktordruckbehältern. In: DGZfP (ed.): 4th Int. Conf. NDT Nuclear Techniques, Lindau 1981, Vol. 8, p. 263–267

340 Dressler, K.: Zur Beurteilung von Anzeigen bei der mechanisierten Ultraschallprüfung an Siedewasserreaktoren. Deutsch—Schweiz. Sem. Ausgew. Aspekte Zerstörungsfr. Prüf. Reaktorkomp., Stuttgart, 1983. Ed. Bundesmin. Forsch. Technol., Bonn, 1984

341 Dreumel van, W. H. M.; Speijer, J. L.: Nondestructive composite laminate characterization by means of ultrasonic polar-scan. Mater. Eval. 39 (1981) 922–925.

342 Droney, B. E.; Klinman, R.: Ultrasonic techniques for determining the mechanical

properties of steels. Conf. Proc. Physics in the Steel Industry, Lehigh University, 1981. (Schwerer, F. C., Ed.). New York, Am. Inst. Phys. 1982, pp. 210–228.

343 Dubresson, J.: Application des ultrasons pour la détection des corrosions internes dans des canalisations en service. Paper Conf. Comp. Sofranel. Paris 1968

344 Dubresson, J.; Evrard, M.; Le Penven, Y.: Contrôle non-destructif des soudures d'angle. Soudage Tech. Connexes 27 (1973) 23–37

345 Dünnwald, H.: Versuche zur Fehlererkennung in Graphit. DAGA Conf. (Dtsch. Arbeitsgemeinschaft f. Akustik) 1980, Munich. VDE-Verlag, p. 463–466

346 Duerinckse, A. J.: Matched Gaussian apodization of pulsed acoustic phased arrays. Ultrason. Imaging 2 (1980) 338–369.

347 Duke, J. C.: NDE of composite materials: a philosophy, an approach and an example. Symp. Composite Materials Quality Assurance, St. Louis 1981. Browning, C.E. (Ed.) ASTM STP 797 (1983), pp. 75–95.

348 Duke, J. C.; Russel, S. S.: The investigation of imperfections in sheet molding compound. Mater. Eval. 40 (1982) 566–571.

349 Dumanchin, R.; Michon, M. et al.: Extension of TEA CO_2 laser capabilities. IEEE J. QE-8 (1972) 163–165.

350 Dunegan, H. L.; Tetelmann, A. S.: Nondestructive characterization of hydrogen-embrittlement cracking by acoustic emission techniques. Eng. Fract. Mech. 2 (1971) 387–402.

351 Dunlop, J. I.: Testing of poles by acoustic pulse method. Wood Sci. Technol. 15 (1981) 301–310.

352 Durbin, P. F.; Armstrong, G. H.; Kuramoto, A.: Microcomputer-based ultrasonic inspection of solder bonds in superconducting cable. Mater. Eval. 41 (1983) 101–105.

353 Dussik, K. Th.: Über die Möglichkeit, hochfrequente mechanische Schwingungen als diagnostisches Hilfsmittel zu verwerten. Z. ges. Neur. Psych. 174 (1942) 153–168.

354 Eberhard, J. W.: Quantitative imaging in nondestructive evaluation by ultrasonic time-of-flight tomography. Mater. Eval. 40 (1982) 68–77.

355 Eberhardt, N.; Tverdokhlebov, A.: A resonance method for measurement of longitudinal and transverse ultrasonic wave velocities and their attenuations. In: Thompson, D. O.; Chimenti, D. E. (Eds.): Quantitative NDE Vol. 1, 1982, pp. 639–651.

356 Edelmann, X.: Zur Fehlergrößenabschätzung bei der Ultraschallprüfung von Schweiß-verbindungen an unlegierten und niedriglegierten Stählen. Diss. ETH Zürich 1984.

357 Edelmann, X.: Wiederkehrende Prüfung mit Ultraschall an austenitischen Schweiß-verbindungen im Hauptkühlmittelsystem von Druckwasserreaktoren. In: DGZfP (Eds.): Int. Symp. Neue Verfahren der zerstörungsfreien Werkstoffprüfung und deren Anwendungen insbesondere in der Kerntechnik, Saarbrücken 1979, pp. 177–198

358 Edelmann, X.: Application of ultrasonic testing techniques on austenitic welds for fabrication and in-service inspection. Non Destr. Test. Int. 14 (1981) 125–133.

359 Edelmann, X.; Hornung, R.: Investigation of an ultrasonic technique for detection of surface flaws during inservice inspection of dissimilar metal welds. In: Clough, R. B. (Ed.): Quantitative NDE in the nuclear industry. Proc. 5th Int. Conf. NDE in the Nuclear Industry, San Diego 1982. Metals Park: ASM 1983, pp. 180–188.

360 Edelmann, X.; Hornung, R.: Erfahrungen im Prüfen von austenitischen Schweiß-verbindungen mit Ultraschall. Mater. u. Tech. 5 (1977) 19–22.

361 Edelmann, X.; Iversen, S. E.: New developments and practical applications of the P-scan technique. 3rd Europ. Conf. NDT Florence 1984. Vol. 1, pp. 454–469.

362 Edwards, P. L.; Cook, B. D.; Dardy, H. D.: Comparison of the experimental and theoretical pressure fields in the nearfield of ultrasonic transducer-lens systems. J. Acoust. Soc. Am. 68 (1980) 1528–1530.

363 Edwards, D. L.; Gearhart, S. W.; Juppenlatz, J. W.: Practical use of ultrasonic testing for steel castings. Trans. Am. Foundrymen's Soc. 88 (1980) Paper 80-30 pp. 457–462.

364 Egelkraut, K.: 20 Jahre Ultraschallprüfung an Achswellen, bewährte Verfahren und

neue Entwicklungen bei der Deutschen Bundesbahn und anderen Eisenbahnen. Schienen der Welt (1970) 594–616.

365 Egelkraut, K.: Activities of the German society for NDT in the field of education, training and professional qualification. Br. J. Non Destr. Test. 15 (1973) 50–54.

366 Egelkraut, K.: On site ultrasonic rail testing. Non Destr. Test. 1 (1968) 297–305.

367 Egelkraut, K.: Ultraschallprüfungen an Schienen bei der Deutschen Bundesbahn. Elsners Taschenbuch der Eisenbahntechnik 1978, pp. 71–98.

368 Egelkraut, K.: Ultraschallprüfungen bei der Deutschen Bundesbahn — ein Beitrag zur Sicherheit. Tech. Überwach. 19 (1978) 379–384.

369 Egelkraut, K.; van Herwijnen, H. G.; Lambert, B.: Internationaler Vorschlag zur Ausbildung von ZfP-Personal. Materialprüfung 16 (1974) 282–284.

370 Egelkraut, K.; van Herwijnen, H. G.; Lambert, B.: Draft recommendations concerning the education, training and certification of NDT-personnel. Br. J. Non Destr. Test. 17 (1975) 76–79.

371 Eichler, R. H.: Apparatus for measurement of sound velocity in a workpiece US Pat. 3.690.155 (1972).

372 Eisenblätter, J.: Verfolgung der Rißbildung in einer dicken Platte bei und nach dem Unterpulverschweißen mit Schallemissionsanalyse (SEA). In: DGZfP (Eds.): Int. Symp. Neue Verfahren der ZfP und deren Anwendungen insbesondere in der Kerntechnik, Saarbrücken 1979, pp. 353–368

373 Eisenblätter, J.; Erlenkämper, S.; Jax, P.; Votava, E.: The influence of wave propagation on the accuracy of locating acoustic emission sources in thick-walled and thin-walled structures. In: Charyulu, V. H. (Ed.): NDE in the nuclear industry — 1980. Metals Park: ASM 1981, pp. 463–477.

374 Eisenmann, K.; Steinkamp, G.: Messung der Tiefen und Weiten von Betonrissen mittels Ultraschall. Beton- u. Stahlbetonbau 49 (1954) 36–38.

375 Eisenmenger, W.: Elektromagnetische Erzeugung von ebenen Druckstößen in Flüssigkeiten. Acustica 12 (1962) 185–202.

376 Elagin, V. I.; Teleshov, V. V.; Grishina, V. M.: The use of ultrasonic inspection for determining overheating of aluminium alloy parts. Sov. J. Non Destr. Test. 14 (1978) 569–570.

377 Elias, C. M.; Moran, T. J.; McCormick, W. S.: A continuous wave pseudorandom binary noise nondestructive ultrasonic correlation system. Proc. 13th Symp. NDE. (Leonard, B. E., Ed.) Southwest Res. Inst., San Antonio 1982, pp. 377–382.

378 Elion, H. A.: Recent advances in new areas of NDT. Non Destr. Test. 18 (1960) 180–182.

379 Elion, H. A.: Metallurgical structure analysis by ultrasonics. Proc. Nat. Electronics Conf., Chicago 1957, Vol. 13.

380 Elion, H. A.: Recent advances in stress measurement by ultrasonics. Proc. 3rd Int. Congr. Acoustics, Stuttgart 1959. Amsterdam: Elsevier 1960.

381 El-Sherbiny, S. M.: Determination of the attenuation coefficient of a scattering medium from the ultrasound back-scattering characteristic. Acustica 48 (1981) 10–14.

382 Elsley, R. K.; Tittmann, B. R.; Nadler, H. L.; Ahlberg, L. A.: Defect characterization by ultrasonic signal processing techniques. IEEE Ultrasonics Symp. Proc. 1977, pp. 48–52.

383 Elvery, R. H.; Vale, D. W.: Developments in the measurements of ultrasonic pulse velocity in concrete. 7th Int. Conf. NDT Warszawa 1973, paper J-17

384 Ely, R. W. J.; Hall, G. D.; Johnson, A.; Pascoe, P. T.; Short, K. A.: Ultrasonic recording and display techniques for the inspection of nuclear power plant. Central Electricity Generating Board, North Western Region, Scientific Services Department, Rep. No. NWR/SSD/83/0128/R, 1983.

385 Emerson, P. J.: Ultrasonic NDT in the iron foundry. Ultrasonics for industry 1970, London, Conf. Pap., pp. 46–48

386 Emerson, P. J.; Lavender, J.; Levene, B.: Ultrasonic testability of cast engineering metals: attenuation characteristics. Ultrasonics for industry 1971, London, Conf.

Pap., pp. 46–48

387 Engl, G.; Elsner, H. J.: Comparison of requirements for inservice inspection in Germany with Section XI, ASME, BAPV Code. In: Charyulu, V. H. (Ed.): NDE in the nuclear industry — 1980. Metals Park: ASM 1981, pp. 291–302.

388 Engl, G.; Figlhuber, D.; von Bernus, L.; Meier, W.: A new concept for steam generator tubing inspection. Proc. 10th World Conf. NDT, Moscow 1982, Vol 7, pp. 336–347 (Acad. Sci. USSR).

389 Engl, G.; Heumüller, R.; Kastl, H.; Koehler, W.: Erfahrungen mit einem neuen Konzept für mechanisierte Ultraschallprüfungen an Primärkreiskomponenten und Rohrleitungen. In: DGZfP (Ed.): 4th Int. Conf. NDT in Nuclear Techniques, Lindau 1981. Vol. 8, pp. 409–416

390 Engl, G.; de Raad, J. A.; Thiel, B.: Entwicklungsarbeiten für die Stutzenkantenprüfung an Reaktordruckbehältern. In: DGZfP (Ed.): Int. Symp. Neue Verfahren der ZfP und deren Anwendungen insbesondere in der Kerntechnik, Saarbrücken 1979, pp. 481–489

391 Engl, G.; Rathgeb, W.; Wüstenberg, H.; Barbian, O. A.; Grohs, B.: A second view on the German results used in the defect detection trials. UKAEA DDT Symp. 1982, Birchwood.

392 Enselke, W.; Schleithoff, K.; Jestrich, H.-A.: Design, operating and inspection considerations to control stress corrosion of LP turbine disks. Proc. Am. Power Conf. Chicago 1983, Vol. 45, pp. 196–206, Illinois Inst. Technol. Chicago.

393 Erdman, D. C.: Ultrasonic inspection using automatic recording and frequency modulated flaw detector. Non Destr. Test. 11 (1953) 17–31, und: Ultrasonic flaw detector. US Pat. 2,593,865 (1950).

394 Erhard, A.; Kutzner, J.; Wüstenberg, H.; Mundry, E.: Abhängigkeit der Echoanzeige von nutartigen Reflektoren vom Prüfkopfschallfeld und der Frequenz. Materialprüfung 19 (1977) 379–382.

395 Erhard, A.; Kröning, M.: Erzeugung, Ausbreitung und Anwendung von Ultraschall-Kriechwellen. Materialprüfung 26 (1984) 323–326.

396 Erhard, A.: Rathgeb, W.: Einfluß des Ankoppelspaltes auf den Schallübergang bei der Ultraschallprüfung mit Schrägeinschallung. Ber. BAM, Berlin 1976.

397 Erhard, A.; Wüstenberg, H.; Engl, G.; Kutzner, J.: Reliability and redundancy in ultrasonic flaw sizing methods. In: Charyulu, V. H. (Ed.): NDE in the nuclear industry — 1980. Metals Park: ASM 1981, pp. 255–268.

398 Erhard, A.; Wüstenberg, H.; Haufe, U.; Möhrle, W.: Berechnung und Bau von Gruppenstrahler-Prüfköpfen. 3rd Europ. Conf. NDT Florence 1984, Vol. 3, pp. 156 bis 170.

399 Erhard, A.; Wüstenberg, H.; Möller, D.: Der Einsatz der akustischen Holographie an plattierten Bauteilen zur Fehlergrößenbestimmung. In: Österr. Ges. ZfP (Ed.): 2nd Europ. Conf. NDT Vienna 1981, pp. 117–119

400 Erhard, A.; Wüstenberg. H.; Schulz, E.; Mundry, E.: Anwendungen der longitudinalen Kriechwelle in der zerstörungsfreien Prüfung mit Ultraschall und Erfahrungen beim Einsatz von Kriechwellenprüfköpfen. Materialprüfung 24 (1982) 43–48.

401 Erhard, A.; Wüstenberg. H.; Schulz, E.: Kriechwellen in der Ultraschallprüfung — Physikalische Grundlagen, Anwendung bei Schweißkonstruktionen. Schweißen u. Schneiden 35 (1983) 220–223.

402 Ermert, H.; Schaefer, J. O.: Flaw detection and imaging by high-resolution synthetic pulse holography. In: Alais, P.; Metherell, A. F. (Ed.): Acoustical imaging, Vol. 10. New York: Plenum Press 1982, pp. 629–642.

403 Ermolov, I. N.: Methods of Calculating the Acoustic Section of an Ultrasonic Flaw-Detector. I. The Acoustic Field of a Normal Probe. (in Russian). Defektoskopija 3, No. 3 (1967) pp. 41–50. II. The acoustical component of reflection by a disc-shaped defect and by an infinite flat surface (in Russian). Defektoskopija 3, No. 4 (1967) pp. 15–23. III. The acoustic component of reflection by spherical and cylindrical defects. Defektoskopija 3, No. 5 (1967) pp. 32–34

404 Ermolov, I. N.: The choice of the optimum frequency for ultrasonic testing of thick welded seams (in Russian). Zavodskaja Laboratorija 26 (1969) 452–454

405 Ermolov, I. N.: Reflection of ultrasound from various types of defects. Sov. J. NDT (1971) 374–380. — Orig.: Defektoskopija (1970) No. 4, 17–24

406 Ermolov, I. N.: Reflection of ultrasound from flaws of different shapes. Sov. J. NDT (1970) 374–380

407 Ermolov, I. N.: On the echo-field of a normal probe. Defektoskopija 6 (1970) 2, pp. 51–57

408 Ermolov, I. N.: The reflection of ultrasonic waves from targets of simple geometry. Non Destr. Test. 5 (1972) 87–91

409 Ermolov, I. N.: The reflection of ultrasonic waves from artificial targets for the angle probe testing. 7th Int. Conf. NDT Warszawa 1973, paper H-08

410 Ermolov, I. N.; Lapin, Yu. V.; Staseev, V. G.: Radiation and reception field along the axis of a rectangular probe taking the pulsed mode into account. Sov. J. Non Destr. Test. 15 (1979) 689–694.

411 Ermolov, I. N.; Razygraev, N. P.; Shcherbinskii, V. G.: Attenuation of ultrasonic head waves with distance. Sov. J. Non Destr. Test. 15 (1979) 28–30.

412 Ermolov, I. N.; Razygraev, N. P.; Shcherbinskii, V. G.: Study of shaping process for acoustic field of a head-type wave in a test medium. Sov. J. Non Destr. Test. 14 (1978) 953–957.

413 Ermolov, I. N.; Razygraev, N. P.; Shcherbinskii; V. G.: The use of head-type waves for ultrasonic monitoring. Sov. J. Non Destr. Test. 14 (1978) 27–33.

414 Ermolov, I. N.; Shcherbinsky, V. G.: Automatization of ultrasonic testing of vessels of nuclear power plants. 3rd Europ. Conf. NDT Florence 1984, Vol. 2, pp. 124–130.

415 Ermolov, I. N.; Shcherbinskij, V. G.: On the use of DGS-diagrams when testing with shear probes. Sov. J. Non Destr. Test. 6 (1970), 665–669.

416 Ermolov, I. N.; Shcherbinskij, V. G.: Measurement of defect size in ultrasonic flaw detection. Sov. J. Non Destr. Text. 3 (1967) 17–23.

417 Ermolov, I. N.; Zenkova, L. S.; Nishnevich, M. M.: Focusing probes for ultrasonic flaw detection. Sov. J. Non. Destr. Text 19 (1979) 139–147.

418 Erwin, W. S.: Supersonic measuring means. US Pat. 2,431,233 (1944).

419 Escoffier, R.: Installation automatique de contrôle par ultrasons. 3rd Europ. Conf. NDT Florence 1984, Vol 3, pp. 431–441.

420 Espinola, R. P.; Waterman, P. C.: US interferometer for the measurement of the temperature dependence of elastic constants. J. Appl. Phys. 29 (1958) 718–721

421 Evans, D. J.: New ultrasonic techniques for the chemical and petroleum industries. Mater. Eval. 12 (1964) 164–168.

422 Evans, D. J.: Ultrasonic inspection in the oil refining and related industries. Non Destr. Test. 15 (1957) 156–160.

423 Evans, J. D.: Corrosion-rate data can be exact. Marine Eng./Log (May 1958).

424 Evrard, M.: Intérêt des blocs d'étalonnage dans le contrôle non destructif par les ultrasons. Mém. Sci. Rev. Métall. 56 (1959) 111–123.

425 Evsyukov, V. N.; Berezovskii, L. B.; Gergel, P. I.: Attenuation of transverse ultrasonic waves in rolled aluminium and aluminium alloy sheet. Sov. J. Non Destr. Test. 14 (1978) 418–420.

426 Ewald, J.; Berger, C.; von Hofe, D.; Röttger, G.; Staif, F.: Überlegungen zur Prüfung und Beurteilung von Fehlern im Stahlguß von Sattdampfturbinen. VGB Konf. Werkstoffe und Schweißtechnik im Kraftwerk, 1983.

427 Farley, P. G.: Ultrasonic inspection of railway traction and rolling stock axles. The three main techniques used by British Rail. Non Destr. Test. Int. 11 (1978) 287–293.

428 Farley, P. G.: Ultrasonic testing of alumino-thermic rail welds. Met. Constr. 12 (1980) 678–684.

429 Farley, J. M.; Dikstra, B. J.; Scruton, G.: Developments in ultrasonic instrumen-

tation to improve the reliability of NDE of pressurized components. In: Periodic inspection of pressurized components, I. Mech. E. Conf. Publ. 1982-9, London: Mech. Eng. Publ. 1982, pp. 217–227.

430 Farrow, C.: Supersonic testing of hot articles. US Pat. 2,697,936 (1954).

431 Fay, B.: Theoretische Betrachtungen zur Ultraschallrückstreuung. Acustica 28 (1973) 354–357.

432 Fay, B.: Gefügebestimmung mit Ultraschall. Fortschritte der Akustik. Plenarvorträge und Kurzreferate der 3. Tag. d. Dtsch. Arbeitsgemeinschaft f. Akustik DAGA-73, Aachen. Düsseldorf: VDI-Verlag 1973, pp. 129–132

433 Fay, B.: Ermittlung der Korngröße von Stahl mit dem Verfahren der Ultraschall-rückstreuung. Arch. Eisenhüttenwes. 47 (1976) 119–126.

434 Fay, B.: Ausbreitung von Ultraschall in streuenden Substanzen. Acustica 48 (1981) 218–227.

435 Feist, W. D.: NDT of felt-metal bonding in aero engines. 3rd Europ. Conf. NDT Florence 1984, Vol. 1, pp. 40–51

436 Feldmann, J.: Inspektion von aktivierten Reaktordruckgefäßen. Paper No. 20 of the Conf. No. 9 of the Nuclear Industry (Nuclex '72), Basel Oct. 1972

437 Fenkner, M.: Die metallkundliche Bedeutung der Schallgeschwindigkeit, dargestellt an der Strukturanalyse wärmebehandelter Stähle. 6th Int. Conf. NDT Hanover 1970, Vol. E, 1–10

438 Fessler, P. A.; Michaud, W. E.: A high sensitivity ultrasonic test system for welds. Contract AG-(29-2)-656 US Atomic Energy Commiss., 1970.

439 Figlhuber, D.; Fischer, E.: Experiences with in service inspection of reactor pressure vessels, pipe-lines and steam generator heating tubes. 3rd Europ. Conf. NDT Florence 1984, Vol. 2, pp. 184–195

440 Filipczynski, L.: Measurement of mode conversion of ultrasonic waves on a solid-solid boundary. Proc. of Vibration Problems 4 (1963) 255–263.

441 Filipczynski, L.: Scattering of a plane longitudinal wave on a free surface of a disc in solid medium. Proc. of Vibration Problems 2 (1961) 41–56.

442 Filipczynski, L.: Measurements of longitudinal and transverse waves radiated by a compressional source into elastic semispace. Proc. of Vibration Problems 5 (1964) 89–93.

443 Filipczynski, L.: Absolute measurements of particle velocity, displacement or intensity of ultrasonic pulses in liquids and solids. Acustica 21 (1969) 174–180.

444 Filipczynski, L.; Etienne, J.: Theoretical study and experiments on spherical focusing tranducers with Gaussian surface velocity distribution. Acustica 28 (1973) 121–128.

445 Filipczynski, L.; Crzenkowicz, I.: Ultrasonic concrete tester BI-2. Proc. 2nd Conf. Ultrasonics, Warszawa 1956, pp. 251–252.

446 Filippi, F. J.: Qualitative analysis of brazed sandwich. Non Destr. Test. 17 (1959) 39–45.

447 Fink, E. W.: Ultrasonic testing as a method of determining variables in pro-cessing zircalloy and hafnium. Symp. NDT in the Field of Nuclear Energy. ASTM Spec. Tech. Publ. No. 223 (1958) 175–179.

448 Fink, K.; Ries, K.; Weber, H. P.: Zerstörungsfreie Fehlerprüfungen im Produk-tionsfluß bei der Herstellung von längsnahtschmelzgeschweißten Großrohren für Fernleitungen. Schweißen u. Schneiden 22 (1970) 119–123.

449 Fink, K.: Stand und Entwicklungstendenzen der zerstörungsfreien Prüfung von Schweißverbindungen. Schweißen u. Schneiden 24 (1972) 375–380.

450 Fink, K.; Richter, F.; Lotter, U.; Schrecke, K.: Physikalische Eigenschaften von Stählen, insbesondere von warmfesten Stählen. Thyssenforsch. 2 (1970) 65–80.

451 Firestone, F. A.: Flaw detecting device and measuring instrument. US Pat. 2,280,226 (1940).

452 Firestone, F. A.: Resonance inspection method. US Pat. 2,439,131 (1943).

453 Firestone, F. A.: Surface and shear wave method and apparatus. US Pat. 2,439,139 (1943).

454 Firestone, F. A.: Supersonic reflectoscope, an instrument for inspecting the interior of solid parts by means of sound waves. J. Acoust. Soc. Am. 17 (1945) 287–299.

455 Firestone, F. A.; Frederick, J. R.: Refinements in supersonic reflectoscopy. Polarized sound. J. Acoust. Soc. Am. 18 (1946) 200–211.

456 Firestone, F. A.: Tricks with the supersonic reflectoscope. Non Destr. Test. 7 (1948) 5–19.

457 Firestone, F. A.; Ling, D. S.: Method and means for generating and utilizing vibrational waves in plates. US Pat. 2,536,128 (1951).

458 Fischer, H.; Fröhlich, L.; Klinge, A.: Zerstörungsfreie Prüfung von Sandwichbau-teilen mit Al-Deckschichten. Schweißtechnik 31 (1981) 254–256.

459 Fischer, E.; Kröning, M.; Berens, M.; Schober, H.: New inspection concept for the ultrasonic in-process inspection of thick-walled reactor components. Proc. 10th World Conf. NDT Moscow 1982, Vol. 7, pp. 328–335 (Acad. Sci. USSR).

460 Fitting, D. W.; Adler, L.: Ultrasonic spectral analysis for NDE. New York: Plenum Press 1981.

461 Forch, K.; Frank, E.: Ultraschallbefund und wahrer Fehler in schweren Schmiede-stücken, Einfluß auf das Betriebsverhalten. 2. Seminar Eisen- und Stahlforschung, Berlin 1982. (Neumann, R., ed.). Vol. 1, pp. 177–186/KFA Jülich 1982

462 Fortunko, C. M.: Ultrasonic evaluation of austenitic stainless steel welds using shear horizontal waves. Appl. Phys. Lett. 39 (1981) 699–700.

463 Fortunko, C. M.; Moulder, J. C.: Ultrasonic inspection of stainless steel butt welds using horizontally polarized shear waves. Ultrasonics 20 (1982) 113–117.

464 Fortunko, C. M.; King, R. B.; Tan, M.: NDE of planar defects in plates using low-frequency shear horizontal waves. J. Appl. Phys. 53 (1982) 3450–3458.

465 Fortunko, C. M.; MacLauchlan, J.: Pulsed electromagnets for EMATs. Proc. DARPA/AFWAL Progress in Quantitative NDE, Rep. AD/A 108 741 (1981) pp. 528–534.

466 Fortunko, C. M.; Schramm, R. E.: Evaluation of pipeline girth welds using low-frequency horizontally polarized waves. J. Non Destr. Eval. 3 (1982) 155–173.

467 Fortunko, C. M.; Thompson, R. B.: Optimization of electromagnetic transducer parameters for maximum dynamic range. IEEE Ultrasonics Symp. Proc. 76 CH 1120-5 SU, pp. 12–16.

468 Foster, F. S.; Hunt, J. W.: The design and characterization of short pulse ultra-sound transducers. Ultrasonics 16 (1978) 116–122, 282–283.

469 Fowler, K. A.; Lynnworth. L. C.: Ultrasonic measurements of temperature using extensional and torsional waves. Proc. 6th Temperature Measurement Soc. Conf., Hawthorne, Calif. (1969) 191–208.

470 Fraatz, M.; Kuhlow, B.: Lichtoptische Abbildung fokussierter Ultraschallfelder. Materialprüfung 21 (1979) 359–363.

471 Francis, R. A.: On-line ultrasonic testing of rails at Whyalla. NDT Australia 21 (1984) 8–10

472 Francke, W., de Gee, A. W. J.: A nondestructive method for the measurement of the adhesive bond strength of thermally sprayed nonfused coatings. Int. Conf. Advance in Surface Coating Techniques, London 1978, pp. 99–109.

473 Frappier, J. C.; Birac, A. M.; Saglio, R.: The "Stadus" ultrasonic data acquisition and processing system. In: Clough, R. B. (Ed.): Quantitative NDE in the nuclear industry. Proc. 5th Int. Conf. NDE in the Nuclear Industry, San Diego 1982, Metals Park: ASM 1983, pp. 419–422.

474 Frederick, J. R.; Ganapathy, S.; Vanden Broek, C. J.; Elzinga, M. B.: Improved characterization of dicontinuities in thick walled pressure vessels. In: Proc. Conf. Periodic Inspection of Pressurized Components, London, 1981, pp. 163–173.

475 Freedman, A.: Sound field of a rectangular piston. J. Acoust. Soc. Am. 32 (1960) 197–209.

476 Freitag, W.; Martin, H. J.: Ergebnisse beim Aufbau eines elektronischen Ultra-schall-Bildwandlers. Acustica 8 (1958) 197—200.

477 Friant, C. L.; Rosen, M.; Green, J. R.: Ultrasonic study of precipitation hardening of 2024 aluminium. Proc. 13th Symp. NDE (Leonard, B. E., Ed.). Southwest Res. Inst., San Antonio 1982, pp. 123–134.

478 Frielinghaus, R.: Ultraschallmessungen an Grauguß. Diss. TH Braunschweig 1963.

479 Frielinghaus, R.: Praktische Ergebnisse der zerstörungsfreien Keramikprüfung mit Ultraschall. In: Handbuch der Keramik. Freiburg: Schmidt 1971.

480 Frielinghaus, R.: The ultrasonic inspection of plastics. 7th Int. Conf. NDT Warszawa 1973, paper J 18

481 Frielinghaus, R.: Über den Stand der Gefüge- und Eigenschaftsbeurteilung von Guß-eisen mit Kugelgraphit durch Ultraschall. Paper Conf. of the VDG (Verein Deutscher Gießereifachleute). Düsseldorf 1967 (not published)

482 Frielinghaus, R.: Beitrag zur Korngrößenbestimmung durch Schallschwächungs-messungen. Proc. 10th Int. Conf. Acoustics Ultrasound, Prag 1972, Sec. II, pp. 238–243.

483 Frielinghaus, R.: Zur Ersatzfehlergrößenbestimmung von Schweißnahtfehlern mit Ultraschall. Schweißen u. Schneiden 25 (1973) 552–555.

484 Frielinghaus, R.: The influence of probe frequency on the indication of weld defects. Proc. Qual. Contr. NDT. Weld. Conf. Welding Institute (Ed.). Abington, London 1974, pp. 92–97.

485 Frielinghaus, R.: Untersuchungen zur besten Prüffrequenz beim Schrägeinschallen an schweißplattierten Blechen. Schweißen u. Schneiden 26 (1974) 172–174.

486 Frielinghaus, R.: Die Ultraschallprüfung austenitischer Werkstoffe auf innere Un-gänzen. VGB Kraftwerkstech. 61 (1981) 105–108.

487 Frielinghaus, R.: Beitrag zur Ultraschallprüfung von Aluminium-Schweißnähten. Große Schweißtechnische Tag. Berlin 1982. DVS-Ber. Vol. pp. 74, pp. 96–98

488 Frielinghaus, R.: Ultraschallprüfen von austenistischen Schweiß- und Mischverbin-dungen. Große Schweißtechnische Tag. Aachen 1983. DVS-Ber. Vol. 83, pp. 185–187

489 Frielinghaus, R.; Ganglbauer, O.; Wallner, F.: Zur Amplitudenbewertung beim Ultraschallprüfen von Schweißverbindungen aus austenitischem Stahl. Schweißen u. Schneiden 33 (1981) 320–325.

490 Frielinghaus, R.; Koppelmann, J.: Genaue Schallschwächungsmessungen mit han-delsüblichen Ultraschall-Impulsecho-Geräten. Materialprüfung 6 (1964) 337–342.

491 Frielinghaus, R.; Schlengermann, U.: Über die Bestimmung der Nahfeldlänge von Winkelprüfköpfen für die Ultraschall-Werkstoffprüfung. Materialprüfung 9 (1967) 437–442.

492 Frost, H. M.: Electromagnetic ultrasound transducers: Principles, practice, and applications. In: Physical acoustics, Vol. 14. New York: Academic Press 1979, pp. 179–270.

493 Fujikake, Y.; Hayama, S.; Kawashima, S.: Fundamental experiment on surface defect detection by electromagnetic surface ultrasonic waves (jap.). J. NDI 32 (1983) 758–759.

494 Fujimori, T.: A consideration on the methods for estimating the sizes of the defects of steel welds by ultrasonic beam testing. IIW-Doc. V 454-71.

495 Fukuoka, H.: Experimental residual stress analysis by velocity measurement of transverse waves (jap.). Theses Book of Japan Machinery Academy, 49 (1983) 403–412.

496 Fukuhara, H.; Kimura, K.: Effects of thickness of couplant layer and surface roughness of test object on sensitivity in ultrasonic angle-beam technique. Trans. Nat. Res. Inst. Met. 22 (1980) 35–42.

497 Fuller, A. G.: Effect of graphite form and fatigue properties of pearlitic ductile irons. Am. Foundrymen Soc. Trans. 85 (1977) 527–536.

498 Furgason, E. S.; Newhouse, V. L.; Bilgutay, N. M.; Cooper, G. R.: Application of random signal correlation technique to ultrasonic flaw detection. Ultrasonics 13 (1975) 11–17.

499 Furlan, J.; Soleille, G.; Mogavero, R.; Chalaye, H.: Ultrasonic testing of steam generator tubes using an internal probe. In: Clough, R. B. (Ed.): Quantitative NDE in the nuclear industry. Proc. 5th Int. Conf. NDE in the Nuclear Industry, San Diego 1982, Metals Park: ASM 1983, pp. 110–112.

500 Gabor, D.: A new microscopic principle. Nature 161 (1948) 777–778.

501 Gabor, D.: Microscopy by reconstructed wavefronts. Proc. R. Soc. A 197 (1949) 454–487.

502 Galan, A.: Two methods of measurement of transverse ultrasound waves in concrete of structures and elements. 10th World Conf. NDT, Moscow 1982, Vol. 5, pp. 57–66. (Acad. Sci. USSR).

503 Ganapathy, S.: Ultrasonic imaging techniques in NDE. CSNI — Specialists Meeting Reliability Ultrasonic Inspection Austenitic Stainless Steel Components, Brüssel 1980. OECD Paris.

504 Ganapathy, S.; Wu, W. S.; Schmult, B.: Analysis and design considerations for a real-time system for NDE in the nuclear industry. Ultrasonics 20 (1982) 249–256.

505 Ganglbauer, O.; Weissteiner, R.; Wallner, F.; Frielinghaus, R.: Vergleich der Schallgeschwindigkeitsverteilung in austenitischen Grundwerkstoffen sowie im Schweißgut und deren Auswirkungen auf die Prüfung. 2nd Europ. Conf. NDT Vienna 1981, pp. 261–262

506 Ganglbauer, O.; Wallner, F.; Außerwöger, J.; Rose, J. L.; Niklas, L.: Fehlerklassifikation in Schweißverbindungen mit Ultraschall unter Einbeziehung des Echodynamikverhaltens. 3rd Europ. Conf. NDT Florence 1984, Vol. 1, pp. 360–370.

507 Gardner, W. E.; Hawker, B. M.; Highton, B.; Martin, R.; Whitehead, N. P.; Johnson, P. C.: Automated inspection of British rail track. Proc. 9th World Conf. NDT Melbourne 1979, Rep. 1C-2.

508 Gardner, W. E.; Hudson, J. A.: Ultrasonic inspection of thick section pressure vessel steel by the time of flight diffraction method. In: Clough, R. B. (Ed.): Quantitative NDE in the nuclear industry, Proc. 5th Int. Conf. NDE in the Nuclear Industry, San Diego 1982, Metals Park: ASM 1983, pp. 250–257.

509 Gautesen, A. K.; Achenbach, J. D.; McMaken, H.: Surface-wave rays in elastodynamic diffraction by cracks. J. Acoust. Soc. Am. 63 (1978) 1824–1831.

510 Gazanhes, C.; Hérault, J. P.; Stephanakis, K.: Reflection coefficient identification by means of correlation: application to a layered medium. J. Acoust. Soc. Am. 69 (1981) 720–727.

511 Gebhardt, W.: Ultraschall-arrays. Fraunhofer Ges., IZfP Saarbrücken Ber. Nr. 770117-TW (1977).

512 Gebhardt, W.; Bonitz, F.; Woll, H.; Schmitz, V.: Ultraschallfeldsteuerung, Fehlerklassierung und Fehlerrekonstruktion mittels "Phased Arrays". Materialprüfung 21 (1979) 437–443.

513 Gebhardt, W.; Bonitz, F.; Woll, H.; Schmitz, V.: Fehlercharakterisierung und Fehlerrekonstruktion mittels elektronischem Sektorscan und Verbundscan; Fraunhofer Ges., IZfP Saarbrücken, Ber. 790520-TW (1979).

514 Gebhardt, W.; Bonitz, F.; Woll, H.: Das phased array als neuer, elektrisch steuerbarer Ultraschallwandler in der Werkstoffprüfung. FhG-Berichte 3 (1978) 60–65.

515 Gebhardt, W.; Bonitz, F.; Woll, H.; Schwarz, H. P.: Einsatz phasengesteuerter Array-Prüfköpfe in der Kerntechnik. In: DGZfP (ed.): 4. Int. Conf. NDT in the Nuclear Field, Lindau 1981, Vol. 8, pp. 691–701

516 Gebhardt, W.; Bonitz, F.; Woll, H.: Defect reconstruction and classification by phased arrays. Mater. Eval. 40 (1982) 90–95.

517 Gebhardt, W.; Schwarz, H. P.; Bonitz, F.; Woll, H.: Application of phased arrays in basic and in-service inspection. 5th Int. Conf. NDE in the Nuclear Industry, Zürich 1983.

518 Geimer, H.; Overkott, E.: Anwendung der zerstörungsfreien Werkstoffprüfung zur Beurteilung feuerfester Steine. Ber. d. Dt. Keram. Ges. 43 (1966) 440–442.

519 Gemesi, J.: Messung mit Ultraschall zur Feststellung der optimalen Bedampfungszeit von Beton. Wiss. Z. der Hochsch. f. d. Bauwesen, Leipzig No. 5 (1967) pp. 99–103

520 Gericke, O. R.: Dual frequency ultrasonic pulse-echo testing. J. Acoust. Soc. Am. 36 (1964) 313–322.

521 Gericke, O. R.: Theory and NDT applications of ultrasonic pulse-echo spectroscopy. Symp. Fut. Ultrason. Spectroscopy, London 1970, Paper 1.

522 Gerken, C.; Wittkopp, H.: Automatic ultrasonic wheel set testing stand for railway axles with data recording. Proc. 10th World Conf. NDT Moscow 1982, Vol. 4, pp. 5–12.

523 Gerlach, J.: Echolotmessungen als Hilfsmittel für die Zuchtwertschätzung beim Schwein. 4. Mitt.: Untersuchungen über die Selektion von Zuchtsauen unter besonderer Berücksichtigung einer Eigenleistungsprüfung im Zuchtstall. Z. f. Tierzücht. u. Züchtungsbiol. 86 (1970) 325–348.

524 Gerlach, M.: Porositätsuntersuchungen an Hochspannungsisolatoren mit Ultraschall und ihre Bedeutung für die Energieversorgung. Silikattechnik 2 (1951) 371–374.

525 Gerstner, R.: Die Ultraschallprüfung von Gußeisen. Materialprüfung 3 (1961) 213–217.

526 Gerstner, R.: Dehnungsmessung mit Ultraschall. Materialprüfung 6 (1964) 43–46.

527 Gerstner, R.: Die automatische Prüfung von widerstandsgeschweißten Rohren mit Ultraschall. Materialprüfung 6 (1964) 320–322.

528 Gilmore, R. S.; Torreno, M. L.; Czerw, G. J., Burnet, L. B.: High-frequency ultrasonic testing of bonds: application to silicon powder devices. Mater. Eval. 37 (1979) 65–72.

529 Gitis, M. B.; Kopanski, A. G.: Installation for the inspection of ball bearing steel rods. Sov. J. Non Destr. Test. 15 (1979) 630–632.

530 Glenn, W. E.; Hirshman, J.: High resolution ultrasonic system for the real time video imaging of internal flaws. Mater. Eval. 40 (1982) 96–100.

531 Glover, G. H.: Computerized time-of-flight ultrasonic tomography for breast examination. Ultrasound in Medicine and Biology 3 (1977) 117–127.

532 Goebbels, K.: Structure analysis by scattered ultrasonic radiation. In: Sharpe, R. S. (Ed.): Research techniques in NDT, Vol. 4. London: Academic Press 1980.

533 Goebbels, K.: Ultrasonic measurement of material properties. In: Sharpe, R. S. (Ed.): Research techniques in NDT, Vol. 4. London: Academic Press 1980.

534 Goebbels, K.; Blauel, J. G.: Ultrasonic structure and stress characterization for the improved determination of defect criticality by fracture mechanics. In: Clough, R. B. (Ed.): Quantitative NDE in the nuclear industry. Proc. 5th Int. Conf. NDE in the Nuclear Industry, San Diego 1982. Metals Park: ASM 1983, pp. 237–242.

535 Goebbels, K.; Höller, P.: Quantitative determination of grain size and detection of inhomogeneities in steel by ultrasonic backscattering measurements. In: Berger, H.; Linzer, M. (Eds.): Ultrasonic Materials Characterization. Spec. Publ. 596, 1980, pp. 67–75. Nat. Bur. of Stand., Gaitersburg, MD.

536 Goebbels, K.; Neumann, E.; Hecht, A.; Reimers, P.: Ultraschallprüfung und Computertomographie an Kunstharz-Hochspannungsisolatoren. 3rd Europ. Conf. NDT Florence 1984, Vol. 5, pp. 23–34.

537 Goebbels, K.; Reiter, H.: Hochauflösende zerstörungsfreie Prüfung an Lötverbindungen mittels Hochfrequenz-Ultraschall. Koll. Hart- und Hochtemperaturlöten und Diffusionsschweißen. DVS Essen, 1981, Vol. 69, pp. 172–175

538 Goebbels, K.; Reiter, H.; Hirsekorn, S.; Arnold, W.: NDT of high temperature and high strength ceramics. Sci. Ceram. 12 (1983) 483–494.

539 Goebbels, K.; Römer, M.; Crostack, H. A.: Quantitativer Vergleich verschiedener

Ultraschall-Prüfverfahren zur Verbesserung des Signal/Rausch-Abstandes beim Vorliegen kohärenten Untergrundes. Materialprüfung 21 (1979) 261–267.

540 Goebbels, K.; Römer, M.; Crostack, H.-A.: On the state-of-the-art and advanced techniques to improve the signal-to-noise ratio for the ultrasonic testing of coarse grained materials. In: Charyulu, V. H. (Ed.): NDE in the Nuclear Industry — 1980. Metals Park: ASM 1981, pp. 75–99

541 Göhlert, C.; Kanngießer, P.; Weiss, H.; Wilke, W.: Akustische Wandler mit piezoelektrischem Element. DE Pat. 2951075 (1979).

542 Golis, M. J.; Brown, S. D.; NDE of steam turbine rotors. An analysis of the systems and techniques utilized for in-service inspection. Interim Rep. 1978 EPRI NP-744, Project 502-2.

543 Götz, J.: Über den Schalldurchgang durch Metallplatten in Flüssigkeiten bei schrägem Einfall einer ebenen Welle. Akust. Z. 8 (1943) 145–168.

544 Goncharov, V. S.: Detection of a corner reflector with irradiation angles close to the critical. Sov. J. Non Destr. Test. 18 (1982) 303–305.

545 Goldman, R. G.; Auger, M. E.: Improved ultrasonic instrumentation for the quality control of turbine-generator components. 3rd Int. Conf. NDT Tokyo 1960, paper 204

546 Goldman, R. G.; Auger, M. E.: Automatic ultrasonic examination of large rotor forgings. IRE Convention Rep. 9 (6) (1961) 316–326.

547 Goldmann, R. G.: Electric acustic image converter. J. Acoust. Soc. Am. 34 (1962) 514–515.

548 Goldschmidt, S.; Buch, A.; Yaron, S.: Relationship between density and sound velocity in sintered materials. 6th Int. Conf. NDT Hanover 1970, Vol. G, pp. 65–75

549 Good, M. S.; Rose, J. L.; Goldberg, B. B.: Application of pattern recognition technique to breast cancer detection. Ultrasonic Imaging 4 (1982) 378–396.

550 Goodman, G.: Ferroelectric properties of lead metaniobate. J. Am. Ceram. Soc. 36 (1953) 368–372.

551 Goodsitt, M. M.: Madsen, E. L.; Zagzebski, J. A.: Field patterns of pulsed, focused, ultrasonic radiators in attenuating and nonattenuating media. J. Acoust. Soc. Am. 71 (1982) 318–329.

552 Gournay, L. S.: Conversion of electromagnetic to acoustic energy by surface heating. J. Acoust. Soc. Am. 40 (1966) 1322–1330.

553 Grabendörfer, W.: Über die Bedeutung des Testfehlers bei automatischen Ultraschall-Prüfanlagen. Materialprüfung 6 (1964) 261–265.

554 Grabendörfer, W.: Untersuchung von dünnen runden Werkstoffen mit Überschall-Oberflächenwellen. Stahl u. Eisen 75 (1955) 1273–1275.

555 Grabendörfer, W.: Untersuchung an Kunststoffen mit Ultraschall nach dem Impulsverfahren. Gummi u. Asbest 10 (1957) 544–548.

556 Grabendörfer, W.; Krautkrämer, J.: Über Impuls-Echo-Prüfung an plattenförmigen Körpern. Z. Metallkde. 49 (1958) 22–26.

557 Grabendörfer, W.; Weber, H.: Ultraschallprüfung von Blechen, Schweißnähten und Rohren. Industrie-Anz. 50 (1960) 775–780.

558 Graff, K. F.: A history of ultrasonics. Phys. Acoust. 15 (1981) 2–90.

559 Granato, A.; Lücke, K.: Theorie of mechanical damping due to dislocations. J. Appl. Phys. 27 (1956) 583–593.

560 Granato, A.; Truell, R.: Frequency dependence of ultrasonic attenuation in germanium. J. Appl. Phys. 27 (1956) 1219–1226.

561 Grasshoff, H. W.; Lex, A.: Bestimmung der Nachweisgrenze kleiner Fehlergrößen mittels Ultraschallprüfung bei der Querdurchschallung von Warmband nach dem Plattenwellenverfahren. 6th Int. Conf. NDT Hanover 1970, paper K 4

562 Grasshoff, H. W.; Tobolski, J.: Erfahrungen mit einer kontinuierlichen Ultraschall-Bandprüfanlage. Bänder, Bleche, Rohre 8 (1967) 736–743, 809—814.

563 Grayeli, N.; Stanke, F.; Shyne, J. C.: Prediction of grain size in copper using acoustic attenuation measurements. In: McAvoy, B. R. (Ed.): IEEE Ultrasonics

Symp. San Diego 1982, Vol. 2, pp. 954–959.

564 Grebennik, V. S.; Taits, M. Z.: Calculation of the directivity pattern of an oblique-entry probe. Sov. J. Non Destr. Test. 17 (1981) 67–78.

565 Grebennik, V. S.: Methods of nondestructive inspection in nuclear power stations (review). Sov. J. Non Destr. Test. 17 (1981) 645–661.

566 Green, P. S.: Methods of acoustic visualization. J. Non. Destr. Test Int. 1 (1969) 1–27.

567 Green, P. S.; Schaefer, L. F.; Jones, E. D.; Suarez, J. R.: A new, high-performance ultrasonic camera. Acoust. Holograph. 5 (1974) 493–503.

568 Greenleaf, J. F.; Johnson, S. A.; Lee, S. L.; Herman, G. T.; Wood, E. H.: Algebraic reconstruction of spatial distributions of acoustic absorption within tissue from their two-dimensional acoustic projections. Acoust. Hologr. 5 (1974) 591–603.

569 Gregory, A. R.; Podio, A. L.: Dual-mode ultrasonic apparatus for measuring compressional and shear wave velocities of rock samples. IEEE Trans. SU-17 (1970) 77–85.

570 Greguss, P.: Ultraschall-Hologramme. Res. Film 5 (1965) 330–337.

571 Greguss, P.: A new liquid crystal acoustical-to-optical display. Acustica 29 (1973) 52–58.

572 Greguss, P.: Ultrasonic imaging. London: Focal Press 1980.

573 Griffin, D. R.: Listening in the dark. Yale University Press 1958.

574 Griffice, Ch. P.; Seydel, J. A.: Spherical wave decomposition approach to ultrasonic field calculations. J. Non Destr. Eval. 2 (1981) 241–247.

575 Grohs, B.: Theoretische Ermittlung von Laufzeit-Ortskurven für Ultraschall-Impuls-echo-Prüfungen — ALOK 4. Materialprüfung 25 (1983) 63–66.

576 Grohs, B.; Barbian, O. A.; Kappes, W.; Paul, H.: Fehlerbeschreibung nach Art, Lage und Dimension mit Hilfe von Laufzeitortskurven aus Ultraschallprüfungen — ALOK 2. Materialprüfung 23 (1981) 427–432.

577 Grohs, B.; Barbian, O. A.; Kappes, W.; Paul, H.; Licht, R.; Höh, F.: Characterization of flaw location, shape and dimensions with the ALOK-system. Mater. Eval. 40 (1982) 84–89.

578 Gruber, G. J.: Defect identification and sizing by the ultrasonic satellite pulse technique. J. Non Destr. Eval. 1 (1980) 263–276.

579 Gruber, G. J.; Hendrix, G. J.; Schick, W. R.: Characterization of flaws in piping welds using satellite pulses. Mater Eval. 42 (1984) 426–432.

580 Grubin, H. L.: Direct electromagnetic generation of compressional waves in metals in static magnetic fields. IEEE Trans. SU-17 (1970) 227–229.

581 Gubernatis, J. E.; Domany, E.; Krumhansl, J. A.: Formal aspects of the theorie of scattering of ultrasound by flaws in elastic materials. J. Appl. Phys. 48 (1977) 2804–2811.

582 Gubernatis, J. E.; Domany, E.; Krumhansl, J. A.; Huberman, M.: The Born approximation in the theorie of scattering of elastic waves by flaws. J. Appl. Phys. 48 (1977) 2812–2819.

583 Guild, F. J.; Philips, M. G.; Harris, B.: Acoustic emission studies of damage in GRP. Non Destr. Test. Int. 13 (1980) 209–218.

584 Gundtoft, H. E.; Nielsen, N.: Fast and accurate nondestructive testing system for inspection of canning tubes. Non Destr. Test. 6 (1973) 34–37

585 Gundtoft, H. E.; Nielsen, N.; Agerup, C. C.: Results of nondestructive examination of tubes by means of a new inspection system. 7th Int. Conf. NDT, Warszawa 1973, paper C01

586 Guo, C. B.; Zhao, W. Q.; Meng, G. L.; Zhu, G. S.; Mao, Q. L.: Automatic grain size testing of metal bars by ultrasonic through-transmission technique. Proc. 10th World Conf. NDT Moscow 1982, Vol. 2, pp. 275–282. (Acad. Sci. USSR).

587 Gupta, P. N.: A few materials for acoustic lenses for use in acoustic imaging. Acustica 42 (1979) 273–277.

588 Gurvich, A. K.; Kuzmina, L. J.: Investigation of methods of measuring the apparent height of defects in the case of scanning with an inclined probe. Sov. J. NDT (1970) 678–684.

589 Gutmann, G.: Hardware components and performance of in-service inspection. Int. Symp. Mechanization and Automation of Inspection of Pressurized Plants, Tokyo 1973.

590 Gutmann, G.; Müller, G.; Oellrich, K.: Ultraschall — Wiederholungsprüfung an Reaktordruckbehältern. Stand der Technik 1978, dargestellt am Beispiel der Einrichtungen für das Kernkraftwerk Krümmel. VGB Kraftwerkstech. 58 (1978) 722–728.

591 Hadden, W. J.; Chew, C. H.: Ultrasonics in determining characteristics of coal. 1981 Ultrasonics Symp. Proc. IEEE, New York 1981, Vol. 1, pp. 465–468.

592 Häusler, E.: Die Anwendung elastischer Oberflächenwellen in der zerstörungsfreien Materialprüfung. Materialprüfung 2 (1960) 51–55.

593 Hagemaier, D. J.: Bonded joints and NDT. Non Destr. Test. 4 (1971) 401–406; 5 (1972) 38–48.

594 Hagemaier, D. J.: Automated ultrasonic inspection of adhesive bonded structure. Mater. Eval. 40 (1982) 572–578.

595 Hagemaier, D. J.: Nondestructive detection of exfoliation corrosion around fastener holes in aluminum wing skins. Mater. Eval. 40 (1982) 682–685.

596 Hagemaier, D. J.; Posakony, G. J.: Ultrasonic testing of melt-through-welds in small diameter, thin-walled tubing couplers. Mater. Eval. 26 (1968) 221–226.

597 Hall, K. G.: Crack depth measurement in rail steel by Rayleigh waves aided by photoelastic visualization. Non Destr. Test. Int. 8 (1976) 121–126.

598 Hall, K. G.: Visualization techniques for the study of ultrasonic wave propagation in the railway industry. Mater. Eval. 42 (1984) 922–933

599 Hall, E. T.; Crecraft, D. I.: NDT of resistance spot, roll spot, stitch and seam welds. Non Destr. Test. 4 (1971) 181–191

600 Halsey, G. .H.: The NDT of passenger tires. Mater. Eval. 26 (1968) 137–142.

601 Hamidzada, W.: Letcher. S.: Candau. S.: Investigation of a liquid crystal acousto-optic conversion cell. In: Acoustical imaging. Vol. 10. New York: Plenum Pess 1982. pp. 711–716.

602 Hanafy, A.: Visualization of multimode radiation patterns of acoustic transducers by acousto-optic diffraction. Ultrason. Imaging 1 (1979) 295–302.

603 Hanstead, P. D.: Direct ultrasonic visualization of defects: a new inspection method. Br. J. Non Destr. Test. 16 (1974) 34–44.

604 Hanstead, P. D.: Simplified digital synthesis of ultrasonic images. Proc. R. Soc. London A 374 (1981) 491–502.

605 Hanstead, P. D., Eng, C.: Ultrasonic visualisation. Br. J. Non Destr. Test. 14 (1972) 162–169.

606 Hanstead, P. D.; McElwee, I.: Automatic ultrasonic inspection of nozzle welds in nuclear reactor pressure vessels. Proc. 4th Int. Conf. NDT London 1963. London: Butterworths Sci. 1964, pp. 255–260.

601 Hamidzada, W.; Letcher. S.; Candau, S.: Investigation of a liquid crystal acousto-optic conversion cell. In: Acoustical imaging. Vol. 10. New York: Plenum Press 1982.

608 Hanstock, R. F.: Development of radiographic and ultrasonic methods of inspection nuclear reactor pressure vessels. Proc. 4th Int. Conf. NDT, London 1963. London: Butterworths Sci. 1964, pp. 249–254.

609 Haran, M. E.: Visualisation and measurement of ultrasonic wavefronts. Proc. IEEE 67 (1979) 454–466.

610 Hardy, G. J.; Turner, T. W.; Ashbee, K. H. G.: Detection of defects in opaque solids using visualized ultrasound. Metal. Sci. 12 (1978) 406–410.

611 Harris, G. R.: Review of transient field theory for a baffled planar piston. J. Acoust. Soc. Am. 70 (1981) 10–20.

612 Harris, G. R.: Transient field of a baffled planar piston having an arbitrary

vibration amplitude distribution. J. Acoust. Soc. Am. 70 (1981) 186–204.

613 Harris, R. V.: Resonance testing without contact. Ultrasonic News (Branson Instruments), Ed. Winter 1960, pp. 10–15

614 Harrold, S. O.: Ultrasonic focusing techniques. In: Sharpe, R. S. (Ed.): Research techniques NDT, London: Academic Press 1982, 49–105

615 Hartmann, K.; Berner, K.: Gütesicherung, neue Prüfmethoden und Erkenntnisse für die Qualitätskontrolle von schraubenliniennahtgeschweißten Großrohren 3R — International 17 (1978) No. 8/9, pp. 525–529

616 Harumi, K.; Igarashi, T.; Saito, T.: Computer simulation of elastic waves by a new model of mass-particles with potentials. Hihakai Kensa 27 (1978) 807–816.

617 Harumi, K.; Okada, H.; Saito, T.; Fujimori, T.: Numerical experiments of reflections of elastic waves by a corner or crack having a corner on a surface. In: McAvoy, B. R. (Ed.): Proc. IEEE Ultrasonic Symp. San Diego 1982. Piscataway: IEEE 1982, Vol. 2, pp. 904–909.

618 Harumi, K.; Okada, H.; Sasaki, S.: Numerical experiments of edge waves of incident transverse waves, 3rd Europ. Conf. NDT Florence 1984, Vol. 5, pp. 246–257.

619 Harumi, K.; Watanabe, N.; Murata, K.: Scattering of a plane longitudinal wave by a cavity disc in a solid. 8th World Conf. NDT Cannes 1976, paper 3 H 3

620 von Haselberg, K.; Krautkrämer, J.: Ein Ultraschallstrahler für die Werkstoffprüfung mit verbessertem Nahfeld. Acustica 9 (1959) 359–364.

621 Hastings, C. H.; Lopilato, S. A.; Lynnworth, L. C.: Ultrasonic inspection of reinforced plastics and resin-ceramic composites. Non Destr. Test. 19 (1961) 340–346.

622 Hatfield, P.: An ultrasonic phase lag method for measuring the thickness of rubber. Br. J. Appl. Phys. 3 (1952) 326–328.

623 Hauptmann, P.; Herold, H.; Rothe, B.; Zenker, R.: Ultraschallverfahren zur Bestimmung des Weichmachergehalts in PVAC-Dispersionen. Plaste, Kautsch. 26 (1979) 307–309.

624 Havlice, J.; Quate, C. F.; Richardson, B.: Visualization of sound beams in quartz and sapphire near 1 GHz. IEEE Trans. SU-15 (1968) 68.

625 Havlice, J. F.; Kino, G. S.; Kofol, J. S.; Quate, C. F.: An electronically focused acoustic imaging device. Acoust. Hologr. 5 (1974) 317–333.

626 Hayford, D. T.; Henneke, E. G.; Stinchcomb, W. W.: The correlation of ultrasonic attenuation and shear strength in graphite-polyamide composites. J. Compos. Mater. 11 (1977) 429–444.

627 Hayman, A. J.: Schlieren visualization of focused ultrasonic images. Ph. D. Thesis, City University London 1977.

628 Hayman, A. J.; Hanstead, P. D.: Developments in direct ultrasonic visualization of defects. Ultrasonics 17 (1979) 105–112.

629 Hayman, A. J.; Weight, J. P.: Transmission and reception of short ultrasonic pulses by circular and square transducers. J. Acoust. Soc. Am. 66 (1979) 945–951.

630 Hecht, A.: Ultraschallprüfung keramischer Isolatoren. Stemag-Nachr. 37 (1963) 1002–1013.

631 Hecht, A.; Cherian, P.; Neumann, E.; Mundry, E.: Effekte bei der Ausbreitung kurzer Impulse in streuenden Werkstoffen. Materialprüfung 23 (1981), 301–304.

632 Hecht, A.; Mundry, E.; Neumann, E.: Einfluß der Bandbreite auf die Prüfbarkeit streuender Werkstoffe. Berichtsband „Ultraschallprüfung grobkörniger Werkstoffe unter besonderer Berücksichtigung von Austeniten". DGZfP, Berlin 1980, pp. 85–91

633 Hecht, A.; Neumann, E.; Rux, P.: Vorstudie über die Leistungsfähigkeit eines Verfahrens zur Wanddickenmessung mit Ultraschall an in Betrieb befindlichen Verzinkungskesseln. BAM, Berlin DECHEMA-Projekt Nr. 10.3/2. BAM-Vorhaben Vh 06245 (Mai 1981).

634 Hecht, A.; Thiel, R.; Neumann, E.; Mundry, E.: Nondestructive determination of grain size in austenitic sheet by ultrasonic backscattering. Mater. Eval. 39 (1981) 934–938.

635 Hecht, A.; Thiel, R.; Neumann, E.; Nabel, E.; Mundry, E.: Einsatz und Erprobung eines Meßverfahrens zur Korngrößenbestimmung an austenitischen Feinblechen mit Hilfe der Ultraschallrückstreuung. Materialprüfung 21 (1979) 275–276.

636 Hecht, A.; Thiel, R.; Voß, U.; Neumann, E.: A computer controlled equipmont for different ultrasonic measurement techniques. 3rd Europ. Conf. NDT Florence 1984, Vol. 3, pp. 145–155.

637 Hecht, D. L.: Multifrequency acousto optic diffraction. IEEE Trans. SU-24 (1977) 7–18

638 Heckhäuser, H.; Richter, H.: Limits of correlation between defect depths and indication heights testing steam generator tubing by ultrasonic test methods. In: Charyulu, V. H. (Ed.): NDE in the Nuclear Industry — 1980. Metals Park: ASM 1981, pp. 577–596

639 Heffan, H.; Mauch, J. W.; Smith, R. C.; Cusick, J. H.: Quality evaluation of missile structure spot weld joints. Mater. Eval. 25 (1967) 15–19.

640 Heimsohn, K.: Zerstörungsfreie Untersuchungen zur Nahtwertigkeit von Abbrennstumpfschweißungen. ZIS-Mitt. 13 (1971) 1466–1475.

641 Heinrich, D.: Bestimmung der Dichte und Größe von Fehlstellenanhäufungen in Schmiedestücken mit Ultraschall. Forschungsber. Verbrennungskraftmaschinen Nr. 324 (1983) 237–284.

642 Heinrich, D.; Müller, G.; Weiß, M.: Mechanisierte Ultraschall-Wiederholungsprüfung austenitischer Schweißnähte in Kernkraftwerken. In: DGZfP (Ed.): 4. Int. Conf. NDT in the Nuclear Field. Lindau, 1981, Vol. 8, pp. 199–210

643 Heinrich, D.; Müller, G.; Weiß, M.: Untersuchungen der Prüfbarkeit von Stutzenkanten bei Prüfung von der Außenseite des Reaktordruckbehälters. MAN AG, Nürnberg, Tech. Ber., MAN-Werk-Nr. 853503 (1975).

644 Heinrich, D.; Müller, G.; Weiß, M.: Mechanized in-service ultrasonic inspection of austenitic welds in nuclear plants. Non Destr. Int. 15 (1982) 179–184.

645 Heisterkamp, W.: Erfahrungen bei der Ultraschallprüfung geschweißter Tankböden. Tech. Überwach. 4 (1963) 304–306.

646 Herrmann, H.: Ultraschallprüfung an Schweißverbindungen aus Polyäthylen hart. Kunststoffe 63 (1973) 535–536.

647 Herrmann, H.: Güteprüfung an Kunststoff-Erzeugnissen mit Hilfe von Ultraschall- und Durchstrahlungsverfahren. Kunststoffe 61 (1971) 839–842.

648 Herman, M.: Mechanisierung der Betriebsprüfungen von kernenergetischen Anlagen in der ÇSSR. 3rd Europ. Conf. NDT Florence 1984, Vol. 2, pp. 54–65.

649 Herment, A.; Demoment, G.; Vaysse, M.: Algorithm for online deconvolution of echographic signals. In: Metherell, A. F. (Ed.): Acoustical imaging, Vol. 10. New York: Plenum Press 1982, pp. 325–345.

650 Hess, A.; Thomas, Ch.: Möglichkeiten der Rißtiefenbestimmung mit Ultraschall nach dem Rißspitzenverfahren. Materialprüfung 25 (1983) 340–344

651 Hetherington, M. J.: Continuous and complete testing of tubes. Engineering (June 1964) 845–846.

652 Hetzler, M.; Michalski, A.: Ultraschallprüfung von Preßpassungen. Werkstattstech. u. Maschinenbau 43 (1953) 321–325.

653 Hetzler, M.; Michalski, A.: Ultraschall-Schrumpfsitzprüfung von Blockaufnehmern für Strangpressen Z. Metallkde. 46 (1955) 5–11.

654 Heyman, J. S.: Phase insensitive acoustoelectric transducer. J. Acoust. Soc. Am. 64 (1978) 243–249.

655 Hiedemann, E.: Wellenausbreitung in festen Körpern. Ultraschall. Fiat-Review of German Science 1939–1946. Physics of Solids, Part 1. Wiesbaden: Dieterichsche Verlagsbuchh. 1948, pp. 154–178

656 Hiedemann, E.; Hoesch, K. H.: Optische Untersuchung von Ultraschallfeldern in Flüssigkeiten und Gläsern. Z. Phys. 104 (1937) 197–206.

657 Highmore, P. J.; Willetts, A. J.; Clough, P.: "Circe" — a versatile ultrasonic digital data recording, analysis and display system. In: Periodic inspection of

pressurized components, I. Mech. E. Conf. Publ. 1982-9. London: Mech. Eng. Publ. 1982, pp. 209–215.

658 Hikata, A.: Ultrasonic attenuation in polycrystallic steel. Government Mech. Lab. Bull. (Japan) 1954, No. 1.

659 Hikata, A.; Truell, R.; Granato, A.; Chick, B.; Lücke, K.: Sensitivity of ultrasonic attenuation and velocity changes to plastic deformation and recovery in aluminium. J. Appl. Phys. 27 (1956) 396–404.

660 Hildebrand, B. P.: An analysis of pulsed ultrasonic arrays. In: Metherell, A. F. (Ed.): Acoustical imaging, Vol. 8. New York: Plenum Press 1980, pp. 165–185.

661 Hildebrand, B. P.: Acoustic holography. In: Edmonds (Ed.): Methods of experimental physics, Vol. 19. New York: Academic Press 1981, pp. 533–562.

662 Hildebrand, B. P.; Harrington, T. P.: Mapping of materials stress with ultrasonic tomography. Proc. Symp. Microstructural Characterization and Reliability Strategies, Pittsburgh 1980. Metall. Soc. AIME 1981, pp. 349–365.

663 Hiller, D.; Ermert, H.: The application of transducer arrays in ultrasound computerized tomography. Conf. Proc. Ultrasonics Int. Graz 1979. Guildford: IPC Sci. and Technol. Press 1979, pp. 540–544.

664 Hillger, W.: Entwicklung einer speziellen Ultraschallprüfelektronik zur Qualitätskontrolle von Fertigteilen aus Beton. Materialprüfung 9 (1984) 310–315.

665 Hillger, W.: Ultraschallprüfung von CFK-Laminaten mit hoher Auflösung und Reproduzierbarkeit in Impuls-Echo- und Durchschallungstechnik. 3rd Europ. Conf. NDT Florence 1984, Vol. 5, pp. 12–22.

666 Hinsch, K.: Akustische Holographie. Tagungsber. d. Dtsch. Arbeitsgemeinschaft Akustik und Schwingungstechnik, Sept. 1972. Berlin: VDE-Verlag 1972.

667 Hirao, M.; Sotani, Y.; Takami, K.; Fukuoka, H.: Love wave propagation in a solid with a coldworked surface layer. J. Non Destr. Eval. 2 (1981) 51–55.

668 Hirao, M., Fukuoka, H.: Scattering of Rayleigh surface waves by edge cracks: Numerical simulation and experiment. J. Acoust. Soc. Am. 72 (1982) 602–606.

669 Hirone, T.: Quality inspection of materials by ultrasonic methods in Japan. 3rd Int. Conf., Tokyo 1960. Keynote Paper No. 34.

670 Hislop, J. D.: Flaw size evaluation in immersed ultrasonic testing NDT 2 (1969) 183–192.

671 Hislop, J. D.: Summing up symposium on ultrasonic spectroscopy. Symp. Future Ultrason. Spectroscopy, London, Oct. 1970.

672 Hitt, W. C.; Ramsey, J. B.: Ultrasonic inspection and evaluation of plastics materials. Ultrasonics 1 (1963) 9–13.

673 Hobaek, H.: Relation between plane and spherical piston fields. In: Novak, Z. (Ed.): Ultrasonics international 1981, pp. 123–128.

674 Högström, K. E.: Schwedische Erfahrungen bei der Ermittlung von Nietlochanrissen an Kochern mittels Ultraschall. Papier 14 (1960) 671–673.

675 Höller, P.; Dick, W.; Lechky, E.: Ultraschallprüfung von Grobblechen im Herstellungsfluß. Stahl u. Eisen 81 (1961) 1116–1122.

676 Höller, P.; Salzburger, H.-J. Neuere Entwicklungen und Lösungspotential zur Prüfung kalter und warmer Brammen auf Oberflächenfehler. Stahl u. Eisen 102 (1982) 576–578.

677 Höller, P.; Smit, H.: Ultraschallprüfung von Grobblechen im Herstellungsfluß nach einem Impulsechoverfahren. Materialprüfung 7 (1965) 296–303.

678 Höller, P.; Smit, H.: Ultraschallprüfung von Kaltband mit Plattenwellen nach dem Echoverfahren. Materialprüfung 11 (1969) 329–335.

679 Höller, P.; Smit, H.: Zur Ankopplung von Ultraschall über Wasser bei der automatischen Grobblechprüfung im Temperaturbereich 0 bis 400 °C. Paper Conf. DGZfP, Mainz 1967

680 Hoent', P. J.: Aperture apodization to reduce the off-axis intensity of the pulsed mode directivity function of linear arrays. Ultrasonics 20 (1982) 231–236.

681 Holman, C. J.: The navy automated weld scanner and recording system. Br. J. Non Destr. Test. 14 (1972) 11–13.

682 Holmes, E.: Ultrasonic behaviour of austenitic stainless steel. Appl. Mat. Res. 2 (1963) 181–184.

683 Holt, A. E.; Brophy, J. W.: Non-destructive inspection of thick section materials using advanced nondestructive examination techniques. In: Nichols, R. W. (Ed.): Nondestructive examination in relation to structural integrity. London: Appl. Sci. Publ. 1980, pp. 233–249.

684 Homès, G. A., Ots, I. H.: Contrôle non destructif des matériaux par les ultrasons. Bull. Sci. AIM Belg. 62 (1949) 23–54.

685 Homès, G. A.: Die Prüfung der Schweißungen im Kunststoff. Paper Conf. DGZfP and VDEh, Düsseldorf, 9. 10. 1959

686 Honeycutt, C. R.; Sattler, F. J.; Williams, L. P.; Griffith, E. G.: Computerized ultrasonic inspection of reactor vessels. Mater. Eval. 32 (1974) 181–186.

687 Horn, C. H.: Ultrasonic testing device. US Pat. 2,846,874 (1958).

688 Hornung, R.: Erfahrungen bei der Fehlersuche mit Ultraschall und Röntgenstrahlen. Stahl u. Eisen 83 (1963) 298–304.

689 Hornung, R.: Erfahrungen mit der Ultraschallprüfung von Schweißnähten. Konstruktion 14 (1962) 41–46.

690 Horst, P.: Entwicklung eines Verfahrens zur Durchführung von Ultraschallmessungen beim lebenden Schwein. Z. f. Tierzücht. u. Züchtungsbiol. 80 (1964) 341–364.

691 Horst, P.: Ein neues Ultraschall-Meßprinzip für den Einsatz in der Schweinezucht. Schweinezucht. u. Schweinemast 19 (1971) 379–382.

692 Hübschen, G.; Walter, F.; Werneyer, R.: Zur zerstörungsfreien Prüfung von Löt- und Diffusionsschweißverbindungen. Koll. Hart- und Hochtemperaturlöten und Diffusionsschweißen. DVS Essen, 1981. Vol. 69, pp. 176–182

693 Hütter, A.: Methoden zur Prüfung des Betons mit Ultraschall. Bauplanung-Bautechnik 9 (1955) 385–389.

694 Hughes, E. T.; Burstein, F. B.: The evaluation of bond quality in honeycomb panels using ultrasonic surface wave techniques. Non Destr. Test. 17 (1959) 373–377.

695 Hughes, R.; Clark, A. V.: Characteristics of the reflection of SV waves from submicron thickness liquid layers. In: Thompson, D. O. (Ed.): Quantitative NDE, Vol. 1. New York: Plenum Press 1982, pp. 181–186.

696 Hullin, Ch.: Homogenisierung der Fokusspur linienfokussierter Ultraschallprüfköpfe. Materialprüfung 21 (1979) 304–305.

697 Hullin, Ch.: Die Apertur-Impulsantwort als Hilfsmittel zur Berechnung monochromatischer und transienter Schallfelder. DAGA Conf. (Dtsch. Arbeitsgemeinschaft f. Akustik) 1980, Berlin: VDE-Verlag, pp. 575–578

698 Hullin, Ch.; Barbian, O. A.; Haralamb, G.; Raeder, E.: Experiences with computer aided evaluation of ultrasonic test data in a heavy plate mill. 3rd Europ. Conf. NDT Florence 1984, Vol. 4, pp. 41–50.

699 Hunter, D. O.: Ultrasonic velocities and critical-angle-method changes in irradiated A 302-B und A 542-B steels. BNWL-988; UC-40, Radiation effects on materials, April 1969.

700 Hurwitz, M. J.: A high resolution ultrasonic imaging system. In: International advances NDT, Vol. 5. New York: Gordon and Breach 1977, pp. 133–160.

701 Husarek, V.: Etat actuel du contrôle automatique par ultrasons des billettes en France. Mém. Sci. Rev. Métall. 62 (1965) 711–719.

702 Husarek, V., Castel, J. G.: Evolution de la conception des appareils à ultrasons grâce au microprocesseur. 3rd Europ. Conf. NDT Florence 1984, Vol. 3, pp. 126–133 und Rev. Pratique de Contrôle Industriel 23 (1984) 68–77.

703 Husarek, V.; Ceccato, S.; Fournel, L.: Réalisation entre l'indication donnée par les ultrasons et le type de défaut lors de l'appréciation de la qualité des billettes par contrôle en continu. 6th Int. Conf. NDT, Hanover 1970, paper H 1

704 Husarek, V.; Ruault, P.: Emploi des méthodes de contrôles nondestructifs pour la vérification des soudures des canalisations de transport de gaz. Materialprüfung 6 (1964) 37–42.

705 Hutchins, D. A.: Field structures of disk transducers with specialized electrode configurations. In: Novak, Z. (Ed.): Ultrasonics Int. Conf. Borough Green, Butterworth, 1983, pp. 307–312.

706 Hutton, P. H.; Schwenk, E. B.; Kurtz, R. J.: Progress toward acoustic emission characterization for continuous monitoring reactor pressure vessels. In: DGZfP (Ed.): Int. Symp. Neue Verfahren der ZfP und deren Anwendungen insbesondere in der Kerntechnik. Saarbrücken 1979, pp. 337–342

707 Iida, K.: Japanese activities in NDE of nuclear structural components. In: DGZfP (Ed.): Papers of the 4th intern. Conf. NDT in the Nuclear Field, Lindau 1981, Vol. 8, pp. 639–654

708 Imoto, K.; Jimbo, J.: On the calculations of sound fields from nonuniformly-distributed source. Proc. 9th World Conf. NDT, Melbourne 1979, Rep. 4E-2

709 Isono, E.; Shibano, H.: Progress of plate wave inspection of steel sheets. 6th Int. Conf. NDT Hanover 1970, Paper K 3

710 Ito, S.; Kadowaki, T.; Sasaki, S.; Yamaguchi, H.; Fujisawa, K.: Development of a wall thickness measuring system for hot seamless pipe using a electrodynamic transducer (jap.). J. NDI 32 (1983) 765–769

711 Ivanov, F. I.; Akulin, M. A.: Sizing of internal defects in metals by ultrasonics (in Russian). Zavodskaja Lab. 23 (1957) 309–311

712 Jackson, J. L.; Hamlin, D. R.: Inservice inspection application of the synthetic aperture focusing technique for ultrasonic testing (SAFT UT). In: Proc. 9th Water Reactor Safety Research Meeting, Gaithersburg, Nat. Bur. Stand. 1981, pp. 1–21.

713 Jackson, G.; Anderson, B. R.: Testing adhesive bonded structural assemblies for aircraft. Non Destr. Test. 4 (1971) 299–300.

714 Jacobs, B. M.: Computer-automated inspection and lifetime analysis for large steam turbine rotors. Mater. Eval. 42 (1984) 1631–1637.

715 Jacobs, J. E.; Collis, W. J.; Berger, H.: An evaluation of an ultrasonic inspection system employing television techniques. Mater. Eval. 22 (1964) 209–212.

716 Jacobs, J. E.: Performance of an ultrasonic camera tube utilizing pyroelectric conversion layers. Acoust. Hologr. 6 (1975) 661–670.

717 Jacobs, J. E.: Ultrasonic imaging systems, particularly the Sokolov tube. In: International advances in NDT Vol. 6. Gordon and Breach 1979, pp. 299–349.

718 Jacobs, J. E.; Reimann, K.; Buss, L.: Use of color display technique to enhance sensitivity of the ultrasound camera. Mater. Eval. 26 (1968) 155–158.

719 Jacobs, J. E.; Peterson, D. A.: The use of discrete, shaped matching sections to increase the aperture of the Sokoloff tube. Conf. Proc. Ultrasonics International, London 1973. Guildford: IPC Sci. and Technol. Press 1973, pp. 275–283.

720 Jaffe, B.; Cook, W. R.; Jaffe, H.: Piezoelectric ceramics. London, New York: Academic Press 1971.

721 Jaffe, H.: Piezolelectric ceramics. J. Am. Ceram. Soc. 41 (1958) 494–498.

722 Jakowatz, C. V.; Kak, A. C.: Computerized tomographic imaging using X-rays and ultrasound. Res. Rep. TR-EE 76-26. School of Electr. Eng. Purdue University 1976.

723 Jansky, J.; Krolop, S.; Stegmeyer, R.; Pfeffer, P.; Deuster, G.; Brinette, R.: Pressurized thermal shock loading at nozzle corner area of HDR-RPV, ASME-PVP Conf. 1984, San Antonio, Texas.

724 Jax, W.; Gaar, H.: Verfolgung von Bruchvorgängen im Mikro- und Makrobereich an Gläsern und Glaskeramik mit Hilfe der Schallemissionsanalyse. Glastech. Ber. 30 (1977) S. 229–236.

725 Jedrzejczak, Z.; Skorupa, A.: Forschungsergebnisse der polnischen technischen Überwachung bei der Verwendung von AVG-Skalen für die Fehlergrößenbestimmung an

Schweißverbindungen. 3rd Symp. d. Werkstoffprüfung. Pula/Jugoslavia (Sept. 1970). Vol. 1. No. 16

726 Jessop, T. J.; Mudge, P. J.; Charlesworth, J. P.: Size measurement and characterization of weld defects by ultrasonic testing, Part 1: Non-planar defects in ferritic steels, Abington Hall, Welding Inst. 1979.

727 Jessop, T. J.; Mudge, P. J.; Harrison, J. D.: Size measurement and characterization of weld defects by ultrasonic testing, Part 2: Planar defects in ferritic steels. Abington Hall, Welding Inst. 1982.

728 Jestrich, H. A.; Ewald, J.: Ultraschall-Prüfung der aufgeschrumpften Radscheiben von Niederdruckläufern. Materialprüfung 27 (1985) 119–122

729 Jipson, V.; Quate, C. F.: Acoustic microscopy at optical wavelengths. Ginzton Lab. Rep. No. 2790. Stanford University, Stanford, Calif. 94305.

730 Johnson, A.: DRUID — A colour graphic ultrasonic imaging device. Br. J. Non Destr. Test. 26 (1984) 203–207.

731 Johnson, G. C.: On the applicability of acoustoelasticity for residual stress determination. Trans. ASME/J. Appl. Mech. 48 (1981) 791–795.

732 Jones, H. W.; Kwan, H. W.: A study of acoustic lenses. Ultrasonics Int. Proc. 1981. Novak, Z., (Ed.). Guildford: IPC Sci. and Technol. Press, 1981, pp. 291–296.

733 Johnson, J. A.: Numerical calculations of ultrasonic fields: Transducer near fields. J. Non. Destr. Eval. 3 (1982) 25–35.

734 Johnson, P. C.; Wise, S.: Significance of a detection of defects in rails. Non Destr. Test. 3 (1970) 111–116.

735 Jolly, W. D.: Die Anwendung von Schallemissionverfahren für die Schweißnaht-kontrolle. Z. f. Werkstofftechnik 2 (1971) 97–101.

736 Jones, R.: The ultrasonic testing of concrete. Ultrasonics 1 (1963) 78–82.

737 Joshi, N. R.: Precrack damage and crack propagation study with ultrasonic attenuation. Mater. Eval. 37 (1979) 57–61.

738 Jünke, H.: The propagation of ultrasonic Lamb waves in plane hardened glass plates. 7th Int. Conf. NDT, Warszawa 1973, Paper C 30

739 Jungerman, R. L.; Khuri-Yakub, B. T.; Kino, G. S.: Optical detection of acoustic displacement for the characterization of surface defects. Mater. Eval. 42 (1984) 444–450.

740 Jurenka, H. J.: Development of the ultrasonic technique for examination of centrifugally-cast stainless steel in pressure piping. In: Clough, R. B. (Ed.): Quantitative NDE in the nuclear industry. Metals Park: ASM 1982, pp. 194–197.

741 Jusino, A.; Adamonis, D. C.; Beith, M.: Improvement of the ultrasonic inspection of the centrifugally cast stainless steel pipe weldments adaptive learning network. In: Clough, R. B. (Ed.): Quantitative NDE in the nuclear industry. Metals Park: ASM 1982, pp. 443–448.

742 Juva, A.; Haarvisto, M.: On the effects of microstructure on the attenuation of ultrasonic waves in austenitic stainless steels. Br. J. Non Destr. Test. 19 (1977) 293–297.

743 Kadleček, V.; Dohnálek, J.: Zur Frage der Ultraschallgeschwindigkeitsdispersion in Beton. Wiss. Ber. TH Leipzig 1979, pp. 43–51

744 Kaiser, J.: Erkenntnisse und Folgerungen aus der Messung von Geräuschen bei Zugbeanspruchung von metallischen Werkstoffen. Arch. Eisenhüttenwes. 24 (1953) 43–45.

745 Kaiserlik, J. H.; Pellerin, R. F.: Stress wave attenuation as an indicator of lumber strength. For. Prod. J. 27 (1977) 39–43.

746 Kalderon, D.: Steam turbine failure at Hinkley Point "A". Proc. Inst. Mech. Eng. 186 (1972) 341–377

747 Kanagy, J. R.; Robinson, M.: Studies on leather by means of a sonic technique. J. Am. Leather Chemists'. Assoc. 51 (1956) 174–197.

748 Kappes, W.; Grohs, B.; Barbian, O. A.: Berechnung von Laufzeit-Ortskurven für die Tandemprüfung mit Ultraschall und Fehlerlage-Rekonstruktion aus Tandem-Lauf-

zeit-Ortskurven beim ALOK-Verfahren — ALOK 3. Materialprüfung 24 (1982) 161–165.

749 Kappes, K.; Barbian, O. A.; Croks, B.; Höh, F.: Fehlerbeschreibung nach Lage und Größe durch iterative Rekonstruktion aus Laufzeitortskurven ALOK. 3rd Europ. Conf. NDT Florence 1984, Vol. 5, pp. 224–233.

750 Kaprano, P. A.: Compression crack closure effect (ccce) — a basis for an NDE technique. Mater. Eval. 42 (1984) 458–462.

751 Karbach, B.: Prüfprobleme bei der Ultraschall-Rohrprüfung sowie grundsätzliche und technische Lösungsmöglichkeiten durch rechnergesteuerte Prüfanlagen. DGZfP-Conf. Neuere Entwicklung besonderer Verfahren der ZfP. Mainz 1978. Vol. 3, pp. 689–696.

752 Karlsen, F.: Radiography versus ultrasonic testing. Non Destr. Test. 6 (1972) 340–343.

753 Kassem, M. A.: Echo phantoms. Iron and Steel 29 (1956) 503–509, 547–549.

754 Kaule, W.: Magnetostriktives Ultraschall-Werkstoffprüfverfahren. Technik 16 (1961) 385–389.

755 Kaule, W.: Ultraschall-Meßverfahren mit Ankopplungskòntrolle. DE Pat. 1 573 596 (1966).

756 Kaule, W.: Verfahren und Vorrichtung für die Ultraschall-Werkstoffprüfung. DE Pat. 1 573 627 (1966).

757 Kaule, W.: Magneto-strictive ultrasonic testing of material. Proc. 4th Int. Conf. NDT, London 1963: Butterworths Sci. 1964, pp. 291–294, 316–318.

758 Kaule, W.: Ultraschallmeßverfahren zur Bestimmung der Wanddicke. DE Pat. 2 025 210 (1971).

759 Kaule, W.; Wetzlar, K. E.; Owens, W. T.: A new method of ultrasonic wall thickness measurement: the PREDEF system. Mater. Eval. 32 (1974) 103–106.

760 Kaule, W.: Streuflußprüfung für magnetisierbares Material. DE Pat. 1 938 107 (1969).

761 Kaule, W.; Primbsch, E.: Optische Nachweismethoden für Ultraschall. Messen u. Prüfen 10 (1974) 427–433.

762 Kaule, W.; Wetzlar, K. E.: Neuartiges Wandstärkenmeßverfahren für Wandstärken bis herab zu 0,2 mm bei einer Meßgenauigkeit von 10 µm. 6th Int. Conf. NDT, Hanover 1970. Paper B 1

763 Kawai, H.: The piezoelectricity of PVDF. Jap. J. Appl. Phys. 8 (1969) 975.

764 Kawashima, K.: Theory and numerical calculation of the acoustic field produced in metal by an electromagnetic ultrasonic transducer. J. Acoust. Soc. Am. 60 (1976) 1089–1099.

765 Kawashima, K.; Murota, S.; Nakamori, Y.: Soga, H.; Suzuki, H.: Electromagnetic generation of ultrasonic waves in absence of external field and its applications to steel production lines. Proc. 9th World Conf. NDT Melbourne 1979, Paper 443.

766 Kay, L.: Ultrasonic image synthesis. In: Research techniques in NDT, Vol. 2. London: Academic Press 1973, pp. 393–418.

767 Keck, R.; Proegler, H.: Application of electromagnetically excited plate waves for the lamination tests of ferritic strip. Proc. 10th World Conf. NDT Moscow 1982, Vol. 3, pp. 15–22. (Acad. Sci. USSR).

768 Kecskés, S.; Réti, P.; Virág, I.: Ultrasonic as a means of safety in railroad transport. Proc. 10th World Conf. NDT Moscow 1982. Vol. 6, pp. 50–57. (Acad. Sci. USSR.)

769 Kecskés, S.; Réti, P.; Virág, I.: Ultrasonic testing as a means of safety in railway transport. Materialprüfung 25 (1983), 26–30.

770 Kecskés, S.; Virág, I.: Evaluation of oval flaws in rails by ultrasonic testing. 7th Int. Conf. NDT, Warszawa 1973, Paper C 36

771 Kemeny, L. G.: Automated nondestructive testing techniques for the computerised inspection of wheels in motion. Proc. 9th World Conf. NDT Melbourne 1979, Rep. 1 C-1.

772 Kesler, N. A.; Merkulov, L. G.; Shmurun, Yu.; Tokarev, V. A.: Ultrasonic spectral method for attenuation measurement and device for automatic testing of micro-structures of materials. 7th Int. Conf. NDT, Warszawa 1973. Paper J 34

773 Kesler, N. A.; Kucheva, R. G.; Lyalin, A. V.; Shmurun et al.: Equipment for the ultrasonic structural inspection of ultrathinwalled tubing. Sov. J. Non Destr. Test. 13 (1977) 390–395.

774 Kessler, L. W.: Imaging with dynamic-ripple diffraction. In: Wade, G. (Ed.) Acoustic imaging. New York: Plenum Press 1976. pp. 229–239.

775 Kesler, N. A.; Shinkarev, V. V.; Kovrik, I. A. u. a.: Instrument for direct measurements of the ultrasonic propagation velocity and the attenuation factor in solid materials. Sov. J. Non Destr. Test. 14 (1978) 172–177.

776 Kessler, L. W.; Yuhas, D. E.: Acoustic microscopy — a tutorial review. Chap 4: The scanning laser acoustic microscope (SLAM). In: Metherell, A. F. (Ed.): Acoustical imaging, Vol. 8 New York: Plenum Press 1980, pp. 275–299.

777 Kharitonov, A. V.: The theory fundamentals for the electromagnetic-acoustic detector of transverse elastic waves in ferromagnetic metals. Proc. 10th World Conf. NDT, Moscow 1982, Vol. 3, pp. 23–30. (Acad. Sci. USSR).

778 Khuri-Yakub, B. T.; Kino, G. S.; Evans, A. G.: Acoustic surface wave measurements of surface cracks in ceramics. J. Am. Ceram. Soc. 63 (1980) 65–71.

779 Kiefer, R.; Schmitz, V.; Wendel, H.: Fast recording and numerical reconstruction of holograms. In: Charyulu, V. H. (Ed.): NDE in the nuclear industry — 1980. Metals Park: ASM 1981, pp. 499–512.

780 Kimura, K.: Cylindrical surface echoes in the ultrasonic flaw detection of round bars. Trans. Nat. Res. Inst. Met. 5 (1963) 43–51.

781 Kimura, K.: The measurement of ultrasonic attenuation using the bottom echoes in round bars. Trans. Nat. Res. Inst. Met. 7 (1965) 21–28.

782 Kimura, K.: On the sensitivity multiplication factor of the ultrasonic testing of turbine rotor shafts. Trans. Nat. Res. Inst. Met. 22 (1980) 19–22.

783 Kimura, K.: Calculation of AVG diagram for ultrasonic normal probes. Trans. Nat. Res. Inst. Met. 22 (1980) 29–34.

784 Kimura, K.; Fukuhara, H.; Matsumoto, Sh.: Design procedure of point focusing angle probe for ultrasonic testing. Hihakai Kensa 31 (1982) 2–10.

785 Kimura, K.; Matsumoto, Sh.: DGS-diagrams for angle probes. 3rd. Europ. Conf. NDT Florence 1984, Vol. 3, pp. 93–102.

786 King, R. B.; Fortunko, C. M.: Determination of in-plane residual stress states in plates using horizontally polarized shear waves. J. Appl. Phys. 54 (1983) 3027–3035.

787 Kipka, S.: Dämpfungsmessungen an Stahlguß mit Impuls-Schall-Gerät. Gießerei-technik 9 (1963) 176–178.

788 Kipka, S.; Anhofer, Th.: 18. Mitt.: Zerstörungsfreie Prüfung von Gußerzeugnissen. Ermittlung der Festigkeit an sphärolitischem Gußeisen mit Hilfe der Ultraschall-geschwindigkeit. Gießereitechnik 27 (1981) 84–85.

789 Kising, J.: Winkelprüfkopf mit Array. DE Pat. 3147482 (1981).

790 Kising, J.; Rost, M.; Viehmann, H.; Warkowski, W.: Isobarenkarte und isome-trische Projektion der Schalldruckverteilung. Das Echo 31 (1983) 40–42.

791 Kitson, N. K.; Low, S. A.; Turner, T. W.: Photoelastic visualization experiments and a computer model for nondestructive testing. Conf. Proc. Ultrasonics Int. Graz 1979. Guildford: IPC Sci. and Technol. Press 1979, pp. 524–533.

792 Kittmer, C. A.: Acoustic lenses — focusing in on defects. J. Can. Soc. Non Destr. Test. 5 (1983) 36–42, 44.

793 Kleesattel, C.: Zur Aufspaltung der Vickers-Härte durch die Einführung neuer Prüfverfahren. VDI-Ber. 308 (1978) 39–47.

794 Kleesattel, C.: Resonant sensing devices US Pat. 3 153 338 (1961); und: Ver-fahren zum Prüfen und Messen von Oberflächeneigenschaften fester Körper. DE Pat. 1287334 (1969).

795 Kleesattel, C.; Gladwell, G. M. L.: The contact impedance meter. Ultrasonics 6 (1968) 175–180, 244–251; 7 (1969) 39–44; 8 (1970) 38–48, 256–257.

796 Klein, M.; Werneyer, R.: Ultraschallspekstroskopische Untersuchungen zur Unterscheidung zwischen Rissen und Poren. Komm. d. Europ. Gemeinsch., Techn. Forsch. Stahl, Abschlußber., 1979, Eur 6343/IV, ed. by Generaldirektion Wissenschaftliche und Technische Information und Informationsmanagement

797 Klein, W. R.; Cook, B. D.: Unified approach to ultrasonic light diffraction. IEEE Trans. SU-14 (1967) 123–134

798 Kleinmann, G.: Bildschirm-Vorsatzskalen zur vereinfachten Bestimmung der Ersatzfehlergröße in Schmiedestücken. Krautkrämer-Echo, No. 22, p. 299

799 Kleint, R. E.: Relationship between defect orientation and ultrasonic indications. Non-Destr. Test. 15 (1957) 30–36

800 Kleint, R. E.; Johnson, C. H.: Ultrasonic inspection of liquid propellant rocket motor components. Non-Destr. Test 19 (1961) 418–421

801 Klemmt, W.-B.; Tober, G.; Funke, G.; Lemwerder: Rechnergestützte Ultraschallprüfung an faserverstärkten Flugzeugteilen. Conf. DGZfP Essen 1984, Paper No. 34

802 de Klerk, J.: Ultrasonic transducers. 3. Surface wave transducers. Ultrasonics 1 (1971) 35.

803 Kliesch, J.; Horst, P.: Untersuchungen zur Methode der Ultraschallmessungen am lebenden Schwein unter Verwendung eines Schnittbildgerätes. Züchtungskde. 34 (1962) 350.

804 Kline, R. A.: The origin of localized weak areas in sheet molding compound composites. Mater. Eval. 40 (1982) 874–879.

805 Klinman, R.; Stephenson, E. T.: Ultrasonic prediction of grain size and mechanical properties in plain carbon steel. Mater. Eval. 39 (1981) 1116–1120.

806 Klot, von, R.; Sahm, A.: Vergrößerung des Störabstandes bei der Ultraschallprüfung auf Fehler unter austenitischen Auftragsschweißplattierungen. Int. Symp. Neue Verfahren der zerstörungsfreien Werkstoffprüfung, Saarbrücken 1979. DGZfP Berlin 1980, pp. 163–175

807 Kluivingh, F.: Erfahrungen mit der Ultraschallprüfung von nichtmagnetisierbarem austenitischen Gußeisen. Gießerei 68 (1981) 75.

808 Knollman, G. C.; Hartog, J. J.: Shear modules gradients in adhesive interfaces as determined by means of ultrasonic Rayleigh waves. J. Appl. Phys. 53 (1982) 1516–1524.

809 Knollman, G. C.; Hartog, J. J.: Shear modulus gradients in adhesive interfaces as determined by means of ultrasonic Rayleigh waves, Part II. J. Appl. Phys. 53 (1982) 5514–5517.

810 Knollman, G. C.; Bellin, J. L.; Weaver, J. L.: Variable-focus liquid-filled hydroacoustic lens. J. Acoust. Soc. Am. 49 (1971) 253–271.

811 Knop, K.; Höller, P.; Pohlman, R.: Zur Reflexion von Plattenwellen an Dopplungen. Materialprüfung 12 (1970) 351–352.

812 Knopf, H. D.: Möglichkeiten der automatischen Ultraschallprüfung geschweißter Kraftfahrzeug-Hohlventile. Materialprüfung 11 (1969) 293–297.

813 Knorr, W.; Ricken, H. G.: Untersuchung zur Messung der Schallschwächung und Ermittlung der Fehlergröße mit Ultraschall. Arch. Eisenhüttenwes. 33 (1962) 317–326.

814 Knott, M. A.; Stinchcomp, W. W.: NDE of fatigue damage in boron aluminium composites with initial defects. Proc. 12th Symp. NDE. San Antonio 1979, pp. 245–259.

815 Kobayashi, H.; Yamamoto, E.; Uetake, N.; Ota, K.; Harumi, K.: Array transducers for ultrasonic testing and their applications. Proc. 9th World Conf. NDT, Melbourne 1979, Rep. 4H-11.

816 Koch, F. O.; Wahl, H. J.: Combination of US- and X-ray-tests for quality assurance of spiral welded pipes for pressure gas transmission lines. Proc. 10th World Conf. NDT, Moscow 1982. Vol. 4, pp. 111–118, (Acad. Sci. USSR).

817 Kolb, K.; Wölfel, R.: Ultraschallprüfung von Kunststoffschweißverbindungen als Grundlage für die Abnahme. Materialprüfung 18 (1976) 167–170.

818 Koltonski, W.: Investigation of rock and raw materials of rock by means of ultrasonics. Proc. 2nd Conf. Ultrasonics, Warszawa 1956, pp. 155–161

819 Koltonski, W.; Malecki, I.: Ultrasonic method for the exploration of the properties and structure of mineral layers. Acustica 8 (1958) 307–314.

820 Konarski, B.; Wazny, J.: Zusammenhang zwischen der Ultraschallgeschwindigkeit und den mechanischen Eigenschaften pilzbefallenen Holzes. Holz als Roh- u. Werkstoff 35 (1977) 341–345.

821 Kondrat'ev, Yu. A.: Ultrasonic field of a flat transducer with a nonuniform pressure amplitude destribution on its surface. Sov. J. Non Destr. Test. 17 (1981) 47–57.

822 Kondo, H.: Investigation by ultrasonic inspection of the relations between flaw pattern on flaws in steel forgings made for marine vessels. Proc. 4th Int. Conf. NDT, London 1963. London: Butterworths Sci. 1964, pp. 235–242.

823 Kopec, B.: Attenuation of ultrasound as a phenomenon depending of fatigue limit in the structure of railway axles. In: Novak, Z.; Baileyl, S. L. (Eds.): Ultrasonics Int. 1982. Guilford: IPC Sci. and Technol. Press 1981, pp. 147–152.

824 Kopec, B.: Ultrasonic testing of the railway axle structure. Proc. 10th World Conf. NDT, Moscow 1982, Vol. 2, pp. 267–274. (Acad. Sci. USSR).

825 Kopineck, H. J.; Krächter, H.; Rauterkus, W.: Ultraschallprüfung von Erzeugnissen der Eisen schaffenden Industrie in der laufenden Fertigung. Stahl u. Eisen 79 (1959) 786–797.

826 Kopineck, H. J.; Sommerkorn, G.: Zur Physik der Ultraschallprüfung von Feinblechen mit künstlichen und natürlichen Fehlern. Materialprüfung 6 (1964) 196–200

827 Kopineck, J.; Sommerkorn, G.; Böttcher, W.: Prüfung warm- und kaltgewalzter Bänder mit Ultraschall. Stahl u. Eisen 79 (1969) 1198–1201.

828 Koppelmann, J.: Schallgeschwindigkeits- und Schallschwächungsmessungen mit handelsüblichen Ultraschallimpulsgeräten an Platten mit sehr hoher Schallabsorption. PTB-Mitt. 68 (1964) 531–533.

829 Koppelmann, J.: Härtetiefenmessung an Stahlwalzen mit Ultraschall. Materialprüfung 9 (1967) 401–405.

830 Koppelmann, J.: Ultraschall-Impuls-Rückstreuungsmessungen in Metallen. Proc. 10th Int. Conf. Acoustics Ultrasound, Prag 1972, Sec. II, pp. 234–237.

831 Koppelmann, J.: Untersuchungen zur Härtetiefenmessung mit Ultraschall an Stahlwalzen bei Frequenzen zwischen 6 und 20 MHz. Materialprüfung 13 (1972) 382–387.

832 Koppelmann, J.: Ultraschallmeßeinrichtung für Härtetiefenmessungen an Stahlwalzen. Materialprüfung 14 (1972) 156–159.

833 Kordina, K.; Roy, V.; Waubke, N. V.: Ultraschallmessungen an bewehrten Kiesbetonen. Materialprüfung 9 (1967) 81–85.

834 Korpel, A.: Visualisation of the cross-section of a sound beam by Bragg-diffraction of light. Appl. Phys. Lett. 9 (1966) 425–427.

835 Korpel, A.; Kessler, L. W.; Palermo, P. R.: Acoustic microscope operating at 100 MHz. Nature 232 (1971) 110.

836 Korpel, A.; Kessler, L. W.: Comparison of methods of acoustic microscopy. Acoust. Hologr. 3 (1971) 23–43.

837 Kosoff, G.: The effects of backing and matching on the performance of piezoelectric ceramic transducers. IEEE Trans. SU-13 (1966) 20–30.

838 Kotval, C.: Ultrasonic evaluation of aluminium master cylinder die castings for porosity. Mater. Eval. 38 (1980) 23–27.

839 Kowalski, W.: Ultraschallschwächung während des Aushärtens von Aluminiumlegierungen. Aluminium 55 (1979) 795–797.

840 Krächter, H.: Ein neuartiges Verfahren zur Messung von Druckkräften mit Ultraschall. Werkstatt u. Betrieb (1958) 246–248.

841 Krächter, H.; Krautkrämer, J. u. H.: Schweißnahtprüfung mit Ultraschall. Schweißen u. Schneiden 5 (1953) 305–314.

842 Krainer, E.: Experience with the assessment and interpretation of ultrasonic indications in the testing of forgings. Mater. Res. 1 (1962) 47–54.

843 Krainer, E.: Messung der Ultraschallschwächung als Mittel der Qualitätskontrolle. Materialprüfung 4 (1962) 463–469.

844 Krainer, H.; Krainer, E.: Überschallprüfung nach dem Durchschallungs- und Impulsecho-Verfahren. Arch. Eisenhüttenwes. 24 (1953) 229–236.

845 Kramorov, G. A.: Sensitivity in ultrasonic monitoring of forgings on untreated surfaces. Sov. J. Non Destr. Test. 15 (1979) 411–413.

846 Kraus, S.; Goebbels, K.: Improvement of signal to noise ratio for the ultrasonic testing of coarse grained materials by signal averaging techniques. In: Berger, H.; Linzer, M. (Eds.): Ultrasonic materials characterization. Spec. Publ. 596, 1980, pp. 551–559. Nat. Bur. Stand. Gaithersburg, MD.

847 Kraus, S.; Goebbels, K.: Improved ultrasonic inspection of austenitic stainless steel components by signal averaging techniques. CSNI-Specialists Meeting Reliability Ultrasonic Inspection Austenitic Stainless Steel Componentts, Brussels, 1980, OECD Paris (1980).

848 Krautkrämer, J.: Ultrasonic weld testing in Europe and the attitude of technical control authorities. Non Destr. Test. 20 (1962) 319–324.

849 Krautkrämer, J.: Datenverarbeitung bei der Ultraschallprüfung. Materialprüfung 6 (1964) 279–282.

850 Krautkrämer, J.: Determination of the size of defects by the ultrasonic impulse echo method. Br. J. Appl. Phys. 10 (1959) 240–245.

851 Krautkrämer, J.: Die Messung der Ultraschall-Schwächung nach dem Echolotverfahren. Gießerei, tech.-wiss. Beih. 20 (1958) 1067–1075.

852 Krautkrämer, J.: Fehlergrößenermittlung mit Ultraschall. Arch. Eisenhüttenwes. 30 (1959) 693–703.

853 Krautkrämer, J.: Unkonventionelle Verfahren zur Erzeugung, zum Nachweis und zur Ankopplung von Ultraschall bei der Werkstoffprüfung. Materialprüfung 15 (1973) 37–42.

854 Krautkrämer, J.; Krautkrämer, H.: Verfahren und Gerät zur Messung von Wandstärken mit Ultraschallimpulsen. DE Pat. 920515 (1951).

855 Krautkrämer, J.; Krautkrämer, H.: Blechprüfung mit Ultraschall. Mitt. d. Forsch.-Ges. Blechverarb. 1955, No. 8, pp. 97–103

856 Krautkrämer, J.; Niklas, L.: Neue Hilfsmittel zum Einstellen des Tiefenausgleichs bei der Ultraschallprüfung. 6th Int. Conf. NDT, Hanover 1970, Paper B 12

857 Kreitz, K.; Ivens, G.: Routinemäßige Prüfung von Schmiedestücken mit Ultraschall. Materialprüfung 2 (1960) 240–244.

858 Kremer, K. J.: Qualitätssicherung bei der Herstellung von Knüppelhalbzeug, Stabstahl und Draht. Stahl u. Eisen 103 (1983) 359–365.

859 Krimholtz, R.; Leedom, D.; Matthaei, G.: New equivalent circuits for elementary piezoelectric transducers. Electron. Lett. 6 (1970) 398–399.

860 Kröning, M.; Fischer, E.: Automated volume and root examination. Proc. 10th World Conf. NDT, Moscow 1982, Vol. 7, pp. 467–474. (Acad. Sci. USSR).

861 Krohn, G.: Zerstörungsfreie Prüfverfahren für Hüllrohre. Atomwirtsch. (1970) 392–393.

862 Kruse, F.: Zur Werkstoffprüfung mittels Ultraschall. Akust. Z. 4 (1939) 153–168.

863 Kruse, F.: Untersuchungen über Schallvorgänge in festen Körpern bei Anwendung frequenzmodulierten Ultraschalls. Akust. Z. 6 (1941) 137–149.

864 Kubiak, E. J.; Rowand, R. R.: Lamb wave inspection system for thin sheet metals. 6th Int. Conf. NDT, Hanover 1970, Paper K 5

865 Kubo, S.: Flaw inspection of rolling stock axles and other parts. Jap. Railway Eng. 20 (1980) 9–13.

866 Kudo, Y.; Yamamoto, I.; Kawamura, K.: Automatic ultrasonic dimensioning system for small diameter seamless tube. Non Destr. Test. J. (Jap.) 1 (1983) 89–91.

867 Kügler, J.; Berner, K.: Kontinuierliche Ultraschall-Prüfung von Bändern und Blechen für Spiralrohre. Bänder, Bleche, Rohre 13 (1972) 583–586.

868 Kügler, J.; Berner, K.: Einfache Prüfanlage für eine 100%ige Fehleranzeigewahr-scheinlichkeit bei der Ultraschallflächenprüfung von Blechen und Bändern. Material-prüfung 15 (1973) 42–49.

869 Kühn, G. J.; Lutsch, A.: Elastic wave mode conversion at a solid-solid boundary with transverse slip. J. Acoust. Soc. Am. 33 (1964) 949–954.

870 Kühne, G.: Zerstörungsfreie Prüfung von Grobblech im Produktionsfluß. 6th Int. Conf. NDT, Hanover 1970, Paper L 5

871 Kuhlow, B.; Neumann, E.; Wüstenberg, H.; Nabel, E.; Mundry, E.: Ultrasonic testing of austenitic steel weld joints. Int. Symp. on Reliability of Nuclear Power Plants. Innsbruck 1975. IAEA — SM — 195/24.

872 Kupperman, D. S.; Caines, M. J.; Winiecki, A.: Assessment of ultrasonic NDE methods for ceramic heat-exchanger tubes. Mater. Eval. 40 (1982) 774–782.

873 Kuppermann, D. S.; Reimann, K. J.: Effect of shearwave polarisation on defect detection in stainless steel weld material. Ultrasonics 16 (1978) 21–27.

874 Kupperman, D. S.; Reimann, K. J.; Winiecki, A.: Computer-assisted spatial averaging for ultrasonic inspection of stainless steel welds. Mater. Eval. 39 (1981) 527–532.

875 Kupperman, D. S.; Reimann, K. J.; Yuhas, D.: Visualization of ultrasonic beam distortion in anisotropic stainless steel. In: Claugh, R. B. (Ed.): Qualitative NDE in the Nuclear Industry. Proc. 5th Int. Conf. NDE in the Nuclear Industry, San Diego 1982. Metals Park: ASM 1983, pp. 172–175

876 Kurz, W.; Lux, B.: Ortung der Erstarrungsfront in Stahl durch Ultraschall. Arch. Eisenhüttenwes. 39 (1968) 521–530.

877 Kurz, W.; Lux, B.: Ultraschall-Ankopplung an heiße Metalle durch Abkühlen der Oberfläche. Arch. Eisenhüttenwes. 39 (1968) 299–306.

878 Kuttruff, H.; Sung, K. M.: Piezoelektrische Ultraschallsender mit ungebündelter Schallabstrahlung. Acustica 43 (1979) 162–166.

879 Kutzner, J.: Zur Bündelversetzung bei der Reflexion von transversalen Ultraschall-wellen an freien Grenzflächen. Acustica 45 (1980) 25–29.

880 Kutzner, J.: Grundlagen der akustischen Holographie und deren Anwendung in der Schweißnahtprüfung. Part 1: Schweißtechnik 2 (1981) 25–28. Part 2: Schweißtechnik 3 (1981) 46–47

881 Kutzner, J.; Erhard, A.; Wüstenberg, H.; Zimpfer, J.: Quasi-Flächenholographie, ein Hilfsmittel zur Fehlergrößenbestimmung. Int. Symp. Neue Verfahren der zer-störungsfreien Werkstoffprüfung, Saarbrücken 1979. DGZfP Berlin 1980, pp. 293–307

882 Kutzner, J.; Wüstenberg, H.; Möhrle, W.; Schulz, E.: Zonenaufteilung, Empfindlich-keitseinstellung und Prüfkopfhalterung bei der manuellen Ultraschallprüfung mit dem Tandemverfahren. Materialprüfung 17 (1975) 246–250.

883 Kutzner, J.; Wüstenberg, H.: Akustische Linienholographie, ein Hilfsmittel zur Fehleranzeigeninterpretation in der Ultraschallprüfung. Materialprüfung 18 (1976) 189–194.

884 Kutzner, J.; Wüstenberg, H.: Akustische Holographie in Tandemanordnung, ein Hilfsmittel zur Fehleranzeigeninterpretation in der Ultraschallprüfung. Material-prüfung 18 (1976) 462–465.

885 Lack, B. J.: Ultrasonic examination of welds in thick plate using a double probe incline technique. Br. Weld. J. (Febr. 1962) 54–60.

886 Lacy, L. L.; Daniel, A. C.: Measurements of ultrasonic velocities using a digital averaging technique. J. Acoust. Soc. Am. 52 (1972) 189–195.

887 Lam, F. K.; Hui, M. S.: An ultrasonic pulse compression system for non-destructive testing using maximal-length sequences. Ultrasonics 20 (1981) 107–112.
888 Lamb, H.: On Waves in an elastic plate. Proc. R. Soc. London, Ser. A, 93 (1916) 114.
889 Lampić, M.: Prüfbarkeit von Gußeisen mit Lamellengraphit mit Ultraschall. Konstruieren, Gießen 3 (1978) 28–33.
890 Lang, R.; Exner, S.: Ultraschallprüfanlage für Rotationsrohre. Int. Symp. Neue Verfahren des ZfP. Saarbrücken 1979. DGZfP Berlin 1980, pp. 499–510
891 Langevin, M. P.; Chilovsky, N. C.: Procédé et appareil pour production de signaux sousmarins dirigés et pour la localisation à distance d'obstacles sousmarins. FR Pat. 502913 (1918).
892 Lapin, Yu. V.; Ermolov, I. N.: Curves of the directivity of emission of rectangular probes under impulse conditions. Sov. J. Non Destr. Test. 14 (1978) 1034–1036.
893 Larmande, M. Th.; Alais, P.: A theoretical study of the transient behaviour of ultrasonic transducers in linear arrays. In: Ash, E. A. (Ed.): Acoustical imaging, Vol. 12. New York: Plenum Press 1982, pp. 361–370.
894 Launay, J. P.; Valibus, L.: The new French code for design and construction of pressurized-water reactors (P.W.R.). Proc. 10th World Conf. NDT, Moscow 1982, Vol. 7, pp. 403–417. (Acad. Sci. USSR).
895 Lauprecht, E.: Bericht über Ergebnisse von Messungen mit dem Ultraschall-Echolot an Schweinen. Züchtungskde. 32 (1960) 441–449.
896 Lauprecht, E.; v. Schutzbar, W.: Ein Beitrag zur Messung der Querschnittsfläche des langen Rückenmuskels am lebenden Schwein mit Hilfe des Ultraschall-Schnittbildgerätes. Schweinezucht u. Schweinemast 12 (1964) H. 6.
897 Lautzenheiser, C. E.: Experiences gained in more than 40 preoperational and inservice inspection of nuclear power systems. 7th Int. Conf. NDT, Warszawa 1973. Paper G-11
898 Lautzenheiser, C. E.; Whiting, A. R.; Flach, W. T.: Problems associated with repetitive inspection of reactor pressure vessels and research toward solutions. In: Nichols, R. W. (Ed.): Advances in nondestructive examination for structural integrity. London: Appl. Sci. Publ. 1982, pp. 107–111.
899 Lautzenheiser, C. E.; Clayton Jr., W. T.: Developments in data handling, data recording and data analysis — some US developments. In: Nichols, R. W. (Ed.): Advances in nondestructive examination for structural integrity. London: Appl. Sci. Publ. 1982, pp. 191–201.
900 Lautzenheiser, C. E.; Doherty, J. E.; Singh, G. P.: Review of US activities in NDE data recording, signal processing, and analysis. In: Nichols, R. W. (Ed.): Advances in nondestructive examination for structural integrity. London: Appl. Sci. Publ. 1982, pp. 203–212.
901 Lavender, J. D.: Transmission of ultrasound in liquid steel and measurement of ultrasonic attenuation during cooling. Non Destr. Test. 5 (1972) 107–109.
902 Lavender, J. D.; Wright, J. C.: A new philosophy in the application of ultrasonic techniques in the foundry industry. Trans. Am. Foundrymen's Soc. 84 (1976) pp. 155–168.
903 Lee, D. A.; Moran, T. J.; Crane, R. L.: Practical considerations for estimating flaw sizes from ultrasonic data. Mater. Eval. 42 (1984) 1150–1158.
904 Lee, S. S.; Williams, J. H.: Stress wave attenuation in thin structures by ultrasonic through-transmission. J. Non Destr. Eval. 1 (1980) 277–286.
905 Lefevre, G.; Maurer, A.; Rauscher, R.: Ultrasonic inspection facility monolithic composite components. 3rd Europ. Conf. NDT, Florence 1984, Vol. 1, pp. 79–87.
906 Legros, D.; Lewiner, J. et al.: Generation of ultrasound by a dielectric transducer. J. Acoust. Soc. Am. 52 (1972) 196–198.
907 Lehfeldt, W.: Reifenprüfung mittels Ultraschallwellen. ATZ 56 (1954) 134–136.

908 Lehfeldt, W.: Methoden der Blechprüfung mittels Ultraschall. Industrieblatt (Stutt-gart) (1958) 425–433.

909 Lehfeldt, W.: Drahtprüfung durch Ultraschall. Draht-Welt 46 (1960) 156–159.

910 Lehfeldt, E.:Plattenwellen in geschichteten Blechen. Materialprüfung 14 (1972) 1–5.

911 Lehtinen, A.: Eine neue Untersuchungsmethode zur Qualitätskontrolle des Guß-eisens mittels Ultraschall. Paper No. 7 Int. Gießerei-Kongr. Zürich 1960

912 Leijsen, W.: Ultraschallresonanz-Wanddickenmessung über eine Flüssigkeitszwi-schenstrecke. Materialprüfung 4 (1962) 407–410.

913 Leisure, R. G.; Prieur, J.-Y.: An improved interferometer for ultrasonic attentuation or velocity measurements. Rev. Phys. Appl. 15 (1980) 781–784.

914 Leith, E. N.; Upatnick, J.: Wavefront reconstruction with diffused illumination and three-dimensional object. J. Opt. Soc. Am. 54 (1964) 1295–1301.

915 Lemon, D. K.; Posakony, G. J.: Linear array technology in NDE applications. Mater. Eval. 38 (1980) 34–37.

916 Lemons, R. A.; Quate, C. F.: Acoustic microscope-scanning version. Appl. Phys. Lett. 24 (1974) 163–165.

917 Lemons, R. A.; Quate, C. F.: Acoustic microscopy. In: Physical acoustics, Vol. 14. New York: Academic Press 1979, pp. 1–92.

918 Le Penven, Y.: Application of NDT-methods to the inspection of stress corrosion crack affected weld structures. Non Destr. Test. 5 (1972) 23–27.

919 Leslie, J. R.; Chefsman, W. J.: An ultrasonic method of studying deterioration and cracking in concrete structures. J. Am. Concr. Inst. 21 (1949) 17–36.

920 Levitt, A. P.; Martin, A. G.: Ultrasonic determination of elastic constants of metals at elevated temperatures. Non Destr. Test. 18 (1960) 333–336.

921 Lewis, R.; Cornforth, A. R.: Automatic rotary probe system for the ultrasonic inspection of steel tube. Non Destr. Test. 3 (1970) 128–131.

922 Liang, K.; Khuri-Yakub, B. T.; Chou, C. H.; Kino, G. S.: A three-dimensional synthetic focus system. In: Acoustical imaging, Vol. 10. New York: Plenum Press 1982, pp. 643–668.

923 Lichodziejewski, W.: Nondestructive inspection of track shoe rubber pads. Int. J. Non Destr. Test. 4 (1972) 199–214.

924 Licht, H.: Ein Beitrag zur berührungslosen Anregung von Plattenwellen. Acustica 27 (1972) 131–144.

925 Licht, H.; Hallet, J. B.: Mapping the ultrasonic defect shadow in a pitch-catch mode. In: DGZfP (Ed.): 4th Int. Conf. NDT in the Nuclear Field, Lindau 1981, Vol. 8, pp. 427–434

926 Light, G. M.: Lautzenheiser. C. E.; Gruber. G. J.; Singh. G. P.: New developments in detection, characterization and sizing of discontinuities. In: Periodic inspection of pressurized components. I. Mech. E. Conf. Publ. 1982-9. London: Mech. Eng. Publ. 1982, pp. 135–145.

927 Li Ming Xuan; Ding Wei Zhi; Chen Ji Mao: Principles of an acoustic impedance method for detection and location of non-bonds in adhesive-bonded multilayered joints. Non Destr. Test. Int. 15 (1982) 137–142.

928 Linhardt, F.: Über den Einfluß der Schallfeldinterferenzen auf den Fehlernachweis in Festkörpern. Metall 12 (1958) 1085–1092; 13 (1959) 1133–1138.

929 Linke, D.: Zur Anwendung des AVG-Diagrammes bei der Bestimmung der Ungänzengröße in der Ultraschall-Schweißnahtprüfung. ZIS-Mitt. 11 (1969) 1243 bis 1259.

930 Liversidge, D. B.; Fearn, G. A.; Dodgson, M. W.: Ultrasonic assessment of unbored rotor forgings. Non Destr. Test. 1 (1968) 385–400.

931 Lloyd, E. A.: Wide-band ultrasonic techniques. Symp. Fut. Ultrason. Spectroscopy, London 1970, Paper 2.

932 Lord Jr., A. E.: Acoustic emission — an update. In: Physical acoustics, Vol. 15. New York: Academic Press 1981, pp. 295–360.

933 Lovelace, J.: Polarization effects in shear wave testing. Mater. Eval. 38 (1980) 61–67.

934 Lovelace, J. F.; Luini, L. A.: Ultrasonic theory applied to the automatic inspection of welds. Mater. Eval. 26 (1968) 204–210.

935 Lucas, R.; Biquard, P.: Nouvelles propriétés optique des liquides, soumis à ondes ultrasonores. C.R. Acad. Sci. 194 (1932) 2132–2134.

936 Lucas, B. G.; Muir, Th. G.: The field of a focusing source. J. Acoust. Soc. Am. 72 (1982) 1289–1296.

937 Ludwig, B.; Wüstenberg, H.: Phasenempfindliche Auswertung von impulsförmigen Ultraschallsignalen bei der akustischen Holographie zur Rekonstruktion von Materialfehlern. Mater. u. Tech. 3 (1981) 142–152.

938 Lücke, K.; Lenz, D.: Ultraschallabsorption in Metallen. In: Neuere metallkundliche Untersuchungsverfahren. Düsseldorf: VDEh 1970, pp. 187–210

939 Lüscher, H. G.: Omyson: direkte Extruderführung durch Ultraschall. Kunststoffe — Plastics 23 (1976) 16–23.

940 Lücke, K.; Lenz, D.: Ultraschallabsorption in Metallen. In: Neuere metallkundl. Untersuchungsverfahren. Düsseldorf: VDEh 1970, pp. 187–210

941 Lukas, G.; Lutsch, A.: Bestimmung der Seigerungszone im Gußblock einer Aluminium-Magnesium-Silizium-Legierung mit dem Ultraschall-Reflexionsverfahren. Z. f. Metallkde. 45 (1954) 158–160.

942 Lumb, R. F.: Nondestructive testing of high pressure gas pipelines. Non Destr. Test. 2 (1969) 259–268.

943 Lund, S. A.: Application of ultrasonics for NDT of materials (dänisch). Ingenioren (1954) 794–803.

944 Lund, S. A.; Jensen, P.: P-scan documentation, a new method for recording and visualizing data from ultrasonic weld inspection. 6th Int. Conf. NDT, Warszawa 1973, Paper C-34

945 Lund, S. A.: Ultrasonic P-scan-system for weld inspection. Proc. 9th World Conf. NDT, Melbourne, 1979, 3B-15.

946 Lutsch, A.; Kühn, G. J.: Generation and reception of elastic waves via a plane boundary. J. Acoust. Soc. Am. 36 (1964) 428–436.

947 Lutsch, A.; Müller, E. A. W.: Anordnung zur Prüfung von Stoffen mit Ultraschallimpulsen. DE Pat. 971891 (1952).

948 Lutsch, A.: Zerstörungsfreie Prüfung der Werkstoffe nach dem Ultraschall-Impuls-Echoverfahren. Arch. Eisenhüttenwes. 23 (1952) 57–65.

949 Lutsch, A.: Grundlagen und Verfahren zur zerstörungsfreien Werkstoffprüfung mittels Ultraschall-Wellen. ATM-Blätter V 91 193-1-4 (1953–1954).

950 Lutsch, A.: Ultraschallschwingeranordnung zur zerstörungsfreien Werkstoffprüfung mittels Ultraschallimpulsen. DE Pat. 1 013 898 (1954).

951 Lutsch, A.: Ultraschall-Schwingeranordnung zur zerstörungsfreien Werkstoffprüfung mittels Ultraschall-Impulsen. DE Pat. 929153 (1953).

952 Lutsch, A.; Böhme, W.: Dickenmessung mittels Ultraschallwellen. ATM-Blatt B 1124–1126 (1957).

953 Lutsch, A.: Ultrasonic reflectoscope with an indicator of the degree of coupling between transducer and object. J. Acoust. Soc. Am. 30 (1958) 544–548.

954 Lutsch, A.: The experimental determination of the extent and degree of fracture of rock faces by means of an ultrasonic pulse reflection method. J. South African. Inst. Mining and Metallurg. (1959) 412–429.

955 Lutsch, A.: Bariumtitanate adhesion- und paste-transducers; ultrasonic generators for the analysis of solids. Proc. 3rd Int. Congr. Acoustics, Stuttgart 1959. Amsterdam: Elsevier 1960; Nature 184 (1959) 1458–1462.

956 Luukkala, M.; Meriläinen, P.: Metal plate testing using airborne ultrasound. Ultrasonics 11 (1973) 218–227.

957 Luukkala, M.; Meriläinen, P.: Plate wave resonance — a contactless test method. Ultrasonics 9 (1971) 201.

958 Lynnworth, L. C. et al.: Ultrasonic measurement of elastic moduli at elevated temperatures using momentary contact. J. Acoust. Soc. Am. 36 (1964) 1678–1684.

959 Lynnworth, L. C.; Patch, D. R.: New sensors for ultrasound: Measuring temperature profiles. Mater. Res. Stand. (Aug. 1970) 6–11.

960 Lynnworth, L. C.: Ultrasonic probes using shear wave crystals. Part 1 — Principles. Mater. Eval. 25 (1967) 265–277.

961 Lynnworth, L. C.: Sound ways to measure temperature. Acoustical techniques. Meas. Control 2 (1969) 414–418.

962 Lynnworth, L. C.: Use of ultrasonics for high-temperature measurements. Mater. Eval. 27 (1969) 60–66.

963 Lynnworth, L. C.: Attenuation measurements using the pulse-echo AB method, without multiple echo reverberations in specimen. Mater. Eval. 31 (1973) 6–16.

964 Lynnworth, L. C.; Papadakis, E. P.; Fowler, K. A.: Ultrasound propagation measurements and applications. In: McGonnagle, W. (Ed.): International advances in NDT, Vol. 5. New York: Gordon and Breach 1977, pp. 71–115.

965 Macecek, M.: Metallurgical causes of difficulties with ultrasonic inspection of austenitic welds. 1. Joint ASME/CSME Pressure Vessels and Piping Conf.; Montreal 1978, ASME-Paper 78 PVP 8.

966 Mackenzie, J. K.: The elastic constants of a solid containing spherical holes. Proc. Phys. Soc. B 63 (1) (1950) 2–11.

967 Macovski, A.: Theory of imaging with arrays. In: Wade, G. (Ed.): Acoustic imaging. New York: Plenum Press 1976, pp. 111–126.

968 Madeyski, A.; Logsdon, W. A.; Brenneman, C. B.: Correlation of ultrasonic tests, material evaluation and spin test results for a CrMoV turbine rotor forging. Congr. Int. Grosse Forge, Paris 1976, Vol. 2, pp. 933–981.

969 Madhava, M. R.; Raman, S.; Rohatgi, P. K.; Surappa, M. K.: Influence of certain microstructural parameters on the ultrasonic velocities and elastic constants of cast aluminium-alumina particle composites. Scr. Metall. 15 (1981) 1191–1195.

970 Maeda, T.; Miyake, S.; Kanekuni, A.: Ultrasonic flaw detection of austenitic stainless steel longitudinally welded pipe and tubing. In: Clough, R. B. (Ed.): Quantitative NDE in the nuclear industry, Proc. 5th Int. Conf. NDE in the Nuclear Industry, San Diego 1982. Metals Park: ASM 1983, pp. 167–171.

971 Maginness, M. G.; Plummer, J. D.; Meindl, J. D.: An acoustic image sensor using a transmit-receive array. Acoust. Hologr. 5 (1974) 619–631.

972 Magnusson, E. J.; Burton, L. M.: Detection of cracks in skirt attachment welds of a rocket motor case using contact pulse echo ultrasonic test methods. Thiokol Chemical Corp., Alabama, Res. Rep. U 68 4505 A (Nov. 1968).

973 Mahmoud, M. A.: Double-inclination probe for sizing steep fatigue cracks. Mater. Eval. 42 (1984) 1041–1046.

974 Mailer, H.: Pavement thickness measurement using ultrasonic testing. Highway Res. Rec. 378 (1972) 20–28.

975 Mak, D. K.: A universal plot for locating maximum sound pressure along the axis of a circular transducer. J. Can. Soc. Non Destr. Test. 5 (1983) 32, 34, 36.

976 Makow, D. M.: Ultrasonic detection of defects in wood. Non Destr. Test. 2 (1969) 197–199.

977 Mansfield, Th. L.: Ultrasonic technology for measuring molten aluminium quality. Mater. Eval. 41 (1983) 743–747.

978 Marcillet, M.; Rispal, M.: Les examens par ultrasons. Cas des essieux-difficultés rencontrées. Rev. Gen. Chem. Fer 3 (1963) 155–168.

979 Marini, J.; Werneyer, R.: Mesure de l'atténuation de la propagation ultrasonore dans les pièces de révolution présentant un alésage central. Materialprüfung 15 (1973) 167–171.

980 Markham, M. F.: Investigation of errors in ultrasonic thickness meters for use on glass reinforced plastics. Br. J. Non Destr. Test. 23 (1981) 187–190.

981 Marsh, D. M.: Means of visualizing ultrasound. In: Research techniques in NDT, Vol. 2. London: Academic Press 1973, pp. 317–367.

982 Martin, E.: Überschalluntersuchung an Achsen von Schienenfahrzeugen. Stahl u. Eisen 72 (1952) 176–185.

983 Martin, E.; Werner, K.: Fehleraufzeichnung beim Überschall-Impuls-Laufzeit-Verfahren. Arch. Eisenhüttenwes. 27 (1956) 579–594.

984 Martin, E.; Werner, K.: Schienenprüfung mit Ultraschall und der Ultraschall-Schienenprüfwagen der Dtsch. Bundesbahn. Eisenbahntech. Rdsch. 5 (1956) 487 bis 505.

985 Martin, E.; Werner, K.: Statistische Auswertung von Ultraschall-Reihenunter-suchungen an Achswellen von Schnellzug-Dampflokomotiven. Glasers Ann. 78 (1954) 1–8, 31–35.

986 Martin, E.; Werner, K.: Prüfung verwickelt geformter Teile mit Überschall. Arch. Eisenhüttenwes. 24 (1953) 411–422.

987 Martin, E.; Werner, K.: Einrichtung zur Schwächung von störenden Neben-echos bei dem Ultraschall-Impulsverfahren der zerstörungsfreien Werkstückprüfung. DE Pat. 934504 (1953).

988 Martin, J. F.; Munn, B. J.: Application of the ultrasonic testbed to graphite/organic composites. In: Thompson, D. O.; Chimenti, D. E. (Eds.): Quantitative evaluation, Vol. 1, 1982, pp. 287–293.

989 Martin, R.: Ultrasonic techniques for 'on-line' thickness measurements. Br. J. Non Destr. Test. 12 (1970) 79–83.

990 Mason, W. P.: Piezoelectricity, its history and applications. J. Acoust. Soc. Am. 70 (1981) 1516–1566.

991 Mason, W. P.: Sonics and ultrasonics: Early history and applications. In: de Clerk, J. (Ed.): IEEE Ultrasonics Symp. Proc. 1976, New York: IEEE 1976, pp. 610–617.

992 Mason, W. P.; McSkimin, J. H.: Attenuation and scattering of high frequency sound waves in metals and glases. J. Acoust. Soc. Am. 19 (1947) 464–473.

993 Mason, W. P.; McSkimin, H. J.: Energy losses of sound waves in metals due to scatter-ing and diffusion. J. Appl. Phys. 19 (1948) 940–946.

994 Mason, W. P.; McSkimin, H. J.; Shockley, W.: Ultrasonic observation of twinning in tin. Phys. Rev. 73 (1948) 1213/1214.

995 Masuyama, I.; Kisigami, M.; Irisawa, T.: Ultrasonic testing of aluminium alloy weldments and proposed defect acceptance criteria determined with their effect on strength taken into consideration. Br. J. Non Destr. Test. 19 (1977) 185–188.

996 Mathers, G. B.: Nondestructive inspection technique for multilayer circuit boards. Mater. Eval. 25 (1967) 148–152.

997 Matiss, I. G.; Slava, H. E.; Shtrauss, V. D.: Automatization of the acoustic and dielectric spectrumetry for nondestructive quality control of composite materials. Proc. 10th World Conf. NDT, Moscow 1982, Vol. 5, pp. 361–369. Acad. Sci. USSR).

998 Matsumura, Y.; Nishifuji, K.: Automatic ultrasonic testing of plates by reflection method. 7th Int. Conf. NDT, Warszawa 1973, Paper C 10

999 Matsumura, Y.: Automatic ultrasonic testing of plates for large diameter welded pipe by reflection method using TR-probes. 6th Int. Conf. NDT, Hanover 1970, Paper L 6

1000 Mätthies, K.; Neumann, E.; Mrasek, H.; Beyer, R.: Neue Entwicklungen bei Ultra-schallwinkelprüfköpfen für die Prüfung bei erhöhten Temperaturen. DGZfP-Conf. Essen 1984

1001 Matting, A.; Schaper, H.: Die Anwendung statistischer Methoden bei der Ultra-schallprüfung von Lagerschalen. Metall 22 (1968) 306–309.

1002 Matting, A.; Wilens, G.: Die Prüfung von Punktschweißungen durch Ultraschall. Schweißtechnik Vol. 35. Düsseldorf: Deutscher Verlag f. Schweißtechnik 1963

1003 Maxfield, B. W.; Hulbert, J. K.: Electromagnetic acoustic wave transducers (EMATS). Their operation and mode patterns. Proc. 10th Symp. NDE, San Antonio 1975, pp. 44–62.

624   References

1004 Mayer, W.; Neumann, A.; Streicher, V.; Dannehl, G.: Ergebnis von Ultraschall-messungen am Reaktordruckbehälter des Kernkraftwerkes Philippsburg. Tech. Ber. KWU AG, R 214-2987, April 1974.

1005 Mayer, W. G.; Ngoc, T. D. K.: Some aspects of ultrasonic nonspecular reflection. Georgetown University, Washington, Rep. AD-A105225 (1981).

1006 McClung, R. W.; Cook, K. V.: Ultrasonic detection of non-bond in clad structures. Proc. 4th Int. Conf. NDT, London 1963. London: Butterworths Sci. 1964, pp. 267–271.

1007 McConnell, G.; Klinman, R.: The nondestructive inspection of aircraft tires by use of pulse-echo ultrasonics. Rep. NADC-72035-VT/AD 747633, Naval Air Development Center, Warminster, Pa. (May 1972).

1008 McGowin, M. L.; Beyer, N. S.: Ultrasonic non-bond inspection to tubular fuel elements. Mater. Eval. 26 (1968) 17–20.

1009 McDonald, K. A.: Application of ultrasonics in the wood industry. Ultrasonics Int. Conf. Proc. Graz 1979, pp. 360–365.

1010 McElroy, J. T.; Briers, K. F.: Annular array search units and their potential application in conventional ultrasonic testing systems. Mater. Eval. 37 (1979) 41–46.

1011 McGaughey, W. C.: Ultrasonic examination of welds: Comparison of ASME and AWS procedures. Mater. Eval. 30 (1972) 44–48.

1012 McGonnagle, W. J.; McLain, St.; Wood, E. C.: Application of NDT to fuel elements for nuclear reactors. Non Destr. Test. 15 (1957) 86–90.

1013 McKinney, R. L.: Digital ultrasonic signal processing used for the clarification of ultrasonic signals. Lawrence Livermore Lab., Livermore Rep. UCRL-87805 (1982).

1014 McNamara, F. L.; Rogers, T. F.: Direct viewing of an ultrasonic beam in a transparent solid. J. Acoust. Soc. Am. 25 (1953) 338/339.

1015 McSkimin, H. J.; Bond, W. L.: Elastic moduli of diamond. Phys. Rev. 105 (1957) 116–121.

1016 Mech, S. J.; Martin, J. D.: Ultrasonic inspection of liquid metal filled austenitic stainless steel piping welds. In: Clough, R. B. (Ed.): Quantitative NDE in the nuclear industry. Proc. 5th Int. Conf. NDT in the Nuclear Industry, San Diego 1982. Metals Park: ASM 1983, pp. 189–193.

1017 Meindl, J. D.: Integrated electronics for acoustic imaging arrays. In: Acoustic imaging. New York: Plenum Press 1976, pp. 127–188.

1018 Meister, P. et al.; Jacobs, B.: NDT of large steam turbine rotors. EPRI Final Rep. of Res. Project 502-2/NP 2763/Dec. 82.

1019 Meixner, S.; Houfek, K.: Die kontinuierliche Prüfung auf Oberflächen- und Kernfehler von Stabstahl im Abmessungsbereich von 30 bis 190 mm Durchmesser. Stahl u. Eisen 100 (1980) 1542–1547.

1020 Melkanovich, A. F.; Zonov, I. V.: Determining the directivity of transducers operating in a pulse mode. Sov. J. Non Destr. Test. 13 (1977) 281–286.

1021 Mellmann, G.: Erfahrungen mit Ultraschall-Laufzeitmessungen am Bauwerk aus Beton. 2nd Europ. Conf. NDT Vienna 1981, pp. 375–377

1022 Mercier, N.; Belleval de, J. F.: Use of the phase of the signal in ultrasonic spectral analysis to evaluate flaws. Proc. Ultrasonics Int. 1981 (Novak, Z. Ed.), pp. 141–146.

1023 Merkulov, L. et al.: Attempt for systematizing the amplitude relationships in the reflection of the ultrasonic Lamb waves from surface grooves. 7th Int. Conf. NDT, Warszawa 1973, Paper C-15

1024 Mesh, W. E.: Variable angle ultrasonic transducer. US Pat. 2,602,101 (1950).

1025 Metherell, A. F.; Spinak, S.; Pisa, E. J.: Temporal reference acoustical holography. In: Metherell, A. F.; Larmore, L. (Eds.): Acoustical holography, Vol. 2. New York: Plenum Press 1970, pp. 69–85.

1026 Meyer, E.; Bock, E.: Hörschall- und Ultraschalluntersuchungen von Betonbalken mit Rissen. Akust. Z. 4 (1939) 231–237.

1027 Meyer, H.-J.: Ultraschall-Wandstärken-Messung an Grauguß-Laufbuchsen von Fahrzeug-Dieselmotoren. Materialprüfung 5 (1963) 293–297

1028 Meyer, H.-J.: Beispiele für die Einsatzmöglichkeit der Ultraschallschwächungsmessung zur Bestimmung von Werkstoff- und Festigkeitseigenschaften an Bauteilen. Metall 19 (1965) 435–441

1029 Meyer, H.-J.: Inspection of grey iron castings by ultrasonic attenuation. Non Destr. Test. 3 (1970) 99–110

1030 Meyer, H.-J.: Neue Möglichkeiten der Serienprüfung von Graugußteilen durch Ultraschall-Schwächungsmessungen, dargestellt am Beispiel von Lagerdeckeln für Dieselmotoren. Materialprüfung 11 (1969) 335–341.

1031 Meyer, H.-J.; Rath, W.: Ultrasonic equipments for in-service inspection of reactor pressure vessels. Paper on the Conf. Nuclex 1972, Basel 1972

1032 Meyer, H. J.: Present status of manipulating inspection systems. Int. Symp. Mechanization and Automation of Inspection of Pressurized Plants, Tokyo 1973.

1033 Meyer, H.-J.: The international state of the art in NDT of welds with special emphasis on flaw characterization. Mater. Eval. 42 (1984) 793–802.

1034 Meyer, P. A., Rose, J. L.: Ultrasonic attenuation effects associated with physical modelling of adhesive bonds. J. Appl. Phys. 48 (1977) 3705–3712.

1035 Mezrich, R. S.; Etzold, K. F.; Vilkomerson, D. H. R.: System for visualizing and measuring ultrasonic wavefronts. RCA Rev. 35, No. 4 (1974) 483–519.

1036 Mezrich, R.; Etzold, K.; Vilkomerson, D.: System for visualizing and measuring ultrasonic wavefronts. In: Acoustical holography, Vol. 6. New York: Plenum Press 1975, pp. 165–191.

1037 Michael, T. E.; Michaels, J. E.; Ronca, G. E.: Analysis methods for ultrasonic inspection of steam turbine discs. In: IEEE, Ultrasonic Symp. 1981, pp. 868–873.

1038 Michalski, F.; Krächter, H.: Kennzeichnung von Überschallanzeigen an Stahlerzeugnissen. Arch. Eisenhüttenwes. 28 (1957) 213–222.

1039 Michalski, F.: Ultraschallprüfung von heißen Schmiedestücken. Conf. DGZfP, Remscheid 1971, Paper No. 30

1040 Midecke, P.: Über die Ultraschallschwächung in austenitischen Chrom-NickelStählen. Materialprüfung 3 (1961) 1–4.

1041 Mikhailov, J. G.; Solov'ev, V. A.: Eine einfache Methode zur Messung der Absorption von Ultraschallwellen in stark absorbierenden Festkörpern (russ.). Doklady Akademii Nauk SSSR 78 (1951) 245–248.

1042 Miklowitz, J.; Achenbach, J. D. (Ed.): Proc. of Modern Problems in Elastic Wave Propagation. Symp. Evanston, 1977. New York: Wiley 1978.

1043 Miller, E. B.; Smith, S. W.; Thurstone, F. L.: A study of near field ultrasonic beam patterns from a pulsed linear array. In: Green, Ph. S. (Ed.): Acoustical Holography, Vol. 5. New York: Plenum Press 1973, pp. 287–293.

1044 Miller, G. F.; Pursey, H.: The field and radiation impedance of mechanical radiators on the free surface of a semi-infinite isotropic solid. Proc. R. Soc. A 223 (1954) 521–541.

1045 Miller, J.: Quality control of brazed joints for critical applications. Koll. Hart- und Hochtemperaturlöten und Diffusionsschweißen. DVS Essen 1981, Vol. 69, pp. 128–131

1046 Minton, W. C.: Ultrasonic inspection of pipeline welds. Proc. Pipeline Welding and Inspection, Houston 1980, pp. 65–76.

1047 Miyagawa, K.; Sasaki, Y.; Matsuda, N.; Sato, S.: Ultrasonic testing of steel products by electromagnetic transducers. Proc. 9th World Conf. NDT, Melbourne 1979. Paper 4 H 4.

1048 Möller, P.: Rationelles automatisches Prüfen mit Ultraschall an Rohren und Rundmaterial. Bänder, Bleche, Rohre 14 (1973) 16–20.

1049 Möller, P.; Berner, K.; Gallus, W.: Fully automatic ultrasonic plate inspection

using a freely programmable electronic system. Proc. 10th World Conf. NDT, Moscow 1982, Vol. 7, pp. 65–71. (Acad. Sci. USSR).

1050 Möller, P.; Röhrich, H.: Rechnergesteuerte Ultraschall-Prüfelektronik zur automatischen Untersuchung von Kernreaktor-Komponenten im Rahmen der Fertigungsprüfung. Materialprüfung 25 (1983) 66–69.

1051 Mohan, R.; Prathrap, G.: An acoustic emission energy analysis and its use to study damage in laminated composites. J. Non Destr. Eval. 1 (1980) 225–234.

1052 Mohr, W.: Erfahrung bei der Ultraschallprüfung schwerer Rotorschmiedestücke und Möglichkeiten zur Verbesserung der Aussagemöglichkeit durch Automatisierung. Materialprüfung 9 (1967) 73–80.

1053 Mohr, W.: Verfahren zur Messung des zeitlichen Impulsabstandes von zwei elektrischen Impulsen. DE Pat. 2 607 187 (1981).

1054 Mohr, W.: Zerstörungsfreie Prüfung von Schweißnähten, insbesondere bei Rotoren. BBC-Nachr., Sept. 1969, pp. 531–536

1055 Mohr, W.: Personal communication

1056 Mohr, W.; Brandstätter, K. W.: In-service inspection of 1800 RPM nuclear turbine rotors. Proc. EPRI WS-80-133, 1981: Nondestructive Evaluation of Turbine and Generator Rotors.

1057 Mohr, W.; Repplinger, W.: Elektrodynamische berührungslose Anregung freier Ultraschallwellen. Materialprüfung 20 (1978) 147–153, 221–225.

1058 Mondot, J.; Braouezec, F.: Ultraschallprüfung von hochfrequenzgeschweißten Rohren (160–144 mm Durchmesser). Materialprüfung 15 (1973) 344–345.

1059 Moore, F.: Development of ultrasonic testing techniques for Saturn honeycomb heat shields. Mater. Eval. 25 (1967) 25–32.

1060 Moore, M. J.; Dodd, F. J.: Real-time signal processing in an ultrasonic imaging system. Mater. Eval. 40 (1982) 976–981.

1061 Morgan, J. B.: Ultrasonic can rate cleanliness fatigue life of steel. Metals Eng. Quarterly 13 (1973) 1–4.

1062 Morgan, J. B.: Ultrasonic as a means of rating steel cleanliness. Mater. Eval. 28 (1970) 121–134, 144.

1063 Morimoto, K.; Ariota, N.; Fukui, S.; Watanabe, Y.: Development of a electro-dynamic transducer for testing heat exchanger tubes (jap.). NDI-Data paper No. 2993 (1983).

1064 Morisada, N.; Muto, T.; Shiono, K.; Takeiri, T.: Relationship between shape of ferrite and low level echo in ultrasonic flaw detection for 0.35% carbon steel forging. Congr. Int. de la Grosse Forge. Paris 1975, pp. 857–879.

1065 Morris, C. J.; Becker, F. L.: State-of-practice review of ultrasonic in-service inspection of class I system piping in commercial nuclear power plants. US Nuclear Regulatory Commission, Washington, Rep. NUREG/CR-2468.

1066 Morris, W. E.: Method and apparatus for ultrasonic testing. US Pat. 2,378,237 (1945).

1067 Morris, W. E.; Stambauch, R. B.; Gehmann, S. D.: Ultrasonic method of tire inspection. Rev. Sci. Instrum. 23 (1952) 729–734.

1068 Mucciardi, A. N.; Dau, G. J.: ALN 4000 ultrasonic pipe inspection system. Electric Power Res. Inst., Palo Alto, Rep. EPRI-NP-2088 (1982) 4.0–4.32.

1069 Mudge, P. J.; Jessop, T. J.: Size measurement and characterization of weld defects by ultrasonic testing: Findings of a collaborative programme. In: Nichols, R. W. (Ed.): Advances in nondestructive examination for structural integrity. London: Appl. Sci. Publ. 1982, pp. 337–355.

1070 Mudge, P. J.: Size measurement and characterization of weld defects by ultrasonic testing, Part 3: The effect of metallurgical features in ferritic steels. Abington Hall, Welding Inst. 1982.

1071 Mühlhäuser, O.: Verfahren zur Zustandsbestimmung von Werkstoffen, besonders zur Ermittlung von Fehlern darin. DE Pat. 569 598 (1931).

1072 Mueller, F.; Jäger, W.; Rockstroh, B.; Kittner, M.: Ultrasonic testing of austenitic

components of nuclear power plants. Proc. 10th World Conf. NDT, Moscow 1982, Vol. 4, pp. 179–186 (Acad. Sci. USSR).

1073 Müller, G.: Fernbediente Ultraschall-Basis- und -Wiederholungsprüfungen an Reaktordruckbehältern. Kerntechnik 20 (1978) 114–119.

1074 Mueller, R. K.; Sheridon, N. K.: Sound holograms and optical reconstruction. Appl. Phys. Lett. 9 (1966) 328–329.

1075 Müller, W.; Schmitz, V.; Schäfer, G.; Langenberg, K. J.; Hoppstädter, K.; Gräber, B.: Erfahrungen bezüglich Ortungs- und Rekonstruktionstreue der Ultraschall — Holographie. Materialprüfung 25 (1983) 9–12.

1076 Mueller, W.; Schmitz, V.; Schaefer, G.: Flaw sizing and flaw charakterization with HOLOSAFT. Mater. Eval. 42 (1984) 439–443.

1077 Müller, W.; Walte, F.; Werneyer, R.: Rekonstruktion aus Signalortskurven — Amplitudenortskurven. Fraunhofer Inst., IZfP Saarbrücken, Ber. 810820-TW (1981).

1078 Münschke, J.: Nachweis von Oberflächenfehlern bei Ventilfederstahldrähten mit einer automatisch arbeitenden Ultraschalldrahtprüfanlage. Draht 21 (1970) 217–221.

1079 Mundry, E.: Über die Anwendung verschiedener Kontrollkörper zur Justierung von Ultraschall-Impulsecho-Geräten. Materialprüfung 5 (1963) 298–306.

1080 Mundry, E.: Über das Verhalten teildurchlässiger Zwischenflächen bei der Materialprüfung mit Ultraschall, Part 1: Theorie. Materialprüfung 8 (1966) 433–444. Part 2: Modellversuche und Anwendungsmöglichkeiten. Materialprüfung 9 (1967) 120–130

1081 Mundry, E.: Untersuchungen über die zerstörungsfreie Prüfung von Schweißpunkten an dicken Blechen mit Ultraschall. Schweißen u. Schneiden 19 (1967) 165–171.

1082 Mundry, E.: Defect evaluation by ultrasonics. Some results of work in progress at the BAM. Non Destr. Test. 5 (1972) 290–297.

1083 Mundry, E.; Krautkrämer, J.: Ultrasonic recommendations for test methods test objects and equipment. 7th Int. Conf. NDT, Warszawa 1973, Paper C 41

1084 Mundry, E.; Schnitger, D.: Über die Leistungsfähigkeit zerstörungsfreier Prüfverfahren zum Fehlernachweis in Schweißnahtverbindungen. In: Fachbuchreihe „Schweißtechnik", Vol. 53. Düsseldorf: Deutscher Verlag für Schweißtechnik 1968

1085 Mundry; E.; Wüstenberg, H.: Beitrag zum AVG-Diagramm für Winkelprüfköpfe. Paper Conf. DGZfP, Freudenstadt 1969

1086 Mundry, E.; Wüstenberg, H.: Ultrasonic defect-size determination with double-probe and single-probe techniques. 5th Int. Conf. NDT, Montreal 1967, Paper 26

1087 Mundry, E.; Wüstenberg, H.: Zum Problem quantitativer Aussagen bei der Ultraschallprüfung mit Winkelprüfköpfen. NDT-Conf. Pula (Sept. 1970), Paper 21a

1088 Munger, D. W.; Weighart, F. G.: Ultrasonic inspection apparatus. US Pat. 3,688,562 (1972)

1089 Murashima, S.; Domon, H.; Miyawaki, H.; Kozima, Y.; Matsuyama, H.: Fully automatic, on-line and 100% testing density ultrasonic testing installation for heavy plate. Proc. 10th World Conf. NDT Moscow 1982, Vol. 7, pp. 313–318. (Acad. Sci. USSR).

1090 Murakami, Y.; Kino, G. S.: An application of Weiner filtering to NDE. Appl. Phys. Lett. 33 (1978) 685–687.

1091 Muratore, J. F.: Carleton, H. R.: The ultrasonic properties of impregnated graphite. 1981 Ultrasonics Symp. Proc. IEEE, New York 1981, Vol. 2, pp. 940–944.

1092 Murgatroyd, R. A.: Automated defect location and sizing by advanced ultrasonic techniques. In: Clough, R. B. (Ed.): Quantitative NDE in the nuclear industry. Proc. 5th Int. Conf. NDE in the Nuclear Industry, San Diego 1982, Metals Park: ASM 1983, pp. 243–249.

1093 Murphy, R. V.: Focussed ultrasonic probes for contact inspection. Mater. Eval. 38 (1980) 53–58.

1094 Murphy, R. V.: Toroidal, conical and spherical lenses in ultrasonic inspection. Mater. Eval. 39 (1981) 391–395.

1095 Murray, E. E.: Ultrasonic in-process control of spot welding quality. Mater. Eval. 25 (1967) 226–230.

1096 Murray, R. M.: Ultrasonic attenuation in cast ferritic steels. J. Steel Castings Res. (Dec. 1968) No. 45, pp. 1–14.

1097 Nabel, E.; Just, E.: Diskussionsbeitrag zur Verbesserung des Signal/Rausch-Verhältnisses bei der US-Prüfung grobkörniger Werkstoffe. DGZfP-Symp. Neue Verf. Analys. Ultrasch. Befunden. Berlin 1977.

1098 Nabel, E.; Mundry, E.: Beitrag zur Formunterscheidung von Ungänzen bei der Ultraschallprüfung. Symp. Neue Verf. der NDT Saatbrücken 1980, pp. 53–60

1099 Nagai, S.; Iizuka, K.: A practical ultrasound axicon for NDT. Ultrasonics 20 (1982) 265–270.

1100 Nakajima, H.; Tanaka, H.; Shimazaki, O.; Yamanaka, K.; Kinoshita, T.; Wada, Y.: New instrument for rapid and accurate measurement of ultrasonic velocity and attenuation using a minicomputer system. Jap. J. Appl. Phys. 18 (1979) 1379–1385.

1101 Nakamura, T.; Matsuyama, H.; Yamamoto, S.: Automatic ultrasonic testing systems for seamless and ERW pipes, 3rd Europ. Conf. NDT, Florence 1984, Vol. 4, pp. 51–66.

1102 Nanda, M. M.; Sinckair, N. A.; Lovelage, J. F.: Ultrasonic inspection of brazed pipe joints. Mater. Eval. 22 (1964) 315–320.

1103 Naumann, F.: Meßanordnung zur Messung von Schall an der Oberfläche von festen Körpern. DE Pat. 1097721 (1959).

1104 Neelakantan, K.; Subramanian, V.; Gopal, V.: Ultrasonic flaw detection in cast iron by boxcar integration. Non Destr. Test. Int. 13 (1980) 102–104.

1105 Neely, H. H.: Sodium-water reaction testing — NDE requirements and approach for ISI of the LMFBR steam generator. In: DGZfP (Ed.): 4th Int. Conf. NDT in the Nuclear Field, Lindau 1981, Vol. 8, pp. 533–540

1106 Neubert, S.; Fischer, H. Ch.: Zerstörungsfreie Prüfung von Gummi-Stahl-Verbunden in der polygraphischen Industrie. Schweißtechnik 30 (1980) 317–318

1107 Neumann, E.: Über den Stand der Entwicklung von Ultraschallprüfverfahren für grobkörnige austenitische Werkstoffe. In: Dorn, L. (Ed.): Schadensfälle und Fehler an Schweißbauteilen — ihre Ursachen und Vermeidung, Grafenau: Expert Verlag 1985

1108 Neumann, E.; Brekow, G.; Römer, M.; Behrendt, B.: Optimierung der Impulsform und Anwendung von A-Bildsignalmittelungstechniken für eine verbesserte Ultraschallprüfung austenitischen Gefüges. DGZfP Conf. Berlin 1983, Paper B 7

1109 Neumann, E.; Hecht, A.; Schnitger, D.; Voß, U.; Gieschler, U.: Rechnergestützte Ultraschallprüfung von faserverstärkten Kunststoffen. 3rd Europ. Conf. NDT Florence 1984, Vol. 5, pp. 35–47

1110 Neumann, E.; Wüstenberg, H.; Nabel, E.; Leisner, W.: Ultraschallprüfung von Schweißverbindungen austenitischer Stähle. Materialprüfung 16 (1974) 395

1111 Neumann, R.; Gebhardt, W.: Ein modernes phased-array-Gerät für die zerstörungsfreie Prüfung im Industriebereich. 3rd Europ. Conf. NDT Florence 1984, Vol. 3, p. 353 und 11th World Conf. NDT Las Vegas 1985, Vol. II, pp. 852–859

1112 Neumann, R.; Goebbels, K.: Geräteprototyp zur Gefügebeurteilung mittels Ultraschall-Rückstreuung. In: DGZfP (Ed.): 4th Int. Conf. NDT in the Nuclear Field, Lindau 1981, Vol. 8, pp. 337–346

1113 Neumann, R. K.; Barbian, O. A.: Hardware equipment for automatic ultrasonic inspection by the ALOK-technique. New procedures in nondestructive testing. Proc. Germany-US Workshop. Saarbrücken 1982. Berlin: Springer 1983

1114 Newhouse, V. L.; Bilgutay, N. M.; Saniee, J.; Furgason, E. S.: Flaw-to-grain echo enhancement by split spectrum processing. Ultrasonics 20 (1982) 59–68.

1115 Newman, D. R.: Ultrasonic thickness measurement for control of machine tools. Br. J. Non Destr. Test. 14 (1972) 73–79.

1116 Newman, D. R.: Ultrasonic Schlieren system using a pulsed gas laser. IEEE Trans. SU-20 (1973) 282–285.

1117 Nichols, R. W.: Recent developments in NDT for UK power applications. In: DGZfP (Ed.): 4th Int. Conf. NDT in the Nuclear Field, Lindau 1981, Vol. 8, pp. 491–498

1118 Nichols, R. W.: NDE effectiveness in relation to reactor pressure vessel integrity. In: Clough, R. B. (Ed.): Quantitative NDE in the nuclear industry, Proc. 5th Int. Conf. NDE in the Nuclear Industry, San Diego 1982, Metals Park: ASM 1983, pp. 6–11.

1119 Nickerson, R. A.: A new view of the elastic theory upon which ultrasonic testing is based. Int. J. Non Destr. Test. 2 (1970) 81–97.

1120 Nickerson, R. A.: Wave propagation theory for ultrasonic testing. 7th Int. Conf. NDT, Warszawa 1973, Paper C-14

1121 Nielsen, N.: P-scan system for ultrasonic weld inspection. Br. J. Non Destr. Test. 23 (1981) 63–69.

1122 Nielsen, N.: P-Scan-System zur Ultraschallprüfung von Schweißnähten. Material-prüfung 23 (1981) 22–24.

1123 Niklas, L.: Eine neue Methode der Dicken- bzw. Schallgeschwindigkeitsmessung. Z. Metallkde. 49 (1958) 152–155.

1124 Niklas, L.: Plattenwellen. Materialprüfung 4 (1962) 12–20.

1125 Niklas, L.: Gruppenlaufzeit und Bündelversetzung bei der Schrägreflexion. Auswirkungen auf die praktische Werkstoffprüfung mit Ultraschall. Materialprüfung 7 (1965) 281–288.

1126 Niklas, L.: Schallfeldberechnungen für kurze Impulse und Stoßwellen. 2nd Europ. Conf. NDT Vienna 1981, pp. 19–24

1127 Nikolov, Ch. D.: Mecanisme de contrôle ultra sonore continu de barres rondes de cuivre ou d'alliages de cuivre et resolution de quelques autres problèmes. 3rd Europ. Conf. NDT Florence 1984, Vol. 5, pp. 1–7.

1128 Nisselroy van, J. J. M.; 'T Hooft, N.; Whillas, R. J.: Mechanised ultrasonic underwater inspection of girth welds in platform legs. Br. J. Non Destr. Test. 26 (1984) 347–353.

1129 Nongaillard, B.; Rouvean, J. M.; Saisse, H.: Scanning acoustic microscopy inside ceramic samples. In: Ash, E. A.; Hill, C. R. (Eds.): Acoustical imaging, Vol. 12. New York: Plenum Press 1982 pp. 125–136.

1130 Nulk, D. E.: A comparison of various nondestructive inspection processes using hot isostatically pressed powder turbine parts. General Electric, Lynn (USA). Rep. AD-A 040 333 (1976).

1131 Nusbickel, E. M.; Cressman, R. N.: Development of a manual operated multiple transducer ultrasonic instrument for inspection of plates. Mater. Eval. 28 (1970) 1–7.

1132 Nußmüller, E.: Aktuelle Probleme bei der Ultraschallprüfung von Freiformschmiede-stücken. Arch. Eisenhüttenwes. 53 (1982) 489–494.

1133 Nußmüller, E.; Gründler, O.: Probleme der zerstörungsfreien Prüfung von präzi-sionsgeschmiedeten Teilen für die Luftfahrtindustrie. 3rd Europ. Conf. NDT Florence 1984, Vol. 1, pp. 66–77.

1134 Obraz, J.: A new method and equipment for measuring the ultrasonic attenuation caused by scattering. 7th Int. Conf. NDT, Warszawa 1973, Paper J-03

1135 Obraz, J.: Bewertung der Fehlergrößen und der Materialschwächung mittels eines AVG-Rechnerprogramms. 3rd Europ. Conf. NDT Florence 1984. Vol. 5, pp. 304–311.

1136 Odru, R.; Riou, C.; Vacher, J.; Deterre, Ph. et al.: New instrument for continuous and simultaneous recording of changes in ultrasonic attenuation and velocity. Rev. Sci. Instrum. 49 (1978) 238–241.

1137 Öhnfeldt, C. G.: Mechanized inspection of generator retaining rings with ultrasound and eddy current. Paper Eurotest Experts Meeting Stockholm 1980

1138 Ogura, T.; Kojima, T.; Uesugi, N.: Ultrasonic image converter. Jap. Electr. Eng. 2 (1968) 66–68.

1139 Ogura, Y.; Ishii, Y.: A measurement of the height of internal defects using the mode converted surface wave at the defect. Proc. 9th World Conf. NDT, Melbourne 1979. Rep. 4G-5.

1140 Ohigashi, H.: Electromechanical properties of polarized polyvinylidene fluoride films as studied by the piezoelectric resonance method. J. Appl. Phys. 47 (1976) 949–955.

1141 Ohkubo, Y.; Saikudo, R.; Goto, M.; Tanaka, H.: Development of automatic ultrasonic examination system for heavy section steel forgings. 6th Int. Conf. Quantitative NDE Nuclear Industry, Zürich 1983.

1142 Ohta, K.; Yamamoto, E.: Direct display and recording instrument for ultrasonic testing by means of multiple distance gate. 7th Int. Conf. NDT Warszawa 1973, Paper C-18

1143 Okyere, J. G.; Cousin, A. J.: On flaw detection in live wood. Mater. Eval. 38 (1980) 43–46.

1144 O'Neil, H. T.: Theory of focusing radiators. J. Acoust. Soc. Am. 21 (1949) 516–526.

1145 O'Neil, R.; Adams, A. L.: Plate inspection steering committee (PISC), a description and results of the round robin ultrasonic examination of three thick plates to the 1974 PVRC procedure based on the ASME XI code. In: Charyulu, V. H. (Ed.): NDE in the Nuclear Industry — 1980. Metals Park: ASM 1981, pp. 321–343.

1146 O'Neil, R.: OECD-EEC plate inspection steering committee the PSC 1-programme — a brief review. In: Nichols, R. W. (Ed.): Advances in nondestructive examination for structural integrity. London: Appl. Sci. Publ. 1982, pp. 295–313.

1147 Onodera, S.: Ultrasonic testing indications in large forgings for nuclear steam supply systems. Trans. Nondestr. Exam. Conf. TÜV-B & W Washington 1976, pp. 77–109.

1148 Onodera, S.; Ohkubo, Y.; Takeya, M.; Wataya, M.: Defects and their inspectability by UT in current heavy section steels for nuclear power plant. In: Clough, R. B. (Ed.): Quantitative NDE in the nuclear industry, Proc. 5th Int. Conf. NDE in the Nuclear Industry, San Diego 1982. Metals Park: ASM 1983, pp. 231–236.

1149 Onozawa, M.; Ishii, Y.: Industrial application of improved narrow beam probes for ultrasonic inspection. Proc. 4th Pan Pac. Conf. NDT Sydney 1983, Vol. 1, Rep. U6.

1150 Opel, P.; Ivens, G.: Fehlergrößenermittlung mit Ultraschall an Schmiedestücken. Arch. Eisenhüttenwes. 33 (1962) 311–316.

1151 Oppermann, W.; Crostack, H. A.: Einfluß des Spektralgehalts von Ultraschall-impulsen auf die Fehlerbewertung nach der AVG-Methode. Materialprüfung 23 (1981) 234–238.

1152 Oppermann, W.: Crostack, H. A.: Untersuchungen zur Verbesserung der Nachweis-empfindlichkeit und der Fehlergrößenbestimmung von Korrosionsrissen. 3rd Europ. Conf. NDT, Florence 1984, Vol. 2, pp. 22–35.

1153 Ortwig, H.; Boese, U.: Erfahrungen auf dem Gebiet der Ultraschallprüfung an geschweißten Polyäthylen-Hart-Rohrleitungen. Proc. Welding, Bratislava 1975, S. 44 bis 49.

1154 Ors, L.; Cabezon, F.: Ultraschall, Betrachtungen, Kriterien und Faktoren im Zu-sammenhang mit der Prüfung von Kehlschweißverbindungen. 6th Int. Conf. NDT, Hanover 1970, Paper H 5

1155 Osterhammel, K.: Optische Untersuchungen des Schallfeldes kolbenförmig schwin-gender Quarze. Akust. Z. 6 (1941) 73–86.

1156 Otsuki, T.: Diffraction by a rectangular aperture. J. Acoust. Soc. Am. 68 (1980) 329–333.

1157 Pancholy, M.; Kumar, S.: Ultrasonic attenuation in carbon steels. Indian J. Technol. 19 (1981) 493–498.

1158 Panhuise, V. E.; Richmond, L.; Novak, R.: The implementation of a computerized scan system. Mater. Eval. 42 (1984) 231–238.

1159 Panian, F. C.; van Valkenburg, H. E.: Development of ASTM reference blocks for ultrasonic inspection. Non Destr. Test. 19 (1961) 45–57.

1160 Papadakis, E. P.: Absolute accuracy of the pulse-echo overlap method and the pulse-superposition method for ultrasonic velocity. J. Acoust. Soc. Am. 52 (1972) 843–846.

1161 Papadakis, E. P.: Ultrasonic attenuation and velocity in three transformation products in steel. J. Appl. Phys. 35 (1964) 1474–1482.

1162 Papadakis, E. P.: Ultrasonic attenuation caused by scattering in polycristalline media. In: Mason, W. P. (Ed.): Physical acoustics, Vol. IVB. New York, London: Academic Press 1968.

1163 Papadakis, E. P.: Buffer-rod system for ultrasonic attenuation measurements. J. Acoust. Soc. Am. 44 (1968) 1437–1441.

1164 Papadakis, E. P.: Adhesive disbond testing by impulse-induced-resonance utilizing damping. IEEE Ultrasonics Symp. Proc. 1975. 75CHO 994-4SU pp. 612–615.

1165 Papadakis, E. P.: Ultrasonic attenuation caused by Rayleigh scattering by graphite nodules in nodular cast iron. J. Acoust. Soc. Am. 70 (1980) 782–787.

1166 Papadakis, E. P.; Petersen, B. W.: Ultrasonic velocity as a predictor of density in sintered powder metal parts. Mater. Eval. 37 (1979) 76–80.

1167 Papadakis, E. P.; Fowler, K. A.; Lynnworth, L. C.: Ultrasonic attenuation by spectrum analysis of pulses in buffer rods: Method and diffraction corrections. J. Acoust. Soc. Am. 53 (1973) 1336–1343.

1168 Papadakis, E. P.; Lynnworth, L. C.; Fowler, K. A.; Carnevale, E. H.: Ultrasonic attenuation and velocity in hot specimens by momentary contact method with pressure coupling and some results on steel to 1200 °C. J. Acoust. Soc. Am. 52 (1972) 850–857.

1169 Papke, W. H.: Schweißnahtprüfung mit Ultraschall. Schweißen u. Schneiden 10 (1958) 131–135.

1170 Papke, W. H.: Vorschlag zur dokumentarischen Erfassung des Befundes von Ultraschall-Schweißnahtprüfungen. Schweißen u. Schneiden 13 (1961) 457–463.

1171 Papke, W. H.: Prüfen mit Ultraschall — neue Erfahrungen. Praktiker/Schweißen u. Schneiden 20 (1968) 269–275.

1172 Pardee, W. J.; Thompson, R. B.: Half-space radiation by EMATs. J. Non Destr. Eval. 1 (1980) 157–181.

1173 Park, S. K.; Bertoni, H. L.: Elastic wave propagation in hexagonal honey combs. I: Method of analysis and low frequency characteristics. J. Acoust. Soc. Am. 70 (1981) 1445–1455. II: High frequency characteristics. J. Acoust. Soc. Am. 70 (1981) 1456–1462.

1174 Paschalis, P.: Bestimmung der Korrelation zwischen ausgewählten Festigkeitseigenschaften und Strukturmerkmalen von Holz mit Anwendung des Resonanz- und Ultraschallverfahrens. Holztechnologie 19 (1978) 14–17.

1175 Passerell, N. D.; Foster, A. C.: Ultrasonic inspection of large solid-fuel booster nozzles. Mater. Eval. 25 (1967) 53–57.

1176 Patel, H. B.: Ultrasonic testing of uranium metal. Paper on the ASNT 31. Nat. Fall Conf., Detroit 1971

1177 Patterson, W.; Bodmer, E.: Ultraschalluntersuchungen an Gußeisen mit lamellarer und kugeliger Graphitausbildung. Gießerei, tech.-wiss. Beih. 17 (1957) 909–917.

1178 Patterson, B. R., Bates, C. E.: Nondestructive property prediction in gray cast iron using ultrasonic techniques. Am. Foundrymen Soc. Trans. 89 (1981) 369–378.

1179 Patterson, M. S.; Foster, F. St.: Acoustic fields of conical radiators. IEEE Trans. SU-29 (1982) 83–92.

1180 Pawlowski, Z.; Gustkiewicz, J.; Cislowski, W.; Gutkiewicz, P.: Measuring of acoustic parameters of rocks subjected to hydrostatic pressure. 3rd Europ. Conf. NDT Florence 1984, Vol. 1, pp. 132–141.

1181 Peck, J.; Thompson, V.: Remote measurement of oxide thickness at Oldbury-on-

Severn Power Station using ultrasonic spectroscopy. Br. Nucl. Energy Soc., Proc. of the Western Branch Symp. Inspection of UK Reactors, 1980.

1182 Penttinen, A.; Luukkala, M.: Sound pressure near the focal area of an ultrasonic lens. J. Phys. D: Appl. Phys. 9 (1976) 1927–1936.

1183 Pelseneer, J. P.; Louis, G.: Ultrasonic testing of austenitic steel castings and welds. Br. J. Non Destr. Test. 16 (1974) 107–113.

1184 Perdijon, J.: An ultrasonic method for the internal inspection of tubing. 10th World Conf. NDT Moscow 1982, Vol. 5, pp. 21–27. (Acad. Sci. USSR).

1185 Perdrix, M.; Baboux, J. C.; Lakestani, F.: Etude théorique et expérimentale de l'influence de la couche de couplant sur la réponse d'un transducteur ultrasonore large bande. J. Phys. D: Appl. Phys. 13 (1980) 185–194.

1186 Perevalov, S. P.; Raikhman, A. Z.: Acoustic circuit of a sloped probe for an angular type reflector, Part I. Sov. J. Non Destr. Test. 15 (1979) 923–931.

1187 Perevalov, S. P.; Raikhman, A. Z.: Acoustic channel of inclined scanner for corner reflector, Part II. Sov. J. Non Destr. Test. 15 (1979) 1036–1041.

1188 Peterson, D. K.; Bennett, S. D.; Kino, G. S.: Real-time NDE of flaws using a digital acoustic imaging system. Mater. Eval. 40 (1982) 1256–1262.

1189 Peterson, D. K.; Bennett, S. D.; Kino, G. S.: Locating and sizing surface-breaking cracks with a synthetic-aperture acoustic-imaging system. Mater. Eval. 42 (1984) 451–457.

1190 Pieper, K.: Ultraschallprüfung und Schallgeschwindigkeitsmessung von GGG-Sicherheitsteilen für die Automobilindustrie mit einer Tauchtechnik-Prüfanlage. 2nd Europ. Conf. NDT, Vienna 1981, pp. 112–116

1191 Pieper, K.: Bindungsprüfung an Silber/Kupfer-Lötungen. DGZfP Conf. Essen 1984, Paper Nr. 39

1192 Pies, W.: Vollautomatische US-Prüfung von Grobblechen. Process. Eng. (1979) 4-11.

1193 Pies, W.: Auswirkungen der Mikroelektronik auf die automatische Ultraschall-prüfung, aufgezeigt am Beispiel einer neukonzipierten Prüfelektronik. Fachber. Hüttenpraxis Metallweiterverarb. 22 (1984) 172–182.

1194 Piggins, J. M.; Farley, J. M.: A compact electronically-scanned variable-angle probe for nondestructive testing. Proc. Ultrasonics Int., Graz 1979, pp. 339–344.

1195 Piltner, R.: Die Finite-Element-Methode bei akustischen Problemen. VDI-Z. 120 (1978) 483–490.

1196 Pirs, J.: Ultraschallschwächungsmessungen an plattenförmigen Körpern aus Guß-eisen mit Kugelgraphit. Gießereiforschung 20 (1968) 116–120.

1197 Pittaway, R. G.: Ultrasonic testing of resistance spot welds. Weld. Met. Fabr. 35 (1967) 443–447.

1198 Pitts, L. E.; Plona, Th. J.; Mayer, W. G.: Theory of nonspecular reflection effects for an ultrasonic beam incident on a solid plate in a liquid. IEEE Trans. SU-24 (1977) 101–110.

1199 Podgorski, J.: Piezokeramischer elektroakustischer Wandler. DE Pat. 2646389 (1976).

1200 Pohl, D.: Ermittlung der Zugfestigkeit von Sintermetallen mit Ultraschallmessungen. Arch. Eisenhüttenwes. 40 (1969) 647–650.

1201 Pohl, E.: Homogenitätskontrolle sowie Ermittlung der Betondeckung und des Kon-taktes zwischen Bewehrung und Beton in Stahlbetonbauteilen. Wiss. Ber. T. H. Leipzig, No. 12 (1979) 57–62

1202 Pohlman, R.: Verfahren zum bildmäßigen Sichtbarmachen und Messen einer Energie-verteilung von thermischer, elektrischer, Schall- oder Ultraschallenergie. DE Pat. 710413 (1937).

1203 Pohlman, R.: Über die Möglichkeit einer akustischen Abbildung in Analogie zur optischen. Z. Phys. 113 (1939) 697–709.

1204 Pohlman, R.; Kopineck, J.; Sommerkorn, G.; Böttcher, W.: Prüfung von Blechen und Bändern mittels mehrerer, simultan angeregter Ultraschall-Plattenwellen. 6th Int.

Conf. NDT, Hanover 1970. Paper K 7

1205 Popescu, N. D.: Zerstörungsfreie Prüfung von Beton mit dem Ultraschallimpuls-verfahren. Materialprüfung 13 (1971) 85–88.

1206 Posakony, G. J.: Acoustic imaging — a review of current techniques for utilizing ultrasonic linear arrays for producing images of flaws in solids. Symp. Elast. Waves NDT Mater. ASME 1978 pp. 10–15.

1207 Potschtowik, G. J.; Termettschikow, M. K.; Stoljarowa, E. A.: Eine Ultraschall-Schnellmethode zur Prüfung der Festigkeit keramischer Werkstoffe. Ziegelindustrie 24 (1971) 431–434.

1208 Pralus, Y.; Lambert, A.; Flambard, C.; Moulin, P.; Sauve, P.; Pocheron, G.; Bertin, G.: Installation de contrôle par ultrasons des soudures de conduites forcées. 3rd Europ. Conf. NDT, Florence 1984, Vol. 1, pp. 325–337.

1209 Preston, T. E.: The NDT of bonding by ultrasonics. Br. J. Non Destr. Test. 12 (1970) 17–20.

1210 Wehrmeister, A. E.: Weld monitoring with acoustic emission. J. Met. 30 (1978) 28–30.

1211 Proegler, H.: Neuere Ultraschallmethoden zur Unterscheidung verschiedener Schweiß-nahtfehler. Symp. Neue Verfahren der NDT, Saarbrücken 1980, pp. 45–52

1212 Proegler, H.; Kräske, W.: Anwendung der Ultraschallspektrometrie zur Ermittlung von Fehlerart und Fehlergröße bei der Schweißnahtprüfung. Betriebsforschungsinst. d. VDEh, Rep. No. 706. Düsseldorf 1978

1213 Pronyakin, V. T.; Anikheev, Ya. F.; Gorshkov, A. V.; Lovyakin, E. M.; Nemirowskii, M. G.; Zagorul'ko, V. S.: Ultrasonic flaw detection in finned tubes. Sov. J. Non Destr. Test. 6 (1970) 13–15.

1214 Pronyakin, V. T.; Kol'tsov, Yu. A.; Korshunov, A. V.; Kolomeitsev, L. P.: Instrument for recording the inspection results on nuclear reactor vessels. Sov. J. Non Destr. Test. 14 (1978) 687–690.

1215 Prot, A.: Contrôle des gaines du réacteur Phenix par ultrasons. 12e Coll. de Métallurgie, Saclay 1968 (Institut National des Sciences et Techniques Nucléaires).

1216 Pursey, H.: The launching and propagation of elastic waves in plates. Quart. J. Mech. Appl. Math. 10 (1957) Part I.

1217 Pursian, G.; Kipka, S.; Schiebold, K.-H.: Zur Schrecktiefenbestimmung an Hart-gußwalzen durch Ultraschall. Neue Hütte 16 (1971) 36–43.

1218 Quate, C. F.: Imaging using lenses. In: Wade, G, (Ed.): Acoustic imaging. New York: Plenum Press 1976, pp. 241–305.

1219 Raad de, J. A.; Engl. G.; Bergh, H.: Inside ultrasonic inspection of innernozzle radius corners of nuclear pressure vessels — Contact and immersion technique. In: DGZfP (Ed.): 4th Int. Conf. NDT in the Nuclear Field, Lindau 1981, Vol. 8, pp. 293–301

1220 Raad de, J. A.; Dijkstra, F. H.: Ultrasonic inspection of some critical areas of nuclear pressure vessels. In: Clough, R. B. (Ed.): Quantitative NDE in the nuclear industry. Proc. 5th Int. Conf. NDE in the Nuclear Industry, San Diego 1982, Metals Park: ASM 1983, pp. 47–51.

1221 Raad de, J. A.: Systeme für die Ultraschallprüfung des Primärkreises eines Druckwasserreaktors. Rotterdam: Röntgen Technische Dienst (RTD) 1983.

1222 Raeder, E.: System zur manuellen Bewertung von Ultraschallanzeigen einer im Fluss der Produktion installierten Grobblechprüfanlage. 3rd Europ. Conf. NDT, Florence 1984, Vol. 4, pp. 30–40.

1223 Raeder, E.; Sauer, U.: Praxiserfahrungen mit einer 100 % flächenprüfenden Ultra-schall-Grobblechprüfanlage im Produktionsfluß. 2nd Europ. Conf. NDT, Vienna 1981. pp. 399–400

1224 Rankin, A. W.: Boyle, C. J.; Moriarty, C. D.; Seguin, B. R.: Thermal cracks in turbine and generator rotor forgings. Mech. Eng. (1955) 559–566.

1225 Rankin, A. W.. Moriarty, C. D.: Acceptance guides for ultrasonic inspection of large rotor forgings. ASME Paper 55A 194 (1956).

1226 Rankin, C. A.: Autosonics — Problems and experiences in automatic production testing. Materialprüf. 2 (1960) 421–428.

1227 Rankin, C. A., Brooks, H. C.; Brown, A.: Ultrasonic inspection of the Nimrod power plant alternator rotors. Proc. 4th Int. Conf. NDT, London 1963. London: Butterworths Sci. 1964, pp. 196–202.

1228 Rasmussen, J. G.: Ultrasonic inspection of turbine and compressor rotor blades for cracks and other flaws. Non Destr. Test. 16 (1958) 228–236.

1229 Rasmussen, J. G.: Prediction of fatigue failure using ultrasonic surface waves. Non Destr. Test. 20 (1962) 103–110.

1230 Rassweiler, G. M.; Erwin, W. S.: Automatic sonic measuring means. US Pat. 2,431,234 (1944).

1231 Rath, R.; Thivin, M.: Some examples of non-destructive test methods used by Electricité de France. Proc. 4th Int. Conf. NDT, London 1963. London: Butterworths Sci. 1964, pp. 222–229.

1232 Rath, W.: In-service inspection of reactor pressure vessels. Power Eng. (July 1973) 40–43.

1233 Rath, W.: Possibilities and requirements for repetitive test on nuclear reactors. Int. Symp. Mechanization and Automation of Inspection on Pressurized Plants. Dec. 1973, Tokyo, Japan.

1234 Rath, W.: Erfahrungen mit Ultraschallprüfungen an Kernreaktoren. Kerntechnik 16 (1974) 538–542.

1235 Rathgeb, W.; Winter, R.: Einsatz der Ultraschallholografie zur Fehlergrößenbestimmung bei wiederkehrenden Prüfungen an nuklearen Komponenten. Siemens Forsch.- u. Entwickl.-Ber. 8, No. 2 (1979) 82–85

1236 Rauscher, R.: Computerized ultrasonic tube testing systems with special reference to the installation in tube mills for nuclear tubing of fuel fabrication facilities. In: Clough, R. B. (Ed.): Quantitative NDE in the Nuclear Industry. Metals Park ASM 1982, pp. 225–228.

1237 Rauterkus, W.: Schwerer Stahlguß in der Ultraschallprüfung. Gießerei 17 (1960) 475–486.

1238 Rauterkus, W.: Vorschlag zur zahlenmäßigen Kennzeichnung von Ergebnissen der Ultraschallprüfung an Schmiedestücken. Arch. Eisenhüttenwes. 34 (1963) 601–604.

1239 Rawding, H.: Ultrasonic testing standards. Ultrasonics 1 (1963) 35–38.

1240 Razygraev, N. P.; Ermolov, I. N.: Probes for surface-layer inspection by means of head-waves. Sov. J. Non Destr. Test. 17 (1981) 40–47.

1241 Read, T. A.: The internal friction of single metal crystals. Phys. Rev. 58 (1940) 371–380.

1242 Rechner, W.: Praktische Ultraschallergebnisse bei der Fehlergrößenbestimmung nach dem AVG-Diagramm. ZIS-Mitt. 11 (1969) 1227–1234.

1243 Rechner, W.: Einfluß der Oberflächenrauhigkeit und des Schweißgutes bei der US-Prüfung mit Winkelprüfköpfen. ZIS-Mitt. 8 (1968) 1365–1375.

1244 Rechner, W.: Prüftechnologien für die Ultraschallprüfung an speziellen Schweißverbindungen. ZIS-Mitt. 5 (1971) 644–653.   [No ref. 1245]

1246 Redwood, M.: A study of waveforms in the generation and detection of short ultrasonic pulses. Appl. Mater. Res. 2 (1963) 76–84.

1247 Redwood, M.: Ultrasonic waveguides — a physical approach. Ultrasonics 1 (1963) 99–105.

1248 Regalbuto, J. A.: Correlation of pulse-echo measurement with tensile strength of diffusion bonded joints. Mater. Eval. 30 (1972) 66—72.

1249 Regazzo, R.; Regazzo, M.; Cermak, F.: Correlation between ultrasonic attenuation and transition temperature to brittle fracture of steels. 10th World Conf. NDT Moscow 1982. Vol. 5, pp. 46–56. (Acad. Sci. USSR).

1250 Reimann, K. J.: A brazed high-temperature ultrasonic transducer. 7th Int. Conf. NDT, Warszawa 1973, Paper C 27

1251 Renken, C. J.; Selner, R. H.: Refractory metal tubing inspection using ultrasonics and pulsed eddy current methods. Mater. Eval. 24 (1966) 257–262.

1252 Réti, P.: Evaluation of shrinkage bond quality by an ultrasonic test method. 7th Int. Conf. NDT, Warszawa 1973. Paper C 31

1253 Réti, P.: Gütekontrolle von kugelgraphitischem Gußeisen mit Ultraschall. Wiss. Z. Hochsch. Schwermaschinenbau Magdeburg 3 (1959) 195–202.

1254 Reverey, G.: Die zerstörungsfreie Prüfung von Isolatoren. ETZ-A 73 (1952) 451–455.

1255 Reynolds, W. N.: Nondestructive examination of composite materials — a survey of European literature. Atomic Energy Research Establishment, Harwell (May 1980) AD-A086 165

1256 Reynolds, W. N.; Wilkinson, S. J.: The nondestructive physical analysis of concrete Br. J. Non Destr. Test. 21 (1979) 35–38.

1257 Reynolds, W. N.; Smith, R. L.: The detection of small defects in ceramic materials: a comparison of ultrasonic and radiographic methods. Br. J. Non Destr. Test. 24 (1982) 145–151.

1258 Richard, B.; Fink, M.; Alais, P.: New arrangements for Fresnel focusing. In: Wang, K. Y. (Ed.): Acoustical Imaging, Vol. 9. New York: Plenum Press 1980 pp. 65–73.

1259 Richter, H. U.; Fischer, C.: Some properties of polarized shear waves. In: Proc. 10th World Conf. NDT, Moscow 1982, Vol. 3, pp. 396–402. (Acad. Sci. USSR).

1260 Richter, H.-U.: Zur Ultraschallprüfung austenitischer Schweißverbindungen. Technik 23 (1968) 610–618; 692–696.

1261 Richter, H. U.: Vergleich und Tendenzen internationaler Richtlinien zur Ultraschallprüfung von Schweißverbindungen. Schweißtechnik 21 (1971) 151–159.

1262 Richter, H. U.: Zur Bestimmung der wirklichen Ungänzengröße bei der Ultraschallprüfung von Schweißverbindungen. ZIS-Mitt. 11 (1969) 1235–1242.

1263 Richter, H. U.: Ist ein ‚Materialfehler' ein Materialfehler? Technik 29 (1974) 320–322.

1264 Richter, H. U.: Herstellen und Prüfen von sprengplattierten Verbundwerkstoffen. Schweißen u. Schneiden 24 (1972) 52–55.

1265 Richter, H. U.: Prüfgerechte Konstruktionen. Spezifische Bedingungen der zerstörungsfreien Werkstoffprüfung. Schweißtechnik 23 (1973) 77–81.

1266 Richter, H. U.; Linke, D.: Automatische Ultraschallimmersionsprüfanlage mit A- und B-Bild sowie Digitalanzeige für schwere Schmiedestücke. Neue Hütte 9 (1964) 455–460.

1267 Richter, H. U.; Linke, D.; Jahn, P.: Zur ultraakustischen Prüfung von Verbundmetallen. Maschinenbautechnik 14 (1965) 169–176.

1268 Rieckmann, P.: Über den Nachweis von Fehlstellen bei der Reifenprüfung nach dem Ultraschall-Durchstrahlungsverfahren. Z. Angew. Phys. 8 (1956) 386–391.

1269 Ries, K.; Thiele, H.; Völker, J.: Verbesserung der Qualitätssicherung durch Verwendung von Dialoggeräten. 3rd Europ. Conf. NDT, Florence 1984, Vol. 3, pp. 342–352.

1270 Ries, K.; Wiedenhoff, W.: Einsatz neuer Prüfverfahren bei der zerstörungsfreien Prüfung von Großrohren. 1st Europ. Conf. NDT, Mainz 1978, Paper 25

1271 Rittler, A.: Echolotmessungen als Hilfsmittel für die Zuchtwertschätzung beim Schwein. 3. Mitt: Abschätzung des Fleisch- und Fettanteils auf Grund von Echolotmessungen am lebenden Schwein. Z. Tierzücht. u. Züchtungsbiol. 85 (1969) 78–89.

1272 Rivecuz, J.: Determination non destructive de la resistance de joints collés par analyse fine d'échos ultrasonore. 3rd Europ. Conf. NDT, Florence 1984, Vol. 5, pp. 117–126.

1273 Robba, M.; Martelli, C.: Controlli non distruttivi di fabbricazione su tubi di guaina aleatti per elementi combustibili nucleari tipo Orgel. Metallurgia Ital. 4 (1968) 293–307.

636   References

1274 Robinson, D. E.; Lees, S.; Bess, L.: Near field transient radiation patterns for circular pistons. IEEE Trans. Acoust. Speech Signal Process. 22 (1974) 395–403.
1275 Roderick, R. L.: The radiation pattern from a rotationally symmetric stress source on a semi infinite solid. Metals Res. Rep. Brown University 1950 (USA).
1276 Roderick, R. L.; Truell, R.: The measurement of ultrasonic attenuation in solids by the pulse technique and some results in steel. J. Appl. Phys. 23 (1952) 267–279.
1277 Röhrich, H.; Figlhuber, D.; Kunz, A.; Ganglbauer, O.; Lodder, M.; Tokaya, M.: Automatisierung der Ultraschall-Fertigungsprüfung. In: Österr. Ges. ZfP (Ed.): 2nd Europ. Conf. NDT, Vienna 1981, pp. 139–142
1278 Römer, M.; Matthies, K.; Schmid, R.; Neumann, E.: Schallfeldfokussierung mit Zonenplatten-Prüfköpfen — eine einfache Methode zur Fehlergrößenabschätzung. In: Österr. Ges. ZfP (Ed.): 2nd Europ. Conf. NDT, Vienna 1981, pp. 282–284
1279 Römer, M.; Neumann, E.; Kuhlow, B.; Mundry, E.: Fresnelsche Zonenplatte zur Schallfeldfokussierung. Materialprüfung 21 (1979) 363–365.
1280 Rogel, A. P.; Moore, S. E.: Use of Boeing portable ultrasonic scanner for inspection of fastener hole cracks on a fatigue tested aircraft wing. ASNT Fall Conf. 1977, Detroit, Mich.
1281 Rogerson, A.; Poulter, L. N. J.; Dyke, A. V.; Tickle, H.: Near surface defect detection and sizing studies at Risley Nuclear Laboratories (RNL). In: Periodic inspection of pressurized components, I. Mech. E. Conf. Publ. 1982-9. London: Mech. Eng. Publ. 1982, pp. 147–154.
1282 Rokhlin, S. I.: Interaction of Lamb waves with elongated delaminations in thin sheets. In: McGonnagle, W. J. (Ed.): International Advances, Vol. 6. London: Gordon and Breach, 1979, pp. 263–285.
1283 Rokhlin, S. I.: Resonance phenomena of Lamb waves scattering by a finite crack in a solid layer. J. Acoust. Soc. Am. 69 (1981) 922–928.
1284 Rokhlin, S. I.: Evaluation of the curing of structural adhesives by ultrasonic interface waves, correlation with strength. J. Compos. Mater. 47 (1983) 15–25.
1285 Roll, K. H.: Inspection and testing lead linings. Non Destr. Test. 16 (1956) 20–24.
1286 Rollins, F. R.: Ultrasonic reflectivity of single and polycrystalline samples of copper. Int. J. Non Destr. Test. 1 (1969) 127–145.
1287 Rollins, F. R.: Study of methods for non-destructive measurement of residual stress. W. A. D. C. Tech. Rep. 59–561 (Dec. 1959).
1288 Rollins, F. R.: Ultrasonic methods for non-destructive measurement of residual stress. W. A. D. C. Tech. Rep. 61-42 (May 1961).
1289 Rooney, J.: NDT of silicon carbide tubes. Int. J. Non. Destr. Test. 6 (1973) 146–153.
1290 Rose, J. L.; Meyer, P. A.: Ultrasonic procedures for predicting adhesive bond strength. Mater. Eval. 31 (1973) 109–114.
1291 Rose, J. L.: Effects of selected electrode shapes on basic ultrasonic field parameters. Mater. Eval. 34 (1976) 114–120.
1292 Rose, J. L.: Elements of feature based ultrasonic inspection system. Mater. Eval. 42 (1984) 210–218.
1293 Rose, J. L.; Avioli, M. J.; Zeger, A.; Abrams, B.; Lapides, M.: Development and qualification of a feature based ultrasonic piping inspection system for the nuclear industry. In: DGZfP (Ed.): 4th Int. Conf. NDT in the Nuclear Field, Lindau 1981, Vol. 8, pp. 109–115
1294 Rose, J. L.; Avioli, M. J.; Bilgram, R.: A feasibility study on the nondestructive evaluation of an adhesively bonded metal to metal bond: an ultrasonic pulse echo approach. Br. J. Non Destr. Test. 25 (1983) 67–71.
1295 Rose, J. L.; Mortimer, R. W.; Chou, P. C.: Applications of dynamic photo-elasticity in flaw detection analysis. Mater. Eval. 30 (1972) 242–247.
1296 Rose, J. L.; Nestleroth, J. B.: Flaw classification in welded plates with a microprocessor controlled flaw detector. Rep. ADA 086755 (1980).
1297 Rose, J.; Nestleroth, J.; Niklas, L.; Ganglbauer, O.; Ausserwoeger, J.; Wallner,

F.: Flaw classification in welded plates employing a multidimension feature-based decision process. Mater. Eval. 42 (1984) 433–438, 443.

1298 Rose, J. L.; Singh, G. P.: A pattern recognition reflector classification feasibility study in the ultrasonic inspection of stainless steel pipe welds. Br. J. Non Destr. Test. 21 (1979) 308–311.

1299 Rosen, M.; Horrowitz, E.: An investigation of the precipitation hardening process in aluminium alloy 2219 by means of sound wave velocity and ultrasonic attenuation. Mater. Sci. Eng. 53 (1982) 163–177.

1300 Ross, J. D., Leep, R. W.: Ultrasonic transmission tester for detection of unbonded areas. Symp. NDT in the Field of Nuclear Energy. ASTM Spec. Tech. Publ. No. 223 (1958) 246–258

1301 Roth, W.: Scattering of ultrasonic radiation in polycrystalline metals. J. Appl. Phys. 19 (1948) 901–910.

1302 Roth, W.: Piezoelectric transducers. IRE 37 (1949) 750–758.

1303 Roule, M.: Émetteur-récepteur à ultrasons fonctionnant à haute température. Thèse présentée à la Faculté des Sciences de l'Université de Lille 1971.

1304 Roule, M.; Birac, A. M.; Saglio, R.: Système de visualisation de type B — Scan — examples d'application. In: Österr. Ges. ZfP (Ed.): 2nd Europ. Conf. NDT, Vienna 1981, pp. 137–138

1305 Rumbold, J. G.; Krupski, S.: Ultrasonic thickness variation measurement of hot forged cannon tubes. Mater. Eval. 39 (1981) 939–942.

1306 Ruppert, W.; Hesse, J.: Bestimmen der Betonfestigkeit durch Ultraschallverfahren. Baustoffindustrie 13 (1970) 259–262.

1307 Ryden, J.: NDT of small diameter stainless steel fuel clad tubing. Mater. Eval. 28 (1970) 67–71.

1308 Sachse, W.; Pao, Y.: Signals in the far-field of an AE source. Ultrasonics Int. 81 (1981) 116–122.

1309 Sachse, W.; Hsu, N. N.; Eitzen, D. G.: Visualization of transducer-produced sound fields in solids. Ultrasonics Symp. Proc. (1978) 139–143. IEEE Cat. No. 78 CH 1344-1 SU.

1310 Saglio, R.: In-service inspection of PWR reactor. IAEA Training Course on Assuring Pressure Boundary Integrity, Argonne Nat. Lab. Argonne, USA, 1982.

1311 Saglio, R.: Data acquisition system used in France for the inservice inspection of PWR vessels. In: Nichols, R. W. (Ed.): Advances in NDE for structural integrity. London: Appl. Sci. Publ. 1982, pp. 237–245.

1312 Saglio, R.; Birac, A. M.; Frappier, J. C.; Viard, J.: Special development made in France for the surveillance of subcladding defects. In: Periodic inspection of pressurized components, I. Mech. E. Conf. Publ. 1982-9. London: Mech. Eng. Publ. 1982, pp. 187–195.

1313 Saglio, R.; Verger, B.: Automatic examination of nuclear reactor vessels with focused search units — status and typical application to inspections performed in accordance with ASME code. In: DGZfP (Ed.): 4th Int. Conf. in the Nuclear Field, Lindau 1981, Vol. 8, pp. 371–378

1314 Saito, S.; Takahashi, M.: An automatic calibration system of the sensitivity in the ultrasonic testing equipment for the seamless steel pipe and tube (jap.). J. NDI 29 (1980) 705–711.

1315 Salokangas, J.: Das Dämpfungsvermögen als Kriterium der Festigkeit von Gußeisen. 6th Int. Conf. NDT, Hanover 1970, Vol. E, pp. 63–74

1316 Salzburger, H. J.: Blech- und Bandprüfung mit elektromagnetisch angeregten Platten- wellen. Materialprüfung 27 (1985) 297–300

1317 Salzburger, H. J.; Repplinger, W.; Hickethier, M.: Verfahren, Anordnung und Schaltung zur zerstörungsfreien Prüfung der Lauffläche von Eisenbahnrädern. DE Pat. 3 218 453 (1983).

1318 Sasaki, S.; Kanda, K.: Ultrasonic flaw detection technique using point-focused variable angle probes (jap.). Hihakai Kensa 30 (1981) 2–6.

1319 Sato, S.; Sasaki, S.; Kubota, J.; Ito, S.; Kadowaki, T.; Yomaguchi, H.; Fujisawa, K.; Murayama, R.: Ultrasonic testing of high temperature billet with electromagnetic transducer (jap.). J. NDI-Data Paper No. 2992 (1983).

1320 Sato, T.; Ueda, M.: Ultrasonic imaging using Debye-sears diffraction of light. Ultrasonics 12 (1974) 16–21.

1321 Sato, Y.: Reflection and diffraction at a crack or a corner. Simulation of an elastic medium by a network system of mass-particles (jap.). Hihakai Kensa 27 (1978) 180–185.

1322 Schaper, H.: Beitrag zur zerstörungsfreien Prüfung von glasfaserverstärkten Kunststoffen. Materialprüfung 10 (1968) 50–54.

1323 Schaper, H.; Stelling, H. A.: Beitrag zur Ultraschallprüfung von glasfaserverstärkten Kunststoffen. Grenzen der Meßgenauigkeit bei der Schallgeschwindigkeitsmessung. Materialprüfung 10 (1968) 337–342.

1324 Scharpenberg, R.; Bäro, G.: Erfahrungen mit einem Brennstab-Schaden-Nachweis-system (BSN) im Kernkraftwerksbereich. In: DGZfP (Ed.): 4th Int. Conf. NDT in the Nuclear Field, Lindau 1981, Vol. 8, pp. 441–446

1325 Schickert, G.: Results of test concerning combined non-destructive testing of concrete. In: Österr. Ges. ZfP (Ed.): 2nd Europ. Conf. NDT, Vienna 1981, pp. 378–380

1326 Schiebold, K.; Pesslies, H.; Koehler, K.: Technological determination of usability limits in ultrasonic testing of forgings. 7th Int. Conf. NDT, Warszawa 1973, Paper C 47

1327 Schiebold, K. H.; Tietz, H. D.: AVG-Vorsatzskalen zur Fehlergrößenabschätzung bei der Ultraschallprüfung von Schmiedestücken. Neue Hütte 15 (1970) 557–560.

1328 Schiebold, K. H.; Wrobel, H. J.; Pohl, H. J.: Investigations into ultrasonic inspection of forgings at elevated temperatures by means of dry pressure contact. 10th World Conf. NDT, Moscow 1982, Vol. 7, pp. 298–306. (Acad. Sci. USSR).

1329 Schijve, J.: Ultrasonic resonance testing of glued metal joints. Aircraft Eng. 30 (1958) 269–271.

1330 Schinn, R.; Wolff, U.: Einige Ergebnisse der Überschallprüfung schwerer Schmiedestücke mit dem Impuls-Echo-Verfahren. Stahl u. Eisen 72 (1952) 695–702.

1331 Schlengermann, U.: Über die Verwendung der Begriffe Nahfeld und Fernfeld in der Ultraschall-Werkstoffprüfung. Materialprüfung 15 (1973) 161–166.

1332 Schlengermann, U.: Schallfeldausbildung bei ebenen Ultraschallquellen mit fokussierenden Linsen. Acustica 30 (1974) 291–300.

1333 Schlengermann, U.: Bestimmung des Schalldruckverlaufs und der Nahfeldlänge von Ultraschall-Prüfköpfen mit der Mehrfachechofolge. Materialprüfung 15 (1973) 337–341.

1334 Schlengermann, U.: Ultraschallverfahren zur Bestimmung der Anzahl von Einschlüssen in Materialproben — eine kritische Betrachtung empfohlener Methoden. Z. Werkstofftechnik 5 (1974) 242–248.

1335 Schlengermann, U.; Frielinghaus, R.: Beitrag zur Fehlergrößenbestimmung mit Ultraschall durch Fehlerabtastung mit relativer Schwelle. Materialprüfung 15 (1973) 50–56.

1336 Schlengermann, U.: Bemerkungen über die Nahfeldlängen-Bestimmung bei Ultraschall-Kolbenstrahlern verschiedener Form. Materialprüfung 16 (1974) 129–131.

1337 Schlengermann, U.: Schallfeldausbildung bei ebenen Ultraschallquellen mit fokussierenden Linsen. Acustica 30 (1974) 291–300.

1338 Schlengermann, U.: Beitrag zur Fehlergrößenbestimmung mit Ultraschall durch Fehlerabtastung mit fester Schwelle. Materialprüfung 16 (1974) 319.

1339 Schlengermann, U.: Schallfelder der Ultraschall-Werkstoffprüfung. Vortrag zur Verleihung des Berthold-Preises, Conf. DGZfP 1975, Berlin

1340 Schlengermann, U.: Die Abhängigkeit zwischen Ultraschallfeld und Prüfzone bei der Rohrprüfung. Materialprüfung 18 (1976) 366–372.

1341 Schlengermann, U.: Vergleichende Überlegungen zum Schallfeld von rechteckigen

Ultraschallwandlern. DAGA (Dtsche Arbeitsgemeinschaft Akustik) 1976, Düsseldorf: VDI-Verlag, pp. 385–388

1342 Schlengermann, U.: Beurteilung effektiver Schallfelddaten aus dem Entfernungsgesetz des Schalldrucks. Materialprüfung 19 (1977) 53–58.

1343 Schlengermann, U.: Kriterien zur Auswahl fokussierender Ultraschall-Prüfköpfe. Materialprüfung 19 (1977) 416–420.

1344 Schlengermann, U.: On the efficiency of installations for testing tubes ultrasonically. Proc. 9th World Conf. NDT, Melbourne 1979. Rep. 1C-7.

1345 Schlengermann, U.: The characterization of focusing ultrasonic transducers by means of single frequency analysis. Mater. Eval. 38 (1980) 73–75, 79. ·

1346 Schlengermann, U.: Normalizing distance-amplitude-curves of side-drilled holes in ultrasonic testing. Mater. Eval. 39 (1981) 1138–1142.

1347 Schlengermann, U.: Charakterisierung von Reflektoren mit Ultraschallmethoden. Vortrag beim Erfahrungsaustausch ZfP. Schweißtechnische Lehr- und Versuchsanstalt Duisburg, 1982

1348 Schlengermann, U.; Frielinghaus, R.: Beitrag zur Fehlergrößenbestimmung mit Ultraschall durch Fehlerabtastung mit relativer Schwelle. Materialprüfung 15 (1973) 50–56.

1349 Schlengermann, U.; Frielinghaus, R.: Erläuterungen zum Ultraschallprüfen mit fokussierenden Prüfköpfen. DGZfP Symp. Neue Verf. Analys. Ultraschall Befund, Berlin 1977, pp. 9–22

1350 Schlengermann, U.; Wielpütz, U.: Beitrag zur Ersatzfehlergrößenbestimmung beim Ultraschallprüfen nach der Tandemmethode. Schweißen u. Schneiden 26 (1974) 169–172.

1351 Schliekelmann, R. J.: NDT of adhesive bonded metal-to-metal joints (2). Non Destr. Test. 5 (1972) 144–153.

1352 Schlusnus, K. H.; Koch, F. O.: Prüfung von Spiralrohren. Bänder, Bleche, Rohre 6 (1963) 282–286.

1353 Schlusnus, K. H.; Krenzer, P.; Stadler, A.: NDT for laminar defects by shock wave method. 7th Int. Conf. NDT, Warszawa 1973, Paper C 45

1354 Schmerling, J. M.; Hammon, J. C.: Investigation of the Tenessy Valley Authority Gallatin Unit No. 2 turbine rotor burst. Proc. Am. Power Conf. 1976, Vol. 38, pp. 545–548.

1355 Schmauch, H.: Über ein neues Verfahren zur Messung von Schallgeschwindigkeit mit hoher Genauigkeit. Ann. Univ. Sar. 3 (II) (1953) 257–269.

1356 Schmidt, B.; Sell, B.: Praxis der Ultraschallprüfung zur Fehlerermittlung bei Gußeisen. Gießerei 66 (1979) 716–720.

1357 Schmidt, P.: Die Ultraschallanalyse als zerstörungsfreie Werkstoffuntersuchung an Hartkohle und Elektrographiten. Schunk & Ebe-Blätter Nr. 29 (1978) 13–16.

1358 Schmidt, W.; Egelkraut, K.: Der Einfluß von Fettspuren in der Grenzschicht des Schrumpfsitzes auf die Ergebnisse seiner Ultraschallprüfung. Conf. DGZfP, Mainz 1978, Vol. 2, pp. 309–314

1359 Schmitt-Thomas, K. G.; Hagn, L.: Aussagekraft zerstörungsfreier Schrumpfsitzprüfungen unter besonderer Berücksichtigung von Ultraschall- und Wärmeflußverfahren. Maschinenschaden 43 (1970) 25–31.

1360 Schmitz, V.: Bedeutung der Ultraschall-Holographie als Abbildungsverfahren von Werkstoffehlern. Fraunhofer-Ges.-Ber. 3 (1978).

1361 Schmitz, V.; Goebbels, K.: Improvement of signal-to-noise ratio for the ultrasonic testing of coarse grained material by digital RF-digital averaging. IEEE Ultrasonics Symp. San Diego 1982 (McAvoy, B. R., Ed.). Vol. 2, pp. 950–953.

1362 Schmitz, V.; Langenberg, K. J.; Jackson, J.; Wüstenberg, H.: Improved methods for ultrasonic defect classification reconstruction and reliability. In: Clough, R. B. (Ed.): Quantitative NDE in the nuclear industry, Proc. 5th Int. Conf. NDE in the Nuclear Industry, San Diego 1982. Metals Park: AMS 1983, pp. 258–264.

1363 Schmitz, V.; Müller, W.; Schäfer, G.: A new ultrasonic imaging system. Mater. Eval. 40 (1982) 101–108.

1364 Schmitz, V.; Wosnitza, M.: Experiences in using ultrasonic holography in the laboratory and in the field with optical and numerical reconstruction. In: Metherell, A. F. (Ed.): Acoustical imaging, Vol. 8. New York: Plenum Press 1980, pp. 651 to 683.

1365 Schneider, E.; Goebbels, K.: Zerstörungsfreie Bestimmung von (Eigen-)Spannungen mit linear polarisierten Ultraschallwellen an Reaktorbaustählen. In: DGZfP (Ed.): 4th Int. Conf. NDT in the Nuclear Field, Lindau 1981, Vol. 8, pp. 313–319

1366 Schneider, E.; Goebbels, K.: Determination of mechanical stress by polarized shear waves. In: Höller, P. (Ed.): New procedures in NDT. Proc. Germany-US Workshop, Saarbrücken 1982. Berlin: Springer 1983, pp. 551–560.

1367 Schneider, H.: Mathematisches Simulationsprogramm für die Ultraschall-Schweiß-nahtprüfung von Großrohren. MAN Forschungsinst. GmbH, Duisburg 1980. Status-ber. Eisen- und Stahlforschung KFA Jülich, pp. 504–510

1368 Schneider, H.: The NDT of tubes and pipes for nuclear application. Nucl. Eng. Des. 81 (1984) 69–76.

1369 Schneider, H.; Baethman, H. J.; Peters, P.: Computer-controlled ultrasonic testing of plates for line-pipes. Proc. 10th World Conf. NDT, Moscow 1982, Vol. 6, pp. 136–152 (Acad. Sci. USSR).

1370 Schneider, H.; Bäthmann, H. J.: Neue Erkenntnisse bei der ZfP. Bänder, Bleche, Rohre 19 (1978) 329–332.

1371 Schroeder, K.: NDT of plastic joints. Proc. 10th World Conf. NDT, Moscow 1982, Vol. 5, pp. 386–394 (Acad. Sci. USSR).

1372 Schröder, K.: ZfP von Plastverbindungen. ZIS-Mitt. 24 (1982) 808–814.

1373 Schoch, A.: Seitliche Versetzung eines total reflektierten Strahls bei Ultraschall-wellen. Acustica 2 (1952) 18–22.

1374 Schöder, K. H.: Ultraschall-Kontrolle der Graphitausbildung bei Gußeisen mit Kugelgraphit. Conf. DGZfP. Saarbrücken 1972

1375 Scholte, J. G.: On the large displacements commonly regarded as caused by Love-waves and similar dispersive surface waves. Proc. Koninkl. Ned. Akad. Wetenschap 51 (1948) 533–543.

1376 Scholz, A.: Zerstörungsfreie Werkstoffprüfung von Generator-Rotor-Zähnen mittels Ultraschall. Europ. Pat. 82000492.5 (1983) und: Nondestructive method and device for ultrasonic testing of the material of generator rotor teeth. US Pat. 4,457,176 (1984).

1377 Schork, L.: Semi automatic ultrasonic testing of brazed components. 7th Int. Conf. NDT, Warszawa 1973. Paper C 06

1378 Schrodt, H.: Werkstoffprüfung mit Ultraschall bei der Deutschen Bundesbahn, insbesondere in der Anwendung bei Fahrzeugachsen. Eisenbahntech. Rdsch. 9 (1960) 245–255.

1379 Schubert, K.: Ultraschallprüfung von Wärmeaustauscherrohren mit rotierenden Prüfköpfen. Kerntechnik 20 (1978) 218–220.

1380 Schütze, R.: Delaminationen und deren Auffindung in CFK-Laminaten. In: Österr. Ges. ZfP (Ed.): 2nd Europ. Conf. NDT, Vienna 1981, pp. 381–384

1381 Schulz, E.; Wegner, W.; Wüstenberg, H.; Mundry, E.: Automatisierung der Wand-dickenmessung mit US an Rohren bei der Prüfung von der Innenseite. In: Österr. Ges. ZfP (Hrsg.): 2nd Europ. Conf. NDT, Vienna 1981, pp. 159–160

1382 Schulz, E.; Wüstenberg, H.; Erhard, A.: Nachweis von Rissen an der Stutzenkante bei Prüfung von aussen an Siedewasserreaktoren. 3rd Europ. Conf. NDT, Florence 1984, Vol. 2, pp. 143–155

1383 Schumann, B.; Herman, K.; Busse, H.: Praktische Erfahrungen bei der zerstörungs-freien Prüfung von Stahlguß auf innere Fertigungsfehler. In: DGZfP (Ed.): 4th Int. Conf. NDT in the Nuclear Field, Lindau, 1981, pp. 237–245

1384 Schuster, K.: Ultraschall-optische Abbildung nach dem Reliefbild-Verfahren. Jenaer Jb. 1951, pp. 217–228

1385 Schwenk, E. B.; Shearer, C. D.: Measuring projection weld strength by acoustic emission. Non Destr. Test. 6 (1973) 29–33.

1386 Schwindt, D.: Zerstörungsfreie Prüfungen an Gußstücken aus Kupfer und Kupfer-legierungen. Gießerei 66 (1979) 90–94.

1387 Scruby, C. B.; Dewhurst, R. J.; Hutchins, D. A.; Palmer, S. B.: Laser generation of ultrasound in metals. In: Sharpe, R. S. (Ed.): Research techniques in NDT, Vol. 5. London: Academic Press 1982, pp. 281–325.

1388 Searles, C. E.; Kleinberg, K. E.: Advanced ultrasonic inspection system for the Lockheed L-1011 adhesive bonded fuselage panels. Tech. Paper for 1971 Western Metal and Tool Conf. and Exposition 1 Q 71-746.

1389 Secco, E.; Canapari, C.: Esame con ultrasuoni (metodo dell'eco-impulso) di saldature in AISI 304 die grosso spessore problemi e considerazioni. Metall Ital. 71 (1979) 185–190.

1390 Seifert, H.; Machts, H.: Zerstörungsfreie Prüfung von Feuerbetonen. Baustoff-industrie 21, Nr. 4 (1978) 9–12.

1391 Seiger, H.: Zur Ultraschallprüfung der sphärischen Lochfeldbereiche von Leicht-wasser-Reaktordruckbehältern. Krautkrämer GmbH, Köln, Ber. A/1/258 (1975).

1392 Seiger, H.: Comparison of three flaw-location methods for automated ultrasonic testing. Non Destr. Test. Int. 15 (1982) 131–135.

1393 Seiger, H.; Engl, G.: Experimentelle Untersuchungen am Kugelboden eines Siede-wasser-Reaktors zur Bestimmung einer geeigneten Ultraschall-Prüftechnik für die Lochfeldbereiche von Leichtwasser-Reaktoren. Krautkrämer GmbH, Köln; KWU AG, Erlangen (Eds.). Krautkrämer-Ber. A/1/315, Teil 1 u. Teil 2, (1976).

1394 Seiger, H.; Engl, G.: Ultrasonic inspection of the spherically shaped perforated areas of light water reactor pressure vessels. Non Destr. Test. Int. 10 (1977) 293–296.

1395 Seiger, H.; Günther, W.; Klein, V.; Rehrmann, M.: Ultraschallprüfkopf mit variablen Schallfeldparametern. In: Österr. Ges. ZfP (Ed.): 2nd Europ. Conf. NDT, Vienna 1981

1396 Seiger, H.; Wagner, J.: Experimentelle Bestimmung der optimalen Prüfkopf-Ankop-pelspaltdicke für mechanisierte Kontakttechnik-Ultraschallprüfungen. In: DGZfP (Ed.): 4th Int. Conf. NDT in the Nuclear Field, Lindau 1981, Vol. 8, pp. 303–311

1397 Seiger, H.; Wagner, J.: Flaw classification by a spectral division of ultrasonic echoes. Non Destr. Test. Int. 16 (1983) 195–200. — dito in: 3rd Europ. Conf. NDT, Florence 1984, Vol. 3, pp. 191–204.

1398 Seki, H.; Granato, A.; Truell, R.: Diffraction in the ultrasonic field of a piston source and their importance in the accurate measurement of attenuation. J. Acoust. Soc. Am. 28 (1956) 230–238.

1399 Serabian, S.: Influence of geometry upon an ultrasonic defect size determination in large rotor forgings. Non Destr. Test. 14 (1956) 18–21

1400 Serabian, S.: Frequency and grain size dependency of ultrasonic attenuation in polycristalline materials. Br. J. Non Destr. Test. 22 (1980) 69–77.

1401 Serabian. S.: An assessment of the detection ability of the angle beam interrogation method. Mater. Eval. 39 (1981) 1243–1249.

1402 Sette. D.: Ultrasonic lenses of plastic materials. Ric. Sci. 18 (1948) 831–842.

1403 Seydel, J. A.: Ultrasonic synthetic-aperture focusing techniques in NDT. In: Sharpe, R. S. (Ed.): Research techniques in NDT. Vol. 6. London: Academic Press 1982, pp. 1–42.

1404 Sharpe, R. S.; Aveyard. S.: The visualization of an ultrasonic extinction network in coarse grained uranium. Appl. Mat. Res. 1 (1962) 170–175.

1405 Shcherbinskij, V. G.; Belij, V.: New information index for the nature of flaws in ultrasonic inspection. Sov. J. Non Destr. Test. 11 (1975) 279–288.

1406 Sheikin, A. A.; Bogdanov, G. P.; Lebedev, L. K.: Inspecting the porosity of

support rod insulators with the use of ultrasonics. Sov. J. Non Destr. Test. 16 (1980) 677–683.

1407 Shenefelt, G. A.: Ultrasonic testing: Requirements of the AWS 1969 building code and bridge specifications. Weld. J. 50 (1971) 342–349.

1408 Shirai, T.; Nosaka, H.; Matsubara, T.; Fukui, S.: Development of ultrasonic inspection tool for reactor vessels. In: DGZfP (Ed.): 4th Int. Conf. NDT in the Nuclear Field, Lindau 1981, Vol. 8, pp. 277–284

1409 Shiraiwa, T.; Yamaguchi, H.; Tomabechi, M.; Kobayashi, Y.: Automatic Ultrasonic Testing Equipment for Pipeline Girth Welds. Proc. 9th World Conf. NDT, Melbourne 1979. Rep. 1C-16.

1410 Shirley, D. J.; Diercks, K. J.: Analysis of the frequency response of simple geometric targets. J. Acoust. Soc. Am. 48 (1970) 1275–1282.

1411 Shraiber, D. S.: Einige Probleme der Fehlerprüfung mit Ultraschall (russ.). Zawodskaja Laboratorija 11 (1945) 1052.

1412 Silber, F. A.: Entwicklung einer Ultraschall-Anlage zur automatischen Prüfung vorgewalzter Brammen. Berg- u. hüttenm. Monatsh. 108 (1963) 8–14.

1413 Silber, F. A.; Ganglbauer, O.: Die Ultraschallprüfung heißer Schweißnähte. Schweißtechnik 23 (1969) 125–128.

1414 Silk, M. G.: Defect sizing using ultrasonic diffraction. Br. J. Non Destr. Test. 21 (1979) 12–15.

1415 Silk, M. G.: A time approach to crack location and sizing in austenitic welds. Br. J. Non Destr. Test. 22 (1980) 55–61.

1416 Silk, M. G.: Ultrasonic techniques for inspecting austenitic welds. In: Sharpe, R. S. (Ed.): Research techniques in NDT, Vol. 4. London: Academic Press 1980, pp. 393–449.

1417 Silk, M. G.: Ultrasonic developments in the UK for reactor pressure vessel weldments. In: Nichols, R. W. (Ed.): Advances in nondestructive examination for structural integrity. London: Appl. Sci. Publ. 1982, pp. 101–116.

1418 Silk, M. G.: Sizing crack-like defects by ultrasonic means. In: Sharpe, R. S. (Ed.): Research techniques in NDT, Vol. 3. London: Academic Press, Chap. 2.

1419 Silk, M. G.; Bainton, K. F.: The propagation in metal tubing of ultrasonic wave modes equivalent to Lamb waves. Ultrasonics 17 (1979) 11–19.

1420 Simmank, D.; Fischer, H. Ch.: Entwicklungsstand einer Ultraschall-Schweißnaht-prüftechnologie für Schweißnähte in Druckgefäßen aus AlMg3F18. ZIS-Mitt. 23 (1981) 1190–1194.

1421 Singh, A.; Burger, C. P.; Schmerr, L. W.; Zachary, L. W.: Dynamic photoelasticity as an aid to sizing surface cracks by frequency analysis. In: Mechanics of NDT. New York: Plenum Press 1980, pp. 277–292.

1422 Singh, G. P.: A technique for notch depth determination using pulse-echo Rayleigh waves. Mater. Eval. 39 (1981) 1232–1236.

1423 Singh, G. P.; Manning, R. C.: A portable system for classification of ultrasonic indications. In: Clough, R. B. (Ed.): Quantitative NDE in the nuclear industry. Proc. 5th Int. Conf. NDE in the Nuclear Industry, San Diego 1982. Metals Park: ASM 1983, pp. 423–426.

1424 Singh, G. P.; Rose, J. L.: A simple model for computing ultrasonic beam behaviour of broad-band transducers. Mater. Eval. 40 (1982) 880–885.

1425 Sipek, M.: Zur Anwendbarkeit des Plattenwellenverfahrens bei der Ultraschall-prüfung. Materialprüfung 8 (1966) 294–297.

1426 Skordev, A.: Criteria and indizes for the selection of reference reflectors in ultrasonic metrology of discontinuities. 3rd Europ. Conf. NDT, Florence 1984, Vol. 3, pp. 517–527.

1427 Skordev, A.; Merkulov, L. G.; Nikolov, R.; Petrov, A.: Attempt for systematizing the amplitude relationships in the reflection of ultrasonic Lamb waves from surface grooves. 7th Int. Conf. NDT, Warszawa 1973, Paper C 15

1428 Skorupa, A.; Hyrnik, E.; Jedrzejczak, Z.: Bestimmung der wirklichen Fehlergröße in Stumpfschweißnähten mit Hilfe der AVG-Skalen. Krautkrämer Echo 26 (1972) 433–434.

1429 Skorupa, A.: Ausgewählte Probleme zur Interpretation der Ergebnisse von Ultraschallprüfungen an Stumpfschweißverbindungen (poln.). Wiss. H. Stanislaw Starsic Akad. Kraków 1974, Nr. 429.

1430 Skorupa, A.; Jedrzejczak, Z.; Hyrnik, E.: Qualitätskriterien von Schweißnähten nach dem Ultraschallverfahren. 2nd Europ. Conf. NDT Wien 1981, pp. 123–125.

1431 Sloushch, V. G.; Reznik, L. A.: An ultrasonic defectoscope for detection pressing cracks in unfired fireclay articles. Ogneupory No. 5 (1968) 13–17.

1432 Smit, H.; Berner, K.; Künne, G.: Fehlergrößenermittlung mit Ultraschall zur Klassifizierung von Grobblechen nach den Stahl-Eisen-Lieferbedingungen 072/US geprüftes Blech. Stahl u. Eisen 100 (1980) 1555–1559.

1433 Smit, H.; Paassen, H.: Automatisierte Ultraschallprüfung von Warmband nach dem Impuls-Echo-Verfahren mit Lamb-Wellen. Arch. Eisenhüttenwes. 46 (1975) 465–469.

1434 Smith, R. et al.: Surface acoustic wave Weiner filtering. IEEE Ultrasonics Symp. 1976.

1435 Smith, R. L.; Reynolds, W. N.; Wadley, H. N. G.: Ultrasonic attenuation and microstructure in low-carbon steels. Metal. Sci. 15 (1981) 554–558.

1436 Smith, R. L.; Rusbridge, K. L.; Reynolds, W. N.; Hudson, B.: Ultrasonic attenuation, microstructure, and ductile to brittle transition temperature in Fe-C alloys. Mater. Eval. 41 (1983) 219–222.

1437 Smith, R. T.: Stress-induced anisotropy in solids, the acousto-elastic effect. Ultrasonics 1 (1963) 3.

1438 Smyth, C. N. et al.: The ultrasound image camera. Proc. IEEE 110 (1) (1963) 16–28.

1439 Smyth, C. N.: The ultrasound camera — recent considerations. Ultrasonics 4 (1966) 15–20.

1440 Söderström, G.; Thörnquist, R.: Ultrasonic testing of scanning tubes for the Marviken reactor boiler fuel elements. 12ᵉ Coll. de Métallurgie, Saclay 1968 (Institut National des Sciences et Techniques Nucléaires).

1441 Sokolov, S. Ja.: Zur Frage der Fortpflanzung ultraakustischer Schwingungen in verschiedenen Körpern. ENT 6 (1929) 454–461.

1442 Sokolov, S. Ja.: Ultrasonic waves and their application (in Russian). Tech. Phys. 2 (1935) 522–544

1443 Sokolov, S. Ja.: Ultrasonic methods for detecting internal defects in metallic objects (in Russian). Zawodskaja Laboratorija 4 (1935) 527, 1468–1473

1444 Sokolov, S. Ja.: Means for indicating flaws in materials. US Pat. 2,164,125 (1937)

1445 Sokolov, S. Ja.: Ultrasonic methods for investigation of the properties of heat treated steel and for detecting internal defects in metallic objects (in Russian). Tech. Phys. 11 (1941) 160–169

1446 Sokolov, S. Ja.: Uses of ultrasound in technology and physics. Industrial Lab. 14, No. 11 (1949) 1328–1335.

1447 Sorel, M.; Aubert, J.; Brand, A.: Assemblages boulonnés — mesure de la tension de serrage par méthode ultrasonore. CETIM-Inf. No. 78 (1982) 1–7.

1448 Souquet, J.; Kino, G. S.; Waugh, T.: Chirp focused transmitter theory. In: Kessler, L. W. (Ed.): Acoustical holography, Vol. 7. London: Plenum Press 1977, pp. 475–493.

1449 Spaan, C.: Ultrasonics in metal cutting research: Measurement of the chiptool contact length. Ultrasonics 9 (1971) 3–5.

1450 Speidel, M. O.: Nichtmagnetisierbare Stähle für Generator-Kappenringe, ihr Widerstand gegen Spannungsrißkorrosion und Wasserstoffversprödung. VGB Kraftwerkstechnik 61 (1981) No. 5

1451 Sproule, D. O.: Improvements in or relating to apparatus for flaw detection and velocity measurement by ultrasonic echo methods. GB Pat. 774675 (1952).

1452 Stäger, H.; Schütz, E.; Meister, R.: Untersuchungen mit Ultraschall an aushärtenden Leichtmetallgußlegierungen. Tech. Mitt. 47 (1954) 149–157.

1453 Stäger, H.; Schütz, E.; Meister, R.: Untersuchungen mit Ultraschall an verschieden hergestellten Kupferlegierungen. Tech. Mitt 48 (1955) 34–45.

1454 Stäger, H.; Studer, H.: Untersuchungen an elektrotechnischem Porzellan mit dem Elektronenmikroskop und mit Ultraschall. Tech. Mitt. 49 (1956) 170–178.

1455 Stäger, H.; Meister, R.: Der Ultraschall als Mittel der Werkstoff-Forschung. Berg- u. hüttenm. Monatsh. 105 (1960) 60–74.

1456 Stein, F.; Einspruch, N. G.; Truell, R.: Temperature dependence of fractional velocity changes in a silicon single crystal. J. Appl. Phys. 30 (1959) 820–825.

1457 Stein, G.; Günther, W.; Römisch, H.: Ultraschallprüfung von austenitischen Kappenringen in einer rechnergesteuerten Tauchtechnikprüfanlage. Materialprüfung 21 (1979) 309–312.

1458 Steinkamp, G.: Ultraschall-Impulsgerät für Beton. Diss. TH Braunschweig 1953. Elektron. Rdsch. 10 (1956) 172–173.

1459 Stelling, H. A.: Einflußfaktoren auf die Meßgenauigkeit bei der Werkstoffprüfung mit Ultraschall. Schweißen u. Schneiden 23 (1971) 452–457.

1460 Stelling, H. A.; Diekmann, H.-U.: Wechselwirkungen zwischen Prüftechnik und objektspezifischen Zulässigkeitsgrenzen bei der Bauteilabnahme mit Ultraschallnachweis und Bewertung von Rissen. Schweißen u. Schneiden 32 (1980) 105–108.

1461 Stenger, H.: Zerstörungsfreie Prüfung mit Hilfe der Laser-Holographie. Materialprüfung 13 (1971) 301–302.

1462 Stepanishen, P. R.: Wide bandwidth acoustic near and far field transients from baffled pistons. IEEE Ultrasonics Symp. Proc. (1977) 113–118.

1463 Stepanishen, P. R.; Fisher, G.: Experimental verification of the impulse response method to evaluate transient acoustic fields. J. Acoust. Soc. Am. 69 (1981) 1610–1616.

1464 Stepanishen, P. R.; Strozeski, B.: Reflection and transmission of acoustic wideband plane waves by layered viscoelastic media. J. Acoust. Soc. Am. 71 (1982) 9–21.

1465 Sterke de, A.: The practical application of automatic ultrasonic inspection of circumferential welds in pipelines. 2. Int. Conf. on Pipewelding, London 1979. Rep. 19.

1466 Sterke de, A.: Automatic ultrasonic inspection of pipeline welds. Non Destr. Test. Int. 13 (1980) 275–284.

1467 Sterke de, A.: Some aspects of radiography and ultrasonic testing of welds in steel with thickness from 100–300 mm. Br. J. Non Destr. Test. 9 (1967) 94–107.

1468 Sterke de, A.: Ultrasonic inspection of welds in nuclear reactor pressure vessels. Vortrag auf dem Int. Symp. NDT of Nuclear Power Reactor Components, Rotterdam 1970.

1469 Sterke de, A.; de Raad, J. A.; Dijkstra, F. H.: Eine mobile Ultraschallanlage mit Mehrfachprüfkopfsystem für die mechanisierte Prüfung von Druckbehältern während der Herstellung. 2nd Int. Conf. TÜV Rheinland, Cologne 1979: Die Qualität der Kernkraftwerke aus amerikanischer und deutscher Sicht, pp. 296–317

1470 Sternischa, M.; Becker, H.; Wallheinke, H.: Anwendungen neuerer Ultraschallprüftechniken an austenitischen Schmiedestücken. Diskussionsstand zur KTA-Regel 3201 und erste Ergebnisse. In: DGZfP (Ed.): Int. Symp. Neue Verfahren der ZfP und deren Anwendungen insbesondere in der Kerntechnik, Saarbrücken 1979, 199–212

1471 Stössel, A.; Boulanger, G.; Furlan, J.; Mogavéro, R.: Ensemble intègre automatique de contrôle non destructif et d'aquisition pour les tubes minces entrainés par simple translation. In: Österr. Ges. ZfP (Ed.): 2nd Europ. Conf. NDT, Vienna 1981, pp. 351–354

1472 Stojanov, Z.; Schmidt, H.; Lenz, J.: Bestimmung der Porisität gesinterter FeNi-

Legierungen durch Messungen von Ultraschallabsorption und -geschwindigkeit. Materialprüfung 22 (1980) 200–207.

1473 Stokes, R. J. M.: The influence of graphite nodularity on ultrasonic nondestructive testing of iron castings. Br. Foundryman 75 No. 7 (1982) 7–10.

1474 Stoll, H.: Wanddickenmessung an heißen, korrodierten Rohren mit dem Impulsecho-verfahren. Paper Conf. DGZfP, Vienna 1965

1475 Stoneley, R.: Elastic waves at the surface of separation of two solids. Proc. R. Soc. London, Ser. A 116 (1924) 416–428.

1476 Stouffer, J. R.; Wallentine, M. V.; Wellington, G. H.; Dieckmann, A.: Development and application of ultrasonic methods for measuring fat thickness and rib-eye area in cattle and hogs. J. Anim. Sci. 20 (1961) 759.

1477 Strassburger, Ch.: Beitrag zur Ultraschallprüfung von Vormaterial für Breitband nach dem Impulsechoverfahren. Stahl u. Eisen 81 (1961) 885–893.

1478 Stüber, C.: Zerstörungsfreie Untersuchung von Hochspannungsisolatoren mit Hilfe des Ultraschall-Impulsverfahrens. Proc. 3rd Int. Congr. Acoust., Stuttgart 1959. Amsterdam: Elsevier 1960.

1479 Stüber, C.: Private communication (Deutsches Bundesbahn-Versuchsamt, Munich)

1480 Sturm, D.; Doll, W.; Deuster, G.: Full size reactor pressure vessel programme. 2nd Japanese-German Joint Seminar on NDE and Structural Strength of Nuclear Power Plants, 1983, Tokyo.

1481 Suchanek, H. J.: Zerstörungsfreie Prüfung von Schweißnähten an Kunststoffrohren. 3R Int. 17, Nr. 10 (1978) 653–656.

1482 Suckling, E. E.; Mac Lean, W. R.: Method of transducing ultrasonic shadowgraph or image for display on oscilloscope. J. Acoust. Soc. Am. 27 (1955) 297–300.

1483 Sugiyama, S.: Nondestructive inspection by frequency spectrum resolution. US Pat. 4.428,235 (1984).

1484 Sugiyama, S.; Suzuki, K.; Kajiyama, S.; Naruse, A.; Takeda, H.; Ooba, K.; Kawai, K.; Masu, T.; Oda, M.: Development of ultrasonic testing system for nuclear power plants. In: DGZfP (Ed.): 4th Int. Conf. NDT in the Nuclear Field, Lindau 1981, Vol. 8, pp. 117–123

1485 Sully, A. H.; Lavender, J. D.: Fehlernachweis in Stahlguß mit Ultraschall. Gießerei 48 (1961) 571–579.

1486 Sully, A. H.; Lavender, J. D.: Correlation between destructive and nondestructive testing of a large steel casting. Eng. Mater. Des. (1963) 354–357.

1487 Sulmont, A.; Mondot, J.; Mantelle, J.: Installation industrielle de contrôle ultrasonore rapide pour tubes sans soudure de grand diamètres. 6th Int. Conf. NDT, Hanover 1970, paper B 14

1488 Sussner, H.: Ursache und Anwendung des starken piezoelektrischen Effekts in dem Hochpolymer PVF$_2$ (Polyvinylidenfluorid). Diss. Max-Planck-Inst. für Festkörperforschung und Centre de Recherche sur les Très Basses Températures, C.N.R.S. Grenoble (1976).

1489 Sussner, H.; Michas, D.; Assfalg, A.; Hunklinger, S.; Dransfeld, K.: Piezoelectric effects in polyvinylidene fluoride at high frequencies. Phys. Lett. 45A (1973) 574–576.

1490 Swanson, G. D.: Development of fracture toughness measurement capability by ultrasound. Bendix Corp., Kansas City. Rep. No. BDX-613-2625 (1981).

1491 Swift, G.; Moore, W. M.: Investigation of applicability of acoustic pulse velocity measurements to evaluation of quality of concrete in bridge decks. Highway Res. Rec. 378 (1972) 29–39.

1492 Swindlehurst, W.: Acoustic emission. Non Destr. Test. 6 (1973) 152–158.

1493 Szabó, T.: Use of ultrasonics to evaluate or characterize wood composites. 4th NDT Wood Symp., Washington 1978, pp. 239–260.

1494 Szabó, T. L.; Slobodnik, A. J.: The effect of diffraction on the design of acoustic surface wave devices. IEEE Trans. SU-20 (1973) 240–251.

1495 Szczepanik, Z. R.; Czerniawski, B.: Bestimmung der elastischen Eigenschaften von

Packstoffen mit Hilfe der Ultraschallmessung. Verpackungs-Rdsch. 21, No. 4 (1970), Tech. Wiss. Beil., pp. 27–31

1496 Szilárd, J.: Ultrasound penetration through very thin gas layers embedded in solid bodies. In: Proc. 4th Int. Conf. NDT London 1963: London: Butterworth 1964, pp. 159–161.

1497 Szilard, J.: On the ultrasonic detectability of thin slag inclusions in steel plates. Non Destr. Test. 1 (1967) 45–47.

1498 Szilard, J.; Kidger, M. J.: Ultrasonic Fresnel lenses. Ultrasonics Int. Proc. 1981, (Novak, Z., Ed.).

1499 Szilard, J.: Ultrasonic Fresnel lenses, Part II: Cylindrical lenses. Ultrasonics 20 (1982) 103–106.

1500 Szilard, J.; Hanstead, P. D.: New imaging techniques. In: Ultrasonic testing, non-conventional testing techniques Chichester: Wiley 1982, pp. 53–102.

1501 Szilard, J.; Scruton, G.: Revealing the grain structure of metals by ultrasonics. Ultrasonics 11 (1973) 114–120.

1502 Tancrell, R. H.; Callerame, J.; Wilson, D. T.: Near field, transient acoustic beam forming with arrays. Proc. IEEE Ultrasonics Symp. 1978, pp. 339–343.

1503 Takahashi, S.: On the sound field of a plane radiator with an arbitrary contour shape. Acustica 44 (1980) 336–338.

1504 Takahashi, A.; Nosetani, T.; Kanamori, T.: Ultrasonic testing of naval brass tube sheets for surface condensers and heat exchangers. Sumitomo keikinzoku gihó (Sumitomo Light Metal Tech. Rep.) 23 (1982) 1–11.

1505 Tamburelli, C.: Systematic application of NDT in pipe mill. Non Destr. Test. 5 (1972) 104–106.

1506 Tarnóczy, H.: On the propagation of ultrasonic energy through thin air layers. Proc. 2nd. Conf. Ultrasonics, Warszawa 1956, pp. 91–94.

1507 Tarnoczy, T.; Illenyi, A.: Akustische Zonenlinsen. Proc. 3rd Int. Congr. Acoust., Stuttgart 1959. Amsterdam: Elsevier 1960.

1508 Tawil, E. P.: Sur les variations des propriétés optiques du quartz piézo-electrique soumis à des courants de haute fréquence. C. R. Acad. Sci. 183 (1926) 1099–1101.

1509 Tawil, E. P.: Erratum C. R. Acad. Sci. Paris 191, (1930) 168.

1510 Taylor, J. L.; Millard, C. N.: The evaluation of sintered metal products. Br. J. Non Destr. Test. 20 (1978) 248–253.

1511 Teagle, P. R.: Recent advances in mechanical impedance analysis. Instrumentation for the evaluation of adhesive bonded and composite structures. 3rd Europ. Conf. NDT, Florence 1984, Vol. 5, pp. 139–162.

1512 Temple, J. A. G.: Time-of flight inspection: theory. Nucl. Energy 22 (1983) 335–348.

1513 Teutonico, L. J.; Granato, A.; Truell, R.: Effect of copper on ultrasonic attenuation in germanium. Phys. Rev. 103 (1956) 832–833.

1514 Thaer, A.; Hoppe, M.; Patzelt, W. J.: Akustomikroskop ELSAM. In: Leitz-Mitt. Wiss. u. Tech. VIII 3/4, 1982, pp. 61–67

1515 Thieme, J.: Untersuchungen von Proben zur ultraakustischen Prüfung von Hart- und Walzenguß. Gießerei 46 (1959) 552–558.

1516 Thiessen, W.; Herrmann, H.: Schweiß- und prüftechnische Gesichtspunkte zur Konstruktion von Chemieapparaten. Chem. Ing. Tech. 44 (1972) 763–770.

1517 Thompson, D. O.; Braezeale, M. A.; Gauster, W. B.: A capacity microphone for ultrasonic measurements at megacycle frequencies. Proc. Conf. on Acoustics of Solid Media, Warszawa 1966, pp. 223–232.

1518 Thompson, D. O.; Breazeale, M. A.; Gauster, W. B.: A capacity microphone for ultrasonic measurements at megacycle frequencies. Proc. Conf. on Acoustics of Solid Media, Warszawa 1966, pp. 223–232.

1519 Thompson, R. B.: A model for the electromagnetic generation of ultrasonic guided waves in ferromagnetic metal polycrystals. IEEE Trans. SU-25 (1978) 7–15.

1520 Thomson, J. L.; Farley, J. M.: Rapid inspection of thick section components using a

compact, electronically controlled, variable angle ultrasonic probe. In: Clough, R. B. (Ed.): Quantitative NDE in the nuclear industry. Metals Park: ASM 1982, pp. 431–436

1521 Thomson, R. N.: A portable system for high resolution ultrasonic imaging on site. Br. J. Non Destr. Test. 26 (1984) 281–285

1522 Thurstone, F. L.: Ultrasound holography and visual reconstruction. Proc. Symp. Biomed. Eng. 1 (1966) 12–15.

1523 Thurstone, F. L.; Ramm von, O. T.: A new ultrasound imaging technique employing two-dimensional electronic beam steering. Acoust. Hologr. 5 (1974) 249–259.

1524 Tietz, H. D.: Methoden der Fehlerabschätzung mit Ultraschall — Vergleichende und kritische Betrachtung. Wiss. Z. Techn. Hochsch. Magdeburg 15 (1971) 429–445.

1525 Tietz, H. D.: Fehlergrößenabschätzung mit Ultraschall nach einem Kugelersatzfehler. Feingerätetechnik 20 (1971) 463–467.

1526 Timo, D. P.; Placek, R. J.: Inspection and evaluation of in-service turbine rotor forgings. Proc. Am. Power Conf. Chicago 1977, Vol. 39. Illinois Inst. Technol. Chicago, pp. 270–281.

1527 Tittmann, B. R.; Ahlberg, L. A.; Buck, O.: Crack closure effects in ultrasonic nondestructive evaluation for real part-through fatigue crack in Al-alloy. In: Thompson, D. O.; Chimenti, D. E. (Eds.): Quantitative NDE, Vol. 1, 1982 pp. 551–555.

1528 Tjoetta, J. N.; Tjoetta, S.: An analytical model for the nearfield of a baffled piston transducer. J. Acoust. Soc. Am. 68 (1980) 334–339.

1529 Tjoetta, J. N.; Tjoetta, S.: Nearfield and farfield of pulsed acoustic radiators. J. Acoust. Soc. Am. 71 (1982) 824–834.

1530 Toepler, A.: Über die Methode der Schlierenbeobachtung als mikroskopisches Hilfsmittel, nebst Bemerkungen zur Theorie der schiefen Beleuchtung. Ann. Phys. 127 (1866) 556–580.

1531 Tomlinson, J. R.; Wagg, A. R.; Whittle, M. J.: Ultrasonic inspection of austenitic welds. Proc. Int. Conf. NDE in the Nuclear Industry, Salt Lake City 1979. ASME, pp. 64–83.

1532 Tomsett, H. N.: The practical use of ultrasonic pulse velocity measurements in the assessment of concrete quality. Mag. Conc. Res. 32 No. 110 (1980) 7–16.

1533 Tripathi, R. C.; Verma, G. S.: Ultrasonic attenuation as function of temperature in a 1% carbon steel. J. Acoust. Soc. Am. 53 (1973) 1344–1345.

1534 Trost, A.: Nachweis von Werkstofftrennungen in Blechen durch Ultraschall. Z. VDI 87 (1943) 352–354.

1535 Truell, R.; Hikata, A.: Fatigue and ultrasonic attenuation. ASTM Spec. Tech. Publ. No. 213 (1957).

1536 Truell, R.; Chick, B.; Picker, A.; Anderson, G.: The use of ultrasonic methods to determine fatigue effects in metals. WADC Tech. Rep. 59-389 (Wright Air Development Center Wright-Patterson Air Force Base, Ohio, USA).

1537 Trumpff, B.; Launay, J. P.; Olivera, J. J.; Thomas, A.: Progress in ultrasonic methods for testing austenitic welds in PWR main reactor coolant systems. Proc. 10th World Conf. NDT. Moscow 1982, Vol. 7, pp. 48–56 (Acad. Sci. USSR).

1538 Trumpfheller, R.: Abnahmeprüfungen an Schweißnähten nach dem Ultraschall-prüfverfahren. Schweißen u. Schneiden 18 (1966) 268–279.

1539 Trumpfheller, R.: Realiability and standards. In: Charyulu, V. H. (Ed.): NDE in the Nuclear Industry — 1980. Metals Park: ASM 1981, pp. 13–21.

1540 Trumpfheller, R.: Zuverlässigkeit der Zerstörungsfreien Prüfung. In: DGZfP (Ed.): 4th Int. Conf. NDT in the Nuclear Field, Lindau 1981, Vol. 8, pp. 247–261

1541 Tsao, M. C.; Grills, R. H.; Simpson, R. P.; Andrew, G. A.: Ultrasonic color imaging and stress analysis of piping coupler shrink fit. Mater. Eval. 42 (1984) 1393–1400.

1542 Tschudi, T.: Holographie in der Meßtechnik. Messen u. Prüfen (1971) 147–153.

1543 Tsuchidana, T.: New rail testing system for Shinkansen. Non Destr. Test. J. (Jap.) 1 (1983) 92–94.

1544 Tsvetyanskii, V. L.: Transmission of ultrasound through the bonding layer in acoustical investigations of solids. Sov. Phys. Acoust. 27 (1981) 338–341.

1545 Turpin, R. J. B.: A metallurgical assessment of ultrasonic billet testing.. Steel Times (1966) 348–352.

1546 Uchida, K.; Kashiwaya, H.; Mori, T.; Honda, H.: Fundamental study of phased array ultrasonic testing method. In: Chlough, R. B. (Ed.): Quantitative NDE in the nuclear industry. Metals Park: ASM 1982, pp. 427–430.

1547 Udagawa, T.; Ueno, T.; Isono, E.: Automatic ultrasonic testing and recording system for welds utilizing a microcomputer. Mater. Eval. 40 (1982) 305–311.

1548 Uno, Y.; Orito, K.; Morita, H.; Aoki, M.; Hoshijima, T.: Automatic surface and internal inspection system for round bar. Proc. 9th World Conf. NDT Melbourne 1979. Rep. 1C–11.

1549 Uozumi, S.; Narushima, I.: Continous ultrasonic inspection of steel plate at high temperature by U.I. roll system. 6th Int. Conf. NDT Hanover 1970, Paper L 8

1550 Ushakov, V. M.; Shcherbin'skii, V. G.: Acoustic field of an inclined probe with a spherical interface. Sov. J. Non Destr. Test. 18 (1982) 14–19.

1550a Vacelet, H.: Controles non destructits des assemblage collés. 3rd Europ. Conf. NDT Florence 1984, Vol. 5, pp. 172–191.

1551 Vadder de, D.; Azou, P.; Saglio, R.; Birac, A. M.: Determination of orientation and size of badly oriented quasi plane defects by means of focused probes. 9th World Conf. NDT, Melbourne 1979. Rep. 4G-1.

1552 Vadder de, D.; Dosso, M.: Caracterisation ultrasonore des bords de fissure par traitement numerique du signal. 3rd Europ. Conf. NDT Florence 1984 Vol. 5, pp. 362–374.

1553 Vainblat, Yu. M.; Pavlov, S. V.: Ultrasonic testing of microscopic defects in hot-rolled aluminium-alloy plates. Proc. 10th World Conf. NDT Moscow 1982, Vol. 7, pp. 7–14 (Acad. Sci. USSR).

1554 Valkenburg van, H. E.: Ultrasonic inspection device. US Pat. 2,667,780 (1951); Transducer control. US Pat. 2,651,012 (1952).

1555 Valkenburg van, H. E.; Cook, E.: Vorrichtung zur Materialprüfung mittels Ultraschall, DE Pat. 1 057 356 (1959).

1556 Valkenburg van, H. E.; Sharpe, D. E.: Improving the effectiveness of electronic distance-amplitude-compensation in ultrasonic nondestructive testing. In: Österr. Ges. ZfP (Ed.): 2nd Europ. Conf. NDT, Vienna 1981, pp. 272–273

1557 Vary, A.: Simulation of transducer couplant effects on broadband ultrasonic signals. National Aeronautics Space Administration, Cleveland, Rep. NASA-TM-81489 (1980).

1558 Vary, A.: Concepts for interrelating ultrasonic attenuation, microstructure and fracture toughness in polycrystalline solids. Mater. Eval. 46 (1988) 642–649

1559 Vasile, C. V.; Houston, R. H.; Thompson, R. B.: Investigation of EMAT base system for the detection of bolt hole type cracks. Part 1: Detection of cracks in the inacessible lower half of wing lap joints using EMATs. Rockwell Int. Corp., Thousand Oaks Report. AD-A 094349 (1980).

1560 Vaubert, Y.; Birac, A. M.; Saglio, R.: System of acquisition and analysis of ultrasonic data. Proc. 10th World. Conf. NDT Moscow 1982. Vol. 6, pp. 110–128. (Acad. Sci. USSR).

1561 Venhuizen, W., Sawatzky, G. A.: A versatile pulse generator and coupled fast signal averager for pulse-echo experiments. J. Phys. E.: Sci. Instrum. 11 (1978) 24–26.

1562 Veremeenko, S. V.; Ignatinskii, I. L.; Meierson, V. G.: An ultrasonic unit for inspecting thin wire and fibers. Sov. J. Non. Destr. Test. 15 (1979) 450 451.

1563 Veretennikov, E. S.; Bakhtinova, N. D.: Determining the optimum frequency of

ultrasonic vibrations in the testing of tubes. Sov. J. Non Destr. Test. 3 (1972) 311–314. Orig.: Defektoskopiya 3, No. 3 (1972), pp. 68–71

1564 Verger, B.; Saglio, R.: Nozzle inservice inspection, detection and characterization of undercladding cracks. In: Clough, R. B. (Ed.): Quantitative NDE in the nuclear industry. Proc. 5th Int. Conf. NDE in the Nuclear Industry, San Diego 1982. Metals Park: ASM 1983, pp. 440–442.

1565 Verhoef, W. A.; Cloostermans, M. J. T. M.; Thijssen, J. M.: The impulse response of a focused source with an arbitrary axisymetric surface velocity distribution. J. Acoust. Soc. Am. 75 (1984) 1716–1721.

1566 Vetter, G.: Zerstörungsfreie Prüfung von Gußerzeugnissen. 17. Mitt.: Erfahrungen bei der Ultraschallprüfung schwerer Stahlgußteile. Gießereitechnik 27 (1981) 53–54.

1567 Vezetti, D. J.; Aks, S. O.: Ultrasonic scattering theory, II: Scattering from composites. Ultrasonic Imaging 2 (1980) 195–212.

1568 Viktorov, I. A.: Rayleigh waves on cylindrical surfaces (in Russian). Akust. J. Akad. Nauk SSSR 4 (1958) 131–136

1569 Viktorov, I. A.: Influence of surface roughness on the propagation of Rayleigh-waves (in Russian). Doklady Akademia Nauk SSSR 119 (1958) 463–465

1570 Viktorov, I. A.: Rayleigh-type waves on cylindrical surface. Sov. Phys. Acoust. 4 (1958) 131–136.

1571 Vilkomerson, D.; Mezrich, R.; Etzold, K.: An improved system for visualizing and measuring ultrasonic wavefronts. Acoustic. Hologr. 7 (1977) 87.

1572 Visser, A.: Laser oder Elektronenstrahlen. Laser u. angew. Strahlentechnik 2 (1970) 5–14.

1573 Vogt, M.: Zwei moderne automatische Ultraschall-Knüppelprüfanlagen. Messen u. Prüfen (1969) 717–719.

1574 Volkwein, A.: Zerstörungsfreie Prüfung von Naturstein durch Ultraschall-Schwächungsmessungen. Materialprüfung 24 (1982) 119–124.

1575 Vopilkin, A. Kh.; Ermolov, I. N.; Staseev, V. G.: Experimental investigation of an ultrasonic spectral method of determining the nature of defects. Sov. J. Non Destr. Test. 14 (1978) 34–43.

1576 Vorobev, V. A.; Gorshkov, V. A.; Kaledin, A. N.; Syrkov, V. B.: Möglichkeit der Schätzung des Spannungszustandes in Beton mit der Ultraschallspektroskopie. Wiss. Ber. d. Techn. Hochsch. Leipzig (1979) No. 14, pp. 47–50

1577 Voskresenskaya, E. V., Kamchatnyi, Yu. G., Marchenko, A. T.: Determining the mean grain size of tungsten alloys by the acoustic method Sov. J. Non Destr. Test. 13 (1977) 145–150.

1578 Votava, E.; Jax, P.; Meier, V.; Mika, C.: Ergebnisse bei der Anwendung der Schallemission bei Druckproben an Primärkreiskomponenten von Kernreaktoren. In: DGZfP (Ed.): Int. Symp. Neue Verfahren der ZfP und deren Anwendungen insbesondere in der Kerntechnik, Saarbrücken 1979, pp. 377–397

1579 Votava, E.; Jax, P.; Eisenblätter, J.: New results on the surveillance of nuclear reactor components by acoustic emission during hydrotests. In: Charyulu, V. H. (Ed.): NDE in the nuclear industry — 1980. Metals Park: ASM 1981, pp. 437–461.

1580 Vries de, D.; Berkhout, A. J.: Wave theoretical approach to acoustic focusing. A. Acoust. Soc. Am. 70 (1981) 740–748.

1581 Waas, A.: Automatische Ultraschallwiederholungsprüfung von Kernreaktorbehältern. Modell zur Verknüpfung der Teilvolumen-Integrations-Methode mit der Ersatzreflektorgröße. Materialprüfung 19 (1977) 382–385.

1582 Wade, G.: Ultrasonic imaging by reconstructive tomography. In: Wang. K. J. (Ed.): Acoustical imaging. Vol. 9. New York: Plenum Press 1980, pp. 379–431.

1583 Wahl, H. J.; Koch, F. O.: Zerstörungsfreie Prüfung von HF-geschweißten Rohren. In: Österr. ZfP (Ed.): 2nd Europ. Conf. NDT, Vienna 1981, pp. 355–357

1584 Waid. J. S.; Woodman, M. J.: A nondestructive method of detecting diseases in wood. Nature 180 (1957) 47.

1585 Wallace, W. D.: Electromagnetic generation of ultrasound in metals. Int. Non Destr. Test. 2 (1971) 309–334.

1586 Walte, F.: Praktische Hinweise zur Prüfung geschichteter Medien. DGZfP-Conf. Essen 1984. Paper No. 18

1587 Walte, F.; Müller, W.: Das Verhalten flächiger, rißartiger Reflektoren in fokussierten Schallfeldern. Materialprüfung 25 (1983) 155–158/235–237.

1588 Walte, F.; Müller, W.: Die Punktquellensynthese als Rechenmodell zur Berechnung von Amplitudenortskurven in fokussierten Schallfeldern. Fraunhofer Inst. ZfP, Saarbrücken, Ber. 830114-TW (1983).

1589 Wardley, J.; Brown, P. H.; Croucher, R. C.: The design and performance of an improved ultrasonic image converter tube. Conf. Proc. Ultrasonics Int., Brighton 1977. Guildford. IPC Sci. and Technol. Press 1977, pp. 121–124.

1590 Wallner, F.; Ganglbauer, O.; Frielinghaus, R.: Der Einfluß der Schallgeschwindigkeit auf die Prüfbarkeit austenitischer Schweißverbindungen. Schweißtechnik 35 (1981) 155–158.

1591 Warren, J. M.: Nondestructive measurement of plate glass temper. Proc. 12th Symp. NDE, San Antonio 1979, pp. 96–108.

1592 Waschkies, E.: Übertragungsfunktionen als Kennzeichen der Ausbreitung von Schallemissionssignalen. In: Höller, P. (Ed.): New procedures in NDT. Proc. Germany—US Workshop, Saarbrücken 1982.

1593 Waschkies, E.; Hepp, K.: Schallemissionsmessungen zum Nachweis von Thermoschockrissen an einer plattierten Stahlplatte. In: DGZfP (Ed.): Int. Symp. Neue Verfahren der ZfP und deren Anwendungen insbesondere in der Kerntechnik, Saarbrücken 1979, pp. 369–375

1594 Watkins, B.; Ervine, R. W.; Cowburn, K. J.: The UKAEA defect detection trials. In: Nichols, R. W. (Ed.): Advances in nondestructive examination for structural integrity. London: Appl. Sci. Publ. 1982, pp. 371–379.

1595 Watkins, B.; Jackson, H.: Technique for inspection of light water reactor pressure vessels. Conf. on Periodic Inspection of Pressure Vessels, London 1972.

1596 Watkins, R. D.; Cooper, W. H. B.; Gillespie, A. B.: The attenuation of Lamb waves in the presence of a fluid. Ultrasonics 20 (1982) 257–264.

1597 Waubke, N. V.; Märkl, J.: Einsatz der Ultraschall-Impulslaufzeitmessung für die Sortierung von Bauhölzern, Teil 1: Vorversuche mit Kanthölzern. Holz Roh Werkst. 40 (1982) 189–192.

1598 Weight, J. P.; Hayman, A. J.: Limitations on the use of wide-band transducers in practical nondestructive testing. Proc. 9th World Conf. NDT, Melbourne 1979, Rep. 4H–12.

1599 Weigler, H.; Kern, E.: Über die Anwendungsmöglichkeiten des Ultraschallverfahrens zur Beurteilung der Betongüte. Betonstein-Ztg. Nr. 5 (1965) 279–286.

1600 Weis, W.; Lampic, M.; Orths, K.: Untersuchungen über die Prüfbarkeit von Gußeisen mit Lamellengraphit mittels Ultraschall. Gießereiforschung 27 (1975), 1–11.

1601 Westkämper, G.; Berner, K.: Ultraschallprüftechniken bei der Gütekontrolle von Gußstücken. Materialprüfung 18 (1976) 321–325.

1602 Wellekens, Ch. J.: Vibrations of backed piezoceramic disk-transducers with annular electrodes and matching layers, Part 1. IEEE Trans. SU-29 (1982) 26–42

1603 Wells, F. H.; Martin, R.: Apparatus for measuring thickness. US Pat. 3,690,154 (1970)

1604 Wenzel, K.: Die Bestimmung elastischer Eigenschaften von anstehendem Fels durch Ultraschall-Sondierung. Schweiz. Bauztg. 77 (1959) 479–484.

1605 Werner, K.: Fortschritte der Schienenprüfung mit Ultraschall bei der Deutschen Bundesbahn. Eisenbahntech. Rdsch. 10 (1961) 417–437.

1606 Werneyer, R.; Schlengermann, U.: Über die Reflexion von Ultraschallwellen an Oberflächenrissen und nutförmigen Testfehlern, Teil I: Einführung und Modellvorstellungen. Materialprüfung 13 (1971) 213–218.

1607 Werneyer, R.; Schlengermann, U.: Über die Reflexion von Ultraschallwellen an Oberflächenrissen und nutförmigen Testfehlern, Teil II: Folgerungen für die Praxis. Materialprüfung 13 (1971) 298–300.

1608 Weston-Bartholomew, W.: Temperature considerations when evaluating materials using the ultrasonic goniometer. Ultrasonics 11 (1973) 132–135.

1609 Weyl, D.: Möglichkeiten der Prüfung von Porzellanisolatoren mit Ultraschall. ATMV 8242/43. Lieferung 257 (June 1957)

1610 Weyns, A.: Radiation field calculations of pulsed ultrasonic transducers, Part 1: Planar circular, square and annular transducers. Ultrasonics 18 (1980) 183–188.

1611 Weyns, A.: Radiation field calculations of pulsed ultrasonic transducers, Part 2: Spherical disk- and ring-shaped tranducers. Ultrasonics 18 (1980) 219–223.

1612 Whalen, M. F.; Mucciardi, A. N.: Pressure vessel nozzle inspection using adaptive learning techniques. In: Nichols, R. W. (Ed.): Nondestructive examination in relation to structural integrity. London: Appl. Sci. Publ. 1980, pp. 45–57.

1613 Whalen, M. F.; Zuralov, M.; Barber, J. H.; Mucciardi, A. N.: Advanced signal processing of turbine rotor bore waveforms. Adaptronics, McLean, Rep. EPRI-NR-2203 (1982).

1614 Whaley, H. L.; Cook, K. V.; McClung, R. W.; Snyders, L. S.: Optical methods for studying ultrasonic propagation in transparent media. 5th Int. Conf. NDT, Montreal 1967, p. 125.

1615 Whaley, H. L.; Cook, K. V.: Ultrasonic frequency analysis. Mater. Eval. 28 (1970) 61–66.

1616 White, R. M.: Generation of elastic waves by transient surface heating. J. Appl. Phys. 34 (1963) 3559–3567.

1617 Whiting, A. R.; Stolle, D. E.: Automated data handling systems for inservice inspection. Conf. on Periodic Inspection of Pressure Vessels, London 1972.

1618 Whittaker, V. N.: A review of nondestructive measurement of flaw size. Non Destr. Test. 5 (1972) 92–100.

1619 Whittington, K. R.: Electronic steering and focusing of ultrasound for tube testing. In: Sharpe, R. S. (Ed.): Research techniques NDT, Vol. 3. London: Academic Press 1977, pp. 135–173.

1620 Whittington, K. R.: Electrodynamic probes-principles, performance and applications. Br. J. Non Destr. Test. 23 (1981) 127–132.

1621 Wickham, G. R.; Coffey, J. M.: An improved theory of ultrasonic shear wave probes. Proc. Conf. Evaluation Calibration Ultrasonic Transducers, London 1977, pp. 1–11.

1622 Wiegand, H.; Hentze, H.: Bestimmung von Werkstoffkennwerten an Eisen-Graphit-Werkstoffen mit Ultraschall. Metall 33 (1959) 1110–1113.

1623 Wiese, A.: Reflektorbewertung mit hochbedämpften Prüfköpfen bei Berücksichtigung der Gleichrichterart. 3rd Europ. Conf. NDT, Florence 1984 Vol. 5, pp. 269–279.

1624 Wild, H. W.: Die Ultraschallprüfung von gußeisernen Tübbingen. Glückauf 98 (1962) 231–235.

1625 Wild, J. J.; Neal, D.: The use of high frequency ultrasonic waves for detecting changes of texture in living tissues. Lancet 1 (1951) 655–657.

1626 Wilhelm, E.: Zurichtungsanlagen für die Herstellung von Halbzeug für besondere Verwendungszwecke. Stahl u. Eisen 99 (1979) 54–60.

1627 Williams, J. H.; Yüce, H.; Lee, S. S.: Ultrasonic attenuation of a void containing medium for very long wavelengths. Mater. Eval. 42 (1984) 219–224.

1628 Williams, J. H.; Doll, B.: Ultrasonic attenuation as an indicator of fatigue life of graphite fiber epoxy composites. Mater. Eval. 38 (1980) 33–37.

1629 Williams, R. S.; Zwicke, P. E.: Assessment of adhesive properties using pattern recognition analysis of ultrasonic NDE data. Mater. Eval. 40 (1982) 312–317.

1630 Williamson, R. C.: Echo-phase-comparison technique and measurement of sound velocity in water. J. Acoust. Soc. Am. 45 (1969) 1251–1257.

1631 Willard, G. W.: Ultrasound waves made visible. Bell Lab. Rec. 25 (1947) 194–200.

1632 Wilson, D. M.; Cole, P. T.; Whittington, K. R.: The development of an electro-magnetic-acoustic system for NDT of steel bar at elevated temperature. Proc. 8th World Conf. NDT, Cannes 1976, Paper 1 A 5.

1633 Wilson, D. M.; Cole, P. T.; Whittington, K. R.: Electromagnetic-acoustic techniques for internal and surface inspection of round steel bars. Conf. Proc. Ultrasonics Int. Brighton 1977, pp. 378–384.

1634 Winter, H.: Schweißen und Schweißnahtprüfung beim Bau der Rohölleitung Wilhelmshaven-Köln. Schweißen u. Schneiden 11 (1959) 270–279.

1635 Winters, D. C.: End-on crack measurement. IEEE Ultrasonics Symp. Proc. 1975, pp. 572–574.

1636 Winterstein, H.; Fischer, C. H.: Güteprobleme beim Schweißen von Bleilegierungen. ZIS-Mitt. 22 (1980) 1165–1172.

1637 Wolitz, K.; Brockmann, W.; Fischer, T.: Prüfung von glasfaserverstärkten Kunststoffbehältern mit Schallemissionsanalyse. DGZfP-Conf. Mainz 1978, Vol. 3, pp. 789–795

1638 Wolter, H.: Schlieren, Phasenkontrast- und Lichtschnittverfahren. In: Handb. der Phys. 24 (Berlin 1956), pp. 555 ff.

1639 Wolters, W. J.; Seydel, J. A.; Novak, R. E.: CUSS — An automated ultrasonic inspection system with interactive graphic displays. Mater. Eval. 40 (1982) 109–114.

1640 Wood, F. W.; Borg, J. O.: Ultrasonic inspection of arc-cast zirconium and its alloys. US Bureau of Mines, Rep. of Investigation 5126 (March 1955).

1641 Wooldridge, A. B.; Denby, D.; Allen, D. J.: Predicting and minimising the adverse effects of austenitic cladding on ultrasonic inspection of PWR primary circuit components. In: Periodic Inspection of Pressurized Components, I. Mech. E. Conf. Publ. 1982-9. London: Mech. Eng. Publ. 1982, pp. 109–116.

1642 Worlton, D. C.: Ultrasonic testing with Lamb waves. Non Destr. Test. 15 (1957) 218–222.

1643 Wright, F. J.; Berry, M. V.: Wave-front dislocations in the sound field of a pulsed piston radiator. J. Acoust. Soc. Am. 75 (1984) 733–748.

1644 Wüstenberg, H.: Untersuchungen zum Schallfeld von Winkelprüfköpfen für die Materialprüfung mit Ultraschall. Diss. TU Berlin 1972.

1645 Wüstenberg, H.: Bestimmung der Richtcharakteristik von Winkelprüfköpfen für die Ultraschallprüfung am Kontrollkörper nach DIN 54 120. Materialprüfung 11 (1969) 311–315.

1646 Wüstenberg, H.: Characteristical sound field data of angle probes. Possibilities for their theoretical and experimental determination. 7th Int. Conf. NDT, Warszawa 1973, Vortrag H 03.

1647 Wüstenberg, H.: Research and development programmes on nuclear in-service inspection in West Germany. Int. Symp. Mechanization and Automation of Inspection on Pressurized Plants, Tokyo 1973.

1648 Wüstenberg, H.: Untersuchungen zum Schallfeld von Winkelprüfköpfen für die Materialprüfung mit Ultraschall. BAM Berlin. Ber. BR-027 (1974).

1649 Wüstenberg, H.: Contribution of the acoustical holography to the ultrasonic inspection. Proc. Int. Conf. New Trends in NDT Brussels 1982, Paper SV-5.

1650 Wüstenberg, H.; Engl, G.: Recent developments in ultrasonic inspection of reactor pressure vessel weldments in the Federal Republic of Germany. In: Nichols, R. W. (Ed.): Advances in nondestructive examination for structural integrity. London: Appl. Sci. Publ. 1982, pp. 59–75.

1651 Wüstenberg, H.; Erhard, A.: Development of ultrasonic techniques for sizing defects; nondestructive examination in relation to structural integrity. Essex: Appl. Sci. Publ. 1980, pp. 59–83.

1652 Wüstenberg, H.; Erhard, A.; Möhrle, W.: Verfahren und Anordnung zum Nachweis von oberflächennahen Fehlern bei der ZfP. DE Pat. 2802278 (1978).

1653 Wüstenberg, H.; Haufe, U.; Erhard, A.: Contribution to the ultrasonic detection and sizing of inner wall surface-breaking cracks in pipes. Mater. Eval. 42 (1984) 1142–1149.

1654 Wüstenberg, H.; Kutzner, G.; Engl, C.: Dependence of echo amplitude on defect orientation in ultrasonic examinations. 8th World Conf. NDT, Cannes 1976.

1655 Wüstenberg, H.; Kutzner, J.; Möhrle, W.: Fokussierende Prüfköpfe zur Verbesserung der Fehlergrößenabschätzung bei der Ultraschallprüfung von dickwandigen Reaktorkomponenten. Materialprüfung 18 (1976) 152–161.

1656 Wüstenberg, H.; Kutzner, J.; Schulz, E.; Erhard, A.: Ultraschallanzeigen von Rißkanten. Proc. 1st Europ. Conf. NDT, Mainz 1978, Vol. 1, pp. 99–106

1657 Wüstenberg, H.; Mundry, E.: Properties of cylindrical boreholes as reference defects in ultrasonic inspection. Non Destr. Test. 4 (1971) 260–265.

1658 Wüstenberg, H.; Mundry, E.: An approach to a system-theoretical description of information sources in ultrasonic testing. Abstracts 9th Conf. NDT, Loughborough 1972, p. 11.

1659 Wüstenberg, H.; Mundry, E.: Beitrag zur Halbwertstiefenausdehnung von Reflexionsstellen in der Materialprüfung mit Ultraschall. Materialprüfung 13 (1971) 329–335.

1660 Wüstenberg, H.; Mundry, E.: Nuten und Kanten als Bezugsreflektoren in der Materialprüfung mit Ultraschall. Materialprüfung 14 (1972) 58–61.

1661 Wüstenberg, H.; Schenk, G.; Haufe, U.: Dynamische Fokussierung in Schrägeinschallung bei der Ultraschallprüfung. Proc. 4th Int. Conf. NDT in the Nuclear Field 1981, pp. 703–716

1662 Wüstenberg, H.; Schenk, E.; Möhrle, W.: Vergleich der Leistungen von fokussierenden Prüfköpfen mit Linsen oder elektronisch gesteuerten Ringstrahlern. In: Österr. Ges. ZfP (Ed.): 2nd Europ. Conf. NDT, Vienna 1981, pp. 32–35

1663 Wüstenberg, H.; Schenk, E.; Möhrle, W.; Neumann, E.: Comparison of the performances of probes with different focusing techniques and experiences. Proc. 10th World Conf. NDT Moscow 1982. Vol. 7, pp. 563–587 (Acad. Sci. USSR)

1664 Wüstenberg, H.; Schulz, E.: Versuche zur Feststellung plattierungsnaher Reflexionsstellen an Reaktorteilen mit Ultraschall. Conf. DGZfP, Saarbrücken 1972

1665 Wüstenberg, H.; Schulz, E.: Investigations concerning the influence of austenitic cladding on the sound fields of ultrasonic probes. 7th Int. Conf. NDT, Warszawa 1973. Paper H 04.

1666 Wüstenberg, H.; Schulz, E.: The influence of membrane size and form on the sound field of angle probes. Proc. Conf. Evaluation Calibration Ultrasonic Transducers, London 1977, pp. 12–17.

1667 Wüstenberg, H.; Wegner, W.; Möhrle, W.; Bertus, N.; Hiller, F.: Automatische Wanddickenmessung von Rohren mit vernarbten Oberflächen und bildliche Darstellung des Rohrquerschnittes. BAM Berlin, BAM-Vorhaben 06260, Projekt Nr. 11.2/4F (1982).

1668 Wulff, F.; Rechner, W.: Die Ultraschallprüfung von Schweißverbindungen an Chrom-Nickel-Stählen. ZIS-Mitt. 4 (1962) 644–664.

1669 Wyatt, R. C.: Visualization of pulsed ultrasound using stroboscopic photoelasticity. Non Destr. Test. 5 (1972) 354–358.

1670 Yamada, K.; Shimizu, H.: Conical and toroidal piezoelectric polymer transducers for long range focusing. Proc. IEEE Ultrasonics Symp. 1982, pp. 837–840.

1671 Yamamoto, S.; Tsukikawa, T.; Nakano, M.; Ueyama, H.: Acoustic emission testing of pressure vessels made of $2^1/_4$Cr–1Mo steel. In: Nichols, R. W. (Ed.): Nondestructive examination in relation to structural integrity. London: Appl. Sci. Publ. 1980, pp. 19–39.

1672 Yee, B. G. W.; Gardner, A. H.; Hillhouse, L.; Russell, D. R.: Evaluation and optimization of the advanced signal counting techniques on weldments. Rep. of Marshall Space Flight Center, Huntsville, Alabama, FZM-5917 (31. Jan. 1971).

1673 Yew, Ch. H.: Using ultrasonic shear horizontal waves to estimate the quality of adhesive bonds: preliminary study. J. Acoust. Soc. Am. 75 (1984) 525–531.

1674 Ying, C. F.; Truell, R.: The effect of hydrogen on ultrasonic attenuation and velocity measurements in titanium. Acta Metall. 2 (1954) 374–379.

1675 Ying, C. F.; Truell, R.: Scattering of a plane longitudinal wave by a spherical obstacle in an isotropically elastic solid. J. Appl. Phys. 27 (1956) 1086–1097.

1676 Yoneyama, H.; Takama, S.; Kishigami, M.; Sasahara, T.; Ando, H.: Ultrasonic pattern recognition study of feedwater nozzle inner radius indication. In: Clough, R. B. (Ed.): Quantitative NDE in the nuclear industry, Proc. 5th Int. Conf. NDE in the Nuclear Industry, San Diego 1982. Metals Park: ASM 1983, pp. 436–439.

1677 Yoneyama, H.; Shibata, S.; Kishigami, M.: Ultrasonic testing of austenitic stainless steel welds. 9th Int. World Conf. NDT, Melbourne 1979, Paper 3 B 11.

1678 Youshaw, R. A.: Development of an ultrasonic guide for the inspection of butt welds in commercial ships. Rep. (May 1970) US Naval Ordnance Lab.

1679 Youshaw, R. A.: Ultrasonic inspection of T-joint welds. Mater. Eval. 24 (1966) 16–22.

1680 Yuozonene, L. V.: Elastic longitudinal surface waves and their use for nondestructive inspection. Sov. J. Non Destr. Test. 16 (1980) 574–581.

1681 Zabinska, T.: Industrial quality control of stoppers and ladle bricks by means of ultrasonic methods. 6th Conf. Silicate Industry, Budapest 1961, pp. 459–469.

1682 Zachary, L. W.: Quantitative use of Rayleigh waves to locate and size subsurface holes. J. Non Destr. Eval. 3 (1982) 55–63.

1683 Zanker, A.: Nomograph for the velocity of sound in solid media. Ultrasonics 10 (1972) 180–181.

1684 Zeiger, A.; Jassby, K.: Measurement of acoustoelastic coefficients of Rayleigh waves in steel alloys. J. Non Destr. Eval. 3 (1982) 115–124.

1685 Zellmann, W.: Ultraschallprüfung von Stahlgußarmaturen. Tech. Information Armaturen 1 (1966) 23–30.

1686 Zemanek, J.: Beam behavior within the nearfield of a vibrating piston. J. Acoust. Soc. Am. 49 (1971) 181–191.

1687 Zettler, E.: Ermittlung elastischer Kenngrößen von Gußwerkstoffen mit Hilfe von Ultraschallgeschwindigkeits- und Schwächungsmessungen. 3rd Conf. NDT, Budapest 1964

1688 Ziegler, R.; Gerstner, R.: Die Schallgeschwindigkeit als kennzeichnende Größe für die Beurteilung von Grauguß. Gießerei 45 (1958) 185–193.

1689 Ziegler, R.; Gerstner, R.: Anwendungsmöglichkeiten des Ultraschallverfahrens bei Schalenhartguß. Gießerei 47 (1960) 112–117.

1690 Zimmermann, R.: Zerstörungsfreie Güteprüfung von Glasschweißverbindungen. Silikattechnik 31 (1980) 310–311.

1691 Zonov, I. V.: Some peculiarities of directional patterns for transducers that radiate pulses of various shapes. Sov. J. Non Destr. Test. 18 (1982) 129–136.

1692 Zottmann, W.: Beitrag zur Fehlergrößenermittlung beim Ultraschall-Impuls-Echo-Verfahren. Arch. Eisenhüttenwes. 35 (1964) 353–358.

1693 Zuidema, J.; van Soest, Th. M.: An acoustic determination of the direction of the vibration of ordinary acoustic shear wave transducers. J. Non Destr. Eval. 3 (1982) 77–84.

3. Publications without named author by Institutes, Corporations etc.

1694 ASM: Metals Handbook, Vol. 11: Nondestructive inspection and quality control. Metals Park 1976.
1695 ASME Boiler and Pressure Vessel Code, Sect. V: Nondestructive examination (1983). ASME Boiler and Pressure Vessel Code, Sect. XI: Rules for in-service inspection of nuclear power plant components (1983).
1696 ASTM E588-82 (1982): Standard practice for detection of large inclusions in bearing quality steel by the ultrasonic method.
1697 ASTM: Recommended practice for evaluating the microstructure of graphite in gray iron. A 247-47-78.
1698 ASTM: NDT in the missile industry. ASTM Spec. Tech. Publ. No. 278 (1959).
1699 ASNT: Proc. 2nd Int. Conf. NDT Chicago 1957. Non Destr. Test. 16 (1958) 84–187.
1700 Ateliers de Constructions Electriques de Charleroi (ACEC): Übertrager für elastische Wellen. DE Pat. 966 392 (1950).
1701 Automation Ind., Inc.: Ultrasonic inspection of plywood panel. US Pat. 3,423,991 (1969).
1702 Babcock-Brown Boveri Reaktor GmbH: Das Brennstab-Schaden-Nachweissystem. Firmenprospekt (1980).
1703 BAM, Labor 6.21: Untersuchungen zum Einfluß der Plattierung und der Geometrie auf die Prüfbarkeit von dickwandigen Reaktorkomponenten mit Ultraschall bei der Tandem- und der Einkopftechnik (1973).
1704 BAM: Ultraschallprüftechnik zur Null- und Wiederholungsprüfung von Schnellbrutreaktoren, Teil I und Teil II. Förderungsvorhaben RS 244 des Bundesministers für Forschung und Technologie (1981).
1705 BATELLE-Institut, Frankfurt: Einführungskurs und Praktikum Schallemission, Batelle-Institut Frankfurt 1980.
1706 Boeing Service Bull. No. 1995 (R-2) A 1964.
1707 Branson Instruments Inc.: Ultrasonic inspection method and apparatus. US Pat. 3,485, 087 (1969).
1708 CEGB: Ultrasonic bracelet probe for tube butt weld inspection. Non Destr. Test. Int. 2 (1969) 137–139.
1709 DAMW Gerätetest (Deutsches Amt f. Maß u. Gewicht): Durchführung und Problematik der Teste von Ultraschall-Materialprüfgeräten. Technik 22 (1967) 397–398.
1710 Deutsche Bundesbahn, Versuchsamt für mechanische Stoffprüfungen, Minden: Richtlinien für die Untersuchung von Radsätzen der Dampflok und sonstigen Lok mit Stangenantrieb auf Querrisse in den Achswellen mittels Ultraschall (1960).
1711 DGZfP: Richtlinie über Eigenschaften von Prüfeinrichtungen mit Ultraschall-Impuls-Echo-Geräten und ihre Kontrolle. (1971.)
1712 DGZfP. Richtlinie über Schweißnahtprüfung mit Ultraschall (1974).
1713 DGZfP: Richtlinie über die Qualifikation und Zertifikation von Personal der ZfP (Qualifikationsrichtlinie). Neuausgabe 12, 1984, c.f. DIN 65 450 (1983), Kap. 34
1714 DIN 54 119: Ultraschallprüfung, Begriffe (1981).
1715 DIN 54 120: Kontrollkörper 1 und seine Verwendung zur Justierung und Kontrolle von Ultraschall-Impulsecho-Geräten (1973).
1716 DIN 54 122: Kontrollkörper 2 und seine Verwendung zur Justierung und Kontrolle von Ultraschall-Impulsecho-Geräten (1973).
1717 DIN 54 124, T 1: Kontrolle der Eigenschaften von Ultraschall-Prüfsystemen, einfache Kontrollen (1983).
1718 DIN 54 125: Prüfung von Schweißverbindungen mit Ultraschall, Anwendungshilfen zur Norm, Beibl. 1 (1982).

1719 DIN 25 435, T 1: Kerntechnische Anlagen, Wiederkehrende Prüfungen, Mechanisierte Ultraschallprüfung (1979). — T 5: Kerntechnische Anlagen, Wiederkehrende Prüfungen, Vordrucke zur Dokumentation der Daten mechanisierter Ultraschallprüfeinrichtungen (1981).

1720 ESI (Electricity Supply Industry) Standard 98-2 (1979): Ultrasonic Probes: medium frequency, miniature shear wave, angle probes.

1721 ESI Standard 98-7 (1982): Ultrasonic probes: normal (0°) compression wave probes for contact testing.

1722 ESI Standard 98-8 (1982): Ultrasonic probes: low frequency single crystal shear wave, angle probes.

1723 Hüttenwerk Oberhausen AG: Schallkopf für die Durchführung von Ultraschallprüfungen an Werkstücken hoher Temperatur. DE GbM 1 979 891 (1968).

1724 IIW/IIS: Handbook on the ultrasonic examination of welds. Welding Inst., Abington, 1977.

1725 IIW/IIS: Doc. 205-66: Draft recommended practice for the ultrasonic inspection of butt welds. Weld. in the World 4 (1966) 62–69.

1726 IIW/IIS: Handbook on the ultrasonic examination of austenitic welds. IIW Doc. V C 422-84.

1727 ISO: Welds in steel. Reference blocks for the calibration of equipment for ultrasonic examination. ISO 2400 (1972).

1728 ISO: Welds in steel. Calibration block No. 2 for ultrasonic examination of welds. ISO DIS 7963 (1983).

1729 ISO: SI units and recommendations for the use of their multiples and of certain other units. ISO 1000 (1973).

1730 ISO 4386, Part 1 (1982): Plain bearings — metallic multilayer plain bearings — nondestructive ultrasonic testing of bond for bearing metal layer thicknesses ≦2 mm.

1731 JIS Z 3060 (1975): Method of ultrasonic manual testing and classification of test results for steel welds.

1732 KTA Sicherheitstechnische Regeln:
     KTA 3201   Komponenten des Primärkreises von Leichtwasserreaktoren.
     KTA 3201.1 (1979): Werkstoffe.
     KTA 3201.2 (1979): Auslegung, Konstruktion und Berechnung.
     KTA 3201.3 (1979): Herstellung.
     KTA 3201.4 (1982): Wiederkehrende Prüfungen und Betriebsüberwachung.

1733 Krautkrämer GmbH: Fehlergrößenbestimmung Das Echo 19 (1967), 195–211.

1734 Kretztechnik GmbH: Ultrasonic plant for testing cast steel billets. Non Destr. Test. Int. 1 (1968) 332–334.

1735 Lockheed Spezification T. O. 1 F-4C-36S-42 (1976).

1736 Materials Evaluation: Redi Reference Guide. Mater. Eval. 46 (1988) 286–287

1737 Material Research and Standards (Sept. 1969 pp. 21–24): Detection of inclusions in bearing quality steel by the ultrasonic method.

1738 NASA: Phasenunempfindlicher Ultraschallwandler. DE Pat. 2 929 766 (1980).

1739 NRC (USA): Standard review plan. NUREG-0800.

1740 NRC: NRC-Regulatory Guides.

1741 Rail Engineering Int.: Rail condition evaluation by ultrasonic car. (May 1971).

1742 La vie du rail (1984) No. 1939, N. N.: La V 4.

1743 Renco Corp.: Dickenmeßgerät, insbesondere für die Dicke von Rückenfett. DE GbM 7 915 059 (1979).

1744 Round Oak Steel Works: Methods of measurement and analysis automatic NDT for the assessment of steel quality. Commission of the European Communities, Final Report (1980). EUR 6656 EN

1745 RSK: RSK-Leitlinie für Druckwasserreaktoren 3rd Ed. (Oct. 1981). — RSK-Leitlinie für Siedewasserreaktoren, Draft (Sept. 1980)

1746 Firma Tube Investments (Ed.): E. M. A. surface inspection. Further developments. T.I.R.L. Rep. No. PR 1029, Cambridge 1976

1747 Firma Tube Investments (Ed.): R.O.S.W. in-line surface wave system description and performance. T.I.R.L. Rep. No. PR 1070, Cambridge 1979

1748 Ultrasonic Imaging. An International Journal. Since 1979. New York: Academic Press.

1749 United Aircraft Corp.: Vorrichtung zur Erzeugung hochfrequenter akustischer Schwingungen in Form akustischer Impulse hoher Energie. DE Pat. 1,772,530 (1968).

1750 VDEh: Stahl-Eisen-Prüfblatt (SEP) 1915 (1977): Ultraschallprüfung auf Längsfehler von Rohren aus warmfesten Stählen.

1751 VDEh: Stahl-Eisen-Lieferbedingungen (SEE) 072 (1977): Ultraschallgeprüftes Grobblech.

1752 VdTÜV: AD-Merkblatt HP 5/3 (1977): Herstellung und Prüfung der Verbindungen. Zerstörungsfreie Prüfung der Schweißnähte.

Supplementary References

1. Textbooks and Handbooks

S 1 McGonnagle, W. J. (Ed.): International advances in nondestructive testing. New York: Gordon & Breach Publ. Vol. 1 (1969), vol. 2 (1970), vol. 3 (1971), vol. 4 (1972), vol. 5 (1977), vol. 6 (1979), vol. 7 (1981), vol. 8 (1981), vol. 9 (1983), vol. 10 (1984), vol. 11 (1985)

S 2 Millner, R. (Ed.): Wissensspeicher Ultraschalltechnik. Leipzig: VEB Fachbuchverlag 1987

S 3 Thompson, D. O.; Chimenti, D. E. (Eds.): Review of progress in quantitative nondestructive evaluation. New York: Plenum Publ. Corp. Vol. 1A, B (1982), vol. 2A, B (1983), vol. 3A, B (1984), vol. 4A, B (1984), vol. 5A, B (1985)

2. Publications with named author

S 4 Adler, L.; Rokhlin, St. I.; Bolland, K.; Nagy, P. B.: Scattering of elastic waves from isotropic and anisotropic boundaries. Proc. 11th World Conf. NDT Las Vegas 1985, Vol. 2, pp. 860–867

S 5 Aindow, J. D.; Markham, M. F.; Puttick, K. E.; Rider, J. G.; Rudman, M. R.: Fibre orientation detection in injectionmoulded carbon fibre reinforced components by thermography and ultrasonics. NDT Intern. 19 (1986) 24–29

S 6 Alers, G. A.; Burns, L. R.: EMAT designs for special application. Mater. Eval. 45 (1987) 1184–1189

S 7 Anderson, M. R.: Nondestructive testing of offshore structures. NDT Intern. 20 (1987) 17–21

S 8 Aoyama, Sh.; Asai, K.: Device for inspecting spot welds. USA-patent No. 4, 208, 917 (1980)

S 9 Arakawa, T.; Hirose, S.; Senda, T.: The detection of weld cracks using ultrasonic testing. NDT Intern. 18 (1985) 9–16

S 10 Baligand, B.; Grozellier, M.; Romy, D.: Improvement in ultrasonic examination of austenitic steels. Mater. Eval. 44 (1986) 577–581

S 11 Balluet, J. C.: Separation of two close echoes. Ann. Telecomm. 36 (1981) 7–8

S 12 Bartsch, R.; Schmitz, V.: Ultraschallprüfung mit dem LSAFT-Verfahren an dem Druckbehälter und der Hauptkühlmittelleitung des Kernkraftwerks Obrigheim. Conf. DGZfP 1987 Lindau

S 13 Batra, N. K.; Chaskelis, H. H.: Determination of minimum flaw size detectable by ultrasonics in titanium alloy plates. NDT Intern. 18 (1985), 261–264

S 14 Berner, K.: Automatische Prüfung und Bewertung von Proben mit wasserstoff-induzierten Rissen. Proc. Seminar DGZfP Moderne Methoden zur quantitativen Bewertung von Ultraschall-Anzeigen, Düsseldorf 1987, pp. 190–204

S 15 Bhatt, M.; Hogg, P. J.: Test conditions in stress wave factor measurements for fibre-reinforced composites and laminates. NDT Intern. 21 (1988) 3–10

S 16 Bilgutay, N. M.; Newhouse, V. L.; Amir, I.: Theoretical analysis and performance of the minimization algorithm in nondestructive testing applications. Proc. 11th World Conf. NDT Las Vegas 1985, Vol. 2, pp. 1048–1053

S 17 Böttger, W.; Graff, A.; Schneider, H.: Dickenmessung an Stahl — mit elektromagne-tischer Ultraschallanregung bei Temperatur bis 1200 °C. Materialprüfung 29 (1987) 124–128

S 18 Bossi, R. H.; Hildebrand, B. P.: Stepped frequency ultrasonic holography. Mater. Eval. 46 (1988) 659–670

S 19 Bossi, R.; Boyd, D.; Oberg, D.; Steffens, R.: Automated detection and sizing of defects in complex geometries. Proc. 11th World Conf. NDT Las Vegas 1985, Vol. 3, pp. 1540–1547

S 20 Bray, D. E.; Leon-Salamanca, T.: Zero-force travel-time parameters for ultrasonic head-waves in railroad rail. Mater. Eval. 43 (1985) 854–858/863

S 21 Bray, D. E.; Najm, M.: Ultrasonic angle-beam inspection through the coldworked layer in railroad rail. NDT Intern. 18 (1985), 139–144

S 22 Brekow, G.; Wüstenberg, H.; Möhrle, W.; Schulz, E.: Ultraschallprüfung am Kugel-boden von Siedewasserdruckgefäßen mit Gruppenstrahlerprüfköpfen. Conf. DGZfP 1987 Lindau

S 23 Brokowski, A.; Deputat, J.: Ultrasonic measurements of residual stresses in rails. Proc. 11th World Conf. NDT Las Vegas 1985, Vol. 1, pp. 592–598

S 24 Brosey, W. D.; Dews, T. W.: Ultrasonic girth-weld evaluation of aluminium test mandrels. Mater. Eval. 45 (1987) 358–362

S 25 Brunk, J. A.: Ultrasonic examination of absorbent materials. Mater. Eval. 46 (1988) 584–585

S 26 Burch, S. F.; Bealing, N. K.: A physical approach to the automated ultrasonic characterization of buried weld defects in ferritic steel. NDT Intern. 19 (1986) 145–153

S 27 Bussiere, J. F.: Online measurement of the microstructure and mechanical properties of steel. Mater. Eval. 44 (1986) 560–567

S 28 Buynak, C. F.; Crame, R. L.: A novel acoustic coupling device using permeable membrane. Mater. Eval. 45 (1987) 743–746

S 29 Canella, G.; Monti, F.: Ultrasonic inspection of hot thick steel products. NDT Intern. 13 (1980) 10–14

S 30 Capener, E. L.: Regression analysis to assess ultrasonic inspection results. Mater. Eval. 46 (1988) 671–678

S 31 Cartwright, D. K.: Validating the inspection of PWR pressure vessels. Brit. J. NDT 29 (1987) 409–410

S 32 Castel, J. G., Husarek, V.: Utilisation pratique pour les matériaux composites d'un appareil à ultrasons portatif numérique. Matériaux et Techniques 1987, 229–233.

S 33 Chaloner, C. A.; Bond, L. J.: Ultrasonic signal processing using Born inversion. NDT Intern. 19 (1986) 133–140

S 34 Chen, W. H.; Chung, I. S.; Kou, C. S.: Application of weiner filtering and pulse compression techniques to ultrasonic nondestructive testing. Proc. 11th World Conf. NDT Las Vegas 1985, Vol. 2, pp. 1056–1063

S 35 Clark, G. A.; Tilly, D. M.; Cook, W. D.: Ultrasonic signal/image restoration for quantitative NDE. NDT Intern. 19 (1986) 169–176

S 36 Clark, R.; Dover, W. D.; Bond, L. J.: The effect of crack closure on the reliability of NDT predictions of crack size. NDT Intern. 20 (1987) 269–275

S 37 Collingwood, J. C.: Nuclear NDT development at Harwell. NDT Intern. 20 (1987) 33–41

S 38 Cross, N. O.: Ultrasonic flaw analysis without a computer. Proc. 11th World Conf. NDT Las Vegas 1985, Vol. 2, pp. 827–832

S 39 Crostack, H. A.; Oppermann, W.: Investigations to improving the detection sensitivity and evaluation of corrosion cracks with ultrasound testing. Proceed. 11th World Conf. NDT, Las Vegas 1985, Vol. 2, pp. 868–873

S 40 Crostack, H. A.: Roye, W.: Ultrasonic multifrequency technique — a new method for the description of defects. Proceed. 11th World Conf. NDT Las Vegas 1985 (1985). Vol. 3, pp. 1648–1653

S 41 Crutzen, S.; Jehenson, P.; Borloo, E.: The PISC II RRT plates and their intended defects. Brit. J. NDT 29 (1987) 307–317

S 42 Deuster, G.; Schmülling, W.: Zerstörungsfreie Prüfungen im Rahmen des PISC II-Programms. Proc. Conf. DGZfP 1987 Lindau

S 43 Deutsch, V.; Platte, M.; Vogt, M.: Technische Maßnahmen zur Verbesserung der Reproduzierbarkeit von Ultraschall-Prüfbefunden. Proc. Seminar DGZfP Moderne Methoden zur quantitativen Bewertung von Ultraschall-Anzeigen, Düsseldorf 1987, pp. 171–189

S 44 Doctor, S. R.; Hall, T. E.; Reid, L. D.: SAFT — the evolution of a signal processing technique for ultrasonic testing technology. NDT Intern. 19 (1986) 163–167

S 45 Durstberger, R.; Hackl, M.; Putz, E.: Fehlerbeurteilung mit Hilfe eines Expertensystems. Proc. Seminar DGZfP Moderne Methoden zur quantitativen Bewertung von Ultraschall-Anzeigen, Düsseldorf 1987, pp. 160–170

S 46 Dzenis, W.: Anwendung von Ultraschall zur Prüfung von Beton und Baukeramik auf Fehler und Festigkeit. Materialprüfung 28 (1986) 109–115

S 47 Edelmann, X.: Vergleichende Gegenüberstellung verschiedener Bewertungsmöglichkeiten. Proc. Seminar DGZfP Moderne Methoden zur quantitativen Bewertung von Ultraschallanzeigen, Düsseldorf 1987, pp. 92–120

S 48 Edelmann, X.: Voraussetzungen für eine erfolgreiche mechanisierte wiederkehrende Ultraschallprüfung an Rohrleitungen in Kernkraftwerken. Proc. Conf. DGZfP 1987 Lindau

S 49 Erhard, A.; Wüstenberg, H.; Szafarska, E.; Schulz, E.; Rathgeb, W.: Auswertung und Bewertung der Meßergebnisse von Ultraschall-Stutzenkantenprüfungen. Proc. Conf. DGZfP 1987 Lindau, Vol. 10, pp. 129–142

S 50 Fiore, St. R.; Peist, W. D.; Walther, H.: Small defect characterization in powder metallurgy materials. Proc. 11th World Conf. NDT Las Vegas (1985), Vol. 3, pp. 1625–1632

S 51 Frielinghaus, R.: Ultrasonic testing of industrial ceramics. Fachber. Hüttenpraxis Metallweiterverarb. 25 (1987) 315–319

S 52 Fuller, M. D.; Avioli, M. J.; Rose, J. L.: Sizing of intergranular stress corrosion cracking using low frequency ultrasound. Proc. 11th World Conf. NDT Las Vegas (1985), Vol. 3, pp. 1480–1486

S 53 Generazio, E. R.: The role of the reflection coefficient in precision measurement of ultrasonic attenuation. Mater. Eval. 43 (1985) 995–1004.

S 54 Gladwell, G. M. L.: The calculation of mechanical impedances relating to an indenter vibrating on the surface of a semi-infinite elastic body. J. Sound and Vibration 8 (1968) 215–220

S 55 Goebbels, K.: Gefügebeurteilung mittels Ultraschall-Streuung. Materialprüfung 17 (1975) 231–233

S 56 Goebbels, K.: Material characterization by ultrasonic backscattering. Proc. 11th World Conf. NDT Las Vegas (1985), Vol. 3, pp. 1594–1599

S 57 Graf, P.; Baumann, J.; Grad, G.; Klofac, P.: Prozeßintegrierte Ultraschall-Wanddickenmessung an Kabeln und Leitungen mit hoher Meßgenauigkeit durch automatische Kompensation von Temperatureinflüssen. Proc. DGZfP Conf. Lindau 1987, Vol. 10, pp. 602–609

S 58 Granville, R. K.; Taylor, J. L.: Improvement in Signal-to-Noise Ratio during the Ultrasonic Testing of Titanium Alloys. Br. J. NDT 28 (1986) 228–231

S 59 Gruber, G. J.; Hamlin, D. R.; Grothus, H. L.; Jackson, J. L.: Imaging of fatigue cracks in cladded pressure vessels with the SLIC 50. NDT Intern. 19 (1986) 155–162

S 60 Gruber, J. J.; Smith, J. M.; Brockelman, R. H.: Ultrasonic velocity C-scans for ceramic and composite material characterization. Mater. Eval. 46 (1988) 90–96

S 61 Guyott, C. C. H.; Cawley, P.: Evaluation of the cohesive properties of adhesive joints using ultrasonic spectroscopy. NDT Intern. 21 (1988) 233–240

S 62 Hagemaier, D. J.; Fassbender, R. H.: Ultrasonic inspection of carbon-epoxy composites. Mater. Eval. 43 (1985) 556–560

S 63 Haines, N. F.; Crutzen, S.; Vinche, C. J.: A review of the major PISC II Round Robin Test results. Brit. J. NDT 29 (1987) 411–417

S 64 Hall, K. G.; Booth, G.: Ultrasonic defect evaluation for high fatigue strength bridge welds. Brit. J. NDT 29 (1987) 403–408

S 65 Harumi, K.: Computer simulation of ultrasonics in a solid. NDT Intern. 19 (1986) 315–332

S 66 Hayman, A. J.: An improved ultrasonic Tip-Corner Timing Method for sizing shallow surface-breaking cracks. Brit. J. NDT 27 (1985) 295–299

S 67 Hecht, A.; Neumann, E.; Rose, P.: Computer-aided ultrasonic testing of non-oxide ceramics. NDT Intern. 19 (1986) 401–406

S 68 Heinrich, D.; Meyer, H.-J.; Prestel, W.: Bewertung von Ultraschallbefunden an Schmiedestücken. Proc. Seminar DGZfP Moderne Methoden zur quantitativen Bewertung von Ultraschallanzeigen, Düsseldorf 1987, pp. 59–91

S 69 Henneke, E. G.; Duke, J. C.: Analytical ultrasonics for evaluation of composite material response. Mater. Eval. 43 (1985) 740–745/753

S 70 Henrique, L. M. dos Reis;; Bergman, L. A.; Bucksbee, J. H.: Adhesive bond strength quality assurance using the acousto-ultrasonic technique. Brit. J. NDT 28 (1986) 357–359

S 71 Highmore, P. J.; Rogerson, A.; Poulter, I. N.: The ultrasonic inspection of PISC II Plate 2 by the Risley Nuclear Laboratories. Brit. J. NDT 30 (1988) 9–17

S 72 Hirsekorn, S.: The scattering of ultrasonic waves in polycrystalline materials with texture. J. Acoust. Soc. Am. 77 (1985) 832–843

S 73 Hirsekorn, S.: Directional dependence of ultrasonic propagation in textured polycrystals. J. Acoust. Soc. Am. 79 (1986) 1269–1279

S 74 Hirsekorn, S.: The scattering of ultrasonic waves by multiphase polycrystals. J. Acoust. Soc. Am. 83 (1988) 1231–1242

S 75 Hirsekorn, S.; Goebbels, K.; Schneider, E.: Stress determination in textured polycrystals using ultrasonic technique. Workshop on "Experimental Techniques of Texture Analysis", 25.–29. 3. 1985, Clausthal-Zellerfeld

S 76 Hull, D. R.; Kautz, H. E.; Vary, A.: Measurement of ultrasonic velocity using phase-slope and cross-correlation methods. Mater. Eval. 43 (1985) 1455–1460

S 77 Hutchins, D.; Hu, J.; Lundgren, K.: A Comparison of Laser and EMAT Techniques for Noncontact Ultrasonics. Mater. Eval. 44 (1986) 1244–1253

S 78 Imoto, K.: Calculations on the sound fields of various pulse shape. Proc. 11th World Conf. NDT Las Vegas (1985), Vol. 2, pp. 756–759

S 79 Jestrich, H.-A.; Prestel, W.; Heinrich, D.; Schmalenbeck, W.: Die Bedeutung der Ultraschall-Reflektorgröße für die Bruchmechanik. Materialprüfung 29 (1987) 13–16

S 80 Johnson, J. A.; Carlson, N. M.: Weld energy reduction by using concurrent non-destructive evaluation. NDT Intern. 19 (1986) 190–196

S 81 Johnston, J.: Optimization of accuracy in ultrasonic velocity measurement of nodular cast iron. Proc. 11th World Conf. NDT Las Vegas (1985), Vol. 3, pp. 1741–1745

S 82 Jones, M. P.; Blessing, G. V.; Robbins, C. R.: Dry-coupled ultrasonic elasticity measurements of sintered ceramics and their green state. Mater. Eval. 44 (1986) 859–862

S 83 Just, T.: Die weitere Entwicklung der mechanisierten wiederkehrenden Prüfungen in Kernkraftwerken. Conf. DGZfP 1987 Lindau

S 84 Karbach, B.: Ultrasonic testing according to api Specifications at different production steps of seamless and welded tubes. Proc. 11th World Conf. Las Vegas (1985), Vol. 2, pp. 1139–1145

S 85 Kautz, H. E.: Ultrasonic evaluation of mechanical properties of thick, multilayered filament-wound composites. Mater. Eval. 45 (1987) 1404–1412

S 86 Kleesattel, C.: On the measurement of elasticity, hardness, creep and relaxation of plastics with a Vickers indenter by an electro-acoustic method. Materialprüfung 20 (1978) 112–119

S 87 Kleesattel, C.: Das UCI-(Ultrasonic-Contact-Impedance) Härteprüfverfahren. Das Echo (1973) 27, 467–478

S 88 Kline, R. A.; Egle, J.: Application of digital methods to ultrasonic materials characterization. NDT Intern. 19 (1986) 341–347

S 89 Kline, R. A.; Hashemi, D.: Ultrasonic guided wave monitoring of fatigue damage development in bonded joints. Mater. Eval. 45 (1987) 1076–1082

S 90 Kröning, M.; Schmid, R.: Statische und dynamische A-Bild-Bewertung. Proc. Seminar DGZfP Moderne Methoden zur quantitativen Bewertung von Ultraschall-Anzeigen. Düsseldorf 1987, pp. 33–58

S 91 Kubota, J.; Sasaki, S.; Sato, I.; Ito, S; Kadowaki, T.; Yamaguchi, H.; Fujisawa, K.; Murayama, R.: An improved electromagnetic ultrasonic testing technique for flaw detection for hot steel. Mater. Eval. 46 (1988) 523–527

S 92 Kupperman, D. S.; Reimann, K. J.; Abrego-Lopez, J.: Ultrasonic NDE of cast stainless steel. NDT Intern. 20 (1987) 145–152

S 93 Kuppermann, D. S.; Reimann, H. J.; Abrego-Lopez, J.: Ultrasonic NDE of cast stainless steel. NDT Intern. 20 (1987) 145–152

S 94 Kutty, T. R. G.; Chandrasekharan, K. N.; Panakkal, J. P.; Ghosal, S. K.; De, P. K.: Use of ultrasonic velocity for nondestructive evaluation of ferrite content in duplex stainless steels. NDT Inter. 20 (1987) 359–361

S 95 Lahure, P.: Ultrasonic test method for the detection of cracking in steam turbine blade roots. Mater. Eval. 45 (1987) 24–25

S 96 Langenberg, K. J.; Berger, M.; Kreutter, Th.; Mayer, K.; Schmitz, V.: Synthetic aperture focussing technique signal processing. NDT Intern. 19 (1986) 177–189

S 97 Leon-Salamanca, T.; Bray, D. E.: Application of ultrasonic P-wave for nondestructive stress measurement. Proc. 11th World Conf. NDT Las Vegas (1985), Vol. 1, pp. 651–653

S 98 Leviston, D.; Bridge, B.: Evaluation of the subsurface microstructure of quenched and tempered carbon steel by ultrasonic backscatter. NDT Intern. 21 (1988) 17–25

S 99 Light, G. M.; Joshi, N. R.; Liu, S.-N.: Ultrasonic detection of stress-corrosion cracks in reactor pressure vessel and primary coolant system anchor studs (bolts). Mater. Eval. 45 (1987) 1413–1418

S100 Ludwig, R.; Lord, W.: A finite-element study of ultrasonic wave propagation and scattering in an aluminium block. Mater. Eval. 46 (1988) 108–113

S101 Mackiewicz, S.; Gorzny, J.; Kiersnowski, M.; Pawlowski, Z.: Ultrasonic detection and depth measurements of cracks in thick welds. Proc. 11th World Conf. NDT Las Vegas (1985), Vol. 2, pp. 1124–1129

S102 Mahmoud, M. A.: Low-melting alloys used as ultrasonic couplants at high temperature. Mater. Eval. 43 (1985) 196–200/205

S103 Mahmoud, M. A. M.; Hewitt, G. A.; Burns, D. J.: Sizing of planar defects by use of double-angle ultrasonic beams and tip-echo times. Mater. Eval. 44 (1986) 1125–1131

S104 Mak, D. K.: Ultrasonic inspection of tubular goods using two probes in tandem. Mater. Eval. 45 (1987) 386

S105 Maldague, X.; Cield, P.; Jen, C. K.: Nondestructive testing applications of laser-generated focused acoustic waves. Proc. 11th World Conf. NDT Las Vegas (1985),

S106 Maldague, X.; Cielo, P.; Jen, C. K.: Nondestructive applications of laser-generated focused acoustic waves. Mater. Eval. 44 (1986) 1120–1124

S107 Mansour, T. M.: Ultrasonic inspection of spot welds in thin-gage steel. Mater. Eval. 46 (1988) 650–658

S108 Martin, B. G.: Modelling material acoustic properties by use of equivalent multilayer systems. Mater. Eval. 44 (1986) 1139–1140

S109 Maxfield, B. W.; Kuramoto, A.; Hulbert, J. K.: Evaluating EMAT designs for selected applications. Mater. Eval. 45 (1987) 1166–1183

S110 McNab, A.; Campbell, M. J.: Ultrasonic phased arrays for nondestructive testing. NDT Intern. 20 (1987) 333–337

S111 Meyer, P. A.; Carodiskey, T. J.: Ultrasonic B boreside array for rapid heat-exchanger tube inspection. Mater. Eval. 45 (1987) 1190–1194

S112 Monchalin, J.-P.; Héon, R.: Laser Ultrasonic Generation and Optical Detection with a Confocal Fabry-Pérot Interferometer. Mater. Eval. 44 (1986) 1231–1237

S113 Morgner, W.; Schiebold, K.-H.; Krause, H.: Ultrasonic high-temperature materials evaluation — a solved problem? Mater. Eval. 45 (1987) 569–571

S114 Mott, G.; Taszarek, B. J.: Ultrasonic characterization of an interference fit. Mater. Eval. 43 (1985) 990–994

S115 Müller, G. P.; Hallenmeier, L.; Heinrich, D.; Grabendoerfer, W.: Automatic ultrasonic pre-service and in-service inspection of pressurized components of the primary circuit of a nuclear reactor. Proc. 11th World Conf. NDT Las Vegas (1985), Vol. 3, pp. 1469–1472

S116 Murphy, J. C.; Wetsel, G. C.: Photothermal methods of optical characterization of materials. Mater. Eval. 44 (1986) 1224–1230

S117 Nagy, P. B.; Jungman, A.; Adler, L.: Measurements of back-scattered Lamb waves in composite plates. Mater. Eval. 46 (1988) 97–100

S118 Najm, M.; Bray, D. E.: Experimental investigations of the effect of cold-working on the refraction of head waves in railroad rail. Mater. Eval. 44 (1986) 453–470

S119 Nichols, R.; McDonald, N.: An introduction to the PISC II project-programs for the inspection of steel components. Brit. J. NDT 29 (1987) 223–227

S120 Noujaillard, B.; Logette, P.; Rouvaen, J. M.; Suisse, H.; Fevier, H.: Acoustic microscopy: a tool for non-destructive evaluation of ceramics. NDT Intern. 19 (1986) 77–82

S121 Nussmüller, E.; Meyer, W.; Bauer, R.: Improved method of defect evaluation in ultrasonic examination of forgings by considered production parameters. 4th. Conf. NDT, London 1987, paper SS 07/05

S122 Ogawa, N.; Ohnishi, E.; Gotoh, K.; Okamoto, K.: Automatic ultrasonic testing equipment for rail during production. Proc. 11th World Conf. Las Vegas (1985), Vol. 3, 1884–1891

S123 Ogilvy, J. A.: Computerized ultrasonic ray tracing in austenitic steel. NDT Intern. 18 (1985) 67–77

S124 Ogilvy, J. A.: A model for elastic wave propagation in anisotropic media with applications to ultrasonic inspection through austenitic steel. Brit. J. NDT 27 (1985) 13–21

S125 Ogilvy, J. A.: The influence of austenitic weld geometry and manufacture on ultrasonic inspection of welded joints. Brit. J. NDT 29 (1987) 147–156

S126 Ogilvy, J. A.: On the use of focused beams in austenitic welds. Brit. J. NDT 29 (1987) 238–246

S127 Ohmatsu, K.; Goto, M.; Itabashi, Y.; Komura, I.: Computerized ultrasonic examination system for shrunk-on wheels of turbine rotor. Proc. 11th World Conf. NDT Las Vegas (1985), Vol. 3, pp. 1838–1845

S128 Ostrovsky, B.: Determination of residual stress by nondestructive methods. Proc. 11th World Conf. NDT Las Vegas (1985), Vol. 1, pp. 599–606

S129 Panhuise, V. E.; Richmond, L.; Novak, R.: The implementation of computerized ultrasonic scan system. Mater. Eval. 42 (1984) 231–238

S130 Paradis, L.; Serruys, Y.; Saglio, R.: A time-of-flight method for crack evaluation using focused ultrasonic probes. Mater. Eval. 44 (1986) 568–570

S131 Paradis, L.; Serruys, Y.; Saglio, R.: Ultrasonic signal processing for thickness measurement and detection of near-surface defects. Mater. Eval. 44 (1986) 1344–1349

S132 Piché, L.; Champagne, B.; Monchalin, J.-P.: Laser ultrasonic measurements of elastic constants of composites. Mater. Eval. 45 (1987) 74–79

S133 Pilarski, A.: Ultrasonic evaluation of the adhesion degree in layered joints. Mater. Eval. 43 (1985) 765–770

S134 Pilarski, A.; Rose, J. L.: Ultrasonic oblique incidence for improved sensitivity in interface weakness determination. NDT Intern. 21 (1988) 241–245

S135 Posakony, G. J.: Experimental analysis of ultrasonic responses from artificial defects. Mater. Eval. 44 (1986) 1567–1572

S136 Poulter, L. N. J.: Signal processing methods applied in the ultrasonic inspection of PWR inlet nozzles. NDT Intern. 19 (1986) 141–144

S137 Pritchard, S. E.: The use of ultrasonics for residual stress analysis. NDT Intern. 20 (1987) 57–60

S138 Reynolds, W. N.: The inspection of engineering ceramics. 4th Conf. NDT London 1987, paper SS 18/09

S139 Rivera, O.; Vitale, F. V.: Airborne ultrasonic scanning. Mater. Eval. 46 (1988) 614–615

S140 Rogerson, A.; Poulter, L. N. J.; Clough, P.; Cooper, A. G.: RNL automated ultrasonic inspection of the PISC II PWR inlet nozzle (Plate 3). Brit. J. NDT 30 (1988) 86–93

S141 Rogovsky, A. J.; Holmquist, G. R.: Nondestructive inspection of miniature aluminium welds in composite structures. Mater. Eval. 42 (1984) 318–324

S142 Rose, J. L.; Karpur, P.; Newhouse, V. L.: Utility of split-spectrum processing in ultrasonic nondestructive evaluation. Mater. Eval. 46 (1988) 114–122

S143 Rose, J. L.; Pilarski, A.: Surface and plate waves in layered structures. Mater. Eval. 46 (1988) 598–605

S144 Rosenberg, R.: Hochauflösendes Ultraschall-C-Bild-System. Proc. DGZfP Conf. Lindau 1987, Vol. 10, pp. 402–410

S145 Roth, D. J.; Generazio, E. R.; Baaklini, G. Y.: Quantitative void characterization in structural ceramics by use of a scanning laser acoustic microscope (SLAM). Mater. Eval. 45 (1987) 958–966

S146 Salzburger, H. J.; Repplinger, W.; Schmidt, W.: Entwicklung, Betriebstest und Einsatz eines automatischen Systems zur wiederkehrenden Prüfung der Laufflächen von Eisenbahnrädern. Proc. DGZfP Conf. Lindau 1987, Vol. 10, pp. 253–264

S147 Sandhu, J. S.: Acoustography: A new imaging technique and its application to nondestructive evaluation. Mater. Eval. 46 (1988) 608–613

S148 Schiebold, K.; Morgner, W.; Krause, H.: Untersuchungen zur Ultraschallprüfung bei höheren Temperaturen durch Langzeitdruckkontaktverfahren. Neue Hütte 30 (1985), 304–308

S149 Schmitz, V.: Stellenwert abbildender Verfahren zur quantitativen Bewertung von Ultraschallbefunden. Proc. Seminar DGZfP Moderne Methoden zur quantitativen Bewertung von Ultraschall. Anzeigen, Düsseldorf 1987, pp. 139–159

S150 Schramm, R. E.; Siewert, Th. A.: Weld flaw sizing using back-scattered and forward-scattered low frequency ultrasound. Proc. 11th World Conf. Las Vegas (1985), Vol. 2, pp. 1286–1293

S151 Schwarz, H.-P.: Development of a divided-ring array for three-dimensional beam steering in ultrasonic nondestructive testing: Theoretical and experimental results of a prototype. Mater. Eval. 45 (1987) 951–957

S152 Scruby, C. B.; Smith, R. L.; Moss, B. C.: Microstructure monitoring by laser-ultrasonic attenuation and forward scattering. NDT Intern. 19 (1986) 307–313.

S153 Serabian, S.: Amplitude independent flaw characterization — use of frequency domain Displays. Proc. 11th World Conf. NDT Las Vegas (1985), Vol. 2, pp. 1030–1037

S154 Serabian, S.: Amplitude independent flaw characterization — use of maximum amplitude location. Proc. 11th World Conf. NDT Las Vegas (1985), Vol. 2, pp. 1072–1079

S155 Serabian, S.; O'Callahan, J. C.: Pulsed ultrasonic flaw detection model. Mater. Eval. 43 (1985) 873–878

S156 Sharp, R. D.; Chan, R. W. Y.; Hay, D. R.: Welding defect sizing by ultrasonic echo signal interpretation using advanced pattern recognition techniques. Proc. 11th World Conf. NDT Las Vegas (1985), Vol. 2, pp. 1316–1323

S157 Silk, M. G.: Changes in ultrasonic defect location and sizing. NDT Intern. 20 (1987) 9–14

S158 Simpson, W. A.: Time-domain deconvolution: a new technique to improve resolution for ultrasonic flaw characterization in stainless steel. Mater. Eval. 44 (1986) 998–1003

S159 Sinclair, A.: Analysis of the ultrasonic frequency response for flaw detection: a technical review. Mater. Eval. 43 (1985) 105–107

S160 Singh, G. P.; Udpa, S.: The role of digital signal processing in NDT. NDT Intern. 19 (1986) 125–132

S161 Smith, B. J.: ZIPSCAN — A new concept in ultrasonic instrumentation. Brit. J. NDT 28 (1986) 9–16

S162 Smith, P. H.: Practical Application of 'creeping' Waves. Brit. J. NDT 29 (1987) 318–321

S163 Smith, R. L.: Ultrasonic materials characterization. NDT Intern. 20 (1987) 43–48

S164 Spengler, F.; Außerwöger, J.; Frielinghaus, R.; Ganglbauer, O.; Niklas, L.: Comson flaw-diagnosis system. 4. Conf. NDT, London 1987 paper SS 09/09

S165 Stanke, F. E.; Kino, G. S.: A unified theory for elastic wave propagation in poly-crystalline materials. J. Acoust. Soc. Am. 75 (1984) 665–681

S166 Swanson, Ch. E.: Ultrasonic testing of nozzle attachment welds in pressure vessels. Mater. Eval. 46 (1988) 566–572

S167 Szelazek, J.: Ultrasonic detection of cracks in wheel set axles. NDT Intern. 20 (1987) 177–180

S168 Teodoru, G. V.: Mechanical strength of concrete at early ages as reflected by Schmidt rebound number, ultrasonic pulse velocity and ultrasonic attenuation. Paper SP 95-8. Conf. Am. Concrete Inst. Chicago 1985, pp. 139–153.

S169 Teodoru, G. V.: Effect of hydrothermal curing of concrete on its compressive strength and on the mechanical properties determined by NDT, Durability of Building Materials 2 (1985) 351–364.

S170 Vary, A.; Lark, R. F.: Correlation of fiber composite tensile strength and the ultra-sonic stress wave factor. NASA Lewis Research Center, Cleveland, Ohio USA, NASA TM 78846, 1978.

S171 Vary, A.; Klima, S. J.; Abbe, P. A.; Baaklini, G. Y.: Ultrasonic NDE of structural ceramics for power and propulsion systems. 4th Conf. NDT London 1987 paper SS 10/05

S172 Volkmann, K.; Opara, U.; Viehmann, H.: Modelling an ultrasonic system using rational functions in the complex frequency plane. Proc. 11th World Conf. NDT Las Vegas (1985), Vol. 2, pp. 1040–1047

S173 Wagner, J. W.: High reolution holographic techniques for visualization of surface acoustic waves. Mater. Eval. 44 (1986) 1238–1243

S174 Walker, D.; Opara, U.: Neues Ultraschall-System zur Strukturanalyse mit C-Bildern. Proc. DGZfP Conf. Lindau 1987, Vol. 10, pp. 438–446

S175 Walker, D.; Opara, U.: Mikro NDT on powder metals and technical ceramics. 4th Conf. NDT London 1987, paper SS 18/10

S176 Walte, F.: Prüfung geschichteter Medien mittels Ultraschall. Teil I: Grundprinzip. Materialprüfung 27 (1985) 191–193; Teil II: Zwei- und mehrfach geschichtetes Medium. Materialprüfung 27 (1985) 265–268

S177 Werden, D.: Beitrag der Ultraschallprüfung zur Bauteilsicherung unter Berücksichtigung der Bruchmechanik. Proc. Seminar DGZfP Moderne Methoden zur quantitativen Bewertung von Ultraschall-Anzeigen. Düsseldorf 1987, pp. 121–138

S178 Wiese, A.; Opara, U.: High frequency ultrasonic equipment for detection of flaws smaller than 1/16 inch flat bottom hole. Proc. 11th World Conf. Las Vegas (1985), Vol. 3, pp. 1669–1676

S179 Williams, J. H.; Karaguelle, H.; Lee, S. S.: Ultrasonic testing of plates containing edge cracks. Mater. Eval. 44 (1986) 100–107

S180 Promising quantitative nondestructive evaluation techniques for composite materials. Mater. Eval. 43 (1985) 561–565

S181 Wüstenberg, H.; Erhard, A.: Bewertungskriterien für Qualitätssicherung und Betriebs-sicherheit. Proc. Seminar DGZfP Moderne Methoden zur quantitativen Bewertung von Ultraschallanzeigen, Düsseldorf 1987, pp. 7–32

S182 Wüstenberg, H.; Erhard, A.; Schenk, G.; Montag, H.-J.: Anwendung der Ultra-schalltomographie an Turbinen und Generatorwellen. Materialprüfung 29 (1987) 297–302

S183 Wüstenberg, H.; Möhrle, W.; Wegner, W.: Winkelprüfköpfe mit Schielwinkel-schwenk durch laufzeitgesteuerte Gruppenstrahler. Proc. DGZfP Conf. Lindau 1987, Vol. 10, pp. 538–550

S184 Wüstenberg, H.; Wegner, W.; Möhrle, W.; Schenk, G.: Nachweis von Spannungs-rißkorrosion (SpRK) mit Ultraschall-Gruppenstrahlern. Materialprüfung 28 (1986) 20–24

S185 Wu Nansong; Shi Jihua: Quasi three-dimensional display of flaws images detected ultrasonically. Proc. 11th World Conf. NDT, Las Vegas (1985), Vol. 2, pp. 980–986

S186 Zhang Jiao-Ping; Wei Yu: Flaw plane identification: a new imaging technique in nondestructive testing. NDT Intern. 20 (1987) 355–358

S187 Zhang, S. Y.; Shen, J. Z.; Ying, C. F.: The reflection of the Lamb wave by a free plate edge: Visualization and theory. Mater. Eval. 46 (1988) 638–641

3. Publications without named author by Institutes, Corporations etc.

S188 Bundesanstalt für Materialforschung und -prüfung und Deutsche Gesellschaft für Zerstörungsfreie Prüfung: Literaturrecherche zum Seminar über Moderne Methoden zur quantitativen Bewertung von Ultraschall-Anzeigen. Düsseldorf 1987 (Bibliography to the Symposium on modern methods for the quantitative evaluation of ultrasonic defect indications, Düsseldorf 1987, 70 papers.)

S189 DGZfP (Ed.) Ultrasonic Testing Basic Course U 1 e, Training Course of Ultrasonic Testing with Exercises and Drawings U 10 e, Ultrasonic Testing, Advanced Course U 2 e. Deutsche Gesellschaft für Zerstörungsfreie Prüfung, e. V. Unter den Eichen 87, D 1000 Berlin 45

S190 DGZfP and IzfP (Eds.): Proc. 3rd Intern. Symp. on Nondestructive Characterization of Materials, Saarbrücken 1988

S191 DGZfP (Ed.) Proc. Seminar on "Automatisierung in der Ultraschallprüfung", Berlin 1988

Subject Index